Contributing Editors

Loren A. Jacobson
Los Alamos National Laboratory, Retired
Dennis R. Floyd
Science Applications International Corp.
Gilbert London
U.S. Naval Air Systems Command, Retired
George Fulton
Lawrence Livermore National Laboratory
Don H. Hashiguchi
Brush Wellman, Inc.
Mark N. Emly
Brush Wellman, Inc.
Warren Haws
Brush Wellman, Inc.
Christopher Dorn
Brush Wellman, Inc.
Robert J. Hanrahan
National Nuclear Security Agency
Richard Alan Patterson
Los Alamos National Laboratory
James C. Foley
Los Alamos National Laboratory
Frank Gibbs
Colorado School of Mines
Curtis Salmon
Colorado School of Mines
Angelique Lasseigne
Colorado School of Mines
Erik A. Pfeif
Colorado School of Mines
Donald J. Kaczynski
Brush Wellman, Inc., Retired

About the cover:

The James Webb Space Telescope scheduled to launch in 2013 is a large infrared telescope. The 6.5 m (21 ft) primary mirror contains 18 hexagonal segments made of beryllium. Credit: NASA (www.jwst.nasa.gov)

Beryllium Chemistry and Processing

Kenneth A. Walsh
Deceased

Edited by

Edgar E. Vidal
Brush Wellman, Inc.

Alfred Goldberg
Lawrence Livermore National Laboratory

Edward N.C. Dalder
Lawrence Livermore National Laboratory

David L. Olson
Colorado School of Mines

Brajendra Mishra
Colorado School of Mines

www.asminternational.org

First printing, July 2009

Comments, criticisms, and suggestions are invited, and should be forwarded to ASM International.

Prepared under the direction of the ASM International Technical Book Committee (2008–2009), Lichun L. Chen, Chair.

ASM International staff who worked on this project include Scott Henry, Senior Manager of Product and Service Development; Charles Moosbrugger and Eileen DeGuire, Technical Editors; Ann Britton, Editorial Assistant; Bonnie Sanders, Manager of Production; Madrid Tramble, Senior Production Coordinator; Diane Whitelaw, Production Coordinator; Patty Conti, Production Coordinator; and Kathryn Muldoon, Production Assistant

Library of Congress Control Number:2009923299
ISBN-13: 978-0-87170-721-5
ISBN-10: 0-87170-721-7
SAN: 204-7586

ASM International®
Materials Park, OH 44073-0002
www.asminternational.org

Printed in the United States of America

Dedication

Dr. Kenneth A. Walsh

Kenneth Walsh was a scientist, technologist, and corporate leader in the beryllium industry. Dr. Ken Walsh was a South Dakota native who attained the love of chemistry from Dr. Gregg Evans, professor of chemistry at Yankton College in South Dakota. Ken received his A.B. degree in chemistry from Yankton College in 1942. He continued his studies in chemistry at Iowa State University at Ames, Iowa until his education was interrupted in 1943 by an invitation to join the Manhattan Project. He started his professional career at Los Alamos where he was working on the task to convert enriched uranium from oxide to fluoride which was then reduced to metal. His Los Alamos experiences allowed him to be a contributor to chemical metallurgy at the beginning of the atomic energy age. He also worked on the chemistry of transuranic-metals and compounds. In addition, Ken met his future wife, Dorothy, at Los Alamos. In 1946, he returned to Iowa State University to continue his research for the Atomic Energy Commission and finish his Ph.D. degree. He returned to Los Alamos in 1951.

During the period from 1957 to 1960, Dr. Walsh did inorganic chemical research for the International Mineral and Chemical Company in Mulberry, Florida. In 1960, Dr. Walsh joined the Brush Wellman Company as Research Manager and focused the rest of his career in the science and engineering of beryllium metal and its compounds and alloys. He made many contributions to the chemical and metallurgical processing of beryllium. From his contributions and experiences, he was recognized as an expert in most of the scientific and technology issues associated with production of beryllium. He has numerous publications and patents and was often called upon to give presentations on beryllium to the broader mineral and metallurgical engineering community. He retired as Associate Director of Technology in 1986 and moved to Tyler, Texas.

Kenneth A. Walsh
1922–1999

Preface

With the downturn in beryllium production due to changes in the international political, environmental, health and safety issues, there has been a curtailment in beryllium research and development and a significant loss in beryllium intellectual capacity. Dr. Walsh, knowing that beryllium exhibits unique and advantageous properties as a primary material and as an alloying addition, foresaw that beryllium offers significant advantages that can not be ignored if technology is to advance. Dr. Walsh envisioned a book, which would serve the function as an instructional tool to educate a scientist and engineer as to the chemistry and chemical and metallurgical processing of beryllium. This book should serve as a textbook for a short course or be complete enough to be used by an individual in self-education. This book is, also, to serve as an archive of the tremendous amount of generated knowledge, which does not need to be rediscovered. And finally, this book should offer the user a one stop resource for the necessary chemical and physical data that is often required by practitioners of the chemistry and/or chemical processing of beryllium. Dr. Walsh was concerned about the education of young engineers and wanted them to be fully prepared with both beryllium science and technology, but, also, to have cognizance about the health issues and the proper practices to handle and process beryllium ore, metals, chemicals and waste.

The book is presented in the manner of an introduction of what beryllium is, its history, and its chemical and physical properties. The mineralogy of beryllium, the preferred sources, and the global source of ore bodies are presented. The identification and specifics of the industrial metallurgical processes used to form oxide from the ore and then metal from the oxide are thoroughly described. The special features of beryllium chemistry are introduced, including analytical chemical practices. Beryllium compounds of industrial interest are identified and discussed. Manufacturing processes of alloying, casting, powder metallurgy processing, forming, metal removal, joining, and others are introduced. The industrially interesting alloys are also identified and specified for their content and applications. The physical metallurgy chapter is offered to bring some conformity between chemical and physical metallurgical processing of beryllium, metal, alloys, and compounds. The environmental degradation of beryllium and its alloys both in aqueous and high temperature condition are presented. The health issues are thoroughly presented in one chapter written by experienced professionals. Another chapter is offered to describe the various requirements to handle beryllium in the workplace and the established practices that are available to meet these continuing requirements. A thorough list of references will assist the user of this book in further investigation.

Contributors to this book come from industry, the academic world, and national laboratories. Each group provides their insight on beryllium technology. We would like to extend a special note of appreciation for the support of Lawrence Livermore National Laboratories in this project.

David L. Olson
Colorado School of Mines
Edgar E. Vidal
Brush Wellman, Inc.
January 2009

Contents

Preface . . . . . **vii**

Chapter 1 **Introduction** **1**
1.1 Physical Properties 4
1.2 Chemical Properties 4

Chapter 2 **History of Beryllium** **7**
2.1 Early History 7
2.2 Description of the Origin of the Domestic Beryllium Industry 8
2.3 Description of Foreign Beryllium Production 12
2.4 Current Status of the Beryllium Industry 17

Chapter 3 **Sources of Beryllium** **19**
3.1 Mineralogy 20
3.2 Geological Outcroppings 22
3.3 Summary Statement 25

Chapter 4 **Physical and Nuclear Properties** **27**
4.1 Introduction 27
4.2 Atomic/Crystal Structure 27
4.3 Elastic Properties 27
4.4 Thermal Properties 32
4.5 Nuclear Properties 42
4.6 Miscellaneous Properties 46

Chapter 5 **Thermodynamics of Extraction** **55**
5.1 Thermodynamic Data 55
5.2 Sources of Thermodynamic Data 55
5.3 Reduction of BeO 59
5.4 Reduction of Beryllium Halides 61
5.5 Hydrogen Reduction 61
5.6 Thermal Decomposition of BeI_2 62
5.7 Electrolytic Reduction 62
5.8 Refining of Beryllium by Distillation 63

Chapter 6 Mineral Processing 65
6.1 Bertrandite and Phenacite Flotation 65
6.2 Beryl Concentration from Pegmatitic Gangues and Low-Grade Deposits 66
6.3 Concentration of Beryl Using Hydrofluoric Acid Activation 66
6.4 Concentration of Beryllium Ores 66
6.5 Tall Oil Fatty Acid Flotation of Phenacite and Bertrandite 69

Chapter 7 Extractive Metallurgy 71
7.1 Extraction from Beryl 71
7.2 Kjellgren-Sawyer Sulfate Extraction from Beryl 71
7.3 Degussa Extraction of Beryllium from Beryl 73
7.4 Copaux-Kawecki Fluoride Extraction from Beryl 74
7.5 Extraction from Bertrandite and Solvent Extraction 78
7.6 Beryllium from Leaching and Settling 78
7.7 Solvent Extraction from Sulfate Solutions 79
7.8 Electrolytic Extraction of Beryllium 85
7.9 Cell Configuration 86
7.10 Theoretical Rate Expression 86
7.11 Electrorefining of Beryllium 90

Chapter 8 Chemistry of Beryllium 93
8.1 General Chemical Character of Beryllium 93
8.2 Solution Chemistry of Hydrated Be^{2+} Ions 97
8.3 Beryllium Fluoride 99
8.4 Chemical Behavior of Beryllium 103

Chapter 9 Analytical Chemistry of Beryllium 107
9.1 Sample Preparation for Beryllium Analysis 107
9.2 Quantitative Procedures for Beryllium Determination 107
9.3 Other Methods for Beryllium Separation 110
9.4 Radiochemical Separation Procedures 110
9.5 Radiometric Methods of Beryllium Analysis 111
9.6 Spectrometric Methods 112
9.7 Polarographic Methods 113

Chapter 10 Beryllium Compounds 117
10.1 Beryllium Borides 117
10.2 Beryllium Carbide 117
10.3 Beryllium Carbonates 118
10.4 Beryllium Carboxylates 118
10.5 Beryllium Halides 118
10.6 Beryllium Hydride 121
10.7 Beryllium Hydroxide 121
10.8 Beryllium Nitrate 121

10.9 Beryllium Nitride 122
10.10 Beryllium Oxide 122
10.11 Beryllium Oxide Carboxylates 123
10.12 Beryllium Oxalate 125
10.13 Beryllium Phosphates 125
10.14 Beryllium Perchlorate 126
10.15 Beryllium Sulfate 126
10.16 Beryllium Sulfide 127

Chapter 11 Beryllium Intermetallic Compounds 131
11.1 Background and Historical Information 131
11.2 Structures of the Beryllides 132
11.3 Other Beryllium Intermetallics 133
11.4 Mechanical Properties 134
11.5 Oxidation Behavior 138
11.6 Thermal and Electrical Properties 139
11.7 Sputter Deposition 140
11.8 Diffusion 140
11.9 Hydrogen Storage 141
11.10 Fabrication of Beryllides 142
11.11 Conclusions and Future Work 142

Chapter 12 Amorphous Alloys That Contain Beryllium 145
12.1 Introduction 145
12.2 Early Work on Amorphous Alloys 145
12.3 Recent Efforts 147
12.4 Applications 148

Chapter 13 Physical Metallurgy of Beryllium 151
13.1 Beryllium Phases and Phase Transformations 151
13.2 Beryllium Physical Properties 151
13.3 Mechanical Properties 153
13.4 Heat Treatment 156
13.5 Alloying 157

Chapter 14 Alloying of Beryllium 163
14.1 Introduction 163
14.2 Alloys and Composites 163
14.3 Beryllium-Aluminum Alloys 164
14.4 Aluminum-Beryllium Production 165
14.5 Beryllium-Antimony Alloys 170
14.6 Beryllium-Copper Alloys 171
14.7 Transition Metals 173
14.8 Beryllium-Iron Alloys 173
14.9 Beryllium-Titanium Composites 174

Chapter 15 Beryllium Binary Phase Diagrams 179
15.1 Beryllium-Silver (Ag-Be) 179
15.2 Beryllium-Aluminum (Al-Be) 180
15.3 Beryllium-Gold (Au-Be) 180
15.4 Beryllium-Boron (B-Be) 180
15.5 Beryllium-Barium (Ba-Be) 181
15.6 Beryllium-Calcium (Be-Ca) 181
15.7 Beryllium-Cobalt (Be-Co) 181
15.8 Beryllium-Copper (Be-Cu) 182
15.9 Beryllium-Iron (Be-Fe) 182
15.10 Beryllium-Gallium (Be-Ga) 183
15.11 Beryllium-Germanium (Be-Ge) 183
15.12 Beryllium-Lithium (Be-Li) 183
15.13 Beryllium-Magnesium (Be-Mg) 183
15.14 Beryllium-Molybdenum (Be-Mo) 183
15.15 Beryllium-Sodium (Be-Na) 186
15.16 Beryllium-Nickel (Be-Ni) 186
15.17 Beryllium-Niobium (Be-Nb) 186
15.18 Beryllium-Plutonium (Be-Pu) 187
15.19 Beryllium-Silicon (Be-Si) 187
15.20 Beryllium-Tin (Be-Sn) 187
15.21 Beryllium-Titanium (Be-Ti) 187
15.22 Beryllium-Uranium (Be-U) 188
15.23 Beryllium-Tungsten (Be-W) 188
15.24 Beryllium-Yttrium (Be-Y) 189
15.25 Beryllium-Zinc (Be-Zn) 189
15.26 Beryllium-Zirconium (Be-Zr) 189

Chapter 16 Metallography of Beryllium and Beryllium Alloys 199
16.1 Specimen Extraction 199
16.2 Grinding Procedures 199
16.3 Polishing Procedures 200
16.4 Etching Procedures 202
16.5 Identification of Constituents 205
16.6 Optical Microscopy 206
16.7 Electron Microscopy 206
16.8 Microstructures of Beryllium 207
16.9 Toxicity Issues 207

Chapter 17 Mechanical Properties of Beryllium 209
17.1 Vacuum Hot-Pressed Block Properties 209
17.2 Hot-Isostatic-Pressed Properties 213
17.3 Yield-Point and Portevin-Le Chatelier Effects 214
17.4 Microyield Properties 217
17.5 Fracture Toughness and Ductile-to-Brittle Transition 219
17.6 Notched-Tensile and Notched-Bend Properties 228

17.7 Fatigue Properties 229
17.8 Creep Strength 231
17.9 Grain Size Effects, Recrystallization, and Grain Growth 233
17.10 Control and Effect of Impurities 243
17.11 Hydrostatic Tests 246

Chapter 18 Casting of Beryllium 253
18.1 Solidification of Beryllium 253
18.2 Cast Structure 255
18.3 Grain Refinement 255
18.4 Melting Techniques 257
18.5 Metal Purification 262

Chapter 19 Powder Metallurgy 267
19.1 Introduction 267
19.2 Powder Production 268
19.3 Powder Consolidation 271
19.4 Sintering 277
19.5 Elevated-Temperature Consolidation 280
19.6 Properties of Powder Metallurgy Beryllium 285

Chapter 20 Metalworking 295
20.1 Powder Consolidation 295
20.2 Formability 297
20.3 Rolling 300
20.4 Forming 305
20.5 Forging 311
20.6 Extrusion 316
20.7 Wire Drawing 322
20.8 Spinning 327
20.9 Near-Net Shaping 328

Chapter 21 Metal Removal 339
21.1 Overview 339
21.2 General Machining Guidelines 341
21.3 Machining-Surface Damage 342
21.4 Machining Operations 348

Chapter 22 Beryllium Coating Processes 361
22.1 Beryllium Coatings 361
22.2 Physical Vapor Deposition 363
22.3 Sputtering 370
22.4 Ion Plating 384
22.5 Plasma Arc Spraying 387
22.6 Chemical Vapor Deposition 393
22.7 Electroplating (Electrodeposition) 395

Chapter 23 Welding and Joining of Beryllium and Beryllium Alloys 401
23.1 Fusion Welding 401
23.2 Brazing 413
23.3 Solid-State Bonding 421
23.4 Soldering 438

Chapter 24 Adhesive Bonding and Mechanical Fasteners 441
24.1 Introduction 441
24.2 Classification of Adhesive Materials 443
24.3 Some Structural-Adhesive Types 445
24.4 Storage Life and Exposure of Adhesives 447
24.5 Surface Preparation 447
24.6 Applying Adhesives 451
24.7 Curing Adhesives 451
24.8 Mechanical Properties 452
24.9 Mechanical Fasteners 453

Chapter 25 Aqueous Corrosion of Beryllium and Beryllium Alloys 459
25.1 Corrosion in Various Environments 459
25.2 Corrosion of Beryllium in Rainwater and Seawater 463
25.3 Observations Related to Carbides and Other Inclusions 464
25.4 Polarization Studies 465
25.5 Pitting Corrosion 467
25.6 Crystallographic-Orientation Effect on Corrosion 472
25.7 Contamination Sources and Corrosion Prevention 474
25.8 Effect on Mechanical Properties 478

Chapter 26 High-Temperature Corrosion of Beryllium and Beryllium Alloys 485
26.1 Beryllium in Gaseous Atmospheres 485
26.2 High-Temperature Corrosion-Resistant Alloys 490

Chapter 27 Beryllium Waste Recycling 493
27.1 Introduction 493
27.2 Resource Recovery and Process Facility 493
27.3 Summary 498

Chapter 28 Medical Aspects of the Toxicity of Beryllium and Beryllium Alloys 499
28.1 Introduction 499
28.2 Beryllium Diseases 500
28.3 Some Statistical Observations 503
28.4 Contamination Sources 506
28.5 First-Aid Procedures and Precautions 508
28.6 Protective and Preventive Actions 509
28.7 Acronyms 511

Chapter 29 Hygienic Practices for Handling Beryllium and Its Components 513
29.1 Introduction 513
29.2 Implementation of Handling Practices 513
29.3 Applications 516
29.4 References of Regulations 517

Appendix Bibliography 523

Index 561

ASM International is the society for materials engineers and scientists, a worldwide network dedicated to advancing industry, technology, and applications of metals and materials.

ASM International, Materials Park, Ohio, USA
www.asminternational.org

Publication title	Product code
Beryllium Chemistry and Processing	05223G

To order products from ASM International:

Online Visit www.asminternational.org/bookstore

Telephone 1-800-336-5152 (US) or 1-440-338-5151 (Outside US)

Fax 1-440-338-4634

Mail Customer Service, ASM International
9639 Kinsman Rd, Materials Park, Ohio 44073, USA

Email Cust-Srv@asminternational.org

In Europe American Technical Publishers Ltd.
27-29 Knowl Piece, Wilbury Way, Hitchin Hertfordshire SG4 0SX, United Kingdom
Telephone: 01462 437933 (account holders), 01462 431525 (credit card)
www.ameritech.co.uk

In Japan Neutrino Inc.
Takahashi Bldg., 44-3 Fuda 1-chome, Chofu-Shi, Tokyo 182 Japan
Telephone: 81 (0) 424 84 5550

Beryllium Chemistry and Processing, p 1-5
By Kenneth A. Walsh
Edited by Edgar E. Vidal, Alfred Goldberg,
Edward N.C. Dalder, David L. Olson, and Brajendra Mishra

CHAPTER 1

Introduction

Kenneth A. Walsh, Brush Wellman Inc., Retired

BERYLLIUM, with a symbol of Be, was originally identified as glucinium (Gl) and is located in the upper left corner of the periodic table of the elements, as seen in Fig. 1.1. Beryllium sits atop the group IIA elements (alkaline earths). It is uniquely located near the beginning of the first short period of the periodic table. Beryllium has an atomic number of 4 and an atomic weight of 9.012182, and it is unique among the elements of even atomic number in that it has a single, stable, naturally occurring isotope ($_4Be^7$). Table 1.1 shows the radioisotopes for beryllium. Its electronic structure in its ground state is given as $ls^2 2s^2$, which has an outer shell of two s-electrons, characteristic of members of the group IIA family. It chemically operates in the electronic hybrid state of $1s^2 2s^1 2p^1$, which gives it a valence of two. The position of beryllium between lithium and boron in the periodic table explains its low density of 1.85 g/cm^3. The density is the second lowest of all the metals. Its melting point of 1551 K (1287 °C) is consistent with its periodic table position.

Beryllium has found commercial outlets for the metal, its oxide, and in alloys, especially copper, aluminum, and nickel-beryllium alloys. Metal usage is prevalent in nuclear and structural applications, which comprise approximately 10% of the annual beryllium consumption. Beryllia ceramic ware used for substrates in high-density electronic circuits requires 15% of the annual beryllium production. High-strength and high-conductivity copper-beryllium alloys represent 75% of the annual beryllium usage.

The nuclear properties of beryllium are unique because it has a low atomic mass, a low x-ray absorption cross section, and a high neutron scattering cross section. With its low mass x-ray absorption coefficient, one of the earliest uses of beryllium was for radiation windows in diagnostic x-ray equipment. As early as 1951, beryllium was selected as a reflector or moderator in nuclear reactors. Quantities of beryllium used in reactors ranged from a few kilograms in systems for nuclear auxiliary power devices to 1600 kg in the Advanced Test Reactor at Idaho National Laboratory. Until the cessation of nuclear weapon construction, large amounts of beryllium metal were used in the triggering device in nuclear warheads.

Beryllium possesses certain unique mechanical and physical properties that make it a special engineering material and an important alloy addition, particularly in copper, nickel, and aluminum alloys. With the highest modulus of elasticity and strength-to-weight ratio coupled with a high melting point, tensile strength, and specific heat and low coefficient of thermal expansion in comparison with most of the structural materials (Table 1.2), beryllium has potentially large applications in aircraft, aerospace, nuclear power, and optical component industries [Clement et al. 1992]. However, almost all of the beryllium in use is from a powder metallurgy product since castings of beryllium generally contain porosity and other casting defects due to its high melting point, high melt viscosity, and narrow solid-liquid range [Stonehouse and Marder 1990]. Beryllium also is an excellent addition for developing specific alloy properties, particularly copper-beryllium alloys. The high specific heat, high thermal conductivity,

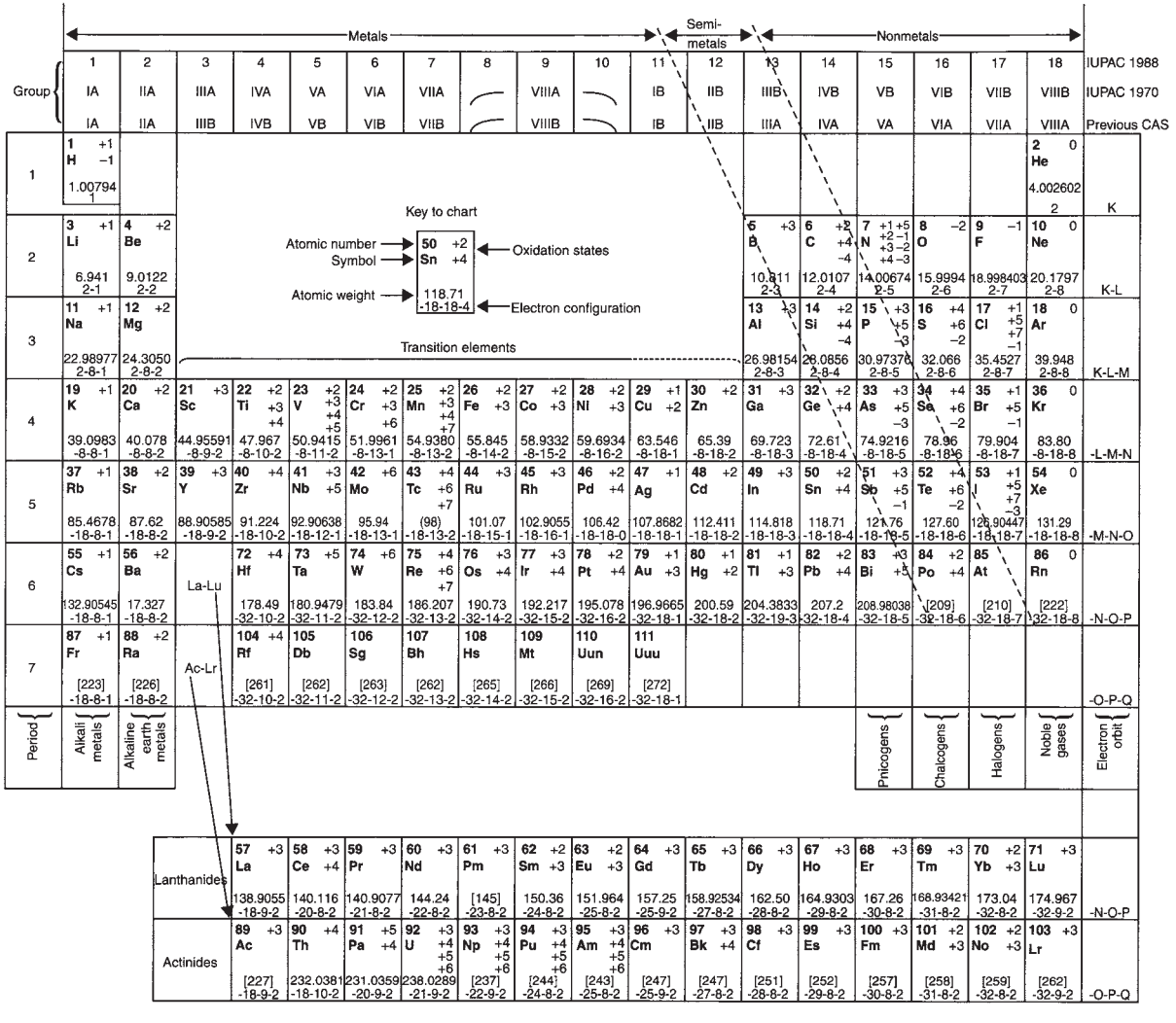

Fig. 1.1 Periodic table of the elements. Beryllium (Be) is located at the top of the second column, group IIA. This column is known as the alkaline earth metals.

Table 1.1 Radioisotopes of beryllium

Isotope	Mass	Half-life	Mode of decay	Nuclear spin
^{6}Be	6.01973	5.9×10^{-21} s	2p to ^{4}He	0
^{7}Be	7.016929	53.28 d	EC to ^{7}Li	$^{3}/_{2}$
^{8}Be	8.0053051	approx 7×10^{-17} s	2α to n	0
^{10}Be	10.013534	1.52×10^{6} y	β^- to ^{10}B	0
^{11}Be	11.02166	13.8 s	β^- to ^{11}B; β^- + α to ^{7}Li	$^{1}/_{2}$
^{12}Be	12.02692	0.024 s	β^- to ^{12}B; β^- + n to ^{11}B	0
^{13}Be	13.0428	0.004 s	β^- to ^{13}B; β^- + n to ^{12}B; β^- + 2n to ^{11}B	0

Source: Lide 1998

Table 1.2 Application of beryllium and its alloys

Class	Usage	Properties utilized
Nuclear	Moderator and reflector in reactors	Low atomic weight Low-absorption and high-scattering cross section to neutrons
	Photoneutron source in reactors	Low photoneutron threshold
	X-ray windows	Low mass absorption cross section High melting point and thermal conductivity
Aerospace	Structures	High modulus as the temperature rises with advanced speeds High strength-to-weight ratio High specific heat
	Instruments, e.g., gyroscope gimbals, torque tubes, high-speed rotating elements	Light weight High toughness Dimensional stability
	Heat sink	High specific heat and thermal conductivity
	Antenna	High specific heat and thermal conductivity
	Structure and radiator fins of thermoelectric power for moon exploration	High specific heat Light weight High thermal output in oxidation
Others	Copper-beryllium springs	Greater corrosion resistance High electrical and thermal conductivity Nonmagnetic
	Copper-beryllium dies for plastic pressing	High hardness and thermal conductivity
	Copper-beryllium electrodes for resistance welding	High hardness and electrical conductivity
	Safety tools in mines and oil tankers	High strength and nonsparking characteristics

Source: Lide 1998

low density, high melting point, and rigidity of the metal aroused substantial interest among space scientists after the U.S.S.R. *Sputnik* success in 1957. Its high stiffness, light weight, and dimensional stability over a wide temperature range made beryllium useful in satellite and space vehicle structures, inertial guidance systems, military aircraft brakes, and space optical components. In the U.S. space shuttles, several structural parts and the brake components use beryllium. Other applications of metallic beryllium include high-speed computer components, audio components, and mirrors.

Its low density, high reactivity, and high melting point along with its occurrence in the form of a very stable beryl ore, which contains approximately 5% Be, make its extraction difficult. The electrowinning of beryllium from molten beryllium and sodium chloride salt-mix is a low-temperature commercial process. Conversion of beryl ore into beryllia precedes the fused salt electrolysis, and several purification techniques are followed to produce high-purity beryllium metal.

A new modified beryllium chloride-beryllium fluoride fused salt electrolysis process is suggested for the production of beryllium on similar principles but with an added advantage of a semicontinuous high-efficiency process. A beryllium fluoride-lithium fluoride fused salt electrolysis at 700 °C is proposed, using theoretical considerations where beryllium may be deposited on a molten aluminum metal cathode. A possible basic cell design has also been proposed. The product, aluminum-beryllium alloy, can be used as a master alloy for aluminum alloy production or as a lightweight, high-strength material. The physical metallurgy

of beryllium, including the powder processing, has been discussed. The metal processing, including joining of beryllium, has also been qualitatively described.

The high cost of production and the associated health hazards have restricted the application of beryllium in many branches of engineering, in spite of its excellent combination of physical, mechanical, and nuclear properties. The health issues are described, and the proper handling of beryllium metal and compounds is described.

The beryllium industry can tailor products to industrial requirements. Beryllium mill products are now available in ingot, lump, chip, powder, block, billet, rod, bar, tube, foil, sheet, plate, wire, and other specialty shapes. Beryllia is an excellent heat conductor as well as an electrical insulator. The material has high hardness and strength. Its specific heat of 1088 J/kg · °C at room temperature is the highest of any ceramic and is greater than that of all metals except beryllium. To avoid overheating, most communication equipment and high-powered communication tubes use beryllia heat sinks. Likewise, heat generated in resistor cores and substrates is rapidly dissipated, thereby minimizing hot spots and reducing temperatures of critical components. The substrates serve in high-speed computers and automotive ignition systems. The number of commercial beryllium alloys is limited by inherent high cost, the toxicity of beryllium, and such metallurgical problems as severe segregation in the alloys. The most important alloys are with copper, which are essentially ternary alloys of copper, beryllium, and cobalt with traces of other elements. The two general categories of copper-beryllium alloys are the high-strength and the high-conductivity materials.

The high-strength alloys contain 1.6 to 2.9 wt% Be, with cobalt additions of up to 1 wt% in the copper matrix. The most important of the high-strength compositions is alloy 25 (UNS C17200), with 1.80 to 2.00 wt% Be. By solution annealing at 750 to 825 °C for 5 min or more, followed by water quenching, the beryllium is left in solid solution at room temperature. The alloy can then be cold worked and machined into finished product shapes. Precipitation hardening can be accomplished by aging for 0.5 to 3 h at 315 to 400 °C. Tensile strengths as high as 1500 MPa (218 ksi) have been observed for the fully age-hardened condition. The electrical conductivity of alloy 25 is 22 to 25% IACS (International Annealed Copper Standard). A leaded version of this alloy has improved machinability.

A slightly less costly high-strength composition with 10% lower tensile properties is used for small electrical components. Alloy 165 (UNS C17000) is slightly less costly because of its lower (1.6 wt%) beryllium content. It is used for electrical contacts, springs, clips, switches, bellows, and Bourdon pressure gages. Strip product in the range of 0.03 to 0.40 mm thickness is commonly used as the manufacturing base for these products.

The high-conductivity alloys have low beryllium levels of 0.3 to 0.8 wt% with high cobalt contents of 1.4 to 2.7 wt%. The most commonly used alloy has 0.5 wt% Be and 2.5 wt% Co. It can be solution annealed at 900 to 940 °C. Aging is performed at 425 to 540 °C for 1 to 4 h. The maximum strength for these alloys is in the range of 700 to 900 MPa (101 to 130 ksi). Beryllium metal has an electrical and a thermal conductivity that is approximately 40% that of copper. An electrical conductivity of 40 to 60% IACS is typical.

1.1 Physical Properties

Beryllium is a steel-gray, lightweight, hard, metallic element. One of its chief useful characteristics is as an alloying element to harden and strengthen other metals. It has a specific gravity of 1.846 and a melting temperature of 1285 °C. It exhibits a hardness from 6 to 7 on the Mohs scale. The oxide film that forms quite readily on the surface of the metal is hard enough to scratch glass. The speed of sound is 2.5 times faster than that of steel. The principal physical data are given in Table 1.3 [Lide 1998].

1.2 Chemical Properties

Pure beryllium is rather stable and tarnishes slightly at room temperatures in dry air and pure oxygen. When it is finely ground and blown into a flame, it burns with brilliant scintillations. Compounds of beryllium have a sweet taste, which accounts for the name glucinum or glucinium, which was first applied to the element. When beryllium is heated in air, a thin, almost invisible oxide layer develops, similar to oxide formation of aluminum. This oxide protects the metal.

Table 1.3 Physico-chemical properties of beryllium compared with other elements commonly used as the solvent for commercial alloys

Properties	Aluminum	Magnesium	Iron	Titanium	Beryllium
Atomic weight	26.98	24.30	55.85	47.9	9.0122
Crystal structure at 25 °C(a)	fcc	hcp	bcc	hcp	hcp
Density, g/cm^3	2.70	1.74	7.87	4.507	1.85
Melting point, °C	660	649	1537	1660	1285
Boiling point, °C	2494	1090	2750	3287	2770
Electronegativity [Pauling 1960]	1.5	1.2	1.8	1.5	1.5
Latent heat of fusion, kJ/mol	10.79	8.59	13.80	15.45	12.2
Electrical conductivity at 20 °C, $[\mu\Omega \cdot cm]^{-1}$	0.372	0.256	0.103	0.0182	0.25
Thermal conductivity, W/m · K	247	156	80.2	21.9	210
Specific heat, cal/g · °C	0.215	0.245	0.107	0.125	0.436
Nature of oxide	Amphoteric	Basic	Basic	Acidic	Amphoteric
Elastic modulus, GPa	9.9	45	28.5	16	303
Coefficient of thermal expansion, 10^{-6}/°C	23.2	2.5	11.9	8.7	11.5
Mass absorption coefficient (Cu-kα), cm^2/g	. . .	. . .	. . .	. . .	1.007
Specific modulus, m*10^{-6}	3.66	2.48	3.62	3.55	16.7

(a) fcc, face-centered cubic; hcp, hexagonal close-packed; bcc, body-centered cubic.
Source: Lide 1998

Beryllium presents the designer with a combination of desirable properties not found in any other material. Strength-to-weight and stiffness-to-weight ratios of beryllium are outstanding. It has the highest specific heat of any metal, as well as excellent thermal conductivity, and it has excellent properties at both elevated and cryogenic temperatures. The unique physical properties of beryllium make it the material of choice for x-ray and nuclear applications. The high stiffness-to-weight ratio, combined with excellent damping properties, make it the premier material for acoustics applications.

REFERENCES

Clement, T.P., Parsonage, T.B., and Kuxhaus, M.B., 1992. Near-Net-Shape Processing Cuts Cost of Beryllium Optics, *Adv. Mater. Process.*, Vol 141 (No. 3), p 37–40

Lide, D.R., 1998. *Handbook of Chemistry and Physics*, 79th ed., CRC Press, Boca Raton, FL

Pauling, L., 1960. *The Nature of the Chemical Bond*, 3rd ed., Cornell University Press, Ithaca, NY

Stonehouse, A.J., and Marder, J.M., 1990. Beryllium, *Properties and Selection: Nonferrous Alloys and Special-Purpose Materials*, Vol 2, *ASM Handbook*, ASM International, p 683–687

SELECTED REFERENCES

- ASM, 1955. *The Metal Beryllium*, American Society for Metals
- Griffith, R.F., 1955. Chap. IIA, *The Metal Beryllium*, American Society for Metals
- Hausner, H.H., 1965a. *Beryllium: Its Metallurgy and Properties*, University of California Press, Berkeley and Los Angeles, CA
- Herman, M., and Spangler, G.E., 1961. *The Metallurgy of Beryllium*, Institute of Metals, London, p 28–75
- Klein, J.L., Macres, V.G., Woodard, D.H., and Greenspan, J., 1955a. Chap. VII, *The Metal Beryllium*, American Society for Metals
- Marder, J.M., and Batich, R., 1985. Beryllium, *Metallography and Microstructures*, Vol 9, *Metals Handbook*, 9th ed., American Society for Metals, p 389–390

Beryllium Chemistry and Processing, p 7-18
By Kenneth A. Walsh
Edited by Edgar E. Vidal, Alfred Goldberg,
Edward N.C. Dalder, David L. Olson, and Brajendra Mishra

CHAPTER 2

History of Beryllium

Kenneth A. Walsh and Donald J. Kaczynski, Brush Wellman Inc., Retired
Loren A. Jacobson, Los Alamos National Laboratory, Retired
David L. Olson, Colorado School of Mines

2.1 Early History

In its purest form, beryl was known and treasured in ancient times as a precious stone. It was found in the oldest known Smaragd mines, which have been traced back to approximately 1650 B.C. The mines are reported to have been located in the Zabarah Mountains of Egypt, south of Kosseir. Smaragd beryl is green in color, a result of its Cr_2O_3 impurity content.

Beryl and emerald were well known as far back in history as Pliny's day (circa 77 A.D.), but they were not suspected of being one and the same mineral. The French mineralogist, Hauy, observed their crystallographic similarity and induced Vauquelin in 1797 to determine the possible similar chemical composition of the two minerals. Not only did Vauquelin confirm their chemical identicalness, but in 1798 he discovered the presence of a new element, which he first named earth of beryl and which later, at the suggestion of Annales de Chemie er de Physique, he referred to as glucine. Glucine was derived from the Greek word *glykys*, which means sweet. These salts have a sweet taste. The element is now known as beryllium, but for many years in France it has been known as glucinum or glucinium [National Security Research Board (NSRB) 1953].

Vauquelin [1798] reported the isolation of a new oxide from beryl. In Vauquelin's procedure, gemstone emerald was finely pulverized before melting with three times its mass of potassium hydroxide. The cooled melt was dissolved in water and the silica removed by filtration. The filtrate was diluted with potassium hydroxide solution and boiled to precipitate beryllium hydroxide contaminated with a trace of aluminum hydroxide. The precipitate was dissolved in hydrochloric acid and then reprecipitated by aqueous potassium carbonate. This precipitate, after recovery by filtration, was dissolved in very dilute sulfuric acid and evaporated after the addition of aqueous ammonium carbonate. The resulting solids were filtered, washed, and dried. Ignition yielded the new oxide, BeO. The new oxide differed from alumina in that it did not form an alum. It was soluble in aqueous ammonium carbonate. Salts formed from the oxide had a sweet taste, prompting Vauquelin to name it glucinium, from the corresponding Greek term.

Pure beryllium was simultaneously and independently produced in 1828 by Wöhler [1828 a,b] and Bussy [1828] by reducing beryllium chloride with potassium in a platinum crucible. Wöhler initiated a nomenclature controversy by referring to the new oxide as berylerde, from which the element was named beryllium. The quarrel was perpetuated by Bussy, who employed the glucinium label. The final choice between beryllium and glucinium was made by the International Union of Pure and Applied Chemistry. The name beryllium and the symbol beryllium became official in 1957. Everest gives a concise description of the early disagreement over the valency of beryllium [Everest 1964]. Berzelius first gave it a value of two, but he later changed this value to three in view of the strong chemical relationship between beryllium and aluminum. The combining ratio of beryllium was 4.7, so the trivalency implied its atomic weight of 14. This value was supported by the Dulong-Petit rule:

$$\text{Atomic weight} = 6.3/\text{Specific heat} = 6.3/[0.397 \text{ for Be}] = 15.8 \quad \text{(Eq 2.1)}$$

Mendeleev could not accommodate an element of atomic weight 14 in his periodic table. He suggested the valency of two, from which its atomic weight of 9.0121 would fit beryllium comfortably between lithium and boron. Mendeleev's prediction was confirmed by the accurate vapor density measurement on beryllium chloride made by Nilson and Pettersson [1878].

Much progress was made by numerous investigators during the late 19th and early 20th centuries to determine the physical properties and chemical relationships of beryllium. Several investigators attempted to prepare beryllium electrolytically. The initial success is attributed to Lebeau in France. In 1898, he used an electrolyte of fused beryllium fluoride and sodium fluoride and liberated beryllium metal. In 1913, Flichter in Germany used Lebeau's method to obtain the first manipulatable quantity of pure (98 wt%) beryllium. In Germany, Oesterheld published the equilibrium diagrams of beryllium-copper, beryllium-aluminum, beryllium-iron, and beryllium-silver [Oesterheld 1916]. Also in 1916, Hugh Cooper produced the first sizeable ingot of beryllium in the United States, which suggested the potential for commercialization. In 1918, Cooper patented a beryllium-aluminum alloy [NSRB 1953].

There was not enough metal to study the properties of beryllium until Lebeau's electrowinning success in 1898 [Lebeau 1898, 1899]. Lebeau selected an electrolyte containing the double salts $2NaF \cdot BeF_2$ and $NaF \cdot BeF_2$. The electrolyte was contained in a nickel crucible that also served as the cathode. A carbon plate or rod was used as the anode. After melting by means of a Bunsen burner, the heating effect of the electric current of 20 A at a potential of 80 V maintained the fluidity of the molten mixture. At the end of the electrolysis, the melt was comminuted and leached with water to remove the fluorides. To remove the last traces of impurities and water, the pure crystallized beryllium flakes were washed with alcohol and dried in a vacuum.

2.2 Description of the Origin of the Domestic Beryllium Industry

Hugh Cooper's success in producing the first sizeable ingot of beryllium [NSRB 1953] led to the laboratory investigations of Stock and Goldschmidt, starting in 1920, to produce liquid beryllium by high-temperature electrolysis. The developmental aspects of their work were continued by Siemens and Halske Konzern in Germany. The formation of the Brush Laboratories in 1921 initiated developmental work in the United States under the direction of Sawyer. The commercial importance emerged from the developmental programs with the discovery of the exceptional mechanical properties of metals alloyed with beryllium. The ability of beryllium, with the addition of small amounts of nickel, to age harden copper was discovered by Corson in 1926. Michael G. Corson was a metallurgist for the Electro-Metallurgical Corporation, a subsidiary of Union Carbide and Carbon Corporation.

In 1929, the first specimen of ductile beryllium metal had been prepared and reported by Rosenhain in England [NSRB 1953]. The beryllium industry had an uncertain but progressive industrial growth up to 1939, when the engineering usefulness of the metal in a variety of alloy products was definitely established.

In 1927, the Beryllium Corporation of America, later to become the Beryllium Corporation, was organized in Cleveland, and in 1932, at Marysville, MI, produced the first significant quantity of domestic beryllium-copper. In 1936, the Beryllium Corporation moved its plant from Marysville, MI, to Reading, PA.

The commercial-scale beryllium ore producers as of 1940 [NSRB 1953] were:

- The Beryllium Corporation of Pennsylvania, Reading, PA (later, the Beryllium Corporation), processed ore to beryllium oxide and to 4 wt% Be-Cu alloys. This company also fabricated various mill shapes, parts, and nonsparking tools.
- The Brush Beryllium Company of Cleveland, OH, processed beryllium ore to beryllium oxide and to 4 wt% Be-Cu master alloy. Small amounts of beryllium metal were produced for experimental purposes. Fluorescent-grade beryllium oxide, fused beryllium oxide, and beryllium-aluminum alloys were also being produced.
- Clifton Products Incorporated of Painesville, OH, produced beryllium oxide. The fluorescent grade was sold mainly to fluorescent lighting-tube manufacturers and the metallurgical grade to other beryllium producers for further processing.

The Beryllium Corporation and Brush Beryllium accounted for approximately 95% of the total beryllium production. The Beryllium Cor-

poration produced primarily the beryllium-copper master alloy and brass mill products. Brush Beryllium produced primarily the beryllium-copper master alloy, beryllium metal, beryllium-aluminum alloy, and a special grade of beryllium oxide for fluorescent phosphors, refractories, and so on. Clifton Products, on a very small scale, was producing special beryllium oxide for fluorescent lighting and also some beryllium metal. After 1949, Clifton Products Company was engaged in research activities.

2.2.1 The Beryllium Corporation

The Beryllium Corporation was organized as the operating company in 1936. The Beryllium Corporation was initially organized and incorporated under Delaware laws on August 14, 1929, as a development and research company under the name of The Beryllium Development Corporation. The business was originally at Marysville, MI, and late in 1935 was moved to a location near Reading, PA, to procure more advantageous plant and transportation facilities. In the latter part of 1936, the company set up a foundry for casting beryllium alloys and shortly thereafter purchased the beryllium safety tool business of the Stanley Tool Company of New Britain, CT. The company, in like manner, also completed a transaction for absorbing, through purchase, the safety tool business from the Super Heater Company of East Chicago, Inc. In both transactions, the purchases included patents, machinery, stocks of tools, and the forwarding of subsequent orders to the company. Most of the activities of the parent organization's activities had been centered on the production of alloys. During World War II, the War Production Board Expansion Program of Domestic Beryllium Industry increased the productive capacity of beryllium products in the domestic industry. As of April 1942, this company was processing approximately one-third of the beryl ore used in United States' production. It reduced ore to beryllium oxide; processed the oxide to a 4 wt% Be-Cu master alloy; prepared beryllium-copper commercial alloys averaging approximately 2 wt% Be content; produced sheet, strip, wire, and rod; and fabricated various mill shapes, tools, and so on [NSRB 1953].

Under the Defense Plant Corporation's expansion program and fabricating facilities at the Beryllium Corporation's plant, the production of 4 wt% Be-Cu master alloy in 1942 and 1943 amounted to 621,064 and 844,777 kg (1,369,211 and 1,862,414 lb), respectively. By 1953, this company was the largest producer of beryllium products in the world [NSRB 1953].

2.2.2 The Brush Beryllium Company

The Brush Beryllium Company, an Ohio corporation chartered in January 1931 by Charles B. Sawyer, was established to exploit certain patents developed by an affiliated unit, The Brush Laboratories Company, for the production of beryllium for commercial uses. The Brush Laboratories Company was chartered under Ohio laws in 1921 to do research and experimental work and was founded by Charles F. Brush, Jr. and Dr. C.B. Sawyer. Although that concern transferred certain of its patents to the subject company and to the Brush Development Company for exploitation, it has continued to conduct a well-equipped laboratory, doing metallurgical and chemical experimental work [NSRB 1953].

The Brush Beryllium Company of Cleveland was incorporated in 1931 by Charles B. Sawyer on the basis of beryllium investigations conducted since 1921 by the Brush Laboratories Company. The company, which was later licensed under the Corson patent, received its first substantial order for beryllium-copper in December 1934 [NSRB 1953].

The Brush Development Company, an Ohio corporation chartered in 1930, grew out of the Brush Laboratories Company in a similar manner. It manufactured piezoelectric devices, scientific instruments, recording devices, and so on. It also did research on piezoelectric devices. The Brush Beryllium Company manufactured beryllium metal, compounds, and alloys, which were sold to phosphor manufacturers, refractories users, rolling mills, foundries, and other industrial users in the United States, Canada, and European countries. Production facilities are confined to one plant, which is in Elmore, OH, and fabrication work was done in its Cleveland plant. The company operated a government-owned plant at Luckey, OH, for the Atomic Energy Commission. Large-scale production of 4 wt% Be-Cu master alloy and casting-alloy ingots was resumed in a plant that was destroyed by fire [NSRB 1953].

As of April 1942, the Brush Beryllium Company supplied approximately one-third of the United States' output of beryllium-copper master alloy from ore. Its facilities were designed for processing ore to beryllium oxide and beryllium oxide to 4 wt% Be-Cu master alloy, which

was sold to commercial alloy manufacturers. Brush was the first company to produce commercially, on a large scale, fused beryllium oxide, pure beryllium oxide, and beryllium-aluminum alloys. Early in 1942, it appeared that the Brush Company's beryllium-copper plant capacity had been reached.

In 1942, the War Production Board, as a result of the growing demands for the master alloy and the indicated lack of adequate productive capacity, recommended that the Defense Plant Corporation expand the Brush Beryllium Company plant in Lorain, OH. The expanded facilities resulted in an appreciable increase in production totals of 4 wt% Be-Cu master alloy, with growth from 408,000 kg (900,000 lb) in 1942 to 590,000 kg (1,300,000 lb) in 1943 [NSRB 1953].

In the post-World War II period, the Brush Beryllium Company was the world's largest producer of pure beryllium metal and pure beryllium oxide.

2.2.3 Clifton Products Incorporated

Clifton Products, Inc. of Painesville, OH, was organized by the late Dr. Robert E. Windecker and C.E. Windecker in 1939 and produced beryllium oxide of high purity for use in fluorescent lamps and refractories and also planned in 1944 to 1945 to reclaim beryllium-copper scrap. The first oxide was produced in this plant by late 1940. By 1942, the company had produced high-quality commercial oxide. Experimental quantities of pure beryllium had also been produced. The War Production Board recommended expansion for especially pure-quality beryllium-copper, alloys, prompting a program of expansion at this company's plant in Painesville, OH. The expansion was planned to provide for output of up to 7545 kg (16,600 lb) monthly of 4 wt% high-purity beryllium-copper master alloy that would be suitable for use, after dilution to approximately 2 wt% Be content, in production of delicate springs for instruments and small pieces of apparatuses needed for more exact control of aircraft, radio, radar, artillery, and other war equipment. The demand for these high-purity products disappeared before production developed, with the result that only a few pounds of beryllium-copper master alloy and beryllium metal were produced and sold at a loss. In 1943, the company's beryllium oxide capacity was expanded approximately ten times, and production facilities for electrolytic flake beryllium were installed. The beryllium department was put in operation in October 1943 [NSRB 1953].

Late in 1943 and during the following year, the company constructed a plant for recovering beryllium-copper scrap for the national stockpile. This stockpile of scrap had been built up by the War Production Board to prevent loss of all beryllium by the return of such scrap to copper smelters [NSRB 1953].

Production in the new oxide facilities continued from the time of their completion in the spring of 1944 through the peak year 1947, when the entire industry was struck with the impact of beryllium toxicity. At this time, the major customer for pure beryllium oxide was the fluorescent-tube industry. In January 1948, the entire fluorescent-tube industry discontinued all further purchases of beryllium oxide. The company continued to produce against a backlog of orders through September 1948, when all oxide production ceased. From September 1948 to the mid-1950s, the company continued fundamental research on beryllium and beryllium oxide. The company's interest in the remarkable properties of beryllium oxide as a ceramic material led to development of a means of producing a fully fused refractory material in 1945. Late in 1949, this interest was strongly renewed, and in 1950, facilities were constructed at the Painesville plant for the production of this material. In engineering the plant, modern safety engineering was employed, with production under strict surveillance [NSRB 1953].

In 1945, the company developed a process for quartz sand and an allied process for purifying graphite shapes. This material was being used in quantity for the production of fused quartz tubing. In early 1949, the company adapted some of its obsolete beryllium facilities to the production of plater's nickel salts. Early in 1951, the company started on development and production of special chemicals for the petroleum industry while continuing basic research on beryllium. After the death of Dr. Robert E. Windecker in 1943, the management was directed by C.E. Windecker; the research department and laboratory had been under the direction of Dr. Anton Schormuller [NSRB 1953].

Copper-beryllium alloy was first marketed in 1931 as a competitor for phosphor bronze. Commercial production by carbon reduction of beryllium oxide in the presence of metallic copper began in the United States in 1934 [Kjellgren 1946]. A copper-beryllium alloy, which contains approximately 2 wt% Be and 0.25 wt% Co, re-

mains the most important alloy. Like copper, the alloy in the annealed condition is ductile and can be processed into all of the usual mill product forms—strip, rod, wire, and tubing. After heat treatment for 2 to 3 h at (315 °C), the formed alloy acquires great mechanical strength in combination with comparatively good electrical conductivity. The alloys accounted for approximately 75% of all beryllium consumption.

Since metallic beryllium was not needed for copper alloy production, its manufacture was not pursued until the 1940s. At that time, the best known use for the metal was in the field of nuclear energy [Bellamy and Hill 1963]. Beryllium was electrowon and cast into billets for these applications. The metal always solidified with very large grain size. Consequently, cast beryllium could not be precision machined, and the fabricated parts had low strength and extreme hot shortness.

In 1952, the contracts between Clifton Products and the Atomic Energy Commission to supply beryllium products were terminated. In 1956, Lubrizol bought the Clifton Products company.

2.2.4 Kawecki Berylco Industries (NGK Metals)

In 1968, Kawecki Chemical Co. and the Beryllium Corporation merged into Kawecki Berylco Industries (KBI). In 1979, under increasing pressures from aging equipment and agency regulation, KBI (having recently become a wholly-owned subsidiary of Cabot Corp.) exited the pure beryllium business. KBI had previously ceased production of beryllium oxide and was working with Brush Wellman to supply its oxide customers. This left KBI only in the beryllium alloy business. Interestingly, Brush Wellman was also planning to exit the pure beryllium business and was only weeks away from announcing this intention when KBI made its announcement. Having acquired all the western world's pure beryllium and beryllium oxide business has allowed Brush Wellman to remain in the beryllium business today (2008).

In 1978, KBI became a wholly-owned subsidiary of Cabot Corporation. In 1986, Cabot Corporation reached an agreement with NGK Insulators Ltd., Nagoya, Japan, on the sale of the KBI beryllium alloy business. In October 1986, NGK Metals Corporation was established, and it currently has operations in Sweetwater, TN; Nagoya, Japan; and Coueron, France. The primary focus of NGK Metals Corp. is the production of beryllium-copper products.

2.2.5 Brush Wellman, Inc.

In 1948, a fire destroyed the Lorain plant of Brush Beryllium. Brush Beryllium operations moved to Luckey, OH, a few miles south of Toledo. The Luckey plant was owned by the U.S. government, and Brush Beryllium operated it for the Atomic Energy Commission from 1948 until 1960. In 1952, operations began to move ten miles east of Luckey to rural Elmore, OH. By 1960, all of Brush Beryllium's operations were located at the Elmore facility, and the Luckey plant was closed. The Elmore, OH, manufacturing plant, located on a 480 acre site in Harris Township, Ottawa County, is Brush Wellman's flagship facility. Up through 2007, the plant employed over 550 people and had 80,400 m^2 (865,000 ft^2) under roof.

In 1971, Brush Beryllium changed its name to Brush Wellman Inc. after acquiring S.K. Wellman, a friction products manufacturer with products used in brakes and clutches. In 2000, Brush Wellman Inc. became the largest wholly-owned subsidiary of Brush Engineered Materials Inc. Through a series of acquisitions and organic growth, the sales of Brush Engineered Materials Inc. have grown from $500 in 1931 to nearly $1 billion in 2007. The family of businesses selling beryllium-containing materials is approximately 40% of these sales. Brush Wellman Inc. is a fully integrated beryllium production company, with beryllium ore mining operations in Delta, UT, the primary products plant in Elmore, OH, and smaller manufacturing facilities and distribution centers in the United States and around the world.

Brush Wellman Inc. near Toledo was the only U.S. company that produced beryllium until it shut down its aged plant in 1999. The company has a supply of beryllium that is expected to last until 2011. In 2004, an innovative public-private cost-sharing partnership under the Defense Production Act Title III program was established for beryllium production. Brush Wellman will provide technology, land, buildings, and ongoing operation of the facility, while the government will fund engineering, design, and equipment. In 2007, the company selected Elmore, OH, as the site for the proposed new primary beryllium facility, after considering the existing plant sites at Elmore and Delta, UT, for the investment. The new plant is expected to be completed by 2010.

2.3 Description of Foreign Beryllium Production

Small-scale production of beryllium metal and alloys was begun in France, Italy, and Japan in the late 1930s. German output grew during the period; the United States has been and continued until 2009 to be the dominant world producer of beryllium metal, alloys, and compounds. Primary foreign beryllium plants actively engaged in the industry since World War II exist only in France and the former Soviet Union. Pilot plants for experimental purposes were set up in many countries of the world, including England. During the World War II period, the total Italian output was approximately double that of the German industry. The German beryllium industry was subpar even before the war, since it had to import large quantities of beryllium oxide from the Beryllium Corporation from 1936 to 1939. Recoveries in these foreign companies were low, amounting to an average of approximately 50% [NSRB 1953].

After World War II, the French beryllium industry ranked behind those of Germany that produced beryllium-copper and some beryllium metal. The French firm was known as Pechiney (formerly known as Alais, Frogues et Camargues), and the facilities were at St. Jean de Maurienne near Lyon, France.

The French, formerly importing beryllium material from the United States in semiprocessed form, had produced beryllium from ore imported in quantity from Madagascar, French Morocco, and Brazil as well as minor amounts from India. After World War II, the Italian and German beryllium industries were inactivated.

Production of beryllium was prohibited in West Germany by agreement among the United States, France, and the United Kingdom. Since World War II, the Japanese beryllium industry had been reported to be retaining a small interest in the field by producing beryllium oxide on a small scale. India, Argentina, and, more recently, Brazil also have an active beryllium oxide industry.

2.3.1 Argentina

The Sociedad Anonima Berilo Argentina was organized in 1940. This company was formed largely to produce mixed beryllium oxide and carbonate for sale as raw material for the purpose of making beryllium metal. The plant was at Juan Ortiz, Province of Santa Fe, with offices in Buenos Aires. It is understood that the process to be used was invented by a French chemical engineer named Gourden. The plant only produced approximately 230 kg (500 lb) of beryllium hydroxide of questionable quality from 1941 to 1942 and has been inactive since that time.

Federico A. Kubli, in Buenos Aires, had been granted a franchise for selling, in the United States, beryllium oxide-carbonate product of 99% purity, containing approximately 80 wt% BeO, which would be produced in Argentina from local ore [NSRB 1953].

2.3.2 China

For many years, government control of information flow limited the availability of knowledge of beryl mining and extraction in China. This situation was alleviated considerably during the 1970s as China sought foreign currency through export sales of beryl and beryllium products. Construction of production facilities in China had been completed by the Soviet mining engineers, geologists, and technologists in the 1950s. Beryl and extraction products were exported to the former Soviet Union until their personnel were precipitately withdrawn from China in approximately 1962. It has been reported that Japan replaced the former Soviet Union as the consumer of Chinese beryl and beryllium products in the 1960s and 1970s. Japanese beryllium processing facilities had been constructed in areas of high population density. Because of ensuing concern with health problems associated with beryllium toxicity, Japan ceased their extraction operations and relied on the Chinese source. Major mining operations were established by the former Soviet Union engineers at Fuyun (Koktokay) in Xinjiang (Sinkiang) province in the Altay Mountains along the Mongolian border.

China was known to have beryllium metal production in the early 1990s, since Chinese participants presented papers in the United States at a metallurgical conference in 1991. There is a beryllium processing plant in Ningxia province, west of Beijing, but this plant does not produce the basic metal. It does produce beryllium shapes and also makes copper-beryllium alloy for electronic applications. The beryllium metal-producing facility is located in another part of the country and is not known to be operational at this time.

China produces copper-beryllium master alloy in a facility in southern China, Shui Kou Shan Sixth Smeltery. The Shui Kou Shan facility converts purchased beryl ore to beryllium oxide, which is the feed to a carbo-thermic reduction furnace producing copper-beryllium master alloy. Some of this master alloy is sold to NGK, and some is consumed domestically. It is believed that China also has a pure beryllium production plant in the northwestern part of the country.

2.3.3 Former Soviet Union

In the interest of making this publication as comprehensive as possible, a brief summary of beryllium developments in the former Soviet Union (FSU) is given in this section. The first of these, the Ulba Metallurgical plant located in Ust-Kamenogorsk, Kazakhstan, is still the major production center for beryllium and beryllium alloys in the entire FSU. It was started in the early 1950s with the initial objective of producing beryllium hydroxide and beryllium oxide. By the early 1960s, metal production was underway, and structural-grade metal was being produced by the powder metallurgy method in the mid-1960s. By 2001, the plant was also producing copper-beryllium alloys. The other major center, devoted primarily to beryllium and beryllium alloy science and technology, is the Kharkov Institute of Physics and Technology, located in Kharkov, Ukraine. Beryllium activity there was started in the late 1940s, primarily stimulated by the potential nuclear applications for beryllium.

In general, the technology for producing beryllium metal in the FSU is identical to that used in the United States. The starting mineral ore is beryl, rather than bertrandite. A large volume of information on beryllium was published jointly in 1975 by the USSR Academy of Sciences and the USSR Ministry of Geology [Kogan et al 1975]. This book contains extensive descriptions of worldwide distribution of beryllium-containing ores, applications of beryllium gleaned largely from U.S. publications, industrial activities in various countries, and conclusions as to the future of beryllium production and application. Also, the method for producing structural-grade beryllium by powder consolidation is similar. In some cases, near-net shapes are made by a powder-forging process rather than by machining from a large compacted billet.

One of the unusual processes that was implemented in the early 1960s was the employment of vacuum distillation to produce hundreds of kilograms of distilled beryllium each year. A large factory building at the Ulba Metallurgical Plant was devoted to the distillation process, with some 40 units, each with a working volume of 1 m diameter by 2 m high. These units had both mechanical pumps and oil diffusion pumps, the latter without provision for preventing backstreaming of oil. The process was originally developed at the Kharkov Institute, where research to make improvements on the distillation process is still being conducted. The reason given for producing large quantities of distilled beryllium was that the nuclear reactor designers, who wished to use beryllium for its neutron-reflecting or multiplication properties, required that there be zero boron present, since boron will trap neutrons and was therefore thought to reduce the reactor efficiency. However, in the 1980s, the Ulba plant sold some beryllium to Western European countries for use in reactors designed and built there, and those reactor designers did not consider the +50 ppm of boron impurity to be a problem. As a consequence, the Ulba Plant stopped producing distilled beryllium.

The FSU appears to have performed a significant amount of work on beryllium alloying. One of the more important references is the book by Papirov [1981], which treats some 82 binary systems with beryllium. In general, the attempts to alloy pure beryllium in order to improve its mechanical properties were not successful. One of the major differences in alloying beryllium was the composition chosen for their version of beryllium-aluminum alloys. The most-used version is Al-35 wt% Be-5 wt% Mg. The magnesium was added to strengthen the aluminum phase, and the amount of beryllium was probably chosen to make for easier processing. It would have been very difficult to maintain control over the amount of magnesium if the melting temperature had been higher, due to a higher beryllium content. Properties of the alloys with different compositions and processing routes were given in the paper presented by V.V. Savchuk at the TMS Beryllium Symposium in November 1999 and subsequently published [Savchuk and Syrnev 2004].

Very little information is available regarding specific applications of beryllium and its alloys in the FSU, probably because most of the beryllium would have been used in sensitive or defense components. The large volume on beryllium referred to earlier [Kogan et al. 1975] does have information on applications, but all of the

items described are ones that apply to Western systems. Large quantities of beryllium would have been used in nuclear reactors as neutron reflector components.

Since the late 1940s, all beryllium fabrication has been based on powder metallurgy. To produce full-density bodies, the beryllium powder must be heated to 1000 to 1100 °C in a die with concomitant application of pressures up to 4800 kPa (700 psi). The operations must be carried out under vacuum to minimize oxidation. Powder metallurgy blocks of beryllium metal produced by this technique are relatively isotropic with respect to both physical and mechanical properties, have excellent dimensional stability, and can be machined to close tolerances with fine surface finishes. These powder metallurgy techniques helped establish beryllium as a structural material when its use in the nuclear industry declined.

Beryllium gained a role in the space age; its low density and high strength improved the economics for payload delivery with ballistic missiles and space vehicles. Beryllium was designed into inertial guidance systems, using its high-precision elastic limit. Aircraft brakes took advantage of the strength and ductility of beryllium at elevated temperatures up to 700 °C expected during abortive braking. Because of its high cost and its health hazard considerations, beryllium has historically been the target of searches for alternative materials, and it is used only when other materials will not give the desired component performance.

The FSU Kazakhstan facility in Ulba is producing pure beryllium and beryllium master alloys. The Ulba plant has an inventory of beryllium ore concentrates established during the Soviet Union time period that is expected to last, at current consumption, approximately five years. Brush Wellman purchased in the past, beryllium/beryllium master alloy from Ulba. It was through the efforts of Brush Wellman that the carbo-thermic reduction process for making copper-beryllium master alloy was established at Ulba during the 2000 to 2002 time period. Ulba is aggressively competing in the world market with their pure beryllium and beryllium alloy products. Ulba continues to supply Russia with beryllium/beryllium alloys and has business relationships with China, with unknown sales of beryllium/beryllium alloys.

2.3.4 Germany

The large German electrical company Siemens & Halske AG of Berlin was one of the pioneers in the study and commercialization of beryllium and its alloys. In 1934, all of its beryllium activities were transferred to Heraeus-Vacuumschmelze AG, a subsidiary of W.C. Heraeus GmbH of Hanau (near Frankfurt), one of the two firms controlling the German platinum trade. The merger, made in the interest of economy, unified German production of heavy beryllium alloys. Furthermore, agreements involving division of world markets and exchange of technical experience were effected with a leading American producer, the Beryllium Corporation. Another company in Germany interested in beryllium was Deutsche Gold und Silver Scheideanstalt (DEGUSSA) in Frankfurt-am-Main, which controlled the German precious metals production and was also the only processor of beryllium ore in Germany. Its function was to supply beryllium oxide and metal to Heraeus for heavy alloys (and to small consumers for other purposes) and to furnish beryllium chloride and beryllium-aluminum master alloy to I.G. Farben Industries at Bitterfeld for light alloys.

The capacity of DEGUSSA at Frankfurt-am-Main was originally 20 kg of contained beryllium a month, but it was increased to 200 kg by makeshift additions. Bombing destroyed much of this overall plant, but only the initial stage of the beryllium unit was damaged. Commencing in approximately mid-1943, beryl was smelted at DEGUSSA's Rheinfelden plant, and the lime-opened material was shipped to Frankfurt; Operations at Rheinfelden were halted at the end of 1944 by failure of the gas supply. DEGUSSA had intended to transfer all of its beryllium production to the Rheinfelden plant in 1943; the same process was to be used. Equipment on hand in 1945 was able to carry the process only to the stage of beryllium hydroxide; apparatuses for chloriding and electrolysis had been fabricated but not delivered. Original construction was designed for consumption of 25 tons of ore monthly and a capacity of 500 kg of marketed oxide, 1500 kg of chloride, and 200 kg of metal on an 8 h/day basis. However, demand increased enough to call for processing of 50 to 75 tons monthly with the same equipment but using three shifts per day [NSRB 1953].

The Heraeus plant at Hanau had a daily capacity of 600 kg of beryllium-copper master alloy, corresponding to 20 to 25 kg of contained beryllium. However, it was very badly damaged by bombing. The arc furnace for producing the

master alloy was little affected, but the vacuum melting and casting furnaces were put out of operation. Of the total output of Heraeus, only approximately 5% was represented by beryllium alloys.

Deutsche Beryllium GmbH (DEBEGE) was formed in 1943 in Stuttgart to prospect for and mine beryllium ore, to acquire patents in all processes relating to beryllium, and to manufacture and market beryllium metal, alloys, and salts. The company does not seem to have actually engaged in any beryllium operations, but it remained in existence until at least 1945 and was affiliated in some manner with the Societa Anonima Processi Privative Industriali (SAPPI), the Italian beryllium producer. The German beryllium industry ceased to function in 1945, and resumption of operation was prohibited by the Allied Control Authority in April 1946 [NSRB 1953].

The DEGUSSA process was used at its plants in Frankfurt-am-Main and Rheinfelden. In brief, the beryl ore is fused with calcium oxide and then treated with sulfuric acid to render the beryllium and aluminum soluble. This product is then leached and the residue discarded. The residue is subsequently treated with ammonium sulfate to remove the bulk of the aluminum as alum. The resulting solution of beryllium sulfate is treated under controlled conditions to hydrolyze the iron and remaining aluminum. This purified solution is then precipitated with ammonia to produce beryllium hydroxide. The dried beryllium hydroxide is mixed with carbon and briquetted. It is then treated with chlorine in an electrically heated vertical tube to produce vaporized beryllium chloride, which is condensed at elevated temperatures in a nickel tube. A second sublimation takes place in the presence of hydrogen, which results in the production of pure beryllium chloride. The pure beryllium chloride is then mixed with an equal weight of sodium chloride and electrolyzed for 24 h at a temperature of 350 to 400 °C in externally electrically heated nickel containers serving as cathodes. Electrolysis is continued until the beryllium chloride concentrate decreases enough to permit removal of beryllium flake by scoop. This process is continuous by adding more beryllium chloride. The anode is composed of graphite and replaced after a period of four to six weeks [NSRB 1953].

Small quantities of beryl were extracted in Germany, and therefore, its needs for beryllium depended on imports from India, the United States, Brazil, Argentina, and Italy. Known imports of beryl ore from 1937 to 1944 totaled 1130 tons (inclusive of 470 tons confiscated in Italy in 1945). Imports of beryllium oxide from the United States were 498 kg in 1936, 2722 in 1937, 4247 in 1938, and 3031 in 1939. Imports of beryllium oxide from Italy were 305 kg in 1936, 8700 (8.7 metric tons) in 1943, and 8800 (8.8 metric tons) in 1944 [NSRB 1953].

Germany was producing approximately 1 ton of beryllium in all forms annually by 1929. The output was 1 to 2 tons of oxide and 1 ton of metal in 1932, according to a United States consular report, and that level of production seems to have been characteristic of 1933 to 1937. Beryllium compounds, metal, and alloys shipped from 1940 to 1944 totaled approximately 21 tons; ending stocks exceeded beginning stocks by approximately 0.5 ton. Of this total, however, 12 tons were from Italian oxide and master alloys.

Measured at the metal and shipped oxide stage, beryllium production in Germany was approximately 12 tons from 1938 to 1944. Of this total, 1 ton was produced from 1938 to 1939, 8.2 tons from 1940 to 1944 by German processing, and 2.8 tons from 1943 to 1944 from confiscated Italian oxide. There was no output in 1945. The entire production was by DEGUSSA at Frankfurt-am-Main, and nearly all of it was shipped to Heraeus-Vacuumschmelze AG for making beryllium-copper. Exceptions in the case of oxide were 1100 kg (gross weight) purified for fluorescent lamps, 125 kg made into chloride for I.G. Farbenindustrie's beryllium-aluminum, and other small quantities used in preparing refractories, dental cement, and beryllium salts. The special metal disposition included 300 kg to the German army for secret use (perhaps in research on atomic energy) and 300 kg to miscellaneous consumers; approximately 472 kg were consumed in fabricating x-ray windows and 200 kg in making beryllium-aluminum for Farben [NSRB 1953].

From 1939 to 1944, Heraeus-Vacuumschmelze AG at Hanau shipped 346,500 kg (8082 kg beryllium) of beryllium-copper, 6854 kg (58 kg beryllium) of beryllium-nickel, and 410 kg of beryllium-iron and other beryllium alloys. This shipment represented the entire German production of heavy beryllium alloys. During that period, it appears that approximately 55% of the output was from DEGUSSA oxide and metal, 35% from Italian oxide and beryllium-copper master alloy (25 wt% Be), and 10% from American oxide [NSRB 1953].

I.G. Farbenindustrie at Bitterfeld produced approximately 5000 tons of Hydroalium 511, an aluminum alloy containing 0.2 wt% Be, from 1942 to 1944. The alloy was used to make sand-cast cylinder heads for airplane motors. Of the 10 tons of beryllium consumed, nearly half was in the form of the beryllium-aluminum master alloy (25 wt% Be) from Italy, and a couple hundred kilograms were in beryllium-aluminum (20 wt% Be) and beryllium chloride from DEGUSSA. The source of the other 5 tons has not been made clear, but there is a sufficient excess of receipts over recorded shipments and stocks at both the DEGUSSA and Heraeus plants, even after generous allowances for process losses, to suggest an unrecorded plant transfer to I.G. Farbenindustrie of some beryllium material, such as metal or chloride [NSRB 1953].

2.3.5 Italy

The Italian beryllium industry has been virtually nonexistent since 1944 [NSRB 1953]. SAPPI, organized in 1932, financed a program of research and development on beryllium until 1937, at which time a pilot plant was constructed for processing beryllium ore. This pilot plant was followed by erection of a full-scale plant at Chivasso, near Turin, that began production of beryllium compounds and alloys late in 1940. Consumption of beryl was designed to be on a scale of 24 tons monthly, but a maximum of 39 tons was reached during its operation from 1942 to 1943. The Italian beryllium industry was thus twice as large as the German, although considerably smaller than the American beryllium industry. The principal product, beryllium-aluminum master alloy (25 wt% Be), was exported mainly to Germany. The SAPPI works were requisitioned by the Italian Ministry of Aeronautics on December 22, 1941, and shut down for six months for reconditioning of machinery. Renamed Industrio del Berillio, the plant resumed operations in approximately June 1942 and changed its principal product to beryllium-copper master alloy. When Germany occupied Italy in September 1943, the SAPPI plant was seized (September 12, 1943), and sizable stocks of beryl and beryllium-copper were confiscated and shipped to Germany. German troops visited the plant on October 22, 1943, and charged several officials with sabotage against the armed forces of the Reich; favorable consideration of a settlement was to include description and surrender of the Italian beryllium industry and refund to Germany of 0.5 million lire paid for patent licenses. Full production continued under German direction until the end of 1943 [NSRB 1953].

In January 1944, the plant was ordered to concentrate all its capacity on the production of beryllium oxide. Operations ceased on September 30, 1944, due to lack of hydrofluoric acid and caustic soda. Pressure from Berlin was directed toward resumption of operations and even threatened removal of the entire SAPPI plant to Germany, but the Italians were able to procrastinate fulfillment of the demand until the Germans were driven out of Italy. After the war, the plant and its records were examined by H.A. Sloman (National Physics Laboratory, England) and C.B. Sawyer (Brush Beryllium Company, Cleveland), and their comprehensive report is the source of all information on the Italian beryllium industry in this publication, unless otherwise stated. The plant, not expected to produce beryllium again, has been converted to a cast iron foundry [NSRB 1953].

SAPPI produced 14.5 tons of beryllium in marketed oxide and alloys during its 3.5 years of operation. An additional quantity, apparently approximately 2 tons, was contained in treatable beryllium-rich slag. Three-fourths of the oxide was consumed in making fluoride, which in turn was used in producing the master alloys. The oxide contained 85 to 90 wt% BeO, 7 wt% NaF, 1 wt% SiO_2, 0.2 wt% Fe_2O_3, and 2 to 7 wt% H_2O.

The SAPPI process consists of mixing 550 parts by weight of sodium acid fluoride with 1000 parts of ground and moistened beryl, pressing into bricks, baking at 680 °C in a conveyor furnace, and leaching in the presence of potassium permanganate to oxidize and render the iron insoluble. The accompanying extraction of the sodium-beryllium fluoride leaves behind the insoluble sodium-aluminum fluoride. The beryllium-containing solution is then treated with NaOH to form beryllium hydroxide, which is washed and collected on a rotary vacuum filter. It is still wet enough to be repulped and pumped into a hydraulic press, where it is dewatered and formed into a cake. Drying at 280 °C follows, whereupon the cake is mixed with ammonium acid fluoride and heated at 380 °C. The resulting beryllium fluoride is melted (with expulsion of the remaining silicon as tetrafluoride) and then reduced by magnesium in the presence of aluminum or copper directly into an alloy of 25 wt% Be and aluminum or copper [NSRB 1953].

The entire beryllium output of SAPPI, including the slags, was shipped from the plant; there were no stocks of beryllium materials in Italy at the end of the war, except the small quantity of beryl previously mentioned. Virtually all shipments went to Germany as a result of purchase or confiscation. The Germans seized the Italian stockpile of 571 tons in September 1943 and shipped it to the Reich. Approximately 31 tons were on hand in Italy at the end of the war. The only exceptions were the following quantities of beryllium-copper: 50 kg of 25 wt% Be alloy and 4500 kg of 2 wt% Be alloy to Italian consumers, and 1635 kg of 25 wt% Be alloy and 1 kg of 4 wt% Be alloy to Japan. The small Italian consumption was principally by FIAT for aircraft bushings and piston rings [NSRB 1953].

Italy has not been a producer of beryl, importing its entire raw material supply. Italy imported 1400 tons of beryl during the period from 1938 to 1939, principally from Brazil and Argentina. Actual ore consumption totaled approximately 800 tons from 1941 to 1944 [NSRB 1953].

2.3.6 Japan

Mishima [1994] gave a review of the industrial history of the Japanese beryllium industry. He reported that no research on metallic beryllium had occurred before the outbreak of World War II. Studies on beryllium-copper alloys had started in the late 1930s.

It has been reported [NSRB 1953] that Santoku Company has a small beryllium oxide plant in Tokyo capable of producing several hundred pounds of beryllium oxide a month. The Santoku Kogyo Kaisha built a plant in Tokyo in 1939 to produce beryllium-copper containing 1000 kg of beryllium annually. It is not in commercial production. One large shipment of beryllium-copper was received from Italy in 1942. Its known supply was derived mainly from imports of beryl ore: 2 metric tons from Brazil in 1940, 168 metric tons from Argentina in 1941, and some semiprocessed material from the United States before the war, which was stocked for subsequent use. Both Sumitomo Metals and Mitsubishi Metal and Mining were making beryllium bronze at the request of the Japanese Army and Navy. Some of their products were used in military aircraft during World War II. The Cu-Be-Sn alloys, consisting of 1 to 2 wt% Be-1.5 to 2.5 wt% Sn, were prepared for the Japanese Engineering Standard (JES), which was known as JIS before 1949, to be used as watch bearings as a substitute for rubies. University of Tokyo, Tokyo Imperial University, Tohoku University, Nagoya Institute of Technology, and Toyamu University were conducting beryllium research during the 1940s.

By 1955, the Japanese industry had regained interest in beryllium with the beginning of research for the Japanese nuclear reactor program. Nippon Gaishi Kaisha (NGK), Yokozawa Chemicals, and Santoku were all producing beryllium metal and copper-beryllium by the late 1950s. The hazards of beryllium were being discussed by the Beryllium Alloy committee, which was established in January 1960 [Mishima 1994]. In 1986, NGK acquired the Cabot Corporation's beryllium business.

2.3.7 India

India has extensive facilities in Turbhe, near Bombay, to supply its beryllium needs. The Indian facility converts domestic beryl ore to beryllium hydroxide, the precursor for making beryllium, beryllium oxide, and beryllium master alloys. This facility recently reported an annual production capacity for 10 metric tons of 2% Be-Cu alloys and 250 kg of vacuum hot-pressed beryllium billets. This entire production is consumed domestically.

2.4 Current Status of the Beryllium Industry

The current status of the beryllium industry is unclear because of beryllium uses in nuclear weapons and the secret nature of this business. This brief summary is believed to be the status of primary beryllium producers around the world.

Brush Wellman Inc. is the major supplier of beryllium and beryllium products worldwide. Brush Wellman has fully integrated beryllium production with mining and extraction in Delta, UT, and primary beryllium products manufacturing in Elmore, OH.

Brush Wellman has competition in the beryllium alloy business from NGK Metals, a subsidiary of NGK Insulator, Nagoya, Japan. NGK purchases beryllium hydroxide from Brush Wellman to produce, through carbo-thermic reduction, copper-beryllium master alloy that it uses to make copper-beryllium alloy product for the marketplace. NGK also purchases copper-beryllium master alloy from China and possibly

from the FSU facility located in the Republic of Kazakhstan.

REFERENCES

Bellamy, R.G., and Hill, N.A., 1963. Extraction and Metallurgy of Uranium, Thorium, and Beryllium, *A Pergamon Press Book International Series of Monographs on Nuclear Energy,* Division VIII, *Materials,* Vol 1, Macmillan, NY

Bussy, A.A.B., 1828. *J. Chim. Med.*, Vol 4, p 453

Everest, D.A., 1964. *The Chemistry of Beryllium,* Elsevier, New York, NY, p 38

Kjellgren, B.R.F., 1946. The Production of Beryllium Oxide and Beryllium Copper, *Trans. Electrochem. Soc.*, Vol 89, p 247–261

Kogan, B.I., Kapustinskaya, K.A., and Topunova, G.A, 1975. *Beryllium,* Nauka, Moscow

Lebeau, P., 1898. *Compt. Rend.*, Vol 126, p 744

Lebeau, P., 1899. Recherches sur le Glucinium et ses Composes, *Ann. Chim. Phys.*, Vol 7, p 16, 495

Mishima, Y., 1994. Half a Century of Beryllium Industry in Japan, *Miner. Process. Extr. Metall. Rev.*, Vol 13 (No. 1), p 13–18

National Security Research Board (NSRB), 1953. "Materials Survey: Beryllium," Compiled for the National Security Resources Board by the United States Department of the Interior with cooperation of the United States Geologic Survey

Nilson, L.F., and Pettersson, O., 1878. Ueber das Atomgewicht des Berylliums, *Chemische Berichte,* Erwiderung: an Hrn. Lothar Meyer, p 906–910

Oesterheld, G., 1916. Über den Schmelzpunkt und die Schmelzwärme des Berylliums. II. Über die Legierungen des Berylliums mit Aluminium, Kupfer, Silber und Eisen, *Z. Anorg. Allg. Chem,* Vol 97, p 1–40

Papirov, I.I., 1981. *Structure and Properties of Beryllium Alloys,* Energoizdat, Moscow, p 18–19

Savchuk, V.V., and Syrnev, B.V., 2004. Technological Ductility and Properties of Aluminum-Beryllium Alloys, *Tsvetn. Met.*, No. 10, p 65–68

Vauquelin, L.N., 1798. *Ann. Chim. (Phys.)*, Vol 26, p 155, 170, 259

Wöhler, F., 1828a. *Pogg. Ann.*, Vol 13, p 577–582

Wöhler, F., 1828b. Sur le Glucinium et L'Yttrium, *Ann. Chim. (Phys.)*, Vol 39, p 77–84

SELECTED REFERENCES

- Bennett, W.D., 1961. "Annual Report on Beryllium Research—1960," Report AECL-1236, Atomic Energy of Canada, Ltd.
- Rebholz, M.J., and Wolff, G.E., 1964. "Beryllium Design and Development Summary Report," Report A701583, Lockheed Missile and Space Co., Sunnyvale, CA

Beryllium Chemistry and Processing, p 19-26
By Kenneth A. Walsh
Edited by Edgar E. Vidal, Alfred Goldberg,
Edward N.C. Dalder, David L. Olson, and Brajendra Mishra

CHAPTER 3

Sources of Beryllium

Kenneth A. Walsh, Brush Wellman Inc., Retired
Edgar E. Vidal, Brush Wellman, Inc.

BERYLLIUM occupies the 44th place in the terrestrial abundance list of the elements. Its overall concentration in the lithosphere is estimated at six parts per million (ppm). Most of it is present in the mineral beryl, in admixtures of beryl and helvite, and in the mineral bertrandite. Beryllium is an essential ingredient in approximately 45 minerals. The more common minerals are listed with their beryllium content in Table 3.1. Beryllium is an occasional constituent in approximately 50 other minerals.

In ordinary rocks and soils, as well as in bituminous coals, concentrations of beryllium fall in the range of 0.1 to 3.0 ppm. The beryllium content of mineral oils is estimated at less than 100 μg/L and of natural waters at below 1 μg/L. None of these materials have had any value as commercial sources of beryllium.

Beryl has been mined for centuries for its gemstone values. The manufacture of copper-beryllium alloys began in the 1930s, with the beryllium component supplied from beryl. Until 1969, requirements for the production of metal, oxide, and alloys in the United States were supplied solely by the mineral beryl. Extraction processes for recovery of the hydroxide intermediate from beryl required delivery of ore containing 10 to 12 Wt% BeO. Beryl consumption has amounted to approximately 4500 metric tons per year. The beryl mining industry remained relatively small compared with the major mineral commodities. In a few years, world beryl production was expanded by acquisitions of beryl, beryllium-copper master alloy, and beryllium metal by the General Services Administration under the U.S. Strategic and Critical Materials Stock Piling Act of 1946 [Public Law 520, 79th Congress].

Table 3.1 Beryllium minerals

Name	Composition	Concentration, wt% Be
Beryl	$3BeO{\cdot}Al_2O_3{\cdot}6SiO_2$	5.0
Bertrandite	$4BeO{\cdot}2SiO_2{\cdot}H_2O$	15.2
Euclase	$2BeO{\cdot}Al_2O_3{\cdot}2SiO_2{\cdot}H_2O$	6.2
Chrysoberyl	$BeO{\cdot}Al_2O_3$	7.0
Phenacite	$2BeO{\cdot}SiO_2$	16.2
Helvite	$3BeO{\cdot}3[Fe,Zn,Mn]O{\cdot}5SiO_2{\cdot}MnS$	4.6
Epididymite	$2BeO{\cdot}Na_2O{\cdot}6SiO_2{\cdot}H_2O$, rh	3.6
Eudidymite	$2BeO{\cdot}Na_2O{\cdot}6SiO_2{\cdot}H_2O$, mon	3.6
Trimerite	$3BeO{\cdot}CaO{\cdot}2[Mn,Fe,Mg]O{\cdot}3SiO_2$	6.1
Gadolinite	$2BeO{\cdot}FeO{\cdot}Y_2O_3{\cdot}2SiO_2$	3.6
Berylonite	$Na_2O{\cdot}2BeO{\cdot}P_2O_5$	7.2
Herderite	$Be[F,OH]{\cdot}PO_3{\cdot}CaO$	5.0
Leucophanite	$[BeF]NaO{\cdot}CaO{\cdot}2SiO_2$	3.7
Meliphanite	$2BeO{\cdot}2CaO{\cdot}NaF{\cdot}3SiO_2$	4.6
Hambergite	$4BeO{\cdot}B_2O_3{\cdot}H_2O$	19.1
Rhodizite	$4BeO{\cdot}3Al_2O_3{\cdot}6B_2O_3{\cdot}5[Cs,Rb,K,Na,Li,H]_2O$	3.6
Danalite	$BeO{\cdot}3SiO_2{\cdot}5[Fe,Zn,Mn]O{\cdot}[Fe,Zn,Mn]S$	5.0
Alvite	$BeO{\cdot}ZnO{\cdot}SiO_2{\cdot}n\,H_2O$	···
Bityite	$7[Be,Ca,H_2]O{\cdot}4Al_2O_3{\cdot}5SiO_2$	···
Bromellite	BeO	36.0
Barylite	$2BeO{\cdot}BaO{\cdot}2SiO_2$	5.6
Milarite	$4BeO{\cdot}K_2O{\cdot}4CaO{\cdot}Al_2O_3{\cdot}24SiO_2{\cdot}H_2O$	···
Kolbeckite	K, Be, F silicate	3.1

World resources of beryllium have been estimated to be more than 80,000 tons. Approximately 65% of the beryllium resources are concentrated in the United States; the Spor Mountain and Gold Hill areas in Utah and the Seward Peninsula area in Alaska account for most of the total. The world reserves and reserve base are not sufficiently well delineated to report consistent figures for all countries [U.S. Geological Survey 2007]. As of 1985, the world

Table 3.2 World mine production, reserves, and reserve base in metric tons per year

Location	1990	2002	2003	2004	2005	2006
United States	200	80	85	100	110	100
China	55	15	15	15	20	20
Kazakhstan	. . .	4	4	4	. . .	. . .
Mozambique	. . .	. . .	3	3	6	6
Russia	1600	40	40	40	. . .	. . .
Other countries	. . .	1	1	1	1	1
World total	1855	140	148	163	138	127

Source:U.S. Geological Survey 2007

beryllium reserves were estimated to be approximately 380,000 metric tons of contained beryllium and a reserve base of 725,000 metric tons [Petkof 1985]. The principal producers of beryl are Brazil, China, and the Soviet Union. The primary producer of bertrandite is the United States. As of 1984, the capacity of world beryllium production was 1200 metric tons and in 1990 was estimated to be approximately 1350 metric tons. These numbers have been altered by historical events, by the end of the Cold War, reconfiguration of the Soviet Union, the international industrialization of China, and environmental and occupational health concerns leading to much stricter regulations for production and manufacturing [Rao and Sreenivas 1994]. By 1996, the world production was at 347 metric tons per year, reaching a low of 148 metric tons per year in 2003. Global production in recent years is summarized in Table 3.2.

3.1 Mineralogy

Beryllium is a metallic element that is a commonly contained constituent in some 50 minerals. These minerals occur mostly in pegmatites, granites, syenites, and occasionally in gneisses and mica schists. When they occur in heterogeneous pegmatites, the crystals attain large size and good to excellent hexagonal crystal form; such crystals occasionally range up to 0.66 to 1 m (2 to 3 ft) in diameter, several feet in length, and several tons in weight. Crystals grown in cavities and druses in the mother rock are frequently quite transparent and of gem quality. Such transparent gems are beryl (emerald and aquamarine), chrysoberyl (alexandrite), and phenacite. Whereas common beryl is found in pegmatites, emerald occurs in schistose rocks and limestones but in close proximity to granite intrusions. It would appear that any area containing pegmatite dikes of acid character is a potential source of beryllium, but very few pegmatite bodies contain large enough quantities of beryl to permit them to be worked primarily for its recovery, even at the high prices that now prevail. Beryl has also been noted with topaz in tin ores and in mica schists.

3.1.1 Beryl

Large crystals of beryl, sometimes weighing as much as 50 to 60 tons, are occasionally found in pegmatites. The common beryl of pegmatites is nontransparent and has a vitreous luster resembling that of quartz. The BeO content of beryl ranges from 10 to 14 wt%. As the BeO content decreases, the oxides of sodium, potassium, calcium, lithium, cesium, iron, and chromium tend to increase from 0 to approximately 7 wt%. Ordinarily, the BeO content of beryl is between 12 and 13 wt%, but the presence of adhering mineral impurities, such as quartz and feldspar, causes the BeO content of most beryl concentrates to be between 10 and 12 wt%.

Beryl is currently the only beryllium-bearing mineral of industrial importance. It contains up to 5 wt% Be and has been found in commercially acceptable form in many pegmatites. However, these in turn are exposed on less than a small fraction of 1% of the Earth's crust and rarely include over 1 wt% beryl. Because beryl is distributed erratically and sparsely, reserves are difficult to estimate, and mining tends to be costly unless other minerals can be produced at the same time and thus bear part of the expense. When pegmatites weather, many of their constituent minerals remain unattacked, and the heavier substances, such as monazite, tin, tungsten minerals, and columbite-tantalite, may be concentrated in the residual mantle or transported to form placer deposits. Beryl, however, is not recovered from placers because it fractures easily and is light in weight. Although the beryllium content may reappear as a constituent of other secondary minerals, such as bertrandite, herderite, or beryllonite, none of these minerals are heavy enough to be separated by the sorting action of streams or other natural concentrating agencies; consequently, the beryllium is too dilute to be recovered from placer deposits on a commercial basis.

Beryl in pure form is a beryllium-aluminum silicate containing approximately 14 wt% BeO, 19 wt% Al_2O_3, and 67 wt% SiO_2. The precious forms of beryl—emerald and aquamarine—approach the pure form in composition. The commercial grades of beryl ore generally contain

10 to 12 wt% BeO, 17 to 19 wt% Al_2O_3, 64 to 70 wt% SiO_2, 1 to 2% alkali metal oxides, and 1 to 2 wt% Fe and other oxides. Beryl ore, being widely distributed, has rarely been found in quantities extensive enough to permit mining for its own sake and therefore is generally produced as a by-product in mining for other minerals, chiefly the mica, feldspar, and lithium ores. The common mineral associations of beryl are quartz, feldspar, mica, and tourmaline. Only crystals large enough to permit hand sorting are recoverable, since no commercially successful concentration process has yet been perfected, although encouraging results have been obtained. Brazil, the Union of South Africa (including Southwest Africa), Southern Rhodesia, Mozambique, Argentina, and French Morocco are currently the largest producers of beryl ore. The principal sources in the United States are Colorado, South Dakota, New Mexico, and the New England states. Numerous beryl deposits have been found in Canada, but none have major importance.

Other possible future sources of beryllium, in addition to beryl, are idocrue (vesuvianite), helvite, garnet, and associated minerals, which occur in certain deposits formed where igneous rocks have intruded limestone. The rare earth mineral allanite, which is available in commercial quantities, is a possible source, sometimes containing up to a few percent BeO.

3.1.2 Bertrandite

In 1969, development of the large Spor Mountain property in Utah sharply decreased the amount of beryl required for United States' operations. The new bertrandite source led to the reevaluation of the U.S. stock pile targets. Surplus beryl was sold by the U.S. government to private industry. Over the last 25 years, beryllium extraction from beryl imports by the major consumer, the United States, was nil.

The rhyolitic tuffs in the Utah source contain 0.1 to 1.0 wt% BeO. The current lower practical limit is an average 0.65 wt% BeO content of the ore input to processing. Although the ore grade is much lower than that of beryl ore, the beryllium content in the bertrandite component of the tuffs is acid soluble and recoverable by established hydrometallurgical technology.

3.1.3 International Beryllium Sources

The major beryl ore producers are currently Brazil, the Commonwealth of Independent States, and China. In the *Preprints from the U.S. Bureau of Mines Mineral Yearbooks* for 1986 and 1987 [Kramer 1986, 1987] and in the annual reports for 1990 and 1991 [Kramer 1990, 1991], beryl production in the former Union of Soviet Socialist Republics (USSR) is listed at 2000 or 2100 metric tons per year for the period from 1982 through 1989. Production decreased to 1600 and 1300 metric tons for 1990 and 1991, respectively [Kramer 1990, 1991]. Nearly all of the former USSR beryl came from the Republic of Kazakhstan.

Imports of beryl from China were reported as 885 metric tons in 1982 and 715 metric tons in 1983. These imports leveled at 100 to 500 metric tons from 1985 to 1989. Chinese exports also included beryllium hydroxide and beryllium-copper master alloy, with Japan and the United States as the most logical customers. Many of the import shipments of ore from China contained 30 to 70 wt% of its beryllium content in an acid-soluble form that has been identified as helvite. The acid-insoluble component is beryl. Both minerals have nearly the same theoretical beryllium oxide content, so the mixtures had little difficulty meeting the minimum 10 wt% BeO specification for international markets.

In the past, commercial quantities of beryl were obtained from India, Madagascar, Argentina, Zambia, Angola, and Rwanda. Their deposits have been depleted, or their mines have been closed. The installed extraction technologies cannot accept direct substitution of non-beryl minerals. The chrysoberyl deposits of Seward Peninsula, Alaska, are located in strongly faulted areas [Berryhill and Mulligan 1965]. At Seal Lake, Labrador, Canada, barylite occurs in veinlets with quartz and albite. In northern Coahuila, Mexico, bertrandite has been found in fluorite that contains other minerals, such as calcite, quartz, kaolinite, and hematite [Warner et al. 1959].

Waste from emerald mines has been a small-volume source of beryl exports from Colombia, South Africa, and Egypt. Emeralds have been found in the Ural Mountains in wall-rock schist. Most of the emerald mines have been located in Brazil. Other colored varieties of beryl gemstone include smaragd (green colored), aquamarine (bluish-green), gold-beryl (golden yellow), heliodor (yellowish-green), cesium-beryl (light rose), and morganite (light rose). In addition, the gem-bearing gravels in Sri Lanka have yielded minor quantities of chrysoberyl.

The tetrahedral diagram in Fig. 3.1 shows the chemical composition relationship of natural

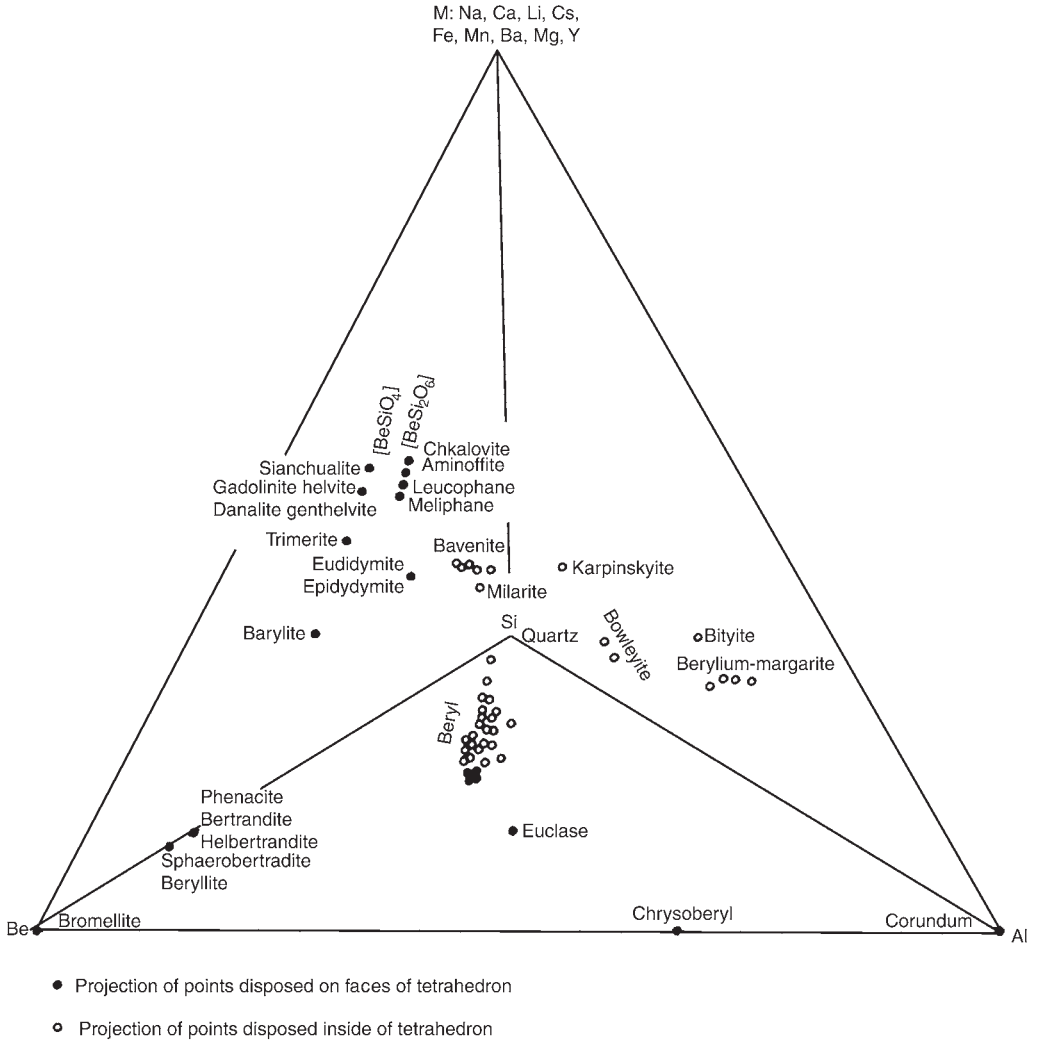

Fig. 3.1 Quaternary composition map of the Be-Al-M-Si-O system. Adapted from Beus 1966

beryllium silicate minerals [Beus 1966]. The minerals of beryllium are listed in Table 3.3.

3.2 Geological Outcroppings

Commercial applications of beryllium began more than 70 years ago, and usage of beryllium alloys, beryllium metal, and beryllium oxide has shown only slow growth over the last 70 years. The discovery of the element in precious gemstone beryl promoted the search for beryl to supply the newborn industry. The precious forms of beryl—emerald and aquamarine—approach the composition of the beryllium-aluminum silicate with 14 wt% BeO, 19 wt% $A1_2O_3$, and 67 wt% SiO_2. Initial requirements were supplied by the waste from emerald mining. There has been limited incentive for the exploration and development of sources other than beryl.

Beryl is widely distributed in fine-grained unzoned pegmatite dikes and in pockets in zoned pegmatite dikes. Pegmatites are not usually mined for their beryl content. Beryl is generally recovered as a by-product of mining other pegmatite minerals such as feldspar, mica, lithium minerals, columbite, tantalite, and cassiterite. Beryl mining is usually begun on an outcrop where commercial pegmatite minerals can readily be seen. Commercial deposits of beryl occur

Table 3.3 Minerals of beryllium

I Oxides

Bromellite BeO
Chrysoberyl Al_2BeO_4
Taaffeite Al_4MgBeO_8

II Silicates

Aminoffite $Ca_2[(Be,Al)Sl_2O_6](OH)_2$
Barylite $BaBe_2[Si_2O_7]$
Bavenite $Ca_4[(Be,Al)_4Si_9(O,OH)_{26}](OH)_2$
Bertrandite $Be_4[Si_2O_7]$
Beryl $Be_3Al_2[Si_6O_{18}]$
Beryllite $Be_6[Si_2O_7](OH)_4 \cdot 2H_2O$
Bityite—bowelyite—beryllium margarite group
Chkalovite $Na_2[BeSi_2O_6]$
Danalite $Fe_4[BeSiO_4]_3 \cdot S$
Epididymite $Na[BeSi_3O_7(OH)$
Eudidymite $Na[BeSi_3O_7(OH)$
Euclase $Al_2Be_2(OH)_2[SiO_4]_2$
Gadolinite $(Y,Ca)_2Fe[BeSiO_4]_2(O,OH)_2$
Genthelvite $Zn_4[BeSiO_4]_3 \cdot S$
Helbertrandite $Be_4[Si_2O_7]\ (OH)_2 \cdot nH_2O$
Helvite $Mn_4[BeSiO]_3 \cdot S$
Karpinskyite $Na[Al,Be,Zn,Si)_4(O,OH)_8]H_2O$
Leucophanite $Na_{1-n}Ca[Be(Si,Al)_2O_6]F_{1-n}$
Meliphanite $Na_{1-n}Ca[Be(Si,Al)_2O_6]F_{1-n}$
Milarite $KCa_2\ (Al,Be)_2[Si_{12}O_{30}] \cdot O \cdot 5H_2O$
Phenacite $Be_2[SiO_4]$
Spherobertrandite $Be_6[Si_2O_7](OH)_4$
Syanchualite $Li_2Ca_3[BeSiO_4]_3F_2$

III Borates

Hambergite $Be_2(OH)[BO_3]$
Rhodizite $(K,NA)_{1-2}(Li,\ Al)_{1.5-4}(O,OH)_4 \cdot Al_4\ [(BeB)_3B_4O_{12}]_2$

IV Antimonates

Swedenborgite $NaBe,Sbo_7$

V Phosphates

Beryllonite $NaBePO_4$
Faheyite $(Mn,Mg)Fe^{3+}_2\ Be_2[PO_4] \cdot 6H_2O$
Herderite $CaBe[PO_4](F,OH)$
Hurlbulite $CaBe_2[PO_4]_2$
Kolbeckite $Ca_{0.4}(Al,Be)_5[(P,Si)O_4]_4 \cdot 8H_2O$
Moraesite $Be_2[PO_4](OH) \cdot 4H_2O$
Vayrynenite $(Mn,Fe)Be[PO_4(OH)]$

VI Carbonates

Beryllium-tengerite $(Y,Ce)Be[CO_3](OH)_3 \cdot H_2O$

Source: Rao and Sreenivas 1994

in the inner zones of pegmatite dikes, the last-to-solidify fractions of low-melting-point magmas. Beryl is found in pockets separated by barren rock. Some beryl crystals are very large, up to 6 m long and weighing several metric tons. Cuts are made or pits are sunk by drilling and blasting the rock. Rock is hand cobbed for beryl and other valuable minerals. In this manual procedure, as much barren rock as practicable is broken off with hand hammers to recover valuable minerals, including beryl. Sometimes, the blasted rock is coarsely crushed. The large hexagonal beryl crystals contained in these deposits yield smaller pieces that retain characteristic shapes, often green or blue in color. The unique shape and color aid the hand sorting and cobbing of beryl crystals from conveyor belts delivering the primary minerals. Hand picking is economic when labor is cheap and beryl fragments are large. The crystals and fragments recovered are seldom less than 2 cm in size. Installed extraction plants usually require beryl input containing greater than 10 wt% BeO. The limitation of ore grade coupled with recognizable crystal size for hand cobbing result in recovery of less than 30% of the beryl from coarse-grained zoned pegmatites. The commercial grades of beryl ore typically contain 11 to 13 wt% BeO, 17 to 19 wt% Al_2O_3, 64 to 70 wt% SiO_2, 1 to 2 wt% alkali metal oxides, and 1 to 2 wt% Fe and other oxides. Table 3.4 lists the typical variation in chemical composition of beryl.

3.2.1 Beryl in Brazil

The availability of beryl from emerald mining waste promoted Brazil as an early supplier of ore for United States' extraction operations. As the market grew, other countries became suppliers of beryl. Commercial quantities were obtained from India, Madagascar, Argentina, Zambia, Australia, Angola, and Rwanda. These sources have been exhausted, or the demand for the major co-produced minerals has diminished. In some cases, the co-produced minerals have become available from other beryl-free sources. Old tailings and old dumps do not and never will provide a substantial quantity of beryl. Brazil remains as a major supplier.

Beryl mining today (2008) is essentially unchanged from that of the 1940s to 1960s, with thousands of hungry *garimperos* (illegal or freelance miners) or sharecroppers sporadically trying to extract small amounts of beryl or other saleable minerals in a primitive manner from selective parts of pegmatites in their areas. In the state of Minas Gerais, the pegmatite can be separated into two areas: the beryl-rich area near Conselheiro Pena and the gemstone-lithium-mica-feldspar-rich area of Governador Valadares. Some of the pegmatite regions extend into the state of Bahia. The pegmatite province of Northeast Brazil is not as extensive as that of Minas Bahia.

Because beryl is considered a strategic mineral, along with monazite, niobium, lithium, and zirconium, export quotas are set and revised every six months by the Comissão Nacional de Energia Nuclear. The export quota for beryl is 1000 metric tons per year. The quota has not been changed since 1970, because export demand has been much lower.

Table 3.4 Typical variation in the chemical composition of beryl

	Alkali-free beryls from pegmatites				Sodium beryls from pegmatites			Sodium-lithium beryl from pegmatites	Lithium-cesium beryl from pegmatites	Alkali-free beryls from India-Average of 7 analysis	Sodium beryl from India
	1	2	3	4	5	6	7	8	9	10	11
SiO_2	64.42	65.54	65.48	65.20	64.70	63.64	62.73	62.66	61.38	64.38	64.62
Al_2O_3	18.03	19.63	18.46	19.10	17.74	20.61	17.57	16.77	17.10	18.31	18.70
Fe_2O_3	0.05	0.63	0.80	0.57	0.40	0.13	0.48	1.39	0.08	0.61	0.26
FeO	Traces	0.13	0.13	. . .	. . .	. . .	. . .	. . .	. . .	. . .	. . .
BeO	14.28	12.38	13.70	12.00	13.80	13.32	12.06	11.93	10.54	13.65	12.36
MnO	0.19	. . .	Traces	. . .	0.05	0.03	. . .	Traces	. . .	. . .	. . .
MgO	0.52	0.18	0.07	0.11	0.06	0.16	0.24	0.20	0.22	. . .	. . .
CaO	0.16	0.46	0.55	1.40	0.15	Traces	0.61	0.43	0.44	. . .	. . .
Na_2O	0.48	0.15	0.07	. . .	0.69	1.18	2.74	2.42	2.50	0.24	0.58
Ll_2O	Traces	. . .	. . .	0.46	. . .	0.45	0.40	0.68	0.60	Traces	0.01
K_2O	0.14	0.36	0.27	. . .	1.44	0.11	0.47	0.67	. . .	0.12	0.17
Cs_2O	. . .	. . .	. . .	. . .	. . .	. . .	. . .	. . .	4.13	. . .	0.01
H_2O	1.60	0.36	0.42	0.57	1.20	0.29	2.59	2.34	2.26	2.38	2.90
Total	100.53	99.82	99.95	99.41	100.23	99.92	99.89	99.49	99.25	. . .	99.61
Source	Emerald from Puuna Australia	Kazak, CIS	Pegmatite Kazak, CIS	Pnumatolyte rock, Kazak, CIS	China	Eastern Siberia, CIS	China	Russia, CIS	Russia, CIS	Bihar, India	Bihar, India

Note: CIS, Commonwealth of Independent States. Source: Rao and Sreenivas 1994

3.2.2 Beryl in China

The major mine at Fuyun, with its pegmatite-hydrothermal deposit classification, is unique in that the crystals of beryl and other minerals have an average size of less than 1 mm. Occasionally, large beryl crystals are found and are hand cobbed. The bulk of the ore is processed through an adjacent flotation mill into powder concentrates of tantalite/niobite, spodumene, and beryl. The flotation mill was constructed and brought into production in 1976, after years of research, development, and pilot plant operation dating back to the 1950s. The capacity of the flotation mill was 300 to 500 metric tons of beryl concentrates per year, depending on the operating demand for the other two mineral concentrates.

Samples of ore imported from China, supposedly from Xinjiang province, exhibited unexpected solubility in acids. From 30 to 70% of the beryllium values along with 30 to 50% of the ore dissolved in hot, dilute hydrochloric or nitric acid. The recovered solution also had a high concentration of manganese, making helvite a candidate as the admixed mineral. The presence of the helvite component was confirmed visually and by thorough chemical and x-ray analysis. The insoluble residue was primarily beryl. The theoretical BeO content of helvite of 13.52 wt% is only slightly less than that for beryl; thus, the Chinese export ore meets the minimum BeO specification but not the beryl requirement for processing in existing equipment.

Additional mines were opened by the former Soviet Union mining engineers in Guangdong province, east of Guangzhou (Canton) near Huidong and Fengshun. The type of mineralization found in Guangdong province is pneumatohydrothermal deposition. This type of ore deposition occurs at a higher temperature than the hydrothermal pegmatite-type deposition found in Xinjiang province. The beryl ore is deposited in a bedding fracture system with openings along the bedding planes. The beryl in this open zone in the bedded plane is associated with greisen-type rock minerals of quartz and greenish-gray mica. This type of deposition also had associated wolframite and molybdenite minerals. The beryl is crystalline with some skeleton crystals. The color is greenish to greenish-white, yellow, green, and sky-blue. The beryl has striations and is irregular and also hexagonal in shape. The grade of the ore varies from 5 to 11 wt%, with an average of 8 wt% BeO. Particle size is 80% +10 mesh. Mining was conducted from 1958 to 1964, during which all mined ore was shipped to the former Soviet Union. The mines were reopened for operations in approximately 1980.

There are two known primary beryl ore extraction plants in China. Former Soviet Union technologists built an extraction plant in 1958 at

Hengyang in Hunan province. It produces two grades of BeO powder and two grades of beryllium pebbles, both grades differentiated by purity. A beryllium-copper master alloy with 3 to 4 wt% Be is also available from the Hengyang plant. A second extraction plant is located at Lanzhou in Gansu province. It offers the same beryllium products as the Hengyang facility, but much of its capacity is interchangeably convertible to the production of rare earth compounds. At both plants, coarse cobbed-lump beryl is required for the extraction process. Domestic Chinese beryllium consumption requires approximately 500 metric tons of lump beryl per year. Capacity is also available for the export of an additional 1000 metric tons of cobbed beryl per year. Xinjiang province supplies over 50% of the lump beryl requirements from pegmatite deposits located at elevations above Fuyun in the Altay Mountains. The remainder of the lump beryl is mined in Guangdong province, with minor contributions from Jiangxi, Hunan, and Hubei provinces. Mining is often continued with the purpose of restricting the flow of rural populations to the overcrowded cities.

3.2.3 Beryl in Russia

With the separation of the USSR into independent states, more information has become available about earlier and current beryllium operations in the region. Kazakhstan produced over 80% of the former USSR's beryllium. The principal production facility, located in Ust-Kamenogorsk, is situated on the Irtysh River in the easternmost part of Kazakhstan. This location is near the Mongolian border of the People's Republic of China. Beryl is recovered from the deposits in the Altay Mountains. It is assumed that their industry was integrated, because little, if any, beryl produced in Russia was traded. Beryllium alloys, metal, and oxide have become available from Kazakhstan.

Geologically, Beus [1966] divided the pegmatites in Russia into three generations of beryl, related to various paragenetic complexes and differing in a number of physical properties and features of chemical composition:

- Alkali-free beryl from block quartz
- Sodium beryl, related to quartz-muscovite, muscovite-albite, and albite replacement complexes
- Alkali-free beryl from cavities and late fissures

In the first group, the beryl crystals form in the central sections of pegmatite bodies before crystallization of the block quartz. Unlike the alkali-free beryl of the first group, the crystals and crystal growths of sodium beryl are the most common in the partly albitized pegmatites. The formation of solid conical sodium beryl is characteristic of the parts of the albite replacement complexes that were formed from the block microcline of the coarse-grained pegmatite, composed of pegmatoid segregations of potassium feldspar and quartz as much as 5 cm and more in diameter. The crystal size varies over wide limits, with the medium size (0.5 by 2 cm to 1 by 5 cm) occurring most frequently. Other beryllium minerals, including chrysoberyl, phenacite, and bertrandite, have a very limited occurrence in the pegmatites under consideration.

3.3 Summary Statement

Production and demand figures up to the 1990s were an order of magnitude higher than today (2008). Today's production and demand figures of beryllium ore and products are very erratic due to restrictions and public concerns of beryllium use and the special needs for beryllium and beryllium compounds in our technical society. The resurgence of the nuclear power industry and the needs of the aerospace industry will only increase the demand for beryllium. It will likely take a decade for the production and demand values to fully recover to pre-1990s values.

REFERENCES

Berryhill, R.V., and Mulligan, J.T., 1965. "Beryllium Investigations of the Lost River Mine, Seward Peninsula, Alaska," Open File Report 1–65, U.S. Bureau of Mines, p 71

Beus, A.A., 1966. *Geochemistry of Beryllium and Genetic Types of Beryllium Deposits,* W.H. Freeman, San Francisco

Kramer, D.A., 1986. Beryllium, *Preprints from the U.S. Bureau of Mines Minerals Yearbook,* Bureau of Mines, U.S. Department of the Interior, Washington, D.C.

Kramer, D.A., 1987. Beryllium, *Preprints from the U.S. Bureau of Mines Minerals Yearbook,* Bureau of Mines, U.S. Department of the Interior, Washington, D.C.

Kramer, D.A., 1990. Beryllium, Annual Report, *Minerals Yearbook, 1990,* Bureau of Mines,

U.S. Department of the Interior, Washington, D.C.
Kramer, D.A., 1991. Beryllium, Annual Report, 1990, Bureau of Mines, U.S. Department of the Interior, Washington, D.C.
Petkof, B., 1985. Beryllium, "Mineral Facts and Problems," Bulletin 675, U.S. Bureau of Mines
Public Law 520, 79th Congress. "Stockpile Report to the Congress July–December 1969," Section 4 of the Strategic and Critical Materials Stockpiling Act
Rao, N.K., and Sreenivas, T., 1994. Beryllium-Geochemistry, Mineralogy and Beneficiation, *Miner. Process. Extr. Metall. Rev.*, Vol 13 (No. 1), p 19–42
U.S. Geological Survey, 2007. "Mineral Commodity Summaries," Jan 2007
Warner, L.A., Holsner, W.T., Wilmarth, V.R., and Cameron, E.N., 1959. "Occurrence of Nonpegmatite Beryllium in the United States," Prof. Paper 318, U.S. Geological Survey

SELECTED REFERENCES

- Lindsey, D.A., Ganow, H., and Mountsoy, W., 1973. "Hydrothermal Alteration Associated with Beryllium Deposits at Spor Mountain, Utah," U.S. Geological Survey
- Montoya, J.W., Havens, R., and Bridges, D.W., 1962. "Beryllium-Bearing Tuff from Spor Mountain, Utah: Its Chemical, Mineralogical, and Physical Properties," Report of Investigations 6084, U.S. Bureau of Mines

Beryllium Chemistry and Processing, p 27-54
By Kenneth A. Walsh
Edited by Edgar E. Vidal, Alfred Goldberg,
Edward N.C. Dalder, David L. Olson, and Brajendra Mishra

CHAPTER 4

Physical and Nuclear Properties

Alfred Goldberg, Lawrence Livermore National Laboratory

4.1 Introduction

This chapter is divided into five subsections: atomic/crystal structure, elastic properties, thermal properties, nuclear properties, and miscellaneous properties. Many of the values reported were extracted from the *Handbook of Chemistry and Physics*, published in 2003 [CRC 2003–2004]. In equations, except where indicated otherwise, temperature (T) is in degrees Kelvin.

4.2 Atomic/Crystal Structure

Beryllium normally exists in the close-packed hexagonal *(hcp)* crystalline form, referred to as α-beryllium, in contrast to β-beryllium, the body-centered cubic form that is stable between 1250 °C and its melting point of 1287 °C. Some characteristics of beryllium related to the beryllium atom and crystal are listed in Table 4.1. In the un-ionized state, beryllium has four electrons, $1s^2$ and $2s^2$. The orbital radii are 0.143 and 1.19 Å for the 1s and 2s electrons, respectively [Stonehouse et al. 1965]. The first and second ionization potentials are 9.320 and 18.206 eV. The valence is 2. The variation of the two lattice parameters (a- and c-axes) of α-beryllium with temperature is given in Table 4.2. Note that the c/a ratio decreases as the crystal (lattice) expands with increasing temperature.

A plot of the change in the crystal-lattice parameters with temperature is shown in Fig. 4.1.

The density, ρ, of beryllium between room temperature and 1227 °C is given by the following expression [Scaffidi-Argentina et al. 2000]:

$$\rho\ (\mathrm{g/cm^3}) = 1.823 - 6.933 \times 10^{-5} T - 1.513 \times 10^{-8} T^2$$

where temperature, T, is expressed in °C.

Table 4.1 Atomic/crystal structure/ characteristic of beryllium

Atomic number	4
Atomic radius, Å	1.125
Atomic volume, $cm^3/g \cdot atom$	4.96
Atomic weight, g	9.01218
Density—pure, g/cm^3	1.8477
Density—commercial grades, g/cm^3	1.82–1.85
Electronic structure	$1s^2 2s^2$
Crystal structure, <1250 °C	Hexagonal close-packed (α-Be)
Crystal structure, >1250 °C	Body-centered cubic (β-Be)
Lattice constants, Å	a = 2.286; c = 3.583; c/a = 1.568; ideal = 1.633

Source: CRC 2003–2004, ASM 1990, Stonehouse 1986

4.3 Elastic Properties

The elastic properties can be given either as a tensorial (matrix) representation or in terms of

Table 4.2 Variation of lattice parameters with temperature

Temperature, °C	a-axis	c-axis	c/a
50	2.287	3.585	1.5679
100	2.288	3.587	1.5676
200	2.292	3.591	1.5670
300	2.296	3.596	1.5664
400	2.300	3.601	1.5658
500	2.304	3.607	1.5652
600	2.309	3.613	1.5646
800	2.319	3.625	1.5633
1000	2.330	3.639	1.5620

Source: Stonehouse et al. 1965

engineering constants. The elastic properties in the tensorial representation are defined by the stiffness (c_{ij}) and compliance (s_{ij}) matrices and are individually referred to as elastic constants. The engineering elastic constants are Young's modulus (E), shear modulus (G), Poisson's ratio (ν), bulk modulus (β), and compressibility (κ). Some variability is reported in elastic properties values, especially for Poisson's ratio. This variability can be attributed to the anisotropy of beryllium. Because of the anisotropic crystalline properties of the hexagonal beryllium crystal and the preferred orientation (texture) of the polycrystalline material, these properties should be related to the corresponding crystallographic axis. Unfortunately, this correlation is not always done. The elastic properties at room temperature are listed in Table 4.3.

Young's modulus as a function of crystallographic orientation for a single crystal of beryllium is shown in Fig. 4.2 [Killpatrick]. Young's modulus as a function of temperature for various grades of beryllium is shown in Fig. 4.3

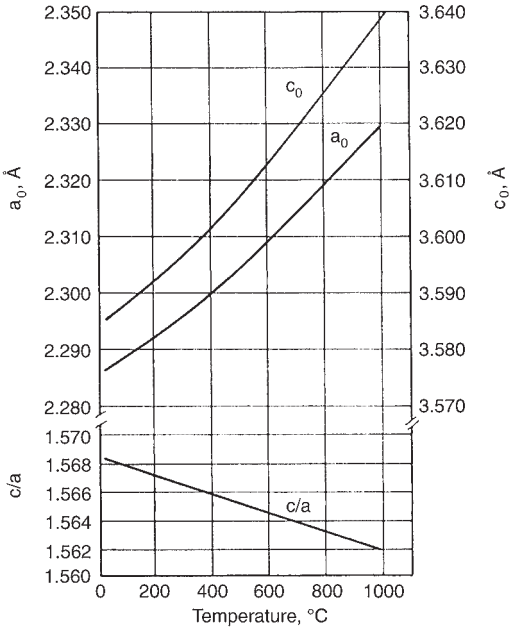

Fig. 4.1 Effect of temperature on the lattice parameters of beryllium. Source: Scaffidi-Argentina et al. 2000

Table 4.3 Elastic properties of beryllium at room temperature

Elastic constants, 100 GPa	
c_{11}	2.923
c_{12}	0.267
c_{13}	0.140
c_{33}	3.364
c_{44}	1.625
Young's modulus, GPa	303
Range	287–321
Shear modulus, GPa	135
Bulk modulus, GPa	110
Poisson's ratio	0.01–0.08
Isothermal compressibility(a), 10^{-10} m^2/N	0.0883
Adiabatic compressibility(a), 10^{-10} m^2/N	0.103

(a) compressibility, κ; $\kappa = \Delta V/V \cdot \Delta P$.
Source: CRC 2003–2004, ASM 1990, Stonehouse 1986, Killpatrick

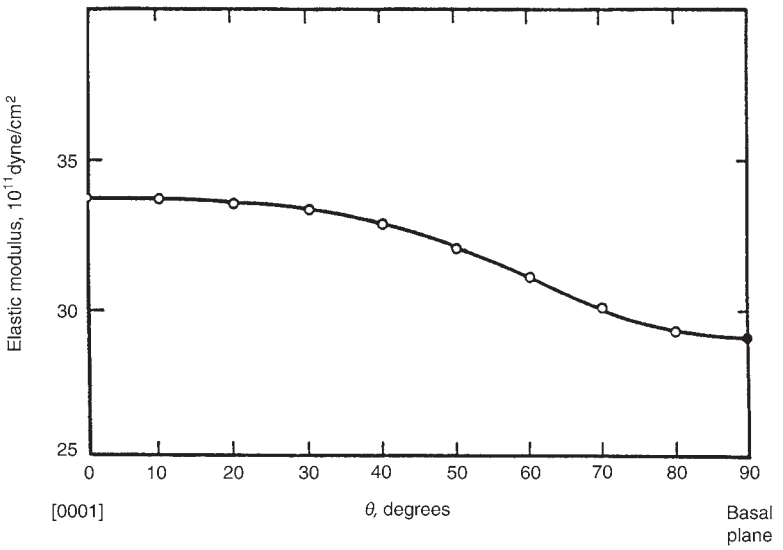

Fig. 4.2 Young's modulus of a single crystal of beryllium as a function of the crystallographic orientation in a plane normal to the basal plane. Source: Killpatrick

[Scaffidi-Argentina et al. 2000]. Young's modulus for two *vacuum* hot pressed *(VHP)* beryllium grades, S-200E and S-65B, are shown in Fig. 4.4 [Smith et al. 1985]. At room temperature, Young's modulus is unaffected by strain rate. Above approximately 425 °C (797 °F), Young's modulus increases with increasing strain rate, which is illustrated in Fig. 4.5, including the change in dynamic modulus with temperature [Killpatrick]. The differences between the static and dynamic values are explained in terms of thermodynamics involving the difference between specific heats at constant pressure and at constant volume as well as being attributed to creep at the elevated temperatures. The dynamic Young's modulus of elasticity of beryllium for two different orientations as a function of temperature is shown in Fig. 4.6. The change in modulus with temperature below 300 K (27 °C) is shown in Fig. 4.7. The grades and histories of the metals for Fig. 4.6 and 4.7 were not given [Killpatrick].

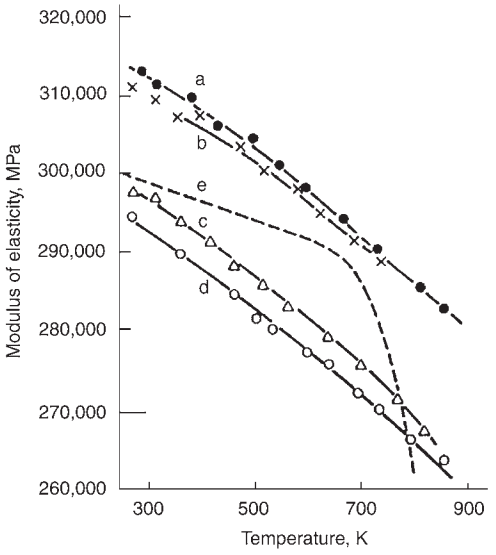

Fig. 4.3 Young's modulus of various grades of beryllium as a function of temperature. a, pressure sintered; b, cast and cross rolled; c, cast and extruded; d, powder metallurgy and extruded; e, pressure sintered (1 wt% BeO). Source: Scaffidi-Argentina et al. 2000

Precision elastic limit (PEL), 0.01% offset yield strength, and Young's modulus for the S-200F material are listed in Table 4.4. The PEL determination followed the Materials Advisory Board specification method [CRC 2003–2004]. Young's modulus was obtained according to ASTM E-111. The PEL is the stress required to produce a permanent strain of 10^{-6}; it is also known as the microyield stress.

The elastic properties are affected by porosity. Young's modulus (E) for a wide variety of as-fabricated beryllium, containing less than 0.3 volume fraction of porosity and at temperatures below 1000 °C, can be represented to within ±15% by:

$$E\,(\text{MPa}) = 3.00 \times 10^5\, e^{-4.574p} \left[1 - 2.016 \times 10^{-4}\,(T - 293)\right]$$

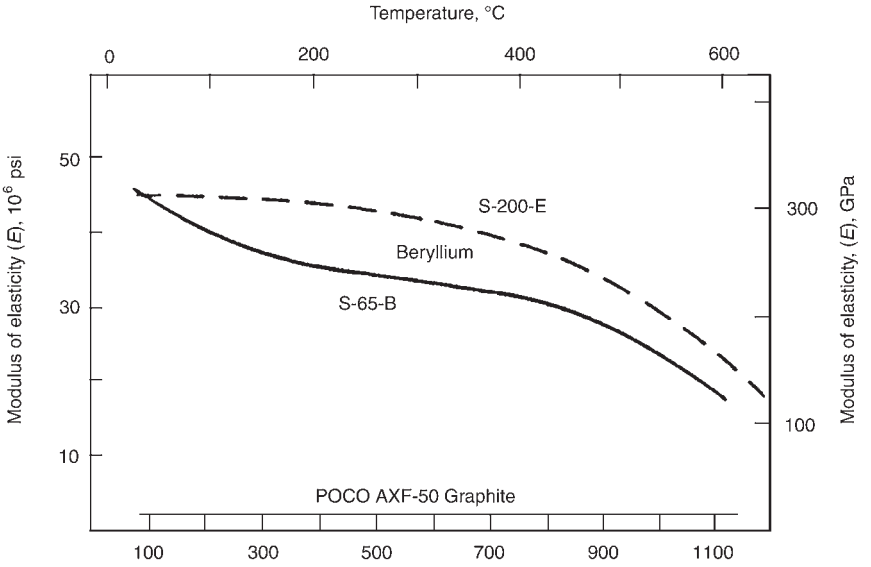

Fig. 4.4 Young's modulus as a function of temperature for smooth-bar specimens from vacuum hot pressed blocks of S-65B and S-200E beryllium. Included are results of a competing graphite product. Source: Smith et al. 1985

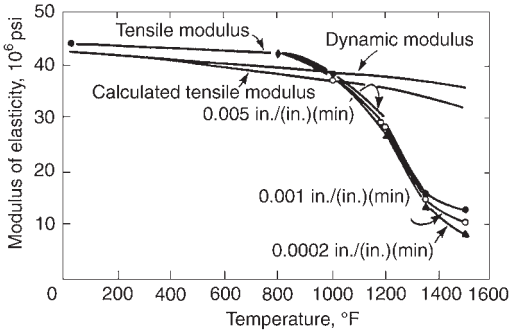

Fig. 4.5 Comparison of dynamic modulus with static modulus of QMV beryllium between room temperature and 815 °C (1500 °F). QMV was an internal designation. Source: Killpatrick

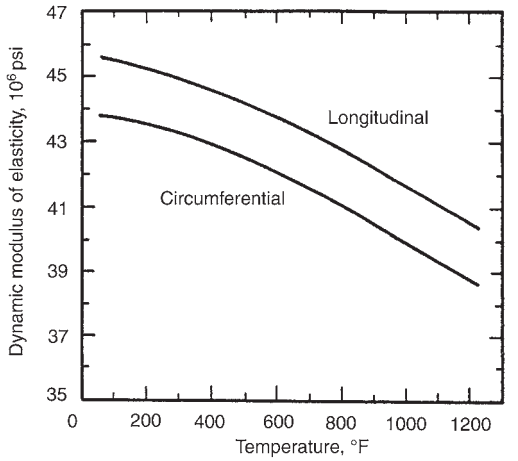

Fig. 4.6 Dynamic Young's modulus between room temperature and 649 °C (1200 °F) for two different orientations of a beryllium sample. Source: Killpatrick

where p is the volume fraction of porosity, and T is the temperature in degrees K [Billone et al. 1995]. The ultimate tensile strength for VHP S-200 beryllium can similarly be represented to within ±10% by:

$$\text{UTS (MPa)} = 324\, e^{-4.733p}\,[1 - 1.925\times10^{-4}(T-293) - 1.750\times10^{-6}(T-293)^2 + 9.198\times10^{-10}(T-293)^3]$$

The shear modulus and Poisson's ratio as a function of temperature for a cross-rolled cast beryllium are shown in Fig. 4.8 [Scaffidi-Argentina et al. 2000]. The shear modulus and Poisson's ratio of beryllium as a function of temperature below 300 K (27 °C) are shown in Fig. 4.9 and 4.10, respectively [Killpatrick]. Inconsistencies can be seen between the values at 300 K in Fig. 4.8 compared to those in Fig. 4.9 and 4.10, namely, 148 versus 141 GPa for the shear modulus and 0.027 versus 0.01 for Poisson's ratio. Such differences are probably due to

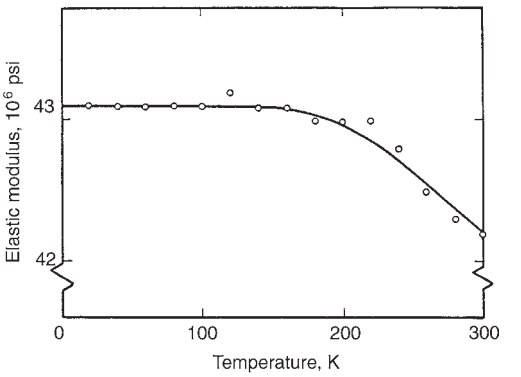

Fig. 4.7 Dynamic Young's modulus as a function of temperature below 300 K (27 °C). Source: Killpatrick

Table 4.4 Tensile elastic limits and yield strength at room temperature for vacuum hot pressed S-200F beryllium

	Test orientation	
Property	**Longitudinal**	**Transverse**
PEL(a), MPa	32.4	34.5
Yield strength(b), MPa	190	203
Young's modulus, GPa	311±7	310±5

(a) PEL, precision elastic limit, (b) 0.01% offset. Source: Haws 1985

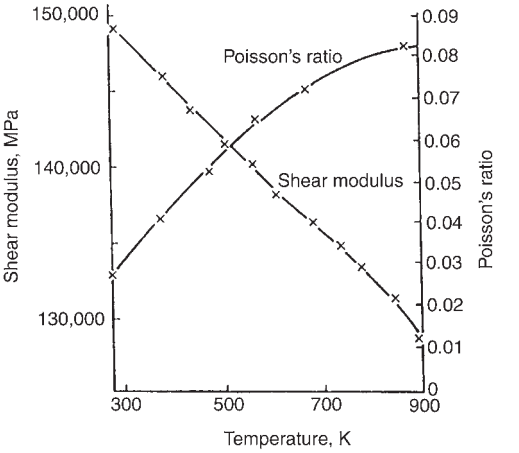

Fig. 4.8 Shear modulus and Poisson's ratio of cross-rolled cast beryllium as a function of temperature. Source: Scaffidi-Argentina et al. 2000

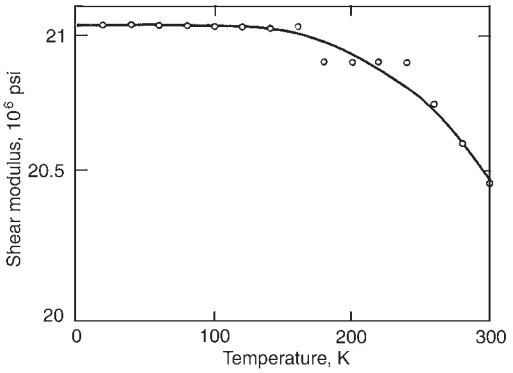

Fig. 4.9 Shear modulus for beryllium between 0 and 300 K. Source: Killpatrick

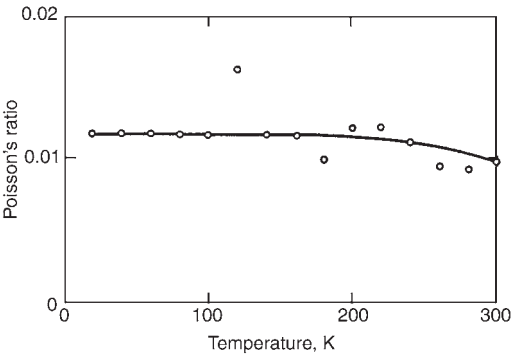

Fig. 4.10 Poisson's ratio for beryllium between 0 and 300 K. Source: Smith et al. 1985

Table 4.5 Shear properties of vacuum hot pressed S-200F obtained from torsion tests at room temperature

Property	Test orientation	
	Longitudinal	Transverse
Shear modulus, GPa	134 ± 5	134 ± 3
Shear rupture modulus, MPa	297 ± 12	309 ± 8

Source: Christman and Feistmann 1972

material composition, processing history, and sample orientation. The room-temperature shear properties for VHP S-200F reported for torsion tests are listed in Table 4.5 [Christman and Feistmann 1972]. The shear values close to 300 K are given as 134 GPa.

A number of elastic properties reported for VHP S-200E are listed in Table 4.6 [Killpatrick]. Tests were performed in the pressing direction and in two orthogonal directions perpendicular to the pressing direction. The measured values indicated that there was little anisotropy in the pressed beryllium; however, the calculated values (Lamé's parameter and Poisson's ratio) showed significant differences. (Lamé's parameter, λ, is defined as: $\lambda = \nu E/(1+\nu)(1-2\nu)$, where ν is Poisson's ratio.) The elastic stiffness constants from six different published sources were compared to illustrate the variable results obtained for beryllium [Killpatrick]. These data are tabulated in Table 4.7. Table 4.8 compares results obtained for compliance constants from four published sources. Table 4.9 lists Poisson's ratio values calculated for six different compliance directions.

Figure 4.11 shows the shear modulus (G_L, longitudinal; G_T, transverse) as a function of temperature calculated from experimental data of Young's modulus for three different values of

Table 4.6 Elastic properties of vacuum hot pressed S-200E beryllium

Property	Pressing direction (*Z*)	Average of transverse (*X* and *Y*) directions
Dilatational wave velocity, mm/μs	12.84 ± 0.04	12.57 ± 0.1
Shear-wave velocity, mm/μs	8.86 ± 0.04	8.82 ± 0.1
Shear modulus, MPa	1.453×10^5	1.440×10^5
Bulk modulus, MPa	1.114×10^5	1.005×10^5
Young's modulus, MPa	3.038×10^5	2.923×10^5
Lamé's parameter	145.6	44.8
Poisson's ratio	0.046	0.015

Source: Killpatrick

Table 4.7 Beryllium stiffness constants at room temperature reported by six different sources (10^{10} Pa)

c_{11}	c_{12}	c_{13}	c_{33}	c_{44}	c_{66}
29.23	2.67	1.40	33.64	16.25	13.28
30.8	−5.8	8.7	35.7	1.0	17.5
29.54	2.59	−0.10	35.61	17.06	13.48
30.87	2.16	1.05	34.25	15.54	14.04
29.39	2.69	1.4	33.78	16.33	13.35
29.2	2.4	0.6	34.9	16.3	13.4
29.65	2.50	0.87	34.44	16.30	13.51

Note: The bottom row consists of averages (of five rows), excluding the second row. The author excluded this row since its values differed considerably from the other reported values. c_{66} is calculated by: $c_{66} = \frac{1}{2}(c_{11} - c_{12})$.

Source: Killpatrick

Table 4.8 Beryllium compliance constants at room temperature reported by four different sources (10^{-11} Pa^{-1})

S_{11}	S_{12}	S_{13}	S_{33}	S_{44}	S_{66}
0.341	−0.0299	0.001	0.2808	0.5862	0.7420
0.35	−0.03	−0.01	0.30	0.61	0.76
0.326	−0.023	−0.009	0.292	0.644	0.712
0.345	−0.028	−0.005	0.287	0.616	0.746
0.341	−0.0.028	−0.006	0.290	0.614	0.740

Note: The bottom row consists of averages of the prior four rows. S_{66} is calculated by: $S_{66} = 2(S_{11} - S_{12})$. Source: Killpatrick

Poisson's ratio. Averaging published data from 14 different sources gave a value of 0.0476, which was suggested as the most probable value for Poisson's ratio. The shear modulus as a function of temperature for three different values of Poisson's ratio is shown in Fig. 4.12. The compressibility, which is the reciprocal of the bulk modulus, is shown in Fig. 4.13 as a function of temperature [Killpatrick].

Assuming isotropic properties, the shear modulus (G) can be calculated from Young's modulus (E) and Poisson's ratio (ν) using the relationship:

$$E = 2G\,(1 + \nu)$$

4.4 Thermal Properties

Some room-temperature thermal properties of beryllium are listed in Table 4.10. Results of several thermal-property measurements of grade S-65B beryllium are listed in Table 4.11 [Smith et al. 1985].

Table 4.9 Poisson's ratio (ν) for different directions in beryllium single crystals

$\nu_{12} = E_{100} \times S_{12} = 0.07$	$\nu_{31} = E_{001} \times S_{13} = 0.03$
$\nu_{21} = E_{101} \times S_{12} = 0.07$	$\nu_{23} = E_{010} \times S_{23} = 0.03$
$\nu_{13} = E_{100} \times S_{13} = 0.03$	$\nu_{32} = E_{001} \times S_{23} = 0.03$

Source: Killpatrick

The mean coefficient of thermal expansion from room temperature to 900 °C is shown in Fig. 4.14 [Pinto 1979b]. The average coefficient of thermal-expansion values for VHP S-200E

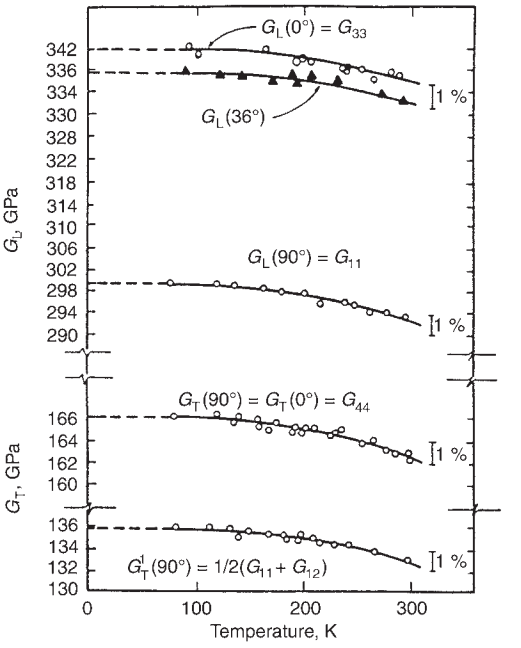

Fig. 4.11 Shear modulus as a function of temperature calculated from experimental Young's modulus values for different values of Poisson's ratio. Source: Killpatrick

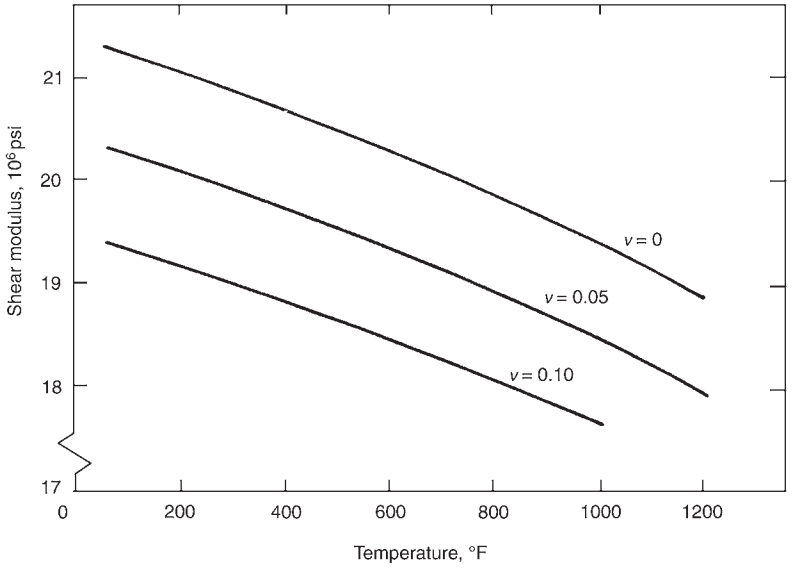

Fig. 4.12 Shear modulus of beryllium as a function of temperature for three different values of Poisson's ratio (ν). Source: Killpatrick

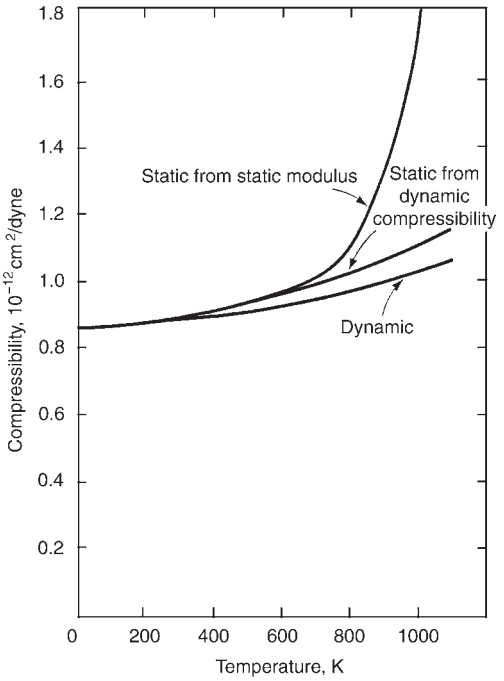

Fig. 4.13 Typical compressibility curves for beryllium as a function of temperature. Source: Killpatrick

Table 4.10 Some room temperature thermal properties of beryllium

Melting point, °C	1287
Latent heat of fusion, kcal/g · atom	1.89 (1.89–2.92)
Boiling point (760 torr), °C	2471
Heat of sublimation, kcal/g · atom	75.56 (75.5–78.8)
Heat of evaporation, kcal/g · atom	53.55 (53.5–74.1)
Specific heat (25 °C, constant pressure), cal/g · atom/°C	3.92
Enthalpy at 25 °C, cal/g · atom	465
Heat of transformation (α to β), cal/g · atom	1.80
Entropy (25 °C), cal/g · atom	2.28
Thermal conductivity, W/m · °C	216
Thermal diffusivity (room temperature), m^2/h	0.18
Temperature coefficient of linear expansion, $\times 10^{-6}$/°C	11.3 (0–50 °C)
Temperature coefficient of resistivity, $\Delta\rho/\rho_o$/°C	0.025
Contraction on solidification, %	3

Source: CRC 2003–2004, Kirk-Othmer 2002, ASM 1990, Stonehouse 1986, Yaws 1999

and S-200F over the range of 5 to 65 °C (278 to 338 K) for the longitudinal and two transverse directions are listed in Table 4.12 [Haws 1985]. The author points out that measurements were made on only one sample of each material. Table 4.13 lists the change in length relative to the length at 20 °C and the coefficient of thermal expansion over a range of temperatures from −268 to 27 °C (5 to 300 K) for hot isostatic pressed (HIP) beryllium. The specimens were manufactured by Brush Wellman from

Table 4.11 Some thermal-property measurements of grade S-65B beryllium covering a range of temperatures

Temperature °C	Temperature K	Thermal conductivity, W/cm · °C	Heat capacity, cal/g · °C	Thermal diffusivity, cm^2/s	Density, g/cm^3
51	324	1.873	0.455	0.540	1.820
139	412	1.523	0.535	0.376	1.814
183	456	1.438	0.560	0.339	1.808
242	515	1.338	0.583	0.304	1.806
291	564	1.288	0.604	0.283	1.801
336	609	1.252	0.624	0.267	1.797
400	673	1.166	0.637	0.244	1.791
464	737	1.104	0.653	0.225	1.785
543	816	1.018	0.664	0.206	1.777
619	892	0.961	0.683	0.190	1.769
700	973	0.884	0.702	0.171	1.760
854	1127	0.758(a)	0.737(a)	0.141	1.742
996	1269	0.638(a)	0.769(a)	0.115	1.725

(a) Extrapolated value. Source: Smith et al. 1985

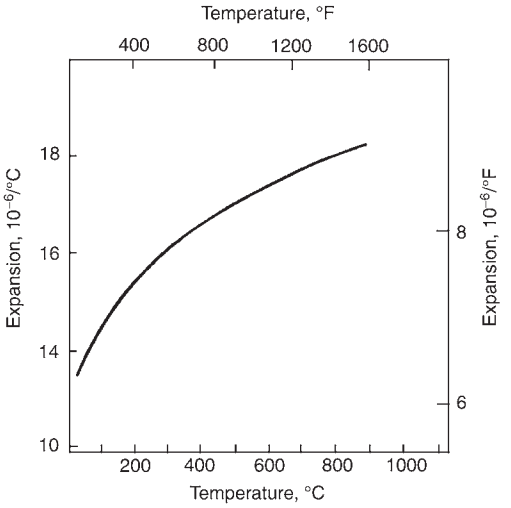

Fig. 4.14 Mean coefficient of thermal expansion from room temperature to indicated temperature of normal-purity beryllium block and sheet. Source: Pinto 1979b

Table 4.12 Average coefficient of thermal expansion (α) for vacuum hot pressed S-200E and S-200F from 5 to 65 °C

Direction	S-200E α (10^{-6}/°C)	S-200F α (10^{-6}/°C)
Longitudinal	11.39	11.39
Transverse 1	11.57	11.76
Transverse 2	11.45	11.82

Source: Haws 1985

material designated as 0–50 HIP. Average coefficients of thermal expansion of beryllium over temperature ranges from 25 to 100 °C up to 25 to 1000 °C are listed in Table 4.14 [ASM 1990]. The coefficients of thermal expansion of beryllium single crystals at low temperatures,

Table 4.13 Coefficient of thermal expansion (α) and length change relative to 293.16 K for hot isostatic pressed beryllium metal

T, K	α, K^{-1}	$\Delta L/L_{293}$, 10^{-6}	T, K	α, K^{-1}	$\Delta L/L_{293}$, 10^{-6}
0	0.00	−1298	110	1.77×10^{-6}	−1254
5	3.16×10^{-10}	−1298	120	2.27	−1234
10	9.60	−1298	130	2.82	−1209
15	2.31×10^{-9}	−1298	140	3.41	−1178
20	4.83	−1298	150	4.01	−1140
25	9.14	−1298	160	4.62	−1097
30	1.61×10^{-8}	−1298	170	5.24	−1048
35	4.83	−1298	180	5.84	−993
40	4.24	−1298	190	6.43	−931
45	6.48	−1298	200	7.00	−864
50	9.61	−1297	210	7.54	−791
55	1.38×10^{-7}	−1297	220	8.07	−713
60	1.94	−1296	230	8.57	−630
65	2.66	−1295	240	9.04	−542
70	3.56	−1293	250	9.50	−449
75	4.67	−1292	260	9.94	−352
80	5.99	−1289	270	1.04×10^{-5}	−251
85	7.52	−1286	273.16	1.05	−218
90	9.26	−1281	280	1.08	−145
95	1.12×10^{-6}	−1276	290	1.11	−35
100	1.32	−1270	293.16	1.13	0
105	1.54	−1263	300	1.15	+78

Source: Swenson 1991

Table 4.14 Average coefficients of thermal expansion of beryllium for several ranges of temperature

Temperature range, °C	Average coefficient of expansion, 10^{-6}
25–100	11.6
25–300	14.5
25–600	16.5
25–1000	18.4

Source: ASM 1990

perpendicular and parallel to the c-axis, are reported in Table 4.15 [Stonehouse et al. 1965, Meyerhoff and Smith 1961].

Low-temperature results of the thermal expansion relative to 300 K and the coefficient of thermal expansion are shown in Fig. 4.15 and 4.16, respectively, for VHP S-200F beryllium. Only one sample was used that had been machined, stress relieved at 788 °C for 1 h, final machined, etched to remove any machining damage, nickel plated, and finally polished to a $\frac{1}{4}$-wavelength finish [Haws 1988]. The thermal expansion results reported for HIPed beryllium made using impact-ground powder are shown in Fig. 4.17. The process was evaluated in its use for large precision mirrors (space applications), where anisotropy cannot be tolerated [Billone et al. 1995].

Figure 4.18 compares the thermal linear expansion between a polycrystalline beryllium and that of a single beryllium crystal in directions parallel to the a-axis and c-axis, respectively.

Table 4.15 Coefficients of thermal expansion of beryllium single crystals at low temperatures

Temperature, K	Perpendicular to c-axis, 10^{-6}	Parallel to c-axis, 10^{-6}	Volume coefficient, 10^{-6}
273–270	10.6	7.7	29.0
265–260	10.2	7.3	27.6
255–250	9.5	6.9	26.0
250–245	9.2	6.7	25.1
240–235	8.5	6.3	23.4
230–225	7.9	5.9	21.7
225–220	7.6	5.7	20.9
220–215	7.3	5.5	20.1
210–205	6.7	5.0	18.3
200–195	6.1	4.6	16.9
190–185	5.6	4.1	15.2
180–175	5.0	3.6	13.5
175–170	4.7	3.3	12.7
165–160	4.1	2.7	10.9
160–155	3.8	2.5	10.1
150–145	3.2	1.9	8.3
140–135	2.7	1.5	6.8
130–125	2.1	1.0	5.3
125–120	1.9	0.9	4.6
115–110	1.3	0.5	3.2
105–100	0.9	0.3	2.1
100–95	0.7	0.2	1.6
95–90	0.6	0.1	1.3
85–80	0.4	. . .	0.8

Source: Stonehouse et al. 1965, Meyerhoff and Smith 1961

The curves are based on the equations shown in Table 4.16 [Touloukian, Kirby, et al. 1975]. Figure 4.19 shows expansion-versus-temperature curves recommended for polycrystalline beryllium and single crystals of beryllium. The curves are based on data obtained from 38 sources [Touloukian, Kirby, et al. 1975]. Figure 4.20 compares the average degree of anisotropy of thermal expansion for beryllium of essentially constant chemical composition for a structural-grade beryllium (indicated as "comp A") produced by five different fabrication techniques [Hausner 1965c]. Also included is an instrument-grade hot pressed beryllium having a high oxide content and a very fine grain size (indicated as "comp B") [Jennings et al. 1966]. The results are based on two specimens per material with 12 determinations on each specimen. The authors state that the thermal expansion results are consistent with the degree of preferred orientation that was observed.

The temperature coefficients for unrelaxed thermal microstresses that were calculated for beryllium are listed in Table 4.17, together with values reported for other *hcp* polycrystalline materials [Armstrong and Borch 1971]. (Anisotropic dimensional changes occur during heating or cooling of hcp metals. In polycrystalline materials, microstrains and corresponding microstresses are developed by the mutual restrictions of adjacent grains to these dimensional changes.) The

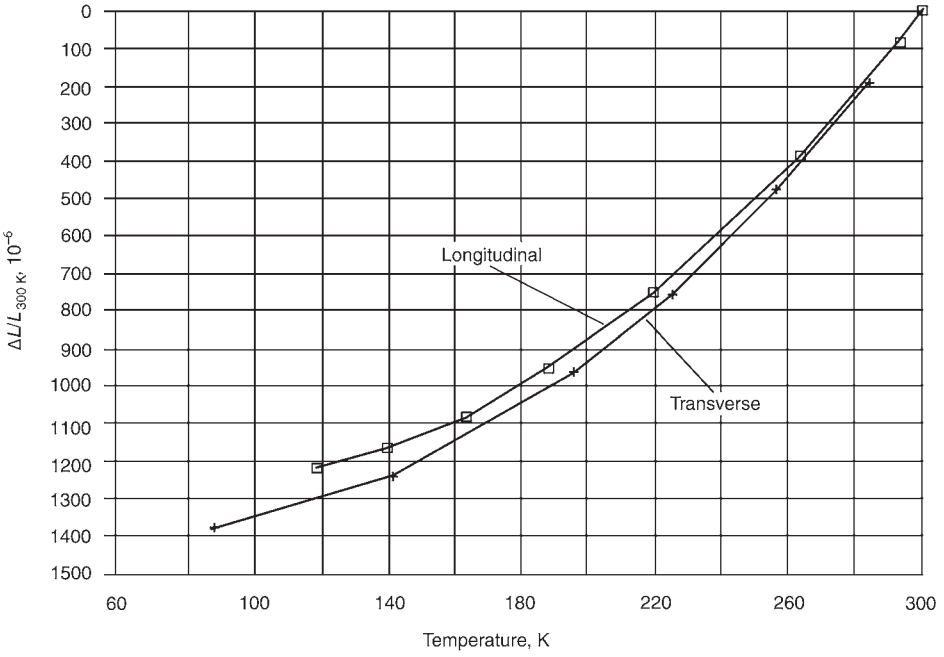

Fig. 4.15 Low-temperature thermal expansion, $\Delta L/L_{300\ K}$, for vacuum hot pressed S-200F relative to 300 K (27 °C). Source: Haws 1988

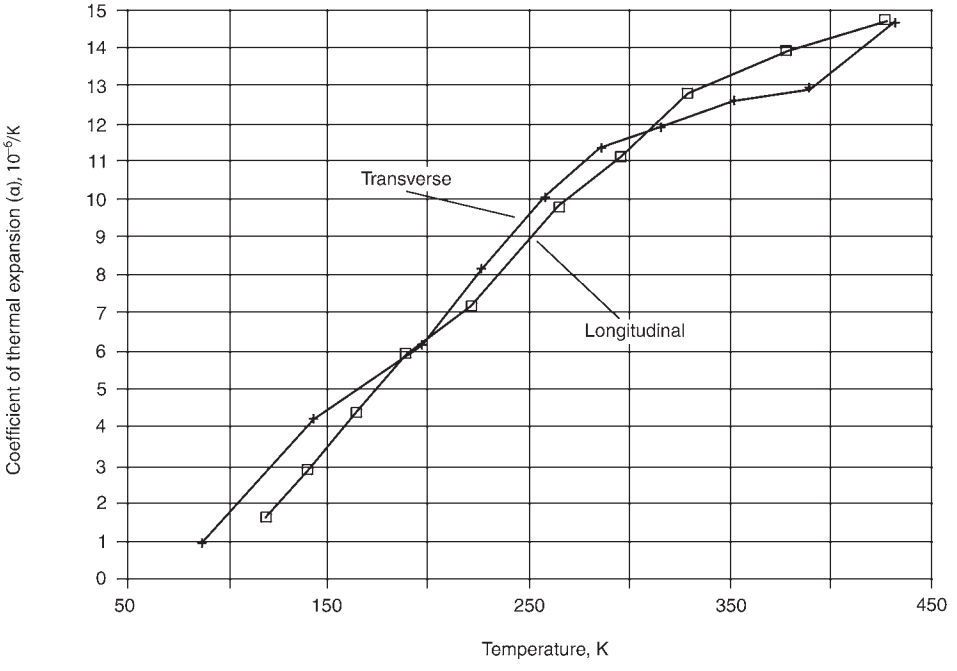

Fig. 4.16 Coefficient of thermal expansion (α) of beryllium versus temperature for vacuum hot pressed S-200F. Source: Haws 1988

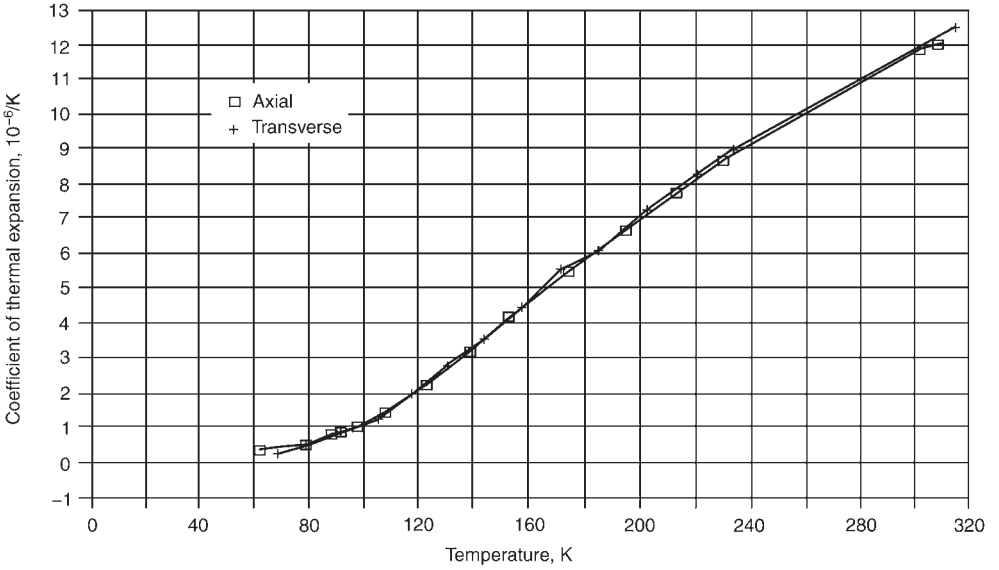

Fig. 4.17 Coefficient of thermal expansion of a beryllium cube in two orthogonal directions, showing excellent isotropy. The cube was hot isostatic pressed beryllium using impact-ground powder. Source: Billone et al. 1995

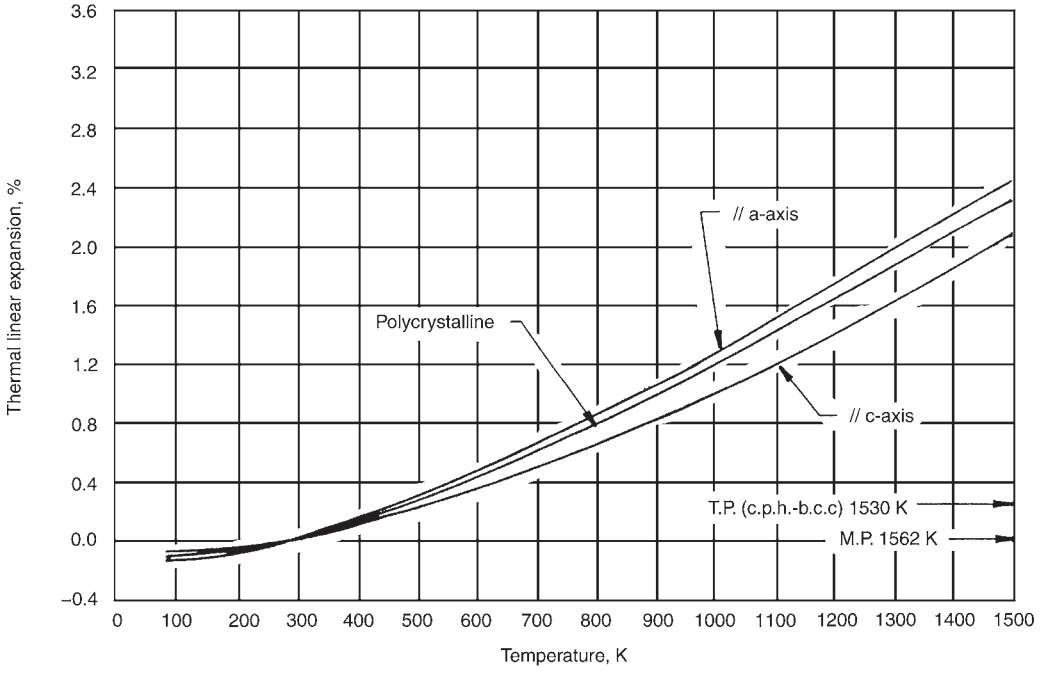

Fig. 4.18 Thermal linear expansion relative to 293 K of polycrystalline beryllium and of a beryllium single crystal parallel to the a-axis and c-axis, respectively. MP, melting point; TP (cph-bcc), transition temperature. Source: Touloukian, Powell, et al. 1975

authors suggest that in beryllium the residual stresses may greatly influence cracking in textured materials, for example, in rolled or extruded plate.

The thermal expansion relative to 298 K (25 °C) of beryllium, having 100% density, in the range of 298 to 1500 K (25 to 1227 °C) is given as [Billone et al. 1995]:

Table 4.16 Equations for curves shown in Fig. 4.18

Orientation/type	Thermal linear expansion, $(L - L_0)/L_0$	Temperature range, K
|| a-axis, single crystal	$1.242\times10^{-3}\,(T-293)+1.144\times10^{-6}\,(T-293)^2-4.567\times10^{-10}\,(T-293)^3$	293–895
|| a-axis, single crystal	$1.063+2.123\times10^{-3}\,(T-895)+3.197\times10^{-7}\,(T-895)^2-1.373\times10^{-10}\,(T-895)^3$	895–1500
|| c-axis, single crystal	$9.881\times10^{-4}\,(T-293)+5.475\times10^{-7}\,(T-293)^2+7.916\times10^{-11}\,(T-293)^3$	293–895
|| c-axis, single crystal	$0.809+1.733\times10^{-3}\,(T-895)+6.904\times10^{-7}\,(T-895)^2-1.519\times10^{-10}\,(T-895)^3$	895–1500
Polycrystalline	$1.148\times10^{-3}\,(T-293)+9.724\times10^{-7}\,(T-293)^2-2.978\times10^{-10}\,(T-293)^3$	293–895
Polycrystalline	$0.978+1.995\times10^{-3}\,(T-895)+4.346\times10^{-7}\,(T-895)^2-1.307\times10^{-10}\,(T-895)^3$	895–1500

Source: Touloukian, Kirby, et al. 1975

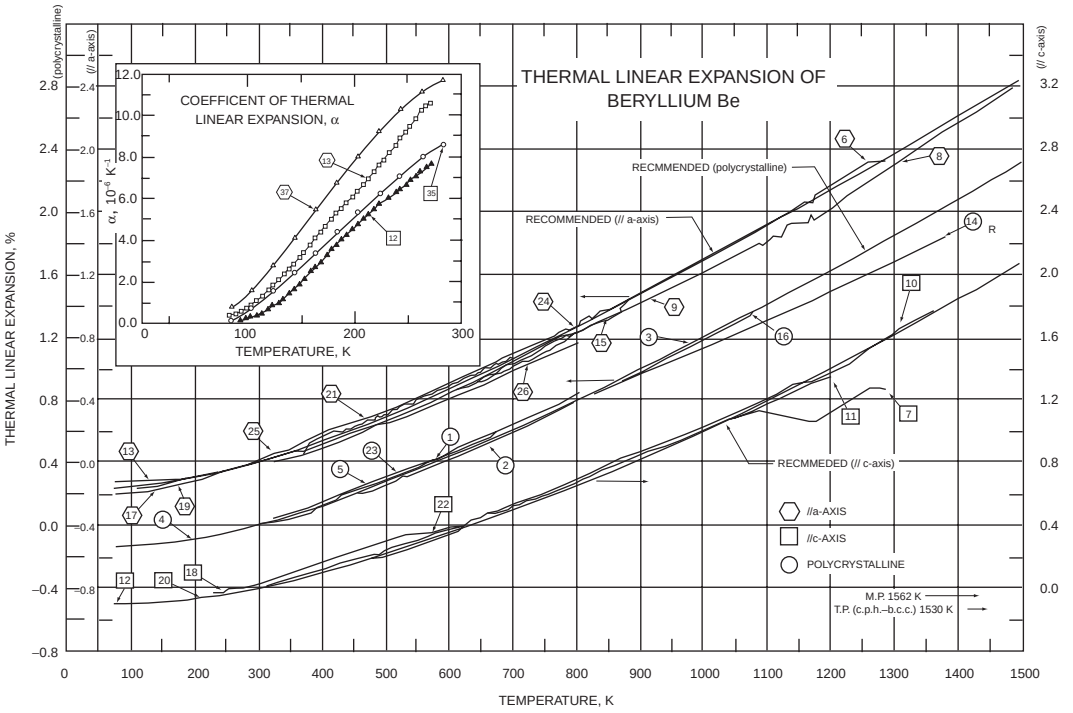

Fig. 4.19 Linear thermal properties. (a) Recommended thermal linear expansion curves for beryllium based on a large number (38) of investigations. The vertical axes from left to right are for polycrystalline material and for single crystals parallel to the a-axis and c-axis, respectively. Details on the temperature ranges, the materials evaluated, and the original references are presented in the current reference. (b) Coefficient of thermal expansion (α) versus temperature. MP, melting point; TP (cph-bcc), transition temperature. Source: Touloukian, Powell, et al. 1975

$$\Delta L/L_{298} = 8.43\times10^{-4}(1 + 1.36\times10^{-3}T - 3.53\times10^{-7}T^2)(T - 298)$$

The mean coefficient of thermal expansion for a near-isotropic S-65B beryllium over the temperature range from 20 to 1200 °C is given as [Scaffidi-Argentina et al. 2000]:

$$\alpha\ (10^{-6}\mathrm{K}^{-1}) = 11.0388 + 1.0859\times10^{-2}T - 4.4735\times10^{-6}T^2 + 8.6305\times10^{-10}T^3$$

In both expressions, T is temperature in degrees K.

A study on thermal expansion and dimensional stability performed on several different beryllium histories showed that cast, hot pressed, and isopressed forms were found to have nearly isotropic expansion properties. By contrast, the difference between anisotropic and isotropic thermal expansion ranged from 0.09×10^{-6}/°C for hot pressed beryllium to 2.07×10^{-6}/°C for heavily forged beryllium. The average value for the hot pressed material was 11.5×10^{-6}/°C [Jennings et al. 1966]. For isotropic sintered blocks such as S-65, differences in thermal expansion in different directions are small (not more than a few percent); for heavily deformed grades, differences in thermal expansion could exceed 20% [Scaffidi-Argentina et al. 2000].

Both the specific heat and thermal conductivity of beryllium are claimed to be relatively

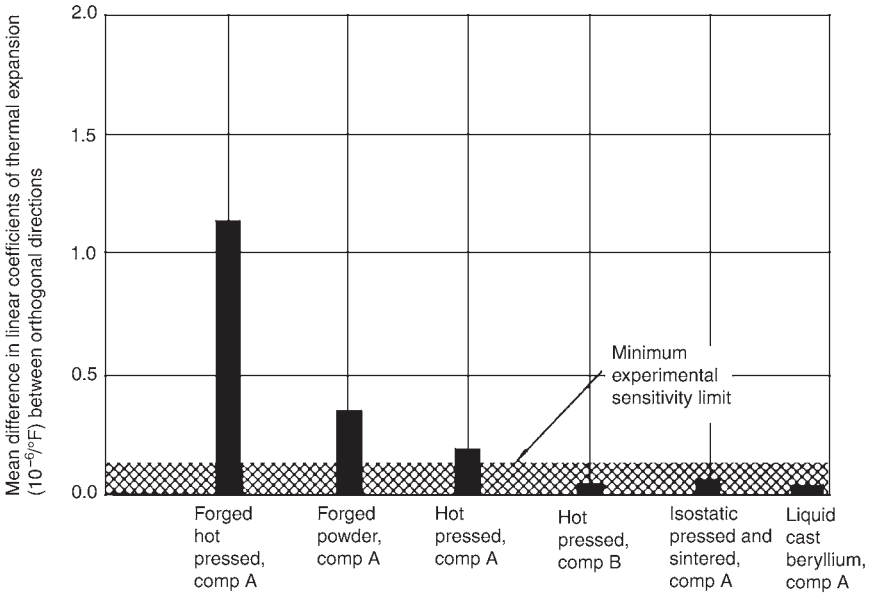

Fig. 4.20 Comparison of the degree of thermal expansion anisotropy for beryllium fabricated by several techniques. A, 2% max BeO; B, 4% min BeO. Source: Jennings et al. 1966

Table 4.17 Temperature coefficient of thermal microstresses in hexagonal close-packed polycrystals

Material	$\sigma_{11}/\Delta T$, 10^2 MPa	$\sigma_{33}/\Delta T$, 10^2 MPa	$\tau_{max}/\Delta T$, 10^2 MPa	$\sigma_{max}/\Delta T$, 10^2 MPa
Cd	2.8	−21	2.5	6.3
Zn	4.9	−3.7	4.3	12.2
Mg	0.17	−0.34	0.26	0.67
Be	−0.74	1.55	−1.14	−2.3
BeO	−0.635	1.27	−0.95	−2.3

Source: Armstrong and Borch 1971

insensitive to fabrication method, low levels of impurity, and, to a certain extent, radiation in a neutron environment above room temperature [Scaffidi-Argentina et al. 2000]. Small levels of impurities and displacement damage have little effect on thermal conductivity [Billone et al. 1995]. However, the presence of as-fabricated porosity and/or helium bubbles can cause a large reduction in the effective thermal conductivity. The following expression is claimed to be a relatively good fit to data of both vacuum hot pressed and foam (low-density) beryllium for porosities up to 50% [Billone et al. 1995]:

$$k_{eff} = (1 - p)(1 + 3.7p^2)^{-1}k_o$$

where k_{eff} is the effective thermal conductivity, p is the volume fraction of porosity, and k_o is the thermal conductivity for virtually zero porosity. Plasma-sprayed beryllium shows a significantly lower value than that predicted by this expression. The thermal conductivity of a normally dense beryllium over the temperature range from 27 to 550 °C is given as [Billone et al. 1995]:

$$k_o = 291(1–1.650\times10^{-3}\,T + 1.464\times10^{-6}T^2 - 5.125\times10^{-10}T^3)\text{W/m·°C}$$

A number of expressions reported for the specific heat at constant pressure (C_p) of beryllium are presented here. The temperature range for the first expression was not given. The next two expressions cover the range between room temperature and 1283 °C, the fourth between 327 and 1287 °C, and the fifth between 1287 and 1927 °C. (As previously indicated, throughout this report, except where noted, T refers to degrees K.):

$$C_p = 4.54 + 2.12\times10^{-3}T - 0.82\times10^5T^{-2}$$
cal/g-atom · °C [Stonehouse 1986]

$$C_p = 5.238 + 13.378\times10^{-4}T - 15.31\times10^4T^{-2}$$
cal/g-atom · °C [Billone et al. 1995]

$$C_p = 3.752 + 7.185\times10^{-3}T - 6.704\times10^{-6}T^2 + 2.746\times10^{-9}T^3 \text{ cal/g-atom} \cdot °C$$
[Scafffidi-Argentina 2000]

$$C_p = 4.322 + 2.18\times10^{-3}T \text{ cal/g-atom} \cdot °C$$
[Stonehouse et al. 1965]

$$C_p = 6.079 + 5.138\times10^{-4}T \text{ cal/g-atom} \cdot °C$$
[Stonehouse et al. 1965]

The specific heat as a function of temperature covering both solid and liquid beryllium is shown in Fig. 4.21 [Pinto 1979b]. A plot of specific heat as a function of temperature is also shown in Fig. 4.22 [Lillie 1955]. The plot consists of data reported for nine different investigations and shows excellent agreement between these various studies. Some low-temperature results reported for specific heat and enthalpy are shown in Table 4.18 [Stonehouse et al. 1965]. Figures 4.23 [Touloukian 1967] and 4.24 [Touloukian and Buyco 1970] show the specific heat as a function of temperature covering both solid and liquid regions, with the curve in Fig. 4.24 extending down below 40 K.

The thermal conductivity as a function of temperature for several different sources of beryllium is shown in Fig. 4.25 [Pinto 1979b] and 4.26 [Lillie 1955]. The thermal conductivity as a function of temperature of beryllium from six

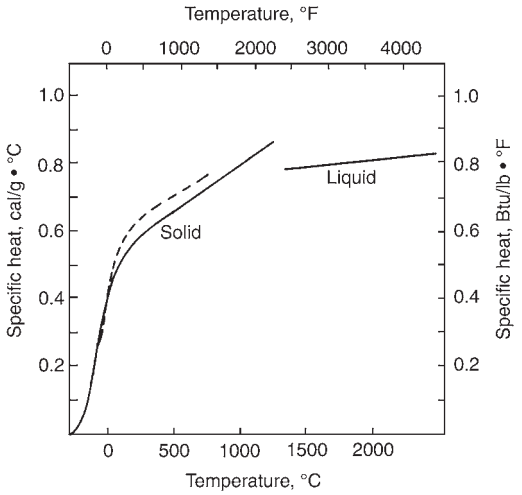

Fig. 4.21 Specific heat of beryllium as a function of temperature. Results from two different sources. Dashed line is for a brake grade of normal-purity block. Source: Pinto 1979b

Table 4.18 Specific heat and enthalpy at low temperatures

Temperature, K	C_p, cal/g · K	ΔH, cal/g
1	0.000006	0.000003
3	0.000019	0.000028
6	0.000043	0.000119
10	0.000093	0.00038
20	0.00038	0.0025
40	0.00238	0.026
60	0.0081	0.125
80	0.0217	0.404
100	0.0476	1.08
140	0.125	4.42
180	0.220	11.3
220	0.308	21.9
260	0.392	36.1
300	0.471	53.3

Source: Stonehouse et al. 1965

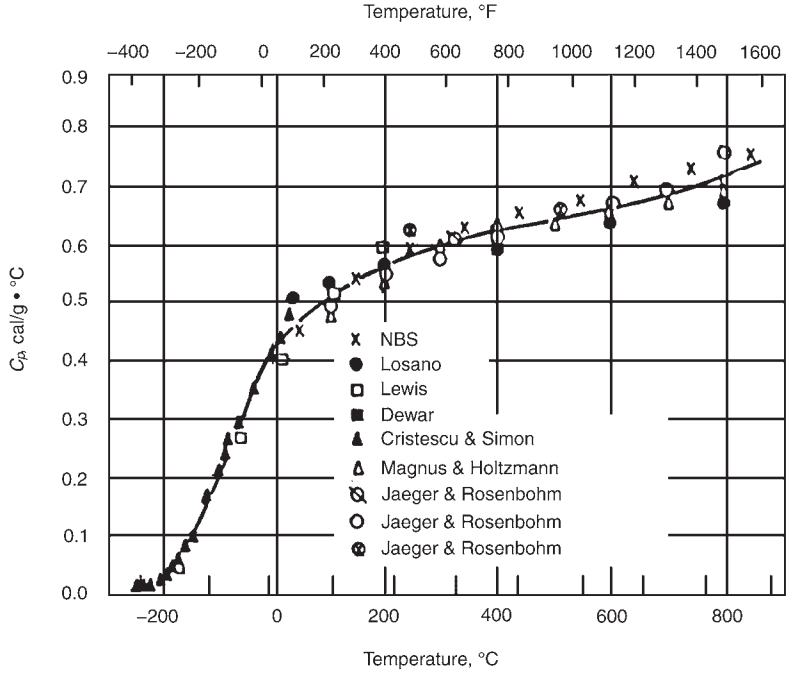

Fig. 4.22 Specific heat of beryllium (per gram) as a function of temperature. Source: Lillie 1955

different sources plotted on the same graph is shown in Fig. 4.27 [Touloukian 1967]. The thermal conductivity as a function of temperature for well-annealed high-purity beryllium over a wide range of temperatures (2 to 1000 K) is shown in Fig. 4.28 [Touloukian, Powell, et al. 1975]. A peak value in the conductivity is seen at approximately 35 K (−238 °C).

Thermal diffusivity (m^2/h) as a function of temperature is shown in Fig. 4.29. The thermal diffusivity determines the rate of heat propagation by conduction. It can be calculated by the following expression [Pinto 1979b]:

$$\alpha = \lambda/\rho C_p$$

where α is thermal diffusivity, λ is thermal conductivity, ρ is density, and C_p is specific heat [Pinto 1979b]. Thermal diffusivity as a function of temperature for well-annealed high-purity beryllium is shown in Fig. 4.30 [Touloukian 1973].

The self-diffusion in beryllium single crystals perpendicular to the basal plane over a series of temperatures is listed in Table 4.19. A plot of D versus 1/RT yields a straight line with the following expression [Lee et al. 1966]:

$$D_{\perp} = 0.19 \times \exp(-38{,}600/RT)$$

where $D_{\perp}$ is the self-diffusion perpendicular to the basal plane. In a different investigation, the

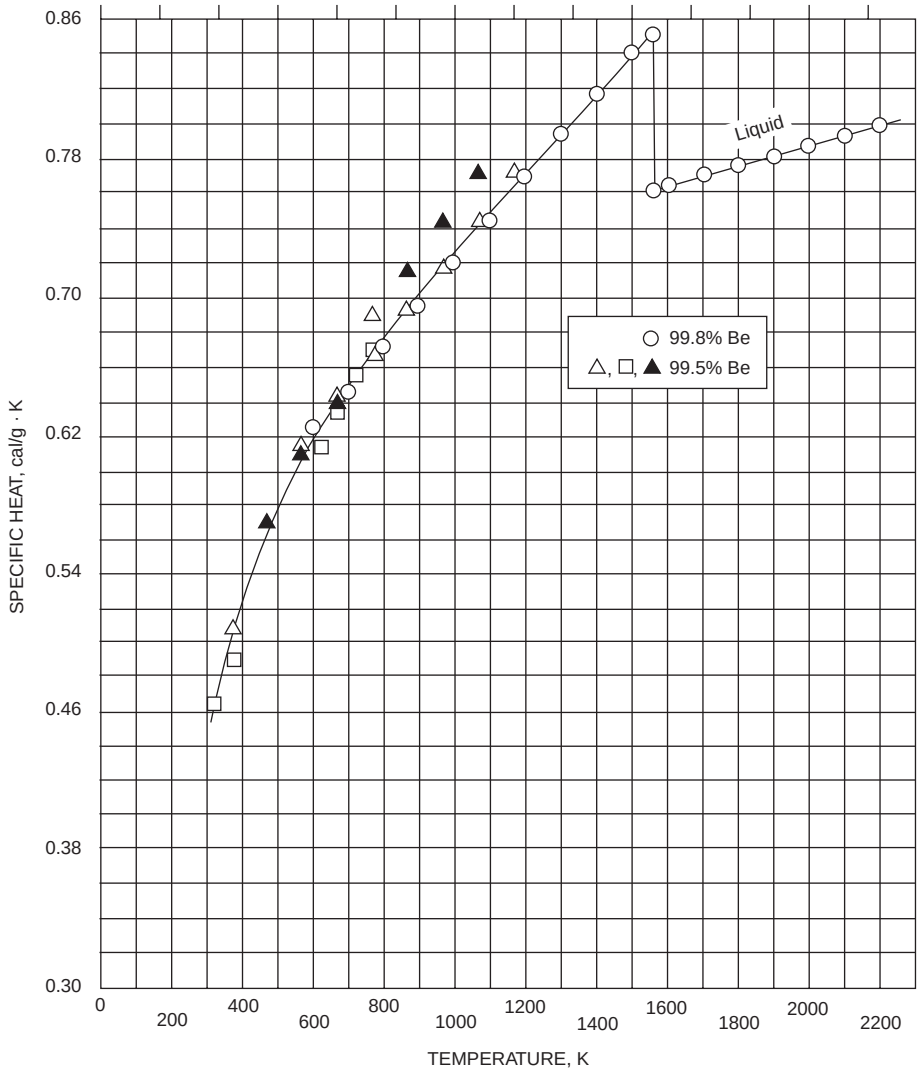

Fig. 4.23 Specific heat of beryllium as a function of temperature from four different sources for both solid and liquid regions. Source: Touloukian 1967

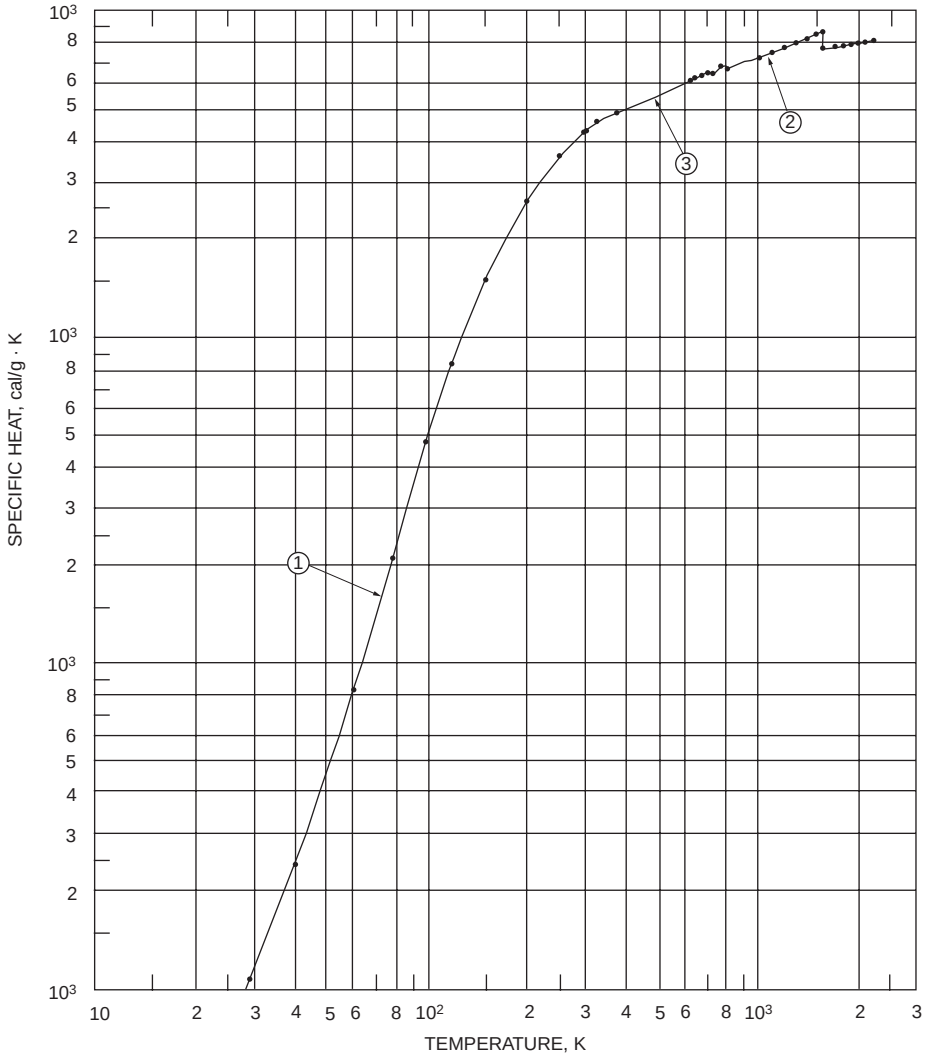

Fig. 4.24 Specific heat of beryllium covering a wide temperature range, from 40 to 2200 K. 1: 0 to 300 K, 99.5% Be, high-temperature extrusion of powder; 2: 600 to 2200 K, 99.8% Be, pulverized and tightly filled into ampoules; 3: 323 to 773 K, 99.8% Be, history not given. Source: Touloukin and Buyco 1970

expressions for self-diffusion of beryllium perpendicular and parallel ($D_{\|}$) to the basal plane are given as [Dupouy et al. 1966]:

$$D_{\perp} = (0.62 \pm 0.15) \times \exp\left[(-39{,}400 \pm 700)/RT\right]$$

and

$$D_{\|} = (0.52 \pm 0.15) \times \exp\left[(-37{,}600 \pm 700)/RT\right]$$

The authors note that the ratio $D_{\|}/D_{\perp}$ is greater than 1. This is consistent with the ratio of c/a being less than c/a ideal for beryllium. The authors also discuss diffusion of iron and silver in beryllium [Dupouy et al. 1966].

The vapor pressure of beryllium as a function of reciprocal temperature between 900 and 1283 °C is shown in Fig. 4.31 for three different beryllium processes [Lillie 1955] and in Fig. 4.32 [Touloukian 1967] for two different beryllium compositions. Both figures cover approximately the same temperature range (900 to 1283 °C). The vapor pressure over this temperature region, which is in the range of 10^{-10} to 10^{2} Pa, is given by the following expression [Scaffidi-Argentina at al. 2000]:

$$\log p\ (\text{Pa}) = 11.192 + 1.45 \times 10^{-4}\, T - 1.6734 \times 10^{4}\, T^{-1}$$

for T in K.

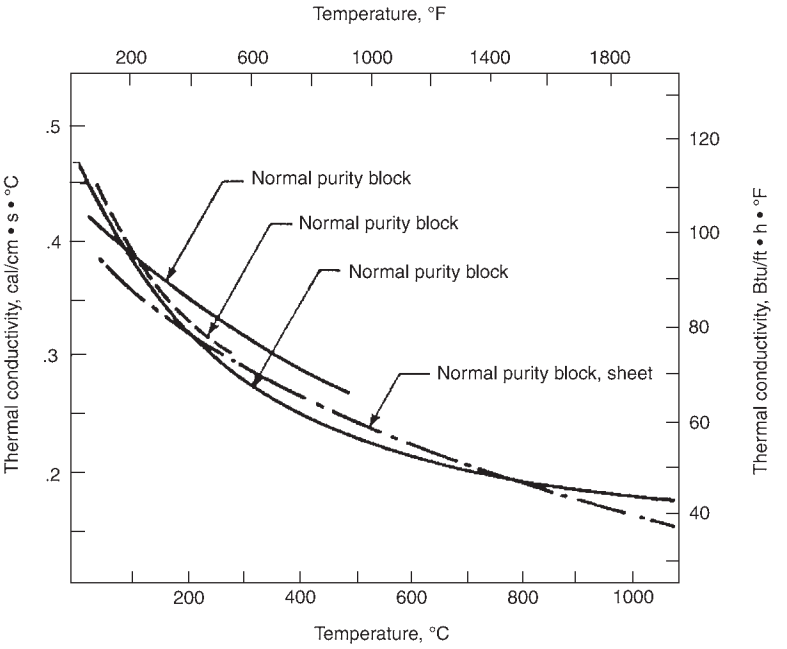

Fig. 4.25 Thermal conductivity of normal-purity beryllium block and sheet as a function of temperature. Each curve indicated in the plot comes from different authors referenced by Pinto 1979b

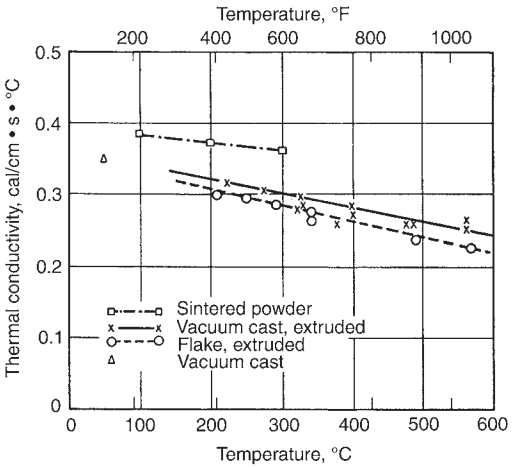

Fig. 4.26 Thermal conductivity of several types of beryllium as a function of temperature. Source: Lillie 1955

4.5 Nuclear Properties

Natural beryllium contains 100% of the ^{9}Be isotope. The principal isotopes of beryllium that have been identified are ^{6}Be, ^{7}Be, ^{8}Be, ^{9}Be, and ^{10}Be [Stonehouse 1986]. Additional isotopes listed are ^{11}Be, ^{12}Be, and ^{14}Be [General Electric Company 1984]. Some properties of the principal beryllium isotopes are listed in Tables 4.20 and 4.21. In searching for data on beryllium isotopes, the published data could, in some cases, differ significantly. Irradiated beryllium yields gas-producing nuclear reactions. The major nuclear reactions are given in Table 4.22. The nuclear reactions listed in Table 4.22 [Stonehouse 1986, Khomutov et al. 2002] are calculated to produce approximately 2.2 to 2.6 cm^3 of gas per cm^3 of beryllium following a fluence of 10^{21} N/cm^2. The first of these reactions has a threshold of approximately 12 MeV. The second one has a threshold of 600 keV, as well as a strong resonance at 3 MeV [Khomutov et al. 2002].

The beryllium atom has a reluctance to acquire additional neutrons while readily parting with one of its neutrons. It has a low neutron-capture cross section (probability of capture) and a high neutron-scattering (large number of collisions with direction change and energy loss) cross section, making the metal an excellent moderating material. Both of these cross-sectional areas are dependent on the energy of the neutrons and the condition of the metal (e.g., impurities and grain size). (The neutron cross section measures the probability of interaction of a neutron with matter. The cross section is visualized as a target area presented to the neutron by the nucleus. It is usually meas-

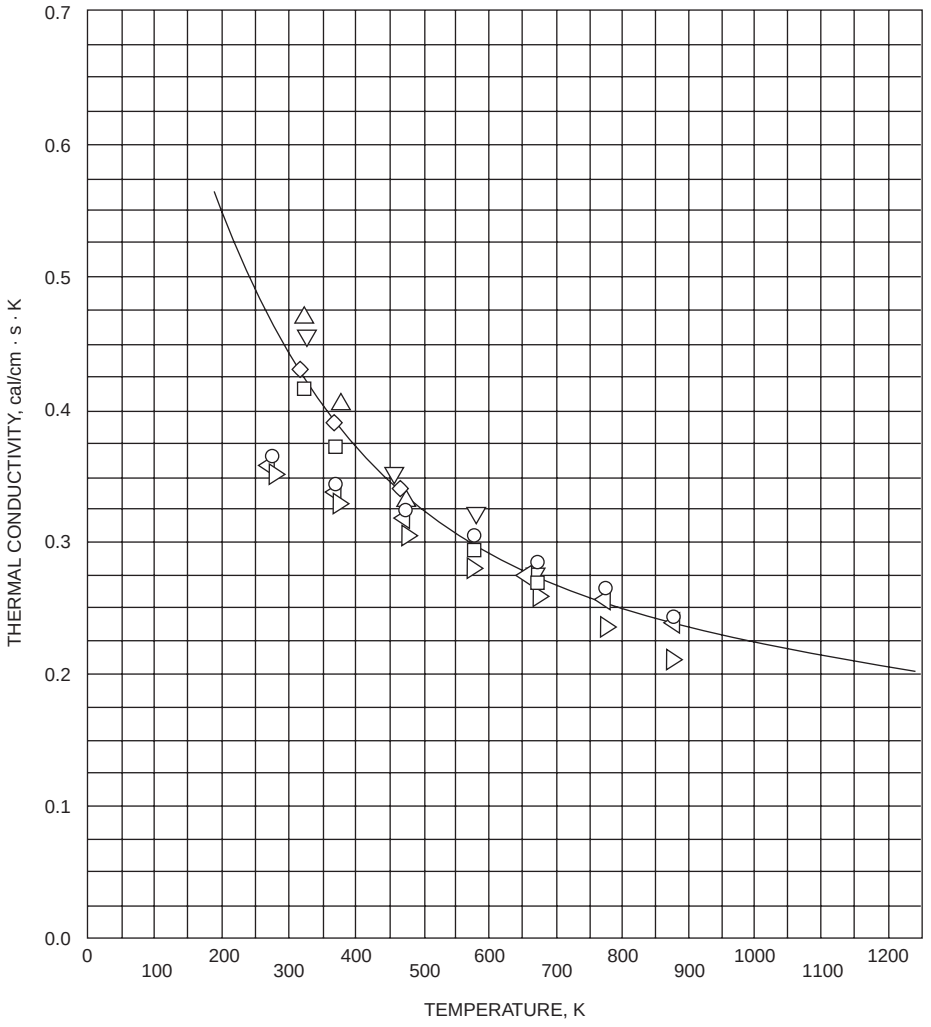

Fig. 4.27 Thermal conductivity of beryllium as a function of temperature. □: data from 322 to 672 K, listed as as-received condition with a density of 1.829 g/cm^3; Δ: 322 to 72 K, as previously described plus heat treated to above 700 °C; ◊: 322 to 672 K, listed as as-received condition with a density of 1.865 g/cm^3; ∇: 322 to 672 K, as previously described plus heat treated to above 700 °C; O: 273 to 875 K, no additional information; ◁: 273 to 875 K, vacuum-cast and extruded pure Be; ▷: 273 to 875 K, flake, extruded pure Be. Source: Touloukian 1967

ured in units of barns, or 10^{-24} m^2 per atom. Absorption and scattering cross section refers to the capture and scattering of neutrons, respectively. The thermal-neutron absorption cross section is the sum of the cross sections of all reactions, except that of the scattering cross section.) The effect of impurities on the thermal-neutron-capture (absorption) cross section is illustrated in Table 4.23 [Hausner 1965c]. With these nuclear properties, beryllium is used as a neutron moderator in nuclear-chain reactions, as a source of neutrons, and as a window in x-ray tubes.

The (n, 2n) reaction with a high-reaction cross section enables beryllium to function as a neutron multiplier. Beryllium is the leading neutron-multiplier candidate material for fusion applications. The combination of high neutron multiplication, low absorption, and high scattering characteristics provides excellent neutron thermalization. Therefore, beryllium can provide a high performance-breeding blanket for fusion systems [Stonehouse 1986]. The absorption cross section for thermal neutrons is 0.008 barns (a barn is a unit of 10^{-24} m^2/atom); the scattering cross section for fast neutrons is

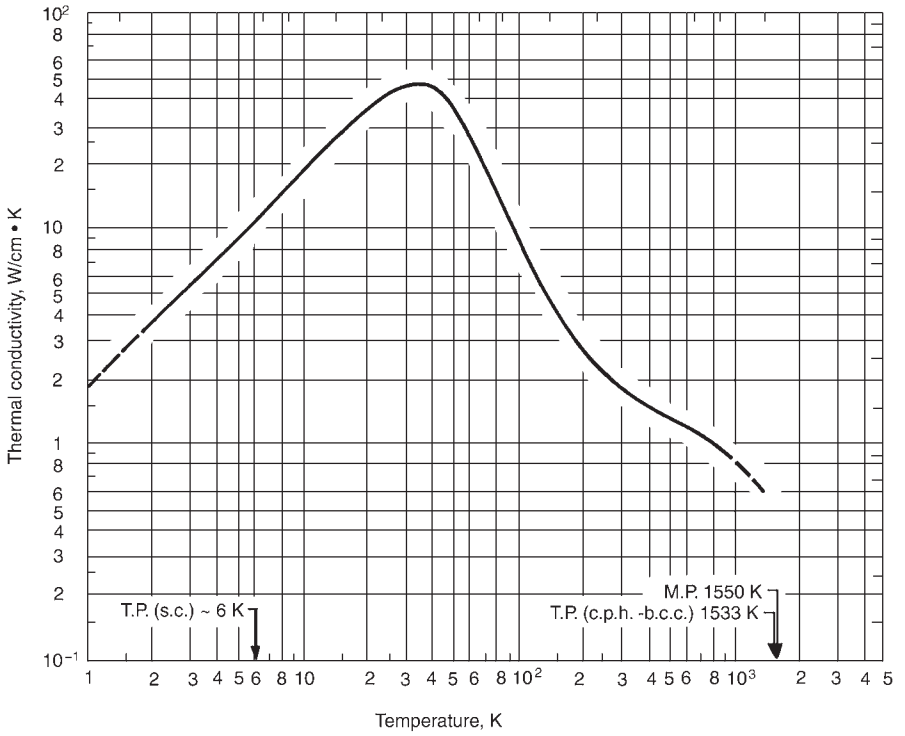

Fig. 4.28 Thermal conductivity for well-annealed high-purity beryllium, showing a maximum in conductivity at approximately 360 K. Data are believed to be accurate to 5% near room temperature and from 5 to 15% at other temperatures. MP, melting point; TP (sc), super conduction transition temperature; TP (cph-bcc), phase transition. Source: Touloukian, Powell, et al. 1975

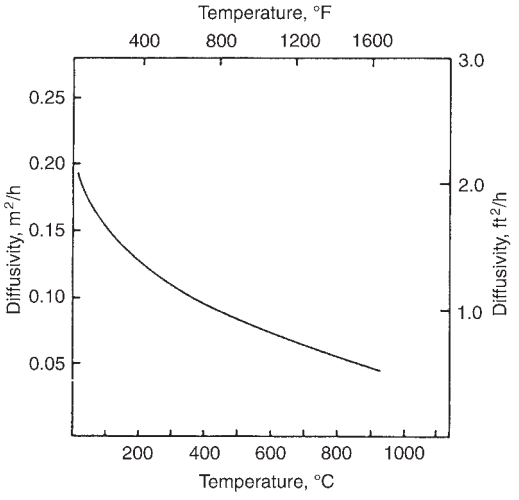

Fig. 4.29 Thermal diffusivity of normal-purity block and instrument-grade block of beryllium. Source: Pinto 1979b

6 barns [General Electric Company 1984]. The resonance integral is 0.004 barns. (Narrow peaks, at exceptionally high rates of reaction, in a plot of cross section versus energy are referred to as resonances. The resonance integral is the integral of the cross section as a function of neutron energy multiplied by the flux density.) The mass-absorption coefficient for copper K-alpha radiation is 1.007 cm^2/g [ASM 1979a].

The adsorption and desorption of deuterium have been measured on clean and on oxidized beryllium surfaces corresponding to the basal plane. The oxidized surfaces released all the adsorbed deuterium by approximately 177 °C. By contrast, for the clean surfaces, the desorption was not complete until the temperature was above 327 °C. The electron-affinity energy (difference between the ground state of the neutral atom and the lowest state of the corresponding negative ion) is indicated as being unstable for beryllium [CRC 2003–2004].

Irradiated beryllium exhibits an increase in yield strength with a loss in ductility and a decrease in fracture toughness. Nil ductility is obtained when tested below 100 °C, whereas a small increase in yield strength with only a small decrease in ductility is obtained above 350 °C. Although the fracture toughness decreases with an increase of neutron fluence, the trend reverses

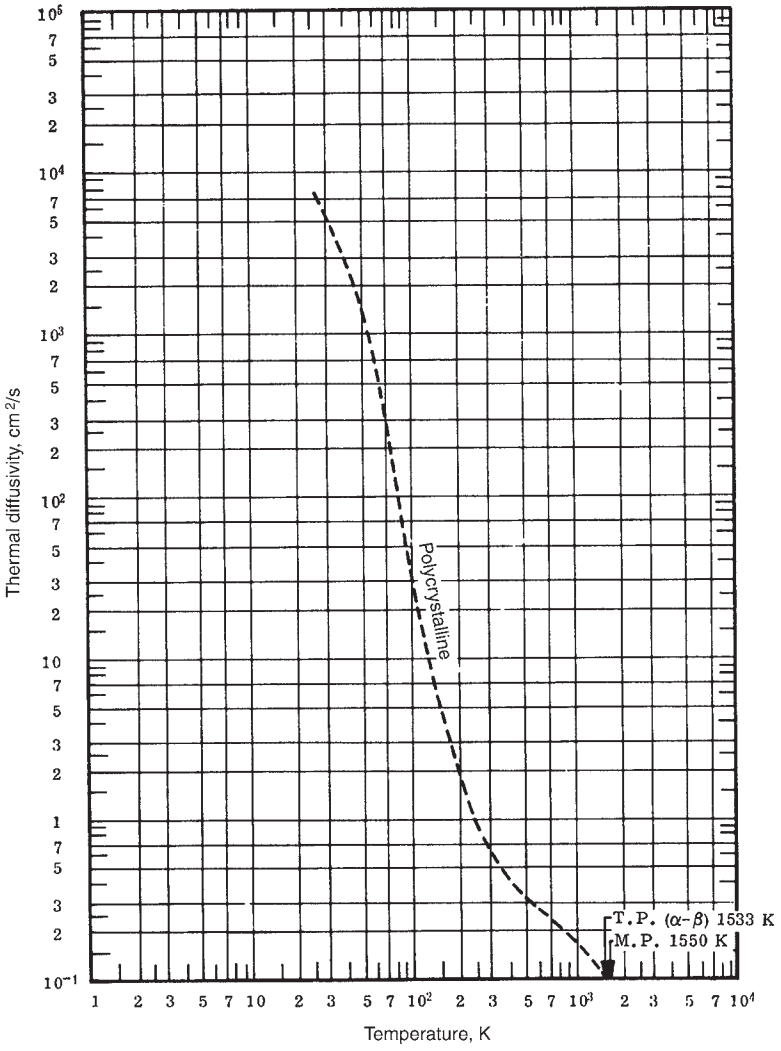

Fig. 4.30 Thermal diffusivity as a function of temperature for well-annealed high-purity beryllium. Uncertainty of ±15% above room temperature and ±25% below, where values are only applicable to beryllium having a residual electrical resistivity of 0.0135 μΩ · cm. MP, melting point; TP (α-β), alpha-beta transition temperature. Source: Touroukin 1973

Table 4.19 Diffusivities in beryllium single crystals perpendicular to the basal plane

Temperature (*T*),°C	Diffusivity (D), cm^2/s	Inverse temperature $(1/T) \times 10^4$, K^{-1}
553	1.3×10^{-11}	12.10
553	1.5×10^{-11}	12.10
607	4.3×10^{-11}	11.35
607	4.4×10^{-11}	11.35
703	5.1×10^{-10}	10.25
804	4.0×10^{-9}	9.27
804	4.8×10^{-9}	9.27
902	1.4×10^{-8}	8.50
1002	5.3×10^{-8}	7.85
1002	4.8×10^{-8}	7.85
1025	6.3×10^{-8}	7.70

Source: Lee et al. 1966

at high fluences. It is suggested that all the beryllium grades exhibit approximately the same fracture toughness response to irradiation. At the lower temperatures, the helium atoms remain in the matrix; at the higher temperatures, the atoms diffuse and agglomerate, causing swelling. As the fluence increases, the temperature required to produce complete annealing appears to increase, and the temperature to produce 1% swelling decreases [Stonehouse 1986].

The total neutron cross section of beryllium is a function of neutron energy and the grain size. This is illustrated in Fig. 4.33, which shows the

much greater transparency of the coarser-grained material in the lower energy range [Hausner 1965c]. Apparently, there is no difference in the transparency at the higher energies. The figure depicts the behavior over the low-energy thermal range, where the neutrons are in thermal equilibrium with the moderator and where the cross-sectional area increases with energy, and in the intermediate region, where the neutrons have been moderated but have not yet reached equilibrium. In the latter region, also known as the slowing-down region, the cross section changes little with energy. In this range, the neutrons have wavelengths comparable with the crystal lattice spacings, and thus, diffraction plays a role here, with interactions occurring between incoming and scattered neutron-wave fronts due to coherent scattering. For beryllium, a pronounced backward scattering occurs for neutrons having an energy of 0.00525 eV and a wavelength of 3.96 Å, which is twice the longest lattice spacing of 1.98 Å for beryllium [Stehn 1965]. In the fast region (above approximately 1 eV), where the neutrons are produced by fission, the cross section decreases significantly with increasing energy. Other reactions, which may be similarly discussed, are nuclear reactions produced by gamma rays, alpha particles, deuterons, and protons [Stehn 1965].

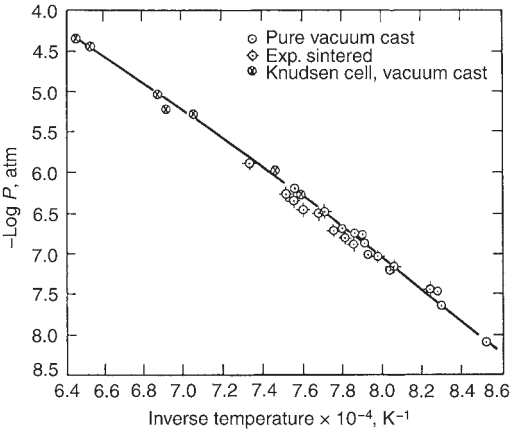

Fig. 4.31 Vapor pressure of beryllium as a function of $1/T$ (K). Source: Lillie 1955

4.6 Miscellaneous Properties

Properties that were not presented in the previous sections are listed in Table 4.24.

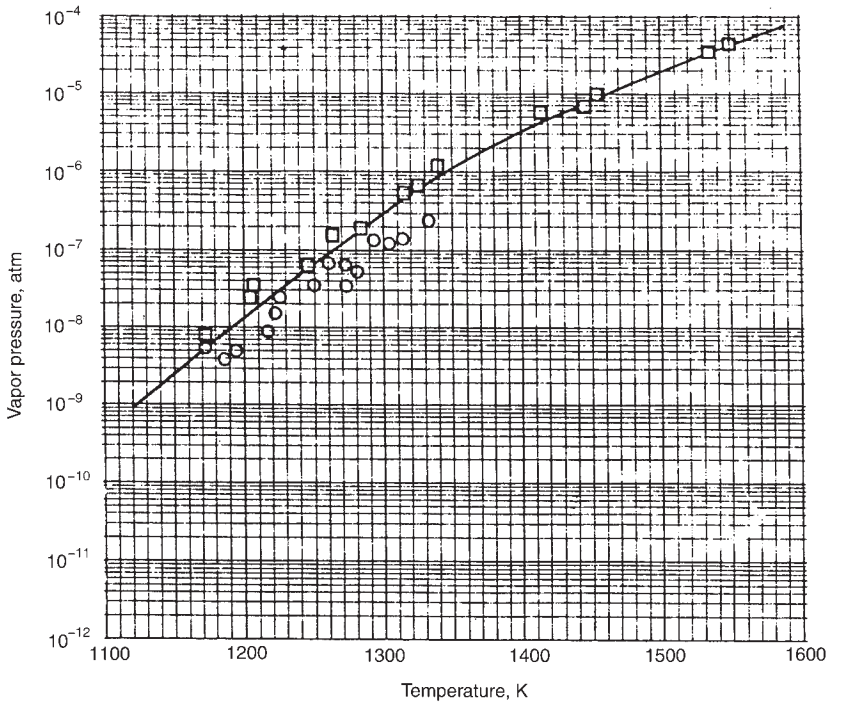

Fig. 4.32 Vapor pressure of beryllium as a function of temperature. O: 1174 to 1336 K, 0.03 Fe, 0.022 Si, 0.008 Al, 0.004 Mg; □: 1172 to 1552 K, vacuum cast, 0.14 Al, 0.07 Fe, 0.04 Si, 0.02 Mg, 0.01 each of Cr, Cu, Na, Ni, and Zn. Source: Touloukian 1967

The electrical resistance of beryllium as a function of temperature from room temperature to 1080 °C is shown in Fig. 4.34 [Pinto 1979b]. A similar plot is shown in Fig. 4.35 [Lillie 1955]. The data in the two figures are similar at the lower temperatures but differ at the higher temperatures; for example, these values at 800 °C are approximately 26 and 31 $\mu\Omega \cdot$cm in Fig. 4.34 and 4.35, respectively. The author [Lillie 1955] states that the electrical conductivity (or resistivity) varies considerably with purity and method of fabrication (as is generally the case for essentially all metals and their alloys). He also states that the conductivity values for beryllium range from 35 to 42% of the IACS values. Figure 4.36 shows a significant spread in resistivity values of beryllium having various densities (1.823 to 1.865 g/cm^3), impurity levels, and processing levels [Touloukian 1967].

Table 4.25 lists the electrical resistivities of polycrystalline beryllium over a range of temperatures from −263 to 673 °C (10 to 900 K). Electrical resistivity measurements were reported on 4 mm beryllium rods, grades CR and CS (French). Billets were extruded into rods in the temperature range between 1000 and 1050 °C and then annealed at 800 °C, producing a recrystallized structure with polygonization (substructure within the grains). The extruded rods had similar textures that were not appreciably altered by the anneal. Both as-swaged and swaged-and-annealed rods were evaluated at four temperatures. The results are shown in Table 4.26 [Logerot 1966]. The author points out that the resistivity varies considerably with metallic impurity, and, the lower the temperature, the greater is this variation. The electrical resistivity at room temperature and at 4.2 K and the residual resistance ratios for various purity levels of beryllium are listed in Table 4.27. (The residual resistance ratio is the ratio of the resistance at room temperature to that at 4.2 K.) The purity level appears to have an appreciable effect on the resistance at 4.2 K, while only a minor effect at room temperature. Significant effects are seen for the relative resistance ratios ($\Omega_{RT}/\Omega_{4.2\ K}$) [Stonehouse et al. 1965]. Different processing histories are also indicated in Table 4.27. The electrical resistance as a function

Table 4.20 Some properties of beryllium isotopes

Isotope	Half-life	Radiation, MeV	Source
^{6}Be	3×10^{-21} s	...	...
^{7}Be	53.5 days	γ	^{6}Li (d, n)
		0.453–0.485	^{7}Li (p, n)
			^{10}B (p, d)
			^{10}B (p, α)
			^{10}B (d, α, n)
^{8}Be	1.4×10^{-16} s	α	^{9}Be (γ, n)
		0.055	^{9}Be (n, 2n)
^{9}Be	Stable	...	...
^{10}Be	2.7×10^6 years	β	^{9}Be (α, p)
		0.56–0.65	9Be (d, p)
			9Be (n, γ)
			^{10}Be (n, p)
			^{13}C (n, α)

Nuclear reactions of the stable isotope ^{9}Be—Gamma-ray bombardment ^{9}Be(γ, n)^{8}Be; Neutron bombardment ^{9}Be(n, α)^{6}He, ^{9}Be(n, γ)^{10}Be, ^{9}Be(n, 2n)^{8}Be. Source: Petzow et al. 2002a

Table 4.21 Some additional properties of beryllium isotopes

Isotope	Half-life	Thermal-neutron cross section, barns	Resonance integral (RI), barns	Coherent scatter length (a), fm
^{7}Be	53.28 days	$\sigma_p = 3.9 \times 10^4$ b(b)	$RI_p = 1.75 \times 10^4$ b	...
		$\sigma_a = 0.1$ b		
^{9}Be	Stable	8.8 mb	3.9 mb	7.79
^{10}Be	1.52×10^6years	<1.0 mb	...	...

(a) fm = 10^{-13} cm. (b) σ_p and σ_a, proton and alpha production, respectively. Source: CRC 2003–2004

Table 4.22 Irradiated beryllium yielding gas-producing nuclear reactions

Irradiation source	Reaction
Fast neutrons	$Be^9 + n_f \rightarrow Li^7 + H^3$
	$Be^9 + n_f \rightarrow Be^8 + 2n$
	$Be^8 \rightarrow 2He^4$
	$Be^9 + n_f \rightarrow He^6 + He^4$
	$He^6 \xrightarrow{B^-} Li^6$
Thermal neutrons	$Li^6 + n_t \rightarrow H^3 + He^4$

Source: Stonehouse 1986

Table 4.23 Effect of various impurities on the thermal-neutron-absorption cross section of beryllium

Impurity	Thermal-neutron cross section, barns	Addition cross section to Be, mb
Boron	766	638
Cobalt	37.0	5.7
Manganese	13.2	2.2
Nickel	4.8	0.7
Iron	2.73	0.44
Calcium	0.44	0.10
Aluminum	0.24	0.08
Magnesium	0.07	0.03

Source: Hausner 1965c

of pressure relative to the resistance at 10 GPa and 25 °C is shown in Fig. 4.37 [Reichlin 1983].

The thermoelectric power of hot pressed beryllium relative to copper as a function of temperature at low temperatures is shown in Fig. 4.38. Curves for both parallel and perpendicular to the pressing direction are presented [Stonehouse et al 1965]. The thermoelectric power of beryllium against platinum is given as 1.6 and 2.6 μV/°C for 99.96 and 99.78% purity, respectively. A straight-line increase from 8.2 μV/°C at 336 °C to 18 μV/°C at 800 °C is reported for beryllium against platinum, as shown in Fig. 4.39 [Stonehouse et al. 1965, Lillie 1955].

The normal spectral reflectance at a series of wavelengths of beryllium anodized by two different methods is listed in Table 4.28 [Stonehouse et al. 1965]. Figure 4.40 is a plot of normal spectral reflectance of beryllium as a function of wavelength using 0.625 mm thick samples [Touloukian 1967]. The data reflect the use of three different hohlraum (target chamber) temperatures (523, 773, and 1273 K).

The normal total emittance of beryllium in air as a function of temperature is shown in Fig. 4.41 [Touloukian 1967]. The composition and history

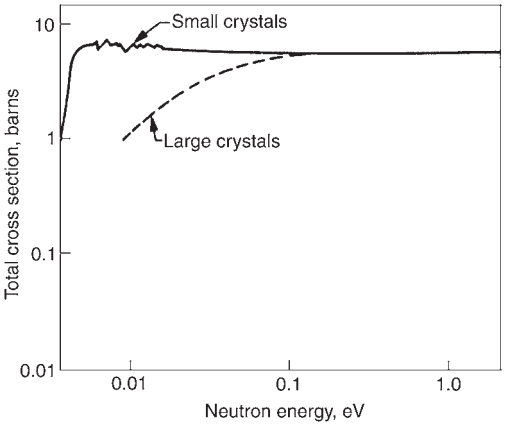

Fig. 4.33 Total neutron cross section as a function of neutron energy of fine-grained and coarse-grained beryllium. The coarse grains were obtained by heat treatment. Source: Hausner 1965c

Table 4.24 Room temperature values of miscellaneous properties of beryllium

Sonic velocity, m/s	12,588
Optical reflectivity (white light), %	50–55
Ultraviolet reflectivity, %	50
Infrared reflectivity (10.6 μm), %	98
Solar absorptivity (polished plate surface), %	46
Electrical conductivity, % of IACS	40.7 (0.24 mho/cm)
Electrical resistivity (25 °C), Ω · m	3.70×10^{-8} (4.31×10^{-8})
Magnetic susceptibility, χ_{mass} (20 °C), cm^3/g	-1.00×10^{-6} (diamagnetic)
Photoelectric work function, eV	3.92
Electron work function (polycrystal), eV	4.98 (depends on surface cleanliness)
Ionization potential for neutral atom, eV	9.3227
Electron-binding energy for 1s (K) level, eV	111.5

Source: CRC 2003–2004, Stonehouse et al. 1965, Kirk-Othmer 2002, ASM 1979a

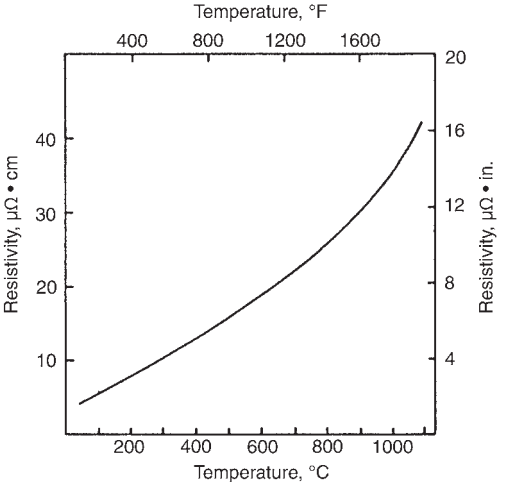

Fig. 4.34 Electrical resistivity as a function of temperature of normal-purity beryllium block. Source: Pinto 1979b

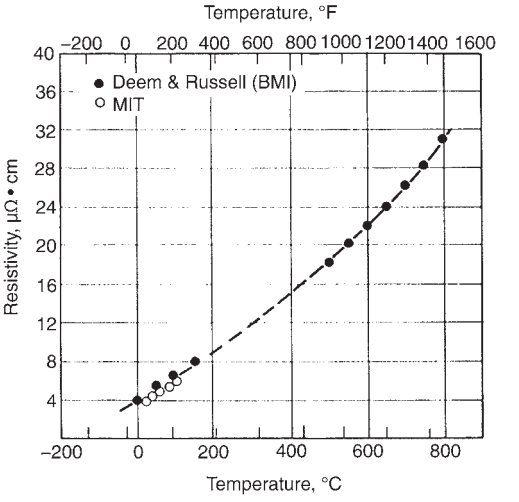

Fig. 4.35 Effect of temperature on the resistivity of beryllium for two investigations. Source: Lillie 1955

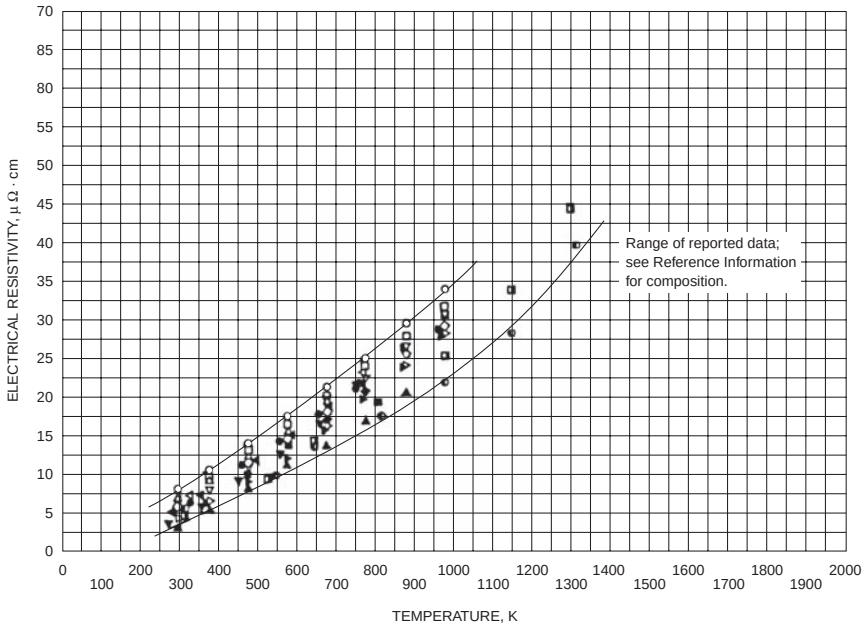

Fig. 4.36 Electrical resistivity as a function of temperature of beryllium having various densities (1.823 to 1.865 cm^3), impurity levels, and processing histories. Source: Touloukian 1967

Table 4.25 Electrical resistivity of polycrystalline beryllium

Temperature, K	Resistivity, 10^{-8} Ω · m
10	0.0332
20	0.0336
40	0.0367
60	0.067
80	0.075
100	0.133
150	0.510
200	1.29
273	3.02
293	3.56
298	3.70
300	3.76
400	6.76
500	9.9
600	13.2
700	16.5
800	20.0
900	23.7

Source: Scaffidi-Argeutina et al. 2000

of the metal were not given. Figure 4.42 shows the normal spectral transmittance of beryllium as a function of wavelength at 298 K [Touloukian and DeWitt 1970]. Measurements were made on aluminum-backed beryllium film (875 ± 100 Å thick), with both aluminum and beryllium being deposited by evaporation on a glass slide. The data were corrected for transmittance of aluminum and glass. Approximately 10% error was indicated for $\lambda > 0.035$ μm and 25% for $\lambda < 0.035$ μm. Geometries of θ and θ^1 were approximately 0° divergent from the normal (90° to surface). Figure 4.43 shows the normal total emittance as a function of temperature during heating (1116 to 1473 K) and cooling (1473 to 1255 K). The geometry was given as incident angle (θ^1) being approximately 0° [Touloukian and DeWitt 1970].

REFERENCES

Armstrong, R.W., and Borch, N.R., 1971. "Thermal Microstresses in Beryllium and Other hcp Metals," UCRL-72915 Rev. 1 Preprint, University of California Lawrence Radiation Lab, Berkeley, CA; also *Met. Trans.*, Vol 2, p 3073–3077

ASM, 1979a. Beryllium, *Properties and Selection: Nonferrous Alloys and Pure Metals*, Vol 2, *Metals Handbook*, 9th ed., ASM International, p 717–718

ASM, 1990. *Properties and Selection: Nonferrous Alloys and Special-Purpose Materials*, Vol 2, *Metals Handbook*, 10th ed., ASM International

Table 4.26 Electrical resistivity of beryllium rods at different temperatures

Rod history	Rod No.	Grade	BeO, %	Total metallic impurities	Grain size, μm	Resistivity, μΩ · cm			
						273 K	77.4 K	20.3 K	4.2 K
As-extruded	1	CR	0.9	0.18	10–80	3.92	1.09	1.03	1.03
	2	CR	1.2	0.10	10–80	3.49	0.65	0.61	0.61
	3	CR	0.1	0.08	30–200	3.28	0.55	0.51	0.51
	4	SR	0.2	0.02	30–200	2.79	0.066	0.037	0.037
Extruded and annealed	1	CR	0.9	0.18	10–80	3.72	0.96	0.88	0.88
	2	CR	1.2	0.10	10–80	3.17	0.41	0.37	0.37
	3	CR	0.1	0.08	30–200	3.15	0.50	0.45	0.45
	4	SR	0.2	0.02	30–200	2.85	0.063	0.37	0.37

Source: Logerot 1966

Table 4.27 Electrical resistivity and residual resistance ratios (relative resistance) for various purity levels of beryllium

Specimen history	Resistivity, μΩ · cm		Relative resistance, $\Omega_{RT}/\Omega_{4.2\,K}$
	Room temperature (Ω_{RT})	4.2 k ($\Omega_{4.2\,K}$)	
Commercial purity, rolled sheet, longitude	5.350	1.068	5.01
Commercial purity, rolled sheet, transverse	4.864	0.967	5.03
Commercial purity, hot pressed	5.543	1.167	4.75
Intermediate purity, hot pressed	4.706	0.394	11.94
High-purity Pechiney SR, hot pressed	4.266	0.027	158
Vacuum-melted Pechiney flake, single distilled	. . .	. . .	80–750
Vacuum-melted Pechiney flake, double distilled	. . .	. . .	200–900

Source: Stonehouse et al. 1965

Billone, M.C., Dalle Donne, M., and Macaulay-Newcombe, R.G., 1995. Status of Beryllium Development for Fusion Applications, *Fusion Eng. Des.*, Vol 27, p 179–190

Christman, D.R., and Feistmann, F.J., 1972. "Dynamic Properties of S-200-E Beryllium," DNA 2785F-MSL 71–23, Materials and Structures Laboratory, General Motors Technical Center, Warren, MI

CRC, 2003–2004. *Handbook of Chemistry and Physics*, 84th ed., CRC Publication

Dupouy, J.M., Naik, M., Adda, M., and Adda, Y., 1966. Self-Diffusion and Diffusion of Foreign Atoms in Beryllium, *Beryllium Technology, Proceedings of the Second International Conference on Beryllium Technology*, Vol 1, Gordon and Breach, Science Publishers, Inc., NY, p 319–333

General Electric Company, 1984. "Chart of the Nuclides with Physical Constants, Conversion Factors and Period Table," 13th ed., San Jose, CA

Hausner, H.H., 1965c. Nuclear Properties, *Beryllium: Its Metallurgy and Properties*, H.H. Hausner, Ed., University of California Press, Berkeley, CA, p 234–239

Haws, W.J., 1985. "Characterization of Beryllium Structural Grade S-200F," Technical Memorandum TM-778, Brush Wellman

Haws, W.J., 1988. "Thermal Expansion of S-200F Beryllium from 100 to 450 K," Technical Memorandum TM-894, Brush Wellman

Jennings, C.G., Gross, A.G., Jr., and Coleteryahn, L.E., 1966. Dimensional Stability and Thermal Expansion Characteristics of Beryllium, *Beryllium Technology, Proceedings of the Second International Conference on Beryllium Technology*, Vol 1, 1964 Conference, Gordon and Breach, Science Publishers, Inc., NY, p 467–478

Khomutov, A., Barabash, V., Chakin, V., Chernov, V., Davydov, D., Gorokhov, V., Kawamura, H., Kolbasov, B., Kupriyanov, I., Longhurst, G., Scaffidi-Argentina, F., and Shestakov, V., 2002. Beryllium for Fusion Application—Recent Results, *J. Nucl. Mater.*, Vol 307–311, p 630–637

Killpatrick, D.H. "Elastic Properties of Beryllium," Internal Report, Logicon (now Northrup Gruman), Albuquerque, NM

Kirk-Othmer, 2002. Beryllium and Beryllium Alloys, *Kirk-Othmer Encyclopedia of Chemical Technology*, John Wiley and Sons, Inc.

Lee, C.H., Drew, J.B., Spangler, G.E., and Herman, M., 1966. Self-Diffusion in Beryllium Single Crystals, *Beryllium Technology, Proceedings of the Second International Conference on Beryllium Technology*, Vol 1, Gordon

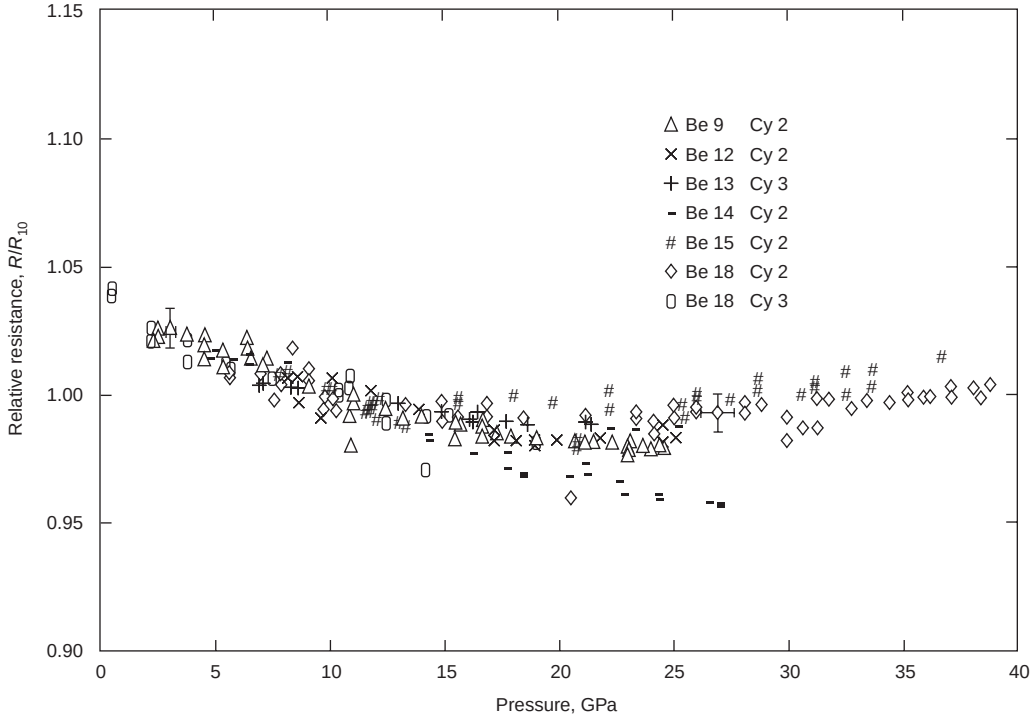

Fig. 4.37 Residual (relative) resistance, R/R_{10}, of beryllium as a function of pressure taken during the second or third cycle (as indicated) while increasing pressure. R_{10} is resistance at 10 GPa. Source: Reichlin 1983

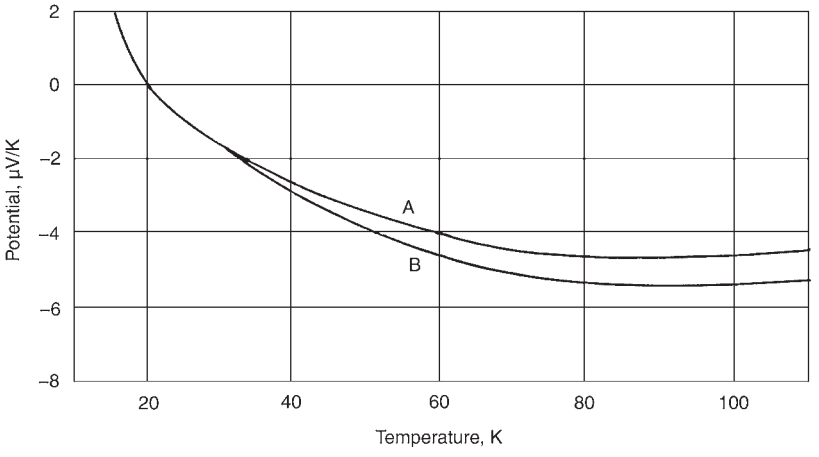

Fig. 4.38 Thermoelectric power of hot pressed beryllium against copper. A, specimen axis parallel to pressing direction; B, specimen axis perpendicular to pressing direction. Source: Stonehouse et al. 1965

and Breach, Science Publishers, Inc., NY, p 307–317

Lillie, D.W., 1955. The Physical and Mechanical Properties of Beryllium, *The Metal Beryllium*, D.W. White, Jr., and J.E. Burke, Ed., American Society for Metals, p 304–327

Logerot, J.M., 1966. Mechanical and Electrical Properties of Beryllium Wire, *Beryllium*

Technology, Proceedings of the Second International Conference on Beryllium Technology, Vol 1, Gordon and Breach, Science Publishers, Inc., NY, p 445–466

Meyerhoff, W., and Smith, J.F., 1961. Anisotropic Thermal Expansion of Single Crystals of Thalium, Yttrium, Beryllium, and Zinc at Low Temperatures, *J. Appl. Phys.*, Vol 33 (No. 1), p 219–224

Petzow, G., Aldinger, F., Jonsson, S., and Preuss, O., 2002a. Beryllium and Beryllium Compounds, *Ullmann's Encyclopedia of Industrial Chemistry,* 6th ed., Wiley-VCH Verlag Chemie, Weinheim, Germany, Table 1

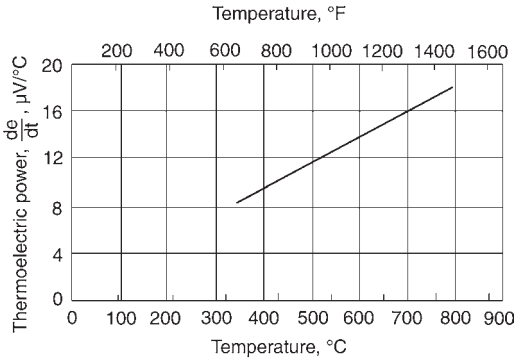

Fig. 4.39 Thermoelectric power of beryllium against platinum as a function of temperature. Source: Lillie 1955

Table 4.28 Normal spectral reflectance of anodized beryllium at a series of temperatures

Wavelength, μm	Anodized in chromic acid	Anodized in sodium hydroxide
0.4	0.172	0.075
0.6	0.179	0.052
0.8	0.168	0.058
1.0	0.165	0.68
2.0	0.280	0.203
4.0	0.355	0.286
6.0	0.335	0.514
8.0	0.317	0.772
10	0.560	0.773
15	0.673	0.606
20	0.494	0.899

Source: Stonehouse et al. 1965

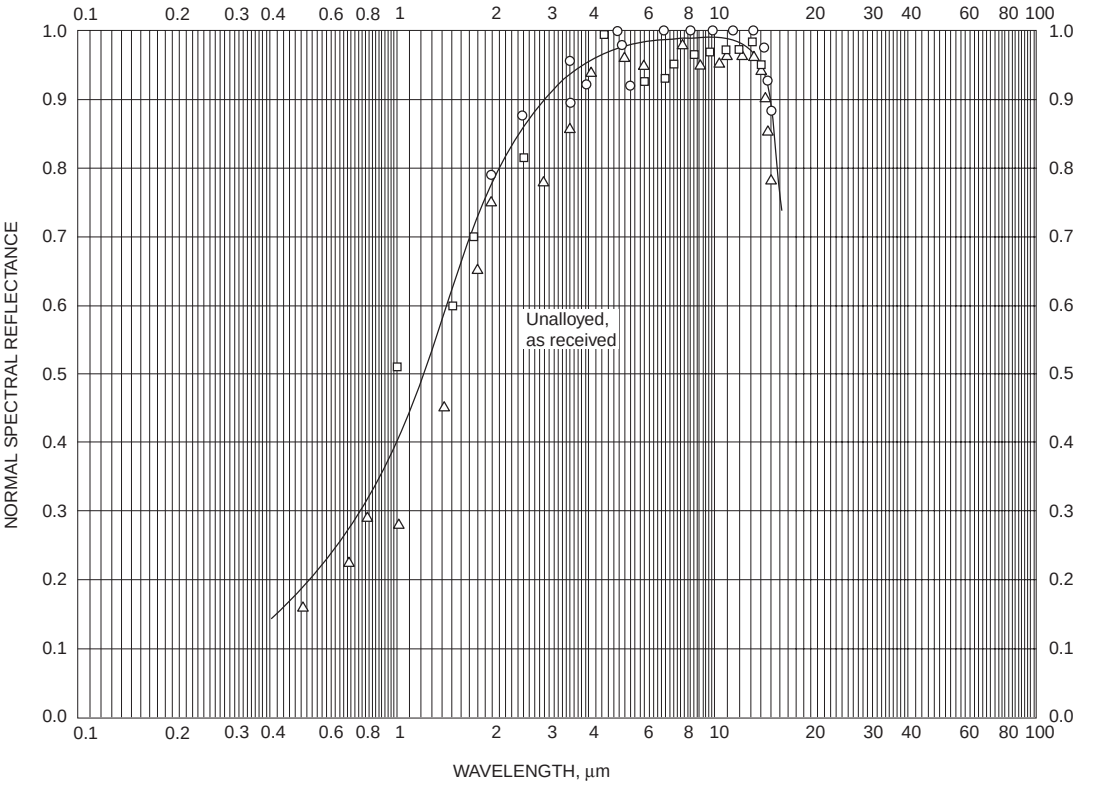

Fig. 4.40 Normal spectral reflectance of as-received, washed, and unalloyed 0.635 mm thick beryllium as a function of wave length. O: hohlraum (h) at 523 K, measuring temperature (mt) < 322 K, wavelength range (wr) 2.00 to 15.00 μm; □: h at 773 K, mt < 322 K, wr 1.00 to 14.00 μm; Δ: h at 1273 K, mt < 322 K, wr 0.50 to 15.00 μm. Source: Touloukian 1967

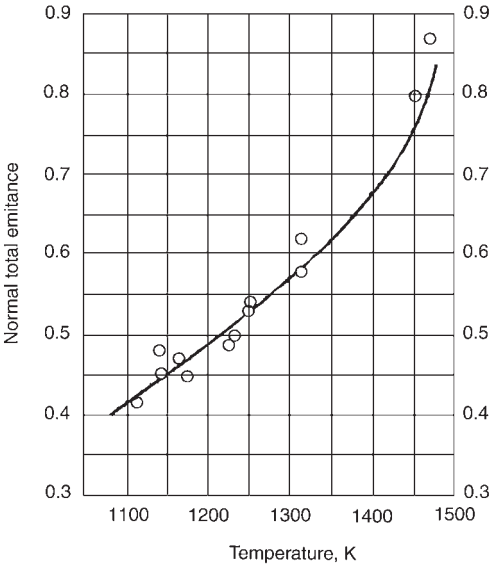

Fig. 4.41 Normal total emittance of beryllium in air as a function of temperature. Source: Touloukian 1967

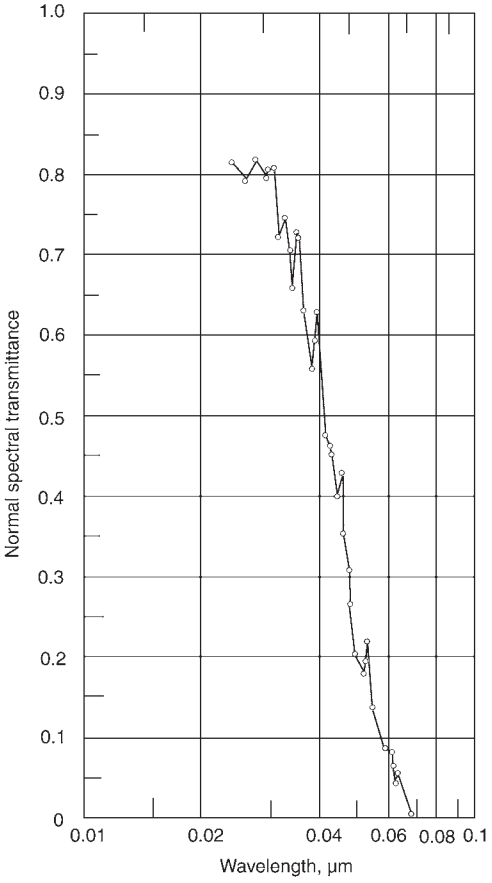

Fig. 4.42 Normal spectral transmittance of beryllium as a function of wavelength at 298 K measured on an aluminum-backed beryllium film (875 ± 100 Å thick). Aluminum and beryllium evaporated at 2×10^{-5} torr on a glass slide. Data corrected for transmittance of aluminum and glass. Approximately 10% error for $\lambda > 0.035$ μm and <25% for $\lambda < 0.035$ μm. Geometry, emittance θ and $\theta^1 \sim 0$. Source: Touloukian and DeWitt 1970

Pinto, N.P., 1979b. Properties, *Beryllium Science and Technology*, Vol 2, D.R. Floyd and J.N. Lowe, Ed., Plenum Press, NY, p 319–350

Reichlin, R.L., 1983. Measuring the Electrical Resistance of Metals to 40 GPa in the Diamond-Anvil Cell, *Rev. Sci. Instrum.*, Vol 54 (No. 12), p 674

Scaffidi-Argentina, A.F., Longhurst, G.R., Shestakov, V., and Kawamura, H., 2000. Beryllium R&D for Fusion Applications, *Fusion Eng. Des.*, Vol 51–52, p 23–41

Smith, M.F., McDonald, J.M., Watson, R.D., and Whitley, J.B., 1985. Thermomechanical Testing of Beryllium for Limiters in ISX-B and JET, *Fusion Technol.*, Vol 8, p 1174–1183

Stehn, J.R., 1965. The Nuclear Properties of Beryllium, *The Metal Beryllium*, D.W. White, Jr., and J.E. Burke, Ed., American Society for Metals, p 328–366

Stonehouse, A.J., 1986. Physics and Chemistry of Beryllium, *J. Vac. Sci. Technol. A*, Vol 4 (No. 3), p 1163–1170

Stonehouse, A.J., Carrabine, J.A., and Beaver, W.W., 1965. Physical Properties, *Beryllium: Its Metallurgy and Properties*, H.H. Hausner, Ed., University of California Press, Berkeley, CA, p 191–205

Swenson, C.A., 1991. HIP Beryllium: Thermal Expansivity from 4 to 300 K and Heat Capacity from 1 to 108 K, *J. Appl. Phys.*, Vol 70, p 3046–3051

Touloukian, Y.S., 1967. *Elements*, Vol 1, *Thermophysical Properties of High Temperature Solid Materials*, Y.S. Touloukian, Ed., MacMillan, NY

Touloukian Y.S., 1973. *Thermal Diffusivity*, Vol 10, *Thermophysical Properties of Matter*, Y.S. Touloukian, R.W. Powell, C.Y. Ho, and M.C. Nicolaou, Ed., IFI/Plenum, NY

Touloukian, Y.S., and Buyco, E.H., 1970. *Specific Heat: Metallic Elements and Alloys*, Vol 4, *Thermophysical Properties of Matter*, IFI/Plenum, NY

Touloukian, Y.S., and DeWitt, D.P., 1970. *Thermal Radiative Properties: Metallic Elements and Alloys*, Vol 7, *Thermophysical Properties of Matter*, IFI/Plenum, NY

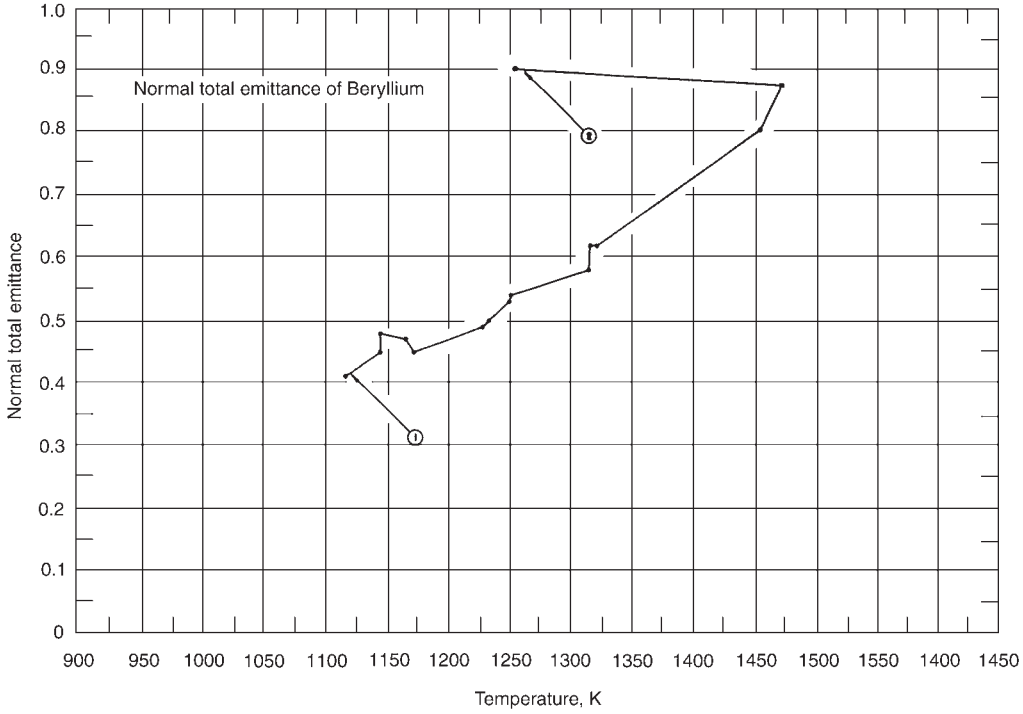

Fig. 4.43 Normal total emittance of beryllium as a function of temperature. 1, heating (1116 to 1473 K); 2, cooling (1473 to 1255 K); geometry, $\theta^1 \sim 0$. Source: Touloukian and DeWitt 1970

Touloukian, Y.S., Kirby, R.K., Taylor, R.E., and Desai, P.D., 1975. *Thermal Expansion: Metallic Elements and Alloys*, Vol 12, *Thermophysical Properties of Matter*, IFI/Plenum, NY

Touloukian, Y.S., Powell, R.W., Ho, C.Y., and Klemenss, P.G., 1975. *Thermal Conductivity: Metallic Elements and Alloys*, Vol 1, *Thermophysical Properties of Matter*, IFI/Plenum, NY

Yaws, C.L., 1999. *Chemical Properties Handbook*, McGraw-Hill

SELECTED REFERENCES

- Sands, D.E., Johnson, Q.C., Zalkin, A., Krikorian, O.H., and Kromholtz, K.L., 1962. The Crystal Structure of $ReBe_{22}$, *Acta Crystallogr.*, Vol 15, p 832–834
- Sands, D.E., Zalkin, A., and Krikorian, O.H., 1959. The Crystal Structures of $NbBe_2$ and $NbBe_3$, *Acta Crystallogr.*, Vol 12 (No. 6), p 461–464
- Von Batchelder, F.W., and Raeuchle, R.F., 1957. The Structure of a New Series of MBe_{12} Compounds, *Acta Crystallogr.*, Vol 10, p 648–649
- Zalkin, A., Bedford, R.G., and Sands, D., 1959. Crystal Structures of $ZrBe_5$ and Zr_2Be_{17}, *Acta Crystallogr.*, Vol 12, p 700
- Zalkin, A., Sands, D.E., and Krikorian, O.H., 1959. Crystal Structure of Nb_2Be_{17}, *Acta Crystallogr.*, Vol 12, p 713–715

Beryllium Chemistry and Processing, p 55-64
By Kenneth A. Walsh
Edited by Edgar E. Vidal, Alfred Goldberg,
Edward N.C. Dalder, David L. Olson, and Brajendra Mishra

CHAPTER 5

Thermodynamics of Extraction

Kenneth A. Walsh, Brush Wellman Inc., Retired
Edgar E. Vidal, Brush Wellman, Inc.
Brajendra Mishra, Colorado School of Mines

THE FUNDAMENTAL understanding of beryllium reduction thermodynamics is essential to effectively read and interpret the following chapters on beryllium extraction, chemical processing, and corrosion. The subsequent tutorial has been extracted from an earlier presentation on the fundamentals of beryllium thermodynamics [White and Burke 1955]. It is presented as a historical brief on the initial efforts to acquire achievable beryllium thermodynamic data. In the appendix, there is a complete listing of currently accepted beryllium thermodynamic data.

The thermodynamic constants of beryllium and its compounds have been compiled, and from these data an attempt is made to explain the difficulties that surround the extraction of beryllium and to predict the thermodynamic conditions for successful extraction by a number of methods. The data are too scarce for complete and accurate prediction in most cases, and, in any event, a large gap exists between prediction of a method by thermodynamic analysis and the engineering of an economical process.

5.1 Thermodynamic Data

Table 5.1 lists the basic thermodynamic constants for beryllium metal and a number of beryllium compounds. Several of the values have been measured. A limitation of the data is the large number of important beryllium compounds (Be_2C, $BeCO_3$, $BeSO_4$, etc.) that do not appear in Table 5.1 because one or more of their major constants are unknown.

Table 5.2 lists the constants to be used in empirical equations that express the temperature variation of the standard free energy of formation of a number of beryllium compounds. These equations were calculated from the basic data of Table 5.1 and the heat capacity relationships of the substances that appear in the equations. In most cases, the heat capacity change for the reactions (ΔC_p) was estimated, since only for Be(c), BeO(c), and Be_3N_2(c) is the heat capacity known as a function of temperature. The estimated uncertainty for each equation is given in the last column of Table 5.2. These uncertainties are large in most cases.

In Fig. 5.1 through 5.3, the standard free energy of formation of a number of oxides, fluorides, and chlorides, respectively, is plotted as a function of temperature. The values for the beryllium compounds were taken from the equations in Table 5.2, whereas the values for the compounds of other metals were mostly taken from previous publications by the author and from other sources mentioned in the figure captions.

5.2 Sources of Thermodynamic Data

The thermodynamic data summarized in Table 5.2 are collected from a variety of sources. The certainty with which the data are known varies.

5.2.1 O_2, N_2, S_2, F_2, Cl_2, Br_2, and I_2

The thermodynamic constants for these cases are accurately known. The values of the heat of

Table 5.1 Thermodynamic constants for beryllium compounds

Substance	$\Delta H°_{f\,298}$, cal mol^{-1}	$S°_{298}$, cal mol^{-1}K^{-1}	Melting point		Heat of fusion at melting point, cal mol^{-1}	Boiling point		Heat of vaporization at boiling point, cal mol^{-1}
			K	°F		K	°F	
Be(c)(a)	0	2.28 ± 0.02	1556	2341	2800 ± 400	2676	4357	72,700 ± 3000
BeO(c)	−143,100 ± 100	3.37 ± 0.05	2823	4622	...	...	...	...
BeS(c)	−56,100 ± 2000	7.4 ± 1	...	...	...	...	...	...
Be_3N_2(c)	−134,700 ± 1500	12.0 ± 2	...	...	...	...	...	...
BeF_2(c)	−227,000 ± 10,000	12.3 ± 3	1070	1466	6000 ± 1000	1600	2420	40,000 ± 3000
	...	...	...	...	...	820(b)	1016(b)	25,000 ± 3000
$BeCl_2$(c)	−109,200 ± 1000	19.1 ± 3	678	761	3000 ± 1000	765(c)	917(c)	24,000 ± 3000
BeCl(g)	+6000 ± 10,000	51.81 ± 0.1	...	...	...	...	...	...
	...	...	...	...	...	800(b)	980(b)	22,000 ± 3000
$BeBr_2$(c)	−78,300 ± 3000	24.7 ± 3	761	910	4500 ± 1000	760(d)	908(d)	27,000 ± 3000
	...	...	...	...	...	760(b)	908(b)	19,000 ± 3000
BeI_2(c)	−39,400 ± 4000	30.1 ± 3	753	896	4500 ± 1000	790(c)	962(c)	18,000 ± 3000
Be_2SiO_4(c)	−12,000 ± 5000(e)	15.4 ± 0.1	...	...	...	...	...	...

(a) "(c)" denotes crystalline state. (b) Vaporization as BeX_2(g). (c) Vaporization as Be_2X_4(g). (d) Sublimation as Be_2Br_4(g). (e) For the reaction 2 BeO(c) + SiO_2(c) = Be_2SiO_4(c). Source: White and Burke 1955

Table 5.2 Free energy of formation for beryllium alloys

$\Delta G = A + B \cdot T \log T + C \cdot T$(a)

Reactions	A, kcal/mol	B, kcal/mol	C, kcal/mol	Range		Uncertainty, ± kcal
				K	°F	
Be(c) = Be(g)	77,810	5.76	−30.14	1172–1556	1650–2341	0.5
Be(l) = Be(g)	78,900	−5.72	−49.23	1556–2676	2341–4357	2
2Be(c) + O_2 = 2BeO(c)	−287,700	−13.82	65.54	298–1556	77–2341	0.5
2Be(l) + O_2 = 2BeO(c)	−298,200	−3.45	98.09	1556–2300	2341–3680	2
2Be(c) + S_2(g) = 2BeS(c)	−143,700	...	54.2	298–1556	77–2341	5
3Be(c) + N_2 = Be_3N_2(c)	134,700	...	40.6	298–1556	77–2341	5
3Be(l) + N_2 = Be_3N_2(c)	−142,100	...	46	1556–2300	2341–3680	8
2BeO(c) + SiO_2(c) = Be_2SiO_4(c)	−12,000	...	1.4	298–1500	77–2240	5
Be(c) + F_2 = BeF_2(c)	−229,000	−15.66	84.1	298–1070	77–1466	8
Be(c) + F_2 = BeF_2(l)	−222,700	−14.97	76.1	1070–1556	1466–2341	10
Be(l) + F_2 = BeF_2(l)	−225,500	−14.97	77.9	1556–1600	2341–2420	10
Be(l) + F_2 = BeF_2(g)	−169,500	8.03	−31.1	1600–2100	2420–3320	15
Be(c) + Cl_2 = $BeCl_2$(c)	−111,300	−15.89	82.7	298–678	77–761	3
Be(c) + Cl_2 = $BeCl_2$(l)(b)	−108,500	−16.58	80.6	678–820	761–1016	4
Be(c) + Cl_2 = $BeCl_2$(g)	−75,500	6.42	−26.45	820–1556	1016–2341	5
Be(l) + Cl_2 = $BeCl_2$(g)	−78,300	6.42	−24.65	1556–2000	2341–3140	7
Be_2Cl_4(g) = 2$BeCl_2$(g)	31,000	11.0	−66.0	400–1200	260–1700	3
2Be(c) + Cl_2 = 2BeCl(g)	13,300	10.1	−75.2	298–1556	77–2341	20
Be(c) + Br_2(g) = $BeBr_2$(c)	−87,600	−15.2	80.4	298–761	77–910	5
Be(c) + Br_2(g) = $BeBr_2$(l)(c)	−83,600	−16.58	79.1	761–800	910–980	6
Be(c) + Br_2(g) = $BeBr_2$(g)	−53,600	6.42	−24.93	800–1556	980–2341	10
Be(l) + Br_2(g) = $BeBr_2$(g)	−56,400	6.42	−23.13	1556–2000	2341–3140	10
Be_2Br_4(g) = 2$BeBr_2$(g)	32,000	11.0	−71.0	400–1200	260–1700	3
Be(c) + I_2(g) = BeI_2(c)	56,200	−14.74	77.3	298–753	77–896	6
Be(c) + I_2(g) = BeI_2(l)	−52,300	−16.58	77.4	753–760	896–908	7
Be(c) + I_2(g) = BeI_2(g)	−25,800	6.42	−23.58	760–1556	908–2341	12
Be(l) + I_2(g) = BeI_2(g)	−28,600	6.42	−21.78	1556–2000	2341–3140	15
Be_2I_4(g) = 2BeI_2(g)	25,000	11.0	−65.0	400–1200	260–1700	3

(a) T = K (b) The partial pressure of Be_2Cl_4 reaches 1 atm (101 kPa) at 765 K (917 °F). (c) $BeBr_2$ is metastable with respect to Be_2Br_4 (g, 1 atm, or 101 kPa) above 769 K (925 °F). Source: White and Burke 1955

formation at 298.16 K ($\Delta H°_{298}$) and the entropy at 298.16 K ($S°_{298}$) were taken from Kelley [1950] and the National Bureau of Standards [Rossini et al. 1952]. Heat capacity relationships were taken from Kelley [1949].

5.2.2 Beryllium

The entropy of solid beryllium is accurately known [Kelley 1950]. The heat of fusion was taken from the compilation of Kubaschewski

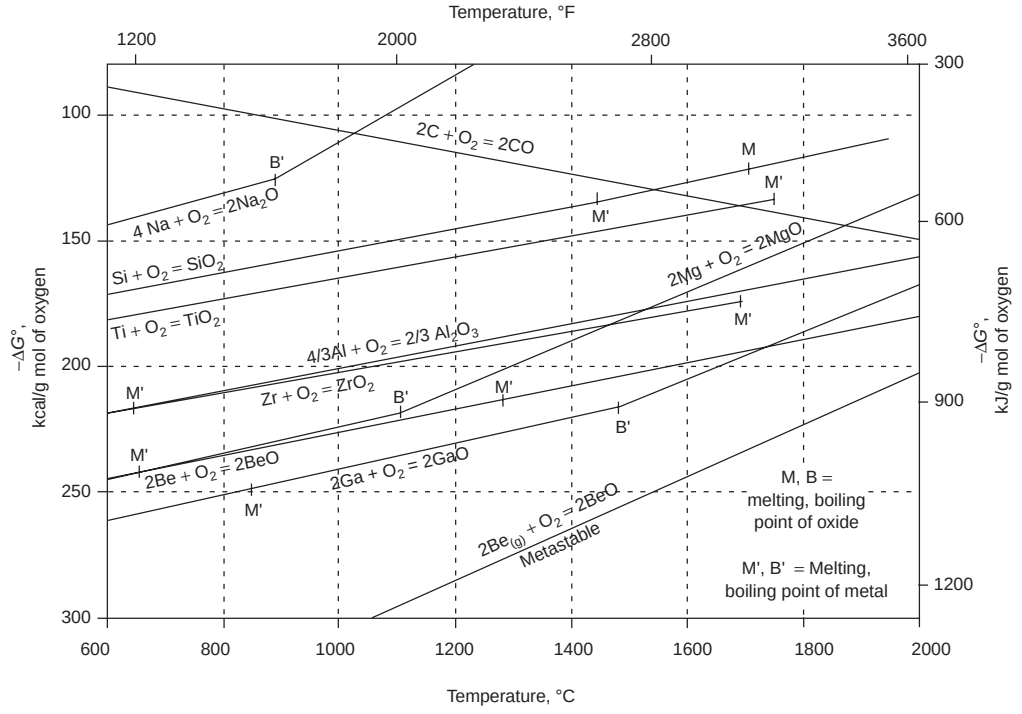

Fig. 5.1 Standard free energy of formation of oxides. Data for BeO from Table 5.2; data for other oxides from Kubaschewski and Evans [1951]

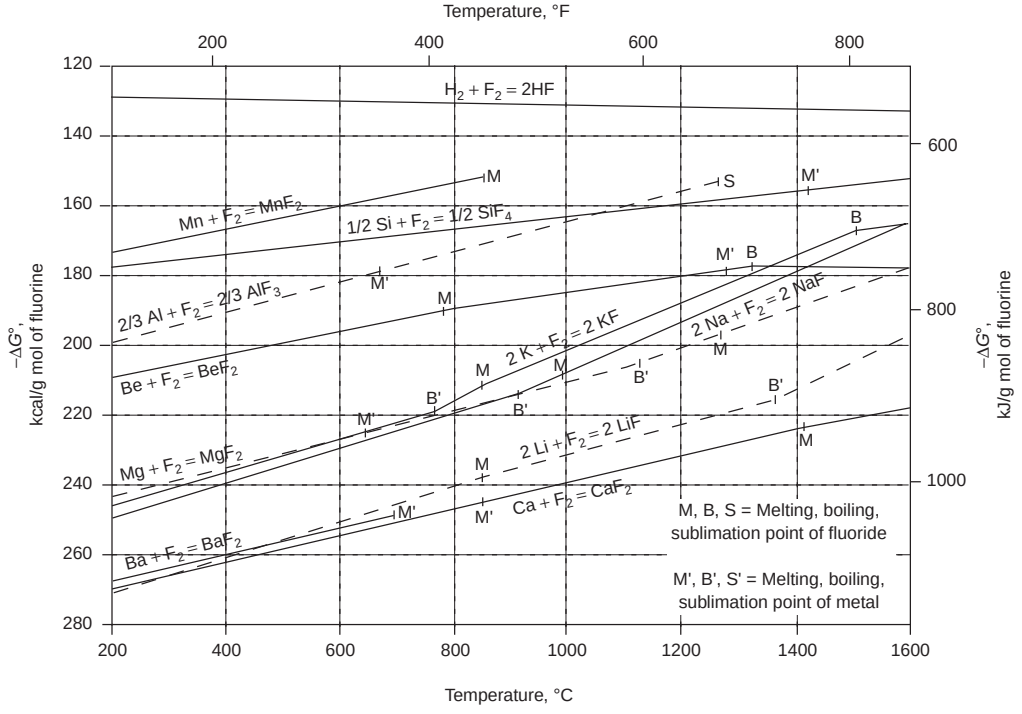

Fig. 5.2 Standard free energy of formation of fluorides. Data for BeF_2 from Table 5.2; data for other fluorides from Kellogg [1951] and Kubaschewski and Evans [1951]

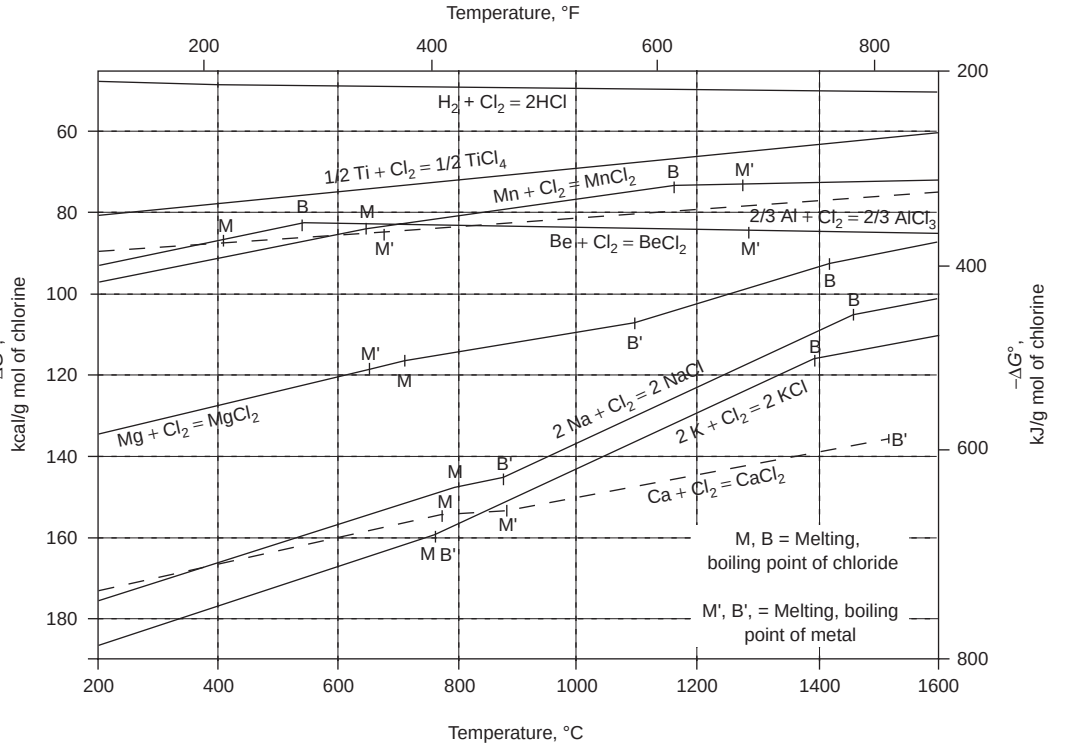

Fig. 5.3 Standard free energy of formation of chlorides. Data for $BeCl_2$ from Table 5.2; data for other chlorides from Kellogg [1951] and Villa [1950]

and Evans [1951]. The sublimation pressure of beryllium was taken from the determination by Holden et al. [1948]. The heat of vaporization, boiling point, and vapor pressure were estimated from the known sublimation pressure [Holden et al. 1948] and the heat of fusion [Kubaschewski and Evans 1951]. The heat capacity of solid beryllium has been redetermined by Ginnings et al. [1951]. The heat capacity of liquid beryllium was estimated as 7.85 $cal \cdot °C^{-1} \cdot mol^{-1}$ (32.84 $J\ K^{-1}\ mol^{-1}$).

5.2.3 BeO

The entropy of BeO(c) is accurately known [Kelley 1950]. The heat of formation was redetermined by Cosgrove and Synder [1953], and their value has been accepted in preference to the results of previous investigators.

The heat capacity of solid BeO is reported by Kelley [1949]. The values of the free energy of formation of BeO, which are calculated from the equation in Table 5.2, agree with recent calculations by Kelley [unpublished calculations] within ± 0.1 kcal (± 0.4 kJ) at all temperatures between 298 and 2000 K (77 and 3140 °F).

5.2.4 BeS, Be_3N_2, and Be_2SiO_4

The values of $\Delta H°_{298}$ and $S°_{298}$ compiled by Kubaschewski and Evans [1951] were accepted. The heat capacity relationship for Be_3N_2 is reported by Kelley [1949]. The change in heat capacity (ΔC_p) for the formation of BeS was estimated.

5.2.5 BeF_2

Brewer [1950a,b] estimated the value of $\Delta H°_{298}$ and allowed for the calculation of $S°_{298}$. The data on fusion and vaporization are those estimated by Brewer [1950a,b]. Because of its relatively high boiling point, the dimer, Be_2F_4, is not an important constituent in the vapor phase. The change in heat capacity (ΔC_p) was estimated for all reactions.

5.2.6 $BeCl_2$, $BeBr_2$, and BeI_2

The values of $\Delta H°_{298}$ compiled by Kubaschewski and Evans [1951] were accepted for $BeBr_2$ and BeI_2. For $BeCl_2$, Siemonsen's [1951] measured value of $\Delta H°_{298}$ was accepted, and the value of $S°_{298}$ for each of these compounds was

estimated. The data for fusion and vaporization are those estimated by Brewer. For each of these compounds, the vapor phase at temperatures below the boiling point is predominantly the dimer, Be_2X_4; as the temperature is raised above the boiling point, the monomer, BeX_2, is the principal vapor species. The proportion of monomer and dimer at any temperature and pressure may be calculated from the dissociation reactions included in Table 5.2.

5.2.7 BeCl(g)

Kelley [1950] reports an accurate value for the entropy of beryllium monochloride. The value of $\Delta H°_{298}$ was estimated from Herzberg's [1950] value for the dissociation energy as determined from molecular spectra.

5.3 Reduction of BeO

The free energy data plotted in Fig. 5.1 (Table 5.2, Kubaschewski and Evans 1951) illustrate some of the difficulties encountered in the reduction of BeO to the pure metal. BeO is an extremely stable oxide—the most stable of all oxides, except CaO, at temperatures in the smelting range.

Reduction of BeO to pure beryllium by other metals takes place according to the reaction:

$$BeO(c) + M(c,l,g) = MO(c) + Be(c,l) \quad \text{(Eq 5.1)}$$

This will be impossible at 1 atm (101 kPa) pressure, except for calcium. (The impossibility could become a possibility, if the activity of MO(c) were reduced below unity by solution in a liquid slag or by formation of a stable complex oxide with some other oxide. However, this reduction in activity would have to be accomplished without simultaneous reduction in the activity of BeO(c), or else the advantage gained would be cancelled.) Reduction by calcium metal according to Eq 5.1 will be possible below 1730 °C (3145 °F), if the pressure is 1 atm (101 kPa). Calcium reduction is not commercially attractive for a number of reasons: calcium is expensive, too much calcium may be alloyed into the product metal, and the physical forms of the products and reactants would probably result in low reaction rates.

Beryllium has low volatility in the temperature range of 1200 to 1300 °C (2190 to 2370 °F) to permit a successful vacuum-retort reduction (similar to the Pidgeon process for magnesium production). This type of process requires that the reducing agent be extremely involatile, which rules out calcium and magnesium as possibilities. Zirconium metal may be used for this purpose (if economics are momentarily neglected) according to the reaction:

$$BeO(c) + \tfrac{1}{2}Zr(c) = \tfrac{1}{2}ZrO_2(c) + Be(g) \quad \text{(Eq 5.2)}$$

At 1300 °C (2370 °F), which is the highest attainable temperature in conventional vacuum retorts, $\Delta G°$ for Eq 5.2 is +42 kcal mol^{-1} (+175 kJ mol^{-1}), and the partial pressure of beryllium vapor would be only 1.4×10^{-6} atm (0.1 Pa). The pressure is far below the practical limit of vapor pressure for vacuum retorting.

If the oxidized form of the reducing agent (MO in Eq 5.1) is a vapor, its activity may also be reduced by vacuum retorting, and spontaneous reduction of BeO to pure beryllium becomes a possibility. The reaction would be:

$$BeO(c) + M(c,l) = Be(c,l) + MO(g) \quad \text{(Eq 5.3)}$$

The only practical reducing agent is carbon, which forms gaseous CO as an oxidation product. With carbon reduction, however, a new difficulty is encountered. Be_2C is known to be a stable carbide at all temperatures up to 2000 °C (3630 °F) and perhaps even higher [Kelley 1949]. If BeO is heated with an excess of carbon, the only possible product is Be_2C, according to the reaction:

$$2BeO(c) + 3C(c) = Be_2C(c) + 2CO \quad \text{(Eq 5.4)}$$

However, if an excess of BeO is heated with carbon, pure beryllium will form if the following reaction can be made spontaneous:

$$BeO(c) + Be_2C(c) = 3Be(c, l) + CO \quad \text{(Eq 5.5)}$$

At all temperatures in the range of 1000 to 2000 °C (1830 to 3630 °F), the pressure of CO in equilibrium with Eq 5.5 is extremely small—in fact, it is less than the vapor pressure of beryllium metal. Hence, it would be impossible to remove CO from the system and leave beryllium metal unvaporized. If beryllium is allowed to vaporize, the reaction becomes:

$$BeO(c) + Be_2C(c) = 3Be(g) + CO \quad \text{(Eq 5.6)}$$

The data in Fig. 5.1 and the estimated value for the free energy of formation of Be_2C permit

calculation of the pressures to be expected from Eq 5.6. At 2000 °C (3630 °F), $\Delta G°$ for Eq 5.6 is found to be $+63$ kcal · mol^{-1} ($+265$ kJ mol^{-1}), and the equilibrium constant is 7.4×10^{-7}. Since:

$$K = p^3_{Be} \cdot p_{CO} = 7.4 \times 10^{-7} \qquad \text{(Eq 5.7)}$$

and

$$p_{Be} = 3p_{CO} \qquad \text{(Eq 5.8)}$$

The equilibrium partial pressures are:

$$p_{Be} = 0.039 \text{ atm (4.0 kPa)}$$
$$p_{CO} = 0.013 \text{ atm (1.3 kPa)}$$

Although these pressures are high enough to allow a vacuum-retorting reaction to take place, other considerations render this reaction unattractive. The principal disadvantages are the very high temperature (below 2000 °C, or 3630 °F), the equilibrium partial pressures for Eq 5.6 decrease very rapidly, and the fact that on cooling below the retort temperature the gases will react with each other to reform BeO and Be_2C. The back reaction could conceivably be prevented by shock cooling, but the chances of a commercial process for production of pure beryllium based on carbon reduction are slight.

Before leaving the subject of carbon reduction of the oxide, the process whereby beryllium-copper alloys are commercially prepared should be discussed. The essence of the process (which is described in Chapter 14, "Alloying of Beryllium," in this book) is the smelting of BeO, carbon, and copper in an electric arc furnace at close to 2000 °C (3630 °F). A beryllium-copper alloy is formed, which also dissolves Be_2C and CO, but these latter compounds are precipitated from the alloy when it is cooled to its casting temperature (1000 °C, or 1830 °F). The final alloy contains approximately 4 wt% Be. The reaction that must be spontaneous in order for this process to be possible is Eq 5.5. The free energy change of Eq 5.5 may be estimated from the data in Table 5.2 and the assumed value for the free energy of formation of Be_2C. The result may be expressed as:

$$\Delta G° = 137{,}400 + 6.91T \log T - 70.0T \qquad \text{(Eq 5.9)}$$

At 2000 °C (3630 °F), $\Delta G° = +31{,}000$ cal mole^{-1}.

$$K = 1.04 \times 10^{-3} = \frac{a^3_{Be} \cdot p_{CO}}{a_{BeO} \cdot a_{Be_2C}} \qquad \text{(Eq 5.10)}$$

If it is assumed that an excess of BeO(c) is present during smelting, then the activity a_{BeO} is unity. It is reported that the liquid alloy is saturated with Be_2C(c); hence, the activity a_{Be_2C} is also unity. The atmosphere near the reaction zone is probably almost pure CO, so that for smelting at atmospheric pressure, p_{CO} is probably close to unity. If these assumptions are incorporated in the equilibrium constant expression, the result is:

$$K = 1.04 \times 10^{-3} = a^3_{Be} \qquad \text{(Eq 5.11)}$$
$$a_{Be} = 0.1$$

The activity-composition relationship for dilute solutions of beryllium in liquid copper is not known. If the relation follows Raoultís law, then the activity of beryllium may be replaced by its mole fraction:

$$X_{Be} = \text{Mole fraction of beryllium in copper}$$
$$= a_{Be} \text{ (for ideal solution)} \qquad \text{(Eq. 5.12)}$$
$$a_{Be} = X_{Be} = 0.1 \text{ (or 1.6 wt\% Be)}$$

If the aforementioned assumptions are correct, the maximum content of beryllium that could be reduced into a copper alloy would be 1.6 wt%. The most doubtful assumption is that the solution of beryllium in copper follows Raoult's law. The phase diagram of beryllium-copper indicates several stable intermediate solid solutions. Therefore, it is very likely that the activity of beryllium in liquid copper shows marked negative deviations from Raoult's law. It is necessary to assume an activity coefficient for beryllium of 0.44 to explain the formation of a beryllium-copper alloy containing 4 wt% Be by smelting at 2000 °C (3630 °F).

The effect of lower temperatures on this equilibrium is to shift Eq 5.5 to the left. Thus, at 1600 °C (2910 °F):

$$\Delta G° = +48{,}600 \text{ cal} \cdot \text{mol}^{-1} \text{ (400 kJ mol}^{-1}\text{)} \qquad \text{(Eq 5.13)}$$
$$K = 2.1 \times 10^{-6}$$

If the same assumptions about the activity of BeO, Be_2C, and CO are made for this temperature, the result is:

$$a^3_{Be} = 2.1 \times 10^{-6}; \; a_{Be} = 1.3 \times 10^{-2} \qquad \text{(Eq 5.14)}$$

If the activity coefficient of beryllium in liquid copper is again assumed to be 0.44, then:

$$a_{Be} = 0.44X_{Be} = 1.3 \times 10^{-2} \qquad \text{(Eq 5.15)}$$
$$X_{Be} = 0.03 \text{ (or 0.4 wt\% Be)}$$

In summary, it is possible to produce a beryllium-copper alloy by smelting of BeO + C + Cu, because the activity of beryllium is reduced below unity by solution in the alloy. The amount of beryllium that can be introduced into the alloy is limited by the equilibrium of Eq 5.5. The higher the temperature, the larger will be the value of $K_{[5.5]}$ and the larger will be the equilibrium content of beryllium in the alloy.

5.4 Reduction of Beryllium Halides

Figures 5.1 to 5.3 illustrate the important fact that beryllium halides are less stable relative to the halides of other metals than was the case with the oxides. Thus, it is possible to reduce beryllium halides with sodium, potassium, lithium, calcium, or magnesium according to the reaction:

$$BeX_2(l) + 2M'(l) = Be(c,l) + 2M'X(c,l) \quad \text{(Eq 5.16)}$$

or

$$BeX_2(l) + M''(l) = Be(c,l) + M''X_2(c,l) \quad \text{(Eq 5.17)}$$

where M′ is an alkali metal, and M″ is an alkaline earth metal. These reactions will be exothermic, and the equilibrium position will be far to the right under most conditions of operation. Magnesium metal is used to reduce BeF_2, according to Eq 5.17, in the commercial production of pure beryllium. This process is described in Chapter 7, "Extractive Metallurgy," in this book. The preferential use of BeF_2 rather than $BeCl_2$ in this process probably results from the high melting and boiling point of the fluoride. $BeCl_2$ boils at 492 °C (920 °F), and therefore, it would be necessary to keep the temperature of the reduction process below 492 °C (920 °F) if $BeCl_2$ were to be reduced at atmospheric pressure in a batch process of the type now used. BeF_2, on the other hand, boils at approximately 1330 °C (2420 °F), and the temperature of the reduction process can be raised to the melting point of beryllium (1283 °C, or 2341 °F) if BeF_2 is the raw material, without recourse to a pressure vessel. Magnesium metal is used because it is the least expensive of the possible reducing agents per pound of BeF_2. Sodium metal would be only slightly more expensive than magnesium, but the low boiling point of sodium (914 °C, or 1677 °F) is a disadvantage for this type of process.

One of the principal disadvantages of the magnesium reduction method for preparation of beryllium is that the reaction product consists of a mixture of MgF_2, Be, and unreacted BeF_2. This mixture must be treated through a series of processes to recover beryllium metal and the unused BeF_2. Only by arc melting of the beryllium can the residual fluoride and magnesium be reduced to a low value.

5.5 Hydrogen Reduction

Reduction of beryllium halides by hydrogen was attempted on a laboratory scale by Hackspill and Besson [1949], but their experiments were only partly successful. Hydrogen reduction is an attractive method because both the reducing agent and its halide are gaseous and cannot contaminate the metal product. The disadvantage of hydrogen reduction lies in the fact that hydrogen is a weak reducing agent for beryllium halides. Table 5.3 lists the values of $\Delta G°$ and K for the reduction of beryllium halides by hydrogen. The data in Table 5.3 are based on the equations in Table 5.2, so that there is considerable uncertainty in all the reported values, but a few general conclusions may be safely drawn. The order of increasing ease of reduction by hydrogen is fluoride, chloride, bromide, and iodide. Even for the iodide, however, the value of the equilibrium constant is small, and the partial pressure of HI would have to be reduced to a low value to obtain spontaneous reduction of BeI_2. At 1250 °C (2280 °F), if the partial pressures of $BeI_2(g)$ and $H_2(g)$ were each 0.5 atm

Table 5.3 Reduction of beryllium halides by hydrogen

	1000 °C (1830 °F)		1250 °C (2280 °F)	
Reaction	$\Delta G°$, cal mol^{-1}	K(a)	$\Delta G°$, cal mol^{-1}	K(a)
$BeF_2(l) + H_2 = Be(c) + 2HF$	53,700	6.1×10^{-10}	47,700	1.45×10^{-7}
$BeCl_2(g) + H_2 = Be(c) + 2HCl$	34,900	1.02×10^{-6}	35,000	9.4×10^{-6}
$BeBr_2(g) + H_2 = Be(c) + 2HBr$	30,300	6.3×10^{-6}	30,000	5.0×10^{-5}
$BeI_2(g) + H_2 = Be(c) + 2HI$	22,700	1.25×10^{-4}	22,000	6.9×10^{-4}

(a) K is the equilibrium constant. Source: White and Burke 1955

(50 kPa), the equilibrium partial pressure of HI would be only 0.013 atm (1.3 kPa). Under the same conditions for the reduction of $BeCl_2$, the equilibrium partial pressure of HCl would be only 0.0015 atm (150 Pa). These reactions could be rendered spontaneous by using a continuous flow system, but the fraction of hydrogen used would be very small.

5.6 Thermal Decomposition of BeI_2

The possibility of preparing pure beryllium metal by thermal decomposition of a volatile halide on a hot wire can be judged from the data given in Table 5.2. Beryllium iodide is the least stable halide; hence, it will be the most easily decomposed. The temperature of the hot wire should be as high as possible to achieve the greatest decomposition, but it should not exceed the melting point of the metal (1283 °C, or 2340 °F). At temperatures close to the melting point of beryllium, $I_2(g)$ is largely dissociated into I(g), so that it is necessary to consider the following two reactions to describe the system:

$$BeI_2(g) = Be(c) + I_2(g) \qquad \text{(Eq 5.18)}$$

$$I_2(g) = 2\,I(g) \qquad \text{(Eq 5.19)}$$

If 1500 K (1230 °C, or 2245 °F) is chosen as a practical hot-wire temperature, then K_1 (for the reaction of Eq 5.18) is calculated from the data in Table 5.2 according to:

$$K_1 = \frac{P_{I_2}}{P_{Be_2}} = 3.5 \times 10^{-5} \qquad \text{(Eq 5.20)}$$

Data from Rossini et al. [1952] are used to calculate K_2 for the reaction of Eq 5.19 according to:

$$K_2 = \frac{P_I^2}{P_{I_2}} = 1.52 \qquad \text{(Eq 5.21)}$$

Simultaneous solution of these equilibrium-constant equations with the relation for the total pressure of the system yields the data in Table 5.4.

The data in Table 5.4 show that the iodine is principally in the form of the monomer, I(g), and that, as the total pressure of the system is reduced, the fraction of BeI_2 decomposed increases. In any case, the fraction of BeI_2 decomposed is small, and it is difficult to predict whether the hot-wire method would produce beryllium metal at a sufficiently rapid rate for commercial exploitation. Decomposition of $BeI_2(g)$ in an arc, at temperatures above the melting point of beryllium, would be much more favorable from an equilibrium viewpoint.

5.7 Electrolytic Reduction

Electrolysis of fused halides has been used successfully in the past to produce pure beryllium [Mantell 1950]. The advantage of this method lies in the fact that the strength of the reducing conditions can be adjusted at will by adjustment of the applied potential, so that the great stability of beryllium compounds does not interfere, except insofar as the cell potential will be large.

Electrolysis of pure beryllium halides, although possible, is complicated by the great volatility of these compounds. The two processes that have been most successful [Mantell 1950] have circumvented this difficulty by using an electrolyte consisting of the beryllium halide dissolved in halides of alkali and alkaline earth metals. The use of the halides of sodium, potassium, lithium, calcium, magnesium, and barium, as added salts in the electrolysis of beryllium halides, does not interfere with the deposition of pure beryllium on the cathodes, because all of these halides are more stable than the respective beryllium halides (Fig. 5.2 and 5.3).

The standard free energy data in Table 5.2 and Fig. 5.1 to 5.3 may be used to calculate the standard decomposition potential, $E°$, of the compound. The relation is:

$$E° = \frac{-\Delta G}{jnF} \frac{-\Delta G}{jnF} \qquad \text{(Eq 5.22)}$$

where j is the conversion factor of joules to calories, 0.239; n is the number of electrons transferred per mole of reaction; and F is the Faraday constant, 96,500 coulombs per mole. The decomposition potential under nonstandard conditions, E, may also be calculated, if the activity of each of the constituents is known.

Table 5.4 Thermal decomposition of $BeI_2(g)$ at 1500 K (2240 °F)

p: Total pressure, atm	Partial pressures, atm			Fraction of BeI_2 decomposed
	p_{BeI_2}	p_{I_2}	p_{I_2}	
1	0.993	3.5×10^{-5}	7×10^{-3}	3.7×10^{-3}
10^{-2}	0.929×10^{-2}	3.3×10^{-7}	7×10^{-4}	3.6×10^{-2}

Source: White and Burke 1955

5.8 Refining of Beryllium by Distillation

The existence of the gaseous, normally unstable monohalides of beryllium, Be*X*, suggests that a method of refining crude beryllium may be developed, based on the reaction:

$$\mathrm{Be(c,1)} + \mathrm{Be}X_2\mathrm{(g)} = 2\mathrm{Be}X\mathrm{(g)} \qquad \text{(Eq 5.23)}$$

Since Eq 5.23 is strongly endothermic, the crude beryllium could be reacted with $\mathrm{Be}X_2$(g) at elevated temperatures and/or reduced pressures, with the resultant partial volatilization of the crude beryllium as Be*X*(g). If this gas is subsequently cooled, or the pressure increased, the reaction must reverse, and pure beryllium will be deposited and $\mathrm{Be}X_2$(g) regenerated. Such a process would be entirely analogous with the proposed process for refining aluminum by volatilization of aluminum monochloride [Gross et al. 1948]. Table 5.5 lists the values of $\Delta G°$ and K for Eq 5.23, where *X* is chloride. The thermodynamic data on BeCl(g) are highly uncertain, so the results shown in Table 5.5 are only a rough indication of what may be expected. Nevertheless, the indicated partial pressures of BeCl(g) are sufficiently large to warrant further investigation of this reaction.

Gross [1952] has patented a somewhat similar process for distillation of beryllium according to the reaction:

$$\mathrm{Be(c)} + 2\mathrm{NaCl(g)} = \mathrm{BeCl_2(g)} + 2\mathrm{Na(g)} \qquad \text{(Eq 5.24)}$$

For this reaction, Gross calculated:

$$\log \mathrm{K} = \frac{-11,740}{T} + 4.59 \quad \log \mathrm{K} = \frac{-11,740}{T} + 4.59 \qquad \text{(Eq 5.25)}$$

where K is the equilibrium constant in atm, and *T* is the absolute temperature.

This reaction is also strongly endothermic, and if crude beryllium is in contact with the vapor at high temperature and reduced pressure, the reaction will proceed to a limited extent from the left to the right side of Eq 5.24. The reaction will reverse, and pure beryllium will deposit if the gas mixture is cooled or the pressure increased.

Table 5.5 Volatilization of beryllium as the monochloride

$\mathrm{Be(c,l)} + \mathrm{BeCl_2(g)} = 2\mathrm{BeCl(g)}$

Temperature		Temperature,	$\Delta G°$, cal		p_{BeCl}(b), atm
°C	°F	K	$\mathrm{mol^{-1}}$	K(a)	
1000	1830	1273	41,300	8.2×10^{-8}	2.9×10^{-5}
1283	2341	1556	31,300	4.0×10^{-5}	6.3×10^{-4}
1527	2781	1800	22,700	1.8×10^{-3}	4.2×10^{-3}

(a) K is the equilibrium constant. (b) The value of the partial pressure of BeCl(g), if the partial pressure of $\mathrm{BeCl_2}$(g) is 10^{-2} atm. Source: White and Burke 1955

REFERENCES

Brewer, L.M., 1950a. Thermodynamic Properties of Common Gases, *The Chemistry and Metallurgy of Miscellaneous Materials*, L.F. Quill, Ed., McGraw-Hill, NY, p 60–75

Brewer, L.M., 1950b. Thermodynamic Properties of Halides, *The Chemistry and Metallurgy of Miscellaneous Materials*, L.F. Quill, Ed., McGraw-Hill, NY, p 76–192

Cosgrove, L.A., and Snyder, P.E., 1953. The Heat Formation of Beryllium Oxide, *J. Am. Chem. Soc.*, Vol 75, p 3102

Ginnings, D.C., Douglas, T.B., and Ball, A.F., 1951. Specific Heat of Beryllium Between 0 and 900°, *J. Am. Chem. Soc.*, Vol 73, p 1236

Gross, P., 1952. Distillation of Metals, U.S. Patent 2,607,675

Gross, P., Campbell, C.S., Kent, P.J.C., and Levi, D.L., 1948. Equilibria Involving Aluminum Monohalides, *Discuss., Faraday Soc.*, No. 4, p 206–216

Hackspill, L., and Besson, J., 1949. La Reduction du Chlorure de Glucinium par L'Hydrogene, *Bull. Soc. Chim. Fr.*, Series 5, Vol 16, p 113–116

Herzberg, G., 1950. *Molecular Spectra and Molecular Structure*, Vol I, *Spectra of Diatomic Molecules*, 2nd ed., Van Nostrand Reinhold Inc., New York, NY

Holden, R.B., Speiser, R., and Johnston, H.L., 1948. The Vapor Pressures of Inorganic Substances, Part I: Beryllium, *J. Am. Chem. Soc.*, Vol 70, p 3897–3899

Kelley, K.K., unpublished calculations

Kelley, K.K., 1949. "Contributions to the Data on Theoretical Metallurgy, X, High-Temperature Heat-Control, Heat-Capacity, and Entropy Data for Inorganic Compounds," Bulletin 476, U.S. Bureau of Mines

Kelley, K.K., 1950. "Contributions to the Data on Theoretical Metallurgy, XI, Entropies of Inorganic Substances," Bulletin 477, Revision 1948 of Data and Methods of Calculation, U.S. Bureau of Mines

Kellogg, H.H., 1951. Metallurgical Reactions of Fluorides, *Trans. Am. Inst. Mining Metall. Eng.*, Vol 191, p 137–141

Kubaschewski, O., and Evans, E.L., 1951. *Metal Physics and Physical Metallurgy,* Butterworth-Springer, London

Mantell, C.L., 1950. *Industrial Electrochemistry,* 3rd ed., McGraw-Hill Book Co., New York, NY

Rossini, D.F., Wagman, D.D., Evans, W.H., Levine, S., and Jaffe, I., 1952. "Selected Values of Chemical Thermodynamic Properties," Circular of the National Bureau of Standards 500, U.S. Government Printing Office, Washington, D.C.

Siemonsen, H., 1951. Uber Die Bildungwarmen Einiger Metallchloride, *Z. Elektrochem.*, Vol 55, p 327

Villa, H., 1950. Thermodynamic Data of the Metallic Chlorides, *J. Soc. Chem. Ind.*, Supplemental Issue, Vol 69 (No. 1), p S9

White, D.W., Jr., and Burke, J.E., 1955. *The Metal Beryllium,* American Society for Metals

SELECTED REFERENCE

- Roboff, S.B., 1965. Reduction of BeO to the Metal, *Beryllium: Its Metallurgy and Properties,* H.H. Hausner, Ed., University of California Press, Berkeley, CA, p 17–32

Beryllium Chemistry and Processing, p 65-70
By Kenneth A. Walsh
Edited by Edgar E. Vidal, Alfred Goldberg,
Edward N.C. Dalder, David L. Olson, and Brajendra Mishra

CHAPTER 6

Mineral Processing

Edgar E. Vidal, Brush Wellman, Inc.
James Foley, Los Alamos National Laboratory
David L. Olson, Colorado School of Mines

BERYLLIUM-CONTAINING ores are treated with conventional mineral processing techniques such as crushing, grinding, desliming, chemical activation, and flotation. Typical ores containing beryl, bertrandite, or phenacite are associated with quartz, calcite, muscovite, micas, feldsparz, tourmaline, and others. To make the extraction of beryllium cost-efficient, these gangue materials must be removed. Many methods have been suggested and tested, and not all are presented here.

Most methods for concentrating beryllium minerals by flotation require the use of an acidic pulp. This acid pulp could pose a problem when the beryllium minerals are combined with complex calcareous minerals. The consumption of reagents would be unacceptable. If the flotation is performed in neutral-to-basic pulps, collectors such as fatty acids will also tend to collect fluorites, scheelites, and apatites. These problems make concentration of beryllium-containing ores rather challenging.

6.1 Bertrandite and Phenacite Flotation

The Federal Bureau of Mines performed flotation tests for the beneficiation of bertrandite and phenacite ores [Havens et al. 1961, Havens 1963]. The ores were associated with calcite, fluorspar, mica, quartz, and other accessory minerals. Two separate ore bodies were tested: from Mount Wheeler, NV, and Lake George, CO. Typically, the ores contained between 0.49 and 0.73 wt% BeO. The beryllium mineralization varied from approximately 66 wt% bertrandite to being completely phenacite.

Sodium fluoride and sodium hexametaphosphate (HMP) modifiers were used while floating the undeslimed pulps at the original starting pH. For the collector, a fatty acid/fuel oil was used. Typically, 2 kg (4 lb) of sodium fluoride along with 1 to 2 kg (2 to 4 lb) of HMP were used per ton of ore. In a typical batch, 82% recovery with a BeO grade of 14 wt% was common when starting with a sample of 0.49 wt% BeO.

In the ore samples obtained from the Mount Wheeler Mine, the liberation of phenacite was found to be roughly 70% between 100 and 325 mesh. All of the bertrandite was liberated below 65 mesh. In the stockpile, though, roughly 10% of the bertrandite was locked with quartz in the 65- to 100-mesh fraction.

Different operating parameters were studied for optimizing the grade and recovery of bertrandite and phenacite: type of water, grinding time and size, pulps in solid, temperature, sequence and quantity of modifying reagents, and conditioning. No effect with changing the type of water was observed (i.e., tap water, distilled water, and zeolite-softened water). A grade of 14.1 wt% BeO and recovery of 82 wt% was obtained after flotation for the 65-mesh nominal grind. Both grade and recovery diminished as the nominal grind size diminished while keeping the flotation conditions constant. The pulp density effect on flotation showed that 25 wt% solids in solution returned the best recovery (82 wt%). This result was obtained when using 2.3 kg (5 lb) of sodium fluoride, 1.4 kg

(3 lb) of HMP, 0.34 kg (0.75 lb) of kerosene, and 0.70 kg (1.5 lb) of oleic acid per ton of ore. The effect of increasing the temperature during conditioning and flotation was not conclusive, but less kerosene and oleic acid seemed to be needed. Details on the sequence and quantities effect can be found in the original reports [Havens et al. 1961, Havens 1963].

6.2 Beryl Concentration from Pegmatitic Gangues and Low-Grade Deposits

Beryl has been concentrated from pegmatitic gangues and low-grade deposits, as reported in literature [Lamb and Banning 1945]. Finely ground and deslimed beryl ore was blunged in an alkali-containing solution to keep the pH between 6 and 9. The mixture was agitated and aerated in the presence of a frothing agent and fatty acid collector. The froth contained the beryl concentrate.

The ore was ground initially to –20 mesh, then further wet ground to –65 mesh in a ball mill, and deslimed by washing with 10 parts of water per part of ore. The ore was then blunged for 10 to 30 min in the same proportions. The water contained 0.5 to 2.3 kg (1 to 5 lb) of caustic soda per ton of ore. The pH was then adjusted to be neutral or slightly alkaline by adding tartatic acid, glycolic acid, citric acid, or lactic acid, or preferably, by washing the ore with water. The pulp was then diluted to 20 wt% solids with water and flotation reagents added.

Once the ore had been washed, it was subjected to froth flotation. The collector was a fatty acid such as caprylic acid, lauric acid, oleic acid, or stearic acid, while the frothing agent was ammonium salt of lauryl diethylene glycol sulfate or a lower-alkyl glycolic ester. The amount of collector was between 0.05 and 0.23 kg (0.1 and 0.5 lb) per ton of ore, while the amount of frothing agent was 0.023 to 0.23 kg (0.05 to 0.5 lb) per ton of ore. The cell was agitated with the collector and frothing agent for 5 to 25 min prior to injecting the air. The froth that formed contained the beryl concentrate. A rougher concentrate was initially obtained, which was then passed to a cleaner cell to produce a finished concentrate, and the middlings were returned to the feed. So, the first stage was carried out for recovery and the second for grade.

Figure 6.1 summarizes in a flow chart the process of concentrating the beryl from the pegmatitic gangues. This process was successfully tested on ores from the Black Mountain deposit near Rumford, ME, from the Weeks Quarry in East Wakefield, NH, and from the Gotta-Walden property in Portland, OR.

6.3 Concentration of Beryl Using Hydrofluoric Acid Activation

Beryllium ores from a reject stockpile in the Ross Mine at Custer, SD, were treated and concentrated by comminution, followed by activation in hydrofluoric acid [Kennedy and O'Meara 1947]. The ore contained 5.3 wt% beryl, or 0.64 wt% BeO. The gangue consisted primarily of quartz, microcline, muscovite, schorlite, feldspar, and cassiterite. The ore particle size was reduced to –100 mesh by crushing and grinding. A 50 wt% H_2O pulp of the ground ore was prepared and mixed with 2.1 kg (4.6 lb) of hydrofluoric acid per ton of ore. The mixture was treated for 30 min prior to separation of the sand and slime. The sands were washed until the pH increased to neutral levels. The sands were again treated with hydrofluoric acid for 15 min and washed with water to neutralize the pH. A rougher concentrate was obtained by flotation using 0.24 kg (0.54 lb) of oleic acid and 0.08 kg (0.18 lb) of pine oil per ton of ore during 4 min. The concentrate was cleaned in four cleaners, the first two used for depressing the gangue, with the exception of the tourmaline, and the other two to depress the beryl while floating the tourmaline. In the first cleaner, 0.16 kg (0.36 lb) of oleic acid and 0.08 kg (0.18 lb) of pine oil were used per ton of concentrate. The total residence time in this cleaner was 2 min. In the second cleaner, no agents were added, and the separation was allowed to progress for another 2 min. In the last two cleaners, beryl is depressed from the tourmaline by adding, for each ton of ore, 1 kg (2 lb) of sulfuric acid and 0.4 kg (0.8 lb) of hydrochlorides of mono-n-octadecyl amine and mono-n-hexadecyl amine. Figure 6.2 shows a flow chart of the process. Tests were also performed on ores from the Iron Mountain in Winston, NM, with successful results.

6.4 Concentration of Beryllium Ores

An example of a complete concentration plant was presented by Johnston [1967]. Figure 6.3

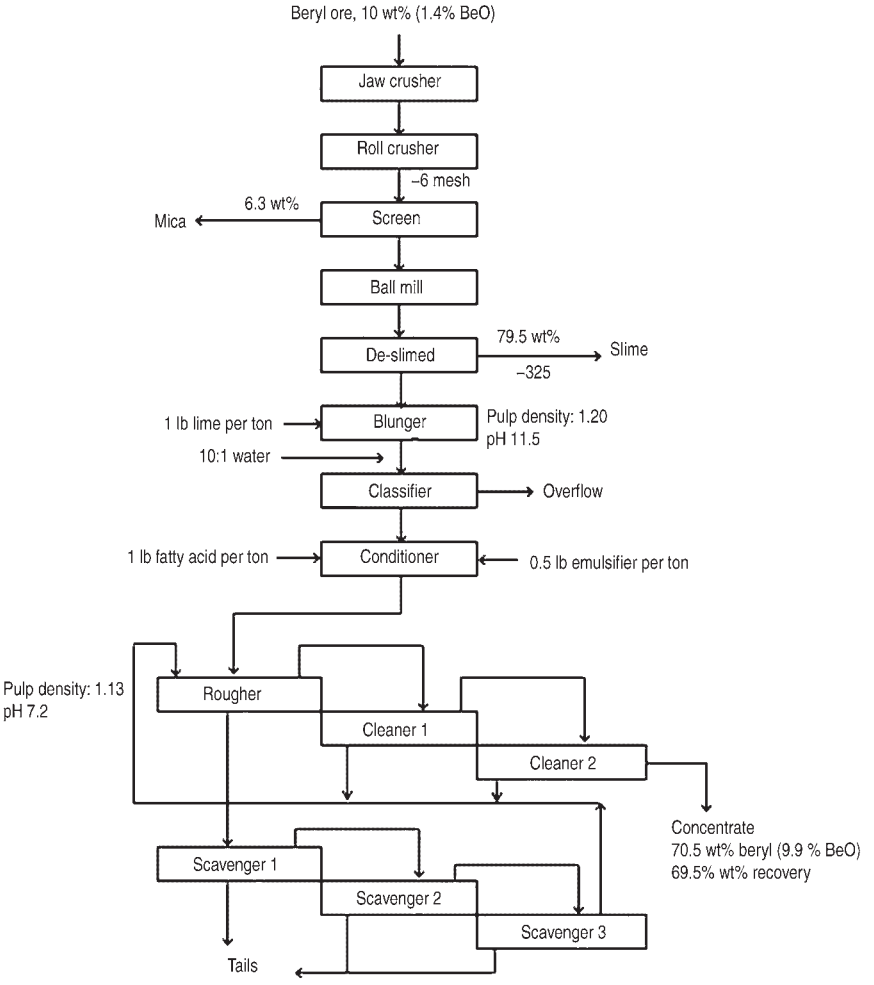

Fig. 6.1 Concentration of beryl from pegmatitic gangues and low-grade deposits. Source: Lamb and Banning 1945

shows a schematic representation of the concentration plant for beryllium ores. It depicts a crushing stage followed by magnetic separation of magnetic impurities. The ore is then moved with a conveyor belt to a surge bin that feeds into a vibrating screen. The larger particles are fed into a cone crusher prior to rejoining the undersized particles in a belt conveyor toward the fine ore bin. The ore at this point is again screened, and the oversized particles are returned to the cone crusher. The fine ore is fed into an ore washer, where it is deslimed and fed using a screw conveyor into a ball mill. The overflow from the ball mill is pumped to a Kreb cyclone, where the smaller particles (–100 mesh) are separated and sent to the conditioning tanks. The temperature of the conditioning tank is kept between 75 and 85 °C (165 and 186 °F) and at a pH above 9.5. The larger particles are fed again into the ball mill. After adding the conditioning agent, sodium sulfide, the pulp (25% solids) is conditioned for 2 to 5 min, after which it is fed into the first stage of the flotation, which are the rougher cells. At this point, the collection and flotation agents are added (oleic acid). The rougher concentrate is reconditioned and fed into a cleaner cell, while the gangue is fed into a scavenger. From the scavenger, the concentrate is fed to the cleaner cell, while the gangue is sent to the tails pond. The concentrate from the cleaner is sent to a thickener and then through a disc filter prior to being fed into a rotary dryer.

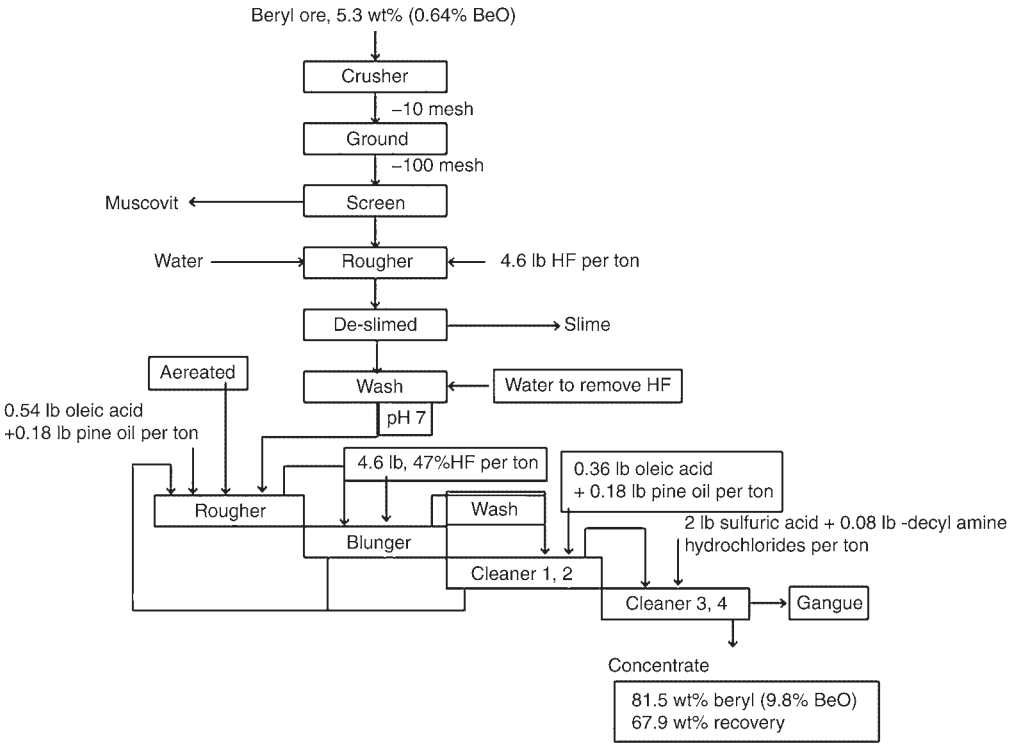

Fig. 6.2 Hydrofluoric acid activation of ores for beneficiation of beryl. Source: Kennedy and O'Meara 1947

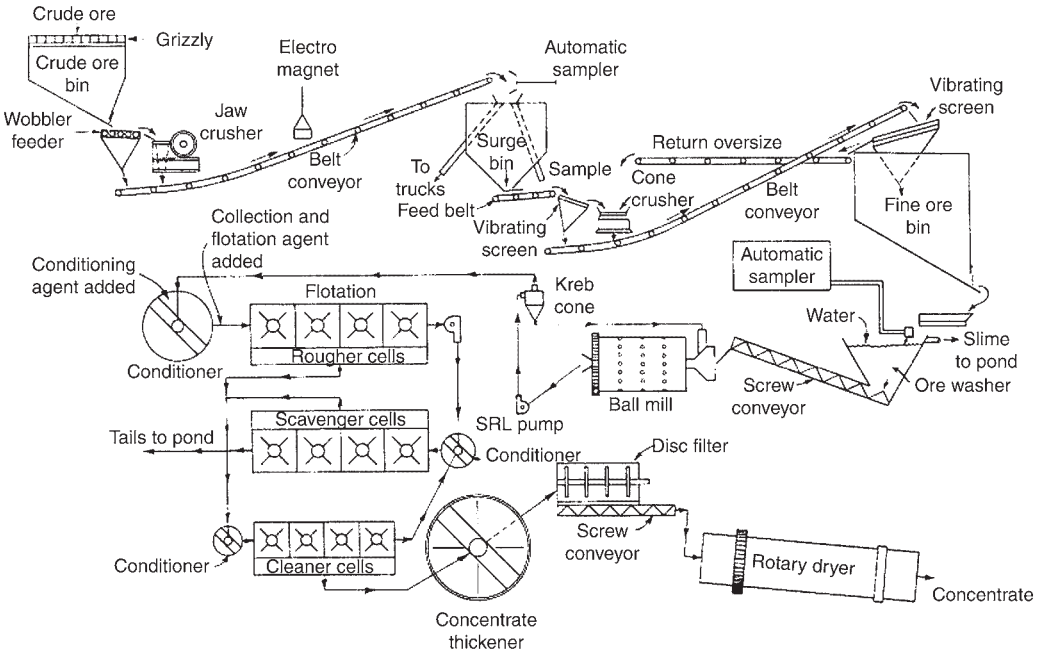

Fig. 6.3 Concentration plant from Mineral Concentrates and Chemical Company, Inc. Source: Johnston 1967

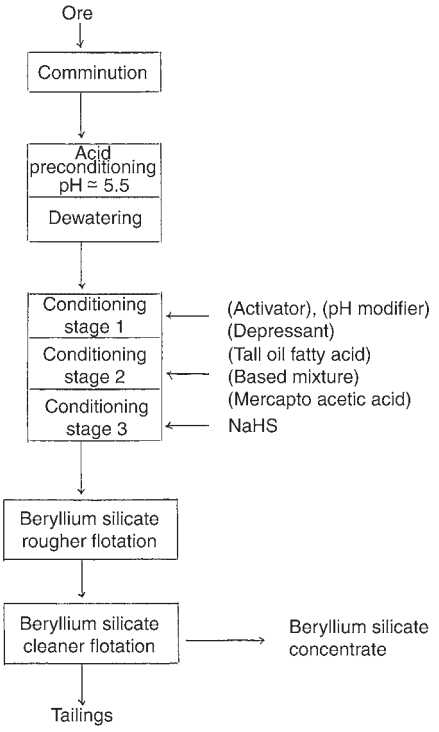

Fig. 6.4 Tall oil fatty acid flotation of phenacite and bertrandite. Source: Bulatovic 1988

6.5 Tall Oil Fatty Acid Flotation of Phenacite and Bertrandite

Bulatovic [1988] patented a process for flotation of phenacite and bertrandite using a so-called tall oil fatty acid base collector. In this process, the ore is ground to a P_{80} (i.e., 80% of the particles), smaller than 37 μm. A magnetic separator is employed to remove any iron-containing materials from the ground ore prior to making a slurry, using water. Sulfuric acid is added as a preconditioner, adjusting the pH between 5 and 5.5. After the pretreatment, the slurry is thickened to 65 wt% solids.

The pretreated slurry is then treated with a modifier, such as sodium carbonate, to adjust the pH to 9.5. Sodium fluoride is typically used as an activator, but sodium silico-hexafluoride can also be used. A depressant such as sodium hexametaphosphate and carboxylmethyl cellulose is used to depress albite, mica, carbonates, fluorite, siliceous gangues, and even yttrium and rare earth minerals. The conditioning stage typically lasts 10 min, followed by the addition of the collector mixture. This collector mixture consists of cresylic acid, an aliphatic alcohol, and kerosene. The conditioning is followed by conventional rougher and cleaner flotation stages. Figure 6.4 shows a flow diagram of the flotation process invented by Bulatovic [1988].

It can be seen from the previous sections that concentration of beryllium ores is rather complicated and not very efficient. Hand sorting is still very common for concentrating beryl and bertrandite minerals, rather than using any of the flotation schemes presented here.

REFERENCES

Bulatovic, S., 1988. Beryllium Flotation Process, U.S. Patent 4,735,710

Havens, R., 1963. Flotation Process for the Concentration of Phenacite and Bertrandite, U.S. Patent 3,078,997

Havens, R., Nissen, W.I., and Rosenbaum, J.B., 1961. "Flotation of Bertrandite and Phenacite from Mount Wheeler, Nevada, Beryllium Ore," U.S. Department of Interior, Bureau of Mines

Johnston, T., 1967. Concentration of Beryllium Ores, U.S. Patent 3,300,147

Kennedy, J., and O'Meara, R., 1947. Beneficiation of Beryllium Ores, U.S. Patent 2,414,815

Lamb, F., and Banning, L., 1945. Beneficiation of Beryllium Ores, U.S. Patent 2,385,819

SELECTED REFERENCES

- Abani, M.C., Murthy, K.B.S., and Iyer, M.R., 1994. Calculation of Burden from Bioassay Analysis for Beryllium Using Icrp Model, *Miner. Process. Extr. Metall. Rev.* Vol 14 (No. 1), p 319–331
- Bunshah, R.F., and Juntz, R.S., 1966. Purification of Beryllium by Crucible-Free Vacuum Melting and Distillation Process, *Beryllium Technology, AIME*, Vol 33, L. McDonald Schetky and H.A. Johnson, Ed., Gordon and Breach, NY, p 1–28
- Gold, L., 1949. "Growth and Perfection of Beryllium Crystals," Report AECD-2643, U.S. Atomic Energy Commission
- Han, K.E., et al., 1994. Mineral Processing and Extractive Metallurgy Review—Special Issue, *Proceedings of the National Workshop on Beryllium*
- Jonsson, S., Freund, A., and Aldinger, F., 1979. Growth of Beryllium Single Crystals

from Neutron Monochromators, *Metall. Verlag*, Vol 12, p 1257–1261

- Livey, D.T., and Williams, J., 1958. "Fabrication Technology of Beryllium and Beryllia," Paper 319, Proceedings of the Second United Nations Conference on the Peaceful Uses of Atomic Energy (Geneva)
- Mitchell, W.R., Mullendore, J.A., and Maloof, R.S., 1961. Zone Purification of Beryllium, *Trans. AIME*, Vol 221, p 824–826
- Williams, J., 1958. The Fabrication and Properties of Commercially Pure Beryllium, *Metall. Rev*., Vol 3, p 1–44
- Williams, J., Munro, W., and Jones, J.W.S., 1955. "The Production of a Stable Beryllium Powder from Electrolytic Flake, Its Fabrication and Properties," Report AERE-M/R-1679, United Kingdom Atomic Energy Authority

Beryllium Chemistry and Processing, p 71-92
By Kenneth A. Walsh
Edited by Edgar E. Vidal, Alfred Goldberg,
Edward N.C. Dalder, David L. Olson, and Brajendra Mishra

CHAPTER 7

Extractive Metallurgy

Kenneth A. Walsh, Brush Wellman Inc., Retired
Edgar E. Vidal, Brush Wellman, Inc.
Brajendra Mishra, Colorado School of Mines

7.1 Extraction from Beryl

Because of its structure, beryl ore is very resistant to acid attack at atmospheric pressure and from intermediate temperatures up to its boiling temperature. The complex structure of the mineral contains $[Si_6O_{18}]^{12-}$ units, each consisting of six SiO_4^{4-} tetrahedra linked in a ring. In beryl, such rings are joined by the coordination of their oxygen atoms to the metallic cations.

Many methods have been explored to recover beryllium from beryl. All are costly due to the low beryllia content of the ore and the necessity for protective measures in handling dusts and spray containing dissolved compounds of beryllium. Some of the usual fusion reagents from analytical chemistry have been successfully used for the decomposition of the ore. The reactants hydrofluoric acid and sodium or potassium hydroxide dissolve beryl ore, but the chemical consumption by the silica component is too expensive. Also included among the rejected candidates are potassium acid sulfate, potassium acid fluoride, sodium, carbonate, and others.

The search for less expensive sources of alkali led to the lime fusion process of Bayliss and Derry [1963]. The addition of large amounts of $CaCO_3$ to beryl before fusing yielded glasses from which the beryllium was extracted by sulfuric acid leaching. Appreciable amounts of silica were also taken into solution. Silica dissolution was controlled by using intermediate quantities of $CaCO_3$ with the beryl. The beryllium became soluble in dilute acid, with no SiO_2 passing into solution. The addition of the metal oxide is postulated to convert the complex $[Si_6O_{18}]^{12-}$ anions into orthosilicate forms through:

$$(Si_6O_{18})^{12-} = nSiO_2 + (6 - n)\ SiO_4{}^{4-} + (2n - 6)O^{2-} \qquad \text{(Eq 7.1)}$$

here, $n = 3$ to 6.

The lime fusion process has the disadvantage of reagent consumption by the calcium cation, for example, conversion for precipitation as calcium sulfate. At least three processes have been commercially practiced for the extraction of beryllium from beryl. Each is described in detail, because some of the so-called abandoned methods may still be of interest for use with the ores of China or the Commonwealth of Independent States.

7.2 Kjellgren-Sawyer Sulfate Extraction from Beryl

The sulfate extraction method is an acidic method for decomposing the ore and recovering its BeO content [Sawyer and Kjellgren 1935, Kjellgren 1946, 1955]. The method is based on the fact that the reactivity of beryl with acids is enhanced by heat treatment. The effect becomes apparent at 1000 °C and increases with rising temperature. The maximum effect can be obtained by completely melting the beryl and then quenching the melt in cold water. Beryl ore at its melting point is extremely active chemically

and rapidly attacks all ordinary refractory linings of furnaces. Initially, a carbon-lined electric furnace was used for melting beryl, with protection from excessive oxidation by a reducing gas atmosphere. In approximately 1965, the carbon liner was replaced by a water-cooled jacketed, rammed beryl liner, which could be employed for over a year without replacement. The furnace of the Heroult type is fitted with three 15 cm diameter top electrodes. The furnace is started with an open arc; as soon as a molten bath is formed by the heat of the arc, the electrodes are immersed into the molten beryl, and the heating is continued by passing the current directly through the bath. Energy consumption for fusion at 1600 to 1625 °C amounts to 1045 kWh per metric ton. This energy cost imposes the economic limit of the method to the use of high-grade beryl ore containing more than 10 wt% BeO. Dust evolution during fusion is limited through the use of pieces of beryl larger than 2 cm. A carbonate content limit is specified to help control dust from gaseous carbon dioxide evolved during fusion.

In the sulfate process for beryllia production, water-soluble beryllium and aluminum sulfates are formed by reacting beryl with sulfuric acid at 400 °C. Silica is precipitated out as an insoluble compound. However, a pretreatment is required to render beryl amenable to sulfation, since direct digestion of the ore in sulfuric acid gives low yields of 40 to 60%. The first pretreatment process to improve the reactivity of beryl in the sulfation step is based on a two-step heat treatment. Beryl is melted at 1650 °C and water quenched, followed by another heat treatment at 900 °C, which allows a 95% recovery of beryllium by changing its crystal structure and dissociating beryllia from the existing compounds in the ore. This process is commercially used. The second pretreatment process practiced industrially requires heating of beryl with lime and sodium carbonate at 1000 °C to form a sinter of beryllium oxide mixed with a silicate-aluminate matrix. A hot dilute acid treatment of this sinter leaves beryllia and silica behind, which is amenable to sulfation. Alkali-decomposed beryllia is even more easily converted to sulfate by dilute sulfuric acid, but the acid quantity required is high. The primary reaction of the sulfate process is as follows:

$$3BeO{\cdot}Al_2O_3{\cdot}6SiO_2 + 6\,H_2SO_4 = 3BeSO_4 + Al_2(SO_4)_3 + 6SiO_2 + 6H_2O \quad \text{(Eq 7.2)}$$

Many processes have been suggested for separating aluminum, iron, and other heavy metals from beryllium sulfate. Reaction with ammonium or potassium sulfate to form an alum is the process predominantly used by beryllium manufacturers. Granular beryllium hydroxide is precipitated by boiling beryllium sulfate with alkali at slightly basic pH through an intermediate sodium beryllate:

$$BeSO_4 + 2NaOH = Na_2SO_4 + Be(OH)_2\ \text{(gelatinous)} \quad \text{(Eq 7.3)}$$

$$Be(OH)_2 + 2NaOH = Na_2BeO_2 + 2H_2O \quad \text{(Eq 7.4)}$$

$$Na_2BeO_2 + 2H_2O = Be(OH)_2 + 2NaOH \quad \text{(Eq 7.5)}$$

Beryllia is produced by calcining beryllium hydroxide above 500 °C.

The cooling rate from the fusion temperature is critical. Rapid cooling rates are obtained by pouring the liquid beryl as a stream from the furnace and striking it with a stream of water. The beryl glass product is no longer crystalline, the structure having been destroyed by the melting and quenching. Grinding the glass and reacting it with hot concentrated sulfuric acid renders only 25 to 30 wt% of the beryllium content water soluble.

Reheating the glass to 900 to 1025 °C causes partial devitrification, a result of which is an increase in the fraction of acid-reactive beryllium oxide. For a given lot of beryl frit, the preferred heat treating temperature is determined by operating a gas-fired rotary kiln at incrementally increasing temperatures above 925 °C for sixty-minute intervals. Samples are removed, treated with hot concentrated sulfuric acid, diluted, and filtered. The filtrate is analyzed for solubilized beryllium. From a plot of solubilized beryllium in terms of heat treating temperature, the maximum yield determines the operating temperature for heat treating the entire lot, usually the quantity needed for one month's production.

The heat treated frit is ground to −200-mesh powder. A slurry of the powder in 93% sulfuric acid is heated to 250 to 300 °C by impinging a jet stream of the slurry onto a surface heated by burning gas. The beryllium and aluminum are converted to their hydrated sulfates, while the silica is retained in a dehydrated, water-insoluble form. The nearly dry sulfated powder is leached with a dilute sulfate solution from the decantation train. If the water vapor present during sulfation is insufficient, anhydrous sulfates are also formed. In the leaching stage, anhydrous

beryllium sulfate is much more slowly dissolved than the rapidly solubilized tetrahydrate. The leached, sulfated slurry is processed through a countercurrent decantation washing system to recover the soluble sulfates from the siliceous solids. The typical overflow leach solution contains 11 g/L Be, 25 g/L Al, and 2 g/L Fe in approximately 0.5 *M* free sulfuric acid. The leach solution contains approximately 92 wt% of the beryllium content of the input beryl. Subsequent processing consists of a series of purification steps to reject the impurities before beryllium hydroxide recovery.

Crystallographic changes resulting from the fusion, quenching, and postheating operations were studied by Bayliss and Derry [1963]. Quenching rates of fused, high-grade beryl needed to be in the 100 to 1000 °C/s range to assure the formation of x-ray amorphous glasses. At slower quenching rates of 10 to 100 °C/s, the formation of phenacite was observed. At still slower quenching rates of 1 to 10 °C/s, beryllia and mullite were found with the phenacite.

Rapid postheating of the glasses was performed by placing the samples in a muffle furnace already at the desired temperature. Below 900 °C, no crystallization was observed. A rapid postheating rate of 500 °C/min to temperatures above 920 °C, followed by very brief holding times of less than 5 min, was favorable for the formation of crystalline beryllia and mullite. After 2 h at the holding temperature, additional crystalline phases were formed and identified as chrysoberyl and α-cristobalite.

A slower postheating temperature rise of 10 °C/min from 920 to 1000 °C with negligible holding time produced beryllia and mullite. At least 50 wt% of the contained beryllium was present as crystalline BeO. Higher temperatures and longer soak times sharpened the BeO lines in the x-ray diffraction pattern to give an intensity sufficient to account for nearly all of the contained beryllium. The mullite lines also became more intense, and α-cristobalite crystallized. At the highest holding temperatures of 1120 to 1200 °C with 2 h soak time, $BeO{\cdot}Al_2O_3$ and $BeSiO_4$ were formed through the reaction of beryllia with mullite.

Purification of the beryl frit acidification leach liquor employed the historical alum and chelation steps, with beryllium hydroxide recovery described by Schwenzfeier [1964], Walsh [1979], and Sloman [1932]. This process had been installed in China by former Soviet technologists before 1960. It was also employed in the former Soviet Union and remains in use in the Commonwealth of Independent States. In the mid-1960s, purification by solvent extraction was installed in the United States.

Neutralization of the free sulfuric acid in the leach liquor with aqueous ammonia to pH = 1 creates enough ammonium sulfate to form ammonium alum. Cooling to 15 °C causes crystallization of ammonium alum, $Al_2(SO_4)_3{\cdot}(NH_4)_2SO_4{\cdot}24H_2O$. Centrifugation removes the crystals. Organic chelating agents, such as the sodium salt of ethylenediamine tetraacetic acid and triethanolamine, are added to the centrifugate. Addition of sodium hydroxide yields the reactions:

$$BeSO_4 + 2\ NaOH \rightarrow Na_2SO_4 + \alpha\text{-}Be(OH)_2 \quad \text{(Eq 7.6)}$$

$$\alpha\text{-}Be(OH)2 + 2\ NaOH \rightarrow Na_2BeO_2 + 2\ H_2O \quad \text{(Eq 7.7)}$$

Passage of the sodium beryllate solution through a jacketed heat exchanger hydrolyzes the sodium beryllate, which precipitates a granular β-beryllium hydroxide by:

$$Na_2BeO_2 + 2\ H_2O \rightarrow 2\ NaOH + \beta\text{-}Be(OH)_2 \quad \text{(Eq 7.8)}$$

The resulting granular hydroxide is readily separated in continuous centrifuges, where it is effectively washed and subsequently dewatered to less than 15 wt% free water. The overall extraction yield from beryl frit acidification and purification is approximately 85 wt%.

7.3 Degussa Extraction of Beryllium from Beryl

The quest for alternative methods for extracting beryllium from beryl was focused on reducing the energy consumption by lowering the fusion temperature and using cheaper lower-BeO-grade beryl. This approach was pursued by Deutsche Gold und Silber Scheide Anstalt (Degussa), located in Frankfurt, Germany. After the German collapse in World War II, Potvin and Farnham issued a report on the inspection of the Degussa works by a British Intelligence Objectives Sub-Committee [Potvin and Farnham 1946]. A more readily available process description is summarized by Darwin and Buddery [1960a]. Both reports describe the beryl decomposition and

conversion to beryllium hydroxide, from which followed the preparation of beryllium chloride for the electrolytic reduction to metallic beryllium. Maximum production reached 160 to 180 kg/month pure beryllium.

The Degussa process employed beryl containing 10 to 12 wt% BeO. The ore was milled to approximately −72 mesh in a cascade ball mill. The milled ore was blended in a 2 to 1 weight ratio with finely powdered quicklime. The quantity of lime was equivalent to that required for the formation of $CaO{\cdot}Al_2O_3 + CaO{\cdot}2SiO_2$, with 12 wt% excess. The mixture was heated to 1400 to 1500 °C for 1.5 h in a gas-fired rotary furnace. The fused mass was discharged into cold water to yield a glassy product. After drying, the glass was ground to −72 mesh. Charges of 300 kg of milled glass were hand mixed with 480 kg technical-grade sulfuric acid. The heat of dilution from a 40 L addition of water gradually warmed the mixture. Following a 2 h reaction period, 420 kg sulfated product was leached with 350 L water, with heating to near boiling. The insoluble calcium sulfate and most of the silica were rejected by filtration. The addition of 77 kg ammonium sulfate to the hot filtrate, followed by cooling to 15 °C, formed ammonium aluminum sulfate (ammonium alum) crystals, separable by centrifugation.

The 600 L of solution of beryllium and iron sulfates was diluted with 1200 L water. The addition of 3 L hydrogen peroxide oxidized the iron, which was then precipitated by stirring a slurry containing 75 kg calcium carbonate into the hot solution to a pH of 3.8 to 4.2. The calcium sulfate and the ferric and aluminum hydroxides, thus formed, were filtered off.

The filtrate was a solution containing primarily beryllium sulfate. To it was added ammonia to precipitate the beryllium hydroxide in the form of a slurry. The precipitate was recovered by filtration and dried on flat trays in a drying oven at 100 °C. The dried product consisted of beryllium hydroxide containing 50 wt% BeO. Ignition of the hydroxide at 1000 °C gave a product having the following approximate composition:

Component	Amount, wt%
BeO	98.5–99
Impurities, total	1
CaO	0.2–0.7
Fe_2O_3	0.02
Al_2O_3	≤0.1
MgO	Trace
SO_3	≤0.8
Na_2O	≤0.4
Loss on ignition	≤1

The recovery of beryllium from the ore was approximately 78 to 80 wt%. The low recovery can be overcome by using current standard engineering techniques. Energy consumption during fusion was not lowered because of the 1.5-fold increase in mass over the beryl alone. Nevertheless, the process may be energy saving with the Chinese flotation product or their fine as-mined beryl. Both avoid pulverization of the beryl. Postheat treatment of the glass is also avoided. Figure 7.1 summarizes the flow sheet of the Degussa process.

7.4 Copaux-Kawecki Fluoride Extraction from Beryl

The second important process for beryllia production, the silicofluoride process, consists of heating beryl with sodium silicofluoride in 1 to 2 by weight proportions at 750 °C according to the following reaction [Copaux 1919]:

$$3BeO{\cdot}Al_2O_3{\cdot}6SiO_2 + 6\,Na_2SiF_6 = 3\,Na_2BeF_4 + 2\,Na_3AlF_6 + 9\,SiO_2 + 3\,SiF_4 \quad \text{(Eq 7.9)}$$

Many variations have been suggested with additions of other cryolites, hydrofluoric acid, sodium carbonate, and so on, but the formation of Na_2BeF_4 occurs in all the cases. The soluble Na_2BeF_4 is separated as a fairly pure beryllium solution by aqueous leaching. Some $NaBeF_3$ and BeF_2 have been reported to form and join the beryllium solution [Lundin 1945]. The precipitation of beryllium hydroxide from Na_2BeF_4 is carried out with an alkali boil by a similar process used in the sulfate route, which is further decomposed to beryllia [Jaeger 1950]:

$$Na_2BeF_4 + 4NaOH = Na_2BeO_2 + 4\,NaF + 2H_2O \quad \text{(Eq 7.10)}$$

$$Na_2BeO_2 + 2H_2O = Be(OH)_2 + 2NaOH \quad \text{(Eq 7.11)}$$

Other processes involving conversion of beryl to beryllium chloride by direct chlorination of the ore have also been developed, which forms the basic raw material for further processing to beryllium [Spitzin 1930].

The recovery of beryllium directly from the ore or beryllia by a thermal reduction is an impractical proposition, since calcium is the only metal that will reduce beryllium oxide under normal thermodynamic conditions, and a stable

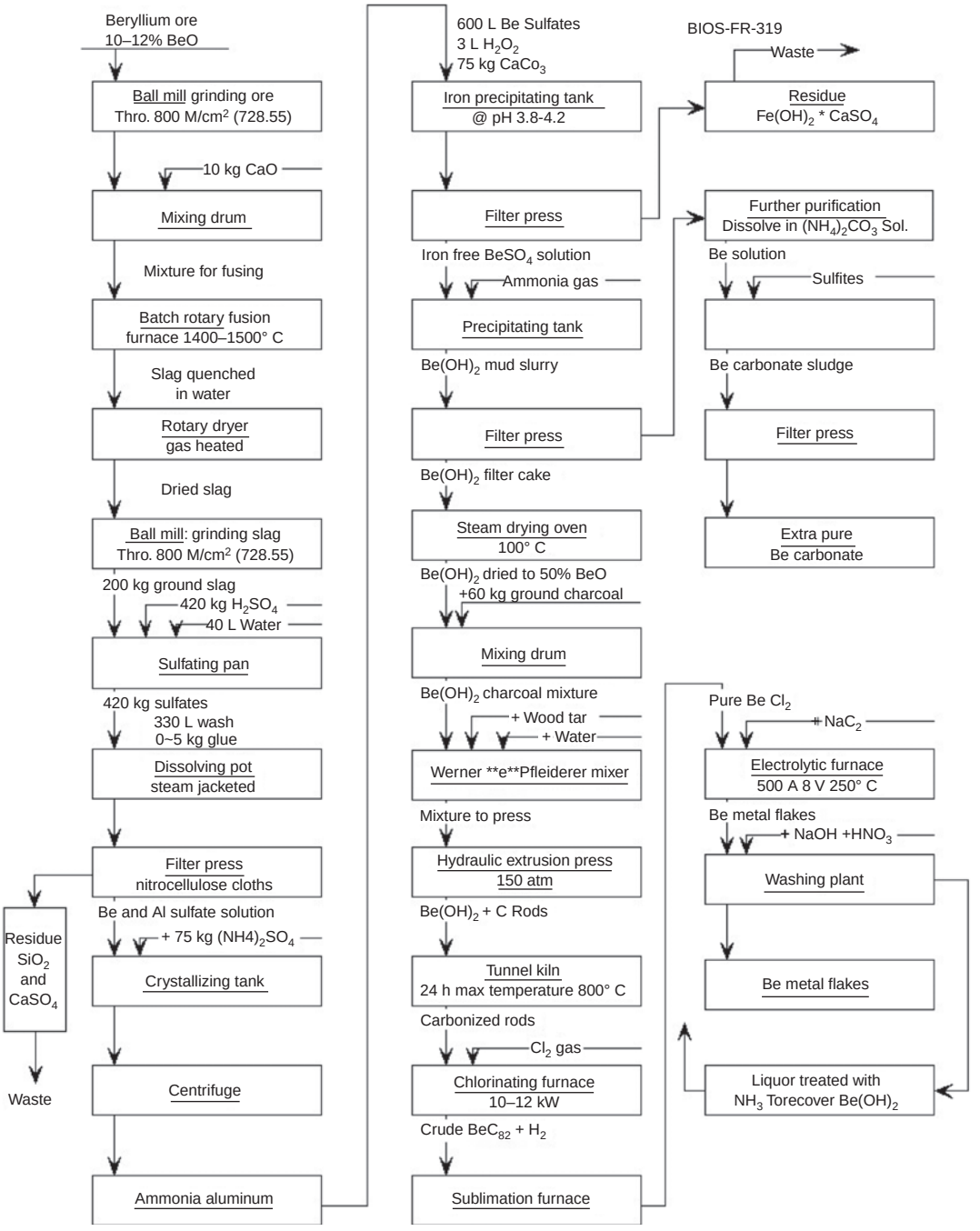

Fig. 7.1 The Degussa production flow sheet. Note: "Thro. 800 M/cm² indicates that particles of approximately 800 mesh/cm² pass. Source: Darwin and Buddery 1960

calcium-beryllium intermetallic forms that does not decompose easily. The relatively high melting point, high stability of the oxide, and high chemical reactivity at high temperatures of beryllium are the three causes attributable to the difficulties in reducing beryllia. Electrolytic methods to produce beryllium from the ore or beryllia through a fluxed medium are also not feasible, because a salt system with good solubility for the oxide is not known. Therefore, the oxide must be

converted to another form, such as halides, to be able to reduce it thermally or electrolytically, since beryllium chloride and fluoride are relatively less stable than the oxide and therefore reduce more easily.

The two commercial methods practiced for producing beryllium are based on converting the oxide into a chloride or a fluoride. The processing temperature must be above the melting point of beryllium to have a molten product that can be easily separated from the slag. However, it imposes daunting material problems, forcing a low-temperature reduction. Therefore, a solid beryllium product, intimately mixed with the slag, is formed.

The major production process for beryllium is the reduction of beryllium fluoride with magnesium at 1300 °C:

$$BeF_2 + Mg = MgF_2 + Be \qquad \text{(Eq 7.12)}$$

The production of beryllium fluoride from hydroxide takes place in two steps. Beryllium hydroxide is reacted with ammonium bifluoride, producing ammonium fluoroberyllate, which, in turn, is decomposed at elevated temperatures (>125 °C) to produce beryllium fluoride and volatile ammonium fluoride:

$$Be(OH)_2 + 2NH_4{\cdot}HF_2 = (NH_4)_2BeF_4 + 2H_2O \qquad \text{(Eq 7.13)}$$

$$(NH_4)_2BeF_4 = BeF_2 + 2\ NH_4F \qquad \text{(Eq 7.14)}$$

Using an excess amount of beryllium fluoride, which helps in fragmenting the slag and releasing the entrapped beryllium globules, enhances the yield of beryllium. Fairly large pieces of beryllium coalesce once the temperature goes above the melting point of beryllium. The rate of reaction picks up beyond 850 °C, after both magnesium and beryllium fluorides are molten. Reduction of fluoride or chloride with sodium has also been attempted by vapor-phase reduction [Wöhler 1828a, b, Fischer and Peters 1933].

In the commercial electrolytic process for beryllium production, beryllia is mixed with carbon and a binder and extruded into short sticks, calcined to form a porous beryllia-carbon mixture, and subsequently heated in chlorine to form beryllium chloride. This chloride is purified by sublimation and fused with an equal weight of sodium chloride and electrolyzed at 350 °C in a nickel cell. Cathodically deposited beryllium flakes are leached free by washing in water [Potvin and Farnham 1946]. An equimolar mixture of sodium and beryllium chloride melts eutectically at 224 °C, providing the opportunity to produce 99.5 wt% pure beryllium at a low temperature, thereby preventing beryllium oxidation as well as corrosion of the cell components.

Other high-temperature electrolysis methods and thermal reduction processes that have been developed have very little commercial value, although these processes have the advantage of a better beryllium separation from the slag or the electrolyte, if the process is carried out above the melting point of beryllium. Several electrolytes, such as beryllium fluoride-sodium fluoride mixture and beryllium fluoride-barium fluoride mixture, have been electrolyzed [Hopkins and Meyer 1924, Vivian 1926]. Magnesium-calcium reduction [Schofield 1954] and thermal decomposition of beryllium iodide [Sloman 1932] are other methods that have been developed at laboratory scale.

The refining of crude beryllium produced by the primary reduction is essential, since the electrolytic beryllium contains significant levels of chlorine, and the reduced beryllium contains magnesium and magnesium fluoride as impurities. Due to the criticality of applications, beryllium needs to be purified to very high levels of cleanliness. Vacuum distillation, zone refining, and electrorefining have been attempted. Remelting under a beryllium fluoride flux and argon atmosphere can give a 99.6 wt% pure beryllium from the thermally reduced pebbles. However, much higher purity levels can be obtained by vacuum induction melting, which can reduce the magnesium contamination to below 500 ppm and fluorine below 50 ppm [Ivanov and Shmelev 1958]. Milling and leaching to produce high-grade powder from electrolytic beryllium flakes has also been practiced [Blainley et al. 1954]. Halide and vacuum distillation also are known successful methods. Soluble anode electrolysis is a viable method that can provide beryllium with greater cleanliness, but the process is not commercially established. Molten salt electrorefining is also not a viable proposition, since the cell will have to operate above the melting point of beryllium to obtain a liquid beryllium anode and liquid cathodic deposit for acceptable refining efficiency. However, the concept of molten salt electrorefining is technically feasible. A potassium, lithium, beryllium chloride electrolyte has been used to produce 99.95 wt% pure beryllium

flakes from scrap metal containing iron, nickel, and aluminum [Mitchell et al. 1989].

This article suggests electrolytic methods for the extraction of beryllium based on beryllium halide-alkali halide salt systems, which could allow a higher efficiency of recovery. Schematic cell arrangement has been suggested to electrowin beryllium through a molten salt electrolyte.

When beryl is made acid soluble by fusion and quenching, with (Degussa) or without (Kjellgren-Sawyer) lime addition, the process is unselective, and separation of beryllium and aluminum must follow. Rendering beryllium ores into a reactive condition was devised by Copaux [1919]. In the Copaux process, beryl is heated with sodium fluorosilicate at 750 °C for 1 h, using a weight ratio of sodium fluorosilicate to beryl of 0.8–1 to 1. The idealized result from the roasting process is:

$$3BeO{\cdot}Al_2O_3{\cdot}6SiO_2 + 3\ Na_2SiF_6 \rightarrow 3BeF_2 + 2\ Na_3AlF_6 + 9\ SiO_2 \qquad \text{(Eq 7.15)}$$

The pulverized ore is mixed with sodium fluorosilicate. Water is added to aid the formation of briquettes. Early modifications included the addition of soda ash at 10 wt% of ore to improve bonding during briquetting. Heating of the briquettes requires a close control of the temperature gradient during roasting. Heating the briquettes too rapidly tends to cause disintegration. If the temperature is maintained at too low a level, the gaseous silicon tetrafluoride resulting from the decomposition of sodium fluorosilicate will escape from the system without reacting with the beryl. To achieve the objective of combining the by-product sodium fluoride and aluminum fluoride, the temperature must be raised very closely to the upper permissible limit. This upper limit is below 800 °C to avoid fusion in the briquette, which would form insoluble beryllium compounds.

The mechanism of the Copaux reaction has been studied by Hyde et al. [1961a, b]. In the early stages, the proportion of sodium fluoride to fluorosilicate is low, so the product species are the glassy, x-ray-amorphous beryllium fluoride; synthetic cryolite, Na_3AlF_6; and α-cristobalite, SiO_2. During this stage, a high proportion of the beryllium is rendered water soluble in a comparatively short time period, for example, 62 wt% in 15 min at 750 °C. During the second stage, the proportion of sodium fluoride to fluorosilicate is higher. This change is accompanied by the appearance of albite, $NaAlSi_3O_8$. As the roasting continues into the third stage, there is a decrease in the proportion of water-soluble beryllium, with a parallel decrease in the amount of α-cristobalite and cryolite. There is an increase in the amounts of albite and sodium fluoride. Because the briquettes are poor thermal conductors, the surface temperature allows all three stages to occur at the surface before the center reaches the temperature required for the first-stage formation of water-soluble beryllium fluoride. After roasting, the cooled briquettes are crushed, then wet milled in water or recycled weak liquor. The resulting slurry is treated in a leaching tank with potassium permanganate and hydrogen peroxide to oxidize any ferrous iron in the system. The pulp is filtered as rapidly as possible, giving a primary filtrate containing approximately 13 g/L beryllium fluoride. The filter cake is washed thoroughly in a countercurrent washing system.

Speed of operation is critical, because some free sodium fluoride is inevitably present in the roast. This will gradually react in aqueous solution with the very soluble beryllium fluoride to give sodium fluoroberyllate, which has a low solubility.

The loss of fluoride values vaporized as silicon tetrafluoride was avoided by Kawecki [1946]. Sodium ferric fluoride is substituted for sodium silicofluoride in the Copaux-Kawecki process. Ore is pulverized, wet or dry, to approximately 70 wt% −200 mesh (74 μm). It is mixed with sodium ferric fluoride and made into wet briquettes. These briquettes are heated for approximately 1 h at 750 °C to give the net reaction:

$$3BeO + 2\ Na_3FeF_6 \rightarrow 3\ Na_2BeF_4 + Fe_2O_3 \qquad \text{(Eq 7.16)}$$

Kawecki [1946] made the assumption that the alumina, silica, and iron oxide components of the beryl do not react. The reported concentration of 3 g/L BeO resulting from leaching slightly exceeds the literature value for the solubility of sodium fluoroberyllate [Novoselova 1934, 1959].

After the baking operation, the material is in a sintered, friable condition. The sodium fluoroberyllate is the only soluble portion of the pulverized sinter. It is leached with water at ambient temperature to give a concentration of 3 g/L BeO. Approximately 95 wt% of the beryllium contained in the ore is put into solution. The insolubles are removed by filtration, washed, and discarded.

Caustic soda is added to a portion of the sodium fluoroberyllate solution to precipitate the gelatinous α-beryllium hydroxide. Additional caustic soda is added to dissolve the gelatinous material and form a sodium beryllate solution. This preparation is heated to approximately 85 °C, and more sodium fluoroberyllate solution is added with vigorous agitation, while maintaining temperature, until all of the beryllium is precipitated as a crystalline hydroxide. The slurry is filtered, and the beryllium hydroxide is washed. The filtrate is a sodium fluoride solution formed by the reaction:

$$2NaOH + Na_2BeF_4 = Be(OH)_2 + 4\ NaF \qquad \text{(Eq 7.17)}$$

The hydroxide cake is calcined at 800 °C, which converts it to the anhydrous oxide. This reaction leads to the intermediate product, BeO.

The sodium fluoride solution is neutralized with a small amount of sulfuric acid. A solution of ferric sulfate is added, which precipitates all of the fluoride as sodium ferric fluoride [Kawecki 1943]:

$$12\ NaF + Fe_2(SO_4)_3 = 2\ Na_3FeF_6 + 3\ Na_2SO_4 \qquad \text{(Eq 7.18)}$$

The sodium ferric fluoride is filtered off. The wet filter cake is used directly in the mixture with pulverized ore. The dilute sodium sulfate solution is discarded. The Kawecki modification has the advantage that the soluble fluoride is recovered and recycled.

The Copaux-Kawecki process was operated for many years in the United States, but it has not been used there since 1970. Expanding from the small-scale examples from the patent literature cited previously, material losses were experienced in the commercial operations. Sintering was conducted for 2 h at 750 °C. The crushed and wet-milled sinter was leached as a slurry containing 35 wt% solid. After recovery of the sodium fluoroberyllate solution, the red mud retained approximately 25 wt% of the input sodium fluorosilicate and sodium ferric fluoride as losses. Therefore, the briquettes had to contain 115% of the theoretical amount of sodium and fluorine required for conversion of the beryllium in the ore into Na_2BeF_4. After conversion to the granular beryllium hydroxide, addition of ferric sulfate to the sodium fluoride filtrate recovered only 67 wt% of the fluoride in the sodium ferric fluoride precipitate for recycling. The lost fluoride was replaced with sodium fluorosilicate. An average analysis of the briquettes is:

Component	Mass, g
Beryl	1000(a)
Na_2CO_3	90
Na_2SiF_6	315
Na_3FeF_6	400
H_2O	325

(a) 11 wt% BeO. Source: Kawecki 1943

Bonding of the briquettes was promoted by the sodium carbonate addition. The beryllium hydroxide product recovered 85 wt% of the beryllium content of the ore.

7.5 Extraction from Bertrandite and Solvent Extraction

The volcanic tuff beds in the Topaz-Spor Mountain, Utah, are a source of beryllium that contains only 0.1 to 1.0 wt% beryllium oxide in the commercial-quality deposits. The ores are economically competitive with beryl because they are accessible by open-pit mining, and the bertrandite component of the ore is acid soluble. Between 1960 and 1967, extensive geologic exploration and development were completed in the Topaz-Spor Mountain area. During this period, research at the Salt Lake City Metallurgy Research Center, U.S. Bureau of Mines, generated much of the early published literature concerning the domestic ore. Research efforts performed by government and private agencies were directed toward the development of improved methods of extracting beryllium from the ore and of improved methods of purifying the crude beryllium solutions and compounds recovered as intermediates during the extraction process.

7.6 Beryllium from Leaching and Settling

At the Salt Lake City laboratories, Crocker et al. [1963] directed research on the leaching of beryllium from −35-mesh Spor Mountain ore samples and the settling characteristics from the clayey solid suspensions. For economic reasons for the future, sulfuric acid as the leaching agent was emphasized. It was found that approximately 95% of the beryllium was dissolved from most of the ore samples by agitation leaching with 272 kg (600 lb) H_2SO_4 per short ton of ore

for 24 h using 35% solids at 65 °C. Settling of the leached pulp, after dilution to 15% solids, required 0.27 to 0.36 kg (0.6 to 0.8 lb) of a polyacrylic flocculant (Separan 2610, Dow Chemical Co.) per ton of ore leached with 272 kg (600 lb) of H_2SO_4 per ton. Comparatively, ore leached with 362 kg (800 lb) of H_2SO_4 per ton required only 91 to 136 g (0.2 to 0.3 lb) of flocculant per ton. Terminal densities of the settled pulps were approximately 28 and 35% solids, respectively, from leaches using 272 and 362 kg (600 and 800 lb) of H_2SO_4 per ton. Thickener requirements for washing by countercurrent decantation were calculated from the test data.

There was no effect on leaching whether the clay minerals were montmorillonite, saponite, or a mixture of the two clays. Roasting the ore at 500 °C for 4 h before leaching increased the limiting pulp density for effective mixing to 50 wt% solids, but acid requirements were not diminished. Roasting above 500 °C adversely affected beryllium extraction.

Chemical composition of a pregnant leach liquor showed 0.54 g/L Be, 5.7 g/L Al, 1.5 g/L Fe, 2.1 g/L Mg, and 4.3 g/L fluoride as the major components. Minor amounts of divalent manganese, potassium, sodium, and zinc were also reported.

Brush Wellman, Inc. designed and constructed facilities for processing low-grade bertrandite ore near Delta, Utah, during 1968 and 1969. Production began in September 1969. Summaries of the process have been published [Walsh 1979, Kramer 1990, 1991]. A flow sheet of the process is reproduced in Fig. 7.2 and 7.3. Ore is transported by truck 50 miles from the mine to the Delta mill. After removal of large blocks with a grizzly, a screenlike device with large openings, the ore is passed through a jaw crusher.

Wash water from the thickener train sluices the ore to ball milling, where a thixotropic slurry of −20-mesh (841 μm) particles is produced. The milled pulp has 40 to 45 wt% solids. The thickener overflow used for sluicing contains 0.4 g/L Be, which is precipitated when the free acid is neutralized to a final pH of 6 in the liquid phase by the alkaline dolomitic carbonate in the ore.

Atmospheric digestion of the ore is conducted in a co-current series of eight tanks. Leaching is continued for 6 h at 90 °C. Acid consumption amounts to 450 lb H_2SO_4 per ton of ore. Over 96 wt% of the beryllium content of the ore is dissolved. The leached slurry is diluted to 15 wt% solids with thickener overflow. Flocculating agents are added, and the solids are washed by countercurrent decantation through eight thickeners. The resulting solution contains 0.4 to 0.7 g/L Be, 4.0 to 7.0 g/L Al, 0 to 5.0 g/L Mg, 1.5 g/L Fe, and 8 to 11 g/L fluoride, plus assorted other minor impurities. The higher fluoride dissolution, as compared with the laboratory results of Crocker et al. [1963], can be attributed to the higher leaching temperature [Walsh 1979].

7.7 Solvent Extraction from Sulfate Solutions

The extraction of beryllium from beryl or bertrandite creates an acidic beryllium sulfate solution. With its chemical similarity to beryllium, co-extracted aluminum requires selectivity of separation to yield purified beryllium concentrates. In the Kjellgren-Sawyer sulfate extraction from beryl, this separation is accomplished by rejection of most of the aluminum as ammonium alum. Selective hydrolysis of sodium beryllate-sodium aluminate solution yielded purified beryllium hydroxide. The low concentrations of beryllium and aluminum in sulfate solutions recovered from bertrandite leaching precluded the alum approach.

Early efforts of Hardy et al. [1961] concentrated on the solvent extraction of tracer levels of ^7Be. Ion-exchange-type alkyl phosphoric acid extractants were dissolved in a nonpolar solvent such as benzene or kerosene. Monohydrogen and dihydrogen alkyl phosphoric acids testing by Wells et al. [1963] eliminated those with high aqueous solubilities. This situation could be linked with excessive extractant losses into the element raffinate. Comparative screening tests reduced the list of promising esters to di-[2-ethylhexyl] phosphoric acid, which was commercially available due to its use in the uranium industry. The rate of extraction of beryllium is slow relative to that of other bivalent metal ions, such as the uranyl ion.

The extraction of cations from aqueous solutions by dialkylphosphoric acids (HA), which exist as dimers $(HA)_2$ in nonpolar solvents, proceeds by:

$$M^{n+}_{(aq)} + n\,(HA)_{2(org)} \rightarrow MA_n\,(HA)_n,\ org + nH^+_{(aq)} \qquad \text{(Eq 7.19)}$$

where aq and org refer to aqueous and organic phases, respectively. Quantitative comparisons

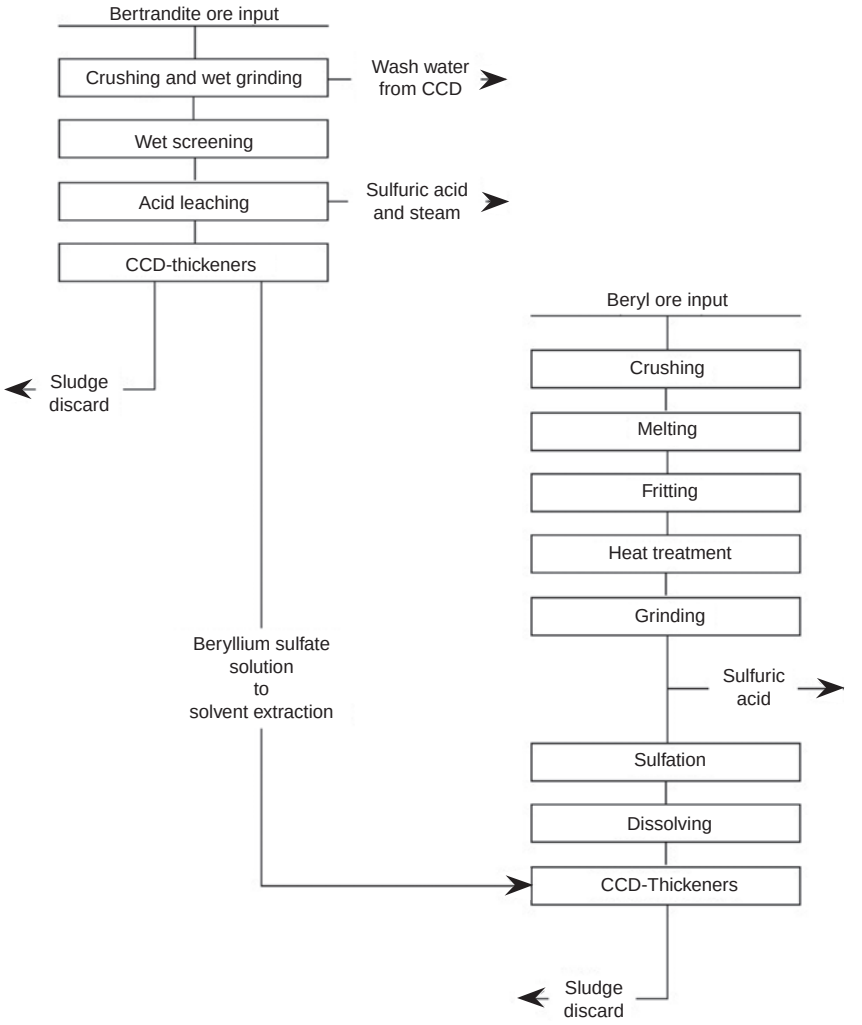

Fig. 7.2 Beryllium extraction from beryl and bertrandite ores at the Delta Plant in Utah by Brush Resources, Inc. Note: CCD thickeners are used in the countercurrent decantation (CCD) process to separate sludge and concentrate from solution.

of extraction under various conditions are made with the extraction coefficient, the ratio of the concentration of the species in the organic phase to that in the aqueous phase. Simple application of the law of mass action indicates that the extraction of divalent beryllium relative to the trivalent aluminum is favored by decreasing the acidity of the aqueous phase. The slow rate of extraction of beryllium by dialkyl phosphoric acids decreases further as the initial pH of the aqueous phase is lowered. The slowness of the reaction has been ascribed to steric hindrance to the attachment of a number of HA or A^- species around the small beryllium cation and the need to displace the strongly-bound water molecules in the primary hydration sheath. It is significant that for di-(2-ethylhexyl) phosphoric acid (HDEHP), equilibrium is attained much more rapidly with uranyl ions, which have a lower ratio of charge to radius than beryllium ions.

The unit cost of organic diluent favored the use of kerosene because of its low solubility in the aqueous phase. Fortunately, extraction coefficients were slightly higher with the kerosene diluent as compared with carbon tetrachloride, benzene, chloroform, toluene, and hexane.

The formation of a third phase was observed on conversion of the extractant to the sodium or ammonium form. This third-phase formation occurred when the extracted species were stripped from the organic phase with sodium hydroxide, ammonium fluoride, or ammonium bifluoride

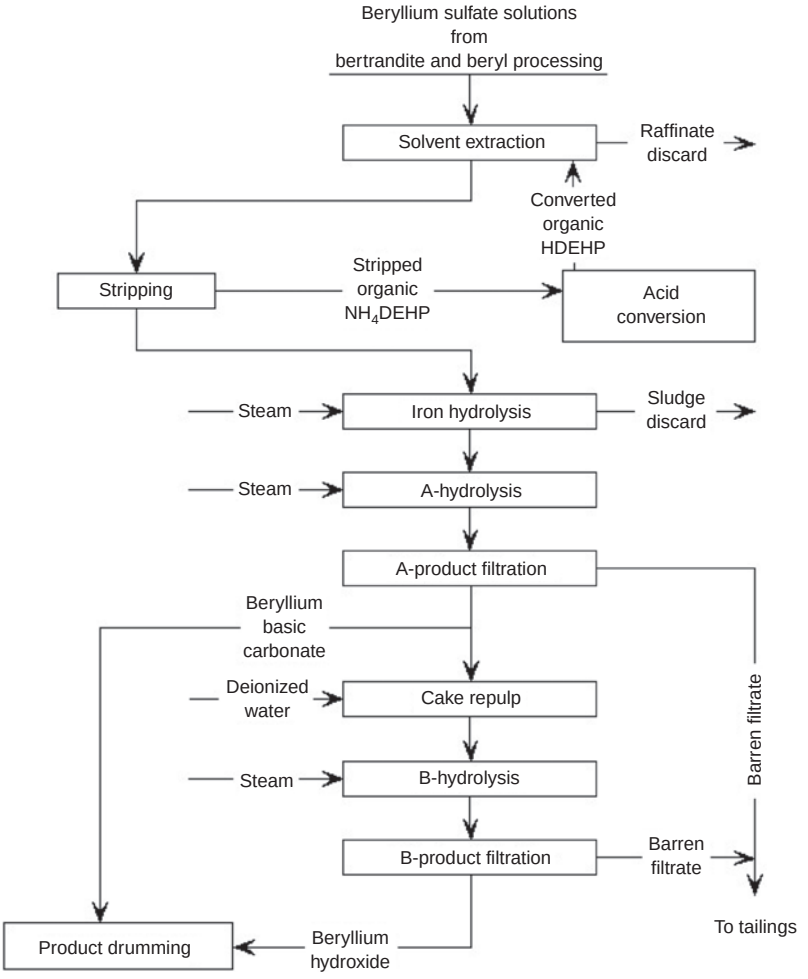

Fig. 7.3 Solvent extraction of beryllium from sulfate solutions at the Delta plant in Utah by Brush Resources, Inc. HDEHP, di-(2-ethylhexyl) phosphoric acid

solution. Third-phase formation was avoided by the inclusion of 4 wt/vol% octan-2-ol ($C_8H_{18}O$) in the organic solvent. This amount of modifier also enhanced the selectivity of beryllium extraction by suppressing the extraction coefficient for aluminum.

Parallel to its study of beryllium leaching of Spor Mountain ore, the Salt Lake City Metallurgy Research Center conducted solvent extraction studies with HDEHP in kerosene. Crocker et al. [1963] defined the major problem as the separation of beryllium from aluminum, iron, and magnesium. The extraction of beryllium is preferential to aluminum over the pH range of 0 to 3. It was also shown that beryllium displaces aluminum. Consequently, high-beryllium loadings in countercurrent operations improve selectivity. For the Spor Mountain solution containing 0.5 to 0.6 g/L Be, the increase in aqueous acidity is not sufficient to require neutralization. When neutralization was beneficial in the seven-stage mixer-settler circuit operations, spent caustic solution from beryllium hydrolysis of strip solution was added to the third and seventh stages.

Ferric iron is more readily co-extracted with beryllium than is aluminum. Ferric iron is not displaced from the extract by beryllium, so the solvent-loading capacity for beryllium is decreased. Because ferric iron is precipitated during caustic stripping, significant losses of entrained beryllium may be incurred unless the iron hydroxide precipitate is further processed. Extraction of ferric iron was controlled by reduction of ferric iron in the leach liquor to the ferrous state with sulfur dioxide or sodium hydrosulfide. For the Spor Mountain solution, prior

reduction of ferric iron with sodium hydrosulfide resulted in only approximately 3 wt% of the iron being extracted.

At pH 2, magnesium and calcium are coextracted when the extractant is in the sodium form, but their extraction by the hydrogen form is negligible. Extraction of aluminum and manganese is also enhanced with NaDEHP. Therefore, after the loaded organic has been stripped with caustic soda, it is preferably scrubbed with acid for conversion back to the hydrogen form before recycling to the extraction train.

Continuous countercurrent extraction testing was conducted by Crocker et al. [1963] in a seven-stage system. The ferric iron content of the leach solution was reduced to the ferrous form by treatment with 5 g/L NaHS. The flow rate of the aqueous feed at pH 2 was 1.5 times the organic rate. The organic feed was 0.25 *M* HDEHP in kerosene to which isodecanol was added at 2 wt/vol%. Contact time was 17 min/stage at the extraction temperature of 45 °C. This practice gave a loaded organic solvent containing 0.9 g/L Be, 0.13 g/L Fe, and 0.3 g/L Al from a leach solution feed with 0.58 g/L Be, 2.0 g/L Fe, and 4.9 g/L Al.

The loaded organic was stripped with 4 *M* NaOH at a flow rate designed to give a Na_2O:BeO molar ratio of approximately 2. Such strip solutions contained 5.4 to 7.2 g/L Be and 1.5 *M* free NaOH. Beryllium was recovered by diluting and boiling the strip solution to precipitate beryllium hydroxide. Scrubbing of the stripped organic solvent with sulfuric acid converted the extractant to the hydrogen form for return to the solvent extraction train. Overall recovery of beryllium from leach solution was 96 to 98 wt%.

During the same period as the Bureau of Mines research, commercial research studies were being conducted at Brush Wellman Inc. and other laboratories. The solvent extraction carbonate process of Maddox and Foos [1966] was installed at the Elmore, Ohio, plant of Brush Wellman Inc. in 1963 to produce 318 to 454 kg (700 to 1000 lb) of beryllium per day as the hydroxide. It replaced the old purification process for beryllium hydroxide from beryl ore. The Kjellgren-Sawyer process was repeated through the steps in which beryl ore is melted, quenched, heat treated, and ground to −200 mesh. The ground ore is reacted with sulfuric acid and leached with thickener overflow to dissolve the beryllium, aluminum, and iron, the major soluble sulfate components. After removal of the silica sludge by countercurrent decantation, the solution was neutralized with ammonium hydroxide and cooled to crystallize ammonium alum for rejection by centrifugation. The feed solution to solvent extraction had a typical analysis of 10.4 g/L Be, 3.1 g/L Al, and 1.6 g/L Fe. The feed solution at pH 1.5 was contacted with a 0.3 *M* NH_4DEHP in kerosene solution in a five-stage mixer-settler countercurrent system. Organic-to-aqueous flow-rate ratios were 10 to 1 to give 80 to 95 wt% organic-phase loading. The near-50 °C temperature of the system was employed to accelerate the rate of beryllium extraction. Heating lowered the viscosity of the organic phase to enhance phase separation. A high-molecular-weight alcohol, 2-ethylhexanol, was added to the organic to reduce emulsification from third-phase separation during stripping. A 1 to 15 volume ratio of 2-ethylhexanol to kerosene was employed. Mixing times were 10 min/stage, with mixing energy approximately 10 hp/1000 gal. The pH of the aqueous phase in the first mixer was approximately 2.0. The terminal raffinate pH was approximately 5.5. Acidity in each stage was controlled by varying the ratio of NH_4DEHP to HDEHP in the input organic.

Under these conditions, the beryllium, aluminum, and iron were completely transferred into the organic phase, with a simultaneous rejection of ammonium and hydrogen ions from the organic to the aqueous phase. Minor impurities, such as sodium, cobalt, nickel, potassium, calcium, magnesium, manganese, silicon, and so on, did not transfer to the organic phase. Some entrainment contamination of the organic phase was observed. Beryllium loss in the raffinate was less than 0.020 g/L. Some of the raffinate, which contained approximately 1.5 *M* ammonium sulfate, was recycled to the ammonium alum crystallization step to take advantage of the common ion effect to further suppress the aluminum concentration in the extraction feed.

Stripping of the metal ions from the loaded organic phase was accomplished with a 3.0 to 3.5 *M* $(NH_4)_2CO_3$ solution in a two-stage mixer-settler operation. The stripping temperature was near 55 °C. The input organic-to-aqueous flow-rate ratio was 3.28 to 1, resulting in an aqueous pH of 9.2 and 9.0 for the first and second stages, respectively. Conversion of the organic phase to NH_4DEHP during stripping is accompanied by a 4% increase in volume. There is a corresponding shrinkage of the aqueous volume. Transfer of the cations was essentially complete in one stage, using a 10 min contact. The stripped

organic, free of all metallic ions, was recycled for reconditioning, in which part of it was converted to the hydrogen form by scrubbing with dilute H_2SO_4.

The strip solution, which is actually a slurry containing precipitated aluminum hydroxide, holds the beryllium and iron in solution. Heating the aqueous carbonate strip solution to 75 °C for approximately 45 min precipitated the iron, while the unaffected beryllium remained as a solution of tetraammonium beryllium tricarbonate. Approximately 2% of the beryllium co-precipitated with the aluminum and iron hydroxides. An additional 4 to 6 wt% of the beryllium was occluded in the filter cake.

The aluminum-iron sludge with its beryllium content was dissolved in sulfuric acid. The iron was extracted from this aqueous solution into a 10 wt% Primene JMT (Rohm and Haas Co.)-kerosene solution in a one-stage mixer-settler system. The beryllium and aluminum solution as the raffinate was recycled to the countercurrent decantation silica wash train.

The impurity level in the strip solution was further lowered by treatment with ammonium sulfide. It reduced the ferric iron, so ferrous sulfide precipitation followed. After filtration to remove the sulfides, chelation with the ammonium salt of ethylenediamine tetraacetic acid further reduced calcium and magnesium levels in the final hydroxide product. Entrainment of the aqueous feed remained the main source of minor impurities, which were effectively controlled by the chelating agent in the strip solution.

Beryllium hydroxide was recovered from the filtered, chelated ammonium beryllium carbonate solution by heating to 140 to 160 °C at 1.0 to 1.4 MPa (150 to 200 psi). Under these conditions, the tetraammonium beryllium tricarbonate dissociates into NH_3CO_2 and beryllium hydroxide. The reaction is rapid, taking only a few minutes to complete. A filterable beryllium hydroxide product was recovered. Starting with the beryllium sulfate feed solution from the beryl ore, overall yield of beryllium in the product was approximately 98%.

The solvent extraction process for recovery of beryllium from bertrandite ore leach solution resembles that for beryl, with some modifications. There is considerable difference in the concentrations of the key components. For the bertrandite leach solution, these become 0.70 g/L Be, 6.6 g/L Al, 1.5 g/L Fe, and 11 g/L fluoride. Focusing on the beryllium concentrations, the total volume in the Utah solvent extraction plant must be over four times as large as the combined organic and aqueous volumes in the Ohio facility. Consequently, the flow-rate ratio had to be shifted from 10:1 to 1:1 for organic-to-aqueous flow. The extraction train for bertrandite was expanded to ten stages. The operating temperature was stabilized at 55 °C, with a contact time of 17 to 20 min/stage.

Since all of the iron is extracted into the organic phase at both plants, the Utah solvent extraction plant must cope with eleven times as much total iron as the Ohio system. The $Fe(DEHP)_3$ forms a more stable complex, $Fe(DEHP)_3$ $(HDEHP)_3$, than the beryllium and aluminum analogs. This iron complex is very viscous and hinders phase separation. The viscosity problem was overcome by increasing the input HDEHP concentration to 0.50 *M*, limiting the organic loading to approximately 70 wt% of the total NH_4 branch sites by adjusting the organic-to-aqueous flow-rate ratio, and by increasing the operating temperature to 55 °C.

The bertrandite feed has much higher magnesium and manganese concentrations than the beryl leach solution. Neither was extracted into the organic phase at the low pH levels of approximately 1. The 2-ethylhexanol vaporized from the system under the revised operating temperature. No effort was made to restore its original concentration, since there was no significant loss of NH_4DEHP in the raffinate or into the ammoniacal strip solution.

The high levels of aluminum and fluorine concentrations in bertrandite promote the formation of AlF^{2+}, the extracted species. This behavior has two negative effects on the process. During stripping with ammonium carbonate, the amount of aluminum hydroxide is increased, causing an increase in loss as occluded beryllium. The fluorine moves forward with the ammonium beryllium carbonate solution and is precipitated with the beryllium hydroxide. Product containing 5 wt% F on a BeO basis was observed during the early periods of the Utah mill operations. Although the rate of extraction of beryllium was sacrificed, lowering the pH of the feed solution and the stage 1 aqueous to 1.0 or below was beneficial. The fluorine-aluminum ionic equilibrium was shifted toward the $(AlF_6)^{3-}$ ionic species, thereby limiting the amount of AlF^{2+} available for extraction. Thereafter, typical beryllium hydroxide product contained approximately 1.0 wt% F (BeO basis).

During the mid-1970s, part of the beryl equipment at the Elmore, Ohio, site of Brush

Wellman Inc. was moved to the Delta, Utah, mill. Beryl ore was treated by the initial steps of the Kjellgren-Sawyer process. As before, the ore was fused, quenched, heat treated, and ground to −200 mesh (74 μm). The ground ore was reacted with sulfuric acid and leached with thickener overflow. The leach solution was recovered from the silica sludge by a countercurrent decantation washing system. Ammonium alum crystallization with solution cooling and the subsequent processing steps to recover beryllium hydroxide were eliminated.

When available and economically practical, beryl leach solution with 11.0 g/L Be, 25 g/L Al, and 2 g/L Fe can be combined with the bertrandite leach solution as feed to the solvent extraction plant. Several benefits in the solvent extraction operation result from the mixed leach solution feed. The beryllium concentration of the blend can become several times that of the bertrandite feed alone, with no increase in iron concentration. With bertrandite leach solution, organic loading was limited to 1.0 g/L Be, above which the $Fe(DEHP)_3 \cdot 3HDEHP$ complex seized control through its adverse viscosity effect. With the blended feed, the organic phase could be loaded up to 1.66 g/L Be, with decreased concentration of the iron complex. At the same ratio of aqueous-to-organic volume flow rates, the higher maximum organic loading level could be achieved with as little as 5 wt% of the beryllium input from beryl. The blended leach solutions have a higher beryllium-to-fluorine concentration ratio, with a corresponding increase in the aluminum-to-fluorine concentration ratio. This combination improved the control of fluorine contamination of the final hydroxide product. Trace impurities of bertrandite origin were diluted by extraction feed blending so that product purity was enhanced.

Following the solvent extraction train, an extra tank was installed as a settler to decrease the volume of entrained impurity-rich aqueous moving forward with the loaded organic solvent. Stripping of the loaded organic with 3.0 to 3.5 *M* ammonium carbonate solution was the same as in the practice of the Maddox-Foos process at Elmore, Ohio. When the blend of beryl and bertrandite leach solutions became available, the increased loading of the organic phase gave as much as a 40% decrease in the ammonium-to-beryllium consumption ratio for the conversion to NH_4DEHP. The aluminum hydroxide slurry from stripping of the organic was heated to 75 °C for approximately 45 min to precipitate the iron. After filtering, ammonium sulfide treatment gave the reduction for precipitation of ferrous sulfide. Ethylenediammine tetraacetic acid solid was dissolved in the ammoniacal sulfide filtrate to chelate the metallic impurities.

The plant design had provided a preliminary hydrolyzer in which the 5.8 to 7.2 g/L Be strip solution was heated to approximately 95 °C. From a solution of the approximate tetraammonium beryllium tricarbonate composition, the solid phase was nearly quantitatively precipitated as beryllium basic carbonate, $2BeCO_3 \cdot Be(OH)_2$. Evolved carbon dioxide and ammonia were recovered for recycling. A subsequent high-temperature hydrolyzer, operating at 140 to 170 °C and 1.0 to 1.4 MPa (150 to 200 psi), had been incorporated in the plant design to basic carbonate, $2BeCO_3 \cdot Be(OH)_2$. Evolved carbon dioxide and ammonia were recovered for recycling.

A subsequent hydrolyzer, operating at 140 to 170 °C and 1.0 to 1.4 MPa (150 to 200 psi), had been incorporated in the plant design. In it, the beryllium basic carbonate solids were converted to beryllium hydroxide slurry, with additional evolution of carbon dioxide recovered for recycling. Heat released during the pressure let-down from the high-temperature hydrolyzer was used to heat the low-temperature hydrolyzer.

The strip solution obtained from bertrandite extraction and stripping contained several trace impurities, including uranium, zirconium, titanium, the yttrium rare earths, and thorium. The chelate complexes of the impurities were relatively unstable compared with the solubility product of their hydroxides and of ammonium diuranate. Consecutive operation of the two hydrolyzers precipitated a highly contaminated beryllium hydroxide in the high-temperature hydrolyzer. Fortunately, the carbonate complexes of the impurities were soluble, so rejection with the filtrate resulted by adding a slurry filtration step between the hydrolyzers. The wet beryllium basic carbonate filter cake was resuspended in water and decomposed in the high-temperature hydrolyzer. Except for fluorine content, the beryllium hydroxide product had much higher purity. The wet beryllium hydroxide cake had higher bulk density than wet beryllium basic carbonate solids, so a shipping volume advantage was also realized. Shipping of the wet beryllium hydroxide cake rather than a dried product gave protection against airborne dust evolution resulting from accidental spillage during transport or

during transfer into or within the Elmore, Ohio, operations.

7.8 Electrolytic Extraction of Beryllium

The electrolytic reduction of beryllium chloride in a molten sodium chloride medium is one of the available commercial processes for beryllium production with a relatively higher degree of purity. Besides the achievable purity, the electrolytic method also has the advantage of a low-temperature operation and avoids the use of expensive reductants in a thermal reduction process. Other low-temperature electrolytes that can be used are $BeCl_2$-6wt%LiCl (500 °C) [Schmidt 1926], BeF_2-24wt%KF (500 °C) [Moore et al. 1959], $BeCl_2$-20wt%BeF_2 (450 °C) [Kuvyrkin et al. 1958, Breusov et al. 1958], and BeF_2-30wt%LiF (500 °C) [Jones et al. 1962].

Since the commercial methods use beryllium chloride or fluoride as the starting material for producing beryllium, these electrolyte systems are attractive as an alternative solution, particularly to the process of magnesium thermal reduction of beryllium fluoride at above 1300 °C. Also, for the electrolytic method of beryllium production, these electrolytes can be used with minimal modification in equipment and only a 100 to 150 °C increase in temperature. The advantage of increasing the temperature can be readily seen from Table 7.1. The recovery of beryllium per unit mass of salt increases six- to eightfold, depending on the salt system, which can improve the process efficiency significantly since the salt must be removed for beryllium recovery and recycled back to the cell.

Table 7.1 Possible salt systems for beryllium electrowinning

Salt system	Cell temperature, °C	Composition, wt% Initial	Composition, wt% Final	Be/100 g salt, g
$BeCl_2$-BeF_2	450	80–20	25–75	8.25
BeF_2-LiF	500	70–30	30–70	10.94
BeF_2-KF	500	76–24	50–50	9.95
$BeCl_2$-LiCl	500	94–6	20–80	10.40
$BeCl_2$-NaCl	350	50–50	43–57	1.38

Source: Mishra et al. 1992

The removal of salt is necessary since, in all the cases, beryllium flakes will be formed, which will have to be separated from the salt, unless a liquid cathode is used. However, beryllium does not form any kind of alloy with common low-melting metals, such as tin, aluminum, lead, magnesium, zinc, and so on. and exhibits complete immiscibility. Very small solubility at high temperatures is observed with aluminum. Therefore, a liquid cathode application is only feasible in producing a stirred mixture of beryllium and other liquid cathode metal.

Table 7.1 shows the possible salt compositions that can be used and the amount of metal recoverable in a batch process. Alternatively, the process can be semicontinuous if a series of alternate anodes and cathodes are used and beryllium chloride or fluoride is continuously fed at a predetermined rate. The critical factors to be controlled are the electrolyte density, electrical conductivity, and beryllium separation. Table 7.2 lists some of the relevant physico-chemical parameters for these salt systems. Beryllium is the only water-insoluble phase in the process and hence can be separated out. Graphite anode and steel cathodes can be used in an inert or chlorine atmosphere. Carbon will serve as an inert anode at the cell temperature of 450 to 500 °C, but beryllium has a strong tendency to form carbide. A porous ceramic sheath could be placed around the graphite anode to prevent the formation of beryllium carbide [Mishra et al. 1992].

Electrical conductivity needs to be improved if the beryllium chloride-beryllium fluoride salt system is used. The $BeCl_2$-BeF_2 electrolyte will require additions of sodium, potassium, or lithium halides to improve its electrical conductivity, since the covalent bonding in beryllium halides tends to give poor conductivity. These additions can also help lower the melting point

Table 7.2 Physical-chemical properties of various relevant halides

Material	Melting point, K	Boiling point, K	Density, g/cm^3	$\Delta G°_f$, 750 K, kcal/mole halogen	Standard dissociation potential, V	Solubility hot water, g/100 cm^3	Mole wt
Be	1550	3243	1.85	. . .	. . .	Insoluble	9.01
$BeCl_2$	678	793	1.9	−91.6	0.475	Very soluble	79.9
BeF_2	1073(a)	. . .	1.99	−217.0	1.124	Complete	47.0
LiCl	878	1623	2.07	−166.0	0.860	130	42.4
LiF	1118	1949	2.64	−260.0	1.347	0.50	25.9
NaCl	1074	1686	2.17	−163.0	0.844	39.12	58.4
NaF	1266	1968	2.56	−236.0	1.228	8.5	42.0
KCl	1043	1773(a)	1.98	−174.0	0.902	56.7	74.6
KF	1131	1778	2.48	−235.0	1.218	Very soluble	58.1

(a) Sublimates. Source: Mishra et al. 1992

of the salt mixture. LiF and NaCl are known to lower the electrolyte density, melting point, and viscosity and can improve the electrical conductivity (Table 7.2). All these attributes are beneficial to a low-temperature salt electrolysis, when a light metal is cathodically produced. Therefore, additions of LiF and NaCl to the beryllium chloride-beryllium fluoride bath are desirable.

7.9 Cell Configuration

Figure 7.4 shows a possible cell configuration for the production of beryllium. The design shown consists of a cylindrical metallic shell, lined with a ceramic, as the primary electrolyte container. A cylindrical anode and a cylindrical ring steel cathode are concentrically placed. The heights of these electrodes can be adjusted within the melt to control the current densities. A ceramic hood placed over the anode is shown to provide a small suction for the anodic gases. Since most of the cathodically deposited beryllium will float at the top or will be mixed with the top layer of the salt, the salt tap hole is located at a height rather than at the bottom of the cell. The salt can be tapped and cooled to recover beryllium, and the cell can be charged with an additional amount of chloride, fluoride, and the additives, based on the salt analysis.

The cell can be operated at 450 to 500 °C, with an external heating arrangement of the cell. Both the tapped salt after beryllium removal and the anodic gases can be recycled. This type of cell arrangement can be used with essentially any combination of beryllium halide-alkali halide salt system.

7.10 Theoretical Rate Expression

Fundamental reaction rate theory can be applied to predict the rate of beryllium deposition on the cathode for a given current density and to determine the cell potential required. The analysis is based on the beryllium chloride-beryllium fluoride salt system, assuming that the fluoride will be an inert molten salt medium and that the beryllium chloride salt will dissociate to form beryllium flakes. The graphite anode will function as an inert anode, unlike the Hall cell, since chlorine or fluorine gas will not attack the anode to any appreciable extent at the process temperature of 450 to 500 °C.

The forward reactions in the beryllium electrowinning cell are:

(a) Chlorine anodic reaction:

$$BeCl_2 = Be^{2+} + 2Cl^- \quad \text{(electrolyte)} \qquad \text{(Eq 7.20)}$$

$$Be^{2+} + 2\,e^- = Be \quad \text{(cathode)} \qquad \text{(Eq 7.21)}$$

$$Cl^- = Cl_2 + 2\,e^- \quad \text{(anode)} \qquad \text{(Eq 7.22)}$$

$$BeCl_2 = Be + Cl_2 \quad \text{(cell reaction)} \qquad \text{(Eq 7.23)}$$

(b) Fluorine anodic reaction:

$$BeF_2 = Be^{2+} + 2F^- \quad \text{(electrolyte)} \qquad \text{(Eq 7.24)}$$

$$Be^{2+} + 2\,e^- = Be \quad \text{(cathode)} \qquad \text{(Eq 7.25)}$$

$$2F^- = F_2 + 2\,e^- \quad \text{(anode)} \qquad \text{(Eq 7.26)}$$

$$BeF_2 = Be + F_2 \quad \text{(cell reaction)} \qquad \text{(Eq 7.27)}$$

$$\text{Boundary condition: } R_{Be} = R_{Cl} + R_F \qquad \text{(Eq 7.28)}$$

where all the rates, R, are in moles/s.

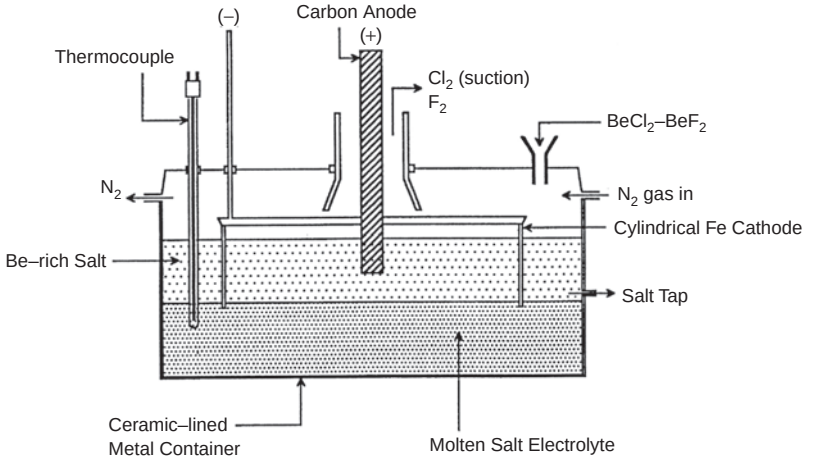

Fig. 7.4 Solid cathode electrolysis cell for beryllium production. Source: Mishra et al. 1992

Figure 7.5 shows the dependence of equilibrium cell potential on the beryllium chloride content of the salt. The dissociation of beryllium chloride (Eq 7.20), a desirable reaction in the present cell, is thermodynamically feasible up to a very low beryllium chloride content ($<10^{-36}$ wt%) in the salt, below which fluoride also can be thermodynamically dissociated. Therefore, it is possible to dissociate all the beryllium chloride in an inert beryllium fluoride salt medium. Accordingly, the boundary condition would reduce to:

$$R_{Be} = R_{Cl_2} \qquad \text{(Eq 7.29)}$$

Calculation of R_{Be} (based on Eq 7.28 and 7.29) is:

$$\nu_{fwd} = \nu_o \cdot \exp\,[-(\Delta G^* + \Delta G')/RT] \qquad \text{(Eq 7.30)}$$

$$\nu_{bkwd} = \nu_o \cdot \exp\,[-\Delta G^*/\mathrm{RT}] \qquad \text{(Eq 7.31)}$$

where ν_o is the atomic vibrational frequency, s^{-1}:

$$\nu_{net} = \nu_{fwd} - \nu_{bkwd} = \nu_o \exp\,[-\Delta G^*/RT] \exp\,[[-\Delta G'/RT]-1] \qquad \text{(Eq 7.32)}$$

$$\nu_{net} = \nu_o \exp\,[\Delta S^*/R] \exp\,[-\Delta H^*/RT] \exp\,[[-\Delta G'/RT]-1] \qquad \text{(Eq 7.33)}$$

where ν_{net} is the net jump frequency of beryllium ions that produce metal on the cathode (Fig. 7.6), and ΔG^* is the free energy activation barrier/mole. The driving force/mole, $\Delta G'$, can be expressed as:

$$\Delta G' = +\, n\mathrm{F}\eta_{Be} + RT \ln\,[[Be]/[Be^{++}]] \qquad \text{(Eq 7.34)}$$

$$\eta_{Be} = E^c_{appl} - E_{Be} \qquad \text{(Eq 7.35)}$$

$$E_{Be} = E_o^{Be} - [RT/n\mathrm{F}] \ln\,[[Be]/[Be^{++}]] \qquad \text{(Eq 7.36)}$$

where η_{Be} is the cathodic overpotential in (−) volts, E^c_{appl} is the cathodic applied potential, E_o^{Be} is the standard beryllium half-cell potential (−1.85 V), and E_{Be} is the equilibrium beryllium half-cell potential:

$$\exp[-\Delta G'/RT] = \exp[-n\mathrm{F}\eta_{Be}/RT] \cdot \exp[\ln\,[Be^{2+}/Be]] = [Be^{2+}]/[Be]\exp[-n\mathrm{F}\eta_{Be}/RT] \qquad \text{(Eq 7.37)}$$

where nF is $2 \times 96{,}500$ A-s/mol, R is the universal gas constant (8.314 J/K-mol), and T is the cell temperature at 450 °C (723 K):

$$\begin{aligned} R_{Be} = \text{mole/s} &= \nu_{net} / \text{Average No.} = 1.66 \times 10^{-24} \cdot \nu_{net} \\ &= 1.66 \times 10^{-24}\, \nu_o \cdot \exp\,[\Delta S^*/R] \\ &\quad \cdot \exp\,[-\Delta H^*/RT]\,[\exp\,[[-\Delta G'/RT] - 1] \\ &= 1.66 \times 10^{-24}\, \nu_o \cdot \exp\,[\Delta S^*/R] \\ &\quad \cdot \exp\,[-\Delta H^*/RT] \cdot [[Be^{2+}]/[Be] \\ &\quad \exp\,[-n\mathrm{F}\eta_{Be}/RT] - 1] \end{aligned}$$

$$R_{Be} = A' \cdot \exp\,[-n\mathrm{F}\eta_{Be}/RT] \qquad \text{(Eq 7.38)}$$

where A' is a coefficient $= 1.66 \times 10^{-24}\ \nu_o \cdot \exp\,[\Delta S^*/R] \cdot \exp\,[-\Delta H^*/RT] \cdot [[Be^{2+}]/[Be]$ in moles/s, and $-n\mathrm{F}\eta_{Be}/RT \gg 1$.

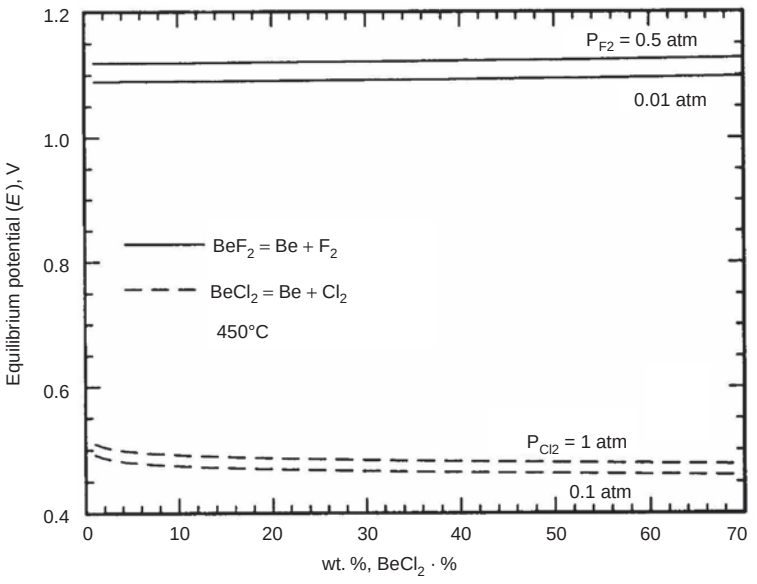

Fig. 7.5 Dependence of the equilibrium cell potential with the beryllium chloride content of the salt. Source: Mishra et al. 1992

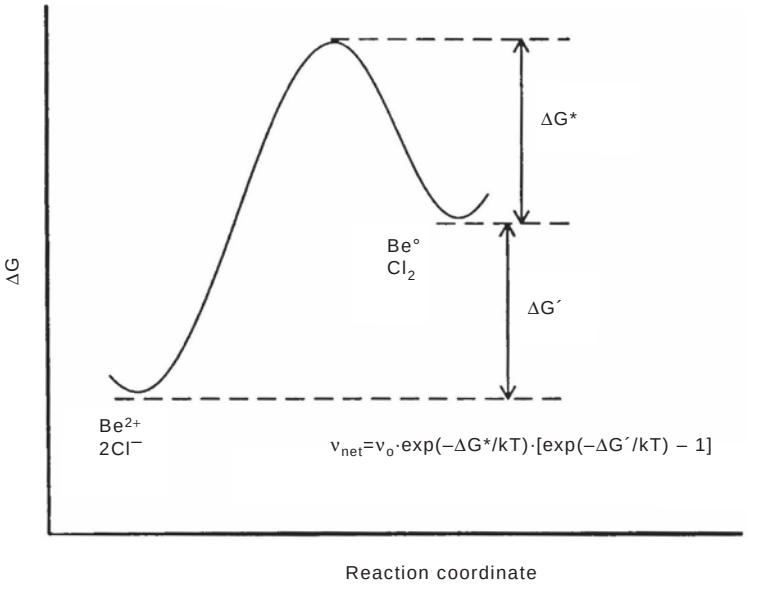

Fig. 7.6 Activated complex plot for beryllium reduction. Source: Mishra et al. 1992

For a cell current efficiency of 100% and a given current of "*I*" amperes:

$$R_{Be} = 5.2 \times 10^{-6} \cdot I \text{ mole/s} \qquad \text{(Eq 7.39)}$$

$$R_{Be} = 5.2 \times 10^{-6} \cdot i_c \cdot C_{area} \qquad \text{(Eq 7.40)}$$

where i_c is the cathodic current density in A/cm^2, and C_{area} is the cathodic area. Combining Eq 7.38 and 7.40:

$$i_c = A^* \cdot \exp\left[-n\mathrm{F}\eta_{Be}/RT\right] \qquad \text{(Eq 7.41)}$$

where A^*, in A/cm^2, is a new coefficient and incorporates the cathodic area. Equation 7.41 is the familiar Tafel equation and can be expressed in the form:

$$\log i_c = \beta - n\mathrm{F}\eta_{Be}/RT \qquad \text{(Eq 7.42)}$$

where $\beta = \log A^*$. Equation 7.42 can be rearranged as:

$$-\eta_{Be} = \alpha \log i_c + \beta' \qquad \text{(Eq 7.43)}$$

where α is $RT/n\mathrm{F} = 0.0312$ V; β' is $-\alpha \cdot \beta$; and β is dependent on the atomic jump frequency of beryllium ions, the free energy activation barrier, ΔG^*, and the cathodic area. Thus, β is a constant at a given temperature and cathode area. For a given cathodic current density, i_c, (i.e., rate of beryllium deposition), η_{Be} can be thus calculated.

A similar analysis can be done to develop a rate equation for the anodic reaction of chlorine evolution, and an equation similar to Eq 7.41 can be obtained:

$$R_{Cl_2} = A'' \cdot \exp\left[n\mathrm{F}\eta_{Cl_2}/RT\right] \qquad \text{(Eq 7.44)}$$

where A'' is a coefficient $= 1.66 \times 10^{-24}\ \nu_o \cdot \exp\left[\Delta S^*/R\right] \cdot \exp\left[-\Delta H^*/RT\right][[\mathrm{Cl}^-]^2/p\mathrm{Cl}_2]$ in moles/s:

$$R_{Cl_2} = 5.2 \times 10^{-6} \cdot I \text{ moles/s} \qquad \text{(Eq 7.45)}$$

$$R_{Cl_2} = 5.2 \times 10^{-6} \cdot i_a \cdot A_{area} \qquad \text{(Eq 7.46)}$$

where i_a is the anodic current density in A/cm^2, and A_{area} is the anodic area.

Combining Eq 7.44 and 7.46 yields:

$$i_a = A^{**} \exp\left(n\mathrm{F}\eta_{Cl_2}/RT\right) \qquad \text{(Eq 7.47)}$$

where A^{**}, in A/cm^2, is a new coefficient incorporating the anodic area. From Eq 7.47:

$$\log i_a = \beta^* + n\mathrm{F}\eta_{Cl_2}/RT \qquad \text{(Eq. 7.48)}$$

where $\beta^* = \log A^{**}$. Equation 7.48 can be rearranged as:

$$\eta_{Cl_2} = \alpha^* \log i_a + \beta'' \qquad \text{(Eq 7.49)}$$

where α^* is $RT/n\mathrm{F} = 0.0312$ V; β'' is $-\alpha^* \cdot \beta^*$; and β^* is a function of the atomic jump fre-

quency of chlorine ions, the free energy activation barrier, ΔG^*, and the anodic area. Thus, β^* is a constant at a given temperature and anode area. For a given anodic current density, i_a, (i.e., rate of chlorine evolution), η_{Cl_2} can be thus calculated.

Equations 7.43 and 7.49 have been plotted in Fig. 7.7. The required applied potential of the cell can be calculated for a given applied current density for the two electrodes (Fig. 7.7). For total applied potential:

$$E_{appl} = E_{Be} + E_{Cl_2} + \eta_{Be} + \eta_{Cl_2} + IR_{drop\ (salt)} \quad \text{(Eq 7.50)}$$

where $E_{Be} + E_{Cl_2} = E_o^{Be} + E_o^{Cl_2} + 0.0173 \log Q$, and η_{Be} and η_{Cl_2} are given by Eq 7.43 and 7.49:

$$\eta_{Be} + \eta_{Cl_2} = \log [i_a^{\alpha^*} / i_c^{\alpha}] + [\beta'' - \beta'] \quad \text{(Eq 7.51)}$$

The current densities, i_c and i_a, and therefore the cell efficiency or the beryllium deposition rate is not only driven by the applied overpotentials, η_{Be} and η_{Cl_2}, but the respective anodic and cathodic areas, A_{area} and C_{area}. In other words, the cell behavior can be controlled by controlling the electrode configurations and applied potential. Under standard condition, that is, $Q = 1$, the applied cell potential can be accurately calculated by Eq 7.50. The term $\log [i_a / i_c]$ in Eq 7.51 translates to a function of the ratio of cathode to anode areas for a given applied current, I. However, as discussed earlier, $\beta'' - \beta'$ also has an equal but opposite dependency on the respective electrode areas, and therefore, the overpotentials are independent of the electrode areas. In a practical situation in a cell, where the electrode areas are different, the overpotential can be determined by using Fig. 7.7. Equation 7.50 completely describes the cell reactions. The voltage components can be described for the condition of a graphite anode application. In Eq 7.50, the following values can be substituted to align with Eq 7.51 and to calculate the applied potential:

$$E^\circ_{Be} + E^\circ_{Cl_2} = 0.475\ \text{V}$$
$$Q = [a_{Be} \cdot p_{Cl_2} / [Be^{2+}] \cdot [Cl^-]^2] \quad \text{(Eq 7.52)}$$

The activity of beryllium ions, a_{Be}, can be assumed as unity, since both the chloride and

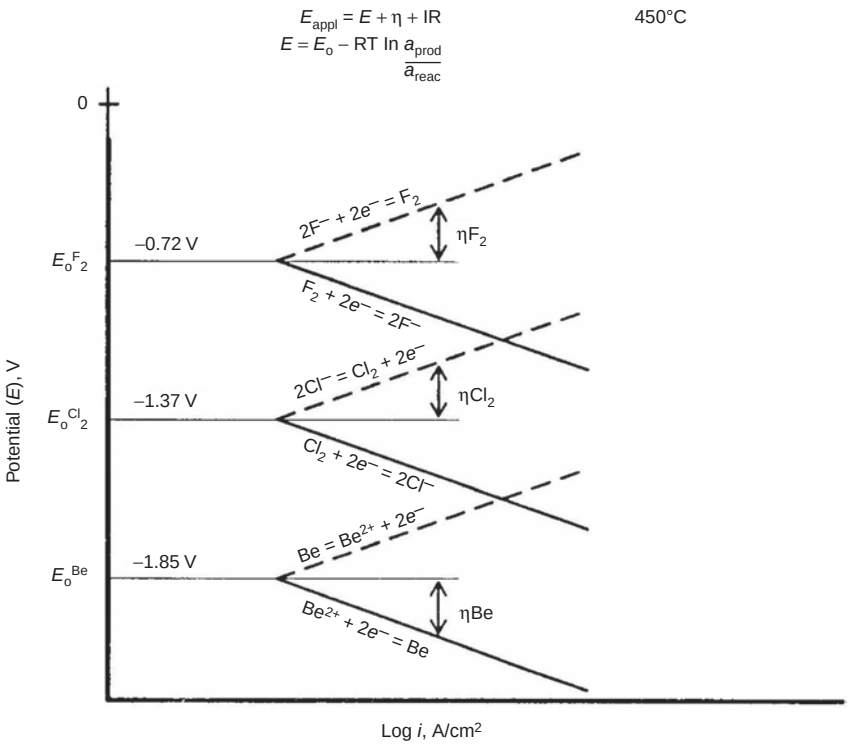

Fig. 7.7 Mixed-potential diagrams for chlorine, fluorine, and beryllium. Source: Mishra et al. 1992

fluoride electrolyte provide the source for beryllium ions. The activity of beryllium metal will be determined by the solubility of the metal in the salt, which is known to be insignificant. Beyond the solubility limit of beryllium in the salt, if any, the metal will have an activity of unity. Therefore, the constitutive constant, *Q*, will depend on the efficiency of removal of chlorine or fluorine gas from the anode and will be a function of time. The removal of the anodic gases is controlled by the flow of inert gas within the cell enclosure at 1 atm pressure. This discussion therefore suggests that a near total depletion of chlorine ions (if beryllium chloride is not intermittently added) from the electrolyte can raise the equilibrium potential of the cell to a level where the evolution of fluorine becomes thermodynamically feasible, and fluorine gas would then start to evolve on the anode (Fig. 7.7). In an event where fluorine depletion also takes place, that is, complete dissociation of the electrolyte, the cell will effectively shut off. The reaction between carbon and chlorine gas is not feasible at 450 °C. However, the evolution of fluorine can be used as an indication for charging beryllium chloride. As shown in Table 7.1, the cell can be operated in the range of 80 wt% beryllium chloride to 20 wt% beryllium chloride at 450 °C maintaining a complete liquid phase, particularly with additions of sodium chloride and lithium fluoride. The dissociation of other alkali fluoride or chloride added to the salt bath for conductivity, density, or viscosity adjustment is not possible at the low applied cell potentials.

7.11 Electrorefining of Beryllium

The fabrication of beryllium articles from hot pressed block converts approximately 25 wt% of the starting material into the product. The remainder becomes machining chips, sawdust, and scrap. The waste material can be upgraded by physical processing such as degreasing, magnetic separation, and sink-float density recovery. For many years, the upgraded waste was converted to powder, which was blended with pebble-grade beryllium powder for recycling to hot pressing. Metallic iron and aluminum, carbon, and beryllium oxide impurities accumulated, resulting in progressively lower-purity hot pressed blocks. Through the use of higher-purity beryllium blocks, it was postulated that the brittleness of beryllium may be overcome. In this way, quality may be achieved for advanced applications.

Conversion of impure beryllium scrap to ultrapure beryllium flake was achieved by electrorefining in nonaqueous, fused salt melts. Prior to 1965, commercial electrorefining operations were conducted in the United States by General Astrometals Corporation and by Beryllium Metals & Chemical Corporation. For proprietary reasons, few details have been recorded about the commercial operations.

The problems and limitations of the electrorefining process tested at the U.S. Bureau of Mines have been described by Wong et al. [1962]. Their laboratory-scale study was expanded by Schimmel [1962]. In the U.S. Bureau of Mines work, the cell was charged with 22.7 kg (50 lb) LiCl-KCl at a molar ratio of 1.44, the eutectic composition. The system was evacuated and dried at 200 °C for 24 h, followed by 24 h at 400 °C. The system was backfilled with helium and heated to 650 °C. The beryllium chloride component of the bath was introduced in situ by reacting anhydrous HCl gas with metallic beryllium in a graphite tube partially immersed in the molten salt. Beryllium chloride passed from the tube and dissolved in the melt. When the target beryllium chloride concentration had been reached, the chloridizing apparatus was removed, and the cell temperature was lowered to 450 or 550 °C. A 19 mm (¾ in.) diameter iron cathode rod was inserted. A 63.5 mm (2½ in.) diameter iron basket containing 6.4 to 12.7 mm (¼ to ½ in.) beads or turnings of technical-grade beryllium became the anode. Atmospheric contamination, especially by moisture, in the cell must be avoided.

Upon completion of the deposition cycle, the cathode was raised just above the melt and allowed to drain. The cathode deposit was raised into a receiving chamber and cooled to ambient temperature. Outside the cell, the deposit was stripped from the cathode, crushed to free the flakes, leached in a dilute nitric acid solution, filtered, washed with water, rinsed with acetone, and dried in a hood.

The beryllium chloride concentration at the three levels of 3.5, 10.3, and 16.5 mol% was among the variables studied. Depositions were made at 450 or 550 °C, with current densities of approximately 3800 A/m^2 (350 A/ft^2). Deposited metal was steel gray and generally in clusters of thin, flat, platelike crystals or long fibers of platelets. Beryllium chloride of high concentration in the bath and low current density favored the formation of clusters of the flat, platelike crystals. Low concentration of beryllium chloride

and high current density favored the formation of fibers of the platelets. Metal deposited at 550 °C adhered to the cathode better than that produced at the lower temperature. Less electrolyte was entrained in the higher-temperature deposit because of improved drainage. Cathode current efficiencies, based on the quantities of metal recovered from the cathode, were in the range of 70 to 90%.

The product was remarkably improved in purity from the 94%-grade beryllium anode feed. Wong et al. [1962] observed a decrease in oxygen content from 3.27% to an average of 0.04%. magnesium content fell from 2.66 to 0.0003 wt% or less. Aluminum, nickel, chromium, and cobalt contents were lowered below their calibration limits of detection by spectrographic analysis. Iron content was reduced from 0.32 wt% in the feed to 0.03 wt% in the flakes, while silicon was lowered from 0.1–1 to 0.004 wt%. Carbon increased from 0.011 to 0.02–0.08 wt%, which was attributed to the use of a graphite crucible. This conclusion is confirmed by Schimmel's reduction of carbon to 260 to 800 ppm using a glass or stainless steel container [Schimmel 1962]. It was necessary to melt the flakes to lower the lithium, potassium, and chlorine contents so the metal would be acceptable for nuclear applications. The expected gains in mechanical properties of beryllium were not realized, so commercial expansion of electrorefining of beryllium was not encouraged.

REFERENCES

Bayliss, R.K., and Derry, R., 1963. "Further Studies of the Breakdown of Beryl and Beryl Concentrates by Fusion Methods," National Chemical Laboratory

Blainey, A., Johnston, T.L., and Jones, J.W.S., 1954. "The Sintering of Beryllium Powder Prepared from Electrolytic Flake," A.E.R.E. M/R-1442, Gt. Brit. Atomic Energy Research Establishment, Harwell, Berks, England

Breusov, O.N., Novoselova, A.V., and Simanov, Yu.P., 1958. Thermal and X-Ray Analysis of the CsF-BeF_2 System and Its Interrelations with the MeF-BeF_2 Systems, *Dokl. Akad. Nauk SSSR*, Vol 118, p 935–937

Copaux, M.H., 1919. *C.R. Acad. Sci., Paris*, Vol 163, p 610

Crocker, L., Dannenberg, R.O., and Bridges, D.W., 1963. "Acid Leaching of Beryllium Ore from Spor Mountain, Utah," Report BM-RI-6322, U.S. Bureau of Mines

Darwin, G.E., and Buddery, J.H., 1960, *Beryllium*, Academic Press Inc., New York, NY

Fischer, H., and Peters, N., 1933. Untersuchungen uber die Reduzierbarkeit von Berylliumchlorid mit Metallischem Aluminum," *Metall. Erz.*, Vol 30, p 390–391

Hardy, C.J., Greenfield, B.F., and Scargill, D., 1961. The Solvent Extraction of Beryllium from Aqueous Solutions of Mineral Acids by Alkyl Esters of Phosphoric Acid, *J. Chem. Soc*., p 174–182

Hopkins, B.S., and Meyer, A.W., 1924. The Electrolytic Production of Beryllium, *Trans. Am. Electrochem. Soc*., Vol 45, p 475–480

Hyde, K.R., Robinson, P.L., Waterman, M.J., and Waters, J.M., 1961a. Reaction of Beryl with Sodium Fluorosilicate Used in Extracting Beryllium from the Mineral, *Bull. Inst. Min. Metall*., Vol 70, p 397–406

Hyde, K.R., Robinson, P.L., Waterman, M.J., and Waters, J.M., 1961b. Structural Evidence on the Beryl-Sodium Fluorosilicate Reaction, *J. Inorg. Nucl. Chem*., Vol 19, p 237–244

Ivanov, E.S., and Shmelev, V.M., 1958. Melting and Casting of Beryllium. Report A/CONF. 15/P/2048, also *Proc. of Second U.N. Conf. on Peaceful Uses of Atomic Energy*, Vol 4, p 302

Jaeger, G., 1950. On the Winning of Beryllium, *Metall*., Vol 4, p 183–191

Jones, L.V., Etter, D.E., Hudgens, C.R., Huffman, A.A., Rhinehammer, T.B., Rogers, N.E., Tucker, P.A., and Wittenberg, L.J., 1962. Phase Equilibria in the Ternary Fused Salt System Lithium Fluoride-Beryllium Fluoride-Uranium Fluoride, *J. Am. Ceram. Soc*., Vol 45 (No. 2), p 79–83

Kawecki, H.C., 1943. Process for Extracting Beryllium Compounds from Silicate Minerals, U.S. Patent 2,312,297

Kawecki, H.C., 1946. The Production of Beryllium Compounds Metal and Alloys, *Trans. Electrochem. Soc*., Vol. 89, p 229–236

Kjellgren, B.R.F., 1946. The Production of Beryllium Oxide and Beryllium Copper, *Trans. Electrochem. Soc*., Vol 89, p 247–261

Kramer, D.A., 1990. Beryllium, Annual Report, *Minerals Yearbook, 1990*, Bureau of Mines, U.S. Department of the Interior, Washington, D.C.

Kramer, D.A., 1991. Beryllium, *Annual Report*, 1990, Bureau of Mines, U.S. Department of the Interior, Washington D.C.

Kuvyrkin, O.N., Breusov, O.N., and Novoselova, A.V., 1958. Thermal Analysis of the System

$BeCl_2$-BeF_2, *Auch. Dok. Vysshei Shkoly Khim. Khim. Tekhnol*., Vol 4

Lundin, H., 1945. Production of Beryllium Oxide, *Trans. Am. Inst. Chem. Eng*., Vol 41, p 671

Maddox, R.L., and Foos, R.A., 1966. Process for Producing Basic Beryllium Metal of High Purity, U.S. Patent 3,259,456

Mishra, B., Olson, D.L., and Averill, W.A., 1992. Application of Molten Salts in Pyrochemical Processing of Reactive Metals, *Molten Salts*, Vol 92-16, R.J. Gale, G. Blomgren, and H. Kojima, Ed., Electrochemical Society p 184–203

Mitchell, D.L., Nieweg, R.G., Ledford, J.A., Richen, M.J., Burton, D.A., Harder, R.V., Watson, L.E., and Thomas, R.L., 1989. "Beryllium Electrorefining," Report RFP-4188, Rockwell International Corp., Rocky Flats Plant, Golden, CO

Moore, R.E., Barton, C.J., Grimes, W.R., Meadows, R.E., Bratcher, LM., White, G.O., McVay, T.N., and Harris, L.A., 1959. *Phase Diagrams of Nuclear Reactor Materials*, ORNL-2548, R.B. Thoma, Ed., Oak Ridge National Lab., p 37

Novoselova, A.V., 1934. *J. Gen. Chem. USSR*, Vol 4, p 1206–1210

Novoselova, A.V., 1959. Beryllium Fluorides and Fluoroberyllates, *Usp. Khim*., Vol 28, p 33–43

Potvin, R., and Farnham, G.S., 1946. The Chloride Process for Production of Beryllium in Germany, *Trans. Can. Inst. Mining Metall*., Vol 49, p 525–538

Sawyer, C.B., and Kjellgren, B.R.F., 1935. Beryllium and Aluminum Salt Production, Canadian Patent CA 354,080

Schimmel, F.A., 1962. "Reclamation of Beryllium Chips by Electrolysis," Atomic Energy Comission

Schmidt, J.M., 1926. Analyse Thermique des Systemses Binaires Formes par le Chlorure de Glucinium Anhydre avec Divers Chlorures Metalliques, *Bull. Soc. Chem*., Vol 39, p 1686–1703

Schofield, T.H., 1954. Research Notes: An Apparatus for Heat-Treatment and Quenching Small Specimens in a Vacuum from High Temperature, *Proc. Phys. Soc., Section B*, Vol 67 (No. 11), p 845–847

Schwenzfeier, C.W., Jr., 1964. Beryllium and Beryllium Alloys, *Kirk-Othmer Encyclopedia of Chemical Technology*, Interscience, Vol 3, NY

Sloman, H.A., 1932. Researches on Beryllium, *J. Inst. Met*., Vol 49, p 365–388

Spitzin, V., 1930. Das Chlorieren von Oxyden und ihren Gemischen mit Kohlenstoff, *Z. Anorg. Chem*., Vol 189, p 337–366

Vivian, A.C., 1926. Beryllium, *Trans. Faraday Soc*., Vol 22, p 211–225

Walsh, K.A., 1979. Extraction, *Beryllium Science and Technology*, Vol 2, D.R. Floyd and J.N. Lowe, Ed., Plenum Press, NY, p 1–10

Wells, R.A., Everest, D.A., and North, A.A., 1963. Solvent Extraction, Recovery, and Purification of Beryllium from Ores, *Nucl. Sci. Eng*., Vol 17, p 259–267

Wöhler, F., 1828b. Sur le Glucinium et L'Yttrium; *Ann. Chim. (Phys.)*, Vol 39, p 77–84

Wöhler, F., 1828a. *Pogg. Ann*., Vol. 13, p 577–582

Wong, M.M., Campbell, R.E., and Baker, D.H., Jr., 1962. "Electrorefining Beryllium. Studies of Operating Variables," Report BM-RI-5959, U.S. Bureau of Mines

SELECTED REFERENCES

- Eigeles, M.A., and Leviush, I.T., 1958. "Flotability of Beryl," Paper 2065, Proceedings of the Second United Nations Conference on the Peaceful Uses of Atomic Energy (Geneva)
- Morana, S.J., 1965. The Extraction of BeO, *Beryllium: Its Metallurgy and Properties*, H.H. Hausner, Ed., University of California Press, Berkeley, CA, p 7–16
- Opatowski, R.S., 1941. Process for the Preparation of Beryllium Compounds, U.S. Patent 2,209,131
- Runke, S.M., 1954. "Petroleum Sulfonate Flotation of Beryl," Report BM-RI-5067, U.S. Bureau of Mines, Rapid City, SD
- Srinivasan, N.R., and Aswath, H.S., 1956. Studies on the Beneficiation of Low Grade Beryl, *J. Indian Inst. Sci. B*, Vol 38, p 135–142

Beryllium Chemistry and Processing, p 93-106
By Kenneth A. Walsh
Edited by Edgar E. Vidal, Alfred Goldberg,
Edward N.C. Dalder, David L. Olson, and Brajendra Mishra

CHAPTER 8

Chemistry of Beryllium

Kenneth A. Walsh, Brush Wellman Inc., Retired
Edgar E. Vidal, Brush Wellman, Inc.
Brajendra Mishra, Colorado School of Mines

8.1 General Chemical Character of Beryllium

Beryllium has an atomic number of four and a gram atomic weight of 9.013 g. This element lies in the first short period of the periodic table at the top of the group IIA column, known as the alkaline earths and including magnesium, calcium, strontium, barium, and radium. All these elements have an electronic ground state of $1s^2$ $2s^2$, and below this ns^2 shell, every element has a complete inert gas core of electrons. With the s shell completed, the chemistry of beryllium and the other alkaline earth elements is dependent on the ns^1np^1 excited state, which allows for a valence of two. Beryllium is usually classified as having ionic bonding, but the bonds in many beryllium compounds have considerable covalent bonding character. This behavior is consistent with its high electronegativity (1.5 eV). Halides react with beryllium and produce gaseous monomeric molecules, which are known as linear molecules. Because these molecules have mixed bonding character (ionic and covalent), they are classified as electron-deficient molecules, having insufficient electrons present to form the expected number of two electron bonds. Examples of such beryllium electron-deficient molecules are beryllium hydride and the beryllium alkyls. The energy difference between the ground state $1s^2$ $2s^2$ and the excited state $1s^2$ $2s^1$ $2p^1$ is 62 kcal (260 kJ), which is significantly less than the 460 kcal (1925 kJ) needed to promote the electron in the helium atom from the 1s to the 2s state. Table 4.1 gives some of the basic physical properties of beryllium and the other alkaline earths. All of the alkaline earths have primarily a close-packed hexagonal structure. Beryllium has a hexagonal alpha phase with room-temperature (20 °C, or 68 °F) lattice parameters of a = 2.286 Å, c = 3.583 Å, and c/a = 1.568.

Beryllium is a gray color and is similar to aluminum in resisting oxidation. Its oxide is less dense than the metal, which allows for a surface oxide that prevents the metal from further attack.

Beryllium also forms compounds in which it shares extra electrons and achieves the excited electronic state of sp^3, which forms tetrahedral hybrid bonds. These shared electron bonds cause some beryllium compounds to have considerable polarity, which is illustrated as:

$$Be^{\delta+} - X^{\delta-}$$

The polarized complexes give some beryllium compounds an ionic character. Beryllium is not capable of expanding its coordination number to six, like other alkaline earth elements. This behavior is the result of the small size of the beryllium atom and the inaccessibility of the 3d orbital, which is required to achieve $s^1p^3d^2$ hybridization. This hybridization electron characteristic is a feature of all the other elements of the first short period of the periodic table.

The beryllium ion, Be^{2+}, occurs in hydrated form in aqueous solution and in hydrated beryllium salts. A hydrous beryllium compound is only partly ionic. Beryllium exhibits an ionic radius of 0.31 Å, resulting in a high charge-to-radius ratio

(z/r) of 6.45 [Pauling 1960]. With this high z/r value, beryllium compounds have a covalent character. The z/r value compares well with aluminum (6.00) and is sharply different from lithium (1.67), magnesium (3.07), and calcium (2.02). Beryllium is chemically similar to aluminum. A comparison of the first and second ionization potentials (Table 8.1) between beryllium and other close-packed hexagonal elements suggests that beryllium should show similar chemical behavior to zinc [Pfeiffer et al. 1951]. This similarity to zinc is most likely due to the polarizability of the eighteen-electron subshell of the transition-metal-type Zn^{2+} ion ($3s^2\ 3p^6\ 3d^{10}$) being greater than that of the inert-gas-type Ca^{2+} ion ($3s^2\ 3p^6$). Apparently, the total polarization interaction of Zn^{2+} and an anion is nearly as strong as the interaction between an anion and the less polarizable but more strongly polarizing Be^{2+} ion, and greater than the interaction between the Ca^{2+} ion and an anion.

When the first ionization potential of beryllium is compared with other elements across the short period of the periodic table, the influence of the electronic structure of beryllium can be better understood. The first ionization potential of lithium (5.34 eV) is less than beryllium because both electrons are 2s; however, beryllium has a greater nuclear charge than lithium, making it harder to extract an outer electron from the atom. The first ionization potential of beryllium is also larger than that of boron (8.30 eV) because the boron electron is in the 2p orbital and experiences a greater screening effect from the nuclear charge by the closed 2s shell, which is sufficiently large to overcome the effect of the increased nuclear charge. Advancing through the period to carbon and nitrogen, the 2p orbitals continue to be filled with electrons, and, with the increased nuclear charge and uncharged 2s screening, the ionization potential increases to 11.285 and 14.545 eV, respectively.

Table 8.1 Ionization potentials of selected elements, in eV

Element	I	II	III
Be	9.3227	18.21116	153.89661
Mg	7.64624	15.03528	80.1437
Ca	6.11316	11.87172	50.9131
Zn	9.3942	17.96440	39.723
Sr	5.6949	11.03013	42.89
Cd	8.9938	16.90832	37.48
Ba	5.21170	10.00390	. . .
Hg	10.43750	18.756	34.2

Note: 1 eV = 8065.541 cm^{-1}. Source: Lide 2002

8.1.1 Reactions of Metallic Beryllium

Freshly exposed surfaces of bulk beryllium metal exhibit a bright, silvery color. Even after 40 years of exposure in a normal atmosphere, the metal did not tarnish. An oxide surface film protected the metal from further attack, because the volume of beryllium oxide is greater than that of the metal from which it is formed [Everest 1973].

Sulfuric acid and hydrochloric acid dissolve beryllium and cause the evolution of hydrogen. The metal is not attacked by cold nitric acid up to 6 *M* concentration. It is reported in the literature that beryllium is dissolved by dilute nitric acid [Everest 1973]. When dissolving beryllium metal samples in nitric acid for chemical analysis, a trace of halide or sulfate ion promotes dissolution. It is suspected that the trace of residual chloride present in electrowon beryllium flakes was responsible for the reported reactivity with nitric acid. Beryllium is rapidly dissolved by aqueous ammonium bifluoride:

$$2\ NH_4HF_2 + Be = (NH_4)_2BeF_4 + H_2 \qquad \text{(Eq 8.1)}$$

The metal is also dissolved in an aqueous solution of sodium or potassium hydroxide, with the generation of hydrogen and the formation of a beryllate:

$$2\ NaOH + Be = Na_2BeO_2 + H_2 \qquad \text{(Eq 8.2)}$$

The concentration of the alkaline hydroxide solution determines whether this reaction takes place in the cold condition or at higher temperature. Organic acids, such as tartaric acid and citric acid, react initially with beryllium metal until a protective film of oxyhydrate is formed [Illig 1932]. The metal does not react with aqueous ammonia.

At elevated temperatures, beryllium has a great affinity for oxygen. Research [Beaver, 1955a, b] found that heating bulk beryllium in air above 700 °C (1290 °F) causes spallation of a gray-black powder. Heating this powder at higher temperature in air results in a weight gain such that the original powder must have been a mixture of metal and oxide. A mixture of oxide and nitride would be white. As a deoxidizing agent, beryllium readily reduces borates, silicates, and phosphates at red heat to form beryllium oxide [Illig 1932]. The direct action of ammonia or nitrogen on beryllium metal at 1100 °C (2010 °F) yields beryllium nitride, Be_3N_2, a white crystalline material [Beaver 1955a, b].

8.1.2 Beryllium Hydroxide and Basic Carbonate

In total commercial volume, beryllium hydroxide is the most important beryllium compound. It is the product of the extraction processes used for beryl, helvite, and bertrandite ores. This beryllium hydroxide has variable degrees of purity. It becomes the intermediate for the production of metallic beryllium, ceramic-grade beryllium oxide, and beryllium-containing alloys as commercial products.

8.1.3 Forms of Beryllium Hydroxide Precipitates

Beryllium hydroxide precipitates from beryllium salt solutions in three forms: a gelatinous material and two crystalline forms. Most common is the gelatinous amorphous form obtained when the stoichiometric quantity of aqueous alkali is added to a cold beryllium-salt solution. The amorphous material transforms into one of the two crystalline forms on aging, which is accelerated by boiling the slurry. The stable orthorhombic crystalline form and the metastable tetragonal modification are formed directly by precipitation from a hot solution or by boiling a beryllate solution.

Seitz et al. [1950] showed that boiling a beryllate solution can yield either polymorph, depending on hydrolytic conditions. Precipitation of the denser orthorhombic form is preferred, because it is more readily filtered than the lighter tetragonal variety. Mercer and Miller [1966] showed that only the orthorhombic form of $Be[OH]_2$ is precipitated by boiling a beryllate solution containing more than 1.0 *M* free NaOH. X-ray diffraction examination of the orthorhombic $Be(OH)_2$ by Mercer and Miller [1966] gave a crystal structure with a = 4.61 Å, b = 7.02 Å, and c = 4.52 Å. The Be^{2+} ions are surrounded tetrahedrally by OH^-. Unlike the majority of hydroxides of bivalent metals, it is not a layered structure. The difference may arise from the high field strength of the Be^{2+} ion, which draws the hydroxyl groups into a more closely packed structure than the layer lattice allows. Orthorhombic $Be(OH)_2$ is analogous to the isostructural $Zn(OH)_2$.

As the concentration of free NaOH in the beryllate solution is decreased, precipitation by boiling increases the amounts of the tetragonal polymorph. When the free NaOH falls below 0.5 *M* and the Na_2O:BeO ratio is decreased to 1.5 or below, only a trace of the orthorhombic form is detected in the $Be[OH]_2$ product. After precipitating the metastable form by hydrolysis of the beryllium chloride solution with urea, Miller and Mercer [1966] indexed it on a tetragonal cell with a = 10.88 Å and c = 7.83 Å.

8.1.4 Hydrolytic Complexes in Aqueous Beryllium Solutions

Much effort has been devoted to the study of hydrolysis of the Be^{2+} ion. It is generally agreed that additions of alkali to an aqueous beryllium salt results in a clear solution up to $z = 1$, where z is the average number of OH^- ions bound per Be^{2+} ion. Above that value, precipitation begins, suggesting the formula $Be_n[OH]_n^{n+}$ for the soluble hydrolytic complex. The generally favored value is $n = 3$, obtained by Kakihana and Sillen [1956]. They showed that $Be_3(OH)_3^{3+}$ is the most important polymer, followed closely by $Be_2(OH)^{3+}$, and these polymers exist over a wider range of pH as the beryllium concentration in solution increases. Kakihana and Sillen [1956] suggested a structure for the $Be_3(OH)_3^{3+}$ complex in which beryllium atoms are linked by hydroxyl bridges, the four coordinations of beryllium being preserved by extra water molecules. This structure is shown in Fig. 8.1. Mesmer and Baes [1967] have shown that the species $Be_5(OH)_7^{3+}$ is formed at higher beryllium concentrations.

With halide salt solutions, precipitation is complete at $z = 2$, but with sulfate or nitrate solutions it is complete at $z = 1.8$ to 1.9. The latter precipitate is not pure $Be(OH)_2$ because it contains some of the coprecipitated salt anion.

8.1.5 Thermal Decomposition of Beryllium Hydroxide

In thermogravimetric analysis tests, Duval and Duval [1948] showed that dehydroxylation of

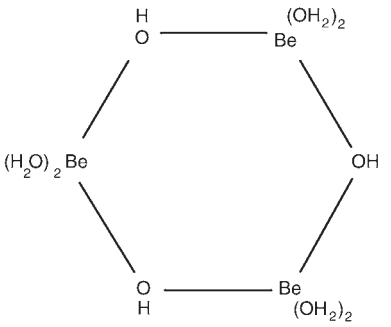

Fig. 8.1 Molecular structure for the $Be_3(OH)_3^{3+}$ complex. Source: Everest 1964

orthorhombic $Be(OH)_2$ begins at 220 °C (430 °F). The bulk of the water is quickly lost up to 280 °C (535 °F), when the composition lies approximately between the empirical $6BeO \cdot H_2O$ and $7BeO \cdot H_2O$ compositions. Thereafter, the remaining water is not released until 500 °C (930 °F) is reached. The initial decomposition of the tetragonal polymorph appears to occur at significantly lower temperatures than for the stable orthorhombic variety. Two-stage dehydroxylation is also observed with the tetragonal form. Duval and Duval [1948] showed further that temperatures above 950 °C (1740 °F) are required for the complete conversion of analytical chemical samples of $Be(OH)_2$ to BeO. There is evidence of beryllium hydroxide in the vapor phase at 1200 °C (2190 °F) and above. Young [1960] recorded the partial pressure of beryllium hydroxide over beryllium oxide as 0.55 mm (7×10^{-4} atm) at 1550 °C (2820 °F).

8.1.6 Beryllium Basic Carbonate Preparation

Everest [1973] observed beryllium basic carbonate ($BeCO_3$) precipitation when sodium carbonate is added to an acidic beryllium solution, with carbon dioxide being evolved. The precipitate is described as a mixture of beryllium hydroxide and the normal carbonate, and it usually contains from two to five molecules of $Be(OH)_2$ to each one molecule of $BeCO_3$. The ratio of hydroxide to carbonate increases as the precipitation temperature increases.

Industrially, in the solvent extraction process described by Maddox and Foos [1966], beryllium is stripped from the loaded organic solvent at 55 °C (130 °F) with 3 *M* ammonium carbonate solution kept near pH 9.3. The organic extractant is converted to NH_4DEHP during stripping, removing some of the ammonium ions from the aqueous system. By analogy with the chemistry of uranium, the beryllium is thought to be present as the $Be(CO_3)_3^{4-}$ anion. After removal of the iron and aluminum precipitates, the filtrate is hydrolyzed at 9 °C (50 °F) to precipitate the impure beryllium basic carbonate used in the manufacture of beryllium products.

Laboratory preparation of high-purity beryllium basic carbonate begins with solid beryllium sulfate. Commercial beryllium hydroxide is dissolved in sulfuric acid, after which evaporation and fractional crystallization yields purified beryllium sulfate. After filtration and drying, the beryllium sulfate crystals are redissolved in water. With vigorous agitation of the sulfate solution, gaseous ammonia is passed over the solution to slowly form and precipitate beryllium hydroxide contaminated with coprecipitated sulfate anion. After filtering and washing, the wet hydroxide cake is dissolved at 55 °C (130 °F) in an ammonium/carbonate solution. The aqueous solvent contains NH_4HCO_3 and $(NH_4)_2CO_3$ in a 2 to 1 molar ratio with a constant volume to form the $(NH_4)_4Be(CO_3)_4$ solution at a beryllium concentration of 5 to 8 g/L. Filtration removes calcium sulfate with iron, aluminum, and other insoluble hydroxides. Addition of ethylenediamine tetraacetic acid to chelate magnesium, calcium, and so on precedes steam hydrolysis at 95 °C (200 °F) to yield a pure beryllium basic carbonate precipitate.

After filtration and washing, the wet precipitate can be further purified. Using plastic ware to redissolve it in a bicarbonate/carbonate solution at 55 °C (130 °F) reduces silica and boron contamination. After filtration to reject trace impurities, chelation and steam hydrolysis at 95 °C (200 °F) are repeated. This process reliably yields a product with a uniform composition of $2BeC \cdot O_3 \cdot Be(OH)_2$.

8.1.7 Decomposition of Beryllium Basic Carbonate

Maddox and Foos [1966] prepared beryllium basic carbonate according to the method described and dried it to constant weight at 100 °C (212 °F). After 1 to 2 days at 200 °C (390 °F), a dried sample had a 52.9 wt% weight loss. Ignition of the residue from 200 to 700 °C (390 to 1290 °F) to constant weight gave an additional loss equal to 4.6 wt% of the original dried sample weight. Empirical calculations from these weight losses led to the formulation $2BeCO_3 \cdot Be(OH)_2$ for the dried material. This composition was confirmed by chemical analysis for CO_2 content.

Thermogravimetric analysis by Konieczny [1992] of a sample heated at a rate of 10 °C/min (18 °F/min) showed the loss of free water below 100 °C (212 °F). A weight loss of 5.07% between 52 and 218 °C (125 and 425 °F) was recorded. A rapid increase in rate of weight loss occurred between 218 and 320 °C (425 and 608 °F). This rapid change was followed by slow, gradual loss up to 740 °C (1365 °F). Differential thermal analysis of the dried beryllium basic carbonate at a scan rate of 10 °C/min (18 °F/min) showed a matching endothermic reaction at 270 °C (520 °F).

Purified beryllium basic carbonate can be slurried in water and hydrolyzed at 165 °C (330 °F) to yield a high-purity beryllium hydroxide. Either the hydroxide or basic carbonate can be used for the preparation of other pure beryllium chemicals. In gaseous reactions, the hydroxide is preferred for its higher density and reduced tendency to become airborne.

8.2 Solution Chemistry of Hydrated Be^{2+} Ions

The high charge-to-radius ratio has a strong influence on the behavior of the Be^{2+} ion in solution. Gurney [1953] describes the beryllium ion as a strong order-producing ion, suggesting that the water molecules adjacent to the ion are more highly oriented. This behavior is evident by the low partial molar entropy, *S*, for beryllium ions compared to the ions of magnesium, calcium, strontium, and barium, respectively. The beryllium ions promote an increase in the viscosity of an aqueous solution [Fricke and Schwetzdeller 1923]. It was concluded that the Be^{2+} ion was the most heavily hydrated of all the bivalent ions. The high charge-to-radius ratio and the resulting high-charge density on the surface of the ion polarizes the surrounding water molecules and orients them with the negative end of their dipole toward the beryllium ion. The protons of the water molecules are so strongly repelled that thermal agitation will be sufficient to transfer the proton to a more distant water molecule. This behavior leaves the OH^- ion in contact with the beryllium ion. This process is most likely to occur when the pH of the solution is increased. The reaction can be written as:

$$N\mathrm{Be}^{2+} + n\mathrm{H_2O} = (\mathrm{BeOH})_N^{n+} + n\mathrm{H}^+ \qquad \text{(Eq 8.3)}$$

Cartledge [1930] described an ion potential criterion to characterize amphoteric properties. The ionic potential (ϕ) of an ion was defined as (ϕ) = z/r, where z is the charge and r is the radius. Ions with a ($\phi^{1/2}$) value less than 2.2 are basic. Those ions greater than 2.2 but less than 3.2 are amphoteric, and those greater than 3.2 are acidic. The ($\phi^{1/2}$) value for Be^{2+} is 2.54, compared to Mg^{2+}, which is 1.76. This criterion suggests that beryllium should exhibit amphoteric behavior, while the rest of the alkaline earth elements are basic.

A dominant behavior of the hydrated Be^{2+} ion is that, during hydrolysis, it produces polynuclear species. The result of this behavior is that beryllium-salt solutions dissolve up to several mole proportions of beryllium oxide [Parsons 1907].

Sidgwick and Lewis [1926] suggested that the complex $Be(OHBe)_x$ ion is formed during normal hydrolytic reactions of the hydrated Be^{2+} ion. These hydrolytic reactions are intensified because the beryllium oxide addition increases both the pH and the beryllium concentration in solution. These two factors increase the promotion of hydrolytic polymerization of the Be^{2+} ion.

It is usually agreed that the addition of an alkali ion to an aqueous beryllium salt establishes the solution at $Z = 1$, where Z is the average number of OH^- bonds per Be^{2+} ion. When Z is above 1, precipitation occurs. With halide salt additions, precipitation is complete by $Z = 2$. With oxoacid salts, such as beryllium sulfate and beryllium nitrate, the precipitation is complete by $Z = 1.8$ to 1.9. This result indicates that the precipitation is not pure $Be(OH)_2$, and it contains some of the salt anion [Everest 1964]. Because precipitation starts at $Z > 1.0$, this behavior suggests the formula $Be_n(OH)_n^{n+}$ for the soluble hydrolytic complex. Prytz [1937] suggested that the complex has $n = 2$. Schaal and Faucherre [1947], Teyssedre and Souchay [1951], and Souchay [1948] suggest that $n = 4$. Mattlock [1954] reported that a variety of ionic species of increasing polymolar complexity exist in the solution. Schindler and Garrett [1960] and Kakihana and Sillen [1956] recommend $n = 3$. Kakihana and Sillen [1956] also report the equilibria and equilibrium constants for complexes with $n = 3$, which are given as follows:

$$3\mathrm{Be}^{2+} + 3\mathrm{H_2O} = \mathrm{Be_3(OH)_3}^{3+} + 3\mathrm{H}^+$$
$$\log \beta^*_{33} = -8.66 \qquad \text{(Eq 8.4)}$$

$$2\mathrm{Be}^{2+} + \mathrm{H_2O} = \mathrm{Be_2(OH)}^{3+} + \mathrm{H}^+$$
$$\log\beta^*_{12} = -3.24 \qquad \text{(Eq 8.5)}$$

$$\mathrm{Be}^{2+} + 2\mathrm{H_2O} = \mathrm{Be(OH)_2} + 2\mathrm{H}^+$$
$$\log \beta^*_{2} = -10.9 \qquad \text{(Eq 8.6)}$$

The symbols used are consistent with the tables of stability constants [Bjerrum et al. 1957].

From Fig. 8.2, it is apparent that $Be_3(OH)_3^{3+}$ is the most dominant polymer, followed closely by Be_2OH^{3+}. It can also be seen that these poly-

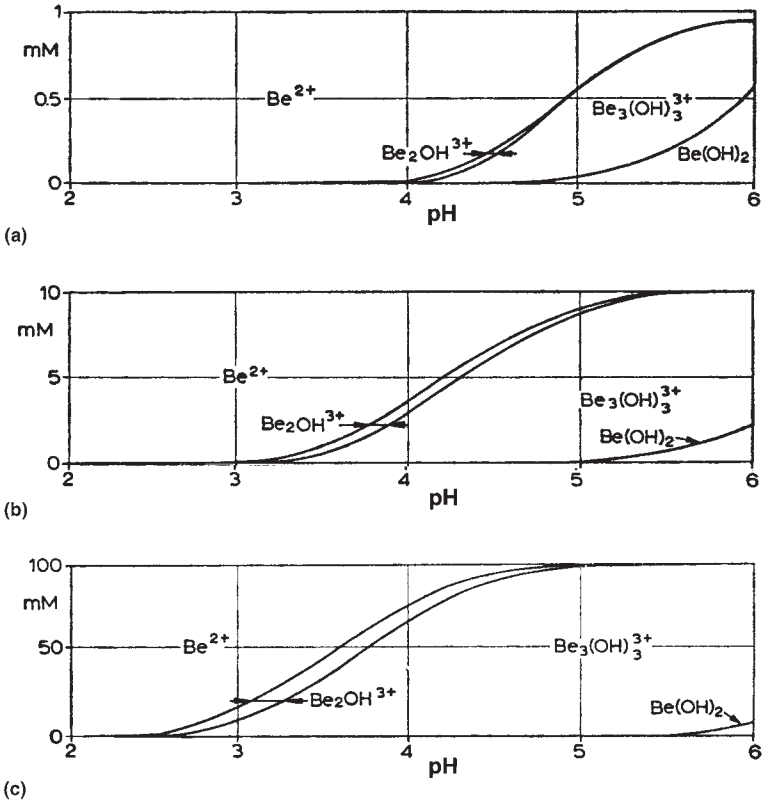

Fig. 8.2 Complex species distribution with respect to the pH, for a total beryllium concentration of (a) 1 mM, (b) 10 mM, and (c) 100 mM. Source: Everest 1964

mers exist over a wider pH range as the beryllium concentration in solution increases.

The molecular structure for the $Be_3(OH)_3^{3+}$ complex was introduced by Kakihana and Sillen [1956]. Their structure consists of beryllium atoms being linked by hydroxyl bridges. The four coordinations of the beryllium are being preserved by extra molecules. This structure is illustrated in Fig. 8.1.

Kakihana and Sillen [1956] recommend even higher complexes at Z greater than 0.9 when there is an increase in the beryllium concentration. Their suggestion is supported by the observation that a sulfonic and cation-exchange resin (Zeo-Karb 225) takes up 2.92 g atoms of beryllium per equivalent resin from an 0.5 M beryllium sulfate solution of pH 5.1. This large loading was accounted for by assuming the absorption of the ion complexes $[Be_n(BeO)_{2n}]^{2n+}$ by resin [Aveston and Milward 1959, Zhukov et al. 1962]. Sidgwick [1950] suggests that it is possible to dissolve more beryllium oxide in a beryllium salt solution than can be explained by the formation of $[(BeOH)_n]^{n+}$ complexes.

Using ultrasonic absorption analysis on beryllium sulfate solutions, Diebler and Eigen [1959] suggested a series of reactions for producing $BeSO_4$. Note the role of water in the inner hydration sphere:

$$\begin{aligned} Be^{2+} + (SO_4)^2 &= Be^{2+}O^{-H}_{-H}O^{-H}_{-H} \\ &= Be^{2+}O^{-H}_{-H}SO_4^{2-} = BeSO_4 \end{aligned} \quad \text{(Eq 8.7)}$$

The first two steps of this series of reactions are rapid, with average mean time of:

$$\tau_1, \tau_2 > 10^{-9}\ \text{s} \quad \text{(Eq 8.8)}$$

The last step involves the replacement of a water molecule in the inner hydration sphere of the beryllium by the sulfate ion. This step proceeds much slower, and the reaction rate was reported to be controlled by the cation. The reaction time, τ_3, is 88×10^{-4} s, which is much greater than the typical 2^+ metal sulfate ion.

Beryllium, being a 2^+ ion, has a limiting step for producing beryllium sulfate that is dependent on the acidity of the entering ligand and the beryllium ion concentration. Most 2^+ ions have a rate-limiting step that is independent of the entering ligand. Between pH 3 and 4.5, Diebler and Eigen [1959] found two additional reaction time effects (τ_4 and τ_5) and suggested reactions (Fig. 8.3) involving hydrolytic complexes.

8.3 Beryllium Fluoride

Beryllium fluoride is described separately because of the sharp difference between its chemistry and that of the other halides. The basic difference results from the variance in degree of ionic character of the beryllium-halide bond. From Pauling's relationship between the electronegativities of the two atoms, it has been calculated that the beryllium-fluorine bond is 80% ionic [Pauling 1960]. This calculated value is much greater than the values of 42, 35, and 25% ascribed to the beryllium-chlorine, beryllium-bromine, and beryllium-iodine bonds, respectively.

8.3.1 Preparation of Beryllium Fluoride

Beryllium fluoride cannot be made by aqueous reactions, because the $BeF_2 \cdot 4H_2O$ produced by dissolution of the hydroxide in aqueous hydrofluoric acid hydrolyzes during dehydration. It can be made by direct action at 220 °C (430 °C) of gaseous hydrogen fluoride on beryllium oxide [Hyde et al. 1958]. It is usually made by Lebeau's method [Lebeau 1898] in which ammonium fluoroberyllate, $(NH_4)_2BeF_4$, is thermally decomposed. Ammonium fluoroberyllate is made by dissolving beryllium hydroxide in aqueous ammonium bifluoride and evaporating the solution.

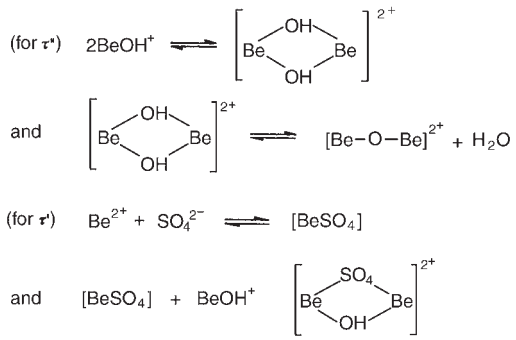

Fig. 8.3 Hydrolytic complex reactions. Source: Everest 1964

Novoselova [1959] states that when ammonium fluoroberyllate is slowly warmed and steadily raised in temperature between 220 and 230 °C (430 and 445 °F), decomposition occurs without the formation of intermediate phases; this research also asserted that when maintained at 240 °C (465 °F), the material decomposes by way of two intermediate ammonium compounds:

$$(NH_4)_2BeF_4 \rightarrow NH_4BeF_3 \rightarrow NH_4Be_2F_5 \rightarrow BeF_2 \quad \text{(Eq 8.9)}$$

Several other versions of a stagewise decomposition have been offered. At temperatures below 240 °C (465 °F), the reaction product retains some of the intermediate phases, and the yield of beryllium fluoride is poor.

8.3.2 Beryllium Fluoride Glass

An important aspect of the chemistry of beryllium fluoride and the fluoroberyllates is the structural relationship between these compounds and silica and the silicates, respectively [Goldschmidt 1926, Roy et al. 1950, 1953]. This relationship arises from the similar radii of 1.40 and 1.36 Å [Wells 1961] and polarizabilities of the O^{2-} and F^- ions. Like silica and germanium dioxide, beryllium fluoride possesses a radius ratio of beryllium to fluorine of ~0.3, a figure that Goldschmidt believed will allow compounds of the AX_2 type to form glasses [Goldschmidt 1926]. Beryllium fluoride is rather difficult to crystallize and for many years was known only as a glass. Based on x-ray methods for determining the structure of the glass, Warren and Hill [1934] suggest that beryllium fluoride has a random network structure in which beryllium atoms are surrounded tetrahedrally by four fluorine atoms, and two fluorine atoms, by two beryllium atoms. The three-dimensional network structure is analogous to that of vitreous silica.

Another aspect of the relationship is the existence of polymorphic crystalline forms of beryllium fluoride analogous to the polymorphic forms of silica. The cristobalite and quartz forms of beryllium fluoride are well established [Roy et al. 1950, 1953]. Beryllium fluoride glass crystallizes spontaneously into the α-quartz modification at 227 °C (440 °F). Russian workers, whose results Novoselova summarized [1934, 1959], believe that beryllium fluoride has a β-quartz form that is stable at room temperature, similar to the

low-temperature quartz form of silica. It is transformed into an α-quartz form at 220 °C (430 °F), corresponding to the high-temperature quartz form of silica. The α-quartz form, when slowly heated, is transformed at 420 to 450 °C (790 to 840 °F) into a tridymite form. At 680 °C (1255 °F), this phase itself is converted into an α-cristobalite form of beryllium fluoride, corresponding to the high-temperature cristobalite form of silica. The α-cristobalite modification of beryllium fluoride is reported by Novoselova to melt at 800 °C (1470 °F), a value confirmed by Sense et al. [1954], who obtained a melting point of 803 °C (1477 °F). When rapidly heated, the α-quartz form of beryllium fluoride melts in a range of 540 to 548 °C (1005 to 1020 °F), but these values were later raised to 552 °C (1026 °F) by Taylor and Gardner [1965], who had higher-purity beryllium fluoride available. There is general agreement that the reconstructive transformations between the three forms of beryllium fluoride are very sluggish, as is the case for silica.

The beryllium fluoride-silica relationship is further illustrated by the properties of the molten fluoride. It has a high viscosity, higher than that of most molten halides by a factor of 10^6, and a low electrical conductivity. Both properties indicate that the liquid beryllium fluoride possesses a nonionic network structure similar to that of molten silicon dioxide or diboron trioxide [Neumann and Richter 1925, Mackenzie 1960]. Beryllium fluoride begins to sublime at 740 °C (1365 °F). It is not dimeric in the vapor phase and shows considerable thermal stability, being less than 50% dissociated at 3000 K and 2×10^{-6} atm [Brewer 1950a, b]. The sublimation pressure at 740 to 803 °C (1365 to 1475 °F) is given by Sense et al. [1954] as:

$$\log P\ [\text{mm Hg}] = 11.822 - 12{,}385/T \qquad \text{(Eq 8.10)}$$

where T is the temperature in degrees Kelvin. The vapor pressure of beryllium fluoride for the temperature range of 803 to 868 °C (1475 to 1600 °F) is obtained from:

$$\log P\ [\text{mm Hg}] = 10.651 - 11{,}125/T \qquad \text{(Eq 8.11)}$$

The extrapolated boiling point is 1159 °C (2120 °F).

Beryllium fluoride is a hygroscopic material with a very high solubility in, and affinity for, water, although its rate of dissolution is very slow. The solubility of beryllium fluoride in water is limited to approximately 25 mol/L at 25 °C (75 °F). This value corresponds to 2 moles of water per mole of beryllium fluoride, for which Linnell and Haendler [1948] suggest the complex in solution as shown in Fig. 8.4.

The presence of the complex is consistent with beryllium fluoride being a weak electrolyte in water. Using electromotive force (emf) and conductivity methods, measurements have disclosed the presence of BeF^+, BeF_2, BeF_3^-, and BeF_4^{2-} ions in these solutions [Tananaev and Vinogradova 1960]. As would be expected, salts of the anions can be crystallized under the correct conditions. Phase equilibria studies by Novoselova [1959] show that fluoroberyllates containing a greater proportion of beryllium can be crystallized from more concentrated solutions when the fluorine-to-beryllium ratio is 4 to 1. The compounds $(NH_4)_2BeF_4$ and NH_4BeF_3 occur in the NH_4F-BeF_2-H_2O system. In the NaF-BeF_2-H_2O system, the compounds Na_2BeF_4, $NaBeF_3$, and 4NaF-3BeF_2-2H_2O have been identified. The compounds K_2BeF_4, $KBeF_3$, and KBe_2F_5 have also been isolated.

The preparation of the BeF_4^{2-}-type fluoroberyllates has been studied [Perfect 1952]. The alkali and alkaline earth salts were readily obtained by adding the appropriate nitrate or chloride to a hot, nearly saturated solution of ammonium fluoroberyllate, resulting in the precipitation of the corresponding fluoroberyllate. The ammonium fluoroberyllate was prepared by reacting beryllium hydroxide and ammonium bifluoride as a dry salt mixture or in solution. The heavy metals were oxidized with ammonium persulfate, and most of the remaining impurities were precipitated with ammonium sulfide prior to removal by filtration. Perfect claims that $MgBeF_4$ can be prepared in this way if care is taken to avoid exposing the salt to prolonged boiling. At the boiling point, the degree of dissociation of the fluoroberyllate ion exceeds that of magnesium fluoride to the extent that magnesium fluoride is being formed continuously until the solid phase becomes almost pure MgF_2. A similar behavior is observed, but at a slower rate, when

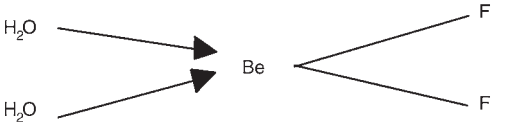

Fig. 8.4 Complex molecule formed by dissolution of beryllium fluoride in water. Source: Linnell and Haendler 1948

$CaBeF_4$ slurries are boiled. Magnesium fluoroberyllate does not appear to exist, according to a fusion diagram by Venturello [1941]. Only a solid solution is indicated for the MgF_2-BeF_2 system.

The similarity between the BeF_4^{2-} fluoroberyllates obtained from solution and the corresponding sulfates has been established [Ray 1932]. Thus, the Co^{2+}, Ni^{2+}, and Zn^{2+} fluoroberyllates crystallize with five, six, and seven molecules of water of crystallization, respectively, as do the corresponding sulfates with which these hydrates are isomorphous. The similarities between the fluoroberyllates and the sulfates appear to be due to the similar size of the BeF_4^{2-} and SO_4^{2-} anions. The analogy is not entirely complete, since the fluoroberyllates can form glasses, whereas the sulfates do not.

Beryllium fluoride represents an extreme among transparent optical materials. In its glassy form, BeF_2 is an isotropic material exhibiting a refractive index $\eta_d = 1.275$, a dispersive power (reciprocal Abbe number) $\nu^{-1} = 9.3 \times 10^{-3}$, and a nonlinear coefficient of refractive index at 1.06 μm of $\eta_2 = 2 \times 10^{-14}$ esu [Williams et al. 1981]. All three of these values are the lowest yet measured for any material that is solid at room temperature and atmospheric pressure. The unusually low nonlinear refractive index has led to active research in beryllium fluoride glasses. These glasses are hygroscopic and difficult to handle experimentally. This problem is surmounted by utilizing the fluoroberyllate systems. The greater the proportion of beryllium fluoride in the system, the more readily glasses are obtained. Too low a proportion of beryllium fluoride leads to the formation of turbid glasses due to the occurrence of immiscibility or the onset of crystallization.

Work on molten fluoride systems was undertaken in the United States in conjunction with the development of a molten salt reactor for atomic energy purposes. In their study of potential systems, Thoma et al. [1960] observed the compounds NaF-BeF_2-ThF_4 and NaF-BeF_2-UF_4. In the NaF-LiF-BeF_2 system, the compounds $NaLiBe_3F_8$, $Na_5LiBe_3F_{12}$, and Na_2LiBeF_5 were identified.

8.3.3 Metal Production from Beryllium Fluoride

Practical methods for producing pure beryllium on a commercial scale are founded on the use of beryllium fluoride. Beryllium fluoride can be reduced by magnesium, sodium, and calcium, all of which are available in commercial quantities. Reduction with sodium is reported to be only partial because stable NaF-BeF_2 is formed, and it cannot be reduced by an excess of sodium [Kroll 1945]. Reduction of beryllium fluoride with calcium is accompanied by the evolution of a large amount of heat, which melts the metal and slag, but the cost of calcium is excessive for this purpose. Alloys of magnesium and calcium have been suggested for reducing beryllium fluoride. For the commercial reduction of beryllium fluoride, magnesium is the preferred reducing agent, especially on the basis of cost per unit of BeF_2 consumed, when considering the reaction:

$$BeF_2 + Mg = Be + MgF_2 \qquad \text{(Eq 8.12)}$$

It is to be noted that at 800 °C (1470 °F), both reactants are molten. It has been found experimentally that the reaction is initiated near the melting point of magnesium. The reaction products are both refractory. Beryllium metal and magnesium fluoride have melting points of 1283 °C (2340 °F) and 1263 °C (2305 °F), respectively [Derham and Temple 1957]. It is therefore necessary to heat the charge to a temperature above 1283 °C (2340 °F) and to add an agent that will flux the magnesium fluoride before the metal particles can coalesce and rise to the surface of the fluoride slag. Kjellgren [1945] suggested the use of excess beryllium fluoride, which has become the standard commercial mode.

The first stage in the production of beryllium metal involves the conversion of beryllium hydroxide to beryllium fluoride. The dry fluorination of calcined beryllium hydroxide with solid ammonium bifluoride may be employed:

$$BeO + NH_4HF_2 = NH_3 + H_2O + BeF_2 \qquad \text{(Eq 8.13)}$$

The reaction between solids makes it impossible to obtain an oxygen-free material. The dissolution of beryllium hydroxide in aqueous ammonium bifluoride gives:

$$Be(OH)_2 + 2NH_4HF_2 = (NH_4)_2BeF_4 + 2\,H_2O \qquad \text{(Eq 8.14)}$$

The separation of the ammonium fluoroberyllate salt by evaporation crystallization gives purification from several elements. The salt is

thermally decomposed to yield beryllium fluoride in a finely divided state. This dust-prone material has been associated with health problems.

In commercial operations, beryllium hydroxide is dissolved in ammonium bifluoride solution to give a level of 20 g/L Be at pH = 5.5 [Walsh 1979]. This solution is made basic by the addition of solid calcium carbonate and heating to 80 °C (175 °F). A small portion of the ammonium fluoroberyllate is sacrificially decomposed through:

$$(NH_4)_2BeF_4 + CaCO_3 + H_2O = NH_4OH + CaF_2 + BeF_2 + CO_2 \quad \text{(Eq 8.15)}$$

for the precipitation of aluminum impurities from the solution with the calcium fluoride as a carrier. The amount of calcium carbonate added is determined empirically from the aluminum content of the beryllium hydroxide. Ammonium hydroxide formed by the calcium carbonate reaction raises the pH of the solution to 8.3.

Lead dioxide is added to the solution to oxidize the manganese impurities to insoluble MnO_2 and to precipitate the chromium as lead chromate. The solution, after treatment with calcium carbonate and lead dioxide, is filtered to remove the insoluble impurities. Ammonium sulfide is added to the filtrate to remove heavy-metal impurities introduced with the hydroxide and solubilized lead from the lead dioxide treatment. The solution is filtered to remove all solid particles.

The ammonium fluoroberyllate solution is analyzed and adjusted to give the balanced ratio needed to yield $(NH_4)_2BeF_4$. The ammonium fluoroberyllate salt is recovered by concurrent evaporation and crystallization under vacuum. The salt is continuously removed by centrifugation and washed lightly. The mother liquor and washings are returned to the evaporator.

In the second stage of the process, fused and solidified beryllium fluoride glass is produced. The $(NH_4)_2BeF_4$ salt is charged into inductively heated, graphite-lined furnaces, where the ammonium fluoride is vaporized into fume collectors for recycling to the dissolving process. Molten beryllium fluoride flows continuously from the bottom of the furnace and is solidified as a glassy product on water-cooled casting wheels [Schwenzfeier 1964].

The third stage of the process consists of the thermal reduction of beryllium fluoride with magnesium metal. The fundamental reaction:

$$BeF_2 + Mg = Be + MgF_2 \quad \text{(Eq 8.16)}$$

has not been forced above an 85% yield. With the high value and high cost of processing to this stage, complete recovery of beryllium from the slag is mandatory. At the 85% reduction yield, leaching of the slag for beryllium fluoride for recycling is incomplete because much is entrapped in the magnesium fluoride matrix.

Employing the approach of Kjellgren [1945], the process developed uses 70% of the stoichiometric magnesium addition and settles for a 50% yield of beryllium metal. This practice leaves 50% of the beryllium fluoride to flux the magnesium fluoride slag. Magnesium metal and beryllium fluoride are charged in solid form into a graphite crucible at a temperature of 900 °C (1650 °F). When the exothermic reaction is completed, the reaction products are heated to ~1300 °C (2370 °F) to allow the molten beryllium to float on the slag. Slag and metal are poured into a graphite receiving pot, where both solidify. Beryllium solidifies in the form of beads or pebbles, roughly spherical in shape and up to 25 mm (1 in.) in diameter, throughout the massive slag mixture of solidified magnesium fluoride and beryllium fluoride.

The final treatment of the mixed, reacted mass is to crush it before water-leaching in an autogeneous ball mill. The excess beryllium fluoride is quickly dissolved, causing disintegration of the reaction mass and liberation of the beryllium pebbles. The leach liquor is continuously recycled through the ball mill, removing the magnesium fluoride particles and leaving the beryllium pebbles in the mill body. The magnesium fluoride is removed from the leach liquor and discarded. The leach liquor is recycled to the ammonium fluoroberyllate preparation process.

The beads or pebbles contain ~97 wt% Be, being contaminated with trapped slag and unreacted magnesium. To remove these impurities, the metal is vacuum melted in induction furnaces. The free magnesium and excess beryllium fluoride vaporize during the melting under vacuum. Nonvolatiles, such as beryllium oxide, magnesium fluoride, and beryllium carbide, separate from the molten metal by sinking as a dross adhering to the bottom of the crucible. The purified metal is poured into an ingot mold capable of containing 75 to 150 kg beryllium.

8.3.4 Electrolysis of Beryllium Chloride

Liquid beryllium chloride is a poor electrical conductor. The addition of even small quantities

of alkali metal chlorides considerably increases the conductivity. Delimarski and coworkers [1955, 1957], by means of electrical conductivity and emf measurements, reported evidence for both anionic and cationic beryllium species in NaCl-$BeCl_2$ melts, depending on the relative concentrations of the components. Schmidt [1926] showed that the chloroberyllates M_2BeCl_4, in which M is sodium, lithium, or thallium, could be isolated from fused salt mixtures under the correct conditions.

Schmidt [1926] included an early rendition of the NaCl-$BeCl_2$ phase diagram. Furby and Wilkinson [1960] determined the melting points of NaCl and $BeCl_2$ combinations. A eutectic mixture of 55 mol% $BeCl_2$ was found with a melting point of 210 °C (410 °F), as compared with Schmidt's figures of 51 mol% and 215 °C (420 °F). The compound $BeCl_2 \cdot 2NaCl$ is unstable in contact with the liquid above its incongruent melting point of 320 °C (610 °C).

Everest [1964] summarized the electrowinning of beryllium using an electrolyte consisting of equal parts by weight of sodium and beryllium chlorides. The cathode was usually iron or nickel, and graphite or iron was used as the anode.

The operating temperatures of 350 to 400 °C (660 to 750 °F) were selected to limit vapor losses of beryllium chloride from the melt. The beryllium flake product was of very good quality, especially with its low oxygen content. The method was used by Degussa in Germany, by Clifton Products Inc. in the United States, and by Pechiney in France to produce beryllium commercially.

Germany was one of the first countries to produce beryllium commercially [Potvin and Farnham 1946]. The Degussa plant in Frankfurt was the sole producer of beryllium metal during World War II. Purified beryllium chloride was mixed with an equal weight of sodium chloride and fused. The melt was electrolyzed in a nickel crucible at a temperature of 350 °C (660 °F), using 40 to 50 V and 500 A. The nickel crucible was 50 cm in diameter and 120 cm long. After 24 h of operation, the current was interrupted. The electrolyte was siphoned off at 500 °C (930 °F) into a preheated crucible, replenished with fresh beryllium chloride, and electrolysis was resumed in the new cell. Anodes lasted for approximately six months in service.

Beryllium metal had deposited on the first cell wall as glittering dendritic flakes. A perforated ladle was used to recover the hot flakes, still at 300 to 350 °C (570 to 660 °F). After the metal had cooled to room temperature, the ladle was plunged into an ice water bath to absorb the heat of solution of adhering beryllium chloride. To remove traces of aluminum and beryllium oxides, the flakes were washed successively with diluted sodium hydroxide and diluted nitric acid. After a second rinse with water, the flakes were centrifuged to dryness. The beryllium content of the flakes at this stage was 99 wt% or above.

The dried flakes were pressed into briquettes of 40 mm diameter and approximately 40 mm high. The briquettes were premelted at 1400 °C (2550 °F) in a beryllium oxide crucible under a hydrogen atmosphere. The crucible had a slight taper to ease the removal of the solid ingot. After melting, the metal was cooled and the regulus tapped from the crucible. Any beryllium oxide collected on the top surface was removed by brushing or grinding.

Final melting and casting were conducted in a vacuum of 10^{-3} mm Hg. Remelting was performed in a beryllium oxide crucible, 5 to 8 cm in diameter and 130 to 140 cm tall. On the upper part of this crucible, a refractory sleeve or tube was placed that served to convey the molten metal to the mold enclosed in the vacuum chamber. Permanent split molds of iron or steel were heated electrically to 150 °C (300 °F). They were of various dimensions, and the most common for rods was 10 mm in diameter by 150 to 160 mm long. The wall thickness was approximately 15 mm. Before dropping the vacuum, the mold and its contents were cooled quickly by a water-cooling arrangement outside the furnace. Large cylindrical bars and flat plates were also cast. The beryllium, after remelting and casting, had a purity of 99.8%, the rest being mainly oxide.

Annual production of flakes amounted to 210 to 1690 kg per year from 1940 to 1944, with a total of 4105 kg. These production levels were attained in the period before acute and chronic beryllium-related diseases were recognized. The problems associated with controlling industrial risk were undoubtedly a factor in the early demise of the electrolytic process in the United States and France.

8.4 Chemical Behavior of Beryllium

Beryllium is a reactive metal, which is difficult to purify. The interstitial alloy addition or contaminant elements can significantly alter

properties. The removal of these impurities has a marked effect on plasticity of beryllium. Since beryllium is chemically closely related to aluminum, it is difficult to completely separate beryllium from aluminum.

Beryllium alloys are subject to oxidation, which occurs at 700 °C (1290 °C), while nitrogen attack becomes apparent at 900 °C (1650 °F). They exhibit respectable passivity at room temperatures. Beryllium maintains a polished surface for years.

Clean beryllium that is free of surface contamination has good corrosion resistance in low-temperature, high-purity water. Under these conditions, the corrosion rate is less than 0.03 mm/year (1 mil/year). Beryllium of normal commercial purity is susceptible to localized pitting, when exposed to impure water. Chloride and sulfate ions are most often the critical contaminants. This pitting has been correlated to the alloy impurity distribution occurring at sites with high concentrations of iron, aluminum, or silicon [Wright and Silver 1963].

Beryllium reacts readily with H_2SO_4 and HCl. Boiling water and alkalis react with beryllium and give off hydrogen. Beryllium will react with molten alkali halides but exhibits no reaction with molten alkaline earth metal halides. It will reduce aluminum halides and halides of heavier elements. Carbon reacts exothermically with liquid beryllium.

Fluoride coatings, which have a glossy appearance, are water insoluble and can provide protection in water containing a 150 ppm concentration of chloride ions. Anodized coatings also have been used to improve the corrosion resistance of beryllium in corrosive aqueous solutions. The technology is similar to anodizing of aluminum. Anodized films of 0.003 mm to several thousandths mm (0.1 mil to several mils) thickness are often produced [Mueller and Adolphson 1979].

REFERENCES

Aveston, J., and Milward, G.L., 1959. Scientific report, N.C.L./A.E. 185, The National Chemical Laboratory; originally in A.I. Zhukov et al., *Zh. Neorg. Khim.*, Vol 7, 1962, p 1448

Beaver, W.W., 1955a. Fabrication of Beryllium by Powder Metallurgy, *The Metal Beryllium*, American Society for Metals

Beaver, W.W., 1955b. *The Metal Beryllium*, American Society for Metals

Bjerrum, J., Schwarzenbach, G., and Sillen, L.G., 1957. Stability Constants, Part 1: Organic Ligands, *Stability Constants of Metal-Ion Complexes*, 1st ed., The Chemical Society, London

Brewer, L.M., 1950a. Thermodynamic Properties of Common Gases, *The Chemistry and Metallurgy of Miscellaneous Materials*, L.F. Quill, Ed., McGraw-Hill, NY, p 60–75

Brewer, L.M., 1950b. Thermodynamic Properties of Halides, *The Chemistry and Metallurgy of Miscellaneous Materials*, L.F. Quill, Ed., McGraw-Hill, NY, p 76–192

Cartledge, G.H., 1930. Studies on the Periodic System: III Relation between Ionizing Potential and Ionic Potentials, *J. Am. Ceram. Soc.*, Vol 52, p 3076–3083

Delimarski, Y.K., et al., 1955. *Zh. Fiz. Khim.*, Vol 29, p 1489

Delimarski, Y.K., et al., 1957. *Zh. Fiz. Khim.*, Vol 31, p 2589

Derham, L.J., and Temple, D.A., 1957. "Preparation of Beryllium Metal by Thermal Reduction of the Fluoride," Symposium on Extraction Metallurgy of Some of the Less Common Metals (London), Institute of Mining and Metallurgy

Diebler, H., and Eigen, M., 1959. Das Relaxationszeitspectrum der Chemischchen Gleichgewichtseinstellung in Wasserigen Losungen von Beryllium Sulfat, *Z. Phys. Chem. Neue Folge*, Vol 20, p 299–306

Duval, T., and Duval, C., 1948. Thermogravimetrics of Analytical Precipitates, Part VI: Determination of Beryllium, *Anal. Chim. Acta*, Vol 2, p 53–56

Everest, D.A., 1964. *The Chemistry of Beryllium*, Elsevier, New York, NY, p 38

Everest, D.A., 1973. Beryllium, *Comprehensive Inorganic Chemistry*, J.C. Bailar, H.J. Emeleus, R. Nyholm, and A.F. Trotman-Dickenson, Ed., Pergamon Press Ltd., Oxford, England

Fricke, R., and Schwetzdeller, H., 1923. Untersuchungen über Hydrate in Wäβriger Lösung. I. Mitteilung. Das Berylliumion, *Z. Anorg. Chem.*, Vol 131, p 130–139

Furby, E., and Wilkinson, K.L., 1960. The Melting and Boiling Points of Beryllium Chloride and an Investigation of the NaCl/$BeCl_2$ System, *J. Inorg. Nucl. Chem.*, Vol 14, p 123–147

Goldschmidt, V.M., 1926. Skrifter Norske Videnskaps-Akad, *Matemot. Naturuid Klasse 6*, Oslo, p 104

Gurney, R.W., 1953. *Ionic Processes in Solution*, McGraw-Hill, New York, NY

Hyde, K.R., O'Connor, D.J., and Wait, E., 1958. Preparation of Beryllium Fluoride from Beryllia, *J. Inorg. Nucl. Chem.*, Vol 6, p 14–18

Illig, K., 1932. "Beryllium and Its Alloys," Report in *Scientific Publications of the Siemens Company Chemical Catalog*, Siemens Company, NY

Kakihana, H., and Sillen, L.G., 1956. Studies on the Hydrolysis of Metal Ions XVI: The Hydrolysis of the Beryllium Ion, Be(II), *Acta Chem. Scand.*, Vol 10, p 985–1005

Kjellgren, B.R.F., 1945. Process for Producing Beryllium, U.S. Patent 2,381,291

Konieczny, J.L., 1992. "A Study of the Thermal Decomposition of Beryllium Oxalate and Other Beryllium Oxysalts," University of Toledo, OH

Kroll, W.J., 1945. "Extractive Metallurgy of Beryllium," Information Circular 7326, U.S. Bureau of Mines

Lebeau, P., 1898. *Compt. Rend.*, Vol 126, p 744

Lide, D.R., 2002. *CRC Handbook of Chemistry and Physics*, 83rd ed., CRC Publication

Linnell, R.H., and Haendler, H.H., 1948. Beryllium Fluoride in Water and Ethanol Solutions, *J. Phys. Chem.*, Vol 52, p 819

Mackenzie, J.D., 1960. Structure of Glass Forming Halides, Part I: Liquid Beryllium Fluoride, *J. Chem. Phys.*, Vol 32, p 1150–1152

Maddox, R.L., and Foos, R.A., 1966. Process for Producing Basic Beryllium Metal of High Purity, U.S. Patent 3,259,456

Mattlock, G., 1954. The Hydrolysis and Aggregation of the Beryllium Ion, *J. Am. Chem. Soc.*, Vol 76, p 4835–4838

Mercer, R.A., and Miller, R.P., 1966. The Preparation and Properties of Some Hydroxy Compounds of Beryllium, *J. Inorg. Nucl. Chem.*, Vol 28, p 61–76

Mesmer, R.E., and Baes, C.F., 1967. The Hydrolysis of Beryllium (II) in 1 M NaCl, *Inorg. Chem.*, Vol 6 (No. 11), p 1951

Mueller, J.J., and Adolphson, D.R., 1979. Corrosion, *Beryllium Science and Technology*, Vol 2, D.R. Floyd and J.N. Lowe, Ed., Plenum Press, NY, p 417–433

Neumann, B., and Richter, H., 1925. *Z. Electrochem.*, Vol 31, p 484

Novoselova, A.V., 1934. *J. Gen. Chem. USSR*, Vol 4, p 1206–1210

Novoselova, A.V., 1959. Beryllium Fluorides and Fluoroberyllates, *Usp. Khim.*, Vol 28, p 33–43

Parsons, C.L., 1907. Solution in a Dissolved Solid, *J. Phys. Chem.*, Vol 11 (No. 9), p 651–680

Pauling, L., 1960. *The Nature of the Chemical Bond*, 3rd ed., Cornell University Press, Ithaca, NY

Perfect, F.H., 1952. *Proc. Penn. Acad. Sci.*, Vol 26, p 54

Pfeiffer, P., Schmitz, E., Dominik, F., Fritzen, A., and Werdelmann, B.R., 1951. Zur Stellung von Beryllium und Magnesium im Periodischen System der Elemente, *Z Anorg. Chem.*, Vol 264, p 188–201

Potvin, R., and Farnham, G.S., 1946. The Chloride Process for Production of Beryllium in Germany, *Trans. Can. Inst. Min. Metall.*, Vol 49, p 525–538

Prytz, M., 1937. Das Verhalten von Berylliumchlorid und Berylliumfluorid in Wäβrigen Lösungen, *Z. Anorg. Allg. Chem.*, Vol 231 (No. 3), p 238–248

Ray, N.N., 1932. Fluoberyllate und ihre Analogie mit den Sulfaten. II. Fluoberyllate einiger Zweiwertiger Metalle, *Z. Anorg. Allg. Chem.*, Vol 205 (No. 3), p 257–267

Roy, D.M., Roy, R., and Osborn, E.F., 1950. Phase Relations and Structural Phenomena in the Fluoride-Model Systems LiF-BeF_2 and NaF-BeF_2, *J. Am. Ceram. Soc.*, Vol 33 (No. 3), p 85–90

Roy, D.M., Roy, R., and Osborn, E.F., 1953. Fluoride Model Systems, Part III: The System NaF-BeF_2 and the Polymorphism of Na_2BeF_4 and BeF_2, *J. Am. Ceram. Soc.*, Vol 36 (No. 6), p 185–190

Schaal, R., and Faucherre, J., 1947. Sur la Variations de pH en Fonction de la Dilution, II. Application a l'Etude des Sels Basiques Solubles, *Bull. Soc. Chim. Fr.*, Series 5, Vol 14, p 927–932

Schindler, P., and Garrett, A.B., 1960. Löslichkeitsprodukte von Metalloxiden und Hydroxiden. 5. Mitteilung. Die Löslichkeit von $Be(OH)_2$ in Verdünnten Säuren, *Helv. Chim. Acta*, Vol 43, p 2176

Schmidt, J.M., 1926. Analyse Thermique des Systemses Binaires Formes par le Chlorure de Glucinium Anhydre avec Divers Chlorures Metalliques, *Bull. Soc. Chem.*, Vol 39, p 1686–1703

Schwenzfeier, C.W., Jr., 1964. Beryllium and Beryllium Alloys, *Kirk-Othmer Encyclopedia of Chemical Technology*, Vol 3, Interscience, NY

Seitz, A., Rosler, U., and Schubert, K., 1950. Kristallstruktur von Beta-$Be(OH)_2$, *Anorg. Chem.*, Vol 261 (No. 1–2), p 94–105

Sense, K.A., Snyder, M.J., and Clegg, J.W., 1954. The Vapor Pressure of Beryllium

Fluoride, *J. Phys. Chem.*, Vol 58 (No. 3), p 223–224

Sidgwick, N.V., 1950. *Chemical Elements and Their Compounds*, Vol 1, Oxford University Press, p 211

Sidgwick, N.V., and Lewis, N.B., 1926. The Solubility of Beryllium Oxide in Solutions of Its Salts, *J. Chem. Soc.*, p 1287–1302

Souchay, P., 1948. Contribution a l'Etude des Phenomenes de Condensation en Chemie Mineral Utilization de la Cryoscopie en Mileu Salin, *Bull. Soc. Chim. Fr.*, Series 5, Vol 15, p 143–156

Tananaev, I.V., and Vinogradova, A.D., 1960. The Composition and Strength of Fluoferrate and Fluorberyllate Complexes in Solution by Solubility Determinations, *Zh. Neorg. Khim.*, Vol 5, p 321–326

Taylor, A.R., Jr. and Gardner, T.E., 1965. "Some Thermal Properties of Beryllium Fluoride from 8 °K to 1200 °K," Reports of Investigation 6664, U.S. Bureau of Mines

Teyssedre, M., and Souchay, P., 1951. Relations Entre Courbes de Titrage Cryoscopique et Potentiometrique en Milieu Heterogene, *Bull. Soc. Chim. Fr.*, Series 5, Vol 18, p 945

Thoma, R.E., Weaver, C.F., Friedman, H.A., and Harris, L.A., 1960. The Compounds $NaF \cdot BeF_2 \cdot 3ThF_4$ and $NaF \cdot BeF_2 \cdot 3UF_4$, *J. Am. Ceram. Soc.*, Vol 43 (No. 11), p 608–609

Venturello, G., 1941. *Atti. Reale Accad. Sci. Torino*, Vol 76, p 559

Walsh, K.A., 1979. Extraction, *Beryllium Science and Technology*, Vol 2, D.R. Floyd and J.N. Lowe, Ed., Plenum Press, NY, p 1–10

Warren, B.E., and Hill, C.F., 1934. *Z. Krist.*, Vol 89, p 484

Wells, A.F., 1961. *Structural Inorganic Chemistry*, Oxford University Press

Williams, R.T., Nagel, D.J., Klein, P.H., and Weber, M.J., 1981. Vacuum Ultraviolet Properties of Beryllium Fluoride Glass, *J. Appl. Phys.*, Vol 52 (No. 10), p 6279–6284

Wright, W.J., and Silver, J.M., 1963. The Extrusion of Beryllium, *The Metallurgy of Beryllium*, Monograph No. 28, The Institute of Metals, London, U.K., p 734–742

Young, W.A., 1960. The Reactions of Water Vapor with Beryllia and Beryllia-Alumina Compounds, *J. Phys. Chem.*, Vol 64 (No. 8), p 1003

Zhukov, A.I., Onosov, V.N., and Krasil'nikov, M.T., 1962. Temperature Effects on Sorption and Elutriation of Hydrolyzed Thorium Ions, *Zh. Neorg. Khim.*, Vol 7, p 1448–1551

SELECTED REFERENCES

- Campbell, A.N., Sukava, A.J., and Koop, J., 1951. The Hydrates of Beryllium Sulfate, *J. Am. Chem. Soc.*, Vol 73, p 2831
- Carell, B., and Olin, A., 1961. Studies on the Hydrolysis of Metal Ions. 37. Application of the Self-Medium Method to the Hydrolysis of Beryllium Perchlorate, *Acta Chem. Scand.*, Vol 15, p 1875–1884
- Fleischer, M., and Cameron, E.N., 1946 and 1955. "Geochemistry of Beryllium," Report MDDC-643 (1946) and TID-5212 (1955), U.S. Atomic Energy Commission, p 80–92
- Gulbransen, E.A., and Andrew, K.F., 1950a. The Kinetics of the Reaction of Beryllium with Oxygen and Nitrogen and the Effect of Oxide and Nitride Films on Its Vapor Pressure, *J. Electrochem. Soc.*, Vol 97, p 383
- Kanazawa, E., and Packer, C.M., 1960. "Specific Heats of Beryllium and an Alloy at Room and Elevated Temperatures," Report LMSD-288140, Vol 2, Lockheed Aircraft Corporation
- McDonald, R.A., and Oetting, F.L., 1965. The Thermodynamic Properties and Allotropy of Beryllium Chloride between 13 and 715 K, *J. Phys. Chem.*, Vol 69 (No. 11), p 3839
- Misumi, S., and Taketatsu, T., 1959. Indirect Complexometric Titration of Beryllium with Ethylenediaminetetraacetic Acid, *Bull. Chem. Soc. Jpn.*, Vol 32 (No. 6), p 593–596

Beryllium Chemistry and Processing, p 107-115
By Kenneth A. Walsh
Edited by Edgar E. Vidal, Alfred Goldberg,
Edward N.C. Dalder, David L. Olson, and Brajendra Mishra

CHAPTER 9

Analytical Chemistry of Beryllium

David L. Olson, Colorado School of Mines
Edgar E. Vidal, Brush Wellman, Inc.

BERYLLIUM belongs to the ammonium hydroxide analytical group. Beryllium is completely precipitated by ammonia, along with iron, aluminum, and chromium, at a pH of 8.5. This precipitation requires the absence of fluoride, silica, phosphate, and organic matters. Beryllium can be separated from aluminum using 8-hydroxyquinoline. Aluminum is precipitated from an acetate-buffered acetic acid solution of pH 5.7. Iron and titanium can be precipitated by cupricferron since beryllium does not form a precipitate with it. Iron, chromium, nickel, cobalt, tin, molybdenum, zinc, and lead can be separated by electrolysis using a mercury cathode, while beryllium is left in the electrolyte.

9.1 Sample Preparation for Beryllium Analysis

Beryllium and beryllium-mineral-containing samples must first be fused with sodium carbonate, potassium hydroxide, or sodium fluoride, because their complete dissolution is usually difficult. Fritting with sodium peroxide or low-temperature fusion with ammonium fluoride can also be done. When finely powdered, beryllium minerals can be dissolved by prolonged treatment with hydrofluoric acid mixed with nitric or perchloric acids.

Fluoride fusions have the advantage of quickly and completely removing silica as silicon tetrafluoride, but their use usually involves the removal of fluoride by fuming with sulfuric acid. General laboratory experience shows that fusion with sodium fluoride or fritting with sodium peroxide are the best methods for dissolving beryllium minerals. Potassium hydroxide fusions are best for beryllium oxide and similar products based on it, which have been heated to a high temperature (>1550 °C, or 2820 °F). Ammonium fluoride fusions, which always require a large excess of flux (25 g NH_4F/5 g sample), are of use in geochemical prospecting, where field operation imposes the use of low fusion temperatures. The procedure of simply dissolving by fusion with potassium bisulfate only incompletely attacks beryl, but, because beryllium in this form is considered nontoxic, the method does not thereby suffer.

9.2 Quantitative Procedures for Beryllium Determination

9.2.1 Gravimetric Methods

Gravimetric methods are employed where accuracy takes precedence over speed and ease of analysis, for instance, in the accurate determination of beryllium in a high-grade ore.

Two main procedures are employed, based either on the precipitation of beryllium hydroxide [Vinci 1962, Brewer 1952, Rogers and Prather 1959] or beryllium ammonium phosphate [Huré et al. 1952]. The precipitate is ignited and then weighed as BeO or $Be_2P_2O_7$, respectively. The phosphate has the advantage of giving 3.838 times as much mass per equivalent of beryllium as the oxide. Although ethylenediamine tetraacetic acid (EDTA) forms strong complexes with many metals, it has a low stability

with beryllium. Therefore, it is possible to selectively precipitate beryllium hydroxide in the presence of this reagent. As in all precipitations of beryllium from aqueous solutions, fluoride must be absent because it strongly complexes beryllium and prevents complete precipitation.

For solutions relatively free from interfering ions, precipitation of beryllium hydroxide at a pH of 8.5 with ammonia in the absence of complexing agents, followed by ignition at 1100 to 1200 °C (2010 to 2190 °F) in a platinum crucible, is satisfactory. Ammonia is preferred to sodium hydroxide because co-precipitated sodium ions are not driven off on ignition but remain and contaminate the beryllium oxide that is finally produced. For solutions of greater impurity, such as are obtained in the analysis of minerals, more precautions are necessary. Describing the analysis of beryl, Brewer [1952] says that, after the precipitation of beryllium hydroxide in the presence of EDTA (added as the ammonium salt), the ignited precipitate should be fused with sodium carbonate, and the cooled melt should be leached with water to remove the aluminum or phosphate. The residue is ignited and weighed as BeO.

In general, beryllium amounts determined by the hydroxide method tend to be high, due to absorption of impurities by the beryllium hydroxide. There is a small loss of beryllium due to solubility at the precipitation stage and a rather larger one during the leaching of the sodium carbonate fusion. However, these losses are counterbalanced by impurities (sodium, silica, and aluminum) in the oxide after its last ignition [Hunt and Martin 1960].

In the phosphate method of Huré et al. [1952], $BeNH_4PO_4$ is precipitated at a pH of 5.2 in the presence of the ammonium salt of EDTA, the phosphate being added as ammonium dihydrogen phosphate to the solution buffered by means of ammonium acetate. For the highest accuracy, the precipitate is redissolved in dilute hydrochloric acid, reprecipitated, ignited at 1000 °C (1830 °F), and weighed as $Be_2P_2O_7$. The alkali metal ions in the solution should be kept to a minimum since these contaminate the precipitate. They give a "fused" appearance to the ignited $Be_2P_2O_7$ and cause it to stick to the sides of the platinum dish. A significant advantage of the method is that it does not require phosphate to be separated from the solution before the precipitation of beryllium.

Another gravimetric procedure is that described by Pirtea and Constantinescu [1959]. In it, beryllium is selectively precipitated by hexamminocobaltic chloride as the complex $(Co(NH_3)_6)[(H_2O)_2Be_2(CO_3)_2(OH)_3] \cdot H_2O$ and is weighed as such. Satisfactory results are obtained with pure beryllium solutions, but great care is needed during the drying of the precipitate to achieve constant composition. This elegant method has shown some uncertainty in operation, which has prevented its general use.

9.2.2 Volumetric Methods

Only one satisfactory volumetric procedure for beryllium exists; it is both empirical in character and applicable only to relatively pure solutions. Beryllium is first precipitated with ammonia (pH 8.5) from a sulfate or chloride solution, and an excess of alkali fluoride is added as potassium or sodium fluoride. An almost quantitative reaction occurs:

$$Be(OH)_2 + 4F^- \leftrightarrow BeF_4^{2-} + 2OH^- \qquad \text{(Eq 9.1)}$$

The amount of alkali liberated is proportional to the beryllium present and is titrated with standard acid [Melick 1958, Wallace 1959a, b]. Aluminum reacts in a similar manner and must either be absent or a correction made for its presence. The same is true of zirconium, rare earths, uranium, and thorium, which should also be absent. Because the reaction is not stoichiometric, all the operations must be precisely standardized, and the acid used must be standardized by an exactly similar method. In particular, the titration must be performed slowly, to give sufficient time for the reaction to reach equilibrium after each addition of reagent.

The method is useful in practice because of its simplicity, speed, and reasonable accuracy and should be of value for the determination of beryllium in relatively pure solutions. The low equivalent weight of beryllium is an advantage in volumetric analysis, since it causes large titrates to be given by relatively small amounts of beryllium.

9.2.3 Colorimetric and Fluorometric Methods

Very large numbers of colorimetric or fluorometric reagents have been described for the determination and detection of beryllium. Of these reagents, Zenia (p-nitrophenyl-azoorcinol) [Stross and Osborn 1944] and, in particular, Berillon (the tetra-sodium salt of 8-hydroxynaphthalene-3, 6-disulfonic acid-(I-azo-2′)-1,8′-di-hydroxynaphthalene-3′,6′-disulfonic acid) [Karanovich 1956] have proved the most important. Although Zenia

is widely used for beryllium analysis, its sensitivity is rather low, the color intensity of the complex is temperature dependent (indicating approximately 2.5 wt% increase per degree), and the conditions in which the reagent blank is found are very critical and must be carefully controlled.

In practice, Berillon seems to be the most satisfactory absorptiometric reagent for beryllium [Hunt and Martin 1960]. In strong alkali solutions, Berillon is magenta to violet, depending on its concentration, and its beryllium complex is blue. Karanovich [1956] increased the selectivity of the reagent by adding EDTA, to complex most other metals, and ascorbic acid, to reduce iron to the noninterfering ferrous state. However, it is doubtful whether these reagents can effectively eliminate interference due to ferric iron in the strongly alkaline solutions employed. Other possible sequestering agents for iron have been examined, and it is recommended that Nervanaid-F (N,N-bis-(2-hydroxyethyl) glycine) be used in place of ascorbic acid when much iron is present. The solution at the time of measurement should contain not more than 16 μg Be/50 mL. Its absorbency is measured at 630 mμ (Unicam SP 500 spectrophotometer-red photocell) from 10 to 30 min after mixing the reagents. However, the plot of absorbency against beryllium concentration is not linear; the curvature is considerable at concentrations above 16 μg Be/50 mL.

The Berillon method has been adapted to field conditions to provide a rapid and sensitive beryllium analytical procedure for use in geochemical prospecting [Hunt et al. 1959–1960]. The colors obtained are compared visually with those of standards.

The most sensitive chemical test known for beryllium is that based on the fluorescence developed when beryllium reacts with Morin (3,5,7,2′,4′-pentahydroxyflavone) in a sodium hydroxide solution of pH greater than 11.0 [Wallace 1959a, b]. Careful control of conditions (temperature and the reagent concentrations) is said to give a detection limit of 0.004 μg Be and a precision of 0.8 wt% on 0.2 μg Be at the 95% confidence level. However, the method is not specific for beryllium and is subject to many interferences, so that beryllium must first be separated from the other elements present [Sill and Willis 1959, Florence 1959]. An important application of the Morin fluorescence method is for the routine determination of microgram or submicrogram amounts of beryllium in filter paper; such samples arise in large numbers in beryllium laboratories from the operation of health-monitoring services. Separation of beryllium from bulk impurities (such as may be present in a smear sample) is carried out by chelating the latter with sodium diethyl dithiocarbamate (which does not complex beryllium) and then extracting the thiocarbamate complexes with ethyl acetate [Berkeley and Smith 1962, Vanossi 1957]. Trace impurities (such as would be present in airborne dust samples) are effectively sequestered with EDTA. Iron, which is not complexed by EDTA at the high pH values used in the Morin method, is sequestered by citric acid and triethanolamine.

It should be noted that the purity of the Morin reagent is of importance; even the best-quality commercial material always gives high blank readings. These blanks are reduced by one-half by dissolving the Morin in alcohol, holding the solution over activated charcoal, and reprecipitating the Morin by the addition of ether [Berkeley and Smith 1962].

Another very sensitive reagent for beryllium is Chrome Azurol S (the sodium salt of 3″-sulfo-2″,6′-dichloro-3,3′-dimethyl-4-hydroxy-fuchson-5,5′-dicarboxylic acid). This compound gives a pink to purple-blue color with beryllium in neutral or weakly acidic solutions [Theis 1955, Wood 1955]. Silverman and Shideler [1958] have shown that for optimum results, the solution should be buffered to pH 6.0 ± 0.1 by means of pyridine-hydrochloric acid, since the intensity of color varies with the pH. The time for reading is not critical, but consistent results are assured when the liquid is allowed to stand for 15 min before measuring the color intensity. Unfortunately, the method is susceptible to interferences: positive by metals such as Fe^{3+}, Al^{3+}, Zr^{2+}, and Pb^{2+}, and negative with complexing agents such as acetate, tartrate, or EDTA. It appears that to obtain maximum sensitivity, and to ensure accurate results, all interfering species must be absent. Under these ideal conditions, from 0.2 to 10 μg Be/50 mL can be determined with a precision of 0.2 μg. Like all the metal-Chrome Azurol S complexes, the complex formed by beryllium is destroyed (bleached) by fluoride. Indeed, this reaction is employed as a sensitive method for fluoride analysis; from 1 to 30 μg F/50 mL can be determined with a precision of 1 μg [Silverman and Shideler 1958].

Eriochrome Cyanine R is another sensitive, although not specific, reagent for beryllium [U.T. Hill 1958]. Combined with the ring-oven

technique, this reagent has been used for the rapid analysis of beryllium in air-monitoring samples [West and Mohilner 1962]. Determinations can be made on 0.05 μg Be with an average error of ±7%.

9.3 Other Methods for Beryllium Separation

In the procedures already outlined, selectivity was introduced by the addition of reagents, such as EDTA or 8-hydroxyquinoline, which either complex or precipitate the impurities rather than the beryllium. Besides these, there are a number of separation procedures that use the newer separation techniques. Thus, beryllium can be separated from aluminum or iron by passing a solution of these metals at a pH of 3.5, and containing EDTA, through a column of a sulfonic acid cation-exchange resin. The uncomplexed Be^{2+} ions are absorbed by the resin, while the anionic or neutral iron and aluminum complexes pass on [Nadkarni et al. 1957]. Rather better results are obtained with a phosphonic acid or a diallylphosphate polymer resin [Kennedy and Wheeler 1959], since these possess a much greater affinity for the Be^{2+} ions. Alternatively, beryllium can be separated from aluminum, iron, and other trivalent metals by selective elution from a sulfonic acid resin with 1.0 *N* hydrochloric or 1.2 *N* nitric acids, the beryllium being eluted in a band ahead of the trivalent metals [Strelow 1961].

Solvent extraction procedures involving direct beryllium extraction have used mainly acetylacetone. Typical is the method of Adam et al. [1952] in which beryllium is separated from other elements by a double extraction of beryllium acetylacetonate into chloroform from aqueous media at a pH of 7 to 8. The addition of EDTA to the aqueous solution before each extraction avoids interferences. The light absorption of the beryllium complex is measured in the final chloroform extract at 295 mμ against a chloroform blank. Between extractions, the chloroform layer is evaporated, the organic matter is destroyed by wet oxidation with nitric or perchloric acids, and the residue is redissolved in water.

Paper chromatographic methods have also been employed. Beryllium is separated from aluminum by downward elution with a solvent consisting of 80 vol% methylethyl ketone and 20 vol% hydrochloric acid. The beryllium band is detected by spraying with Morin or alizarin solution; the particular strip is excised, ashed, and the beryllium is dissolved in dilute sulfuric acid and determined absorptiometrically.

An improved procedure has been described [Ader and Alon 1961] in which the chromatogram is developed on paper impregnated with the disodium salt of EDTA or methylethyl ketone-hydrochloric acid; or, ethanol-hydrochloric acid-water is used as the developing solvent and Eriochrome Cyanine R the color-forming reagent. The blue-violet beryllium-dye complex is compared with standard chromatograms for quantitative work, and as little as 0.002 μg Be can be visually detected. Impregnation with EDTA reduces interference from metals that form colored complexes with Eriochrome Cyanine R. However, it does cause the beryllium band to be somewhat diffuse and trailing, a difficulty that is overcome by allowing the band to migrate only a short distance (4 cm). The sheet is finally air dried, exposed to ammonia gas, and then sprayed with 0.075% Eriochrome Cyanine R solution.

9.4 Radiochemical Separation Procedures

These are dealt with separately from the macro methods because the active components in most of the solutions encountered in radiochemistry are in extremely dilute solution. Aspects of beryllium chemistry that are of little importance at macro concentrations become significant at high dilutions. For example, the ready hydrolysis of the Be^{2+} ion leads to the adsorption of beryllium onto the walls of the containing vessel, presumably as a polymeric hydrolytic species. It has been found that up to 20 wt% of the ^{7}Be from a carrier-free solution in 0.1 *M* sodium chloride buffered with 0.001 *M* sodium acetate is adsorbed onto the surface of a glass container at pH 6, whereas less than 5 wt% of the ^{7}Be is adsorbed on polyethylene under similar conditions. The adsorption of beryllium onto polyethylene or glass falls to zero at approximately pH 5 and 4.5, respectively [Fairhall 1960]. Thus, for storage of any very dilute beryllium solution, polyethylene vessels should be employed and the pH kept below 4.

Another important consequence of the hydrolysis of the Be^{2+} ion is its ready co-precipitation with almost any precipitate formed at pH ~7. Gelatinous hydroxides, such as those of aluminum or iron, are particularly effective. From

ferric hydroxide used as a co-precipitant, beryllium can be recovered by treatment with cold caustic soda.

Solvent extraction procedures are of importance in connection with beryllium radiochemistry; those involving acetylacetone [Toribara and Chen 1952], thenoyltrifluoro-acetone (TTA) [Bolomey and Wish 1950], and the chloroform extraction of beryllium oxide acetate are typical. Extraction by TTA (0.01 *M* TTA in benzene) differs from that by acetylacetone in being slow; at the optimum aqueous phase pH of 7, it takes approximately 3 h to complete. Aluminum is also removed, but less iron is removed at pH 7 than at a lower pH. Back-extraction of the organic phase with concentrated hydrochloric acid removes all the calcium, iron, strontium, and yttrium in 15 min. These are completely separated from the beryllium; this separation requires at least 80 h for complete back-extraction. However, beryllium is rapidly and completely stripped from the organic phase by a mixture of two parts concentrated formic to one part concentrated hydrochloric acid. Working at tracer concentrations, the TTA method has an advantage over the acetylacetone procedure, since loss of beryllium does not occur through volatilization of the beryllium-TTA complex. Separations based on the extraction of the oxide acetate have the advantage of being nearly specific for beryllium. However, the preparation of beryllium oxide acetate is relatively lengthy, and this tends to limit the use of the method.

Chromatographic ion-exchange methods have been applied to separations of radiochemical beryllium. For example, 1.5 *M* hydrochloric acid has been used for the separation of the alkaline earth elements absorbed on the sulfonic acid resin Dowex 50 (Dow Chemical Co.) [Milton and Grummitt 1957]. The metals are eluted in the expected order, namely, beryllium first, followed by magnesium, calcium, strontium, and barium. Other selective eluting agents have been employed with sulfonic resins: 0.55 *M* ammonium lactate at a pH of 5 for separating beryllium and the alkaline earths [Milton and Grummitt 1957]; 0.02 to 0.10 *M* sulfosalicylic acid [Schubert et al. 1958] at a pH of 3.5 to 4.5 for separating beryllium from Cu^{2+}, UO_2^{2+} and Ca^{2+}; and dilute magnesium or calcium solutions for separating beryllium and aluminum [Honda 1951]. The beryllium is always eluted first, rapidly with >3 *M* hydrochloric acid [Diamond 1955] or by 0.5 *M* sodium acetate in 1.0 *M* acetic acid [Fairhall 1960]. With the sodium acetate, all the beryllium is removed in only 0.5 to 1.5 column volumes of effluent.

9.5 Radiometric Methods of Beryllium Analysis

Following the pioneering work of Gaudin and Pannell [1951], several instruments have been devised for the radiometric assay of beryllium, based on the nuclear reaction:

$$^{9}_{4}\mathrm{Be} + \gamma \leftrightarrow {}^{8}_{4}\mathrm{Be} + {}^{1}_{0}\mathrm{n} \qquad \text{(Eq 9.2)}$$

In this reaction, the number of neutrons produced is directly proportional to the quantity of beryllium present. Provided that the source and the geometry of the system remain unchanged, the beryllium contents of different samples can be compared. This can be achieved by beryllium assay equipment with a γ source of an aluminum capsule containing antimony that has been pile irradiated to give ^{124}Sb (60 day half-life) and ^{122}Sb (3 day half-life). It is the 2.39 MeV γ-radiation from the ^{124}Sb that liberates neutrons from the beryllium atoms. The ^{122}Sb merely causes an increase in the background gamma radiation. The source is usually 100 to 125 millicuries (mC) of ^{124}Sb and is used for approximately six weeks before re-irradiation. The neutrons liberated are counted by five boron trifluoride counters appropriately dispersed around the sample. Indeed, the maintenance of correct counter geometry at all times is one of the most important features in the design of this equipment.

The sensitivity and accuracy of the (γ, n) assay equipment is enhanced by an increase in source size; the statistical accuracy of a determination depends on the number of counts. For instance, at least 6000 total counts are required for 2% accuracy. Obviously, with a particular beryllium content, this minimum number of counts can be achieved more rapidly with a larger gamma source. Alternatively, the amount of beryllium required to give sufficient counts in a given time decreases as the intensity of the source is raised. However, large sources present shielding problems, and this limits the power of the source that is convenient to employ.

An advantage of the (γ, n) method is that it provides nondestructive analysis of solid samples. This analysis both eliminates the time-consuming process of sample dissolution and allows valuable experimental material to be preserved. Samples of approximately 50 g are usually employed

in the assay equipment, although simple modifications allow the use of smaller samples. The count rate for the unknown sample is compared with that for a standard under similar conditions, both being corrected for background. The percentage of beryllium in the sample is given by the counts per minute adjusted for its weight.

For accuracy, the volumes of the samples and the standard should be approximately the same, and their densities and particle sizes should be similar. The procedure is applicable to beryllium-containing solutions when the count rates of equal volumes of sample and standard are compared. It provides the only analytical method for beryllium solutions with which fluoride does not interfere. With a ^{124}Sb source of approximately 100 mC, the background count is about four per minute. The count rate for a 50 mL liquid sample containing 1 mg BeO/mL is approximately 120 counts/min; this is about two counts/min per mg BeO. Similar figures apply to solid samples.

The only elements that interfere with the (γ, n) method are the rare earths (particularly gadolinium) and boron [Milner and Edwards 1959], which absorb neutrons and reduce the observed count rate. However, these elements must be present in considerable quantity for their interference to be significant. The (γ, n) method has been adapted for the detection and assaying of beryllium minerals under field conditions [Bowie et al. 1959]. The equipment is handled by means of long, hinged arms that enable the operative portion to be brought into contact with any rock surface, while the operators remain at a safe distance from the gamma source. It provides an extremely powerful tool in beryllium prospecting.

9.6 Spectrometric Methods

The determination of beryllium is better undertaken by either wet analytical methods or the (α, n) procedure than by means of emission spectrometry. Advantages of the latter are its specificity, high sensitivity, and, especially, its ability to cope rapidly with large numbers of samples. The method is empirical, and a range of standard mixtures for each type of samples to be analyzed must be prepared. Although a number of spectrometric procedures have been described for the determination of beryllium in beryl [Kehres and Poehlmann 1954, Alekseeva and Rusanov 1957, Creitz 1958], the method is primarily used for the rapid control of mineral separations and for sorting large numbers of ore samples. Even here, the (α, n) method is preferred if 10 to 100 g samples are available, containing not less than 0.01 wt% Be for a 100 mC source.

Emission spectrometry is very useful for the analysis of trace quantities of beryllium, especially for samples produced by environmental monitoring [Brooks 1958a, b]. An especially important application is the development of portable spectrographic equipment for the continuous analysis of beryllium in air. Churchill and Gillieson [1952] introduced the technique of continuously drawing a constant flow of air across a spark gap. The light from the spark was dispersed by a grating monochromator set for the beryllium doublet at 3130 Å, and the resulting beam was detected and recorded continuously by means of a photomultiplier, direct current amplifier, and chart recorder. An improved version of this monitor has been described [Webb et al. 1959] in which integration over a short time is used rather than continuous recording. It is claimed that by careful design of the spark gap and by using a pulsed-arc discharge axially in the air stream, rather than a condensed spark across it, the results are independent of the particle size and chemical composition of any airborne beryllium dust.

An important use of emission spectrometry is in the determination of impurities in beryllium oxide, beryllium metal, and so on. In this method [Karabash 1959], a 2 g sample is converted to beryllium oxide acetate, which is dissolved in chloroform and the impurities re-extracted into 4 *N* hydrochloric acid together with approximately 5 wt% of the beryllium. This beryllium is reconverted to oxide and contains all the impurities present in the original sample. The impurities are determined by arching the oxide in a graphite cup at 12 A, and the detection limits are stated in Table 9.1.

Table 9.1 Detection limits of impurities using emission spectrometry

Element	Amount, ppm
Zn	5.0
Ca, Al	3.0
Ba, Ti, Fe, Sb, Te, In, Tl	2.0
Mg, Mo, Co, Ni, Sn, Pb, Na	1.0
V, Cr, Bi, Ga	0.5
Cu	0.3
Ag	0.2
Mn	0.1
C	0.05

Source: Everest 1964

9.7 Polarographic Methods

Heyrovsky and Berezicky [1929] did not observe a reduction wave with solutions of pure beryllium salts before the onset of the hydrogen wave caused by the hydrolysis of the Be^{2+} ion. Later, solutions of beryllium sulfate and chloride were shown to give two waves, the first at approximately -1.4 V due to the discharge of hydrogen and the second at -1.8 V versus the saturated calomel electrode due to reduction of the Be^{2+} ion [Kemula and Michalski 1933], but the beryllium wave was not well defined. More recently, it has been reported that an analytically usable wave is produced in a 0.5 *M* lithium chloride supporting electrolyte of pH 3.4, the diffusion current remaining proportional to the beryllium concentration up to 8×10^{-3} *M* [Venkataratnam and Rao 1958]. The beryllium wave is close to that of hydrogen, so the pH must be carefully controlled in order that the height of the beryllium wave can be measured.

REFERENCES

Adam, J.A., Booth, E., and Strickland, J.D.H., 1952. The Determination of Microgram Amounts of Beryllium Using Acetyl Acetone, *Anal. Chem. Acta*, Vol 6, p 462–471

Ader, D., and Alon, A., 1961. Rapid Determination of Beryllium. A Paper-Chromatographic Method, *Analyst*, Vol 86, p 125–129

Alekseeva, V.M., and Rusanov, A.K., 1957. Quantitative Spectrographic Determination of Beryllium in Ores and Minerals, *Zh. Anal. Khim.*, Vol 12 (No. 1), p 23–33

Berkeley, A.M., and Smith, A.H., 1962. Scientific Report NCL/AE 203, The National Chemical Laboratory

Bolomey, R.A., and Wish, L.J., 1950. Thenol Trifluoride Acetone as a Complexing Agent for Isolation and Purification of Carrier-Free Radioberyllium, *J. Am. Chem. Soc.*, Vol 72, p 4483–4486

Bowie, S.H.U., Burke, K.C., Bisby, H., and Hale, F.H., 1959. Electronic Instruments for Detecting and Assaying Beryllium Ores, *Trans. Inst. Min. Metall.*, Vol 69, p 345

Brewer, P.J., 1952. Determination of Be in Beryl by Means of EDTA, *Analyst*, Vol 77, p 539

Brooks, R.O.R., 1958a. Beryllium Handling. Reducing the Health Risk, *Nucl. Power*, Vol 3, p 112–114

Brooks, R.O.R., 1958b. Environmental Monitoring for Beryllium, *Nucl. Power*, Vol 3, p 539–542

Churchill, W.L., and Gillieson, A.H., 1952. A Direct Spectrographic Method for Monitoring of Air for Minute Amounts of Beryllium and Beryllium Compounds, *Spectrochim. Acta*, Vol 5, p 238–250

Creitz, E.E., 1958. "Spectrographic Determination of Beryllium in a Variable Matrix," Report BM-RI-5407, U.S. Bureau of Mines, Washington, D.C.

Diamond, R.M., 1955. Factors Influencing Ion-Exchange Equilibria in Concentrated Solutions: Behavior of Alkaline Earth and Alkali Ions, *J. Am. Chem. Soc.*, Vol 77, p 2978

Everest, D.A., 1964. *The Chemistry of Beryllium*, Elsevier, New York, NY, p 38

Fairhall, A.W., 1960. "The Radiochemistry of Beryllium," Report NAS-NS-3013, Nuclear Science Series of the National Research Council, Department of Chemistry, Washington University, Seattle, WA

Florence, T.M., 1959. A Rapid Routine Method for Determination of Sub-Microgram and Microgram Amounts of Beryllium in Filter Paper, *Anal. Chim. Acta*, Vol 20, p 472

Gaudin, A.M., and Pannell, J.H., 1951. Determination of Beryllium by Photodisintegration, *Anal. Chem.*, Vol 23, 1951, p 1261

Heyrovsky, J., and Berezicky, S., 1929. The Deposition of Radium and Other Alkaline Earth Metals at the Dropping Mercury Cathode, *Collect. Czech. Chem. Commun.*, Vol 1, p 19–46

Hill, U.T., 1958. Photometric Determination of Beryllium, *Anal. Chem.*, Vol 30 (No. 4), p 521

Honda, M.J., 1951. *Chem. Soc. Jpn.*, Vol 72, p 361

Hunt, E., and Martin, J.V., 1960. A.E.A. Report, *Symposium on the Analytical Chemistry of Beryllium* (Blackpool, U.K.), I. Metcalfe and J. Ryan, Ed., p 171

Hunt, E., Stanton, R.E., and Wells, R.A., 1959–1960. Field Determination of Beryllium in Soils for Geochemic Prospecting, *Bull. Inst. Min. Metall.*, Vol 69, p 361–369

Huré, J., Kremer, M., and Le Bekquier, F., 1952. Dosage Gravamétrique Rapide du Béryllium dans les Béryls, *Anal. Chim. Acta*, Vol 7, p 37

Karabash, A.G., Peizulaev, S.I., Slyusareva, R.L., and Lipatova, V.M., 1959. Chemico-Spectrographic Method for the Analysis of Metallic Beryllium and Beryllium Oxide

of High Purity, *Zh. Anal. Khim.*, Vol 14, p 94–99
Karanovich, G.C., 1956. Colorimetric Determination of Beryllium by Means of a New Reagent—Berillon II, *Zh. Anal. Khim.*, Vol 11, p 417–421
Kehres, P.W., and Poehlman, W.J., 1954. Spectrochemical Analysis of Beryllium in Ore, Air and Solutions, *Appl. Spectrosc.*, Vol 8 (No. 1), p 36–42
Kemula, W., and Michalski, M., 1933. *Collect. Czech. Chem. Commun.*, Vol 5, p 436
Kennedy, J., and Wheeler, V.J., 1959. The Separation of Beryllium from Polyvalent Cations with a Diallyl Phosphate Complexing Resin, *Anal. Chim. Acta*, Vol 20, p 412–415
Melick, E.S., 1958. "The Analytical Chemistry of Beryllium," Report TID-7555, First Conf. Analytical Chemistry in Nuclear Reactor Technology, U.S. Atomic Energy Commission
Milner, G.W.C., and Edwards, J.W., 1959. "The Determination of Beryllium by the Photoneutron Method," Report AERE-R-2965, United Kingdom Atomic Energy Authority
Milton, G.M., and Grummitt, W.E., 1957, Ion-Exchange Methods for the Quantitative Separation of the Alkaline Earths, and Their Application to the Determination of Sr90 in Milk Ash, *Can. J. Chem.*, Vol 35 (No. 6), p 541–551
Nadkarni, M.N., Varde, M.S., and Athavale, V.T., 1957. The Separation of Beryllium from Iron, Aluminum and Titanium by Ion Exchange, and Its Application to the Analysis of Beryl, *Anal. Chim. Acta*, Vol 16, p 421–425
Pirtea, J., and Constantinescu, V.Z., 1959. Eine Gewichtsanalytische Bestimmungsmethode für Beryllium in Gegenwart von Anderen Elementen in Legierungen und Mineralien, *Fresenius' J. Anal. Chem.*, Vol 165 (No. 3), p 183–188
Rogers, N.E., and Prather, D.W., 1959. Determination of Uranium and Beryllium in Fused Fluoride Systems, *Anal. Chem.*, Vol 31 (No. 6), p 1081–1084
Schubert, J., Lindenbaum, A., and Westfall, W., 1958. Ion-Exchange Separation of Beryllium by Elution with Salicylate Analogs, *J. Phys. Chem.*, Vol 62 (No. 4), p 390–394
Sill, C.W., and Willis, C.P., 1959. Fluorometric Determination of Submicrogram Quantities of Beryllium, *Anal. Chem.*, Vol 31 (No. 4), p 598–608
Silverman, L., and Shideler, M.E., 1958. "Spectrophotometric Determinations of Beryllium and Fluoride Using Chrome Azurol S," Report NAA-SR-2686, North American Aviation Inc., Canoga Park, CA
Strelow, F.W., 1961. A Separation of Beryllium from Aluminum, Trivalent Iron, Yttrium, Cerium, and the Rare Earths by Cation Exchange Chromatography, *Anal. Chem.*, Vol 33 (No. 4), p 542–545
Stross, W., and Osborn, G.H., 1944. Photometric Determination of Beryllia in the Presence of Alumina, *J. Soc. Chem. Ind.*, Vol 63 (No. 8), p 249–251
Theis, M.Z., 1955. Ein neuer Empfindlicher Nachweis des Berylliums, *Fresenius' J. Anal. Chem.*, Vol 144 (No. 3), p 192–194
Toribara, T.Y., and Chen, P.S., 1952. Separation of Beryllium from Biological Materials, *Anal. Chem.*, Vol 24 (No. 3), p 539–542
Vanossi, R., 1957. *An. Asos. Quim. Argentina*, Vol 45, p 215
Venkataratnam, G., and Rao, B.S.V.R., 1958. Polarography of Beryllium, *J. Sci. Ind. Res. India B*, Vol 17, p 360–362
Vinci, F.A., 1962. *Standard Methods of Chemical Analysis*, 6th ed., N.H. Furman, Ed., D. Van Nostrand, NY
Wallace, C.G., 1959a. "The Volumetric Determination of Beryllium in Beryl Ore," Report AERE-AM-29, United Kingdom Atomic Energy Authority
Wallace, C.G., 1959b. "The Volumetric Determination of Beryllium in Low Grade Ores," Report AERE-AM-30, United Kingdom Atomic Energy Authority
Webb, R.J., Webb, M.S.W., and Wildy, P.C., 1959. Atomic Energy Research Established Report AERE R2868
West, P.W., and Mohilner, R.R., 1962. Estimation of Beryllium with Eriochrome Cyanine R Using the Ring Oven Technique, *Anal. Chem.*, Vol 34 (No. 4), p 558–560
Wood, J.H., 1955. A New Organic Reagent for the Determination of Microgram Quantities of Beryllium by a Spectrophotometric Method, *Mikrochim. Acta*, Vol 43, p 11–24

SELECTED REFERENCES

- Duval, T., and Duval, C., 1948. Thermogravimetrics of Analytical Precipitates, Part VI: Determination of Beryllium, *Anal. Chim. Acta*, Vol 2, p 53–56

- Gaudin, A.M., Dasher, J., Pannell, J.H., and Freyberger, W.L., 1953. Use of an Induced Nuclear Reaction for the Concentration of Beryl, *Min. Eng. (NY)*, Vol 2, p 495–498
- Sill, C.W., Willis, C.P., and Flygare, J.K., Jr., 1961. Improvements in the Fluorometric Determination of Submicrogram Quantities of Beryllium, *Anal. Chem.*, Vol 33 (No. 12), p 1671–1684
- Smythe, L.E., and Whittem, R.N., 1961. Analytical Chemistry of Beryllium—A Review, *Analyst*, Vol 86, p 83–94
- Toribara, T.Y., and Sherman, R.E., 1953. Analytical Chemistry of Micro Quantities of Beryllium, *Anal. Chem.*, Vol 25 (No. 11), p 1594–1597
- Vauquelin, L.N., 1799. *Ann. Chim. (Phys.)*, Vol 30, p 82

Beryllium Chemistry and Processing, p 117-129
By Kenneth A. Walsh
Edited by Edgar E. Vidal, Alfred Goldberg,
Edward N.C. Dalder, David L. Olson, and Brajendra Mishra

CHAPTER 10

Beryllium Compounds

Kenneth A. Walsh, Brush Wellman, Inc., Retired
Edgar E. Vidal, Brush Wellman, Inc.
Brajendra Mishra, Colorado School of Mines

BERYLLIUM forms a wide range of inorganic and organic compounds. Some of the most important families of compounds and their synthesis are summarized in this chapter.

10.1 Beryllium Borides

Beryllium forms three borides: Be_2B, BeB_2, and BeB_6. An additional possible phase is BeB_4. The borides are all obtained by direct interaction of the elements at approximately 1400 °C (2550 °F). It is not possible to account for the formulae of the beryllium borides in terms of the ordinary concept of valency. The boron atoms probably are linked in chains, layers, or three-dimensional networks extending throughout the entire crystal. The beryllium atoms are then accommodated in the boron network. A related compound, CaB_6, possesses a sodium chloride structure in which sodium ions are replaced by calcium. The chloride ions are replaced by regular octahedra of boron atoms. Every octahedron is linked to six neighboring octahedra at a distance of 1.72 Å, which is also the interatomic distance within each octahedron, according to Johnson and Daane [1963].

The most reactive beryllium boride is BeB_2, which is readily hydrolyzed by dilute acids to give boron hydrides. It is copper-red in color and possesses a cubic fluorite structure with a = 4.661 Å. The other beryllium borides are insoluble in acids. These compounds have potential application as refractory materials because they are only slowly attacked on heating in oxygen or nitrogen, due to the formation of protective coatings. They do not melt below 1500 °C (2730 °F). Attack by carbon, carbon monoxide, and carbon dioxide is more rapid, because the beryllium carbide formed on the surface is not protective.

10.2 Beryllium Carbide

Beryllium carbide, Be_2C, is prepared by heating a mixture of beryllium powder and carbon under hot pressing conditions. On reaching 900 °C (1650 °F), an exothermic reaction is initiated that raises the temperature to approximately 1400 °C (2550 °F). The reaction mass is crushed and pulverized to a fine powder and used to make more pure beryllium carbide shapes by hot pressing at temperatures up to 2000 °C (3630 °F). Early efforts to make beryllium metal by reduction of beryllium oxide with carbon resulted in Be_2C on firing the mixture at 1950 to 2100 °C (3540 to 3810 °F) for 8 h.

Beryllium carbide is a hard, translucent, isotropic substance with a trace of amber to dark brown discoloration resulting from traces of residual free carbon. Its abrasive properties are similar to carborundum (silicon carbide). Beryllium carbide is a substitutional derivative of methane, which is evolved when the carbide is hydrolyzed by water or dilute acids. In bulk form, Be_2C is not attacked by moist air at room temperature. It has no value as a ceramic, since it is attacked by nitrogen above 1100 °C (2010 °F), by oxygen above 800 °C (1470 °F), and by sulfur above 1000 °C (1830 °F).

It has been shown that after beryllium powder has been stored for several months under ambient conditions in a loosely covered container, the original beryllium carbide impurity phase

can no longer be identified by x-ray diffraction. Atmospheric moisture slowly hydrolyzes the beryllium carbide to beryllium hydroxide and methane. The minimum residual carbon content of 0.035 wt% is its solubility in beryllium.

10.3 Beryllium Carbonates

Beryllium carbonate tetrahydrate, $BeCO_3 \cdot 4H_2O$, is prepared by passing carbon dioxide through an aqueous suspension of beryllium hydroxide. It is unstable and is obtained only when the solution is under carbon dioxide pressure. Beryllium oxide carbonate is precipitated when sodium carbonate is added to a beryllium salt solution, with carbon dioxide being evolved. The precipitate appears to be a mixture of beryllium hydroxide and the normal carbonate, $BeCO_3$, and usually contains from two to five molecules of $Be(OH)_2$ to each one of $BeCO_3$.

Soluble beryllium carbonate complexes are produced by dissolving beryllium oxide carbonate or hydroxide in ammonium carbonate. Iron and aluminum hydroxides are insoluble in this solution; hence, the reaction can be used to separate these two elements from beryllium. The resulting solution appears to approach the stoichiometry of a solution of tetraammonium beryllium tricarbonate, $(NH_4)_4Be(CO_3)_3$. After removal of insoluble impurities, hydrolysis of $(NH_4)_4Be(CO_3)_3$ just below the boiling point gives a granular precipitate of di(beryllium carbonate) beryllium hydroxide, $2BeCO_3 \cdot Be(OH)_2$. It can be dried to constant weight at 100 °C (212 °F). Decomposition to BeO is nearly complete after five days at 200 °C (390 °F). The continued addition of $2BeCO_3 \cdot Be(OH)_2$ and $(NH_4)_2CO_3$ to a warmed solution of $(NH_4)_4Be(CO_3)_3$ produces solutions containing up to 42 g/L Be in which the empirical composition is $(NH_4)_2Be(CO_3)_2$. The solid beryllium oxide carbonate intermediates are obtained by a laboratory procedure for preparing pure beryllium salt solutions by reaction with aqueous mineral or organic acids.

10.4 Beryllium Carboxylates

The beryllium salts of organic acids can be divided into normal beryllium carboxylates, $Be(RCOO)_2$, and beryllium oxide carboxylates, $Be_4O(RCOO)_6$. The latter are prepared by dissolving beryllium oxide, hydroxide, or oxide carbonate in an organic acid, followed by evaporation to give either a solid or an oily liquid. The oxide carboxylate is extracted with chloroform or petroleum ether and recrystallized from the solvent. These compounds are nonelectrolytes, soluble in organic solvents, insoluble in cold water, possess sharp melting points, and can usually be sublimed or distilled without decomposition. The oxide formate requires special preparation by heating the normal formate to 250 to 260 °C (480 to 500 °F) or by boiling it with a water suspension containing the calculated amount of beryllium oxide carbonate. The normal beryllium carboxylates must be prepared under strictly anhydrous conditions. The normal acetate is made by treating the oxide acetate with glacial acetic acid and acetyl chloride.

10.5 Beryllium Halides

Beryllium is a member of the group of elements whose stabilities of their halide complexes lie in the order $F > Cl > Br > I$. The bonding in the halide complexes of these elements is essentially electrostatic. The strongest bonds are formed by ligands combining a small ionic radius with a low polarizability, parameters that decrease monotonically from I^- to F^-. The relatively greater stability of the fluoride complex arises from the very small size of the fluoride ion relative to that of the other halides (radii of F^-, Cl^-, Br^-, and I^- are 1.36, 1.81, 1.95, and 2.16 Å, respectively).

Beryllium chloride, bromide, and iodide, like the fluoride, are very soluble in water. Unlike beryllium fluoride, all give solutions containing only the hydrated beryllium cation. Chloroberyllates, bromoberyllates, or iodoberyllates have never been established as existing in aqueous or nonaqueous solutions. Despite much effort, all attempts to prepare chloroberyllates from aqueous solution have failed; $BeC1_2 \cdot 4H_2O$ and the other metal chloride were always the only solid phases isolated.

Beryllium bromide and beryllium iodide, $BeBr_2$ and BeI_2, are prepared by the reaction of bromine or iodine vapors, respectively, with metallic beryllium at 500 to 700 °C (930 to 1290 °F). They cannot be prepared by wet methods. Neither compound is of commercial importance, and special uses are unknown.

Beryllium chloride, $BeCl_2$, is prepared by heating a mixture of beryllium oxide and carbon in chlorine at 600 to 800 °C (1110 to 1470 °F). At pressures of 2.7 to 6.7 Pa (0.02 to 0.05 mm Hg)

beryllium chloride sublimes at 350 to 380 °C (660 to 715 °F). It is easily hydrolyzed by water vapor or in aqueous solutions. Beryllium chloride hydrate is obtained by concentrating a saturated aqueous solution of the chloride in a flow of hydrogen chloride. Chloroberyllate compounds have not been isolated from aqueous systems, but they have been isolated from anhydrous fused salt mixtures.

Beryllium fluoride, BeF_2 properties differ sharply from those of the chloride, bromide, and iodide. Beryllium fluoride is essentially an ionic compound, whereas the other three halides are largely covalent. The fluoroberyllate anion is very stable.

Beryllium fluoride is produced commercially by the thermal decomposition of diammonium tetrafluoroberyllate, $(NH_4)_2BeF_4$. The fluoride and the fluoroberyllates show a strong similarity to silica and the silicates. Like silica, beryllium fluoride readily forms a glass that, on heating above 230 °C (445 °F), crystallizes spontaneously to give the quartz crystal structure. This quartz structure exists in two forms; the low-temperature α-form is converted to the high-temperature β-form at 227 °C (440 °F). The melting temperature of the quartz form of beryllium fluoride appears to be 552 °C (1026 °F) [Pearson 1958].

Beryllium fluoride is hygroscopic and highly soluble in water, although its dissolution rate is slow. Fluoroberyllates can be readily prepared by precipitation or crystallization from aqueous solution. Compounds containing the BeF_4^{2-} ion are the most readily obtained, although compounds containing other fluoroberyllate anions can also be obtained, for example, $(NH_4)_2BeF_4$ and NH_4BeF_3, depending on conditions.

10.5.1 Preparation of Beryllium Halides

Although usually formulated as the tetrahydrate, Semenenko and Turova [1964, 1965] consider that the hydrate is formulated as an "onium" compound approaching the composition $BeC1_2 \cdot 4.5H_2O$. Hydrated beryllium chloride can be obtained as a hygroscopic solid by concentrating a saturated aqueous solution of the chloride in a flow of gaseous hydrogen chloride. It is suggested that the complex structure is made up of close-packed layers of $BeC1_2 \cdot 2H_2O$ groups, with the excess water occurring interstitially in the channels between the layers. Hydrated beryllium bromide hydrolyzes during drying and cannot be prepared because it is too easily hydrolyzed [Cupr and Salansky 1928].

Beryllium chloride must be prepared by dry methods due to the ease with which the tetrahydrate undergoes hydrolysis during evaporative drying. Greenfield et al. [1962] studied two approaches for beryllium chloride preparation from beryllia:

- Heating a mixture of the oxide and carbon in chlorine
- Heating the oxide in a stream of either carbon tetrachloride, perchlorethylene, or phosgene

Chlorination of powder mixtures of beryllia and carbon was slow up to 600 °C (1110 °F), above which the rate increased, becoming rapid as 900 °C (1650 °F) was approached. Intimate contact of oxide and carbon was necessary; however, chlorination times up to 5 h were still required with a pressure-bonded compact to produce beryllium halide.

Carbon tetrachloride proved to be a more effective chlorinating agent for beryllia than perchlorethylene and phosgene. A fluidized bed of beryllia was chlorinated with carbon tetrachloride vapors, using nitrogen or argon as carrier gas. There was very little difference between the reactivity of hydroxide dried at 110 °C (230 °F) and oxide calcined from hydroxide at 500 °C (930 °F). The chlorination was initiated at 400 °C (750 °F) but proceeded satisfactorily in the fluidized bed only above 600 °C (1110 °F). The physical condition of the oxide residue was unexpected, since its volume was approximately the same as that of the input material, in spite of approximately 90 wt% loss. Chlorination was completed in 2 h at 600 °C (1110 °F) and in 1 h at 700 °C (1290 °F). At higher temperatures, some pyrolysis of the carbon tetrachloride occurred, leaving traces of carbon in the beryllium chloride condensate. Subsequent semiscale chlorination by Vil'komiskii et al. [1961] of beryllia compacts with carbon tetrachloride at 650 to 700 °C (1200 to 1290 °F) yielded quantities of beryllium chloride up to 10 kg.

The preferred method of synthesizing beryllium bromide is by action of bromine gas at 1100 to 1200 °C (2010 to 2190 °F) on a mixture of beryllium oxide and carbon. Alternative methods involve the action of bromine gas on beryllium metal or beryllium carbide at 500 to 600 °C (930 to 1110 °F). Similarly, beryllium iodide is prepared by passing a mixture of nitrogen and hydrogen iodide over beryllium metal or beryllium carbide at 600 to 700 °C (1110 to 1290 °F). In all halogenations, care must be

taken to exclude moisture because of the ease of hydrolysis of the products.

10.5.2 Polymorphism in Beryllium Halides

Beryllium chloride exists in a number of polymorphic forms. Everest discusses this topic using several literature references as source material [1964, 1973]. The transitions between the various forms of beryllium chloride are complex in character, mainly due to the existence of parallel stable and metastable equilibria [Kuvyrkin et al. 1958, McDonald and Oetting 1965]. Crude beryllium chloride was prepared by Furby and Wilkinson [1960] using the methods of Greenfield et al. [1962]. Their product was purified by sublimation at 350 to 380 °C (660 to 715 °F) and 20 to 50 μm of mercury. The sublimate was collected as fibrous crystals (mainly α′-form with some β) reminiscent of cotton wool. Novoselova [1959] obtained the same α′-form with rapid cooling of molten beryllium chloride [Kuvyrkin et al. 1960].

On heating the α′-phase to 250 °C (480 °F), it changes into the β′-phase, which itself becomes the stable β-phase at 340 °C (645 °F). Slow cooling of molten beryllium chloride causes the crystallization of a fourth phase, α-phase, which is converted into the stable β-phase with further slow cooling to 405 °C (760 °F). Furby and Wilkinson [1960] cooled molten sublimate samples at 4 °C/ min (7 °F/min). In addition to the thermal arrest at the melting point, there was a second halt in the cooling curve at 335 °C (635 °F), yielding the β′-phase. McDonald and Oetting [1965] have summarized the transformations in Table 10.1.

X-ray studies by Rundle and Lewis [1952] showed the α′-phase of beryllium chloride was orthorhombic, a = 9.86 Å, b = 5.36 Å, c = 5.22 Å, and z = 4. It is possible that the α′- and α-forms are identical. The β′-form is cubic, a = 8.27 Å and z = 8, while the β-phase is orthorhombic, a = 16.08 Å, b = 14.48 Å, c = 10.10 Å, and z = 36.

Table 10.1 Polymorphic transformations of beryllium chloride

Transition temperature, °C (°F)	Transition
250 (480)	$\beta \rightarrow \beta'$ (stable) $\alpha' \rightarrow \beta'$ (metastable)
340 (645)	$\beta' \rightarrow \beta$ (stable) $\beta' \rightarrow \alpha$ (metastable)
403 (755)	$\beta \rightarrow \alpha$ (stable)
410 (770)	$\beta \rightarrow$ liquid (metastable)
415 (780)	$\alpha \rightarrow$ liquid (stable)

The α′-phase consists of continuous chains of distorted $BeCl_4$ tetrahedra linked together at opposite edges and situated parallel to the c-axis. The polymorphism of beryllium chloride arising from such causes is associated with relatively small heat changes and is thereby characterized by slow rates of transformation.

The beryllium-chlorine bond angles in the crystalline halide indicate that all bonds contain an electron pair, so that the chlorine atoms must use an unshared pair of electrons to form the chlorine bridge bonds [Rundle and Lewis 1952]. Thus, beryllium chloride can be considered to contain a different type of bonding compared with electron-deficient molecules such as dimethylberyllium.

In its properties, beryllium bromide is similar to the chloride, although the quantity of published work is relatively limited. Beryllium bromide is orthorhombic, a = 10.32 Å, b = 5.52 Å, and c = 5.54 Å [Semenenko and Naumova 1963]. It does not appear to possess any polymorphic forms. On the other hand, beryllium iodide exists in polymorphic forms [Semenenko and Naumova 1963]. The low-temperature form is orthorhombic, a = 11.18 Å, b = 5.94 Å, and c = 6.04 Å. Between 290 and 370 °C (555 and 700 °F), this phase is converted into β′-form, which is body-centered rhombic, a = 18.0 Å, b = 16.69 Å, and c = 11.43 Å. Above 370 °C (700 °F), a tetragonal β-form is obtained, a = 5.84 Å and b = 5.70 Å.

The purified sublimate from crude beryllium chloride of Furby and Wilkinson [1960] gave a spectrographic analysis showing 300 to 400 ppm Fe, 15 to 30 ppm Mg, and 0 to 20 ppm Na, while other elements were not detected. Samples of this material were transferred to silica tubes, where they were melted. Cooling rates of approximately 4 °C/min (7 °F/min) were employed. Thermal arrests on twenty samples gave an average melting point of 399 ± 1 °C (750 ± 2 °F). Boiling point determinations on twelve samples of the same sublimate gave an average value of 482.5 ± 1 °C (900 ± 2 °F) within the accuracy imposed by the measuring equipment. Beryllium chloride is associated in the vapor phase to give the chlorine-bridged dimer (Fig. 10.1).

The dimer dissociates on heating to yield monomeric $BeCl_2$. Dissociation is complete at 1000 °C (1830 °F). Electron diffraction measurements show the monomer to be linear with a beryllium-chlorine distance of 1.77 Å [Akishin et al. 1958]. The beryllium-chlorine bond length in beryllium chloride vapor is shorter than that

of the 2.02 Å length in the solid [Rundle and Lewis 1952]. This difference is compatible with the different bonding involved, that is, sp^3 in the solid and *sp* in the vapor.

Beryllium bromide melts at 488 °C (910 °F) and sublimes below this at 473 °C (883 °F) [Rahlfs and Fischer 1933]. Beryllium iodide melts at 510 °C (950 °F) and boils at 590 °C (1095 °F) [Wood and Brenner 1957]. Beryllium iodide, like the chloride and bromide, is dimeric in the vapor phase. The iodide dissociates into the monomer as the temperature increases above the melting point. The beryllium-iodine bond length in the monomer is 2.12 Å [Akishin et al. 1958]. The vapor of beryllium iodide is relatively stable, and it is not appreciably decomposed into its elements below 1200 °C (2190 °F).

10.6 Beryllium Hydride

In the mid-1960s, considerable interest in beryllium hydride was generated by its potential use with ammonium perchlorate oxidizer in solid propellants for rockets. Beryllium hydride, BeH_2, was prepared by action of ethereal lithium-aluminum hydride with beryllium chloride. A white powder resulted from which the complete removal of ether was difficult. The hydride is not stable above 125 °C (255 °F), decomposing into beryllium and hydrogen.

Beryllium hydride is a three-dimensional polymer, considerably ionic in character and containing Be^{2+} and H^- ions, as shown in Fig. 10.2. Alternatively, it may be considered to be an electron-deficient molecule, similar to beryllium chloride and the beryllium alkyls, with hydrogen bridges between the two beryllium atoms (BeH_2Be).

10.7 Beryllium Hydroxide

Beryllium hydroxide, $Be(OH)_2$, exists in three forms. By adding alkali to a beryllium salt solution until the solution has a slightly basic pH, a slimy, gelatinous beryllium hydroxide is produced. Aging this amorphous product results in a metastable tetragonal crystalline form, which, after months of standing undisturbed, transforms into a stable orthorhombic crystalline form. The orthorhombic phase is also precipitated from a sodium beryllate solution containing more than 5 g/L of beryllium by hydrolysis near the boiling point. This granular beryllium hydroxide is the product from the sulfate extraction processing of beryl (see Chapter 7, "Extractive Metallurgy," in this book), and is readily filtered. When heated, beryllium hydroxide loses water, although temperatures above 950 °C (1740 °F) are required for complete dehydration to the oxide. There is evidence that beryllium hydroxide exists in the vapor phase above 1200 °C (2190 °F) [Young 1960]. Water vapor reacts with BeO to form beryllium hydroxide vapor, which has a partial pressure of 73 Pa (0.55 mm Hg) at 1500 °C (2730 °F).

10.8 Beryllium Nitrate

Beryllium nitrate tetrahydrate, $Be(NO_3)_2 \cdot 4H_2O$, is prepared by crystallizing a solution of beryllium hydroxide or beryllium oxide carbonate from a slight excess of dilute nitric acid. After dissolution is complete, the solution is poured into plastic bags and cooled to room temperature. The crystallization is started by seeding. Crystallization from more concentrated nitric acids yields crystals with less water of hydration. On heating above 100 °C (212 °F), the beryllium nitrates decompose, with simultaneous loss of water and oxides of nitrogen. Decomposition is complete above 250 °C (480 °F).

The compound $Be(NO_3)_2 \cdot 4H_2O$ is most readily prepared by reacting dilute nitric acid with beryllium hydroxide or, preferably, beryllium

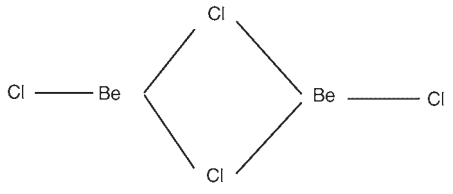

Fig. 10.1 Chlorine-bridged dimer

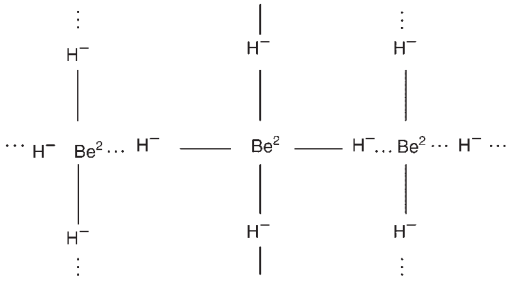

Fig. 10.2 Three-dimensional molecule of beryllium hydride

basic carbonate in stoichiometric ratios in plastic vessels. The product is an outstanding example of a compound that is soluble in its waters of hydration. Evaporation of the neutralized solution with heat is discouraged because of nitrous-oxide-vapor evolution. Subjecting the solution with the prescribed stoichiometry to vacuum or dessication conditions does not yield crystals of the product. After two or three weeks of storage at ambient temperatures, crystals of $Be(NO_3)_2 \cdot 4H_2O$ are very slowly formed, and the entire mass ultimately solidifies. This prolonged relief of supersaturation has produced 20 to 100 lb (10 to 50 kg) quantities of the compound. The use of product crystals to seed the supersaturated solution has not been advantageous.

The crystallization of beryllium nitrate from more concentrated nitric acid solutions leads to the formation of tri-, di-, and monohydrates. The trihydrate is the product obtained under commercial conditions. Differential thermal analysis of the tri- or tetrahydrate shows that the salt first dissolves in its water of crystallization at 60 °C (140 °F) [Gorden and Campbell 1955]. Between 100 and 200 °C (212 and 390 °F), there is a simultaneous loss of water and oxides of nitrogen. Decomposition to beryllium oxide is complete above 250 °C (480 °F). As with other hydrated alkaline earth nitrates, thermal decomposition of beryllium nitrate tri- and tetrahydrates occurs through hydrolysis to give nitric acid, which subsequently decomposes, rather than by thermal breakdown of the nitrate ion itself.

Anhydrous beryllium nitrate has been prepared by the reaction of anhydrous beryllium chloride with an ethylacetate-dinitrogen tetroxide mixture to give $Be(NO_3)_2 \cdot 2N_2O_4$ [Addison and Walker 1963]. When heated above 50 °C (120 °F) in a vacuum, oxides of nitrogen are evolved, leaving anhydrous beryllium nitrate. The anhydrous salt is stable to approximately 125 °C (255 °F), when a sudden decomposition occurs to give nitrogen tetroxide and a volatile compound that separates from the gas phase as colorless $Be_4O(NO_3)_6$ crystals. These crystals are slowly hydrolyzed when added to water.

10.9 Beryllium Nitride

Heating metallic beryllium powder in a gaseous ammonia or nitrogen atmosphere at 1100 °C (2010 °F) yields white crystalline beryllium nitride, Be_3N_2 [Beaver 1955a,b; Markovskii et al. 1955]. It is a sinterable powder, but the cubic crystal structure, a = 8.134 Å, transforms above 1400 °C (2550 °F) into a hexagonal structure, a = 2.841 Å and c = 9.693 Å [Mallett et al. 1954]. Beryllium nitride sublimes in vacuum at 2000 °C (3630 °F) and melts with decomposition above 2200 °C (3990 °F).

Beryllium nitride is rapidly oxidized in air at 600 °C (1110 °F). The compound is decomposed by water (more rapidly with dilute acids or bases), forming ammonium and beryllium salts in solution. Hot pressing mixtures of beryllium nitride and silicon nitride, Si_3N_4, at 1700 °C (3090 °F) produces beryllium silicon nitride, $BeSiN_2$. This compound is chemically inert and may have potential use as a ceramic material.

10.10 Beryllium Oxide

Beryllium oxide (BeO) is the most important high-purity commercial beryllium chemical. In the primary industrial synthesis process, technical-grade beryllium hydroxide is dissolved in sulfuric acid. The solution is filtered to remove insoluble oxide and sulfate impurities. The resulting clear filtrate is concentrated by evaporation and, upon cooling, high-purity beryllium sulfate crystallizes. This salt is calcined at carefully controlled temperatures between 1150 and 1450 °C (2100 to 2640 °F), selected to give tailored properties of the beryllium oxide powders required by the individual beryllia ceramic fabricators. Commercial beryllium oxide powder calcined at 1150 °C (2100 °F) consists of crystallites that are predominantly 0.1 to 0.2 μm in diameter. Powder particles are made of clusters or aggregates of crystallites.

The alternative commercial process for manufacturing ceramic-grade beryllium oxide involves dissolving the technical-grade beryllium hydroxide in sulfuric acid. Following filtration, organic chelating agents are added to the filtrate. The clear solution is treated with ammonium hydroxide to precipitate high-purity beryllium hydroxide, which is carefully calcined to beryllium oxide powder.

The availability of high-purity beryllium oxide powder has spawned a new industry in the last 20 to 30 years, because the material can be fabricated with classic ceramic-forming processes such as dry pressing, isostatic pressing, extrusion, and slip casting. Additives consisting of the oxides of magnesium, aluminum, or silicon, or their combinations are frequently included

in the green beryllia part to improve the reproducibility in sintering and properties. The green compact of formed beryllia is commonly sintered at 1500 to 1600 °C (2730 to 2910 °F) in dry air or dry hydrogen. Moisture in the sintering atmosphere is detrimental to the surface characteristics, such as roughness, texture, and microstructure. The sintering operation produces beryllia ceramics at 95 to 97% of the theoretical density, with an average grain size from 6 to 30 μm. Higher density can be achieved by hot pressing high-purity beryllia powder.

Beryllia ceramics offer the advantage of a unique combination of high thermal conductivity and heat capacity with high electrical resistivity. Thermal conductivity approaches that of metals; at room temperature, beryllia has a thermal conductivity nearly equal to that of pure aluminum and one-half that of copper. Other properties important to the utility of beryllia ceramics are included in Table 10.2.

Beryllia ceramic parts are frequently used in electronic and microelectronic applications requiring thermal dissipation. Beryllia substrates are commonly metalized with refractory metals such as molybdenum-manganese, chromium, titanium, and nickel-chromium alloys. Semiconductor devices and integrated circuits can be bonded by metallization for removal purposes.

Table 10.2 Properties of high-purity beryllium oxide

Property	Value
Specific heat, J/kg · K	1050
Thermal conductivity	
At 25 °C, W/m · K	290–330
At 100 °C, W/m · K	190–220
Dielectric constant	
1 MHz at 25 °C	6.55–6.72
1 MHz at 100 °C	6.55–6.75
1 GHz at 25 °C	6.72–6.75
1 GHz at 100 °C	6.72–6.81
9.3 GHz at 25 °C	6.77
9.3 GHz at 100 °C	6.77
Loss tangent	
1 MHz at 25 °C	0.00005–0.00016
1 MHz at 100 °C	0.00007–0.00019
1 GHz at 25 °C	0.00006–0.00035
1 GHz at 100 °C	0.00014–0.00051
9.3 GHz at 25 °C	0.00007–0.00031
9.3 GHz at 100 °C	0.00026–0.00047
Volume resistivity	
At 25 °C, Ω · m	2.0×10^{14} to 1.3×10^{15}
At 100 °C, Ω · m	1.4×10^{11} to 5.0×10^{11}
Coefficient of thermal expansion	
At 100 °C	9.7×10^{-6} K^{-1}
Tensile strength, MPa	150
Compressive strength, MPa	1400
Modulus of rupture, MPa	250
Modulus of elasticity, GPa	345
Poisson's ratio	0.164–0.380
Specific gravity of 99.5% BeO	2.86–2.91

10.11 Beryllium Oxide Carboxylates

A very important class of beryllium compounds is the oxide carboxylates, $Be_4O[RCOO]_6$. The oxide acetate, $[Be_4O(CH_3COO)_6]$, is the most familiar. From the many methods described in the literature for the preparation of oxide carboxylates, Everest [1973] has selected three methods [Moeller 1957]:

- Dissolution of beryllium oxide, hydroxide, or basic carbonate in the requisite organic acid or the corresponding acid anhydride. Subsequent evaporation gives either a solid or an oily liquid. The oxide carboxylate is extracted with chloroform or petroleum ether and recrystallized from the solvent.
- The action of the organic acid or acid anhydride on anhydrous beryllium chloride. This gives the oxide carboxylates. Under carefully controlled conditions (especially during drying) to avoid moisture, normal carboxylates form.
- The action of the organic acid or acid chloride on another beryllium oxide carboxylate. This method is used to yield mixed oxide carboxylates, which can also be formed by co-melting the individual carboxylates. Hardt [1962] has prepared a whole range of compounds, given by the composition $Be_4O[CH_3COO]_x[CH_3CH_2COO]_y$, where $[x + y = 6]$. The compounds were synthesized by melting together the oxide acetate or propionate, by action of acetyl chloride on the propionate, or by action of propionic acid on the oxide acetate.

The oxide carboxylates are nonelectrolytes, soluble in organic solvents such as chloroform or benzene, insoluble in cold water, possess sharp melting points, and can usually be sublimed or distilled (Table 10.3) without decomposition. The oxide carboxylates are stable toward heat and oxidation except under drastic conditions. They are only slowly hydrolyzed by hot water. Treatment with mineral acids yields the corresponding beryllium salt and free organic acid.

Table 10.3 Thermal properties of beryllium oxide carboxylates

Compound	Formula	Melting temperatures °C	Melting temperatures °F	Boiling temperatures °C	Boiling temperatures °F
Formate	$Be_4O[HCOO]_6$	Sublimes		...	
Acetate	$Be_4O[CH_3COO]_6$	285	545	330	625
Propionate	$Be_4O[CH_3CH_2COO]_6$	138	280	340	645
Butyrate	$Be_4O[CH_3CH_2CH_2COO]_6$	27	80	239	460
Isobutyrate	$Be_4O[[CH_3]_2CHCH_2COO]_6$	88	190	336	635
Benzoate	$Be_4O[C_6H_5COO]_6$	317	600	...	
o-chlorobenzoate	$Be_4O[C1C_6H_4COO]_6$	255	490	...	

The oxide acetate crystallizes in the cubic system, while other polymorphs include two monoclinic forms [Semenenko and Gordeev 1959]. A high-temperature monoclinic modification is obtained by heating the cubic form to 145 to 150 °C (295 to 300 °F). The second monoclinic modification is obtained by recrystallization of the oxide acetate from hot tetraline. In addition, an order-disorder transition of the cubic form takes place at 40 °C (105 °F). It does not involve a phase change since the crystals can be repeatedly heated or cooled through the transition without any recrystallization taking place. The transition is probably due to a rotation of the carbonyl oxygens around the C-C bonds.

10.11.1 Normal Beryllium Carboxylates

The normal beryllium carboxylates must be prepared under strictly anhydrous conditions, because only a one-quarter mol water equivalent is required for complete hydrolysis to the oxide salt:

$$4Be[RCOO]_2 + H_2O \rightarrow Be_4O[RCOO]_6 + 2\ RCOOH \qquad \text{(Eq 10.1)}$$

The normal acetate is made by treating the oxide acetate with glacial acetic acid and acetyl chloride:

$$Be_4O[CH_3COO]_6 + 2\ CH_3COOH + 2\ CH_3COCl \rightarrow 4Be[CH_3COO]_2 + [CH_3CO]_2 + 2\ HCl \qquad \text{(Eq 10.2)}$$

Other normal organic salts of beryllium have been made by the interaction of anhydrous beryllium chloride with the corresponding acid chloride in the absence of moisture. The normal acetate is decomposed on heating by either:

$$4\ Be[CH_3COO]_2 \rightarrow Be_4O[CH_3COO]_6 + [CH_3CO]_2O \qquad \text{(Eq 10.3)}$$

or

$$Be[CH_3COO]_2 \rightarrow BeO + [CH_3CO\ ]_2O \qquad \text{(Eq 10.4)}$$

These reactions are in contrast to the decomposition of calcium acetate, which gives acetone and calcium carbonate.

The only normal carboxylate, which is more stable than the corresponding oxide salt, is the formate. It is obtained by dissolving beryllium hydroxide or basic carbonate in 50% formic acid, or by the action of formic acid on the oxide acetate. Beryllium formate is an anhydrous solid, insoluble in organic solvents, and slowly hydrolyzed by water. After subliming beryllium formate into an inert carrier gas, impinging the gas stream on a heated surface caused the formate to decompose to beryllium oxide. Using this technique, limited success was obtained in depositing microfilms of beryllium oxide on shaped substrates heated to approximately 200 °C (390 °F).

Normal beryllium carboxylates synthesized with fatty acids result from the drop-by-drop addition of aqueous beryllium sulfate into an agitated solution containing a stoichiometric quantity of the sodium salt of the fatty acid. In the oleate system, continued agitation with heating just below boiling for 10 to 15 min resulted in an oily liquid. Liquid beryllium oleate with a 95% yield was separated from the aqueous system using funnel separation techniques. With sodium palmitate and stearate solutions, a slurry of the beryllium salts was formed. After recovery by filtration and drying, the products were given a final purification by heating to 90 °C (195 °F) in a coarse, fritted-glass crucible, allowing the liquid beryllium salt to filter by gravity. The normal palmitate and stearate salts are recovered as white flaky solids. Beryllium stearate melts at 42 °C (107 °F), and beryllium palmitate melts at 40 °C (104 °F). The three salts are soluble in long-chain organic solvents up to 5 wt%. In the aqueous environment for

preparation, hydrolysis of the carboxylates of the fatty acids should have been observed. Steric factors preventing ring formation of the corresponding beryllium oxide carboxylates apparently prevail.

10.12 Beryllium Oxalate

Beryllium oxalate trihydrate, $BeC_2O_4 \cdot 3H_2O$, is obtained by evaporating a solution of beryllium hydroxide or oxide carbonate in a slight excess of oxalic acid. The compound is very soluble in water. Beryllium oxalate is important for the preparation of ultrapure beryllium oxide by thermal decomposition above 320 °C (610 °F). The latter is frequently used as a standard for spectrographic analysis of beryllium compounds.

Beryllium oxalate differs from the other hydrated beryllium salts in forming a trihydrate rather than a tetrahydrate. It is the only bipositive metal oxalate that is water soluble. Its solubility is 38.22 g/100 mL at 25 °C (75 °F), [CRC 1971–1972].

Beryllium oxalate was prepared by Konieczny [1992] by slowly adding the stoichiometric quantity of purified beryllium basic carbonate to 0.4 *M* oxalic acid until dissolved. The solution was evaporated while subjected to a 55 °C (130 °F) water bath. Beryllium oxalate crystals formed as evaporation proceeded. The crystals were recovered by filtration. Air drying gave a mixture of beryllium oxalate monohydrate and trihydrate. The material was hygroscopic on exposure to water vapor over free-standing water at ambient temperature in a desiccator. Equilibration with water vapor over a saturated solution of ammonium chloride led to a constant weight and the trihydrate composition. Other variations in the partial pressure of water vapor in the desiccator gave mixtures of the monohydrate and trihydrate. Beryllium oxalate can also be prepared by evaporation of a solution of beryllium oxide or hydroxide in a slight excess of oxalic acid.

The Be^{2+} ion is strongly complexed by oxalate anions. The ionic conductivity of an aqueous solution of beryllium oxalate is only approximately one-fourth that of an equivalent beryllium sulfate solution and remains at a constant value over a wide range of concentration; freezing point measurements confirm that beryllium oxalate gives only a few ions in solution. Sidgwick and Lewis [1926] suggest that in beryllium oxalate solutions there is an equilibrium between an un-ionized hydrated monochelate complex and a dichelate complex salt, as represented in Fig. 10.3.

Because metal oxalates usually have one water molecule associated with each oxalate group, either of the previous species can account for the observed trihydrate. The fact that at least part of the beryllium is present as the anionic complex $[Be(C_2O_4)_2]^{2-}$ is demonstrated by the extraction of beryllium from oxalate solutions by anion-exchange resins.

On heating the trihydrate in thermogravimetric analysis (TGA) equipment, a phase change was observed between 50 and 120 °C (120 and 250 °F). This phase change is the dehydration step forming BeC_2O_4-H_2O. Walter-Levy and Perrotey [1966] suggested that BeC_2O_4-H_2O undergoes partial decomposition between 200 and 320 °C (390 and 610 °F) to give a basic salt formulated as $8BeC_2O_4 \cdot 5Be(OH)_2$. Such an intermediate was not observed by Konieczny [1992] using TGA or x-ray diffraction. Instead, a second endothermic peak was observed between 100 and 160 °C (212 and 320 °F) corresponding with a chemical water loss of the oxalate product, yielding an anhydrous/monohydrate mixture. A two-stage endothermic transition was seen in the 300 to 420 °C (570 to 790 °F) range to form beryllium oxide. The mechanism of the decomposition of beryllium oxalate trihydrate follows a route to form the monohydrate and/or anhydrous material, which then decomposes to BeO in a gradual fashion without distinct losses of CO and CO_2. This mechanism is supported by the observation that BeO was found with the intermediate products. Thermal decomposition of the oxalate is employed as a method for the preparation of ultrapure beryllium oxide.

10.13 Beryllium Phosphates

The mono-, di-, and tertiary beryllium phosphates, $Be(H_2PO_4)_2$, $BeHPO_4$, and $Be_3(PO_4)_2$, have been described by Travers and Perron [1924]. The hydrated monoacid phosphate has

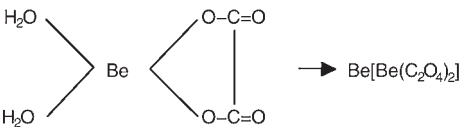

Fig. 10.3 Dichelate complex salt of beryllium

been formulated as $Be(OH)(H_2PO_4)$. A systematic study of the $BeO \cdot P_2O_5 \cdot H_2O$ system is required to define the simple beryllium phosphates and to establish their stability limits [Everest 1973].

The best known phosphate is the compound $BeNH_4PO_4 \cdot xH_2O$, with $x \sim 1$. It is made by adding $(NH_4) \cdot 2HPO_4$ to a beryllium solution at pH 5.2 to 5.5 [Toribara and Chen 1952]. When the pH is much below this, some $BeHPO_4$ is also precipitated, and the material contains less than the theoretical quantity of ammonia. Heating $BeNH_4PO_4$ releases water of hydration at 250 °C (480 °F), ammonia at 400 °C (750 °F), and water of constitution at 500 °C (930 °F). At 700 °C (1290 °F), conversion to $Be_2P_2O_7$ is complete [Bouille and Dupin 1962]. The loss of ammonia at 400 °C (750 °F) produces $BeHPO_4$, but the conversion is never quantitative. The only compound in the sequence to be analytically useful is $Be_2P_2O_7$. $BeNH_4PO_4$ crystallizes in the tetragonal system, a = 12.96 Å and c = 9.65 Å. $BeHPO_4$ is also tetragonal, a = 9.05 Å and c = 9.65 Å. Beryllium phosphite, $BeHPO_3$, is prepared by dissolution of beryllium hydroxide or basic carbonate in phosphorus acid. On heating, it decomposes at 400 °C (750 °F).

10.14 Beryllium Perchlorate

Beryllium perchlorate tetrahydrate was obtained by Sidgwick and Lewis [1926] by dissolving beryllium oxide in a slight excess of perchloric acid. It is very soluble in water, 59.5% at 25 °C (75 °F). The tetrahydrate is thermally stable, not losing water below the temperature at which the perchlorate ion begins to decompose.

10.15 Beryllium Sulfate

Beryllium sulfate is the most important and therefore the most extensively studied oxysalt of beryllium. Because they are formed in ore extraction processes, sulfate solutions are commonly encountered industrially. Subsequent purification steps with minimal beryllium losses are selected in progressing to the recovery step of the beryllium hydroxide intermediate.

In the simplest process to yield beryllium sulfate, the hydroxide intermediate is dissolved in sulfuric acid to give a solution with 44 wt% $BeSO_4$. The heat of reaction raises the temperature to 110 °C (230 °F), causing some removal of water by evaporation. At 11 °C (50 °F), the solubility is greater than 44 wt%, so cooling to 20 °C (70 °F) crystallizes $BeSO_4 \cdot 4H_2O$. The crystalline product contains 75 wt% of the input beryllium. Impurities such as iron, aluminum, magnesium, sodium, and fluorine are left in solution. The crystals are recovered before redissolving in water and filtered to remove SiO_2, MnO_2, and $CaSO_4$. Reprecipitation with ammonia yields a high-purity hydroxide, which can be recycled to sulfuric acid dissolution for preparation of purified beryllium sulfate crystals.

Beryllium sulfate tetrahydrate, $BeSO_4 \cdot 4H_2O$, is produced commercially in a highly purified state by fractional crystallization from a beryllium sulfate solution obtained by reacting beryllium hydroxide with sulfuric acid. The salt is used primarily in the production of beryllium oxide powder for ceramics. By heating $BeSO_4 \cdot 4H_2O$ at 92 °C (200 °F), beryllium sulfate dihydrate is obtained. Anhydrous beryllium sulfate results on heating the dihydrate in air to 400 °C (750 °F). Decomposition to BeO starts at approximately 650 °C (1200 °F). The rate is accelerated by heating up to 1450 °C (2640 °F). At 750 °C (1380 °F), the vapor pressure of SO_3 over $BeSO_4$ is 48.7 kPa (365 mm Hg).

Beryllium sulfate tetrahydrate consists of tetrahedral $[Be(H_2O)_4]^{2+}$ cations and sulfate anions arranged in an approximate body-centered cubic, cesium chloride structure [Wells 1961]. Every water molecule has two external contacts to the oxygen atoms of the sulfate anion. The tetrahydrate is readily soluble in water amounting to 37 and 42.5 g/100 g H_2O at 18 and 25 °C (65 and 75 °F), respectively. Beryllium sulfate has a negligible equilibrium solubility in 100% sulfuric acid. Solubility does not exceed 2.5% $BeSO_4$ in the range of 88 to 98 wt% sulfuric acid.

A concentrated solution of beryllium sulfate continues to dissolve beryllium basic carbonate with brisk effervescence even after the addition of more than 1 mol of base to each mol of salt present. Parsons [1904] found that the solubility of the oxide increased with the concentration of the salt. In strong solution, it exceeded 2 mols/mol of salt. No basic salts were isolated, so the salt solution is acting as a mixed solvent. The mechanism is the formation of the complex cation $[Be(BeO)_x]^{2+}$, which accounts for the small change in ionic conductivity. Solutions saturated with 29.74 wt% $BeSO_4$ at 25 °C (75 °F) dissolved basic carbonate. After boiling and

allowing crystallization of $BeSO_4 \cdot 4H_2O$, solutions were produced containing 31.73 to 37.48 wt% $BeSO_4$ and 2.16 to 7.73 wt% BeO. Molecular ratios of BeO:$BeSO_4$ ranged from 0.286 upward to 0.867, with which the mol ratio of BeO to extra $BeSO_4$ had values between 3.75 and 4.62. Therefore, 1 mol of salt dissolves for every 4 mols of oxide added.

In addition to the tetrahydrate, a number of other hydrates of beryllium sulfate have been described, but the results lack confirmation. Drying $BeSO_4 \cdot 4H_2O$ over P_2O_5 shows no weight change. Transitions on dehydration, according to Campbell et al. [1951], are limited to:

$$BeSO_4 \cdot 4H_2O \xrightarrow{89\,^\circ C} BeSO_4 \cdot 2H_2O \qquad \text{(Eq 10.5)}$$

Novoselova and Levina [1938] confirm that $BeSO_4 \cdot 2H_2O$ is the only intermediate hydrate. Anhydrous beryllium sulfate can be readily prepared by dehydrating the tetrahydrate or dihydrate under vacuum at 250 °C (480 °F) or by heating in air at 400 °C (750 °F). $BeSO_4$ has a cristobalite structure [Grund 1955]. Anhydrous beryllium sulfate has a moderate thermal stability. It is appreciably less stable than the other alkaline earth sulfates such as magnesium sulfate, which is stable up to white heat. Suchkov et al. [1959] report that on heating, beryllium sulfate begins to decompose at 580 to 600 °C (1075 to 1110 °F).

Beryllium sulfate forms double salts with sodium, potassium, and ammonium. The compounds $3Na_2SO_4 \cdot BeSO_4$, $K_2SO_4 \cdot BeSO_4 \cdot 2H_2O$, $(NH_4)_2SO_4 \cdot BeSO_4 \cdot 2H_2O$, and $(NH_4)_2SO_4$-$BeSO_4$ above 50 °C (120 °F) have been isolated by Schroder et al. [1938, 1938, 1939]. Other double salts with beryllium sulfate have not been found in the study of the systems with lithium, silver, ferrous iron, copper, calcium, and aluminum sulfates.

10.16 Beryllium Sulfide

The reaction of gaseous hydrogen sulfide and beryllium powder at 900 °C (1650 °F) gives solid beryllium sulfide, BeS. It can also be prepared by reacting gaseous sulfur with beryllium carbide at 1350 °C (2460 °F). It is a colorless solid with a cubic zinc-blend structure, a = 4.862 Å [Staritzky 1956]. Beryllium sulfide is slowly decomposed by water and is readily attacked by all acids, including atmospheric carbon dioxide.

REFERENCES

Addison, C.C., and Walker, A., 1963. Anhydrous Nitrates of the Group II Metals, *J. Chem. Soc*., p 1220–1226

Akishin, P.A., Spiridonov, V.P., and Sobolev, G.A., 1958. Electron Diffraction Study of the Beryllium Halide Molecular Structures, *Dokl. Akad. Nauk SSR*, Vol 118, p 1134–1137

Beaver, W.W., 1955a. Fabrication of Beryllium by Powder Metallurgy, *The Metal Beryllium*, American Society for Metals

Beaver, W.W., 1955b. *The Metal Beryllium*, American Society for Metals

Bouille, A., and Dupin, A.S., 1962. *Compt. Rend*., Vol 254, p 122

Campbell, A.N., Sukava, A.J., and Koop, J., 1951. The Hydrates of Beryllium Sulfate, *J. Am. Chem. Soc*., Vol 73, p 2831

CRC, 1971–1972. *Handbook of Chemistry and Physics*, The Chemical Rubber Company Press, Cleveland, OH

Cupr, V., and Salansky, H., 1928. Hydrate von Berylliumhalogeniden. I. Experimenteller und Analytischer Teil, *Z. Anorg. Chem*., Vol 176, p 241–257

Everest, D.A., 1964. *The Chemistry of Beryllium*, Elsevier, New York, NY, p 38

Everest, D.A., 1973. Beryllium, *Comprehensive Inorganic Chemistry*, J.C. Bailar, H.J. Emeleus, R. Nyholm, and A.F. Trotman-Dickenson, Ed., Pergamon Press Ltd., Oxford, England

Furby, E., and Wilkinson, K.L., 1960. The Melting and Boiling Points of Beryllium Chloride and an Investigation of the NaCl/$BeCl_2$ System, *J. Inorg. Nucl. Chem*., Vol 14, p 123–147

Gorden, S., and Campbell, C., 1955. Differential Thermal Analysis of Inorganic Compounds, *Anal. Chem*., Vol 27, p 1102

Greenfield, B.F., Hyde, K.R., and Waterman, M.J., 1962. "Conversion of Beryllia to Anhydrous Beryllium Chloride," Report AERE-R-4149, U.K. Atomic Energy Authority

Grund, A., 1955. Crystal Structure of Beryllium Sulfate, *Tschernaks Mineralog. Petrog. Mitt*., Vol 3, p 227–230

Hardt, H.D., 1962. Die Intra-Molekulare Mischverbindung $Be_4O(OOCCH_3)x$ $(OOCCH_2CH_3)y$, *Z. Anorg. Allg. Chem*., Vol 314 (No. 3–4), p 210–221

Johnson, R.W., and Daane, A.H., 1963. Electron Requirements of Bonds in Metal Borides, *J. Chem. Phys*., Vol 38, p 425

Konieczny, J.L., 1992. "A Study of the Thermal Decomposition of Beryllium Oxalate and Other Beryllium Oxysalts," University of Toledo, OH

Kuvyrkin, O.N., Breusov, O.N., and Novoselova, A.V., 1958. Thermal Analysis of the System $BeCl_2$-BeF_2, *Auch. Doklady Vysshei Shkoly Khim. i Khim. Tekhnol*., Vol 4

Kuvyrkin, O.N., Breusov, O.N., Novoselova, A.V., and Semenenko, K.N., 1960. Polymorphism of Beryllium, *Zh. Fiz. Khim*., Vol 34, p 160–163

Mallett, M.W., Durbin, E.A., Udy, M.C., Vaughan, D.A., and Center, E.J., 1954. Preparation and Examination of Beryllium Carbide, *J. Electrochem. Soc*., Vol 101 (No. 6), p 298–305

Markovskii, L.Y., Kondrashev, Y.D., and Kaputovskaya, G.V., 1955. Structure and Properties of Beryllium Borides, *Zh. Obshche. Khim*., Vol 25 (No. 6), p 1045–1052

McDonald, R.A., and Oetting, F.L., 1965. The Thermodynamic Properties and Allotropy of Beryllium Chloride between 13 and 715 K, *J. Phys. Chem*., Vol 69 (No. 11), p 3839

Moeller, T., 1957. *Inorganic Synthesis*, 3rd ed., McGraw-Hill, NY

Novoselova, A.V., 1959. Beryllium Fluorides and Fluoroberyllates, *Usp. Khim*., Vol 28, p 33–43

Novoselova, A.V., and Levina, M.E., 1938. *Zh. Obshchei. Khim*., Vol 8, p 1143

Parsons, C.L., 1904. Equilibrium in the System $BeO \cdot SO_3 \cdot H_2O$, *J. Am. Chem. Soc*., Vol 26 (No. 11), p 1433–1446

Pearson, W.B., 1958. *A Handbook of Lattice Spacings and Structures of Metals and Alloys*, Pergamon Press, NY

Rahlfs, O., and Fischer, W., 1933. Über Thermische Eigenschaften von Halogeniden. 6. Dampfdrucke und Dampfdichten von Beryllium-und Zirkonium-Halogeniden, *Z. Anorg. Allg. Chem*., Vol 211, p 349–367

Rundle, R.E., and Lewis, P.H., 1952. Electron Deficient Compounds, Part VI: The Structure of Beryllium Chloride, *J. Chem. Phys*., Vol 20 (No. 1), p 132

Schroder, W., 1938. Über die Beziehungen des Berylliums zur Gruppe der Vitriolbildner und der Erdalkalimetalle. II, *Z. Anorg. Chem*., Vol 239 (No. 1), p 39–56

Schroder, W., Hompesch, H., and Mirbach, P., 1938. Über die Beziehungen des Berylliums zur Gruppe der Vitriolbildner und der Erdalkalimetalle. III. II. Über die Doppelsulfatbildung zwischen Natrium-und Berylliumsulfat im Vergleich mit der der Vitriole. 2. (Die Polytherme des Ternären Systems $BeSO_4$ $Na_2SO_4H_2O$ Zwischen 0° und 100°), *Z. Anorg. Chem*., Vol 239 (No. 3), p 225–239

Schroder, W., Beckmann, U., and Ausel, W., 1939. Über die Beziehungen des Berylliums zur Gruppe der Vitriolbildner und der Erdalkalimetalle. VI. IV. Über die Doppelsalzbildung Zwischen Ammonium-und Berylliumsulfat im Vergleich mit der der Vitriole. 2, *Z. Anorg. Chem*., Vol 241 (No. 2–3), p 179–195

Semenenko, K.N., and Gordeev, I.V., 1959. Monoclinic Modification of Beryllium Oxyacetate, *Zh. Neorg. Khim*., Vol 4, p 431–432

Semenenko, K.N., and Naumova, T.N., 1963. Polymorphism of Beryllium Bromide and Iodide, *J. Struct. Chem*., Vol 4 (No. 1), p 59–62 (Translated from *Zh. Strukt. Khim*., Vol 4 (No. 1), p 67–72)

Semenenko, K.M., and Turova, N., 1964. Structure of the Beryllium Chloride-Water-Diethyl Ether Addition Compound, *Zh. Neorg. Khim*., Vol 9 (No. 4), p 557–559

Semenenko, K.M., and Turova, N., 1965. The Structure of Hydrated Beryllium Chloride, *Zh. Neorg. Khim*., Vol 10 (No. 1), p 42–45

Sidgwick, N.V., and Lewis, N.B., 1926. The Solubility of Beryllium Oxide in Solutions of Its Salts, *J. Chem. Soc*., p 1287–1302

Staritzky, E., 1956. Crystallographic Data 120: Be_2C; 121: BeS; and 122: K_2PtCl_4, *Anal. Chem. Acta*, Vol 28 (No. 5), p 915

Suchkov, A.B., Borok, B.A., and Morozova, Z.I., 1959. Thermal Decomposition of Certain Sulfates in a Current of Steam, *Zh. Prikl. Khim*., Vol 32 (No. 7), p 1646–1648

Toribara, T.Y., and Chen, P.S., 1952. Separation of Beryllium from Biological Materials, *Anal. Chem*., Vol 24 (No. 3), p 539–542

Travers, P.M., and Perron, M., 1924. Contribution a L'Etude des Orthophosphates Simples et Doubles de Metaux, *Ann. Chem. Fr*., p 298

Vil'komiskii, I.E., Silina, G.F., Berengard, A.S., and Semakin, V.N., 1961. Preparation of Highly Pure Beryllium by the Chloride Method, *At. Energy*, Vol 11 (No. 3), p 828–888

Walter-Levy, L., and Perrotey, J., 1966. Etude de la Thermolyse de Hydrates de L'Oxalates de Beryllium. Analyse Chromatographique Qualitative et Quantative de Gaz Emis, *Bull. Soc. Chim. Fr*., No. 12, p 3964–3969

Wells, A.F., 1961. *Structural Inorganic Chemistry*, Oxford University Press

Wood, G.B., and Brenner, A., 1957. Electrodeposition of Metals from Organic Solutions,

Part IV: Electrodeposition of Beryllium and Beryllium Alloys, *J. Electrochem. Soc*., Vol 104 (No. 1), p 29–35

Young, W.A., 1960. The Reactions of Water Vapor with Beryllia and Beryllia-Alumina Compounds, *J. Phys. Chem*., Vol 64 (No. 8), p 1003

SELECTED REFERENCES

- Coobs, J.H., and Coshuba, W.J., 1952. The Synthesis, Fabrication, and Properties of Beryllium Carbide, *J. Electrochem. Soc*., Vol 99, p 115–120
- Janot, C., and Gibert, H., 1972. Mossbauer Effect Study of the Precipitation of Iron in Beryllium, *Mater. Sci. Eng*., Vol 10 (No. 1), p 23–31
- Kjellgren, B.R.F., Beryllium Compounds, *ECT*, 1st ed., Vol 2, The Brush Beryllium Company, p 505–509
- Lewis, J.R., 1961. Further Evaluation of the Beryllides, *J. Met*., Vol 13, p 829–832
- Opatowski, R.S., 1941. Process for the Preparation of Beryllium Compounds, U.S. Patent 2,209,131
- Schwenzfeier, C.W., Jr., Beryllium Compounds, *ECT*, 2nd ed., Vol 3, The Brush Beryllium Company, p 474–480
- Zalkin, A., Sands, D.E., Bedford, R.G., and Krikorian, O.H., 1961. The Beryllides of Ti, V, Cr, Zr, Nb, Mo, Hf, and Ta, *Acta Crystallogr*., Vol 14, p 63–65

Beryllium Chemistry and Processing, p 131-144
By Kenneth A. Walsh
Edited by Edgar E. Vidal, Alfred Goldberg,
Edward N.C. Dalder, David L. Olson, and Brajendra Mishra

CHAPTER 11

Beryllium Intermetallic Compounds

Christopher Dorn, Brush Wellman, Inc.
Loren A. Jacobson, Los Alamos National Laboratory, Retired
Gilbert London, U.S. Naval Air Systems Command, Retired

11.1 Background and Historical Information

Research on the beryllides was initiated as a part of the search for new materials capable of operating as structural components at very high temperatures in aerospace-defense applications. The initial study identified some beryllides with structural potential, but that interest eventually gave way to their pursuit for use as high-temperature nuclear reactor materials. The projected nuclear uses of the beryllides have included both fuel components and structural hardware. It should be noted that despite the very promising physical and mechanical properties of beryllide intermetallic compounds, various problems have kept these materials from realizing their full potential in the form of a production-level application to date.

Beryllium has been found to form intermetallic compounds with most metallic elements in the periodic table where the binary systems have been examined. Aluminum and silicon are exceptions. The family of beryllides, therefore, includes a large number of intermetallic compounds. Many of the compounds discussed here are high-melting compounds that exhibit excellent oxidation resistance and strength in the 1093 to 1649 °C temperature range. Such beryllides are found in a number of binary systems between beryllium and the transition metals. Some important properties of high-temperature oxidation-resistant beryllides are listed in Table 11.1.

Many of these compounds have unusual properties, and have been intensively investigated intermittently over the last 50 years [Beaver et al. 1964; Paine et al. 1964a, b, c, d; Carrabine 1963; Walsh et al. 1971; Foos et al. 1970]. In the early years, however, the combination of the high melting points of these compounds with the lack of any significant compositional variation in the single-phase compound field, required that blended elemental powders be reacted, ground, reacted again, and finally hot-pressed to full density. This kind of process resulted in significant oxygen, iron, and other impurities, as well as multiple beryllide phases; thus the property measurements made in this time period may not have accurately represented the true capability of many of these materials [Stonehouse et al.

Table 11.1 High-temperature oxidation-resistant beryllides

		Composition, wt% Be	Melting point, °C	X-ray density, g/mL	Crystal structure
Nb-Be	$NbBe_{12}$	53.8	1690	2.92	Body-centered tetragonal
	Nb_2Be_{19}	48.0	1705	3.17	Hexagonal
	Nb_2Be_{17}	45.2	1705	3.28	Rhombohedral
Ta-Be	$TaBe_{12}$	37.4	1850	4.18	Body-centered tetragonal
	Ta_2Be_{17}	29.8	1990	5.05	Rhombohedral
Mo-Be	$MoBe_{12}$	53.2	1705	3.03	Body-centered tetragonal
Ti-Be	$TiBe_{12}$	69.3	1595	2.26	Hexagonal
	Ti_2Be_{17}	61.5	1630	2.46	Rhombohedral
Zr-Be	$ZrBe_{13}$	56.2	1925	2.72	Face-centered cubic
	Zr_2Be_{17}	45.7	1980	3.08	Rhombohedral
Hf-Be	$HfBe_{13}$	39.7	1595	3.93	Face-centered cubic
	$HfBe_{13}$	34.0	1750	4.25	Hexagonal
	Hf_2Be_{17}	30.0	1750	4.78	Rhombohedral

1960; Booker et al. 1962]. There were also some early investigations into simultaneously reacting and consolidating the powders as well as vacuum casting the materials, but these methods were considered less reliable than the "twice-reacted" process.

The properties presented in these investigations generated some interest at the time, but the processing difficulties and expense associated with the beryllium content proved to limit their application.

An extensive compilation of beryllide properties was published by Samsonov [1966]. This article discusses the beryllides as they form with the elements in groups across the periodic table, including some phase-diagram information, and provide 179 references to other work. One very interesting statement in this review article treats the peculiarities of the electronic structure of the beryllium atom. The normally expected electronic configuration of beryllium is $1s^2 2s^2$, but in solid beryllium and its compounds, there can be a single *s* to *p* promotion, giving a configuration of $1s^2 2s2p$. It is the *sp* configuration that brings about the formation of covalent bonds between beryllium atoms, particularly in the lattices of its intermetallic compounds. In the early 1990s, there was renewed interest in the beryllide intermetallics, motivated in part by the National Aero-Space Plane (NASP) project. At that time, a review volume by Dudley and Desai [1996] compiled the data that were then available. This review is very thorough and presents information that includes mechanical property data and oxidation behavior for compounds beginning with $CrBe_2$ and ending with $Zr_2Be_{17} + Ta_2Be_{17}$, arranged in alphabetical order.

Renewed interest in the beryllide intermetallics has been noted over the last 20 years. For example, beryllide intermetallic compounds with the actinide metals exhibit unusual superconducting properties based on a solid-state entity called a "heavy fermion" [Ott et al. 1983; Fisk et al. 1988].

Several other efforts to investigate the structure and properties of beryllides have also been conducted with the aim of developing better understanding of the behavior and potential of these materials. The various types and structures of beryllide intermetallics that have been characterized will first be presented. Information that is currently available will then be given on mechanical, chemical, thermal, magnetic, and other physical properties of these materials. For more complete descriptions of the beryllide intermetallics, their properties and potential uses, the reader is referred to Jacobson, Hanrahan, and Smith [2002].

11.2 Structures of the Beryllides

The structure of important beryllium intermetallics include the following types.

MBe_{22}. Based on the $ZrZn_{22}$ analog, this compound has a cubic structure, with a Pearson symbol of *cF*184 and a space group of *Fd*3*m*. WBe_{22} is one of the phases with this stoichiometry that has been investigated in the past. Paine et al. [1959, 1964a, b, c, d] presented oxidation data showing a weight gain at 1260 °C of 4 mg/cm^2 in 100 h. There is also a $MoBe_{22}$ compound, but it has not been studied to any significant extent.

MBe_{13}. This compound has a face-centered cubic (fcc) structure of the $NaZn_{13}$ prototype with 112 atoms per unit cell. The Pearson symbol for this structure is *cF*112, and the space group is *Fm*3*c*. The elements Mg, Ca, Pu, Sb, Sc, Sr, Zr, Hf, and Y all form such compounds with beryllium. All of the lanthanide and actinide series elements investigated to date also form compounds with beryllium that have the same stoichiometry.

MBe_{12}. This compound has a body-centered tetragonal (bct) structure with 26 atoms in a unit cell, the binary prototype of which is $ThMn_{12}$. The Pearson symbol for this structure is *tI*26. The metallic elements Ag, Au, Cr, Mn, Mo, Nb, Pd, Pt, Ti, V, and W are known to form beryllides with this stoichiometry and structure.

M_2Be_{17}. This compound can exist in two crystal structures, a hexagonal lattice with the Pearson symbol *hP*38 with 38 atoms per unit cell, and a rhombohedral structure, *hR*19. Two compounds, Ti_2Be_{17} and Hf_2Be_{17}, are known to exhibit both structures, while niobium, tantalum, and zirconium appear to exist only in the *hR*19 form. The four higher beryllium content compounds can be characterized as being constructed of beryllium polyhedra surrounding the larger refractory metal.

MBe_5. This compound has the Pearson symbol *hP*6, and the binary prototype is $CaCu_5$. It has been observed in beryllium metal as an impurity phase but has not been investigated as a single-phase intermetallic. This compound has been found in the scandium, niobium, hafnium, and zirconium systems.

MBe_3. This compound is found in the titanium, niobium, and copper systems and has a

Pearson symbol *cF*24. Such compounds have not been investigated to any significant extent.

MBe_2. These compounds with beryllium are generally considered to be in the group of intermetallics called Laves phases, and they have all three of the crystal structures considered to be members of this group, i.e. cubic *C*15, and hexagonal *C*14 and *C*32. Most prior work on these compounds has been related to their potential for storing hydrogen and their unusual magnetic properties. Representative compounds with this stoichiometry are found in the Ti, Cr, Cu, Fe, Hf, Mn, Mo, Nb, Ta, Ti, V, W, and Zr systems with Be.

MBe. These compounds generally have the CsCl or *B*2 crystal structure. The most extensively investigated compound with this structure is NiBe. The Be-Co and Be-Cu systems also have stable compounds with this composition. Other examples of this compound stoichiometry were found in the titanium, zirconium and hafnium systems where they form metastable structures on devitrification of amorphous alloys that were obtained by quenching melts of approximately the eutectic composition between the metal and the nearest stable beryllide, MBe_2 [Tanner and Giessen 1978].

Table 11.2 summarizes the more common structural types found among the beryllides of the transition elements. Generally, MBe_{13} phases are found in the systems. A number of other phases may be found in a given system, particularly on the beryllium-deficient side of the phase diagrams, which were not considered in the preparation of Table 11.2. Thus, the 51 compounds listed in Table 11.2 do not include, by any means, all of the reported beryllides. They do, however, include those compounds which are thus far prime candidates as high-temperature materials; that is the MBe_{17}, MBe_{12} and MBe_{13} series.

Table 11.2 General structural types of beryllides

Phase	Structure	Metals
MBe	Cubic	Ti, Co, Ni, Cu, Pd
	Cubic, T^4	Au
MBe_2	fcc	Ti, Nb, Ag, Ta
	Hexagonal, D^4_{6h}	V, Cr, Mn, Fe, Mo, W, Re
	Hexagonal, D^1_{6h}	Zr, Hf
MBe_5	Cubic	Pd, Au
	fcc	Fe
	Hexagonal	Zr, Hf
M_2Be_{17}	Rhombohedral	Ti, Zr, Nb, Hf, Ta
MBe_{12}	Tetragonal	V, Cr, Nb, Mo, Ta, W
	Hexagonal	Ti
MBe_{13}	fcc	Y, Zr, Hf, La, Ce, Th, U, Np, Pu, Am, Ca, Mg
MBe_{22}	fcc	Mo, W, Re

Considerable confusion persists in the literature as to whether a given compound should be assigned the formula MBe_{12} or MBe_{13}. This particular issue has been addressed by a number of investigators so that it may now be simply stated that the group VB and VIB metals (V, Nb, Ta, Cr, Mo, and W) form the MBe_{12} structure along with titanium, while the lanthanides and actinides along with yttrium, zirconium, and hafnium form MBe_{13} types. It is of interest to note that MBe_{13} compounds have also been identified with magnesium and calcium.

The highest melting-point compounds in this series are found in the Ta-Be, Zr-Be, and possibly Hf-Be systems. The compounds of the Nb-Be system, while not as high melting as those from these other three families, possess some rather remarkable high-temperature properties nonetheless. The densities range from a low of 2.26 g/cm^3 in the case of $TiBe_{12}$ to a high of 5.05 g/cm^3 in the case of Ta_2Be_{17}. The actual density of a beryllide body will change rapidly with composition due to the low density of beryllium. Thus, when determining the porosity of a body, the measured density should not be compared solely with the x-ray density of the compound, or substantial error may be encountered. Pycnometric densities (based on displacement principle) taken on pulverized portions of a body have been used with success for the determination of body porosity.

11.3 Other Beryllium Intermetallics

Several other beryllide intermetallics, and representative compounds are Nb_3Be_2, Mo_3Be, and $BeFe_3$ (a $D0_3$ phase, similar to Ni_3Al). There are also several compounds in the Be-Co and Be-Fe systems with uncertain stoichiometry, and compounds in the Be-Pd, Be-Pt, and Be-Ru systems. None of these compounds has been extensively studied.

Iron, one of the ubiquitous impurities, is usually present in the 500 to 2,000 ppm range. Its solubility increases with temperature, so that at the hot-pressing temperature all of the iron is in solid solution. During cooling from the hot-pressing temperature or with thermal treatment of the beryllium at lower temperatures, the solubility limit is exceeded, and the iron is precipitated as $FeBe_{11}$.

In the presence of aluminum, Carrabine [1963] showed that the ternary beryllide, $AlFeBe_4$, can

be formed as a face-centered cubic phase with a lattice parameter of 6.06 Å. The formation of the ternary beryllide draws iron from $FeBe_{11}$ or from solid solution to the grain boundary. The interactions of iron, aluminum, and beryllium were summarized by Walsh et al. [1971], as shown in Fig. 11.1.

11.4 Mechanical Properties

The refractory-metal beryllides of compositions MBe_{13}, MBe_{12}, and M_2Be_{17} have unique combinations of properties that include high-temperature strength, good thermal conductivity, excellent oxidation resistance, and low density. For example, the strength (modulus of rupture) of Ta_2Be_{17} at 1060 °C is 420 MPa, and its density is 4.99 g/cm^3. At the same temperature the strength of the nickel-base alloy, Inconel 825, is only 42 MPa at a density of approximately 8 g/cm^3. The strength-to-density ratio for the beryllide is thus about 16 times that of the nickel-base alloy at temperature. Another of the high-strength nickel-base alloys, Inconel 718, has a comparable strength to density ratio, but at the lower temperature of 760 °C. Unfortunately, the beryllides have poor ductility and toughness at ambient temperature, which is related to their complex crystal structures, as described above. As a result, their potential usefulness in engineering structures has been quite limited.

An interesting exception is the CsCl (*B*2) structure beryllide, NiBe. Samples of different stoichiometry were prepared by casting, and hardness was measured as a function of composition [Nieh et al. 1989]. A minimum was found at the stoichiometric composition, similar to the aluminides NiAl and CoAl, which have the same crystal structure. Some room-temperature ductility was inferred from the fact that there was no cracking associated with hardness indentations. Later work on extruded NiBe [Nieh et al. 1989] showed that the strain to failure at room temperature is 1.3% in tension and 13% in compression, with failure controlled primarily by the cohesive strength of grain boundaries. At temperatures above 400 °C, 30% compression could be achieved before failure, and the strength levels at elevated temperatures compared favorably with those of NiAl and were somewhat lower than CoAl strengths.

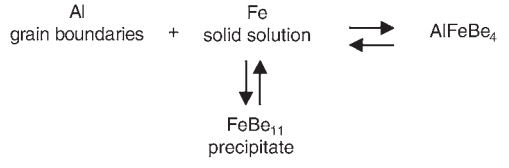

Fig. 11.1 Interactions of iron, aluminum, and beryllium. Source: Walsh et al. 1971

Several investigations have been performed on the relationship between hardness and test temperature for many of the interesting beryllide intermetallics. Fleischer and Zabala [1989] measured the hardness of Nb_2Be_{17}, $ZrBe_{13}$, $NbBe_{12}$, and $TiBe_{12}$; at 1000 °C, the hardness values were 9.5, 6.0, 5.8, and 4.7 GPa, respectively. The data for hardness as a function of temperature for these beryllides did not give a clear indication of a ductile-to-brittle transition temperature (DBTT), but from an observation of the absence of cracking associated with the hardness indentations, the temperatures were estimated to be 1050, 840, 1000, and 840 °C respectively, for the compounds in the order of decreasing hardness listed above. An investigation of the hardness of three of these same beryllides, and substituting $TaBe_{12}$ for $TiBe_{12}$, was also performed at different temperatures [Nieh and Wadsworth 1990]. The materials were prepared by vacuum hot pressing, and hardness samples were sectioned directly from the hot-pressed materials. These investigators found that by plotting the logarithm of the hardness as a function of the reciprocal of temperature, a clearer indication of a ductile-to-brittle transition could be determined. Table 11.3 compares the DBTT results of the above investigations, along with those from Bruemmer et al. [1993].

These high values for DBTT are undoubtedly sufficient to discourage the application of these complex crystal-structure beryllides in low-temperature structural components. The estimate of 750 °C for the DBTT of VBe_{12} by Nieh et al. [1992] comes from a more extensive study of this compound which measured room-temperature properties, including fracture toughness, as well as elevated-temperature creep behavior.

Table 11.3 Ductile-to-brittle transition temperatures (DBTT) for some beryllide compounds

	DBTT, °C		
Compound	Fleischer and Zabala [1989]	Nieh and Wadsworth [1990]	Bruemmer et al. [1993]
$TiBe_{12}$	840	. . .	700
$NbBe_{12}$	1000	770	955
Nb_2Be_{17}	1050	815	. . .
$ZrBe_{13}$	840	740	. . .
$TaBe_{12}$	. . .	790	. . .
VBe_{12}	. . .	750 (estimated)	690

The fracture toughness was estimated from the micro-cracking associated with a hardness indentation and found to be 0.84 MPa$\sqrt{m}$.

Characteristic of intermetallic compounds in general, the beryllides are hard, strong materials. The room-temperature hardness values for several beryllides are given in Table 11.4. For purposes of orientation in the hardness spectrum, aluminum is about 40 on this scale, tungsten about 400, BeO is 1300, and titanium carbide is 3200. The beryllides are, therefore, much harder than common metallic materials, but not among the extremely hard materials.

Table 11.4 Room-temperature hardness values for selected beryllides

Compound	HV, 2.5 kg load
Nb_2Be_{11}	1000
Nb_2Be_{17}	1050
$NbBe_{12}$	500
Ta_2Be_{17}	1120
$TaBe_{12}$	720
Zr_2Be_{17}	1130
$ZrBe_{13}$	1000
$MoBe_{12}$	950
$TiBe_{12}$	960

Source: Stonehouse et al. 1960

The strength of vacuum-hot pressed Ta_2Be_{17} as a function of temperature is illustrated in Fig. 11.2. This modulus of rupture curve is quite typical of the beryllide family in that a gradual increase in strength with temperature is noted up to 871 °C, after which a sharp increase in strength is observed. The peak strength occurs in the 1260 °C region. In this case, the effect of minor variations in stoichiometry was under examination, with 29.8 wt% beryllium being the stoichiometric composition for Ta_2Be_{17}. It was concluded that the minor variations in stoichiometry tested here had little effect upon the observed strength of the material, the results being indicative of the range of values encountered in the modulus of rupture testing. Typical modulus of rupture values for other beryllides are shown in Table 11.5. The highest values are recorded for Nb_2Be_{17}, Nb_2Be_{11}, and Ta_2Be_{17}. The niobium compounds are particularly attractive when their relatively low densities (3.28 and 3.17 g/cm^3, respectively) are considered.

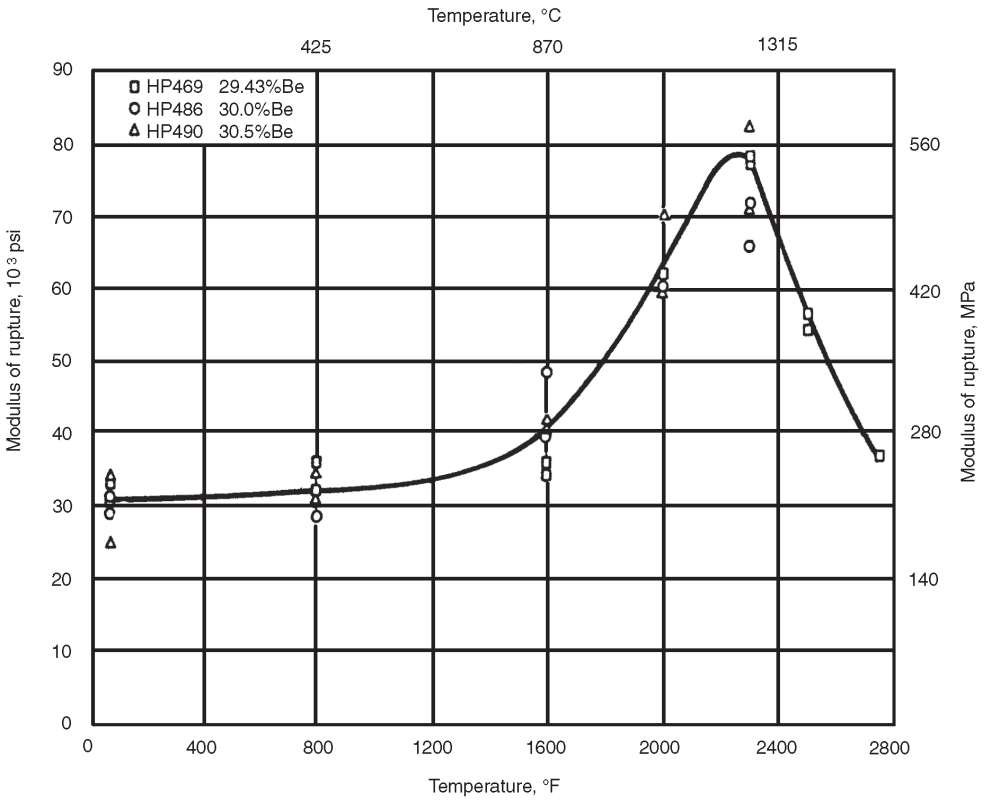

Fig. 11.2 Modulus of rupture of vacuum hot-pressed Ta_2Be_{17} as a function of temperature. Source: Stonehouse et al. 1960

Static Young's modulus values determined in the course of the modulus of rupture test are 43 to 47 × 10^6 psi (296 to 324 GPa) at room temperature, 40 × 10^6 psi (276 GPa) at 871 °C, and 20 to 25 × 10^6 psi (138 to 172 GPa) at 1371 °C for the beryllides under discussion. Dynamic measurements of Young's modulus have indicated anomalies in the behavior of the niobium compounds, and a minimum is recorded at approximately 760 °C after which a rapid rise occurs to peak at 1316 °C in the case of Nb_2Be_{17} [Stonehouse et al. 1960; Truesdale et al. 1961]. The values for Nb_2Be_{17} are 43 × 10^6 psi (296 GPa) at room temperature, 41 × 10^6 psi (283 GPa) at 760 °C, 47 × 10^6 (324 GPa) at 1093 °C, 53 × 10^6 psi (365 GPa) at 1260 °C, and 46 × 10^6 psi (317 GPa) at 1371 °C.

Compressive strength determinations have indicated 1.9 to 2.0 × 10^5 psi (1310 to 1379 MPa) at room temperature, 1.3 to 1.5 × 10^5 psi (896 to 1034 MPa) at 871 °C, and 0.7 to 0.8 × 10^5 psi (483 to 552 MPa) at 1371 °C for $ZrBe_{13}$ and $NbBe_{12}$, respectively.

Table 11.5 Modulus of rupture of niobium, tantalum, and zirconium beryllides

	Modulus of rupture, ksi			
Compound	RT	1260 °C (2300 °F)	1371 °C (2500 °F)	1510 °C (2750 °F)
Nb_2Be_{11}	31	70	63	36
Nb_2Be_{17}	30	70	65	27
$NbBe_{12}$	22	45	40	22
Ta_2Be_{17}	30	78	56	35
$TaBe_{12}$	31	53	43	26
Zr_2Be_{17}	25	40	40	35
$ZrBe_{13}$	25	40	37	25

RT, room temperature

Little capacity for plastic strain is exhibited by the beryllides described in this chapter between room temperature and 1093 °C, but significant plastic deformation has been recorded at higher temperatures. Calculations from the deflection of the modulus-of-rupture bars indicate that a maximum of about 0.1% tensile elongation occurs in the outermost fibers of such bars at room temperature prior to fracture. At 1371 °C, elongations from 1.0 to 2.6% may be calculated for the niobium and the tantalum compounds, but the zirconium compounds remain at approximately 0.1%. $TaBe_{12}$ and Nb_2Be_{17} showed about 5% and 7% elongation, respectively, at 1510 °C, while Zr_2Be_{17} and $ZrBe_{13}$ showed only 0.1% and 0.6%, respectively, at the same temperature. Tensile elongations for Nb_2Be_{17} in the tensile test showed a maximum of 2%. This difference is believed to be due to the design of the specimen which in effect provided a very small gauge section making it necessary to calculate strain from reduction in area.

The chart in Fig. 11.3 shows the breaking strengths at 1371 °C for a number of materials. The chart is based on the tensile strength data for the refractory metals and modulus-of-rupture data for the beryllides, carbides, and oxides. Typical values for the beryllides range

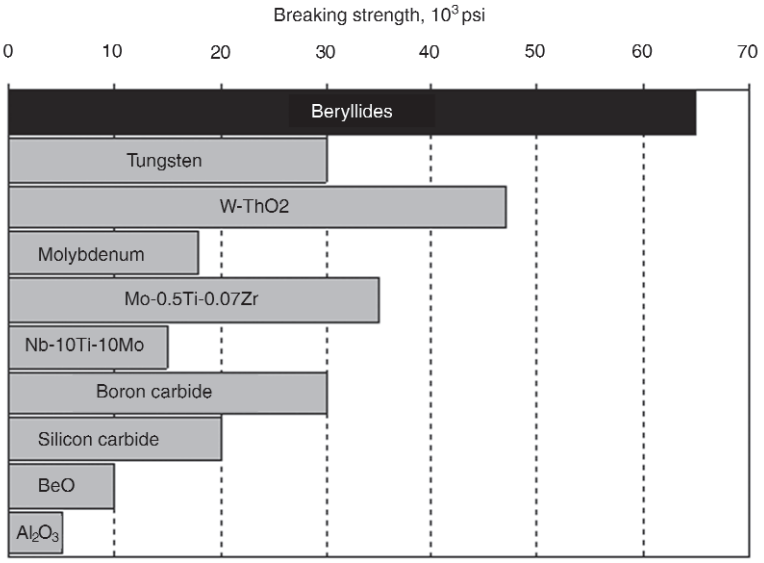

Fig. 11.3 Breaking strength of beryllides at 1371 °C as compared to other compounds

from 37,000 to 65,000 psi (255 to 448 MPa), depending on the compound tested. The refractory metals and their high-temperature alloys break under considerably lower stress at 1371 °C: tungsten, at 30,000 psi (207 MPa); thoriated tungsten at approximately 47,000 psi (324 MPa); molybdenum at 18,000 psi (124 MPa); Mo0.5Ti0.07Zr at 35,000 psi (241 MPa); and Nb-10Ti-10Mo at 15,000 psi (103 MPa).

Although oxides themselves have excellent resistance to oxidation, they have considerably lower strength at higher temperatures than either the beryllides or the refractory metals and their alloys. Boron carbide has a breaking strength of approximately 30,000 psi (207 MPa), while silicon carbide, beryllium oxide, and aluminum oxide rupture at stresses below 20,000 psi (138 MPa).

Specific gravity is an important property for airborne and space applications (see Fig. 11.4). Like beryllium, the beryllides have low specific gravities, ranging from 2.72 to 5.05. The beryllides have a significant weight advantage over such refractory metals as tungsten and molybdenum, which have specific gravities of 19.3 and 10.2, respectively.

Steady-state creep rates were compared for vacuum hot-pressed and hot isostatically pressed material for different stress levels at 1100 and 1150 °C. At low strain rates, the stress exponent was found to be near four, consistent with dislocation climb as the rate-controlling mechanism, which is similar to the stress exponent found for other intermetallics, such as TiAl, Ti_3Al, NiAl, and CoAl. At higher stresses, the power law appears to break down.

At low strain rates, the creep activation energy was found to be 270 kJ/mol and, again, is close to the activation energies observed for the other intermetallic compounds. Nieh et al. [1992] have also investigated the creep behavior of the beryllide Nb_2Be_{17}. In 1993, again using the microcracking associated with a hardness indentation, the room-temperature fracture toughness was found to be 1.1 $MPa\sqrt{m}$. For this compound, the stress exponent for steady-state creep was found to be close to three, a value which is associated with dislocation glide as the rate-controlling mechanism. The activation energy was determined to be approximately 575 kJ/mol, a value which is higher than that found for other beryllides. It was not possible to associate this activation energy with any specific diffusion process due to the lack of diffusion data for the compound. Observation of the absence of intergranular crack formation after 15% deformation in creep was also cited as evidence for dislocation glide as the rate controlling mechanism.

Several research efforts were performed jointly by Battelle-Pacific Northwest Laboratories and Washington State University [Bruemmer et al. 1992; Henager et al. 1992; Henager et al. 1993; Sondhi et al. 1993]. These studies have shed

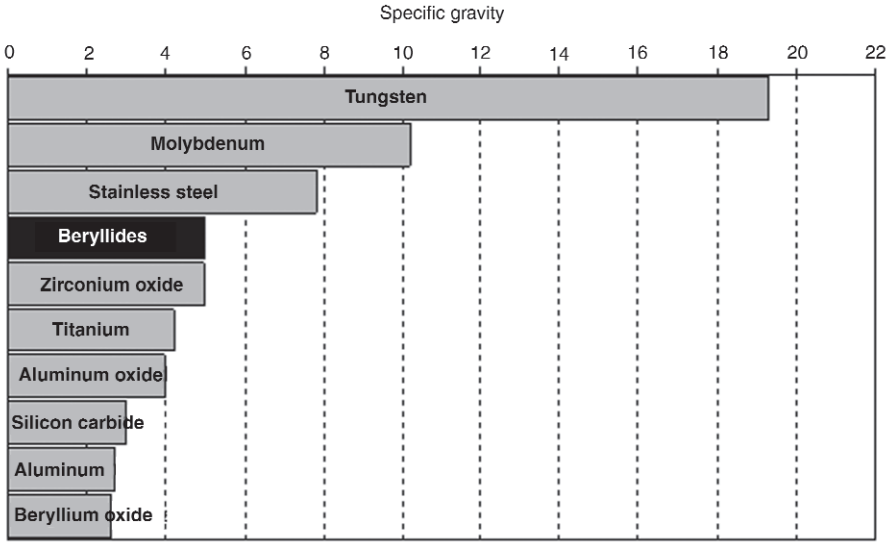

Fig. 11.4 Specific gravity of selected compounds and beryllides

some important new light on deformation mechanisms and dislocation structure in the niobium beryllides, $NbBe_{12}$ and Nb_2Be_{17}. For the former compound, dislocations were observed to be partials bounding planar faults, with slip systems that were identified as 1/2<101>{121}, 1/2<101>{101}, and 1/2<100>{011}. The partial dislocations were related to the possible phase transformation from $NbBe_{12}$ to Nb_2Be_{17} (the latter structure is very closely related to the former) and could account for enhanced dislocation mobility and the promotion of high-temperature deformation. Atomistic modeling has been performed for the a[100] edge and screw dislocations, and the a/2[100] screw dislocation [Sondhi et al. 1992].

Other results of the previous investigations compare favorably with prior measurements. In particular, it was found that the room-temperature fracture toughness of $NbBe_{12}$ was 4 $MPa\sqrt{m}$, which is higher than that measured by other investigators. In general, it was found that hot isostatic pressing (HIP) gave better properties for this compound, but intermediate-temperature tests revealed possible intergranular embrittlement for HIP material. Twinning modes in vacuum hot-pressed and HIP pressed $NbBe_{12}$ were also investigated by these researchers [Charlot et al. 1991], who found that twins and extended faults have {101} habit planes and <011> twinning directions, while shorter range faults have a (001) habit plane. This extensive collection of work should be referred to by future investigations into the mechanical behavior of the MBe_{12} intermetallic compounds.

11.5 Oxidation Behavior

The oxidation behavior of beryllides is enhanced by the fact that beryllium forms a protective oxide, BeO, which has two allotropes of which only the alpha phase is usually observed. Studies by Doychak [1994] and Brady and Doychak [1999] provide a comparison between some thermodynamic and oxidative measurements of beryllium and other metal/oxide systems. Among the beryllides are some of the highest-melting of all intermetallic compounds, as well as some of the lowest-density refractory metallic phases. These densities range from 2 to 4 g/cm^3.

Paine et al. [1964a, b, c, d] published the results of an extensive survey of the oxidation behavior of the transition-metal beryllides. With the exception of $ZrBe_{13}$, the MBe_{13} compounds are not resistant at temperatures as high as 1260 °C, although good resistance below this temperature may be recorded in some literature. Some of the MBe_{13} compounds tested included YBe_{13}, $LaBe_{13}$, $CeBe_{13}$, $GdBe_{13}$, $ThBe_{13}$, and UBe_{13}. The majority of the MBe_{12} and MBe_{17} phases are quite oxidation resistant.

The actinide MBe_{13} compounds are not oxidation resistant in the 1260 to 1371 °C temperature range. The MBe_{13} series is, however, isomorphous, and a continuous solid solution may be formed between $ZrBe_{13}$ and UBe_{13}. The resultant single-phase material has been found to be oxidation resistant at 1371 °C up to at least the equimolar $ZrBe_{13}$-UBe_{13} composition, which contains 42 wt% uranium. The (U,Zr)Be_{13}–10 wt% uranium material exhibits a penetration of 0.013 mm (0.0005 in.) after 100 h of exposure at 1371 °C in air and 0.008 mm (0.0003 in.) after 100 h of exposure at 1598 °C in air, an oxidation behavior essentially equivalent to $ZrBe_{13}$. Other lanthanides and actinides would be expected to form similar solid solutions. These have been prepared and tested with the expected results in the case of $GdBe_{13}$ and $HfBe_{13}$ [Paine et al. 1964a, b, c, d].

To determine oxidation resistance, beryllides have been exposed to streams of air at high temperature for 100 h periods. At 1371 °C, oxide thickness ranges from 0.008 mm (0.0003 in.) in the case of Ta_2Be_{17} to 0.023 mm (0.0009 in.) for $NbBe_{12}$ were found. Even at 1482 °C, the tantalum beryllides show an oxidation layer thickness of only 0.023 mm (0.0009 in.) [Stonehouse 1962].

Oxides exhibit superior oxidation resistance for obvious reasons, but beryllides are close to them in this respect. Refractory metals have extremely poor oxidation resistance at high temperatures—one of their major drawbacks.

Despite the attractive properties of beryllides, only a handful of studies on the oxidation of these compounds have been conducted since the 1960s. In addition to the well-known beryllium health and safety issues that must be dealt with to work with beryllides, there are two technical reasons that are often cited to explain the lack of research into the oxidation of beryllium compounds. Historically, the majority of the research was conducted on complex line compounds, all of which were brittle at very high temperatures. This may have contributed to decisions not to

pursue these efforts further. In the few post-1960s studies that were published on the oxidation of beryllides, significant problems with intermediate-temperature disintegration and/or oxide volatility in the presence of water vapor were found. The reaction between beryllium oxide and water vapor at elevated temperatures [Stuart and Price 1964] may be simplified as:

$$BeO(s) + H_2O\,(g) \leftrightarrow Be(OH)_2\,(g)$$

This reaction has also been implicated in the accelerated oxidation of beryllides at intermediate temperatures (a "pest" reaction, for example Doychak [1994]) and at high temperatures [Aitken and Smith 1962; Perkins 1963; Dudley and Desai 1996]. A review of the effects of moisture on the oxidation of beryllides is provided by Hanrahan [1999]. Based on the early data and recent work on the compounds $TiBe_{12}$, $CrBe_2$, and alloys of NiAl and beryllium, he concludes that the effects of water vapor on compounds that form continuous BeO scales are only significant at temperatures above 1100 °C. The rates observed are comparable to the SiO_2–H_2O reaction [Opila 1999]. Hence in stagnant environments and/or low partial pressures of moisture, beryllides might be successfully employed at considerably higher temperatures. Nonetheless, this temperature may be considered the upper use limit for beryllides exposed in moist environments.

While the beryllides are not as refractory as many ceramics, they possess a stability toward surrounding atmospheres approaching that of the refractory oxides due to the layer of beryllium oxide, an excellent ceramic material, which is formed when the beryllide surface is exposed to high-temperature oxidizing conditions. While the surfaces of the compounds are thus essentially a refractory-oxide surface in service, the beryllide matrix possesses properties quite unlike that of the refractory oxide, most notably high strength at elevated temperature. Significant further increases in the strength of beryllides at temperature are believed possible with the development of techniques for attaining and maintaining very fine-grained bodies. Further gains in mechanical behavior may be possible through the use of metal-working techniques, which have been demonstrated to be feasible [Truesdale et al. 1961].

Beryllide materials are typically not high-purity, single-phase materials. Work has shown that the range of homogeneity for any of the beryllide phases under discussion is quite narrow. For instance, a nominal $ZrBe_{13}$ compound will typically contain 2 to 5 wt% Zr_2Be_{17} or similar levels of free beryllium. The materials discussed in this chapter were always controlled so that the exact composition was on the M_2Be_{17} side of the MBe_{12} or MBe_{13} phase in preparations of these latter compound types and slightly on the MBe_{12} or the MBe_{13} side in the case of M_2Be_{17} preparations. Very pure beryllides have been made, as confirmed by the presence of a single phase in an x-ray diffraction pattern. Chemical impurities include 0.7 to 1.5 wt% BeO, 500 to 800 ppm iron, 300 to 600 ppm silicon, and 300 to 800 ppm of aluminum.

11.6 Thermal and Electrical Properties

The thermal properties of the transitional element beryllides are quite good, generally being intermediate of the more familiar ceramic and metallic high-temperature materials. The coefficients of thermal expansion (CTE) for a number of the members of the beryllide family are presented in Table 11.6.

The coefficients of thermal expansion are of the same order of magnitude as those exhibited by metals and are higher than those of refractory oxides. The CTE versus temperature curves for these materials are quite similar with only small differences between individuals [Booker et al., 1964].

The thermal conductivities of the niobium and tantalum beryllides along with $ZrBe_{12}$ are given in Table 11.7. These values plot as essentially straight lines with a slight increase in

Table 11.6 Coefficient of thermal expansion for several beryllides at different temperature intervals

	Coefficient of thermal expansion, $°C^{-1} \times 10^{-6}$				
Compound	27 to 316 °C	27 to 649 °C	27 to 982 °C	27 to 1316 °C	27 to 1482 °C
Nb_2Be_{17}	6.3	7.3	7.9	8.5	8.8
$NbBe_{12}$	6.7	7.5	8.3	9.0	9.3
Ta_2Be_{17}	6.2	7.1	7.8	8.4	8.7
$TaBe_{12}$	5.8	6.9	7.6	8.1	8.4
Zr_2Be_{17}	5.6	7.0	7.5	8.1	8.4
$ZrBe_{13}$	6.5	7.7	8.6	9.4	9.8
$MoBe_{12}$	6.7	7.8	8.4	9.0	9.3
Hf_2Be_{21}	6.5	7.7	8.2	8.8	9.1

Source: Stonehouse 1971

conductivity with temperature. Specific heat values are given in Table 11.8.

Figure 11.5 shows the electrical conductivity as a function of temperature of the beryllides.

Table 11.7 Thermal conductivity of several beryllides

	Thermal conductivity, W/m · K				
Compound	649 °C (1200 °F)	871 °C (1600 °F)	1093 °C (2000 °F)	1316 °C (2400 °F)	1427 °C (2600 °F)
Nb_2Be_{17}	31.3	32.0	32.7	33.4	33.7
$NbBe_{12}$	30.6	31.0	31.5	32.0	32.2
Ta_2Be_{17}	29.2	30.3	31.5	32.7	31.5
$TaBe_{12}$	28.9	31.7	33.7	36.3	38.6
$ZrBe_{13}$	40.0	38.1	36.3	34.6	33.7

Source: Stonehouse 1971

Table 11.8 Specific heat of beryllides

	Specific heat, kJ/kg · K				
Compound	538 °C (1000 °F)	816 °C (1500 °F)	1093 °C (2000 °F)	1371 °C (2500 °F)	1538 °C (2800 °F)
$NbBe_{12}$	1.61	1.67	1.73	1.80	1.83
Ta_2Be_{17}	0.89	0.95	1.00	1.06	1.09
$TaBe_{12}$	1.13	1.17	1.21	1.24	1.26
$MoBe_{12}$	1.60	1.68	1.77	1.86	1.91
$ZrBe_{13}$	1.60	1.70	1.80	1.91	1.97

Source: Stonehouse 1971

11.7 Sputter Deposition

The technique of sputter deposition to form beryllide intermetallics has been used by Brimhall et al. [1992] to make material specimens that do not have the complications of impurities as cited earlier. There was one finding of particular interest involving alloys of two metals with beryllium. When the compounds with the individual metals were different, the phase found was that which was characteristic of the majority element. For example, in alloys of niobium and zirconium with beryllium, the phase $(Nb_xZr_y)Be_{12}$ was found when x was in excess of 0.5, and the phase $(Nb_xZr_y)Be_{13}$ was present when y was greater than 0.5. One of the possible explanations for these observations is that the cage formed by beryllium can accommodate different metal atoms, and the particular symmetry is defined by the majority element.

11.8 Diffusion

Investigation of reaction rates between liquid rare-earth metals and beryllium has been done

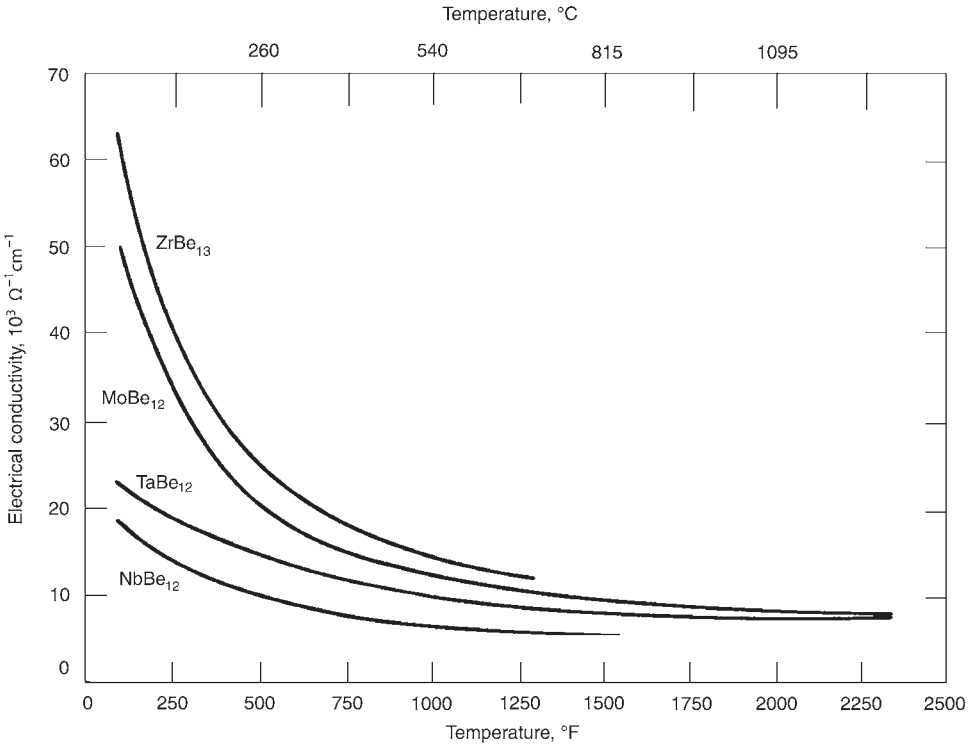

Fig. 11.5 Electrical conductivities of selected beryllides. Source: Stonehouse 1971

by Hanrahan et al. [1997]. The differences in diffusion behavior between the higher atomic-number rare earths (Er, Yb) and the lower members of this grouping (Ce, Nd, Sm) have been clearly demonstrated. For example, the growth rate of the intermetallic compound $YbBe_{13}$, which forms between molten ytterbium and solid beryllium, is governed almost exclusively by the diffusion of beryllium through the compound toward the liquid, and the diffusion of vacancies from the liquid toward the compound-beryllium interface. Conversely, for the lower atomic number rare-earths, such as cerium or praseodymium, the growth of the intermetallic is principally via diffusion of the lanthanide. Intermediate lanthanides, such as $SmBe_{13}$, grow by nearly balanced diffusion of both species. In all cases, lattice diffusion of both species must proceed through vacancies on the beryllium sublattices. Therefore, the concentration of vacancies within a particular compound must control the mobility and hence the growth rate of the intermetallic compound. The mobility of species on the other hand, is dictated by the valance structure of the particular lanthanide and its ability to occupy (albeit temporarily) beryllium sites.

Other work that deals with diffusion and beryllide intermetallics is that of Brimhall and Bruemmer [1992]. This work investigated the reactions between the beryllide $NbBe_{12}$ and the refractory metals molybdenum, tantalum, and tungsten. The ceramics SiC, $MoSi_2$, and Al_2O_3 were also studied. Diffusion couples were prepared between $NbBe_{12}$ and the other materials, and in no case was the diffusion of other metallic elements into the beryllide observed. Rather, it was primarily the diffusion of beryllium from the intermetallic into the other materials that governed the interfacial reaction, with some evidence that the compound Nb_2Be_{17} was formed due to the depletion of beryllium in the intermetallic phase. It was observed that silicon from the silicon-bearing ceramics diffused into the beryllide. The reactions that were observed were considerable, and since this study was done with the possibility in mind that the beryllide could ultimately be combined with the other materials in a composite, it was concluded that some form of reaction barrier would have to be used in order to limit the degradation of the interface. It seems clear that the high mobility of beryllium at elevated temperatures is a factor that contributes to the reactivity of beryllium and high-melting-point beryllides with other refractory materials and molten metals.

11.9 Hydrogen Storage

It has been found that three intermetallic compounds of beryllium form definite hydride phases. These compounds are $TiBe_2$, $ZrBe_2$, and $HfBe_2$ [Maeland and Libowitz, 1983]. When heated to 375 °C at atmospheric pressure, $TiBe_2$ forms a limiting solid solution of composition $TiBe_2H_{0.05}$. This limiting solid solution involves a small expansion of the cubic $TiBe_2$ lattice. When an applied pressure of 15,000 kPa was used, a hydride of approximate composition $TiBe_2H_3$ was formed. However, when the pressure was lowered to atmospheric pressure, all of the hydrogen was released, indicating that the hydride was unstable, with a dissociation pressure between 100 kPa and 15,000 kPa. The compound $ZrBe_2$ reacted spontaneously with hydrogen at atmospheric pressure and room temperature to form the phase $ZrBe_2H_{1.5}$. The dissociation pressure at room temperature was too low to measure accurately. The hydrogen content of the hydride appears to increase with increasing pressure; at 13 kPa the composition was found to be $ZrBe_2H_{2.3}$. The compound $HfBe_2$ behaves similarly to $ZrBe_2$, but the hydrogen content is lower, at a composition $HfBe_2H_{1.1}$. Other beryllium compounds including VBe_2 and $ZrBe_5$ were investigated but not found to have significant hydrogen absorption. The same was true of $HfBe_5$ and $TiBe_3$. The conclusion was that although the hydrogen storage efficiencies of the three group IV di-beryllides were not as great as BeH_2, they still compare favorably with some of the hydrides of other intermetallics that are being investigated as hydrogen storage media, particularly on a weight percentage basis [Schlapbach 1994]. The hope was expressed that additional investigation would uncover practical ways to lower the dissociation pressure of $TiBe_2H_3$ or raise that of $ZrBe_2H_{1.5}$ so that the dissociation pressure of the hydride would fall in a range suitable for practical use.

The possibility of developing a useful hydrogen storage material using a beryllide has not been investigated recently. Study of the structure of the $ZrBe_2H_{1.5}$ phase showed that deuterium occupied tetrahedral sites in a partially ordered configuration at 12 K (−261 °C) and continuously transformed to a disordered structure at 298 K (25 °C), in which it occupied trigonal bipyramidal sites [Hauback et al., 1995]. Hydrogen diffusion in this phase has also been investigated, with the interesting finding that hydrogen diffusion is restricted to two dimensions within

individual powder particles [Kimmerle et al., 1998]. Practical hydrogen storage using beryllide intermetallics could become useful.

11.10 Fabrication of Beryllides

To turn constituent metals into a beryllide intermetallic compound, they are intimately blended in powder form and then reacted at elevated temperatures. The reacted compacts are ground to powder. From this raw material, specific shapes are produced in many ways:

- *Cold pressing and sintering*: This technique is similar to conventional ceramic processes where raw materials are mixed with suitable binders, pressed to shape in steel dies, and fired at high temperatures. Resulting shapes have densities at 98 to 100% of theoretical. Beryllide blocks 25.4 × 203 × 203 mm (1 × 8 × 8 in.) with excellent high-temperature strength and resistance to oxidation can be fabricated. Finishing methods depend on tolerances required, but in general diamond grinding is used.
- *Isostatic pressing and sintering*: Isostatic pressing is satisfactory for fabricating beryllide shapes to close internal dimension tolerances. The process is similar to cold pressing except that pressure is applied hydraulically from all directions instead of axially. Cones and cylinders with high, uniform density are produced.
- *Vacuum hot pressing*: Large shapes are made by hot pressing. Discs 305 mm (12 in.) in diameter and 25.4 mm (1 in.) thick have already been produced, and larger parts are feasible. This technique is similar to that used in powder metallurgy.
- *Flame spraying*: In this technique, the powder is sprayed at a very high temperature onto a shape to coat its surface with a thin layer. Flame spraying can produce a wide variety of shapes of almost any thickness. Plates and cones have been fabricated by this method.
- *Extrusion and slip casting*: These are other processes that have been successfully investigated for fabricating beryllides.

11.11 Conclusions and Future Work

Since their initial investigation in the 1950s, beryllide intermetallic compounds have been a periodic source of interest for a few specialized applications over the years. It is indisputable that on the whole, there are several beryllide compounds that possess an unusual combination of properties, featuring high melting points, with excellent oxidation resistance and good mechanical strength at very high temperatures.

Beryllium metal has long been regarded by the nuclear fusion community as the reference material for the neutron multiplier in fusion blanket designs. Starting in the late 1990s and continuing into the 2000s, there has been particular interest in titanium beryllide with the composition $TiBe_{12}$ for use in this same application. $TiBe_{12}$ stands out from other beryllides for fusion because it has the highest neutron-multiplication characteristic, with the added benefit of higher temperature performance capability compared to beryllium metal. Service demands on the breeder blanket in the first full-scale fusion reactors are expected to reach 900 °C, a temperature at which structural grades of beryllium metal oxidize readily and have diminished mechanical performance due to recrystallization and grain growth. In laboratory-scale work, $TiBe_{12}$ has shown itself to outperform beryllium sufficiently to justify continuing efforts on its development.

Despite all of their promise over the past 50 years, beryllide intermetallic compounds are not known to have been used in a production-scale application to date. With the recent serious specific interest in $TiBe_{12}$ on the part of the fusion community, combined with the technological developments in materials processing over the same timeframe, it seems possible at last that the beryllides are poised to make a major breakthrough in the 21st century.

REFERENCES

Aitken, E.A., and Smith, J.P., 1962. Oxidation of Beryllium Intermetallic Compounds in Moist Atmospheres: *J. Nucl. Mater*., Vol 6, p 119

Beaver, W.W., et al., 1964. Symposium on Compounds of Interest in Nuclear Reactor Technology, University of Colorado, Boulder, CO

Booker, J., Paine, R.M., and Stonehouse, A.J., 1962. "Investigation of Intermetallic Compounds for Very High Temperature Applications," Wright Air Development Center Reports No. WADD-TR-60-889, Part II

Booker, J., Paine, R.M., and Stonehouse, A.J., 1964. Studies on the Vapor Pressure and Oxi-

dation of Certain Beryllides, *Compounds of Interest in Nuclear Reactor Technology*, sponsored by The Metallurgical Society of AIME, at the University of Colorado, p 477–493

Brady, M.P., and Doychak, J., 1999. *High Temperature Oxidation and Corrosion of Intermetallics*, Wiley-VCH, Weinheim, Germany, 1999

Brimhall, J.L., and Bruemmer, S.M., 1992. Compatibility of High Temperature Materials with $Be_{12}Nb$, *Scr. Metall. Mater*., Vol 27, p 1747–1752

Bruemmer, S.A., Charlot, L.A., Brimhall, J.L., Henager, C.H., and Hirth, J.P., 1992. Dislocation Structures in $Be_{12}Nb$ After High-Temperature Deformation, *Philos. Mag. A*, Vol 65 (No. 5), 1992, p 1083–1094

Bruemmer, S.M., Arey, B.W., Brimhall, J.L., and Hirth, J.P., 1993. Hot-Hardness Comparisons Among Isostructural $Be_{12}X$ Intermetallic Compounds, *J. Mater. Res*., Vol 8 (No. 7), p 1550–1557

Carrabine, J.A., 1963. Ternary AlMnBe4 Phases in Commercially Pure Beryllium, *J. Nucl. Mater*., Vol 8, p 278–280

Charlot, L.A., Brimhall, J.L., Thomas, L.E., and Bruemmer, S.M., 1991. Twinning Relationship in $Be_{12}Nb$, *Scr. Metall. Mater*., Vol 25, p 99–103

Doychak, J., 1994. *Oxidation of Intermetallic Compounds*, J.H. Westbrook and R.L. Fleischer, Ed., John Wiley & Sons, New York, 1994

Dudley, R.D., and Desai, P.D., 1996. *Properties of Intermetallic Alloys III, Beryllides and Miscellaneous Intermetallic Alloys*, Metals Information Analysis Center, West Lafayette, Indiana, 1996

Fisk, Z., Hess, D.W., Pethick, C.J., Pines, D., Smith, J.L., Thompson, J.D., and Willish, J.O., 1988. Heavy Electron Metals: New Highly Correlated States of Matter, *Science*, Vol 239, p 33–42

Fleischer, R.L., and Zabala, R.J., 1989. Mechanical Properties of High-Temperature Beryllium Intermetallic Compounds, *Metall. Trans. A*, Vol 20A (No. 7), p 1279–1282

Foos, R.A., Stonehouse, A.J., and Walsh, K.A., 1970. Micro-Alloying Relationships in Beryllium, *Proc. Beryllium Conf*., National Academy of Sciences, Washington, D.C., p 127–147

Hanrahan, R.J. Jr., Thoma, D.J., Jacobson, L.A., Zocco, T.G., Lowery, J.L., and Pereyra, R., 1997. Surrogate Studies of the Pu-Be Reaction II, *21st DOE Compatibility, Aging and Stockpile Stewardship Conference*, Albuquerque, N., Report No. LA-UR–97-3885, 1997

Hanrahan, R.J., Jr., 1999. Moisture Effects on the Oxidation of Beryllides: High Temperature Corrosion and Materials Chemistry, *Per Kofstad Memorial Symposium*, P.Y. Hou et al., Ed., Honolulu, HI, The Electrochemical Society, 1999

Hauback, B.C., Fjellvag, H., and Maeland, A.J., 1995. Temperature-Induced Structural Changes in Be2ZrD1.5 Studied by Powder Neutron Diffraction, *J. Alloy. Compd*., Vol 224 (No. 2), p 241–243

Henager, C.H., Bruemmer, S.M., and Hirth, J.P., 1993. Strength and Toughness of Beryllium Niobium Intermetallic Compounds, *Mater. Sci. Eng. A*, Vol 170 (No. 1–2), p 185–197

Henager, C.H., Jacobson, R.E., and Bruemmer, S.M., 1992. Elevated Temperature Mechanical Properties of Be12Nb, *Mater. Sci. Eng. A*, Vol 153 (No. 1–2), p 416–421

Jacobson, L.A., Hanrahan, R.J., and Smith, J.L., 2002. Beryllide Intermetallic Compounds, *Intermetallic Compounds, Principles and Practice*, J. H. Westbrook and R. L. Fleischer, Ed. John Wiley & Sons, Vol 3, p 37–51, 2002

Kimmerle, F., Majer, G., Kaess, U., Maeland, A.J., Conradi, M.S., and McDowell, A.F., 1998. NMR Studies of Hydrogen Diffusion in ZrBe2H1.4, *J. Alloy. Compd*., Vol 264 (No. 1–2), p 63–70

Maeland, A.J., and Libowitz, G.G., 1983. Hydrides of Beryllium-Based Intermetallic Compounds, *J. Less-Common Met*., Vol 89, p 197–200

Nieh, T.G., and Wadsworth, J., 1990. Hot Indentation Tests of Refractory Metal Beryllides, *Scr. Metall. Mater*., Vol 24 (No. 8), p 1489–1494

Nieh, T.G., Wadsworth, J., and Liu, C.T., 1989. Mechanical Properties of Nickel Beryllides, *J. Mater. Res*., Vol 4 (No. 6), p 1347–1353

Nieh, T.G., Wadsworth, J., Grensing, F.C., and Yang, J.M., 1992. Mechanical Properties of Vanadium Beryllide, VBe12, *J. Mater. Sci*., Vol 27 (No. 10), p 2660–2664

Opila, E.J., 1999. Variation of the Oxidation Rate of Silicon Carbide with Water Vapor Pressure, *J. Am. Ceram. Soc*., Vol 82 (No. 3), p 625–636

Ott, H.R., Rudigier, H., Fisk, Z., and Smith, J.L., 1983. UBe13: An Unconventional Actinide Superconductor, *Phys. Rev. Lett*., Vol 50 (No. 20), p 1595–1598

Paine, R.M., Stonehouse, A.J., and Beaver, W.W., 1959. "An Investigation of Intermetallic Compounds for Very High Temperature Applications," Brush Beryllium Co., WADC TR 59-29, Part I, 1959

Paine, R.M., Stonehouse, A.J., and Beaver, W.W., 1964a. Oxidation of the Beryllides at Intermediate Temperatures-Anomalous Behavior and a Solution, *Met. Soc*., Am. Inst. Mining, Met. Petrol. Engrs., Inst. Metals Div., Spec. Rept., Vol No. 13, p 495–509, 1964

Paine, R.M., Stonehouse, A.J., and Beaver, W.W., 1964b. High Temperature Oxidation Resistance of the Beryllides, *Corros*., Vol 20 (No. 10), p 307–313

Paine, R.M., Stonehouse, A.J., and Beaver, W.W., 1964c. "High Temperature Oxidation Resistance of the Beryllides," paper presented at NACE Symposium on Aerospace Metals, 1964

Paine, R.M., Stonehouse, A.J., and Beaver, W.W., 1964d. Oxidation of Beryllides at Intermediate Temperatures—Anomalous Behavior and a Solution, *Symposium on Components of Interest in Nuclear Reactor Technology*, AIME-TMS, Warrensdale, PA, p 495–509, 1964

Perkins, F.C., 1963. "Intermediate Temperature Oxidation of Beryllides, Final Report," University of Denver Research Inst. Report DRI-2128, 1963

Samsonov, G.V., 1966. The Chemistry of the Beryllides, *Russ. Chem. Rev. (Uspekhii Khimii)*, Vol 35 (No. 5), p 339–361

Schlapbach, L., Meli, F., and Zuttel, A., 1994. Intermetallic Hydrides and their Applications, *Intermetallic Compounds, Principles and Practice*, Vol 4, J.H. Westbrook and R.L. Fleischer, Ed., John Wiley & Sons Ltd., NY, p 475–488, 1994

Sondhi, S., Hoagland, R.G., and Hirth, J.P., 1992. Atomistic Modeling of Dislocations in Be12X Compounds, *Mater. Sci. Eng. A*, Vol 152 (No. 1–2), p 103–107

Sondhi, S., Hoagland, R.G., Hirth, J.P., Brimhall, J.L., Charlot, L.A., and Buremmer, S.M., 1993. "Deformation Mechanisms in Be12X Compounds," Conference: High-Temperature Ordered Intermetallic Alloys V, Boston, MA, 1993

Stonehouse, A.J., and Woodard, D.H., 1971. "Characteristics of Beryllium-Antimony Alloys," Brush Beryllium Co., Report, presented at AIME Meeting, Detroit, 1971

Stonehouse, A.J., Paine, R.M., and Beaver, W.W., 1960. Mechanical Properties of Some Transition Element Beryllides, *Mechanical Properties of Intermetallic Compounds*, J.H. Westbrook, Ed., John Wiley & Sons, Ch 13, 1960

Stonehouse, A.J., 1962. Beryllides for Lightweight, High Temperature Structures, *Mater. Design Eng*., Vol 55 (No. 2), p 84086

Stuart, W.I., and Price, G.H., 1964. The High Temperature Reaction between Beryllia and Water Vapor, *J. Nucl. Mater*., Vol 14, p 417–433

Tanner, L.E., and Giessen, B.C., 1978. Structure and Formation of the Metastable Phase M-TiBe, *Metall. Trans. A*, Vol 9 (No. 1), p 67–69

Truesdale, R.S., Lympany, B.B., Bielawski, C.A., Grala, E.M., and Beaver, W.W., 1961. "Investigation of the Effects of Processing Variables and Fabrication Techniques Upon the Properties of Intermetallic Compounds," ASD-TDR-62-476, 1961

Walsh, K.A., Stonehouse, A.J., et al., 1971. "Altering Beryllium Properties by Heat Treatment and Chemistry Control," ASM-Westec Conference, Los Angeles, CA, 1971

SELECTED REFERENCES

- Carrabine, J.A., Woodard, D.H., Stonehouse, A.J., and Beaver, W.W., 1964, The Effects of AlFeBe4 on Mechanical Properties of Fabricated Polycrystalline Beryllium
- Paine, R.M. and Carrabine, J.A., 1960, Some New Intermetallic Compounds of Beryllium
- Rooksby, H.P., 1962, Intermetallic Phases in Commercial Beryllium

Beryllium Chemistry and Processing, p 145-149
By Kenneth A. Walsh
Edited by Edgar E. Vidal, Alfred Goldberg,
Edward N.C. Dalder, David L. Olson, and Brajendra Mishra

CHAPTER 12

Amorphous Alloys That Contain Beryllium

Loren A. Jacobson, Los Alamos National Laboratory, Retired
Robert Hanrahan, National Nuclear Security Agency

12.1 Introduction

Amorphous alloys, or metallic glasses, have been known since the early 1970s. Amorphous alloys have no long-range order like conventional crystalline materials and are generally made by rapid quenching of molten alloy by a splat process, by a melt spinning process that produces ribbon, by a planar flow casting process that produces wide ribbon, or by atomization to fine powder from a molten state. One of the earliest publications on this class of materials was by Gilman [1975]. The alloy systems that have the greatest potential for forming amorphous alloys are those systems with deep eutectics, where the eutectic temperature is significantly lower than the melting temperature of the individual elements. Also, it is sometimes necessary that there be limited solid solubility of one element in another, although this condition is not a rigid requirement. Several of the amorphous alloys developed in the late 1970s and early 1980s contained beryllium. A bulk amorphous alloy containing beryllium was also developed and is described subsequently.

12.2 Early Work on Amorphous Alloys

The early work on amorphous alloys, performed mainly at Allied Signal Corporation laboratories, was aimed at producing commercial quantities of 30 μm thick ribbon material by rapid quenching from the melt, for potential use in soft magnetic applications such as transformer cores. The mechanical and thermal properties of one of these alloys, $Fe_{80}B_{20}$ glass, were summarized by Davis, Ray, et al. [1976]. The strength and stiffness of other amorphous alloys were given in a parallel article by Davis, Chou, et al. [1976], and are listed in Table 12.1. Data are given for metallic glasses that are made up of a transition metal (TM) and a metalloid (M), in which the compositions are approximated by the ratio of 80 to 20 ($TM_{80}M_{20}$), in atomic percentages. The information in this table shows similar data for several "metal-metal" glasses for which the composition is very nearly equiatomic.

At the time of this work, the detailed mechanism of deformation for these amorphous phases was not known. Because there was a similarity in the relationship between stiffness and hardness for the two types of glass, it was assumed that there must be a common flow mechanism. However, while the correlations were roughly parallel, they were on different curves, implying that there could be a structural difference between transition metal-metalloid glasses and metal-metal glasses.

Note that one of the compositions in Table 12.1 contains a significant amount of beryllium. The designation as a "Metglas" indicates that it was a product of the Allied Signal Corporation laboratories. The physical properties of this glass were measured by Tanner and Ray [1977], and the measurements indicated that this composition had the highest specific strength of metallic glasses known at the time. The Vickers

Table 12.1 Mechanical properties of selected amorphous alloys with comparison to a beryllium amorphous alloy

Alloy	Hardness (H_v), kg/mm^2	Young's modulus (E), $\times 10^3$ kg/m^2	Density (ρ), g/cm^3	Acoustic velocity (VE), $\times 10^5$ cm/s	E/H
$Pd_{80}Si_{20}$	490	8.97	10.3	2.92	18.3
$Pd_{77.5}Cu6Si_{16.5}$	500	8.97	10.3	2.92	17.9
$Pd_{40}Ni_{40}P_{20}$	540	10.0	9.48	3.22	18.5
$Ni_{80}P_{20}$	610	11.6	7.90	3.79	19.0
$Ni_{40}Fe_{40}P_{14}B_6$ Metglas 2826	750	12.7	7.51	4.08	16.9
$Ni_{39}Fe_{38}P_{14}B_6A1_3$	750	13.0	7.52	4.12	17.3
$Fe_{80}P_{20}$	755	13.3	7.10	4.29	17.6
$Ni_{49}Fe_{29}P_{14}B_6Si_2$ Metglas 2826B	790	13.5	7.65	4.15	17.1
$Fe_{80}P_{16}C_3B_1$ Metglas 2615	835	13.8	7.30	4.30	16.5
$Ni_{36}Fe_{32}Cr_{14}P_{12}B_6$ Metglas 2826A	880	14.4	7.46	4.34	16.4
$Fe_{80}B_{20}$ Metglas 2605	1100	16.9	7.4	4.74	15.4
$Cu_{50}Zr_{50}$	580	8.51	7.33	3.38	14.6
$Cu_{64}Zr_{36}$	600	9.17	7.54	3.45	14.8
$Cu_{50}Ti_{50}$	610	9.86	6.25	3.93	16.1
$Cu_{60}Ti_{40}$	685	10.8	6.69	3.98	15.9
$Be_{40}Ti_{50}Zr_{10}$ Metglas 2204	730	10.7	4.13	5.05	14.7

Metglas, Allied Signal Corporation. Source: Davis et al. 1976

hardness was measured as 740 kg/mm^2, and the yield strength was estimated to be approximately 231 kg/mm^2 (328 ksi). The Young's modulus was 10.7×10^3 kg/mm^2 (15.3×10^6 psi), and its density was determined to be 4.13 g/cm^3. It was in this work that TiBe, the metastable ordered phase with B2 (CsCl) structure in which zirconium is substituted for titanium, was described. The competition of this phase with glass formation led to a restricted glass-formation range observed in titanium-beryllium-rich alloys. Formation of an amorphous material required a high critical cooling rate. The structure and formation of this metastable phase in the titanium-beryllium system was further investigated by Tanner and Giessen [1978].

Major contributions to the understanding of the formation and behavior of beryllium-containing glass phases were made by Tanner. One of the more important of these was a thermochemical description of the titanium-beryllium, zirconium-beryllium, and hafnium-beryllium systems, which was coupled with phase diagram data and used to predict the minimum melting temperatures in the three possible ternary systems, Ti-Zr-Be, Ti-Hf-Be, and Zr-Hf-Be.

Kaufman and Tanner [1979] and Tanner and Ray [1979] also made contributions to the information about the glass-forming ability of the binary and ternary systems. In the titanium-beryllium and the zirconium-beryllium systems, the low-temperature hexagonal (alpha) phase of the transition metal has little or no equilibrium solubility of beryllium, but the high-temperature body-centered cubic (beta) phase has a solubility between 3 and 5 at.%. The zirconium-beryllium system has a glass-forming range from 30 to 50 at.% Be, but this range was only 37 to 41 at.% Be in the titanium-beryllium system. They found a metastable ordered phase in the zirconium-beryllium system of the CrB (B33)-type structure, which was also found in quenched alloys in the hafnium-beryllium system and the Zr-Hf-Be ternary system. The equilibrium phase in all three binary systems is a Laves phase of composition MBe_2.

These findings clearly contributed to later work that led to the use of beryllium as a key ingredient in the first alloy system to remain amorphous under relatively slow cooling rates of the order of 10 K/s (18 °F/s) or less [Peker and Johnson 1993]. This alloy had the composition $Zr_{41.2}Ti_{13.8}Cu_{12.5}Ni_{10.0}Be_{22.5}$ and was prepared as ingots weighing 5 to 6 g. It was postulated that the large difference in size of constituent atoms would require large chemical concentration fluctuations to form crystalline-phase nuclei of critical size. Some years later, work at Los Alamos National Laboratory was conducted on this alloy, and arc-melted ingots weighing up to 200 g were prepared that retained the amorphous state [He et al. 1996]. This work explored the changes in Young's modulus and density after annealing at temperatures between 650 and 800 K (710 and 980 °F). At room temperature, the Young's modulus was 100.4 GPa (15×10^6 psi), and after complete crystallization it was 131.8 GPa (19×10^6 psi). The slow cooling rate used to prepare the alloy did not result in a large free volume, and after annealing above the

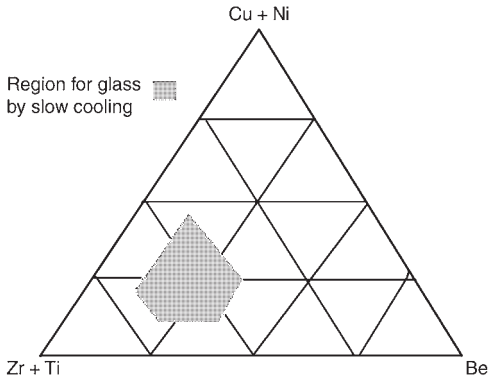

Fig. 12.1 Pseudo-ternary phase diagram showing the region for obtaining glass by slow cooling. Source: Busch et al. 1995

glass transition temperature, the density increased by only approximately 0.1%.

Information on the composition ranges that can be slowly cooled (10 K/s, or 18 °F/s, or less) and still remain amorphous was given in a later publication [Busch et al. 1995]. This work shows a quasi-ternary diagram with Zr+Ti at one corner, Cu+Ni in another corner, and beryllium at the third corner. Figure 12.1 shows the approximate composition range for slowly cooled glass, as presented in the article.

Another alloy system that was investigated in the 1980s was the Be-Al-Ti system, which was thought to have some potential application to the improvement of high-temperature aluminum alloys. The work also dealt with the effect of aluminum on the formation and stability of titanium-beryllium glass [Tanner et al. 1988]. It was found that approximately 5 at.% Al could be added to the Ti-$TiBe_2$ eutectic (37.5 at.% Be) and retain the amorphous structure on splat quenching from the melt.

12.3 Recent Efforts

The bulk metallic glass that contains beryllium allowed for thick enough sections to be prepared so that the fracture mechanics requirements for the determination of plane-strain fracture toughness, K_{Ic}, could be satisfied. Conner et al. [1997] determined K_{Ic} for three specimens and obtained values of 55, 57, and 59 MPa · $m^{1/2}$. For a yield stress of 2 GPa (290 ksi), the thickness is required to be greater than 1.6 mm (0.06 in.), and the specimens used for that study were at least 2.2 mm (0.09 in.) thick. An apparent fracture surface energy of 30,000 J/m^2 was determined, a value very much higher than that for ceramics or other metals, which typically fall in the range of 0.5 to 10 J/m^2. This result suggested that mechanisms other than simply creating new surface were operating during the fracture of the bulk metallic glass.

A later investigation of fracture, fatigue, and environmentally assisted fracture of commercially produced bulk metallic glass gave K_{Ic} values ranging from 18 to 68 MPa · $m^{1/2}$ [Ritchie et al. 2000]. This variability was thought to be due to residual stresses in the samples following processing, and different loading rates. Fatigue crack-growth rates were also measured in air and in NaCl solution. Growth rates in the NaCl solution were 2 to 3 orders of magnitude greater than those in air. Deionized water testing indicated that there was little effect of this environment on fatigue crack growth. Material that had been recrystallized was also tested and proved to be so brittle that plane-strain fracture toughness values had to be determined by the indentation method. The value was very low, approximately 1 MPa · $m^{1/2}$.

Investigators in China have selected a different bulk metallic glass for study. This glass had the composition $Zr_{52.5}Al_{l0}Ni_{10}Cu_{10}Be_{12.5}$, and its properties were compared with a similar glass composition that had 65 at.% Zr and no beryllium. The glass with beryllium was found to have a tensile strength of 1.75 GPa (253 ksi), compared to the other glassy phase that had a tensile strength of 1.33 GPa (193 ksi) [Xiao et al. 2003]. A later work performed by the same group reported on the investigation of the influence of beryllium on the thermal stability of the Zr-Al-Ni-Cu bulk amorphous alloys [Xiao et al. 2004]. With the aluminum, nickel, and copper held at constant atomic percentages of 10, 10, and 15, respectively, the zirconium composition was (65-X) at.%, with X = 0, 3, 6, 9, 12.5, and 16 at.% Be. It was found that the glass-forming ability and thermal stability first increase and then decrease as the alloy first starts as an off-eutectic composition, approaches and then reaches the eutectic, and finally exceeds the eutectic composition. The eutectic is at X = 12.5 at.% Be, and this was the composition investigated in the previous paper.

Work at Lawrence Livermore National Laboratory on beryllium-base coatings identified an amorphous phase in coatings that contained boron [Jankowski et al. 2002]. Sputter-deposited beryllium coatings were prepared with additives

that included copper, iron, and boron. These elements were added in an attempt to refine the grain size of the coatings, and iron and boron were found to be very effective in this role. In addition, increasing amounts of boron were added, and at compositions above 16 at.%, the coatings were amorphous. Hardness values for the amorphous coatings were lower than those for the microcrystalline coatings. Additional work was performed on the beryllium-boron coatings to determine the effect of annealing temperature on the crystallization of amorphous material [Jankowski et al. 2003]. It was found that the crystallization temperature was dependent on the boron concentration. For 16 at.% B, crystallization was seen at 200 °C (390 °F), but a temperature greater than 300 °C (570 °F) was required for the 21 at.% B material. Phase separation in the crystalline phase was also observed, suggesting a mechanism involving eutectic crystallization.

12.4 Applications

The bulk amorphous alloy $Zr_{41.2}Ti_{13.8}Cu_{12.5}Ni_{10.0}Be_{22.5}$ is now being produced on a commercial scale by several firms. Studies of different compositions of this basic alloy have shown that properties can be varied to suit specific applications, but detailed information remains proprietary. Comparison of the yield strength of this alloy, designated VIT-001, with aluminum, titanium, and stainless steel is shown in Fig. 12.2. The related elastic limit comparison is shown in Fig. 12.3 [Jacobson 2006].

While the elastic modulus of this alloy is rather low because of its liquid state, 96 GPa (13.9 Mpsi) [Conner et al. 1997], the high yield strength and elastic limit give articles made from the alloy excellent energy-transfer properties. This situation has led to application in golf club heads (both in irons and in metal woods), tennis racquet frames, baseball bats, and skis. The beryllium content of the alloy is still of concern, despite the rather low weight percent (approximately 3.5 wt% Be), which is not so different from copper-beryllium alloys. This concern has limited, to some extent, the wide application of this unusual material.

It is evident that beryllium has been an important additive to amorphous metal alloys, particularly where lower density and higher strength were desired. Beryllium has also played a significant role in the early compositions of bulk amorphous alloys, which can be slowly cooled and still retain the amorphous structure.

REFERENCES

Busch, R., Schneider, S., Peker, A., and Johnson, W.L., 1995. Decomposition and Primary Crystallization in Undercooled $Zr_{41.2}Ti_{13.8}Cu_{12.5}Ni_{10.0}Be_{22.5}$ Melts, *Appl. Phys. Lett.*, Vol 67, p 1544–1546

Conner, R.D., Rosakis, A.J., Johnson, W.L., and Owen, D.M., 1997. Fracture Toughness Determination for a Beryllium-Bearing Bulk Metallic Glass, *Scr. Mater.*, Vol 37, p 1373–1378

Davis, L.A., Chou, C.P., Tanner, L.E., and Ray, R., 1976. Strengths and Stiffnesses of Metallic Glasses, *Scr. Metall.*, Vol 10, p 937–940

Davis, L.A., Ray, R., Chou, C.P., and O'Handley, R.C., 1976. Mechanical and Thermal Properties of $Fe_{80}B_{20}$ Glass, *Scr. Metall.*, Vol 10, p 541–546

Gilman, J.J., 1975. Metallic Glasses, *Phys. Today*, Vol 28, p 46

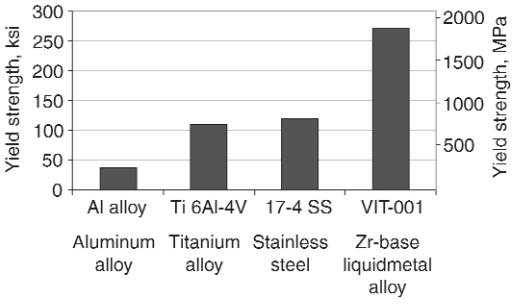

Fig. 12.2 Yield strength of several cast alloys compared to Liquidmetal alloy. Source: Jacobson 2006

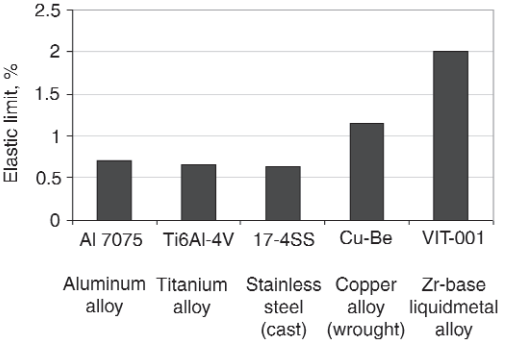

Fig. 12.3 Elastic limit of various metals compared to Liquidmetal alloy. Source: Jacobson 2006

He, Y., Schwarz, R.B., Mandrus, D., and Jacobson, L., 1996. Elastic Moduli, Density and Structural Relaxation in Bulk Amorphous $Zr_{41.2}Ti_{13.8}Cu_{12.5}Ni_{10.0}Be_{22.5}$ Alloy, *J. Non-Cryst. Solids*, Vol 205–207, p 602–606

Jacobson, L.A., 2006. Los Alamos, NM, private communication

Jankowski, A.F., Wall, M.A., and Nieh, T.G., 2003. Crystallization of Beryllium-Boron Metallic Glasses, *J. Non-Cryst. Solids*, Vol 317, p 129–136

Jankowski, A.F., Wall, M.A., Van Buuren, A.W., Nieh, T.G., and Wadsworth, J., 2002. From Nanocrystalline to Amorphous Structure in Beryllium-Based Coatings, *Acta Mater.*, Vol 50 (No. 19), p 4791–4800

Kaufman, L., and Tanner, L.E., 1979. Coupled Phase Diagrams and Thermomechanical Descriptions of the Titanium-Beryllium, Zirconium-Beryllium and Hafnium-Beryllium Systems, *CALPHAD*, Vol 3, Pergamon Press Ltd., p 91–107

Peker, A., and Johnson, W.L., 1993. A Highly Processable Metallic Glass: $Zr_{41.2}Ti_{13.8}Cu_{12.5}Ni_{10.0}Be_{22.5}$, *Appl. Phys. Lett.*, Vol 63 (No. 17), p 2342–2344

Ritchie, R.O., Schroeder, V., and Gilbert, C.J., 2000. Fracture, Fatigue and Environmentally Assisted Failure of a Zr-Based Bulk Amorphous Metal, *Intermetallics*, Vol 8 (No. 5–6), p 469–475

Tanner, L.E., and Giessen, B.C., 1978. Structure and Formation of the Metastable Phase M-TiBe, *Metall. Trans. A*, Vol 9 (No. 1), p 67–69

Tanner, L.E., Jacobson, L.A., and Wall, M.E., 1988. Formation and Crystallization of Amorphous Phases in the Ti-Be-Al System, *Mater. Sci. Eng.*, Vol 97, p 379–383

Tanner, L.E., and Ray, R., 1977. Physical Properties of $Ti_{50}Be_{40}Zr_{10}$ Glass, *Scr. Metall.*, Vol 11 (No. 9), p 783–789

Tanner, L.E., and Ray, R., 1979. Metallic Glass Formation and Properties in Zr and Ti Alloyed with Be—1. The Binary Zr-Be and Ti-Be Systems, *Acta Metall.*, Vol 27 (No. 11), p 1727–1747

Xiao, X., Fang, S., Wang, G., Hua, Q., and Dong, Y., 2004. Influence of Beryllium on Thermal Stability and Glass-Forming Ability of Zr-Al-Ni-Cu Bulk Amorphous Alloys, *J. Alloy. Compd.*, Vol 376, p 145–148

Xiao, X., Fang, S., Xia, L., Li, W., Hua, Q., and Dong, Y., 2003. Thermal and Mechanical Properties of $Zr_{52.5}Al_{l0}Ni_{10}Cu_{10}Be_{12.5}$ Bulk Metallic Glass, *J. Alloy. Compd.*, Vol 351, p 324–328

SELECTED REFERENCE

- Tanner, L.E., and Ray, R., 1980. Phase Separation in Ti-Zr-Be Metallic Glasses, *Scr. Metall.*, Vol 14 (No. 6), p 657–662

Beryllium Chemistry and Processing, p 151-162
By Kenneth A. Walsh
Edited by Edgar E. Vidal, Alfred Goldberg,
Edward N.C. Dalder, David L. Olson, and Brajendra Mishra

CHAPTER 13

Physical Metallurgy of Beryllium

Alfred Goldberg, Lawrence Livermore National Laboratory
David L. Olson, Colorado School of Mines
Loren A. Jacobson, Los Alamos National Laboratory, Retired

13.1 Beryllium Phases and Phase Transformations

Beryllium is an unusual metal in many ways. Its atomic number is 4, making it the only element with an even atomic number that has only one stable isotope. This stable isotope has mass number 9, but a number of radioactive isotopes are known, and they have mass numbers that range from 6 to 11. The electronic configuration is also unusual. As the first member of group IIA in the periodic table, it is expected to have a configuration of $1s^2$-$2s^2$, but in light of the directional bonding observed in the pure metal and also in many of the intermetallic compounds of beryllium, it is more likely that the electronic configuration is $1s^2 2s^1 2p^1$.

At 1 atm pressure, two solid phases exist for pure beryllium between room temperature and its melting temperature. There is an allotropic transformation in beryllium at approximately 1250 °C (2280 °F), only about 35 °C (65 °F) below the melting temperature. The lower-temperature alpha phase is hexagonal close-packed (hcp), and the higher-temperature beta phase is body-centered cubic (bcc). In this regard, beryllium is similar to titanium and zirconium, which have the hcp structure at ambient temperature and also transform to bcc at elevated temperature. The beta phase of beryllium is stable over a very small temperature range of approximately 30 °C (55 °F), but the temperature range of beta-phase stability increases with increasing pressure to become approximately 300 °C (540 °F) wide at 295 atm (300 bar) pressure [Adhikari and Mukhopadhyay 1994]. Some alloying additions can also increase the temperature range over which bcc beryllium is stable (i.e., cobalt, nickel, and copper). The solidification of pure beryllium does not reveal evidence of this phase transformation, probably because liquid beryllium can undercool below the transformation temperature, such that the first phase to nucleate is the hcp low-temperature phase. The lattice parameter of beta (bcc) beryllium is 0.2549 nm. The alpha (hcp) phase of beryllium has lattice parameters of $a = 0.2285$ nm and $c = 0.3585$ nm. The hcp lattice parameters give an axial ratio of 1.5688, which is less than the ideal value of 1.632. At the alpha-to-beta transformation, the bcc phase is denser than the hcp phase, resulting in a negative volume change on heating, an unusual transition [Gupta 1994]. Based on the Engel-Brewer theory, the alkaline earth metals have an sp electronic hybrid state that promotes the hcp structure at lower temperatures, while at higher temperatures, the entropy contribution results in free energy for the bcc phase to be more energetically favorable.

13.2 Beryllium Physical Properties

The sp hybrid electronic state contributes to a number of unusual properties of beryllium metal. For example, the bonding in the basal plane appears to be metallic in nature, while the bonding perpendicular to the basal plane has a covalent character. This bonding anisotropy leads to the anisotropy of ambient-temperature

elastic constants and slip properties, described as follows.

Some of the physical properties for beryllium are given in Tables 13.1 and 13.2 [Singh 1994]. The elastic constants, in terms of compliance coefficients, are given. Note that C_{13} is equal to zero (or very nearly so). This suggests that there is little or no shear coupling between the "a" and "c" directions and accounts for the fact that pyramidal (or c/a) slip does not occur at ambient temperatures. Dislocations that have Burgers vectors with c-axis components are not energetically favored and therefore are not found in samples that have been deformed at low temperatures. These elastic compliances give an elastic modulus of over 300 GPa, which is higher than that of almost all other metals. Coupled with its low density, this elastic modulus gives beryllium a specific stiffness, or modulus-to-density ratio, that is six times higher than that of any other structural material.

Table 13.1 Elastic properties of beryllium

	Elastic modulus	
Compliance coefficients	**GPa**	**$\times 10^6$ psi**
C_{11}	292.3	42
C_{33}	336.4	49
C_{12}	26.7	4
C_{13}	0.0	0.0
C_{44}	162.5	24

Table 13.2 Thermal properties of beryllium

Thermal expansion coefficient	$\alpha_{11} = 13.9$, $\alpha_{35} = 10.4 \times 10^{-6}\ K^{-1}$
Specific heat	0.481 cal/g (2 J/g) (highest of any metal)

The thermal expansion coefficients are also given. Note that the anisotropy is not as strong as may be expected with the low c/a ratio. Specific heat as a function of temperature is presented in Fig. 13.1. This figure also presents specific heat information for several other metals for comparison (magnesium, aluminum, titanium, and steel).

The fact that beryllium has the highest specific heat of any metal is a property that promotes beryllium application in a variety of components where heat absorption is very important. Examples are found among electro-optical devices such as position sensors and inertial guidance systems. The latter components also benefit from the high Young's modulus of beryllium.

Because of its low atomic number and low atomic weight, beryllium has a low mass absorption coefficient. This property makes it virtually transparent to x-rays and other high-energy radiation; for example, beryllium transmits x-rays 17 times better than an equivalent thickness of aluminum. Beryllium is therefore

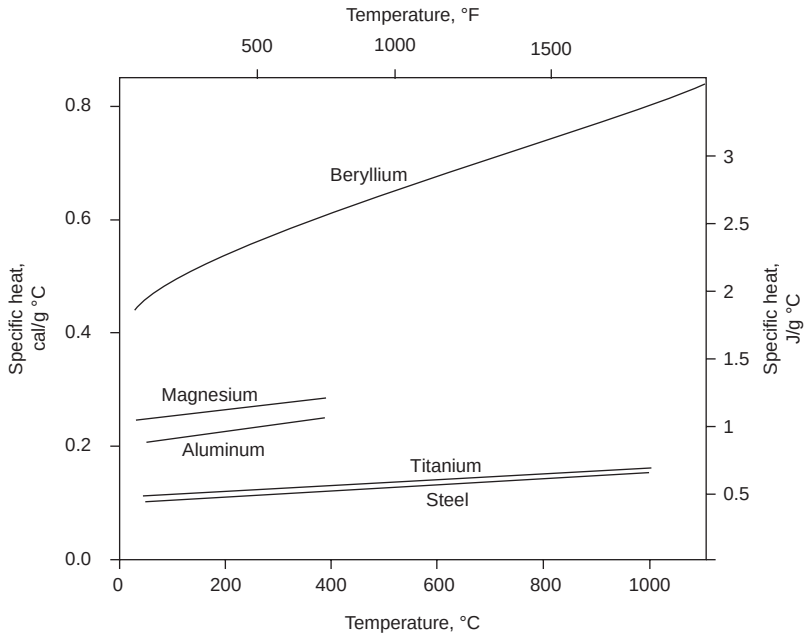

Fig. 13.1 Specific heat of beryllium, titanium, magnesium, aluminum, and steel, plotted as a function of temperature. Source: Greenfield 1971

used as a window material in x-ray tubes and in energy-dispersive x-ray detectors. Another very attractive property of beryllium is its reflectivity in the infrared wavelength range. At these longer wavelengths, beryllium reflects more than 99% of the intensity that is incident upon it. Beryllium is thus a very suitable material for use in mirrors for surveillance systems and satellites [Adhikari and Mukhopadhyay 1994].

13.3 Mechanical Properties

13.3.1 Deformation Mechanisms

The alpha phase, with its hcp structure, has a variety of different deformation modes, including slip on the basal plane, slip on the prismatic and pyramidal planes, cross slip, and twinning, as illustrated in Fig. 13.2. There are three first-order and three second-order prismatic planes and six first-order and six second-order pyramidal planes [Adhikari and Mukhopadhyay 1994]. The primary slip planes are those lattice planes on which dislocations are glissile with low flow stress. The primary slip planes in hcp metals commonly are the basal planes or possibly first-order prismatic planes. The axial ratio is important in the selection of the primary slip plane. Among the hcp metals, alpha-beryllium has the lowest axial ratio, which strongly influences the mechanical properties and behavior. The basal slip occurs for $c/a > 3^{1/2}$, and prismatic slip occurs for $c/a < 3^{1/2}$. Alpha-beryllium does not behave this way, since it exhibits basal slip. These

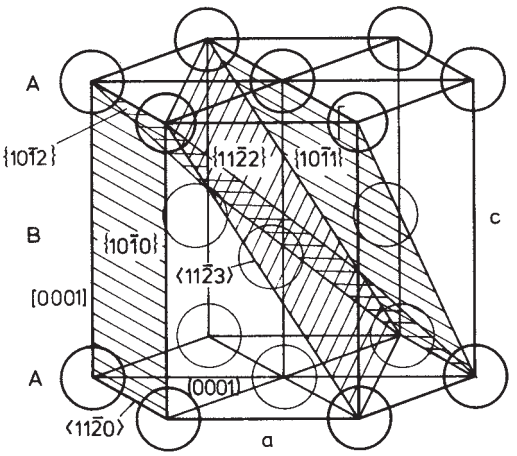

Fig. 13.2 Hexagonal crystal structure showing important planes for possible deformation. Source: Aldinger 1979

slip planes are glissile with low flow stress. The secondary slip plane becomes active if the primary slip planes are unfavorably oriented or if constraints increase the stress in these planes. The extent to which any of these modes operate depends on the axial c/a factor, temperature, strain rate, stacking fault energy, and impurity level. The critical resolved shear stress (CRSS) as a function of temperature for the different slip systems is shown in Fig. 13.3. Notice the temperature ranges necessary to have basal slip compared to prismatic slip [Aldinger 1979].

The operative slip systems at ambient temperature consist of two independent basal slip systems, with one plane and two Burgers vectors, and two independent prismatic slip systems, with two planes and one dislocation Burgers vector. These Burgers vectors are parallel to the basal plane at ambient temperature, so there is not a c-axis component to any of these systems. Thus, there are only four independent systems at ambient temperature, and this is insufficient for full polycrystalline plasticity. (Five independent systems would be required for extensive polycrystalline plasticity to be achieved.) Thus, grain size must be small to limit the extent of dislocation pile-up stress at grain boundaries and to keep any resulting cleavage cracks as short as possible. Twinning is also a potential deformation mode but does not contribute at any significant extent to ambient temperature ductility of polycrystalline beryllium.

The mobile dislocation Burgers vector is [0001], which lies in the basal plane and can also move on the prism planes, {10$\bar{1}$0}, and this combination gives the four independent slip systems that can be active at ambient temperature in beryllium.

The peak in CRSS for prismatic slip near room temperature is thought to be due to the ease of cross slip from prismatic planes to basal planes, along with a greater difficulty of cross slip from basal to prismatic planes [Aldinger 1979].

Unfortunately, the basal plane is also a plane on which cleavage can easily occur, so the polycrystalline ductility of beryllium is further compromised. The flow stress of single-crystal beryllium as a function of temperature for various possible slip systems is given in Fig. 13.4. The solid lines are for single-crystal properties, and the data points represent various grades of polycrystalline beryllium.

Twinning is another possible deformation mode, and the fact that the c/a ratio of beryllium

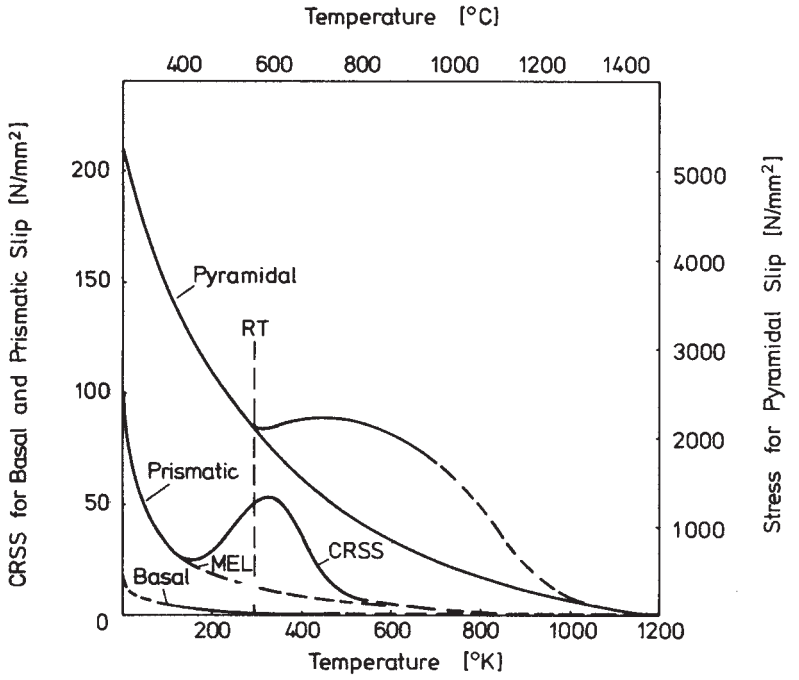

Fig. 13.3 Critical resolved shear stress (CRSS) for different slip systems in beryllium as a function of temperature. Source: Aldinger 1979

is less than the ideal value means that tensile stress parallel to the c-axis, or compressive stress perpendicular to this axis, can lead to the formation of twins on the {1012} <1011> system. The effect of loading conditions and temperature on the CRSS for twinning is shown in Fig. 13.5.

Twinning is not a deformation mode that makes any significant contribution to the ductility of polycrystalline beryllium, since the formation of a twin within a grain can cause significant tensile stresses perpendicular to basal planes and thus promote early cleavage. Dislocation pileups can also lead to early fracture initiation in beryllium, as illustrated in Fig. 13.6.

A micrograph showing a crack that was nucleated by bend-plane splitting is shown in Fig. 13.7. The ease with which basal plane cracks are nucleated is mainly responsible for the low strain to failure of beryllium. However, if the grain size in polycrystalline material is small enough, even though individual grains may be cracked in this way by bend-plane splitting, a larger amount of strain is required to generate a crack of critical length to cause overall fracture.

Past efforts to improve the ductility of beryllium have focused on improving its purity level. However, this was found to have little positive effect, particularly in terms of reducing the CRSS for pyramidal slip, which could have the effect of improving the possibility of true polycrystalline ductility [Aldinger 1979]. Other approaches have included alloying, but not many elements have significant solid solubility in beryllium. The major exception is copper, which has a maximum solid solubility in beryllium of 42.5 wt% (9 at.%) at 1110 °C (2030 °F) and at 250 °C (480 °F) is soluble up to approximately 15 wt%. Much smaller amounts of copper were added to beryllium, and the CRSS was measured for both basal and prismatic planes as a function of temperature. The results are shown in Fig. 13.8 and 13.9 [Avotin et al. 1974, 1975].

It is clear that small amounts of copper raise the CRSS for basal slip to a greater degree than for prismatic slip, bringing the two critical stresses closer together. However, the critical stresses are both raised to such an extent that cleavage fracture is more likely to occur, and so, the hoped-for improvement in ductility was not realized.

13.3.2 Polycrystalline Beryllium

The mechanical properties of various grades of polycrystalline beryllium, which are a strong

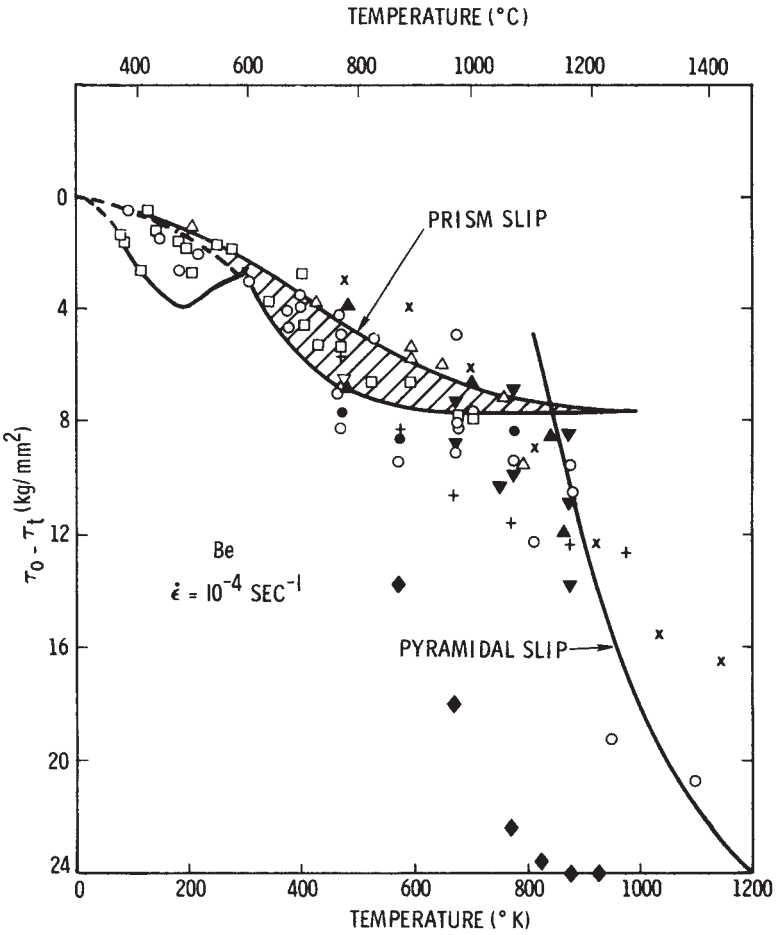

Fig. 13.4 Effect of temperature on the yield stress of beryllium. Data points are for various polycrystalline materials; solid lines represent single-crystal performance. Source: Aldinger 1979

function of impurity content and grain size, are shown in Table 13.3 [Pinto 1979b]. This table lists the ultimate tensile strength, yield strength, and elongation at room temperature. Only fine-grained material has been found to have sufficient plasticity to be useful for structural applications. Mechanical working can generate significant preferred crystallographic orientation, or texture, and can enhance ductility in some directions, for example, in the plane of a rolled sheet. However, the ductility perpendicular to the plane of such sheet is essentially nil, which is illustrated in Fig. 13.10. It must be recognized that many of the types of beryllium referred to in this table are no longer commercially available.

As a consequence of the unavoidable development of preferred orientation for highly deformed beryllium, it has proven necessary to use powder processing to achieve the required fine grain size. Even though the ductility of hot-pressed polycrystalline block is relatively low, at least it is nearly isotropic. The temperature dependence of tensile, yield strength, and elongation of normal-purity hot pressed beryllium block is illustrated in Fig. 13.11. The influence of higher purity on the strength of hot-pressed block is shown in Fig. 13.12.

Beryllium is reported to have excellent fatigue properties when compared to other metals on the basis of fatigue strength/density and is considered to be a favorable factor in the application of beryllium to components subjected to cyclic loading. The creep strength of beryllium is sensitive to aluminum, silicon, and magnesium contents. The fact that these impurities tend to segregate to grain boundaries, and thus lead to hot shortness, is very well known and can be reduced by certain heat treatments [Borch 1979].

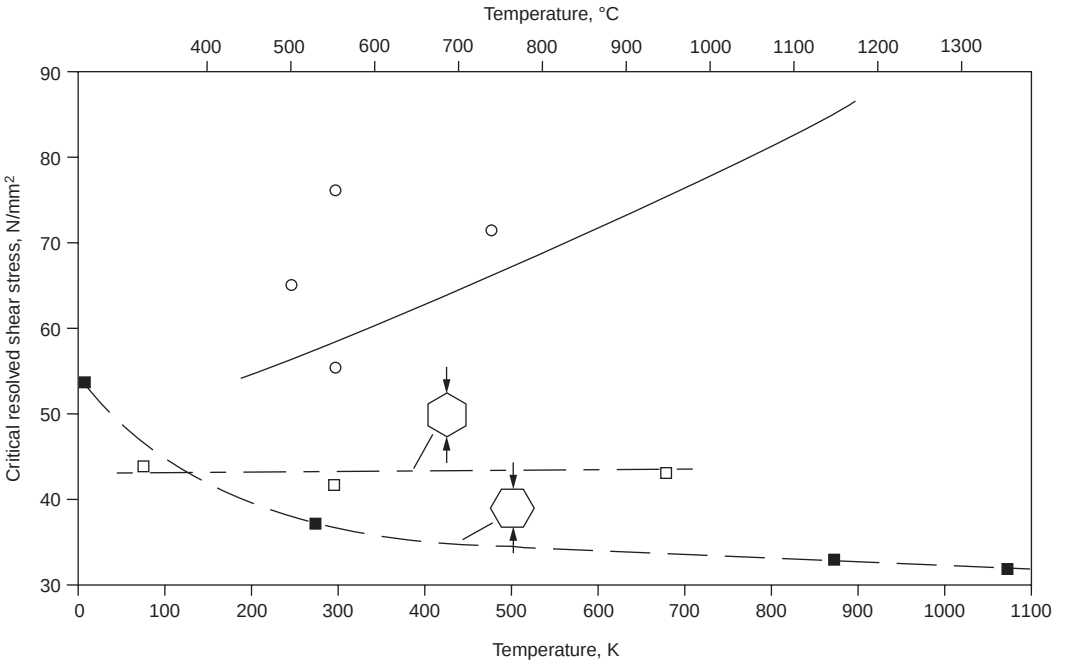

Fig. 13.5 Effect of loading and temperature on the critical resolved shear stress for twinning in beryllium. Source: Aldinger 1979

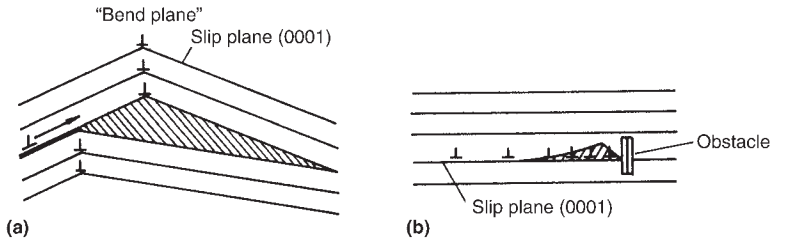

Fig. 13.6 Nucleation of basal cleavage by (a) bend-plane splitting and (b) dislocation pileups. Source: Aldinger 1979

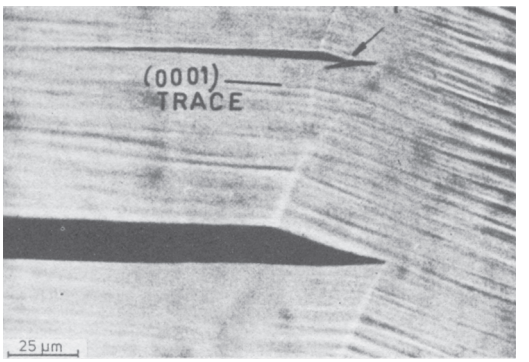

Fig. 13.7 Optical micrograph of a basal plane crack due to bend-plane splitting. Source: Herman and Spangler 1963a,b, taken from Aldinger 1979

It should be noted that the plane-strain fracture toughness, K_{Ic}, is approximately 10 MPa · $m^{1/2}$, and the plot of crack-growth rate as a function of stress-intensity range has a high slope, much higher than that of high-strength aluminum alloys. Hence, the fatigue life of beryllium components is probably more controlled by the number of cycles to cause crack initiation than by the crack-growth life.

13.4 Heat Treatment

Commercial beryllium products, consolidated from powder, are often given heat treatments in

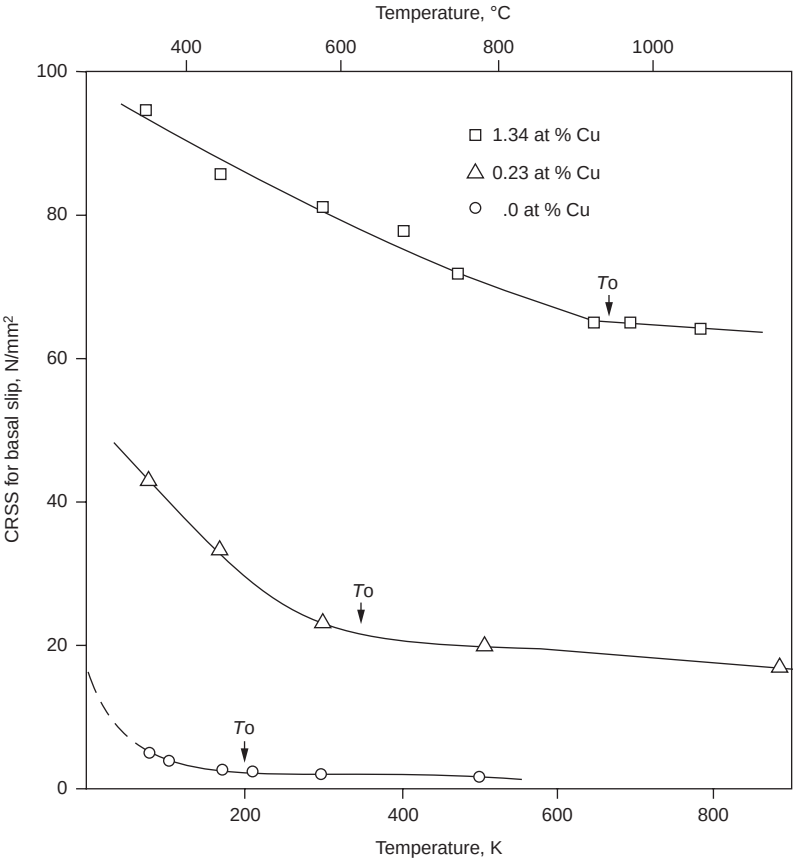

Fig. 13.8 Critical resolved shear stress (CRSS) for basal slip (T_o) in beryllium and beryllium-copper alloys in terms of temperature. Source: Avotin et al. 1974, 1975

order to eliminate high-temperature brittleness, often termed hot shortness. Typically, impurities such as aluminum and silicon will segregate to grain boundaries and form low-melting phases. These impurities can lead to intergranular failure if beryllium components are welded, brazed, or subjected to high-temperature structural loads. The consequences are illustrated in Fig. 13.13. Iron is also a common impurity in commercial beryllium, and the objective of heat treatment is often to promote the formation of a ternary compound, such as $FeAlBe_4$, that will prevent the aluminum from segregating to beryllium grain boundaries. An important practical question has to do with how much iron impurity is necessary for the ternary compound to be stable in the ternary system Be-Fe-Al. Detailed investigation of the beryllium-rich corner of this ternary system was performed by Myers and Smugeresky [1976, 1978]. Their conclusion was that the aluminum-iron ratio for ternary compound stability should be at least 0.5. This finding is consistent with Soviet work that suggests there should be at least twice the concentration of transition metal impurity in beryllium as that of aluminum [Papirov 1981].

Figure 13.13 illustrates the effect of a heat treatment that effectively ties up the elements that are responsible for low ductility of beryllium at elevated temperatures.

13.5 Alloying

Beryllium has a very small atomic diameter of 0.2256 nm. There are only a few elements, such as hydrogen, boron, carbon, nitrogen, and oxygen, that have still smaller atomic diameters. Because of this small atomic diameter, the interstitial holes in alpha-beryllium are very small in size. It is possible to calculate the diameters of tetrahedral and octahedral sites, which are

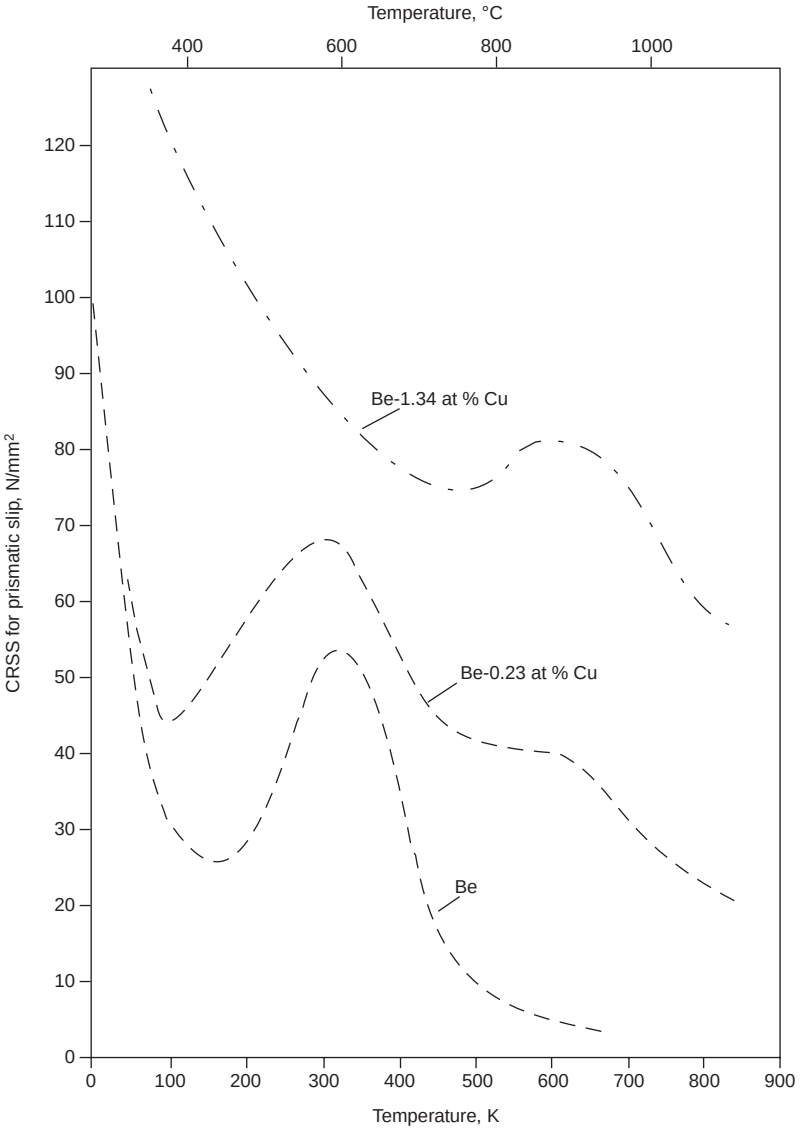

Fig. 13.9 Macro elastic limit (critical resolved shear stress, or CRSS) for prismatic slip of beryllium and dilute beryllium-copper alloys as a function of temperature. Source: Avotin et al. 1974, 1975

0.025 nm and 0.046 nm, respectively. As a consequence, the interstitial solid solubility in alpha-beryllium is extremely limited. The solid solubilities of carbon, nitrogen, and oxygen are less than 0.005 at.%. However, it is somewhat uncertain whether these elements act as interstitial or as substitutional solutes in alpha-beryllium, because their atomic sizes are much larger than the size of the available octahedral sites. Even though hydrogen would be small enough to be accommodated as an interstitial solute, its solubility remains negligible, possibly due to a relative valence effect.

Most of the other elements also exhibit very limited substitutional solubility. A few elements do have a solubility that exceeds approximately 1 at.%, including copper, nickel, cobalt, silver, gold, palladium, and iron. Of these elements, copper has the highest solid solubility in the hcp as well as the bcc phases of beryllium, approach-

Table 13.3 Room-temperature mechanical properties for various beryllium grades

Reference	Material	Grain size, μm	Ultimate tensile strength (UTS) (a), MN/m^2	Yield strength (b), MN/m^2	Tensile elongation, %
Bunce and Evans [1961]	Rolled electrolytic flake	80	112	131 (c)	~4
Papirov and Tikhinskiy [1970]	Complexed, worked, high-purity ingot	13	?	596 (d)	7.5 (e)
Webster and Crooks [1975a]	Upset-forged high-purity ingot	70	120	45	1.5
Heiple [1972]	Diffusion-bonded rolled ingot laminates	16	221	284	18
Levine *et al.* [1964]	Commercial purity (Brush QMV), extruded	6	492	329	7.3
	High purity (Pechiney CR), extruded	20	166	382	9.7
Greenspan [1968]	Hot pressed, forged and aged, high purity	~20 (powder)	373	219	18
London *et al.* [1975]	High purity, hot isostatically pressed (HIP), and extruded	1.6	676	484	12.7
	High purity, HIP, and rolled	2.8	586	305	27.5
Webster and Crooks [1975a]	HIP, upset forged, and heat treated, high purity	?	284	315	13.6
Webster *et al.* [1974]	Hot pressed, commercial purity	10	321	108	4.8
London *et al.* [1975]	As-HIP, Pl	7.0	284	215	6.7
Webster and Crooks [1975a]	As-HIP, Pl	?	238	214	7.1
Keith [1976]	As-HIP, Pl	3.8	420	205	5.9
Turner and Lane [1977]	As hot pressed, Pl	7.9	240	250 (c)	5.7

(a) 0.2% Proof stress. (b) σ_e calculated from UTS × (1 + strain). (c) Measured. (d) Fracture stress. (e) Average value, maximum 10%. Source: Pinto 1979b

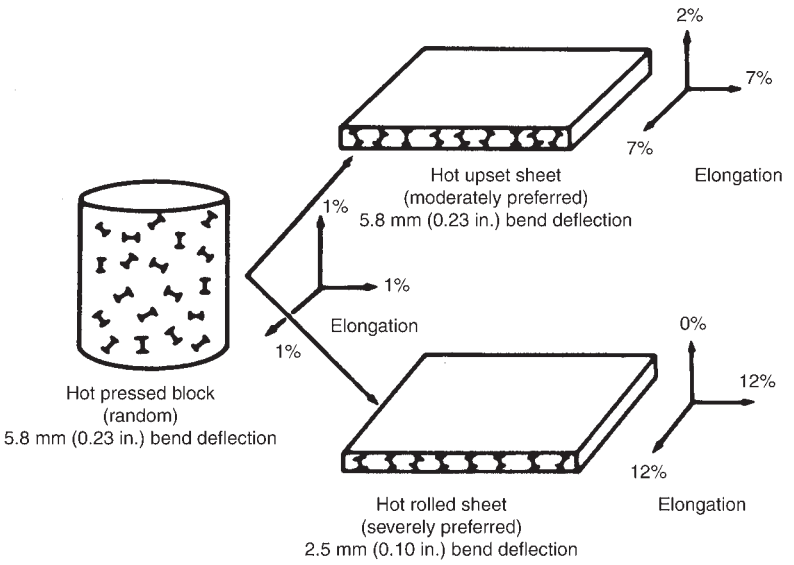

Fig. 13.10 Effect of working and degree of preferred orientation on tensile ductility of beryllium hot pressed block and sheet. Source: Pinto 1979b

ing 10 at.% in the former phase. Most of the alloying elements that have low substitutional solid solubility in beryllium conform to the empirical Hume-Rothery rules with respect to electronegativity and relative atomic size [Adhikari and Mukhopadhyay 1994]. Aldinger and Petzow [1979] have presented a detailed review on alloy theory concepts and phase stability behavior for beryllium alloys.

The formation of intermetallic phases and compounds of beryllium is discussed in Chapter 11, "Beryllium Intermetallic Compounds," in this

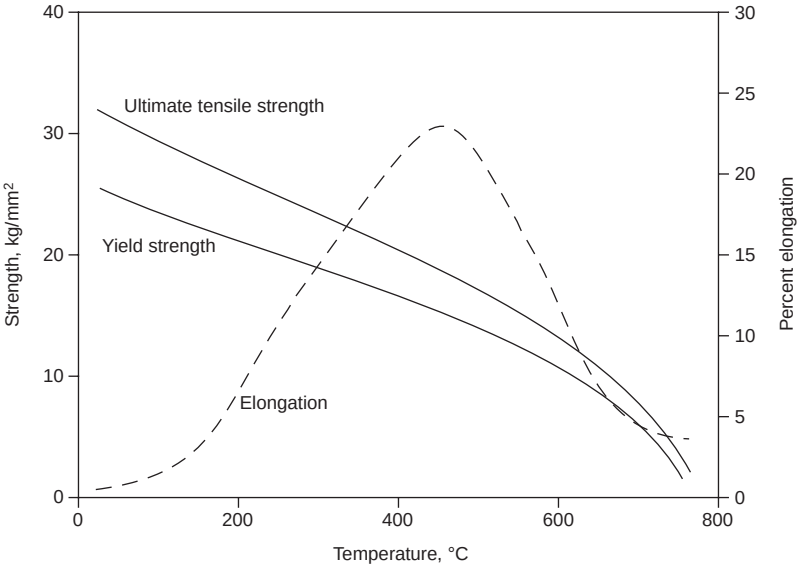

Fig. 13.11 Temperature dependence of strength and ductility for normal-purity hot-pressed beryllium block. Source: Pinto 1979b

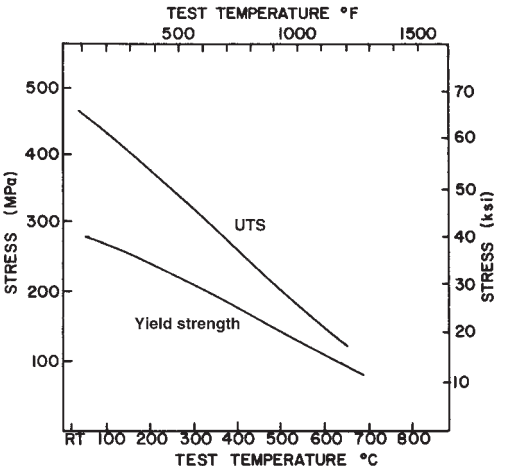

Fig. 13.12 Temperature dependence of the ultimate tensile strength (UTS) and yield strength of high-purity hot-pressed beryllium block. Source: Pinto 1979b

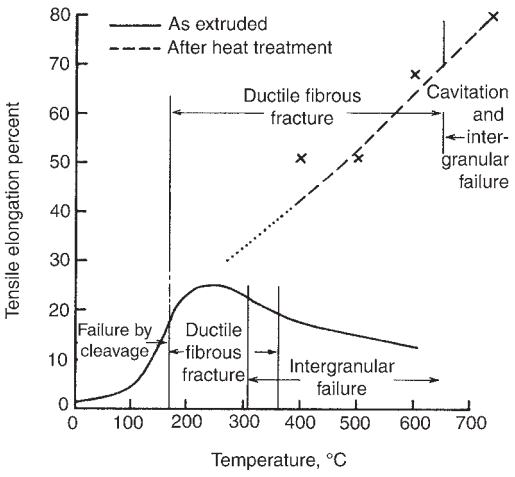

Fig. 13.13 Effect of heat treatment on the ductility of cast and extruded beryllium. Heat treatment at 780 °C (1435 °F) for 120 h. Source: Brown et al. 1960

book. Beryllium is an important alloying addition to copper and nickel, where it provides for a precipitation-hardenable alloy. It is also useful for the control of aluminum melting and casting because of its strong affinity for oxygen.

REFERENCES

Adhikari, S., and Mukhopadhyay, P., 1994. Physical Metallurgy of Beryllium and Its Alloys, *Miner. Process. Extr. Metall. Rev.,* Vol 14 (No. 1), p 253–299

Aldinger, F., 1979. Flow and Fracture of Single Crystals (Beryllium Crystal Dislocations), *Beryllium Science and Technology,* Vol 1, D. Webster and G.J. London, Ed., Plenum Press, New York and London

Aldinger, F., and Petzow, G., 1979. Constitution of Beryllium and Its Alloys, *Beryllium Science and Technology,* Vol 1, D. Webster and G.H. London, Ed., New York, p 235–305

Avotin, S.S., Kapcherin, A.S., Papirov, I.I., Puar'e, Z.P, and Tikhinskii, G.F., 1974. Influence of Copper on Prismatic Slip in Beryllium Single Crystals, *Phys. Met. Metallogr.*, Vol 38 (No. 1), p 165–171

Avotin, S.S., Papirov, I.I., Tikhinskii, G.F., and Kapcherin, A.S., 1975. Investigation of Basal Slip Nature in Beryllium and Its Alloys, *Phys. Status Solidi*, Vol 30, p 39–46

Borch, N.R., 1979. Elevated Temperature Behavior, *Beryllium Science and Technology*, Vol 1, D. Webster and G.J. London, Ed., Plenum Press, New York and London, p 307–330

Brown, A.B., Morrow, F., and Martin, A.J., 1960. An Improvement in the Ductility of Beryllium at High Temperature, *Nature*, Vol 187, p 494–496

Bunce, J.E.J., and Evans, R.E., 1961. A Study of the Effect of Grain Size, Texture, and Annealing Treatment on the Properties of Wrought Beryllium Ingot, *Conf. Met. Beryllium 1961*, Institute of Metals, London, p 246–263

Greenfield, P.G., 1971. *Engineering Applications of Beryllium*, Mills and Boon, London

Greenspan, J., 1968. Some Effects of Powder Particle Size on the Physical Behavior of Press Forged Beryllium, *Second European Symposium on Powder Metallurgy* (Stuttgart, Germany), Vol 1A, Section 2.7, p 1–19

Gupta, C.K., 1994. National Workshop on Beryllium Technology, *Proceedings Mineral Processing and Extractive Metallurgy Review*, Vol 13, Gordon and Breach Science Publications, Amsterdam

Heiple, C.R., 1972. Mechanical Properties of Diffusion Bonded Beryllium Ingot Sheet, *Metall. Mater Trans. B*, Vol 3 (No. 4), p 807–812

Herman, M., and Spangler, G.E., 1963a. Basal Plane Fracture of Beryllium Single Crystals, *Proc. of Conference on the Metallurgy of Beryllium* (Conf.-170), ORNL, Oak Ridge, TN, p 48–68

Herman, M., and Spangler, G.E., 1963b. The Flow and Fracture Characteristics of Zone Melted Beryllium, *The Metallurgy of Beryllium*, Institute of Metals Monograph 28, Chapman and Hall Ltd., London, p 75–83

Keith, G.H., 1976. "Fine-Grained Low Oxide Beryllium," Report F-1876, Kawecki Berylco Industries, Reading, PA

Levine, E.D., Pemsler, J.P., and Gelles, S.H., 1964. Characteristics of Vacuum-Distilled Beryllium, *J. Nucl. Mater.*, Vol 12 (No. 1), p 40–49

London, G.F., Keith, G.H. and Pinto, N.P., 1975. Effect of Grain Size and Oxide Content on the Strength and Ductility of High-Purity Beryllium, submitted to *Met. Trans.*

Myers, S.M., and Smugeresky, J.E., 1976. Phase Equilibria and Diffusion in the Be-Al-Fe System Using High Energy Ion Beams, *Metall. Mater. Trans. A*, Vol 7 (No. 5), p 795–802

Myers, S.M., and Smugeresky, J.E., 1978. Phase Equilibria in the Be-Al-Fe System Using High Energy Ion Beams, Part II, *Metall. Mater. Trans. A*, Vol 9 (No. 12), p 1789–1794

Papirov, I.I., 1981. *Structure and Properties of Beryllium Alloys*, Energoizdat, Moscow, p 18–19

Papirov, I.I., and Tikhinskiy, G.F., 1970. Stucture and Mechanical Properties of Fine-Grained Deformed Beryllium, *Phys. Met. Metallogr.*, Vol 29 (No. 5), p 167–169

Pinto, N.P., 1979b. Properties, *Beryllium Science and Technology*, Vol 2, D.R. Floyd and J.N. Lowe, Ed., Plenum Press, NY, p 319–350

Singh, A.J., 1994. Beryllium—Extraordinary Metal, *Miner. Process. Extr. Metall. Rev.*, Vol 13 (No. 1), p 177–192

Turner, G.I., and Lane, R.A., 1977. "The Effects of Powder Particle Size on the Mechanical Properties of Hot Pressed P1 Beryllium," Met. Soc. Conf. on Beryllium

Webster, D., and Crooks, D.D., 1975a. Factors Influencing the Creep Strength of Hot Pressed Beryllium, *Metall. Trans. A*, Vol 6 (No. 11), p 2049–2053

Webster, D., Greene, R.L., and Lawley, R.W., 1974. Factors Controlling the Strength and Ductility of High Purity Beryllium Block, *Metall. Trans.*, Vol 5, p 91–96

SELECTED REFERENCES

- Bonfield, W., Sartell, J.A., and Li, C.H., 1963. The Effect of Surface Condition on the Microstrain of Beryllium, *Trans. AIME*, Vol 227 p 669–673
- Carrabine, J.A., Woodard, D.H., Stonehouse, A.J., and Beaver, W.W., 1964. The Effects of $AlFeBe_4$ on Mechanical Properties of Fabricated Polycrystalline Beryllium, *Beryllium Technology*, Vol 1, L.M. Schetky and H.A. Johnson, Ed., Gordon and Breach, NY, p 239–257

- Coobs, J.H., and Coshuba, W.J., 1952. The Synthesis, Fabrication, and Properties of Beryllium Carbide, *J. Electrochem. Soc.*, Vol 99, p 115–120
- Dupouy, J.M., Poirier, J.P., Antolin-Beaudier, J., and Adda, Y., 1964. Contribution a L'etude de la Deformation et de la Restauration du Beryllium Pur, *J. Nucl. Mater.*, Vol 12, p 277–290
- Garber, R.I., Gindin, I.A., Kogan, V.S., and Lazarev, B.G., 1955. Investigation of the Plastic Properties of Beryllium Single Crystals, *Fiz. Met. Metalloved. I*, p 529–537
- Jacobson, M.I., Almeter, F.M., and Burke, E.C., 1962. Surface Damage in Beryllium, *Trans. Am. Soc. Met.*, Vol 55, p 492–504
- Klein, J.L., Macres, V.G., Woodard, D.H., and Greenspan, J., 1955b. *Ductility of Beryllium as Related to Preferred Orientation and Grain Structure*, American Society for Metals, p 425–465
- Matthews, C.O., Jacobson, M.I., Jahsman, W.E., and Ward, W.V., 1960. "Beryllium Crack Propagation and Effects of Surface Condition," Report WADD-TR-60-116, Lockheed Aircraft Corp. Missiles and Space Division, Sunnydale, CA
- Rebholz, M.J., 1966. Buckling Strength of Curved Beryllium Panels in Compression, *Beryllium Technology*, Vol 2, Gordon and Breach, NY, p 857–877
- Scholz, U., Plachke, D., Yuan, W., Carstanjen, H.J., Petzow, G., and Mucklich, F., 1996. On the Influence of Impurities in Beryllium Single Crystal Growth, *J. Cryst. Growth*, Vol 169 (No. 3), p 575–577
- Siergiej, J.M., 1965. Extrusion of Beryllium Structural Shapes, *Beryllium: Its Metallurgy and Properties*, University of California Press, Berkeley and Los Angeles, CA, p 86–101
- Stonehouse, A.J., Paine, R.M., and Beaver, W.W., 1964. "Physical and Mechanical Properties of Beryllides," Spec. Report, Vol 13, Met. Soc., Am. Inst. Mining, Met. Petrol. Eng., Inst. Metals Div., p 445–455
- Taylor, W., and White, J.S., 1973. Grinding Induced Machining Damage in Beryllium, *J. Mater. Sci.*, Vol 9 (No. 4), p 569–575
- Tuer, G.L., and Kaufman, A.R., 1955. Ductility of Beryllium as Related to Single Crystal Deformation and Fracture, *The Metal Beryllium*, D.W. White, Jr., and J.E. Burke, Ed., American Society for Metals, p 372–424
- Watson, R.D., and Whitley, J.B., 1986. Thermal Fatigue Tests of a Prototype of Beryllium Limiter for JET, *Nucl. Eng. Des./Fusion*, Vol 4 (No. 1), p 49–60

Beryllium Chemistry and Processing, p 163-178
By Kenneth A. Walsh
Edited by Edgar E. Vidal, Alfred Goldberg,
Edward N.C. Dalder, David L. Olson, and Brajendra Mishra

CHAPTER 14

Alloying of Beryllium

Gilbert London, U.S. Naval Air Systems Command, Retired
David L. Olson, Colorado School of Mines

14.1 Introduction

Most of the work done over the last 60 years or so to investigate alloying of beryllium has focused on the attempt to discover alloying approaches that will alleviate low-temperature brittleness. The specific alloying approaches can be divided into several general categories:

1. Alloying additions that will bond with harmful impurities that promote the embrittlement of the metal
2. Alloying to change the *c*/*a* ratio of the beryllium lattice to approach that of the ideal hexagonal close-packed lattice, which is 1.633
3. Modifications that will reduce the grain size and increase the uniformity of cast beryllium ingots
4. Addition of elements that stabilize the high-temperature beta, or body-centered cubic, phase, of beryllium
5. Development of alloys with a plastic matrix
6. Alloying additions that are directed at the elimination of a low-melting eutectic, which leads to hot shortness, by bonding of aluminum or silicon, the main components of this low-melting eutectic, into refractory compounds

The first four alloying approaches have not led to any great success. The fifth approach has resulted in several families of beryllium-aluminum materials that are discussed later. Consideration of the sixth approach has resulted in greater attention being paid to the ratio of various impurity elements. If such a ratio is in the appropriate range, the hot shortness, or high-temperature brittleness, problem can usually be eliminated by appropriate heat treatment.

An excellent monograph on the structure and properties of beryllium alloys has been published by Papirov [1981]. Unfortunately, this extensive compilation of alloying information on beryllium is available only in the Russian language. A limited-circulation English translation has contributed to the points made in the earlier introduction. Another valuable source was presented by London [1979].

14.2 Alloys and Composites

Only a few alloying elements form substantive solid solutions in beryllium metal, that is, copper, nickel, cobalt, and, to a lesser extent, iron. Silver has limited solid solubility in beryllium. Most solid-solution alloys are substantially stronger than the purified metal, that is, metal from which microalloying-type impurities have been removed. Ductility improvement through solid-solution alloying, however, has not been realized and is not considered a likely product of future development studies [London 1979].

Beryllium forms many intermetallic compounds that often play an important role in both alloy-development studies and efforts to produce beryllium composites. Processing of beryllium-titanium composites, for instance, is limited by the formation of significant quantities of $TiBe_{12}$ at temperatures above 705 °C (1300 °F).

Aluminum is a major alloying addition that forms no intermetallic compound with beryllium. Neither does aluminum exhibit significant solid solubility in beryllium nor beryllium in aluminum, so beryllium-aluminum alloys appear as mixtures of the two essentially pure metals. The mechanical properties of such alloys are usually analyzed as though they are composites (i.e., mixtures of two dissimilar metals), their formulation being based on melting and solidification practices rather than the mixing or cofabricating techniques generally associated with composites [London 1979].

14.3 Beryllium-Aluminum Alloys

Alloying beryllium with large percentages of aluminum addition results in a mixture of two phases, because beryllium and aluminum have insignificant mutual solid solubility. Thus, these beryllium-aluminum alloys are classified as composites. The spatial distribution of the two phases can be quite different, depending on the relative quantities of each element and the method used to process the material. Tensile stress, tensile modulus, and tensile elongation decrease somewhat with increasing aluminum content. However, by annealing, the higher-aluminum alloys achieve elongations of greater than 8%. An aluminum 38 wt% Be alloy, known as Lockalloy, was manufactured by a powder metallurgy practice, and the beryllium content was chosen to give an elastic modulus equivalent to that of steel (2.1×10^5 MPa, or 3.0×10^4 ksi).

Beryllium-aluminum alloys have been under development and studied since approximately 1961. Properties of a series of alloys containing 24 to 43 wt% Al were reported by Fenn et al. [1966]. These alloys were generally produced by a rapid-solidification technique, which forms a finely dispersed mixture of essentially pure beryllium and aluminum. The aluminum is usually the continuous phase in the as-solidified material, but subsequent warm working causes the two phases to be intermixed. Notice this partitioning in the beryllium-aluminum phase diagram shown in Fig. 14.1.

Lockalloy has a structure typical of a pure component eutectic; that is, it shows a very fine dispersion or beryllium and aluminum phases. In powder form, the aluminum matrix is the

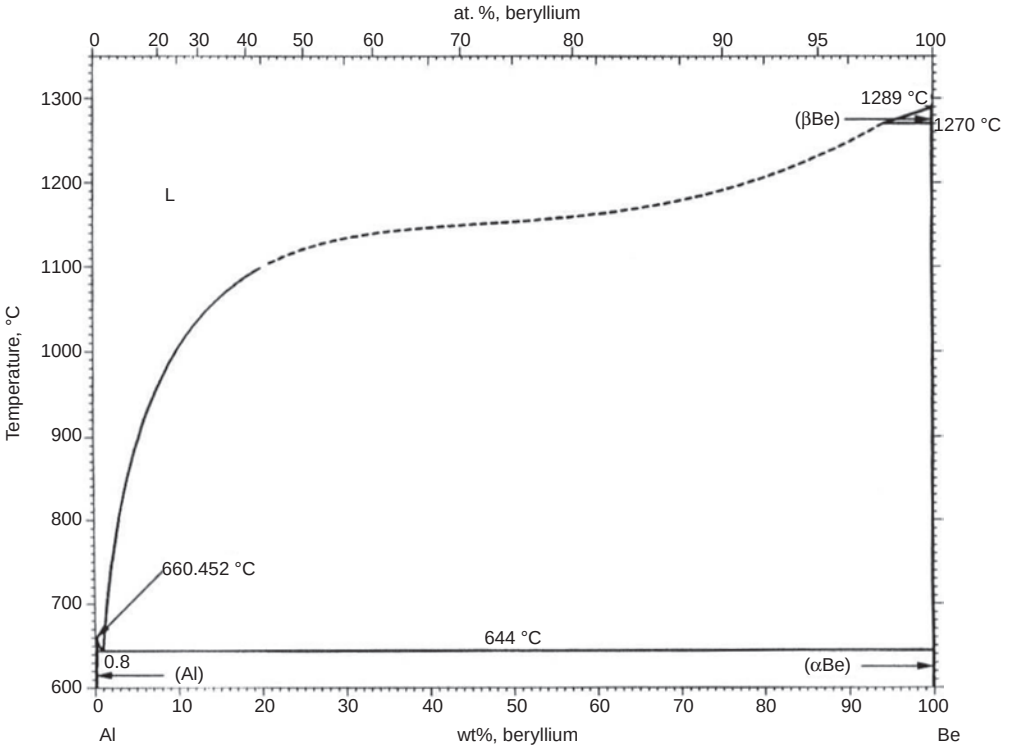

Fig. 14.1 Beryllium-aluminum phase diagram. Source: Murray and Kahan 1988

continuous phase. After hot extrusion, the beryllium and aluminum phases become intermixed with the larger-volume-percent beryllium phase, appearing as more continuous. Extrusions have a tendency to exhibit some aluminum stringers parallel to the extrusion direction, but hot rolled sheet has a relatively isotropic structure [London 1979].

The mechanical properties are a function of aluminum content, as shown in Fig. 14.2 for extruded and annealed material. It can be seen that tensile properties, including tensile modulus, generally decrease with increasing aluminum content. Tensile elongation decreases somewhat in the as-extruded condition with increased aluminum, but annealing the higher-aluminum-content alloys gives elongations of greater than 8% [London 1979].

The most-used beryllium-aluminum alloy generally contained 38 wt% Al and was produced as extrusions and sheet hot rolled from extruded bar stock. This alloy had been used in several aerospace applications [Ind. Heat. 1971, Duba et al. 1976], principally because of its good extrudability, ease of machining, better formability, and generally better fabricability than unalloyed beryllium [London 1979].

14.4 Aluminum-Beryllium Production

Beryllium-38wt%Al (Lockalloy) was vacuum annealed, inspected, and consolidated by cold isostatic pressing into billets suitable for extrusion. Billet size varied depending on the type of extrusion desired. Billets had been extruded to 27.94 cm (11 in.) diameter by 63.5 cm (25 in.) long. For rolling subsequent to extrusion, the extruded sheet bar was cut to length, jacketed in steel plates, and hot rolled to approximately 50% reduction. The material was then annealed, rejacketed, and rerolled as necessary to produce the final thickness of plate or sheet material required [London 1979].

Extrusion and rolling were conducted in the 510 to 565 °C (950 to 1050 °F) range. Both extruded and hot rolled sheet material were generally supplied in the annealed condition [Alloys Digest 1971], a condition where the alloy exhibits its maximum ductility and formability. Both tensile and yield strength are lowered by annealing [London 1979].

Unlike pure beryllium, Lockalloy was readily fusion welded by both gas tungsten arc (GTA) welding and electron beam (EB) welding techniques. Weld efficiencies of 60 to 70% for GTA and 85 to 100% for EB welding have been reported [London 1979]. The microstructure after welding is similar to that of a powder metallurgy part but varies in fineness, depending on the cooling rate experienced by the weld metal.

In the annealed condition, Lockalloy had only moderate yield (YS) and tensile strength (UTS). Average values for both extrusions (parallel to the extrusion direction) and hot rolled sheet are 345 to 379 MPa (50 to 55 ksi) UTS and 276 to 310 MPa (40 to 45 ksi) YS. Elastic modulus was high, with exceptionally high specific modulus, second only to that for pure beryllium [Duba et al. 1976].

The fracture toughness of Lockalloy was generally higher than that for pure beryllium. Lockalloy extrusions exhibit fracture toughness values of approximately twice beryllium (4.38 $MPa \cdot m^{1/2}$) when the crack propagation direction is normal to the extrusion direction; cracks propagating in this direction are blunted as they intersect the aluminum stringers described previously. Fracture toughness tests with cracks propagating parallel to the extrusion direction, an unusual failure direction for many extruded shapes, show fracture toughness values of approximately that for pure beryllium. Lockalloy sheet exhibits more isotropic toughness values and compares favorably to other structural sheet and plate materials [London 1979].

In the as-extruded or as-hot-rolled condition, Lockalloy was considerably stronger and somewhat less ductile than indicated previously. On annealing in the range of 425 to 595 °C (800 to 1100 °F), tensile and yield strength fall with progressively increased tensile ductility. Figure 14.3 shows the tensile strength, yield strength, and ductility versus annealing temperature for a representative Lockalloy (LX62) extrusion. The crack-growth characteristics of Lockalloy sheet have been measured by Duba et al. [1976].

Although the Be-38wt%Al was the first composition to be called Lockalloy, other beryllium-aluminum compositions had been produced by the Lockalloy process. The original Be-38wt%Al alloy was modified by a small magnesium addition, providing solid-solution strengthening to the relatively soft pure-aluminum component of the alloy. The magnesium addition to the Be-38wt%Al alloy was found to improve tensile and yield strength by 69 to 103 MPa (10 to 15 ksi), with the same or improved ductility. The magnesium also lowered the maximum permitted

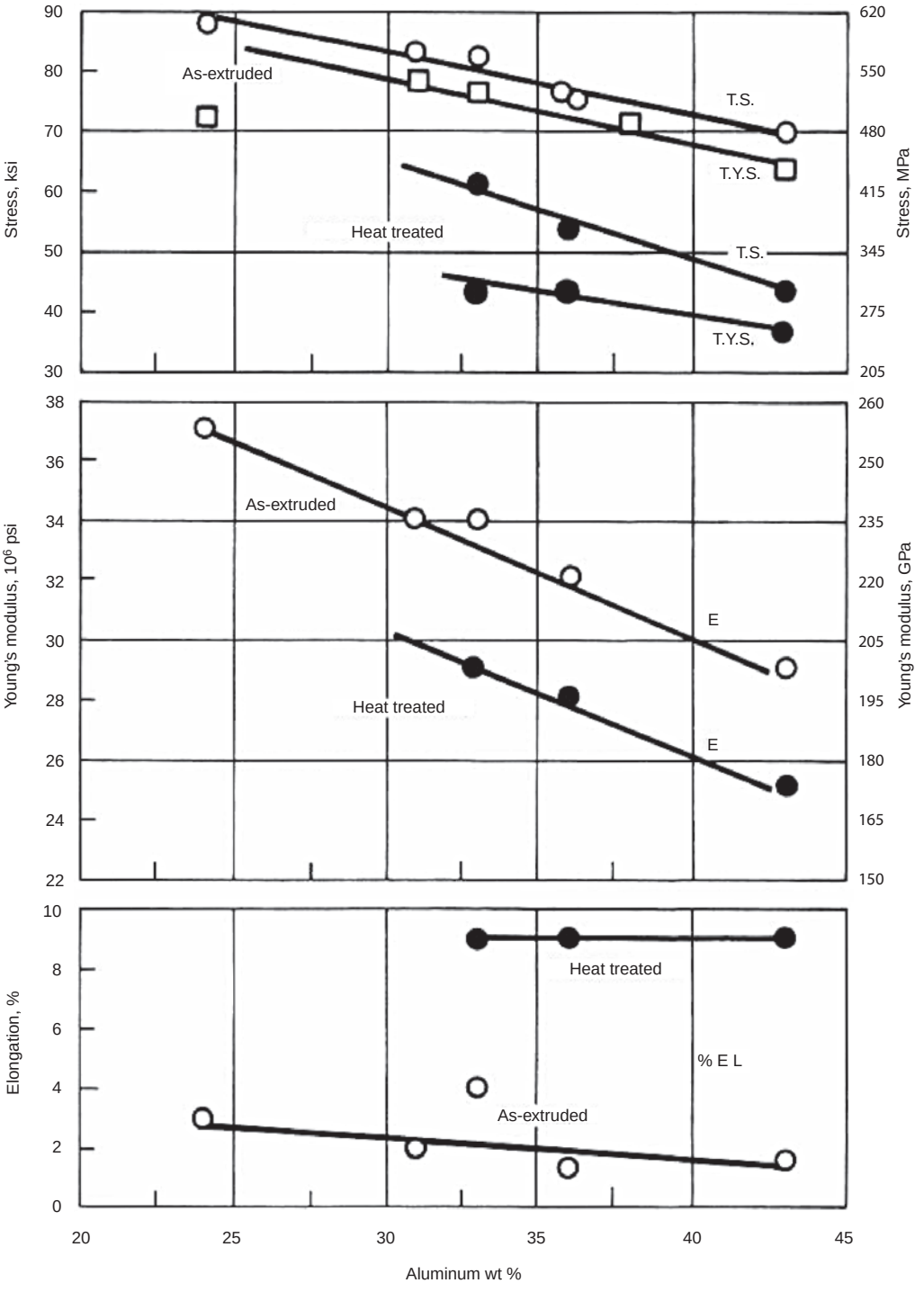

Fig. 14.2 Longitudinal properties of as-extruded and heat treated (annealed) beryllium-aluminum alloy extrusions as a function of aluminum content. Source: London 1979

exposure temperature to approximately 480 °C (895 °F) as compared to approximately 565 °C (1050 °F), because of the low solidus temperature of the aluminum-magnesium system.

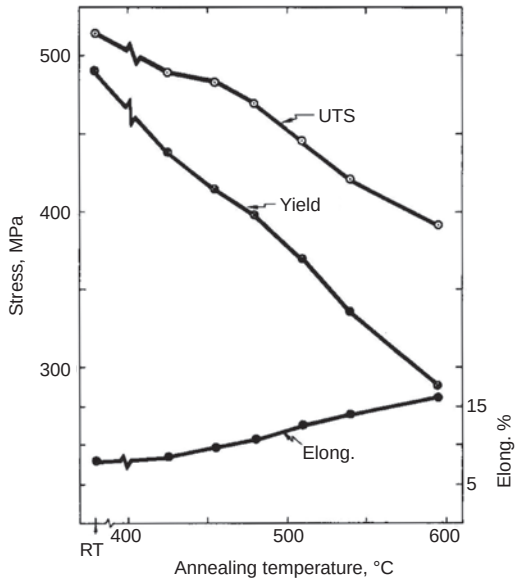

Fig. 14.3 Tensile strength (UTS), yield strength, and elongation as a function of temperature for extruded Lockalloy LX62. Source: London 1979

Table 14.1 shows the tensile properties of the modified Be-38wt%Al alloy at room and elevated temperature (150 °C, or 300 °F).

The higher-aluminum-content alloys have an outstanding combination of strength, modulus, and ductility. This improvement is especially true for the Be-57-Al-3Mg (wt%) alloy. The alloy was reported to be readily rollable to sheet.

Work had been done since the 1970s in the former Soviet Union on beryllium-aluminum alloys. One of the most intensely investigated compositions is the ternary alloy Al-30Be-5Mg (wt%). In this system, the magnesium performs a useful role as a solution-strengthening element for the aluminum phase. Some of the reported results for an alloy with lithium and zirconium additions are strengths for extruded material ranging from 379 to 448 MPa (55 to 65 ksi) and elongations up to 8%, depending on heat treatment. Major conclusions reached were:

- Alloying of aluminum-beryllium alloys with magnesium significantly improves the mechanical properties of extruded semiproducts. The more promising alloys for structural application with acceptable processing characteristics are the alloys with beryllium content of 30 to 50 wt% and magnesium content of 3 to 6 wt%.

Table 14.1 Results of mechanical and design properties tests for Be-38Al (wt%) alloy at room and elevated temperatures

Property		Temperature(b)		
		Specimen orientation(a)	Room temperature	600 °F
Tensile				
	Tensile strength, ksi	L	47.1–52.6	23.9–25.0
		LT	49.6–51.8	23.2–24.5
		ST	13.7–17.2	. . .
	Yield strength, ksi	L	36.2–37.8	21.8–23.5
		LT	34.8–36.2	21.2–23.5
	Young's modulus(c), 10^6 psi	. . .	27.0–31.0	19.0–24.5
	Elongation, %	L	5–12	7–12
		LT	8–13	9–11
Compression	Yield strength, ksi	L	31.9–34.8	21.9–23.6
		LT	31.6–32.6	22.4–23.3
	Modulus, 10^6 psi	. . .	. . .	17.2–21.8
Shear	Ultimate, ksi	. . .	29.5–40.2	16.3–21.0
	Modulus, 10^6 psi	. . .	11.6–13.6	7.9–10.8
Poisson's ratio	. . .	. . .	0.142–0.163	0.140–0.19
Bearing	Ultimate, ksi	$e/D = 1.5$	69.8–85.0	34.2–43.6
	. . .	$e/D = 2.0$	89.7–104.3	44.0–53.3
	Yield, ksi	$e/D = 1.5$	58.0–74.3	31.9–42.3
	. . .	$e/D = 2.0$	61.9–80.0	40.5–46.6
Notch sensitivity	Strength ($K_t = 3$)/unnotched strength	L	0.934–1.016	1.336–1.37
		LT	0.990–1.020	1.249–1.34
Creep	Stress to produce 0.5% deformation in 100 h at 600 °F	L	. . .	7.5–10.5
		LT	. . .	9.0–10.0
Joint	Strength, lb/fastener			
	0.125 in. thick	3/16 in.(d)	1812–2065	1235–146
	0.15 in. thick	3/16 in.(d)	2212–2412	1455–152
	0.15 in. thick	1/4 in.(d)	3225–3275	2105–230

(a) L, longitudinal; LT, long transverse; ST, short transverse. (b) Tested after 100 h exposure at 600 °F (315 °C). (c) Based on strain gage data. (d) Flush titanium screw diameter. Source: London 1979

- Alloying of Al-Be-Mg alloys with lithium increases their strength properties and allows the use of heat treatment to improve properties. This alloying practice leads to the much greater opportunity for the control of properties during the fabrication of final products [Savchuk and Syrnev 1999].

The National Aerospace Plane program explored the use of rapid-solidification processing for aluminum-beryllium alloys. Silver was added to the binary system to allow for precipitation strengthening of the aluminum phase. A composition of 50Be-47.5Al-2.5Ag (wt%) was centrifugally atomized and hot isostatically pressed to make a dense compact. One of the main features of the microstructure of this alloy was that the beryllium and aluminum phases were continuous, a consequence of rapid solidification accompanied by phase separation in the liquid. This microstructure occurs because there is a temperature range of approximately 500 °C (900 °F) between the liquidus and solidus temperatures at these compositions, and a subliquidus miscibility gap probably exists. Peak-aged samples gave properties approximately equal to aluminum 2024-T6, with yield strength of 393 MPa (57 ksi), ultimate tensile strength of 448 MPa (65 ksi), and elongation of 10%. There has been no further development of this alloy system or process procedures [Jacobson 2006].

Newer alloys produced since the mid-1990s are AlBeMet 140 and AlBeMet 162, marketed by Brush Wellman, Inc. These alloys have similar compositions as Lockalloy but are made by an inert gas atomization process that results in a finer microstructure.

The physical properties for AlBeMet 140 and 162 are given in Table 14.2, while the mechanical properties are shown in Table 14.3 [Brush Wellman]. Tensile properties with temperature are show in Fig. 14.4. Axial fatigue tests have been performed on AlBeMet 140, as shown in Fig. 14.5. In the transverse direction, this composite material seems to have a better fatigue limit compared to the longitudinal direction.

Figure 14.6 shows a typical EB weld on AlBeMet 140. The base material on the right side shows a coarser microstructure compared to the resolidified region on the left after the EB has passed. The dark-colored phase corresponds to beryllium, while the light phase corresponds to the aluminum.

A schematic of the aluminum-beryllium alloy production and processing is shown in Fig. 14.7. The aluminum and beryllium powders are blended, annealed, and hot isostatically pressed before being extruded into plates. The extrusion is performed by jacketing the alloy in between mild steel. The reduction process is carried out in multiple stages to avoid cracking of the alloy.

Table 14.2 Physical properties of AlBEMet 140 and 162

Property	AlBeMet 162	AlBeMet 140
Elastic modulus at 25 °C (77 °F), GPa (10^6 psi)	200 (29)	158 (23)
Elastic modulus at 200 °C (390 °F), GPa (10^6 psi)	195 (28)	. . .
Poisson's ratio	0.167	. . .
Density, g/cm^3	2.01	2.28
Linear coefficient of thermal expansion at 25–100 °C, 10^{-6}/°C	16.35	16
Thermal conductivity at 25 °C (77 °F), W/m · K (Btu · in · ft^2 · h · °F)	212 (14.7)	210 (14.6)
Specific heat, J/g · °C (Btu/1b · °F)	1.500 (0.36)	1.280 (0.31)
Electrical resistivity, μΩ · cm	3.43	8.27
Solidus temperature, °C (°F)	644 (1190)	644 (1190)
Melting temperature(a), °C (°F)	1082 (1980)	1082 (1980)

(a) Estimated values based on the Al-Be phase diagram

Table 14.3 Specification mechanical properties for AlBeMet 162 aluminum-beryllium alloy

Specification and product form	0.2% offset yield strength, MPa	0.2% offset yield strength, ksi	Ultimate tensile strength, MPa	Ultimate tensile strength, ksi	Elongation, %
AMS 7913, sheet	276	40	386	56	5
AMS 7911, hot isostatic pressed block	193	28	262	38	2
AMS 7912,extrusions (longitudinal)	276	40	358	52	7

In the 1990s, Nuclear Metals Corp., and subsequently a spinoff company called Starmet, developed several beryllium-aluminum alloys that were tailored for applications as cast components. Two compositions, Beralcast 363 and 191, were reported in the literature, and their alloy content and properties are given in Table 14.4.

Beralcast 191 was developed to improve the thermal conductivity of Beralcast 363, which it appears to have achieved at a roughly one-third reduction in strength [Nachtrab and Levoy 1997]. The thermal conductivity requirement was driven by electro-optical components that required significant heat dissipation during operation.

The potential applications of beryllium-aluminum alloys have not been fully realized, partly due to the higher cost of these materials and also because of the increase in concern for beryllium toxicity. Nevertheless, studies continue to be performed on the performance comparison between beryllium-aluminum and other aerospace structural materials. One such study compared AlBeMet 162 to aluminum and titanium alloys and

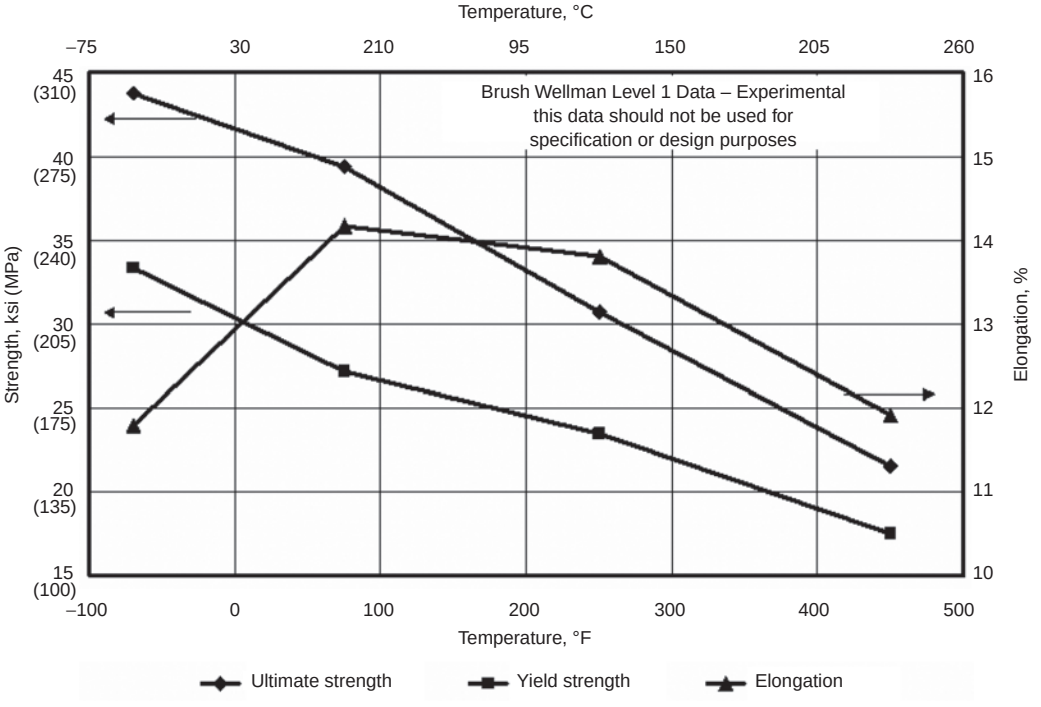

Fig. 14.4 Tensile properties as a function of temperature for AlBeMet 140. Source: Brush Wellman 2004

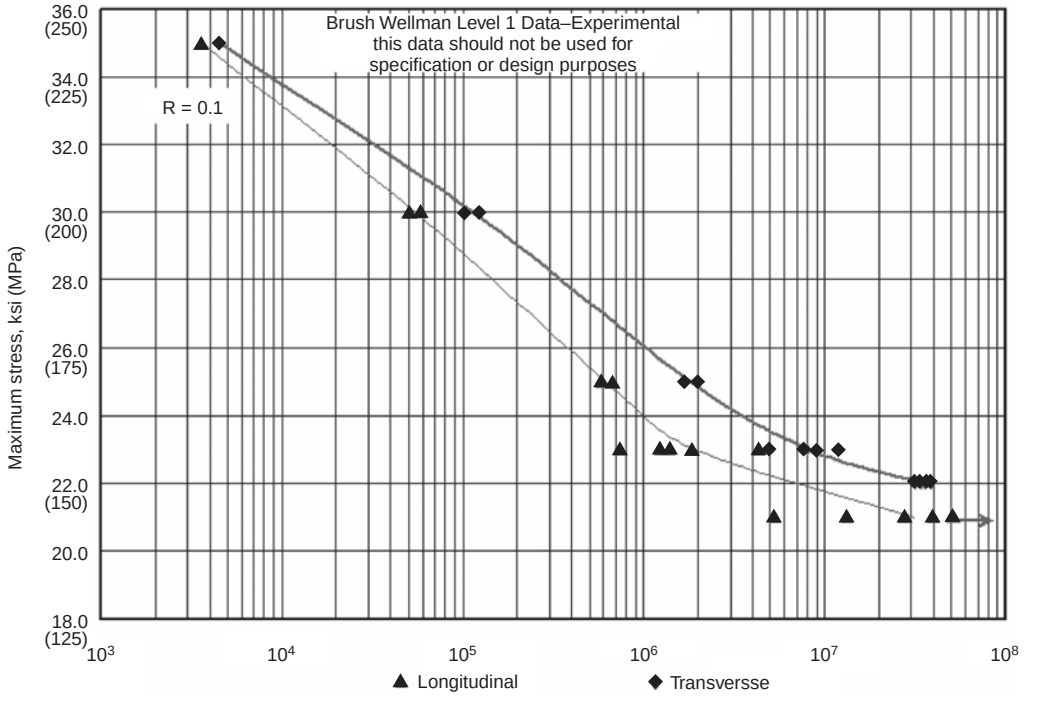

Fig. 14.5 Axial fatigue plot for AlBeMet 140 in the longitudinal and transverse direction. Source: Brush Wellman

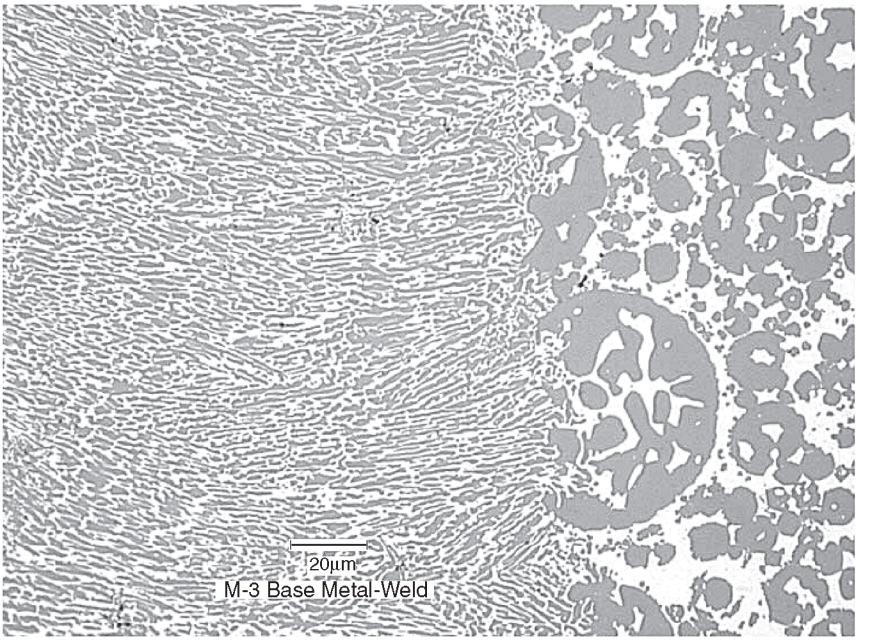

Fig. 14.6 Electron beam welding of a 1.25 cm thick section of AlBeMet 162 showing the base metal on the right

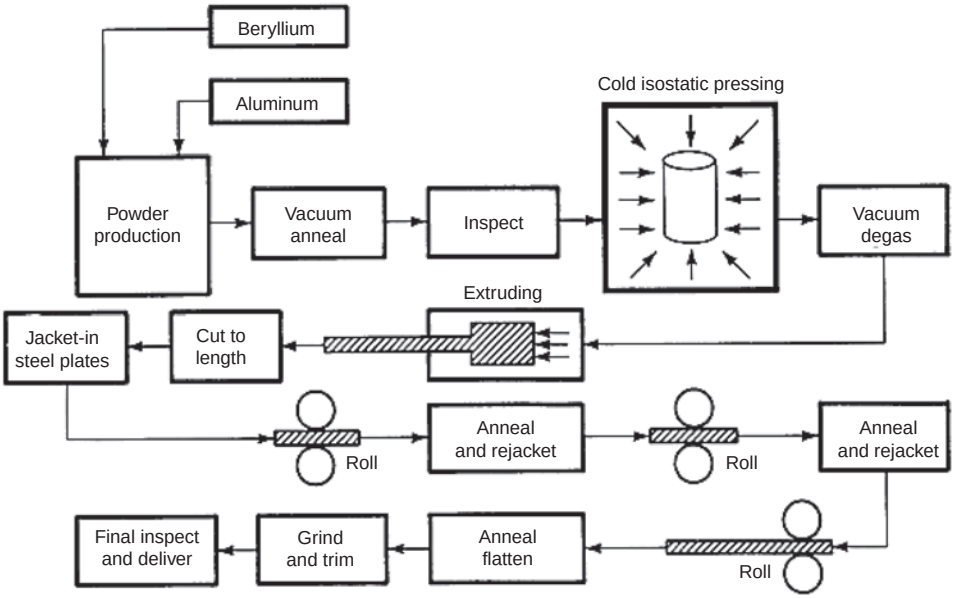

Fig. 14.7 AlBeMet aluminum-beryllium alloy sheet and plate manufacturing sequence

found that AlBeMet 162 was superior in potential performance for all stiffness-limited components and was only slightly lower than titanium for strength-limited designs [Speer and Es-Said 2004].

14.5 Beryllium-Antimony Alloys

Beryllium-antimony alloys in the range 0.1 to 16 wt% have been studied by Stonehouse and Woodard [1971], who report that antimony

Table 14.4 Beralcast alloys

Composition		
Element	**Beralcast 363**	**Beralcast 191**
Beryllium	bal	bal
Aluminum	27.5–34.5	27.5–34.5
Silver	2.65–3.35	1.65–2.35
Cobalt	0.65–1.35	N/A
Germanium	0.55–0.95	N/A
Silicon	N/A	1.65–2.35

Properties		
Property	**Beralast 363**	**Beralcast 191**
Density, max, g/cm^3 at 25 °C (lb/in.^{3} at 77 °F)	2.19 (0.079)	2.19 (0.079)
Modulus of elasticity in tension, GPa at 25 °C (10^6 psi at 77 °F)	206.8 (30.0)	206.8 (30.0)
Ultimate tensile strength, MPa at 25 °C (ksi at 77 °F)	289.6 (42.0)	196.5 (28.5)
Yield strength, MPa at 25 °C (ksi at 77 °F)	213.6 (31.0)	137.9 (20.0)
Elongation (2.54 cm, or 1 in., gage) All orientations at 25 °C (77 °F)	4.0	2.0
Thermal conductivity, W/m · K at 25 °C (Btu/h · ft · °F at 77 °F)	108 (62.4)	190 (109.8)

Source: Starmet Corp. 2004

additions in the range of 4 to 8 wt% produce enhanced machining characteristics, with room-temperature tensile properties similar to those machining behaviors of unalloyed beryllium for both the hot pressed and sheet materials. Elongation and strength properties of the beryllium-antimony alloys are lower than those for beryllium at elevated temperatures.

Fracture toughness values measured in Be-6wt%Sb sheet 1.561 mm thick were approximately 49 MPa · m$^{1/2.}$ See Section 17.5 in Chapter 17 of this book for a discussion of the effect thickness has on fracture toughness.

14.6 Beryllium-Copper Alloys

Copper-beryllium alloys were one of the primary early uses for beryllium, especially in a structural material. Alloys in the range of 0.008 to 5 wt% Cu have been produced both by vacuum casting plus hot rolling and by vacuum casting and extrusion followed by hot rolling [London et al. 1968]. Both copper and nickel alloys have significant improvements in mechanical properties with beryllium additions of up to approximately 2 wt%. The principal strengthening mechanism involves precipitation. Figure 14.8 shows a typical microstructure for a C82200 alloy casting. The temperature range for age hardening and solution anneal is illustrated on the phase diagram in Fig. 14.9.

The competitiveness of beryllium as an effective and economical alloy addition to copper, nickel, aluminum, magnesium, and zinc alloys centers around the ability to make master alloys. Beryllium-copper master alloys were produced in the early 1900s by electrolysis. It was replaced by carbothermic reduction of BeO in 1939 by Sawyer and Kjellgren [1939]. An arc furnace charged with molten copper and BeO was reacted with carbon to reduce the BeO. The process operated in the temperature range from 1800 to 2100 °C (3270 to 3810 °F). This process has remained approximately the same today with the use of a three-phase alternating-current arc furnace practice. Cribb and Ali [1994] outlined and described the chemistry and unit process of making beryllium-copper master alloys.

Copper-beryllium alloys are known for their ability as a wrought alloy to give high strength, formability, high-fatigue strength, acceptable elastic modulus, and still maintain acceptable levels of electrical and thermal conductivity. In bearings, copper-beryllium alloys offer antigalling properties. For magnetic-sensing housings, these alloys have low magnetic susceptibility, and for resistance welding tips, copper-beryllium alloys offer an acceptable combination of both hot hardness and conductivity [Cribb and Ali 1994]. Alternative methods for the production of copper-beryllium master alloys, especially with the use of plasma processing, have been explored [Scammon 1972, Segsworth and Alcock 1977, Jarrett et al. 1986].

Copper addition has been reported to influence plastic anisotropy in beryllium single crystals by promoting nonbasal slip. Beryllium-copper alloys consist of a complete solid solution [Jepson 1965]. Copper additions have been reported to make beryllium more difficult to hot roll at fabrication temperatures. No slip systems were made operative by the copper addition.

Herman and Spangler [1961] reported that copper additions favorably influenced plastic anisotropy of beryllium single crystals. London et al. [1968] and Damiano et al. [1968] showed that copper in solid solution promoted nonbased $(c + a)$ slip in beryllium. Carson and Denny [1967], Taylor and Carson [1967], and Evans et al. [1968] also performed investigations on beryllium-copper hot rolled sheet material. Alloys in the range of 0.008 to approximately 5 wt% Cu content were produced both by vacuum casting plus hot rolling [Evans et al.1968] and by vacuum casting and extrusion followed

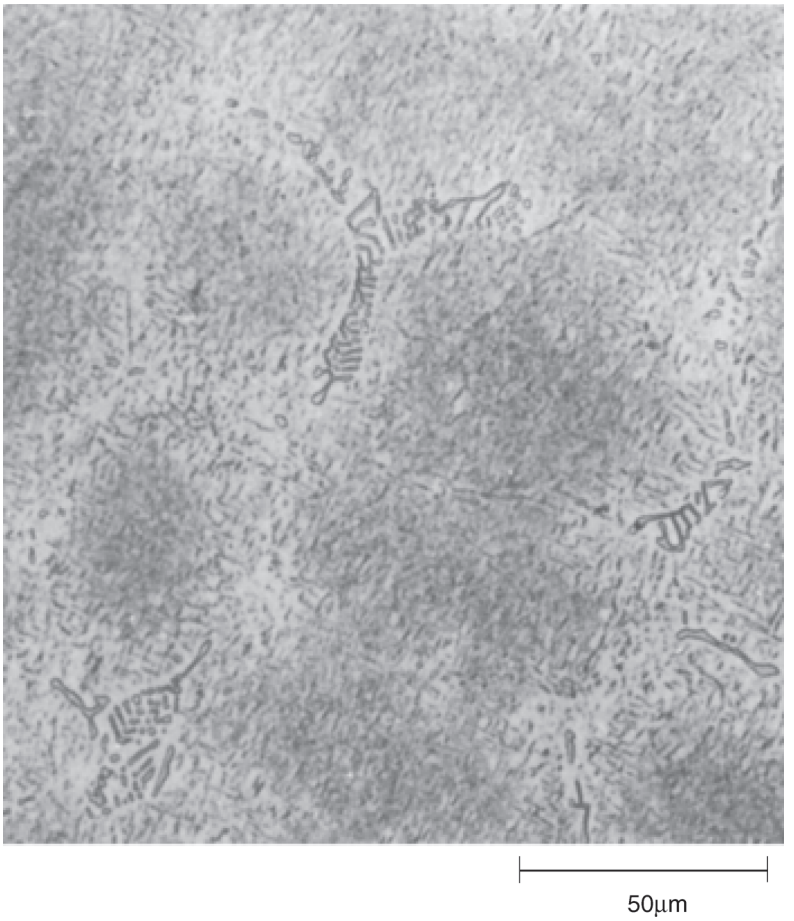

Fig. 14.8 The C82200 alloy casting is an as-cast microstructure that shows an interdendritic network of large primary beryllide phase in a matrix of α solid solution. Preferred orientation of small secondary beryllides is observed with the matrix. Original magnification: 400×

by hot rolling [Carson and Denny 1967, Taylor and Carson 1967]. The results of these studies generally showed that copper made beryllium more difficult to hot roll at all fabrication temperatures. Carson and Denny [1967] and Taylor and Carson [1967] reported on rolling 0.008, 1.00, 2.79, and 4.65 wt% Cu alloys at 760, 650, 540, 425, 350, and 250 °C (1400, 1200, 1000, 800, 600, and 480 °F). The 0.008 and 1.0 wt% Cu alloys were successfully rolled at all temperatures studied, while the higher-copper-content alloys developed surface fissures and grooves below 650 °C (1200 °F). All alloys were reported to be in complete solid solution. Texture evaluation of the sheet showed that copper had essentially no effect on the final texture produced. This result suggests that contrary to expectations, no slip systems were made operative by the copper addition.

Taylor and Carson [1967] reported on an extended evaluation of Be-1.0wt%Cu ingot sheet also prepared by vacuum casting hot extrusion (1010 °C, or 1850 °F) and hot rolling using a decreasing temperature rolling schedule from 790 °C (1455 °F) at the start or rolling to 250 °C (480 °F) as reduction proceeded. This practice was expected to produce the finest possible final grain size. The copper alloy showed substantial cracking. Evaluation of sound material showed that the 1 wt% Cu addition produced approximately a 10% strength increase, with lower ductility in both tensile and bend tests below 205 to 315 °C (400 to 600 °F).

Alloys containing up to 5 wt% Cu were evaluated after vacuum casting and hot rolling by Evans et al. [1968]. The study concluded that only moderate strength improvement was produced by the copper addition (principally up to

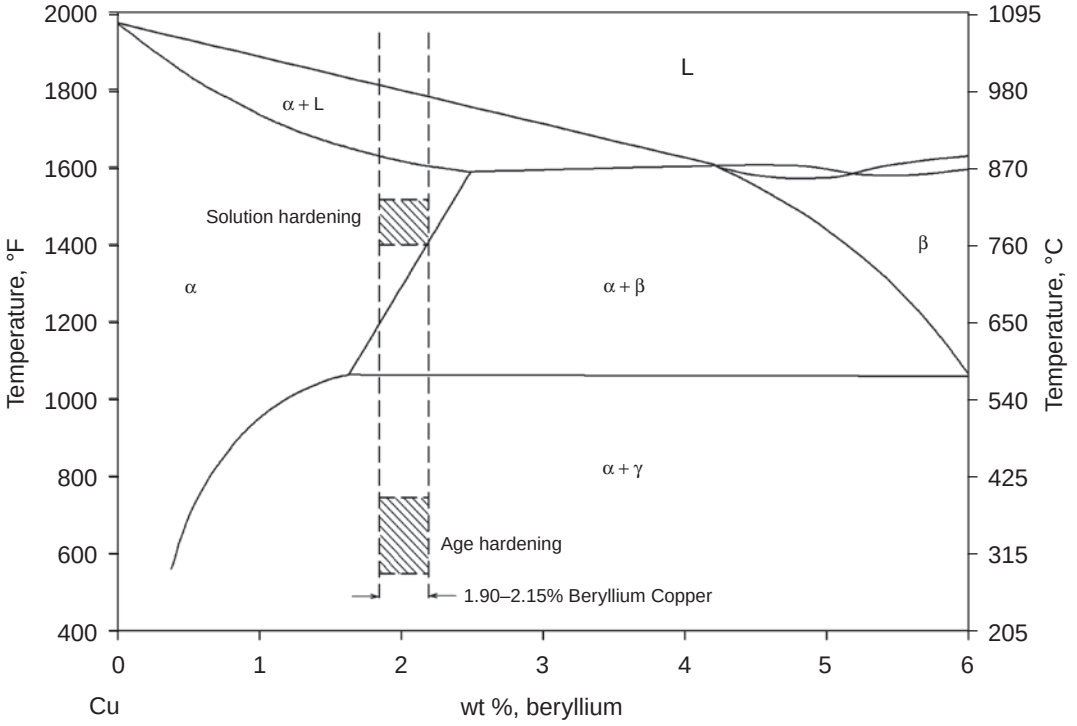

Fig. 14.9 Beryllium-copper equilibrium phase diagram in the copper-rich section

1 wt% Cu), with progressively increasing rolling difficulty as the copper content was increased to 5 wt%. Increased casting defects were also noted with increased copper content.

Aldinger and Wilhelm [1975] showed that copper addition to beryllium single crystals greatly increased its cleavage resistance. Polycrystalline beryllium-copper alloy ingots produced by hot isostatic pressing of prealloyed powder showed improved strength with nearly constant ductility up to approximately 5 wt% Cu. Further copper additions resulted in decreased elongation. Fracture toughness was found to decrease with copper content in direct contrast to the single-crystal results [Smugeresky 1979].

14.7 Transition Metals

Work on rapidly solidified alloys of beryllium with small amounts (0.5 to 2 wt%) of transition metals or rare earth metals (titanium, yttrium, and zirconium) showed that potentially useful dispersions of beryllium intermetallic compound particles could be realized. Such dispersions, made up of particles of MBe_{12} or MBe_{13}, were particularly stable when exposed to elevated temperature (above 700 °C, or 1290 °F), because of the very low solubility of these metals in beryllium and the high thermodynamic stability (high melting temperature) of the compounds. The effort did not progress to the point of making large quantities of material on which useful mechanical properties data could be obtained, but this approach holds promise if the high-temperature properties of beryllium need to be improved.

A publication from the Kharkov Institute of Physics and Technology presents some information on several beryllium alloys, including aluminum, nickel, and yttrium. The latter element appeared to stabilize grain size during superplastic deformation to a much more effective extent than was found for the other elements [Karpov et al. 1980].

14.8 Beryllium-Iron Alloys

Iron is a commonly occurring impurity in most commercially available forms of beryllium metal. It occurs both in the originally refined metal (in very low concentration levels in electrolytic flake material) and as an impurity

accumulated during power processing (chipping. comminution, etc.). The commonly occurring range is from approximately 100 to 500 ppm (0.01 to 015 wt%).

Several investigators have studied iron levels greater than 0.15 wt% to determine the nature of the precipitation in these higher-iron-content beryllium-iron alloys. Scott and Lindsay [1966] reported extensive cracking in rolling a Be-1.2wt%Fe alloy at 750 °C (1380 °F). Extensive precipitation of a hexagonal $FeBe_{11}$ intermetallic compound was found by Morozumi et al. [1969] and Janot and Delcroix [1972]. Scott and Lindsay [1966] also suggest that precipitation of $FeBe_{11}$ is enhanced in the more dilute alloys studied by prior plastic deformation such as rolling or extrusion.

14.9 Beryllium-Titanium Composites

The beryllium-titanium composite system has been of interest principally for improved specific modulus with better retention of base-metal ductility than either boron or boron-SiC composite systems. This improvement is because beryllium, although not as strong as boron or boron-SiC reinforcements, exhibits useful tensile ductility, especially in the form of fine wire or extruded filaments. A second attractive feature of this composite system is that both components achieve substantial ductility in the 450 to 750 °C (840 to 1380 °F) temperature range. This behavior means that composite and component fabrication may be accomplished using normal metalworking techniques such as extrusion and forging. This accomplishment is an important economic factor bearing on the ultimate applications to be found for such generally costly products. Beryllium appears as a unique reinforcement since it is a high-specific-modulus metal with relatively low yield and ultimate strength. Thus, specific modulus is improved, but yield and ultimate tensile strength are generally reduced compared to values for titanium alloys.

Early composites in this system were fabricated by vacuum hot pressing. Fine wire (0.13 mm, or 0.005 in., diameter) was co-wound with Ti-6Al–4V wire to form composite tape interlayered with titanium alloy foil and vacuum hot pressed to produce consolidated material. Properties of this type composite were excellent, but the unfavorable economics of manufacture led to evaluation of other fabrication methods. Coextrusion has been used to produce two distinct beryllium-titanium composite systems:

- A continuous filamentary composite with the final appearance closely resembling conventional wire composites is produced by multiple coextrusion.
- Discontinuous filament composites are produced by coextrusion of mixed beryllium and titanium or titanium alloy powders.

Secondary fabrication by isothermal forging and hot rolling has been applied successfully to both of these composite types.

Properties achieved with these composite systems are a function of volume percent filament, titanium alloy extrusion reduction ratio, and the stress-strain history of the composite. Two factors contribute to the low proportional limit of composites in the beryllium-titanium system. The thermal expansion coefficient for beryllium is three times that of titanium. Cooling from the forming temperature therefore produces a residual tensile stress in the beryllium component. This, combined with the high beryllium modulus and relatively low (compared to boron-beryllium) yield strength, results in an unusually low proportional limit followed by very rapid strain hardening in the 0 to 0.2% strain region. Figure 14.10 shows a schematic diagram of the modulus effect described.

Two interesting effects consistent with the presence of a high residual stress in the beryllium-titanium composites are as follows. First, compressive proportional limit is much higher than that in tension (Table 14.5), Second, tensile proportional limit increases or remains approximately constant with increased testing temperature. Small tensile prestrain treatment therefore would be expected to have a significant effect on the relative tensile and compressive properties of beryllium-titanium composites.

Beryllium-titanium composites show good strength properties parallel to the filament axis. These composites are not as strong as comparable boron-aluminum composite, but both show superior off-axis tensile properties. Figure 14.11 shows a comparison of tensile properties for beryllium-titanium, B-SiC-Ti, and boron-aluminum composites containing 50% composite filament. The extruded filamentary beryllium-titanium composites show virtually no loss in properties in the 90° direction because of the abovementioned flat ribbon aspect of the extruded flat composite forging preforms. Extruded mixed-powder beryllium-titanium composites do

not show this transverse strengthening effect and exhibit a drop in properties at the 90° orientation roughly comparable to those shown for the B-SiC-Ti composites. This transverse strengthening effect is apparently because, with the extruded powders, it is either difficult to achieve good bonding in the transverse direction, or the flattened aspect ratio of the fine powder particles is not sufficient to effect the strengthening observed with the larger continuous filaments. True tensile plasticity is an important attribute of the beryllium-titanium composites. The B-SiC-Ti composites show essentially linear elastic stress-strain behavior, with no plasticity in the 0° direction at room temperature. The composites show 1.5 to 3% tensile elongation in off-axis tests, where matrix properties become predominant.

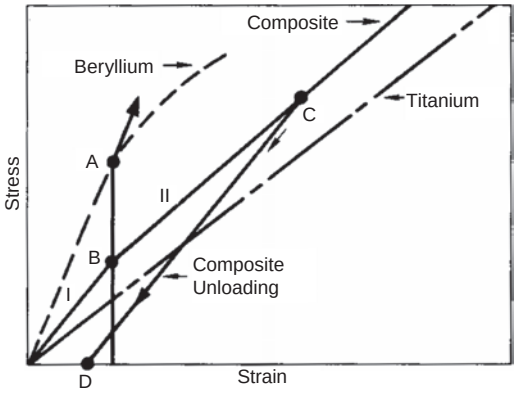

Fig. 14.10 Composite stress-strain behavior based on the moduli and elastic limits. A: beryllium elastic limit; B: composite elastic limit; I: fully elastic; II: elastic plastic; C: unloading point. Source: London et al. 1979

Both beryllium-titanium and B-SiC-Ti composite systems show a relatively small decrease in tensile properties of approximately 10 to 15% with increased temperature up to 315 °C (600 °F), the usually considered operating temperature range. Hot forging at 705 °C (1300 °F), an operation unique to beryllium-titanium composites, results in some tensile property reduction. Beryllium-titanium composites appear, at this time, to be a viable composite system for structural applications requiring high specific modulus, moderate strength, good formability/fabricability, and good toughness properties [London et al. 1971].

Other composite studies involving beryllium have included beryllium wire used as a composite reinforcement, beryllium laminate systems, and second-phase materials added to beryllium to enhance or modify its basic properties. Fine beryllium wire, usually of 0.127 mm (0.005 in.) diameter, has been used in several composite studies. Beryllium wire-aluminum- and beryllium wire-titanium-matrix composites were studied by Goodwin and Herman [1970]. Properties of the wire composites were good, but the composite fabrication was considered to be uneconomic compared to coextrusion. Mahiew and Schwartz [1967] studied the properties of beryllium-wire-reinforced plastic composites. Properties of the composites studies were good, with specific ultimate strength of 2.3×10^6 cm (0.90×10^6 in.) and specific yield strength (0.27 offset) of 2.2×10^6 cm (0.86×10^6 in.).

Shyne et al. [1969] studied the behavior of beryllium with added dispersoids. Systems studied were Be-BeO, Be-Be_2C, Be-Si, and Be-$Be_{32}W$. All were prepared using powder techniques. All

Table 14.5 Tensile and compressive properties of beryllium-titanium powder composites showing the proportional limit effect

Test conditions	Be, vol%	Proportional limit, MPa (ksi)	Tensile strength, MPa (ksi)	Elongation, %	Modulus, GPa (10^6 psi)
Tensile					
25 °C	50	104 (15.1)	846 (122.7)	1.5	192 (27.8)
	60	131 (19.0)	766 (111.1)	1.0	180 (26.1)
	20–30	90 (13.1)	1075 (155.9)	1.4	143 (20.7)
315 °C	50	141 (20.4)	685 (99.3)	4.1	154 (22.3)
	60	133 (19.2)	590 (85.6)	1.6	153 (22.1)
	20–30	227 (32.9)	868 (125.9)	3.0	107 (15.5)
			Compressive ultimate strength, MPa (ksi)		
Compression					
25 °C	50	1030 (149)	1282 (186)	...	...
	60	992 (144)	1269 (184)	...	...
315°C	50	848 (123)	1175 (170)	...	...
	60	977 (142)	1113 (161)	...	...

Source: London 1979

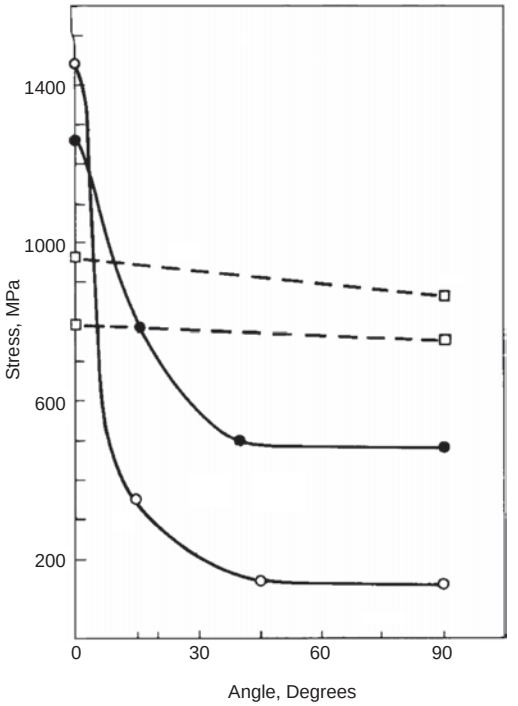

Fig. 14.11 Off-axis tensile strength (50% composites). °, B-Al-6061; ● , B-SiC-Ti(6Al-4V); □, Be-Ti(6Al-4V). Source: London et al. 1979

dispersoids tended to strengthen and embrittle the beryllium. Highest strength was obtained with a Be-20vol%BeO system (compression strength 1034 MPa, or 150,000 psi) but with only 4% compressive strain at fracture compared to 40% compressive failure strain for the beryllium-base material (276 MPa, or 40,000 psi, compressive yield strength).

REFERENCES

Alloys Digest, 1971. Lockalloy—High Modulus, Low Density Material, *Engineering Alloys Digest*, Upper Montclair, NJ, Sept 1971

Aldinger, F., and Wilhelm, M., 1975. "Influence of Copper on Crack Propagation in Be Single Crystals," Technical Report BMFT-FB-W-75-07

Carson, C., and Denny, J.P., 1967. "Solid Solution Strengthened Beryllium Alloy Sheet," Contract NOW-66.0563-C, Final Report 112167, The Beryllium Corp., Reading, PA

Cribb, W.R., and Ali, S., 1994. Production of Cu-Be Master from Beryllium Oxide, *Miner. Process. Extr. Metall. Rev*., Vol 13, p 157–164

Damiano, V.V., London, G.J., and Conrad, H., 1968. Microstrain Compression of Beryllium and Beryllium Alloy Single Crystals Parallel to the [0001], Part II: Slip Trace Analysis and Transmission Electron Microscopy, *Trans. Metall. Soc. AIME*, Vol 242, p 987–994

Duba, R.J., Haramis, A.C., Marks, R.F., Payne, L., and Sessing, R.C., 1976. "YF-12 Lockalloy Ventral Fin Program," Final report, Vol 1, NASA CR-144971

Evans, R.E., Beasley, D., and Lowe, J.N., 1968. "Fabrication and Evaluation of Beryllium Ingot Sheet Alloyed with Copper and Silver," Technical Report AFML-TR-68-135, Atomic Weapons Research Establishment, Air Force Materials Laboratory

Fenn, R.W., Jr., Crooks, D.D., Cons, W.C., and Underwood, E.E., 1966. Properties and Behavior of Beryllium-Aluminum Alloys, *Beryllium Technology*, Vol 1, Gordon and Breach, New York, NY, p 108–143

Goodwin, V.L., and Herman, M., 1970. "Structural Requirements of Compressor and Fan Blading of Beryllium Composite Materials," National Materials Advisory Board Conference on Beryllium (Washington, D.C.)

Herman, M., and Spangler, G.E., 1961. *The Metallurgy of Beryllium*, Institute of Metals, London, p 28–75

Ind. Heat., 1971. Beryllium-Aluminum Alloy Extrusions Save Weight in Minuteman III Missile, *Ind. Heat*., Vol 38, p 666–672

Jacobson, L.A., 2006. Los Alamos, NM, private communication

Janot, C., and Delcroix, P., 1972. Study of Mechanically-Strained Beryllium-Iron Alloys by the Mossbauer Effect, *Acta Metall*., Vol 20 (No. 4), p 637–643

Jarrett, N., Szekely, J., and Roman, W., 1986. NMAB Report on Plasmas, *J. Met*., Vol 38 (No. 1), p 41–45

Jepson, W.B., 1965. The Corrosion Behavior of Beryllium, *Beryllium*, Atomic Energy Research Establishment, Harwell, England, p 221–256

Karpov, E.S., Papirov, I.I., and Tikhinski, G.F., 1980. Superplasticity Investigation of Beryllium Alloys, *Fiz. Khim. Obrab. Mater*., No. 4, p 96–100

London, G.J., 1979. Alloys and Composites, *Beryllium Science and Technology*, Vo. 2, Plenum Press, NY, p 297–318

London, G.J., Damiano, V.V., and Conrad, H., 1968. Microstrain Compression of Beryllium and Beryllium Alloy Single Crystals Parallel to the [0001], Part I: Crystal Preparation and Microstrain Properties, *Trans. Metall. Soc. AIME*, Vol 242, p 979–986

London, G.J., Taylor, W., and Herman, M., 1971. "Co-Extruded Beryllium-Titanium Composites for Light Weight Structures," National SAMPE Technical Conference, Space Shuttle Materials

Mahiew, W., and Schwartz, H.S., 1967. "Time Dependent Mechanical Behavior of Beryllium Wire Reinforced Plastic Composites, Parts I and 2," 12th National SAMPE Symposium on Advances in Structural Composites (Anaheim, CA)

Morozumi, S., Tsuno, N., and Doda, S., 1969. *Trans. Jpn. Inst. Met*., Vol 10, p 64–69

Murray, J.L., and Kahan, D.J., 1988. The Beryllium-Aluminum Phase Diagram, *Phase Diagrams of Binary Beryllium Alloys*, ASM International

Nachtrab, W.T., and Levoy, N., 1997. Beryllium-Aluminum Alloys for Investment Castings, *Adv. Mater. Process*., Vol 151 (No. 5), p 23–25

Papirov, I.I., 1981. *Structure and Properties of Beryllium Alloys*, Energoizdat, Moscow, p 18–19

Savchuk, V.V., and Syrnev, B.V., 1999. "Technological Ductility and Properties of Aluminum-Beryllium Alloys," ASM Conference on Beryllium (Cincinnati, OH)

Sawyer, C.B., and Kjellgren, B.R.F., 1939. Production of Alloys Containing Beryllium, U.S. Patent 2,176,906

Scammon, L.W., 1972. Material Treatment Apparatus, U.S. Patent 3,661,764

Scott, V.D., and Lindsay, H.M., 1966. Some Electron Microscope Observations on Precipitation in Beryllium, *Beryllium Technology*, Gordon and Breach, NY, p 145–l78

Segsworth, R.S., and Alcock, C.B., 1977. Extended Arc Furnace and Process for Melting Particulate Charge Therein, U.S. Patent 4,037,043

Shyne, J.C, Sherby, O.D., and Moberly, J.W., 1969. "Investigation of Beryllium with Added Dispersoids," Report 863648, Stanford University of California Dept. of Materials Science and Engineering

Smugeresky, J., 1979. Sandia Laboratories, Livermore, CA, private communication

Speer, W., and Es-Said, O.S., 2004. Applications of an Aluminum-Beryllium Composite for Structural Aerospace Components, *Eng. Fail. Anal*., Vol 11 (No. 6), p 895–902

Starmet Corp., 2004. Concord, MA

Stonehouse, A.J., and Woodard, D.H., 1971. "Characteristics of Beryllium-Antimony Alloys," Report presented at AIME Meeting (Detroit), Brush Beryllium Co.

Taylor, W., and Carson, C., 1967. "Solid Solution Strengthened Beryllium Alloy Ingot Sheet," Report, The Beryllium Corp., Reading, PA

SELECTED REFERENCES

- Armelin, J.P., Blodin, W.C., and King, D.B., 1970. The Minuteman Beryllium Spacer, *Proceedings of the Beryllium Conference*, Vol 1, Publication NMAB-272, National Academy of Sciences-National Academy of Engineering, Washington D.C., p 337
- Cox, A.R., 1975. "Beryllium/Titanium Bimetal System," Naval Air System Command Contract: N00019-74-C-0017, Report AD-A-019657, Pratt and Whitney Aircraft Division, United Technologies Company
- Cullity, B.D., Bitsianes, G., Chandler, W.T., and Neher, M., 1945. "Alloys of Gold and Beryllium," Report MDDC-97 (Declassified: 1946), Atomic Energy Commission
- Harkness, J.C., Spiegelberg, W.D., and Cribb, W.R., 1990. Beryllium Copper and Other Beryllium Containing Alloys, *Properties and Selection: Nonferrous Alloys and Special-Purpose Materials*, Vol 2, *Metals Handbook*, 10th ed., ASM International
- Hurd, J.N., Lohrer, R.J., and O'Rourke, R.G., 1970. "The Development of Beryllium Alloys for High Strength Beryllium Wires," WPAFB Report AFML-TR-69-306
- Isserow, S., and Rizzitano, F.J., 1974. Titanium-Beryllium Microcomposites, A State-of-the-Art Review, *Composites*, Vol 5 (No. 4), p 141–150
- Kawecki Berylco Industries, Inc., 1984. Product Specification, Lockalloy, File 303 3 SP1
- Kovacs, W.J., and London, G.J., 1977. Synthesis and Material Characterization of Beryllium/Ti-5Al-4V Composites, *Metall. Trans. A*, Vol 8 (No. 1), p 179–185
- Marder, J.M., 1997. Aluminum Beryllium Alloys, *Adv. Mater. Process.*, Vol 152 (No. 4) p 37–40

- Sippel, G.R., and Herman, M., 1974. "Optimization and Design Criteria for Beryllium/Titanium, Composites," Naval Air Systems Command Contract N00019-74C-0103, Report EDR8159, Detroit Diesel Allison Division of General Motors
- Tanner, L.E., 1980. The Stable and Metastable Phase Relations in the Hf-Be Alloy System, *Acta Metall.*, Vol 28 (No. 12), p 1805–1816

Beryllium Chemistry and Processing, p 179-197
By Kenneth A. Walsh
Edited by Edgar E. Vidal, Alfred Goldberg,
Edward N.C. Dalder, David L. Olson, and Brajendra Mishra

CHAPTER 15

Beryllium Binary Phase Diagrams

Loren A. Jacobson, Los Alamos National Laboratory, Retired

IMPORTANT BERYLLIUM binary phase diagrams are presented and summarized in this chapter. More detailed phase diagram information can be found in the *ASM International Monograph Series on Alloy Phase Diagrams*, *Phase Diagrams of Binary Beryllium Alloys*, edited by H. Okamoto and L. Tanner, ASM International, 1987.

15.1 Beryllium-Silver (Ag-Be)

Figure 15.1. This system has one incongruent melting compound, $AgBe_2$. The compound melts peritectically at a temperature of 1010 °C (1850 °F), and it decomposes at temperatures below 760 °C (1400 °F). The eutectic between

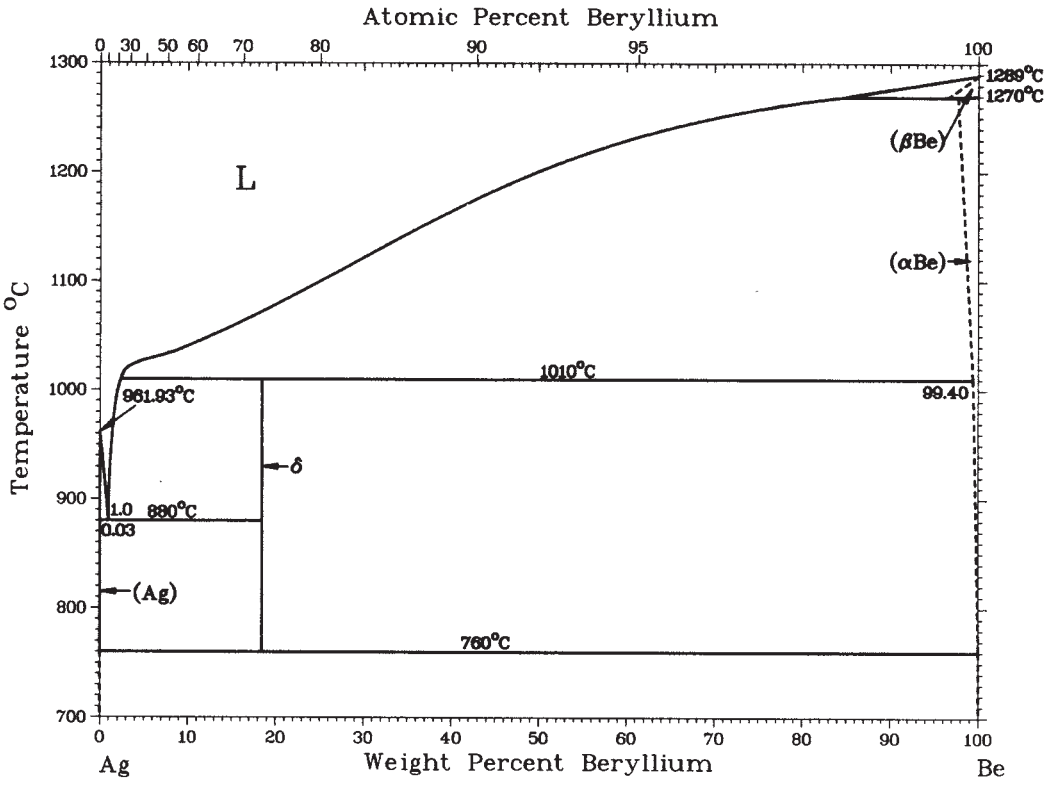

Fig. 15.1 Binary phase diagram of beryllium-silver. Source: Okamoto and Tanner 1987e

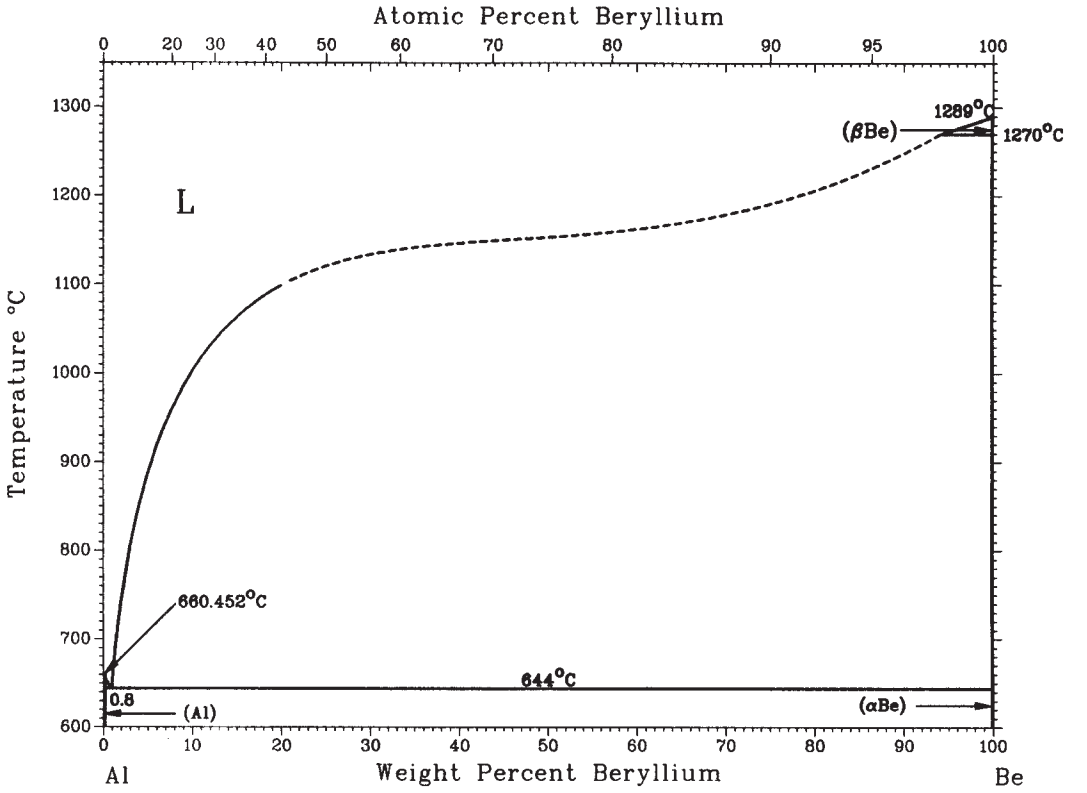

Fig. 15.2 Binary phase diagram of aluminum-beryllium. Curves are from thermodynamic calculations, and their position do not always correspond to the assessed values. Source: Murray and Kahan 1988

this compound and pure silver is at 880 °C (1615 °F) and a composition of approximately 10.5 at.% Be. The maximum solid solubility of silver in beryllium is approximately 0.7 at.%.

15.2 Beryllium-Aluminum (Al-Be)

Figure 15.2. This system is a simple eutectic, with the eutectic temperature at 644 °C (1190 °F) and a composition of 2.5 ± 0.2 at.% Be. There is negligible solid solubility of the metals in one another, with approximately 0.3 at.% Be in aluminum and less than 0.007 at.% Al in beryllium. It has been reported that Guinier-Preston zones form in aluminum from the beryllium that remains in solid solution. It has also been reported that there may be a metastable miscibility gap in the liquid-plus-solid region of the diagram. If this is so, it allows a rapidly cooled alloy to separate into two phases in the liquid state and the subsequent formation of a fine, interconnected microstructure in the solidified alloy.

15.3 Beryllium-Gold (Au-Be)

Figure 15.3. The system has several intermediate phases, none of which have been extensively studied. Three of these phases appear to melt congruently: AuBe, $AuBe_3$, and $AuBe_5$. Additional phases include Au_4Be_3, Au_2Be with the $MoSi_2$ structure, and Au_3Be. The eutectic temperature and composition between pure beryllium and $AuBe_5$ have not been precisely determined. The maximum solubility of beryllium in gold is approximately 0.2 at.%. The solid solubility of gold in hexagonal beryllium is estimated to be approximately 3 at.% but is not precisely known.

15.4 Beryllium-Boron (B-Be)

Figure 15.4. This is a very complex binary system, with five intermediate phases and two more possible intermediate phases shown as dotted lines. It is evident that the stability ranges

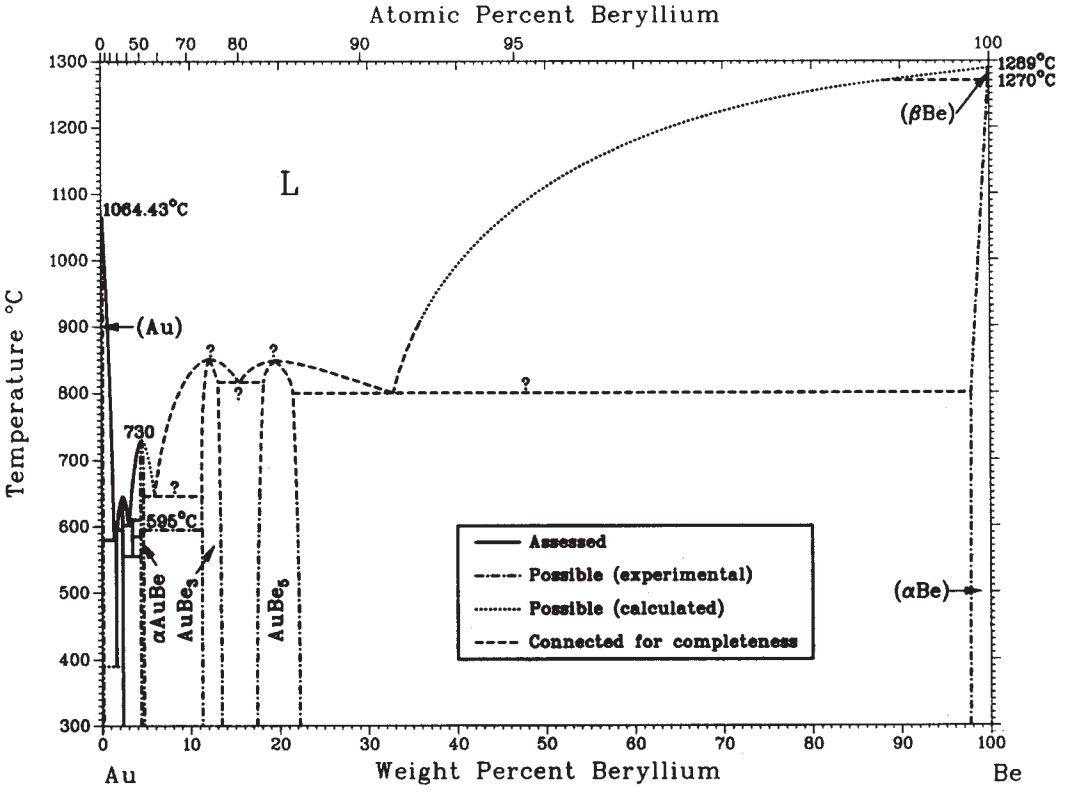

Fig. 15.3 Binary phase diagram of beryllium-gold. Source: Okamoto and Massalski 1987

and melting points have not been well established for many of these phases. The two elements have no mutual solid solubility.

15.5 Beryllium-Barium (Ba-Be)

Figure 15.5. This system has one intermetallic compound with the stoichiometry $BeBa_{13}$, which melts congruently at 1807 ± 50 °C (3285 ± 90 °F). There may be a metastable subliquidus miscibility gap on the barium-rich side of the system. The solubility of each of the elements in the other is very low.

15.6 Beryllium-Calcium (Be-Ca)

Figure 15.6. Note that this diagram includes solid, liquid, and gas phases. The solid solubility of beryllium in calcium is not known, and the solid solubility of calcium in beryllium is very low, less than 0.02 at.%. There is one compound in the system, $CaBe_{13}$, which decomposes to beryllium liquid plus calcium gas at temperatures in excess of 1583 °C (2880 °F).

15.7 Beryllium-Cobalt (Be-Co)

Figure 15.7. Cobalt is one of the elements that stabilizes body centered cubic beryllium, with a maximum solubility of 6 at.% or 28 wt% Co. The maximum solubility of cobalt in hexagonal beryllium is approximately 3 at.% or 14 wt%. The maximum solid solubility of beryllium in cobalt is approximately 12 at.% or 3 wt%. There are two congruent melting phases: The beta phase, with a cesium chloride-ordered cubic structure, melts at 1420 °C (2590 °F), and the gamma phase melts at 1400 °C (2550 °F). Gamma and gamma prime are closely related, with gamma being a disordered version of gamma prime. There are two other phases, both of which have a hexagonal crystal structure.

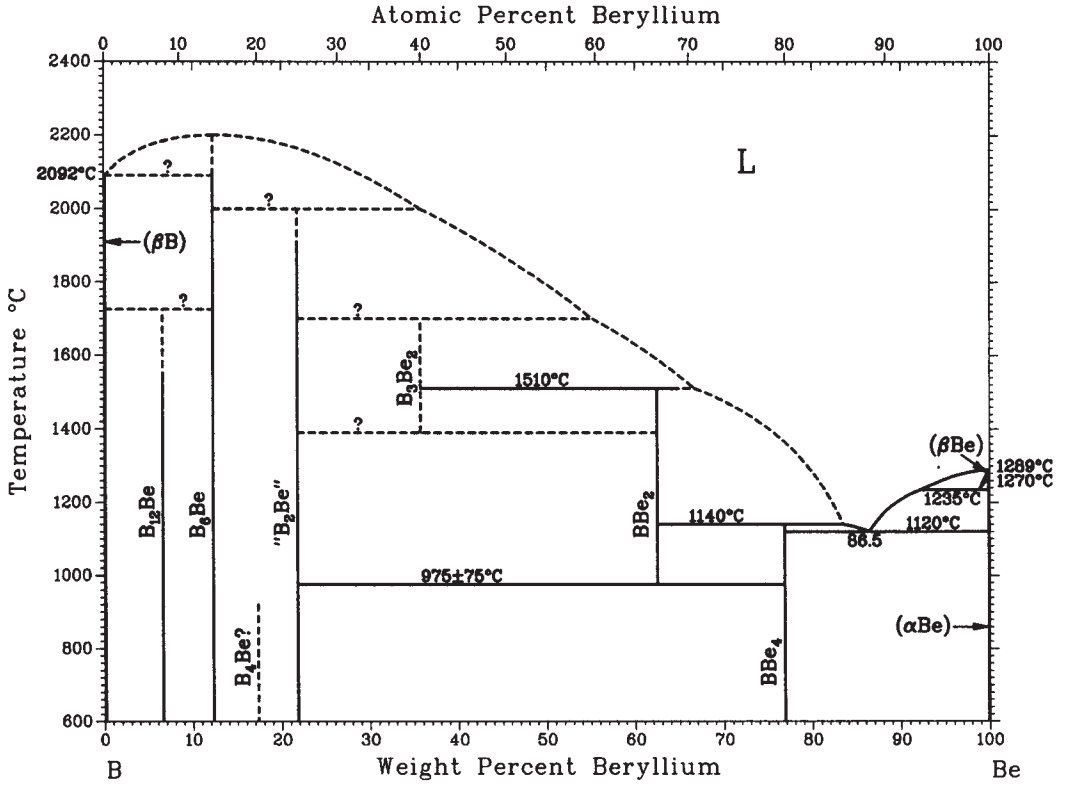

Fig. 15.4 Binary phase diagram of beryllium-boron. Source: Okamoto and Tanner 1988

Neither the epsilon nor the zeta phases are stable above 1100 °C (2010 °F). The nature of the beta phase is unresolved at the present time.

15.8 Beryllium-Copper (Be-Cu)

Figure 15.8. Copper is the element with the highest solid solubility in hexagonal beryllium, at 9.5 at.% or 42.5 wt% at the eutectoid transformation temperature of 1109 °C (2030 °F). Copper also stabilizes the body-centered cubic form of beryllium with a maximum solubility of nearly 60 wt%. The minimum temperature for the eutectoid transformation is 1109 °C (2030 °F) at a composition of approximately 15 at.% Cu. or 52.8 wt%. There are three intermediate phases. The delta phase is a C-15 Laves phase that melts congruently at 1219 °C (2225 °F). The gamma phase melts peritectically at 930 °C (1705 °F) and has a CsCl ordered cubic structure. The beta phase is a disordered solid solution stable above 620 °C (1150 °F). The solid solubility of beryllium in copper is sufficient to yield useful age-hardenable alloys with good electrical, strength, and wear properties.

15.9 Beryllium-Iron (Be-Fe)

Figure 15.9. Iron is one of the principal impurities found in commercial beryllium materials and has a maximum solubility of 0.9 at.% or 5.3 wt% in hexagonal beryllium at 1205 °C (2200 °F), The maximum solubility of beryllium and iron at a temperature of 1165 °C (2130 °F) is 6 wt% or 30 at.% There are three intermediate phases: epsilon, which decomposes at 1050 °C (1920 °F) and has the stoichiometry of Be_7Fe; delta, which is a C-15 cubic Laves phase with unknown stoichiometry; and zeta, which is a C-14 hexagonal Laves phase with a stoichiometry of $FeBe_2$. This phase melts congruently at 1463 °C (2665 °F). All of the intermediate phases appear to have an extensive homogeneity range of composition.

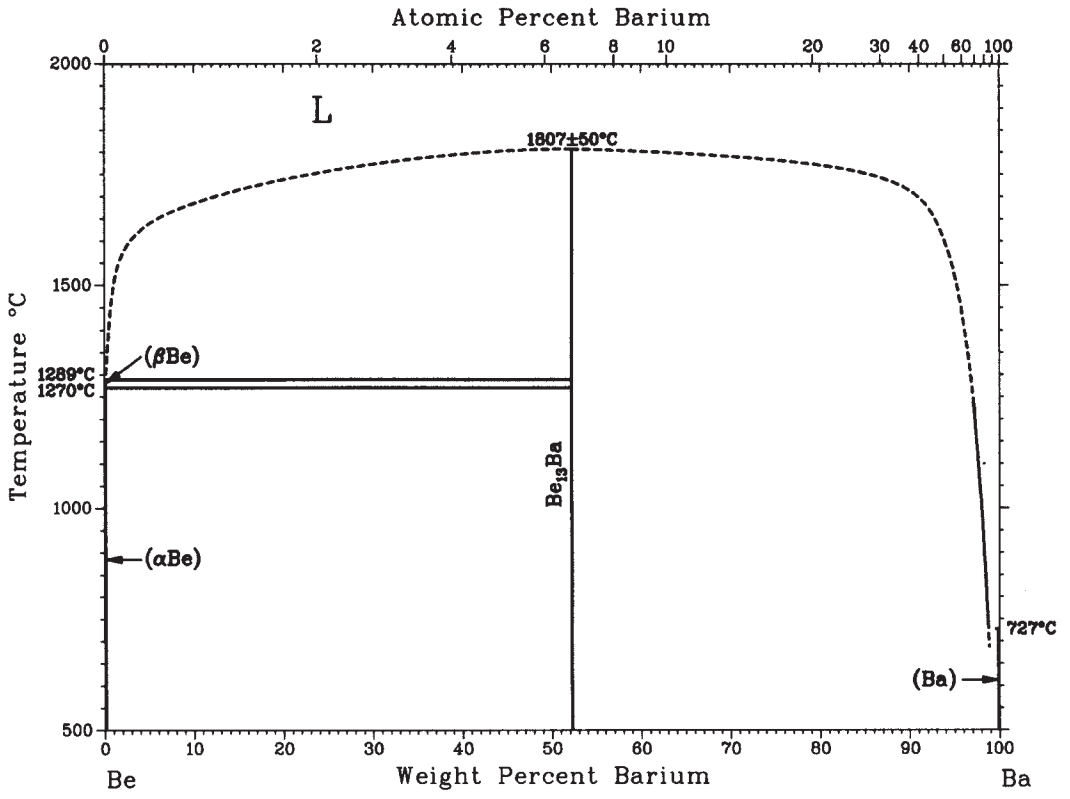

Fig. 15.5 Binary phase diagram of beryllium-barium. Source: Okamoto, et al. 1987

15.10 Beryllium-Gallium (Be-Ga)

Figure 15.10. Gallium and beryllium are not soluble in one another, and this monotectic system has a very large two-liquid range. The monotectic temperature is 1260 °C (2300 °F).

15.11 Beryllium-Germanium (Be-Ge)

Figure 15.11. The beryllium-germanium system is a monotectic system with an extensive two-liquid region. There does not appear to be any solid solubility of germanium and beryllium. The solubility of beryllium in germanium is estimated to be 0.023 at.%.

15.12 Beryllium-Lithium (Be-Li)

Figure 15.12. The solid solubility of each of these elements in the other is extremely small. The solubility of beryllium in liquid lithium at 732 °C (1350 °F) was measured at 0.23 at.%, and at 1016 °C (1860 °F) at 1.08 at.%. There is also a very low solubility of lithium in liquid beryllium. The maximum extent of the two-liquid region is not known.

15.13 Beryllium-Magnesium (Be-Mg)

Figure 15.13. The very low solid solubility of each element in the other has an important practical consequence, because magnesium is used to reduce beryllium fluoride in the commercial process for producing beryllium metal. The only intermediate phase, $MgBe_{13}$, decomposes at approximately 950 °C (1740 °F).

15.14 Beryllium-Molybdenum (Be-Mo)

Figure 15.14. The solid solubility of beryllium in molybdenum is less than 0.5 at.% at the

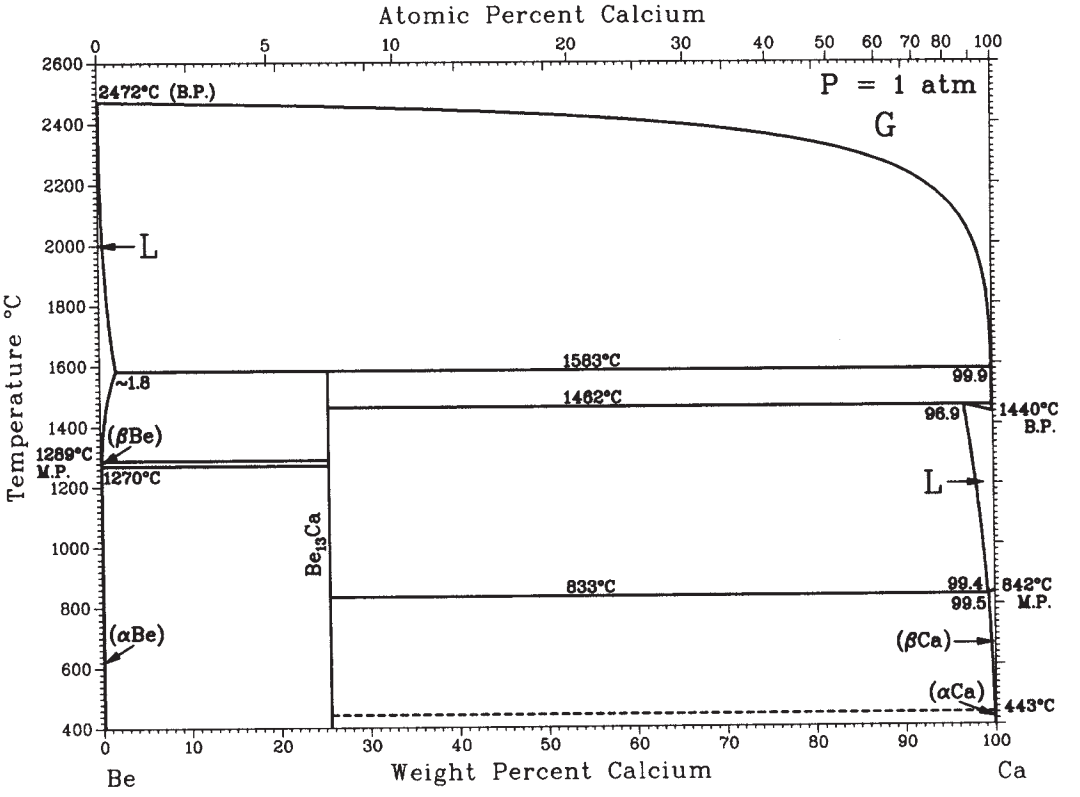

Fig. 15.6 Binary phase diagram of beryllium-calcium. Source: Itkin et al. 1987

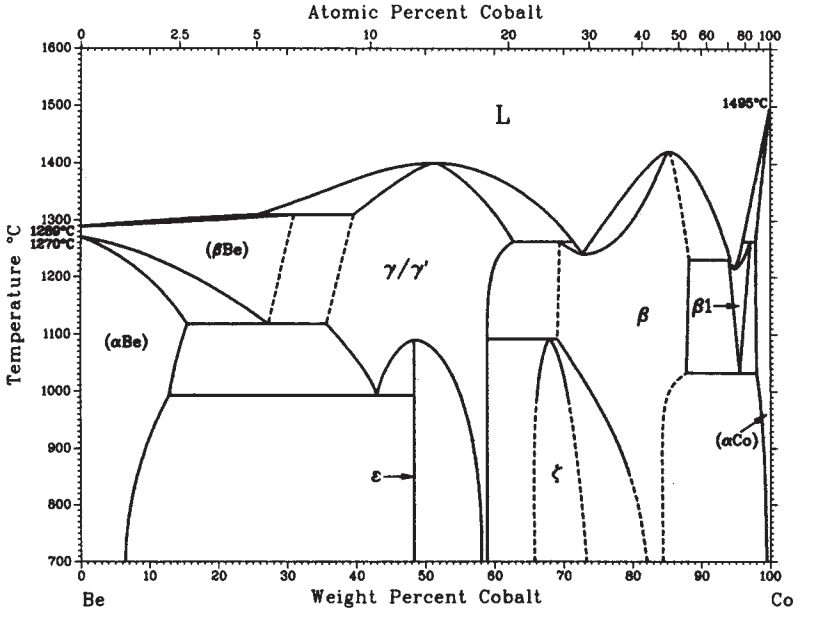

Fig. 15.7 Binary phase diagram of beryllium-cobalt. Source: Okamoto et al. 1988

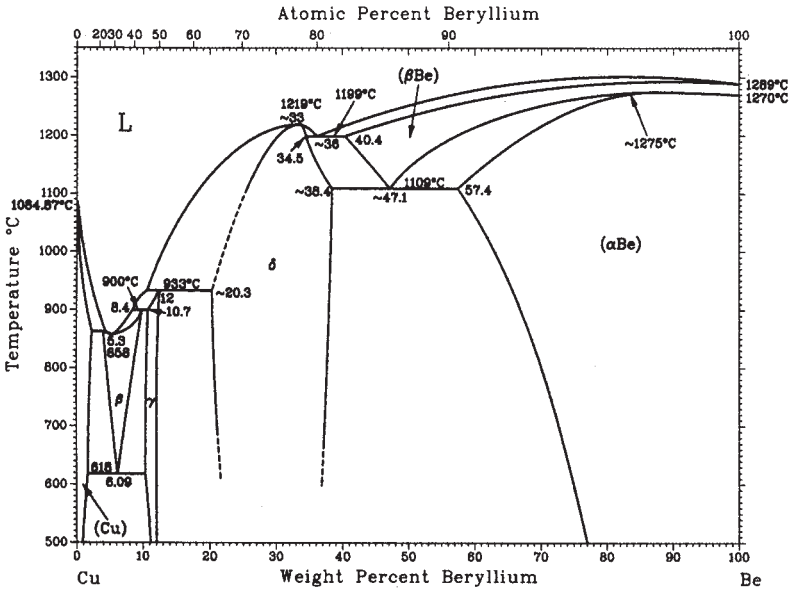

Fig. 15.8 Binary phase diagram of beryllium-copper. Source: Chakrabarti et al.1987

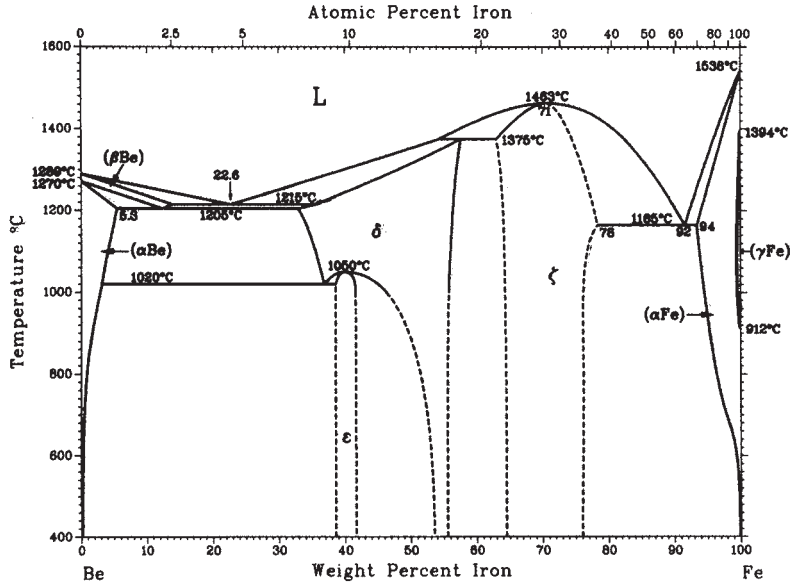

Fig. 15.9 Binary phase diagram of beryllium-iron. Source: Okamoto et al. 1993

eutectic temperature of 1827 °C (3320 °F), and the solid solubility of molybdenum in beryllium is very small. There are four intermetallic compounds in this system, one of which, $BeMo_3$, is not stable above 900 °C (1650 °F). The congruent melting phase, $BeMo_2$, is a C-14 Laves phase that melts at 2027 °C ± 200 °C (3680 ± 360 °F). $MoBe_{12}$ melts congruently at 1690 °C (3075 °F), and $MoBe_{22}$ melts peritectically at approximately 1300 °C (2370 °F).

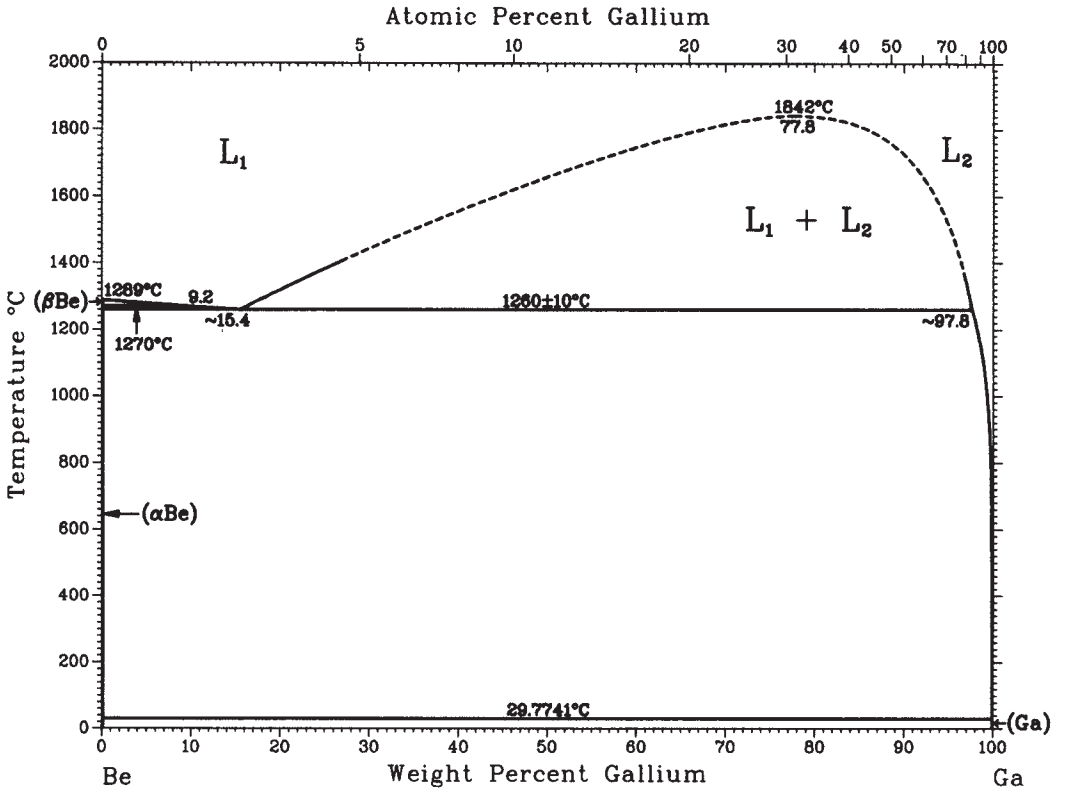

Fig. 15.10 Binary phase diagram of beryllium-gallium. Source: Okamoto et al. 1987a

15.15 Beryllium-Sodium (Be-Na)

Figure 15.15. At the melting point of pure sodium, 97.8 °C (208 °F), the solubility of beryllium is approximately 0.6 at.%. At the melting point of beryllium, 1289 °C (2350 °F), the solubility of beryllium in liquid sodium is approximately 4.5 at.%. The solubility of sodium in either liquid or solid beryllium is very low. The maximum temperature of the two-liquid region has not been determined.

15.16 Beryllium-Nickel (Be-Ni)

Figure 15.16. Nickel is another of the elements that stabilizes the body-centered cubic phase of beryllium. Its maximum solubility is 10.5 at.% or 42 wt% Ni, and the eutectoid composition is 37.7 wt% Ni at a temperature of 1062 °C (1945 °F). The maximum solubility of nickel in hexagonal beryllium is 4.5 at.% or 23.5 wt%. The gamma phase extends from 47 to 60 wt% Ni or 12 to 20 at.% and melts congruently at 1395 °C (2545 °F). This phase has a distorted gamma brass structure in which gamma is disordered and gamma prime is ordered. The approximate stoichiometry is $Be_{21}Ni_5$. The beta phase, NiBe, has an ordered CsCl structure, melts congruently at 1605 °C (2920 °F), and has a large homogeneity range on the beryllium-rich side out to approximately 75 at.% Be at the eutectic temperature.

15.17 Beryllium-Niobium (Be-Nb)

Figure 15.17. Beryllium has a very small solid solubility for niobium of approximately 0.015 at.%. However, niobium has a maximum solubility for beryllium of approximately 16 at.% or 4 wt% at the peritectic with Be_2Nb_3 at 1590 °C (2895 °F). This system has six intermetallic compounds, only two of which melt congruently. One of these, Nb_2Be_{17}, is not stable below 1415 °C (2580 °F), and $NbBe_{12}$ melts peritectically at 1672 °C (3040 °F). The highest melting

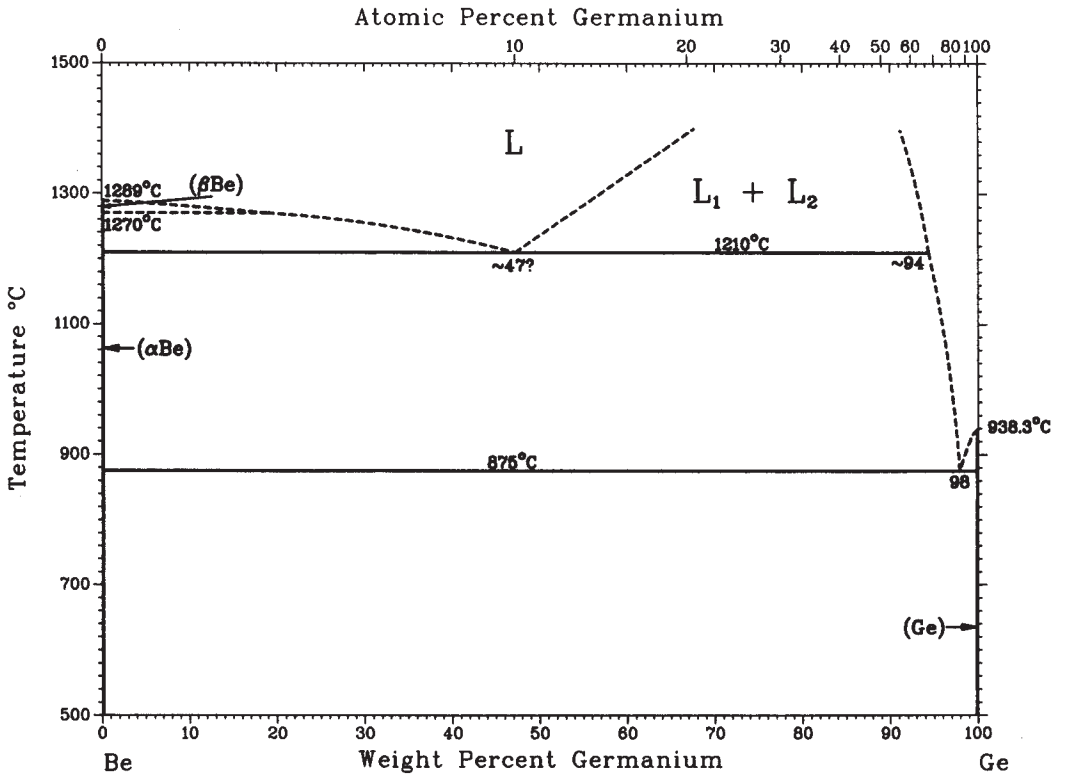

Fig. 15.11 Binary phase diagram of beryllium-germanium. Source: Okamoto et al. 1987b

intermediate phase, Be_3Nb, melts at approximately 1920 °C (3490 °F).

15.18 Beryllium-Plutonium (Be-Pu)

Figure 15.18. This system has only one intermetallic compound, $PuBe_{13}$, which melts congruently at approximately 1950 °C (3540 °F). There is no solid solubility of plutonium in beryllium or of beryllium in any of the allotropic forms of plutonium. There could be a subliquidus miscibility gap on the plutonium-rich side of this system.

15.19 Beryllium-Silicon (Be-Si)

Figure 15.19. This system is a simple eutectic with a eutectic composition of 64 wt% Si or 36 at.% Si and a eutectic temperature of 1090 °C (1995 °F). There is a negligible solid solubility of beryllium in silicon, and less than 0.3 at.% Si is soluble in beryllium.

15.20 Beryllium-Tin (Be-Sn)

Figure 15.20. This system is a monotectic with a wide liquid miscibility gap and a monotectic temperature of approximately 1276 °C (2330 °F). There is no solid solubility of tin in beryllium, and approximately 1 at.% Be is soluble in solid tin. The reaction at the tin-rich side may be a peritectic, but the temperature is not known accurately.

15.21 Beryllium-Titanium (Be-Ti)

Figure 15.21. This system has four intermediate intermetallic phases, only one of which, Ti_2Be_{17}, melts congruently. There may be two allotropic forms of this compound, but these are not shown in the diagram. The $TiBe_{12}$ melts peritectically at 1550 °C (2820 °F), and there are conflicting reports about its structure, which could be either tetragonal or hexagonal. There is no reported solubility between titanium and beryllium up to 882 °C (1620 °F).

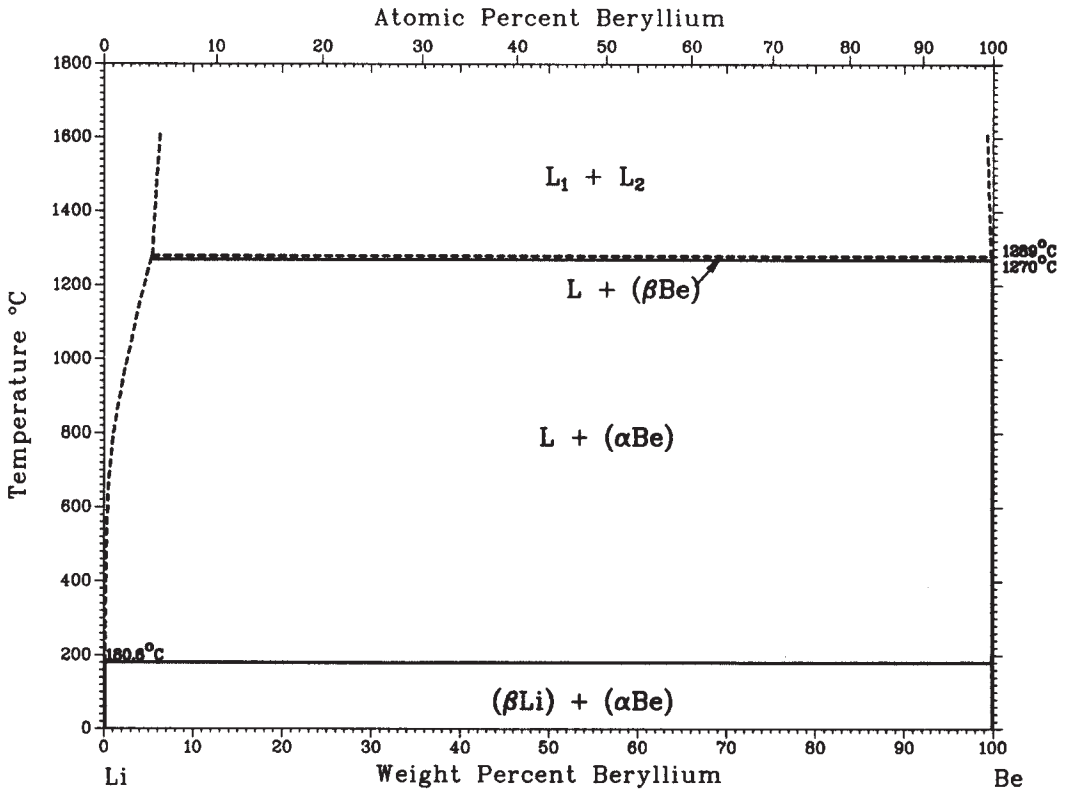

Fig. 15.12 Binary phase diagram of beryllium-lithium. Source: Pelton 1987a

However, the maximum solid solubility of beryllium in body-centered cubic titanium is 5 at.% or approximately 2 wt%. The eutectic temperature between beta-titanium and $TiBe_2$ is approximately 960 °C (1760 °F), and the eutectoid transformation temperature is approximately 810 °C (1490 °F). The compound $TiBe_2$ melts peritectically at 1360 °C (2480 °F) and is a C-15 Laves phase. There is a metastable compound, TiBe, which has the ordered cubic CsCl crystal structure. It can be formed by quenching from the liquid or by precipitation from the amorphous phase that is formed by quenching molten alloy compositions near the eutectic temperature.

15.22 Beryllium-Uranium (Be-U)

Figure 15.22. No solid solubility of beryllium in any of the allotropic forms of uranium or of uranium in beryllium has been observed. There is one compound, UBe_{13}, that melts congruently at approximately 2000 °C (3630 °F). The monotectic on the beryllium-rich side of this diagram is somewhat controversial, and it may be more appropriate to consider this as a metastable miscibility gap lying below the liquidus temperature, similar to the beryllium-aluminum system.

15.23 Beryllium-Tungsten (Be-W)

Figure 15.23. The solid solubility of tungsten in beryllium is not measurable, while the solubility of beryllium in tungsten ranges from 3 at.% between 1000 and 1500 °C (1830 and 2730 °F) up to 5 at.% at 2100 °C (3810 °F). This is approximately the temperature of the Be_2W:W eutectic. Be_2W melts congruently at 2250 °C (4080 °F) and appears to have a homogeneity range between 3 at.% and 5 at.% Be. $Be_{12}W$ melts peritectically at approximately 1750 °C (3180 °F), and the compound $Be_{22}W$ melts

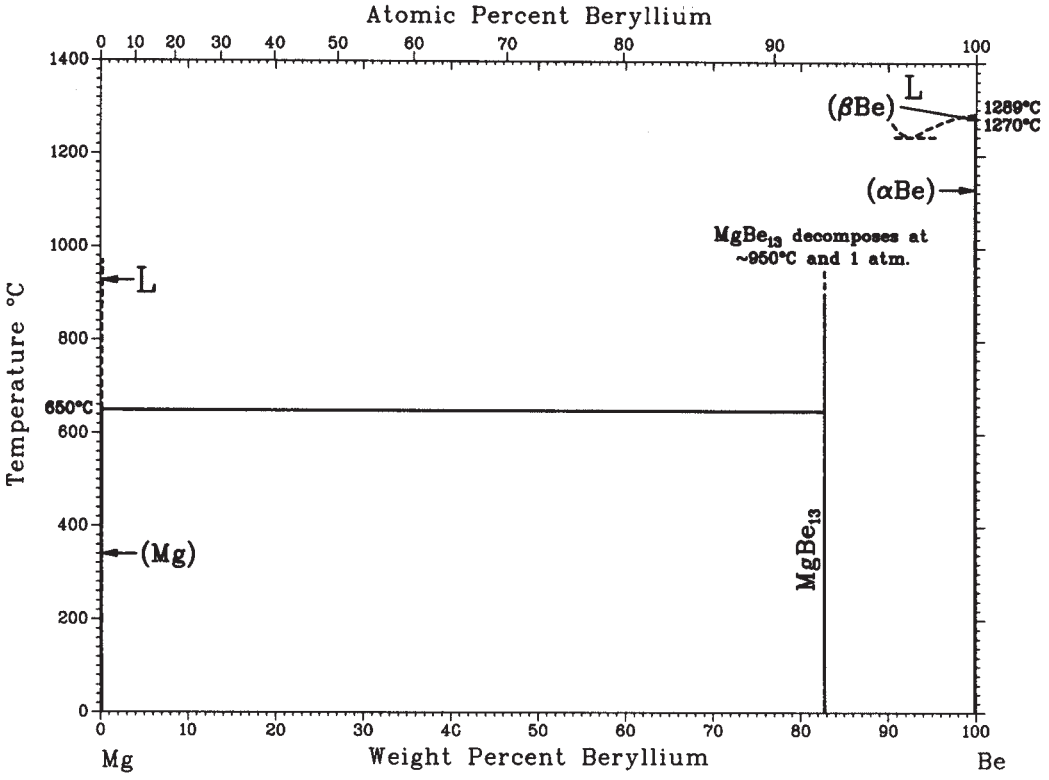

Fig. 15.13 Binary phase diagram of beryllium-magnesium. Source: Nayeb-Hashemi and Clark 1987

peritectically at a lower but as yet unmeasured temperature.

15.24 Beryllium-Yttrium (Be-Y)

Figure 15.24. The beryllium-yttrium system has only one intermetallic compound, YBe_{13}, which melts congruently at approximately 1920 °C (3490 °F). There is no solid solubility of either element in the other. The eutectic composition at the beryllium-rich end of the diagram is approximately 0.5 to 1 wt% Y.

15.25 Beryllium-Zinc (Be-Zn)

Figure 15.25. This system exhibits a classic monotectic at a temperature somewhat below 1200 °C (2190 °F). The solubility of zinc in beryllium at this temperature is approximately 0.8 at.%. There is no solid solubility of beryllium in zinc. The peak of the two-liquid phase region is at approximately 1578 °C (2870 °F) and 50 at.% Zn.

15.26 Beryllium-Zirconium (Be-Zr)

Figure 15.26. The beryllium-zirconium system is a very complex one, with four stable intermetallic compounds and one metastable compound. The beryllium terminal solid solution contains only 0.03 at.% Zr. Beginning with the compound $ZrBe_{13}$, the melting point is 1800 °C (3270 °F), and it melts congruently. The next compound, Zr_2Be_{17}, melts peritectically at 1590 °C (2895 °F), and Be_5Zr melts at 1475 °C (2690 °F), also peritectically. The compound $ZrBe_2$, a Laves phase, melts peritectically at 1235 °C (2255 °F). Body-centered cubic zirconium has a maximum solubility of beryllium of approximately 4 at.% at 965 °C (1770 °F). This is the eutectic melting point at a eutectic composition of approximately 65 at.% or 95 wt% Zr. Alpha, or hexagonal, zirconium below 863 °C (1585 °F) has

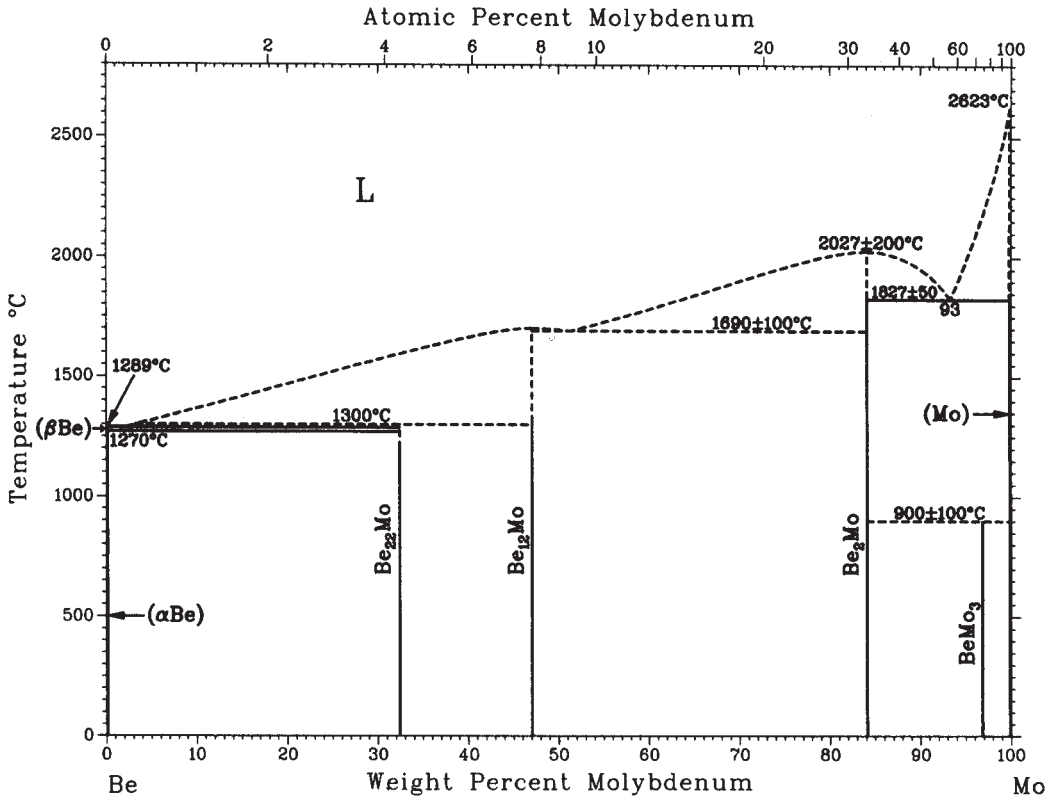

Fig. 15.14 Binary phase diagram of beryllium-molybdenum. Source: Okamoto et al. 1987c

practically no solubility for beryllium. Compositions between 55 and 70 at.% can be quenched from the melt and retained in an amorphous state. A metastable phase, BeZr, can be formed from the quenched liquid but does not form upon recrystallization of the glass.

REFERENCES

Chakrabarti, D.J., Laughlin, D.E., and Tanner, L.E., 1987. Copper-Beryllium Phase Diagram, *Bull. Alloy Phase Diagrams*, Vol 8 (No. 3)

Gschneidner, K.A., Jr., and Calderwood, F.W., 1987. Beryllium-Yttrium Phase Diagram, *Phase Diagrams of Binary Beryllium Alloys*, ASM International

Itkin, V.P., Alcock, C.B., Okamoto, H., and Tanner, L.E., 1987. Beryllium-Calcium Phase Diagram, *Phase Diagrams of Binary Beryllium Alloys*, ASM International

Murray, J.L., 1987. Beryllium-Titanium Phase Diagram, *Phase Diagrams of Binary Beryllium Alloys*, ASM International

Murray, J.L., and Kahan, D.J., 1988. The Beryllium-Aluminum Phase Diagram, *Phase Diagrams of Binary Beryllium Alloys*, ASM International

Nayeb-Hashemi, A.A., and Clark, J.B., 1987. Beryllium-Magnesium Phase Diagram, *Phase Diagrams of Binary Magnesium Alloys*, ASM International

Okamoto, H., and Massalski, T.B., 1987. The Beryllium-Gold Phase Diagram, *Phase Diagrams of Binary Beryllium Alloys*, ASM International

Okamoto, H., and Tanner, L.E., 1987a. Beryllium-Niobium Phase Diagram, *Phase Diagrams of Binary Beryllium Alloys*, ASM International

Okamoto, H., and Tanner, L.E., 1987b. Beryllium-Silicon Phase Diagram, *Phase Diagrams of Binary Beryllium Alloys*, ASM International

Okamoto, H., and Tanner, L.E., 1987c. Beryllium-Tin Phase Diagram, *Phase Diagrams of Binary Beryllium Alloys*, ASM International

Okamoto, H., and Tanner, L.E., 1987d. Beryllium-Zinc Phase Diagram, *Phase Diagrams of Binary Beryllium Alloys*, ASM International

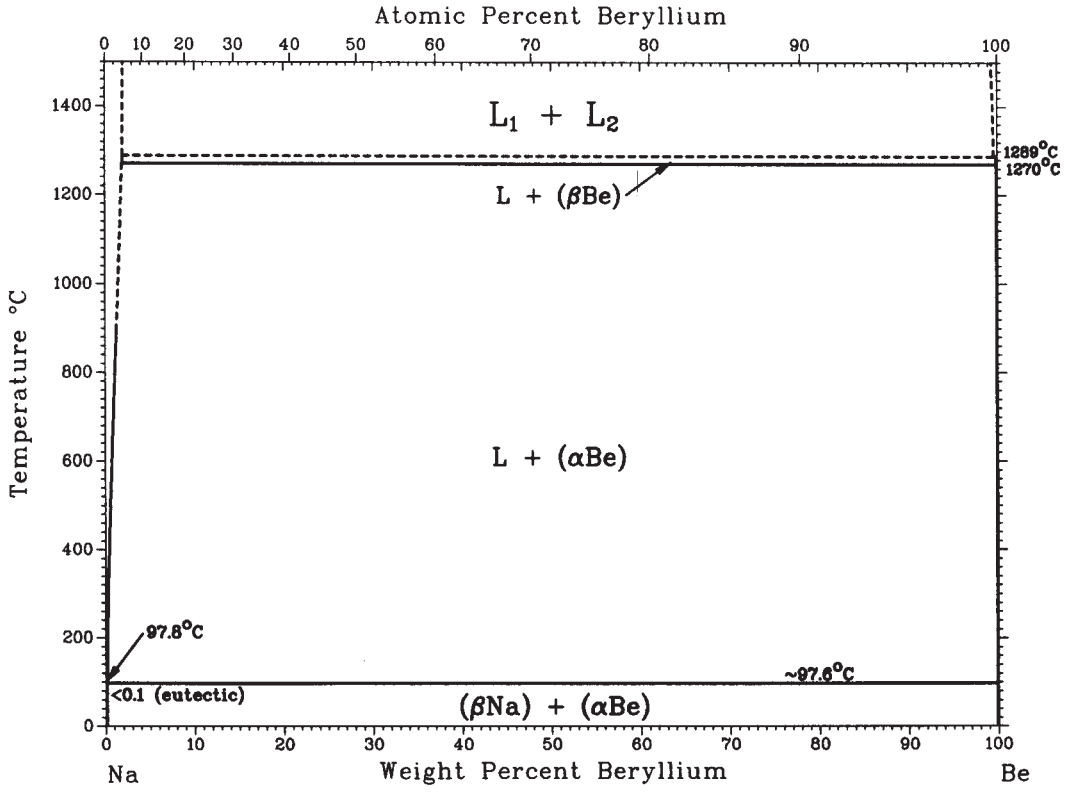

Fig. 15.15 Binary phase diagram of beryllium-sodium. Source: Pelton 1987b

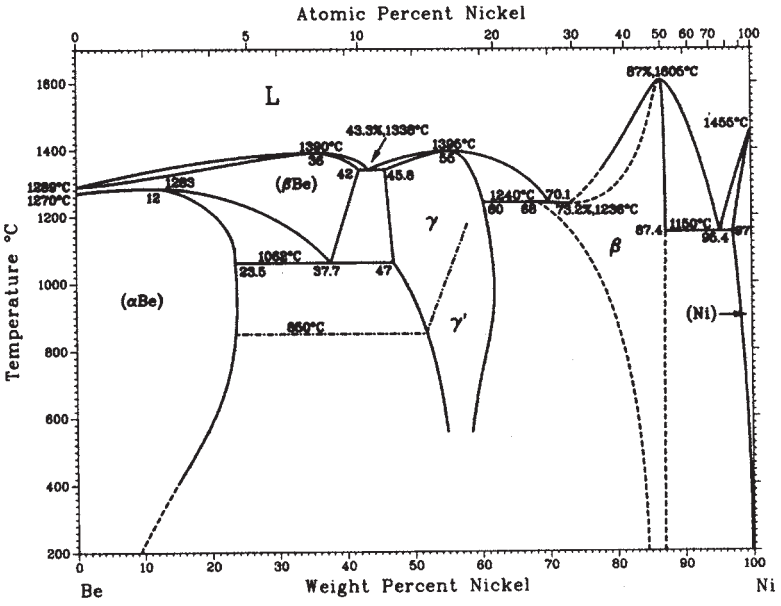

Fig. 15.16 Binary phase diagram of beryllium-nickel. The placement of the dashed line in the γ/γ′phase field is arbitrary. Source: Okamoto et al. 1991

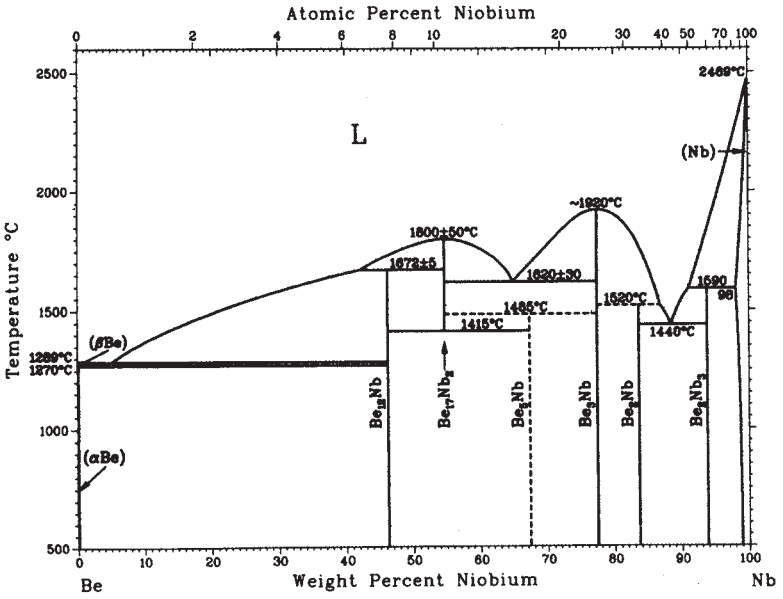

Fig. 15.17 Binary phase diagram of beryllium-niobium. Source: Okamoto and Tanner 1987a

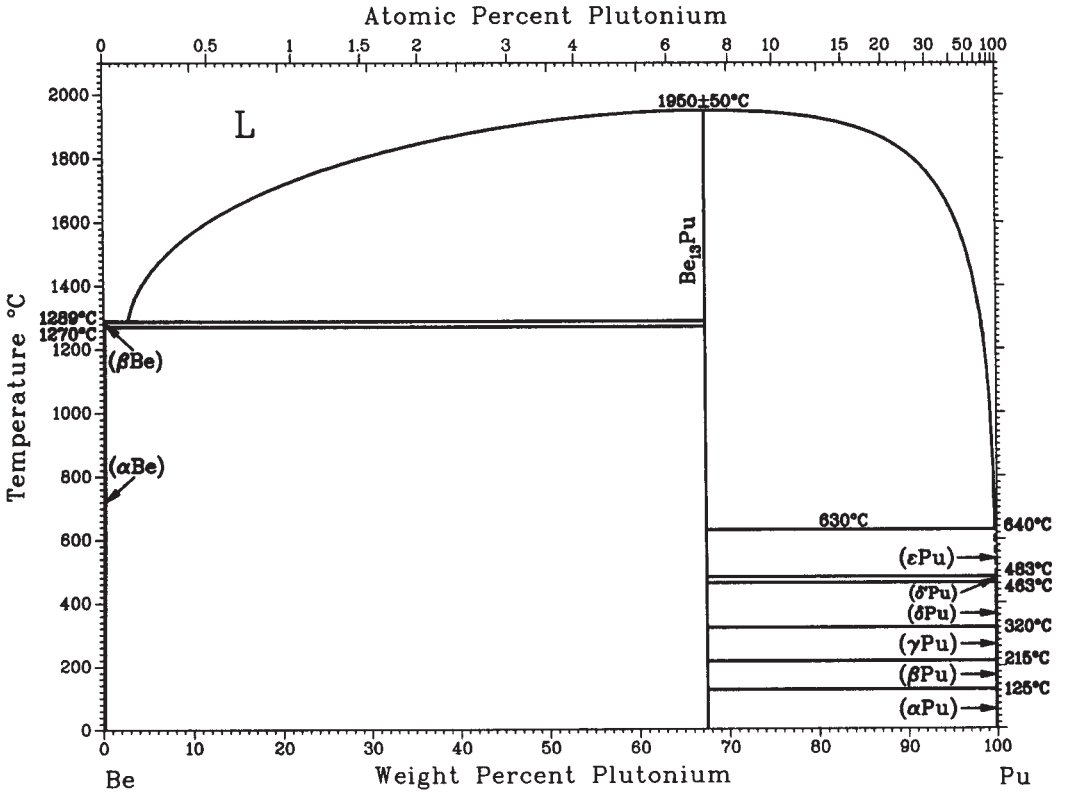

Fig. 15.18 Binary phase diagram of beryllium-plutonium. Source: Okamoto et al. 1987d

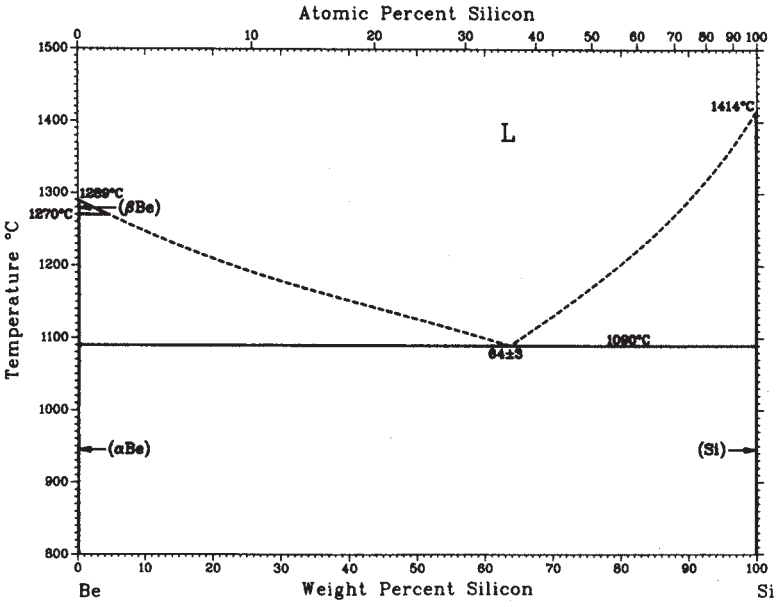

Fig. 15.19 Binary phase diagram of beryllium-silicon. Source: Okamoto and Tanner 1987b

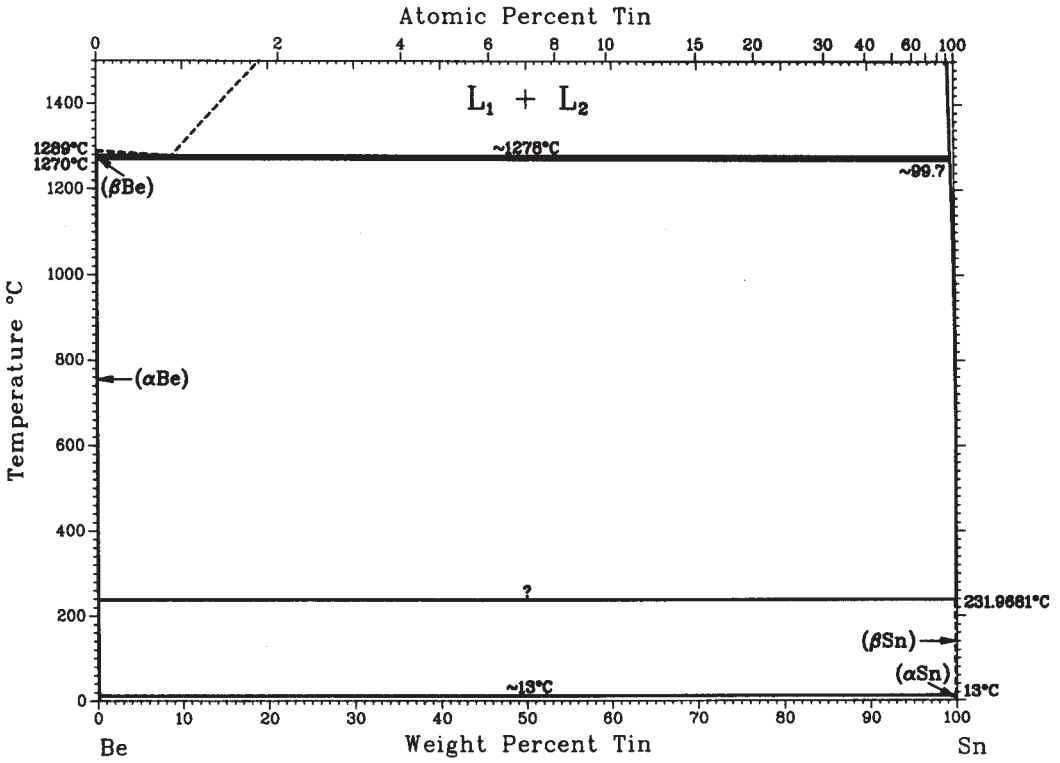

Fig. 15.20 Binary phase diagram of beryllium-tin. Source: Okamoto and Tanner 1987c

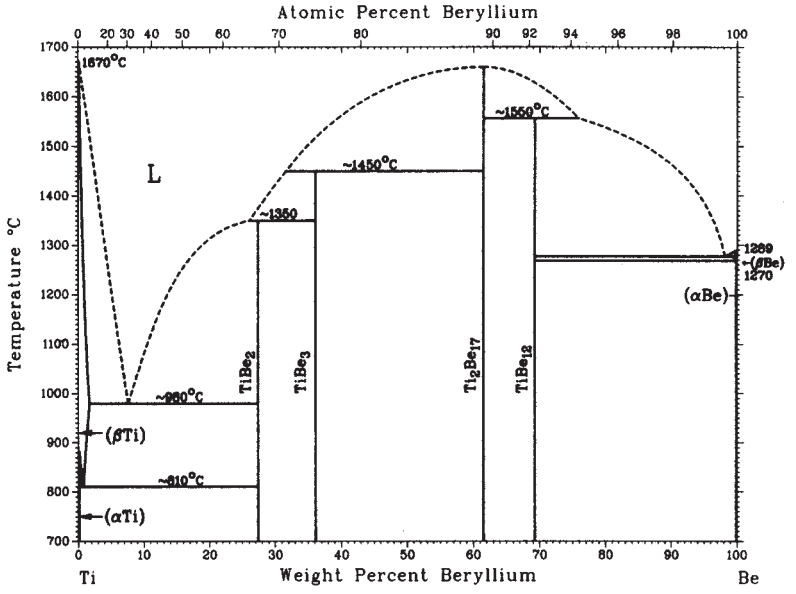

Fig. 15.21 Binary phase diagram of beryllium-titanium. Source: Murray 1987

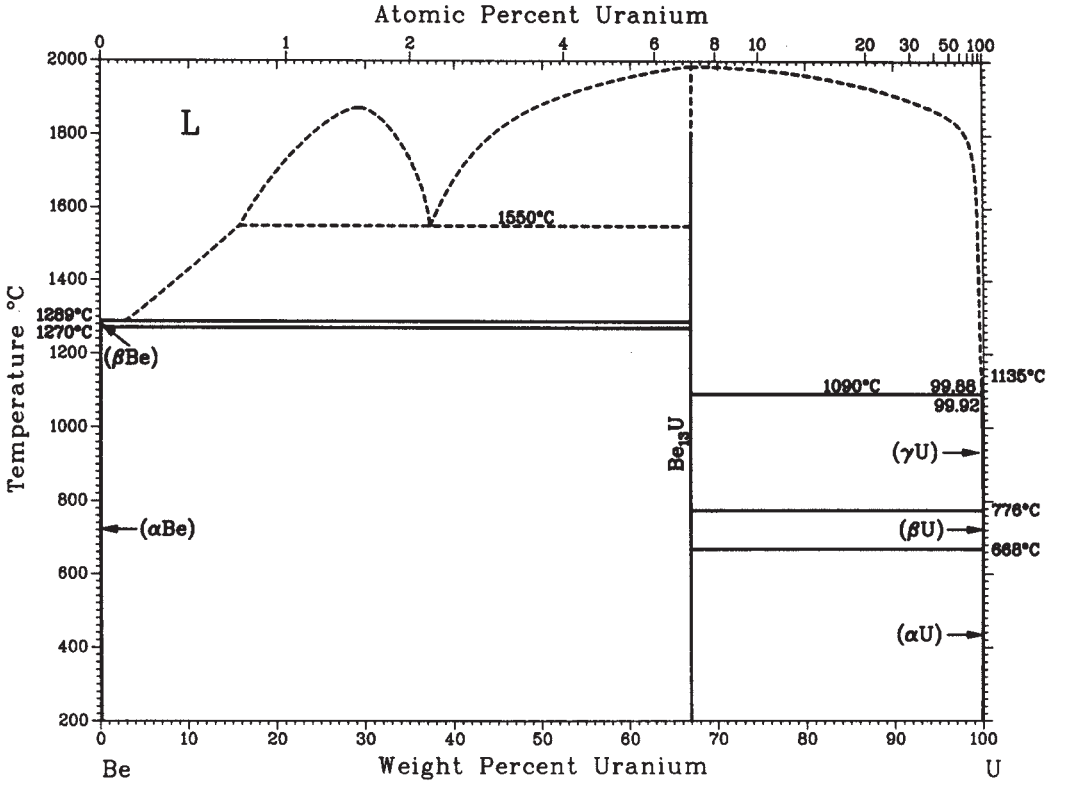

Fig. 15.22 Binary phase diagram of beryllium-uranium. Source: Okamoto et al. 1987e

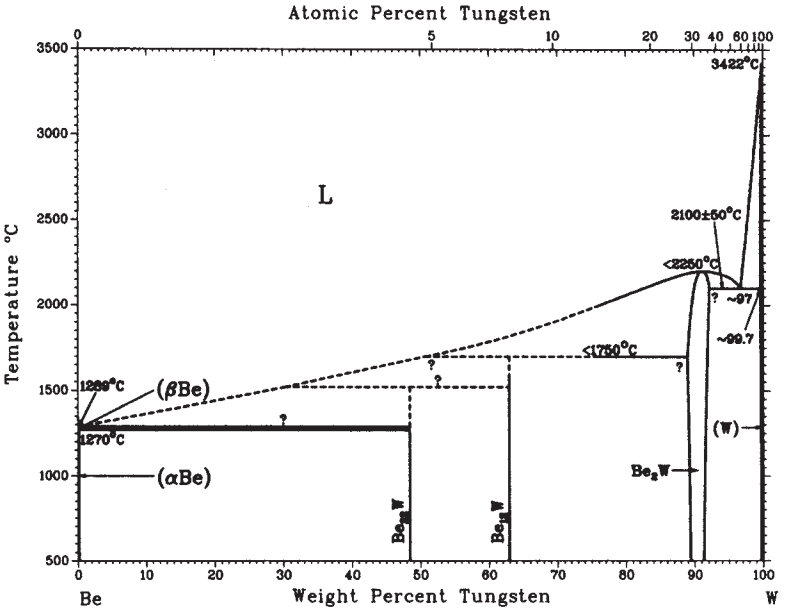

Fig. 15.23 Binary phase diagram of beryllium-tungsten. Source: Okamoto and Tanner 1991

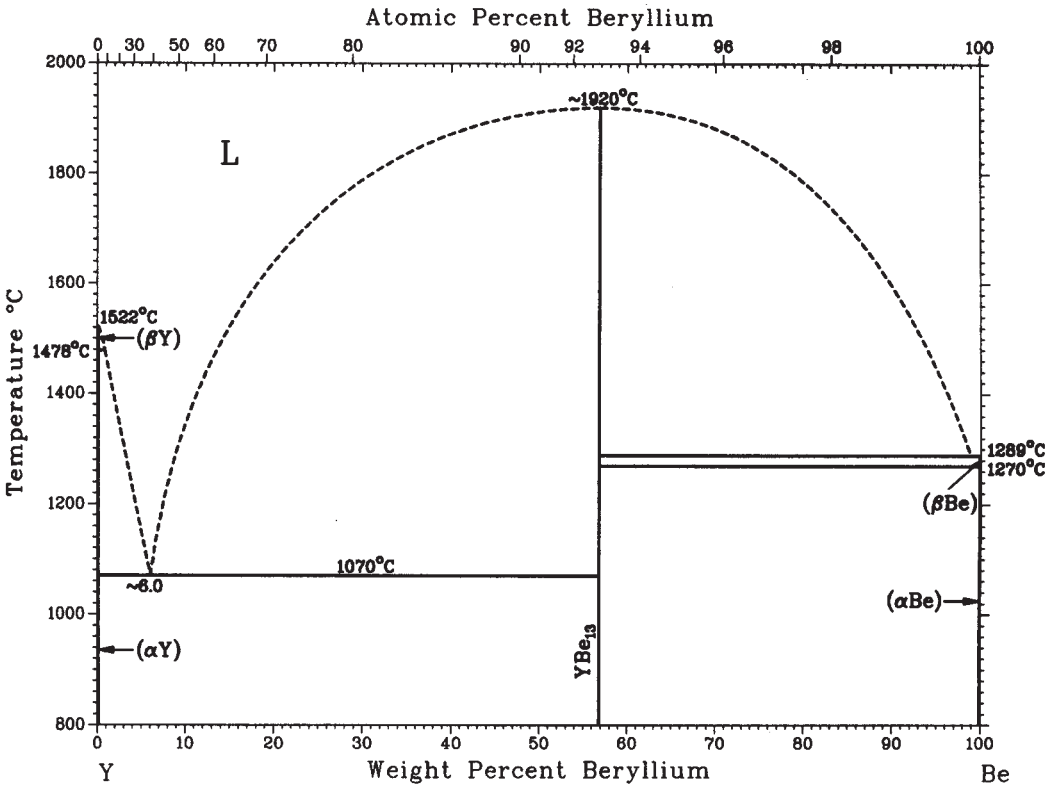

Fig. 15.24 Binary phase diagram of beryllium-yttrium. Source: Gschneidner and Calderwood 1987

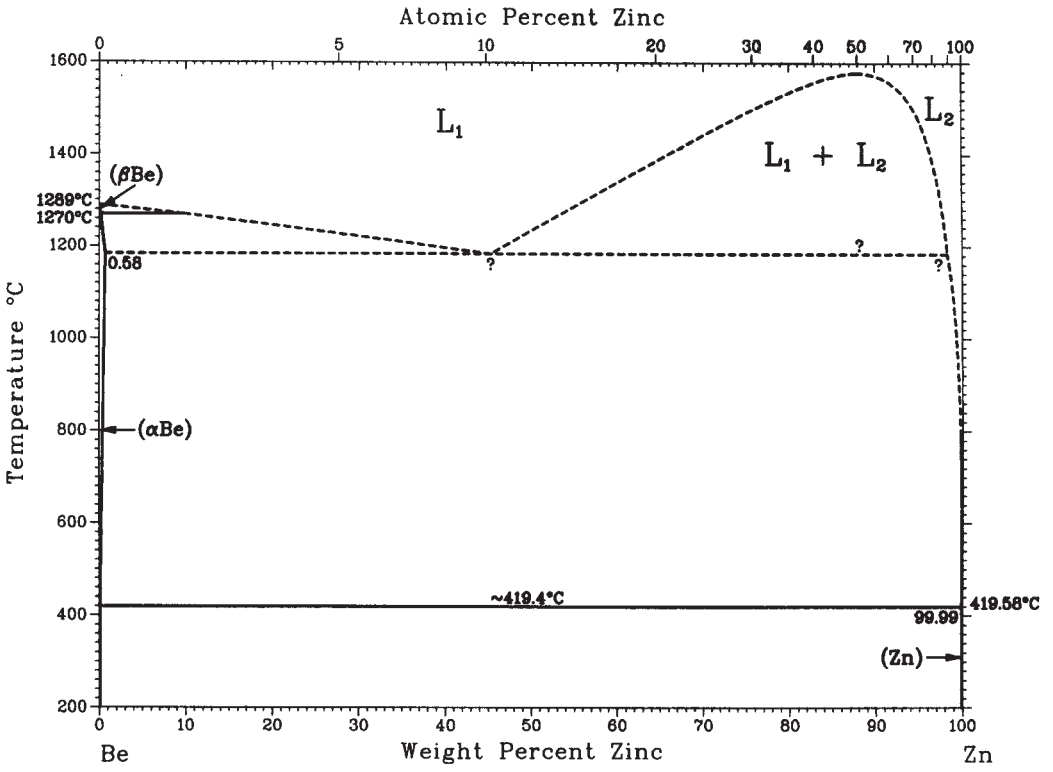

Fig. 15.25 Binary phase diagram of beryllium-zinc. Source: Okamoto and Tanner 1987d

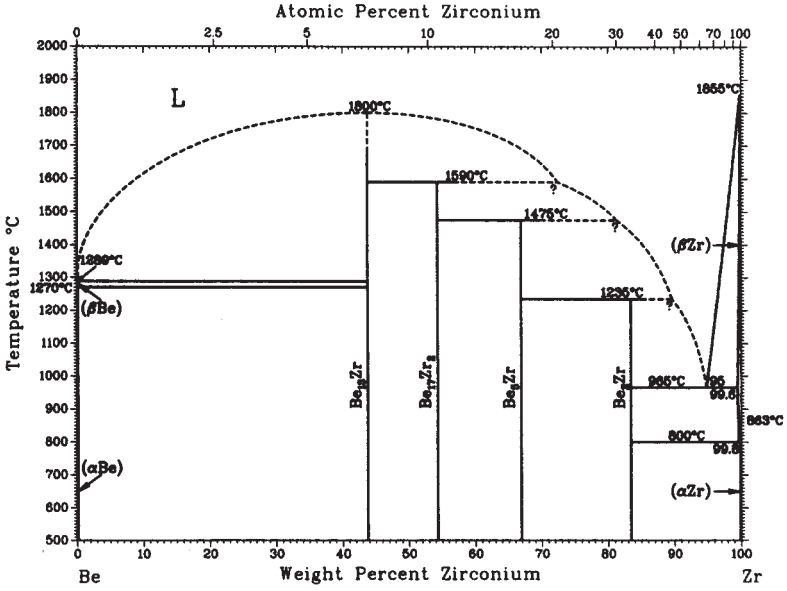

Fig. 15.26 Binary phase diagram of beryllium-zirconium. Phase boundaries are based on a thermodynamic model. Source: Okamoto, et al. 1987

Okamoto, H., and Tanner, L.E., 1987e. The Silver-Beryllium Binary Phase Diagram, *Phase Diagrams of Binary Beryllium Alloys*, ASM International

Okamoto, H., and Tanner, L.E., 1988. Beryllium-Boron Phase Diagram, *Phase Diagrams of Binary Beryllium Alloys*, ASM International

Okamoto, H., and Tanner, L.E., 1991. Beryllium-Tungsten Phase Diagram, *Phase Diagrams of Binary Tungsten Alloys*, The Indian Institute of Metals

Okamoto, H., Tanner, L.E., and Abriata, J.P., 1987. Beryllium-Zirconium Phase Diagram, *Phase Diagrams of Binary Beryllium Alloys*, ASM International

Okamoto, H., Tanner, L.E., Itkin, V.P., and Alcock, C.B., 1987. Beryllium-Barium Phase Diagram, *Phase Diagrams of Binary Beryllium Alloys*, ASM International

Okamoto, H., Tanner, L.E., and Nishizawa, T., 1988. Cobalt-Beryllium Phase Diagram, *Bull. Alloy Phase Diagrams*, Vol 9 (No. 5)

Okamoto, H., Tanner, L.E., and Peterson, D.E., 1987a. Beryllium-Gallium Phase Diagram, *Phase Diagrams of Binary Beryllium Alloys*, ASM International

Okamoto, H., Tanner, L.E., and Peterson, D.E., 1987b. Beryllium-Germanium Phase Diagram, *Phase Diagrams of Binary Beryllium Alloys*, ASM International

Okamoto, H., Tanner, L.E., and Peterson, D.E., 1987c. Beryllium-Molybdenum Phase Diagram, *Phase Diagrams of Binary Beryllium Alloys*, ASM International

Okamoto, H., Tanner, L.E., and Peterson, D.E., 1987d. Beryllium-Plutonium Phase Diagram, *Phase Diagrams of Binary Beryllium Alloys*, ASM International

Okamoto, H., Tanner, L.E., and Peterson, D.E., 1987e. Beryllium-Uranium Phase Diagram, *Phase Diagrams of Binary Beryllium Alloys*, ASM International

Okamoto, H., Tanner, L.E., and Peterson, D.E., 1991. Beryllium-Nickel Phase Diagram, *Phase Diagrams of Binary Nickel Alloys*, ASM International

Okamoto, H., Tanner, L.E., and Peterson, D.E., 1993. Iron-Beryllium Phase Diagram, *Phase Diagrams of Binary Iron Alloys*, ASM International

Pelton, A.D., 1987a. Beryllium-Lithium Phase Diagram, *Phase Diagrams of Binary Beryllium Alloys*, ASM International

Pelton, A.D., 1987b. Beryllium-Sodium Phase Diagram, *Phase Diagrams of Binary Beryllium Alloys*, ASM International

SELECTED REFERENCES

- Geller, R.F., Yavorsky, P.J., Steieman, B.L., and Creamer, A.S., 1946. Studies of Binary and Ternary Combinations of Magnesia, Calcia, Baria, Beryllia, Alumina, Titania, and Zirconia in Relation to Their Use as Porcelains, *J. Natl. Bur. Stand.*, Vol 36, p 277–308
- Golbeck, O., 1965. Phase Diagrams, *Beryllium: Physico-Chemical Properties of Its Compounds and Alloys*, O. Kubaschewski, Ed., Atomic Energy Review-UNIPUB, New York, NY, p 45–61
- Hansen, M., and Anderko, K., 1958. *Constitution of Binary Alloys*, McGraw-Hill, New York, NY
- Harkness, J.C., Spiegelberg, W.D., and Cribb, W.R., 1990. Beryllium Copper and Other Beryllium Containing Alloys, *Properties and Selection: Nonferrous Alloys and Special-Purpose Materials*, Vol 2, *Metals Handbook*, 10th ed., ASM International
- Stonehouse, A.J., 1971. Beryllium-Antimony Composition, U.S. Patent 3,574,608
- Tanner, L.E., 1980. The Stable and Metastable Phase Relations in the Hf-Be Alloy System, *Acta Metall.*, Vol 28 (No. 12), p 1805–1816

Beryllium Chemistry and Processing, p 199-208
By Kenneth A. Walsh
Edited by Edgar E. Vidal, Alfred Goldberg,
Edward N.C. Dalder, David L. Olson, and Brajendra Mishra

CHAPTER 16

Metallography of Beryllium and Beryllium Alloys

David L. Olson, Colorado School of Mines
Edgar E. Vidal, Brush Wellman, Inc.

METALLOGRAPHY OF BERYLLIUM has been reported as early as the 1930s when Sloman [1932] identified phases attributable to carbon, iron, and silicon. In general, the metallography of beryllium has not been found to offer much difficulty, with the exception of the important issues of dealing with the toxicity of the dust that develops during cutting, grinding, and polishing. All these procedures should be carried out under a hood, and the necessary safety precautions in handling beryllium are to be applied. Proper preparation of the specimens presents a considerable problem. Since most beryllium metal contains a certain amount of hard constituents (primarily BeO), which are readily pulled out of the metallic matrix, the beryllium specimens must be polished very carefully.

16.1 Specimen Extraction

For preparation of metallographic specimens, beryllium is either sawed or cut on an abrasive wheel to a convenient size, which should not be more than 6.35 mm (0.25 in.) square. For best results in mounting and polishing, Bakelite mountings are preferred.

16.2 Grinding Procedures

Two alternative grinding procedures have been reported by Dingle and Moore [1962]. Mechanical grinding through a series of abrasive disks with successively finer grit sizes gives satisfactory results. The specimen should be rotated 90° between disks.

In one procedure, specimens are ground successively on 120-, 240-, 400-, and 600-grit wet or dry metallographic discs. Depending on the initial condition of the specimen, the coarsest disk, 120 grit, may sometimes be omitted. In other instances, the grinding may be terminated after the 400-grit disk, thus eliminating the 600-grit operation. Water may be used on all but the final disk, which is best used dry. Kerosene lubrication may also be used. Pressures should be extremely light, barely enough to keep the specimen against the disk. Only sharp disks should be used. The abrasive discs are revolved at 1750 rpm on a conventional pedestal grinder. The coarsest disc (120 grit) is used either wet or dry, and it can usually be eliminated from the procedure. Grinding on the two finer discs (240 and 400 grit) is accompanied by the application of kerosene. The technique consists of holding an oil can containing kerosene in one hand and the mounted specimen in the other hand. While the grinding is being done, several drops of kerosene are applied every few seconds close to the center of the disc. Light oils and water are not satisfactory for the finer grinding operations.

Wet rough grinding holds and carries away dust generated during operation. Disks of waterproof silicon carbide grinding paper are mounted on a wheel rotating at approximately 1150 rpm. Grit sizes of 120, 240, 320, 400, and 600 are used. Care must be taken to prevent deformation

twinning, and ample time must be allowed at each grinding step to remove damage caused by previous operations.

The second procedure is perhaps slightly slower than the first and requires a more careful technique, but it eliminates the use of kerosene. The specimen is first ground wet on a 240-grit disc, followed by dry grinding on a 400-grit disc.

In a third procedure, rough polishing is performed using a 550 rpm wheel, a chemo-textile cloth with adhesive backing, and a medium-light concentration of 8 to 22 μm diamond compound. The specimen should be frequently rotated counter to the direction of wheel rotation. Heavy pressure is used to maximize material removal, although excessive pressure may introduce mechanical twins. Polishing time is approximately 2 min.

Fine polishing is carried out using a 550 rpm wheel, an adhesive-backed rayon cloth, and a medium-light concentration of 1 to 5 μm diamond compound. The mount should be frequently rotated counter to the direction of wheel rotation. Heavy-to-medium hand pressure is used to maximize removal of material. Polishing time is approximately 3 min.

The final fine polishing is performed using a 550 rpm wheel, an adhesive-backed rayon cloth, and a 0.05 μm deagglomerated alumina (Al_2O_3) in a water slurry. Final polishing takes approximately 3 to 5 min. The specimen should appear flat and essentially free of most scratches.

An attack-polish procedure may also be used. Initial polishing is performed using Al_2O_3 abrasive on a short-nap cloth at 1750 rpm. A 5 to 10% aqueous oxalic acid solution is used with the Al_2O_3 to achieve simultaneous chemical attack and mechanical polish. Final polishing is then performed using γ-Al_2O_3 and the aqueous oxalic acid solution on a medium-nap cloth at 1750 rpm. Water, instead of oxalic acid solution, is used to keep the wheel moist during the last few seconds of final polishing. Care must be taken to maintain the proper balance between chemical attack and abrasive action to achieve optimal polishing conditions. Polishing times are approximately 1 min for each wheel. Vibratory polishing and electrolytic polishing of beryllium have also been used [Buchheit et al. 1959].

The hard constituents are readily chipped and pulled out of the matrix and may seriously scratch the specimen. On the other hand, soft constituents are easily gouged out or embedded with abrasive or other material. The matrix itself is easily deformed, which makes it difficult to remove the effects of scratching. In addition, rough handling can cause twinning. As a further difficulty, the matrix and some of the constituents are readily pitted during etching, which makes the structure difficult to develop.

The preparation of the specimen may be considered more than half done when a satisfactory rough grind has been obtained. The specimen should be examined, for example, at a magnification of 500×, before starting the polishing operation. The operator, after some experience, is able to judge whether or not grinding has been accomplished without deforming the surface of the matrix or removing any hard, brittle constituents. If there is evidence that successful grinding has not been accomplished, it is well to start over, since it is a waste of time to polish an improperly ground surface.

Grinding procedures of various metallographers are compared in Table 16.1. The only practice notably different from that described previously is that of Frye [1953], whose technique is used for corroded metal and is intended to preserve the corrosion products. It uses a series of three conventional lead laps with carefully sized emery abrasives.

Battelle Memorial Institute [Buchheit et al. 1959] has suggested procedures for the metallographic preparation of beryllium, which recommends grinding of the specimens with extremely light pressure on a disc grinder, using successively finer and sharper grits to No. 400, followed by hand polishing, using a 5 vol% solution of oxalic acid to etch and polish simultaneously. This method, however, has the disadvantage that inclusions such as BeC are lost during the polishing cycle by the use of oxalic acid. For etching, a 10 vol% solution of 48 vol% HF in 19-proof ethyl alcohol is provided. Most of the beryllium specimens, however, are examined unetched in polarized light.

16.3 Polishing Procedures

16.3.1 Mechanical Polishing

Bennett [1960] gives the following information on the metallography of beryllium: The samples were machined to size, mounted in Bakelite, and ground by hand on a series of graded silicon carbide papers, using kerosene as a lubricant. Three different methods of polishing have been used. The first involved polishing through 6, 3, and 1 μm grades of diamond compound, using kerosene lubrication; the method introduces a minimum of cold work and surface deformation

Table 16.1 Grinding procedures used at various laboratories

Procedure	Remarks	Metallographer
1. Mechanical grinding on 120-, 240-, and 400-grit polishing papers. Rotate 90° between papers. Lubricant not indicated	To be followed by electrolytic polishing and etching	Noland et al. [1948]
2. Mechanical grinding (1750 rpm) on successive 120-, 240-, and 400-grit discs. Use 120-grit disc wet or dry; may usually be eliminated. Finer discs lubricated with kerosene	Pressures should be extremely light. Discs should be sharp, then discarded when they show evidence of becoming dull or loaded. To be followed by mechanical polishing	Udy et al. [1949]
3. Mechanical grinding (1750 rpm) on 240- and 400-grit discs. Use 240-grit disc wet and 400-grit disc dry. Occasionally, it is necessary to go through a 600-grit disc. Only the final disc is used dry	Pressures should be extremely light. Discs should be sharp, then discarded when they show evidence of becoming dull or loaded. To be followed by mechanical polishing	Udy et al. [1949], Doig and Schwartz [1953]
4. Mechanical grinding wet on 150-, 320-, 400-, and 600-grit silicon carbide papers. Rotate specimen 90° between each paper	To be followed by mechanical or electrolytic polishing	Beaver and Magalski [1953]
5. Careful mechanical grinding on 120-, 240-, 400-, and 600-grit papers. Lubricant not indicated	To be followed by mechanical or electrolytic polishing	Czarkowski [1953]
6. Hand grinding, dry 320-grit silicon carbide, followed by 2/0 and 3/0 emery. Light pressure on final papers	To be followed by mechanical or electrolytic polishing	Kaufmann et al. [1950], Roth [1953]
7. Grinding through series of three conventional lead laps using carefully sized emery abrasive	To be followed by mechanical polishing	Frye [1953]
8. Mechanical grinding on 180-grit belt, then on 2/0 and 3/0 discs lubricated with kerosene	To be followed by mechanical polishing	Hausner and Pinto [1951]
9. Wet grinding on 240- and 600-grit paper	To be followed by etching and examination at relatively low magnification	Brick et al. [1950]

but is time-consuming and leaves fine surface scratches. No success was obtained with the ¼ μm size of diamond. The second method consisted of approximately 2 min on a high-speed, silk-covered wheel, using Linde B alumina (union carbide), followed by approximately 2 min on a high-speed wheel covered with Microcloth (Buehler Ltd.) and also using Linde B alumina. This method is rapid and effective but has not been adopted as regular practice because the fast polishing wheel is situated in an area where cleaning and ventilation services were considered inadequate. The third method, which was finally adopted, was, in some ways, a compromise between the first two methods just described. Because it appears to be the most satisfactory, the following description of the three steps involved is given in some detail:

1. A 6 μm diamond paste was spread on photographic paper mounted on a 152 mm (6 in.) wheel rotating at 500 rpm. Kerosene was used as a lubricant, and the specimen was considered satisfactory after 2 to 2.5 min.
2. A 3 μm diamond paste was spread on Microcloth mounted on an 89 mm (3.5 in.) wheel rotating at 500 rpm. Kerosene was used as a lubricant, and the polishing time was 2 to 2.5 min.
3. Polish-etch technique: Linde B alumina was used on a 152 mm (6 in.) wheel covered with Microcloth and rotating at 500 rpm. During polishing, ten drops of a 0.3 Vol% solution of oxalic acid were added to the center of the pad every 20 s. After approximately 2 min, the specimen surface was satisfactory for examination under polarized light.

Some difficulty was experienced in clearly outlining the grain boundaries of longitudinal-cut specimens under polarized light. The effect has been attributed to the high degree of preferred orientation in the part. To overcome this effect, numerous etchants recommended in the literature were tried, and although most produced heavy pitting at the oxide inclusions, an oxalic acid etch has been modified to give very satisfactory grain-boundary definition. The etch involves dipping the specimen in 3 vol% oxalic acid at 100 °C (212 °F) for 1 min.

Straight mechanical polishing is carried out in two steps. The initial polishing is accomplished on a high-speed wheel with a hard, short-nap cloth. An alumina abrasive is preferred, although silicon carbide, rouge (iron oxide), or diamond paste may be used. Except for special purposes, which are noted later, water suspensions of the abrasives are satisfactory. Only a short polishing time is needed.

Final polishing is accomplished on a high-speed wheel covered with a softer, longer-napped cloth than that used for the initial polish. Fine gamma-alumina powder is the preferred abrasive, but rouge, chromic oxide, or diamond paste also give good results. Water suspensions are

suitable, except as noted later. Times of the order of 1 min are usually sufficient.

Frye [1953] reported a procedure that preserves corrosion products in their beryllium specimen by using a diamond paste lubricated with suitable oils for both polishing operations, thus avoiding water.

A technique reported [Udy et al. 1949] for preserving certain soft constituents, such as the magnesium-rich phase sometimes present in beryllium, consists of polishing the specimen in one operation on a high-speed wheel covered with billiard cloth that has been loaded with magnesium oxide. The magnesium oxide is applied as a freshly prepared suspension in 30 vol% hydrogen peroxide. The peroxide holds the abrasive on the cloth better than water does and also inhibits reaction of soft inclusions with water. The polishing is actually done on a layer of magnesium oxide.

For mechanical polishing with an etchant on the wheel, the same types of cloths are used as for straight mechanical polishing. The abrasive, usually fine alumina, is suspended in a 5 to 10 vol% oxalic acid solution. Generally, only one polishing operation is needed: the final one with the finest abrasive. In this case, the hard, short-napped cloth is preferred.

16.3.2 Electropolishing

Various methods of electropolishing beryllium have been proposed, and, where details were available, experiments were made with the electrolytes. Two solutions proved successful with the 1arge-grained Pechiney beryllium, and conditions for use of these two solutions are given as follows. Both procedures originate from a Harwell method described by White and Burke [1955]:

Solution	Processing parameters
Solution 1	
100 mL phosphoric acid	Current density = 0.2 A/cm^2
100 mL H_2SO_4	2 min polishing time
100 mL absolute ethanol	Molybdenum cathode
300 mL glycerol	
Solution 2	
100 mL phosphoric acid	Current density = 2.0 A/cm^2
30 mL H_2SO_4	1 min polishing time
30 mL absolute ethanol	Molybdenum cathode
30 mL glycerol	

For the bulk of beryllium used, electropolishing produces severe pitting at the finely dispersed oxide inclusions. It has therefore been abandoned in favor of mechanical polishing for the routine preparation of beryllium. The polishing procedures used at various laboratories and production plants where beryllium metallography is done vary to a large extent, as revealed in Table 16.2.

16.3.3 Electrolytic Polishing

The electrolytic polishing procedure practiced in this country uses the following solution: 900 mL H_3PO_4, 240 g CrO_3, and 200 mL H_2O. The specimen is anodically treated for 1 min at 70 to 80 °C (160 to 175 °F) with a current density of 250 A/cm^2. An inert cathode such as lead, stainless steel, or graphite is used. The amount of water should be kept to the minimum necessary to keep the CrO_3 in solution. The proportion of CrO_3 may be decreased to 200 g to minimize the necessary water. This polishing procedure always causes pitting and therefore is almost useless for impure or worked metal. It is good for pure metal in the cast or annealed condition.

A British-developed electrolytic polishing method may offer the advantage of less pitting and therefore more widespread useful application. The method uses the following solution: 100 mL H_3PO_4, 30 mL H_2SO_4, 30 mL glycerol, and 30 mL absolute ethanol. The specimen is anodically treated at room temperature at a current density of 2 to 4 A/cm^2. An inert cathode is used.

16.4 Etching Procedures

Once a beryllium or beryllium-rich alloy specimen has been properly prepared, microscopic examination presents no problem. It can be examined under polarized light for grain structure or under bright-field illumination for identification of inclusions or second phases. It can be photographed for record or report purposes, in black and white or in color.

The hard constituents are readily chipped and pulled out of the matrix and may seriously scratch the specimen. On the other hand, soft constituents are easily gouged out or embedded with abrasive or other material. The matrix itself is easily deformed, which makes it difficult to remove the effects of scratching. In addition, rough handling can cause twinning. As a further difficulty, the matrix and some constituents are readily pitted during etching, which makes the structure difficult to develop.

For examination under polarized light, etching after the polishing operation is not always necessary. Even for bright-field examination, some of the polishing procedures, electrolytic

Table 16.2 Polishing procedures used at various laboratories

Procedure	Remarks	Metallographer
1. Electrolytic with lead cathode. Current density: 250 A/cm^2 at 70–80 °C *Solution:* 900 mL H_3PO_4 240 g CrO_3 200 mL H_2O	Polish directly from 400-grit paper. Complete in 60 s. Cannot be done in Bakelite mount. To be followed by electrolytic etching	Sloman [1932]
2. Electrolytic with inert cathode. Current density: 2–4 A/cm^2 *Solution:* 100 mL H_3PO_4 30 mL H_2SO_4 30 mL glycerol 30 mL absolute ethanol	For examination of grain structure under polarized light. No further etching necessary	Mott and Haines [1951]
3. Mechanical. Worsted serge on wheel. 5 vol% oxalic acid in water used on wheel in conjunction with abrasive. Fine alumina is used sparingly. When soft constituents are present, levigated commercially pure ferric oxide is preferred.	Longer-nap cloths promote pitting. Proper polishing depends on a balance between chemical and abrasive action. Polishing can be completed in a few minutes.	Udy et al. [1949]
4. Mechanical. Linde A powder suspended in 5–10 vol% oxalic acid in water on billiard cloth or Forstmann's cloth. Same abrasive gave good results when used in silk first, followed by Gamal cloth.	. . .	Dickerson [1953]
5. Mechanical. Billiard cloth on wheel; Merck's heavy commercially pure MgO suspended in 30 vol% hydrogen peroxide is used liberally.	Usefulness of cloth improves with use. Polishing is actually done on layer of MgO instead of cloth. Peroxide holds MgO on cloth better than water with some alloy constituents. Suspension is unstable; it must be made fresh several times daily. Polishing can be completed in a few minutes.	Udy et al. [1949]
6. Mechanical. 600-grit silicon carbide on Buehler Metcloth followed by 1-μm Cr_2O_3 powder in water suspension on Buehler Miracloth	Polish first to study and photograph inclusions, then continue polishing before studying and photographing grains	Beaver and Magalski [1953]
7. Electrolytic with lead or graphite cathode. 250 A/cm^2 at 70–80 °C *Solution:* 225 mL H_3PO_4 60 g CrO_2 50 mL H_2O	This is the same solution used by Argonne National Laboratory.	Beaver and Magalski [1953]
8. Mechanical. Coarse Precisionite on Gamal cloth with minimum amount of water and heavy pressure. Followed, when necessary, by fine Precisionite on Gamal cloth	In most cases, final wheel is not necessary.	Czarkowski [1953]
9. Electrolytic: 2 mL HCl, 2 mL HNO_3, 2 mL $HClO_4$ (perchloric acid), 94 mL ethylene glycol; 10–16 V dc, 0.1 A/cm^2	. . .	Price and McCall [1968]
10. Electrolytic. Use stainless steel cathode. May decrease CrO_3 from 60 to 50 g	. . .	Czarkowski [1953]
11. Mechanical: (1) Silk cloth, Linde A in 10 vol% oxalic acid aqueous solution. 5–10 min. (2) Long-nap wool cloth such as Botany or fleece, Linde A in 10 vol% oxalic acid aqueous solution, 5–10 min. (3) Long-nap wool cloth, Linde B in 10 vol% aqueous solution, 2 min	For examination under polarized light. No etch needed	Kaufmann et al. [1950], Roth [1953]
12. Mechanical: (1) Silk cloth, Linde A in 10 vol% oxalic acid aqueous solution, 2 min	For examination under bright light. Followed by etch, if necessary	Kaufmann et al. [1950], Roth [1953]
13. Electrolytic: Minimum amount of water used	This procedure always causes pitting and therefore is almost useless for impure or worked metal. It is good for pure metal in the cast or annealed condition.	Roth [1953]
14. Mechanical: 30 μm diamond paste on canvas wheel; then 6 μm diamond paste on a woven, napped cloth; and finally, 1 μm diamond paste on a synthetic metallographic cloth. Polishing is done in absence of water using recommended oils as a lubricant.	No etchant used	Frye [1953]
15. Mechanical: Silk-covered bronze disc 2–5 min. Solution of 10 g oxalic acid in 100 g H_2O to which 5–8 g Linde A powder is added. Followed by 2–3 min on Gamal cloth with Linde B in the oxalic acid solution	Additional etching needed for bright-field examination	Hausner and Pinto [1950]
16. No polishing needed. Etch directly from 600-grit paper	For examination under relatively low magnification	Brink et al. [1950]

Table 16.3 Etching procedures used at various laboratories

Procedure	Remarks	Metallographer
1. Electrolytic: Room temperature. Stainless steel cathode. 20–40 s in fuming nitric acid	. . .	Noland et al. [1948]
2. For examination under polarized light, no etch is necessary. To develop contrast for bright-field work, 2 vol% hydrofluoric acid may be used.	. . .	Mott and Haines [1951]
3. Room temperature for 10–30 s in solution of 10 mL of 48 vol% hydrofluoric acid and 90 mL of 95 vol% ethyl alcohol	This etchant outlines and produces many color distinctions in the different alloy constituents. The etchant seems to increase in activity for several hours.	Udy et al. [1949]
4. Swab gently with 10 vol% solution of ammonium bifluoride diluted 50 vol% with glycerol. May be followed with 2 vol% HNO_3 in water	. . .	Dickerson [1953]
5. Immerse specimen in boiling 20 vol% solution of oxalic acid in water	. . .	Dickerson [1953]
6. A brief etch with 2 vol% hydrofluoric acid in glycerine is used to increase the contrast between the metal and the inclusions.	. . .	Beaver and Magalski [1953]
7. A bright-field etch of 10 vol% hydrofluoric acid in glycerine is used for 1–4 min. This is a swab etch.	For examination under polarized light, no etchant is used.	Czarkowski [1953]
8. A brief etch with 2 vol% hydrofluoric acid in water may be used to increase the contrast between the metal and the inclusion.	For bright-field examination. No etch is used.	Kaufmann et al. [1950], Roth [1953]
9. No etchant used. Specimens examined in as-polished state	Examination of corrosion specimens	Frye [1953]
10. At 100 °C for 1–3 min in 20 vol% oxalic acid.	For bright-field photography	Hausner and Pinto [1950]
11. Tucker's reagent (45 mL conc. HCl, 15 mL HNO_3, 15 mL of 40 vol% HF, 25 mL H_2O)	For grain-size studies at relatively low magnification	Brink et al. [1950]
12. The 2-2-2 etch: Consists of 2 vol% conc. sulfuric acid, 2 vol% diluted (48 wt%) hydrofluoric acid, 2 vol% conc. nitric acid, and remainder distilled water. Swabbed 5–10 s at 20 °C	Method reveals grain boundaries and oxide	Marder and Batich [1985]
14. 100 mL H_2O, 0.5–2 mL HF	Increases contrast between inclusion or constituent particles and matrix. HF can also be used in glycerol.	Price and McCall [1968]
15. 95 mL H_2O, 5 mL H_2SO_4. Immerse 1–15 s.	Reveals grain boundaries	Price and McCall [1968]
16. 100 mL H_2O, 3–20 g oxalic acid. Use boiling	Immerse 2 min to reveal precipitates. Immerse 16 min to reveal grain boundaries	Price and McCall [1968]
17. Electrolytic: 2 mL HCl, 2 mL HNO_3, 2 mL $HClO_4$ (perchloric acid), 94 mL ethylene glycol; etch of 5 V dc for 5–7 s. Standard cathode	. . .	Price and McCall [1968]
18. Electrolytic: 2 mL HCl, 98 mL ethylene glycol; etch at ~70 V dc for 1–4 min. Stainless steel cathode at 10–15 °C	If structure is not etched, reduce to 6–8 V dc for 3–5 s, stir solution, and wash specimen in boiling water. Specimen can be examined under bright-field illumination.	Price and McCall [1968]
19. Electrolytic: 100 mL H_3PO_4, 30 mL glycerol, 30 mL ethanol; cathode covered with cotton, and specimen swabbed lightly in a circular pattern. Use standard steel cathode, 25 V dc for 1–3 min, 30 s cycles at 10 °C	Polarized light improves contrast.	Price and McCall [1968]
20. Electropolishing: 100 mL H_3PO_4, 30 mL glycerol, 30 mL ethanol; 10–16 V dc, 0.1 A/cm^2 (0.65 A/in^2.)	. . .	Price and McCall [1968]

or mechanical with etchant on the wheel, may leave the specimen in a sufficiently etched condition. In most cases, however, an etchant is desired to develop suitable contrast between the phases in bright-field examination and may also be beneficial for use with polarized light. The etching procedures used by the various laboratories are compared in Table 16.3. A solution of 2 to 10 vol% concentrated hydrofluoric acid in water, alcohol, or glycerine is satisfactory as a swab or dip etch. A 10 vol% ammonium bifluoride solution, diluted 50 vol% with glycerine, can be substituted for the aforementioned etchant and behaves similarly. A 1 to 3 min dip etch in boiling 20 vol% oxalic acid solution also gives satisfactory results. Either of these etchants, in or-

Table 16.4 Appearance of the microconstituents in beryllium

Element	Composition range, wt%	Description	References
Bismuth	. . .	Two-liquid melts (monotectic reaction). No bismuth remains in beryllium phase.	Czarkowski [1953]
Boron	. . .	BeB_4-beryllium eutectic in grain boundaries. Red, unetched. Stained purple by 10 vol% alcoholic HF etch. Compatible with yellow aluminum eutectic. Same hardness as silicon eutectic	Udy et al. [1949]
Calcium	10	Primary compound in beryllium matrix. Light yellow	Kaufmann et al. [1950], Udy et al. [1949]
Carbon	. . .	Not appreciably affected by HF in alcohol. Same hardness as beryllium matrix	Kaufmann et al. [1950]
Cerium	1	Second phase as fine precipitate	Kaufmann et al. [1950]
Chromium	10	Produces eutectic network	Kaufmann et al. [1950]
Cobalt	5	Some second phase at grain boundaries	Kaufmann et al. [1950]
Cobalt	10	Some second phase at grain boundaries	Kaufmann et al. [1950]
Copper	. . .	Alloys quenched from 500 °C showed a single-phase structure up to approximately 20 wt% Cu, while similar alloys quenched from 1100 °C showed single-phase structure to approximately 35 wt% Cu. Above these limits, a eutectic structure is formed.	Kaufmann et al. [1950]
Germanium	10	Light-colored second phase at grain boundaries as well as in isolated globules. Probably a eutectic	Kaufmann et al. [1950]
Gold	. . .	Very low solid solubility in beryllium. A eutectic with $AuBe_5$ is formed.	Cullity et al. [1945]
Hydrogen	. . .	No phase attributable to hydrogen has been identified. Solubility in the liquid is appreciable.	Udy et al. [1949]
Manganese	10	Similar in appearance to iron eutectic. Has a pink cast compared to matrix. Unstained by HF in alcohol but outlined by it	Udy et al. [1949]
Molybdenum	. . .	Eutectic network. Barely distinguished from matrix in unetched condition. 10 vol% alcoholic. HF first stains the eutectic chocolate brown and then black.	Kaufmann et al. [1950]
Nickel	10	Single phase, indicating high solid solubility	Kaufmann et al. [1950]
Niobium	10	Second phase at grain boundaries	Kaufmann et al. [1950]
Osmium	10	20–30 wt% eutectic in structure	Kaufmann et al. [1950]
Palladium	. . .	A 5 wt% Pd alloy was entirely single phase, while a 10 wt% alloy showed a very small amount of second phase. Alloys quenched from 1200 °C were single phase to approximately 28 wt% Pd.	Kaufmann et al. [1950]
Platinum	20	20 wt% second phase as eutectic network	Kaufmann et al. [1950]
Rhodium	10	Second phase as eutectic network	Kaufmann et al. [1950]
Ruthenium	10	20 wt% eutectic as fine precipitate in primary beryllium	Kaufmann et al. [1950]
Selenium	1	No observable inclusions at 500×	Kaufmann et al. [1950]
Silicon	1	No observable inclusions at 500×	Kaufmann et al. [1950]
Silver	10	Mostly single phase. Small amount of white compound	Kaufmann et al. [1950]
Sulfur	1	No observable inclusions at 500×	Kaufmann et al. [1950]
Tantalum	1	Tan-colored eutectic network	Kaufmann et al. [1950]
Thorium	10	10 wt% second phase as angular compound in long stringers Lower alloys showed separate angular particles.	Udy et al. [1949]
Tin	. . .	Two-liquid melts. No appreciable tin in beryllium part of melt	Udy et al. [1949]
		Carbides and other inclusions carried down with tin. Beryllium-rich phase in tin is eutectic, resolved at 2000×.	Kaufmann et al. [1950]
Titanium	1	Eutectic network	Udy et al. [1949]
	10	Primary compound. Not affected by HF in alcohol. Traces of eutectic	Kaufmann et al. [1950]
Tungsten	1	Tan-white eutectic network	Kaufmann et al. [1950]
Uranium	5	Second phase not distinguishable without etching. 10 vol% HF in alcohol stains the dendritic compound a series of colors from yellow to green.	Udy et al. [1949]
Zinc	. . .	Zinc distills out and does not remain to form second phase in beryllium.	Kaufmann et al. [1950]
Zirconium	5	Dendritic phase scarcely distinguishable from the matrix until etched. 10 vol% alcoholic HF stains it light blue and outlines it.	Udy et al. [1949]

dinary cases, may be followed by a brightening treatment consisting of swabbing the surface with 2 vol% HNO_3 in water.

For low-magnification work, where inclusions are unimportant, an etchant such as Tucker's reagent (45 mL concentrated HCl, 15 mL concentrated HNO_3, 15 mL of 48 wt% HF, and 25 mL H_2O) is satisfactory.

16.5 Identification of Constituents

Table 16.4 lists descriptions of the appearance of the microconstituents in beryllium and beryllium-rich alloys. Many of these constituents are usually characterized by a variety of colors, and color microphotography has therefore been found to be a useful tool in the metallography of beryllium, especially in the determination of small amounts of impurities.

16.5.1 Principal Constituents

The most prominent constituents found as separate phases in "pure" beryllium have been traced to aluminum, carbon, and silicon. Very little beryllium is seen that does not have constituents containing these elements. In addition,

powder metallurgy beryllium almost always contains an oxide constituent.

Aluminum [Udy et al. 1949, Kaufmann et al. 1950] produces a bright yellow eutectic phase in beryllium. Sometimes, this phase has a speckled appearance. The components of this eutectic are the elements. The yellow aluminum phase is soft and difficult to polish. Etching with 10 vol% HF in alcohol does not affect the color but outlines the phase. The yellow aluminum eutectic is often closely associated with the bright-blue silicon eutectic.

Carbon [Udy et al. 1949, Kaufmann et al. 1950] is present as the carbide Be_2C. It is hard, angular, and usually gray. When exposed to a moist atmosphere, the carbide readily stains, first to all colors of the rainbow and eventually to brown. The color of the carbide phase is not affected by etching with 10 vol% HF in alcohol. It has been suspected that silicon may also be present in beryllium as SiC. Carbides are sometimes seen in a dendritic pattern.

Oxygen [Udy et al. 1949, Kaufmann et al. 1950] has not yet been identified graphically in any phases in cast beryllium. However, an oxide phase is most often present in powder metallurgy beryllium. The BeO phase is the darkest inclusion segregated in the grain boundaries. Carbide inclusions are also evident.

16.5.2 Minor Constituents

Inclusions resulting from iron, magnesium, and nitrogen occur less frequently in beryllium than the constituents already described. They are distinctive, however, and easily recognized.

Iron [Udy et al. 1949, Kaufmann et al. 1950] appears to have some slight solid solubility in beryllium. It is difficult to identify a second phase attributable to iron when it is present in small amounts. The shadowy network is difficult to distinguish from the background in this unetched specimen. Other eutectics seem to have been absorbed in the iron phase. The 10 vol% HF in the alcohol etchant colors the iron phase to a reddish brown, thus giving a method for distinguishing it from certain other similar-appearing phases.

Magnesium [Udy et al. 1949] may occur in certain beryllium melting stock to the extent of 1 wt% or more. Materials containing as low as 0.35 wt% Mg have been found to contain a phase attributable to that element. It may also occur in powder metallurgy beryllium. It is soft and exceedingly difficult to retain during grinding. In addition, it is somewhat attacked by water and may disappear during polishing.

Nitrogen [Udy et al. 1949, Kaufmann et al. 1950] is seldom found in beryllium unless it is deliberately added. The shape and color of the nitride phase are distinctive. It is gray but darker than the carbide. It is not affected by the 10 vol% HF in alcohol etch and is usually present in needlelike form. However, in larger amounts, it may have a more massive appearance.

16.6 Optical Microscopy

16.6.1 Macroexamination

Commercially available beryllium is predominantly a powder metallurgy product. Structural castings have poor strength and ductility because of their coarse grain size, and forgings tend to be highly anisotropic. Therefore, macroexamination is seldom used for beryllium, because vacuum hot pressing does not produce substantial flow, and the grain size it too small for macroexamination to be a valuable tool.

16.6.2 Microexamination

Microexamination of beryllium is generally carried out using polarized light. Polarized light techniques cause color differences between grains as a result of crystallographic orientation differences. Polarized light is generally used for metallographic examination instead of chemical etchants, although grain-boundary etchants have been used in some investigations. The fine grain size of the most common commercial forms of beryllium (vacuum hot pressed block and rolled sheet) limits the value of magnifications less than 250×. Polarized light also shows the positions from which oxide particles have been "pulled out" of the structure during polishing. These locations generally appear bright white.

16.7 Electron Microscopy

Saulnier [1958, 1960] developed electron microscopic methods for the examination of substructures and dislocations in beryllium. He also demonstrated by this method the disappearance

of subgrains and dislocations during recrystallization after annealing at 800 °C (1470 °F). Saulnier operated with thin metallic specimens prepared from a beryllium sample with perfectly parallel faces, electropolished in a semiautomatic Disapol apparatus with an electrolyte consisting of 300 g copper nitrate, 900 mL methyl alcohol, and 30 mL nitric acid, and polished at a potential of 50 V, alternating every 5 to 10 s from one face of the sample to the other. Perfectly clear slides can be prepared in this way, with adequate contrast for substructures, dislocations, and foreign phases.

16.8 Microstructures of Beryllium

The microstructure of vacuum hot pressed beryllium consists of grains of beryllium and particles of beryllium oxide (BeO) as major constituents. The microstructural differences between grades are subtle; grain size and oxide content are the only distinguishing characteristics.

Rolled beryllium sheet begins as a hot pressed block, which is subsequently subjected to warm rolling. The final microstructure consists of the usual elongated grains; aspect ratios depend on the actual reduction performed.

Intentional alloying does not occur in the production of pure beryllium, because beryllium has low solubility for most elements, and the introduction of alloying elements generally compromises the desirable density and modulus of this metal. Microalloying, which is essentially performed by controlling the proportions of iron and aluminum, is used primarily to prevent the formation of grain-boundary films.

The predominant second-phase constituent is BeO, which has the hexagonal close-packed crystal structure and acts as a grain-boundary pinning agent. Because the strength of beryllium is strongly dependent on grain size, there is a strong correlation among oxide content, grain size, and strength. The amount of oxide also correlates inversely with ductility.

16.9 Toxicity Issues

Beryllium is considered extremely hazardous to health when sufficient quantities of dusts, mists, or fumes containing particles small enough to enter the lungs (typically 10 μm or less) are inhaled. Sectioning, grinding, and polishing operations that produce dusts or fumes should be performed under adequately vented hoods equipped with special filters. Metallographic preparation equipment and laboratory work surfaces should be damp wiped periodically to prevent accumulation of dry particles. For additional information, see Chapters 28 and 29 in this book.

REFERENCES

Beaver, W.W., and Magalski, R., 1953. Brush Beryllium Corporation, private communication

Bennett, W.D., 1960. "Annual Report on Beryllium Research Project, 1959," Report AECL-1029, Atomic Energy of Canada, Ltd.

Brick, R.M., et al., 1950. "Recrystallization and Grain Growth Characteristics of Beryllium and Zirconium," Interim Report, University of Pennsylvania Thermodynamics Research Laboratory, Philadelphia, PA

Buchheit, R.D., Brady, C.H., and Wheeler, G.A., 1959. "Procedures for the Metallographic Preparation of Beryllium, Titanium, and Refractory Metals," DMIC-Memo-37, Defense Materials Information Center, Battelle Memorial Institute

Cullity, B.D., Bitsianes, G., Chandler, W.T., and Neher, M., 1945. "Alloys of Gold and Beryllium," Report MDDC-97 (Declassified: 1946), Atomic Energy Commission

Czarkowski, J.W., 1953. Knolls Atomic Power Laboratory, private communication, Sept 2, 1953

Dickerson, R.F., 1953. Battelle Memorial Institute, private communication, Sept 24, 1953

Dingle, J.H., and Moore, A., 1962. A Rapid Electrolytic Method for the Preparation of Metallographic Surfaces on Fabricated Beryllium, *J. Inst. Met.*, Vol. 90, p 270–271

Doig, J.R., and Schwartz, C.M., 1953. Battelle Memorial Institute, private communication, Sept 21, 1953

Frye, J.J., 1953. Oak Ridge National Laboratory, private communication

Hausner, H.H., and Pinto, N.P., 1951. The Powder Metallurgy of Beryllium, *Trans. ASM*, Vol 43, p 1052–1071

Kaufmann, A.R., Gordon, P., and Lillie, D.W., 1950. The Metallurgy of Beryllium, *Trans. ASM*, Vol 42, p 785–844

Marder, J.M., and Batich, R., 1985. Beryllium, *Metallography and Microstructures*, Vol 9,

Metals Handbook, 9th ed., American Society for Metals, p 389–390

Mott, R.W., and Haines, H.R., 1951. "The Examination of Metals Under Polarized Light," AERE-M/R-791, Oct 16, 1951

Noland, R., et al., 1948. "Electropolishing and Electroetching Beryllium for Microexamination under Bright Field Illumination," Argonne National Laboratory, unpublished work

Price, C.W., and McCall, J.L., 1968. "A Review of Metallographic Preparation Procedures for Beryllium and Beryllium Alloys," DMIC Memorandum 237, Defense Metals Information Center, Battelle Memorial Institute, Columbus, OH

Roth, H.P., 1953. Massachusetts Institute of Technology, private communication, Oct 1, 1953

Saulnier, A., 1958. Electron Micrography of Films of Beryllium Reduced from Bulky Specimens, *Compt. Rend.*, Vol. 246, p 1688

Saulnier, A., and Mirand, P., 1960. Electron Micrography of Films of Beryllium Reduced from Bulky Specimens, Exhibiting Substructure and Dislocations, *Compt. Rend.*, Vol 250, p 709

Sloman, H.A., 1932. Researches on Beryllium, *J. Inst. Met.*, Vol 49, p 365–388

Udy, M.C., Manning, G.K., and Eastwood, L.W., 1949. Metallographic Examination of Beryllium Alloys, *Trans. AIME*, Vol 18, p 799–784

White, D.W., Jr., and Burke, J.E., 1955. *The Metal Beryllium*, American Society for Metals

SELECTED REFERENCE

- Venkataratnam, G., and Rao, B.S.V.R, 1958. Polarography of Beryllium, *J. Sci. Ind. Res. India. B*, Vol 17, p 360–362

Beryllium Chemistry and Processing, p 209-252
By Kenneth A. Walsh
Edited by Edgar E. Vidal, Alfred Goldberg,
Edward N.C. Dalder, David L. Olson, and Brajendra Mishra

CHAPTER 17

Mechanical Properties of Beryllium

Alfred Goldberg, Lawrence Livermore National Laboratory
David L. Olson, Colorado School of Mines

THE EFFECT of the many variables of the material, in the processing and in testing (such as temperature, grain size, impurities, and strain rate), on the mechanical properties of beryllium is reported in this chapter. In general, ductility and strength improve as the grain size is reduced. An increase in BeO content generally results in a decrease in ductility and an increase in strength. The degree of isotropy (texture) and porosity is also an important factor. Heat treatment is important in controlling the distribution of some impurities between grain boundaries and matrix as well as controlling grain size, yield points, and precipitation hardening. The properties discussed are tensile properties, fracture toughness, creep, fatigue, ductile-to-brittle transition, notch sensitivity, microyield, and yield phenomena.

17.1 Vacuum Hot-Pressed Block Properties

The effect of temperature on moduli (*E* and *G*), yield and ultimate tensile (transverse and longitudinal) strengths, and elongation for grade S-200F is shown in Fig. 17.1 and 17.2 [Brush

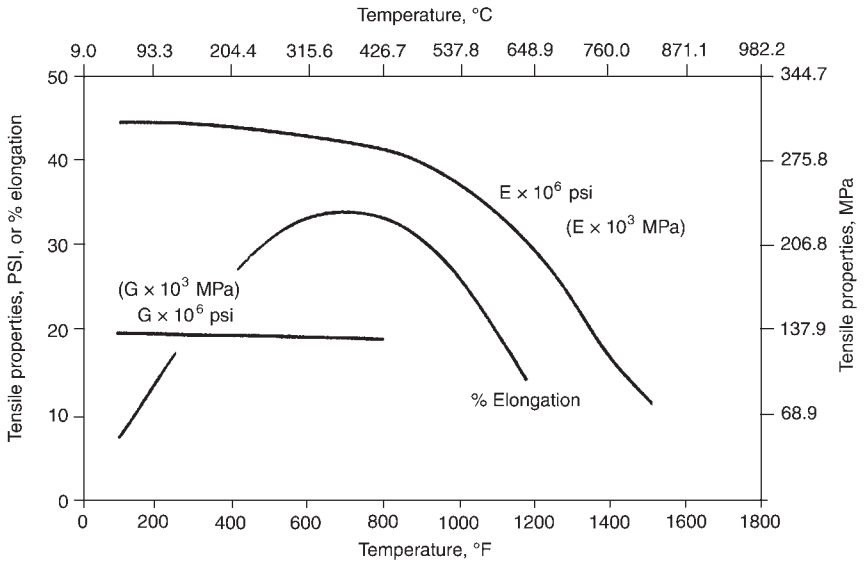

Fig. 17.1 Modulus and elongation properties for hot-pressed block, grade S-200F. Source: Brush Wellman 2001

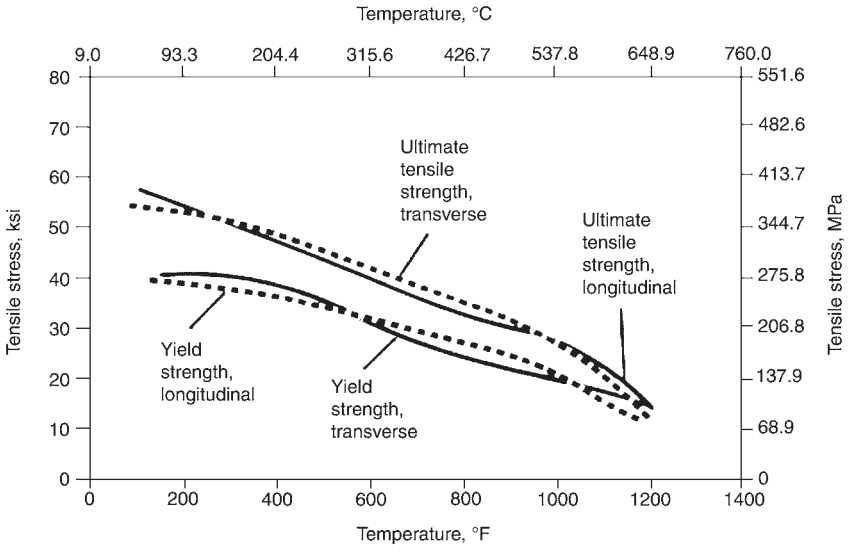

Fig. 17.2 Tensile properties of hot-pressed block, grade S-200F. Source: Brush Wellman 2001

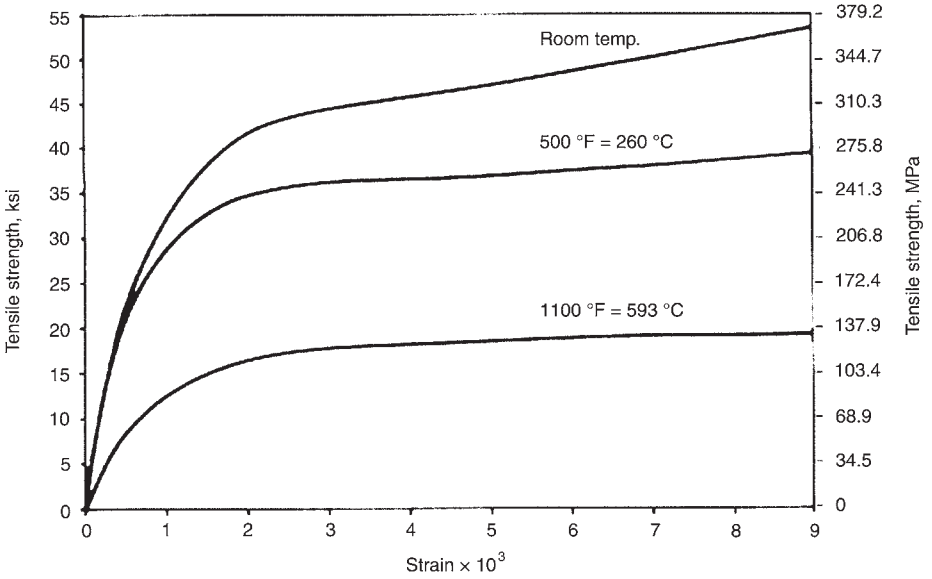

Fig. 17.3 Stress-strain curves for hot-pressed block, grade S-200F. Source: Brush Wellman 2001

Wellman 2001]. Corresponding stress-strain curves at three temperatures are shown in Fig. 17.3. The effects of temperature on tensile yield strength and ultimate tensile strength for grade S-65C, tested at an initial strain rate of $1.1 \times 10^{-4}\ s^{-1}$, are shown in Fig. 17.4 and 17.5, respectively [Goods and Dombrowski 1997]. The powders for both S-65C and S-200F are obtained by impact grinding, which reduces the anisotropy from that normally obtained from disk-ground powders. It can be seen that the differences in mechanical properties between the longitudinal and transverse directions in S-65 are relatively minor and considerably less than those values obtained for grade S-200F. The main difference between the two grades is in the oxide content; of the two grades, S-65C has the lower BeO content. It may be that the S-65C grade was compacted using better technology than that used for the S-200F grade resulting in a more isotropic

product. The properties of vacuum hot-pressed (VHP) grade S-65B at several temperatures from 20 to 60 °C are listed in Table 17.1 [Stonehouse 1986].

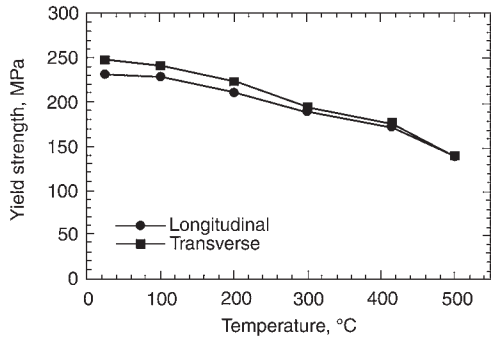

Fig. 17.4 Drop in yield strength with increase in temperature for grade S-65C. Source: Goods and Dombrowski 1998

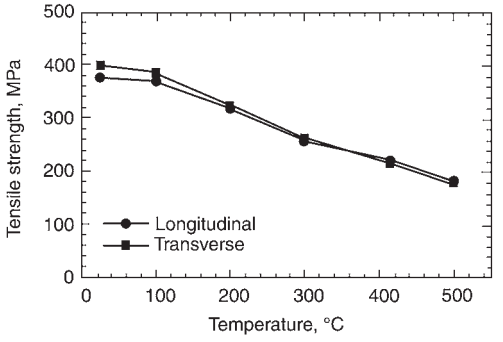

Fig. 17.5 Drop in ultimate tensile strength with increase in temperature for grade S-65C. Source: Goods and Dombrowski 1998

Tensile results of a study performed on VHP grade S-200E over a temperature range from 300 to 1100 °C are shown in Tables 17.2 and 17.3 for the longitudinal and transverse directions, respectively [Henshall et al. 1995]. The beryllium contained 1.6, 0.06, and 0.03 wt% BeO, iron, and aluminum, respectively. S-200E powder is typically produced by disk grinding. The data were obtained on specimens machined from a billet measuring 254 mm in diameter by 762 mm long (10 by 30 in.). The billet had an average as-received grain size of 27 μm (6 to 45 μm) and contained a small number of inclusions approximately 10 μm in diameter. The billet had not been given any postconsolidation anneal. Tests were performed on specimens in the as-machined condition in a high-purity argon atmosphere at a strain rate of approximately 5.5×10^{-4} s^{-1}. The corresponding stress-strain curves did not reveal any yield point, which is frequently observed in beryllium. The absence of either a yield point or any serrations in the stress-strain curve was attributed to the lack of a

Table 17.1 Tensile properties for vacuum hot-pressed grade S-65B beryllium

Temperature, °C	Orientation(a)	Yield strength (σ_y), MPa	Ultimate tensile strength, MPa	Elongation, %
20	L	270	421	3.0
20	T	273	454	5.4
200	L	232	382	10.2
200	T	234	389	23.4
400	L	179	270	50.0
400	T	177	268	49.5
600	L	119	160	25.2
600	T	122	167	31.9

(a) L, longitudinal, and T, transverse, are parallel and perpendicular to the pressing pressure, respectively. Source: Stonehouse 1986

Table 17.2 Tensile data for longitudinal direction of as-machined S-200E beryllium

Temperature, °C	Yield strength (σ_y) (0.2% offset), MPa	Ultimate tensile strength, MPa	Elongation, %	Reduction in cross-sectional area, %	Fracture stress(a), MPa
300	219.8	304.8	5.30	9.2	328.7
300	202.4	294.8	9.95	16.9	333.0
400	193.8	258.8	15.80	32.2	323.1
400	203.8	261.8	13.15	. . .	. . .
500	185.9	230.4	12.53	22.9	255.9
600	159.6	181.4	6.38	8.5	177.3
600	142.4	159.6	4.15	. . .	. . .
600	161.1	185.9	6.58	. . .	. . .
700	122.4	127.4	3.27	4.0	107.7
700	96.3	102.7	4.08	2.4	104.9
700	112.9	117.9	2.99	3.7	. . .
800	52.2	53.0	3.62	3.9	. . .
800	34.3	34.8	4.02	1.2	. . .
800	48.2	48.2	2.10	4.0	. . .
900	15.4	15.7	8.48	. . .	. . .
1000	6.67	6.99	15.98	35.3	. . .
1000	2.86	3.07	55.43	37.8	. . .
1100	2.60	2.64	64.80	45.3	. . .

(a) Fracture stress refers to true stress: load/area at fracture. Source: Henshall et al. 1995

Table 17.3 Tensile data for transverse direction of as-machined S-200E beryllium

Temperature, °C	Yield strength (σ_y) (0.2% offset), MPa	Ultimate tensile strength, MPa	Elongation, %	Reduction in cross-sectional area, %	Fracture stress(a), MPa
300	197.3	297.3	25.40	39.4	413.8
400	183.9	248.8	30.40	45.7	333.4
500	162.6	196.4	15.16	29.6	237.1
500	158.1	189.6	14.73	22.6	222.0
600	155.1	185.1	9.89	18.9	202.2
700	60.0	60.5	8.87	5.1	. . .
700	59.5	60.5	5.34	3.8	. . .
700	58.0	59.5	5.82	5.1	. . .
800	20.7	21.1	6.58	5.8	. . .
900	7.99	8.04	15.18	15.0	. . .
1000	2.56	2.90	60.33	39.9	. . .
1100	0.69	0.72	114.0	57.6	. . .

(a) Fracture stress refers to true stress: load/area at fracture. Source: Henshall et al. 1995

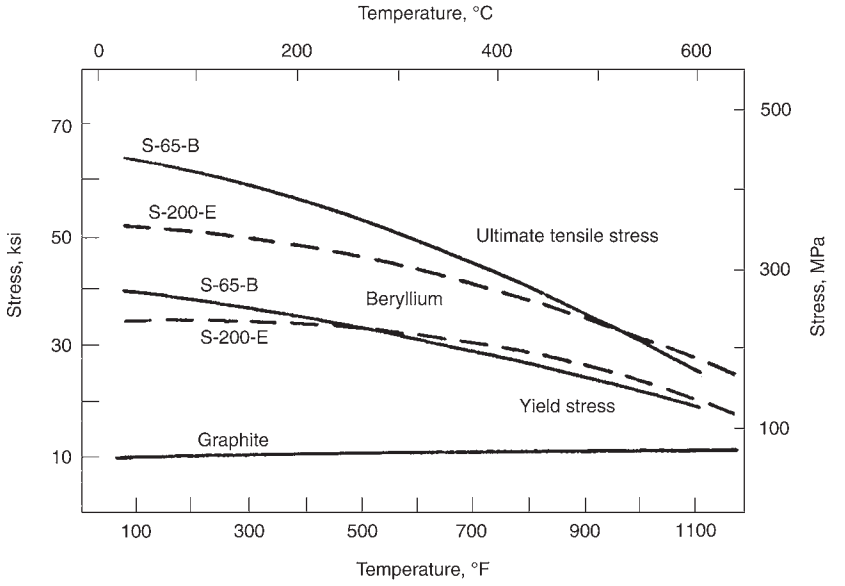

Fig. 17.6 Yield and ultimate tensile strengths as a function of temperature for smooth bar specimens from vacuum hot-pressed blocks of S-65B (solid lines) and S-200E (broken lines) beryllium. Included are results of a competing graphite product. Source: Smith et al. 1985

postconsolidation anneal. The dip in elongation in the 600 to 800 °C range was attributed to free aluminum segregation at grain boundaries.

Studies on the mechanical properties of several grades of VHP beryllium were performed to evaluate their use as material for contact with the plasma in magnetic-confinement fusion devices. Tests were performed on smooth tensile-bar specimens. The results reported for grade S-65B and S-200E are shown in Fig. 17.6 and 17.7 for strength and ductility, respectively [Smith et al. 1985]. The large increase in ductility starting at approximately 200 °C is attributed to a shift from basal-plane cleavage to a shear fracture. The peak in ductility and its subsequent fall is attributed partly to the decrease in tensile strength and partly to the formation of low-melting phases along the grain boundaries, the latter depending on the impurities present. The large difference in the ductility between the two grades is attributed to differences in the powder source and processing method. The powder for S-200E was produced by grinding beryllium chips between two beryllium disks, which produced somewhat platelike particles, while S-65B, which was a newer grade, used impact-ground powder combined with improved powder-handling methods. Also included in the two figures are curves for a competitive graphite product.

Compressive stress-strain curves obtained at a high strain rate of 10^3 s^{-1} at 20 and 300 °C are shown in Fig. 17.8 for S-200F beryllium [Ansart and Naulin 1991]. Grade S-200F is a modification of S-200E in using impacted powder rather

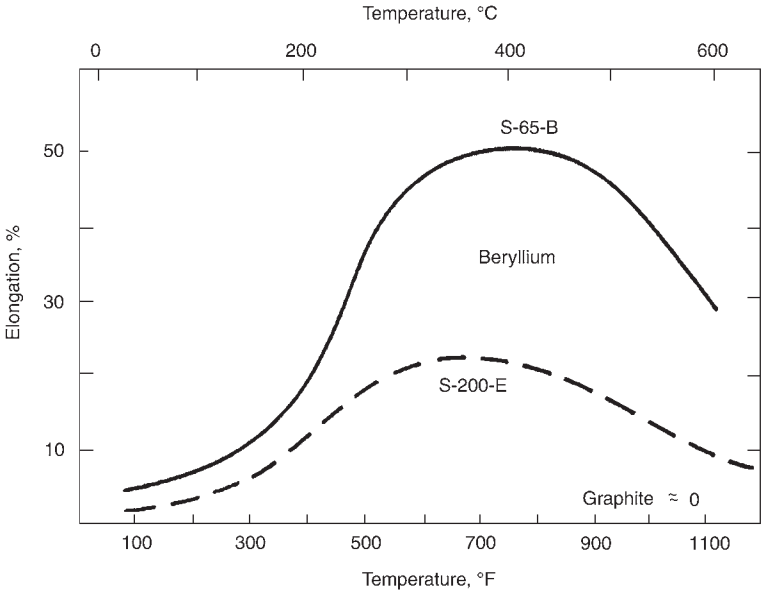

Fig. 17.7 Elongation as a function of temperature for smooth bar specimens from vacuum hot-pressed blocks of S-65B (solid line) and S-200E (broken line) beryllium. Included are results of a competing graphite product. Source: Smith et al. 1985

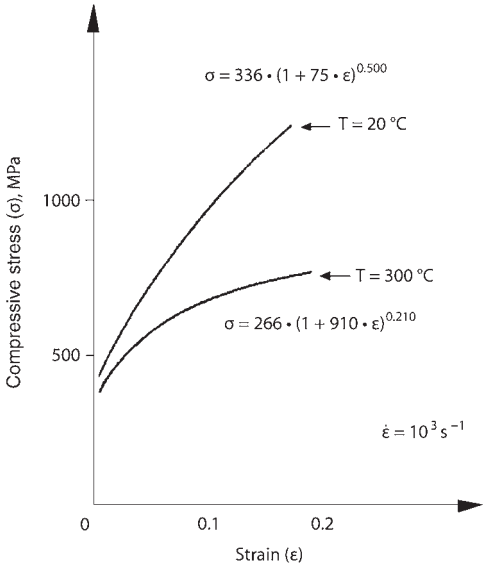

Fig. 17.8 Compressive stress-strain curves obtained at a high strain rate of 10^3 s^{-1} at 20 and 300 °C for vacuum hot-pressed S-200F beryllium. Source: Ansart and Naulin 1991

than disc-attritioned powder, starting with a blocky rather than a flakelike powder and thereby yielding a more isotropic product. Haws reported room-temperature compressive-yield strengths for S-200F of 280 and 271 MPa for the longitudinal and transverse directions, respectively [Haws 1985]. The tensile properties of S-200F at several temperatures from room temperature to 649 °C (1200 °F) are listed in Table 17.4. A comparison between the yield and ultimate strengths and the ductility of the two grades, S-200E and S-200F, can be seen in Fig. 17.9 to 17.11, respectively [Haws 1985]. The average hardness values for three specimens of the S-200F material were 85.5 and 85.4 Rockwell B for the longitudinal and transverse directions, respectively, relative to the pressing direction.

17.2 Hot-Isostatic-Pressed Properties

A study on the effect of hot isostatic pressing (HIPing) temperature on ultimate tensile strength (UTS) and elongation was performed on powders produced by three different methods (ball mill, disk, and impact). The UTS increased by approximately 50 MPa in going from 950 to 1075 °C. The corresponding elongations increased, adding approximately 1%, with an increase in temperature up to 1050 °C and subsequently dropped to the 950 °C values [Henshall et al. 1995]. The results are shown in Fig. 17.12.

Tensile properties of a grade S-65B part that was fabricated by cold pressing/sintering/HIPing are shown in Table 17.5 for three test temperatures. Results are averages of four or more tests. At room temperature, the fracture toughness ranged from 9.9 to 10.4 MPa$\sqrt{m}$, Young's

Table 17.4 Tensile properties of grade S-200F vacuum hot-pressed beryllium

Temperature, °C (°F)	Orientation(a)	Yield strength (σ_y) (0.2% offset), MPa	Ultimate tensile strength, MPa	Upper yield point, MPa	Lower yield point, MPa	Elongation, %	Reduction in cross-sectional area, %
RT	L	263	382	268	263	3.4 ± 0.3	3.3 ± 0.3
	T	262	407	273	262	6.1 ± 0.5	5.9 ± 0.2
204 (400)	L	256	332	260	255	12.0 ± 1.3	11.2 ± 1.4
	T	260	334	262	256	29.5 ± 4.1	25.9 ± 3.3
427 (800)	L	203	244	204	197	30.4 ± 2.4	52.5 ± 1.2
	T	188	236	190	183	33.8 ± 0.2	54.0 ± 0.2
538 (1000)	L	143	199	(b)	(b)	22.4 ± 0.8	29.4 ± 2.2
	T	144	196	146	144	25.7 ± 0.6	33.9 ± 1.7
649 (1200)	L	90	108	93	86	8.8 ± 1.4	7.3 ± 0.4
	T	95	107	(b)	(b)	10.9 ± 2.1	9.7 ± 2.0

(a) L, longitudinal; T, transverse. (b) Did not have a yield point. Source: Haws 1985

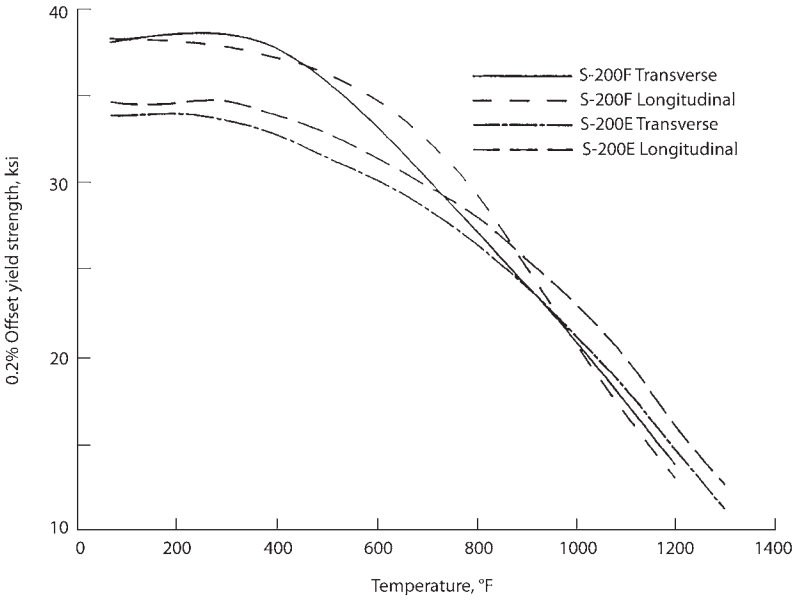

Fig. 17.9 Tensile yield strength of hot-pressed blocks as a function of temperature, comparing grade S-200F with grade S-200E beryllium in transverse and longitudinal directions. Source: Haws 1985

modulus was 3.03×10^5 MPa, and Poisson's ratio was 0.08 [Stonehouse 1986].

The yield and ultimate tensile strengths and the ductility of grade HP21 as a function of temperature are shown in Fig. 17.13 and 17.14, for both transverse and longitudinal directions. Upper and lower yield strengths are present throughout the entire temperature range [Borch 1979]. (The prefix HP refers to a VHP product.)

17.3 Yield-Point and Portevin-Le Chatelier Effects

Under certain conditions, beryllium exhibits upper and lower yield points and a related phenomenon, the Portevin-Le Chatelier (PLC) effect. An example of the former is shown for VHP grade S-65C in Fig. 17.15. An example of the PLC effect in the form of serrations along the lower-yield plateau in VHP beryllium is shown in Fig. 17.16 [Goldberg et al. 1982]. With prior strain hardening of the material during manufacturing, the amplitude of the serrations is greatly reduced, and the serrations disappear. The termination of both the plateau region and the serrations is due to the exhaustion of particle-pinned dislocations that caused both phenomena to have taken place.

The relative difference between upper and lower yield points has been given in terms of a yield-point factor defined as:

$$(\sigma_{yp} - \sigma_{pl})/\sigma_{pl}$$

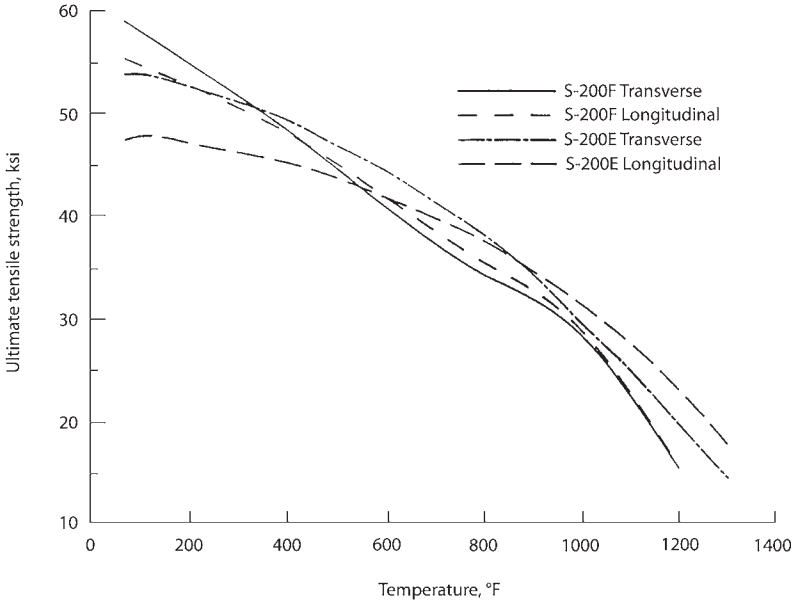

Fig. 17.10 Ultimate tensile strength of hot-pressed blocks as a function of temperature, comparing grade S-200F with grade S-200E beryllium in transverse and longitudinal directions. Source: Haws 1985

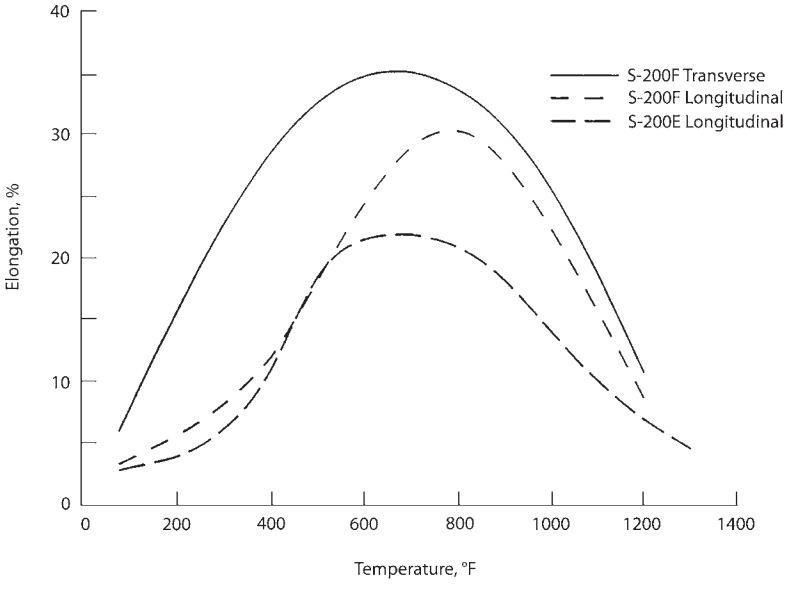

Fig. 17.11 Elongation of hot-pressed blocks as a function of temperature comparing grade S-200F (broken line) with grade S-200E (dot-dash line) beryllium in longitudinal direction. Elongation of grade S-200F transverse (solid line) also given. Source: Haws 1985

where σ_{yp} and σ_{pl} are the upper and lower yield values, respectively. The yield-point factor as a function of temperature for S-65C is shown in Fig. 17.17 [Goods and Dombrowski 1997]. The data show that only the transverse orientation exhibited a yield drop at ambient temperature. The variation of fracture strain and reduction in area with temperature for this material is shown in Fig. 17.18 and 17.19. The authors state that the yield point has been attributed to dislocation pinning by $AlFeBe_4$ and/or FeB_{11} precipitates [Goods and Dombrowski 1997]. Evidence

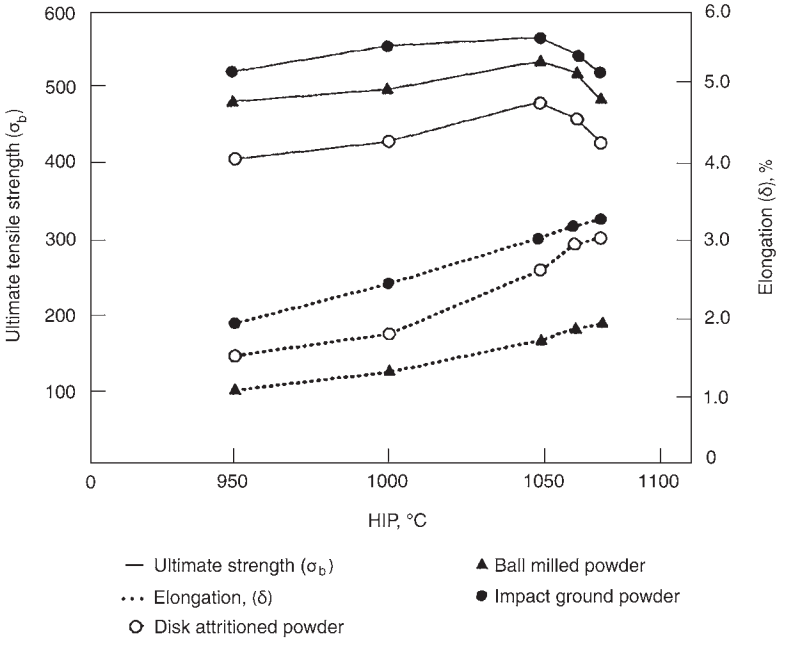

Fig. 17.12 Effect of hot isostatic pressing (HIPing) temperature on the tensile properties of beryllium with powders from three different attrition methods. ○, disk-attritioned powder; ▲, ball-milled powder; ●, impact-ground powder. Source: Henshall et al. 1995

Table 17.5 Tensile properties of grade S-65B fabricated by cold pressing/sintering/hot isostatic pressing

Temperature	Yield strength (σ_y), MPa	Ultimate tensile strength, MPa	Elongation, %	Reduction in cross-sectional area, %
Room	211	342	5.2	. . .
370 °C	133	228	49.4	66.9
650 °C	81	123	38.5	29.5

Source: Stonehouse 1986

indicates that FeB_{11} is the more likely precipitate causing the yield phenomenon [Stonehouse 1979]. The yield-point behavior can be eliminated by a solution heat treatment at 1040 °C for 6 h, followed by rapid cooling. It can be made to reappear by aging at 760 °C for 1 h, followed by slow cooling [Smugeresky 1986]. In beryllium of commercial purity, slow cooling below 650 °C can induce or enhance its appearance. Except where a large yield drop is obtained, the presence of the yield point has a negligible effect on the total elongation to failure [Smugeresky 1986]. If pinning persists up to the UTS, the metal will become brittle with little plastic deformation. In commercial practice, yield points are eliminated or controlled by limiting the availability of iron for the precipitation of FeB_{11} or by the heat treatment that favors the formation of $AlFeBe_4$ over that of FeB_{11} [Stonehouse 1979].

The PLC effect refers to discontinuous yielding during plastic deformation. Its occurrence depends on temperature and strain rate. Kharinov et al. reported the development of the PLC effect in a hot-pressed beryllium of commercial purity (TGP-50); its chemical composition is given in Table 17.6 [Kharinov et al. 1990]. Yield points and discontinuous flow were observed in the temperature ranges of 325 to 425 °C and 355 to 525 °C, respectively. Figure 17.20 is an example of discontinuous yielding for this material. The authors conclude that the interaction of carbon with dislocations is responsible for the observed PLC effect [Kharinov et al. 1990].

In evaluating the yield-point phenomenon in a hot isostatic pressure forging from beryllium powder tested at 300, 77, 50, 40, 30, and 4.2 K, it was observed that the yield point disappeared at and below 77 K (−196 °C). The purity was given as no lower than 98.7 wt% Be. Similar behavior was observed for both orientations, transverse and parallel to the forging axis. In agreement with observations reported by other investigators, the authors noted that the yield point can be reduced or eliminated by reducing the iron content [Lavrent'ev et al. 1987].

17.4 Microyield Properties

The microyield strength is defined as the stress required to produce a plastic strain of 10^{-6}. High microyield strengths are required with applications that cannot tolerate distortions, for example, for use in space mirror structures.

A study was reported on the microyield behavior of two experimental beryllium grades: HIP-50 and X-520 [Kumar et al. 1985]. Grade HIP-50 was produced by Kawecki-Berylco using HIPing of electrolytic-flake, high-purity, impact-attritioned beryllium powder. Grade X-520 was fabricated by Brush Wellman using hot pressing of impact-attritioned powder of lower purity. A summary of the results of the two grades follow-

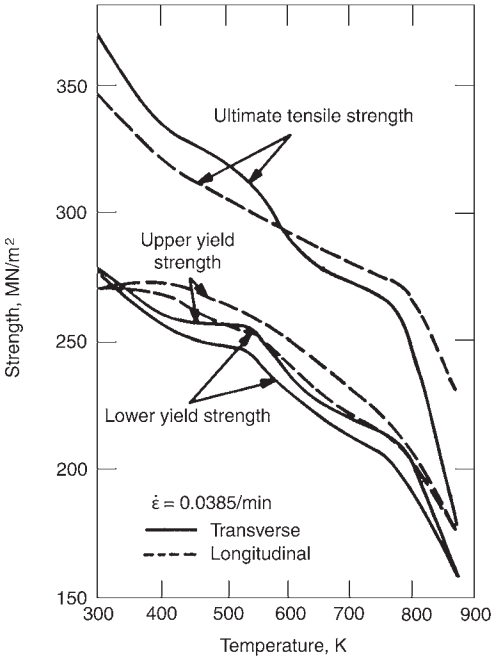

Fig. 17.13 Temperature dependence of yield and ultimate tensile strengths of HP21 beryllium. Source: Borch 1979

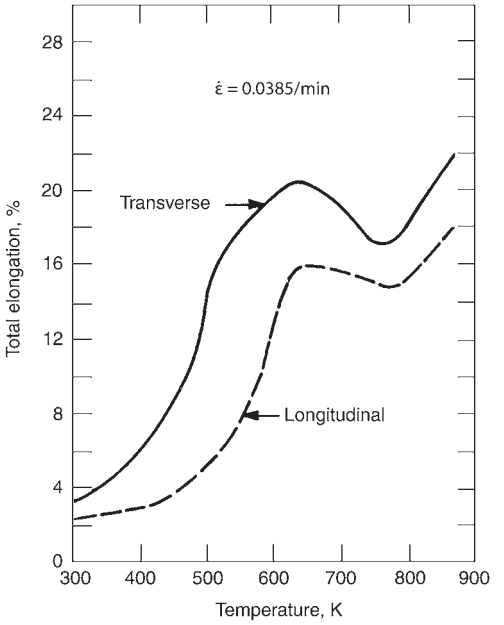

Fig. 17.14 Temperature dependence of total elongation of HP21 beryllium. Source: Borch 1979

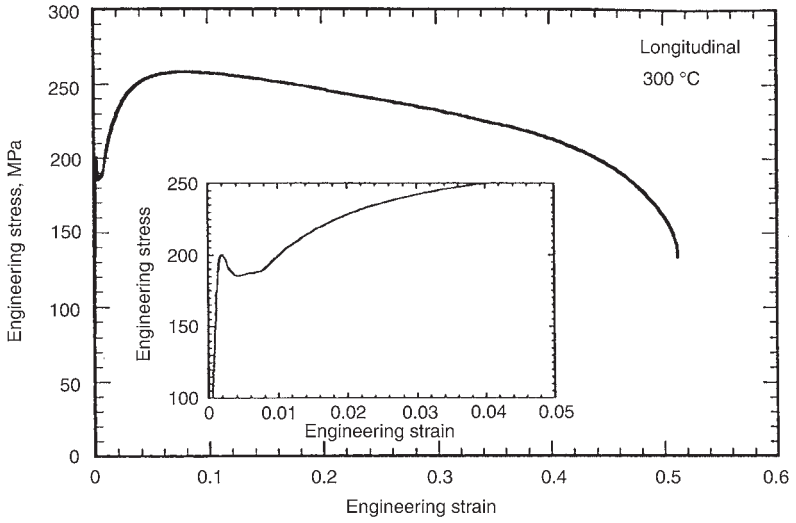

Fig. 17.15 Yield point obtained in longitudinal tensile test of S-65C. Source: Goods and Dombrowski 1997

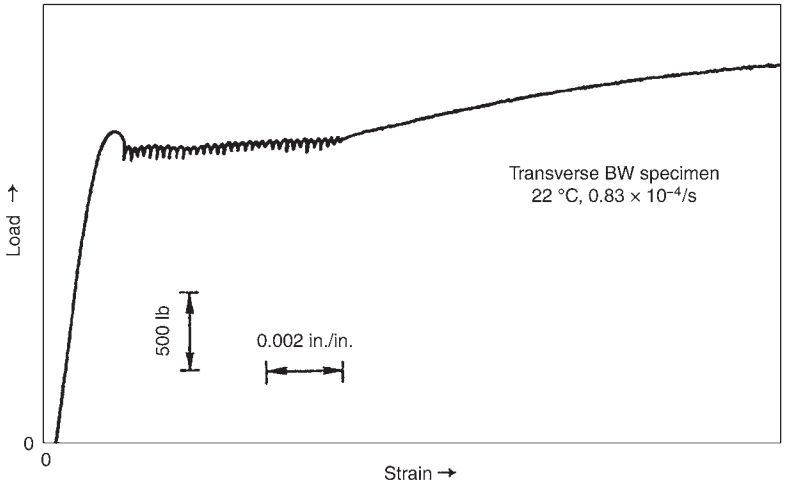

Fig. 17.16 Analog recording of the load-strain response of a vacuum hot-pressed beryllium specimen transverse to the pressing direction. Serrations (Portevin-Le Chatelier effect) can be seen along the lower-yield plateau. Source: Goldberg et al. 1982

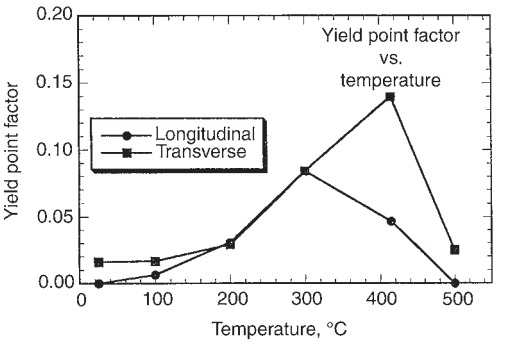

Fig. 17.17 Yield-point factor $[(\sigma_{yp} - \sigma_{pl})/\sigma_{pl}]$ as a function of temperature for S-65C beryllium. Source: Goods and Dombrowski 1997

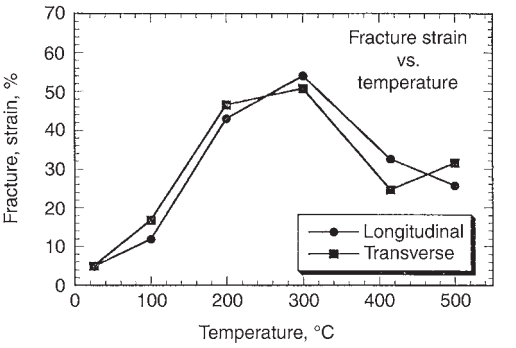

Fig. 17.18 Influence of temperature on ductility (fracture strain) for S-65C beryllium. Source: Goods and Dombrowski 1997

ing different treatments is given in Table 17.7. Grade HIP-50 is considered to be isotropic, and the effect of orientation was not considered for this grade. The microyield stresses for the experimental alloy, HIP-50, which had the higher microyield stress, are significantly greater than the values reported for the VHP commercial structural and instrument grades, respectively, listed in Tables 17.8 and 17.9.

The authors attributed the difference in the microyield strength of the two experimental materials to the differences in the oxide particle size and silicon content. A finer particle size results in a higher concentration of particles at the grain boundary, which, in turn, offers a higher resistance to the initiation of plastic flow at these boundaries. Excessive amounts of silicon result in agglomeration of particles due to the formation of Be_2SiO_4. The silicon contents were 300 and 40 ppm for X-520 and HIP-50, respectively, with an as-received grain size of 5 μm listed for both materials. All the heat treated samples of X-520 showed a particle size of approximately 0.1 μm diameter compared to the as-received size of roughly 0.25 μm. The corresponding values for HIP-50 in the as-received and HT1 conditions were 0.05 and 0.03 μm, respectively.

The results of a study on the effect of grain size on the microyield strength of a VHP beryllium are given in Table 17.8. The effect of BeO content and loading rate were also reported, and the results are shown in Table 17.9. Unfortunately, the authors did not attempt to vary independently one of the variables (grain size or BeO content) while

maintaining the other constant [Naik and Singhal 1991]. It must be assumed that the finer grain sizes are associated with the higher BeO contents.

Vapor-deposited beryllium from a high-purity source was evaluated for microyield properties using four-point-bend tests. Using a stationary substrate, fully dense columnar grains were formed with the major crystallographic axis being parallel to the direction of incidence of the depositing atoms. The structure had a grain-aspect ratio of approximately 20. When using a rotating substrate, the microstructure consisted of interwoven helical columnar grains. In both structures, shear occurred on the basal plane. The microyield strengths for the stationary and rotating substrates were 57.3 and 213.5 MPa, respectively. The large increase in the strength is attributed to the higher dislocation density predicted as being present in the rotated-produced substrate to accommodate the curvatures in the helical structure [Nieh and Wadsworth 1998].

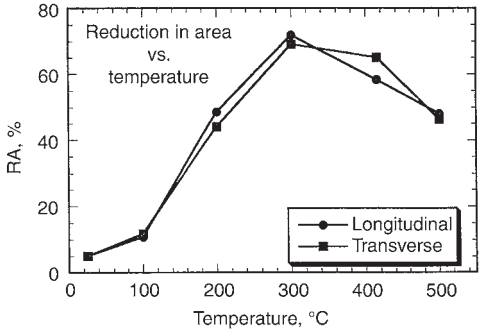

Fig. 17.19 Influence of temperature on reduction in area (RA) for S-65C. Source: Goods and Dombrowski 1997

17.5 Fracture Toughness and Ductile-to-Brittle Transition

Generally, as with most brittle materials, the maximum tensile stress has been used to predict fracture for beryllium. Where parts must be designed to perform close to their potential limit, a more reliable fracture criterion, such as fracture toughness, may be required. Fracture toughness, as defined by K_{Ic}, provides a quantitative measure of the resistance to fracture in a material containing a flaw of known dimensions. It is defined by the relationship:

$$K_{Ic} = \sigma\sqrt{(\alpha\pi a)}$$

Table 17.6 Chemical composition and room-temperature mechanical properties of TGP-50

Impurity content, wt%										Mechanical properties		
Fe	Al	Mn	Si	Ni	Cr	Cu	Mg	C	O	Yield strength $(\sigma)_y$, MPa	Ultimate strength, tensile MPa	Elongation, %
0.086	0.0073	0.0043	0.011	0.01	0.027	0.0032	0.003	0.0075	1.23	480	330	3.7

Source: Kharinov et al. 1990

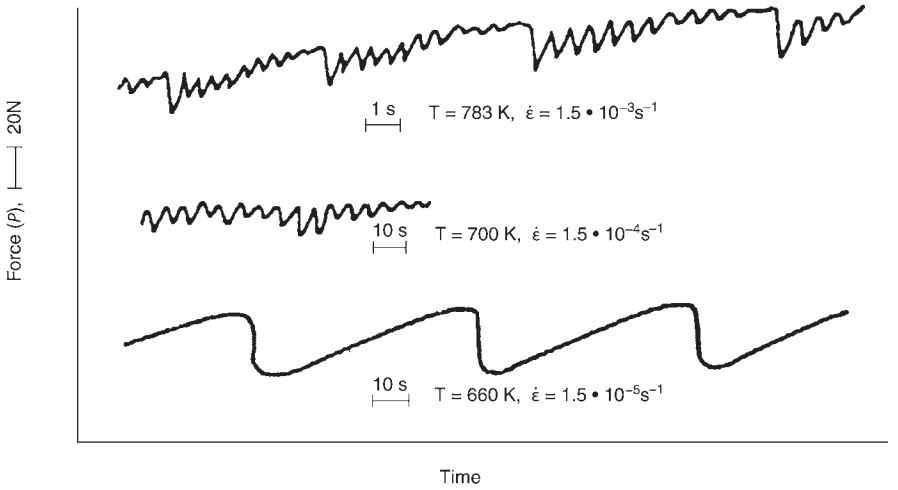

Fig. 17.20 Discontinuous flow in TGP-beryllium in "load-time" coordinates. Source: Kharinov et al. 1990

where K_{Ic} is the critical stress-intensity factor (at the crack tip), σ, is the tensile stress required to produce failure, a is the radius of the flaw, and α is a geometrical factor. The number I refers to the crack-opening fracture mode, which is the most common failure mode; II and III are used to refer to an edge (sliding) mode and screw mode, respectively. The three modes are illustrated in Fig. 17.21. Calculation of critical flaw sizes for beryllium yields values between 0.2 and 1 mm [Pinto 1979b]. Depending on the type of test, the value may refer either to the radius, the length, or half-length of the flaw.

The ASTM International specimen-size criterion to obtain a valid K_{Ic} for plane strain is given by the following condition:

$$b \geq 2.5 (K_{Ic}/\sigma_y)^2$$

where b is the minimum specimen thickness. Using this condition, and depending on the yield and K_{Ic} values obtained, the minimum thickness can range from approximately 1.6 to 7 mm. The ASTM E-24 subcommittee on fracture-toughness testing of beryllium, however, recommends a minimum thickness of 12.7 mm for beryllium. The most common approved specimen used is the wedge-opening load specimen or its variant, the compact-tensile specimen, although the single-edge-notched-bend specimen is also approved by ASTM International. Other specimens, such as the double-cantilever beam (DCB) and the tapered double-cantilever beam (TDCB), have also been used. Illustrations of several different types of fracture-toughness specimens are shown in Fig. 17.22. The DCB and TDCB specimens generally have side grooves to guide the growth of the crack. A schematic illustration of the variation of stress intensity with thickness, as well as indicating the regimes of plane strain and plane stress, is shown in Fig. 17.23 [Cooper 1979].

No substantial differences in toughness have been found for the S-65, S-200E, and S-200F grades with K_{Ic} values ranging from 8.8 to 12.2 MPa√m [Marder 1986]. The toughness increases with temperature; the corresponding range in values at 260 °C is from16.5 to 22 MPa√m. An average value of 11 MPa√m was reported for a modified VHP S-65 grade of beryllium tested at room temperature [Mayville 1980].

Mayville [1980], in evaluating fracture criteria for beryllium, noted that the tensile stress required to cause fracture was significantly higher under triaxial than under biaxial conditions [Mayville 1980]. This difference is attributed to

Table 17.7 Summary of microyield (10^{-6} permanent strain) data on Brush Wellman X-520 and Kawecki-Berylco HIP-50

	Microyield stress, MPa		
Specimen history(a)	Longitudinal X-520	Transverse X-520	Longitudinal HIP-50
As-received	55	59	117
HT1	57	62	186
HT2	56	55	122
HT3	66	57	143

(a) HT1, As-pressed (AP) + 100 h at 600 °C. HT2, AP + 2 h at 1055 °C, quench, +24 h at 370 °C, furnace cool. HT3, AP + 2 h at 870 °C + slow cool with step age 20 h at 750 °C, 20 h at 720 °C and 20 h at 695 °C, followed by furnace cool to room temperature. Source: Kumar et al. 1985

Table 17.8 Effect of grain size in vacuum hot-pressed beryllium on microyield strength

Average gain size, μm	20	15	12	10	8.0	6.0	5.5
Microyield strength, MPa	30.4	34.3	36.7	41.2	50.0	54.9	72.6

Source: Naik and Singhal 1991

Table 17.9 Effect of loading rate on microyield strength

	Loading method and microyield strength, MPa		
BeO content, wt%	Very slow speed	Slow speed	High speed
2.0	33.3	35.3	37.3
4.0	48.1	52.0	53.9
6.5	70.6	73.1	76.5

Very slow is manual; slow and high speeds are motorized. Source: Naik and Singhal 1991

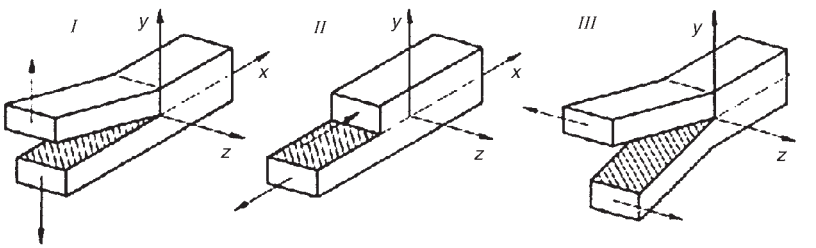

Fig. 17.21 Illustration of the three principal loading modes for the determination of fracture toughness: I, crack-opening mode; II, edge or sliding mode; III, screw or twist mode

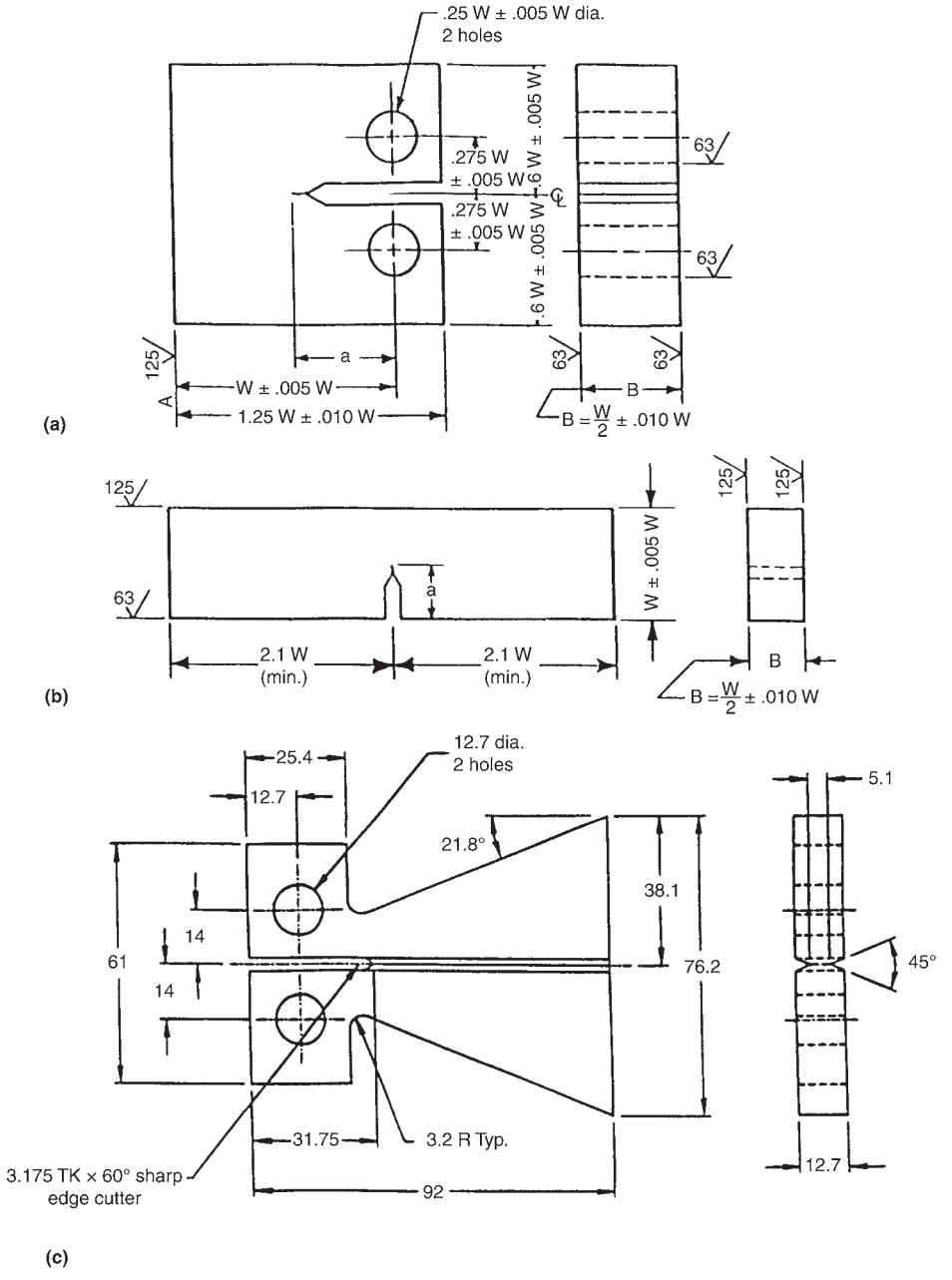

Fig. 17.22 Examples of fracture-toughness specimens: (a) compact tensile, (b) single-edge-notched, (c) tapered double-cantilever beam. The wedge-opening load geometry differs from that of the compact-tensile in the w dimension being relatively greater; this dimension is still greater for the double-cantilever beam.

the high triaxiality that is associated with a notch, which leads to considerably less plastic deformation than that obtained under biaxial or uniaxial tensile conditions. Furthermore, sharper notches can withstand higher maximum tensile stresses, since the overall magnitudes of the strains are less. The aforementioned reasoning assumes that the tensile stress required to cause fracture is dependent on the amount of damage in the material, which, in turn, is a function of the plastic strain. Therefore, maximum stress may not always be a valid criterion in designing to avoid fracture.

The increase in toughness with increasing temperature is associated with a corresponding

increase in ductility. Following an initial slow gradual increase in tensile elongation with increasing temperature, a sharp, large increase then occurs over a narrow temperature range. This behavior is typical of materials exhibiting a ductile-to-brittle transition temperature (DBTT). It is to be noted that while impact toughness is generally used for most materials in defining the DBTT, elongation is frequently also used for beryllium. The DBTT, T_c, is typically taken at midpoint between the maximum and minimum along the sharp rise in the toughness or elongation values.

Theoretical analysis, together with fitted experimental data, indicated that T_c would fall to room temperature at grain sizes of 10 and 1 μm for two sets of data, respectively [Turner 1979]. Limited data indicate that T_c increases with an increase of impurities, while the influence of strain rate is unclear. A study on hot-pressed HY beryllium showed that embrittlement was induced at a moderately high strain rate at temperatures above room temperature, with a corresponding drop in elongation. The latter can be seen in Fig. 17.24 [Borch 1979].

In the tensile testing of a HIP forging of powdered beryllium, the fractured cleavage surfaces were examined on a scanning electron microscope. Tests were performed between 4.2 and 300 K (−269 and 27 °C). It was noted that with decreasing test temperatures, the inclusion particles become more evident on the fractured surfaces. Because the insoluble impurities tend to be preferentially concentrated at grain boundaries, this situation suggests that the grain boundaries, in contrast to the grain, play an increasing role in the deformation as the temperatures are lowered. A corresponding decrease in the UTS was obtained, as shown in Fig. 17.25. At 27 °C, a mixed (grain/grain-boundary) fracture was observed that changed to a grain-boundary fracture at the lower temperatures [Lavrent'ev et al. 1987].

It was noted that the fracture toughness of beryllium depends primarily on the texture and oxide content and, to a lesser degree, on the grain size and impurity levels [Grensing et al. 1990]. The authors investigated the fracture toughness of VHP beryllium made from both impact-ground powder (S-200F) and atomized spherical powder (ASP). Precracked compact-tension specimens were instrumented and tested in accordance with ASTM E 9 and E 399-83, respectively. Because of difficulty in initiating a fatigue crack, a stress ratio (minimum stress divided by maximum stress) of −2 rather than the ASTM International value of 0.1 was used. Their results were compared with those of VHP S-200E, which typically used attritioned powder. The chemical compositions, tensile properties, and fracture-toughness values are given in Tables 17.10 to 17.12.

Fractured surfaces, which were examined with the scanning electron microscope, revealed brittle transgranular cleavage with some regions of ductile shear along grain boundaries. Since the grain size is largely dependent on oxide content, it is difficult to separate the effects of grain size from oxide content. Nevertheless, consistent with other reported observations, it appears that the oxide content has the greatest influence on the fracture toughness, whereas the effect of grain size is somewhat unclear. A decrease in oxide content and, apparently, an increase in grain size increase fracture toughness. Pole figures revealed texturing in the S-200F material, whereas the ASP material was essentially isotropic. The improved fracture toughness of orientation TL over that of orientation LT (Table 17.12) for grade S-200F is attributed to the alignment of the basal planes being parallel to the direction of crack propagation. Slip ahead of the crack tip would absorb energy [Grensing et al. 1990]. It is commonly found that VHP block has better tensile properties normal to the pressing direction than parallel to it. Similar relative behavior is observed for fracture toughness [Cooper 1979].

An extensive investigation was performed on VHP S-200E and, to a lesser extent, on VHP S-65 [Lemon and Brown 1985]. For cracks with their planes normal to the pressing direction, the mean K_{Ic} for S-200E was 9.86 MPa$\sqrt{m}$, while parallel to the pressing direction, the mean value was 11.05 MPa$\sqrt{m}$. It was noted that special processing did not have any significant effect. The authors obtained results from eight different pressings of VHP S-200E with powder from the same source and, together with results of other investigators, made the following conclusion. The plane-strain fracture toughness of hot-pressed beryllium for cracks with their plane parallel to the pressing direction decreases with an increase of tensile yield and ultimate strengths. This effect of tensile strength on toughness was not observed for cracks with their planes normal to the pressing direction. This influence of crack orientation can be seen in Fig. 17.26 [Lemon and Brown 1985].

Pinto reported that K_{Ic} for most grades of VHP blocks falls within the range of 9 to 13 MPa$\sqrt{m}$, with the values increasing with an increase of temperature, as seen in Fig. 17.27 [Pinto 1979b].

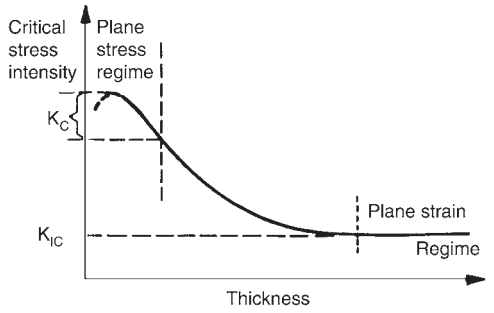

Fig. 17.23 Schematic illustration showing the variation of the critical stress intensity with thickness. Source: Cooper 1979

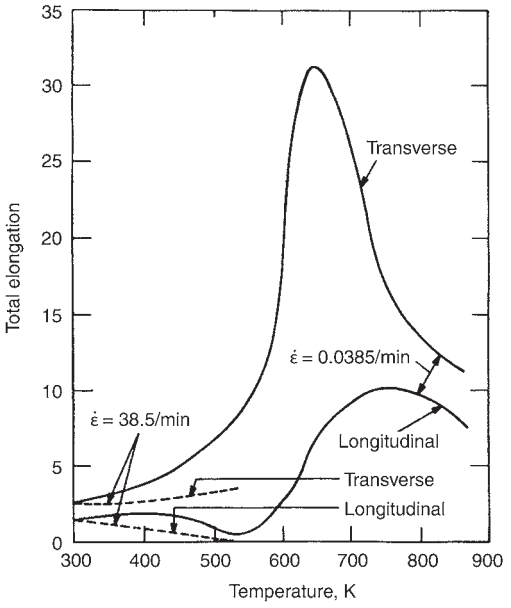

Fig. 17.24 Temperature and strain-rate dependence of total elongation of hot-pressed HY beryllium. Source: Borch 1979

Figure 17.28 contains a summary of results reported by three different investigators for VHP S-200-grade beryllium. The curves show a smooth increase with an increase in temperature, and, with the exception of the 1.6 mm material, which is in a state of plane strain, the results are relatively close. Differences are likely to be mainly due to the different types of specimens used [Cooper 1979]. High-purity block was

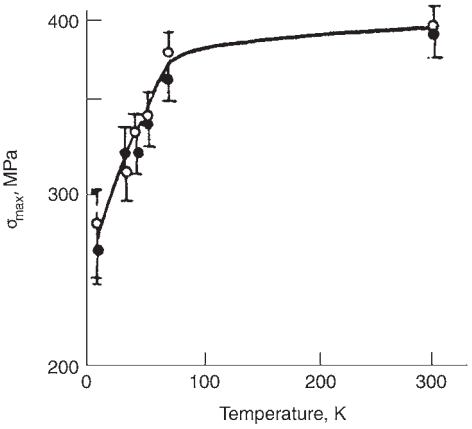

Fig. 17.25 Temperature dependence of ultimate tensile strength of a polycrystalline isostatic pressure forging of beryllium. ○, parallel to forging direction; ●, perpendicular to forging direction. Source: Lavrent'ev et al. 1987

Table 17.10 Chemical composition and grain size of three grades of vacuum hot-pressed (VHP) beryllium used for fracture-toughness tests

Element, wt%	VHP S-200E	VHP S-200F	VHP ASP(a)
BeO	1.1	0.67	0.37
C	. . .	0.08	0.10
Fe	0.07	0.07	0.08
Al	0.03	0.03	0.03
Si	. . .	0.02	0.02
Mg	. . .	0.02	0.0005
Grain size, μm	11.3	8.7	13.2

(a) ASP, atomized spherical powder. Source: Grensing et al. 1990

Table 17.11 Tensile properties of three grades of vacuum hot-pressed (VHP) beryllium used for fracture-toughness tests listed in Table 17.10

Property	Orientation(a)	VHP S-200E	VHP S-200F	VHP ASP(b)
Yield strength, MPa	LT	266	256	224
	TL	271	259	223
Ultimate tensile strength, MPa	LT	364	357	346
	TL	406	377	357
Elongation,%	LT	1.7	4.0	2.5
	TL	3.1	6.4	2.9

(a) First and second letters refer to sample and crack orientation, respectively, relative to the VHP billet. L, longitudinal, and T, transverse, to the pressing direction. (b) ASP, atomized spherical powder. Source: Grensing et al. 1990

Table 17.12 Fracture-toughness values of four grades of vacuum hot-pressed (VHP) beryllium

VHP grade	Crack orientation(a)	Specimen thickness, mm	Fracture toughness, MPa$\sqrt{m}$
S-200E	LT	12.7	10.11
	TL	12.7	11.43
S-200F	LT	25.4	10.62
	TL	25.4	12.31
ASP(b)	LT	1.27	13.59
S-65	LT	25.4	9.7
	TL	25.4	9.9

(a) First and second letters refer to sample and crack orientation, respectively, relative to the VHP billet. L, longitudinal, and T, transverse, to the pressing direction. (b) ASP, atomized spherical powder. Source: Grensing et al. 1990, Lemon and Brown 1985

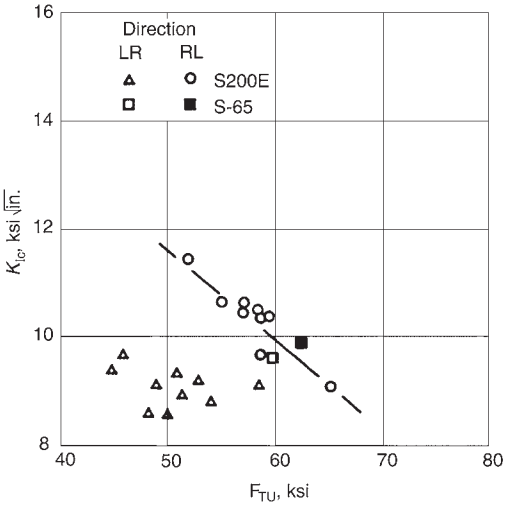

Fig. 17.26 Plane-strain fracture toughness as a function of the ultimate tensile strength for vacuum hot pressed (VHP) S-65 and VHP S-200E. First and second letters refer to sample and crack orientation, respectively, relative to the VHP billet. L, longitudinal (parallel to the pressing direction), and R, radial (normal or transverse to the pressing direction). Source: Adapted from Lemon and Brown 1985

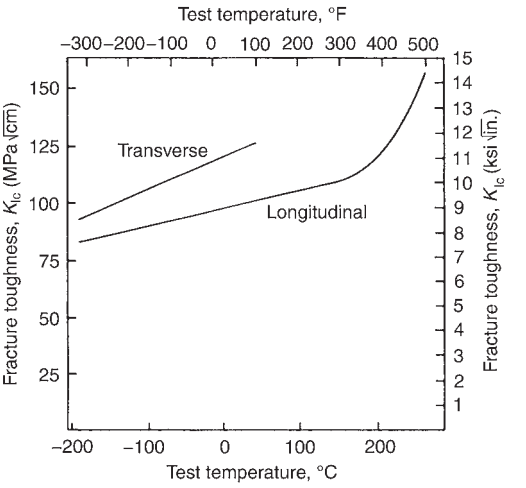

Fig. 17.27 Plain-strain fracture toughness of normal-purity beryllium block as a function of temperature. Orientation refers to direction of load application. Source: Pinto 1979b

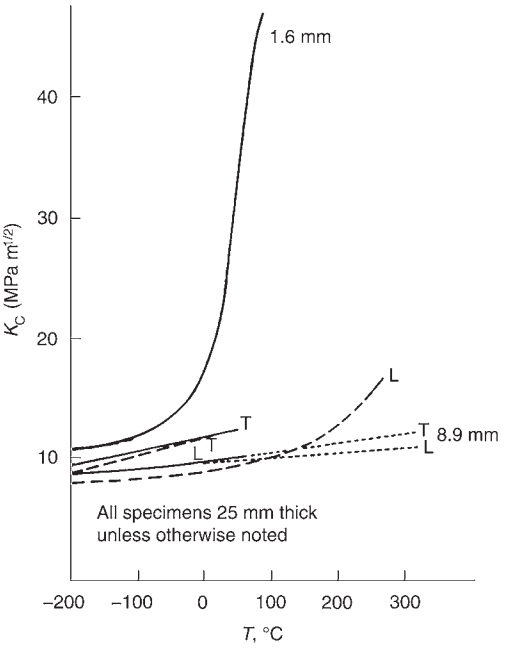

Fig. 17.28 Fracture toughness as a function of temperature for S-200 beryllium from three different investigations. Source: Cooper 1979

reported to have K_{Ic} values at room temperature of approximately 16.5 MPa, being near 50% higher than that for normal-purity block, with some evidence that the value for ultrapure beryllium is still higher [Pinto 1979b]. Perra and Finnie, using 8.92 mm thick double-cantilever beam specimens, evaluated the fracture toughness of a high-yield-strength (338 MPa at 0.2% offset and 2.1% elongation) grade of VHP beryllium, with the chemical analysis being within the limits of grade S-200F and with a grain size of 8.8 ± 0.3 μm [Perra and Finnie 1975]. Specimens were obtained with the crack plane in both the transverse (18 specimens) and longitudinal (10 specimens) directions relative to the pressing direction. Tests were performed mostly at room temperature, with several tests at 300 °C and one at 150 °C. Only a weakly increasing function of temperature (9.0 to 10.8 MPa$\sqrt{m}$) and no appreciable orientation effect were observed (8.6 and 9.1 MPa$\sqrt{m}$ for the longitudinal and transverse directions of the crack plane, respectively).

In a cooperative study performed by three laboratories, two in the United States and one in the United Kingdom, the mechanical properties of 12 different powders that had been HIPed to full density were studied. The powders consisted of four different levels of purity and three different powder-size fractions; each purity sample set had sizes of −44, −44 + 10, and −20 μm. Fracture toughness was determined in the United Kingdom using single-edge-notch (SEN) specimens, while wedge-opening load specimens were used in the United States. Both types had machined notches. The results are shown in Fig. 17.29. The powders are designated as P10, XP-10,

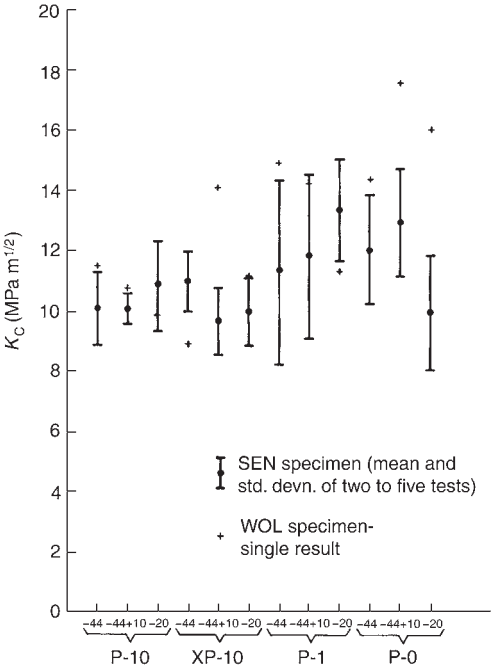

Fig. 17.29 Fracture toughness of various powder-size fractions (in μm) of P-10, XP-10, P-1, and P-0 grades of beryllium. Test details are given in the text. SEN, Single-edge notch; WOL, wedge-opening load. Source: Cooper 1979

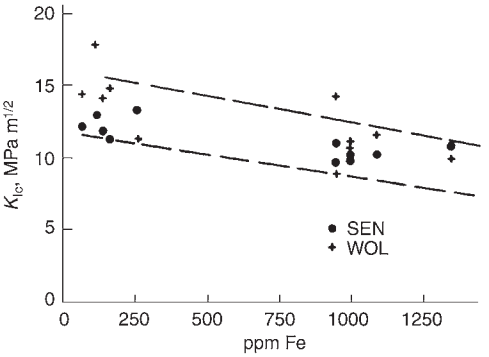

Fig. 17.30 Effect of iron content on the fracture toughness of hot-pressed beryllium. SEN, single-edge notch; WOL, wedge-opening load. Source: Cooper 1979

P-1, and P-0, with increasing levels of purity, respectively. Although there is considerable scatter in the results, there is a general trend of an increase of fracture toughness with an increase of purity level. The effects of iron alone, as well of the oxide content, are shown in Fig. 17.30 and 17.31. A definite trend is indicated for iron; the influence of the oxide content is unclear here [Cooper 1979].

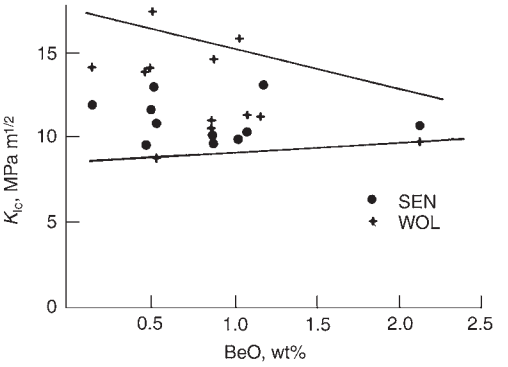

Fig. 17.31 Effect of BeO content on the fracture toughness of hot-pressed beryllium. SEN, single-edge notch; WOL, wedge-opening load. Source: Cooper 1979

Low values for plane-stress fracture toughness have been reported for unrecrystallized sheet material. When fully recrystallized, however, high toughness was attainable. Testing was performed on flat sheet that had an initiation flaw that was introduced by electrodischarge milling. The sheet specimen was then subjected to fatigue cracking. Values obtained from these tests could be used to calculate the critical flaw stress for a given stress leading to rapid crack propagation and failure. Figure 17.32 shows the results of such calculations for ingot and powder sheet [Pinto 1979b]. Opposite to the trend seen in block material, it appears that an increase in oxide content may increase the fracture toughness of sheet.

The author also reported on the role of porosity on toughness in VHP block. The fracture toughness values were calculated from data obtained on notched Charpy specimens. The results, which are shown in Fig. 17.33 for normal-purity and high-purity beryllium, indicate that a maximum in toughness is obtained at some intermediate low porosity.

The effect of thickness on fracture toughness has been examined by a number of investigators. It appears that there is very little variation in fracture toughness with thickness greater than approximately 6 mm. By contrast, significant increases can be seen for thicknesses of 2.5 mm or less. Values of 16 to 22 MPa$\sqrt{m}$ are reported for this lower-thickness range as compared to 10 to 11 MPa$\sqrt{m}$ under plain-strain conditions [Cooper 1979]. Values in the range of 28 to 32 MPa$\sqrt{m}$ were reported for 0.8 mm thick sheet by Tardiff [Tardiff 1974].

Tardiff evaluated the fracture toughness of ingot sheet and powder sheet using both SEN

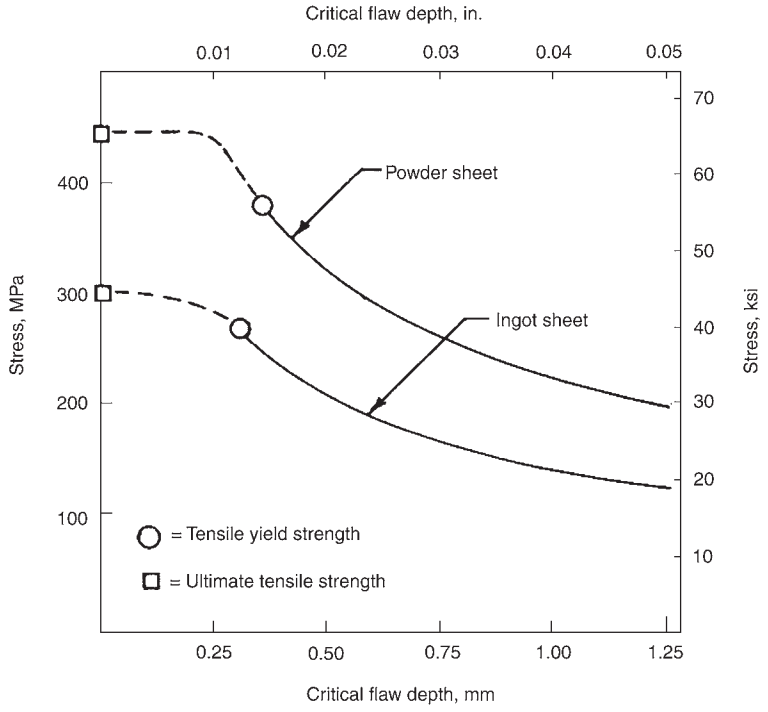

Fig. 17.32 Critical flaw depth of beryllium sheet calculated from fracture toughness data. Source: Pinto 1979b

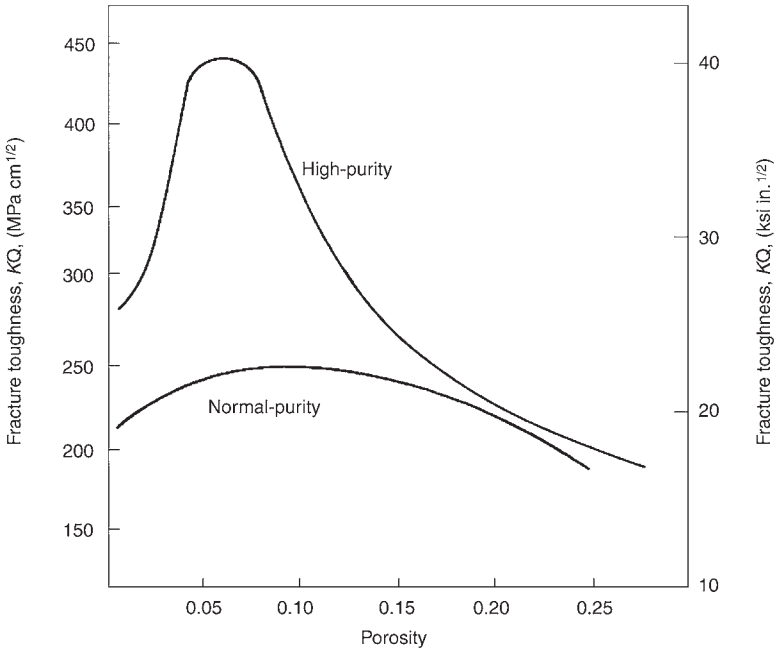

Fig. 17.33 Calculated fracture toughness versus porosity for notched Charpy specimens of vacuum hot-pressed beryllium. Source: Pinto 1979b

and double-edge-notch specimens [Tardiff 1974]. Both materials had been cross rolled to a thickness allowing for cleanup to a final thickness of 0.80 mm. The ingot sheet was of commercial purity. The powder sheet was rolled from an HP-8 block material (hot-pressed block from Kawecki Berylco Industries, Inc.). The effect of annealing temperature on fracture toughness for the ingot sheet is shown in Fig. 17.34. The large increase observed at approximately 750 °C, was attributed to changing from plane-strain to plain-stress conditions. A constant grain size was maintained until approximately 750 °C, above which recrystallization was initiated, with subsequent grain growth increasing from 40 μm at 750 °C to 120 μm at 880 °C. The corresponding tensile properties are shown in Fig. 17.35. The continuous drop in yield strength with increasing annealing temperature up to 750 °C is attributed to an increase in subgrain size and a decrease in dislocation density. Many of the recrystallized grains did not contain any substructure, as was observed in all the grains annealed below 750 °C. The author thus attributes the initial low fracture toughness to the presence of these subgrains. Studies of the fractured SEN samples annealed at 680 and 780 °C showed that the fatigue precracking changed from cleavage or quasi-cleavage for the lower temperature to largely intergranular for the higher temperature. Mostly, cleavage was observed in both cases for the fast-fracture region. Several different heat treatments were performed yielding a range of grain sizes that followed the Hall-Petch

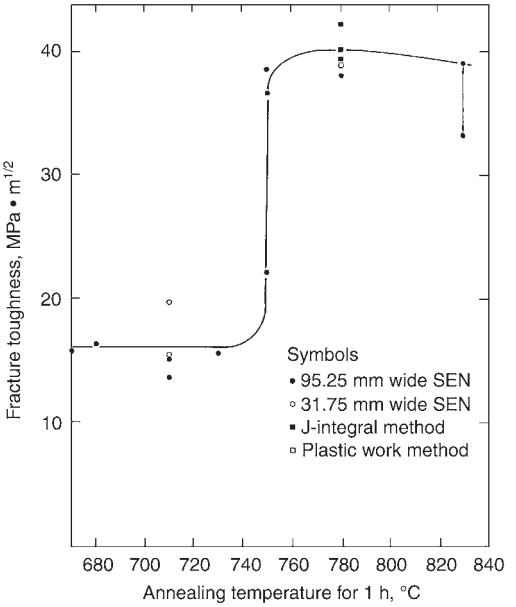

Fig. 17.34 Effect of annealing temperature on the fracture toughness of warm-rolled beryllium ingot sheet. SEN, single-edge notch. Source: Tardiff 1974

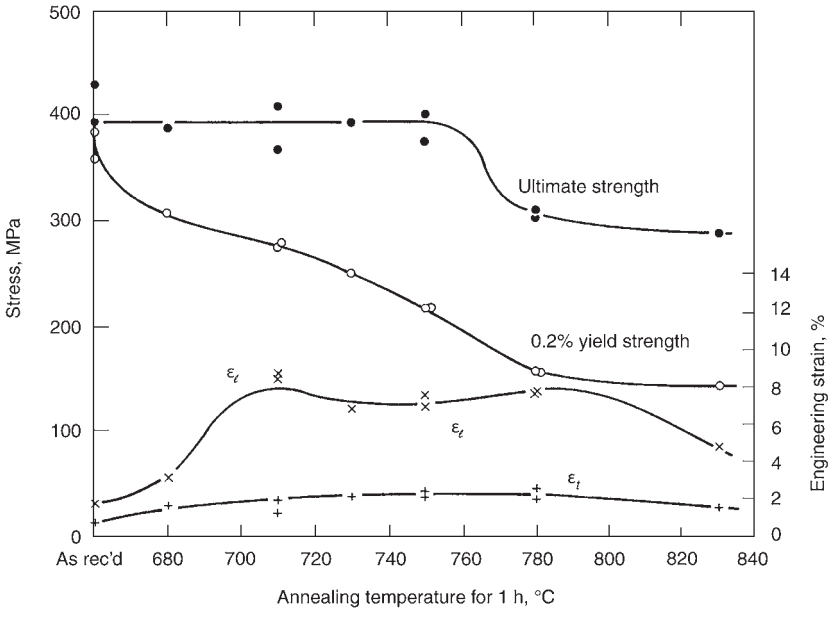

Fig. 17.35 Effect of annealing temperature on the tensile properties of warm-rolled beryllium ingot sheet. ε_l, longitudinal engineering strain; ε_t, tangential engineering strain. Source: Tardiff 1974

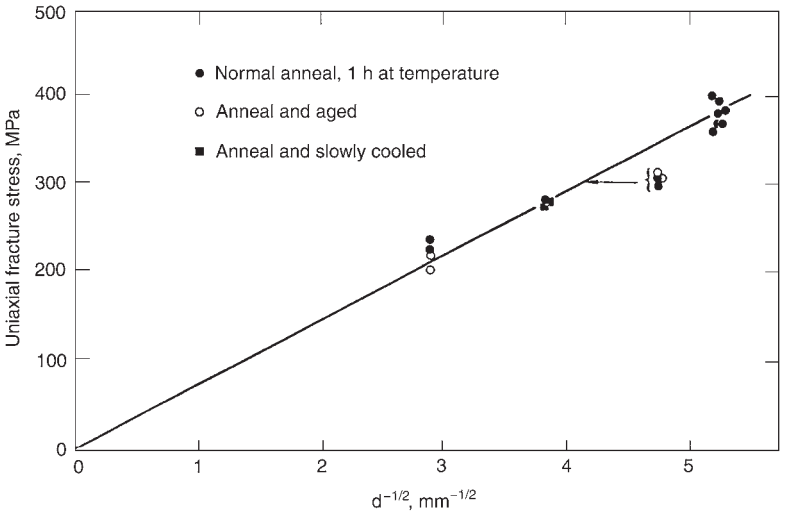

Fig. 17.36 Hall-Petch relationship of fracture stress versus grain size for beryllium ingot sheet following various heat treatments: normal cool, 0.5 °C/s; slow cool, 0.14 °C/s; age, 2 h at 700 °C + 2 h at 600 °C. Source: Tardiff 1974

relationship (see section 17.9 in this chapter) for fracture stress, as shown in Fig. 17.36. Limited tests were performed with the powder sheet. Following similar heat treatment, the powder sheet, although having the finer grain size, showed the lower fracture toughness of the two materials. This was attributed to the powder sheet having a higher degree of anisotropy than that of the ingot sheet.

17.6 Notched-Tensile and Notched-Bend Properties

The constraint imposed by the triaxiality developed at the root of a notch can, at low stress concentrations, result in the notched to notch-free strength ratio (NSR) being greater than 1. Notched tensile data for a VHP S-200F block are shown in Fig. 17.37 [Marder 1986]. As can be seen, above a temperature of approximately 100 °C, the NSR exceeds 1.0 for stress-concentration factors (K_t) of 1.9 and 3.0, suggesting that beryllium is not notch sensitive above this temperature for stress concentrations up to this value. Following the increase in the room-temperature tensile strength obtained by rolling, the notched strength also increases. Figure 17.38 shows the notch strength as a function of temperature for cross-rolled sheet exhibiting similar behavior as that seen for the as-VHP block [Marder 1986].

Loaded bend specimens can be considered to represent simple structures having a distribution of stresses and strains, especially in the vicinity of a notch. Figure 17.39 shows the results of slow-rate three-point-bend tests of notched specimens for four grades of beryllium [Saxton and London 1979]. The results indicate that a significant loss in load-carrying capacity can occur with notch radii less than approximately 5 mm. Furthermore, examination of polished fractured specimens revealed microcracks in the vicinity of the notch in all specimens with notch radii equal to or greater than 1.6 mm. The microcracks were oriented perpendicular to the maximum tensile stresses in the loaded specimens, indicating that grains favorably oriented for cleavage will fracture first. The microcracks were localized within a single grain, in that the adjacent grains acted as crack arresters if they had the proper combination of smallness and basal-plane orientation. It had been suggested that the larger grains will fracture first [Saxton and London 1979]. Interestingly, microcracks were not observed for notches at and below 0.254 mm (0.01 in.).

Notched tensile data obtained at room temperature and at 204 °C (400 °F) for VHP structural-grade S-200F are listed in Table 17.13. Impact-ground powder was used. At room temperature, with an NSR of approximately 1.01, the material does not exhibit any noticeable notch sensitivity. The increase in the NSR at 204 °C (notch-strength hardening) is attributed to the increased ductility obtained at the higher temperature [Haws 1985]. Grade S-200E showed similar behavior.

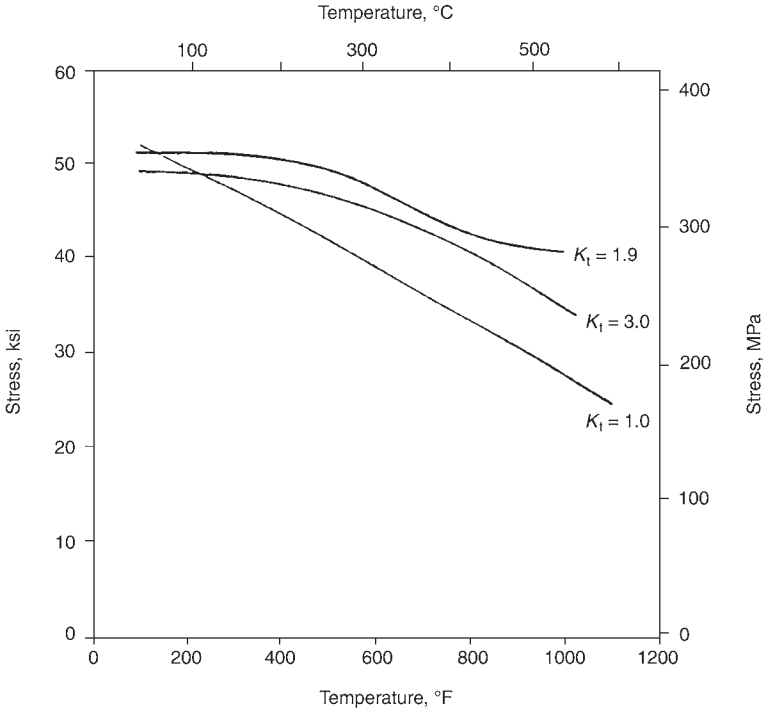

Fig. 17.37 Notched strength as a function of temperature for beryllium block. Source: Marder 1986

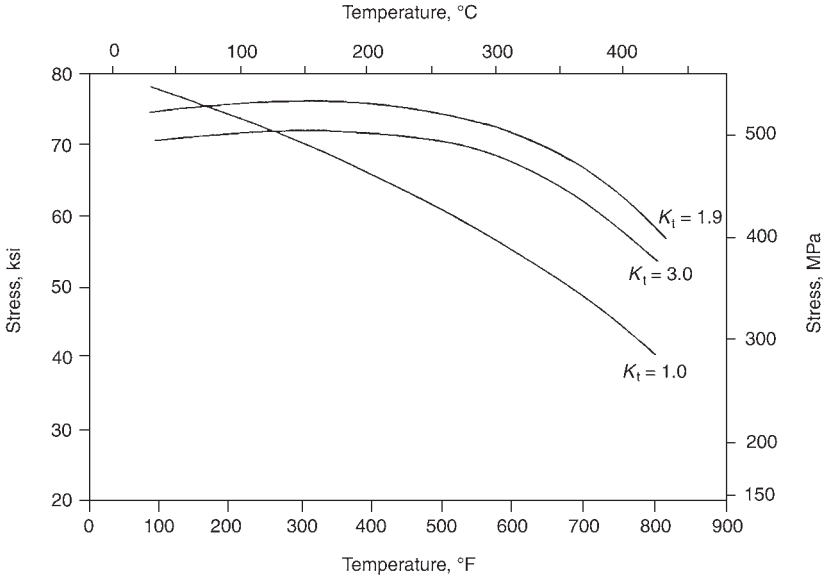

Fig. 17.38 Notched strength as a function of temperature for beryllium sheet. Source: Marder 1986

17.7 Fatigue Properties

Fatigue results at room temperature reported for VHP-grade S-200F are listed in Table 17.14 [Haws 1985]. Smooth fatigue tests were performed according to ASTM specification E 466 using a Krouse rotating-beam fatigue machine having cantilever fully reversed bending (ratio

of maximum to minimum stress equal to −1). Specimens were 9.53 mm (0.375 in.) at the grips, with a minimum diameter of approximately 6.1 mm. The fatigue life at 10^7 cycles is given as 262.0 and 265.5 MPa for the longitudinal and transverse directions, respectively.

Fatigue crack growth rates as a function of fracture toughness for VHP S-65 and S-200E are shown in Fig. 17.40 [Lemon and Brown 1985]. The data were obtained on compact-tension specimens used in a study on fracture toughness with the precrack being either parallel (L) or transverse (T or R) to the pressing direction of the billet. In the figure, the first letter refers to the load direction and the second to the crack direction. The relationship between crack growth rate, *da/dN*, and ΔK (the stress-intensity factor range, i.e., the difference between the upper and lower stress intensities in fatigue crack growth rate tests) can be seen to be dependent on the orientation, with the growth rate being lower for the RL than the LR orientation. The corresponding relationships are given, respectively, as:

$$da/dN = 8.9 \times 10^{-16} \Delta K^{8.76} \quad \text{(Eq 17.1)}$$

$$da/dN = 4.2 \times 10^{-27} \Delta K^{21.45} \quad \text{(Eq 17.2)}$$

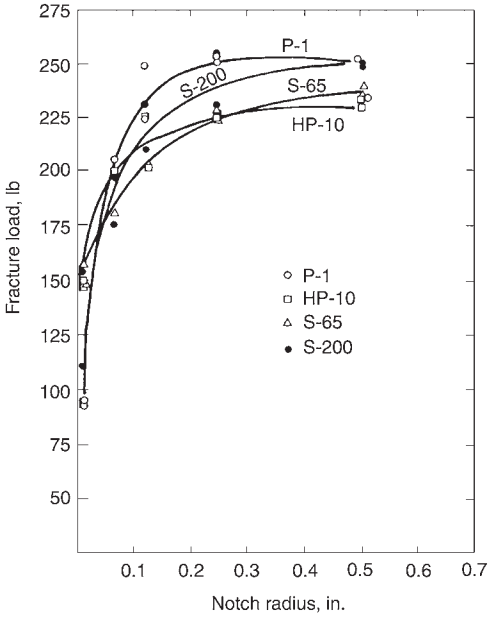

Fig. 17.39 Effect of notch radius on the fracture load in three-point bending for four grades of beryllium. Source: Saxton and London 1979

Auten and Hanafee evaluated the crack growth rate of five experimental grades of beryllium that were either of higher purity or used different processing steps compared to the previous hot-pressed commercial grades such as S-200E [Auten and Hanafee 1976]. Characteristics of the grades evaluated are listed in Table 17.15. Tests were performed using compact-tension specimens having five different thicknesses. A fatigue-stress ratio (minimum to maximum stress), *R*, of −1 was used. Since tensile properties and microstructures showed a high degree of isotropy, distinction between specimen orientation was not indicated. The authors stated that they obtained markedly lower fatigue crack growth rates than rates previously reported for beryllium. They obtained, however, considerable scatter in their results, which they claim is a real effect. The characteristics ahead of the crack front, such as encountering grains with different orientations or localized heavy oxide deposits, will affect the nature and morphology of the failure and the rate of cracking. In addition, the authors point out that quite often a higher maximum tensile stress will yield lower crack growth rates. The stress intensity was increased in increments, and if an increase was stopped, the rate would decrease, eventually leading to crack arrest.

Figure 17.41 shows results of crack growth rate versus K_{fmx} obtained for one of the grades (grade C) where K_{fmx} is the maximum applied stress-intensity factor at the crack tip. The solid line is based on behavior predicted by theory. By contrast, the growth rate shows no dependence on K_{fmx}, and this was typical for all five grades. Figure 17.42 shows the mean fatigue crack growth rate for the different specimen thicknesses. An order of magnitude difference in the rate can be seen for a given grade. The trend of

Table 17.13 Notched tensile properties of an experimental-grade S-200F

Temperature, °C (°F)	Orientation(a)	Stress-concentration factor (K_t)	Notch tensile strength, MPa	Notch-strength ratio (NSR)
Room Temperature	L	3.07 ± 0.04	385.4 ± 15.2	1.01 ± 0.04
	T	3.01 ± 0.05	415.8 ± 7.6	1.02 ± 0.03
204.4 (400)	L	3.05 ± 0.03	400.0 ± 8.3	1.21 ± 0.03
	T	3.02 ± 0.12	403.3 ± 7.6	1.21 ± 0.03

(a) L, longitudinal, T, transverse. Source: Haws 1985

Table 17.14 Room-temperature fatigue properties of S-200F beryllium

Maximum stress, MPa	Cycles, 10^3	Results(a)
Transverse group		
275.8	377	GSF
275.8	686	GSF
268.9	1,309	GSF
268.9	4,033	GSF
268.9	15,766	RO
262.0	210	GSF
262.0	12,262	RO
262.0	30,473	RO
248.2	13,938	RO
248.2	17,186	RO
234.4	14,649	RO
234.4	30,819	RO
Longitudinal group		
275.8	135	GSF
275.78	141	GSF
268.9	229	GSF
268.9	233	GSF
262.0	14,860	RO
262.0	15,609	RO
248.2	18,885	RO
248.2	25,686	RO
234.4	584	GSF
234.4	11,340	RO
234.4	13,554	RO

(a) GSF, gage-section failure; RO, run out. Source: Haws 1985

an increased rate with a decrease in thickness is attributed to a corresponding change from plane strain to plain stress. The thinner specimens enable more plastic strain per cycle, which, in turn, leads to increased fracturing [Auten and Hanafee 1976].

Fatigue properties of S-200F beryllium reported by Brush Wellman, Inc. are presented in Fig. 17.43 through 17.46 [Brush Wellman 2001]. Also included for comparison are curves on aluminum and titanium alloys. Using Krause rotating-beam fatigue tests, S-200F shows essentially no difference in the 10^7 cycle endurance limit between the longitudinal and transverse directions. Furthermore, since the endurance limit is near the static yield strength for VHP block, Brush Wellman states that beryllium components can be expected to undergo 10^7 cycles from -261 to $+261$ MPa ($R = -1$), which corresponds to the specification yield strength of the material. The fatigue ratio (UTS to fatigue-endurance limit) of S-200F is reported as 0.7 compared to 0.5 for steel and 0.35 for aluminum and magnesium [Brush Wellman 2001].

17.8 Creep Strength

Since the specific modulus of beryllium retains an advantage over other structural materials at elevated temperatures, where the strength is still significant, the creep properties of beryllium are important. Figure 17.47 shows a Larson-Miller plot for VHP S-200F, where the stress for different amounts of creep deformation is given as a function of time and temperature [Marder 1986]. The increase in tensile strength produced by rolling is also reflected by a corresponding increase in the creep strength. Figure 17.48 shows a Larson-Miller creep plot for sheet material [Marder 1986]. The increase in creep strength obtained by rolling can be seen by comparing this figure with Fig. 17.47. As with all nonelastic properties, the creep rate of beryllium is highly sensitive to impurities and microstructure. The creep rate of dense VHP S-200F beryllium for applied stresses from 14 to 21 MPa and from 400 to 700 °C is given as:

$$d\varepsilon/dt = 0.75(1 - p^{2/3})^{-3.6} \exp(-2.60 \times 10^4/T)\sigma^{3.6}$$

where p is the volume fraction of porosity, T is the temperature in degrees K, t is in seconds, and σ is the von Mises stress in MPa [Borch 1979].

The BeO together with the low-melting-point impurities tend to segregate at the grain boundaries formed during the hot-consolidation process. This, in turn, will affect the creep behavior. At temperatures above 760 °C, it was observed that the creep strength was related to the presence of such impurities, since liquid grain-boundary phases are generally located at triple points and/or at isolated pools along the grain faces. Thus, grain-boundary separation and sliding occurs, which is not prevented by the BeO particles. By contrast, with high-purity beryllium, where there is a large reduction in the liquid phase, the matrix becomes the weakest link. Slip occurs within the grains, and the strength of the matrix will now be influenced by the size and volume fraction of BeO [Stonehouse 1979].

Figure 17.49 is an illustration of the detrimental influence of impurities on creep strength [Borch 1979]. The role of the oxide particles is illustrated in Fig. 17.50. The creep strength is approximately doubled by having the oxide dispersed along the grain boundaries as compared to that obtained for the same high-purity material in which the oxide was uniformly dispersed in the matrix. The latter condition was obtained by extruding the original HIPed material. Both materials were subsequently recrystallized to obtain the same starting grain size. It may be noted that grain growth at the higher creep temperatures

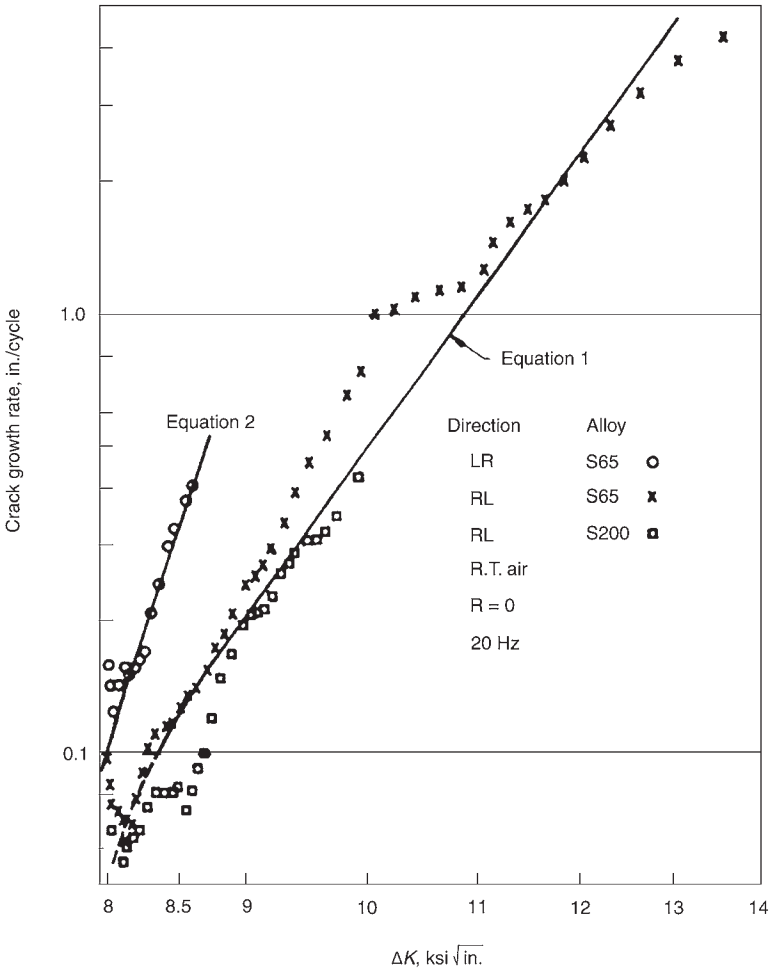

Fig. 17.40 Fatigue crack growth rate versus K_{Ic} for vacuum hot-pressed S-65 and S-200E. Source: Lemon and Brown 1985

Table 17.15 Characteristics of five experimental grades of beryllium compared to two commercial grades

	Chemistry, wt%					Yield strength(a), MPa		
Grade	BeO	Fe	Al	Density, g/cm³	Grain size, μm	L.	T	Processing(b)
A	0.84	0.023	0.002	1.851	15	231	233	I, C, H
B	1.32	0.024	0.006	1.856	10	307	305	I, C, H
C	1.82	0.036	0.006	1.861	5	393	396	I, H
D	0.60	0.06	0.02	1.847	10	233	268	I, HP
E	0.48	0.01	>0.01	NA	14	227	231	I, HP
S-200	1.1	0.16	0.07	1.82	NA	228	241	HP
HP-20	2.0	0.18	0.15	1.84	NA	. . .	207	HP

(a) L, longitudinal, T, transverse. (b) I, impact powder; C, cold isostatic pressing: H, hot isostatic pressing; HP, vacuum hot pressing. Source: Auten and Hanafee 1976

only occurred with the as-HIPed material, whereas the grain size remained stable with the extruded material. With increasing temperature, the increase in grain size offsets the strengthening effect of the grain-boundary oxides, such that differences in the creep strength between the two materials diminished with increasing temperature.

Most pure metals and some alloys exhibit creep behavior that follows an expression of the form:

$$d\varepsilon/dt = K\sigma^{n} \exp(-Q/RT)$$

where $d\varepsilon/dt$ is the creep rate, K is a structure-sensitive parameter, n is the stress exponent, Q is

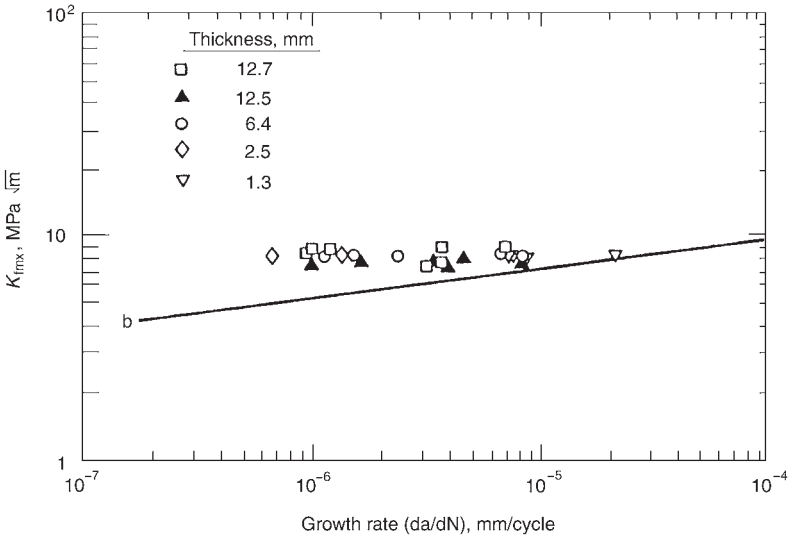

Fig. 17.41 Fatigue crack growth rate for experimental grade C beryllium as a function of maximum applied stress-intensity factor, K_{fmx}, at the crack tip for a range of specimen thicknesses. Solid line *b* is theoretical. Source: Auten and Hanafee 1976

the activation energy, *T* is the temperature, and *R* is the gas constant. Typical of most dispersion-hardened materials, a range of values were obtained for n (2.0 to 14.0) and *Q* (44 to 276 kcal/mol). The introduction of liquid at the grain boundaries, the amount of liquid increasing with increasing temperature, and the coarsening of grains and oxide particles result in a continually changing structure. Correspondingly, a change in the predominant creep mechanism may occur; the oxide coarsening as well as the liquid phase can promote grain-boundary sliding. A study was performed with high-purity HIPed beryllium [Borch 1979]. Steady-state creep behavior of this material showing a small change in slope (n-value) with temperature can be seen in Fig. 17.51. The behavior of different powder-based products is shown in Fig. 17.52. The steady-state creep rate as a function of stress at a series of temperatures is shown in Fig. 17.53 for a high-purity, cast-and-extruded SR-grade beryllium [Borch and Hauber 1968]. The effect of grain size on the creep rate is given in Fig. 17.54 for the same material. The BeO content was given as 1600 ppm, an unusually low oxide content.

Figure 17.54 shows the creep rate of a high-purity HIPed beryllium as a function of grain size at several different temperatures [Webster et al. 1973]. It can be seen that at 982 and 1093 °C (1255 and 1366 K), the usual inverse grain-size relationship with creep rate is obtained. At and below 899 °C (1172 K), however, this relationship reverses for grain sizes below approximately 25 μm, in that the creep rate decreases with increasing grain size. A similar observation was reported for low-purity HIPed beryllium [Borch 1979].

17.9 Grain Size Effects, Recrystallization, and Grain Growth

The tensile yield strength is typically related to grain size through the Hall-Petch (H-P) equation:

$$\sigma_y = \sigma_o + kd^{-1/2}$$

where σ_y is the measured yield stress, σ_o is the yield stress at infinite grain size, *k* is a constant (slope), and *d* is the grain size. A similar relationship exists for the UTS. The relationships between the yield and ultimate tensile strengths and the grain size reported for S-200F structural-grade beryllium are shown in Fig. 17.55 [Hashiguchi et al. 1988]. The values for σ_o and *k* will depend on material variables (e.g., impurities, initial dislocation density, orientation texture, etc.).

Table 17.16 lists the H-P constants for the yield strength of beryllium from different sources with various histories. A detailed critique of the results listed in the table was presented in the paper by Turner [1979]. The Hall-Petch relationship is also used for flow stresses at constant

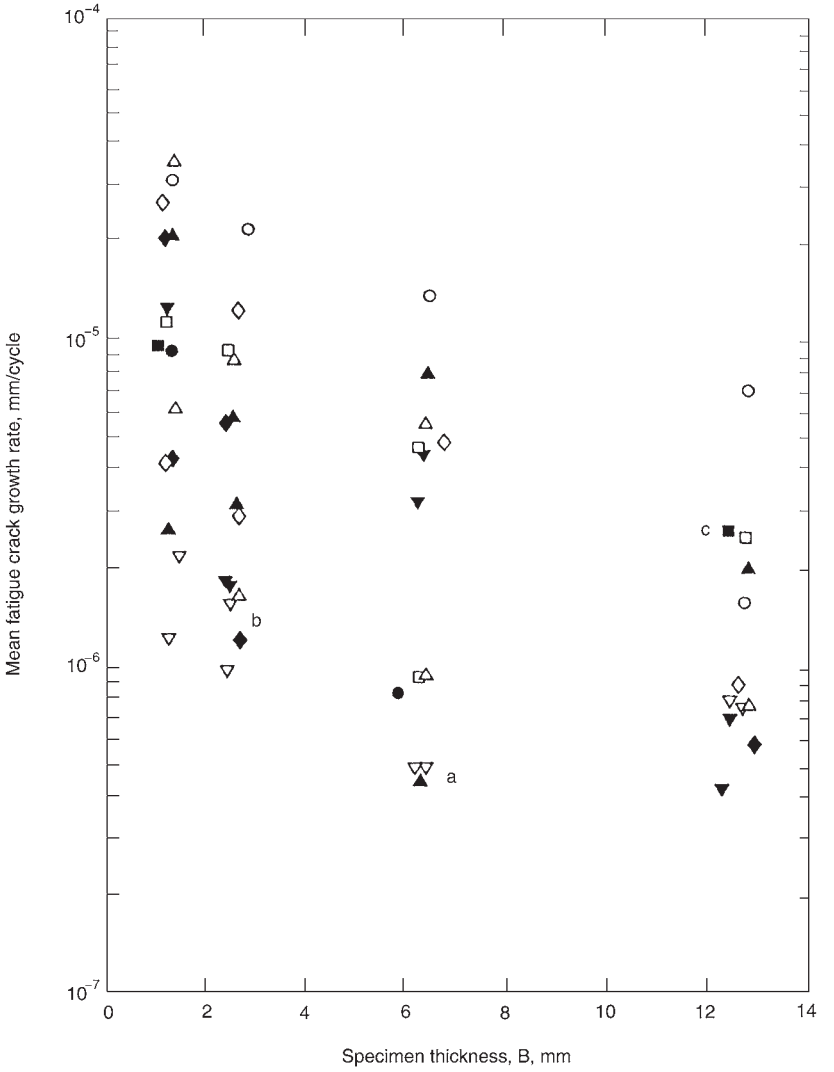

Fig. 17.42 Effect of specimen thickness on mean crack growth rate in five experimental grades of beryllium. △, grade A; ◆, grade B; □, grade C; ○, grade D; ▽, Grade E. Filled and empty symbols represent transverse and perpendicular directions to the pressing direction, respectively. Source: Auten and Hanafee 1976

strains ranging from the yield stress up to the fracture stress. Table 17.17 lists the H-P constants for the fracture strength of various beryllium materials. In general, the slope, k_f, increases with an increase in strain, as illustrated in Fig. 17.56 for hot-pressed, high-purity beryllium [Turner 1979]. The Hall-Petch relationship obtained for tensile stresses is also valid for hardness data, and both properties show similar behavior.

The grain size of as-cast beryllium is generally large, of the order 10^4 μm, which is typical of hexagonal close-packed metals and is largely the result of their strongly preferred growth direction. A common method of obtaining fine grain sizes is through one or more rolling and recrystallization cycles. This method was attempted for beryllium using high-purity ingot that was subjected to a number of repeated rolling-recrystallization cycles involving large deformations (e.g., 90%). The smallest grain size that was developed was approximately 13 μm. Rolling, however, develops a textured structure. To minimize such structures, redundant forging was also attempted; however, this produced a grain size of over 50 μm [Turner 1979]. In con-

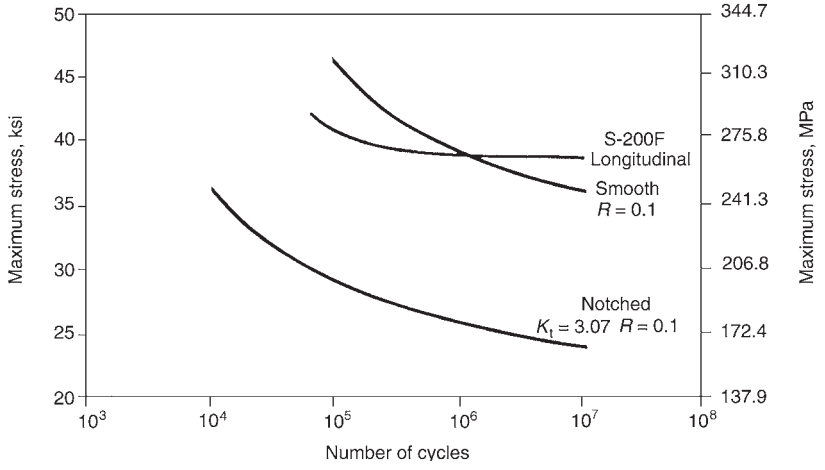

Fig. 17.43 Axial stress-number of cycles (*S-N*) curves for notched and smooth samples of vacuum hot-pressed beryllium block tested at room temperature. Source: Bush Wellman 2001

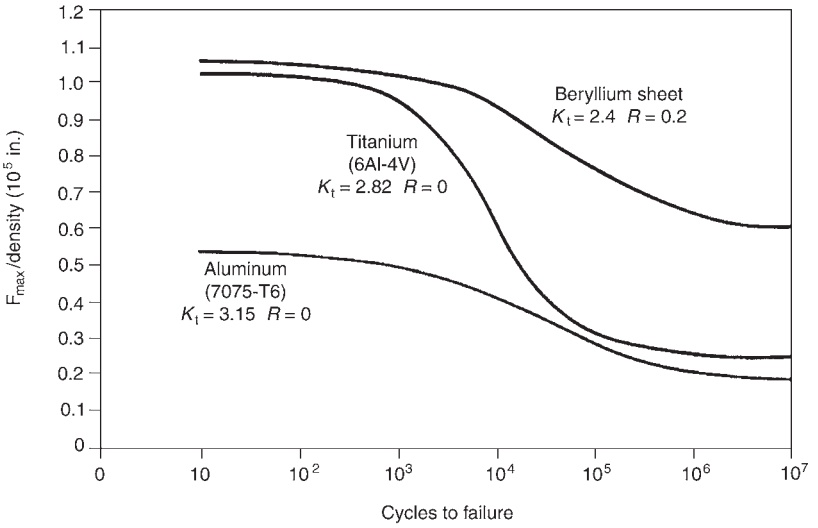

Fig. 17.44 Comparison of fatigue-strength-to-density ratio of notched specimens of beryllium, titanium (Ti-6Al-4V), and aluminum (7075-T6). Source: Bush Wellman 2001

trast with attempts to refine the cast structures, relatively fine grain sizes are achievable by pursuing the powder route, generally followed by mechanical working.

Hall-Petch plots for both yield stress and fracture stress as a function of grain size are shown schematically in Fig. 17.57. Since the difference between the yield stress and fracture stress increases with a decrease in grain size, it follows that the ductility would also increase. Table 17.18 lists the (best-effort) ductilities obtained for different grain sizes of beryllium having various purities and produced by a variety of methods. Also included in the table are the differences between the fracture and yield stresses. The table covered results published over the period from 1961 to 1977 [Turner 1979]. In the case of the bonded laminates, while isotropic high ductility (18% elongation) was obtained in the plane of the sheets, the elongation was reduced to 3 to 5% perpendicular to the bond plane. A detailed discussion referring to this table is presented in the published paper [Turner 1979].

The author points to several cases where the maximum ductility is obtained with an intermediate grain size [Turner 1979]. This ductility

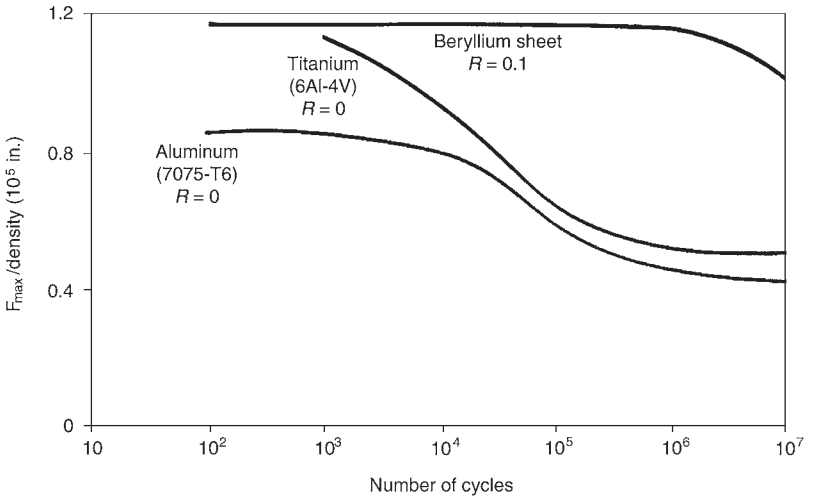

Fig. 17.45 Comparison of axial fatigue strength of smooth specimens of beryllium, titanium (Ti-6Al-4V), and aluminum (7075-T6). Source: Brush Wellman 2001

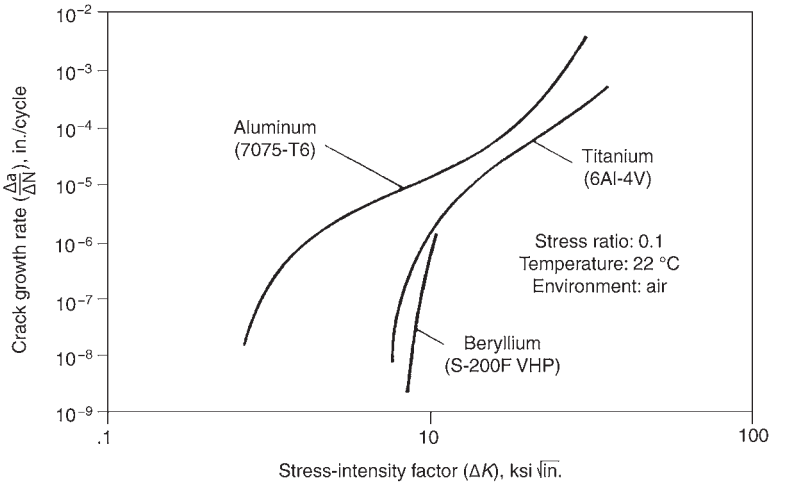

Fig. 17.46 Comparison of fatigue crack growth of beryllium, titanium (Ti-6Al-4V), and aluminum (7075-T6). To convert in./cycle to m/cycle, divide by 39.3; to convert ksi$\sqrt{\text{in.}}$ to MPa$\sqrt{\text{m}}$, multiply by 1.099. Source: Brush Wellman 2001

was attributed to increasing impurity with decreasing grain size as well as a possible change in failure mode. Generally, the minimum grain size attainable decreases and the ductility increases in traversing from cast to attritioned powder to impacted powder to lower oxide content to added deformation. Some limited fracture-toughness results, obtained using Charpy U-notched bars of plasma-consolidated powders, are consistent with the aforementioned results. Bars were tested at a strain rate of 54 s^{-1}. Based on the integrated areas under the impact stress-strain curves, the absorbed impact energy first increased to a peak value with decreasing grain size and subsequently decreased with further reduction of grain size [Turner 1979].

At temperatures above 50% of the melting point, with sufficiently fine grain sizes and of sufficient purity, beryllium can exhibit superplastic properties. That is, a high value of the strain-rate sensitivity coefficient, *m*, which is required to delay the onset of tensile instability, is obtained. The coefficient *m* is defined by the following relationship:

$$m = d\ (\ln \text{stress})/d\ (\ln \text{strain rate})$$

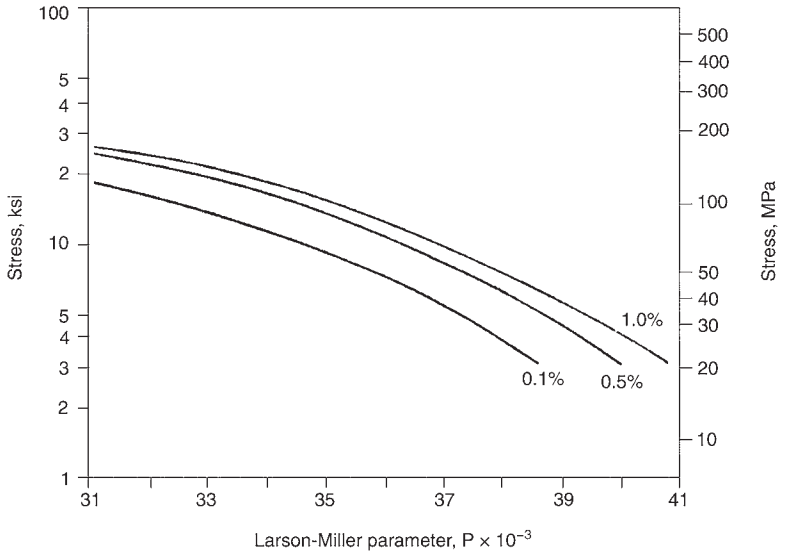

Fig. 17.47 Larson-Miller parameter (P) for beryllium block at three different creep strains. P = (*T* + 460) (c + log *t*), where c is 20, *T* is temperature (°F), *t* is time (s) for data range 1000–1500 °F (538–816 °C). Source: Marder 1986

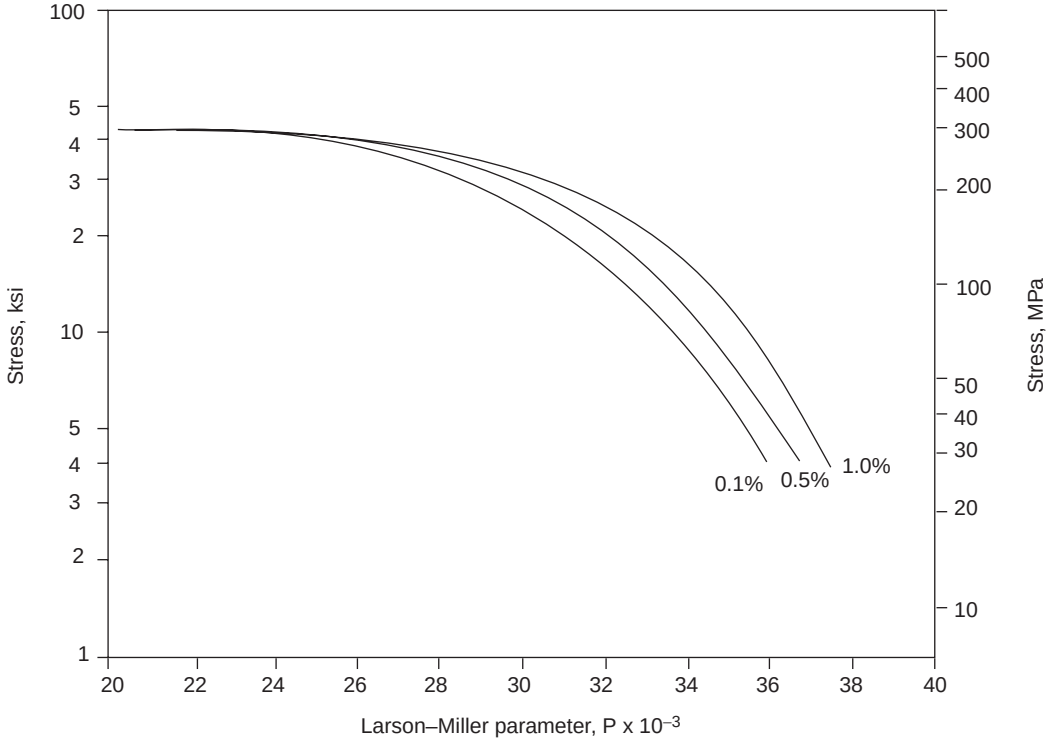

Fig. 17.48 Larson-Miller parameter for beryllium sheet at three different creep strains. P = (*T* + 460) (c + log *t*), where c is 20, *T* is temperature (°F), *t* is time (s) for data range 500–1250 °F (260–677 °C). Source: Marder 1986

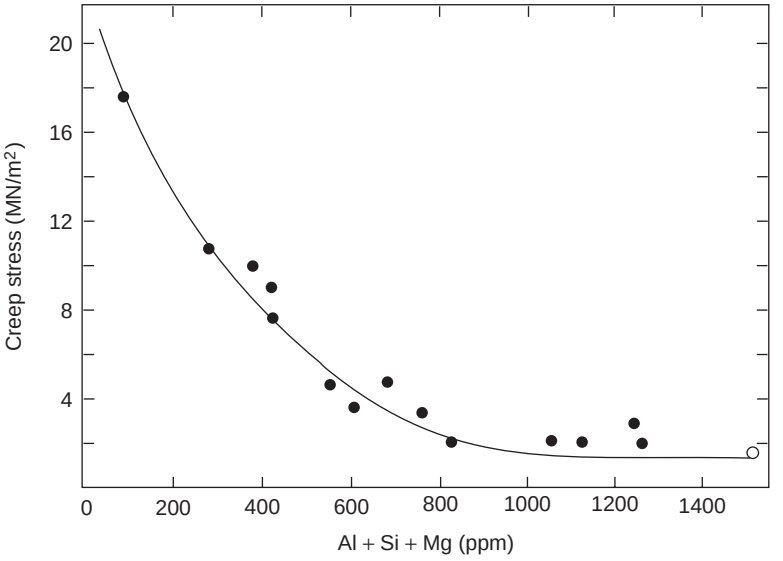

Fig. 17.49 Effect of the sum of Al, Si, and Mg contents on the creep strength of hot-pressed beryllium tested at 982 °C (1800 °F) at a strain rate of 10^{-4}/s. Source: Borch 1979

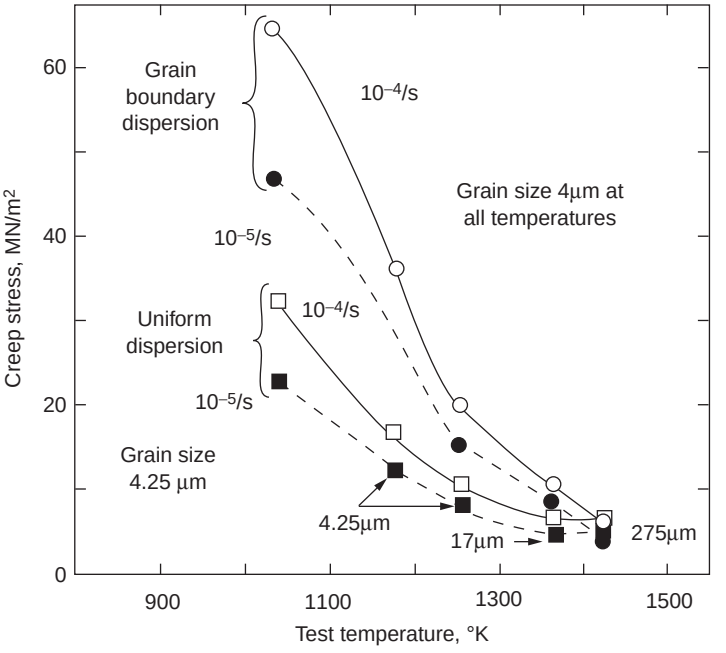

Fig. 17.50 Effect of BeO dispersion on creep strength of high-purity hot isostatic pressed beryllium. Source: Borch 1979

For example, tensile elongations of 90 and 130% were obtained at 752 and 952 °C, respectively, for a grain size of 13 μm. A study on similar material, under optimized strain-rate and temperature parameters, gave a maximum elongation of approximately 200% at $10^{-4}s^{-1}$ at temperatures between approximately 600 to 700 °C. In beryllium of lower-purity-containing oxide, superplasticity was not attainable over a wide range of temperature and strain rate [Turner 1979]. Superplastic behavior was also observed for a fine-grain, 16 μm ingot above approximately 700 °C.

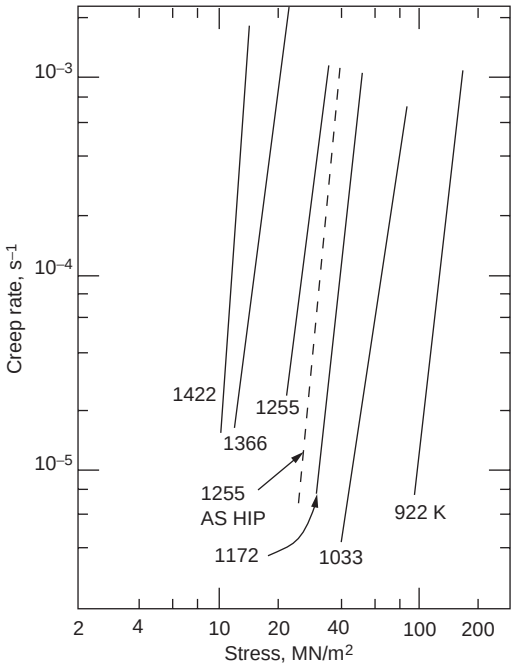

Fig. 17.51 Steady-state creep behavior of high-purity hot isostatic pressed (HIPed) beryllium annealed 3 h at 1163 °C (2125 °F) and tested at several different temperatures (K). Source: Borch 1979

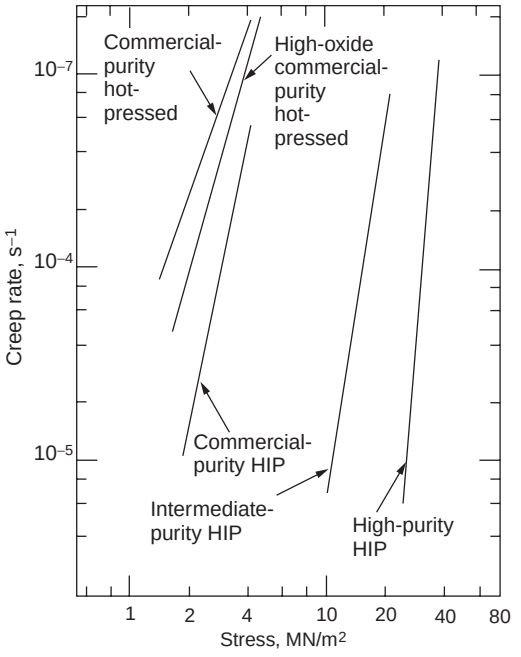

Fig. 17.52 Steady-state creep data at 982 °C (1800 °F) for several powder products of beryllium. HIP, hot isostatic pressed. Source: Borch 1979

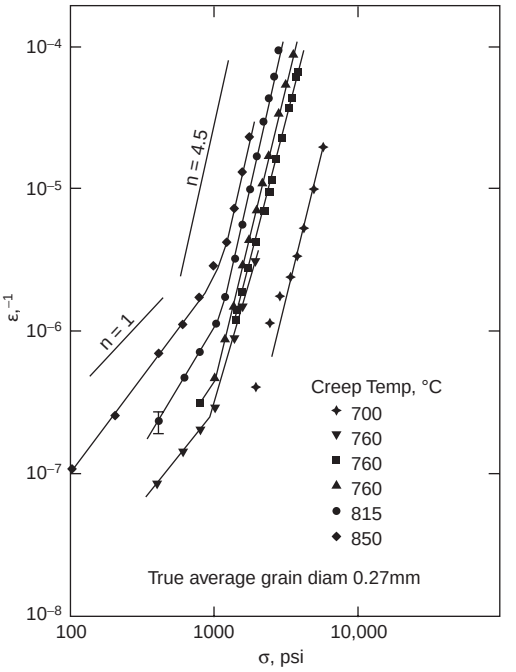

Fig. 17.53 Steady-state creep rate as a function of stress at constant grain size for cast-and-extruded SR-grade beryllium. Source: Borch and Hauber 1968

The impurities listed in ppm are 200 O, 620 Al, 1380 Fe, 500 Si, and 220 Ti. Although a high strain-rate sensitivity coefficient of approximately 0.9 was seen, elongations obtained were only of the order of 100%. At a larger grain size of 33 μm, the superplastic behavior was not seen, although grain-boundary sliding was still observed at the lower strain rates (5×10^{-5} to $5 \times 10^{-4} s^{-1}$). At the higher strain rates (greater than 3×10^{-3}), grain-boundary sliding did not occur [Borch 1979].

Results of several studies indicated that the critical ductile-to-brittle transition temperature is lowered with decreasing grain size, approaching room temperature with sufficiently small grain sizes, for example, a fine-grain, nontextured, recrystallized structure produced by upset forging of ingot beryllium deformed by grain-boundary sliding at room temperature, resulting in a ductile-type failure [Turner 1979].

Recrystallization in beryllium takes place primarily by the formation of low-angle subgrain boundaries, which, with the absorption of dislocations resulting in a corresponding increase in the boundary angles, subsequently form into high-angle grains. The process usually occurs in two stages. Grains that are initially favorably oriented for slip and are more heavily deformed recrystallize most readily, in contrast to grains

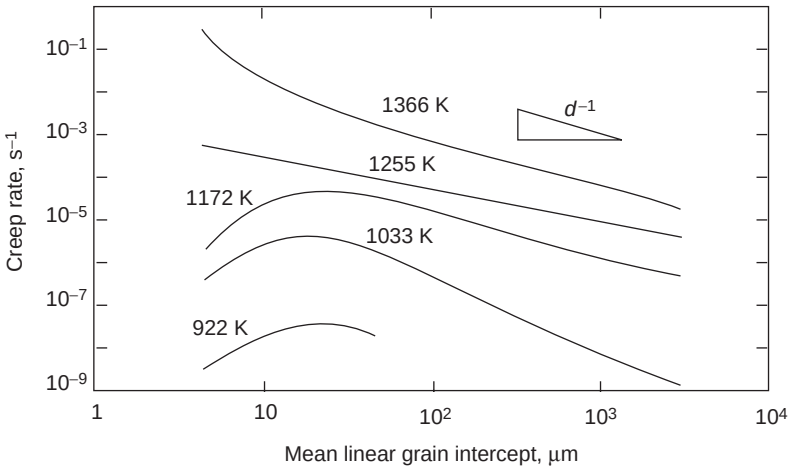

Fig. 17.54 Effect of grain size on the creep rate of hot isostatic pressed high-purity beryllium. Source: Borch 1979

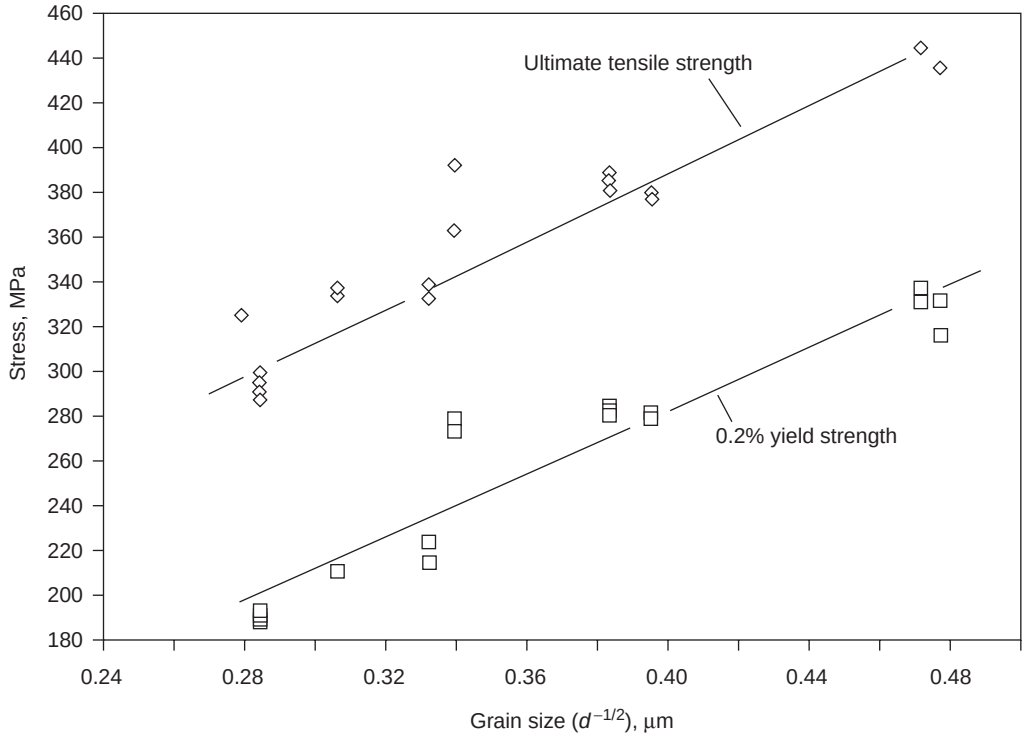

Fig. 17.55 Hall-Petch relationship between tensile strengths and grain size for S-200F structural-grade beryllium. Source: Hashiguchi et al. 1988

that had their basal planes at or near perpendicular to the deformation axis and are less deformed. The temperature required to initiate recrystallization is increased by the following: decreased cold work; decreased BeO particle size; increased BeO particles in grain boundaries in contrast to being uniformly dispersed; and decreased contents of elements that form low-melting-point phases, which facilitate the agglomeration of the particles. The agglomeration of the particles

Table 17.16 Hall-Petch constants for yield strength of beryllium in uniaxial tension reported by a number of different investigators

Material history	Grain-size range, μm	Test temperature, K	σ_o, MN/m^{-2}	k, MN/m$^{-3/2}$
Powder, extruded rod, sheet	16–60(a)	295	86.2	. . .
High-purity electrolytic flake, cast and rolled	80–300	295	22.4	0.80
		373	50.4	0.38
		473	63.1	0.06295
Attritioned powder extruded to flats:				
Low oxide	6–50	295	0	0.81
High oxide	. . .	. . .	158	0.81
High-purity wrought ingot(b)	31–116	295	88.3	2.17
Commercial-purity hot-pressed powder:				
Low iron	20–45	295	17.6	0.94
High iron	10–35	295	47.3	0.94
Hot-pressed + annealed various materials:				
Low iron	4–60	295	73.0	0.48
High iron	4–60	295	130	0.47
Variety of materials and conditions	2–20	295	−37.1	0.94
Uniaxially hot-pressed, high-purity powder	3–17	295	114	0.37
		450	82	0.37
		550	44	0.37

(a) Powder particle size range. (b) Bend-test data. Source: Turner 1979

Table 17.17 Hall-Petch constants for fracture strength of beryllium in uniaxial tension reported by a number of different investigators

Material history	Grain-size range, μm	Test temperature, K	σ_o, MN/m^{-2}	k, MN/m$^{-3/2}$
Various hot-worked conditions	16–100	295	86.2	3.2
Hot extruded	10–100	295	86.2	2.2
Hot-pressed	15–60	295	86.2	0.98
Attrition powder-extruded	6–50	295	200	1.37
High-purity electrolytic flake, cast and rolled	80–100	295	−72.8	2.76
		373	−56.7	2.69
		473	−56.7	2.16
Variety of materials and conditions(a)	2–20	295	−58.4	1.37
High-purity wrought ingot(b)	31–116	295	160.7	5.68
High-purity hot-pressed	3–17	295	152	0.96

(a) Ultimate tensile stress. (b) Bend-test data. Source: Turner 1979

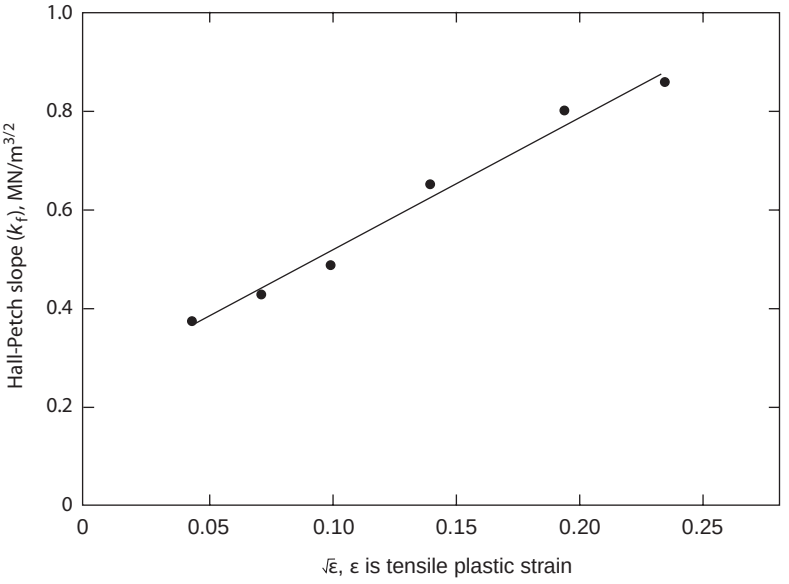

Fig. 17.56 Effect of strain on the Hall-Petch slope for flow stress in hot-pressed, high-purity beryllium. Source: Turner 1979

reduces the number of particles in the grain boundary and thus their effectiveness in inhibiting recrystallization. Subsequent grain growth is affected similarly by the factors that affect recrystallization [Webster 1979].

An example showing the relationship between the degree of cold work and the recrystallization temperature and the influence of the oxide particles can be seen in Fig. 17.58. In the HIPed condition, the oxides remain mainly in the grain boundaries, where they are most effective in restricting grain growth. The HIPed product was then extruded, which resulted in a more uniform distribution of the BeO particles. The extrusion was then recrystallized to provide the same grain size as that of the HIPed condition. Both materials were then cold rolled to give the results shown in the figure. A further reduction of the oxide shows an additional lowering of the recrystallization temperature [Webster 1979].

Hot pressing of beryllium powder to form VHP blocks generally results in a fully annealed condition with some grain growth. Since HIPing may be done at significantly lower temperatures, recrystallization and grain growth may not always occur here. In both processes, however, neither recrystallization nor grain growth will occur with beryllium of sufficiently high purity. The results in Fig. 17.59 for high-purity HIPed beryllium show that no significant growth occurred until reaching a temperature of approximately 1325 °C [Borch 1979].

The effect of grain size on the temperature dependence of elongation in beryllium is shown in Fig. 17.60. Curves 1 and 2 refer to a consolidated-powder product; the material history for curves 3 and 4 was not given; curve 5 refers to a cast commercial-purity beryllium that was thermomechanically processed to provide a fine grain size [Volokita and Tikhinskii 1989]. It can be seen that the peak elongation is increased and occurs at decreasing temperatures, with a decrease in grain size.

An extensive review of mechanical properties of beryllium was published in 1954 that included data on the effect of grain size as a function of temperature [Beaver and Wikle 1954]. Tensile-bar specimens measuring 19 mm in diameter with a gage length of 50.8 mm were used. Figures 17.61 and 17.62 show the effect of grain size on UTS for VHP and VHP plus hot-extruded beryllium, respectively. The powder was obtained by attrition of chips machined from vacuum-cast ingots that were cast from melted beryllium pebbles. It may be seen that at the lower temperatures, the strength increases with decreasing grain size; however, the strengths tend to merge or even reverse at the higher temperatures, whereby the finest-grained condition inverts from the strongest to the weakest condition from 450 to approximately 700 °C.

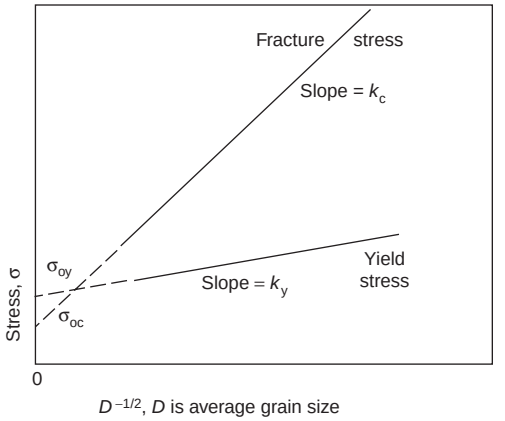

Fig. 17.57 Hall-Petch stress-grain size dependence. Source: Turner 1979

Table 17.18 Comparisons between grain size, room-temperature tensile yield strength, fracture strength minus yield strength, and elongation of beryllium reported by a number of different investigators

Material	Grain size, μm	σ_y(a), MN/m²	($\sigma_c - \sigma_y$(b), MN/m²	Elongation, %
Rolled electrolytic flake	80	112	131(c)	4
Complexed-worked high-purity ingot	13	. . .	596(d)	7.5(e)
Upset-forged high-purity ingot	70	120	45	1.5
Diffusion-bonded rolled ingot laminates	16	221	284	18
Extruded commercial purity (QMV)	6	492	329	7.3
Extruded high purity (Pechiney CR)	20	166	382	9.7
Hot-pressed, forged and aged high purity	−20 powder	373	219	18
Hot isostatic pressed (HIP) and extruded high purity	1.6	676	484	12.7
HIP and rolled high purity	2.8	586	305	27.5
HIP, upset forged and HT high purity	?	284	315	13.6
Hot-pressed commercial purity	10	321	108	4.8

(a) 0.2% proof stress. (b) σ_c calculated from UTS × (1 + strain). (c) Measured. (d) Fracture stress. (e) Average value, minimum 10%. Source: Turner 1979

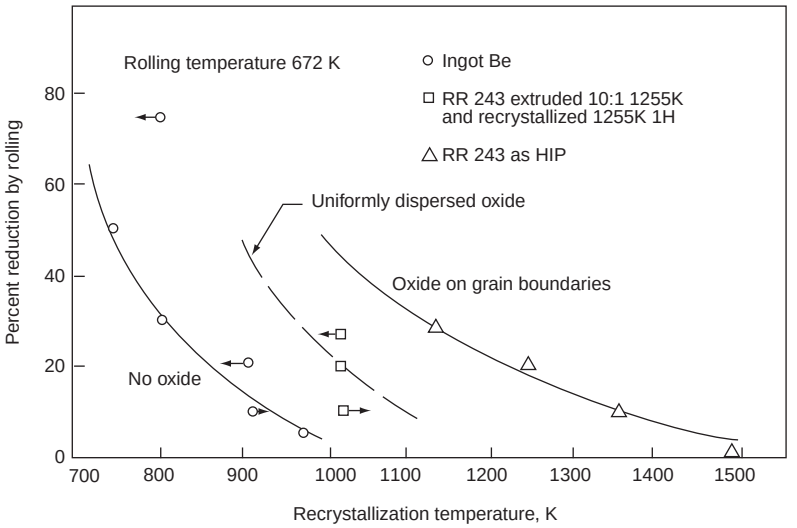

Fig. 17.58 Influence of the presence and distribution of BeO particles on the recrystallization temperature of high-purity vacuum hot-pressed block. Source: Webster 1979

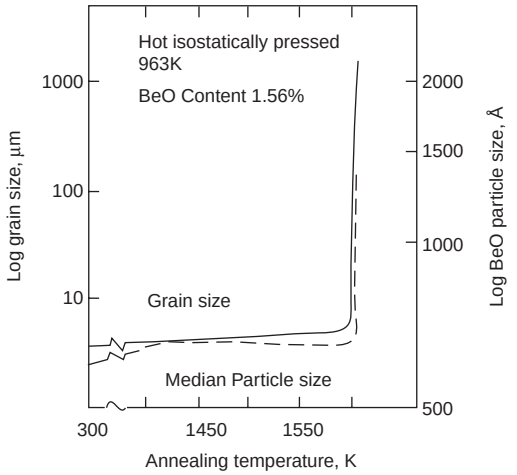

Fig. 17.59 Effect of temperature on the BeO particle size and grain size of high-purity hot isostatically pressed beryllium. Source: Borch 1979

17.10 Control and Effect of Impurities

Aluminum, silicon, and magnesium are elements that are essentially insoluble in beryllium. Consequently, during solidification, these elements become concentrated as low-melting phases in the grain boundary and have the potential of causing significant hot shortness (loss of elevated-temperature ductility). Aluminum is the key element in causing hot shortness. It is well established that free aluminum in the grain boundaries results in a reduction in ductility of beryllium. An example of this loss as affected by the content of free aluminum is shown in Table 17.19 for VHP beryllium. The dramatic drop in elongation obtained over a relatively narrow range in the free-aluminum-content material can be seen in Fig. 17.63 [Stonehouse 1979].

The amount of free aluminum can be reduced by combining with iron to form $AlFeBe_4$. Since the weight relationship of iron to aluminum is close to 2, the free-aluminum content can be controlled by having the iron content be at least twice that of aluminum. In addition, the beryllium must be aged at an elevated temperature for a sufficient length of time to allow the iron to diffuse to the grain boundaries and combine with the aluminum to form $AlFeBe_4$. On cooling from the aging temperature, an additional iron compound precipitates out of solution as the solubility of iron in beryllium decreases with decreasing temperature. The cooling rate from the aging temperature must be slow enough for the iron to diffuse, otherwise $FeBe_{11}$ forms in the matrix instead of $AlFeBe_4$ forming in the grain. The equilibrium amount of $AlFeBe_4$ increases with a decrease in aging temperature; however, the time to reach equilibrium correspondingly increases. A practical range for aging is within 650 to 800 °C. Times could be over 100 h. The changes in ductility and fracture mode that occurred over a range of temperatures as a result of an aging treatment for cast-and-extruded beryllium are depicted in Fig. 17.64.

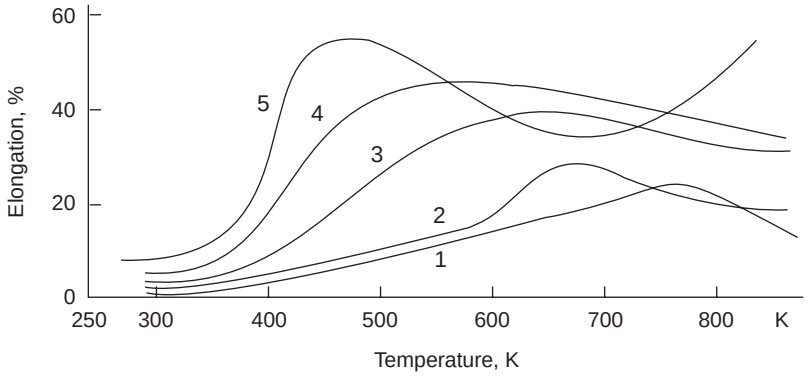

Fig. 17.60 Effect of grain size on the temperature dependency of elongation of beryllium with different maximum grain sizes: curve 1, 300 μm; curve 2, 170 μm; curve 3, 112 μm; curve 4, 80 μm; curve 5, 1.5 μm. Source: Volokita and Tikhinskii 1989

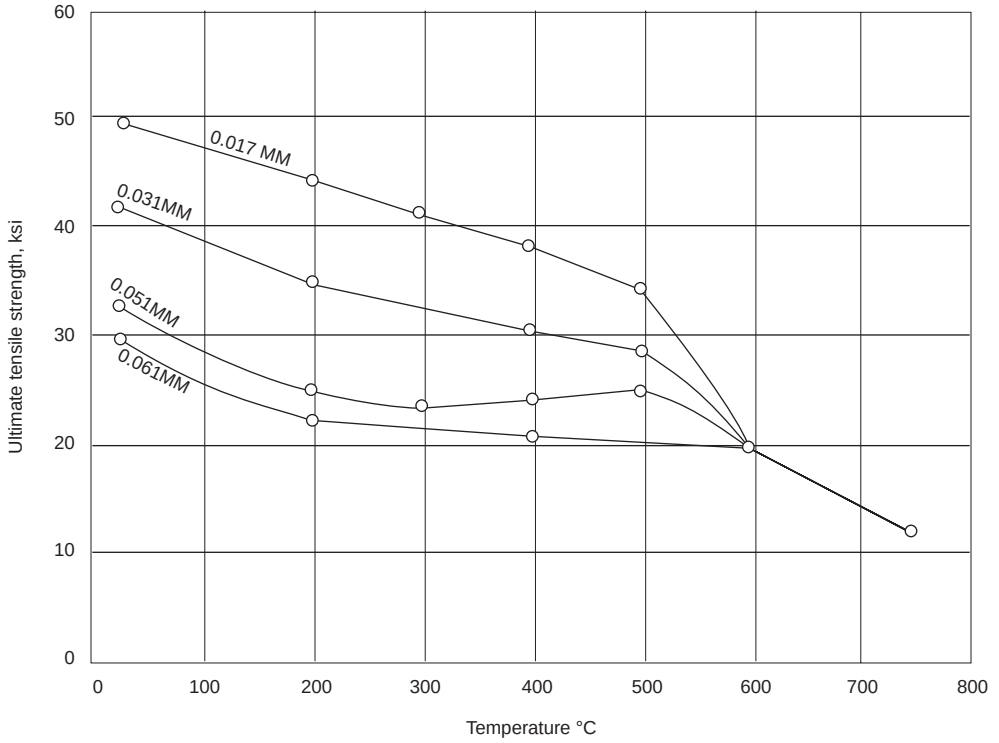

Fig. 17.61 Effect of grain size on the ultimate tensile strength as a function of temperature of vacuum hot-pressed (QMV) beryllium. Source: Beaver and Wikle 1954

The dramatic effect seen above approximately 300 °C is obvious. With increasing temperature, the form of aluminum changes from discrete globules to a continuous grain-boundary film [Stonehouse 1979].

The large dropoff in yield strength with an increase in aluminum content for a series of forged hot-pressed materials with different iron contents can be seen in Fig. 17.65 [Stonehouse 1979]. The curves are shifted to higher yield strengths with increasing iron content. Iron, in solution providing solid-solution hardening and in $FeBe_{11}$ providing precipitation hardening, can result in a significant increase in strength, as revealed in Fig. 17.65. The increase in strength as a result of an increase in matrix iron (i.e., within the grains in contrast to at the grain boundaries), however, may result in a decrease in fracture

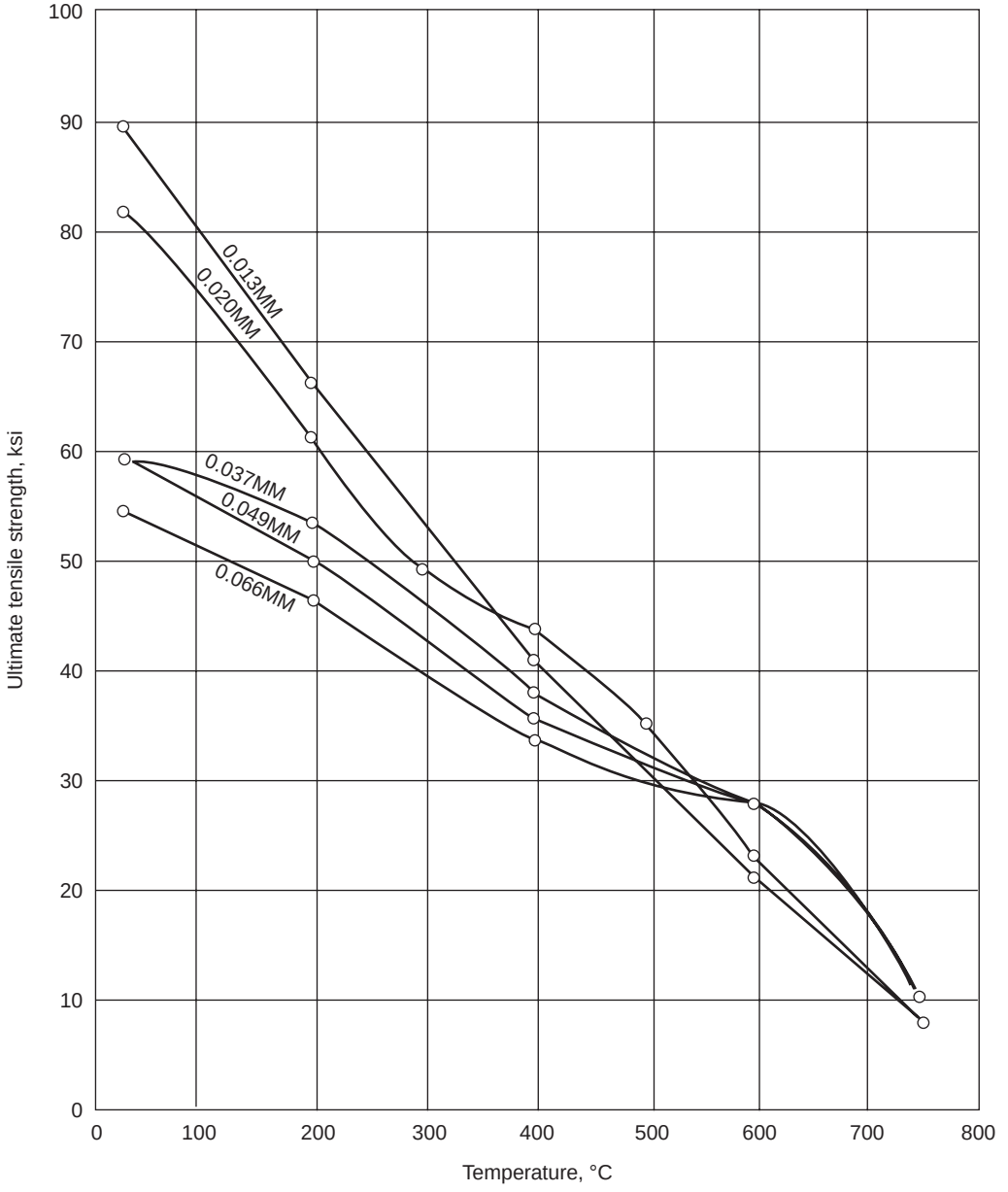

Fig. 17.62 Effect of the average grain size on the ultimate tensile strength as a function of temperature of vacuum hot-pressed and hot-extruded (QMV) beryllium. Source: Beaver and Wikle 1954

Table 17.19 Variations in longitudinal tensile elongation as related to free-aluminum content

	Tensile elongation, %	
Test temperature, °C	400 ppm free Al	10 ppm free Al
25	2.6	4.4
260	32.0	63.9
370	43.9	63.2

Source: Stonehouse 1979

toughness. The effect of inducing precipitation hardening to increase the yield strength is shown in Fig. 17.66 for hot-pressed beryllium having a grain size of approximately 11 μm and tested parallel to the pressing direction at several temperatures. The material was aged to equilibrium at 732 °C (1350 °F). A lower aging temperature would have resulted in higher strength as a result of finer precipitates. However, longer aging

times would have been required to produce equilibrium. The strengthening is due to both solid-solution hardening and precipitation hardening. Upper and lower yield points were obtained at the higher contents of matrix iron that were attributed to dislocation pinning by $FeBe_{11}$ matrix precipitates [Stonehouse 1979].

Beryllium oxide is the impurity having the highest concentration in beryllium. Typical concentrations range from approximately 0.7% to approximately 1.5%, with about 0.3% on the low side and as high as 6% for some instrument grades. High BeO content provides the high stiffness required at high stress levels. In ball milling and attritioning in air, the oxide content increases rapidly as the powder particle size decreases. Finer particle sizes result in correspondingly finer grain sizes. While both the strength and ductility increased with decreasing grain size, it was observed that there was a reversal in the ductility below a grain size of approximately 7 μm. The yield strength, however, still continued to increase, while the UTS remained unchanged with a further decrease in grain size below 7 μm. Impact grinding produces powder with lower oxide contents. The embrittling effect of BeO is attributed to premature fracture originating at BeO sites. Under tensile stress, a void forms around each BeO particle that serves as a nucleus for cleavage and propagation of a crack, leading to failure. The ductility may similarly be affected at elevated temperatures where operations such as forming take place [Stonehouse 1979].

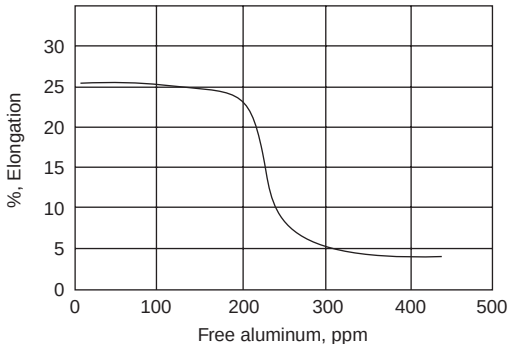

Fig. 17.63 Transverse tensile elongation at 556 °C (1033 °F) as a function of free-aluminum content. Source: Stonehouse 1979

17.11 Hydrostatic Tests

Experimental results of tests performed on SR-grade beryllium deformed under high (nearly

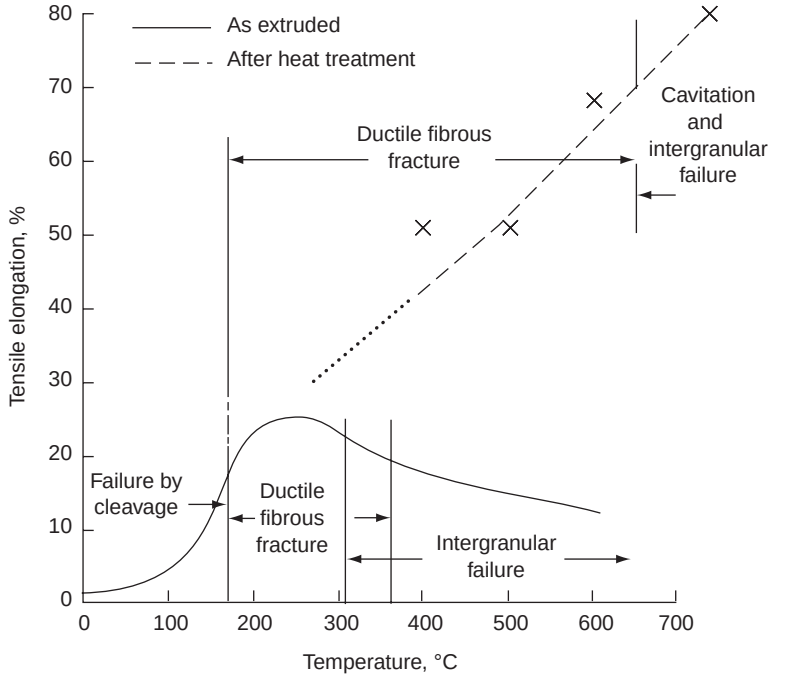

Fig. 17.64 Effect of heating for 120 h at 780 °C (1436 °F) on the ductility of cast-and-extruded beryllium. Source: Stonehouse 1979

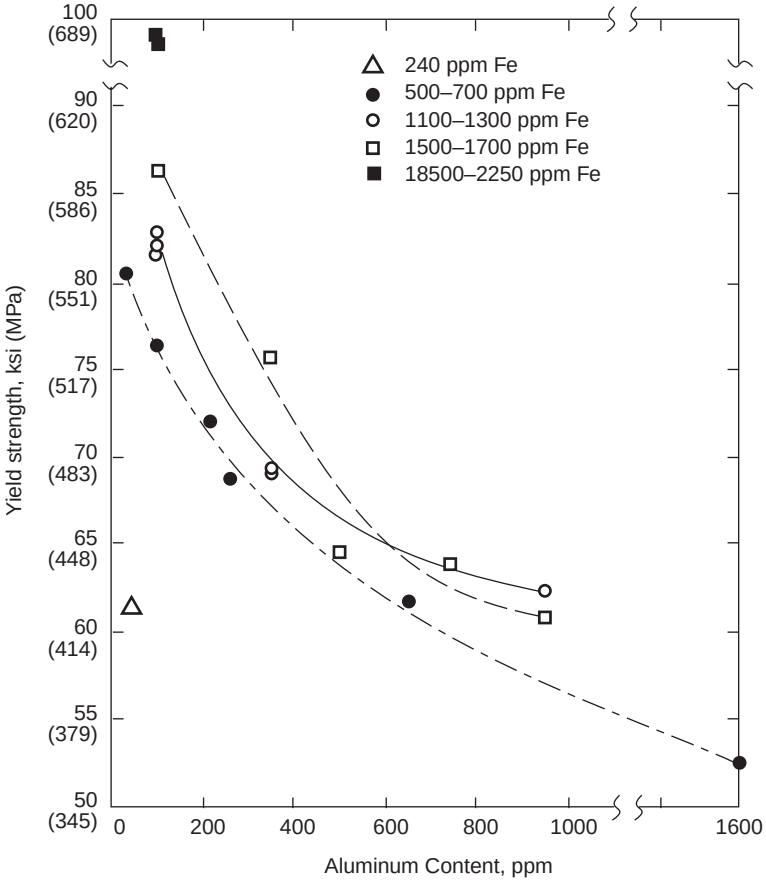

Fig. 17.65 Effect of aluminum content at different iron concentrations on the room-temperature tensile yield strength of forged hot-pressed beryllium. Source: Stonehouse 1979

hydrostatic) pressures at three different strain rates are shown in Fig. 17.67 to 17.69 for small strains and in Fig. 17.70 for large strains [Abey 1970]. Results were reported for the outer radius of the test samples. Experimental uncertainties were given as ±10% for small strains and ±20% for large strains. Data were taken in the form of torque versus angle of twist. Shear stress was obtained from the torque values by assuming that the shear strain was a linear function of the radius. The author's interpretation of the results depicted in Fig. 17.70 is the following. The initial increase in shear stress up to the maximum value is associated with ductile shear, at which point the sample starts to fracture internally, resulting in a corresponding decrease in shear strength under hydrostatic loading. The strain at which the initial fracture occurred (i.e., the amount of ductile strain) increased with an increase in pressure. Extrapolation of the data suggested that ductile strain is not present below a pressure of 600 MPa at a strain rate of 0.37/s.

REFERENCES

Abey, A.E., 1970. Effect of Pressure and Strain Rate on the Shear Strength of Beryllium, *J. Appl. Phys.*, Vol 41 (No. 13), p 5254–5259

Ansart, J.P., and Naulin, G., 1991. Constitutive Model of Several Materials at High Rates of Strain, *Mechanical Behavior of Materials Sixth Conference Proceedings*, Vol 1 (Kyoto, Japan), p 259–264

Auten, T.A., and Hanafee, J.E., 1976. "The Fatigue-Crack Growth Behavior of Some New Grades of Beryllium," Preprint UCRL-78241

Beaver, W.W. and Wikle, K.G., 1954. Mechanical Properties of Beryllium Fabricated by Powder Metallurgy, *J. Met.*, Vol 6, p 559–573

Borch, N.R., 1979. Elevated Temperature Behavior, *Beryllium Science and Technology*, Vol 1, D. Webster and G.J. London, Ed., Plenum Press, New York and London, p 307–330

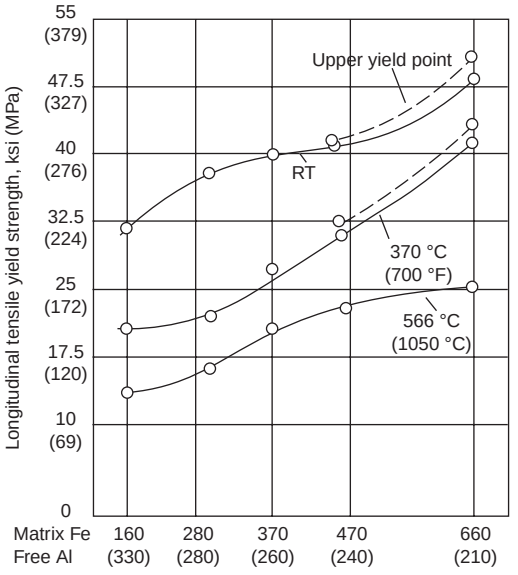

Fig. 17.66 Tensile yield strength of hot-pressed beryllium as a function of matrix iron tested at several temperatures following heating at 732 °C (1350 °F) until equilibrium is reached. Dashed lines indicate pinning by matrix precipitate, FeB_{11}. Source: Stonehouse 1979

Borch, N.R., and Hauber, J.R., 1968. Creep Study on High-Purity Polycrystalline Beryllium, *Trans. Met. Soc. AIME*, Vol 242, p 1933–1936; Preprint UCRL-70779 Rev. 1

Brush Wellman, 2001. "Designing with Beryllium," Brochure 517, Cleveland, OH

Cooper, R.E., 1979. Fracture Mechanics, *Beryllium Science and Technology*, Vol 2 (No. 17), D.R. Floyd and J.N. Lowe, Ed., Plenum Publishing Corp., New York, NY, p 351–378

Goldberg, A., Hanafee, J.E., Scott, R.G., 1982. "Mechanical Properties Evaulation of Some Commercial Beryllium Materials," UCRL-87392 Preprint, Lawrence Livermore National Laboratory, Livermore, CA

Goods, S.H., and Dombrowski, D.E., 1997. Mechanical Properties of S-65C Grade Beryllium at Elevated Temperatures, *JAERI Proceedings of Third International Workshop on Beryllium Technology for Fusion*, p 39–52

Grensing, F., Hashiguchi, D., and Marder, J., 1990. Fracture Toughness of Vacuum Hot-Pressed Beryllium Powder, *Advances in Powder Metallurgy Proceedings*, Metals Powder Industries Federation, Princeton, NJ, p 27–36

Hashiguchi, D.H., Clement, T.P., and Marder, J.M., 1988. Properties of Beryllium Consolidated by Several Near-Net Shape Processes, *International Powder Metallurgy Conference*, Vol 18, p 627–643

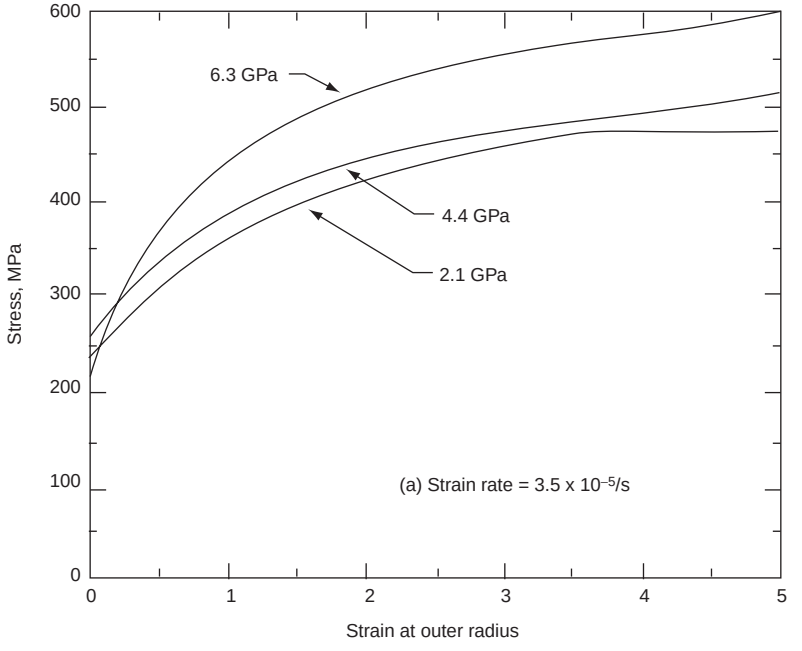

Fig. 17.67 Shear stress versus shear strain at outer radius for SR-grade beryllium tested at a strain rate of 3.5×10^{-5}/s under three different (nearly hydrostatic) pressures. Source: Abey 1970

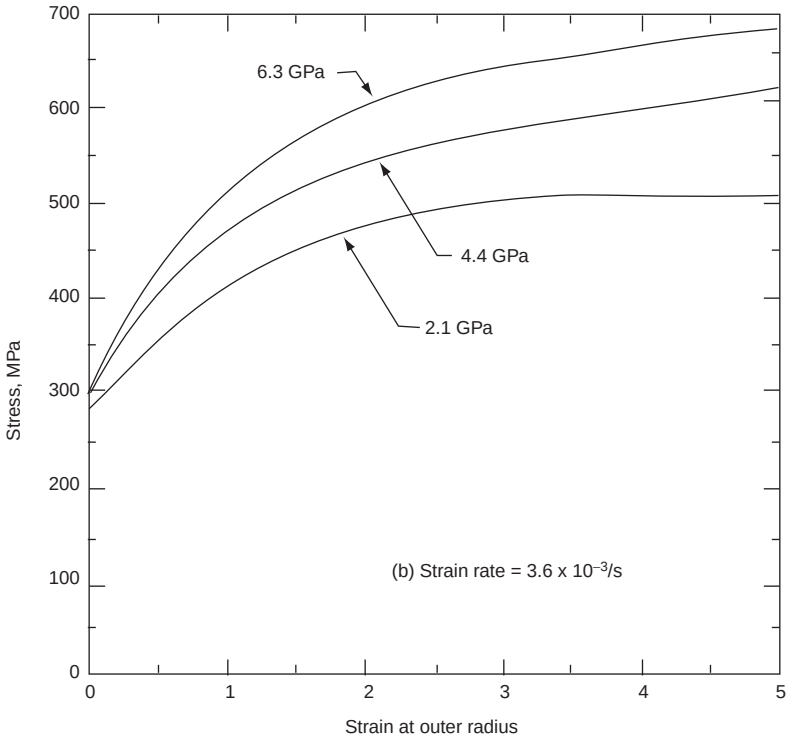

Fig. 17.68 Shear stress versus shear strain at outer radius for SR-grade beryllium tested at a strain rate of 3.6×10^{-3}/s under three different (nearly hydrostatic) pressures. Source: Abey 1970

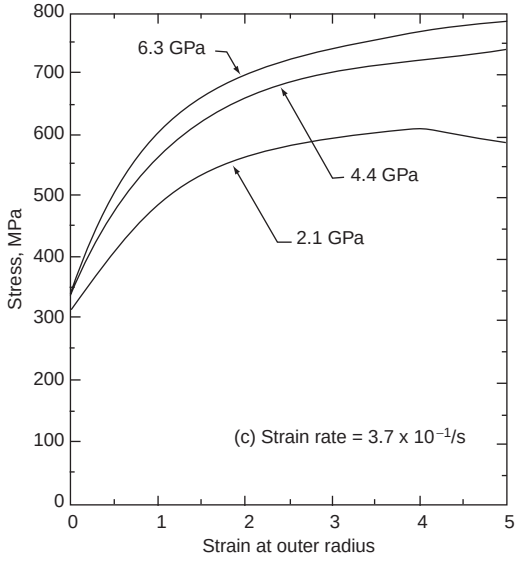

Fig. 17.69 Shear stress versus shear strain at outer radius for SR-grade beryllium tested at a strain rate of 3.7×10^{-1}/s under three different (nearly hydrostatic) pressures. Source: Abey 1970

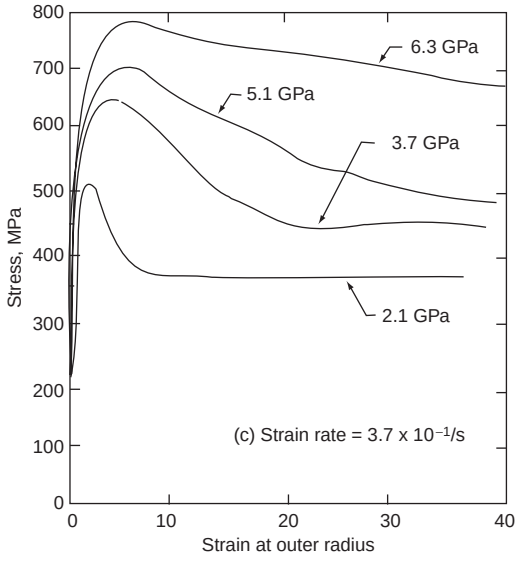

Fig. 17.70 Large-strain data of shear stress versus shear strain at outer radius for SR-grade beryllium tested at a strain rate of 3.7×10^{-1}/s under four different (nearly hydrostatic) pressures. Source: Abey 1970

Haws, W.J., 1985. "Characterization of Beryllium Structural Grade S-200F," Technical memorandum TM-778, Brush Wellman

Henshall, G.A., Torrex, S.G., and Hanafee, J.E., 1995. "The Elevated Tensile Properties of S-200E Commercially Pure Beryllium," UCRL-ID-120258, Lawrence Livermore National Laboratory, Livermore, CA

Kharinov, V.P., Pavlychev, A.N., and Popov, A. B., 1990. The Effects of Dynamic Deformation Aging in Beryllium, *Fiz. Met. Metalloved*., No. 12, p 127–134

Kumar, K., McCarthy, J., and Sande, J.B.V., 1985. Correlation of Microyield Behavior with Silicon in X-520 and HIP-50 Beryllium, *Metall. Trans. A*, Vol 16 (No. 5), p 807–814

Lavrent'ev, F.F., Salita, O.P., Palei, V.V., Matsievskii, O.V., and Khimich, Y.U.P., 1987. Plastic Deformation and Fracture of Polycrystalline Commercial Beryllium, *Phys. Met. Metallogr. (USSR)*, Vol 64 (No. 6), p 177–180

Lemon, D.D., and Brown, W.F., Jr., 1985. Fracture Toughness of Hot-Pressed Beryllium, *J. Test Eval*., Vol 13, p 152–161

Marder, J.M., 1986. Beryllium in Stress-Critical Environments, *J. Mater. Energy Sys*., Vol 8 (No. 1), p 17–26

Mayville, R.A., 1980. "The Use of Notched Beams to Establish Fracture Criteria for Beryllium," UCRL-52866, Ph.D. thesis, University of California, Berkeley CA

Naik, B.G., and Singhal, V.K., 1991. Evaluation of Micro Yield Strength of Beryllium Consolidated by Powder Metallurgy, 17th ATM and National Conference on Powder Metallurgy, *Trans. of the PMAI* (Powder Metallurgy Soc. of India), p 31–35

Nieh, T.G., and Wadsworth, J., 1998. Improved Microyield Strength in Beryllium Produced by Vapor Deposition, *Scr. Mater*., Vol 38 (No. 6), p 863–868

Perra, M., and Finnie, I., 1975. "Fracture-Toughness Tests on a High-Strength Beryllium from Room Temperature to 300 °C," UCRL-51774, University of California, Livermore

Pinto, N.P., 1979b. Properties, *Beryllium Science and Technology*, Vol 2, D.R. Floyd and J.N. Lowe, Ed., Plenum Press, NY, p 319–350

Saxton, H.J., and London, G.J., 1979. Flow and Fracture of Polycrystalline Beryllium, *Beryllium Science and Technology*, Vol 1, Plenum Press, NY, p 115–144

Smith, M.F., McDonald, J.M., Watson, R.D., and Whitley, J.B., 1985. Thermomechanical Testing of Beryllium for Limiters in ISX-B and JET, *Fusion Technol*., Vol 8, p 1174–1183

Smugeresky, J.E., 1986. Beryllium and Beryllium Alloys, *Encyclopedia of Materials Science and Engineering*, Vol 1, Pergamon Press Ltd., p 289–294

Stonehouse, A.J., 1979. Impurity Effects in Beryllium, *Science and Technology*, Vol 1, D. Webster and G.L. London, Ed., Plenum Press, NY, p 181–206

Stonehouse, A.J., 1986. Physics and Chemistry of Beryllium, *J. Vac. Sci. Technol. A*, Vol 4 (No. 3), p 1163–1170

Tardiff, G.E., Jr., 1974. "The Fracture Toughness of Thin Beryllium Sheet," UCRL-51544, Ph.D. thesis, submitted to Michigan Technology University, Houghton, MI

Turner, G.I., 1979. Grain Size Effects, *Beryllium Science and Technology*, Vol 1, D.Webster and G.L. London, Ed., Plenum Press, NY, p 145–179

Volokita, G.I., and Tikhinskii, G.F., 1989. Peculiarities of Deformation of Ultra-Fine-Grained Beryllium in the Temperature Range 77–830 K, *Phys. Met. Metallogr*., Vol 67 (No. 2), p 174–176

Webster, D., 1979. Recrystallization and Grain Growth in Beryllium, *Berullium Science and Technology*, Vol 1, D. Webster and G.L. London, Ed., Plenum Press, NY, p 207–234

Webster, D., Crooks, D.D., and Vidoz, A.E., 1973. Effect of Oxide Dispersions on the Recrystallization of Beryllium, *Metall. Mater. Trans. B*, Vol 4 (No. 12), p 2841–2847

SELECTED REFERENCES

- Beitscher, S., 1968. "Tensile Properties of Rocky Flats Division Ingot-Sheet Beryllium from Room Temp to 250C," Report RFP-1205, Dow Chemical Company, Rocky Flats Division, Golden, CO
- Brown, A.B., Morrow, F., and Martin, A.J., 1960. An Improvement in the Ductility of Beryllium at High Temperature, *Nature*, Vol 187, p 494–496
- Carrabine, J.A., Woodard, D.H., Stonehouse, A.J., and Beaver, W.W., 1964. The Effects of $AlFeBe_4$ on Mechanical Properties of Fabricated Polycrystalline Beryllium, *Beryllium Technology*, Vol 1, L.M. Schetky

and H.A. Johnson, Ed., Gordon and Breach, NY, p 239–257

- Chandler, E., Lindsay, H.M., Pugh, H., Li, D., and White, J.S., 1973. The Effect of Surface Finish on the Pressure-Induced Ductility of Beryllium, *J. Mater. Sci.*, Vol 8 (No. 12), p 1788–1794
- Dupouy, J.M., Poirier, J.P., Antolin-Beaudier, J., and Adda, Y., 1964. Contribution a L'etude de la Deformation et de la Restauration du Beryllium Pur, *J. Nucl. Mater.*, Vol 12, p 277–290
- Eaton, N.F., Longstaff, D.A., and Robinson, J.A., 1961. "Production and Properties of Beryllium Ingots Made by Consumable-Electrode Arc Melting," Paper 65, The Institute of Metals Conference on the Metallurgy of Beryllium, Oct 16–18, The Institute of Metals, London, U.K.
- Fenn, R.W., Jr., Crooks, D.D., Kinder, W.C., 1969. "Test Methods for Evaluating Mechanical Properties of Anisotropic Materials (Beryllium)," Report AFML-TR-68-173, Lockheed Missile and Space Co., Palo Alto, CA
- Floyd, D.R., 1972a. "Technical Data Book for Ingot-Sheet Beryllium," Report RFP-1605, Dow Chemical Company, Rocky Flats Division, Golden, CO
- Garber, R.I., Gindin, I.A., Kogan, V.S., and Lazarev, B.G., 1955. Investigation of the Plastic Properties of Beryllium Single Crystals, *Fiz. Met. Metalloved. I*, p 529–537
- Gross, A.G., and O'Rourke, R.G., 1963. Some Properties and Applications of Beryllium Wire, *Wire and Wire Prod.*, Vol 38, p 1087–1091
- Hanafee, J.E., 1976. "Effect of Machining Damage on Tensile Properties of Beryllium," Report UCID 17248, California University, Lawrence Livermore Lab, Livermore, CA
- Heiple, C.R., 1972. Mechanical Properties of Diffusion Bonded Beryllium Ingot Sheet, *Metall. Mater. Trans. B*, Vol 3 (No. 4), p 807–812
- Hill, N.A., 1958. "A Preliminary Study of the Production and Properties of Beryllium Sheet," A.E.R.E. Report M/M 193
- Hill, N.A., 1961. "The Effect of Various Temperatures upon the Tensile Properties of a Beryllium Sheet"
- Klein, J.L., Macres, V.G., Woodard, D.H., and Greenspan, J., 1955b. *Ductility of Beryllium as Related to Preferred Orientation and Grain Structure*, American Society for Metals, p 425–465
- London, G.J., Damaino, V.V., Stone, G., and Conrad, H., 1967. "Mechanical Properties of Commercial Purity and of Distilled and Zone Refined Beryllium," AFML-TR-67-126, Franklin Inst. Research Labs, Philadelphia, PA
- Nicholas, T., 1975. "Effect of Plastic Prestrain on the Tensile Strain to Failure of Beryllium," Report AFML-TR-75-52, Air Force Materials Lab, Wright Patterson Airforce Base, OH
- Nicholas, T., and Atkins, G.R., 1975. "Notch Tensile Strength of Advanced Structural Grades of Beryllium," Report AFML-TR-74-252, AD-A-011647, Air Force Materials Lab, Wright Patterson AFB, OH
- Nieh, T.G., Wadsworth, J., Chou, T.C., Owen, D., and Chokshi, A.H., 1993. "Creep of a Niobium Beryllide, Nb_2Be_{17}, *J. Mater. Res.*, Vol 8 (No. 4), p 757–763
- Papirov, I.I., and Tikhinskiy, G.F., 1970. Stucture and Mechanical Properties of Fine-Grained Deformed Beryllium, *Phys. Met. Metallogr.*, Vol 29 (No. 5), p 167–169
- Rebholz, M.J., 1966. Buckling Strength of Curved Beryllium Panels in Compression, *Beryllium Technology*, Vol 2, Gordon and Breach, NY, p 857–877
- Rennhack, E.H., 1973. Influence of Machining Temperature on the Surface Damage, Residual Stress, and Texture of Hot-Pressed Beryllium, *Metall. Trans. B*, Vol 5 (No. 5), p 1095–1101
- Stonehouse, A.J., Paine, R.M., and Beaver, W.W., 1964. "Physical and Mechanical Properties of Beryllides," Spec. report, Vol 13, Met. Soc., Am. Inst. Mining, Met. Petrol. Eng., Inst. Metals Div., p 445–455
- Toth, I.J., 1974. Comparison of the Mechanical Behavior of Filamentary Reinforced Aluminum and Titanium Alloys, *Composite Materials, Proceedings of the Third Conference on Testing and Design*, p 542–560
- Tuer, G.L., and Kaufman, A.R., 1955. Ductility of Beryllium as Related to Single Crystal Deformation and Fracture, *The Metal Beryllium*, D.W. White, Jr., and J.E. Burke, Ed., American Society for Metals, p 372–424
- Watson, R.D., and Whitley, J.B., 1986. Thermal Fatigue Tests of a Prototype of Beryllium Limiter for JET, *Nucl. Eng. Des./Fusion*, Vol 4 (No. 1), p 49–60

- Webster, D., and Crooks, D.D., 1976. "Improved Beryllium Ductility Study," Lockheed Missiles and Space Report LMSC-D507268
- Webster, D., Greene, R.L., and Lawley, R.W., 1974. Factors Controlling the Strength and Ductility of High Purity Beryllium Block, *Metall. Trans.*, Vol 5, p 91–96
- Woodard, D.H., Stonehouse, A.J., and Beaver, W.W., 1968. "Development of Beryllium with Improved Impact Resistance," Brush Beryllium Co., Cleveland, OH, Air Force Materials Laboratory

Beryllium Chemistry and Processing, p 253-265
By Kenneth A. Walsh
Edited by Edgar E. Vidal, Alfred Goldberg,
Edward N.C. Dalder, David L. Olson, and Brajendra Mishra

CHAPTER 18

Casting of Beryllium

Loren A. Jacobson, Los Alamos National Laboratory, Retired
Don H. Hashiguchi, Brush Wellman, Inc.

18.1 Solidification of Beryllium

Beryllium solidification phenomena offer extremes to study [Krenzer 1979]. Beryllium differs from most metals in that it has a relatively high melting point (1287 °C), a high latent heat of fusion (7.895 kJ/mol), and a low thermal conductivity (200 W/m · K). Because of the combined effects of these properties, heat removal during solidification becomes difficult. This difficulty in rapidly removing heat contributes greatly to the formation of large columnar grains and generates high thermal stresses during cooling, resulting in an increased susceptibility for hot cracking. Beryllium melts at approximately 1280 °C and has an allotropic transformation approximately 30 °C below the melting temperature. The ingot beryllium exhibits exceptionally rapid grain growth above 900 °C and slow cooling through this temperature region, making it difficult to grain refine. This physical property situation inherent of beryllium results in the typical cast structure consisting of large columnar grains, which becomes more of a problem as the ingot size is increased. There is some promise for grain refinement, because there are several examples of the effect of small intentional additions of other elements and compounds (inoculants) to beryllium to improve casting behavior.

A detailed thermal analysis of cooling within the beryllium mold and radiographic analysis of the cast structure in various sections of the 23 by 23 by 51 cm beryllium ingot have been made. Figure 18.1(b) illustrates three regions with specific casting features. More than 100 ingots, cast from both high-purity and commercial-purity feed, have been characterized, and a qualitative description of the solidification mechanism of beryllium in this ingot size has been provided [Krenzer 1979].

It has been found that the cooling rate has a large effect on the orientation of the grain structure and the extent of segregation in the ingot. Typical cooling curves are shown in Fig. 18.2. Curves Ml and M2 show temperatures in the bottom and side of the graphite mold, respectively, and Cl shows temperatures measured in the graphite crucible. Three distinct regions of different cooling rates are observed. In region I, a sharp temperature increase occurs in the mold temperatures within a few minutes after pour. This rise is due to the superheated melt and release of latent heat during the formation of the chill zone. Following this thermal experience, cooling rates in the mold within region II are high and quite variable. Within region II, it is felt that a certain amount of supercooling occurs before solidification proceeds. Once the supercooled melt adjacent to the chill zone solidifies, release of latent heat brings the melt temperature ahead of the solid-liquid (S/L) interface back up close to the melting point of beryllium.

The final stage of solidification, region III, is believed to be steady-state solidification, controlled by the removal of latent heat. Cooling rates within region III are quite constant, approximately 1 to 5 °C/min, depending on when the furnace power is shut off. In the example shown in Fig. 18.2, the furnace power was shut off 30 min after pour, and total time for solidification of the ingot was 65 min, as shown in the

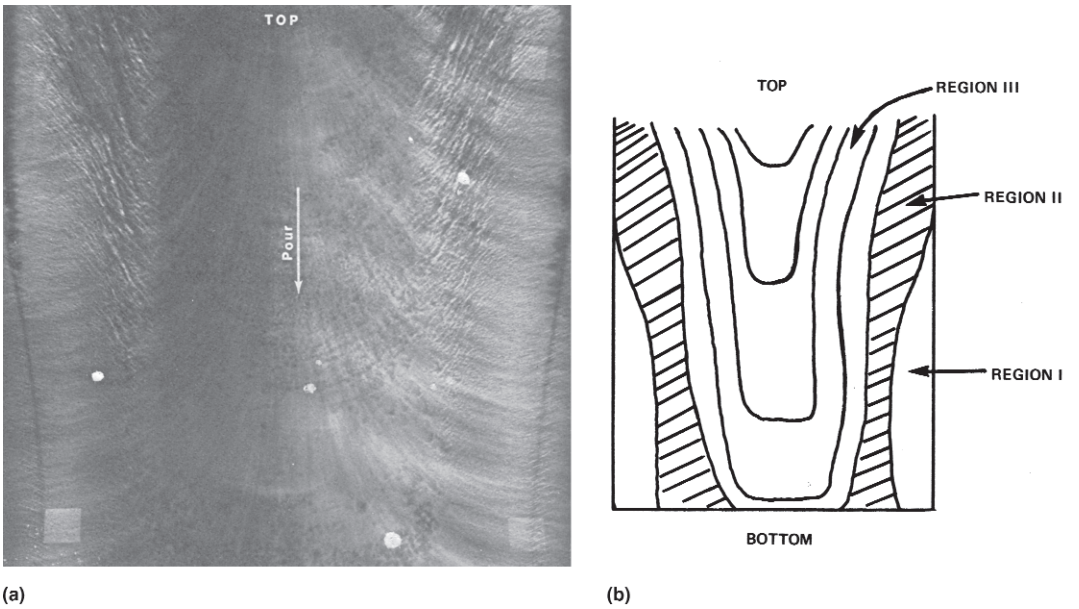

Fig. 18.1 (a) Radiograph showing extensive segregation resulting from rapid cooling in a 23 by 23 cm vertical section in the bottom of an ingot. Note: Lighter regions are higher-density regions. (b) Sketch of equivalent section showing different regions discussed. Source: Krenzer 1979

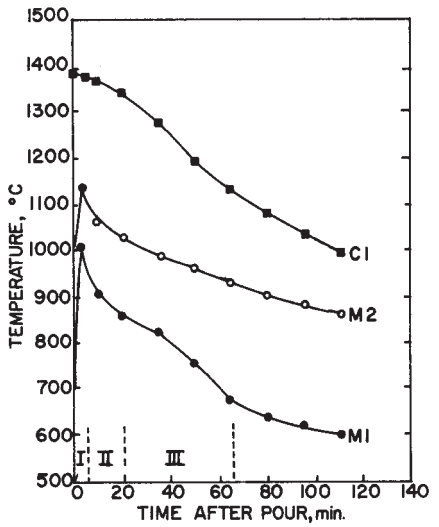

Fig. 18.2 Typical cooling curves for 23 by 23 by 51 cm beryllium ingot. •, mold 1; ○, mold 2; ■, control. Source: Krenzer 1979

M1 curve. Increasing the time for power-off to 120 min results in cooling rates of approximately 1 °C/min. Solidification rates in large beryllium ingots are extremely slow in the final stages of solidification.

Various cooling curves obtained with different thermal conditions during solidification have been compared to radiographs of thin sections taken from different locations in the ingot. Various features, such as grain flow, segregation, and cracking, are revealed in 1.27 cm thick sections by radiographing with 14 kV x-rays. Figure 18.1(a) shows the structure of a vertical section taken from the center of the ingot. The section is parallel to the 23 by 51 cm face of the ingot, showing a region next to the bottom of the ingot. Lighter regions in the radiograph are higher-density regions. The arrow in Fig. 18.1(a) indicates pour direction. The extent of the chill zone is marked on either side by the dark lines. The bottom 20 cm of the ingot is below the furnace coils and accounts for the shape of the chill line. A linear array of high-density stringers (light lines) can be observed along the chill line. Within the center of the section, the mottled light and dark region connecting the ridged pattern on both sides is believed to be associated with region III shown on the cooling curves. This segregation pattern is typical of V-segregation [Mehrabian et al. 1970]. The progress of the S/L interface from bottom to top within region III is readily apparent and appears to be planar in nature. The zone between the chill line (region I) and region III is believed to be the supercooled region (region II), where dendritic solidification is most likely superimposed on these features;

one can see the grain flow, turning upward in the center. The segregation in region III can almost be entirely eliminated by slow cooling at approximately 1 °C/min [Krenzer 1979].

This work has demonstrated that imposed thermal conditions during ingot solidification can greatly modify cast structure. The segregation patterns described, which are not observed in ingots cast from high-purity beryllium, can be almost entirely eliminated in commercial-purity beryllium by controlled cooling. However, refinement of the large columnar grains has not been achieved. The effect of thermal gradients and solidification rates needs a more thorough understanding for casting designers to achieve a sound technical approach to obtain the desirable refined cast grain structure.

18.2 Cast Structure

When a pure metal or alloy freezes, the shape of the S/L interface plays a major role in determining the cast structure and properties of the ingot. Solidification proceeds as the molten metal ahead of the S/L interface becomes supercooled. Several distinct types of supercooling can occur. As heat is removed from the interface regions, either by convection in the molten metal or by conduction through the solid and/or mold, solidification can proceed by thermal supercooling of the melt. This behavior is the predominant mechanism in pure metals. In addition, alloys can freeze by constitutional supercooling [Walton and Chalmers 1959], where rejection of solute by the solid into the melt will lower the melting point in the boundary layer of the remaining liquid, thus widening the freezing range of the alloy.

Depending on the thermal gradients, solidification rate, and alloy composition, other types of S/L interfacial behaviors have been described [Flemings 1974, Morris and Winegard 1969, Tiller 1964]. Their behaviors are categorized as planar, cellular, and dendritic interfaces. With small amounts of supercooling, the metal will freeze by planar growth where the interface is smooth. With increasing supercooling, the planar interface becomes unstable, and the smooth interface will degenerate into a cellular interface. For still larger amounts of supercooling, further degeneration of the S/L interface occurs, and dendritic solidification becomes the predominant mechanism. Constitutional supercooling occurs only in alloys, and thermal supercooling is operative in both pure metals and alloys. In a pure metal with a high latent heat of fusion, such as beryllium, the extent of supercooling is small, and the ability to form dendrites during freezing is restricted. Dendritic solidification is very common in alloys [Krenzer 1979].

Three distinct regions are common in castings. Next to the mold wall, a chill zone is formed consisting of small equiaxed grains. Next to the chill zone, a columnar structure develops where the long columnar grains are oriented parallel to the growth axis and direction of heat removal. Finally, in the central region of the ingot, an equiaxed zone exists comprised of randomly oriented equiaxed grains. All three zones are common to alloys, whereas only the chill zone and columnar structure are typical in ingots of pure metals.

18.3 Grain Refinement

The transformations associated with the columnar-to-equiaxed zone have been thoroughly studied, particularly because of the casting properties relevant to grain refinement during solidification [Haworth and Oliver 1967, Tiller 1959, Chalmers 1964, Jackson et al. 1966].

It is common for the thermal gradients in the liquid to be small for much of the solidification time of an ingot. For pure metals, the temperature of the melt remains relatively constant near the freezing point after the initial superheat has been dissipated. Freezing progresses in a steady-state manner, establishing an equilibrium between the generation of latent heat and removal of heat by conduction through the solid and mold. Such conditions promote growth of columnar grains and a planar growth front. A breakdown of such columnar growth can most easily be achieved by alloy additions and thus constitutional supercooling, and secondarily by controlling heat removal and thermal supercooling [Krenzer 1979].

Because of its high latent heat, beryllium supercooling is difficult to achieve. It can be expected that columnar growth of multibranched dendrites should not occur in beryllium. The ability of a melt to supercool is measured in terms of three factors: alloying content (C_o), thermal gradients (G), and solidification rates (R). These variables are related to those of the solidification structure, as shown in Fig. 18.3 for the lead-tin system [Tiller and Rutter 1956]. Similar relationships are not known for beryllium or its alloys but should be expected. Beryllium casting

investigations have not adequately addressed the question whether substantial grain refinement can be achieved in beryllium by optimizing both alloy content and thermal conditions during freezing. Dendritic growth can be promoted at a given composition by reducing the *G*/*R* ratio, as seen in Fig. 18.3. It has already been reported that low values of *G* exist in large beryllium ingots, but sufficiently high values of *R* can be obtained to promote dendritic growth. Chill casting does produce a finer beryllium structure; however, cracking associated with rapid chilling is undesirable [Krenzer 1979].

The desire to obtain sound ingots free of cracking while achieving a refined cast grain size is the expected difficult choice for beryllium castings. Most research efforts have been directed toward achieving sound ingots. Grain refinement approaches, other than thermal and constitutional combinations, have also been explored. Refinement by inoculation is an option but dependent upon the presence of effective nuclei within the melt for growing new grains.

Bibb and Bishop [1958] identified and investigated some of these factors in their attempts to refine the grain size of cast beryllium. They found that additions of 2.5 wt% Al and Si to beryllium produced a central zone of equiaxed grains, and the alloy ingots exhibited the classical three-zoned structure. They also recognized that other factors, such as pour temperature, may be important, but they did not take into account the effect of the *G*/*R* ratio in their experiments. Lower *G*/*R* ratios could have reduced the aluminum or silicon contents necessary to observe a refinement effect. Mold vibration was observed to have no effect on unalloyed beryllium. Here again, thermal conditions are playing an important role in producing dendritic growth necessary to couple with mold vibration.

Bibb and Bishop [1958] have made several inoculants to unalloyed beryllium and found that the additions did not produce any grain refinement. Experiments at Rocky Flats have shown that in 5 by 10 by 10 cm ingots, the addition of solid beryllium particles to the molten stream at pour produces a refined grain size in the center of the ingot. Stirring the melt was not possible, so the beryllium particles were not uniformly distributed throughout the ingot [Krenzer 1979].

Crossley et al. [1959] have reported interesting measurements on the degree of supercooling (or undercooling) of small 99.14 wt% Be samples. Their results on 5 g samples are plotted in Fig. 18.4 as a function of cooling rate. Their results show that relatively high cooling rates are needed to achieve sufficient supercooling of unalloyed beryllium. Within this range of supercooling, they did not observe any effect on grain size. Alloy additions of germanium gave larger degrees of supercooling and evidence of grain refinement. The maximum amount of supercooling measured is within the same range that the phase transformation occurs in beryl-

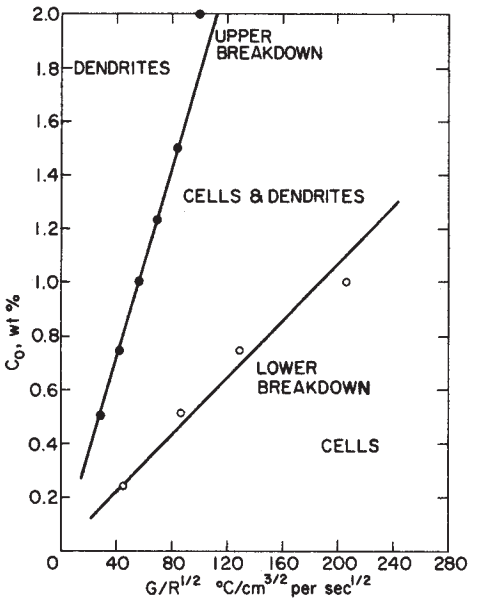

Fig. 18.3 Effect of growth conditions on the transition from a cellular to dendritic interface in lead-tin alloys. Source: Tiller and Rutter 1956

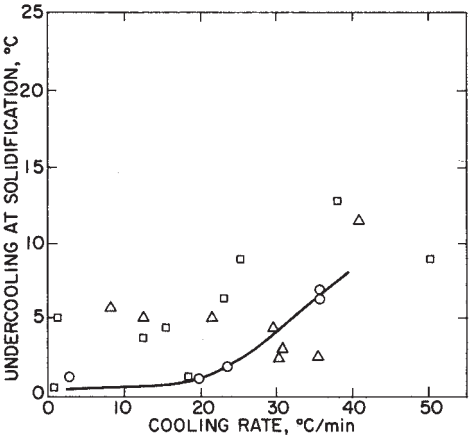

Fig. 18.4 Relationship between supercooling and cooling rate in beryllium and dilute beryllium alloys. ○, Be; Δ, Be-1wt%Th; □, Be-1wt%Ge. Source: Crossley et al. 1959

lium, which may have some bearing on the problem. If this situation is true, germanium would greatly restrict the ability of beryllium to thermally supercool. Three inoculants, TaN_x, TiB_2, and WC, were also reported to be effective nuclei in beryllium. In addition, their work also reported that mold vibration may be beneficial, but thermal conditions during solidification must be considered.

Fergason and Heiple [1973] investigated the use of mold oscillation to refine the grain size of beryllium castings. Oscillation frequencies up to 72 reversals/min and amplitudes up to 75° between reversals failed to produce any refinement effects using vacuum induction melting (VIM) (section 18.4.2 in this chapter). This approach would more likely succeed if the thermal gradients would be lowered, but at the same time, the solidification rate would be sufficient to promote nonplanar solidification. The physical properties of beryllium make it difficult to achieve the desired outcome. At best, these requirements may be satisfied in a small optimum processing range. It is to be seen that these factors could be combined to produce sound, fine-grained ingots. Castings in this study were made in 15 cm diameter by 23 cm in length cylindrical molds and 15 cm square molds 23 cm in length.

Popov et al. [1960] have reported that considerable refinement of beryllium can be achieved using ultrasonics in vacuum arc melting (VAM) (section 18.4.3 in this chapter). This result is contrary to Maropis and Jones [1957], who coupled ultrasonic vibration with VIM without success. It appears that there is an important difference between applying oscillation or ultrasonics to VIM compared to VAM. It was mentioned previously that VAM is more of a steady-state melting process, where the melting rate is more readily controlled. This difference provides possible evidence that sufficiently low *G/R* values may be achieved to produce a change in the cast structure. Further research in VAM appears to be one key in the attempts to produce grain refinement in beryllium [Krenzer 1979].

Gelles and Malik [1975] investigated the feasibility of producing fine-grained beryllium castings in space. Their initial approach was to produce a melt containing a uniform dispersion of BeO to aid nucleation during solidification and to achieve it without gravitational settling forces and gravity-induced convective currents. They reported that neither beryllium particles nor BeO produced a fine-grained cast structure. They then focused on determining if these inoculants are ineffective as nucleating agents and/or if grain growth just below the melting point of beryllium destroys refinement achieved during melting. Three melts, using two different BeO powders, were made in a BeO crucible by heating to a range of 1404 to 1425 °C and cooling through the solidification temperature at a rate of 138 to 282 °C/min. These melts did not show any evidence of grain refinement, including one with an addition of 5 vol% BeO powder.

Webster et al. [1973] reported that agglomeration of BeO due to the presence of a liquid phase in melted samples removes grain growth inhibition by BeO. Agglomeration of beryllium is believed to be due to grain-boundary incipient melting promoted by impurities such as aluminum, silicon, and magnesium.

Wouch et al. [1978], in a related investigation, examined the difference in solidification structure for beryllium with dispersed BeO particles, as produced by melting and solidification in Earth's gravity or in a near-zero-*G* environment during rocket free fall. It was observed that a more uniform distribution of BeO particles was retained in the sample solidified in zero-*G*, but there was virtually no effect on achieving a more refined grain structure. A high-purity powder consolidated beryllium was used for both melting experiments.

18.4 Melting Techniques

The various traditional casting and melting practices are described, including static casting, vacuum induction melting, vacuum arc melting, electron beam melting, and centrifugal casting.

Their historical developments are outlined and referenced to allow for further searching in greater detail on each practice.

18.4.1 Static Casting

Early work on beryllium casting has been reviewed by Corzine and Kaufmann [1955], Darwin and Buddery [1960b], and Denny [1965]. Their conclusion was that the process is only useful as a means of purification. The biggest disadvantage of casting is the large columnar grains inherent to beryllium ingots. As-cast product exhibits poor tensile properties, with tensile strengths between 34 and 68 MPa and nil ductility. Only after severe deformation and recrystallization processing can minimum tensile properties of approximately 270 MPa yield strength,

270 MPa tensile strength, and 3% elongation be achieved [Floyd et al. 1973]. Reliance on powder metallurgy technology seemed to be the only practical route, because cast product could only be considered in cases where mechanical properties were not important.

18.4.2 Vacuum Induction Melting

Kaufmann and Gordon [1947] cast ingots 11 cm in diameter and up to 18 cm long, in addition to clusters of six rods 3 cm in diameter by 41 cm long, using VIM. They used a bottom-pour beryllia crucible and a pour temperature of 1450 °C. They concluded that a medium rate of solidification was necessary to avoid internal cracks from chill casting and large grains produced by slow cooling. Comparison of composition before and after casting showed that magnesium is removed by melting; however, little change in the iron, aluminum, silicon, and copper content occurred.

Kura et al. [1949] also used beryllia crucibles; however, they employed a tilt-pour induction furnace, shown in Fig. 18.5. One disadvantage was that dross was inductively stirred into the melt, resulting in poor microcleanliness. Gas porosity was identified as a specific problem, and it was emphasized that baking out both the feed and the mold was necessary to eliminate moisture and to obtain sound castings.

Ivanov and Shmelev [1958] studied both static and centrifugal casting in a vacuum induction furnace. Melting was done in a beryllia crucible, and molds were fabricated from graphite and steel. After degassing in the initial stages of melting, they backfilled the furnace with purified argon. They reported that sound ingots with 80 to 92% metal yields could be obtained. However, they did not distinguish whether there was a difference between static and centrifugal yields. Argon provided the inert atmosphere and also influenced heat transfer within the furnace and within the conditions present in these experiments, which probably contributed to achieving sound ingots. They also investigated improvement of mechanical properties by extruding centrifugal ingots at 500 °C. A large range of ductility improvement was reported, dependent upon the combined effect of deformation and recrystallization. Although they annealed extruded product at 720, 850, and 1050 °C, no correlation

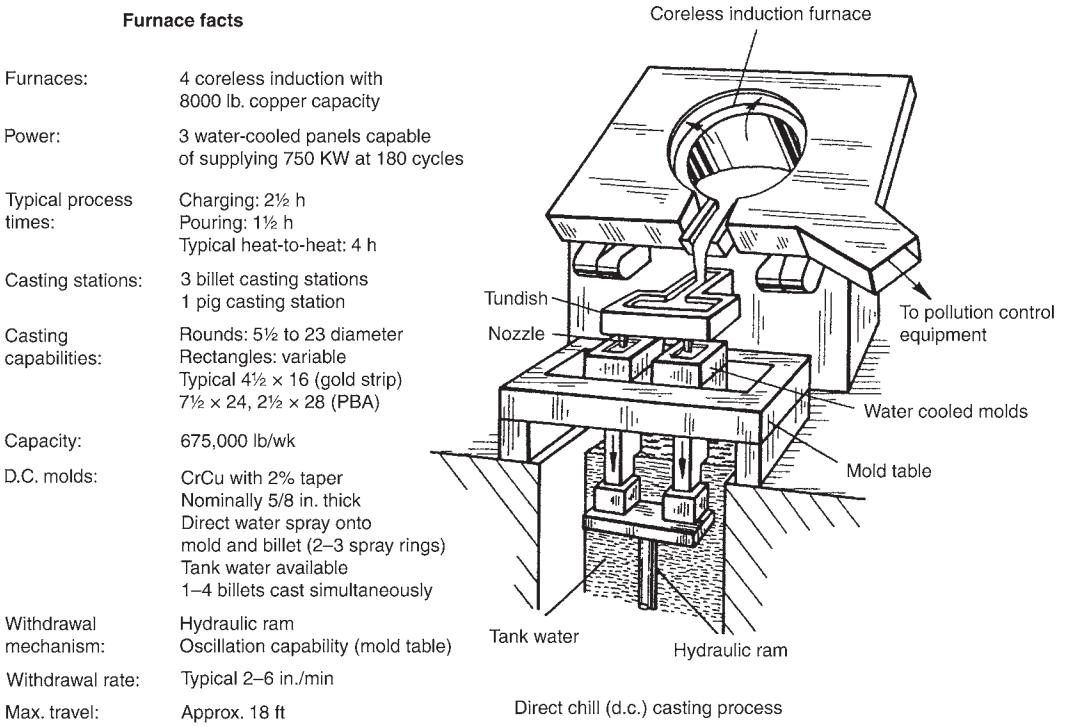

Fig. 18.5 Direct chill casting process for copper-beryllium. Source: Brush Wellman

was given between heat treatment and mechanical properties. Thermomechanical processing of cast beryllium is an attractive area for future research into improving mechanical properties of ingot-source product [Krenzer 1979].

Denny and Hessler [1962] were able to independently vary mold temperatures and pouring temperatures. Mold temperatures up to 600 °C were studied, using a separate mold heater, and pouring temperatures from a range of 1300 to 1400 °C were used. They established the interesting relationship, shown in Fig. 18.6, between cast grain size and pouring temperature. A pour temperature of 1349 °C was determined to give the best results for conditions existing in these experiments. They reported that thermal conditions existing at both time of pour and during solidification have a major influence on the soundness and structure of the ingot. Accelerated directional cooling, promoted by a water-cooled copper plug in the bottom of the mold, was found to be effective in achieving sound, relatively fine-grained ingots. The imposed thermal gradient, from the top to the bottom of the mold, governed the nature of shrinkage voids and porosity in the ingot. It was found that centerline cracking appeared to be associated with ingot purity, possibly caused by rejection of impurities to the center of the ingot during solidification. However, chemical analysis could not verify this assumption.

Goosey et al. [1962] investigated many factors associated with mold design, feed purity, heat flow during solidification, and control of cooling rates during freezing that influence the soundness of beryllium ingots. Typical defects associated with VIM include shrinkage pipe, gas porosity, microcracks, centerline defects, cold shuts, inclusions, and macrosegregation of metallic impurities. They point out that enhancing unidirectional solidification, as was reported for both arc melting and electron beam melting, is useful in reducing typical cast defects in beryllium. They found that the lowest pour temperature of 1375 °C was consistent with good fluidity of the melt, which is desirable to promote rapid solidification and reduce tendency for thermal cracking. A pour rate of 1 kg/20 s appeared to be the best for optimum soundness of ingots cast in this study. Microprobe analysis showed that titanium segregation was associated with centerline defects in ingot cast from thermally reduced pebble. It was suggested that the addition of 0.25 to 0.5 wt% Al be made to the melt to eliminate centerline defects. However, modifying mold design, increasing unidirectional solidification, and preventing radial heat flow during freezing would be a more desirable solution to centerline defects than to intentionally add aluminum to the melt. Aluminum additions promote high-density cast defects.

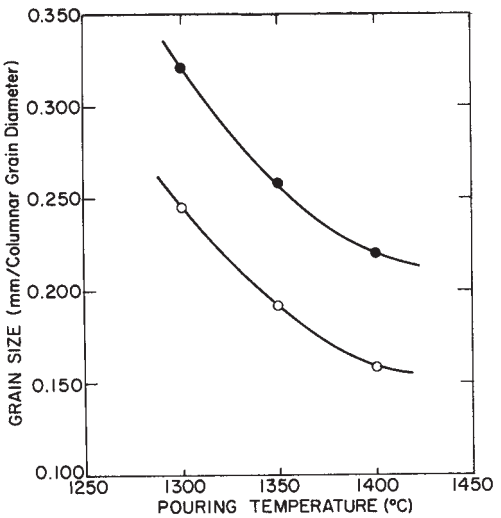

Fig. 18.6 Relationship between grain size and pour temperatures in beryllium ingots. •, elevated mold temperature; ○, ambient mold temperature. Source: Krenzer 1979

Thorne and Lowe [1963] were able to independently control the temperature and cooling rate of the hot top and mold with separate heating coils. Near the melting point of beryllium, the cooling rate could be varied from 6 to 30 °C/min. Within the range of 500 to 1000 °C, the cooling rate in the mold could be varied from 2 to 20 °C/min. Below 500 °C, very slow rates of 1 °C/min were obtainable. Pour temperatures from 1320 to 1400 °C were examined. Directional solidification from the bottom to the top of the mold was established in each ingot by maintaining a steep thermal gradient in the mold. Cast ingots measured 5 by 10 by 10 cm, and the existence of a centerline crack was a common occurrence [Krenzer 1979]. The investigators evaluated the length of the crack in terms of pour temperature, pouring time, and thermal conditions before and after the pour.

Patenaude [1964] and Denny and Patenaude [1966] casted sound, crack-free beryllium ingots, nominally 2 cm in diameter by 25 cm long and of commercial purity, by controlling thermal gradients in the mold. High-purity ingots were reported to be more susceptible to cracking. Mold temperatures were measured as a function of time at three different positions during

solidification, and empirical equations were derived to explain required heat transfer to produce sound ingots of this size. It was found that to produce sound ingots, the superheat transfer rate must be above a critical minimum, and heat must be extracted at a sufficient rate from the bottom of the mold. This observation showed that a chill plate in the bottom of the mold is desirable.

Metallographic and radiographic examination confirmed that, in commercial-purity ingots cast using proper heat-transfer rates, centerline and thermal cracking were not observed. High-purity ingots, cast under the same conditions, were susceptible to cracking and appeared to have a slightly larger grain size.

Meyer [1966] cast larger ingots, 12 and 15 cm in diameter. Ingot soundness was again described in terms of heat-transfer characteristics of the mold. Increased ingot size resulted in larger as-cast grains. Thermal conditions during solidification had a major influence on soundness and grain structure of the ingots. Inducing a vertical thermal gradient in the mold by positioning the top of the mold within the furnace coil and using a chill plate in the mold bottom outside the coil produced the best results. Directional solidification had been reported previously as a necessary condition for casting sound ingots. Comparison of commercial- and high-purity feed showed that high purity was more susceptible to cracking and tended to have a larger grain size. Meyer [1966] verified that susceptibility for cracking is directly related to the chemical composition of the melt.

In 1961, the beryllium ingot-sheet process was established at Rocky Flats. Early work on this process has been reported by Frankeny [1964]. This process developed from a need to recycle both ingot- and powder-source scrap to produce a wide variety of beryllium components. Through this process, the technology was developed to cast large beryllium ingots on a consistent basis. Sound ingots, up to 55 kg in mass, have been cast in production quantities. The most significant variable in the process has been the wide variety of feed scrap used for melting. The constitution of the feed scrap has led to minor effects on ingot soundness but has not led to a measurable effect on the mechanical properties of the wrought product. The type and distribution of impurity phases and inclusions in wrought product have been affected by the quality of the starting feed.

Frankeny and Floyd [1968] reported on the salient features of the ingot-sheet process. Vacuum induction melting was used exclusively in this process. The graphite crucible and mold assembly was designed for bottom pouring. Exposed graphite surfaces were coated with a $BeOBeSO_4$ slurry and baked at 1450 °C for 30 min. Although a protective film of Be_2C formed during use, frequent recoating was required to prevent the reaction of molten beryllium with graphite. A 15% overcharge was used to minimize shrinkage defects. Pour temperatures from 1300 to 1450 °C were investigated, and a temperature of 1400 °C was used with the standard 23 by 23 by 51 cm ingot [Corle et al. 1978].

Centerline defects were eliminated by promoting unidirectional solidification from the bottom to the top of the mold. Graphite felt was wrapped around the sides of the mold to reduce lateral heat transfer, and this practice proved to be one of the best techniques for eliminating internal cracking. Unidirectional solidification was achieved by using a hot top and a water-cooled copper chill plate in the bottom of the mold [Krenzer 1979]. Improved pouring techniques, using a graphite tundish with an offset bung, were used to reduce carbon contamination from the crucible. This practice reduced the number of Be_2C inclusions trapped in the solidified ingot.

Knowledge gained over the past 60 years has shown that VIM of beryllium is a viable source of material for conventional metalworking processes. Investigators have recognized the need for unidirectional solidification and controlling heat transfer and cooling rates during freezing. Beryllium is quite susceptible to gas porosity and internal cracking, and controlling melt composition is a major factor. It has been demonstrated that large, sound ingots can be cast on a production basis. However, lack of chemistry control has restricted the efficiency of the subsequent rolling and fabrication processes. Refining the as-cast grain size is still a major problem. Particularly in larger ingots useful for production, large columnar grains are typical. Only with large amounts of deformation can these grains be refined to obtain acceptable mechanical properties in ingot-sheet product [Krenzer 1979].

18.4.3 Vacuum Arc Melting

Crossley et al. [1959] investigated several ways to produce fine, equiaxed grains in consumable-arc melted ingots. They pointed out that VAM differs significantly from other melting methods. The VAM is a continuous process

characterized by a steady-state melting and solidification rate. The VIM is a batch-type process in which thermal conditions are constantly changing during solidification. The structure of VAM ingots is controlled by the depth of the molten pool, which in turn is primarily influenced by the melting rate of the electrode and rate of heat extraction in the mold. The VAM exhibits an improved ability of controlling solidification, which is a distinct advantage to VIM.

These investigators found that by controlling VAM variables, improvements in grain structure can be achieved. They investigated the combined influence of melting rate, controlled by the electrode current and magnetic stirring, on ingot soundness. It was found that deep-pool melting by periodically reducing the electrode current produced the finest ingot structure. Ingots 8 cm in diameter by 20 cm high were VAM from 3 cm diameter electrodes using a vacuum of 75 to 90 μm of Hg. Increasing the pool depth decreases the grain size. All ingots exhibited fine hairline cracks.

Consumable-arc melting seems to be the preferred method for VAM of beryllium, mainly because of tungsten contamination from the electrode and slower melting rates associated with nonconsumable melting. Denny and Santschi [1963] point out that special preparation is required in making electrodes, and that electrodes extruded from VIM ingots have given the best results. Electrodes compacted from thermally reduced pebble are too brittle, and electrodes produced from electrolytic flake or beads will outgas significantly [Denny and Santschi 1963]. They concluded that VAM is preferred over VIM because lower oxide levels can be achieved and some grain refinement can be achieved in arc melting. Beryllium oxide segregates to the ingot surfaces, causing a poorer-quality ingot surface. This segregation can be removed from the ingot by machining. As-cast grain structure appears to be more readily controlled by VAM in which large columnar grains are promoted by a shallow molten pool, while a mixed columnar and equiaxed grain structure can be obtained with a deeper molten pool. Some grain refinement can be achieved with a deep molten pool and pulsating currents. They also report that double and triple VAM does not appear to improve ingot quality [Krenzer 1979].

Kyffin and Craik [1963] investigated VAM of various grades of beryllium. Electrodes compacted from each of the materials were used to produce ingots up to 15 cm in diameter by 25 cm high. A water-cooled copper crucible was used, maintaining a vacuum between 1 and 10 μm during melting. They experienced extensive gas porosity in ingots produced from electrolytic flake. Thermally reduced pebble produced ingots free from gas porosity. They concluded that starting electrodes should be made by VIM. It was shown that, although chemical refinement does not occur in going from VIM to VAM product, the biggest advantage of the process was in the grain refinement that was achieved. However, microcracking was a problem in VAM ingots. They also reported that the inclusions such as BeO and Be_2C tended to segregate to the top of the ingot, leaving the bulk of the ingot inclusion free [Krenzer 1979].

Eaton et al. [1963] developed a consumable-electrode VAM process for beryllium to avoid contamination from crucible and mold materials and to obtain lower oxygen contents. They pointed out that, economically, the most attractive production process for obtaining high-purity product for fabrication is to use both VIM and vacuum arc remelting (VAR). The second VAR step reduces both impurities and grain size and removes cast inhomogeneities associated with induction-melted product. The double melting of beryllium, that is, VIM followed by VAR of extruded electrodes, would be an attractive area to pursue to achieve optimized outcomes from the two practices. The combined advantages of the chemical refinement by VIM and the grain refinement by VAR offer an interesting alternative to VIM.

18.4.4 Electron Beam Melting

Sumsion and Matthews [1959] investigated if sound beryllium ingots could be produced by electron beam melting (EBM). Essentially, the process consisted of bombarding beryllium with electrons and solidifying the resultant melt in a water-cooled copper crucible. Ingots 8 cm in diameter and up to 61 cm long were produced in this manner. They found that initial attempts to melt unconsolidated pebble, electrolytic flake, and induction-melted chips were unsuccessful, and that it was necessary to compact the material into a feed ingot. Three separate melting stages were used to obtain an ingot of acceptable quality. These steps are listed in Table 18.1. Electron-beam-melted ingots were reported to have a finer grain structure than VIM and VAM product. However, this comparison was difficult to assess from the evidence presented. In addition

Table 18.1 Electron beam melting procedure

Step	Vacuum, μHg	Melting rate, cm/h
Consolidation	0.1–0.3	61
Purification	0.08–0.1	41
Casting	0.08–0.1	122

Source: Krenzer 1979

to differences in melting techniques, one could not determine what effect thermal conditions during solidification and metal purity had on final grain size. No advantage in mechanical properties of EBM product was identified. Data showed that there were no significant differences in metallic impurities between feedstock and the final ingot. Also, there were no differences detected in the composition between the surface and the interior of the ingots. Higher oxygen concentrations were found on the surface of all ingots. This segregation could easily be removed by scalping, thus providing an effective means of reducing oxygen content. Thus, this study showed that small, sound ingots could be produced by EBM. Average vaporization losses for the combined melting steps shown in Table 18.1 amounted to approximately 11.5% [Krenzer 1979].

In summarizing their experiences with EBM of beryllium, Denny and Santschi [1963] concluded that because of the necessity for multiple melting, slow melting rates, and expensive equipment, EBM is less attractive compared to other techniques. Also, vaporization losses are substantially higher than other melting methods.

18.4.5 Centrifugal Casting

Corle et al. [1978] have successfully applied centrifugal casting to beryllium. Several different shapes have been cast by spinning the casting around a vertical axis of rotation. Various-sized hemishells, cylinders, and straight- and tapered-walled cups have been cast in a vacuum induction furnace using a bottom-pour graphite crucible and graphite mold. Wall thicknesses from 0.6 to 2.5 cm can be achieved in these various shapes. Cylinders as large as 33 cm high and 34 cm in diameter have been centrifugally cast. Typically, a 15 cm diameter by 15 cm high straight-walled cup was poured at 1300 °C and 400 rpm. This casting had a relatively smooth bottom and side walls, with a bottom thickness of 1.3 cm and a wall thickness of 2.2 cm.

In addition to casting several different shapes, a wide range of pouring temperatures and spinning speeds have been investigated. Centrifugal casting is a form of pressure casting, where the molten metal is forced against the mold walls. This centrifugal force throws heavier components in the melt toward the outside of the casting. This process behavior is effective in reducing the heavier inclusions in beryllium. Rotational speeds from 100 to 500 rpm have been used. For lower speeds, the molten metal does not work up the walls of the casting properly, and higher speeds are necessary for longer castings. Variable speeds during solidification have also been studied, and gradually increasing the speed and holding at a maximum speed before gradually decreasing the speed have proven successful. More uniform wall thickness can be achieved in this manner. Abrupt stopping of the rotation produces laps in the casting. Typically, the casting was held at 400 rpm for 15 min before slowly reducing the spinning. Centrifugal casting is a useful method for producing beryllium shapes for applications where as-cast mechanical properties are acceptable. The main purpose of this work was to demonstrate that sound beryllium shapes could be centrifugally cast [Krenzer 1979].

Typically, large grains are produced by centrifugally cast beryllium. Constant rotational motion during solidification will suppress the transition from columnar to equiaxed grains [Stewart et al. 1971], thus making columnar grain growth even more difficult to avoid. When the mold is rotated at a constant speed, temperature gradients in the melt will remain high. Centrifugal casting is therefore not a useful approach for grain refinement [Krenzer 1979].

18.5 Metal Purification

The chemical composition of the melt has a significant effect on the solidification grain structure. Impurity segregation during solidification, even with relatively pure metals containing impurities of only a few parts per million, will broaden the freezing range and lower the thermal gradients in the melt. This altering of the solidification mechanism will result in changes in the cast grain structure.

Bunshah and Juntz [1964] investigated the use of VIM of beryllium for purification. During VIM, volatile and insoluble impurities are removed or redistributed by evaporation and segregation. The VIM can result in a reduction in carbon, oxygen, sodium, magnesium, chlorine, fluorine, and manganese during melting,

but, as expected, exhibits very little, if any, reduction of iron, chromium, nickel, aluminum, silicon, and copper concentrations. Beryllium melt reactions with the graphite crucibles and molds can also increase Be_2C content. This type of carbide formation is more evident with induction-melted recycled beryllium.

Herman and Spangler [1963a, b] and Spangler et al. [1964] reported that during zone refining of beryllium using a floating zone and induction heating, BeO, aluminum, chromium, iron, magnesium, calcium, copper, and silicon contents are segregated or partitioned into the liquid. This segregation means that such metallic impurities will concentrate to some extent in the last liquid to solidify and tend to produce high-density regions in various parts of the ingot. It was also reported that nickel inversely segregates to the solid. Chemically homogeneous cast product is difficult to achieve from feed containing substantial amounts of metallic impurities. This situation has made it difficult to consider castings for some specific applications.

Table 18.2 Content of impurities in beryllium (mass%) after single, double, and triple distillation

Element	Initial metal	Distillation cycles 1	2	3
Na	0.001	0.00001	0.000003	0.000001
Mg	0.0003	0.00005	0.000004	0.000002
Al	0.07	0.003	0.000004	0.000002
Si	0.04	0.003	0.0010	0.0003
P	0.003	0.00006	0.000002	0.000002
Cl	0.002	0.0002	0.000003	0.000003
K	0.001	0.0002	0.00001	0.000003
Ca	0.001	0.0001	0.00003	0.000003
Ti	0.005	0.0001	0.000006	0.000004
Cr	0.03	0.00160	0.00006	0.000004
Mn	0.009	0.0045	0.0008	0.00007
Fe	0.036	0.007	0.00025	0.00005
Ni	0.005	0.0001	0.00002	0.000006
Cu	0.01	0.00050	0.00007	0.00002
Zn	0.0005	0.0001	0.000009	0.000009
Amount of impurities	0.21	0.0155	0.0023	0.000478
Be, not less than	99.79	99.98	99.997	99.995

Source: Papirov

Purification of beryllium in large quantities was performed in the former Soviet Union using vacuum distillation. This process was originally developed at the Kharkov Institute of Physics and Technology (KIPT), Ukraine, and was substantially scaled up at the beryllium manufacturing plant located at Ust' Kamenogorsk, Kazakhstan. Motivation for the scaleup of vacuum distillation to industrial-sized quantities (hundreds of kilograms per year) came from the nuclear reactor industry, where designers demanded that beryllium metal used for neutron reflector components have essentially zero boron content [Savchuk]. In more recent times, it was learned that reactor designers in Western Europe were not concerned about the 50 ppm or so of boron in the beryllium, and so the industrial-scale process was shut down.

In recent years, KIPT has improved the vacuum distillation process on a laboratory scale and has demonstrated 99.999 wt% pure metal in only three distillation steps [Papirov]. Detailed results are shown in the Tables 18.2 and 18.3.

REFERENCES

Bibb, A.E., and Bishop, S.M., 1958. "Grain Refinement of Cast Beryllium," Report KAPL-1917, Knolls Atomic Power Laboratory

Bunshah, R.F., and Juntz, R.S., 1964. Purification of Beryllium by Crucibleless Melting, Casting and Distillation Process, *J. Met.*, Vol 16 A138 (No. 9), p 693

Chalmers, B., 1964. *Principles of Solidification*, John Wiley and Sons, NY

Corle, R.R., Voiles, K.E., and Krenzer, R.W., 1978. "Casting Large Beryllium Ingots," Report RFP-2695, Rockwell Corp., Atomics International Div., Golden, CO

Corzine, P., and Kaufmann, A.R., 1955. The Melting and Casting of Beryllium, *The Metal Beryllium*, Section A, *Fabrication*, American Society for Metals, p 136–151

Table 18.3 Content of impurities in beryllium

Material	Impurities, mass% × 10^3 Fe	Si	Al	Mg	Mn	Cu	Cr	Ca
Distilled Be without additions	5.20	2.40	1.60	0.30	0.30	0.37	5.40	0.30
Distilled Be + 5% Nb	0.34	1.00	0.26	0.18	0.16	0.20	0.41	0.20
Distilled Be + 10% Nb	0.30	0.60	0.31	0.22	0.15	0.15	0.11	0.17
Distilled Be + 5% Mo	0.34	0.80	0.16	0.30	0.15	0.15	0.17	0.17
Distilled Be + 10% Mo	0.32	0.52	0.32	0.06	0.14	0.18	0.15	0.27

Source: Papirov private communication

Crossley, F.A., Metcalfe, A.G., and Graft, W.H., 1959. "Beryllium Research for Development in the Area of Casting," Report WADC-TR-59–500, Wright Air Development Center

Darwin, G.E., and Buddery, J.H., 1960b. Beryllium, *Metallurgy of the Rarer Metals*, Butterworths Scientific Publications, London, U.K., p 11–99

Denny, J.P., 1965. Melting and Casting, Chapter 4, The Fabrication of Beryllium, Section B, *Beryllium: Its Metallurgy and Properties*, H.H. Hausner, Ed., University of California Press, Berkeley, p 55–67

Denny, J.P., and Hessler, H.B., 1962. "Beryllium Casting," The Beryllium Corporation Technical Report ASD-TDR-62–390, United States Air Force Contract AF33(COO)-37902

Denny, J.P., and Patenaude, C.J., 1966. Casting of Beryllium Ingots and Shapes, *Beryllium Technology*, Vol 33, L.M. Schetky and H.A. Johnson, Ed., Gordon and Breach, NY, p 807–824

Denny, J.P., and Santschi, W.H., 1963. Melting and Casting of Beryllium, *Met. Prog*., Vol 84 (No.1), p 111–113, 126, 128, 130, 132

Eaton, N.F., Longstaff, D.A., and Robinson, J.A., 1963. The Flow and Fracture Characteristics of Beryllium Made by Consumable Electrode Vacuum Arc Melting, *The Metallurgy of Beryllium*, Institute of Metals Monograph 28, Chapman and Hall Ltd., London, p 687–696

Fergason, D.L., and Heiple, C.R., 1973. "Grain Refinement Trial in Cast Beryllium by Mold Oscillation," Report RFP-1840, Dow Chemical Co., Rocky Flats Div., Golden, CO

Flemings, M.C., 1974. Solidification Processing, *Metall. Trans. B*, Vol 5, p 2121–2134

Floyd, D.R., Leslie, W.W., and Dolechek, L.F., 1973. "Can-Rolling of Beryllium Ingots," Report RFP-2041, The Dow Chemical Company, Rocky Flats Division, Golden, CO

Frankeny, J.L., 1964. Vacuum Induction Casting of Beryllium, RFP-340, *Mod. Cast*., Vol 45 (No. 6), p 348–352

Frankeny, J.L., and Floyd, D.R., 1968. "Ingot-Sheet Beryllium Fabrication," Report RFP-910, Dow Chemical Co., Rocky Flats Div., Golden, CO

Gelles, S.H., and Malik, R.K., 1975. "Process Development for Producing Fine-Grain Casting in Space," Final report, Report N-75-21313, NASA-CR-120739

Goosey, R., Knight, R.A., and Martin, A.J., 1962. The Induction Melting and Casting of Beryllium, *J. Less-Common Met*., Vol 4 (No. 2), p 199–212

Haworth, C.W., and Oliver, B.F., 1967. Solidification Structures in Directionally-Frozen Ingot, *Trans. AIME*, Vol 239 (No. 8), p 1129–1136

Herman, M., and Spangler, G.E., 1963a. Basal Plane Fracture of Beryllium Single Crystals, *Proc. of Conference on the Metallurgy of Beryllium* (Conf.-170), ORNL, Oak Ridge, TN, p 48–68

Herman, M., and Spangler, G.E., 1963b. The Flow and Fracture Characteristics of Zone Melted Beryllium, *The Metallurgy of Beryllium*, Institute of Metals Monograph 28, Chapman and Hall Ltd., London, p 75–83

Ivanov, E.S., and Shmelev, V.M., 1958. "Melting and Casting of Beryllium," Report A/CONF.15/P/2048, also *Proc. of Second U.N. Conf. on Peaceful Uses of Atomic Energy*, Vol 4, p 302

Jackson, K.A., Hunt, J.D., Uhlmann, D.R., and Seward, T.P., 1966. *Trans. Met. Soc. AIME*, Vol 236, p 149–158

Kaufmann, A.R., and Gordon, E., 1947. Vacuum Melting and Casting of Beryllium, *Met. Prog*., Vol 52 (No. 3), p 387–390

Krenzer, R.W., 1979. Casting Beryllium Products, *Beryllium Science and Technology*, Vol 2, Plenum Press, NY, p 31–56

Kura, J.G., Jackson, J.H., Udy, M.C., and Eastwood, L.W., 1949. Preparation and Casting of Beryllium Melts, *J. Met*., Vol 1, p 769–778

Kyffin, P.D., and Craik, R.L., 1963. Consumable-Electrode, Vacuum Arc Melting of Beryllium, *The Metallurgy of Beryllium*, Institute of Metals Monograph No. 28, Chapman and Hall, London, U.K., p 677–686

Maropis, N., and Jones, J.B., 1957. "Investigation of Ultrasonic Grain Refinement in Beryllium," Report NYO-7788, AEC Contract AT(30–1)-1836, Aeroprojects, Inc.

Mehrabian, R., Keane, M., and Flemings, M.C., 1970. Interdendritic Fluid Flow and Macrosegregation; Influence of Gravity, *Met. Trans*., Vol 1 (No. 5), p 1209–1220

Meyer, G.E., 1966. "Bi-Monthly Progress Report on Development of Solution Strengthened High Purity Beryllium Alloy Sheet," Report AD-639838, Beryllium Corp., Reading, PA

Morris, L.R., and Winegard, W.C., 1969. The Development of Cells during the Solidification of Dilute Pb-Sn Alloy, *J. Cryst. Growth*, Vol 5, p 361–375

Papirov, I.I. Kharkov Institute of Physics and Technology, Ukraine, private communication

Patenaude, C.J., 1964. "Casting and Hot Working of Sound Large Diameter Beryllium Ingots," Interim Technical Documentary Report, United States Air Force Contract AF 33(657)-10943

Popov, B.E., Kovtun, S.F., and Amonenko, V.M., 1960. Modification of Beryllium and Chromium Structure by Means of Ultrasonic Irradiation during Arc Melting, *Fiz. Met. Metalloved*., Vol 10 (No. 6), p 853–856

Savchuk, V.V., Ust' Kamenogorsk, Kazakhstan, private communication

Spangler, G.E., Stone, J., and Herman, M., 1964. Automated Zone Melting of Beryllium, *J. Met*., Vol 16 (No. 9), p 693

Stewart, M.J., MacAulay, L.C., and Weinberg, F., 1971., Macrosegregation in Castings Rotated and Oscillated during Solidification, *Metall. Trans. B*, Vol 2 (No. 1), p 169–173

Sumsion, H.T., and Matthews, C.O., 1959. "Vacuum Melting of Beryllium by Electron Bombardment," Report LMSD-480485, Lockheed Aircraft Corp. Missiles and Space Division, Sunnyvale, CA

Thorne, M.A., and Lowe, J.N., 1963. "The Casting of Rolling Slabs from Thermally Reduced Beryllium," Atomic Weapons Research Establishment Report 0–41/63, Nov 1963, Atomic Weapon Research Establishment, Altermaster, U.K.

Tiller, W.A., 1959. Grain Size Control during Ingot Solidification, Part 2: Columnar-Equiaxed Transition, *Trans. Met. Soc. AIME*, Vol 224 (No. 3), p 448–459

Tiller, W.A., 1964. Dendrites, *Science*, Vol 146, p 871–879

Tiller, W.A., and Rutter, J.W., 1956. The Effect of Growth Conditions upon the Solidification of a Binary Alloy, *Can. J. Phys*., Vol 34 (No. 1), p 96–121

Walton, D., and Chalmers, B., 1959. The Origin of Preferred Orientation in the Columnar Zone of Ingots, *Trans. AIME*, Vol 215, p 847–855

Webster, D., Crooks, D.D., and Vidoz, A.E., 1973. Effect of Oxide Dispersions on the Recrystallization of Beryllium, *Metall. Mater. Trans. B*, Vol 4 (No. 12) p 2841–2847

Wouch, G., Frost, R.T., Pinto, N.P., Keith, G.H., and Lord, A.E., Jr., 1978. Uniform Distribution of BeO Particles in Be Casting Produced in Rocket Free Fall, *Nature*, Vol 274, p 235–237

SELECTED REFERENCES

- Meyer, G.E., 1965. "Casting and Hot Working of Sound Large Diameter Beryllium Ingots," United States Air Force Contract AF33(657)-10943, Technical Report AFML-TR-65–361, The Beryllium Corporation
- Nachtrab, W.T., and Levoy, N., 1997. Beryllium-Aluminum Alloys for Investment Castings, *Adv. Mater. Process.*, Vol 151 (No. 5), p 23–25
- Patenaude, C.J., and Denny, J.P., 1964. Casting of Beryllium Ingots and Shapes, *J. Met.*, Vol 16 (No. 9), p 698
- Sumsion, H.T., and Matthews, C.O., 1958. "Electron Bombardment Melting and Casting of Beryllium," Report LMSD-48330, Lockheed Missiles and Space Division, Sunnyvale, CA

Beryllium Chemistry and Processing, p 267-293
By Kenneth A. Walsh
Edited by Edgar E. Vidal, Alfred Goldberg,
Edward N.C. Dalder, David L. Olson, and Brajendra Mishra

CHAPTER 19

Powder Metallurgy

James Foley, Los Alamos National Laboratory
David L. Olson, Colorado School of Mines
Edgar E. Vidal, Brush Wellman, Inc.

19.1 Introduction

Powder metallurgical techniques for beryllium were first developed in 1946. Currently, powder metallurgy is the main processing route to produce beryllium components. The vacuum hot pressing method results in a fine-grained, machinable form of the material. The random orientation and fine grain size of the powder metallurgy ingots enable beryllium to be used in structural applications with relatively uniform mechanical properties in all directions. In contrast, the relatively poor mechanical properties of cast beryllium product led to an emphasis on the powder metallurgy route. Vacuum hot pressing has been a standard consolidation technique throughout the development of beryllium technology, and hot pressed powder is the major form of beryllium in use today. Powder metallurgy beryllium has been further processed by a number of conventional forming methods to produce a wide variety of shapes and to alter the directional mechanical properties of the material. However, the use of standard powder metallurgy techniques to produce near-net shape products has been very limited, and future research is needed.

The most common method to produce beryllium powder uses traditional practices and starts with a cast ingot of inherently coarse grain size that has low ductility and low fracture resistance [Pinto 1979a]. Beryllium cleaves readily along a single (basal) plane, such that particles, made by impacting the beryllium, are thin, jagged, and rather flat. Producing sufficient amounts of a specified particle size distribution requires repeated classification and milling practices. Various processes are used to yield different grades of powders.

Beryllium powder is consolidated using a selected powder grade and consolidation process, resulting in a compact. The powder composition and consolidation practice can be modified to achieve the deserved properties. These compacts are generally machined into shapes or parts that are used directly for their intended applications. The compacts may also be intermediate forms that will be further worked into mill products, such as extrusions, sheet, foil, and wire.

The ease in consolidating normal-purity grades of beryllium is related to the oxide coating and contaminants, especially silicon. Silicon is a sintering aid that permits full densification of the hot pressed billets using hot pressing conditions. Sintering can be performed, but the properties of the sintered billets are not equal to properties of hot pressed material. Plasma-sprayed thin-walled preforms may be sintered into hollow shapes with satisfactory properties. Control of the beryllium particle size distribution and impurity control is essential to achieve extruded products.

During the course of beryllium powder metallurgy development, a better understanding of the influence of input materials and processing methods has evolved. Powder factors such as source, purity, particle-size distribution, and particle shape have been related to the finished density and mechanical properties in a number of investigations. The improvement of beryllium has

Table 19.1 Impurities in beryllium in various stages of manufacturing

	Analysis, ppm					
	Pebble source			Flake source		
Element	Pebble	Ingot	Powder(a)	Flake	Ingot	Powder(a)
O_2	...	300	2500–4000	2300	600	2500–4000
Al	400	450	470	200	200	230
Fe	500	500	550	300	250	325
Ni	100	100	120	150	125	150
Si	50	50	75	75	100	125
B	...	1	...	2	...	...
Cr	100	75	...	20	...	...
Mn	100	50	...	60	...	...
Ca	...	100	...	200	<200	...
Mg	15,000	300	...	50	...	...
Na	...	50	...	300	...	...
C	300	350	400	300	150	250
F_2	20,000	<50	...	...	...	...
Cl_2	...	...	...	1000	<50	...
Be assay		96.0%			96.5%	

(a) Powder, −200 mesh. Source: Hansen and Andarko 1958

been concerned with grain-size control and purity effects, from the standpoint of both improved ductility and beneficial additions to beryllium.

The following covers the production of beryllium powder, consolidation techniques, and some properties of the consolidated product.

19.2 Powder Production

19.2.1 Traditional Impact Grinding

Impact grinding involves attrition of chips made from machining vacuum-melted ingots. Chips machined from vacuum-melted stock are thoroughly inspected and classified [Wikle and Potter 1961]. These chips are then attrited to −200-mesh powder in a water-cooled, beryllium-faced mill. The resulting ground powder is conveyed over 200-mesh screens, where the appropriately sized powder is collected and the oversized powder is returned for recycling through the mill. The −200-mesh powder produced in this manner generally has an average particle size of 19 μm but consists of a wide range of particle sizes, with approximately one-half of the product being −325-mesh material.

The chipping operation greatly increased the surface area of the powder, resulting in contamination. Iron and carbon contents increase slightly. Oxygen contents are increased considerably during the powder-processing operation, with a resultant BeO content ranging from 1 to 2 wt%. Continuous sampling of the powder material and the determination of chemical and screen analyses are employed to permit blending of powders for a uniform product. Typical analyses of two commercial types of −200-mesh powder are given in Table 19.1 [Hausner 1965d]. The composition of the source materials, after melting into ingot form and after attritioning to −200-mesh powder, demonstrates the influence of each stage of the operation. Electrolytic-flake source material represents a higher purity level in all stages but does not appreciably affect the final oxygen content of powder.

With further decreases in particle size, the oxide content of the powder increases appreciably. It has been observed that such finer particle-sized powders are useful in obtaining increased strength and ductility in finished beryllium [Beaver 1966]. A proprietary powder, designated as I-400 which yields pressings with an average particle size of 10 μm, has evolved from efforts to produce fine-particle powders. A typical analysis of this powder compared with several other powders that yielded material of the same grain size after hot pressing is shown in Table 19.2. It is apparent that the I-400 beryllium powder reflects an increase in all impurity levels due to the elaborate method of processing and greater surface area.

Introduction of a different form of impact attrition, in which beryllium particles carried by a high-velocity gas stream impact on a beryllium target, was accomplished in approximately 1977 and led to improved particle morphology (more blocky), which gave greater tap density and, correspondingly, more uniform hot pressed billets. The blocky particles also do not show a

Table 19.2 Chemistry of variant-purity powder lots of beryllium averaging approximately 10 μm grain size after pressing

Composition, ppm	I-400 (typical)	Low-purity thermally reduced metal	High-purity thermally reduced metal	Electrorefined metal
BeO(a)	4.25–4.75	4.57	2.29	2.14
C	2000–4000	1520	1110	420
Al	1000–1500	600	300	40
Cr	200–400	110	120	60
Fe	1300–1700	1400	800	240
Mg	200–450	180	170	20
Mn	400 max	70	90	6
Ni	400 max	210	110	85
Ti	400 max	210	260	6
Cu	400 max	120	100	50
Si	400–800	500	200	55

(a) Unit, %. Source: Hausner 1965d

preferred orientation, and, as a consequence, the texture of the billet was more random.

19.2.2 Grades

There is no uniform system for identifying the different grades of beryllium. The identification system that has been largely used in the United States is based on that evolved at Brush Wellman. Experimental products and materials produced in countries other than the United States usually do not follow the Brush Wellman system. Prefixes refer to the proposed use for the material, for example, "S" for structural, "O" for optical, "I" for instrument, "SR" for rolled sheet, "PR" for rolled plate, and so on. The structural grades are mostly produced by vacuum hot pressing. The structural grades are also produced by hot isostatic pressing (HIP) and cold isostatic pressing (CIP) processes, but to a much lesser extent. Other designations that appear in figures, but are obsolete, include nuclear-grade powder (NP) and QMV, a Brush Wellman grade.

Suffixes relate to changes in the process and to the specific consolidation process; for example, the grade S-200E was improved by changing to the use of impact-ground powder. This modification resulted in changing the designation from S-200E to S-200F. A suffix "H" designates HIP and "C" designates CIP, for example, S-200FH and S-200FC, respectively. Structural-grade S-200F contains 1.5 wt% BeO and relatively high ductility; S-200E and S-65 contain a maximum of 2.0 and 1.0 wt% BeO, respectively. The "S" grades have higher ductility but lower elastic limits than the "I" or "O" grades.

The term *attrition* or *attritioned* with reference to the production of powders is not uniformly used in the literature. For example, Brush Wellman reserves the term for powders produced by grinding and machining processes. Some authors use it as a generic term for powders produced by any mechanical means, including ball milling, whereas Brush Wellman refers to this powder as ball-milled powder.

19.2.3 Atomization

In recent years, several methods of making beryllium powder by atomizing from the melt have been successfully developed. One of these methods is called centrifugal atomization and consists of directing a stream of molten metal onto a rapidly spinning cooled disk, where the molten metal is broken into small droplets as it departs the disk rim at high velocity. A flow of quench gas such as helium is directed perpendicularly to the molten droplets, and they freeze before striking the side wall of the chamber. The gas and powder flow is then directed to a cyclone separator, where the powder is collected in a vessel and the gas escapes. The powder made from this process is typically larger than what can be achieved with gas atomization. The work on centrifugal atomization of beryllium powder was mainly done at Los Alamos National Laboratory and has since been discontinued in favor of gas atomization.

Gas atomization has also been successfully used for beryllium and its alloys, and ultrasonic velocity gas atomization is being developed for this purpose as well. Advantages expected for the ultrasonic atomization are primarily associated with the possibility of obtaining a finer and narrower particle-size distribution than with conventional gas atomization.

Atomized powder has a spherical shape and therefore is expected to give compacted material

with a minimum of texture, or preferred orientation. It also has more uniform and controllable flow properties, making it preferred for plasma spray consolidation techniques. Brush Wellman's gas atomizer was obtained from Valimet, a commercial spherical aluminum powder manufacturer, and modified for beryllium atomization. While the majority of the gas used to make the powder in the Brush Wellman atomizer is inert, there is some oxygen added to the gas stream.

The addition of oxygen to the inert gas is a practice that was carried over from the production of aluminum and aluminum alloy powder. The practice is based on the theory that the powder must be passivated to minimize the likelihood of explosions. The practice of adding oxygen to the inert atomization of aluminum powder has come into question by some researchers [Anderson and Foley 2001]. In addition, beryllium powder is on the other end of the ignition-and-explosibility scale from aluminum, with beryllium being categorized as weak and aluminum as severe [Jacobson et al. 1964]. Another surprising result from the Bureau of Mines study was that certain mixes of beryllium powder with aluminum prevented the ignition of the aluminum [Jacobson et al. 1964.]. The vast majority of the powders that are produced by the Brush Wellman atomizer are aluminum-beryllium alloys, with the next higher fraction being optical-grade powder. All of the mirrors for the James Webb Space Telescope (see book cover) were made from powder produced in Brush Wellman's atomizer.

High-Pressure Gas Atomizer. A research-sized, high-pressure gas atomizer (HPGA) was built at Los Alamos National Laboratory (LANL) to produce beryllium powder without adding oxygen to the atomization gas. The HPGA at LANL uses high pressure (500 to 1300 psig) compared to the relatively lower pressure (100 to 200 psig) of the Brush Wellman atomizer [Foley 2007]. At the time of this writing, the LANL atomizer was still being fine tuned for use and approval as a beryllium atomizer. It is hoped that the reduction of BeO formation during atomization process will generate a final product that is equal or better than the S-grade beryllium product. However, it remains to be demonstrated that consolidation of atomized powder will give a structural product that has the same mechanical properties, particularly ductility, as material hot pressed from attritioned powder. Another possible outcome of the research being performed at LANL is the development of new processing routes that enable near-net shaping of beryllium. Near-net shaping of beryllium would have both a cost and health-and-safety benefit by reducing the amount of machining that is necessary to produce a part.

19.2.4 Other Techniques

Ball Milling. Reduction of powders to a particle size of less than 10 μm by ball milling has been examined [Bufferd et al. 1964, Theodore et al. 1967]. At first, both pebble- and flake-source materials were attritioned by ball milling in methyl alcohol with an argon atmosphere. Although powders with particle sizes on the order of 1 to 5 μm could be produced in this manner, iron contamination resulting from contact with stainless steel components was too high to make ductile beryllium. More recently, contamination has been reduced through the use of beryllium components and prior grinding of scrap beryllium to coat the various grinding components. Powders of less than 20 μm have been produced [Porembka et al. 1967].

Vapor. Several methods for processing submicron beryllium powders have been investigated. One method is based on the condensation of metal vapor in an inert atmosphere at reduced pressure [Raymond 1964]. In this operation, beryllium vapor is given off at a hot source, condensed as spherical particles in free space, and collected on the wall of a cooled rotating drum. Initial studies using a BN-coated carbon crucible to contain the molten beryllium resulted in some BeC_2 contamination. However, submicron-sized particles of beryllium were successfully obtained.

Electrolysis. A second method has involved the electrolysis of beryllium from a molten eutectic mixture of BeC_{12}-NaCl at 300 °C using a mercury cathode and a carbon anode [Gale et al. 1965]. The beryllium is collected in the mercury cathode in the form of a quasi-amalgam. The amalgam is collected, filtered, squeezed, and then distilled to yield a fine beryllium powder with a particle size of approximately 1 μm.

An ablation method using a 50 kW plasma torch with a transferred-arc mode of operation has been studied as a means of powder production [Theodore et al. 1966]. In this operation, the high-velocity, high-momentum plasma flame expels molten metal from the target. Difficulty with iron contamination was experienced, related to the abrasive action of the particles

Table 19.3 Commercially available beryllium powders

Standard powder designations(a)	Nominal mesh size	Chemical composition (maximum unless noted), %							
		Be (min)	BeO	Al	C	Fe	Mg	Si	Other
SP-100-C	−200	98.5	1.2	0.14	0.15	0.15	0.08	0.08	0.04
GB-1	−150								
SP-200-C	−100	98.0	2.0	0.16	0.15	0.18	0.08	0.08	0.04
P-20	−140								
GB-2	−150								
SP-300-C	−100	97.4	3.0	0.18	0.15	0.20	0.08	0.12	0.06
NP-50-A	−200	99.0	0.9	0.075	0.10	0.075	0.03	0.06	. . .
P-8	−140								
NP-100-A	−200	98.5	1.2	0.10	0.12	0.14	0.05	0.08	. . .
P-12	−140								
GB-1N	−150								
NP-200-A	−100	98.0	2.0	0.10	0.15	0.16	0.05	0.08	. . .
CR	−150	99.0	0.9	0.03	0.04	0.05	0.005	0.01	0.04
CR-N	−150	99.0	0.9	0.03	0.04	0.05	0.005	0.01	. . .
CR-IN	−150	99.0	0.9	0.07	0.10	0.10	0.03	0.06	. . .
SR(b)	−200	. . .	0.8	0.008	0.015	0.01	0.006	0.008	. . .
SSR(c)	. . .	. . .	0.45	0.003	0.010	0.0005	0.001	0.0015	. . .

(a) SP designation, Brush Beryllium Co.; P and NP designations, Beryllium Corp.; GB designations, General Astrometals; CR, SR, SSR designations, Pechiney, licensed to General Astrometals. (b) Semicommercial high-purity powder. (c) Semicommercial very high-purity flake

with steel components. The powder particles produced by this technique were generally spherical with a particle size of −200 mesh, although the contamination levels were considered too high for fabrication of ductile beryllium. Plasma spheroidization of beryllium powders has also been studied in an effort to obtain better powder packing characteristics and more random orientation of pressed beryllium [Hodge et al. 1966]. Information on such powders, however, is limited.

Splat cooling offers a means of producing a large-particle beryllium material that consists of small grains (1 to 10 μm) [Kaufmann and Muller 1966]. Since the particles are large and represent a low surface area, oxygen contents can be maintained at a low level. Fabrication of fine-grained pressings from this material avoids the high oxygen contents normally associated with fine-particle-sized beryllium powders. This operation is accomplished by quenching drops of molten beryllium on a rotating copper disk in an inert atmosphere. The molten drops are formed by rotating a beryllium rod or tube about its longitudinal axis while melting the end face with a direct current arc. The splats produced in this manner are ejected from the rotating disk and collected. The resulting material consists of irregularly shaped platelets approximately 5 to 10 μm thick and approximately 1000 to 2000 μm in diameter. The grain structure of the splats appears as equiaxed fine grains when viewed in the plane of the platelet and columnar grains when viewed through the thickness of the splat [Porembka et al. 1967].

19.2.5 Standard Commercial Structural Beryllium Powder

A number of standard beryllium powders are available commercially. Their designations and respective nominal particle sizes and compositions are listed in Table 19.3. It should be noted that some slight variations exist in the powders as produced by the different suppliers, but the groupings in the table represent equivalent powders.

19.3 Powder Consolidation

19.3.1 Cold Compaction

Traditionally, a major part of commercial operations is based on vacuum hot pressing. Some complex configurations have been hydropressed prior to sintering. The compaction behavior of beryllium powders in die pressing, slip casting, explosive pressing, and vibration packing has been studied, and these processes have been applied only to a limited extent. A review of the techniques for compaction of beryllium powder provides considerable insight into the characteristics of this material and is discussed.

19.3.2 Die Pressing

The cold-die-pressing characteristics of beryllium powders are affected by their particle size and method of processing. The addition of coarser particles will generally raise cold-pressed densities, as shown in Fig. 19.1 [Beaver

and Lympany 1965]. At pressures above 830 MPa (60 tsi), densities on the order of 80% of theoretical and greater are readily obtained. The condition of the powders, that is, annealed as opposed to attritioned, will also influence the cold-pressed density. The differences shown in Fig. 19.2 [Beaver and Lympany 1965] are due to the increased work hardening of the beryllium during the attritioning operation and a subsequent resistance to compaction. With annealing, this resistance is reduced.

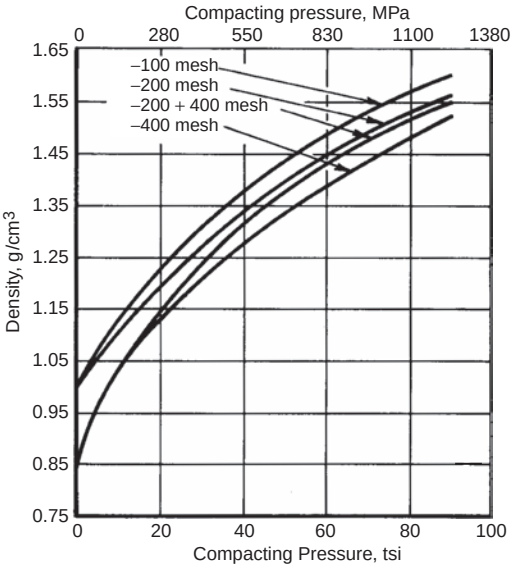

Fig. 19.1 Compactability curves at room temperature for attritioned beryllium powder of various mesh sizes. Source: Beaver and Lympany 1965

Particle shape has been observed to affect cold-pressing characteristics, particularly in the case of attritioned flake beryllium and splat-cooled beryllium. The platelet nature of these two types of particles results in a tendency of the particles to align themselves on loading into the pressing container [Porembka et al. 1967]. This arrangement of particles is then retained in the pressed form. The beryllium powders that are more regular in particle shape appear more equiaxed in the pressed form, although a range of particle sizes is contained within the compact.

19.3.3 Cold Isostatic Pressing

Cold isostatic pressing (CIP) of beryllium powders for large irregular shapes, prior to sintering or elevated-temperature consolidation, provides a major economic advantage by reducing machining time and beryllium scrap [Billman 1965]. Cold isostatic pressing has also been used extensively

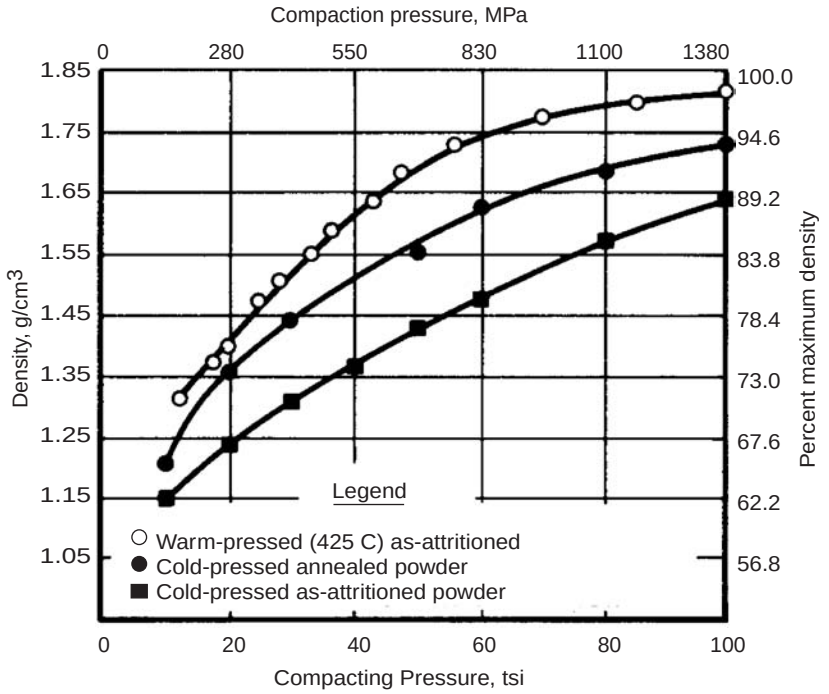

Fig. 19.2 Density as a function of pressure relationships for compacts, 3.81 cm (1.5 in.) diameter by 0.762 cm (0.300 in.) long, of QMV beryllium powder (−200 mesh). Source: Beaver and Lympany 1965

Table 19.4 Porosity in isopressed metal powders

Pressure(a)		Pressed density, percent of theoretical			
MPa	ksi	Beryllium (−20 mesh)	Iron (−200 mesh)	Copper (−200 mesh)	Aluminum (−200 mesh)
172	25	71	74	75.5	87.5
345	50	77.9	82.1	85.3	94.4
646	93	...	...	91.9	98.7
689	100	86.8	89.9	...	98.9
910	132	...	...	94.6	...
1034	150	91.4	94	95.8	99.2
1206	175	92.8	...	...	...

(a) Metric units derived from customary units. Source: Greenspan 1964

to fabricate powder preforms for the hot isostatic pressing (HIP) method [Hodge et al. 1966, Hanes et al. 1964]. In a typical CIP operation, the powder is loaded into a rubber container of the desired size and configuration, the assembly is evacuated and sealed, and an isostatic pressure is applied with a hydraulic pressing medium. The initial loading of powders must be uniform, since any layering effects in this stage will also be present in the finished compact. Frequently, vibration methods are used to ensure proper powder distribution. The application of pressure from all directions results in an essentially uniform density throughout the compact. With this technique, good uniformity is achieved because frictional forces, such as those normally associated with die walls, are avoided [Porembka et al. 1967].

The isostatic pressing behavior of several types of beryllium powders have been characterized by Greenspan [1964]. The compacting behavior of a −20-mesh beryllium powder under pressures of up to 1200 MPa (175 ksi) were evaluated. All compacts pressed at 345 MPa (50 ksi) and above were observed to be sound. Compared with −200-mesh powders of aluminum, copper, and iron, which were also examined, the −20-mesh beryllium powder was found to press to lower densities at all pressures. The results obtained from this comparison are listed in Table 19.4.

Greenspan also studied the influence of strain hardening developed during isostatic pressing of beryllium powder by twice annealing compacts at 816 and 1038 °C (1500 and 1900 °F) between pressings at 1034 MPa (150 ksi). The results of these two sequences of operations are shown in Fig. 19.3, where the density was increased to approximately 98% of theoretical for the 816 °C anneal and 99% for the 1038 °C anneal. The strain hardening observed in this work is related to the particle deformation necessary to accommodate the increase in compact density.

A commercial grade of −200-mesh beryllium powder (P-12) has been CIPd to densities on the order of 80% of theoretical within a practical range of pressures [Hodge et al. 1966]. The density as a function of pressure is given in Fig. 19.4.

It was noted that compacts of this type pressed at 207 MPa (30 ksi) were somewhat friable but could be handled with sufficient care. Higher pressures resulted in improved handling characteristics, and after being pressed at 414 MPa (60 ksi) and above, the compacts could be machined prior to further processing. From limited work with other types of commercial −200-mesh beryllium powders, it appeared that the pressing characteristics of a 0.8% BeO nuclear-grade material and a 2.0% BeO structural-grade material were similar.

Cold isostatic pressing of several types of beryllium-flake materials at pressures to 317 MPa (46 ksi) has been investigated [Bunshah and Juntz 1963]. The final densities achieved (given in Table 19.5) are higher than those obtained at similar pressures with the −20 and −200-mesh powders. This difference may be due to the higher purity of flake material and its tendency to align on loading and compacting. Machine turnings generally pressed to lower densities, which would also indicate an influence of particle shape. The pressing behavior of the beryllium flake material was found to compare favorably with that of titanium sponge [Porembka et al. 1967].

19.3.4 Vibration Packing

Vibration techniques are used during loading of beryllium powders to provide more uniform distribution of the powder and to increase the starting density. The packed density that can be achieved in this manner is a function of the

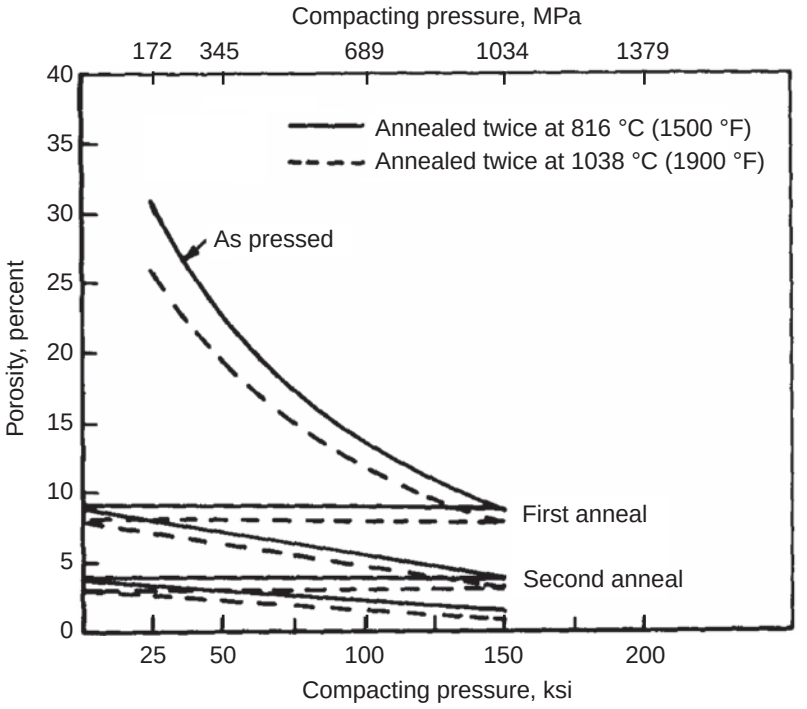

Fig. 19.3 Compacting behavior of beryllium powder annealed twice at 816 °C (1500 °F) and recompacted or annealed twice at 1038 °C (1900 °F) and recompacted. Source: Porembka et al. 1967

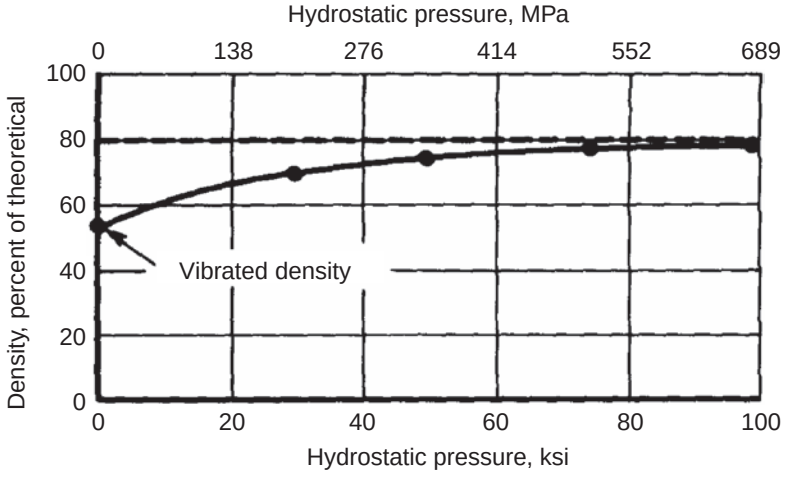

Fig. 19.4 Effect of pressure on the density of hydrostatically pressed Berylco P-12-grade beryllium. Source: Hodge et al. 1966

particle size, particle shape, and particle-size distribution. In general, coarser-sized particles with a narrow range of particle sizes will develop higher packing densities during vibration. Commercial −200-mesh powders can normally be vibration packed to densities slightly over 50% of theoretical within relatively short times. The effect of vibration time is shown in Fig. 19.5, where it is evident that, after 10 min, very little further increase in density is obtained [Beaver and Lympany 1965]. In most cases, vibration frequencies have ranged from 60 to 100 Hz, with little difference in the final results. This procedure is used prior to commercial hot

Table 19.5 Typical data on compaction of different types of beryllium flakes

Material	Initial preform size: Diameter, in.	Initial preform size: Length, in.	Final compact size: Diameter, in.	Final compact size: Length, in.	Weight, g	Compacting pressure, ksi	Liner thickness, mils	Density: g/cm³	Density: % of theoretical	Remarks
Pechiney flake	$2\frac{7}{16}$	$7\frac{3}{4}$	$1\frac{7}{8}$	6	380	25	5	1.47	79	Good
Pechiney flake	$2\frac{7}{16}$	$1\frac{1}{2}$	$1\frac{3}{4}$	$1\frac{1}{6}$	50	46	5	1.672	90	Good
U.S. Bureau of Mines flake	$2\frac{7}{8}$	16	2-$2\frac{1}{4}$	12	1087	46	5	1.63	88	Slightly irregular diameter
Machine turnings	$2\frac{5}{8}$	$11\frac{3}{4}$	$1\frac{7}{8}$	9	525	46	5	1.35	73	Slightly irregular diameter

Source: Bunshah and Juntz 1963

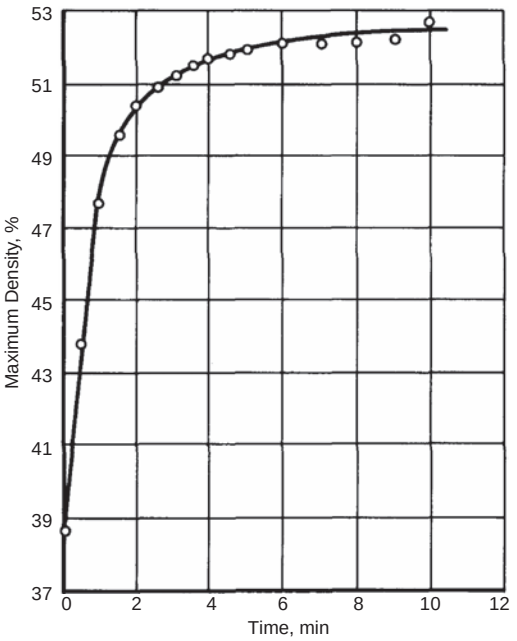

Fig. 19.5 Increase of −200-mesh loose beryllium powder density by vibration. Source: Beaver and Lympany 1965

pressing and has also been employed prior to isopressing and HIP.

The effect of vacuum during vibration compaction of SP-200-C and I-400 beryllium powders has been investigated [Lohrer 1964]. Cylindrical columns of the two types of powders were vibrated at 100 cycles/min with and without vacuum. Presence or absence of vacuum had little effect on the −200-mesh (SP-200-C) beryllium powder. With the finer I-400-type powder, longer vibration times were required to achieve maximum density when the system was under vacuum. In the early stages of vibration, the evacuated system provided higher densities; however, the final density achieved after longer vibration times was lower. It was concluded that a modification of the use of vacuum in vibration packing the I-400 powder would yield the maximum density, namely, evacuation prior to vibration for 10 to 15 min and restoration of atmospheric pressure with continued vibration.

Blending of selected particle-size fractions of beryllium powder to enhance vibration-packed densities has been studied [Hodge et al. 1966]. Size fractions of NP-50A beryllium powder consisting of −60 + 100 mesh, −100 + 200 mesh, and −200 mesh were blended in various amounts and vibrated at 60 cycles/s to the densities shown in Fig. 19.6. The influence of particle size is apparent from this ternary presentation, showing packed densities significantly above and below that normally obtained with a −200-mesh commercial powder.

19.3.5 Slip Casting

Slip casting of powders is an attractive method for producing complex shapes. Development of a successful slip-casting process requires the proper selection of binders, thickeners, and vehicles to maintain the metal in suspension with little relative movement of the particles. In this process, a slip of beryllium powder is poured into a porous absorbent mold of the required configuration. Absorption of water from the slip by the mold deposits the powder particles on the mold surface and, with continued absorption and the introduction of additional slip, the powder preform is made. Hollow shapes can be obtained by pouring out the remaining slip after the required thickness of powder is deposited. The residual binder after dewatering maintains the cast green form, and the green strength of the component can then be increased by low-temperature baking [Porembka et al. 1967].

A satisfactory slip-casting technique for beryllium powder was developed [Hayes and Yoblin 1961]. The method employed a slip consisting of 68.5 wt% −325-mesh beryllium, −0.6 wt%

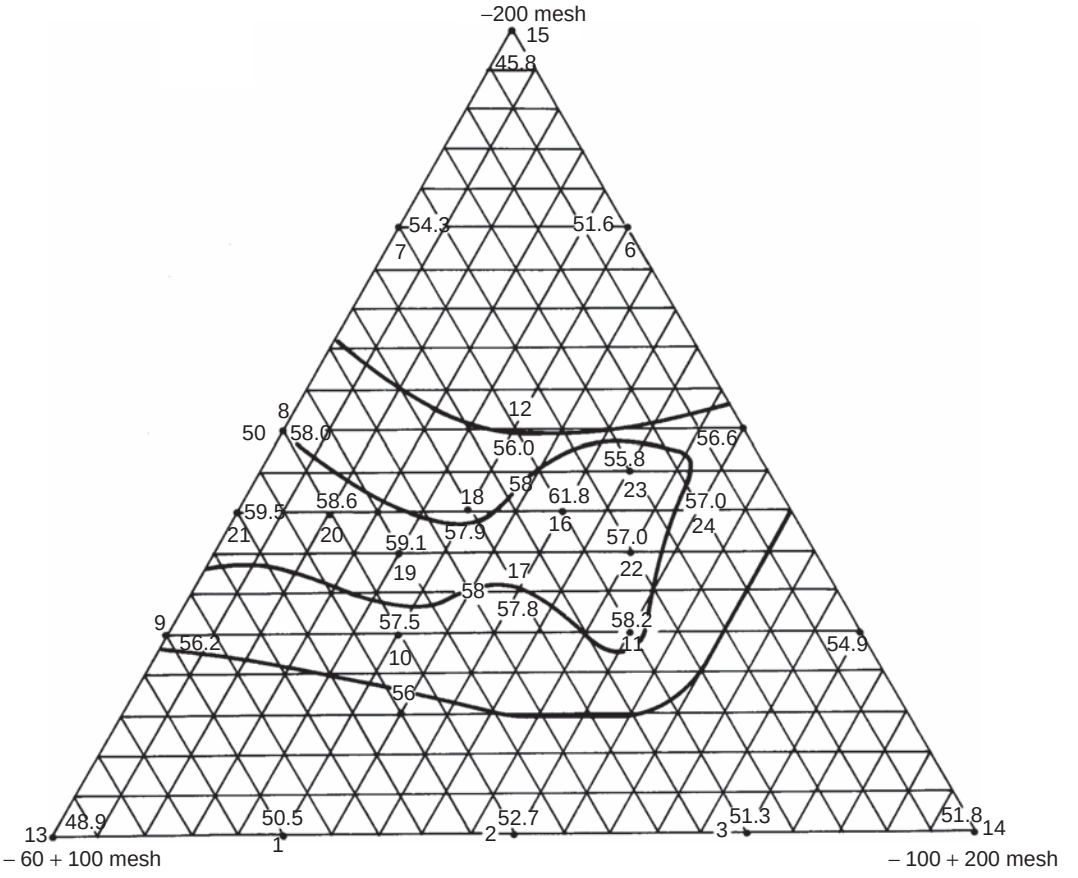

Fig. 19.6 Vibrational-pack densities of selected particle sizings of NP-50A beryllium powder. Source: Hodge et al. 1966

Kelcosol (Merck), and 30.9 wt% water at a pH of 5.8. The constituents were blended in a counterrotating mixer to form a slip with a viscosity of approximately 4000 cP. Several slips were cast into plaster molds and then removed; after baking at 38 °C (100 °F), sufficient green strength was attained to permit final sintering. The transverse rupture strength of the castings after the baking operation averaged approximately 1 MPa (150 psi).

The beryllium powder used in this work did not produce a satisfactory slip, as had been reported earlier [Bielowski et al. 1963, Fisher et al. 1965]. The difference in particle-size distribution between the powder in this later study and that used in the earlier reference was the apparent cause for this difference in behavior. It was found that this powder, which was somewhat coarser in average particle size, provided a better slip when the vehicle consisted of a mixture of equal parts of methyl ethyl ketone and xylene, to which was added 30% of collodion solution (a glue-forming constituent). Mold sticking was experienced with these collodion-containing slips; consequently, various coatings for the plaster molds were examined. The best results were obtained when the mold was coated with an ammonium-alginate solution, dried, and then coated with a polyethylene suspension. This approach proved very successful for simple shapes but did not completely avoid mold sticking with complex shapes. The methods developed for beryllium alone were also found satisfactory for beryllium powder with alloy-powder additions. The latter were for the promotion of liquid-phase sintering on subsequent densification [Porembka et al. 1967].

19.3.6 Explosive Compaction

The very high pressures developed during the detonation of explosives have been used to

compact beryllium powder to high densities [Hodge et al. 1966, Porembka 1963]. The procedure consists of loading the powder into a mild-steel container, wrapping the container with a sheet explosive, and detonating the assembly from one end. A −200-mesh commercial powder, which had been initially loaded to a density of 50% of theoretical by tap packing, was compacted to 96% density in this manner. This method has also been employed for making high-density preforms that were then consolidated to full density by HIP. A principal advantage of the process is that shape can be retained despite heavy material deformation.

19.4 Sintering

The behavior of beryllium powders during conventional sintering has not been investigated extensively, since this method is rarely used in production. Most of the work involving sintering of die-pressed beryllium powders was conducted with materials that would be considered less pure than those now available. It has been noted that the purer materials, such as those derived from electrolytic processes, do not sinter as readily as the pebble-source types. Consequently, efforts have been aimed at achieving activation of sintering through minor additions of other elements. Pressureless sintering of beryllium powders as a means to retain an isotropic finished material has also been studied recently. With the increased interest in isopressing of complex shapes, sintering as a method for final densification has become more important [Porembka et al. 1967].

19.4.1 Conventional Sintering

The sintering of beryllium generally requires a temperature above 1050 °C (l922 °F) to achieve effective increases in density. It has also been observed that the sintering atmosphere influences the final densities obtained. Both of these effects are shown in Fig. 19.7 as a function of initial compacting pressure for a −200-mesh beryllium powder [Hausner and Pinto 1949]. Sintering in vacuum yielded higher densities than sintering in argon, and at 1200 °C (2192 °F), the sintered density was nearly independent of the compacting pressure. Measurements of electrical resistivity with increasing sintering temperature have shown that although the compact density does not change at sintering temperatures from 500 to 900 °C (932 to

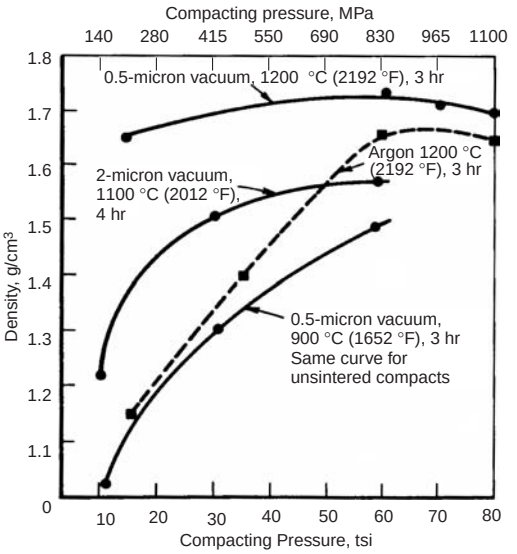

Fig. 19.7 Effect of compacting pressure on the sintered densities of −200-mesh beryllium powder compacts. Source: Hausner and Pinto 1949

1652 °F), the electrical resistivity is markedly reduced [Hausner and Pinto 1949]. This effect is attributed to changes in the pore shape within the powder mass without any corresponding change in pore volume. Material transport to effect the pore changes is related to the vapor pressure of beryllium at elevated temperatures, particularly in vacuum.

In sintering cold-pressed beryllium powders, vacuum is generally preferred. This permits the removal of air that may be entrapped in the compact during the pressing operation. With other sintering atmospheres and very high-pressed densities, blistering and a subsequent density decrease have been experienced [Beaver 1955a]. In addition, vacuum promotes the removal of adsorbed gases from the surfaces of the powder particles, which is also necessary to obtain high final densities [Porembka et al. 1967]. It has been observed in outgassing experiments that gases are evolved from −200-mesh commercial powders in decreasing amounts up to temperatures on the order of 954 °C (1750 °F). Data obtained in such tests are given in Table 19.6, where the amount of gas evolved and its analysis was obtained in successive tests on the same powder sample.

The BeO content of beryllium powders plays several roles during the sintering process. Since BeO is contained on the surface of each powder particle, it tends to restrict grain growth across

Table 19.6 Relative amounts of different gases evolved from QMV beryllium powder(a) at different temperatures

Temperature		Total volume, each step, cm^3	Gas compositions, %					
°C	°F		H_2	CO and/or N_2	CH_4	H_2O	CO_2	C_2H_6
150	300	2.1	0.5	0.07	2.0	92	5.4	0.07
540	1000	19	95	...	4.2	0.3	0.01	0.5
790	1450	1.3	100	...	...	...	...	...
950	1750	1.5	100	...	...	...	...	...
1090	2000	0.1	100	...	...	...	...	...
Total cm^3 atm		24	21	0.001	0.80	2	0.01	0.09
Micrograms		...	1875	1.3	570	1600	196	112
Percent by weight		...	0.02	<0.001	0.005	0.01	0.002	0.001

(a) Obsolete Brush Wellman grade. Source: Porembka et al. 1967

Table 19.7 Effect of sintering temperature and time on the density of loose beryllium powder

	Density at indicated sintering temperature, percent of theoretical					
Sintering time, h	1100 °C (2012 °F)	1125 °C (2057 °F)	1150 °C (2102 °F)	1175 °C (2147 °F)	1200 °C (2192 °F)	1220 °C (2228 °F)
4	...	...	79.6	90.4	95.6	95.5
6	65.5	76.7	86.2	90.7	96.6	97.0
8	...	...	86.1	91.7	96.3	...
12	...	...	...	92.2	97.6	97.9

Source: Hausner 1965d

particles at the higher sintering temperatures. With finer particle-size powders, where the BeO contents are higher, this effect is more pronounced. Normally, a fine-grain powder would have a greater tendency toward grain growth on sintering than would a coarser powder. In addition, movement of BeO within the structure as a result of sintering has been noted [Hausner 1965d]. The BeO particles appear to arrange in the grain boundaries or agglomerate into larger particles at voids during sintering. It has been found that the BeO distribution in vacuum-sintered beryllium is usually different from that in argon-sintered material, which may be a result of differing sintering mechanisms in the two atmospheres.

19.4.2 Pressureless Sintering

Beryllium powder metallurgy parts prepared by pressureless sintering do not exhibit orientation effects, as normally associated with pressure compaction. Loading of powders prior to sintering is accomplished either by tamping or vibrating to packed densities of approximately 45 to 50% of theoretical. As a result, the individual powder particles are not deformed, and the voids within the powder mass are not oriented. During subsequent sintering, the powder mass can then shrink uniformly from all directions, resulting in a uniform grain structure [Porembka et al. 1967].

The initial work in pressureless-sintered beryllium was conducted with a −200-mesh powder produced from electrolytic flake beryllium [Barrett et al. 1958a,b]. Precise control over chipping of the vacuum-melted ingot and ball milling was required to attain a desired particle-size distribution. The powder obtained was placed in a graphite mold, and the surface was covered with BeO to prevent volatization of the beryllium during sintering. The graphite mold was induction heated in vacuum for the sintering operation, and it was observed that good shape retention of the compact was obtained despite high linear shrinkage. The effects of temperature and time on the density achieved by pressureless sintering are shown in Table 19.7. It is apparent that high densities can be achieved only at temperatures of 1175 °C (2147 °F) and above.

The application of pressureless sintering to produce cylindrical and tubular blanks for extrusion was studied by Reeves and Keeley [1961]. Since commercially available powders as used in this work were not designed for pressureless sintering, it was necessary to examine different sintering conditions. The standard powder yielded densities of approximately 97%, which was similar to those reported in previous experiments by another group [Barrett et al. 1958a,b], but the

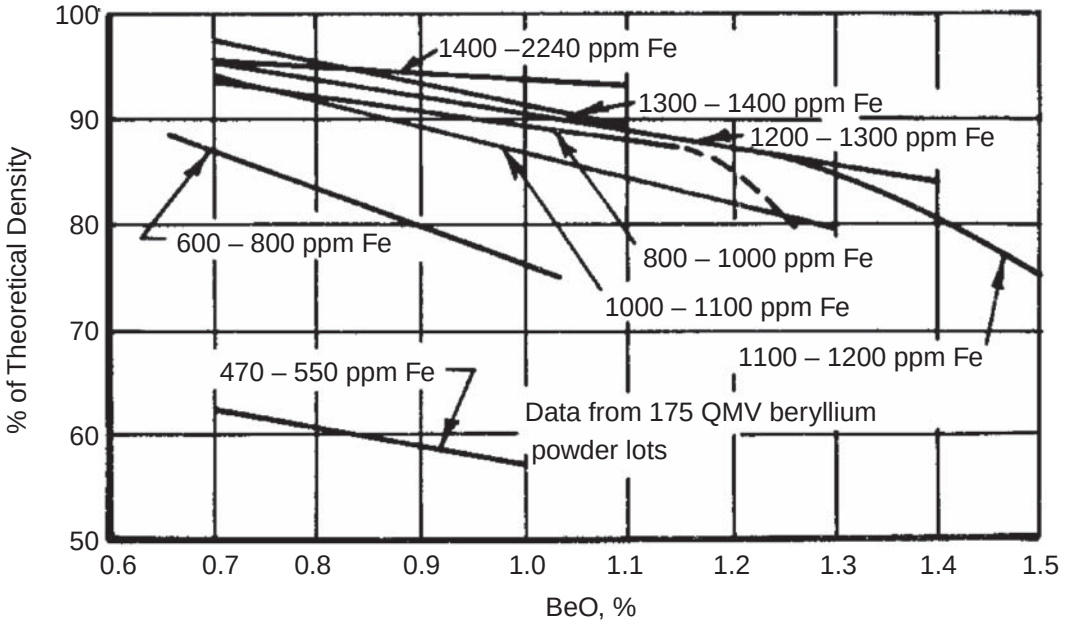

Fig. 19.8 Summary of the relationship between the sinterability of QMV beryllium powder and the beryllium oxide and iron impurity levels at 1200 °C (2152 °F). Source: Lympany et al. 1963

higher-purity powders produced compacts having significantly lower densities. Temperatures higher than 1240 °C (2264 °F) could not be used for the higher-purity powders, since excessive grain growth was encountered. As a result, sintering conditions of 5 h at 1200 °C (2192 °F) for the standard grades and 5 h at 1230 °C (2246 °F) for the high-purity grades were selected. The sintered densities varied from 72 to 98% of theoretical, with the tubular shapes resulting in lower densities than did cylinders.

A regression analysis of composition versus density was performed on the density values obtained in several hundred bars, from approximately 30 batches of beryllium powder, pressureless sintered at 1230 to 1240 °C (2246 to 2264 °F) [Eyre et al. 1966]. The density as a function of chemical composition was determined as:

$$\text{Density} = 1.60 + (1.11\,X_1 + 13.32\,X_2 + 37.83\,X_3 - 0.33\,X_4 - 10.87\,X_5 + 21.44\,X_6) \times 10^{-5}$$

where density is g/cm^3, and X_1, X_2, X_3, X_4, X_5, and X_6 represent iron, aluminum, silicon, oxygen, carbon, and magnesium contents, respectively, expressed in parts per million.

This expression applies only over the range of impurities examined, namely, 410 to 2200 ppm Fe, 350 to 1610 ppm Al, 35 to 255 ppm Si, 1100 to 5500 ppm O, 120 to 690 ppm C, and 40 to 450 ppm Mg. This analysis indicates the importance of impurity contents but does not define the mechanism by which the various elements influence sintering. Several possible mechanisms suggested include liquid-phase formation, oxide-film modification, formation of volatile or liquid oxides, and metal vaporization that disrupts oxide films. Further information on the effects of various elements on sintering is provided in the section on vacuum hot pressing.

The effect of various impurity elements on pressureless sintering has also been investigated [Lympany et al. 1963]. A −200-mesh beryllium powder was sintered for 5 h at 1200 °C (2142 °F), producing densities ranging from 60 to 98% of theoretical. Variations in iron content were found to be the major cause of the differences in sintering behavior observed. In general, it was noted that sinterability increased with increasing iron content and decreased with increasing BeO content. These results are summarized in Fig. 19.8 for 175 powder lots [Lympany et al. 1966]. The effects of iron, aluminum, and silicon were also investigated. The amount of final porosity was found to be a function of both aluminum + silicon level and aluminum/silicon ratio, with decreasing porosity resulting from

increased aluminum + silicon level. A cyclic variation of porosity with aluminum/silicon ratio was noted. It was found that the aluminum and silicon additions were generally located at the grain boundaries after pressureless sintering, thus suggesting a liquid-phase sintering effect. Studies of the effects of other elements on sinterability showed that germanium, silver, and copper have an activating influence, iron by itself does not activate, manganese and ruthenium at 1000 ppm do not activate sintering, and vanadium and tin tend to deactivate sintering.

19.5 Elevated-Temperature Consolidation

Most commercial beryllium products are fabricated by vacuum hot pressing. Components may be machined directly from the pressed block, or portions of the block material may be wrought into other forms by forging, extrusion, and rolling. Direct pressing of shapes from beryllium powder has been accomplished by HIP, which permits higher pressures at lower temperatures, thereby providing a means to closely control the grain structure of pressings. Hot upsetting of powder to flats prior to cross rolling has resulted in favorable orientations in beryllium that have demonstrated appreciable ductility in all directions. Forging of parts from powder has been investigated to a limited extent, and a similar situation exists with the extrusion of beryllium powder. In the past, plasma spraying has also been examined as a method for fabricating preforms of complex shapes [Porembka et al. 1967].

19.5.1 Vacuum Hot Pressing

During the commercial practice of vacuum hot pressing, the beryllium powders are densified primarily through plastic flow. Diffusion, evaporation, and condensation also contribute to the process, particularly in the areas of promoting particle bonding and the final closure of pores. As a result, hot pressed beryllium is virtually free of porosity, and because of the short pressing times, a desirable fine-grain structure is obtained. A slight degree of orientation exists in the material, since the pressing operation is directional, and frictional forces are encountered at the die walls.

The operations involved in vacuum hot pressing beryllium have been outlined in several references [Wikle and Potter 1961, Denny and Moyer 1962]. Although improvements have been made in some aspects of the process, the general procedure remains the same. The operations are as follows:

- Two methods of powder loading have been used: (a) Load powders into steel cans for handling purposes, and insert cans into the pressing die, or (b) load the powders directly into steel, graphite, or carbon hot pressing dies.
- Load the die with the required compaction tooling into a furnace, and seal the furnace vacuumtight.
- Evacuate the furnace to approximately 500 μm Hg.
- Heat so that a powder temperature of 1000 to 1100 °C (1832 to 2012 °F) is attained.
- Apply a pressure of 1.4 to 10 MPa (200 to 1500 psi) to compact the beryllium to full density. The total pressure and rate of application may be varied, and the end point of densification can be determined from the compact height.
- Unload the compacted block, die, and tooling into a special cooling chamber after the furnace cools to 540 °C (1000 °F).
- Unload the pressed block from the die.
- Remove the steel can, if used, or machine the compact surface to remove slight iron and carbon contamination resulting from contact with the die walls.

The behavior of beryllium powders during vacuum hot pressing in a die was found to be similar to that on cold pressing in a die [Wikle and Potter 1961]. In particular, a study of layered compacts consisting of alternate layers of beryllium and beryllium with a 1 wt% metallic additive indicated the relative movements of individual layers of the powder materials during hot pressing. The structures shown in Fig. 19.9 indicate the influence of die-wall friction and pressing direction on the relative movement of the powder during consolidation. From these structures, it was observed that the central body of the powder was first more highly densified, after which the zone of maximum densification spread to the upper corners, to the central wall area, to the area just below the punch, and to the bottom corners, in that order. Porosity, as noted with dye penetrants, substantiated this mode of beryllium densification during vacuum hot pressing.

The effects of pressure, temperature, and time on hot pressing beryllium powder have been in-

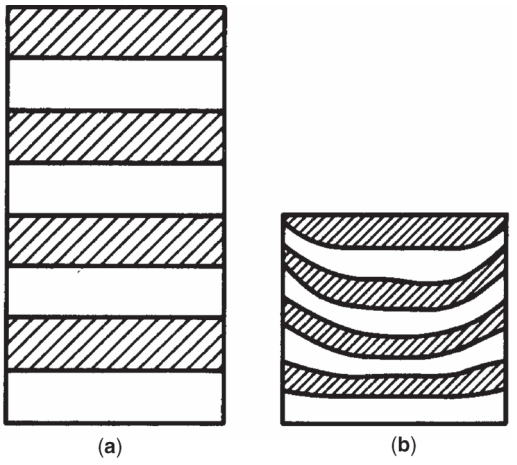

Fig. 19.9 Illustration of relative material movement during vacuum hot pressing of beryllium powder in a die. (a) Vibrated powder column with bands of beryllium powder alternating with bands of beryllium plus additive powder. (b) Vacuum hot pressed compact at +99.5% of theoretical density showing relative movement of powder layers. Source: Wikle and Potter 1961

vestigated by Butcher and Beasley [1964]. A single batch of −200-mesh beryllium powder, designated as a superpure grade, was employed in this work. Compacts measuring 5.08 cm (2 in.) in diameter by 10.16 cm (4 in.) long were fabricated, and hot pressability was assessed as the length of compact exhibiting greater than 98% density. The effects of temperature, pressure, and time are shown in Fig. 19.10 through 19.12. It is apparent that pressure produces the greatest effect, since this was the only series in which a compact exhibited 98% density over its entire length. Density variation experienced in these compacts was related to powder flow and frictional interaction with mold and plunger faces. The effectiveness of increased pressure and temperature was attributed to reductions in the yield stress of the powder columns at high temperatures.

It is apparent that time, temperature, and pressure can be varied to produce high-density

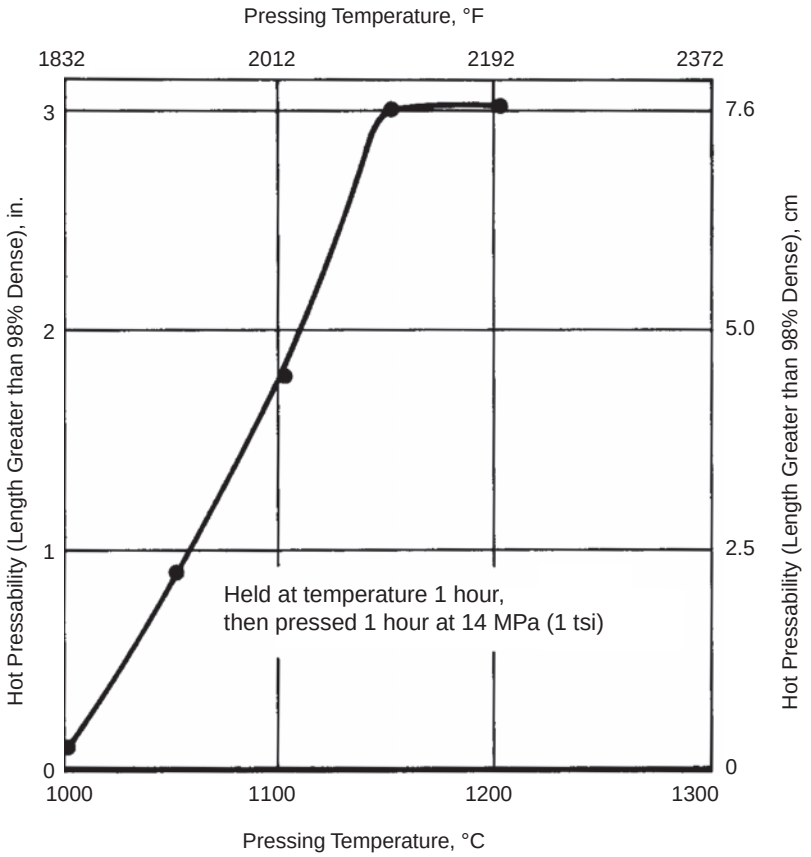

Fig. 19.10 Effect of pressing temperature on hot pressability of beryllium powder. Source: Butcher and Beasley 1964

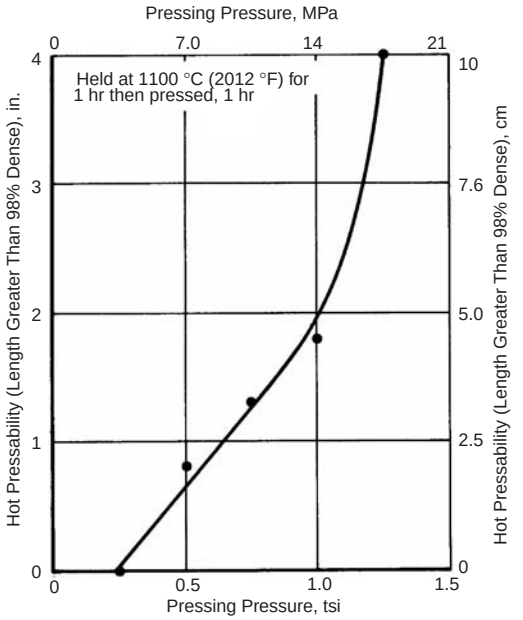

Fig. 19.11 Effect of pressing pressure on hot pressability of beryllium powder. Source: Butcher and Beasley 1964

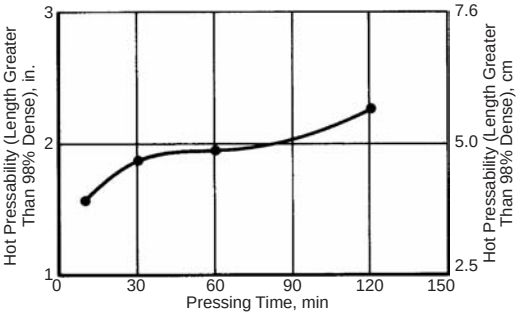

Fig. 19.12 Relationship between hot pressability and pressing time of beryllium powder at 100 °C (212 °F) under 13.8 MPa (1 tsi). Source: Butcher and Beasley 1964

beryllium. Warm pressing, which involves lower temperatures and higher pressures, has been used successfully. It should be noted, however, that die limitations frequently determine the extent to which warm pressing can be effectively employed. A brief comparison of hot and warm pressing conditions and the resulting pressed densities is given in Table 19.8 [Hausner 1965d]. At the lower pressing temperatures, considerable increases in pressure are required to produce high-density beryllium.

As was noted in the section on pressureless sintering, impurities and alloying additions

Table 19.8 Pressure compacting of beryllium at moderately elevated temperatures

Sample	Pressure		Temperature		Time at temperature, min	Density, g/cm³
	MPa	ksi	°C	°F		
1	3.4	0.5	960	1760	30	1.64
2	3.4	0.5	1000	1832	30	1.68
3	3.4	0.5	1115	2039	30	1.83
4	5.2	0.75	1075	1967	30	1.85
5	5.2	0.75	1125	2059	30	1.84
6	6.9	1	1020	1868	30	1.71
7	6.9	1	1078	1972	30	1.87
8	6.9	1	1100	2012	30	1.87
9	345	50	500	932	15	1.77
10	345	50	600	1112	15	1.85
11	345	50	650	1202	15	1.85

Source: Hausner 1965d

markedly affect the sinterability of beryllium powder. The compactibility of commercial beryllium powders during vacuum hot pressing also has been related to chemical composition [Butcher and Beasley 1964]. Pebble-source powders normally contain sufficient quantities of activating elements to permit the attainment of high densities. Electrolytically produced powders, representing a higher purity, cannot be hot pressed to such high densities. The addition of 500 ppm Si to these powders significantly improves their consolidation. The silicon present at the particle surfaces limits particle distortion and permits particle flow during compaction. The activation of powders by silicon, iron, nickel, and chromium additions, or by the existence of these elements in the commercial powder, accounts for variations in hot pressability with different powder batches of the same size and impurity-limit specification.

A study of 20 different elements added in the amount of 0.02 at.% to CR-grade powder identified the desirable features of activating elements [Butcher 1965]. The effects of the additions were evaluated on the basis of the density variations along the length of hot pressed cylinders measuring 50 mm (2 in.) in diameter by 100 mm (4 in.) long. It was found that activation of hot pressing was realized by adding elements that met the following requirements:

- An interatomic distance of less than 2.8 Å
- A valency greater than 2
- Presence of transport mechanism to distribute the added element around the particles during heating

Where large quantities of the elements were added, no benefit was realized.

19.5.2 Hot Isostatic Pressing

Hot isostatic pressing has proven an interesting approach to the consolidation of beryllium powders because of the extended range of useful temperatures and pressures and the adaptability of the process to complex shapes. The low temperature of consolidation results in a fine-grain-sized material of nearly theoretical density, and the isotropic deformation produces an essentially random orientation in the consolidated beryllium.

Various commercial-grade beryllium powders and specialized powders have been consolidated by HIP at temperatures from 700 to 950 °C (1292 to 1742 °F) and pressures from 69 to 103 MPa (10 to 15 ksi) [Hodge et al. 1966]. Powders processed in this manner are loaded into a mild-steel container of the desired configuration, evacuated, and sealed. The assemblies are then inserted in cold-wall autoclaves with internal resistance-wound heaters and subjected to a high gas pressure at an elevated temperature.

The gas pressure acting from all directions on the powder mass forces the particles into intimate contact, and the elevated temperature promotes diffusion across the particle-to-particle interfaces. The temperature is selected to provide sufficient ductility to effect particle deformation, but such that grain growth and chemical interaction with the jacket material will not occur. Upon completion of the pressing, the container is removed by chemical etching or mechanical stripping.

The commercial beryllium powders NP-SO, S-200, and P-l2 have been successfully consolidated by HIP, as have Bureau of Mines beryllium flakes and several size ranges of plasma-spheroidized beryllium. Powders have been prepacked and preformed by vibration packing, hydrostatic pressing, explosive compaction, or plasma arc spraying. The exact parameters for HIP are determined in part by the particle geometry, type of preform, and relative hot strength. The particle shape establishes the geometry of the last pores to close in the powder body. With plasma-spheroidized particles, a regular geometric pattern of porosity is developed, and the last pores to close are located at interstitial points. This structure requires a higher pressure for complete densification than does a structure developed from irregularly shaped particles of smaller size. On this basis, it is expected that partially sintered bodies and powders containing high BeO contents would require higher pressures and temperatures for complete densification.

Commercial SP-200-C beryllium powders have been HIPed directly to sheet, with the result that improved tensile properties, compared with those of commercial hot pressed sheet, were obtained [Porembka et al. 1967]. Preforming of the powders was accomplished by isopressing in the mild-steel sheet jackets prior to evacuation and sealing. Bonding parameters of 1 h at 788 °C (1450 °F) and 69 MPa (10 ksi) produced fine grain structures in which the grains represented the initial powder particle sizes. The material was also characterized by a density close to theoretical, high strength, and an essentially random orientation. Ductility was found to be somewhat lower than that normally reported for commercial hot pressed block but was later substantially improved by low-order deformation in the form of cross rolling. It was also observed that bend ductility was markedly improved by cross rolling in a similar manner.

Hot isostatic pressing has been used as a means to fabricate complex hollow shapes for gyro and stabilized platform components [Hanes et al. 1964, Hanes and Gripshover 1966]. The advantage offered by this approach is that considerable savings in machining time and material can be made possible by fabricating these components to near-finished dimensions. In all cases, the powders were isopressed into the desired configuration as the initial step. Mandrel materials employed to provide hollow areas in the finished form were of porous copper.

Can design in HIP is more critical if the desired outcome is a near-net shape component. Computer models have been devised to assist in can design to be able to predict amounts of deformation of the canned powder from point to point in the part. It may be necessary to vary the wall thickness of the can in order to ensure that the local deformation is limited, so as to preserve desired part geometry.

A copper foil barrier was placed around the beryllium preform to prevent vapor transport from a sodium chloride pressure-transmitting medium to the beryllium. The preform, barrier, and pressure-transmitting medium were contained in a steel can for the HIP operation. After sealing and insertion into the autoclave, the assembly was first heated to 427 °C (800 °F), with only a light pressure. Pressure and temperature were then increased together until 648 °C (1200 °F) and 69 MPa (10 ksi) were reached, and heating was continued to 760 °C (1400 °F).

The assembly was held for 3 h at these conditions, after which the pressure was increased to 103 MPa (15 ksi) for an additional 2 h. On cooling, the autoclave was depressurized to 1.4 MPa (200 psi) in such a manner that the temperature of the assembly did not drop below 482 °C (900 °F). This procedure also ensured a slow cool to room temperature. Disassembly consisted of mechanically removing the steel can, dissolving the salt in a stream of tap water, and removing the copper barrier and mandrels by leaching.

Densities of the finished beryllium averaged 99.5% of theoretical. It was noted that some minor surface cracking was evident; however, the cracks were readily removed by light machining and pickling in a 10% sulfuric acid solution.

19.5.3 Forging

Forgings made directly from beryllium powder have ranged from 2 to 545 kg (5 to 1200 lb) with diameters of 8 to 152 cm (3 to 60 in.) [Orrell 1963a,b]. In this process, a −200-mesh beryllium powder, supplied according to close specifications, is vibration packed into a thin-gage steel can. Packed densities range from 50 to 55% of theoretical, depending on the particle-size distribution of the powder.

After the loading ports are sealed, the cans are handled in an upright position throughout the remaining operations, which include outgassing at 540 °C (1000 °F), final sealing, and preheating at 980 °C (1800 °F). Partial sintering occurs during the preheat, and care must be taken to avoid any cracks in the structure, because these are difficult to heal during forging. The preform is then forged in dies to the desired shape, with a ram speed of approximately 76 cm (30 in.) per minute. It has been generally observed that unit pressures of 172 MPa (25,000 psi) or greater are required to produce full-density parts. After air cooling, the can is removed from the consolidated beryllium by pickling, machining, or mechanical stripping.

A similar procedure, without the use of dies, has been employed to produce hot-upset beryllium sheet [Yans 1959]. In this operation, beryllium powder contained in a steel can is upset at 1010 to 1065 °C (1850 to 1950 °F) to form a flat of consolidated beryllium. The upset ratio is usually 6 to 1 or greater, and the edges of the can are not restricted. The resulting material is fully dense and represents a favorable orientation for ductility in all three directions, since the process simulates random rolling. Hot-upset beryllium has been cross rolled to produce sheet material of larger sizes; however, this degrades the favorable forged properties. The limitation in press capacity to produce larger parts has been a major factor in restricting the further development of hot-upset beryllium.

19.5.4 Extrusion

Although extrusions can be made directly from powder, in commercial practice it is preferable to extrude hot pressed or ingot forms of beryllium [Siergiej 1964]. Hot pressed and powder billets of CR-grade beryllium have been compared and the differences in behavior noted [Lidman and Moyer 1966]. All powder billets were prepared by vibration packing the powders directly into steel cans. With extrusions conducted at 790 to 1065 °C (1454 to 1949 °F), it was found that higher breakthrough pressures were required for the powder billets, apparently due to the powder consolidation prior to entry into the die. Running pressures were approximately the same for both types of billets. Evaluation of the extruded materials showed that the average density of the powder extrusions was slightly lower. The powder billets also exhibited a finer grain size, which resulted in their excellent mechanical properties.

With more recent extrusion developments involving the filled-billet technique for fabricating complex shapes, it is apparent that the use of soli-beryllium components will permit greater dimensional control.

19.5.5 Plasma Spraying

Densification of beryllium powders into complex shapes has been accomplished by plasma spraying [Headman et al. 1964]. Spraying of a −200- plus 400-mesh beryllium powder was conducted in a dry box with a Gianinini Plasmadyne model SF-100 gun. Parameters found to be most successful were a power setting of 500 A and 28 V, an arc gas flow rate of 26 L/min (55 ft^3/h), a powder feed rate of 0.2 g/s (1.75 lb/h), and a work distance of 2.5 to 290 cm (1 to 114 in.). Powder sprayed in this manner adheres but does not bond to the mandrel and results in a beryllium structure of approximately 86% of theoretical density. Sintering at 1120 to 1150 °C (2050 to 2100 °F) in hydrogen or vacuum produced final densities up to 97%. With all fabricated shapes, which included plates, cylinders, and domes, a higher oxygen content, compared to

Table 19.9 Minimum room-temperature tensile properties of vacuum hot pressed beryllium powders

Type	Maximum BeO, wt%	Ultimate tensile strength		Yield strength		Elongation, %
		MPa	ksi	MPa	ksi	
S-100 HP-12 GB-1	1.2	241	35	186	27	1
S-200 HP-20 GB-2	2.0	276	40	207	30	1
S-300 HP-30	3.0	276	40	207	30	1
I-400 HPI-40	4.25	414–552	60–80	345–448	50–65	0–0.5
CR	0.9	241	35	186	27	1
HPN-8	0.8	241	35	172	25	1

Source: Brush Wellman

other processes, was observed. Final consolidation of the beryllium was done by HIP, which resulted in significantly higher tensile properties, probably because of higher densities and finer grain sizes.

19.6 Properties of Powder Metallurgy Beryllium

Both the input material and the method of processing influence the properties of powder metallurgy beryllium. As noted previously, powder factors such as source, purity, particle-size distribution, and particle shape determine the behavior of the powder during compaction and densification. Frequently, conditions for a powder metallurgy process must be altered to accommodate these differences. This need has been particularly evident in processing high-purity beryllium powder or fine-particle-sized beryllium powders. The method of final consolidation and the parameters of temperature, time, atmosphere, and direction of deformation have a direct bearing on the density, grain size, pore characteristics, and orientation of the final structure. Each of these factors affects the mechanical and physical properties of beryllium. Since vacuum hot pressing is the most widely used commercial powder metallurgy method for beryllium, the input material and process factors are best defined for this process. With other processing methods, except for HIP, these factors are not well defined, due to either the limited or proprietary nature of the work.

19.6.1 Vacuum Hot Pressed

The properties of hot pressed block as fabricated from the various grades of commercial powder indicate the effects of the input powder. Equivalent grades of powder are listed in Table 19.9 along with nominal values for the ultimate and yield strengths and elongation. As the average particle size is decreased, with a corresponding increase in BeO content, the strength is increased and elongation is decreased. The I-400 and HPI-40 grades, which are mainly used for instrument applications, represent the finest grain size (~10 μm) and highest BeO content of the group.

The CR and HPN-8 grades generally contain fewer overall impurities and less BeO, which accounts for their lower strength values. Since all grades of powder are attritioned from castings, the general particle shape in each case would be similar, although the degree of cold work in each powder material may vary.

Experimental powders would be expected to produce tensile properties distinctly different from those listed for commercial block materials. A study of closely controlled powder-size fractions from three different source materials has been conducted [Beaver and Lympany 1965]. The results of this work, shown in Table 19.10, demonstrate the effects of both particle size and purity. The smaller particle sizes resulted in generally higher strengths and lower elongations, while increased purity tended to produce lower strengths and higher elongations. Spheroidization of these size fractions yielded pressings in which both the strength and elongations were lowered. In all pressings, the grain sizes measured were a direct function of the powder particle sizes employed. More closely controlled particle-size fractions exhibited a more pronounced effect on the mechanical properties, as shown in Table 19.11. In this case a nearly direct relationship between particle size

Table 19.10 Chemical composition of commercial grades of vacuum hot pressed beryllium (by weight)

Chemical composition	S-65C	S200E	S-200F	I-70B	I-220C	I-400A	I-400
Be, min %	99.0	98.0	98.5	99.0	98.0	94.0	94.0
BeO, max %	1.0	2.0	1.5	0.7	2.2	4.25(a)	4.25(a)
Al, max ppm	600	1600	1000	700	1000	1600	1600
C, max ppm	1000	1500	1500	700	1500	2500	2500
Fe, max ppm	800	1800	1300	1000	1500	2500	2500
Mg, max ppm	600	800	800	700	800	800	800
Si, max ppm	600	800	600	700	800	800	800
Other, each max ppm	400	400	400	400	400	1000	1000

(a) Minimum specified in this instance. Source: Beaver and Lympany 1965

Table 19.11 Tensile properties of commercial grades of vacuum hot pressed beryllium

Property	S-65C	S200E	S-200F	I-70B	I-220C	I-400A	I-400
Ultimate tensile strength, MPa min	290	276	324	241	379	50.0	379
Tensile yield strength, 0.2 % offset, MPa min	207	207	241	172	276	. . .	276
Elongation, % min	3	1.0	2	2	2	. . .	2
Microyield, MPa	. . .	. . .	27 typical	12.4 typical	34 min	5.0	34 min
Standard sizes(a), cm	81 diam × 76 long	. . .	81 diam × 114 long	81 diam × 76 long	81 diam × 76 long	. . .	81 diam × 76 long

(a) Pressing sizes of billets may range from 18 to 186 cm diam and 15 to 168 cm in length, depending on grade and chemistry. Source: Beaver and Lympany 1965

and tensile properties, including the precision elastic limit, is evident. It should be noted that at the extremely fine particle sizes, the BeO and other contaminant contents become very high and may tend to override the effects of fine grain size in the finished pressing.

The hot pressing parameters of pressure, temperature, and time have been discussed previously in terms of hot pressability. These factors influence properties primarily through the density and grain size achieved in the final structure. In commercial practice, these conditions have been standardized, and very few data on the effect of variation in pressing parameters on mechanical properties are available.

As part of a beryllium sheet-rolling program, the influence of several powder blends of virgin and recycled material on the properties in each quadrant of the hot pressings was evaluated [Hornak et al. 1964]. Variations of up to 35 MPa (5000 psi) in ultimate strength and 21 MPa (3000 psi) in yield strength were observed as a result of material differences. For each individual material, these values generally fell within 6.9 MPa (1000 psi). Elongation values were well within 1% for differences in material and pressing quadrant. These results indicate that the input material is a more dominant factor than the process variables, as experienced in a standardized practice. Sampling of concentric rings of material in the same pressings yielded differences approximating those observed as a result of input material. This effect is primarily due to heating (i.e., the time at temperature for the different portions of material).

19.6.2 Hot Isostatic Pressing

The influence of input powder material has been apparent in the properties determined for HIPed beryllium (Tables 19.12 and 19.13). Significant differences were noted in the tensile properties of sheets fabricated from QMV- and CR-grade −200-mesh powders pressed for 1 h at 790 °C (1450 °F) and 69 MPa (10,000 psi) [Porembka et al. 1965]. Full density was achieved with both types of powder, and a near-random orientation was obtained. The CR-grade powder sheet, which represented a high purity level, exhibited ultimate and yield strengths of 386 and 338 MPa (56 and 49 ksi), respectively, as compared with corresponding values of 414 and 391 MPa (60 and 56.7 ksi) for the QMV powder sheet.

Elongation values differed only slightly and fell within the range of 0.5 to 1.0% normally experienced for HIPed beryllium. It has generally been found that HIP produces higher strengths

Table 19.12 Comparison of tensile properties-grain size relationship of beryllium powders from different sources

Powder type	Powder size, μm	Grain size, μm	Tensile strength		Yield strength		Elongation, %	Reduction in area %
			MPa	ksi	MPa	ksi		
Thermally reduced	−20 + 5	11.1	526	76.3	333	48.3	4.46	4.37
	Spheroidized −20 + 5	12.6	384	55.7	236	34.3	1.63	1.56
	−15 +1	8.7	579	84.0	388	56.3	4.67	4.62
Electrorefined	−5 +1	6.3	645	93.6	488	70.8	2.50	2.64
	−20 + 5	12.0	494	71.6	269	39.0	3.99	4.24
	Spheroidized −20 + 5	16.5	390	56.5	212	30.8	3.26	3.68
	−15 +1	9.6	529	76.7	278	40.3	6.04	6.61
Zone refined	−5 +1	6.0	639	92.7	391	56.7	3.76	4.46
	−20 + 5	11.4	476	69.0	252	36.6	5.55	5.69

Note: Longitudinal tensile properties (direction of pressing) lower but with same order; maximum values were used to show spread. This did not apply to pressings of spheroidized powder that had uniform strength properties in all directions at room and elevated temperatures (425 and 565 °C, or 800 and 1050 °F) but had variable plasticity parameters. Source: Porembka et al. 1965

Table 19.13 Room-temperature tensile properties of various fine-particle-sized batches of hot pressed beryllium

Nominal powder type, μm	Ultimate strength		Yield strength		Elongation, %	Reduction in area, %	Precision elastic limit	
	MPa	ksi	MPa	ksi			MPa	ksi
−5	571	82.8	457	66.3	2.40	1.76	91	13.2
−5 + 1	539	78.1	452	65.6	2.77	2.86	70	10.2
−10	548	79.4	401	58.2	...	...	72	10.5
−10 + 1	544.7	79.0	387	56.1	3.11	3.37	62	9.0
−15 + 1	545	79.1	380	55.1	3.45	3.61	50	7.3
−20 + 1	510	74.0	359	52.1	2.84	3.05	33	4.8

Source: Porembka et al. 1965

Table 19.14 Effect of densification temperature on mechanical properties of NP-50A (−200-mesh) beryllium powder consolidated by hot isostatic pressing

Densification temperature(a)	Tension properties							Compression properties				Bend properties		As-pressed density, g/cm³
	0.2% yield stress		Ultimate strength		Strain of fracture, %	Modulus of elasticity		0.2% yield stress		Modulus of elasticity		Modulus of rupture		
	MPa	ksi	MPa	ksi		GPa	10^6 psi	MPa	ksi	GPa	10^6 psi	MPa	ksi	
705 °C (1300 °F)	...	...	311	45.1	...	267	38.7	407	59.0	276	40.0	556	80.6	1.85
		...	375	54.4	0.27	288	41.7	393	57.0		...	648	94.0	1.86
790 °C (1450 °F)		...	339	49.1	0.26		...	379	55.0	248	36.0	758	110.0	1.86
		...	344	49.9	0.27		...		...		...	772	112.0	1.85
870 °C (1600 °F)	341	49.5	372	54.0	0.62		...	376	54.5	248	36.0	674	97.7	1.87
		...	344	49.9	0.31		...	352	51.0	241	35.0	750	108.8	1.85
		...	329	47.7	0.29		...	355	51.5	248	36.0		...	1.85
		...	325	47.2	0.25		...	365	53.0	255	37.0	740	107.3	1.86
	172(b)	25.0(b)	241	35.0(b)	1.0(b)									

(a) Specimens densified 1 h at 69 MPa (10,000 psi) and specified temperature. (b) Minimum specification for N-50 block. Source: Lympany et al. 1966

and lower elongations than does vacuum hot pressing, an effect that is attributed to the lower pressing temperatures and resultant finer grain sizes.

The effects of HIP temperature on tension, compression, and bend properties have been compared for cylinders made from a type NP-50A (−200-mesh) powder [Theodore et al. 1966]. These results are given in Table 19.14 and indicate that high-density material was obtained over the temperature range from 705 to 870 °C (1300 to 1600 °F). The most noticeable change in properties resulted in the compressive yield strength, which decreased with increasing

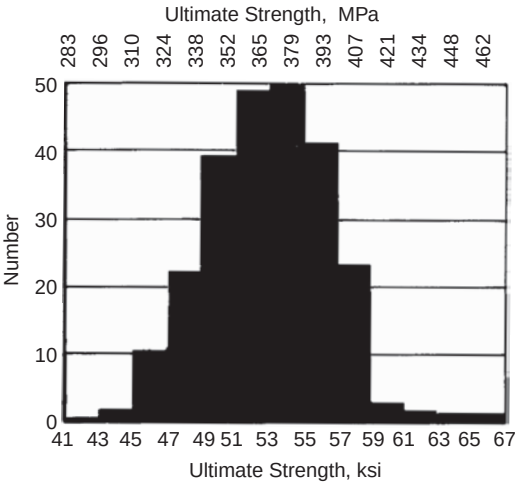

Fig. 19.13 Frequency distribution of ultimate tensile strengths for 241 forged beryllium powder parts. Source: Orrell 1963a,b

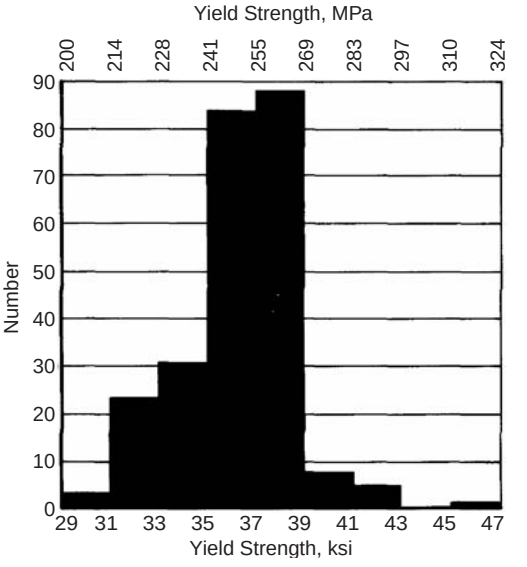

Fig. 19.14 Frequency distribution of yield strengths for 241 forged beryllium powder parts. Source: Orrell 1963a,b

pressing temperature. A scatter in values was obtained for ultimate tensile strength and modulus of elasticity; however, the strength values show some relationship to minor variations in final density. In all cases, the tensile strength values were higher than those given as minimum values for commercial N-50 block. A comparison of strain at fracture shows that lower values were obtained with the HIPed material.

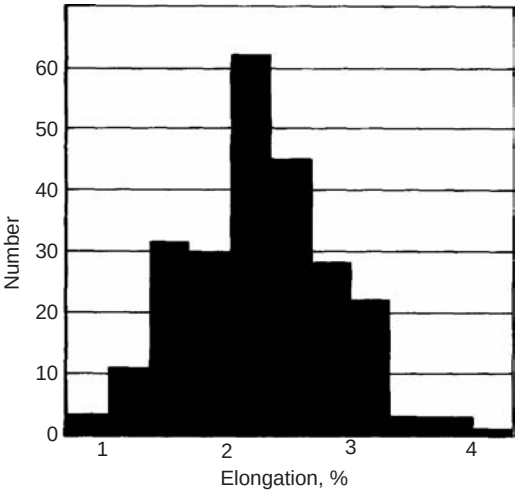

Fig. 19.15 Frequency distribution of percent elongation for 241 forged beryllium powder parts. Source: Orrell 1963a,b

19.6.3 Forged Powder

The mechanical properties of forged beryllium powder are usually at a level between those of hot pressed block and forged block beryllium. The property values will vary according to the part being forged and the degree of work required to complete the required shape. It is apparent that the orientation induced by this working of material will heavily influence the directional mechanical properties. A statistical summary of properties obtained for 241 parts of the same configuration, but with some variations in forging practice during the production run, have been reported [Orrell 1963a,b]. All tests were taken from a location in the part that had been found to give the lowest property values. From the distributions given in Fig. 19.13 to 19.15, it appears that the ultimate strength and elongation are affected more by process variations than is the yield strength. A similar study was made for 516 parts of another configuration, which resulted in wider distributions of values for all tensile properties.

19.6.4 Plasma-Sprayed Powder

Forms plasma sprayed directly from beryllium powders are of low density, and consequently, their strengths are low [Headman et al. 1964]. In order to achieve acceptable strength levels, it is necessary to further densify the material. Both sintering and HIP have been examined in this respect, with the results as summa-

Table 19.15 Properties of beryllium powder (1.55% BeO) preformed by plasma arc spraying

Condition	Density, percent of theoretical	Tensile properties		
		Ultimate strength		Strain of fracture, %
		MPa	ksi	
As plasma sprayed	86	79	11.5	0
As sprayed and sintered at 1150 °C (2100 °F)	97	241	35.0	0.3
Sprayed, sintered, and gas-pressure compacted 1 h at 760 °C (1400 °F) and 69 MPa (10,000 psi)	98.5	406	58.9(a)	0.25

(a) Average of ten tests. Source: Hodge et al. 1966

rized in Table 19.15 [Hodge et al. 1966]. Substantial improvement in ultimate strength was attained through further densification by the two methods. Hot isostatic pressing resulted in a much higher strength, although the strains at fracture were nearly the same. This difference in strength is probably due to the density difference and a grain-size effect. The high sintering temperature employed would be expected to produce a large grain size, which would also be expected to yield a lower-strength material.

19.6.5 Sintered Powder

The property determinations for sintered beryllium have been generally associated with the isopressed or pressureless-sintered forms of the material. The tensile properties of an isopressed −20-mesh powder as a function of sintering conditions and the resultant porosity have been reported [Greenspan 1964]. The sintering temperatures used in this work were somewhat low; consequently, little densification was experienced over the isopressed material. The data listed in Table 19.16 show that the ultimate strength is markedly reduced by porosity. In most cases where the yield strengths were determined, they were found to be nearly equal to the ultimate strength. This effect may be related to the coarse particle size and low sintering temperature.

Isopressed material and sintered material have been compared with equivalent vacuum hot pressed block material for use as stable elements.

Engineering properties of the two forms of beryllium are given in Table 19.17. The isopressed beryllium exhibits slightly lower strengths and elongations, although they are well within the requirements for the intended application. A considerable improvement in the mean difference in thermal expansion between orthogonal directions was realized as a result of isopressing and sintering. A value of $0.075 \times 10^{-6}/°F$ was determined for this material, compared with $0.200 \times 10^{-6}/°F$ for the equivalent hot pressed block.

The effect of pressureless-sintering variables on the ultimate strength of beryllium has been investigated [Reeves and Keeley 1961]. Both time and temperature were varied during sintering of a −200-mesh powder to produce the results plotted in Fig. 19.16. At sintering temperatures of 1000 °C (1832 °F), time has little effect on strength. At higher temperatures, the first 5 h of sintering time have the greatest effect on

Table 19.16 Mechanical properties of isopressed and sintered beryllium compacts

Porosity		Sintering			Modulus of elasticity		Tensile properties				
		Temperature						Yield strength (0.2% offset)		Ultimate strength	
Pressed, %	Sintered, %	°C	°F	Time, h	GPa	10^6 psi	Elongation, %	MPa	ksi	MPa	ksi
23	24	1040	1900	7		...			...	66	9.6
19.9	19.6	1040	1900	8		(a)	...		...		...
18.5	16.8	1040	1900	6		...	...		...	101	14.6
15.2	13	845	1550	6		...	...		...		...
11.4	12.2	1065	1950	8		...	...		...	192	27.8
12.3	12	980	1800	6		...	...		...	181	26.3
10.3	9.5	1065	1950	8		...	...		...	197	28.6
8.2	8.2	1040	1900	6		...	...		...	212	30.7
8.4	8.7	1065	1950	6		...	...		...	215	31.2
2.6	2.7(b)	845	1550	8	234	34	0.6	281	40.8	287	41.6
2.3	2.2(b)	1040	1900	9	241	35	0.3	272	39.5	276	40.0
1.8	1.6(b)	1040	1900	12	241	35	0.3	269	39	272	39.5
1.0	2.7(b)	1040	1900	12	241	35	0.5	276	40.1	296	43
2.5	2.7(b)	1040	1900	12	241	35	0.36	269	39	280	40.6

(a) Not determined. (b) Annealed and recompacted. Source: Greenspan 1964

Table 19.17 Some engineering properties of isopressed and hot pressed beryllium powders

	Hot pressed(a)	Isopressed(a)
Immersion density range, g/cm^3	1.84–1.86	1.78–1.86
Average stress, MPa (ksi), to cause a plastic strain of:		
1×10^{-6}	14 (2.0)	14 (2.0)
5×10^{-6}	34 (4.9)	26 (3.7)
20×10^{-6}	65 (9.4)	49 (7.1)
Minimum yield strength at 0.2% offset, MPa (ksi)	207 (30.0)	172 (25.0)
Minimum tensile strength, MPa (ksi)	276 (40.0)	207 (30.0)
Minimum elongation, %	1.00	0.75

(a) Both powders have the same chemical analysis (Comp. A ABO 170-002) and radiographic quality (Type 1 ABO 170-002). Source: Greenspan 1964

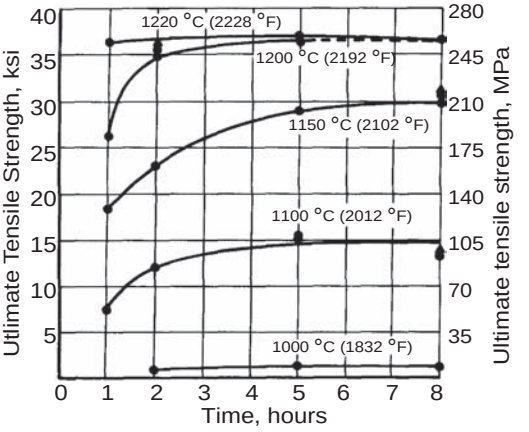

Fig. 19.16 Effects of time and temperature during pressureless sintering on the ultimate tensile strengths of −200-mesh beryllium powder (powder lot Y.9833, 1B). Source: Reeves and Keeley 1961

strength and parallel a similar effect on sintered density. These results demonstrate the importance of using a high sintering temperature in the pressureless-sintering process, although the maximum strength obtained is still slightly below that for hot pressed block.

Sintered beryllium slip castings have been evaluated by Brush. The results are given in Table 19.18; the low strengths and ductilities obtained were related to the partial densities (~1.75 g/cm^3) obtained by sintering for 5 h at 1230 to 1235 °C (2246 to 2254 °F) in vacuum. Little difference in properties as a result of the two binder/vehicle systems used in slip casting was observed.

Forging, extruding, rolling, or drawing of hot pressed block produces wrought forms of beryllium and hence widens the field of application of powder metallurgy beryllium. As a result of these deformation processes, high strength levels and improved directional ductility are obtained that can be used in a structural application. Some recent production applications of wrought hot pressed beryllium are listed in Table 19.19 to demonstrate the extent of its uses [King 1966]. Wrought hot pressed beryllium has also been used experimentally in compressor blades and disks and in the fabrication of box-beam structures. With the development of fine-grained, high-strength types of beryllium, additional structural applications are being examined.

Applications of powder metallurgy forms of beryllium other than wrought hot pressed block have been limited, for the most part, to development studies and test programs. Powder forging, however, has been used in production operations that have involved classified components. Hot isostatic pressing has been employed to produce beryllium gimbals by a procedure developed during the course of a test program on

Table 19.18 Mechanical properties of vacuum-sintered beryllium slip castings

Input beryllium powder(a)	Binder/ vehicle system(b)	Metal loading, wt%	Vacuum sintered density(c), g/cm^3	Ultimate tensile strength		Yield strength		Modulus of elasticity		Elongation, %	Average grain size, μm	Observed grain size range, μm	
				MPa	ksi	MPa	ksi	GPa	10^6 psi			Min	Max
Type A	PVP/MEK	44.8	1.76	164	23.8	152	22.0	275(d)	39.8(d)	0.50	33	13	65
Type B	PVP/MEK	46.1	1.74	182	26.4	161	23.3	264(d)	38.3(d)	0.66	37	10	65
Type C	PVP/MEK	39.7	1.74	...	...	...	...	293	42.5	...	...	...	...
Type A	Collodion/ MEK	43.4	1.77	174	25.3	160	23.2	275(d)	39.8(d)	0.30	30	10	65
Type D	Collodion/ MEK	42.2	1.75	152	22.1	142	20.6	323	46.8	0.50	30	10	65

(a) Type A designates 200 QMV powder with less than 1 μm fines removed. Type B designates blend of 50 wt% −200 + 325 particles, + 25 wt% 200 QMV, + 25 wt% I-400 powders. Type C designates blend of 95 wt% 200 QMV, 4 wt% −200 + 325, + 1 wt% I-400 (<1 μm fines removed) powders. Type D designates blend of 90 wt% 200 QMV + 10 wt% −200 + 325 mesh powders. (b) PVP, polyvinylpyrrolidone; MEK, methyl ethyl ketone. (c) 5 h at 1230–1235 °C (2246–2254 °F) vacuum. (d) Dynamic modulus of elasticity values. Source: Bielowski et al. 1963

Table 19.19 Some production applications of wrought hot pressed beryllium

Component identification	Type of material	Special characteristics
Solar cell boards—Orbiting Geophysical Observatory satellite	Sheet, rod	Beryllium studs brazed to sheet
Gemini shingles	Rolled, plate	Formed, machined, and chemical milled
Minuteman spacer	Ring-rolled block, sheet	Ring-rolled sheet, formed and brazed longerons, chemical milled, riveted
Agena D skin panels	Sheet	Formed, chemical milled, drilled, attached with screws
Telstar antennae	Wire	Hot-formed helical coil brazed to beryllium fittings
Gimbals-Redeye	Forged	Triaxial forgings
Control rods	Extruded	Extruded tubes, brazed end fittings
Mirrors	Plate, block	Brazed sandwich assembly
Scanning head	Extruded	Extruded rod brazed to hot pressed rings

Source: King 1966

this subject. It is expected that further development work with the other powder metallurgy processes will bring about their adaptation to production.

REFERENCES

Anderson, I.E., and Foley, J.C., 2001. Determining the Role of Surfaces and Interfaces in the Powder Metalllurgy Processing of Aluminum Alloy Powders, *Surf. Interface Anal.*, Vol 31 (No. 7), p 599–608

Barrett, T.R., Ellis, G.C., and Knight, R.A., 1958a. "Pressureless Sintered Beryllium Powder," Paper 320, Proceedings of the Second United Nations Conference on the Peaceful Uses of Atomic Energy (Geneva, Switzerland)

Barrett, T.R., Ellis, G.C., and Knight, R.A., 1958b. The Pressureless Sintering of Loose Beryllium Powder, *Powder Metall.*, Vol 1/2, p 122–132

Beaver, W.W., 1955b. *The Metal Beryllium*, American Society for Metals

Beaver, W.W., 1966. A Review of Progress in Beryllium Technology and Applications Since the 1961 International Conference on Beryllium Technology, *Beryllium Technology*, Vol 2, Gordon and Breach, NY, p 879–927

Beaver, W.W., and Lympany, B.B., 1965. Influence of Grain Size-Purity Relationship on the Ability to Fabricate Beryllium and the Resulting Mechanical Properties, *International Conference on the Metallurgy of Beryllium* (Grenoble, France), p 489–506

Bielowski, C.A., Theodore, J.G., and Beaver, W.W., 1963. "Development of a Slip Casting Process for Manufacturing Spherically Shaped Beryllium Gyro Platform Gimbals," NASA Technical Report 334-241

Billman, G.C., 1965. "Minuteman Producibility Study No. 2-A—Beryllium Isopressing for Stable Elements," CS-1050/32, Autonetics

Bufferd, A.S., Widmer, R., and Grand, N., 1964. "Fine Beryllium Powder Made by Attritioning," ASD-TDR-62-509, Vol 3, Beryllium Research and Development Program

Bunshah, R.F., and Juntz, R.S., 1963. "Isostatic Compaction of Particulate Pure Metals without Contamination," UCRL-6932, University of California, Lawrence Livermore National Laboratory, Livermore, CA

Butcher, J.W., 1965. Activated Sintering of Beryllium, *Conference on the Metallurgy of Beryllium* (Grenoble, France), p 555–564

Butcher, J.W., and Beasley, D., 1964. The Influence of Pressure, Temperature, and Time on the Hot Pressing of Commercial Beryllium Powder, *Powder Metall.*, Vol 7 (No. 14), p 313–326

Denny, J.P., and Moyer, K.H., 1962. "Hot Pressing of Beryllium," New York University Conference on Beryllium Metallurgy

Eyre, P.B., Williamson, L.J., and Williams, L.R., 1966. Development of Methods of Producing Beryllium Tubes for Nuclear Fuel Element Cans, *Beryllium Technology*, Vol 2, Gordon and Breach, NY, p 769–806

Fisher, G.W., et al., 1965. "Complex Shapes by Slip Casting—Phase I Progress Report," IR-8-12 (IV), General Electric Company

Foley, J.C., 2007. personal communication

Gale, C.O., Griffiths, V., Habashi, F., and Hanson, G.T., 1965. "The Preparation of Ultra-Fine Beryllium Powder by the Amalgam Process," Report on NASA Contract NASW 1099, General Astrometals Corporation

Greenspan, J., 1964. High Pressure Isostatic and Pressureless Sintering of Some Metal Powder Compacts, *Metals for the Space Age, Fifth Plansee Seminar* (Reute, Austria), p 163–176.

Hanes, H.D. and Gripshover, P.J., 1966. "Fabrication of Beryllium Stabilized Platform Components by Gas-Pressure Bonding,"

Final report to NASA Marshall Space Flight Center

Hanes, H.D., Gripshover, P.J., and Hodge, E.S., 1964. "Gas Pressure Bonding of Beryllium Gyro and Stabilized Platform Components," Final report to George C. Marshall Space Flight Center, Contract NAS8-11559

Hansen, M., and Anderko, K., 1958. Constitution of Binary Alloys, McGraw-Hill, New York, NY

Hausner, H.H., 1965d. "Powder Metallurgy of Beryllium," *Beryllium: Its Metallurgy and Properties*, University of California Press, Berkeley, CA, p 33–54

Hausner, H.H., and Pinto, N.P., 1949. "The Powder Metallurgy of Beryllium," U.S. Atomic Energy Commission Report AECD-2869

Hayes, A.F., and Yoblin, J.A., 1961, "New Concepts for Fabricating Beryllium Through Advanced Forging and Powder Metallurgy Techniques," Paper 53, presented at the Institute of Metals Conference on the Metallurgy of Beryllium (London)

Headman, M.L., Roseberry, T.J., and Parkinson, F.L., 1964. "Process Development and Evaluation of Plasma Sprayed Beryllium," Report N-649-229, Western Gear Corp., Lynwood, CA

Hodge, E.S., Gripshover, P.E., and Hanes, H.D., 1966. Properties of Gas-Pressure-Consolidated Beryllium Powder, *Beryllium Technology*, Vol 2, Gordon and Breach, p 703–728

Hornak, M.B., Grala, E.M., O'Rourke, R.G., Marsh, G.L., and Busch, L.S., 1964. "Final Report on Rolling Improved Beryllium Sheet," ML-TDR-64-193

Jacobson, M., Cooper, A.R., and Nagy, J., 1964. "Explosivity of Metal Powders," Report 6516, U.S. Government Publication, Bureau of Mines, U.S. Department of the Interior, Washington, D.C.

Kaufmann, A.R., and Muller, W.C., 1966. Fine Grain Size in Beryllium by Splatcooling, *Beryllium Technology*, Vol 1, Gordon and Breach, NY, p 629–646

King, B., 1966. A Review of Advances on Beryllium Applications Since the 1961 International Conference on the Metallurgy of Beryllium, *Beryllium Technology*, Vol 2, Gordon and Breach, NY, p 963–990

Lidman, W.G., and Moyer, K.H., 1966. Extrusion of Electrolytic A Grade CR Beryllium, *Beryllium Technology*, Vol 2, Gordon and Breach, NY, p 825–839

Lohrer, R.J., 1964. "Vibratory Compacting of I-400 and SP-200-C Beryllium Powders," Brush Beryllium Corp. Memo M-64-230

Lympany, B.B., Theodore, J.G., and Beaver, W.W., 1963. Factors Controlling the Sintering Characteristics of Beryllium Powder, *The Metallurgy of Beryllium*, Institute of Metals Monograph 28, Chapman and Hall Ltd., London, p 708–723

Lympany, B.B., Theodore, J.G., and Beaver, W.W., 1966. "Micro-Alloying Beryllium for Improved Sintering Characteristics and Mechanical Properties," International Conference on the Metallurgy of Beryllium (Grenoble, France)

Orrell, N.G., 1963a. Beryllium Powder Forging, "Beryllium—Its Properties and Applications," short course, University of California, Berkeley, CA

Orrell, N.G., 1963b. "The Fabrication of Beryllium Powder Forging," Report RD 63-l05, Wyman Gordon Co., Worcester, MA

Pinto, N.P., 1979a. Communication and Consolidation, *Beryllium Science and Technology*, Vol 2, D.R. Floyd and J.N. Lowe, Ed., Plenum Press, NY, p 13–29

Porembka, S.W., 1963. Explosive Compacting, *Ceram. Age*, Dec 1963, p 69–71

Porembka, S.W., Carlson, R.J., and Linse, V.D., 1965. "Fabrication of Beryllium Sheet by Gas-Pressure Bonding," Contract AF 33(615)-1683, Vol 1, AFML-TR-65-83

Porembka, S.W., Hanes, H.D., and Gripshover, P.J., 1967. "Powder Metallurgy of Beryllium," Report DMIC-239, Defense Metals Information Center, Columbus, OH

Raymond, P.L., 1964. "Preparation of Ultra-Fine Beryllium Powder," ASD-TDR-62-509, Vol 3, Beryllium Research and Development Program, Nuclear Metals Inc., West Concord, MA

Reeves, G.L., and Keeley, R.L., 1961. "The Pressureless Sintering of Beryllium Powder to Billets for Hot Extrusion," Paper 11, Institute of Metals Conference on the Metallurgy of Beryllium (London)

Siergiej, J.M., 1965. "Extrusion of Beryllium Structural Shapes:" Beryllium: Its Metallurgy and Properties, University of California Press, Berkeley and Los Angeles, CA, pp. 86–101.

Siergiej, J.M., 1964. "Extrusion of Beryllium Structural Shapes," NMI-TN-53, Nuclear Metals Inc.

Theodore, E.G., Lympany, B.B., and Beaver, W.W., 1966. "Research on Effects of High Purity in Wrought Polycrystalline Sheet," Progress Report 2, BBC-TR-403-251

Theodore, E.G., Lympany, B.B., and Beaver, W.W., 1967. "Research on Effects of High Purity in Wrought Polycrystalline Beryllium Sheet," Progress Report 5, BBC-TR-424-251

Wikle, K.G., and Potter, V.C., 1961. Beryllium Processing by Powder Metallurgy, *J. Met.*, Vol 13 (No. 8), p 537–544

Yans, F.M., 1959. "Third Dimensional Ductility and Crack Propagation in Beryllium Sheet," NMI-1212, Nuclear Metals Inc., Concord, MA

SELECTED REFERENCES

- Butcher, J.W., and Lowe, J.N., 1966. Activated Sintering in Beryllium Powders by Selective Addition of Trace Elements, *Beryllium Technology*, Vol 1, Gordon and Breach, NY, p 501–522
- Greenspan, J., 1968. Some Effects of Powder Particle Size on the Physical Behavior of Press Forged Beryllium, *Second European Symposium on Powder Metallurgy* (Stuttgart, Germany), Vol 1A, Section 2.7, p 1–19
- Hausner, H.H., and Pinto, N.P., 1951. The Powder Metallurgy of Beryllium, *Trans. ASM*, Vol 43, p 1052–1071
- O'Rourke, R.G., and Beaver, W.W., 1969. "A Study to Characterize a Fully Forgeable Grade of Fine-Grained High Strength Beryllium Powder," BBC-TR-436-248 or AFMLTR-69-61, Brush Beryllium Co., Cleveland, OH
- Paquin, R.A., 1985. Hot Isostatic Pressed Beryllium for Large Optics, *SPIE Proceedings*, Vol 571, G.M. Sanger, Ed., p 259–266
- Pinto, N.P., 1954. The Warm Pressing of Beryllium Powder, *Trans. Am. Inst. Miner. Metall. Eng.*, Vol 200 (No. 5), p 629–633
- Pinto, N.P., Denny, J.P., and London, G.J., 1974. Isostatic Pressing of Beryllium Powder, *Metall. Soc. AIME*, TMS A74-50, p 489–511
- Seybolt, A.U., Frandsen, J.P., and Linsmayer, R.M., 1950. Hot Pressing Beryllium Powder, *Steel*, Vol 126, p 71–74
- Turner, G.I., and Lane, R.A., 1977. "The Effects of Powder Particle Size on the Mechanical Properties of Hot Pressed P1 Beryllium," Met. Soc. Conf. on Beryllium
- Webster, D., and Crooks, D.D., 1975a. Factors Influencing the Creep Strength of Hot Pressed Beryllium, *Metall. Trans. A*, Vol 6 (No. 11), p 2049–2053
- Williams, J., 1956. The Powder Metallurgy of Beryllium, Chapter 3.2, *Metallurgy and Fuels*, H.M. Finniston and J.P. Howe, Ed., Pergamon Press, London

Beryllium Chemistry and Processing, p 295-337
By Kenneth A. Walsh
Edited by Edgar E. Vidal, Alfred Goldberg,
Edward N.C. Dalder, David L. Olson, and Brajendra Mishra

CHAPTER 20

Metalworking

Alfred Goldberg, Lawrence Livermore National Laboratory
Dennis Floyd, Science Applications International Corporation
David L. Olson, Colorado School of Mines

THIS CHAPTER COVERS various metalworking methods used to manufacture a beryllium product, including rolling, forming, forging, extrusion, wire drawing, spinning, and near-net shape forming. The method normally used for manufacturing products from conventional metals—fabrication of products directly from ingot-cast material—is unsuitable for beryllium products. Beryllium is a highly reactive metal with a high melting point, making it susceptible to react with mold-wall materials, forming beryllium compounds (such as BeO) that become trapped in the solidified metal. In addition, the as-cast grain size is excessively large, being 50 to 100 μm in diameter, while grain sizes of 15 μm or less are required to meet acceptable strength and ductility requirements [Marder et al. 1990, Haws 2000]. Attempts at refining the as-cast-grain size have been unsuccessful. Because of the large grain size and limited slip systems, the casting will invariably crack during a hot working step, which is an important step in the microstructural-refining process [Haws 2000]. The high reactivity of beryllium, together with its high viscosity (even with substantial superheat), also makes it an unsuitable candidate for precision casting [Marder et al. 1990, Marder 1991].

20.1 Powder Consolidation

To overcome these problems, alternative methods have been developed for the manufacturing of beryllium. The vast majority of these methods involve the use of beryllium powders. The powders are consolidated under pressure in vacuum at an elevated temperature to produce vacuum hot pressed (VHP) blocks and vacuum hot isostatic pressed (HIP) forms and billets. (The term *block*, in contrast to *billet*, is associated with the VHP product.) These typically cylindrical blocks are produced over a wide range of sizes (up to 183 cm, or 72 in., diameter by 61 cm, or 24 in., high). They may be cut or machined into parts or subjected to thermomechanical processing to develop the desired microstructure, properties, and shapes. Vacuum hot isostatic pressing and cold isostatic pressing (CIP) followed by sintering and possibly by a final HIPing (CIP/sinter/HIP) are important in their use for the production of near-net-shaped parts. For the same starting powder, a HIPed product will have less anisotropy than that obtained for a VHP product. A schematic presentation illustrating the difference between VHPing and HIPing is shown in Fig. 20.1 [Marder et al. 1990]. Beryllium can also be deposited as coatings as well as free-standing forms. The microstructure, properties, and various methods used that are related to the deposition of beryllium are discussed in Chapter 22, "Beryllium Coating Processes," in this book.

Briefly, the beryllium ores are chemically processed into beryllium hydroxide, which is then converted into beryllium fluoride. The fluoride is then made to react with magnesium in a high-temperature furnace, forming beryllium fluoride and beryllium "pebbles" (roughly spherical nodules) of 1 to 2 cm (0.4 to 0.8 in.) in diameter. The beryllium pebbles are somewhat

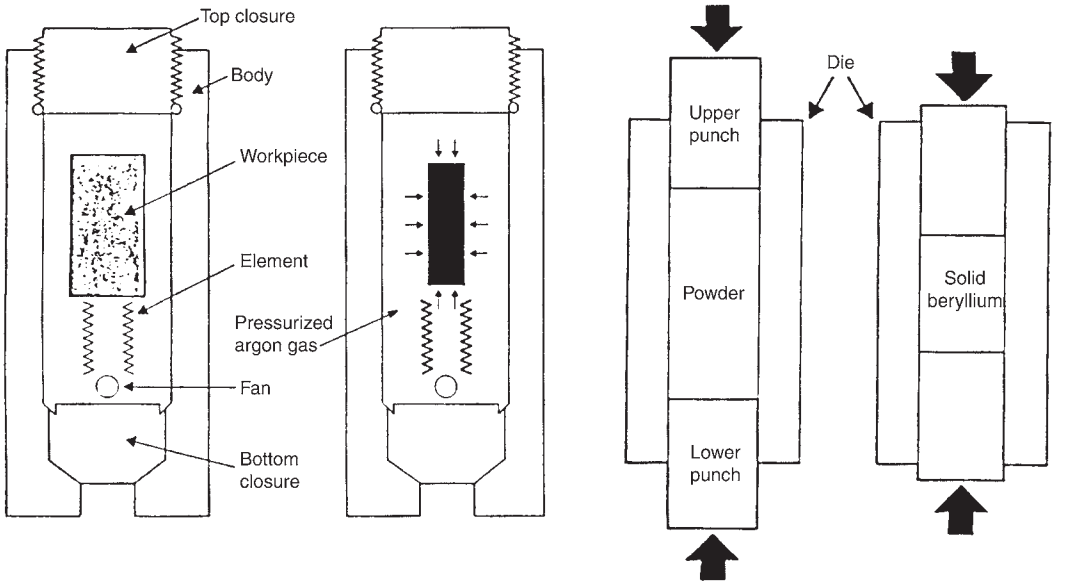

Fig. 20.1 Schematic illustration of two beryllium consolidation processes. Hot isostatic pressing is shown by the two schematics on the left. Vacuum hot pressing is shown on the right. Source: Marder et al. 1990

Table 20.1 Nominal compositions of nuclear and structural grades of beryllium powders

Element or oxide	Nuclear-grade S-65C	Structural-grade S-200F	Element or oxide	Nuclear-grade S-65C	Structural-grade S-200F
Be assay(a)	99.0	98.0–98.5	Pb	0.002	. . .
BeO	1.0	1.5	Li	0.0003	. . .
Al	0.60	0.10	Mg	0.0006	0.08
B	0.0002	. . .	Mn	0.012	. . .
Cd	0.0002	. . .	Mo	0.002	. . .
Ca	0.01	. . .	Ni	0.02	. . .
C	0.10	0.15	N	0.02	. . .
Cr	0.01	. . .	Si	0.06	0.06
Co	0.0005	. . .	Ag	0.0010	. . .
Cu	0.015	. . .	Others(b)	. . .	0.04
Fe	0.0800	0.13			

(a) Indicates maximum content; minimum contents are given for remainder of elements. (b) Indicates other metal impurities. Source: Marder 1998a

impure, containing a number of high-vapor-pressure elements from the reduction processes. The contaminants are removed by induction vacuum melting, and the purified melt is cast into ingots, typically weighing 180 kg (400 lb). The ingots are cut into chips in a lathe with a multihead cutting tool, cleaned, and reduced to the powders used in the consolidation processes [Marder et al. 1990]. Chemical compositions of two common grades of powders are given in Table 20.1 [Marder 1998a].

Powders are formed by ball milling, disk grinding, or impact grinding the chips or by an inert gas atomizing process (gas-pressure spray). Depending on the method used, the powder particles differ mainly in their shape. Gas-atomized powders are spherical and isotropic and have excellent flow and packing characteristics. (In gas atomizing, a stream of molten metal is broken into droplets by a jet of high-pressure gas. Surface tension causes the droplets to form into spheres before they solidify.) The properties of the consolidated materials made with these powders are equal or superior to the properties obtained with those made with comparable mechanically produced powders [Stonehouse and Marder 1990]. In mechanical attrition, especially at the low-impact collision rates that occur within a ball mill, slip and fracture of the (brittle) beryllium chips proceed primarily along basal planes of the hexagonal close-packed crystal structure, yielding platelike particles. During the vibratory loading of the VHP chamber, the flat fracture surfaces tend to become aligned

Table 20.2 Comparison of properties of beryllium with other materials

Material	Modulus-to-density ratio, 10^8 in.	Density (ρ) lb/in.^{3}	Density (ρ) g/cm^3	Young's modulus (*E*) 10^6 psi	Young's modulus (*E*) GPa	Thermal conductivity (*K*), Btu · ft/(h · ft^2 · °F)	Specific heat (*C*), Btu/lb · °F	Coefficient of thermal expansion, 10^{-6} in./in. · °F	Thermal stabilizing factor(a), s/in.^{2}	Natural frequency factor(b)
Beryllium	6.6	0.067	1.85	44.0	303	104	0.46	6.5	1.5×10^{-4}	25.0
Aluminum	1.1	0.098	2.71	10.5	72	128	0.22	12.5	0.9×10^{-4}	10.5
Titanium	1.0	0.160	4.43	16.0	110	4.5	0.13	5.0	23×10^{-4}	10.0
Steel	1.0	0.290	8.03	29.0	200	27	0.12	6.0	6.4×10^{-4}	10.0
Optical dielectric	1.6	0.090	2.49	14.5	100	0.92	0.22	0.2	110×10^{-4}	12.0

(a) Thermal-stabilizing time factor = $(\rho \times C)/(2 \times K)$, s/in.^{2}. (b) Natural frequency factor = $\sqrt{(E/\rho)}/1000$. Source: Grant and Hardesty 1990

perpendicular to the loading direction and thereby impart anisotropic properties to the hot pressed billet. Of the various attrition methods employed, the degree of anisotropy is smallest using the impact process, in which a high-velocity gas stream propels the chips against a beryllium target. The high impact force causes the beryllium chips to fracture on other planes in addition to the basal planes, resulting in blocky-like particles, which have decreased tendency to align during loading of the powder. A reduction in the degree of anisotropy leads to improved overall ductility. Consequently, impact grinding has become the major mechanical-production method for producing beryllium powders. Less anisotropy is obtained under isostatic loading (HIPing) than under uniaxial loading (VHPing). The minimization of anisotropic properties in beryllium is an important factor when used in control and diagnostic systems, especially if involved with optics.

Table 20.2, which compares a number of properties of beryllium with those of some competitive materials, was developed to illustrate the advantages offered by beryllium [Grant and Hardesty 1990]. Applications for beryllium, which were reported in a review paper published in 2000 [Haws 2000] and others [Hunt 1988], include fusion- and fission-nuclear reactors, infrared target-acquisition systems, inertial-guidance systems, space telescopes, satellite structures, optics for space and ground-base systems, commercial optical scanners, audio components, high-speed computer parts, avionics, thermal management, windows for x-ray sources and detectors, missile-guidance systems, structural material for solar energy collectors, and fire-control systems for tanks.

20.2 Formability

The formability of beryllium is low compared with that of most other metals. Beryllium, with its hexagonal close-packed crystal structure, has relatively few slip planes, and its plastic deformation is limited. For this reason, all beryllium products should be formed at elevated temperatures, generally 540 to 815 °C (1000 to 1500 °F) and at slow speeds. The primary factors influencing the formability of beryllium are grain size, texture, impurity content, prior metalworking history, ductility as a function of temperature, and strain rate [Blakeslee 1979, Leslie 1979]. Each of these factors is discussed briefly as follows.

20.2.1 Grain Size

Grain size is important to formability. With very fine-grained material, grain-boundary sliding was the significant mode of deformation. Very fine-grained ingot-source beryllium has exhibited superplastic-like behavior. Grain-boundary sliding was reported to be a significant deformation mode in causing the superplastic behavior. Elongation on the order of 100% in a 16 μm grain size had been observed near 700 °C (1290 °F) [Heiple 1973a].

20.2.2 Texture

Crystallographic texture in any given direction can cause serious anisotropic ductility, resulting in poor formability. The formability of beryllium varies with the texture in powder-source beryllium sheet [Barrow and Craik 1963, Bishop 1963]. A weak 3X random basal texture exists in ingot-source beryllium that exhibits excellent formability [Beitscher and Grimes 1970]. Crystallographic texture in any given direction will cause serious anisotropic ductility, resulting in poor formability [Keeler 1968]. Random texture for any material is recommended, but a weak 3X random basal texture often exists in ingot-source beryllium, and it exhibits excellent formability. The preferred crystallographic orientation in severely worked beryllium produces

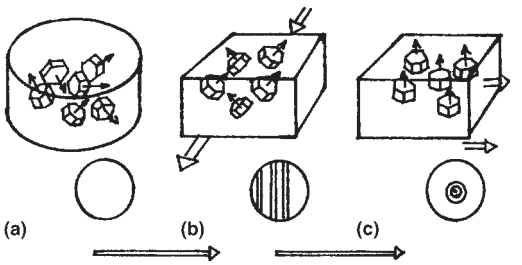

Fig. 20.2 Schematic view showing the texture (small circles replicate basal plane pole figures) resulting from cross rolling of beryllium. (a) Near-random basal plane orientation of hot pressed block. (b) Basal planes align in the plane of the sheet when rolling is unidirectional. (c) Cross rolling aligns basal planes randomly with respect to rolling direction but preferentially in the plane of the sheet.

uniaxial or biaxial ductility, with values in the range above 20% elongation. However, this severe texture also results in nearly zero ductility in the short-transverse or through-thickness direction. Cross rolling is often used to disrupt the tendency to texture [Sharma and Sivasubramanian 1994]. A special forging practice known as triaxial forging, often known as redundant forging, has been used to change the angular inclination of maximum preferred orientation and the degree of orientation but does not completely eliminate preferred orientation [Hayes 1979]. Figure 20.2 shows schematic representations of the texture that can result from cross rolling.

20.2.3 Composition

The oxide content of ingot and powder sheet has a significant effect on formability. As the oxide content increases, yield strength increases and ductility decreases. Poor formability, even at elevated temperature, can also result from excessive beryllium oxide content (>1 wt%). This situation can often be alleviated with the proper selection of process parameters and practices, such as by processing in an inert atmosphere. Quality ingot-source beryllium typically exhibits a BeO content of less than 30 ppm. The ingot-source beryllium process typically produces material with less than 50 ppm BeO.

High ductility with very high-purity, zone-refined, ingot-source beryllium has been reported [Hanafee 1971]. Rolling reductions of 90% at only 200 °C (390 °F) were reported, demonstrating that purity is a strong factor to be reckoned with in beryllium formability. It is not practical to use zone-refined, high-purity beryllium to form engineering structures. It is necessary to deal with the problem of hot shortness, which can plague powder-source beryllium sheet. This condition is caused by free aluminum in the grain boundaries. It has been shown that this condition can be eliminated by controlling the iron-to-aluminum ratio coupled with proper heat treatment to avoid precipitation of aluminum at the grain boundaries [Foos et al. 1970a, b]. The heat treatment involves holding for long times (~24 h) at 780 °C (1450 °F) to allow iron atoms time to migrate to the aluminum sites and form the compound $AlFeBe_4$.

20.2.4 Fabrication History

Beryllium products consolidated by vacuum hot pressing have low ductility, even at a theoretical density of 100%. The ductility of hot pressed beryllium can be increased by hot mechanical working. If beryllium is processed properly, and the parameters controlled properly, it is quite ductile at elevated temperatures and therefore formable.

20.2.5 Preheat Treatment

In most forming applications, both the die and the workpiece must be preheated. Dies are specially constructed to permit heating. Usually, a furnace is preferred for preheating the forming blank. No specially prepared atmosphere is needed. At the maximum temperature normally used for forming beryllium (760 °C, or 1400 °F), surface oxidation in an air atmosphere is usually negligible. However, if desired, the workpiece can be coated with a film of commercial heat-resistant oil to prevent surface discoloration (hard oxide layer). After forming, the oil film can be removed by wet blasting or by degreasing. When forming thin sheet (less than 1 mm, or 0.040 in., thick), cooling of the work between the furnace and the forming equipment is often a problem. Overheating to compensate for this heat loss is not recommended. One satisfactory solution is to "sandwich" thin sheets of beryllium between two sheets of low-carbon steel. This sandwich is retained throughout heating and forming.

20.2.6 Temperature

Beryllium formability is very sensitive to forming temperature. Uniaxial ductility reaches a maximum between 400 and 800 °C (750 and 1500 °F), but most forming operations use a temperature range from 600 to 750 °C (1110 to 1380 °F). If beryllium is processed by properly controlling the material quality and process

parameters, it is very ductile and formable. Beryllium must be heated to have enough slip systems available for deep drawing. Powder-source beryllium is usually formed between 600 and 650 °C (1110 and 1200 °F). Tooling temperature is usually at 400 to 450 °C (750 to 840 °F). Torch, resistance, and induction heating can be used to heat tooling. For rolling, reductions in thickness of 5 to 10% per pass are typical.

The selection of forming temperature for deep drawing ingot-source beryllium depends on the grain size. Since grain refinement in ingot-source beryllium depends on the amount of reduction, the thicker sections have coarse grains. Ingot-source beryllium with blank thickness up to 2.54 mm requires forming temperature between 650 and 700 °C (1200 and 1290 °F). Greater thickness requires higher temperatures: 6.35 and 8.25 mm thick blanks are formed at 700 to 750 °C (1290 to 1380 °F) and at 780 °C (1435 °F), respectively. Higher processing temperatures are avoided due to concerns of oxidation resulting in BeO scale, with a potential promotion of toxicity.

20.2.7 Deformation Characteristics

Plastic deformation studies of single crystals identified the crystallographic planes on which slip, twinning, and fracture occur in beryllium. With its close-packed hexagonal structure, beryllium deforms by slip on the (10$\bar{1}$0) prism plane, in the [11$\bar{2}$0] direction, and, to a lesser degree, on the (0001) basal plane. Twinning occurs on the (10$\bar{1}$2) plane, and fracture readily occurs on the (0001) basal plane.

Hot working preferentially orients the basal planes parallel to the plane of metal movement. Hence, for open-die upset forging of an isotropic billet, the basal plane orientation will be parallel to the radial-circumferential plane of the disk-shaped forging. For solid cylindrical forward extrusion, the basal plane orientation will be parallel to the axial direction of the wrought extrusion. Recrystallization of heavily worked beryllium can initiate at approximately 700 °C (1290 °F) and can be complete at 820 °C (1510 °F), depending on the degree and temperature of prior warm work. Beryllium that is recrystallized from a wrought product retains its anisotropic characteristics, although the degree of preferred orientation may decrease. Change of preferred orientation can be accomplished by further metalworking in a different direction(s).

20.2.8 Strain Rate

The strain rate used in deep drawing varies, depending on the severity of the draw. For deep drawing simple shapes, punch speeds of 760 to 1270 mm/min are used. With optimum die clearance and lubrication, strain rates up to 2500 mm/min can be used. Increasing the strain rate increases the resulting ductile-brittle temperature. Strain rate also affects bend ductility at elevated temperatures.

20.2.9 Equipment and Tooling

Standard mechanical presses or other fast-forming presses are not suitable for forming beryllium. Presses operated by air or hydraulic systems are usually used because slow speeds are required.

Critical components of the equipment must be protected against damage by the heat of forming. This protection usually is achieved by means of simple insulation. Because the tools used for forming beryllium will be heated, allowances must also be made for thermal expansion, high-temperature strength, and oxidation when selecting tool material and designing tools. Since a considerable portion of the blank heat is lost by conduction to the drawing surfaces, reheating to maintain sufficient slip systems for drawing is necessary. Interrupting the draw process to heat also allows an opportunity to replenish the lubricant. For example, a double-action draw of 45% reduction may require up to two reheats. Dies are usually made from hot work die steels, stainless steel, or one of the nickel- or cobalt-base heat-resistant alloys. Gray cast iron is satisfactory for most applications using a punch and die. Drawing surfaces are usually made from a free-machining tool steel or, in the case of very large dies, low-carbon steel that has been carburized after machining.

20.2.10 Lubrication

Lubrication or coating of some type is needed in most beryllium working operations. For less severe operations, such as bending, powdered mica has been used. Lubrication is required to prevent galling between the beryllium workpiece and the die. A lubricant film must be maintained over that portion of the blank surface making contact with the drawing surfaces of the die throughout the entire draw. For operations such as joggling, forming in matched dies, or deep drawing, colloidal graphite in oil is

commonly used. The role of lubrication is especially critical in deep drawing.

Because elevated temperatures (595 to 675 °C, or 1100 to 1250 °F, for the workpiece and 400 to 500 °C, or 750 to 930 °F, for the dies) are required to deep draw beryllium, conventional lubricants applied directly to the blank and die will burn off, causing galling between workpiece and die at high-pressure areas such as the draw ring-to-blank interface. The solution to this problem is best achieved by using die materials that are self-lubricating, such as graphite or an overlay of colloidal suspension of graphite on an insulating paper carrier.

The technique of using consolidated graphite as a self-lubricating die material was initially developed for forming small, thin-walled parts to finished size [Blakeslee 1979]. This technique has evolved to the point that very deep drawing of 6.35 mm (0.25 in.) thick blanks over a graphite draw ring is routine. The disadvantage is that such draw rings have short service life because the graphite is susceptible to wear and fracture.

Organic emulsified suspensions of powdered graphite, aluminum, and copper have been used successfully to lubricate punches to facilitate part removal. These materials can also be applied to the draw ring to improve lubricity of the drawing surface under the graphite-impregnated paper.

20.2.11 Stress Relieving

Stress relieving between stages of forming, or after forming is completed, is needed only when forming relatively thick sheet metal or in severe forming. For some finish-formed parts, stress relieving has proved an effective means of counteracting "oil canning" or excessive warpage. When stress relieving is used, regardless of whether it is an intermediate step or a final operation, holding at 705 to 760 °C (1300 to 1400 °F) for 30 min is recommended. No specially prepared atmosphere is needed.

20.3 Rolling

There are two distinct types of beryllium sheet. One type is produced by rolling block originally consolidated by hot pressing powder and is often called powder sheet. The other type is produced by rolling vacuum-cast ingot and is often called ingot sheet. The powder sheet is characterized by fine grain size (10 μm), high beryllium oxide content (approximately 2 wt%), strong texture, high strength and ductility in the plane of the sheet, and fair formability at elevated temperatures. The ingot sheet, in contrast, exhibits a coarse grain size (50 μm), low beryllium oxide content (approximately 50 ppm), weak texture, moderate strength and ductility, and excellent formability at elevated temperatures [Leslie 1979].

20.3.1 Powder-Source Materials

Flat-rolled products produced from powder-source materials, such as plates, sheets, and foils, are generally produced by encasing the beryllium in steel jackets and rolling, usually at a moderately elevated temperature. Flat-rolled stock 0.508 mm (0.02 in.) thick or less is referred to as foil, between 0.508 and 6.35 mm (0.02 and 0.25 in.) as sheet, and greater than 6.35 mm (0.25 in.) as plate.

Rolling (as well as upset forging) beryllium tends to align the basal planes parallel to the rolled plane and in the direction of rolling. This alignment of basal planes results in anisotropic properties providing increased ductility along the rolling plane, with a corresponding reduced ductility in the thickness direction. Cross rolling (alternating by 90° the direction of rolling the beryllium) is used if uniform biaxial properties are required [Brush Wellman 2001].

20.3.2 Sheet and Plate

The specified grade numbers for sheet and plate are SR-200 and PR-200, respectively. Their chemical composition conforms to that of the VHP block S-200F. Ambient-temperature tensile properties in the plane of the sheet or plate and the maximum sizes available are shown in Table 20.3 [Brush Wellman 2001]. The rolled sheet and strip were made by cross rolling billets of VHP block encased in steel. The relationship of shear strength to tensile strength was reported as being higher than that for most materials at the lower temperature range and lower than expected at temperatures exceeding 482 °C (900 °F).

A study on powder metallurgy sheets describes hot rolling a slab that had been machined from VHP block [Leslie 1979]. The slab was rolled at 650 to 900 °C (1200 to 1650 °F), with reheats in a furnace to maintain temperature. After rolling, the steel jackets were removed by shearing. The

Table 20.3 Tensile properties and sizes available for warm-rolled beryllium sheet and plate

Thickness			Minimum ultimate	Minimum yield strength,	Minimum	Maximum size
mm	in.	Grade	tensile strength, MPa	0.2% offset, MPa	elongation, %	available, cm
0.533–0.762	0.021–0.030	SR-200	482.6	344.7	10	61 by 183
0.763–3.175	0.031–0.125	SR-200	482.6	344.7	10	61 by 213
3.176–6.350	0.126–0.250	SR-200	482.6	344.7	10	61 by 168
6.351–11.430	0.251–0.450	PR-200	448.2	310.3	4	61 by 127
11.431–15.240	0.451–0.600	PR-200	413.7	275.8	3	61 by 102

Source: Brush Wellman 2001

Table 20.4 Comparison of tensile results in the longitudinal and transverse directions for beryllium cross-rolled sheet

Source and material	Orientation(a)	Yield strength, MPa	Ultimate tensile strength, MPa	Elongation, %
Herrera and Staffor [1991]	L(b)	392	517	17.3
SR-200 (2.54 mm thick)	T	415	497	25.2
Kovarik [1984]	L(c)	393	N/A	N/A
SR-200E (0.51–1.19 mm)	T(c)	400	N/A	N/A
Marder [1986]	L(d)	345	483	10
SR-200E (0.53–0.64 mm)	T(d)	345	483	10
MIL-HDBK-5E [1987]	L(d)	296	448	5
SR-200D (1.78–6.35 mm)	T	296	448	5
Fenn et al. [1967]	L	372	538	16
S-200 (1.96 mm)	T	386	552	16
Ingels [1966]	L	352–434	538–586	10–24
(0.51–3.05 mm)	T	345–421	483–593	7–25

(a) L, longitudinal; T, transverse. (b) Average of three tests. (c) Average of 12 tests. (d) Minimum design properties. Source: Henkener et al. 1992

sheet was then flattened and stress relieved between large ceramic plates. Certain large sizes required rejacketing of the beryllium. Sheet sizes as large as 91 by 244 cm (36 by 96 in.) were made. Some commercially available sheet and plate sizes were 2 mm by 1.2 m by 4.6 m, 4 mm by 1.2 m by 4.6 m, and 1.3 cm by 0.8 m by 1.3 m.

Mechanical properties for cross-rolled 2.5 mm (0.1 in.) thick sheet of SR-200E (VHP) beryllium were reported by the National Aeronautics and Space Administration (NASA)/Johnson Space Center [Henkener et al. 1992]. Tensile, biaxial, and shear tests were performed, and the results were compared to the results based on several finite-element models. The tensile results obtained and compared with results reported by other sources are presented in Table 20.4. Some of the tensile sheet specimens that were sanded (not included in the table) showed extensive degradation in the properties. The elongations became limited to approximately 1%; the ultimate tensile strengths decreased approximately 16 and 20% in the transverse and longitudinal directions, respectively; by contrast, the yield strengths were not significantly affected by the sanding. The degradation depended on the coarseness of the papers (280 and 400 grit).

20.3.3. Foil

Foils are usually made by rolling at elevated temperatures in steel cans. Because beryllium cannot be successfully rolled at room temperature, a cold-rolled surface is not available [Brush Wellman 2001]. Due to its use primarily as windows for detector and source applications, which involve special characteristics, close tolerances, and reproducibility, foil is only available in two high-purity grades: PF-60 and IF-19 [Brush Wellman 2001]. Their chemical compositions are listed in Table 20.5. Beryllium foil has also been produced by hot rolling plates of beryllium condensate contained in sheaths (proprietary details were not given) [Krivko et al. 1991]. A fine-grained substructure having an ultimate tensile strength of approximately 475 MPa (69 ksi) and a 0.2% offset yield strength of approximately 395 MPa (57 ksi) was developed. Annealing for 1 h at temperatures up to 500 °C (930 °F) increased the ductility with practically no change in either microstructure or strength. Beryllium foils have been used for domes in loudspeakers. Foils were rolled down from slabs. To obtain sufficient ductility and formability, the foils had to be formed above 300 °C (570 °F). The foils were formed in an hermetically sealed heat-forming chamber.

Table 20.5 Chemical composition of beryllium foils

Composition	Grade IF-19	Grade PF-60
Beryllium, % min	99.8	99
BeO, % max	0.03	0.8
Al, ppm max	100	500
B	3	3
Cd	2	2
Ca	200	100
C	300	700
Cr	25	100
Co	5	10
Cu	50	100
Fe	300	700
Pb	5	20
Li	. . .	3
Mg	60	500
Mn	30	120
Mo	10	20
Ni	200	200
N	. . .	400
Si	100	400
Ag	5	10
Ti	10	. . .
Zn	100	. . .
Available gage	0.008–0.508 mm (0.0003–0.02 in.)	0.008–3.175 mm (0.0003–0.125 in.)

Source: Brush Wellman 2001

20.3.4 Ingot-Source Rolling

The successful processing of vacuum-cast ingot beryllium into usable sheet has been reported [Floyd 1972a, Floyd et al. 1973, Frankeny and Floyd 1968]. They have reported production-type processes for can rolling 22 by 22 by 9 cm (8.5 by 8.5 by 3.5 in.) thick beryllium rolling billets obtained from 23 by 23 by 51 cm (9 by 9 by 20 in.) castings. In their standard process, the billet is encased in uniformly thick (1.6 cm, or 0.6 in.) type 304 stainless steel and reduced in thickness 94%. (can rolling). The beryllium sheet can then be reduced further without the use of cladding (bare rolling). Each of these procedures, can rolling and bare rolling, is discussed as follows. This technology, which was developed in a U.S. government plant, has been successfully transferred to industry and used to produce products by the Manufacturing Sciences Corporation in Oak Ridge, TN.

20.3.5 Can Rolling

Floyd [1972a, 1973] reports that ingot-source beryllium must first be encased in a protective "can" prior to rolling. This "canned-rolling" process is described as follows. All faces of the cast billets are machined, and all edges are chamfered. The machined billets are cleaned with a starch product and water and vacuum

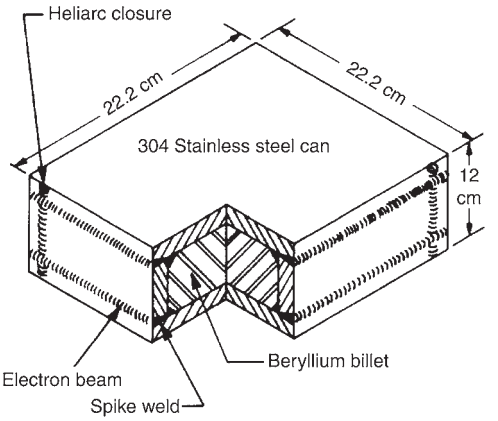

Fig. 20.3 Cutaway of typical canned-rolling billet

baked at 600 °C (1110 °F) to remove volatile material. A parting compound of alumina, sodium silicate, and water is applied to all faces of the billet to prevent bonding between the stainless steel jacket and the beryllium billet during rolling. The billet is jacketed (canned) in type 304 stainless steel in preparation for rolling. The stainless steel can is gas tungsten arc welded in several places along each edge. Final closure is done using electron beam welding. The chamfered edges on the billet prevent beryllium from being drawn up into the weld when the electron beam spikes through the stainless steel can. A cutaway of a typical canned-rolling billet is shown in Fig. 20.3.

Figure 20.4 shows stages of evolution leading to the optimum design described previously. Design No. 1 was used when only round beryllium castings were available and was dropped in favor of design No. 2 due to excessive use of canning materials, excessive welding time, and minimal volume of beryllium. Design No. 2 was used until the development of the 22.9 by 22.9 by 39.4 cm (9 by 9 by 15.5 in.) square casting, at which time design No. 3 was developed. The round rolling billets were not efficient for material utilization and were also awkward to remove. Design No. 3 was dropped in favor of design No. 4, mainly to reduce welding times. Importantly, the use of electron beam welding seals a vacuum within the can. This eliminates problems with bursting of trapped gases during rolling, prevents oxidation of the beryllium, and enables diffusion bonding to heal cracks that form during rolling.

The rolling parameters that must be optimized are billet temperature, reduction per pass, num-

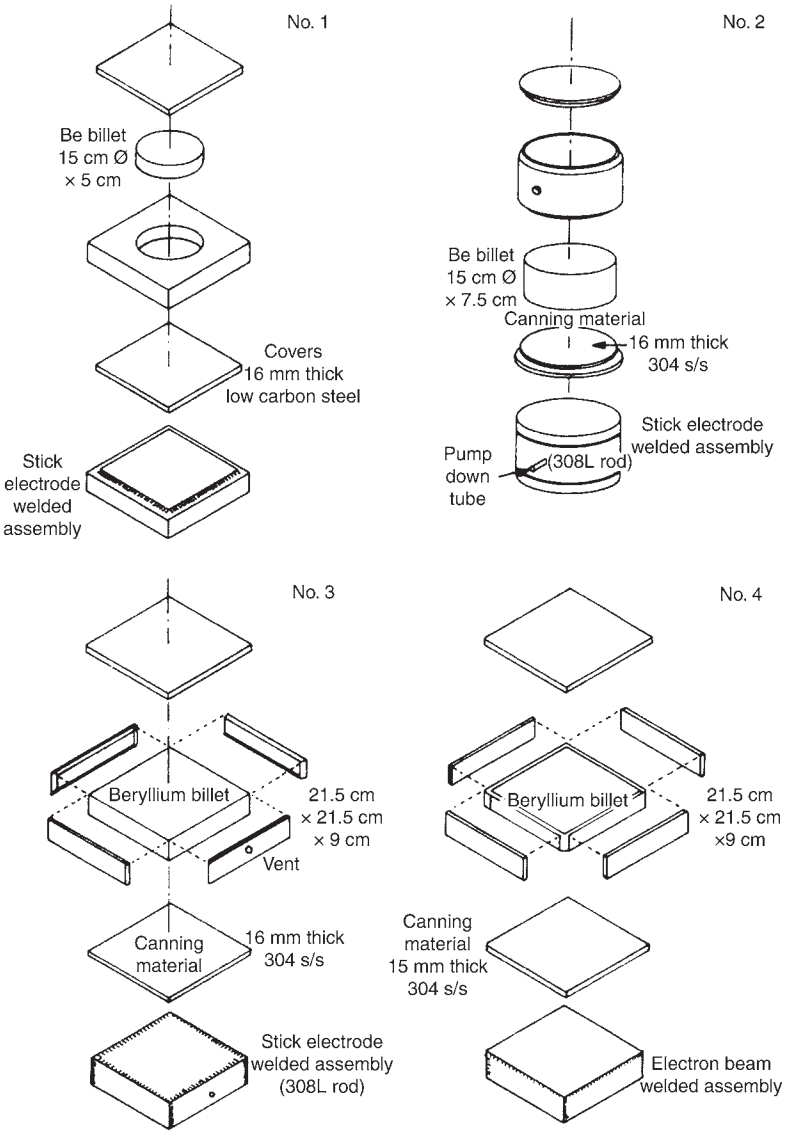

Fig. 20.4 Design sequence of four different methods that have been used to clad beryllium billets for rolling. The symbol "s/s" refers to stainless steel.

ber of passes without reheats, reheat conditions, lubrication of rolls, crown of rolls, and surface finish of rolls. Because as-cast grains are nonuniform, very large, and columnar, a key problem in rolling ingot beryllium is that of achieving a uniform, fine, equiaxed grain size in the finished sheet. Lowering the rolling temperature too early in the schedule will result in retained cast structure in the sheet. Retaining the sheet at too high a final rolling temperature will yield large grains. Skipping the intermediate temperature reheats will produce a duplex microstructure.

Curling of the canned pack during rolling is deleterious because the beryllium sheet can crack and will not necessarily heal during subsequent passes. Also, curling strains frequently rupture the stainless steel can, which normally ruins the beryllium sheet within. Curling occurs at a roll diameter-to-thickness ratio of approximately 12 to 1. For the rolling mill used for this work, this corresponds to a thickness of approximately 2.5 cm (1 in.). Reportedly, the most significant variable controlling curling is friction between the work rolls and the rolling billet [Heiple 1973b].

Friction, in turn, depends strongly on lubrication and the surface finish of the rolls. Curling occurs toward the roll having the higher friction coefficient. Upward curling is undesirable because the workpiece is not restrained in this direction, and a tight radius of curvature may result. Experience has shown that it is best to adjust the friction variable to favor a slight downward curl. This practice is accomplished by lightly lubricating the top roll while keeping the bottom roll dry; also, the bottom roll is given a rougher surface finish (1.5 μm) than the top roll (0.25 μm). These two factors, lubrication and roll surface finish, cause the bottom work roll to have a higher friction coefficient than the top work roll; hence, slight downward curling occurs and is limited by the stripper bar and roll tables.

High-quality sheet metal results from the can-rolling process only after 90% reduction has been achieved (9.0 mm, or 0.35 in., beryllium thickness). Sheet removed from the can earlier in the process does not usually survive subsequent deep-drawing or bare-rolling operations without fracture.

An objective of the can-rolling schedule is to produce sheet metal with isotropic properties. This accomplishment is done by cross rolling after each pass and is important to the success of subsequent deep drawing and structural applications.

The width of the rolls dictates the point in the rolling process where the sheet must be rolled in one direction only. This practice results in tensile properties approximately 30% greater in the rolling direction than transverse to it. Uniform properties can be obtained either by (1) stopping the can rolling before any unidirectional passes are employed, or by (2) removing the beryllium sheet from the can, shearing it to a smaller size, and bare rolling in a direction opposite to the last can-rolling direction for an amount commensurate with the previous unidirectional rolling.

20.3.6 Bare Rolling

Bare rolling (i.e., no cladding used) of ingot material has been performed on a production scale [Leslie 1979]. A specially designed in-line furnace with doors at both ends and mounted on the roll tables allows direct transfer of the machined beryllium billet (or sheets) from furnace to rolls. Preheating and intermediate reheats were performed in an inert-atmosphere annealing furnace held at 790 °C (1455 °F). The beryllium was then transferred to the in-line furnace held at 730 °C (1345 °F) in an inert atmosphere. The rolled material was finally vacuum annealed for 4 to 6 h at 760 °C (1400 °F). Billets up to 46 cm wide by 0.5 cm thick (18 by 0.2 in.) were rolled, the initial dimensions depending on the goal for the final sheet dimensions. A hot flattening procedure was used if curling occurred between any passes, which was required when cross rolling. A combination of can rolling and bare rolling was found to be successful, whereby the final pass or passes are performed bare after removal of the can. The mechanical properties, surface finish, and thickness uniformity of the bare-rolled sheets were superior to those of the can-rolled sheets. Typical mechanical properties of bare-rolled, ingot-source beryllium are listed in Table 20.6 [Brush Wellman 2001].

20.3.7 Foil

Foils ranging from 25 to 250 μm thick were produced by bare rolling on laboratory-type mills, starting with bare-rolled, 1 mm thick sheets [Leslie 1979]. The thinner foils were chemically milled to size after reaching rolled thicknesses of approximately 200 to 250 μm. Attempts at rolling down to 75 μm resulted in a loss of over 75% of the material. The high loss rate was attributed to embrittlement by surface oxidation, edge cracking due to springback and deformation of the rolls, and heat loss and chilling effect on transfer to the rolls. Rolled-and-etched sheets, 15 cm by 23 cm by 25 μm thick, were produced but only had isolated areas (10 cm^2) that were free of pinholes. High-purity beryllium should be used to obtain leaktight, 25 μm foil. Beryllium foil is available in thicknesses from 0.025 to 0.5 mm in panel sizes up to 125 by 300 mm [Marder 1998a].

Although ingots are generally considered too brittle to be worked, very small vacuum-cast ingots having fine grains can be rolled into foils. Successful laboratory rolling of high-purity, bare-ingot sheet from 5 to 8 mm down to 1 mm by preheating for 1 h at 790 ± 14 °C (1455 ± 25 °F) in an inert atmosphere and then rolling at 730 ± 14 °C (1345 ± 25 °F) at a 10 to 16% reduction per pass was reported [Smugeresky 1986]. Room-temperature tensile properties were reported as 175 MPa (25 ksi) yield strength, 230 MPa (33 ksi) ultimate strength, and 3 to 5% elongation. At thicknesses less than 2 mm, the frequency of edge cracking was increased, and

Table 20.6 Typical mechanical properties of bare-rolled, ingot-source beryllium

Thickness, mm	Ultimate tensile strength, MPa	Yield strength, 0.2% offset, MPa	Elongation, %	Typical size, cm	Test direction
1.52	301	182	5.0	30.5 by 107	Transverse
	343	182	6.1		Longitudinal
2.54	308	182	4.9	46 by 132	Transverse
	343	182	6.2		Longitudinal
3.81	280	182	3.5	36 by 107	Transverse
	301	175	5.0		Longitudinal
5.08	252	175	3.0	36 by 107	Transverse
	273	175	4.0		Longitudinal
8.25	231	182	2.7	74 by 74	Transverse
	245	182	2.5		Longitudinal

Source: Brush Wellman 2001

special handling was required to prevent heat losses at the edges. The ingots were produced using electrolytic-flake beryllium, yielding a very high-purity, fine-grained product. This process, which was initially developed to make foil for beryllium windows, was not commercially available at that time (1986). The author stated that by applying special thermomechanical treatments to ingot-processed (high-purity) beryllium, he was able to produce low-oxide products with equiaxed grain sizes of less than 30 μm. With these small grain sizes, grain-boundary sliding was obtained at room temperature, thus providing an additional deformation mode. Ductility as high as 7% with strengths in the range of 250 to 300 MPa (36 to 45 ksi) resulted. Charpy impact values of 4 to 6 J have been reported, which are close to the values obtained for 7075-T6 aluminum alloy. By contrast, conventional hot pressed billets have a Charpy impact value of 0.7 J [Smugeresky 1986].

20.4 Forming

Thin sheets of metal can be shaped by several metal-forming processes, most of which involve applying tensile or compressive (or both) stresses to sheet metal through the use of dies. Usually, there is little or no change in the thickness of the metal sheet as a result of the forming operation.

20.4.1 Deep Drawing

Deep drawing, which is also referred to as cupping, is the forming of deeply recessed parts by means of plastic flow of the material. Tooling consists of a punch and suitable die or draw ring. The process requires that the blank be pulled through the die orifice by being formed over the punch into a cup shape as it advances through the die orifice. For classic deep drawing, there is no strain in the die orifice, and the perimeter of the blank thickens as it passes through the die, with the metal in the bottom of the cup not being deformed [Keeler 1968]. Forming operations that can be considered classic deep drawing are rare. Normally, the deformation is a combination of deep drawing and stretching. That is, deformation occurs in the bottom of the cup in the form of thinning, and thickening of the flange is minimized as a result of the stretching. Since beryllium usually exhibits limited triaxial ductility and resists thinning because of a limited amount of properly oriented slip systems, it follows that deep-drawing operations should be designed to approach classic conditions and avoid stretching where possible.

Deep-drawn, thin-walled beryllium parts can realize considerable savings over the cost of machining [Blakeslee 1979, Grant 1988]. A successful deep-drawing operation involves proper control of friction and hold-down pressure, which is affected by the die design and lubricant selection. Lubrication is required to prevent galling between the beryllium workpiece and the die and to prevent subsequent failure of the drawn part. The lubricant film must be maintained along the contact areas throughout the entire draw. Due to the elevated temperatures that are required (above 595 °C, or 1100 °F, for the workpiece and 400 to 500 °C, or 750 to 930 °F, for the die), conventional lubricants will burn off. Self-lubricating dies or an overlay of a colloidal suspension of graphite on an asbestos paper carrier have been successfully used for deep drawing of small parts. Organic emulsified suspensions of powdered aluminum, graphite, or copper can be applied to the draw ring to improve lubricity of the drawing surface under the graphite-impregnated asbestos paper. The location of the

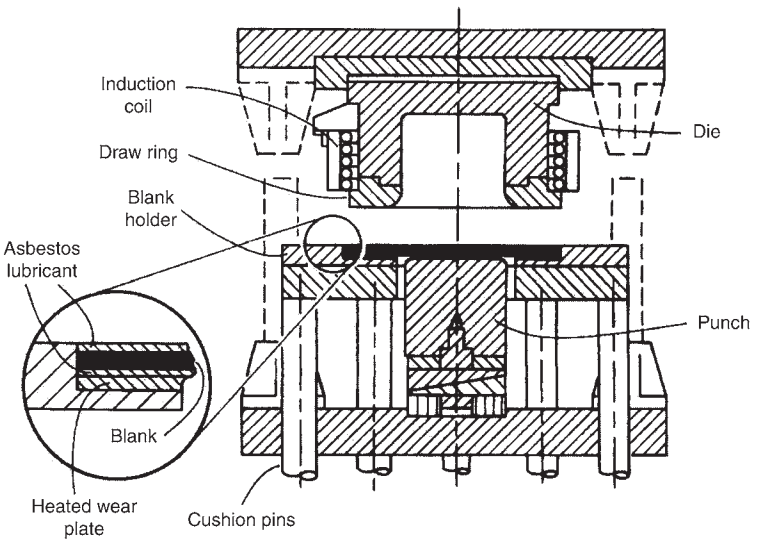

Fig. 20.5 Double-action tool for deep drawing of beryllium that employs the action of the lower-press action for blank restraint. Lubrication shown is insulating paper impregnated with colloidal graphite, as seen in the inset. Source: Blakeslee 1979, Grant 1998

lubricated asbestos paper on the workpiece blank in a double-action tool for deep drawing of beryllium is pointed out in Fig. 20.5 [Blakeslee 1979, Grant 1998]. The double action provides a restraint on the workpiece (blank or preform) to prevent wrinkling, which may occur when using a single-action tool. The restraint is applied by the blank holder and is developed by a lower (additional) ram in the hydraulic press. Both the holder and punch are supported by a set of cushion pins. The die is connected to the main ram, which lowers down over the punch, pushing the blank holder down and drawing the blank over the punch. The draw ring minimizes the transfer of heat from the blank to the blank holder and acts as a stripper to remove the part from the punch. The tooling, however, does not provide for an ejector to remove the part from the die. A modified version of the design does provide a part ejector [Blakeslee 1979]. Restraint is required if the blank is too thin to support itself during the early stages of drawing; excessive thinness causes the blank to buckle and/or wrinkle.

Blank development for deep drawing of beryllium generally follows the same rules as for other metals. Blanks too thin to support themselves during the early stages of drawing will buckle or wrinkle. A restraining force is required to prevent this buckling. There are numerous factors involved in determining whether blank restraint is required during any drawing operation. The two most important are (1) the blank diameter-to-thickness ratio, D/t, where D is the blank diameter, and t is the blank thickness; and (2) the percentage of reduction (R) from one draw to the next draw, where:

$$R = [(D_o - D_f)/D_o] \times 100 \qquad \text{(Eq 20.1)}$$

and D_o is the original blank diameter, and D_f is the drawn part diameter. For parts with a wall thickness greater than 6.35 mm, D should be substituted for the mean shell diameter:

$$D_m = \text{OD} - t \qquad \text{(Eq 20.2)}$$

where OD is the outside part diameter, and t is the part wall thickness.

The relationship between R and D/t is shown graphically in Fig. 20.6 for cylindrical pans or shells having either flat-bottomed or hemispherical cups. The areas under the curves were determined experimentally, with the curves themselves being the normal limit of formability for a given reduction at a given D/t ratio, both with and without blank restraint. A safety limit at approximately 48% is indicated, with the values decreasing with D/t greater than 150 for blank restraint and greater than approximately 40 for no restraint.

Since the curves describe formability limits, some consideration should be given during design to avoid borderline cases. Reductions of

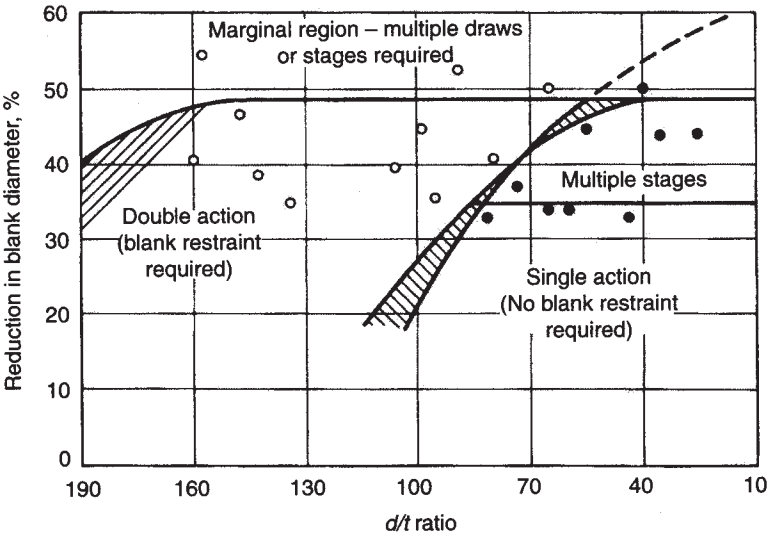

Fig. 20.6 Graphic relationship between reduction and diameter-to-thickness ratio showing the limits for deep drawing cylindrical beryllium shells. The "x" and "o" symbols represent experimental data. Shaded areas are marginal. Source: Blakeslee 1979

more than 50% are possible but will require partial drawing followed by several anneals, and usually, the failure rate is high. Several stages of tooling requiring smaller reductions is a more practical approach.

An overlay technique has been developed for deep drawing foil parts that exceed the formability limits established in Fig. 20.6. Blanks whose *D*/*t* ratio exceeds the formability curve for a given reduction can be made formable by increasing the thickness by sandwiching or simple overlaying of material until a favorable *D*/*t* ratio is achieved. The overlay material is removed from the formed part and discarded. The overlay material must exhibit formability characteristics similar to beryllium. Calculations of the blank size for a given part geometry follow the rules of conventional sheet metal forming.

Figure 20.7 shows a cross section of an early single-action design in which restraint was not applied. This design was used for investigations on forming thick-walled beryllium hemispheres. Failure with this type of design can be high because of unfavorable stress distributions and difficulty in lubricating the draw ring [Blakeslee 1979]. (A draw ring is a ring-shaped die over which the inner edge of a sheet metal is drawn by the punch.) Deep drawing of simple hemispherical shells is done at punch speeds from 760 to 1270 mm/min (30 to 50 in./min) [Grant 1988]. The primary cause of failure in deep-drawn shapes was observed to be due to local-

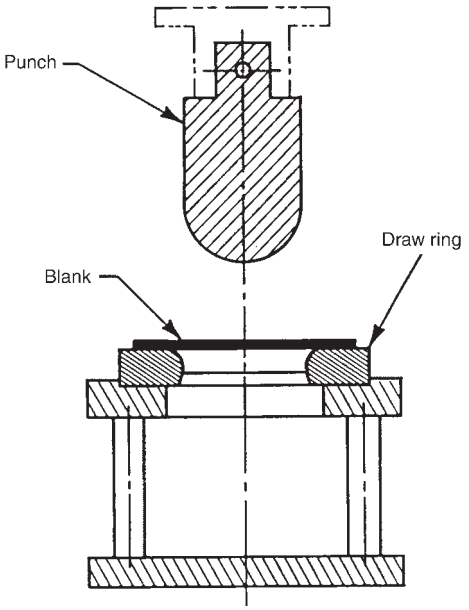

Fig. 20.7 Cross-sectional view of a simple, single-action punch and draw ring used for deep drawing beryllium. Source: Blakeslee 1979

ized tensile strains induced by stresses from the punch. The strains are most severe in the early stages of the draw, when the contact areas are small [Blakeslee 1979].

To minimize this problem, a conical die was developed to reduce the magnitude of localized stresses by increasing the distribution of the

maximum stress over a larger area of the drawing blank. A cross section of the design is shown in Fig. 20.8, in which the blank is supported by the outermost edge of the conical die. Such support introduces a bending mode, requiring less force, especially during the early stages of drawing. A reduction of 20% in drawing forces was achieved using this design [Blakeslee 1979]. Lubrication of the die was achieved by applying a layer of asbestos paper impregnated with a colloidal suspension of graphite on the drawing surface.

An overlay method was developed for deep drawing foil parts. A material having similar formability as beryllium is placed on or both on and under (sandwiching) the beryllium until the desired (safe) *D*/*t* ratio is achieved, as indicated in Fig. 20.6. This material is then discarded after the drawing operation [Blakeslee 1979].

In designing the tools, adequate clearance between punch and die must be considered. Thickening in the flange in a deep-drawn part may be as much as 22% for a simple hemishell. Common design practice for parts with a straight section is to allow for 20% blank thickening at the equator and to add a 2° taper to the straight portion of the die above the equator [Blakeslee 1979]. Cup-shaped parts that require a slightly thicker wall at the equator than at the pole are suited to be formed by deep drawing.

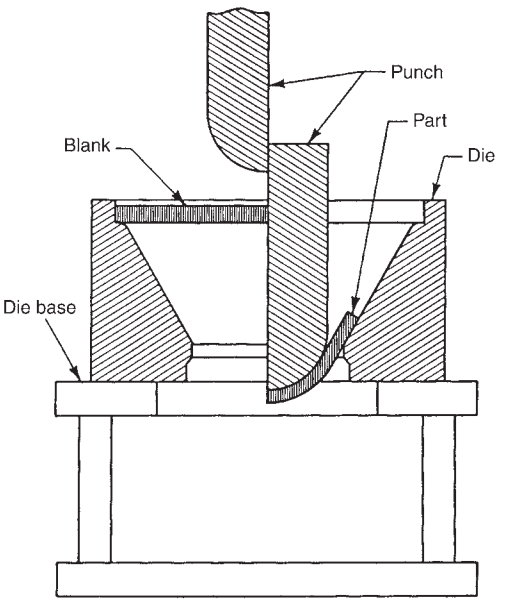

Fig. 20.8 Cross-sectional view of a conical die used to deep draw a thick-walled hemishell of beryllium. Left side shows the die punch with blank in place before forming the part. Right side shows the formed part just prior to exiting the die. Source: Blakeslee 1979

Powder-source (VHP or HIP) beryllium is usually formed between 600 and 650 °C (1110 and 1200 °F), independent of blank size or thickness. The temperature for deep drawing ingot-source material depends to a large extent on grain size, because the grain size influences formability. Since the grain size is largely dependent on the degree of rolling reduction used in producing the sheet from which the blank is obtained, it follows that the drawing temperature can be related to the blank thickness. Larger sections will also require more heat because of the thickness. Thicknesses up to 2.54 mm (0.1 in.) require temperatures between 650 and 700 °C (1200 and 1290 °F). Thicknesses up to 6.35 mm (0.25 in.) require temperatures up to 750 °C (1380 °F). Thicknesses up to 8.255 mm (0.33 in.) have been successfully drawn at 780 °C (1435 °F) [Blakeslee 1979]. Tools may be heated by several methods, such as torch, resistance, induction, and so on, with induction being the preferred method.

Strain rates may vary widely depending on the severity of the draw. For deep drawing simple hemishells, punch speeds between 760 and 1270 mm/min (30 and 50 in./min) are typically used. Where optimum conditions of die clearance and lubrication exist, strain rates in excess of 2500 mm/min (98 in./min) have yielded successful deep draws [Blakeslee 1979]. One would expect that blank thickness would be a factor on limiting the speed.

20.4.2 Roll Bending (Three-Roll Forming)

Three-roll roll forming is a process for forming smoothly contoured parts, such as plates, bars, beams, and so on, into various shapes by applying three-point bending forces progressively along the surface, with usually one or more of the rolls being driven. For beryllium, this usually involves the formation of curved panel sections and cylindrical shapes [Blakeslee 1979]. There are two basic types of three-roll forming machines: the pinch-type and the pyramid-roll-type machines, which are shown in Fig. 20.9. Both types operate with two driven rolls and one bending roll, the latter determining the amount of bend (curvature) to be obtained. Two of the pinch types are shown in views (a) and (b). The ends of the formed part are shown as being flat in view (a). The flat ends, if present, must generally be removed. The pyramid type is

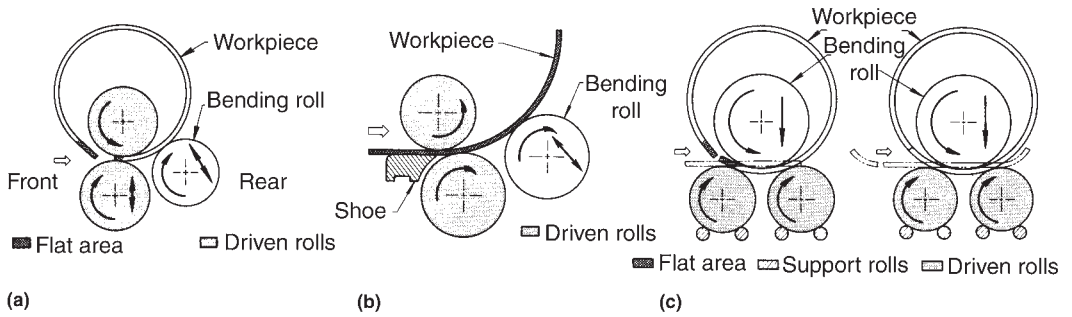

Fig. 20.9 End views of different setups for three-roll forming. (a) Conventional pinch-type machine (note large flat area on the leading end and smaller flat end on trailing end). (b) Shoe-shape machine with two powered rolls. (c) and (d) Arrangement of rolls in a pyramid-type machine. Note flat leading and trailing ends shown in (c) are minimized in (d) by prebending. Source: ASM 1988c

shown in views (c) and (d), the difference between the two being only in that the ends were prebent in view (d) [ASM 1988c]. With the pinch-type machine, the flat ends can be avoided or minimized by preforming the ends. This can be done by reversing the rotation of the rolls and feeding a short length from the rear. With the pyramid-type machine, the ends cannot be flattened by this technique; other flattening means, such as preflatening in a press brake, must be used. A sufficiently longer sheet (e.g., of stainless steel) can be combined with the beryllium sheet to lead through the machine and eliminate flat ends [Blakeslee 1979]. The flat ends can be virtually avoided by incorporating a forming "shoe" at the entry of the pinch-type machine, as shown in the figure. The shoe pinch-type machine lends itself to automation and is therefore used primarily as a production unit. However, it is limited to smaller thicknesses and widths and to round cylinders and is only applicable to cold forming [ASM 1988c].

The pinch-type machine produces a truer cylindrical shape than that which is obtained with a pyramid-type machine. This is because, of the two machines, the pinch-type machine allows the workpiece to be held more firmly against the rolls. In the pinch-type machine, the bending roll is rotated by the friction between it and the workpiece. It is adjusted angularly to produce a specified diameter. The roll is depicted in Fig. 20.9(a) as being at an angle of 30°. In the pyramid-type machine, the bending roll is adjusted vertically to produce a specified diameter. This type of adjustment offers the ability to attach (bolt) dies to the bending roll that permits forming of irregular shapes. Of the two machines, the pinch-type machine provides greater

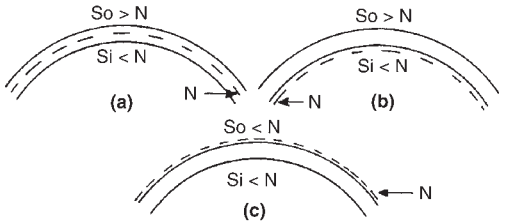

Fig. 20.10 Schematic illustration of three conditions that can exist during bending: (a) plane bending, (b) stretching, and (c) shrinkage. N refers to the neutral axis (and the neutral stress); So and Si refer to the stresses on the outer and inner surfaces, respectively.

accuracy and, for a given machine size, can produce a larger range of thicknesses [ASM 1988c].

The minimum diameter that can be formed is determined by the diameter of the top roll for both machine types. Under optimum conditions, the smallest cylinder diameters that can be formed are 50 mm (2 in.) larger than the top roll diameter for the pinch-type machine and 150 mm (6 in.) larger than the top roll diameter for the pyramid-type machine. Thin-gage products may require support to prevent out-of-roundness. Maximum width and length dimensions are basically limited by roll sizes and available space. Machines having 12.5 m (41 ft) rolls have been built [ASM 1988c]. Heat treatments and intermediate anneals of beryllium would be comparable to those used for other forming operations.

The amount of strain obtainable in a curving process without failure should be at least equal to the uniform strain obtained in a tensile test made under comparable conditions of temperature and strain rate. Three conditions can exist during bending, as illustrated in Fig. 20.10: plane bending, with the neutral axis in the center of the sheet thickness; stretching, where the neutral

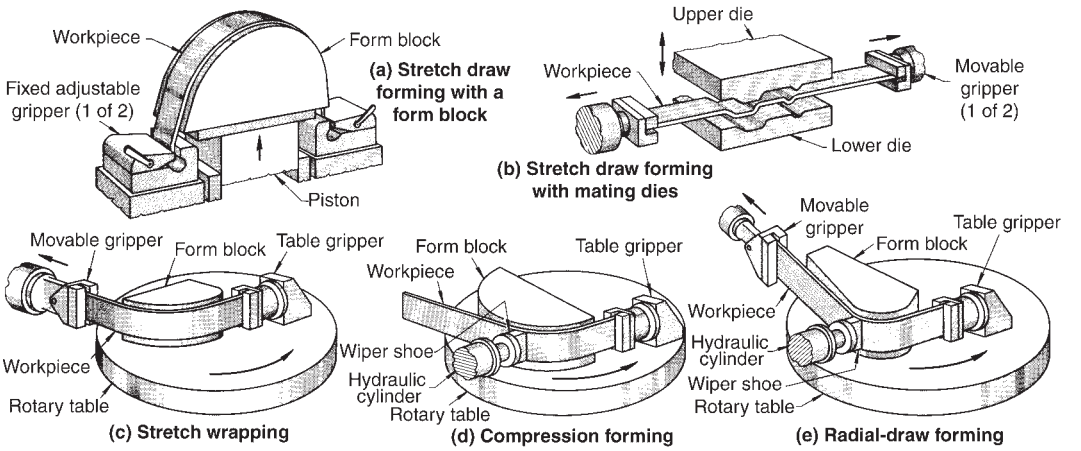

Fig. 20.11 Illustrations of techniques involved in the four basic methods of stretch forming: (a) and (b) stretch draw forming, (c) stretch wrapping, (d) compression forming, and (e) radial-draw forming. Source: ASM 1988b

axis is inside the inner surface; and shrinking, where the neutral axis is outside the outer surface. For simple bending through relatively large radii, the strain, *e*, is approximately related to the radius, *r*, and thickness, *t*, by the following expression [Blakeslee 1979]:

$$e \cong t/2r \qquad \text{(Eq 20.3)}$$

and for stretching, the strain is given approximately by the expression:

$$e \cong t/r \qquad \text{(Eq 20.4)}$$

Two examples of precision three-rolled-formed cylinders were reported, both produced from ingot-source beryllium [Blakeslee 1979]. A 50 mm (2 in.) diameter cylinder was roll formed at room temperature from 0.5 mm (0.02 in.) thick sheet in eleven passes. The cylinder, in which the ends of the formed sheet had been electron beam fusion welded, was round to within ±0.254 mm (±0.01 in.) on the diameter. A 430 mm (17 in.) diameter cylinder was roll formed at 700 °C (1290 °F) from a 6.85 mm thick by 305 mm wide by 1.57 m long (0.27 by 12 by 61.8 in.) blank in five passes. The ends were joined using an electron beam aluminum-shim weld and then machined to a uniform wall thickness of 5 mm (0.2 in.) and a diameter of 475 ± 0.2 mm (19 ± 0.008 in.).

20.4.3 Stretch or Creep Forming

Stretch forming involves shaping a rolled or extruded part by applying tension while wrapping it over or around a block having the desired contour. The metal is stretched just sufficiently beyond its yield point to retain the stretched shape. When applied to beryllium, the wrapping operation usually takes place quite slowly and undergoes some creep. It is also referred to as creep forming [Blakeslee 1979]. Both open- and closed-die tooling can be used, the former tooling being most commonly used for beryllium. It consists of a male die with the desired contour and the means of forcing the blank to assume that contour. In closed-die tooling, the male die is used to force the blank into the female die, forcing it to assume the contour of the male die. Friction forces from the female die help to restrain the part and cause a stretching condition. In closed-die tooling, both dies can be heated, lending itself to heating the part and maintaining the desired temperature. Since the high modulus of beryllium will resist buckling or warping, tension may not be necessary [Blakeslee 1979].

Examples of stretch forming, taken from the *ASM Handbook*, are reproduced in Fig. 20.11 [ASM 1988b]. Four methods of stretch forming are illustrated:

- Stretch draw forming—views (a) and (b)
- Stretch wrapping, also known as rotary stretch forming—view (c)
- Compression forming—view (d)
- Radial-draw forming—view (e)

View (b) can be considered as an example of closed-die stretching.

In general, excessive tension will induce cracking. Insufficient tension may result in poor con-

touring, wrinkling, or springback of the formed part. An estimation of force required for stretching a part is given by the following:

$$F = A(Y + U)/2 \qquad \text{(Eq 20.5)}$$

where F is the stretch-forming force, A is the transverse cross-sectional area of the part, Y is the yield strength, and U is the ultimate tensile strength. This would represent an average force. It does not take into account work hardening, friction, complex contours, and so on. It is suggested that for certain complex parts, an additional 25% may be added to the calculated value [ASM 1988b]. Surface finishes may be protected by using carrier sheets. (The blank, or workpiece, is sandwiched between or covered by protective sheets, called carrier sheets, which are subsequently removed from the blank after stretching.) An alternative method may be to use a polyvinyl chloride coating instead of a lubricant and/or by careful cleaning to eliminate abrasive dust particles.

Several examples of stretch forming beryllium were reported. Beryllium panel blanks, measuring 627 by 716 by 1.4 mm (25 by 28 by 0.06 in.) and 570 by 358 by 1.4 mm (22 by 14 by 0.06 in.), were stretch formed to a radius of curvature of 762 mm (30 in.), using either open- or closed-die tooling. With the open-die tooling, a blank was heated to 732 °C (1350 °F) using quartz lamps and creep formed to the male contour with a weighted wire mesh. Using closed-die tooling, the dies were heated to 732 °C (1350 °F), and a flat blank that was preheated to the same temperature was placed between them; the dies were then closed within 1 to 2 s. To avoid warping during cooling, the curved panels were placed in a set of unheated dies, which resulted in the cooling being more uniform than when cooled in the original dies. In another example, a U-shaped longeron was formed in a closed die heated to 632 °C (1170 °F). The flat blank was heated to 743 °C (1370 °F) and formed at a rate of 13 to 25 mm/min (0.5 to 1.0 in./min). Some of the advantages offered by stretch forming listed in the *ASM Handbook* are [ASM 1988b]:

- Approximately 70% less force is needed than that required with conventional press forming.
- Material costs can be reduced by as much as 15% compared to other forming methods.
- There is little likelihood of buckling and wrinkling since the stretching is done over the entire area of the workpiece.
- Springback is greatly reduced. Although, if there is some springback, it is easily controlled by overforming.
- Residual stresses are low.
- Changeover is easy, since tooling is simple.

Some limitations or disadvantages are the following [ASM 1988b]:

- It is limited in its ability to form sharp contours and reentrant angles. It is at its best in forming shallow or nearly flat contours.
- If the workpiece is not pinched between mating dies, there is no opportunity to coin out or iron out slight surface irregularities.
- In some of the methods, such as in stretch wrapping, the process is relatively slow and not suited to high-volume production. Stretch draw forming with mating dies, however, can be done as rapidly and automatically as forming with conventional press operations.
- Deep forming in the direction of the free edges is not practical.
- This method is best for rectangular blanks.
- Metals with very nearly similar yield and tensile strengths may require automatic equipment to determine and control the amount of strain for uniform results (without the danger of fracturing).

20.5 Forging

Forging involves shaping a material by impact using forging hammers or by pressure in forging machines (presses). It can be done with open dies, closed dies, isothermally, at slow rates, and at high rates. Because of its strain-rate sensitivity, however, forging of beryllium is more amenable to the use of presses rather than hammers, in that slower rates are obtained with presses. Related processes include radial forging, ring rolling, roll forging, rotary forging, and swaging. (Swaging refers to a progressive reduction in cross-sectional area, and corresponding lengthening, by the rapid impact of a revolving pair of mating dies in a swaging machine as the part progresses along the dies. Dies can be changed in the forging machine as necessary for further reduction of the part, or a series of machines with successively smaller die radii can be used.) The material being forged must have the capability to be deformed without fracturing. The brittle characteristics inherent in beryllium would make beryllium a difficult candidate for

swaging. One type of test suggested for evaluating the forgeability of beryllium consists of forging a right-circular cylinder with rounded edges and a height-to-diameter ratio of unity. If it can be forged to a height reduction of 60%, the material should be forgeable for making special shapes [Smugeresky 1986]. To avoid excessive preferred orientation, the amount of deformation should also be limited to 60%. Reductions less than 40% are preferred. Parts forged from HIPed materials show less anisotropy than those forged from VHP materials. The various pressing methods (VHP, HIP, CIP) now used to consolidate powders may be considered as pressure forging. These methods confine the metal in closed-die systems under essentially compressive conditions.

Forging is usually performed between 700 and 760 °C (1290 and 1400 °F), which is claimed to be at or slightly below the recrystallization temperature of beryllium [ASM 1979a]. It is also the temperature range where beryllium oxidizes at a slow enough rate to avoid the need for having elaborate safety measures against the toxicity of BeO. Higher forging temperatures can be used for billets encased in steel jackets, with thicknesses depending on the forging parameters. When encased, billets are forged at temperatures between 760 and 1065 °C (1400 and 1950 °F). Forging can be more readily accomplished by maintaining the part in a compressive mode. The necessary restraint can be achieved by using:

- Expandable support rings (ring-roll forming)
- Appropriate design of the dies
- Controlled forging procedures
- Only a welded steel jacket. When using a steel jacket, the shape of the billet must be such that it will be subjected to high restraint throughout the forging cycle [ASM 1979a].

The early forging studies were performed on beryllium powders that were canned in mild steel containers to minimize tensile stresses, prevent forging tears, and overcome the brittleness problem. Procedures used were somewhat analogous to those employed in making VHP block, namely, fill the container with powder, then degas, preheat to 538 °C (1000 °F), seal, and finally heat the container to 982 °C (1800 °F) (typically heated to between 870 and 1040 °C, or 1600 and 1900 °F, prior to forging). Compacting of the powder, as is done with hot pressed block, was not always performed. To ensure uniform flow of the beryllium and to minimize failure of the can, a high-temperature lubricant should be applied between the can and die surfaces. A schematic of the setup before and after forging is shown in Fig. 20.12 [Hayes 1979]. A significant development of contour is illustrated. After forging, the steel container is removed by machining or acid pickling. Mechanical properties obtained by powder forging, however, were inferior to those developed by forging a solid preform or billet. For example, the yield and ultimate tensile strengths of a powder-forged bowl were approximately 260 and 425 MPa (38 and 62 ksi), respectively, with elongations of approximately 6.5% [Hayes 1979]. Yield and ultimate tensile strengths developed by forging a solid material are typically over 350 and 550 MPa (51 and 80 ksi), respectively. However, the higher strengths are usually associated with reduced elongations.

Cladding was used in ring-roll forming, primarily to prevent forging tears. This was accomplished by rolling the beryllium against the cladding, so that the beryllium was kept under compressive stresses. The cladding also minimized die chill during the process. The preform consisted of a premachined, VHP hollow cylinder. Ring-rolling forming temperatures were between 790 and 850 °C (1455 and 1560 °F). Ring rolling is most applicable to relatively large-diameter seamless parts with heights equal to or less than the billet starting diameter. The process was used to manufacture 788 mm diameter by 330 mm high (31 by 13 in.) Minuteman spacer shells [Hayes 1979].

Because of the costs involved in can or clad forging, development efforts were directed more toward bare forging. In particular, efforts were focused on developing methods for reducing

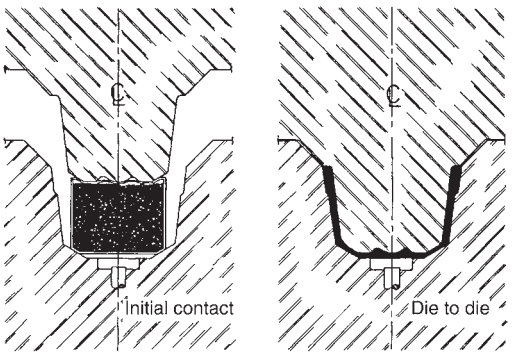

Fig. 20.12 Schematic illustration of forging canned powder. Left side shows canned powder prior to being forged. Right side shows forged part with can prior to removal from die. Source: Hayes 1979

tensile stresses during forging and producing more forgeable grades of VHP beryllium. Tooling was designed to choke the advancing flow of material in solid forgings, which had been a frequent cause of rupture. A different technique had to be developed for producing hollow shapes where significant flow of metal occurs when there is inadequate die-cavity restraint. Compressive restraint was introduced by placing a hot, mild steel expandable compression ring over the forging punch, as illustrated in Fig. 20.13 [Hayes 1979]. As the punch (A) is forced into the beryllium preform (B), which sits in the die cavity, the restraint of the compression ring (C) superimposes compressive stresses on the tensile stresses generated by the deforming metal. The steel ring is forced out of the die cavity by the back extrusion of the beryllium and deforms under the head of the die punch. Depending on the required restraint, the steel ring may be heated to a maximum temperature of 1093 °C (2000 °F).The expandable-ring restraint principle can be used by forging in two stages, as illustrated in Fig. 20.14 [ASM 1970]. Another example involves a two-stage metalforming process. In the first stage, a solid cylinder, with the die contour providing some choke restraint, is forged into the die cavity to produce the external configuration. In the second stage, the forged solid is back-extruded to develop a hollow using the compressive-ring restraint technique. A hollow cylinder with a tapered flat end was forged at 700 °C (1290 °F) by this two-stage operation. If one of the stages had involved forward extrusion, cladding of the beryllium would have been required for that part of the operation [Hayes 1979].

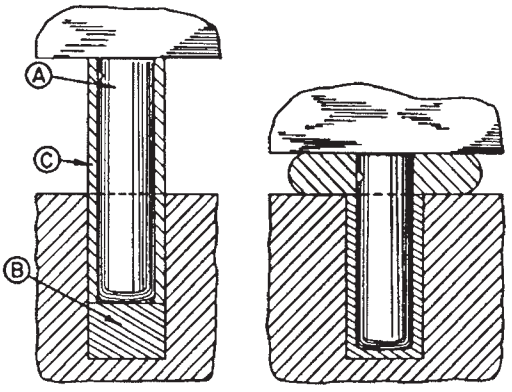

Fig. 20.13 Schematic illustration of hydrodynamic compressive restraint provided by a deformable ring. A, die punch; B, workpiece; and C, deformable restraint ring. Left is before and right is after forging. Source: Hayes 1979

In addition to cracks being attributed directly to the forging process, cracks may arise due to die chill (hot metal shrinking upon contacting the cold, unheated die) and during extraction from the dies as a result of the high stresses developed from the prior shrinking of the hot metal. Isothermal forging eliminates the die-chill problem. Proper forging lubrication will reduce any tendency for cracking of the workpiece, which can result from poor metal flow or galling of the dies. The workpiece may be etched in a $3\%H_2SO_4$-$3\%H_3PO_4$ acid solution and coated with a low-temperature, glass-frit-enamel lubricant. When additional forging operations are required, the cleaning and lubrication procedures are repeated.

As with any of the forming processes, unidirectional forging can lead to significant anisotropy. The term *triaxial forging* was introduced for procedures aimed at either reducing the degree of anisotropy or developing preferred directional properties, where maximum strength or ductility is required in only one direction. This may involve developing a preferred orientation in the preform, redundant forging, upset forging, reversing metal flow during forging sequences, and/or intermittent heat treating [Hayes 1979]. Figure 20.15 illustrates the effect of three different forging procedures on the properties of beryllium cones forged from VHP S-200 [Glenn and Hayes 1969]. Ten forging sequences were used in each case. One involved back extrusion and

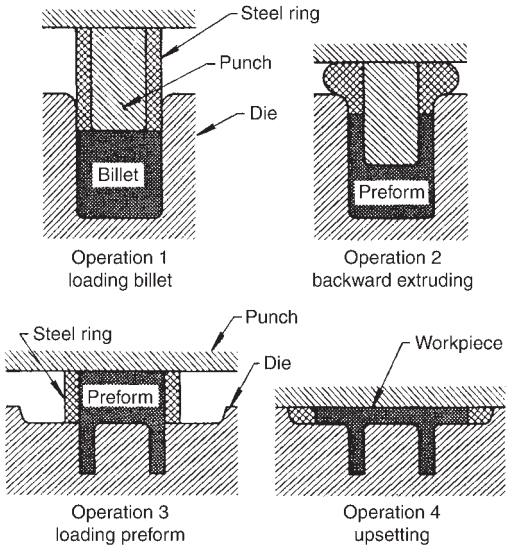

Fig. 20.14 Backward extruding and upset forging of a beryllium part using a deformable steel ring to support the billet during forging. Source: ASM 1970

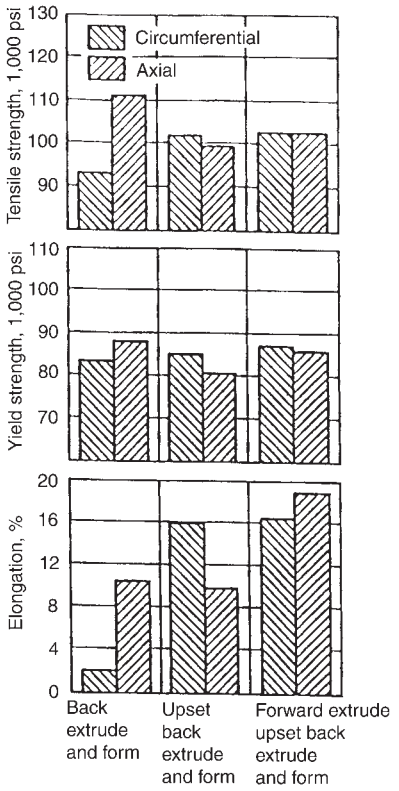

Fig. 20.15 Influence of forging combinations on mechanical properties of forged beryllium cones. Source: Glenn and Hayes 1969

forming; another involved upsetting, back extrusion, and forming; and the third involved forward extrusion, upsetting, back extrusion, and forming. An optimum combination of properties for both circumferential and axial directions is obtained for the third option.

20.5.1 Powder Forging

Powder forging (Fig. 20.12) refers to the process whereby beryllium powder is directly consolidated by forging rather than preconsolidating the powder by VHP or HIP. The forging procedure for the powder forging process entails fabrication of the container, usually a thin, mild steel welded assembly; container cleaning; powder inspection and blending; filling the container with powder; degassing and sealing; heating; and forging. The forger assumes the additional tasks of containerization, powder inspection, and handling but bypasses the need for separate powder compaction and subsequent inspection of the compact. A report of the process details the powder handling and inspection, the powder forging process and attendant experimentation, design criteria and limitations, and mechanical-property levels achieved [Orrell 1963a, b]. Powder evaluation included particle size distribution, chemistry, and 100% x-ray inspection. Canned powder assemblies were vented for degassing, preheated at 538 °C (1000 °F), and sealed. A vacuum could be used but normally was not considered necessary. The canned assemblies were heated to 982 °C (1800 °F) and forged using a pressure of 172 MPa (25 ksi).

The mechanical properties of powder-forged beryllium parts are reported generally at a level intermediate between those of parts produced by press sintering and those shaped by solid forging [Orrell 1963a, b].

20.5.2 Unclad Forging

The forging of unclad beryllium has been developed [Kosinski and Hayes 1966, Hayes and Yoblin 1962, Murphy et al. 1965, Hayes 1967]. This process has limited production requirements, high tooling costs, and directionality effects. Methods were developed for reducing the magnitude of tensile stresses during forging operations without the need to resort to cladding techniques. Higher-strength grades of VHP beryllium having improved forgeability were produced. Mechanical properties of wrought beryllium were increased and characterized with respect to microstructure, preferred orientation, and processing parameters. A variety of configurations were produced in sizes ranging from 25 to 788 mm (1 to 31 in.) diameter and included disks, rings, beams, hollow cylinders, hemispheres, hollow shafts, and cones. Certain shapes were amenable to direct forging without rupturing because tooling could be designed to essentially "choke" the advancing flow of metal as it was deformed and thereby limit the extent of tensile stresses developed [Hayes and Yoblin 1962]. Ruptures that occurred were caused by an excessive amount of metal movement in the rib area during the final forging operation and by use of one of the earlier high-strength grades of beryllium (I-400) that lacked favorable forgeability. These problems were correctable. Hollow shapes, however, entail significant degrees of reduction without the benefit of adequate die-cavity restraint, so that external means of providing compressive restraint were required to minimize or eliminate forging tears. The back extrusion of hollow cylinders was accomplished by using a hot mild steel compression ring.

Forging progresses with superimposed compressive force, provided by the plastic expendable mild steel sleeve, acting on the beryllium, thereby allowing the metal to be worked without generating severe tensile forces.

Application of different methods in a sequence of forging operations was used for two different purposes: to develop the required contour and to control or limit directionality effects [Kosinski and Hayes 1966]. In the initial forging operation, the tapered flat end is formed by forging a solid cylinder directly into the die cavity, using the natural "choke" of the configuration to provide the necessary restraint. Billet cladding was not required for either operation. Forging was conducted at 700 °C (1290 °F), which provided adequate warm work for meeting strength requirements, while at the same time ensuring adequate forgeability. The high elastic modulus, low density, and attractive wrought strength of beryllium generated considerable interest in the aerospace industry.

20.5.3 Forgeability Tests

A standardized forgeability test was developed [Hayes 1967] to qualify beryllium material prior to forging. A description of the test is included, since it not only defines the test but provides a general guide of typical billet preparation for forging. The forgeability test consists essentially of upset forging a representative sample of the lot of beryllium being qualified and determining the percentage of sound material yield after removal of defects. The standard specimen is a 50 mm diameter by 50 mm high (2 by 2 in.) solid cylinder having a 5 mm (0.2 in.) radius on the top and bottom edges. The specimens should have a machined surface of 64 rms or better and be etched in a 6% sulfuric acid solution to remove approximately 0.1 mm (0.004 in.) from all surfaces. The test billet is heated to 760 °C (1400 °F) and held at this temperature for 1 h prior to forging. It is then forged to a height reduction of 60% (20 mm, or 0.8 in.) between flat dies that are preheated to 425 ± 30 °C (800 ± 54 °F). A graphite-in-oil-type die lubricant is used. After cleaning and weighing, all forging defects are removed by machining in such a manner so as to provide the largest sound cylindrical disk from which a percentage of yield by weight can he calculated. The machined disks are inspected, using acid etch and dye-penetrant techniques, and are remachined if necessary to ensure removal of defects. The percent ratio of the weight of the rupture-free disk to the weight of the original billet is the forgeability index.

20.5.4 Anisotropy

The high degree of preferred crystallographic orientation in severely worked beryllium produces extremely attractive uniaxial or biaxial ductility, with values ranging beyond 20% tensile elongation. This effect is accompanied by very poor or no ductility in the true-transverse (short-transverse) structural direction. Tensile stress in the true-transverse direction is perpendicular to the [11$\bar{2}$0] slip direction and to the (0001) basal fracture plane, so that failure occurs in this direction with little opportunity for significant plastic elongation in the highly anisotropic condition.

Attempts to balance the preferred orientation by forging in essentially the three geometric planes were successful in changing the angular inclination of maximum preferred orientation and the degree of preferred orientation but could not approach elimination of preferred orientation. The technique referred to as triaxial forging was used for making a variety of shapes and entailed the use of redundant metalworking during one or more operations in the sequence of forging steps.

A seamless ring, rolled directly from VHP (randomly oriented) beryllium material, preferentially orients basal planes (0001) in the circumferential-axial plane of the ring. Since metal movement is restricted to the circumferential direction, highest tensile properties are developed in this direction (324 MPa, or 47 ksi, yield strength; 552 MPa, or 80 ksi, ultimate strength; and 8.5% elongation). Properties in the axial direction are also increased, since this direction also lies in the plane of preferred (0001) orientation. The ductility in the radial direction, although unmeasured in this instance, would be relatively low due to the 4X random basal plane orientation in the axial-circumferential geometric plane.

When circumferential ring rolling was used after blank upsetting, tensile properties increased to 380 MPa (55 ksi) yield strength and 600 MPa (87 ksi) ultimate tensile strength in the circumferential (now the preferred) direction. Axial tensile properties increased to 345 MPa (50 ksi) ultimate strength with 1% elongation.

An important aspect of the triaxial (redundant) forging concept is that the redundant metalwork imposed is not only time-consuming and

costly, due to required additional tooling and operations, but seriously limits the geometries and degree of contour refinement possible, such that metal input may significantly exceed that used by machining directly from VHP block. The previous investigations showed decreases in the degree of preferred orientation by forging and/or thermally treating at the high limit of the temperature range studied (815 °C, or 1500 °F).

Because beryllium lacks impact resistance, it is expected that uniformity and texture control can be improved, so that a moderate incremental improvement in mechanical properties can be obtained.

The effect of deformation processing parameters on microstructure, crystallographic orientation, impact resistance, and tensile properties has been correlated. Beryllium samples taken from both uniaxial (forward extruded) and biaxial (forward extruded followed by upset forged) forgings have been evaluated for various combinations of uniaxial and biaxial deformation [Floyd 1972b]. Variable parameters correlated included amounts of reduction, forging temperature, and intermediate and postforging thermal treatments.

Yield strength was found to be mainly dependent on forging temperature, amount of reduction, and postforging thermal treatment, while tensile elongation was affected principally by the amount of deformation and test direction. Impact resistance remained consistently low and completely insensitive to the different combinations of thermal-mechanical processing.

The principle of triaxial forging was demonstrated by the development of a forgeability tolerance graph depicting the billet-cracking boundary at approximately a 690 MPa (100 ksi) compressive yield strength as a function of forging temperature and height reduction, as illustrated in Fig. 20.16.

20.6 Extrusion

Beryllium has been extruded into rods, tubes, and structural shapes [Siergiej 1965]. Extrusions can be produced with consistent mechanical properties and within commercial tolerances. They are typically used in aerospace and satellite applications. Input billets for extrusions are usually machined hot pressed blocks. Unsintered pressed billets can also be extruded. The extrusion billets are normally jacketed in low-carbon steel cans with shaped nose plugs and are hot extruded through a steel die between 900 and 1065 °C

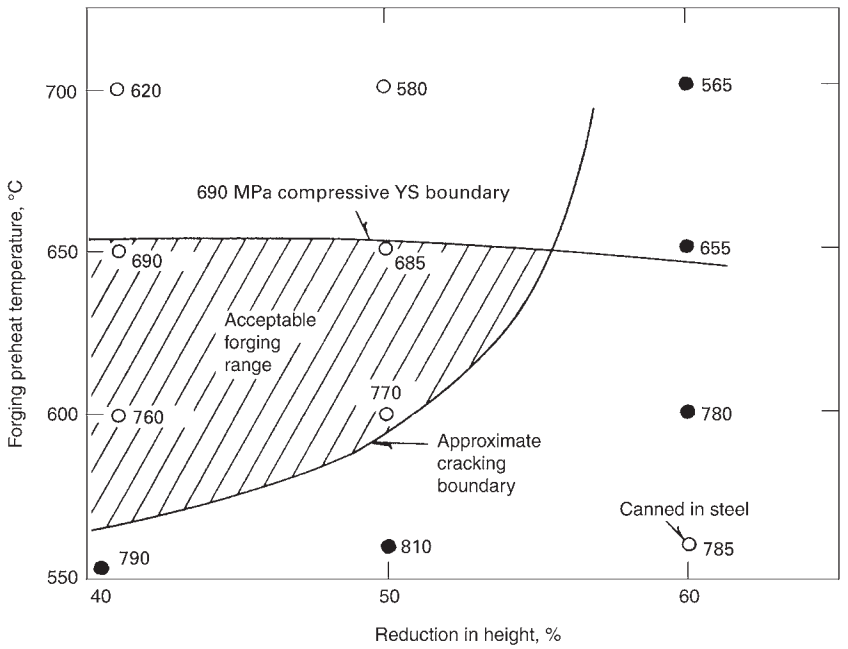

Fig. 20.16 Forgeability tolerance found by compressing solid cylinders of high-strength beryllium at various temperatures to various reductions in height. The compression yield strength of samples taken from the resulting forgings is listed near each data point in units of MPa. Source: Floyd 1972b

(1650 and 1950 °F). Warm extrusions are produced at 400 to 450 °C (750 to 840 °F). Carbon steel jackets are chemically removed from the beryllium [Marder 1991]. Beryllium powders can also be extruded [Marder 1998a].

The type of tooling and equipment necessary to accomplish beryllium extrusion is shown in Fig. 20.17. The dies are usually made of either hot work steels, high-speed steels, or cart high-speed steels.

A schematic for canned extrusion of beryllium is shown in Fig. 20.18 [Loewenstein 1979]. A soft "cutoff" block such as graphite or copper, which is also extruded, is placed between the beryllium and steel dummy block and is cut at the end of a run. This avoids the need to remove the toxic beryllium from the dummy block at the end of a run. Warm extrusions are also produced unclad or bare using very low extrusion speeds, low reduction ratios, and special solid-film lubricants that strongly adhere to the billet. The main advantage is the ability to produce small, complex shapes with very good dimensional control [Loewenstein 1979].

All early attempts at extrusion of unclad or bare beryllium at elevated temperatures and conventional speeds and lubricants failed due to galling and die washout. Limited success with bare extrusion was later obtained by using (1) a low extrusion temperature (between 400 and 450 °C, or 750 and 840 °F), (2) very low extrusion speeds, (3) low reduction ratios, and (4) special solid-film

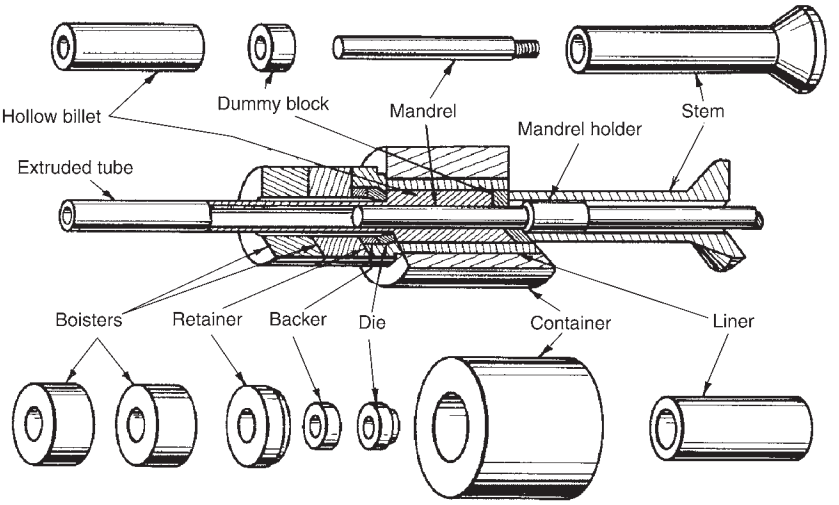

Fig. 20.17 Tooling and setup for the extrusion of beryllium. Courtesy of Brush Wellman Corp.

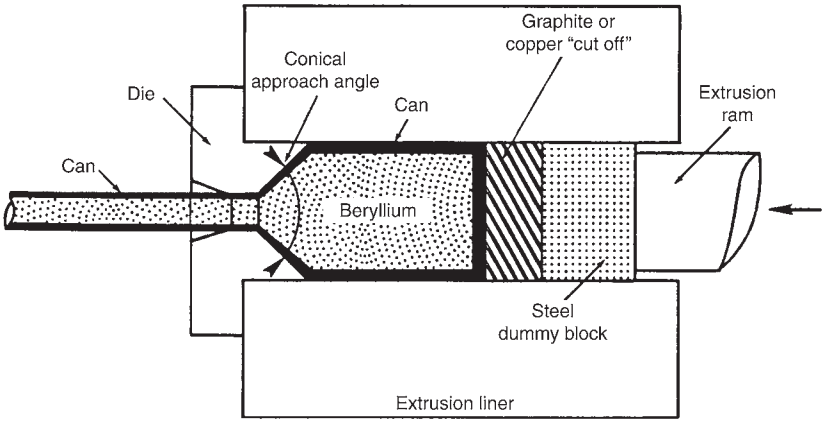

Fig. 20.18 Schematic illustration for canned extrusion of beryllium. Source: Loewenstein 1979

lubricants strongly adhering to the billets [Sawyer et al. 1950, Loewenstein et al. 1955, Darwin and Buddery 1960]. Small rods, shapes, and tubes have been made by the warm extrusion process. The principal advantage of the bare or warm extrusion process is the ability to produce complex shapes with very good dimensional control.

Canning overcomes the strong tendency of beryllium to gall or stick to the extrusion tools. Furthermore, if not canned, abrasive oxides that score tooling would form at the elevated temperatures (above 600 °C, or 1110 °F). Also, when extruding as-cast beryllium, a significant difference in deformation behavior may occur in different regions of the billet. This arises from the coarse-grained structure in the as-cast ingot and the differences in the crystallographic orientation of individual grains relative to the extrusion direction.

Carbon steel is the preferred canning material. It has approximately the same extrusion constant (flow resistance) as beryllium at extrusion temperatures; it does not form low-melting eutectics with beryllium below 1165 °C (2130 °F); it has relatively low solubility in beryllium (0.9% at 1000 °C, or 1830 °F), decreasing rapidly with decreasing temperature; it has reasonable lubricity; it does not stick to tools; and it can be removed from the beryllium by pickling in nitric acid [Loewenstein 1979]. A conical-approach extrusion die (Fig. 20.18), good lubrication, tightly fitting tools, and avoidance of the formation of a skull (shell) in the extrusion liner provide the streamlined metal flow that is necessary for extrusion of beryllium. The main difference between exrusion dies for beryllium extrusion and conventional dies is the requirement of a conical approach to the die aperture. For complex shapes, the approach must be sculptured, shaping it with special attention so as to promote the flow of the canning material into areas where the can may become extremely thin. This aspect of beryllium extrusion definitely requires more “art” than science and relies heavily on the experience of the tool designer.

With the advent of the canned-extrusion technique, it became practical to extrude beryllium in the three available forms: castings, loose powder, and consolidated powder. Cast billets generally have larger grains and lower oxygen content than powder-product beryllium. The large grains, combined with the pronounced crystal anisotropy of the metal, result in a rough, barklike surface after removal of the carbon steel can on shapes extruded from castings compared to the smooth surface of products extruded from consolidated powders. In addition, the grain boundaries of such cast material are relatively weak. Such grain boundaries have a tendency to crack unless they are heavily worked during the compressive part of the extrusion deformation. This deficiency means that cast beryllium must be extruded at relatively high reduction ratios to avoid defects. The extrusion of cast material may become even more of an issue with high-purity beryllium ingot. When extruding loose powder, the billet is compressed close to theoretical density before the metal begins to issue from the die. During the consolidation part of the extrusion step, the billet shortens and the can has a tendency to form folds that, when extruded, would form a defective product [Loewenstein et al. 1955]. This folding is avoided if the powder in the billet has a density over 60%. Therefore, loose powder (which has a pour density of only 30%) is precompacted in the extrusion can in stepwise layers. Special precautions are needed to avoid the abrading of the steel can and the contamination of the beryllium with the canning material. Most of the beryllium extruded today (2008) uses high-density, hot pressed billets as starting stock. This practice avoids all of the problems associated with the extrusion of cast material and of loose powder.

The can for a cylindrical billet consists of outer seamless carbon steel tube and two end plugs. The carbon steel end plugs are 3 to 6 mm (0.125 to 0.250 in.) thick. A groove to facilitate welding to the outer can may be provided. Some producers feel that the front end plug should be in the form of a cone corresponding to the cone of the extrusion die; the end plug is a disk. Other producers feel that a simple flat disk gives equally good results. For a tubular extrusion, the beryllium billet is a hollow cylinder, and a carbon steel can is placed on the inside diameter and welded to the end plates.

The practice of sealing the billets within the cans requires careful evacuation through a tube provided at one end plug. In other cases, the can is simply welded tightly without evacuation. Beryllium is sometimes extruded with intentionally incomplete welding of the end plugs. The choice seems to depend on the density of the starting billet and the importance attached to control of oxygen and nitrogen. A partially welded can and consequent surface oxidation during heating appear to minimize alloying between the can and the beryllium during extrusion [Loewenstein 1979].

The relationship of the thickness of the canning material in the billet to that of the shape after extrusion is governed by two simple principles that apply to all streamlined extrusions: (1) the ratio of the cross-sectional area of the canning material to the cross-sectional area of the billet remains constant, and (2) the cross-sectional area of the canning material after extrusion is equal to the cross-sectional area of the canning material after extrusion divided by the reduction ratio, *R*, where $R =$ (cross-sectional area of billet)/(cross-sectional area of cylindrical die). In the case of a tubular extrusion, the relationship is slightly more complicated.

In the case of a complex shape, such as a "U," the thickness of the cladding is more difficult to determine. The fixed relationship between the total cross-sectional areas of the canning and that of the beryllium is still maintained, but the average can thickness of the extruded section is less than it would be for a corresponding cylindrical extrusion by the ratios of the perimeter of the section to the circumference of a cylinder of equal cross section. Those areas that are difficult to feed, such as the inside of the U-shapes, are likely to be starved of cladding. The cladding may become so thin that it may lead to breakthrough, contact between tools and beryllium, and failure of the extrusion [Siergiej and Nerses 1961, Christensen and Wells 1962, Jenkins et al. 1964]. Increased clad thickness and special die design aimed at channeling canning into the starved areas are used to overcome this potential problem.

Extrusion temperatures for beryllium range between 840 and 1066 °C (1545 and 1950 °F). Temperatures at the lower end of this range are preferred because higher strengths are attainable, since the lower temperatures produce finer grain sizes. Reduction ratios should be above 9 to 1 and not exceed 60 to 1. Low reduction ratios may not develop required properties, while high reductions may lead to excessive alloying between the can and beryllium due to self-heating [Loewenstein 1979]. The pressure required to produce streamlined flow is given by the following expression:

$$P = \mathrm{K} \ln R \qquad \text{(Eq 20.6)}$$

where *P* is the pressure, *R* is the reduction ratio (cross section of billet/cross section of extrusion), and K is the extrusion constant. The constant represents resistance to deformation and is based on past experience for a specific temperature. It can be used as a guide for a specific operating condition for simple shapes. The value of K will vary with temperature, type of material, extrusion shape, and operating parameters. The dependence of the extrusion constant on temperature is shown in Fig. 20.19 for a number of materials. The operating parameters and extrusion shapes were not given [Loewenstein 1979].

20.6.1 Mechanical Properties of Extruded Beryllium

Large differences in mechanical properties are obtained between the directions perpendicular and parallel to the extrusion direction. Increased reduction ratios lead to increased degrees of preferred orientation of the basal plane being parallel to the extrusion direction.

Although the longitudinal yield and ultimate strengths may increase significantly, they are only increased moderately or may even decrease in the transverse direction, depending on the degree of preferred orientation that is obtained. Elongations would increase in the longitudinal direction and decrease in the transverse direction. An example of such property differences for drawn beryllium wire is illustrated in Table 20.7 [Brush Wellman 2001, Loewenstein 1979]. A claim was made that up to 20% ductility can be reliably obtained with beryllium extrusions made from commercial-purity powder billets [Loewenstein 1979].

The effect of reduction ratio on the room-temperature tensile properties of a VHP beryllium, warm extruded at 425 °C (800 °F) and annealed at 750 °C (1380 °F), is shown in Fig. 20.20. The data were published in a review paper in 1954 [Beaver and Wikle 1954]. A large early increase in strength was obtained with increasing reductions, with a peak elongation of approximately 10% at an extrusion ratio of approximately 2 to 1. Figures 20.21 and 20.22 show the effect of extrusion ratio on strength and elongation, respectively, as a function of temperature for VHP beryllium that was hot extruded between 1050 and 1100 °C (1920 and 2010 °F) [Beaver and Wikle 1954]. Although there is a threefold difference in reduction between the highest (38 to 1) and lowest reduction (12.4 to 1), the ultimate tensile strength appears to be affected only slightly by this difference in reduction. At low temperatures, the strength increased and ductility decreased with increased hot-extruded reductions. Reversals on the effect

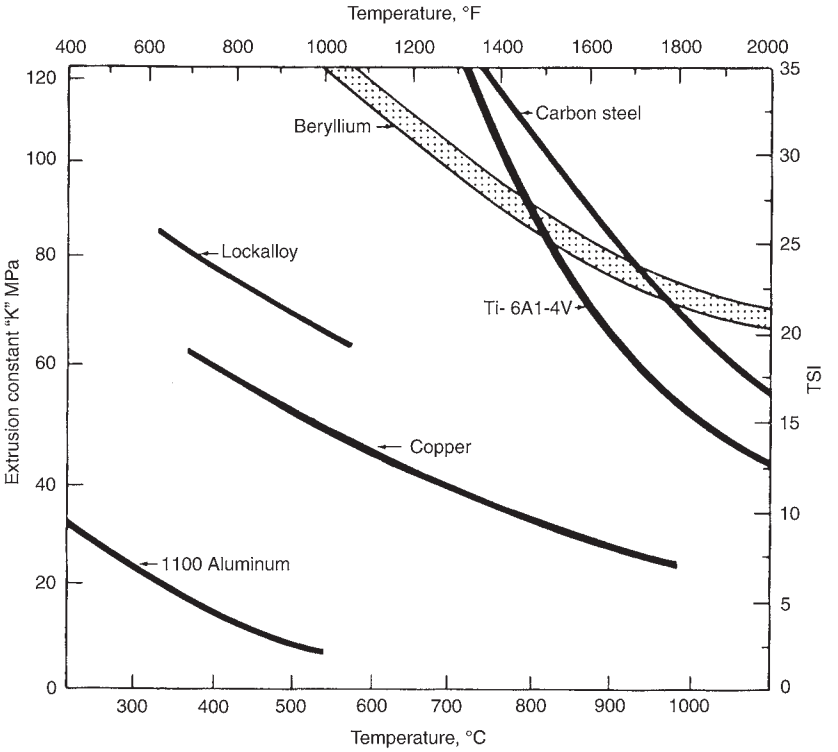

Fig. 20.19 Extrusion constant, K, as a function of temperature for beryllium and other related materials. Source: Loewenstein 1979

Table 20.7 Extruded beryllium tensile properties

Material		Longitudinal			Transverse		
Shape	Diameter, cm	Yield strength, MPa	Ultimate tensile strength, MPa	Elongation, %	Yield strength, MPa	Ultimate tensile strength, MPa	Elongation, %
Rod(a)	2.54–6.35	345	745	10	372	434	0.6
Rod(a)	0.95–1.27	414	765	10	. . .	. . .	. . .
Tubing(a)	16.5 outside diameter (OD) to 9.40 inside diameter (ID)	352	655	13	324	414	0.7
Tubing(a)	3.05 OD to 2.03 ID	434	800	9	. . .	. . .	. . .
Tubing(b)	. . .	345	448	5.0	207	310	0.75

(a) First four shapes reported for S-200; typical values are listed. Source: Brush Wellman 2001. (b) Grade and size are not reported; values indicated are minimum values. Source: Loewenstein 1979

of the amount of reduction on both strength and elongation occurred as the temperature increased. The authors state that "it is not clear why this behavior should occur as the reversals take place at temperatures considerably below the recrystallization temperature, which is above 1000 °C (1830 °F) for beryllium." (The *Metals Handbook* indicates the recrystallization temperature for beryllium is between 725 and 900 °C, depending on the amount of cold work and annealing time, and the hot working temperature is from 800 to 1100 °C. In addition, the recrystallization temperature would be affected by the type and content of impurities.) Furthermore, the reversal along the strength and elongation curves takes place at different temperatures: 350 °C (660 °F) for strength and 200 °C (390 °F) for elongation.

Comparisons between the transverse and longitudinal ultimate tensile strengths and elongations of the hot-extruded VHP beryllium as a function of temperature are shown in Fig. 20.23 and 20.24. Curves A and B were obtained from comparable beryllium extrusions, while the C curves were obtained from a coarse-grained material of lower strength [Beaver and Wikle

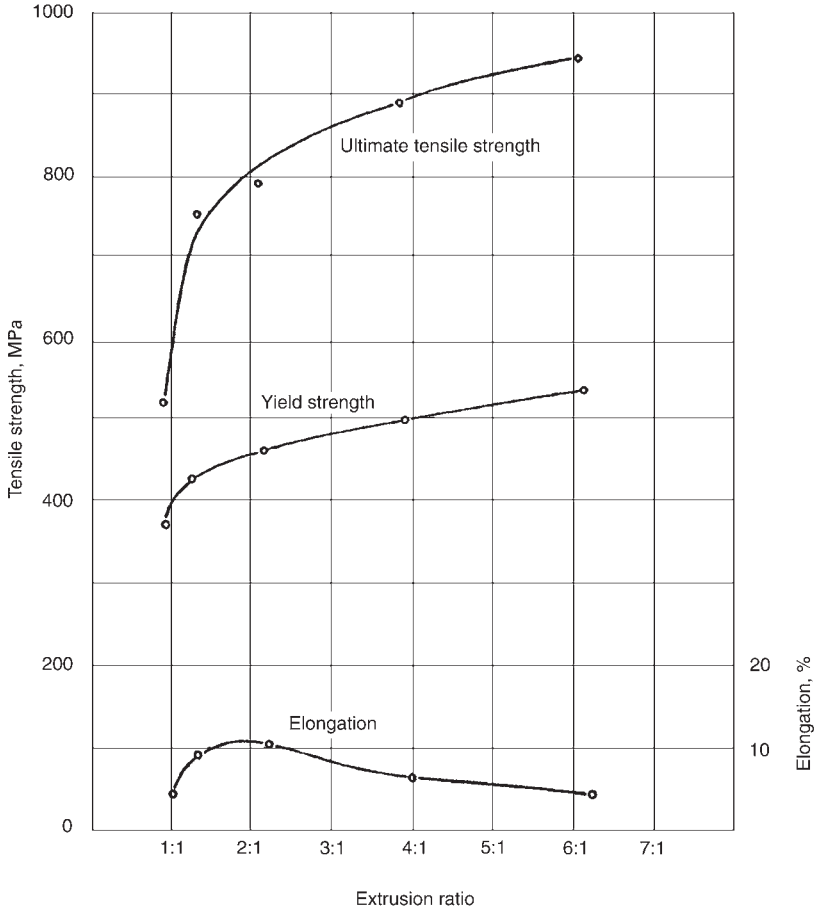

Fig. 20.20 Effect of extrusion-reduction ratio on the tensile properties of vacuum hot pressed (QMV) beryllium warm extruded at 425 °C (800 °F) and annealed Source: Beaver and Wikle 1954

1954]. The large differences in strength seen at room temperature gradually decrease with increasing temperature. The data merge at approximately 450 °C (840 °F), indicating that the influence of preferred orientation disappears at elevated temperatures. Similar behavior was shown for the warm-extruded condition. The convergence of longitudinal and transverse properties is the result of additional slip systems beginning to operate with increasing temperature. Convergence of the elongation also occurs, however, to a lesser degree than that exhibited by the ultimate tensile strength. It is interesting to note that the peak in elongation at approximately 250 °C (480 °F) that is frequently observed only occurs for the longitudinal direction (curve A). A small ductility peak occurs in the transverse direction (curve C) for the coarser-grained material at 500 °C (930 °F); this temperature roughly corresponds to where a rapid decrease in strength is initiated.

20.6.2 Extrusion Conditions and Limitations

Some general factors controlling the extrusion process are discussed subsequently. The pressure, P, required to extrude a metal in streamlined flow is given by the expression:

$$P = \mathrm{K} \ln R \qquad \text{(Eq 20.7)}$$

where R is the reduction ratio (cross-sectional area of billet divided by cross-sectional area of extruded shape), and K is the extrusion constant, which is a function of the material and the billet temperature. The extrusion force, F, determining the required press capacity is calculated

by multiplying the extrusion pressure, *P*, by the cross-sectional area, *A*, of the billet:

$$F = A \times P = AK \ln R \qquad \text{(Eq 20.8)}$$

The extrusion process is limited by the following considerations:

- The extrusion temperature should not exceed 1055 °C (1950 °F), and lower temperatures are more desirable. In recent years, extrusion temperatures of 843 to 954 °C (1550 to 1750 °F) generally have been used for production.
- The unit pressure, *P*, for most extrusion tools should not exceed 1240 MPa (180 ksi), although under special conditions, higher pressures can be accommodated.
- The reduction ratio, *R*, should be greater than 9 and should not exceed 60. Lower reduction ratios are uneconomical and will not develop full properties. Higher reduction ratios lead to excessive alloying between the can and beryllium due to self-heating.
- The diameter of the circumscribed circle around a flat or a complex shape should not exceed three-quarters of the diameter of the extrusion billet. Sections having wall thickness of less than 3 mm (0.125 in.) require special techniques.
- The ram speed for extrusion of beryllium varies from 76 to 127 cm/min (30 to 50 in./min).
- The extrusion press should have the necessary force and speed to carry out the extrusion operation.

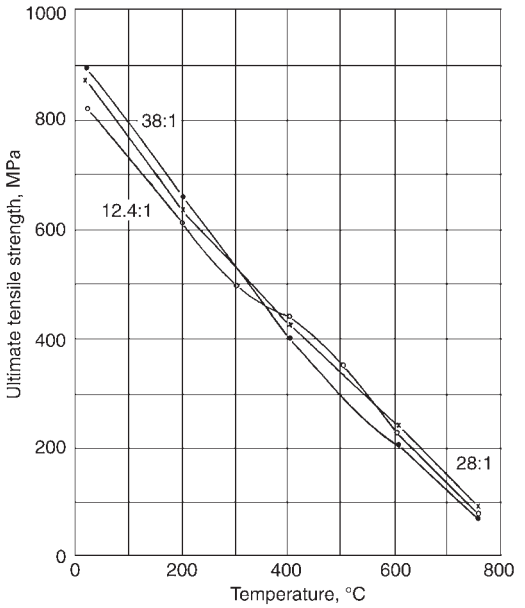

Fig. 20.21 Effect of extrusion-reduction ratio (12.4:1, 28:1, 38:1) on ultimate tensile strength as a function of temperature for vacuum hot pressed (QMV) beryllium hot extruded between 1050 and 1100 °C (1920 and 2010 °F). Source: Beaver and Wikle 1954

20.7 Wire Drawing

Beryllium wire combines the low density, high modulus of elasticity, high thermal conductivity, and high specific heat of beryllium with higher strength levels than are available in other mill forms.

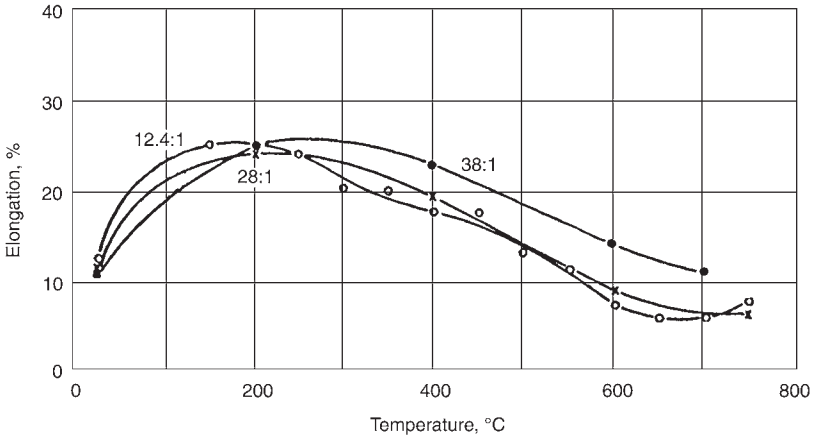

Fig. 20.22 Effect of extrusion-reduction ratio (12.4:1, 28:1, 38:1) on elongation as a function of temperature for vacuum hot pressed (QMV) beryllium hot extruded between 1050 and 1100 °C (1920 and 2010 °F). Source: Beaver and Wikle 1954

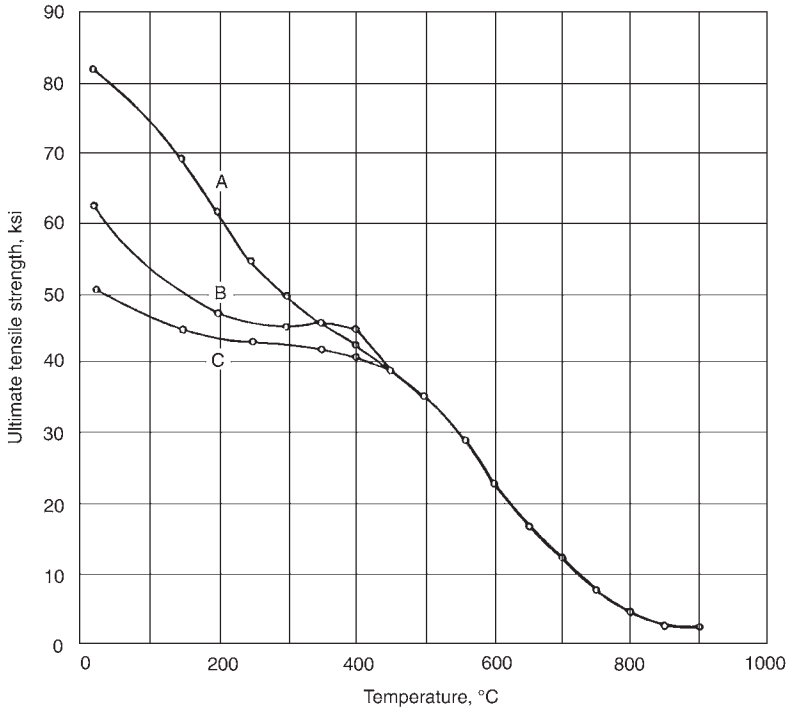

Fig. 20.23 Comparison of longitudinal and transverse ultimate tensile strength as a function of temperature of vacuum hot pressed (QMV) beryllium hot extruded at 1050 °C (1920 °F). Curves A (longitudinal) and B (transverse) are for comparable beryllium extrusions; curve C (transverse) was obtained for a coarser-grained, lower-strength extruded beryllium. Source: Beaver and Wikle 1954

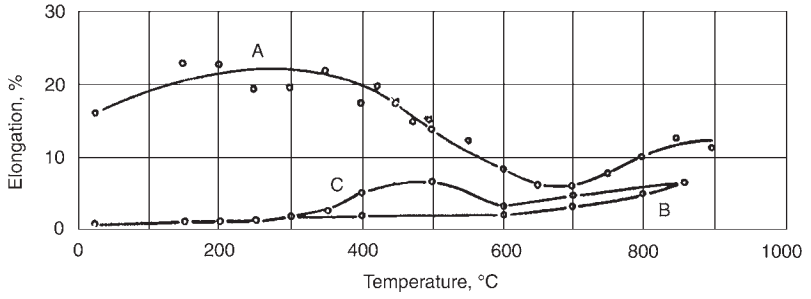

Fig. 20.24 Comparison of longitudinal and transverse elongations as a function of temperature for vacuum hot pressed (QMV) beryllium hot extruded at 1050 °C (1920 °F). Curves A (longitudinal) and B (transverse) are for comparable beryllium extrusions; the C (transverse) curve was obtained for a coarser-grained, lower-strength extruded beryllium. Source: Beaver and Wikle 1954

20.7.1 Technology

Drawing is the reduction of the cross section of a shape (rod, bar, tube, or wire) by pulling it through a die. A number of successive dies may be required to achieve the final dimension. It allows obtaining closely controlled dimensions in long products with constant cross sections. Excellent as-drawn surface finishes are attainable. A number of drawing methods are illustrated in Fig. 20.25.

Excessive draw force can lead to unstable deformation. For practical reasons, the draw force is usually limited to approximately 60% or less of the as-drawn flow stress, giving reductions of approximately 15 to 35%. Depending on the product, much larger single reductions could be attainable by extrusion [ASM 1988d]. For example, a

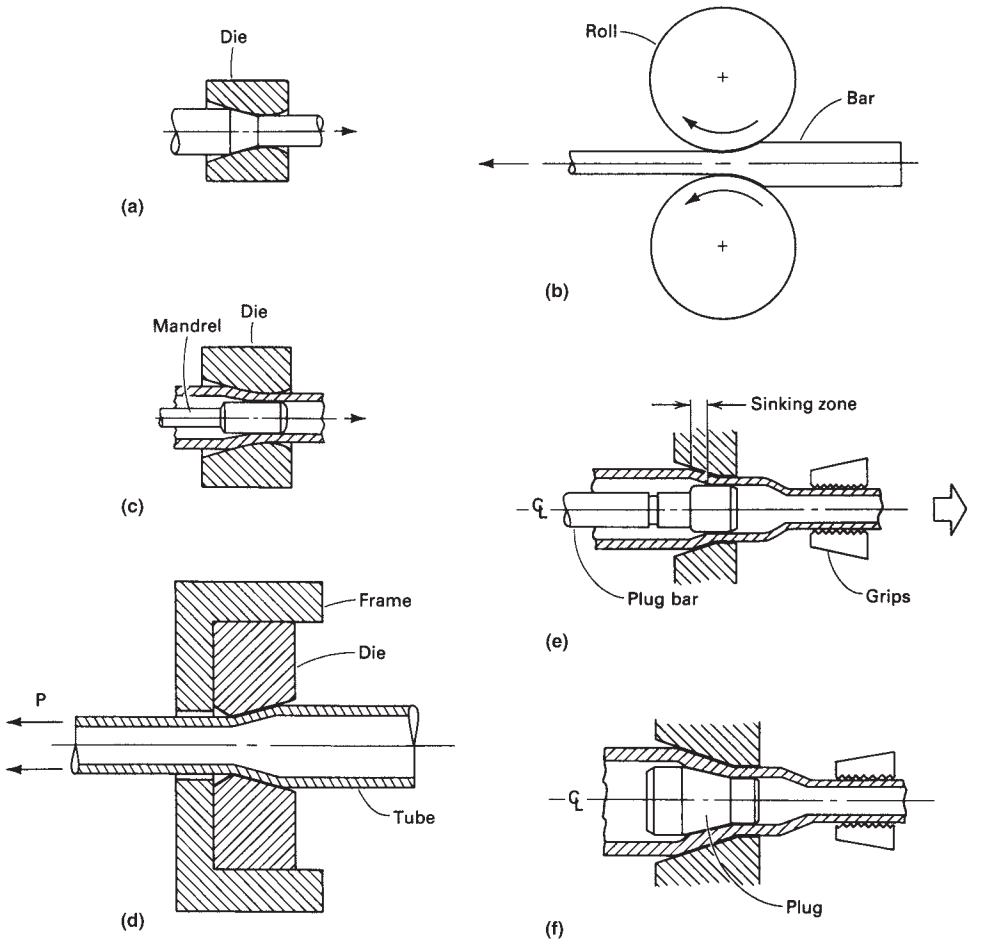

Fig. 20.25 Schematic examples of some drawing methods: (a) wire drawing, (b) bar drawing with undriven rolls, (c), (d), (e), and (f) tube drawing. View (d) shows drawing without any mandrel, (e) with fixed plug, and (f) with floating plug if a fixed plug will stretch or break. Source: ASM 1988d

reduction in cross section of 83% (100 to 17), which can be accomplished by one extrusion pass, would require five drawing passes on corresponding die sizes, assuming 30% reduction per pass. Wire drawing would be used for production of large quantities of small-diameter wire (e.g., 0.01 mm diameter), requiring excellent dimensional control with good surface finish.

Beryllium wires have been produced to sizes down to 0.125 mm (0.005 in.) diameter in 3000 m (9900 ft) continuous lengths using standard equipment. Smaller lengths of 0.025 mm diameter filaments have also been produced. Beryllium undergoes extensive deformation when drawn without intermediate anneals from 9.5 to 0.125 mm (0.4 to 0.005 in.) diameter [Denny 1979a]. This reduction in cross-sectional area is a ratio of 5776 to 1.

The material is produced by warm drawing of ingot or hot pressed stock at 400 to 425 °C (750 to 800 °F). In each case, the production of long, continuous lengths of fine filaments requires material of excellent quality, and close controls are maintained on chemistry and radiographic cleanliness.

Cylindrical billets of ingot or hot pressed block origin, for example, 8.5 cm (3.3 in.) in diameter and 20 cm (8 in.) long, are encapsulated in steel jackets and hot extruded at 950 to 1065 °C (1740 to 1950 °F) to yield 9.5 mm (0.4 in.) diameter rod. The material is dejacketed by pickling in nitric acid, straightened, and etched in $HF\text{-}HNO_3$ solution to yield the drawing stock.

Wire is produced on standard equipment, but the drawing temperature of 400 to 425 °C (750 to 800 °F) presents special problems. Die jaws

must be insulated and provisions made to ensure heat retention during all stages of processing. Special equipment features may include shock absorbers, automatic spoolers, and level winders; precautions are taken to prevent tangling, which can be a source of breakage. Drawing speeds of up to 60 m/min (195 ft/min) are employed. Tungsten carbide dies with an included angle of 12.5° are normally used for diameters above 0.5 mm (0.02 in.), and diamond dies are used at smaller diameters. Molybdenum disulfide and fine graphite powder lubricants are employed during drawing. A reduction per pass of 12.5% is normal, although 25% reductions are feasible.

Beryllium has been drawn bare using a molybdenum disulfide lubricant, but a nickel jacket is often preferred to circumvent galling and seizing. The jacket is placed on the stock during the initial drawing pass by co-drawing and removed at final gage by pickling in concentrated nitric acid. Points for die threading are prepared by pickling the end of the wire in sulfuric acid.

Three types of equipment are used for different wire-size ranges: processing from 9.5 to 1.85 mm (0.4 to 0.07 in.) diameter is conducted on a mechanical drawing bench, from 1.85 to 0.50 mm (0.07 to 0.02 in.) diameter on a capstan-type drawing machine, and below 0.5 mm (0.02 in.) diameter on multiple-pass drawing machines. The latter may consist of as many as 12 drawing stations with individual dies packed in graphite powder. Drawing assemblies are heated to 400 to 425 °C (750 to 800 °F) in all cases.

The previously described procedures represent commercial practice and yield long, continuous lengths of beryllium wire, for example, 3000 m (9900 ft) at 0.125 mm (0.005 in.) diameter. One pound of beryllium wire at 0.125 mm (0.005 in.) diameter is equivalent to a length of 19,400 m (12 miles).

Internal defects, generally known as chevron-type defects, may be produced by improper beryllium drawing procedures. This defect has been observed in other materials and is often associated with low reductions in area and certain die configurations. These, in combination, cause tensile stresses to be generated along the centerline during or immediately after deformation. Inadvertent temperature fluctuations below the desired working temperature can also promote the formation of centerline defects. These may be observed during the etch-pointing operation, wherein the wire breaks away nonuniformly into the etching solution.

Beryllium wire may corrode when stored under conditions of high humidity, and best practice is to store and ship the material in desiccated containers. Exposure to the atmosphere for short periods of time does not adversely affect the material.

Resistance butt welding of beryllium wire is feasible, and flash from the welding operation may be removed by gently abrading the joint with emery paper. Butt welding has been used to produce long lengths of wire at final gage but has not proved feasible as an in-process step to repair breaks during drawing operations. Long columnar grains, for example, 7 by 64 μm, form in the heat-affected zone during welding, and these are associated with reduced joint efficiency. The tensile strength of butt welds in wire of electrolytic flake origin varied from 345 to 690 MPa (50 to 100 ksi), whereas joints in low-oxide wire of thermally reduced origin exhibited tensile strengths of 125 to 200 MPa (18 to 29 ksi) [Denny and Meyer 1966a, b].

Hydrostatic extrusion drawing has been studied as a method for producing beryllium wire [Richardson et al. 1970]. A plated copper cladding and castor oil hydraulic fluid permitted three sequential 60% reductions at 150 °C (300 °F). Lengths of up to 670 m (2200 ft) were produced at drawing speeds in excess of 600 m/min (1970 ft/min). The work was of a prototype nature, and additional development work is required.

Stretch straightening of annealed wire has been shown to be feasible. A camber less than 20 mm/m can be achieved by passing as-drawn nickel-clad wire through a rotary straightener.

20.7.2 Materials

Because of its enhanced purity level and cleanliness, providing greater drawing reliability, electrolytic flake is the preferred beryllium source. The high purity resulted in a drop in strength and an increase in ductility. Attempts were made, unsuccessfully, to increase strength by additions of BeO. Additions of a large number of intermetallic compounds as dispersions were also investigated. These insoluble dispersions (oxides and intermetallics) segregated into striations running parallel to the drawing direction, causing a concurrent decrease in drawability [Denny 1979a].

Ingot-origin wire has a rough surface after jacket removal, caused by nonuniform deformation of the relatively coarse beryllium grains.

A chemical polishing procedure that produces a substantial improvement in surface quality has been developed [Hoffmanner 1965]. A preferred polishing solution contains 450 mL phosphoric acid, 25 mL sulfuric acid, and 52 g of chromic anhydride; immersion of beryllium wire in this solution for 15 s at 120 °C (250 °F) results in the removal of 0.0125 mm from the wire diameter, with greatly improved surface smoothness. It has been reported [Soltis 1962] that good wire ductilities were achieved by chemical milling below 0.0625 mm diameter, as evidenced by the necking of tensile specimens; the effect was not confirmed by tensile elongation values, however. Wire is normally used in the as-drawn condition and is not chemically polished for most applications [Denny 1979a].

20.7.3 Mechanical Properties

Beryllium undergoes extensive plastic deformation when drawn without intermediate anneals from 9.5 to 0.125 mm (0.4 to 0.005 in.) diameter. This corresponds to a reduction in area of over 5000 to 1. Ultimate and yield strength levels increase progressively until the wire is reduced to a diameter of approximately 0.75 mm (0.03 in.). The strength then remains approximately constant on further reduction. Typical tensile properties of as-drawn 0.125 mm diameter ingot-source wire are 1030 MPa (149 ksi) ultimate, 895 MPa yield (130 ksi), and 3.7% elongation.

Higher strength levels can be achieved with starting materials prepared from hot pressed powder-source block. Material of electrorefined origin is best, since the associated high-purity level results in excellent drawability. The highest mechanical-property values for 0.125 mm (0.005 in.) diameter wire were obtained by drawing electrorefined origin block to 0.25 mm (0.01 in.) diameter at 425 °C (800 °F) and then further drawing to 0.125 mm (0.005 in.) diameter at 205 °C (400 °F) [Murphy and O'Rourke 1964]. The resultant tensile properties were 1570 MPa (228 ksi) ultimate, 1170 MPa (170 ksi) yield, and 2.1% elongation. Attempts to achieve an ultimate tensile strength of 2070 MPa (300 ksi) by dispersion and solid-solution strengthening additions to beryllium have been unsuccessful [Murphy and O'Rourke 1964, Carson 1969].

In general, heat treatment at 590 to 700 °C (1095 to 1290 °F) enhances the room-temperature

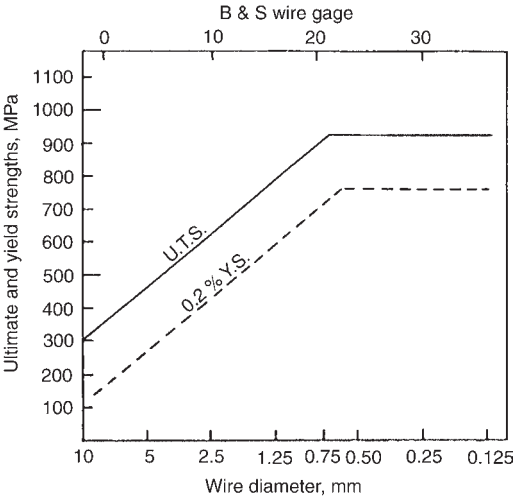

Fig. 20.26 Yield and ultimate tensile strengths of beryllium wires as a function of reduced wire diameter after successive reductions without any intermediate anneals. Source: Denny 1979a

ductility of wire, with concurrent reduction in strength level. Tensile elongations of 11 to 17% were observed after heat treatment of ingot-source wire at 650 °C (1200 °F) [Denny and Meyer 1966b]. The tensile strength was concurrently reduced from 1200 MPa (174 ksi) to 690 to 790 MPa (100 to 115 ksi). The electrical conductivity of beryllium wire varies from 36.6 to 44.8% IACS. The highest values of conductivity are associated with heat treatments of 15 to 30 min at 540 to 760 °C (1005 to 1400 °F).

Yield and ultimate tensile strengths as a function of the reduction of wire diameter are shown in Fig. 20.26. Starting with a diameter of 9.5 mm, the curves indicate that the strengths increase progressively with reduction until a diameter of approximately 0.70 mm is reached (reduction of 184 to 1), with the strengths remaining unchanged with further reduction [Denny 1979a]. In one study, maximum yield and ultimate tensile strengths of 1170 and 1570 MPa (170 and 228 ksi), respectively, with an elongation of 2.1% were obtained by drawing electrorefined-origin block. Heat treatment will generally increase ductility, with a concurrent reduction in strength. Results from different time-temperature treatments are seen in Table 20.8 [Denny 1979a].

20.7.4 Microstructure

The reversals in elongation seen with increasing time or temperature at the higher tempera-

Table 20.8 Effect of heat treatment on mechanical properties of beryllium wire drawn to 0.125 mm diameter

Condition	Ultimate tensile strength, MPa	0.2% yield strength, MPa	Elongation (in 25 cm), %
As-drawn	1198	941	6.3
Heated to 425 °C (800 °F), 24 h	1088	1040	0.8
Heated to 540 °C (1005 °F), 24 h	924	836	5.0
Heated to 595 °C (1105 °F), 0.5 h	972	765	11.0
Heated to 650 °C (1200 °F), 0.5 h	793	538	13.9
Heated to 655 °C (1210 °F), 3 h	780	469	17.3
Heated to 655 °C (1210 °F), 7.5 h	697	427	11.1
Heated to 705 °C (1300 °F), 0.5 h	752	427	11.7
Heated to 760 °C (1400 °F), 0.5 h	629	345	9.0
Heated to 815 °C (1500 °F), 0.5 h	468	276	6.5

Source: Denny 1979a

tures revealed in Table 20.8 were undoubtedly due to recrystallization and/or grain growth, since recrystallization of the heavily worked wire was observed to occur at temperatures as low as 595 °C (1100 °F). Substructures as small as 0.1 μm were reported. Pronounced basal and prism textures parallel to the wire axis and randomly oriented with respect to the radial direction were reported [Denny 1979a].

Substantial reductions in the grain size occur during drawing [Denny and Meyer 1966a]. The average grain size of ingot-origin material decreased from 50 μm in the as-extruded condition to 2 μm in fine wire. Strength levels increase concurrently. The yield strength appears to be a function of the square root of the reciprocal grain diameter. Metallographic examination shows recrystallization at temperatures as low as 595 °C (1100 °F). This behavior is no doubt associated with the large amount of warm work imparted to the wire during drawing.

The texture of beryllium wire was measured from Laue and Debye reflections [Denny et al. 1968]. Results showed that both as-drawn and drawn-plus-annealed wire have a classical texture, with basal planes oriented parallel to the working axis and a [1010] fiber texture. The texture of as-drawn wire appeared more pronounced than annealed wire, as evidenced by higher reflection intensities. Metallographic studies showed that the basal planes are randomly oriented with respect to the radial and tangential directions. Prism-plane textures were found to increase from 5 to 68X random during reduction from 3.7 to 0.86 mm (0.1 to 0.03 in.) diameter. Pronounced basal and prism textures develop early in the wire-drawing process, following which the prism texture continues to increase rapidly to very high values. Transmission electron microscopy showed the development of a subgrain structure, on the order of 1 μm or less, with increasing reduction during the drawing process. The substructure of fine beryllium wire may be as small as 0.1 μm.

20.8 Spinning

Spinning involves forming sheet metal or tubing into seamless, circular shapes (hollow cylinders, hemispheres, cones, domes, etc.) by a combination of rotation and force. The forming can be done by either manual spinning or by power spinning. Manual spinning results in no appreciable thinning and involves relatively little force. It is normally done on a lathe and consists of pressing a spinning tool against a circular sheet (blank) that is forced against a shaped mandrel, which is attached to and rotated by the headstock. The workpiece is clamped to the mandrel by a follower block that is attached to the tail stock. Two spinning setups are illustrated in Fig. 20.27 [ASM 1988a]. Simple shapes, where dimensional tolerances are not critical, may not require a mandrel [ASM 1988a]. In power (shear) spinning, the metal is intentionally thinned by shear forces. Spin forming can generally be performed without heating the metal. Exceptions are for metals having low ductilities, such as beryllium, and for large-thickness blanks used with power spinning. Because of low tooling costs, manual spinning is often used for prototype runs and for relatively small production runs.

Beryllium sheets up to 5.1 mm (0.2 in.) thick have been successfully formed by spinning [Grant 1988]. Beryllium sheets that are less than approximately 1 mm (0.04 in.) thick are usually sandwiched between two 1.5 mm (0.06 in.) sheets of low-carbon steel. The sandwich is heated to 620 °C (1150 °F) prior to spinning. The steel sheets help to prevent buckling and maintain temperature. Sheets larger than 1 mm (0.032 in.) thick are usually not sandwiched and are heated to between 730 and

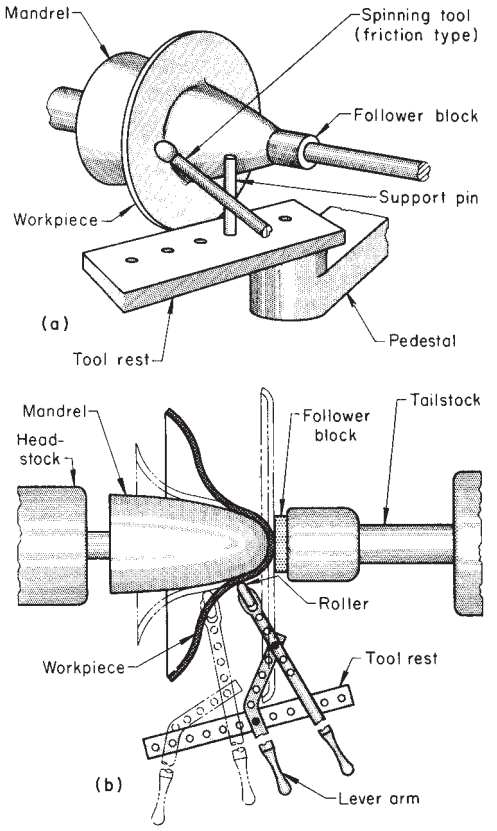

Fig. 20.27 Two examples of manual spinning using a lathe. (a) Simple setup using a hand tool applied as a pry bar. (b) Setup using scissorlike levers with a roller tool. Source: ASM 1988a

815 °C (1345 and 1500 °F). The workpiece and tool may be torch heated during spinning. Lubrication, which is especially important in spinning, is usually done with colloidal graphite or glass [Grant 1988]. Hemispheres up to 79 cm (31 in.) diameter and 0.51 cm (0.2 in.) thick have been produced using glass lubricants.

20.9 Near-Net Shaping

Net shape processing of beryllium was first introduced to reduce the high cost of machining and the high production of scrap in fabricating a complex or intricate geometry. Usually, approximately 65% and as much as 90% of the consolidated material ended in scrap and chips when starting with a typical solid, cylindrical billet [Hanes and Stonehouse 1987]. Net shape or, more commonly, near-net shape (NNS) products can be produced either by direct HIPing or by CIP followed by sintering. Any residual porosity can subsequently be removed by HIP (CIP/sinter/HIP) or by warm forming in a closed die (CIP/sinter/warm form). Both of these operations may also provide for some dimensional adjustment of the part. The viability of producing NNS products was first demonstrated in 1960 when HIP was used to produce a demonstration part [Hanes and Stonehouse 1987]. The first major NNS product was an aircraft brake component formed by CIP/sinter/coining, while the first NNS commercial product produced by HIPing was a mass-mounted sight-sensor support structure [Haws 2000, Marder 1998b]. (Coining, striking or sizing refers to an operation to sharpen or modify a radius or profile. Coining also refers to a closed-die squeezing operation in which all surfaces of a workpiece are confined or restrained, resulting in a well-defined imprint of the die on the workpiece. It can be done warm or cold.)

Table 20.9 Comparison of beryllium specification of mechanical properties for vacuum hot pressing (VHP) and hot isostatic pressing (HIP)

	Beryllium grade					
	S-200		I-70		I-220	
Property	HIP	VHP	HIP	VHP	HIP	VHP
0.2% yield, MPa	296	241	207	172	345	276
Ultimate tensile strength, MPa	414	323	345	241	448	379
Elongation, %	3	2	2	2	2	2

Source: Marder 1998b

Vacuum hot pressing uses uniaxial pressures ranging up to 8.3 MPa (1.2 ksi) at temperatures between 1000 and 1200 °C (1830 and 2190 °F) to produce billets up to 183 cm (72 in.) diameter [Marder 1998b]. A HIP system installed at Brush Wellman in 1985 was capable of processing beryllium at temperatures up to 1250 °C (2280 °F) with isostatic (argon) pressures up to 103 MPa (15 ksi) [Denny 1979a].

The mechanical properties of the HIPed beryllium were found to be equivalent or superior to the VHP billet in all respects. A comparison of tensile properties between VHP and HIP consolidations is shown in Table 20.9 [Marder 1998b].

For NNS products, it is preferable to use atomized spherical powders, since these powders, have much better flow characteristics than those that are obtained with the mechanical-attrited powders. This results in improved fill characteristics (especially for complex parts) and increased

overall packing densities (62 to 65% compared to 50 to 55%).

Many examples of NNS products are presented in the literature [Marder et al. 1990, Marder 1998a, Clement et al. 1992, Hashiguchi et al. 1989]. The most straightforward method of producing an NNS product is the direct HIP process whereby the powder is loaded into a shaped can. The can is evacuated in vacuum at approximately 600 to 700 °C (1110 to 1290 °F), hermetically sealed, and subjected to HIP. The final billet shape takes on the shape of the can. Shaped mandrels can be used to provide cavities in the billet. Cans are usually made of mild steel because they can be cheaply and easily fabricated (formed and welded) and easily removed from the shaped billet by etching or machining [Stonehouse and Marder 1990]. Mandrels are generally made out of copper, although too high a consolidation temperature may limit its use. (Copper and beryllium have a low temperature-congruent melting point of approximately 860 °C, or 1580 °F, at approximately 5 wt% Be.) The copper can be removed by machining, by a nitric acid etch, or by a combination of both. Dilute concentrations of the acid will not attack beryllium. A critical part of the procedure is the degassing step to remove entrapped air and gases adsorbed on particle surfaces and the subsequent hermetic sealing of the can. Residual gases may result in some distortion of the can during heating. Of major concern, however, is the presence of any residual moisture. At elevated temperatures, the water vapor will react with beryllium to form beryllium oxide and hydrogen. The increase in the oxide content may not pose a serious problem. The hydrogen (gas), being virtually insoluble in beryllium, will expand during any subsequent heat treatment of the HIPed product and may significantly increase porosity as well as cause distortion of the product [Marder 1990].

The effect of HIP temperature on mechanical properties for HIPed beryllium using three different types of powders is depicted in Fig. 20.28. The curves show slow continual increases in tensile strength up to 1050 °C (1920 °F), followed by a rapid decrease, while the elongations continue to increase within the same temperature range. The reduction in strength at the highest temperatures could be attributed to the increase in grain size. In a separate study, the results of HIP on impact-ground beryllium powder at 744 and 1000 °C (1370 and 1830 °F) are compared. No difference in the ultimate tensile

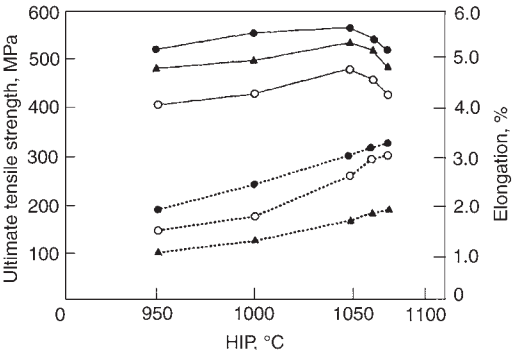

Fig. 20.28 Effect of hot isostatic pressing (HIP) temperature on the ultimate tensile strength and elongation of three types of consolidated beryllium powders. The dotted line is for elongation; the solid line is for ultimate tensile strength; solid circles are for impact-ground powder; triangles are for ball-milled powder; and open circles are for disk-attritioned powder. Source: Benshuang and Xinghai 1996

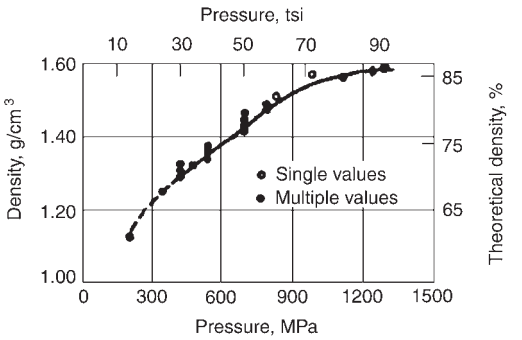

Fig. 20.29 Effect of compacting pressure on the green density of uniaxially cold pressed beryllium powder. Source: Marder 1998b

strength was shown, while the yield strength was lower and the elongation was greater at the higher temperature [Marder et al. 1990]. Since HIP is performed at much higher pressures than the pressures used for VHP, lower temperatures and shorter times can be used with HIP to produce the same densities as those achieved with VHP. Accordingly, finer grain sizes with improved mechanical properties are obtained with HIP products compared to VHP products.

Instead of a shaped-can container, an inexpensive reusable elastic (e.g., neoprene or rubber) bag can be used to create an NNS preform by CIP. Pressure can be achieved by means of liquid. This practice yields a "green" (unsintered compact) with a density between approximately 65 and 80% theoretical density [Stonehouse and Marder 1990, Marder 1998b]. The effect of compacting pressure on the green density of beryllium is shown in Fig. 20.29 [Marder

1998b]. Subsequent sintering can increase the density to up to 98% theoretical density. Greater densities may be achieved by HIPing (CIP/sinter/HIP) the sintered product.

Experimental properties of S-200F consolidated by different NNS processes, which were obtained in an early investigation on NNS, are listed in Table 20.10 [Hashiguchi et al. 1989]. Direct HIP was performed at 1000 °C (1830 °F) under a pressure of 103 MPa (15 ksi) for 3 h. The CIP was performed using a cylindrical rubber bag that was inserted in a perforated aluminum cage to maintain the initial shape. Compacting was done at 276 MPa (40 ksi). The CIPed preform was then placed in a steel HIPing can and embedded in a granular refractory material that served as a pressure-transmitting medium. The can was then degassed, sealed, and subjected to HIP as previously described. The CIP/sinter product was subjected to CIP as described previously and then sintered at 1230 °C (2245 °F) for 5 h in vacuum. Each of the steps for the CIP/sinter/HIP product followed the previously described procedures, respectively. The Hall-Petch relationship between strength and grain size that was obtained is shown in Fig. 20.30 [Hashiguchi et al. 1989].

Hot isostatic pressing can be done without using a can, provided the sintered body has attained a density of approximately 96% theoretical density. In such cases, the HIPing is done at temperatures below those used for HIPing alone. The relatively high temperatures used in sintering, however, may cause sufficient grain growth to lower the strength level below that of a VHP product using the same powder [Hanes and Stonehouse 1987]. When necessary, a final warm shaping step, such as coining or by some other deformation process, may be applied. For example, a closed-die forging may be used to improve flatness of a mirror component; this would be followed by a stress-relief treatment [Clement 1990]. An alternative processing method may be to use a die press instead of CIPing or HIPing, as indicated in the following sequence: die press/sinter/coin, where warm coining is used to achieve dimensional and density requirements. This process has been used for the production of aircraft brakes, where the beryllium, with its high heat capacity and high melting point, also acts as an excellent heat sink [Marder et al. 1990]. Examples of manufacturing cost-savings for parts produced by direct HIPing and by VHPing are shown in Table 20. 11 [Marder et al. 1990]. The cost-savings refer to all processing operations as well as material savings. Additional savings may arise by introducing additional procedures such as CIPing and sintering, which eliminate the cost of can fabrication and can outgassing.

When producing an NNS part, the can dimensions must provide for shrinkage that occurs during consolidation of the powder. The following expression, Eq 20.9, was used to provide these dimensions for a preform that would be machined into a mast-mounted sight structure (MMSS) having final linear dimensions of 235 by 248 by 305 mm (9.3 by 9.8 by 12 in.) [Skillern et al. 1991]:

$$C = P/(D_c \times D_p)^{1/3} \qquad \text{(Eq 20.9)}$$

where C is the HIP-can dimension, P is the fully dense preform dimension, D_p is the relative

Table 20.10 Properties of S-200F consolidated by near-net shape processes

Property	VHP	Direct HIP	CIP/HIP	CIP/sinter	CIP/sinter/HIP
Density, g/cm^3	1.85	1.87	1.86	1.85	1.86
(% theoretical)		(100)	(99.5)	(99.3)	(99.5)
Grain size, μm	8.8	6.6	4.5	12.4	9.9
0.2% yield strength, MPa					
Longitudinal	272	281	334	191	220
Transverse	272	283	323	190	211
Yield point, MPa					
Longitudinal	283	283	336	. . .	. . .
Transverse	278	290	330	. . .	. . .
Ultimate tensile strength, MPa					
Longitudinal	362	378	444	289	336
Transverse	392	385	435	301	336
Elongation, %					
Longitudinal	3.0	3.2	3.9	3.6	3.6l
Transverse	5.7	4.2	3.8	3.8	4.4
Microyield, MPa					
Longitudinal	. . .	39.1	36.2	14.5	15.8
Transverse	. . .	42.7	41.7	13.1	13.1

Note: VHP, vacuum hot pressed; HIP, hot isostatic pressed; CIP, cold isostatic pressed. Source: Hashiguchi et al. 1989

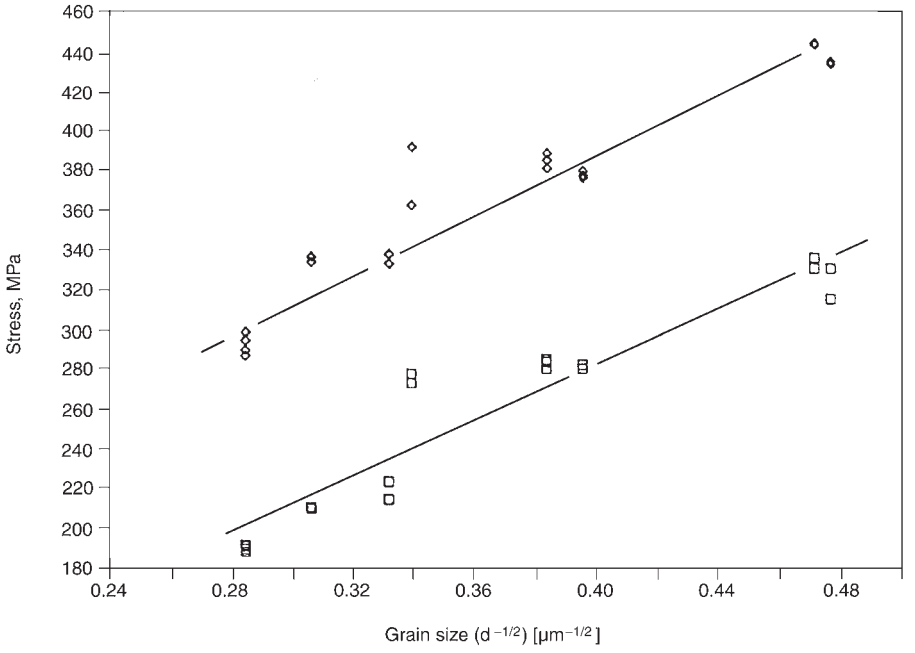

Fig. 20.30 Hall-Petch relationship showing the effect of grain size on tensile yield and ultimate strengths of vacuum hot pressed, structural-grade S-200F beryllium. Source: Hashiguchi et al. 1989

Table 20.11 Cost-savings on comparing direct hot isostatic pressing (HIPing) with vacuum hot pressing

	Vacuum hot pressing		Direct HIPing		Cost saving
Shape(a)	Input, kg	Blank, kg	Input, kg	Blank, kg	by HIPing, %
A	83.2	30.9	40.5	21.8	42
B	30.5	12.7	13.6	11.4	31
C	16.8	7.3	7.7	5.0	27
D	8.0	2.3	3.6	2.3	18

(a) Specific shapes were not reported. Source: Hanes and Stonehouse 1987

preform density, and D_c is the relative tapped density in the HIP can. (The tapped density is the density of the powder prior to applying the consolidation pressure. The density of the powder is increased by a tapping, or vibration action during charging of the powder into the consolidation chamber.) The expression relates the linear shrinkage, given by $(D_c \times D_p)^{1/3}$, to the change in densities.

In previous evaluations made with other preforms, Skillern et al. [1991] found that the shrinkage was isotropic (in the three orthogonal directions), with an average of 14% linear shrinkage. Slight shrinkage differences were attributed to corresponding variations in the tapped density. To accommodate such differences, the HIP-can dimensions were constructed such that there was an excess shell of material around the MMSS preform. In addition, to minimize the amount of required machining, the can has as few welds as possible and has optimized component fit-up to the final structure. The powder-loading system was designed to provide a constant and continuous feed rate to the can, since this leads to better density uniformity of the powder. The system was also designed to avoid any health and safety problems. The cans were sealed, evacuated, leak tested, and then heated in an oven while being evacuated to remove any gases and water vapor trapped on the powder surfaces. The degassing took a number of days before reaching a prescribed pressure ($<10^{-4}$ torr, or 1.3×10^{-2} Pa) [Skillern et al. 1991]. The degassing stems were sealed off, and the can was then subjected to HIP using argon gas at a pressure of 103 MPa (15 ksi) at a temperature of 1000 °C (1830 °F). The preform was then etched in a 40% (by weight) nitric acid solution to remove the steel can, and finally, it was stress relieved at 800 °C (1470 °F) for 4 h and cooled at 50 °C/h (90 °F/h) to room temperature. The resulting preform was machined to create a webbed support structure similar to that shown in Fig. 20.31. With webs that were 2.03 mm (0.08 in.) thick, the 20.5 kg (45 lb) preform was

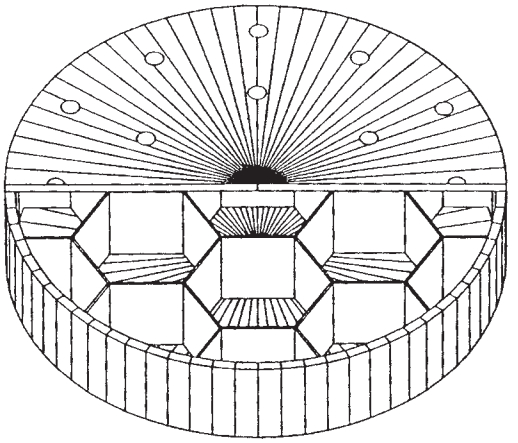

Fig. 20.31 Cutaway view of a lightweight, closed-back, solid beryllium mirror revealing a honeycomb core structure made by using copper mandrels. Holes in the back plate, which were centered above each cell, facilitated removal of the tooling by nitric acid etching after the hot isostatic pressing operation. Source: Marder 1998b

reduced to a 2.73 kg (6 lb) part. A reduction of 50% in material costs was achieved with a part having better mechanical properties and a finer grain size than those developed by starting with the traditional VHP billet [Skillern et al. 1991]. The same final density (1.85 g/cm^3) was obtained in each case.

The low density (1.85 g/cm^3), high elastic modulus (303 GPa), high thermal conductivity (210 W/m/K), and moderate coefficient of thermal expansion (11.3×10^{-6}/°C) of beryllium make it the logical choice for optical components that require high precision and high stability. The high cost of beryllium, however, had prevented it from competing with other materials used for optics, such as metal-matrix composites and silicon nitride ceramics. With the development of NNS processing of beryllium using CIP/sinter/HIP or CIP/sinter/warm forming technology, beryllium became competitive with other optical materials and is now widely used. Furthermore, the NNS processing provides better dimensional control, improved isotropy of thermal and mechanical properties, and improved thermal stability compared to these characteristics obtained with traditional VHP beryllium [Clement et al. 1992]. In addition, design of an all-beryllium optical system is simplified, since compensation for thermal expansion mismatch of different materials is unnecessary, and higher-resolution images are attainable [Clement 1990]. A number of examples of optical systems were reported [Clement et al. 1992, Clement 1990].

In a CIP-HIP study of NNS processing for enhanced optical properties, beryllium powder was vibration fed into a rubber or plastic bag and subjected to CIP at 260 MPa (38 ksi), achieving densities of up to 73% theoretical density. The green CIPed blanks were degassed at 650 °C (1200 °F) for 26 h, followed by 4 h at 750 °C (1380 °F) [Hashiguchi et al. 1989]. The authors state that the HIPing pressure is typically 105 MPa (15 ksi) with temperatures within the range of 760 to 1100 °C (1400 to 2010 °F). A secondary pressure-transmitting medium can be used to fill in the space between the blank and can. Media that have been successfully used are sodium chloride, aluminum oxide, boron nitride, graphite, and glass balls. When using any of these media, it is important to consider the deformation compatibility between the medium and the blank during the HIPing cycle [Benshuang and Xinghai 1996]. Homogeneous parts suitable for optical applications were obtained. The authors describe the properties for three different mirror configurations as examples of NNS products formed either by direct HIPing or by CIP/sinter/form and describe the fabrication of a lightweight mirror structure in some detail.

One structure had a 25 cm (9 in.) diameter, closed-back mirror that consisted of flat front and back plates separated by honeycomb-shaped webs, as shown in the cutaway view of Fig. 20.31 [Clement et al. 1992]. The structure was made by HIPing the beryllium powder, which surrounded copper tooling and was contained in a fabricated steel can. The steel can was degassed and underwent HIPing for 3 h at 103 MPa (15 ksi). Holes in the back plate, centered above each cell, facilitated removal of the copper by nitric acid etching. Copper was selected because of its good machinability; compatibility with beryllium under HIP conditions; higher coefficient of thermal expansion than beryllium, thus avoiding tensile residual stresses upon cooling; and its solubility in dilute nitric acid (unlike beryllium). During final machining, the part underwent a stress-relief heat treatment.

As with all NNS powder processing, shrinkages had to be evaluated. The diametrical and longitudinal shrinkages were 5.6 and 17.1%, respectively. The HIPed mirror structure was observed to be distortion-free, and the copper tooling did not suffer any deformation [Marder 1998b]. It was noted that in direct HIPing, the cost of the copper tooling (mandrels) and its removal was significant. In fabricating solid nickel

or gold-plated beryllium mirrors, total costs were reduced by using CIP/sinter/form instead of direct HIPing. The processing costs using CIP/sinter/form were slightly more for the processing but were only one-third the cost for the beryllium compared to these costs for HIPing [Marder 1998b]. Structures as large as 1.2 m (47 in.) with web thickness as thin as 1 mm (0.04 in.) can be produced by NNS processes [Grant and Hardesty 1990].

Inert-gas-atomized powders are the preferred powders for producing near-net-shaped beryllium products. The improved packing characteristics of the spherical particles, as compared to those produced by mechanical methods, provide for better control of the charge weight on filling the HIP cans. The improved packing leads to higher final densities as well as better dimensional control of the HIPed product [Clement 1990].

20.9.1 Rapid Net-Shape Forming

The term *rapid net-shape forming* applies to a net-shape process for manufacturing intricate and complex components, including those designed with internal passages and very thin walls [Bugle and Stroud 2000]. Parts with hollow passages or cavities contain cores with corresponding geometries. The process is initiated with the design of a sacrificial wax pattern based on the part geometry and adjusted to accommodate shrinkage and shape change that would occur during consolidation of the powder. The pattern is then fabricated using rapid prototyping technology. This involves developing the model using three-dimensional computer-aided design (CAD), converting the CAD data into a stereolithography file, which is used to slice the CAD model into hundreds or thousands of cross-sectional layers. The part (in this case a mold) is then formed, using a stereolithography apparatus by depositing liquid polymer epoxy droplets, layer by layer, onto a rising platform contained in a tank. A laser-generated beam traces out the cross sections and solidifies the polymer, while a controller regulates the deposition rate and geometry of each layer and the rising platform. The speed and low cost of the process allows for many modifications of a design.

The epoxy mold serves as a wax-injection die to produce a wax pattern with close tolerances. Ultrapure nickel is then evenly deposited over the wax pattern by electroforming. The wax pattern is removed from the nickel electroform by investment-casting techniques, and the nickel is cleaned. A seamless nickel canister, which precisely replicates the shape and surface texture of the pattern, is thus obtained for HIPing a part. Sulfur and other contaminants from the electroforming bath must be kept at a minimum. Contaminants, especially sulfur, can impair ductility of the nickel as a result of grain-boundary precipitation during HIPing. Similar loading, evacuation, and pressing procedures as employed in conventional HIPing are used. Free-flowing spherical powder is used to provide the maximum packing density and fill uniformity, reducing the tendency for distortion during HIPing. Distortion can be reduced further by using a ceramic exoskeleton designed to allow the gas to pressurize the seamless canister walls [Haws 2000]. The use of an exoskeleton depends on the contour complexity of the part. The HIP cycles must be compatible with the capabilities of the canister. Beryllium can be processed by HIP at 1010 °C (1850 °F) [Bugle and Stroud 2000]. The nickel, as well as any cores that may have been added for passages and cavities, is dissolved in nitric acid. Parts ranging from a few centimeters to as large as a 60 cm (24 in.) cube have been made [Bugle and Stroud 2000]. Several examples of rapid net-shaped formed parts were reported [Haws 2000, Bugle and Stroud 2000].

REFERENCES

ASM, 1970. Forging of Beryllium, *Forging and Casting*, Vol 5, *Metals Handbook*, 8th ed., American Society for Metals, p 132–133

ASM, 1979a. Beryllium, *Properties and Selection: Nonferrous Alloys and Pure Metals*, Vol 2, *Metals Handbook*, 9th ed., American Society for Metals, p 717–718

ASM, 1988a. Spinning, *Forming and Forging*, Vol 14, *ASM Handbook*, ASM International, p 599–604

ASM, 1988b. Stretch Forming, *Forming and Forging*, Vol 14, *ASM Handbook*, ASM International, p 591–598

ASM, 1988c. Three-Roll Forming, *Forming and Forging*, Vol 14, *ASM Handbook*, ASM International, p 616–623

ASM, 1988d. Wire, Rod, and Tube Drawing, *Forming and Forging*, Vol 14, *ASM Handbook*, ASM International, p 330–342

Barrow, D.A., and Craik, R.L., 1963. Fabrication of Beryllium Sheet by Upset Forging,

The Metallurgy of Beryllium, Institute of Metals Monograph 28, Chapman and Hall Ltd., London, p 743

Beaver, W.W., and Wikle, K.G., 1954. Mechanical Properties of Beryllium Fabricated by Powder Metallurgy, *J. Met.*, Vol 6, p 559–573

Beitscher, S., and Grimes, A.G., 1970. "Tensile Properties of Rocky Flats Division Ingot-Sheet Beryllium from 195 °C to 700 °C," RFP-1194, The Dow Chemical Company, Rocky Flats Division, Golden, CO

Benshuang, S., and Xinghai, S., 1996. Beryllium Benefits from CIP/HIP Pressing, *Met. Powder Rep.*, Vol 51 (No. 5), p 28–30

Bishop, J.F., 1963. "On the Ductility of Polycrystalline Beryllium," U.K. Atomic Energy Authority Report IGR-TN/S-791

Blakeslee, J.J., 1979. Metalworking IV: Forming, *Beryllium Science and Technology*, Vol 2, J.N. Lowe and D.R. Floyd, Ed., Plenum Press, NY, p 107–124

Brush Wellman, 2001. "Designing with Beryllium," Brochure 517, Cleveland, OH

Bugle C.M., and Stroud, V., 2000. Rapid Net-Shape Forming of P/M Parts, *Adv. Mater. Process.*, Vol 158 (No. 1), p 43–45

Carson, C., 1969. "Dispersed Phase Strengthened Beryllium Alloys for High Strength Wire," Report AFML-TR-69-35, Wright Patterson Air Force Base, OH

Christensen, L.M., and Wells, R.K., 1962. "Program for the Development of Extruded Beryllium Shapes," Norair Report NOR-6225, Final technical engineering report

Clement, P., 1990. How the Beryllium Industry Is Building New Markets by Applying Isostatic Processing Technologies, *Proceedings of the Fourth International Conf. on Isostatic Pressing* (Stafford-upon-Avon, U.K.), p 18–1 to 18–11

Clement, T.P., Parsonage, T.B., and Kuxhaus, M.B., 1992. Near-Net-Shape Processing Cuts Cost of Beryllium Optics, *Adv. Mater. Process.*, Vol 141 (No. 3), p 37–40

Darwin, G.E., and Buddery, J.H., 1960. Beryllium, *Metallurgy of the Rarer Metals*, Butterworths Scientific Publications, London, U.K., p 11–99

Denny, J.P., 1979a. Metalworking V: Wire Drawing, *Beryllium Science and Technology*, Vol 2, D.R. Floyd and J.N. Lowe, Ed., Plenum Press, NY, p 125–134

Denny, J.P., London, G.J., and Pinto, N.P., 1968. "Plastic Deformation of Beryllium Wire," 97th AIME Annual Meeting (New York), Feb 29, 1968

Denny, J.P., and Meyer, G.E., 1966a. Beryllium Ingot Wire, *Wire and Wire Prod.*, Vol 41, p l640–l64l, 1712

Denny, J.P., and Meyer, G.E., 1966b. "Development of a Manufacturing Process for the Production of 0.005" Diameter Beryllium Wire," WPAFB Report AFML-TR-66–312

Fenn, R.W., Crooks, D.D., Kinder, W.C., and Lempriere, B.M., 1967. "Test Methods for Mechanical Properties of Anisotropic Materials (Beryllium Sheet)," Report AFML-TR-67-212, Lockheed Missile and Space Co., Palo Alto, CA

Floyd, D.R., 1972a. "Technical Data Book for Ingot-Sheet Beryllium," RFP-1605, Dow Chemical Company, Rocky Flats Division, Golden, CO

Floyd, D.R., 1972b. "Isotropic High Strength Beryllium," Report RFP-l816, United States Atomic Energy Commission, The Dow Chemical Co., Rocky Flats Division, Golden, CO

Floyd, D.R., Leslie, W.W., and Dolechek, L.F., 1973. "Can Rolling of Beryllium Ingots," Report RFP-2041, The Dow Chemical Company, Rocky Flats Division, Golden, CO

Foos, R.A., Stonehouse, A.J., and Walsh, K.A., 1970a. Micro-Alloying Relationships in Beryllium, *Proc. Beryllium Conf.*, National Academy of Sciences, Washington, D.C., p 127–147

Foos, R.A., Stonehouse, A.J., and Walsh, K.A., March 1970b. "Micro-Alloying Relationships in Beryllium," BBC-TR-456, The Brush Beryllium Company

Frankeny, J.L., and Floyd, D.R., 1968. "Ingot-Sheet Beryllium Fabrication," Report RFP-910, Dow Chemical Co., Rocky Flats Division, Golden, CO

Glenn, G., and Hayes, A.F., 1969. New Forging Techniques for Beryllium, *Met. Prog.*, Vol 95 (No. 3), p 131–139

Grant, L.A., 1988. Forming of Beryllium, *Forming and Forging*, Vol 14, *ASM Handbook*, ASM International, p 805–808

Grant L.A., and Hardesty R.E., 1990. Fabrication of Stable Lightweight Beryllium Optical Support Structures, *Dimensional Stability*, Vol 1335, R.A. Paquin, Ed., SPIE, p 140–155

Hanafee, J.E., 1971. "Investigation Including a Testing Program to Study and Develop Methods for Improving Ductility of Beryllium," Final Report F-2574, The Franklin Institute Laboratories

Hanes, H.D., and Stonehouse, A.J., 1987. HIP Beryllium Achieves Full Commercial Status, *Met. Powder Rep.*, Vol 42 (No. 10)

Hashiguchi, D.H., Clement, T.P., and Marder, J.M., 1989. Properties of Beryllium Consolidated by Several Near-Net Shape Processes, *J. Mater. Shaping Technol.*, Vol 7 (No. 1), p 23–31

Haws, W.J., 2000. New Trends in Powder Processing Beryllium-Containing Alloys, *JOM*, Vol 52 (No. 5), p 35–37

Hayes, A.F., 1967. "Beryllium Forging for Turbine Engine Components," Report AFML-TR 67–334, Wright Patterson Air Force Base, Air Force Materials Laboratory, Ladish Co., Cudahy, WI

Hayes, A.F., 1979. Metalworking III: Forging, *Beryllium Science and Technology*, Vol 2, D.R. Floyd and J.N. Lowe, Ed., Plenum Press, New York, NY, p 83–105

Hayes, A.F., and Yoblin, J.A., 1962. "Beryllium Forging Program: Final Technical Engineering Report, May 6, 1958–November 19, 1961," Report TR 62–7–647, Wright Patterson Air Force Base, Aeronautical Systems Division, Ladish Co., Cudahy, WI

Heiple, C.R., 1973a. Extended Ductility in Beryllium, *Metall. Trans.*, Vol 4 (No. 2), p 585–588

Heiple, C.R., 1973b. Factors Affecting Curling in Rolled Sheet, *J. Eng. Mater. Technol. (Trans ASME)*, Ser. H., Vol 95 (No. 5), p 103

Henkener, J.A., Spiker, I.K., and Castner, W.L., 1992. "The Mechanical Behavior of Cross-Rolled Beryllium Sheet," NASA TM-4397, N-92–33485

Herrera, J.M., and Staffor, S.W., 1991. "Fracture Criteria for Beryllium Sheet," Final report for NASA-JSC grant NAG 9-281, University of Texas at El Paso, El Paso, TX

Hoffmanner, A.L., 1965. "Study of Methods to Produce Composite Beryllium Blades," Interim report, Navy Contract NOw-65-028 I-f

Hunt, M., 1988. Surprising Beryllium, *Mater. Eng.*, Vol 105, p 46–49

Ingels, S.E., 1966. "Ductility of Cross-Rolled Beryllium Sheet," NASA-CR-91705, Lockheed Missile and Space Co., Sunnyvale, CA

Jenkins, R.G., Siergiej, J.M., Wolff, A.K., and Klein, J.L., 1964. "Development of Improved Fabrication Methods, Processes and Techniques for Producing Typical Aircraft Shapes from Beryllium," Technical documentary report to the Air Force ML-TDR-64-108, Nuclear Metals Division of Textron, Inc., Concord, MA

Keeler, S.P., 1968. Understanding Sheet Metal Formability, *Mach., NY*, Feb 1968, p 88–96; March 1968, p 94–101; April 1968, p 94–103; May 1968, p 92–99; June l968, p 98–104; July l968, p 78–83

Kosinski, E.J., and Hayes, A.F., 1966. "Recent Advances in Forging Beryllium for Aerospace Applications," Internal report, Ladish Co., Cudahy, WI

Kovarik, D.P., 1984. Precision Stress-Strain Curves of Commercial Beryllium, *25th Structures, Structural Dynamics and Materials Conference*, Technical Papers Part 1 (Palm Springs, CA), American Institute of Aeronautics and Astronautics, NY, p 174–185

Krivko, V.P., Romanko, P.M., Kolesnik, L.I., Vagnibeda, N.V., and Kokovikhin, Y. I., 1991. The Effect of Annealing on the Mechanical Properties and the Structure of Beryllium Foil, *Met. Sci. Heat Treat.*, Vol 33 (No. 1–2), p 12–14

Leslie, W.W., 1979. Metalworking I: Rolling, *Beryllium Science and Technology*, Vol 2, D.R. Floyd and J.N. Lowe, Ed., Plenum Press, NY, p 57–66

Loewenstein, P., 1979. Metalworking II: Extrusion, *Beryllium Science and Technology*, Vol 2, D.R. Floyd and J.N. Lowe, Ed., Plenum Press, NY, p 67–82

Loewenstein, P., Kaufmann, A.R., and Arnold, S.V., 1955. Mechanical Working of Beryllium by Extrusion, *The Metal Beryllium*, D.W. White, Jr., and J.E. Burke, Ed., American Society for Metals, p 241–261

Marder, J.M., 1986. Beryllium in Stress-Critical Environments, *J. Mater. Energy Syst.*, Vol 8 (No. 1), p 17–26

Marder, J.M., 1990. Current Applications of Beryllium Manufactured by P/M Techniques, *P/M in Aerospace and Defense Technologies, Proceedings of the Conference and Exhibition*, Vol 2 (Seattle, WA), Nov 1989, p 133–136

Marder, J.M., 1991. Current Applications of Beryllium Manufactured by P/M Techniques, *Aerospace and Defense Technologies*, Vol 2, Seattle, WA, p 133–136

Marder, J.M., 1998a. Powder Metallurgy Beryllium, *Powder Metal Technologies and Applications*, Vol 7, *ASM Handbook*, ASM International, p 941–946

Marder, J.M., 1998b. Production of Beryllium Powders, *Powder Metal Technologies and Applications*, Vol 7, *ASM Handbook*, ASM International, p 202–205

Marder, J.M., Kuxhaus, M.B., and Stonehouse, A.J., 1990. Near-Net Shape Beryllium Products, *Int. J. Powder Metall.*, Vol 26 (No. 2), p 139–146

MIL-HDBK-5E, 1987. *Military Standardization Handbook: Metallic Materials and Elements for Aerospace Vehicle Structures*, Vol 2, Department of Defense, p 7–8

Murphy, E.A., Hornak, M.B., and O'Rourke, R.G., 1965. "Developing Technology to Forge Unclad Beryllium," Report AFML-TR-65-30, Wright Patterson Air Force Base, Air Force Materials Laboratory

Murphy, E.A., and O'Rourke, R.G., 1964. "Development of Very High Strength Beryllium Wire, Final Report," Technical Report BBC-TR-382-243, Brush Beryllium Co.

Orrell, N.G., 1963a. Beryllium Powder Forging, "Beryllium—Its Properties and Applications," Short course, University of California, Berkeley, CA

Orrell, N.G., 1963b. "The Fabrication of Beryllium Powder Forging," Report RD 63-l05, Wyman Gordon Co., Worcester, MA

Pinto, N.P., and Denny, J.P., 1967. Beryllium Wire: A New Engineering Material, *Met. Prog.*, Vol 91 (No. 6), p 107–108, 110, 112, 114, 118

Richardson, B.D., Meyer, G.E., Uy, J.C., Fiorentino, R.F., and Sabroff, A.M., 1970. "Prototype Production Process for the Fabrication of Wire and Tubing by Hydrostatic Extrusion Drawing," Report AFML TR-70-82, Battelle Memorial Institute, Columbus, OH

Sawyer, C.B., Beaver, N.W., Dodds, H.W., and Rapprich, D.D., 1950. "Fabrication by Powder Metallurgy," Report BBC-50, Brush Beryllium Company

Sharma, V.P., and Sivasubramanian, N., 1994. Processing of Beryllium for High Technology Applications, *Miner. Process. Extr. Metall. Rev.*, Vol 13 (No. 1), p 229–242

Siergiej, J.M., 1965. Extrusion of Beryllium Structural Shapes, *Beryllium: Its Metallurgy and Properties*, University of California Press, Berkeley and Los Angeles, CA, p 86–101

Siergiej, J.M., and Nerses, V., 1961, "Extrusion Development of Beryllium U-Channels: Phases I, II, and III," Report NMI 4469, Final report to Northrup Corporation, Nuclear Metals., Inc., Concord, MA

Skillern, C.G., Hollman, R.R., and Kulkarni, K.M., 1991. Production of Beryllium Mast-Mounted Sights Using Near-Net Shape Technology and Chemical Milling, *Advances in Powder Metallurgy*, Vol 6, *Aerospace, Refractory, and Advanced Materials, Proceedings of the Powder Metallurgy Conference and Exhibition* (Chicago IL), p 381–389

Smugeresky, J.E., 1986. Beryllium and Beryllium Alloys, *Encyclopedia of Materials Science and Engineering*, Vol 1, Pergamon Press Ltd., p 289–294

Soltis, P.J., 1962. "Study of Size Effect of Beryllium Wire," Report NAMC-AML-1550, Naval Air Material Center, Aeronautical Materials Lab

Stonehouse, A.J., and Marder, J.M., 1990. Beryllium, *Properties and Selection: Nonferrous Alloys and Special-Purpose Materials*, Vol 2, *ASM Handbook*, ASM International, p 683–687

SELECTED REFERENCES

- Armstrong, E.T., Dayton, R.W., and Dawes, R.C., 1949. "The Machinability of Beryllium," AECD-3880, BMI-T-II, Battelle Memorial Institute
- Brewer, A.W., 1970. Spark Machining of Beryllium, *Microstructures*, Vol 1, p 25–28
- Colling, L.W., Jr., 1961. Machining the Astro-Metal-Pure-Beryllium, *Machinery*, Vol 67 (No. 10), p 93–97
- Creutz, E., and Gurinsky, D., 1952. Fabrication of Beryllium Metal, *Met. Progr.*, Vol 62, p 82
- Creutz, E.C., Gurinsky, D.G., Chapin, J.H., Yancey, R.W., Foote, F.G., Bethke, H., and Kaufmann, A.R., 1946. "The Extrusion of Beryllium," DEP No. AECD 2883, U.S. Atomic Energy Commission
- Denny, J.P., Meyer, G.E., and Funk, E.A., 1966. Drawing Fine Beryllium Wire, *Beryllium Technology*, Vol 1, L.M. Schetky and H.A. Johnson, Ed., Gordon and Breach Science Publishers, NY, p 661–678
- Denny, J.P., and Patenaude, C.J., 1966. Casting of Beryllium Ingots and Shapes, *Beryllium Technology*, Vol 33, L.M. Schetky and H.A. Johnson, Ed., Gordon and Breach Science Publishers, NY, p 807–824
- Friedman, G., 1937. "Problems in the Extrusion of Structural Beryllium Shapes," Technical Paper MF-67-204, American Society of Tool and Manufacturing Engineers, Dearborn, MI
- Gross, A.G., O'Rourke, R.G., and Beaver, W.W., 1959. "Fabrication of Beryllium Wire," Final report, Navy Contract NOw-59–6030-C0
- Hayes, A.F., 1969. "Production of Forged Beryllium Conical Structural Shapes," Wright Patterson Air Force Base, Air Force Materials

Laboratory, Report TR-69-1 68, Ladish Co., Cudahy, WI
- Hovis, V.M., 1966. "Machining and Finishing Fine-Grained Beryllium," Report Y-1551, Union Carbide Corp.
- Kawecki Berylco Industries, Inc., 1975. "Beryllium—High Purity Extrusion Grade," File 302 6-SP2
- Meyer, G.E., 1965. "Casting and Hot Working of Sound Large Diameter Beryllium Ingots," United States Air Force Contract AF33(657)-10943, Technical Report AFML-TR-65-361, The Beryllium Corporation
- Meyer, G.E., and Henning, H.J., 1970. "Beryllium Wrought Products," DMIC Report S-29, Defense Metals Information Center, Battelle Memorial Institute, Columbus, OH, p 4, 5
- Murphy, E.A., Hornak, M.B., and O'Rourke, R.G., 1965. "Developing Technology to Forge Unclad Beryllium," Report AFML-TR-65-30, Wright Patterson Air Force Base, Air Force Materials Laboratory
- Olofson, C.T., 1959. "The Machining of Beryllium," Batelle DMIC Memo 21, Battelle Memorial Institute
- Pearson, C.E., and Parkons, R.N., 1960. *The Extrusion of Metals*, 2nd ed., Chapman and Hall, London
- Purdon, B., 1968. "Advanced Techniques for Chemical and Mechanical Machining of Beryllium," North American Rockwell Corp., Los Angeles Division
- Taylor, R.D., 1982. Preparation of High Purity Beryllium Foils, *Nucl. Instrum. Methods*, Vol 200, p 135–140
- Webster, D., and Crooks, D.D., 1975b. "Textureless Forming of Beryllium," Lockheed Report LMSC-D462630, U.S. Patent No. 3,954,514, Palo Alto Research Laboratory
- Williams, R.F., Gerds, A.F., and Boulger, F.W., 1966. The Fabrication of Beryllium, *A Survey of Current Technology*, Vol 1, Report NASA TM-X-53453, Lockheed Space and Missile Co., Palo Alto, CA
- Zenuk, C.H., and Loewenstein, P., 1968. "Production Techniques for the Extrusion of Thin Lockalloy Shapes," Technical Report AFML-TR68-238, AFML/AFSC, Wright Patterson Air Force Base, OH

Beryllium Chemistry and Processing, p 339-359
By Kenneth A. Walsh
Edited by Edgar E. Vidal, Alfred Goldberg,
Edward N.C. Dalder, David L. Olson, and Brajendra Mishra

CHAPTER 21

Metal Removal

Alfred Goldberg, Lawrence Livermore National Laboratory
Dennis Floyd, Science Applications International Corporation

21.1 Overview

Beryllium is readily machinable. Excellent surface finishes and close tolerances can be obtained with the fine-grained beryllium produced from powders. By contrast, machined surfaces of cast beryllium are typically rough due to the coarse-grained structure of as-cast beryllium. Although beryllium is relatively soft (Rockwell B 80 to B 90, depending mainly on its oxide content), it is abrasive, producing a discontinuous chip [Brush Wellman 1982]. This characteristic causes tool-edge erosion when using improperly designed tooling or when the wrong material is selected for the cutting tool edge. The chips tend to become more continuous with decreasing oxide content. The abrasiveness of beryllium will rapidly wear down cutting tool edges, degrading accuracy and causing excessive scrap due to the need to repeat machining of machined parts requiring tight tolerances. The abrasiveness (tool wear) decreases with decreasing oxide content. The oxide content appears to have a greater influence on tool wear than does the work-hardening factor of the beryllium. With few exceptions, beryllium has similar machining characteristics to those of chilled (hard) gray cast iron and to heat treated aluminum castings; accordingly, it uses similar machining practices [Brush Wellman 1982, Bunce and Hill 1979]. Beryllium has a machinability factor of 55% of the machinability of grade 1112 free-machining mild steel.

The machining blanks, which are typically cut out from beryllium blocks, are usually in a high state of residual stress, which at times may be quite complex. These residual stresses may cause severe machining problems, especially if they continually vary during the machining. A stress-relief treatment of up to 2 h in the temperature range from 570 to 800 °C (1060 to 1470 °F), followed by controlled slow cooling, is recommended. The cooling rate should not exceed 150 °C/h (270 °F/h). The recommended cooling rate for large sections can be as low as 20 °C/h (36 °F/h) [Bunce and Hill 1979].

Beryllium, being a brittle material, will easily chip or break if roughly handled or if improperly supported. Sharp corners should be avoided. The metal has a tendency to chip or edge crack as the tool enters or leaves the part. To minimize this problem, chamfering of edges, especially corner edges, should be included in the design of the part. Cutting should proceed from the corner edges inward, finishing in the center of the part. Using run-off material as well as light cuts may also be helpful. When drilling or tapping through holes, backup support (brass or free-cutting mild steel fixtures) should be used to minimize breakthrough damage. Any steel scrap can readily be separated magnetically from the beryllium scrap, while both brass and steel can be dissolved by nitric acid. To prevent possible distortion and/or cracking, soft jaw chucks that provide as large a contact area as possible should be used, and excessive pressure should be avoided [Brush Wellman 1982, Bunce and Hill 1979, Paul 1967]. Machining on centers should be done using live (rotating) centers in contrast to stationary centers. In the latter case, carbide centers with lubricants must be used [Paul 1967]. Since beryllium has a relatively

low-precision elastic limit with the possibility of microcreep, care must be taken in cutting, handling, or storing unsupported thin regions to avoid permanent deformation.

Because of the high value of beryllium scrap and the cost of decontamination, where practical, beryllium should be machined dry (i.e., without the use of a lubricant). Dry chips have a higher salvage value than wet chips. Accordingly, heavy stock removal is usually performed dry. Advantages of wet cutting are improved cutting action and a reduction of airborne beryllium dust. Health hazards may also dictate the use of wet machining/cutting. In some operations, wet cutting must be used due to the difficulty in collecting dry chips and/or to flush chips away from the cutting region, such as in grooving and drilling. Coolants should also be used where excessive heat may be generated. For best results, beryllium should be finish machined with coolants [Brush Wellman 1982]. Care must be taken that the wet coolant or cutting oil does not react with the metal and that it does not dry out and allow dust to form. The coolant and/or cutting oil should be washed off in a solvent, and the machined part should be dried. To prevent corrosion, distilled or deionized water should be used for mixing with water-soluble oils, which are the preferred oils (typically one part oil to 20 to 30 parts water). These oils should be changed monthly and the pH level maintained according to specifications. Oils should be without sulfur and without free chlorine.

The beryllium should not be exposed to cutting oils or coolants for an extended period of time, lest the beryllium becomes etched or corrosion is initiated. For example, a galvanic couple can develop between the beryllium and the metal fixture when exposed to the coolant. Operations using brass fixtures while beryllium is in contact with water-soluble coolants should be limited to less than 30 min [Paul 1967]. The galvanic action may be prevented by coating the fixture with a polymer such as polytetrafluoroethylene (PTFE), which is a pure form of Teflon (E.I. duPont de Nemours & Co.), or with trichlorotrifluoroethane (Liquid Freon TF by DuPont), that was shown to be a good coolant and lubricant. A coolant grade especially formulated for beryllium is Prochem Triple C type 5505 [Brush Wellman 1982]. After using coolants, the part should be neutralized before storage, assembly, or packaging. This can be accomplished by immersion in perchloroethane, followed by air drying. Freon is the recommended agent for ultrasonic cleaning. Contact with alcohol or halogens should be avoided [Bunce and Hill 1979].

Government regulations limit the maximum in-plant atmospheric concentration of beryllium to an average of 2 $\mu g/m^3$ (this may soon be changed to 0.2 $\mu g/m^3$) for an 8 h day [Brush Wellman 2001, Gallagher and Hardesty 1989]. Exposures to 25 $\mu g/m^3$ for as long as 30 min are allowed, but exposure to concentrations over this amount for any period of time is considered unsafe. For machining operations, an appropriate hood and exhaust system should be installed, enclosing the workpiece, cutting tool, and chuck. Where a hood may not be practical, an exhaust nozzle alone can be used and should be located no further than 13 mm (0.5 in.) from the cutting tool. Although the speeds and feeds of typical lathe operations are similar to those applicable to cast iron, they are often limited by the efficiency of the dust extraction and chip collection systems. The operation should be approved and monitored by an industrial hygienist. Polishing of the machined workpiece should be done in a glove box or, if using a lathe, under a hood [Gallagher and Hardesty 1989].

Beryllium work hardens during machining, resulting in a susceptibility to microcracking [Beitscher 1979, Bunce and Hill 1979]. The depth of machining damage is approximately 10% of the depth of the cut. Machining damage and tool life are functions of cutting parameters, such as cutting speed and feed rate. Increasing the cutting speed with finer depth of cut may result in an unsafe practice due to the pyrophoric nature of heated beryllium chips. Increasing the feed rate leads to increasing the cutting forces and machining damage.

It is necessary to consider certain precautions to successfully machine beryllium. These precautions are needed to avoid such defects as chipping, edge cracking, tool breakthrough damage during drilling, and permanent deformation when holding thin sections. The beryllium oxide content is a serious factor because the presence of oxides in a powder metal part causes the material to cut with a discontinuous powder chip. The chips become more continuous as the oxide content is reduced. Chip formation is due primarily to brittle fracture. Precision machining of beryllium often requires a stress-relieving treatment after semifinish machining and thermal cycling after finish machining. The stressed layer can be removed by chemical etching, but this is not a recommended

practice since its application affects dimensional accuracy.

21.2 General Machining Guidelines

General guidelines for machining of beryllium are described as follows and apply to the standard processes of turning, milling, grinding, drilling, sawing, and so on [Beitscher 1979, Bunce and Hill 1979]. Some of these guidelines have been mentioned already but are repeated for emphasis and to provide a concise summary of the key variables:

- To reduce chipping or edge cracking as the tool enters or leaves the workpiece, it is advisable to design chamfers into corner edges of components or alternatively modify the machining technique so that cutting takes place from corner edges inward and finishes in the center of a surface.
- Machining between centers should be carried out with live centers (centers that turn with the workpiece) where possible.
- Use soft jaw chucks to provide as large a contact area as possible, since beryllium is a relatively soft material having a hardness in the range of 90 to 150 HV, depending on the purity and fabrication route. It may be advisable to use locating diameters or holes.
- To drill or tap holes, it is necessary to use back-up fixtures to minimize breakthrough damage. Mild steel is recommended, since either magnetic separation or acid leaching can remove steel contamination.
- To accommodate the low-precision elastic limit of beryllium when cutting unsupported surfaces in thin cross sections, the recommended practice is to fill parts with a low-melting-point alloy that can be easily removed after machining.
- Select cutting oils and coolants that do not promote corrosion. Exposure of beryllium to the cutting fluid should be for the minimum amount of time possible.
- Use distilled or deionized water for mixing soluble oils and cleaning contaminated beryllium surfaces.
- To neutralize beryllium surfaces, immerse the part in perchloroethane, followed by air drying. Freon (or a Freon substitute) is recommended as an ultrasonic cleaning agent.
- Exposure of beryllium to mixtures of methanol and Freon (or a Freon substitute) and to alcohols or halogens can be detrimental.
- Recognize and alleviate machining damage in the form of residual stresses, microcracks, and surface scuffing.
- Strictly adhere to recommended feed rates, cutting speeds, cutter geometry, and cutter sharpening or renewal frequency.
- A variety of types of tool cutters with a wide range of tool design may be used. Depth of cut is usually in the range of 0.012 to 8.9 mm (0.0005 to 0.4 in.). When finishing, a good practice is for each new cut to be one-half the depth of the preceding cut, to minimize the residual machining damage.

Machining-induced surface damage includes twinning [Beitscher 1979]. In the lathe-turned material, twins are apparent in approximately one-half of the surface grains. Some grains have a large portion twinned, and other grains exhibit a few individual twins occupying a small portion of the grain area. In milling, the surface grains are heavily twinned. The subsurface grains experience less twinning, which often leaves a sawtooth boundary between the lightly twinned and heavily twinned material. The resulting twinning can rotate cleavage planes of beryllium crystals into the directions that are detrimental to the ductility.

Cracks are observed with less frequency than twins. Cracking is sometimes observed in the machine-damaged layer but only after tensile straining. Most of these cracks are reported to be the result of crack nucleation and propagation during straining and are not present prior to straining.

Residual stresses develop in beryllium during machining. The residual stresses in machined beryllium are always compressive. They can be as high as 280 MPa (40 ksi). The stress-relieving and thermal-cycling operation involves heating the part to be machined to temperatures between 770 and 800 °C (1420 and 1470 °F) for 1 to 2 h in an inert (or slightly reducing) atmosphere or vacuum. The part should be allowed to slow cool ($<$25 °C/h, or 45 °F/h). Grinding will also reduce the stresses but does not totally alleviate the compressive stresses. The finished beryllium part is stabilized by subjecting it to a cyclic heat treatment between two extreme temperatures. The selection of these temperatures varies and depends on the end use of the part. The surface compressive residual stress in beryllium is normally considered favorable to ductility. Most

likely, this stress state hinders the nucleation and propagation of surface cracks.

The passage of the tool over the beryllium surface causes deformation that reorients the grains in the damaged region and generates a possible surface texture. This behavior causes a reduction in strength or ductility if cleavage planes are aligned perpendicular to the direction of stress. It is not expected that the shallow geometrical grooves produced any significant level of reduction on the mechanical properties of beryllium. When used in cyclic stress situations, however, there is a concern that the surface defects will nucleate cracks that will propagate with each cycle, resulting in a reduction in service life.

Proper selection of cutting parameters is essential to avoid machining damage and elevating the tool and workpiece temperature. The cutting forces must be minimized to avoid work hardening, which results in residual stresses, twinning, and microcracking. With proper choice of machining parameters, it is possible to achieve dimensional and geometrical tolerances of better than 1.0 μm. With a cutting speed of 30 m/min (98 ft/min) and a feed rate of 0.12 mm/min (0.005 in./min), overheating can be minimized and the temperature of the workpiece and tool kept below 470 °C (880 °F). Tool life was found to be satisfactory with these optimized parameters. Increasing the cutting speed with finer depth can result in a greater dissipation of heat through the chips, which results in unsafe pyrophoric behavior. The cutting speed for turning and thread cutting is larger than for thread cutting and reaming. Also, the increase in feed rate can result in a higher chip cross section, higher cutting forces, and increased susceptibility to machining damage. If the depth of cut exceeds twice the tool nose radius, the dissipation of heat through the chips decreases, resulting in reduction of tool life. If the depth of cut is very small, a high-frequency vibration results and may lead to microcracking.

The selection of cutting tool material is limited. High-speed steel tools, even with their low tool life, are used for difficult surface contours. Diamond tools are unacceptable because they react with beryllium, causing graphitization of the diamond and resulting in greater wear. Tungsten carbide tools can overcome these difficulties by maintaining an acceptable cutting edge. Tungsten carbide tooling has two to three times the cutting life of high-speed steel tools [Bunce and Hill 1979]. It is suggested that both the tool wear resistance and surface finish may be enhanced by honing or lapping the tool cutting surfaces. The use of a sharp tool is important in reducing the tendency or extent of machining surface damage, which is a common occurrence with beryllium. A grade 2, general-purpose carbide cutting tool used for cast iron and nonferrous materials is recommended, with preference of specific grades within this class, such as Valenite VC-2 or equivalent [Brush Wellman 1982, Brush Wellman 2001]. Excellent results are attainable with this grade for medium-to-light cuts on long workpieces with extensive cutting-edge coverage. In general, carbide tools of ISO K05/K10 grades offer an excellent tool life and produce a good surface finish. Carbide drill bits result in better drill life and produce better hole contours when compared to high-speed steel drill bits. The cutting speed with tungsten carbide tools has been reported to be twice that with high-strength steel tools. Brazed tip-type tools are used for most metal-removal operations.

Conventional tool geometries are appropriate for beryllium metal removal. The conventional cutting angle on twist drills of 118° results in radial circumferential cracks and breakthrough damage. Cutting angles of 90° for drilling thickness up to 3 mm (0.1 in.) and 100° for drilling thickness above 3 mm (0.1 in.) have performed acceptably. Tools with zero or negative rake result in excessive edge cracking at the initiation or exit of a cut. Tools with larger clearance angles can improve metal removal but at a reduced tool life. Suggested tool geometries are given in Fig. 21.1. Tools with multiple points, each with a modified geometry, have worked satisfactorily.

Computer-aided design/computer-aided manufacturing (CAD/CAM), which is increasingly used in the design and manufacture of components and systems, is not discussed in this book. An excellent description of CAD/CAM for machining operations is presented in *Machining*, Volume 16 of *ASM Handbook* [Zimmers 1989].

21.3 Machining-Surface Damage

Beryllium is susceptible to surface damage during machining, which, if not removed, will degrade its mechanical properties. The surface layer of a machined part typically will contain microcracks and a network of twins [Marder et al. 1990] (detected metallographically) that can lead to brittle fracture. The formation of twins is

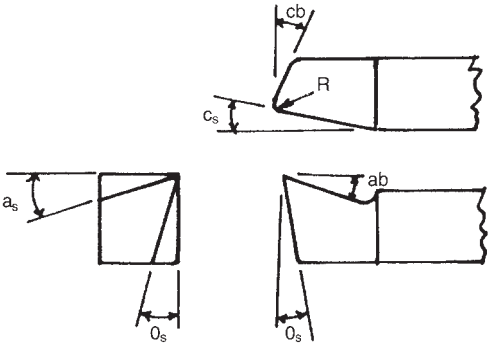

Nomenclature	Value (X°) for SS 304	Be	Cast iron	Nonferrous metal
ab, back rake, deg	0 to (−7)	+7	0 to −7	0 to 10
a_s, side rake, deg	+6 to (−7)	+5	+6 to −7	10 to 20
ϕs, end relief, deg	5 to 10	(+10)	5 to 8	6 to 10
θs, side relief, deg	5 to 10	+10	5 to 8	6 to 10
Cb, end-cutting edge, deg	5 to 15	15	5 to 15	5 to 15
C_s, side-cutting edge, deg	0 to 20	0 to +10	0 to 45	0 to 45
R, nose radius, deg	0.1 to 0.5	0.25	0.1 to 0.5	0.5 to 1.5
Drill angle, deg	118	. . .	118	118
	90° up to 3 mm drilling 100° above 3 mm drilling			

Fig. 21.1 Cutting tool designs used for beryllium and comparison of geometry with other metals

caused by the machining-induced stresses. The depth of the damage is largely dependent on the severity of the machining operation. Twins tend to propagate readily through a grain but propagate with difficulty across a grain boundary. Therefore, the extent of damage is also related to the grain size. It appears that the depth of machining damage increases with increasing grain size, and, accordingly, increasing grain sizes require increasing the depth of surface removal, which is done by chemical machining (an etching process). The depth of the twinned region typically may range from 0.05 to 0.5 mm (0.002 to 0.02 in.), and it appears to be less with a decrease in the grain size [Beitscher 1979]. For fine-grained material, deformation (mechanical) twins have been detected to depths of 250 μm below the machined surface. For a grain size of 25 μm, this depth would correspond to ten grains. It is generally accepted that the damage depth for fine-grained beryllium under normal machining practice is approximately 10% of the depth of the cut [Bunce and Hill 1979]. The surface grains are much more heavily twinned than the subsurface grains, and the degree of twinning decreases with distance from the surface. This observation is illustrated in Fig. 21.2, which shows a plot of the number of twins remaining on the etched surface as a function of

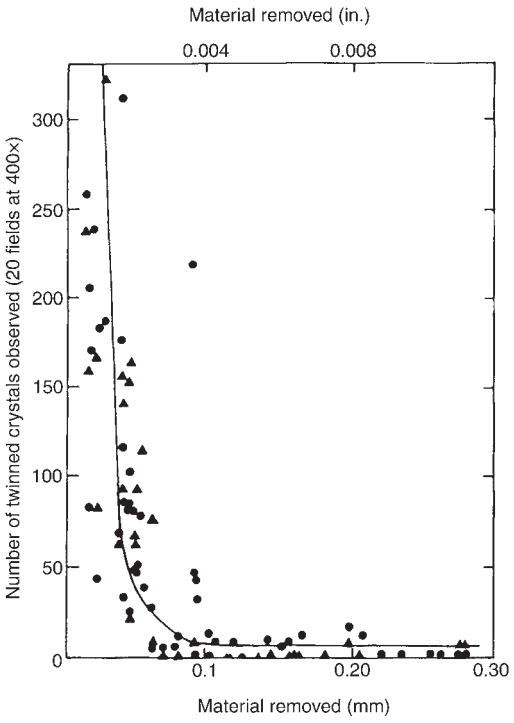

Fig. 21.2 Number of twins observed on the etched surface of a machined beryllium as a function of depth of etching. Δ, direct observation; ●, replica observation. Source: Beitscher 1979

etch depth for machined S-200 beryllium having a grain size ranging from 35 to 50 μm [Beitscher 1979]. The analysis was made using both direct observation and acetate replicas of the surface examined at 400×. In this study, it was noted that microcracks, laminations, and smeared metal were completely absent after an etch depth of 0.025 mm.

Surface damage, if not removed, can result in a large decrease in both fracture strength and elongation. Although the yield strength may not be significantly affected, elongation can be reduced to a fraction of the damage-free elongation [Brush Wellman 1982]. Regardless of grain size, etching to remove approximately 100 μm from each machined surface is recommended [Brush Wellman 1982, Cooper 1979]. This amount of removal, which assumes that proper machining practices were used, generally results in a marked improvement in mechanical properties, even though the calculated critical crack sizes for beryllium are larger than this value, namely, between 0.2 and 1 mm (0.008 and 0.04 in.) [Cooper 1979]. It was generally observed that for tensile test specimens, etching 0.08 to 0.13 mm (0.003 to 0.005 in.) off from each surface was sufficient to remove nearly all the detrimental effects of most machining treatments, even if etching to that depth range did not remove all the metallographically detectable damage [Beitscher 1979].

When fabricating the space shuttle orbiter, it was determined that the removal of 0.152 mm (0.006 in.) of metal by etching was required to eliminate the presence of all machining-induced twinning; this was done without creating excessive dimensional tolerance problems (except for holes in thick sections) [Norwood 1984]. Typical machining damage ranges from 0.025 to 0.10 mm (0.001 to 0.004 in.) for most machining and may extend to a depth of 0.50 mm (0.02 in.), depending on the machining method [Gallagher and Hardesty 1989]. Good practice dictates that the damaged layer should generally not exceed a depth of 51 μm (0.002 in.). However, under severe machining, damaged layers 0.254 mm (0.01 in.) deep may be obtained. Surface damage must be restricted to a maximum depth of 102 μm (0.004 in.) in machined structural surfaces [Brush Wellman 1982]. This depth of damage can be eliminated by either a stress relief or an acid etch. Excessive removal of damaged surface material by etching will decrease dimensional-tolerance control. Experience has indicated that very close tolerances can be maintained with surface removal of as much as 127 μm (0.005 in.) [Brush Wellman 1982].

Etchants commonly used for chemical milling are:

- 2%HF-2%HNO_3-2%HSO_4 [Brush Wellman 1982, Hashiguchi 1992]
- Sulfuric acid solutions
- Nitric/hydrofluoric acid solutions and ammonia bifluoride [Hashiguchi 1992]
- 15% ammonium bifluoride and 20% nitric acid-1% hydrofluoric acid [Beitscher 1979]
- 10% distilled or deionized water, 127 g dry chromic acid, 75% phosphoric acid, with 15% sulfuric acid and 25% nitric acid, 0.25 to 1.0% hydrofluoric acid, and balance distilled or deionized water [Hughes Aircraft Company].

In the absence of microcracks and where the damage is due only to mechanical twinning and where dimensional tolerance is important, a 2 h anneal at 800 °C (1470 °F) may be sufficient to preserve the desired properties. This anneal is also adequate to remove any residual stresses and essentially restore the premachined, room-temperature mechanical properties [Cooper 1979]. The condition of machined parts can be determined by examining polished cross-sectional surfaces (in polarized light, 250× magnification) of machined samples with the same thermal history as the parts [Brush Wellman 2001]. The use of heat treatment may not be feasible for temperature-sensitive structures, for example, structures containing brazed joints.

In general, for tensile-load-bearing components (or any critical components), etching and/or a stress-relief treatment is recommended following machining. Etching (chemical milling) can be used to remove the machining-damaged layer. This is accomplished by immersing the part in an acid solution for a specified length of time. The material removal, however, can be uneven and cause a loss of precision tolerances. Heat treatment, which removes the mechanical twins, will not affect dimensional tolerances, except for possible distortion. Annealing twins may form, but they will not adversely affect mechanical properties. Whereas heat treatment will not remove all surface defects (e.g., machining cracks), etching, while removing damaged metal, will also remove all the possible defects contained in the damage-removed metal. Nevertheless, in general, in the absence or even with a slight presence of machining cracks, annealing

Table 21.1 Transverse tensile properties of as-machined, annealed, and etched grade S-200E beryllium

Condition		Ultimate tensile strength		0.2% yield strength		Elongation, %
		MPa	ksi	MPa	ksi	
Premachining		366	53	227	33	3.7
As-machined		263	38	216	31	0.7
Machined and annealed at °C (°F)	400 (750)	218	32	193	28	0.5
	500 (930)	207	30	199	29	0.3
	600 (1110)	282	41	187	27	2.0
	700 (1290)	353	51	205	30	3.6
	800 (1470)	343	50	230	33	3.1
	900 (1650)	347	50	249	36	3.2
	1000 (1830)	342	50	239	35	3.3
Machined and etched	25 μm	323	47	209	30	2.8
	50 μm	337	49	220	32	2.8
	75 μm	333	48	216	31	3.1

Source: Gallagher and Hardesty 1989

appears to be as effective as etching in restoring mechanical properties of machined parts. Most investigators concluded that machining cracks are less significant than mechanical twins in affecting mechanical properties [Beitscher 1979]. Table 21.1 lists some mechanical properties of S-200E beryllium in the following conditions: before machining, as-machined, machined and annealed, and machined and etched [Gallagher and Hardesty 1989].

A stress-relief-anneal schedule proposed by Brush Wellman is as follows [Brush Wellman 1982]:

- Use a high-vacuum furnace to minimize oxidation and discoloration.
- Heat the part to 760 ± 5 °C (1400 ± 9 °F) and hold for 1 h for each 25.4 mm (1.0 in.) of cross section.
- Vacuum cool in a two-step process from 760 to 690 °C (1400 to 1275 °F) at a maximum rate of 5 °C /h (9 °F/h) and from 690 to 200 °C (1275 to 390 °F) at a maximum rate of 50 °C/h (90 °F/h). An inert-gas atmosphere may be used below 690 °C (1275 °F).

In a more recent Brush Wellman report [Hashiguchi 1992], the parts were heated to 790 °C (1455 °F). Also, it was recommended that the vacuum cooling rate for large pieces be limited to a maximum of 20 °C/h (36 °F/h) in both temperature regimes of the cooling process.

Fatigue properties were shown to be significantly improved after removing the machining-damaged surface by etching and/or annealing, as indicated in Fig. 21.3 for extruded ingot beryllium. An unusual contradiction to these results is shown in Fig. 21.4, where the fatigue behaviors of machined and of machined-and-etched ingot-source sheet material are shown. This unexpected result was attributed to the possibility that the residual surface compressive stresses outweighed the detrimental effects of the surface twins in the as-machined specimens [Beitscher 1979].

Figure 21.5 shows that for ground Charpy unnotched specimens of beryllium, the impact toughness transition temperature was lowered by etching to a depth of 0.05 mm (0.002 in.). Significant improvement by etching was obtained in the ambient temperature region. These and other results show that the two sets of toughness values tend to converge at elevated temperatures. It was also observed that the detrimental effects of a basal orientation that results in basal-plane fracture may actually become more significant than surface damage in affecting impact toughness of beryllium [Beitscher 1979]. Note the low toughness values shown in Fig. 21.5 for the shot-peened specimens independent of temperature.

Some studies have been reported evaluating the effect of machining temperature on surface damage. Lathe turning of hot pressed S-200 fine-grained (10 μm average grain diameter) beryllium at 400 °C (750 °F), which is above its ductile-to-brittle transition temperature (DBTT) range, essentially eliminated the development of twinning, microcracks, and residual stresses. Figure 21.6 shows the effect of cut depth on depth of twinning for the same material at several temperatures below 400 °C (750 °F), namely, ambient, 230, 290, and 340 °C (445, 555, and 645 °F) [Beitscher 1979]. A decrease in machining temperature resulted in a deeper penetration of twinning for a given cut depth, although the differences between the three

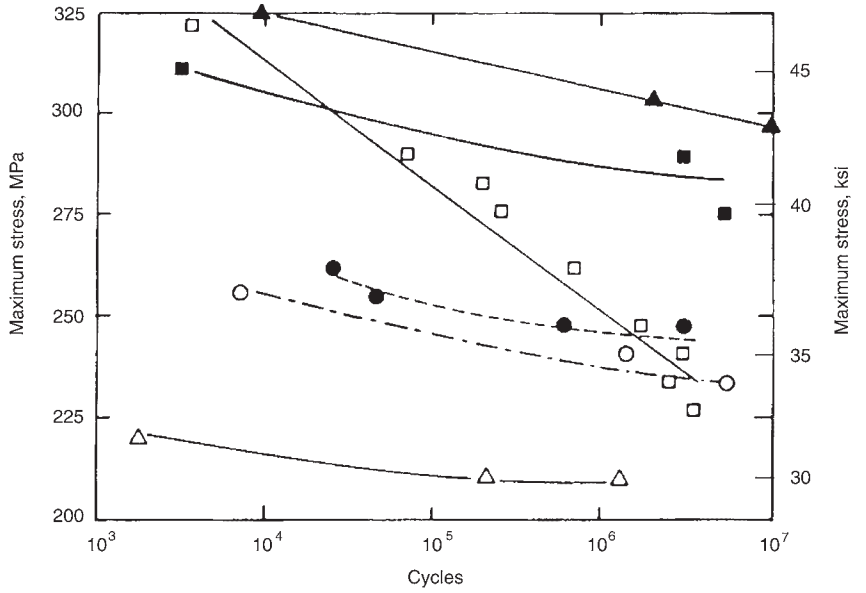

Fig. 21.3 Effect of various treatments on the fatigue life of extruded ingot beryllium. ▲, annealed, etched 0.46 mm (0.02 in.) deep; ■, annealed, etched 0.46 mm deep (245 MPa, or 36 ksi); ●, annealed, etched 0.05 mm (0.002 in.) deep (236 MPa, or 34 ksi); □, annealed (259 MPa, or 38 ksi); °, as-machined, etched 0.05 mm deep (275 to 400 MPa, or 40 to 58 ksi); Δ (210 MPa, or 30 ksi). Numbers in parentheses refer to ultimate tensile strength. Source: Beitscher 1979

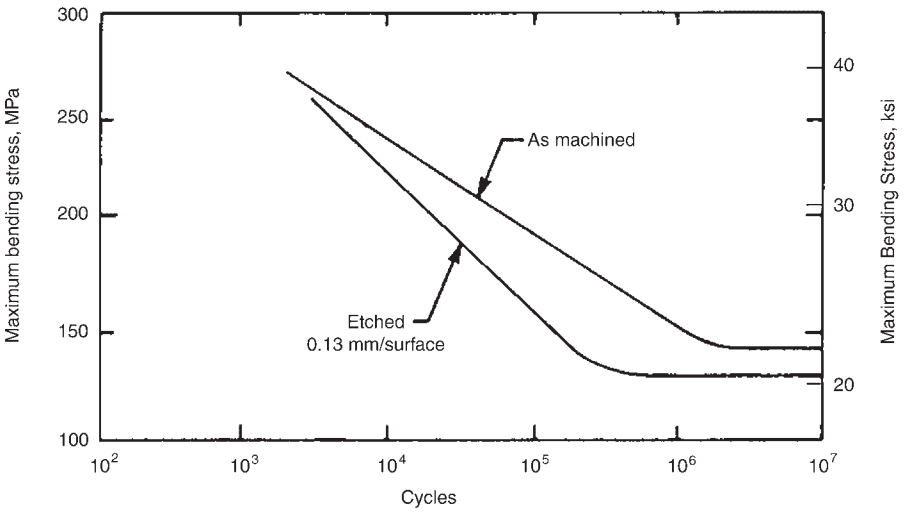

Fig. 21.4 Effect of etching on the fatigue behavior of machined ingot-sheet beryllium. Note that the results are opposite to what would be expected. This was attributed to residual compressive machining stresses dominating over the removal of surface damage. Source: Beitscher 1979

higher temperatures are minor. At ambient temperature, the ratio of twin depth to cut depth is approximately 0.05; at the higher temperatures, it is approximately 0.004. Residual stress after machining at ambient and at 400 °C (750 °F) was also compared, giving residual compressive stresses of 55 and 3 MPa (8 and 0.4 ksi), respectively, above the residual stresses present in unmachined material. Differences obtained between machining at 400 °C (750 °F) and at the lower temperatures were attributed to the additional slip systems operating at the higher temperature, that is, above the DBTT. In contrast to these results, one study reported that no signifi-

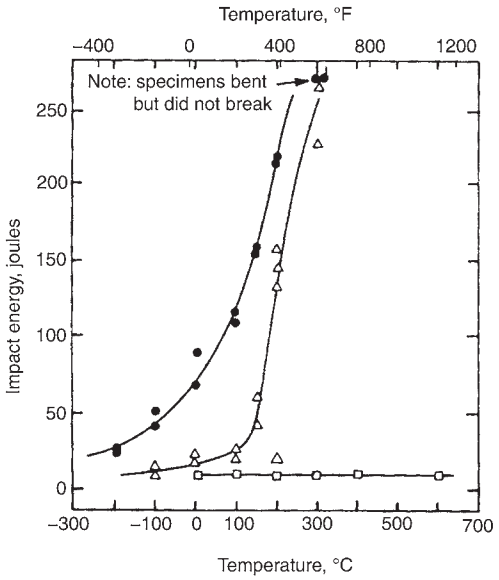

Fig. 21.5 Impact behavior of unnotched Charpy specimens obtained from hot upset beryllium sheet. Δ, as-ground; ●, ground and etched to 0.05 mm (0.002 in.) depth; □, shot peened. Source: Beitscher 1979

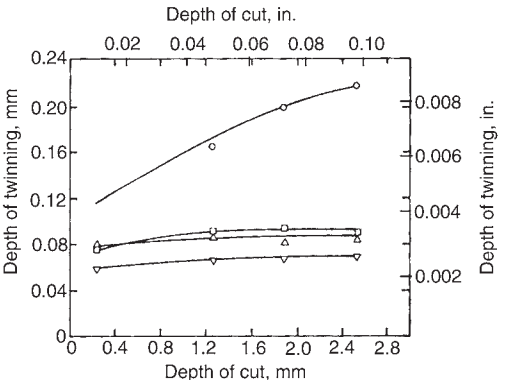

Fig. 21.6 Influence of lathe cutting depth and machining temperature on the depth of twinning in hot pressed beryllium. ○, ambient temperature; □, 230 °C (445 °F); Δ, 290 °C (555 °F); ∇, 340 °C (645 °F). Source: Beitcher 1979

cant difference in twin depth was found (metallographically) by lathe turning at temperatures of −70, 25, and 250 °C (−95, 75, and 480 °F) [Gallagher and Hardesty 1989].

Machining damage can be minimized by adjusting the machining schedule to produce finer and finer successive cuts. For example, each cut should be one-half the depth of the preceding cut. The optimum schedule for a particular case would be determined by pre-evaluations. Cut depths can range from 12.7 μm to nearly 9 mm (0.0005 to 0.35 in.) if required [Bunce and Hill 1979, Paul 1967]. Finishing cut depths should not exceed 0.76 mm (0.030 in.), to avoid developing excessive residual stresses. An example of a partial final sequence of finishing cuts is 0.76, 0.51, 0.25, and 0.127 mm (0.030, 0.020, 0.010, and 0.005 in.) [Brush Wellman 1982].

Hughes Aircraft specifies two procedures for finish machining of beryllium of hot pressed blocks and wrought material, respectively, which includes stress relieving and surface-damage reduction, as follows [Hughes Aircraft Company].

Hot pressed block:

- Machine each surface to within 0.51 mm (0.020 in.) of final dimensions, using 0.76 mm (0.030 in.) maximum cut depths.
- Stress relieve by heating to 871 °C (1600 °F) in a vacuum or inert atmosphere at a rate not exceeding 316 °C/h (570 °F/h). Hold at temperature for 1 h plus an hour for each additional 25.4 mm (1 in.) of thickness.
- Cool to 371 °C (700 °F) at a rate not exceeding 38 °C/h (70 °F/h). While still in the furnace (vacuum/inert), cool to ambient temperature at a rate not to exceed that obtained in still air; that is, avoid quenching.
- Machine each surface to within 0.25 mm (0.010 in.) of final dimensions, using 0.25 mm (0.010 in.) maximum cut depths.
- Machine each surface to within 127 μm (0.005 in.) of final dimensions, using 127 μm (0.005 in.) maximum cut depths.
- Etch after any machining step, if necessary.

Wrought beryllium:

- Machine each surface to within 0.43 mm (0.017 in.) of final dimensions, using 0.84 mm (0.033 in.) maximum cut depths.
- Machine each surface to within 0.18 mm (0.007 in.) of final dimensions, using 0.25 mm (0.010 in.) maximum cut depths.
- Machine each surface to within 51 μm (0.002 in.) of final dimensions, using 127 μm (0.005 in.) maximum cut depths.
- Etch after any machining step, if necessary.

There will be some degree of uncertainty as to the form of damage that may be present. Some published examples relating appearances to the extent of damage are presented here. Visual inspection (naked eye or low magnification) should reveal some aspects of damage from the surface condition. A change in surface finish from a satinlike appearance for light machining damage (0.05 mm, or 0.002 in., depth)

to becoming striated with heavier damage, the degree of which increases with increased depth of damage, was reported for lathe turning of beryllium. Under optical or scanning electron microscopy, surfaces with shallow twinning (0.04 mm, or 0.002 in., depth) displayed a grain-like structure, whereas surfaces with deep twinning (0.11 mm, or 0.004 in., depth) revealed a smooth, smeared surface with shiny tool marks. If direct metallographic observation of the as-machined surface is difficult, replicas of the surface can be used and taken at several stages during machining. With lathe turning, it was observed that a change in twin depth was accompanied with a change in chip appearance. Also, the amount of tool wear (breakdown) was proportional to the degree of surface damage.

The most reliable method for evaluating the extent of surface damage is by metallographic examination of cross sections perpendicular to the surface. Care must be taken during metallographic preparation to remove any damage caused by the sectioning. A uniform amount of twinning across a section, especially extending beyond a reasonable machining-damaged depth, would be indicative of this. Additional evaluations may be made, such as residual-stress measurements, ultrasonic surface-wave measurements, and x-ray diffraction for surface textures. However, surface damage could exist without positive results from these observations. It should be noted that although machining damage can form without the presence of cracks, other forms of damage are probably always present when cracks are present [Beitscher 1979].

21.4 Machining Operations

Machining encompasses a number of different operations: turning, milling, drilling, boring, grinding, sawing, abrasive cutting, thread cutting, chemical machining, electrical discharge machining, electrochemical machining, and trepanning. Feed rates and cutting speeds for lathe turning and milling are comparable to those used for machining cast iron, although they may be dictated by the efficiency of the dust extraction and chip collection systems. To avoid damaging the relatively soft beryllium, soft chuck jaws should be used, providing as large a contact area as possible. Because of its relative softness, a positive rake angle is recommended for all beryllium machining, since soft materials have a tendency to puddle up in front of the cutting tool, which is minimized by having a positive rake angle.

Beryllium is usually machined dry when heavy stock-removal operations are performed. Coolants are used for operations such as deep-hole drilling, threading, and/or where close tolerances, damage-free surfaces, and long tool life are required. When machining with a coolant, and using brass or copper fixtures, the possibility exists of developing a galvanic action between the beryllium and the fixtures, and this possibility should be monitored [Brush Wellman 1982]. Sulfurized and chlorinated oils should be avoided because they corrode or discolor the beryllium. When cutting fluid is used, the beryllium must be thoroughly washed in Stoddard or methyl ethyl ketone solvent and dried after machining. Wet cutting helps to suppress the beryllium dust but increases the cost of reclaiming the beryllium scrap.

A Hughes Aircraft Company document on machining beryllium specifies that “rough machining (turning, milling, and boring) shall be performed to within 1.27 mm (0.050 in.) of the finished surface and to within 2.54 mm (0.100 in.) on a diameter. Roughing cuts by sawing shall not be closer than 2 mm (0.080 in.) to the final surface. A 0.76 mm (0.030 in.) minimum cut shall be made on a mill or lathe prior to finish machining when roughing by sawing or with an abrasive cut-off wheel. Finish machining shall be defined as the removal of the final 1.27 mm (0.050 in.) of metal in order to meet dimensional requirements.”

21.4.1 Turning

Turning is a machining process for generating external surfaces of revolution by a cutting tool on a rotating workpiece. The operation, which is usually performed on a lathe, includes producing thread forms, trepanning, facing, and, in some cases, drilling and boring. Examples of some of the basic turning operations are shown in Fig. 21.7 [ASM 1989c].

Best turning results are obtained with a positive back rake angle of 1 to 5°. Small positive or even negative rake angles are used for abrasive materials. The rake angles define the relationship between the cutting edge and workpiece. It is generally recommended that for most materials positive rake angles be used with high-speed steel cutters and zero or negative rake angles for carbide-tipped cutters. A positive rake angle will generally provide a better-defined edge than

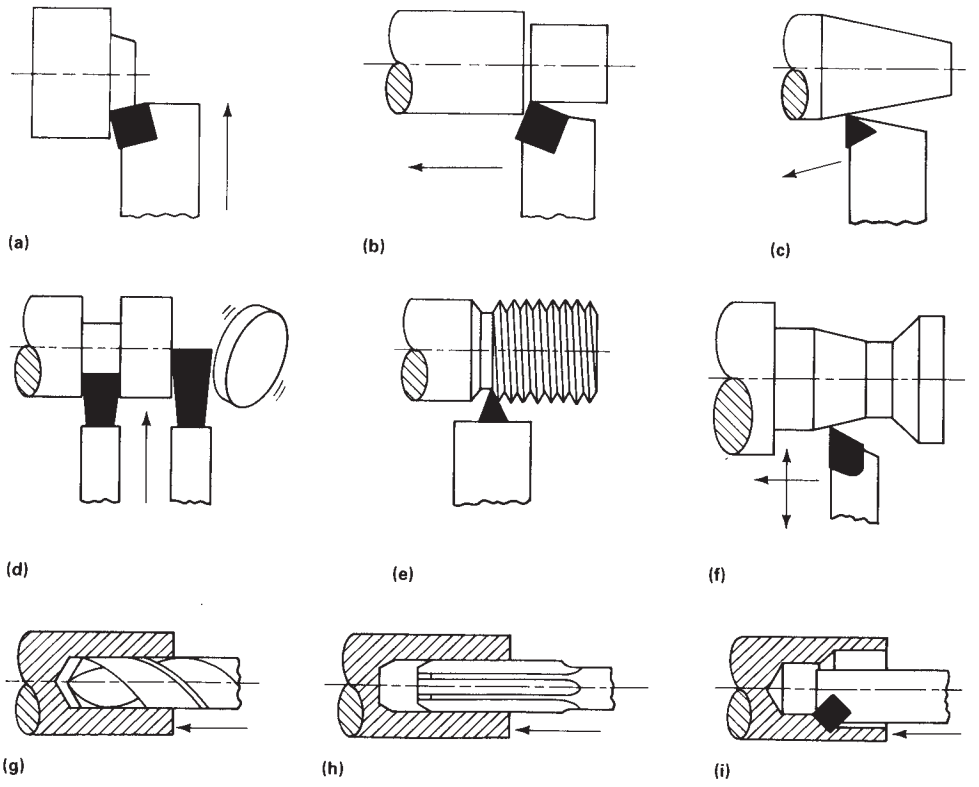

Fig. 21.7 Some basic operations performed on turning equipment. (a) Facing. (b) Straight turning. (c) Taper turning. (d) Grooving and cutoff. (e) Threading. (f) Tracer turning. (g) Drilling. (h) Reaming. (i) Boring. Cutting tool in black. Source: ASM 1989

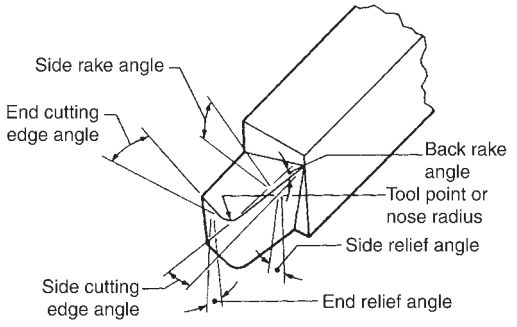

Fig. 21.8 Terms applied to single-point turning tools. The side rake angle shown is positive.

will a negative rake angle. A drawing illustrating the relationship between a single-point cutting tool and workpiece (at cutting edges) and the corresponding terms used is shown in Fig. 21.8 [Hughes Aircraft Company].

Single-point tools must have sharp cutting edges, with a primary clearance angle of approximately 6° and a secondary clearance angle of approximately 10° [Brush Wellman 1982]. It was suggested that for maximum metal removal, the rake angle should be zero, with minimal side clearance. The latter is important to prevent pulling out metal and chipping the machined surface [Beitscher 1979]. To reduce cutting pressure and minimize potential damage to the beryllium part, the nose radius or chamfer should be as small as feasible; a radius of 0.4 mm ($^1/_{64}$ in.) is recommended. Side-cutting angles up to 45° will protect faces from chipping when entering or leaving the workpiece [Paul 1967]. Carbide tools should be used, with the all-tungsten grades being the best. Because of the abrasiveness of beryllium, live centers should be used [Skillern et al. 1991].

Beryllium is commonly rough turned, faced, and bored at speeds of 53.4 to 76.2 m/s (175 to 250 ft/s. Speeds of 30.5 to 61 m/s (100 to 200 ft/s) are recommended for finish turning of critical dimensions. Roughing feeds of 158 to 316 μm (0.006 to 0.012 in.) per revolution are generally used, with finishing feeds as low as 12.4 μm (0.0005 in.) per revolution. Surface roughness is generally in the ranges of 70 to 125 and

30 to 60 rms, respectively [Brush Wellman 1982]. Interrupted cuts should be avoided when turning a round part from a square blank. The use of uncoated inserts with a generous nose radius has been done successfully for roughing cuts. Cut depths could exceed 6.35 mm (0.250 in.) in some cases. Chipping, which may occur as the tool leaves the work at the end of a cut, can be avoided by taking light cuts, using a sequence of short finishing cuts at alternate ends, chamfering both ends prior to turning, and/or using run-off material.

21.4.2 Milling

Milling is a machining operation in which metal is removed by a rotating multiple-tooth cutter, whereby each tooth removes a small amount of metal with each revolution of the spindle. Since both workpiece and cutter can be moved independently in more than one direction at the same time, surfaces having almost any orientation can be machined. Relatively small chips are formed, with variations in thickness within each chip. Basic milling operations and cutters and various surfaces that can be generated are illustrated in Fig. 21.9 [ASM 1989a]. Milling can be done in almost any type of machine that can rigidly hold and rotate a cutter while allowing a workpiece to be fed into the cutter (or visa versa).

Practices for milling are similar to those used for turning beryllium. Up-cut (climb) milling is recommended rather than the more conventional down-cut milling in order to obtain the best surface finish and maximum cutter life [Bunce and Hill 1979]. Edge fracturing (chipping), called breakout, can occur when the cutter moves against and out of an edge of the workpiece. To minimize the tendency to such chipping, up-cutting should be used during the roughing stages, which can be followed by conventional cutting using backup plates (free-cutting steel, polymethyl methacrylate, or beryllium). By beveling (chamfering) the edges of the workpiece, a more gradual exit is provided for the cutter, thereby also reducing the tendency for breakout [Brush Wellman 1982]. Milling parameters may be affected by chip collection problems, because it can be difficult to position the collection piping to the cutter, which is immersed in the workpiece. Thus, except for small vertical-type machines, milling machines are customarily completely enclosed in a glove box [Bunce and Hill 1979].

The axial rake, radial rake, and corner angle in milling are respectively equivalent to back rake, side rake, and side-cutting-edge angle in turning. These angles are usually used to define the relationship between the cutting edge and workpiece. The rake angle affects the shear angle in the chip-forming process and greatly affects the tool force, power requirements, and temperature generated. The tool force decreases as the true rake angle becomes more positive. Face-milling cutters with fine pitches and positive radial and axial tooth rakes should be selected for beryllium. Milling cutters with blade-type inserts can be useful with many variations of blade angles. Carbide insert-type cutters with 30 to 45° corner chamfers or 0.76 to 1.04 mm (0.030 to 0.040 in.) radii are recommended [Brush Wellman 1982]. Interrupted cuts should be avoided; instead, when possible, interrupted cutting should be performed using turning operations [Paul 1967].

Face milling generally uses cutting speeds in the range of approximately 50 to 90 m/min (164 to 295 ft/min) and feed rates of 76 to 127 μm (0.003 to 0.005 in.) per cutting tooth. Finishing-cut depths of from 127 to 254 μm (0.005 to 0.01 in.) will usually yield an acceptable finish [Bunce and Hill 1979]. Beryllium is usually rough milled at surface speeds of 30.5 to 45.7 m/s (100 to 150 ft/s), with a feed rate of up to 0.254 mm (0.010 in.) per tooth and a maximum cut depth of 6.35 mm (0.250 in.). Finish milling occurs at 45.7 to 61 m/min (150 to 200 ft/min), with a maximum cut depth of 762 μm (0.030 in.) and a feed rate of 76 to 203 μm (0.003 to 0.008 in.) per tooth [Brush Wellman 1982]. There is some inconsistency in the data from the two references.

Programming to eliminate exit-edge milling will reduce the tendency for edge damage. Chamfering the edges of the workpiece prior to final milling will also reduce edge damage. The most common method to avoid the edge problem is to cut into a backing plate [Bunce and Hill 1979].

End milling generally uses cutting speeds in the range of approximately 23 to 54 m/min (75 to 177 ft/min) and feed rates of 0.127 mm (0.005 in.) per cutting tooth, the particular parameters being influenced by the exit-edge conditions. Unless special precautions are taken to avoid the tendency of rubbing with shallow cuts (causing surface damage), finishing cuts should be limited to depths of 127 to 254 μm (0.005 to 0.01 in.). Unless provided with rigid spindle construction, end-milling cuts should be limited

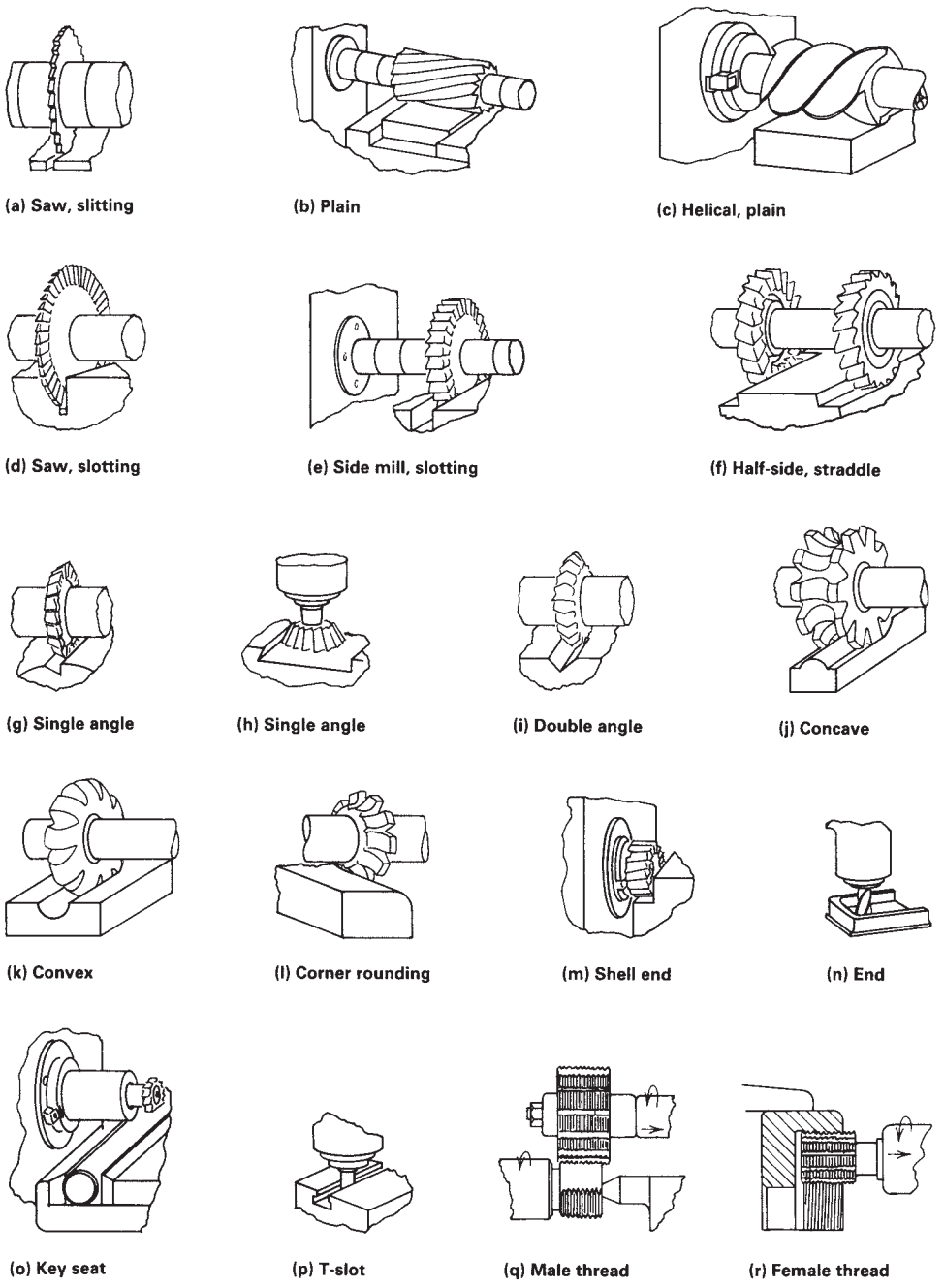

Fig. 21.9 Basic milling operations and cutters illustrating the variety of surfaces and surface combinations that can be generated. Source: ASM 1989a

to 3.175 mm (0.125 in.) [Bunce and Hill 1979]. More flutes, rather than fewer flutes, are recommended for end milling [Brush Wellman 1982].

Roller or slab milling generally uses cutting speeds in the range of approximately 15 to 24 m/min (50 to 80 ft/min) and feed rates of 76 to 127 μm (0.003 to 0.005 in.) per cutting tooth. This milling method is often most effective for finishing because it does not present a trailing-edge problem. The rigidity in the arbor

or fixturing necessary to avoid rubbing cannot be achieved with very shallow cuts. Thus, cut depths are limited to a minimum of 51 μm (0.002 in.). However, it was found that for correct feeds, twin damage was less than 51 μm (0.002 in.) for roller-milling cuts in the 254 to 305 μm (0.010 to 0.012 in.) range [Bunce and Hill 1979].

21.4.3 Drilling

The basic motions of drilling consist of a relative rotation between the workpiece and tool along with longitudinal feeding. These two motions also occur in many other machining operations. Consequently, drilling can be done on a variety of machines. Drill presses are specifically designed for drilling operations with a number of different types of presses available for various drilling operations. The basic requirement is that the spindle (or spindles in a multiple-spindle drilling machine) must rotate accurately and resist any side forces introduced by the drilling. Drilling of long holes offers special problems not generally encountered in typical drilling operations. As the hole length increases, it becomes increasingly difficult to support the workpiece and the drill properly. Rapid removal of the chips, which is necessary to assure accurate drilling, becomes more critical with increased hole length. Deep-hole drilling machines were developed to overcome these problems. Dissipation of heat also is a problem. Holes with depths greater than five times the diameter are considered to be deep holes. The heat problem with deep holes is addressed by using cutting fluids under pressures up to 20.7 MPa (3 ksi) with oil holes or rifle drills [Brush Wellman 1982]. Feed rates for beryllium are generally kept between 25.4 and 254 μm (0.001 and 0.010 in.) per revolution. Cutting speeds range from 7.6 to 30.5 m/min (25 to 100 ft/min), with the higher range being most common. A rigid setup is important for dimensional control and minimization of potential drilling damage. In setups lacking sufficient rigidity, drills with short flutes and tapered shanks should be used [Bunce and Hill 1979]. Cutting speeds were also given as 7.6 to 45.7 m/min (25 to 150 ft/min), with speeds at the lower end of the range used for most applications [Brush Wellman 1982]. Feed rates varied from 15 to 30 μm (0.0006 to 0.0012 in.) per revolution and in special cases may be as high as 254 μm (0.010 in.) per revolution. Prior center drilling is advisable to minimize a bouncing entrance that may cause chipping and, in thin parts, a breakthrough.

The major difficulties with drilling beryllium are tool wear, hole surface damage, chipping, and lamellar cracking or spalling as the drill breaks through the workpiece. The latter can occur when drilling rolled sheet having a high degree of anisotropy (crystallographic preferred orientation). Hole chipping on breakthrough can be minimized by using a backing plate. Beryllium, being notch sensitive, if highly stressed, may stress relieve itself by intergranular cracking. Thus, it is important that drilling parameters, especially feed rate and having the proper drill point [Brush Wellman 2001], are chosen to minimize machining stresses [Bunce and Hill 1979]. Pilot holes should not be used, because enlarging holes by successive drilling can lead to hole damage. For large-diameter holes, final sizing should be performed by boring, which also removes hole-surface damage introduced by drilling [Bunce and Hill 1979].

A slight taper from drill point to shank is important to minimize the resistance due to abrasive wear. For deep holes, tapering in from the drill tip to the shank by approximately 100 μm will reduce heat generation and abrasive wear [Brush Wellman 1982]. Drills with thinned webs are used to reduce thrust force. For through holes, the corners at the outside diameter and the drill point should be chamfered at a 45° angle to prevent chipping when breaking through the beryllium [Paul 1967]. The web thickness should be thin at the drill point and gradually enlarged for strength and rigidity. Two-fluted-tipped drills of tungsten carbide with included angles between 90 and 120° are commonly used. Brush Wellman recommends using an automatic torque-sensing drilling device (Tornetic drilling unit, Dyna Systems, Inc.), which varies the speed and feed rate in order to maintain the cutting force within safe limits for both drill and beryllium [Brush Wellman 2001]. A dull or chipped tool will indicate an increased force and thereby reduce the feed rate [Brush Wellman 1982].

Boring involves the use of a single-point cutter whereby an internal-diameter surface is generated relative to the centerline of the rotating spindle. It is a process used primarily for enlarging or finishing holes. Boring is also used for circular contours other than holes.

According to specifications by Brush Wellman for electrical discharge machining drilling of beryllium, the metal-removal rate for rough

cutting should not exceed 18.0 cm^3/h (1.10 $in.^3$/h), and cuts should not extend any closer than to within 0.102 mm (0.004 in.) from the finished surface. The metal-removal rate for finishing cuts should not exceed 2.05 cm^3 (0.125 $in.^3$). The final finishing cuts prior to a stress-relief treatment should consist of a minimum of 0.102 mm (0.004 in.) of metal removal [Hughes Aircraft Company].

21.4.4 Grinding

Surface grinding is usually not recommended for bulk-metal removal of beryllium. It is primarily used to achieve extremely close tolerances, a very fine surface finish, and/or where sharp edges are required. If machining dry, the glove box must be completely dry to contain the fine powder. As with many metal powders, the fine powder can be pyrophoric, since sparks may develop during the grinding. Because of these problems, grinding of beryllium should be performed wet.

The following recommendations were presented as a guide for grinding beryllium [Bunce and Hill 1979]:

- Use a high cutting surface speed of 150 to 2000 m/min (500 to 6500 ft/min).
- Use a high work speed of 6.1 to 18.3 m/min (20 to 60 ft/min).
- Use a low cross-feed rate of 1.52 mm (0.060 in.) per pass.
- Use a small cut depth of 0.025 to 0.076 mm (0.001 to 0.003 in.) per pass for rough grinding and 2.5 to 12.7 μm (0.0001 to 0.0005 in.) per pass for finishing cuts.
- For rough grinding, use a tough-grained aluminum oxide wheel having a course grain size and a soft, vitrified bond, similar to Norton 38 A46-K5 or A46-K5-VBE.
- For finish grinding, use a sharp-grained silicon carbide wheel having a medium grain size (40 to 80 grit) and a soft to medium-hard bond, similar to Norton 38 A60-K5-VBE or 37046-K + VK.
- Frequently dress the wheel to prevent buildup, which inhibits the process from being speeded up.
- Use a water-soluble oil emulsion, free from sulfur or chlorine, when coolant is required, and ensure that parts are cleaned and given a surface neutralizing treatment using perchloroethylene after machining is finished.
- Side wheeling should be avoided.

21.4.5 Sawing (Cutting)

Cutting of beryllium blocks into sizes suitable for machining operations is usually performed by either band sawing, mill sawing, elastic wheel slitting, or electric discharge sawing. Headers are removed from cast ingots using either band or mill sawing. Rolled plate and sheet are cut into workable sections using either band sawing or elastic wheel slitting. Cutters must be kept in sharp condition. In general, lack of sharpness and/or too few teeth can result in severe machining damage.

Band sawing (surface) speeds vary from approximately 61.0 m/min (200 ft/min) for thin sheet to 30.5 m/min (100 ft/min) for thick-section blocks. The corresponding feed rates vary from 1290 to 6.45 cm^2/min (200 to 1 $in.^2$/min) [Bunce and Hill 1979]. Saw blade widths should be increased as the workpiece thickness is increased. Band widths of 6.35, 12.7, 25.4, and 50.8 mm (0.25, 0.5, 1, and 2 in.) are typically used for thicknesses of 0.635 mm (0.025 in.), up to 3.17 mm (0.125 in.), up to 76.2 mm (3 in.), and up to 76.2 cm (30 in.), respectively. Generally, the greater the number of teeth, the smoother the cut; however, the chance of clogging up the spaces between the teeth correspondingly increases. With hot pressed powder block, it is best to use blades having fewer teeth, in the range of 4 to 10 teeth per 2.54 cm (1 in.), to avoid such clogging. Thin sections should use blades with a smaller teeth spacing of 20 to 30 teeth per 2.54 cm (1 in.).

Mill sawing (surface) speeds are in the range of approximately 30.5 to 45.7 m/min (100 to 150 ft/min). Since the operation can be easily performed without the use of coolants, it offers a high recovery, low-contamination yield of swarf for recycling. Machining conditions are similar to milling. Cut depths of up to 6.35 mm (0.25 in.) are allowable [Bunce and Hill 1979].

Elastic wheel slitting exhibits similar characteristics as those shown for surface grinding. A typical wheel is the Norton A60-QET. The main advantages over other sawing techniques are that there is less machining damage to the beryllium, and breakout and burring are avoided. The elastic wheel saws can have widths as small as 0.635 mm (0.025 in.).

Electrical discharge sawing involves having a conductive electrolyte sprayed through nozzles into the space between the beryllium workpiece (anode) and a continuous moving band of strap steel (cathode). A blade-shaped electrode moves

at approximately 20 m/s (65 ft/s) and is fed toward the workpiece by a control system that maintains the proper arcing and prevents welding between the two electrodes. Feed rate is controlled to maintain successive arc discharges, each one lasting approximately 100 μs. Sawing rates are approximately 19.4 cm^2/min (3 $in.^2$/min), with cut widths of approximately 0.8 mm (0.032 in.). A thinner, smoother cut with a lower stressed surface is achieved compared to that obtained using a comparable mechanical saw. The residual stresses are still sufficiently high as to require a final finish machining to eliminate any microcracks that may have developed. The process is best used for rough cutting [Bunce and Hill 1979].

The abrasive sawing technique is suggested for obtaining straight cuts of beryllium sheet using an abrasive sawing technique [Brush Wellman 2001]. The operation is performed wet, using a resin-bonded, semifriable aluminum oxide wheel rotating such that the surface speed is 35.6 to 45.7 m/s (7000 to 9000 ft/min). A wheel with an abrasive grain size of 80 grit and a relatively soft "L" bond grade is recommended.

21.4.6 Thread Cutting

Threading beryllium is usually done with a single-point tool. Due to its brittleness, care must be taken to avoid chipping both during and after thread cutting of beryllium. The risk of chipping can be reduced by machining external-truncated threads or by drilling oversized holes on internal threads, thereby increasing the crest of the thread. A 55% effective thread depth is recommended to develop a sufficiently wide crest [Bunce and Hill 1979]. The tool angle should be such that only one side of the thread at a time is roughed out. For the final finished cuts, the cutter should be fed straight, so that both sides of the thread are finished simultaneously. Fine cuts are made throughout the threading operation [Bunce and Hill 1979].

21.4.7 Cutting Speeds and Feed Rates

Among the factors that affect cutting speeds and feed rates are chip collection and dust elimination systems, metal-removal rate, tool wear rate, surface finish, and component size [Bunce and Hill 1979]. Replacing a tool may be required to maintain a good surface finish. This practice can cause problems with dimensional tolerances. Increasing feed rate and reducing surface-cutting speed was shown to improve tool wear. Increased feed rate, however, degrades the surface finish, which can be subsequently improved by etching (if a small loss in dimensional tolerance is acceptable). Normal finishes are in the range of 0.76 to 1.52 μm (30 to 60 μin.) rms. Etching machined finishes that were in the range of 1.01 to 2.29 μm (40 to 90 μin.) yielded surface finishes in the range of 0.89 to 1.14 μm (35 to 45 μin.) rms. Suitable feed rates ranged from 50.8 to 381 μm (0.002 to 0.015 in.) per revolution, and surface cutting speeds ranged from 0.38 to 5.08 m/s (75 to 1000 ft/min). Cut depths can range from 12.7 μm to 8.89 mm (0.0005 to 0.35 in.) [Bunce and Hill 1979].

21.4.8 Electrical Discharge Machining

Electrical discharge machining (EDM) is a method of metal removal by erosion from sparks, which are created between the workpiece and a shaped electrode (usually a graphite, copper, or brass cathode) using a pulsed power supply. In using a low mechanical-support force and avoiding any tool-to-workpiece contact, EDM lends itself to precision machining of intricate shapes; fragile thin-walled components; narrow, deep slots; small holes; and trepanning. The sparks travel through a dielectric fluid (which also acts as a coolant) at a controlled distance. Excess heat, however, can cause surface melting and resolidification, alloying with the electrode material, and microcracking, resulting in a defective surface as much as 127 μm deep. This damage can be minimized by operating at low current levels, high frequencies, and low metal-removal rates. A cutting rate of 6.45 mm^2/min (0.010 $in.^2$/min) can be achieved with a brass electrode, providing a smooth surface finish of 0.25 to 0.51 μm (10 to 20 μin.) rms on beryllium [Bunce and Hill 1979]. Low residual stresses are obtainable. An example for having a distortion-free mirror was given where the only stresses following EDM were due to those in the original part [Paul 1967]. High cutting rates result in rough surfaces with numerous microcracks of up to a depth of 0.13 mm (0.005 in.) and in relatively high residual stresses [Beitscher 1979].

The EDM process is claimed to be very effective and practical for machining small features and otherwise inaccessible areas as well as intricate, irregular, and complex curved shapes of beryllium at good production rates. A modified EDM method for cutting beryllium with close

tolerances consists of having a thin traveling metal wire, usually a copper-base alloy, as the electrode (wire EDM machine) [Brush Wellman 2001, Krivko et al. 1991]. A thin, loosely adherent copper residue from the wire can be left on the as-machined surface, which can be removed by a flash etch with nitric acid [Krivko et al. 1991]. Etching EDM beryllium surfaces resulted in slightly better tensile properties than those obtained prior to etching [Hashiguchi 1992]. Since the EDM process may create additional beryllium-recovery problems, alternative methods for machining beryllium should first be considered.

According to specifications by Hughes Aircraft for EDM drilling of beryllium, the metal-removal rate for rough cutting should not exceed 18.0 cm^3/h (1.10 $in.^3/h$), and cuts should not extend any closer than 0.10 mm (0.004 in.) from the finished surface. The metal-removal rate for finishing cuts should not exceed 2.05 cm^3/h (0.125 $in.^3/h$). The finishing cuts prior to stress relief should consist of a minimum of 0.1 mm (0.004 in.) of metal removal from the surface [Hughes Aircraft Company].

21.4.9 Electrochemical Machining

Electrochemical machining (ECM) refers to the controlled removal of metal by anodic dissolution in an electrolytic cell in which the workpiece is the anode and the tool is the cathode. The electrolyte is pumped through the space (cutting gap) between tool and workpiece, while direct current is passed through the cell at a low voltage to dissolve metal from the workpiece. Electrolytes are usually aqueous solutions of inorganic salts [Lievestro 1989]. Sodium nitrate and sodium chloride are electrolytes that have been successfully used for beryllium [Brush Wellman 2001]. Electrodes are usually copper, brass, or stainless steel. The current can range from 50 to 20,000 A, with a current density of 0.155 to 3.1 A/mm^2 (100 to 2000 $A/in.^2$) and 30 V dc applied across a gap of 0.025 to 1.27 mm (0.001 to 0.05 in.) between the tool and workpiece [Lievestro 1989]. The electrolyte flows through the cutting gap at a rate of 30.5 to 61 m/s (100 to 200 ft/s). A schematic of an ECM system is shown in Fig. 21.10 [Lievestro 1989]. Modifications of the cleanup system would be expected for the recovery of the dissolved beryllium and any suspended beryllium solids.

The ECM process has been used successfully for a number of years for trepanning, contouring, slotting, and drilling of complex beryllium parts [Bunce and Hill 1979]. It produces a relatively small degree of surface damage [Brush Wellman 1982]. The machined beryllium surfaces are free of twins, microcracks, and other defects, and rapid machining rates can be achieved. To prevent corrosion following ECM, parts should be rinsed in deionized water and given a light etch to remove traces of salt from surfaces. To further reduce any corrosion tendency, the parts may then be immersed in water-soluble oil, such as may be used as a coolant during mechanical machining.

21.4.10 Electrochemical Grinding

Electrochemical grinding is a modification of ECM, in that the metal is removed by a combination of electrochemical action and mechanical abrasion. The process caused a slight roughening of the surface of a rod, although the surface was found to be free of any metallurgical-related damage [Beitscher 1979].

21.4.11 Chemical Machining

Chemical machining refers to removal of metal by chemical dissolution (etching), with several possible objectives: removal of machining-damaged surfaces, thinning sections to reduce weight, and/or producing detailed precision parts. The typical etching solutions for beryllium are sulfuric acid, a nitric acid-hydrofluoric acid mixture, and ammonium bifluoride. Additional etchants were reported earlier in this chapter. There are two main types of processes: chemical milling (machining) and photochemical machining; the latter process is used for small details, especially where high precision is required.

Chemical milling has been successfully used in the fabrication of parts made from beryllium block, sheet, extrusions, and forgings. Metal removal may be over the entire surface or it may be restricted to selected areas by masking. Chemical milling may be used to remove damaged surface layers and/or to reduce weight by restricting etching (thinning) to specific areas. Thin, uniform, distortion-free webs can be obtained [Skillern et al. 1991]. Masking may also be used to develop certain designs. The removal of damaged surfaces is typically performed by complete immersion in the etchant. Because the etching is unlikely to be uniform throughout the part, such immersion may compromise any high tolerances obtained by previous machining operations, especially for complex designs. Careful

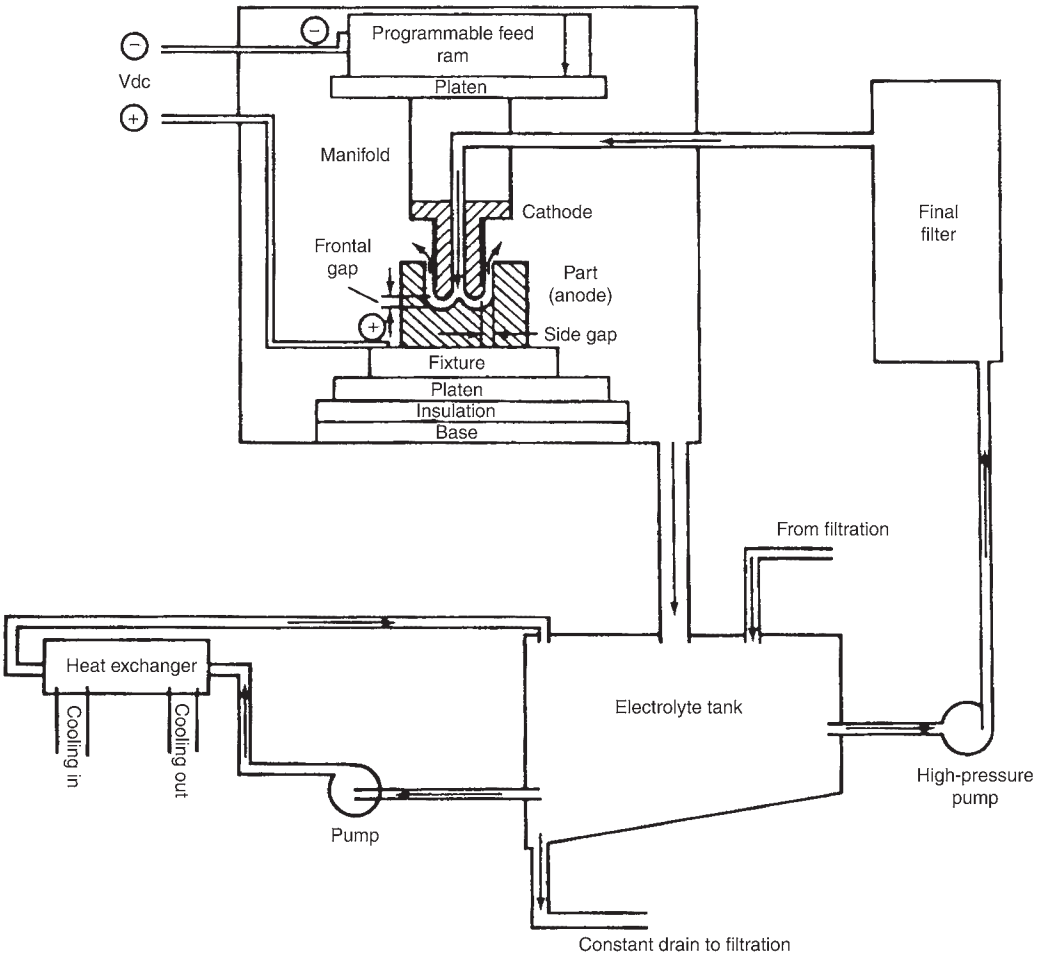

Fig. 21.10 Schematic of an electrochemical machining system, which is applicable to most metals. (Modifications of the cleanup system would be expected for recovery of beryllium.) Source: Lievestro 1989

control of the etching could uniformly remove metal from all surfaces [Skillern et al. 1991]. Surface finishes are generally rougher after chemical milling, depending to a great extent on the prior surface condition.

The maskants (elastomer coatings, or masks, deposited on areas that are not to be attacked by the etchant) are specially designed liquid elastomers that, when cured, are hand strippable and resistant to the etchants. The procedure used is as follows: The cleaned, dried workpiece is coated with the liquid elastomer, which is then dried and cured. A pattern is scribed on the cured elastomer, defining the boundaries between the areas to be etched and unetched. The mask is then peeled off from the areas to be etched, and the part is immersed in etchant for a specific period of time. If differing amounts of thinning are required, a new pattern may be scribed on the remaining mask, or a new mask may be applied over the etched areas and scribed with the pattern. The appropriate parts of the mask are peeled off, and the part is again immersed in the etchant. This gives two sets of areas with different amounts of thinning. The process can be repeated a number of times on the same part. The maskants can be applied either by immersion in the liquid elastomer or by using hot airless spray equipment. The maskant must be cured to provide the proper amount of adhesion. Adhesions that are too low result in poor definition between etched and unetched regions; excessive adhesion makes stripping difficult. Curing can be done at temperatures from ambient to over 90 °C (195 °F); increasing temperatures lead to better adhesion as well as

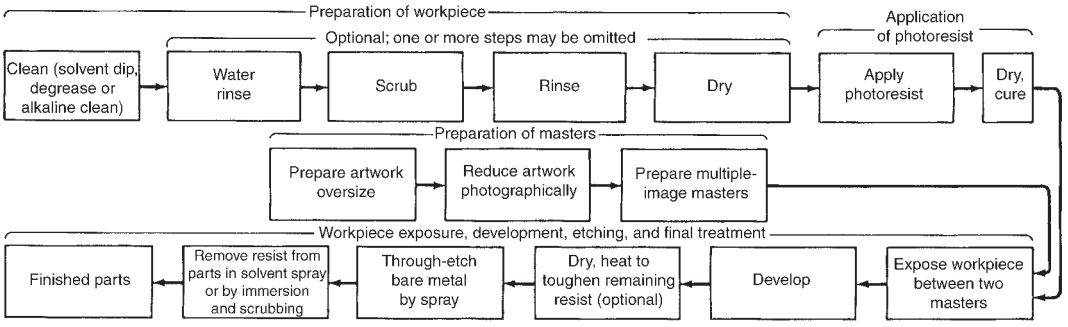

Fig. 21.11 Flow chart of principal process steps for photochemical etching. Source: Friedman 1989

shorter curing times [Langworthy 1989]. Material-removal rates by the etchant vary from 25 to 51 μm/min (0.001 to 0.002 in./min). Tolerances of the final part can be very close to those obtained prior to etching and can be held to ±127 μm (±0.005 in.) and may vary in complex configurations [Brush Wellman 2001].

Photochemical machining (PCM) is a metal-etching process that uses a photoresist maskant to define the location where the metal will be etched. The photoresist can be applied by dipping (immersion), whirl coating, or spraying [Friedman 1989]. Whirl coating yields the best uniformity, while spraying provides the most versatility. The resists are dried at ambient temperature and then baked for approximately 15 min at 120 °C (250 °F) or at ambient temperature for longer periods of time. The photoresist can also be applied as a solid dry film laminated to the part. However, this provides poorer resolution than that of the liquid form. The photoresist mask provides a photosensitive surface that is resistant to the etchant. Etchants used for chemical milling of beryllium are also used for PCM. The PCM process is used to produce detailed precision parts. Best results are obtained on flat material of uniform thickness and having a fine grain size. Thicknesses can range from 0.013 to 1.5 mm (0.0005 to 0.06 in.). Very tight tolerances are attainable with beryllium: ±0.075 mm (±0.003 in.) is easily attainable, and ±0.025 mm (±0.001 in.) can be achieved if required [Gallagher and Hardesty 1989].

A photochemical flow chart of the process is shown in Fig. 21.11 [Friedman 1989]. Basically, the steps are to create the pattern artwork, make the masters, prepare the workpiece, apply the photoresist, cover the workpiece with the masters, and image and develop such that the pattern (detail) is defined by the photoresist. The photoresist that was exposed to the imaging light is washed away by the developing solution and subsequently will be attacked by the etchant. Alternatively, the unexposed photoresist can be made to wash away. The methods are referred to as positive and negative masking, respectively. The masters are reusable, thus providing highly reproducible details in production parts. Various materials and techniques can be used for the artwork and masters, depending on the required precision and dimensions of the details and the desired permanency of the masters. For example, the original artwork may range up to 200 times the actual size and be photographed with a reduction camera. The artwork may be done manually or by computer-aided drafting [Friedman 1989].

21.4.12 Trepanning

Trepanning allows for cost recovery for some of the material and avoids the cost of reprocessing machining chips. It is a machining process for producing a disk, cylinder, or tube from solid stock or for producing a circular groove or hole in the stock. This is accomplished by having a tool containing one or more cutters (usually single point) revolving around a fixed center. Component depths (thicknesses) decrease with increasing part diameter. The unused material, such as a cylinder formed by trepanning a hole, would be available for making some other part or used for higher-value scrap [ASM 1989b]. Holes over 25.4 mm (1 in.) diameter in beryllium are usually trepanned rather than being drilled or bored [Bunce and Hill 1979]. A setup for trepanning a disk is depicted in Fig. 21.12 [Friedman 1989]. The setup contains an adjustable fly cutter mounted on a twist drill, which serves both as driver and pilot. Having

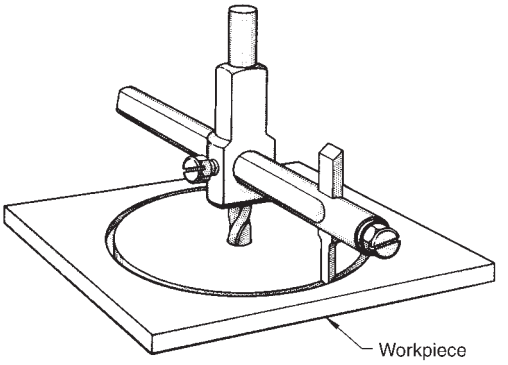

Fig. 21.12 Drill-mounted, adjustable fly cutter used for trepanning various sizes of disks from flat stock. It can also be used for forming grooves around centers. Source: ASM 1989b

the pilot (drill) on the drive unit helps to stiffen the tool, reduce chatter, and retain cutter sharpness. A hole is formed in the center of the disk. If a hole is not acceptable, the drill pilot is replaced with a drill-free pilot; however, there is less rigidity, possibly more tool chatter, and some loss of dimensional control [ASM 1989b, Bunce and Hill 1979]. Trepanning requires that the cutting or parting blades be designed with proper clearance angles to give optimum cutting, and they must be kept sharp; if not, the blades need to be replaced, or severe machining damage may occur. Replacing the tool may cause problems with dimensional tolerances. Cutting-edge clearance should be contoured to the outside and inside diameters with zero to positive rake and a 3 to 5° degree end clearance to be most effective and to reduce tool wear [Bunce and Hill 1979, Paul 1967].

21.4.13 Tapping

Taps with two or three flutes are most effective. The creep characteristics of beryllium should be known, especially in thin cross sections. High-speed steel taps should be surface treated, for example, by nitriding. Lead-screw tappers with fine torque adjustments give the operator good control of tap behavior. A minimum of 1.59 mm ($^1/_{16}$ in.) from an edge is required for tapping beryllium. Tapping lubricants should be used, preferably a sulfur-base oil [Paul 1967].

REFERENCES

ASM, 1989a. Milling, *Machining*, Vol 16, *Metals Handbook*, 9th ed., ASM International, p 303

ASM, 1989b. Trepanning, *Machining*, Vol 16, *Metals Handbook*, 9th ed., ASM International, p 175–180

ASM, 1989c. Turning, *Machining*, Vol 16, *Metals Handbook*, 9th ed., ASM International, p 135

Beitscher, S., 1979. Machining-Induced Surface Damage, *Beryllium Science and Technology*, Vol 2, D.R. Floyd and J.N. Lowe, Ed., Plenum Press, NY, p 197–230

Brush Wellman, Inc., 1982. "Machining Beryllium Metal," Report, Second Revision, Brush Wellman, Inc.

Brush Wellman, 2001. "Designing with Beryllium," Brochure 517, Cleveland, OH

Bunce, J.E.J., and Hill, M., 1979. Machining, *Beryllium Science and Technology*, Vol 2, D.R. Floyd and J.N. Lowe, Ed., Plenum Press, NY, p 177–196

Cooper, R.E., 1979. Fracture Mechanics, *Beryllium Science and Technology*, Vol 2 (No. 17), D.R. Floyd and J.N. Lowe, Ed., Plenum Publishing Corp., New York, NY, p 351–378

Friedman, H., 1989. Photochemical Machining, *Machining*, Vol 16, *Metals Handbook*, 9th ed., ASM International, p 387–393

Gallagher, D.V., and Hardesty, R.E., 1989. Machining of Beryllium, *Machining*, Vol 16, *Metals Handbook*, 9th ed., ASM International, p 870–873

Hashiguchi, D.H., 1992. "Beryllium Machining Technique Evaluation," Technical Report TR1036, Brush Wellman

Hughes Aircraft Company. "Hughes Standard Specification on Machining of Beryllium," Document HP 1–26

Krivko, V.P., Romanko, P.M., Kolesnik, L.I., Vagnibeda, N.V., and Kokovikhin, Y.I., 1991. The Effect of Annealing on the Mechanical Properties and the Structure of Beryllium Foil, *Met. Sci. Heat Treat.*, Vol 33 (No. 1–2), p 12–14

Langworthy, E.M., 1989. Chemical Milling, *Machining*, Vol 16, *Metals Handbook*, 9th ed., ASM International, p 379–386

Lievestro, T.L., 1989. Electrochemical Machining, *Machining*, Vol 16, *Metals Handbook*, 9th ed., ASM International, p 533–541

Marder, J.M., Kuxhaus, M.B., and Stonehouse, A.J., 1990. Near Net Shape Beryllium Products, *Int. J. Powder Metall.*, Vol 26 (No. 2), p 139–146

Norwood, L.B., 1984. Application of Beryllium on the Space Shuttle Orbiter, *SAMPE J.*, Vol 20, p 7–15

Paul, G.R., 1967. "Fabrication and Techniques of Beryllium Metal Removal," Report CONF-671063-2, Aeronautic, Space Engineering, and Manufacturing Meeting (Los Angeles, CA)

Skillern, C.G., Hollman, R.R., and Kulkarni, K.M., 1991. Production of Beryllium Mast Mounted Sights Using Near Net Shape Technology and Chemical Milling, *Advances in Powder Metallurgy*, Vol 6, Aerospace, Refractory, and Advanced Materials, Proceedings of the Powder Metallurgy Conference and Exhibition (Chicago, IL), p 381–389

Zimmers, E.W., 1989. CAD/CAM Applications in Machining, *Machining*, Vol 16, *Metals Handbook*, 9th ed., ASM International, p 627–636

SELECTED REFERENCES

- Cunningham, J.E., 1950. "Deep Hole Drilling of Hot Pressed Beryllium Metal," Report AECD-3722, CF-50-4-110, Oak Ridge National Lab, TN
- Glynn, C.E., and Bayer, J., 1966. "Machinability of Beryllium," Report AFMI TR-66–125, General Electric Co., Cincinnati, OH
- Gurklis, J.A., 1972. "Nontraditional Machining of Beryllium," Metals and Ceramics Information Center, Report MCIC 72-03, Battelle Labs, Columbus, OH
- Hovis, V.M., 1966. "Machining and Finishing Fine-Grained Beryllium," Report Y-1551, Union Carbide Corp.
- King, B., 1976. "Fabrication, Material Characterization and Machining Process Evaluation of S-65 Grade Hot Pressed Beryllium," Report AFML-TR-76-08, Brush Wellman Inc.
- Missel, L., and Shakeen, M.E., 1965. Chemical Milling of Beryllium, *Met. Finish.*, Vol 63 (No. 11), p 69–71
- Terry, E.L., 1963. "Effects of Different Hole Preparation Procedures on Strength of QMV Beryllium Cross-Rolled Sheet," Brush Technical Information Sheet, TIS-100, Brush Beryllium Co.

Beryllium Chemistry and Processing, p 361-399
By Kenneth A. Walsh
Edited by Edgar E. Vidal, Alfred Goldberg,
Edward N.C. Dalder, David L. Olson, and Brajendra Mishra

CHAPTER 22

Beryllium Coating Processes

Alfred Goldberg, Lawrence Livermore National Laboratory

THIS CHAPTER deals with a description of coating methods applicable to beryllium, their relative advantages and disadvantages, the effect of various operating parameters on the microstructures and properties developed, and examples of applications. In exploring the literature on this subject, it may be noted that considerable investigative effort, especially in more recent years, was and is still directed toward repairing the plasma-facing components in the International Thermonuclear Experimental Reactor and Tokamak Fusion Test Reactor. Such studies involved the use of several different physical vapor deposition methods. Another active investigative area is the coating of spheres for use in the National Ignition Fusion facility, and here studies were directed mainly to sputtering methods. Many of these studies were concerned with evaluating the effect of operating parameters on the properties and microstructures developed in the deposits.

In attempting to classify the different coating processes under various categories, difficulties arise since some of the processes overlap the different categories. Accordingly, different classification schemes exist [Bunshah 1982]. In addition, many of these processes are not applicable to beryllium.

22.1 Beryllium Coatings

A number of methods have been used for the deposition of beryllium on substrates to form beryllium coatings or self-standing structures. In this chapter, the focus is primarily on physical vapor deposition (PVD) processes and plasma spraying. To a lesser extent, chemical vapor deposition (CVD) and electroplating are also discussed.

22.1.1 Physical Vapor Deposition

Physical vapor deposition is a process where atoms or molecules are sputtered off from a solid source or vaporized from a melted source, transported in the vapor through a low-pressure gaseous or vacuum environment, and condense on a substrate. Typically, PVD processes are used to deposit films and coatings of thicknesses in the range of a few angstroms (Å) to millimeters, with deposition rates ranging from 10 to over 10,000 Å/s (10^{-3} to 1 μm/s) [Mattox 1998, Beat 2005]. The deposits can consist of single materials, layers with graded compositions, or multilayer coatings. Similar microstructures are obtained for coatings from CVD and PVD processes. There are three categories of PVD processes: thermal evaporation, sputter deposition, and ion plating.

Thermal (Vacuum) Evaporation. The material from a thermal vaporization source reaches the substrate without significant collisions with gas molecules present in the space between the source and substrate. The source may be melted and evaporated by a number of different methods (e.g., electron beam heating, resistance heating, induction heating, laser heating, and radiation). The depositing species (clusters of atoms or molecules) have relatively low energies (less than five electron volts, or eV). Relatively high deposition rates are attainable. The process is generally performed in vacuum, typically at 10^{-3} to 10^{-4} Pa (10^{-5} to 10^{-6} torr), so that the evaporated species undergo an essentially collision-free line-of-sight transport to the

substrate, which is usually at ground potential (not biased).

Sputter Deposition. With sputter deposition, the source of the vaporized material is a target whose surface is being subjected to physical sputtering by positive ions, usually argon, produced in a glow discharge. The sputtered material is emitted as a cosine distribution, depositing on a substrate. (The cosine distribution gives the amount or intensity that is emitted from some source as a function of cosine θ. The form of the function depends on the type of coordinates, for example, Cartesian, polar, and so on, selected and the assumptions that are made. For example, the cosine-distribution plot in Fig. 22.3 uses polar coordinates. The sputtering assumes ideal molecular flow; that is, no collisions occur.) Sputter deposition may be further subdivided into high- and low-pressure sputter deposition, especially when considering film properties. An increase in the partial pressures of the metal vapor and/or the gas species results in an increase in collisions during transport of the sputtered particles to the substrate. The depositing species have relatively moderate energies (on the order of 20 eV). Relatively high energies (on the order of 100 eV) can be obtained with accelerated species such as in ion plating, where only relatively low or moderate deposition rates are attainable.

Ion plating is a process in which a portion of the depositing material from an evaporation or sputtering source is deliberately ionized. Once charged, the ions can be accelerated with an electric field so that the impingement energy on the substrate is greatly increased, producing modification of the microstructure as well as of residual stresses. By ionizing all the depositing material, much higher accelerating energies are attainable, such that the ions can penetrate the substrate surface. The ion bombardment is usually done in an inert-gas discharge system similar to that used in sputter deposition, except that in ion plating the substrate is made a sputtering cathode. This allows surface contaminants and any barrier layers to be removed by sputter cleaning prior to deposition. The term *bias plating* is also used. A reactive gas may be added to deposit a compound. Relatively high deposition rates are attainable [Bunshah 1982].

22.1.2 Plasma Spraying

Plasma (arc) spraying involves the successive buildup of deposited layers of hot and/or molten particles on a substrate, which, on impact, deform and adhere to each other. Plasma spraying of beryllium has received considerable attention with respect to repairs in fusion reactors. It is a process in which the source powder is injected into a plasma jet stream that is produced by a low-voltage, high-current electrical discharge. The plasma is a hot ionized gas, which heats the powder to near or above its melting temperature and accelerates it toward the substrate (workpiece) along a line of sight from the plasma torch. The plasma consists of free electrons, ionized atoms, some neutral atoms, and (if nitrogen or hydrogen is used) some undissociated diatomic molecules.

22.1.3 Chemical Vapor Deposition

Chemical vapor deposition is a chemical process that takes place in the vapor phase very near or on the substrate, so that a reaction product is deposited onto the substrate. The close proximity of the reaction to the substrate offers the ability to deposit uniform coatings on irregularly shaped objects.

22.1.4 Electroplating

Electroplating involves depositing out metal ions from an electrolyte bath containing an anode source (positive polarity) and a cathode substrate (negative polarity). Neither electroplating nor CVD have proven to be viable processes for deposition of beryllium, primarily due to the high reactivity of the metal resulting in entrapment of impurities, mainly oxygen, nitrogen, and/or carbon. Investigations of attempts to solve this problem are reviewed.

Comparisons in operating pressures, substrate temperatures, and deposition rates between different deposition methods are shown in Table 22.1 [Dini 1992].

22.1.5 Adhesion

In any one process, adhesion may vary considerably. For permanent coatings and restored surfaces, adhesion properties are of major importance. Parting agents are usually used for self-standing structures and foils, adhesion to the substrate being just sufficient to enable the deposition to take place. For PVD processes, ion plating is generally superior to normal sputtering, and both of these usually provide better adhesion than that obtained with thermal evaporation. These differences are attributed to differences in the energy (degree of bombardment) of

Table 22.1 Typical coating parameters for different deposition methods

Deposition method	Pressure		Substrate temperature		Deposition rate, μm/min
	Pa	Torr	°C	°F	
Evaporation	10^{-5} to 10^{-3}	10^{-7} to 10^{-5}	Up to 250(a)	Up to 480(a)	1.2–12
Sputtering	10^{-2} to 13	10^{-4} to 10^{-1}	Up to 250(a)	Up to 480(a)	0.012–24
Ion plating	10^{-2} to 13	10^{-4} to 10^{-1}	Up to 250(a)	Up to 480(a)	1.2–12
Electroplating	Ambient(b)		10–100	50–212	0.4–180
Electroless plating	Ambient		15–100	60–212	0.5–2.0

(a) Dependent on temperature and material. (b) Low pressures (200–300 torr, or 0.03–0.04 MPa) have been used to remove hydrogen bubbles in order to prevent the formation of potential pit sites that would usually lead to porosities in the deposit. Source: Dini 1992, Beat 2005

the depositing atoms [Dini 1992]. Excellent adhesion is claimed to be attainable with plating processes, although no examples or references for beryllium were given [Dini 1992].

22.1.6 Thickness

Coatings may range from thin films to relatively thick deposits. Thicknesses can vary from angstroms to millimeters, with 1 μm often considered the boundary between thin and thick deposits. The distinction between thin and thick coatings is somewhat arbitrary. The difference has also been defined in terms of its function: If used for its surface properties (e.g., emissivity), it is characterized as thin; if used for its bulk properties, it is characterized as thick [Bunshah 1982]. A thick film has also been defined as one that is sufficiently thick to permit evolutionary selection processes (such as texture development and grain growth) to develop during the growth of the deposit and influence its structure [Thornton 1977].

Thicknesses of at least several millimeters are achievable by all these processes. Plasma spraying, however, can provide thicknesses considerably greater than obtainable by other deposition methods. Except for plasma spraying, thin films can be produced using any of these methods. Limits in maximum attainable thickness increase in the following order: sputtering, evaporation, CVD, electroplating, and plasma spraying [Beat 2005].

22.2 Physical Vapor Deposition

Physical vapor deposition processes involve the creation and condensation of vapors onto substrates to form coatings or films. Figure 22.1 illustrates schematically the main categories of PVD processes [Dini 1992].

22.2.1 Thermal (Vacuum) Evaporation

In thermal evaporation, the coating rate and substrate temperature are the controlling process parameters. High-quality beryllium films can be produced with relative ease [Adams and Hurd 1969, Hseieh 1988]. Films with smooth surfaces, either amorphous or crystalline, can be deposited on a variety of substrates in various thicknesses. Preferred crystallographic orientations are commonly obtained. The degree of crystallographic orientation of the film depends on substrate temperature, deposition rate, and the type and crystallographic orientation of the substrate [Adams and Hurd 1969]. Formation of solids by condensation can result in a vast array of defects, such as dislocations and stacking faults as well as grain boundaries that look almost as wide as the grains they separate. Very fine grain sizes are attainable. In addition to the high energy of the depositing atoms (actually clusters of atoms) [Beat 2005], diffusion of these atoms in the previously deposited material is initially much higher than is predicted by simple diffusion [Hill 1986]. Differences in vapor pressure and deposition rates of the various constituents present in the melted beryllium often lead to compositional gradients in the deposit.

Of the various heating methods available (e.g., electron beam melting, resistance heating, induction heating, laser heating, and radiation), electron beam melting (EBM) and resistance heating are the most commonly used sources. In EBM, an electron beam, which is a stream of energetic, negatively charged particles, is generated. Upon impacting a solid material, the kinetic energy of the beam is converted into thermal energy. The energy from the electron beam is concentrated on the surface of the target. Therefore, molten target material can be supported by a cooled structure, with the target material providing its own solidified "skull" separating the molten portion from a water-cooled crucible or hearth. This characteristic avoids contamination from the container and makes the electron source an ideal heat source for both the evaporation and purification of materials.

The use of EBM for the successful purification of beryllium, followed by evaporation of

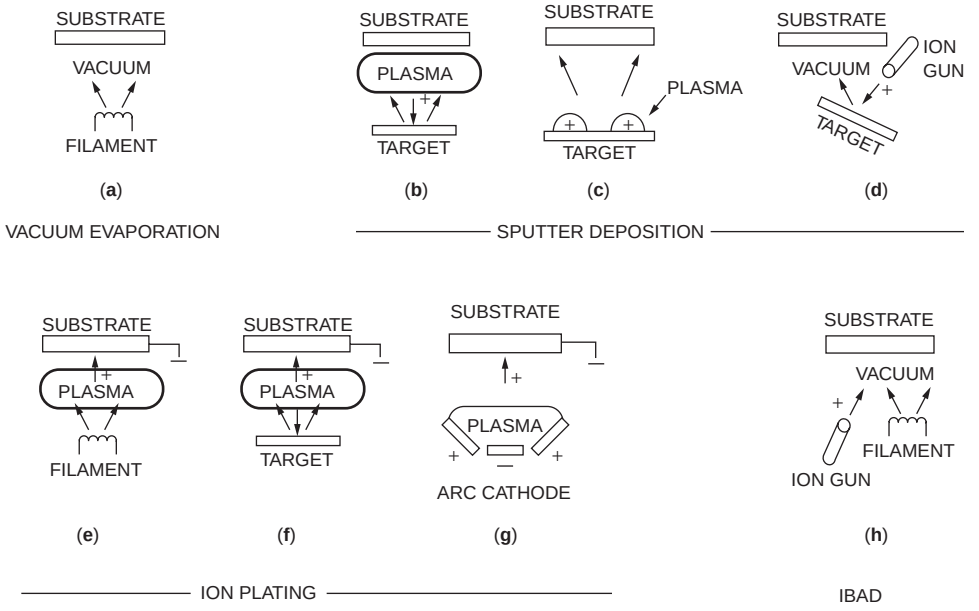

Fig. 22.1 Schematic illustrations of physical vapor deposition processing methods. (a) Vacuum evaporation. (b) and (c) Sputter deposition in a plasma environment. (d) Sputter deposition in vacuum. (e) Ion plating in a plasma environment with a thermal evaporation source. (f) Ion plating with a sputtering source. (g) Ion plating with an arc vaporization source. (h) Ion-beam-assisted deposition (IBAD) consisting of a thermal evaporation source and ion bombardment from an ion gun. Source: Mattox 1998

the purified distillate and deposition onto a substrate, was reported by Bunshah and Juntz [1967]. The deposit was high-purity, full-density beryllium that could be rolled directly into sheet. During evaporation, the chamber pressure ranged from 10^{-4} to 10^{-6} Pa (10^{-6} to 10^{-8} torr) with the substrate, which was at least 200 mm (7.9 in.) from the melt, reaching temperatures from 500 to 1000 °C (930 to 1830 °F). Depending on the beam power and source-to-substrate distance, thicknesses varied from approximately 5 mm (0.2 in.) along the center of the deposits to approximately 1.3 mm (0.05 in.) along the edges. The weight of a deposit ranged from approximately 400 to 500 g (14 to 18 oz) following a condensation rate of approximately 6 g/min (0.21 oz/min) with a collection efficiency of approximately 55%. (The collection efficiency is the fraction deposited compared to the fraction evaporated and depends primarily on the size of the collector, or substrate, and the distance to the molten pool.) A shutter was placed over the molten pool until it was stabilized.

The electron beam gun, which operates on the same principle as a cathode ray tube, consists of a vacuum system operating at less than 5×10^{-2} Pa (5×10^{-4} torr). At pressures below 10^{-4} Pa (10^{-6} torr), electron beam processing is done in an environment of free-electron flow, in that the few remaining gas molecules in the system rarely collide with each other. The electron beam gun contains a filament that is heated to incandescence by a low-voltage current, causing electrons to be emitted thermionically from a heated tungsten cathode and accelerated to the anode, which is at ground potential. The filament is located in the groove of a cathode beam former, and both are connected to the negative terminal of a high-voltage power supply. The heater current in the filament may be either alternating current (ac) or direct current (dc). The dc produces a more precise beam and is used for high-power guns. An important feature is the electromagnetic beam field-deflector system that allows the electron beam emitter (gun) to be placed completely out of the path of the evaporating material or of any falling debris. Various arrangements are possible, one of which is schematically illustrated in Fig. 22.2 [Hill 1986].

An important consideration is the evaporation rate of the molten pool. This can be obtained from the Langmuir-Knudsen equation, which is generally applicable for any material:

$$dm/dt = kAP\sqrt{(M/T)} \qquad \text{(Eq 22.1)}$$

where dm/dt is the evaporation rate, A is the evaporant surface area, P is the evaporant vapor

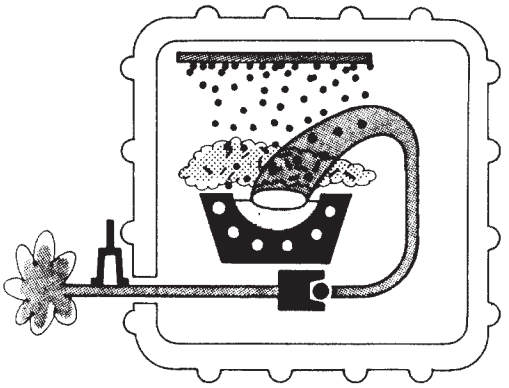

Fig. 22.2 Illustration of an electromagnetic beam deflection through 270° in a vacuum evaporation system using an electron beam heating source. Source: Hill 1986

pressure, *M* is the molecular weight, *T* is the temperature (Kelvin), and k is a constant. In practice, with increasing evaporation rates, viscous flow (interference) effects develop with corresponding deviations from the theoretical rates.

Power losses must be factored in when considering power requirements for a given evaporation rate [Hill 1986]. At low energy densities and low temperatures, losses occur through conduction and convection in the evaporant (first-power losses). As the energy density and temperature increase, heat losses through radiation (fourth-power loss, which refers to losses due to differences in temperature between the molten pool, T_m, and surroundings, T_s, according to $T_m - T_s$ and $(T_m)^4 - (T_s)^4$ for first and fourth powers, respectively) and vaporization become important, with the second loss eventually overtaking the first loss. High beam densities increase the vapor density directly above the source, stimulating ionization in the vapor, which causes a loss in efficiency. Beam positioning and beam-spot size, which are controlled by the strength and direction of the magnetic field, affect temperature.

Optimum beam density varies with the boiling point of the metal being evaporated. If the beam density is increased, the temperature of the beam-impact point increases. This should lead to more efficient evaporation. However, the density of evaporant atoms at the beam-impact point also increases. These atoms intercept the incoming beam, resulting in a reduction of electrons striking the evaporant surface. Thus, increasing the power at high power levels may only provide a marginal increase of electrons striking the target.

For thick coatings, nominal bulk properties are obtained when the substrate is heated to approximately ⅓ to ½ of the absolute melting point of the evaporant. It is important that the evaporation rate be large compared to the rate of bombardment of the substrate by residual gas molecules. For a given gas pressure, as the deposition rate is increased, the damaging effects of occluded gases and other contaminants present are decreased.

A layered deposit may present planes of weakness. This may be due to localized impurities in the beryllium or to a sudden change in deposition rate. Spattering, which is an inherent problem in vapor deposition, could be due to either excessive evaporation rates or explosive outgassing of the source material. The spatter could cause self-shadowing, leading to increased porosity, which can be avoided by decreasing the rate and/or using a premelted source [Wheeler et al. 1982].

Electron beam systems provide much higher evaporation rates (10^2 to 10^4 higher) than any other evaporating system. This increases the proportion of evaporant to contaminant, allowing the attainment of high-purity coatings at an operating vacuum level of 10^{-3} Pa (10^{-5} torr), compared to vacuum levels of 10^{-5} to 10^{-7} Pa (10^{-7} to 10^{-9} torr) with other evaporating methods. At pressures of the order of 10^{-3} Pa (10^{-5} torr), it is possible to produce deposits that have less than one part per million (ppm) impurity pickup from the vacuum environment. Deposition rates of 50 to 75 μm/min are routine [Hill 1986].

Rod feeding is generally used when a large amount of material is to be deposited. The rod also provides a continuous feed of evaporant so that compositional variations of the deposit due to differences in vapor pressure of the constituents are minimized. In evaporation and condensation processes, the absolute value of pressure is often less important than the ratio of evaporant molecules to contaminant molecules. To minimize contaminants, material premelted in vacuum should be used.

During transit, the evaporant species may collide in the vapor cloud, causing a change in its direction and depositing on the substrate from a direction other than from the line-of-site direction [Hill 1986]. When a sufficiently large number of collisions occur between source and substrate, the deposition rate will be effectively controlled by this scattering process. Condensation will then take place on various surfaces of the substrate, with the corresponding deposit

thickness depending on the local concentration of the condensing species. With a pressure level as high as approximately 7 Pa (5×10^{-2} torr), substantial non-line-of-site coating occurs; the evaporation kinetics, however, are not severely suppressed at this pressure [Hill 1986].

For thicknesses greater than several thousand angstroms, the structure or morphology of coatings and deposits becomes dependent on the substrate temperature. When T_s/T_{em} (substrate and evaporant melting point temperatures, respectively, in degrees K) is approximately 0.1, the deposit is usually a nonadherent fine powder. With increasing substrate temperature, the powder becomes coarser and moderately adherent but porous. When T_s/T_{em} reaches 0.3, the structure becomes columnar, still with some porosity. At a T_s/T_{em} of 0.6, the structure may vary from columnar to equiaxed, depending on the material, and be almost fully dense, with properties similar to the bulk material. With T_s/T_{em} near 0.8, epitaxial deposits may form for some combinations of substrate and condensate. (Epitaxial refers to a crystalline orientation in a crystalline material, or substrate, to nucleate and grow the same orientation in the crystalline material being deposited on it.) The substrate temperature may rise during condensation to a temperature where the rate of evaporation may approach the rate of condensation. The latent heat of condensation of the deposit may damage the substrate or even melt it.

For low vaporation rates, the material from a point vaporization source deposits on a substrate according to a source-to-substrate-distance dependence and a substrate-orientation dependence given by the cosine-deposition distribution. This is illustrated in Fig. 22.3 [Mattox 1998], which shows the distribution of atoms vaporized from a point source and the thickness distribution of the film formed on a planar surface above the point source, based on the cosine distribution. The flux distribution departs from the cosine law due to a number of factors, the more important being source geometry, collisions in the vapor during a high vaporization rate, and source surface geometry changing with time. (A dense vapor cloud, the degree depending on the vaporization rate, forms directly above the melt surface. As a result, the cosine distribution is only initiated at some distance above the melt surface, where the cloud density is sufficiently reduced to result in a low-collision rate.) The strong dependence of deposition rate on geometry and time requires that fixtures and tooling be used to randomize the substrate(s) position and angle of incidence of the depositing vapor during deposition in order to optimize the uniformity of deposit thickness.

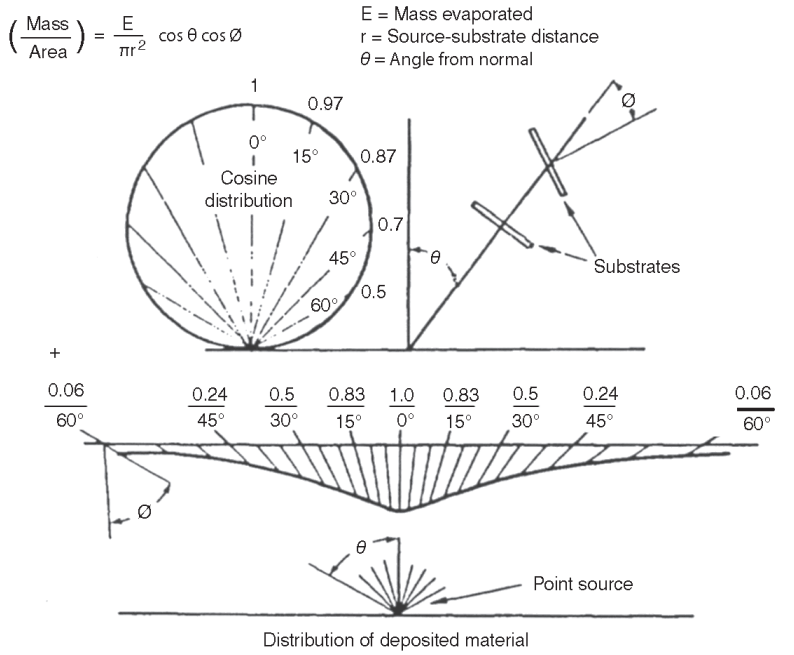

Fig. 22.3 Illustration of the cosine distribution of vapor from a point source. Source: Mattox 1998

The initial closing of a shutter above the melt source allows the evaporant to be heated without exposing the substrate to volatile contaminant material that may first be vaporized from the source. The vaporization rate of each component is proportional to its vapor pressure at a given temperature (Raoult's law). Therefore, during vaporization, the higher-vapor-pressure components will vaporize more rapidly, and the source will become progressively enriched in the lower-vapor-pressure component as evaporation progresses.

Advantages of thermal (vacuum) evaporation are [Mattox 1998]:

- High-purity films can be deposited from high-purity source material.
- High vacuums, 10^{-3} to 10^{-7} Pa (10^{-5} to 10^{-9} torr) (depending on level of gaseous contaminants that can be tolerated), minimize the presence of contaminants.
- Source material may be a solid in any form or purity.
- High vaporization rates can be obtained.
- The line-of-sight trajectory and "limited-area sources" allow the use of shutters and masks.
- Deposition monitoring and control are relatively easy. However, the beam must be swept continuously.
- Deposition system can be pumped at a high rate during the deposition.
- Residual gases and vapors in the vacuum environment can be easily monitored.
- It is the least expensive of the PVD processes.

The disadvantages of thermal (vacuum) evaporation are [Mattox 1998]:

- Many alloy compositions and compounds can only be deposited with difficulty.
- Line-of-site and limited-area sources result in poor surface coverage on complex surfaces without proper fixturing and fixture movement.
- Line-of-site trajectories and limited-area sources result in poor film-thickness uniformity over large areas without proper fixturing and fixture movement.
- Few processing variables are available for film-property control.
- Source-material utilization may be poor.
- High radiant heat loads can develop and persist in the deposition system.

Coating-thickness distribution across the substrate will be affected by the evaporating cone of the source. For example, if a cavity is drilled into the evaporant source by the electron beam the solid angle of the evaporation cone (spread) would decrease with increasing depth of the cavity. A similar effect is obtained for a source contained in a crucible as the level of the source in the crucible drops during evaporation. The thickness of the deposit outside the cone will be less than within the cone. The distance between the source and substrate will also affect the thickness distribution. A number of examples are available for calculating the required source-to-substrate distance to obtain the desired thickness distribution of deposits on stationary-, moving-, and rotating-substrate plates/strips, including calculations for multiple sources [Hill 1986].

The electron beam offers great flexibility for obtaining multilayer and mixed-component deposits. A single gun can be equipped with a multicrucible mount, or, alternatively, several guns can be aimed at several sources. Sharp compositional changes or graded mixed layers can be obtained by varying the source and/or power input. An alloy composition can be deposited uniformly by having a source fed at a rate equal to the vaporization rate or by mixing vapors from different corresponding electron beam sources, which are controlled at the appropriate vaporization rates to provide the desired final composition.

The overall quality of the deposits is affected largely by the deposition rate and the substrate temperature. In an early work, it was reported that there is a substrate temperature, T_s, dependent on the deposition rate, above which the deposited beryllium film appears to be completely undisturbed [Adams and Hurd 1969, Wheeler et al. 1982]. The substrate temperature, T_s, was observed to increase (nonlinearly) from 100 °C (212 °F) at a deposition rate of 0.5 Å/s to 150 °C (300 °F) at 140 Å/s. When films 0.2 to 0.3 μm thick were deposited at temperatures below T_s, cracks nucleated and grew due to the high density of structural defects in the deposits. As the substrate temperature rose, the defect density and the magnitude of the stresses decreased, and the ductility of the film increased. At and above 300 °C (570 °F), surface relief rapidly developed.

The yield strength of beryllium deposited on rotating substrates in an EBM system was reported as being substantially higher than that obtained using stationary substrates, namely 213.5 and 57.3 MPa, respectively [Nieh and

Wadsworth 1998]. The rotation of the substrate resulted in a zigzag pattern of the columnar grains, with the periodicity of the pattern determined by the combination of the deposition and rotation rates. In three-dimensional views, the microstructure consisted of interwoven helical grains. The periodicity was most obvious under a high deposition rate at a slow rotation speed and least obvious under a low deposition rate at high rotation speed. No such pattern was exhibited when the substrate remained stationary. The increased strength was attributed to the increase in dislocation density that is required to accommodate the curvatures associated with the interwoven columnar grain structure.

The substrate was arranged coaxially with a 5 cm (2 in.) diameter high-purity beryllium rod source that was located 20 cm (8 in.) above the substrate [Nieh and Wadsworth 1998]. The substrate, which measured 12.5 cm (5 in.) in diameter, was capable of being rotated from 1 to 60 revolutions per hour. Rectangular four-point bend samples (25 by 10 by 1.25 mm, or 1 by 0.4 by 0.05 in.) were obtained from the deposited beryllium. Carbon was used as a parting agent, which permitted the beryllium deposit to be easily removed. The substrate temperature was controlled at 400 ± 10 °C (750 ± 18 °F). The substrate, made of SAE 4230 steel, was chosen because its coefficient of thermal expansion is close to that of beryllium. The deposits were highly anisotropic, consisting of columnar grains having an aspect ratio of approximately 20, with their major axis (corresponding to the [001] crystallographic direction) always pointing toward the evaporation source. Very fine grain sizes were obtained, initially averaging approximately 1 μm at the interface, which increased laterally as well as with increasing thickness of the deposit.

In comparing a condensed beryllium with the evaporant source, the condensed deposit had lower amounts of the lower-vapor-pressure constituents (iron, BeO, chromium, nickel, copper), coarser grain size, and a columnar structure [Anisimov et al. 1997]. The density, however, was close to that of the source material. The coefficient of thermal expansion of the deposit differed from that of the source, as may be seen in Table 22.2. The thermal conductivities were close (120 W/m · K at 400 °C, or 750 °F). Thermal evaporation was obtained using resistance heating of a crucible to between 1400 and 1500 °C (2550 and 2730 °F), achieving a deposition rate of 0.1 to 0.2 mm/h (0.004 to 0.008 in./h). A compromise exists between an unacceptable short life of equipment at higher temperatures and too slow a deposition rate at lower temperatures. The condensing substrate-surface temperature ranged from 500 to 900 °C (930 to 1650 °F). Where bulk deposits were required, surface-oxidized beryllium or molybdenum substrates were used; both allowed easy separation of the deposit from the substrate. Where good adhesion was required, the substrate was either pure beryllium, copper, or stainless steel. On evaporation, the pressure during deposition was approximately 10^{-3} Pa (7.5×10^{-6} torr). Plates with thicknesses of 1 to 3 mm (0.04 to 0.1 in.) and 10 to 15 mm (0.4 to 0.6 in.) were made, the latter group in stages with 1.5 to 2 mm (0.06 to 0.08 in.) of deposit thicknesses per run. To improve adhesion between the layers, the deposit was subjected to a thermomechanical treatment: 900 °C (1650 °F) for 30 min under a pressure (load) of 5 MPa (0.7 ksi).

Beryllium (98.5% purity) was evaporated from a source temperature of 1500 °C (2730 °F), with the chamber evacuated to 10^{-3} to 10^{-4} Pa (10^{-5} to 10^{-6} torr), and a source-to-substrate distance of approximately 13.5 cm (5 in.) [Dua et al. 1985]. The vapor was deposited on a number of different substrates having relatively rough surfaces. The substrate plates were polished with 600-grit SiC, ultrasonically cleaned, and degreased. The deposition rate (65 to 765 Å/s) did not show any significant effect on coating. Brittle deposits with microcracks were obtained at the lowest substrate temperature of 150 °C (300 °F). The microcracks were attributed to internal stresses caused by the high density of structural defects. With increasing substrate temperature, the defect density and residual stresses decreased, resulting in an increase in ductility and the absence of microcracks in deposits made at both 300 and 450 °C (570 and 840 °F). The coatings became microscopically

Table 22.2 Coefficient of thermal expansion (CTE) for condensed beryllium and a bulk (TShP) beryllium source

Temperature range		Average CTE (∥/⊥), 10^{-6}/ °C	
°C	°F	Deposit	Source
20–10	70–212	10.2/13.0	10.9/11.1
20–200	70–390	12.2/14.0	11.2/11.5
20–300	70–570	13.2/16.0	11.9/12.3
20–400	70–750	14.6/16.8	12.6/13.1
20–500	70–930	15.5/17.6	13.7/13.7
20–600	70–1110	16.2/18.2	14.5/14.5
20–700	70–1290	16.8/18.6	15.0/14.9

Source: Anisimov et al. 1997

smoother with increasing temperature. At the high magnification of 4000× (scanning electron microscope), the surface appearance was shown to depend on the incident deposition angle; at 51° the surface was relatively featureless, while at 90° it had a petal-like structure.

Beryllium foils were produced for x-ray windows using electron beam evaporation under a chamber pressure of 1.3×10^{-4} Pa (10^{-6} torr), with the substrate heated to 550 °C (1020 °F). A deposition rate of approximately 5 μm/min was used to form 7.5 μm thick films. The electron beam power was 3.0 kW (10 kV at 300 mA). Columnar grain growth, which is typical of vapor-deposited beryllium, with an average grain size of 2.0 μm in diameter was obtained. Porosity and pinholes were seen that were attributed to contaminants and roughness of the substrate surface. To minimize diffusion of copper from the substrate into the beryllium, a molybdenum/silicon diffusion barrier was used between the deposit and substrate, creating a Cu/Mo/Si/Be sequence. Silicon has a low solubility in beryllium, while molybdenum limits the diffusion of copper into silicon. Using 0.2 μm thick interlayers of molybdenum and silicon, less than 20 ppm of either copper or molybdenum were detected in the beryllium film. Without the barrier, copper contents were 70 and 700 ppm in deposits made at 350 and 480 °C (660 and 900 °F), respectively.

Using an electron beam melting source, beryllium was vapor deposited on substrates that were masters (negative mirror surfaces) made of AISI 4130 steel polished to optical quality [Wheeler et al. 1982]. Carbon, to a thickness of several hundred angstroms, was deposited on the steel as a release agent for easy removal of the thick beryllium deposit, allowing sufficient adhesion to exactly replicate every detail of the steel surface. Thickness of the carbon-coating releasing agent had no effect on the deposit microstructure. The masters were located coaxially and 18 cm above the source. A movable plate was interposed between source and substrate until a stable molten pool was achieved. Surface asperities can strongly affect the atom flux distribution in the vapor beam.

At low substrate temperatures, fine, tapered crystalline grains (columnar structure) with porosity at the grain boundaries were obtained. Porosity was attributed to vapor beam shadowing that was caused by the preferential columnar growth. At higher temperatures, the increase in surface-atom mobility greatly decreased or eliminated the porosity, resulting in a deposit having higher density with increased toughness. The increase in grain size obtained with increasing thickness suggested that the surface temperature was likely higher than that at the substrate-deposit interface (perhaps exhibiting a temperature gradient).

High deposition rates at low temperatures generally caused deposits to peel spontaneously from the substrate [Wheeler et al. 1982]. This was attributed to the defect structure and high internal stresses obtained at low substrate temperatures. At the higher substrate temperatures, annealing and grain growth occurred, and the rate of growth increased with an increase in deposition rate. It was suggested that the higher deposition rates increased the surface temperature. The microhardness decreased significantly with an increase of substrate temperature (250 to 400 °C, or 480 to 750 °F), as shown in Fig. 22.4. This was attributed to the elimination (by annealing) of the defect structure trapped at the lower temperatures. The effects of temperature and deposition rate on adhesion of the deposit to the substrate are interrelated. For a given deposition rate, there is a lower temperature limit at which the deposit will peel off. For a given substrate temperature, there is an upper deposition rate above which the deposit will separate from the substrate. Higher temperature produces a stronger bond, while higher deposition rates

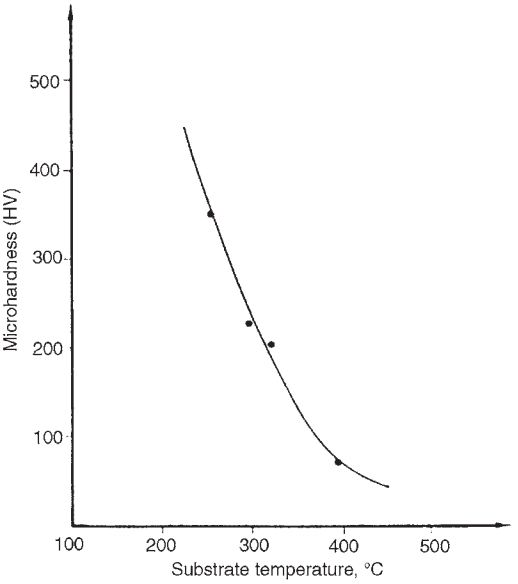

Fig. 22.4 Microhardness of a beryllium deposit as a function of substrate temperature. Source: Wheeler et al. 1982

increase internal stress. Adhesive forces decrease as thickness decreases [Wheeler et al. 1982].

The (102) and (002) planes parallel to the substrate surface were obtained for beryllium deposited at low and high temperatures, respectively. At intermediate temperatures, both (102) and (002) crystalline texture were present. (Texture refers to the structure that may be developed in a material as a result of its prior solidification, deposition, thermal, and/or deformation history. It may reflect compositional variations or preferred crystallographic orientations, where, in the latter case, certain crystalline planes have a preferred orientation, or parallel alignment, with respect to some arbitrary reference in contrast to being randomly oriented.) Because of the anisotropic coefficient of thermal expansion and that of the critical shear stress for slip, the thermal stability and strength of the deposit would be affected by the degree of crystalline anisotropy of the deposit [Wheeler et al. 1982].

A highly textured structure was reported for vapor-deposited beryllium using EBM [Nieh et al. 1982]. An elongated columnar structure with the major axis parallel to the vapor-flux travel direction with an aspect ratio of approximately 20 was obtained, as seen in Fig. 22.5. Fine 1 μm grains were formed at the initial interface, with the grains increasing in size as deposition proceeded. Along the edges of the deposit, the elongated grains formed at an oblique angle consistent with direction of the nonnormal incident angle away from the center of the flux. A 1 to 1 linear relationship was found between the orientation of the column angles and the direction of the incident flux. The major axis of the columns always pointed to the evaporation source. The substrate was maintained at approximately 400 °C (750 °F). The substrate was located 20 cm (8 in.) above and coaxial with the source. Deposition rates were between 0.1 and 0.3 mm/h (0.004 and 0.01 in./h). The deposits were approximately 99% dense, with thicknesses between 1 and 3 mm (0.04 and 0.1 in.).

Adhesion values were obtained for 10 μm thick films deposited on the different substrates at a deposition rate of 270 Å/s at a substrate temperature of 450 °C (840 °F) [Dua et al. 1985]. The adhesion strengths in kg/cm^2 for various substrates were as follows: 304 stainless steel, 509; 316 stainless steel, 700; molybdenum, 318; Monel 400, 664; and copper, 627. The adhesion strength improved with increasing substrate temperature; for example, for 316 stainless steel substrates, values of 265 and 700 kg/cm were obtained for substrate temperatures of 300 and 450 °C (570 and 840 °F), respectively. A 13 μm thick deposit obtained at a deposition rate of 183 Å/s at 300 °C (570 °F) had significant porosity, and the coating-to-substrate bond appeared to be mechanical.

Using an EBM source, high-purity beryllium was deposited at a deposition rate of 25 μm/min on substrates at temperatures ranging from 400 to 700 °C (750 to 1290 °F). Pinpoints developed in films that were formed at the lower substrate temperatures. This was attributed to insufficient cleaning and lack of subsequent protection of the substrate surface prior to deposition. This problem was serious for thicknesses less than 50 μm [Dua et al. 1985]. Deposits produced on substrates that were at temperatures below 400 °C (750 °F) did not reach full (bulk) density and contained pores.

Among the many products formed by thermal evaporation are optical-interference coatings, mirror coatings, decorative coatings, permeation-barrier films on flexible packaging materials, electrically conducting films, and corrosion-protective coatings [Mattox 1998].

22.3 Sputtering

During sputtering, the target is bombarded by ions, which, by a momentum transfer, physically chip atoms off of the target, causing them to be ejected from the surface and subsequently strike and adhere to the substrate. In this manner, a high-quality film is built up. The ions are usually gaseous ions accelerated by a plasma or an ion gun. Sputtering is one of the two principal technologies for vapor deposition of thin films on

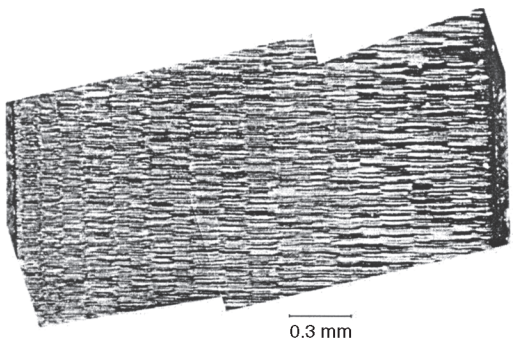

Fig. 22.5 Microstructure of a thick beryllium deposit near the center of the deposition. The axis of the columns is parallel to the normal of the substrate surface (left end of view). Deposited at 400 °C at the rate of 0.12 mm/h. Source: Nieh et al. 1982

silicon, alumina, intermetallics, and glass substrates in the electronics and optical industries.

There are a number of different sputtering methods: planar diode sputtering, triode sputtering, pulse sputtering, radio-frequency sputtering, and magnetically assisted sputtering (magnetron sputtering). The following gives a brief description of each method.

Planar Diode Sputtering. The target and substrate holders act as the cathode and anode, respectively. On applying a high negative potential to the cathode, a plasma glow discharge ignites within the vacuum chamber. The dc diode plasma generally consists of argon gas ions, is usually weakly ionized with perhaps one in 10^4 neutrals, and has a particle temperature of several electron volts [Mattox 1998]. (An electron volt, eV, of energy is the amount of energy acquired by any charged particle carrying unit electronic charge when accelerated through a potential difference of 1 V.) This is the simplest arrangement, but to minimize contamination of the deposit and produce reproducible results requires controlling the ion current density, residual gas pressure, and temperatures of the substrate and cathode within narrow limits.

The dc diode sputtering system has the following advantages [Mattox 1998]:

- Large areas can be sputtered uniformly over long periods of time.
- The target can be made conformal with the substrate.
- The dc diode plasma, which fills the entire chamber, can be used to plasma clean surfaces as part of the in situ cleaning.

It has the following disadvantages:

- It is limited to relatively low sputtering rates.
- The target can be poisoned by reactive contaminants.
- Surface heating is caused by the electrons accelerated away from the target.
- Only electrical conductors can be used as sputtering targets.

Triode Sputtering. There are three electrodes: a sputtering cathode, a substrate anode, and a thermionically heated filament that generates electrons. These electrons accelerate toward the anode, where they ionize a large portion of the gas molecules. The heated filament acts to increase the ion population and to maintain a constant bias voltage, resulting in a higher sputtering rate, increased film density, improved regulation of deposition, and less contamination, compared to the planar diode system. Schematics of planar diode and triode systems are shown in Fig. 22.6. A radio-frequency (rf) sputtering system is essentially similar to that of the triode sputtering system, except that the dc

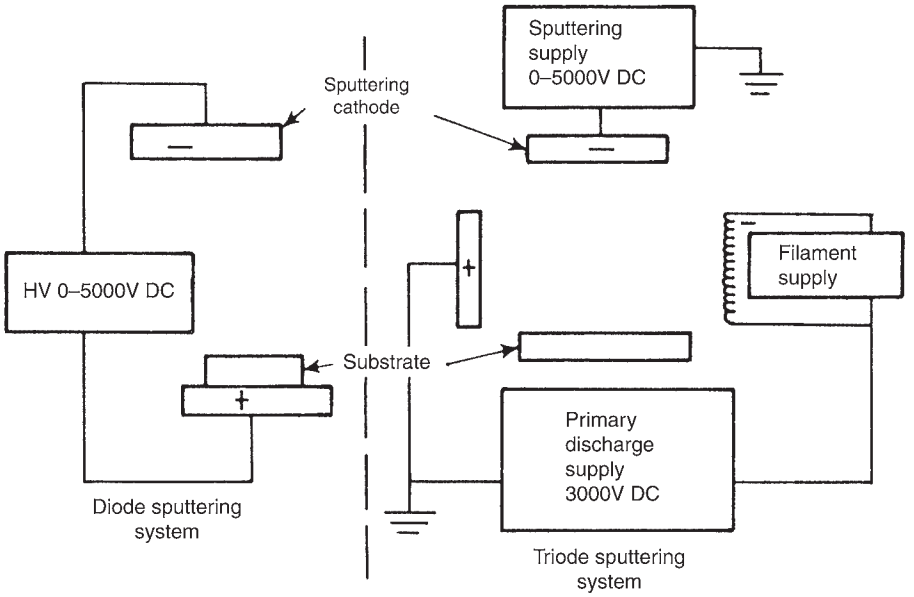

Fig. 22.6 Schematic diagrams of planar diode and triode sputtering systems. Source: Hill 1986

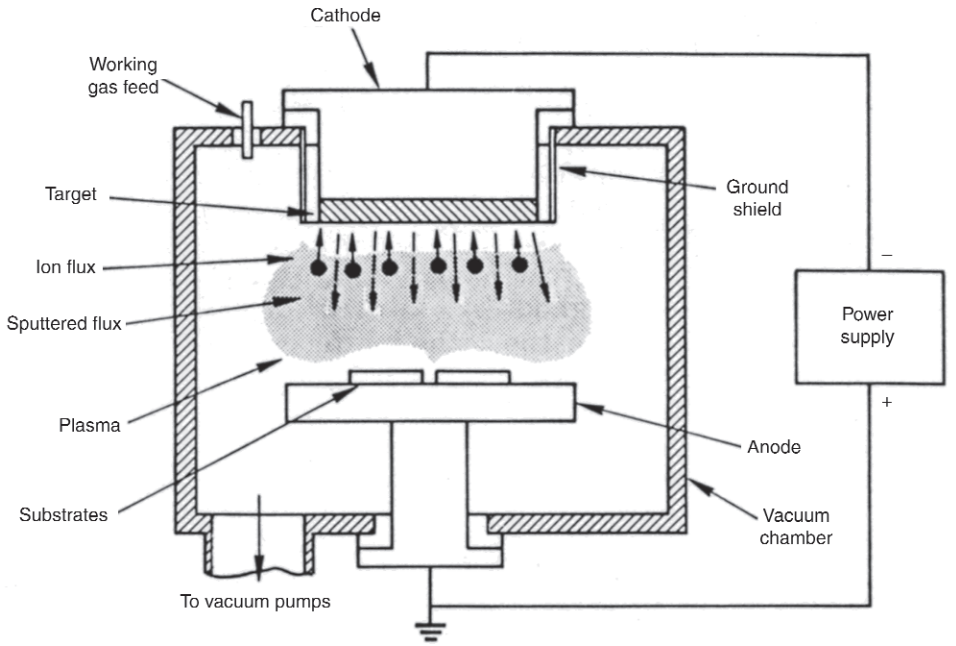

Fig. 22.7 Schematic of a planar electrode system used for sputtering. Source: Thornton 1982b

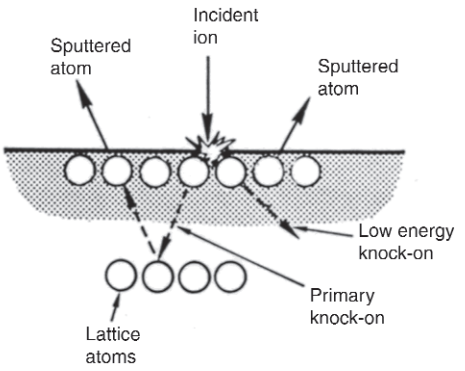

Fig. 22.8 Schematic illustration showing some momentum-exchange processes that occur during sputtering. Source: Thornton 1982a

sputtering supply shown in Fig. 22.6 is replaced by a 13.56 MHz rf power supply [Hill 1986].

Pulse Sputtering. A schematic representation of deposition sputtering by an ion-plasma flux in a planar electrode system is shown in Fig. 22.7 [Thornton 1982b]. Figure 22.8 illustrates a possible scenario with a momentum exchange between an incident ion and two surface atoms of the target [Thornton 1982a]. The atom receiving the major component of the ion momentum transfers this component to one or more atoms below the surface and is reflected back to kick out an atom from the surface. As illustrated, the atom receiving the smaller momentum transfer kicks out an adjacent surface atom.

Radio Frequency. This method of sputtering allows insulators to be sputter coated. With a dc system, the charge buildup on the insulator target cannot be dissipated and interferes with sputtering off material from the target. The rf potential enhances the negative charge on the target. At pressures as low as 3×10^{-2} Pa (2×10^{-4} torr), two difficulties inherent in higher-pressure diode-type sputtering are reduced: gaseous impurity inclusions and nonreproducibility of film properties. Also, a heated filament to sustain the plasma is eliminated, and therefore, contamination from thermionic emission is eliminated.

Magnetron sputtering involves coupling magnetic fields with the sputtering source. The primary reason is to decrease the mean-free path of electrons in the discharge so that more ions can be produced without having to increase the gas pressure in the system. The magnetic field confines the electrons that maintain the discharge ionization, and therefore the resulting plasma, to be near the target surface. This increases the plasma density and the sputtering rate. Because of the much higher sputtering rate, poisoning by reactive contaminants is greatly

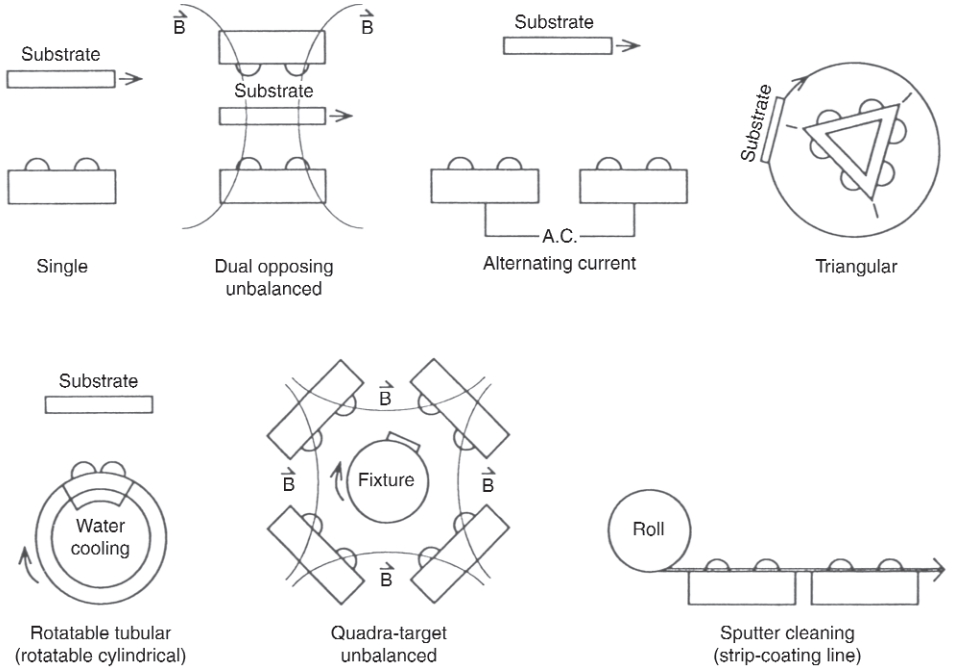

Fig. 22.9 Some schematic arrangements of magnetron sputtering targets. Source: Mattox 1998

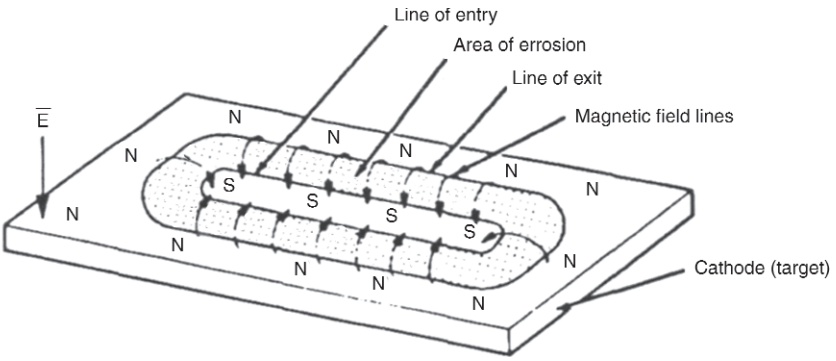

Fig. 22.10 Direct current diode planar magnetron sputtering configuration. Source: Mattox 1998

reduced. By confining the electrons near the surface, the dc gas discharge can be maintained at low pressures (0.1 to 0.5 Pa, or 8×10^{-4} to 4×10^{-3} torr), where collision and charge-exchange collision probabilities are low, and the sputtered atoms pass by line of sight directly to the substrate. This permits substrates to be scaled to large sizes with uniform deposition over very large areas [Thornton 1982b].

Magnetron sputtering configurations use a magnetic field (approximately 200 gauss), usually from permanent magnets near the target (cathode) surface, in order to confine the electrons near the surface. When an electron is ejected from the target surface, it is accelerated away from the surface by the electric field, but it is forced to spiral around the magnetic field lines. By confining the electrons near the surface, the dc gas discharge can be sustained by low pressures where collision probabilities are low. This allows the cathode potential to be low ($<$1000 V) with a high-energy, high-current flux, which gives high sputtering yields and high sputtering rates [Mattox 1998]. A number of planar magnetron sputtering target arrangements are illustrated schematically in Fig. 22.9. An example of a specific magnetic field arrangement is shown in Fig. 22.10.

A large part of the energy flux comes from the electrons generated in the plasma. In the planar magnetron, the electrons are deflected away from the substrate by the magnetic field. Thus, substrate temperatures that are reached in a planar magnetron can be significantly lower than those reached in the substrate using the planar diode, making the magnetron more amenable for coating heat-sensitive materials. A distinct advantage of planar magnetron sputtering over evaporation coating is the ability to deposit films from a target in virtually any direction. The three basic sputtering directions are sputtering up, down, and sideways (away from the source). The relative advantages and disadvantages of each direction are summarized in Table 22.3 [Hill 1986].

Sputtering, in general, offers many advantages (and some disadvantages) over other coating methods. Advantages include [Mattox 1998, Hill 1986]:

- Film-thickness control is simple and easily reproduced.
- With the proper configuration, large-area targets can be used.
- Fast electrons can be kept away from the substrate to prevent substrate heating.
- Nonporous films with surfaces that resemble the substrate surface can be produced.
- There are no difficulties with "spitting" (random dispersion or ejection of material from evaporant), as in thermal evaporation.
- There are no restrictions with respect to gravitational forces in electrode or substrate arrangement.
- Elements, alloys, compounds, refractory materials, and insulating films can be deposited.
- Target provides a long-lived evaporation source with a stable geometry.

Table 22.3 Characteristics of three sputtering-source mountings

Source mounting	Advantages	Disadvantages
Sputtering up	Least particulate contamination on substrates	Possible particulate contamination and arc-downs on source. Materials handling is sometimes complex and will likely require special fixuring.
Sputtering down	Least particulate contamination on target	Possible particulate contamination on substrate
Sputtering sideways	Particulate contamination shared by substrate and source	Materials handling will likely require complex fixturing.

Source: Hill 1986

- In some cases, target can be configured to provide a large-area vaporization source that can be of almost any shape.
- Good film adhesion is assured.
- Low-temperature epitaxy is possible. (Epitaxy refers to a crystalline orientation present in a crystalline material, or substrate, to nucleate the same orientation in the material being deposited onto the substrate. If a material different than that of the substrate is being deposited and the mismatch between the two corresponding lattice planes is small, that is, $<8\%$, the crystallographic mismatch between the two sets of planes can be accommodated by dislocations at their interface. Epitaxial films generally have better adhesive properties.)
- Thickness uniformity over relatively large planar areas can be obtained.
- Depositing atoms are relatively energetic, leading to more compact films.
- By simply applying a voltage bias to the substrate, ambient noble gas ions will bombard the growing film, leading to further densification as well as other microstructural modifications.
- Sputtering is suitable to the introduction of dopants.

Disadvantages of sputter deposition are [Mattox 1998]:

- Sputtering rates are low compared to those that can be obtained by thermal evaporation.
- In many configurations, the deposition flux distribution is nonuniform and requires fixturing to randomize the position of the substrates in order to obtain films of uniform thickness and properties.
- Sputtering targets are often expensive, and material utilization may be poor.
- Targets can be poisoned by reactive contaminants.
- Electrical conductors must be used as sputtering targets, except when powering with rf sources.
- Most of energy incident on the target turns into heat, which must be removed.
- Generally, the pumping speed of the system must be lowered during sputtering, and gaseous contamination is not easily removed from the system.
- Gaseous contaminants are activated in the plasma, thus making film contamination more of a problem than in vacuum evaporation.

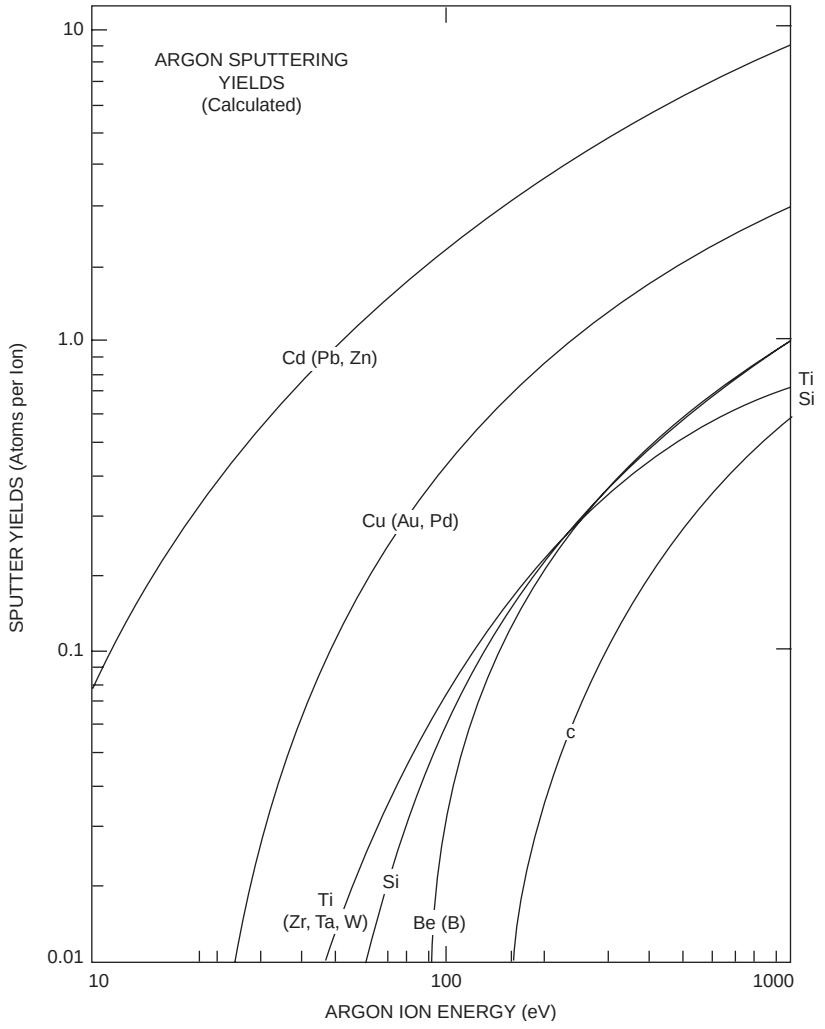

Fig. 22.11 Sputtering yields of several materials bombarded with argon ions at various energies. The materials listed in parentheses have similar sputtering-yield curves. Source: Mattox 1998

- In some configurations, radiation and bombardment from the plasma or sputtering target (cathode) can degrade the substrate.

Other factors to consider are:

- Sputtering yields and corresponding deposition rates vary for different metals, alloys, nonmetals, and insulators.
- Negative biasing of the substrate can be used to improve the adherence of the metal film.
- Negative biasing of the substrate can be used to remove contaminants (oxides, carbides, nitrides, hydrides, etc.).

The sputtering yield is proportional to the energy of the sputtering particle (as well as other factors), and thus, it is preferable to sputter beryllium with argon gas rather than with the lighter helium or neon. The calculated sputtering yields as a function of argon ion energy for a number of metals, including beryllium, are shown in Fig. 22.11 [Mattox 1998]. The angle of incidence and relative masses of the bombarding and target species will also influence the yield. The chemical bond strength of the surface atoms and surface topography of the target are also factors that affect yield. If the gas pressure is too high, the mean-free path will be short, and the probability of the sputtered atom being backscattered to the target is increased. For example, the effect of pressure on the deposition rate for tantalum is shown in Fig. 22.12

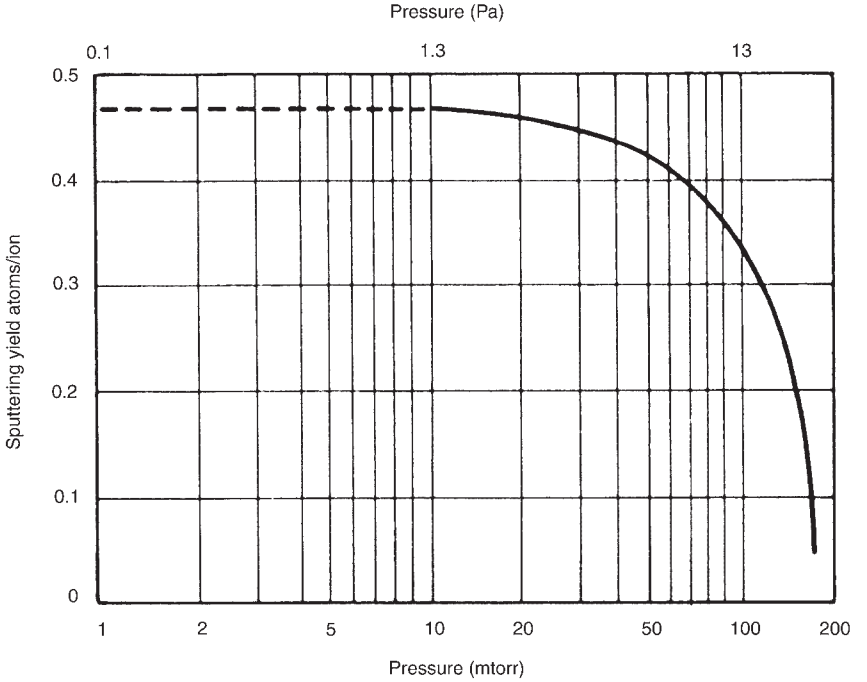

Fig. 22.12 Variation of sputtering yields of tantalum as a function of the total pressure of the vacuum system. Source: Hill 1986

[Hill 1986]. For beryllium, being a much lighter atom, the curve would be shifted to the right.

The presence of oxygen greatly inhibits the sputtering rate of most materials. If the arrival of oxygen ions at the target is equal to or greater than the sputtering rate of oxygen from the target, then the target will not clean up, and the sputtering rate will remain suppressed. This is especially the case for oxygen-active metals such as beryllium, where the bond between the target metal and the oxygen (or nitrogen) is stronger than between the metallic atoms themselves. The oxide (or nitride) films will change the plasma parameters, which will reduce the sputtering rate. The change in chemical composition of the target (cathode) that causes retardation in the sputtering rate is referred to as cathode poisoning. In the extreme case, poisoning will cause bombardment of the cathode to cease. This can occur most readily under a continuous dc potential whereby a positive surface-charge buildup develops, which decreases the bombardment energy. If an insulating surface forms on the (dc) cathode, the charge buildup will cause arcing over the surface. The arc can be suppressed by momentarily turning off the power supply or by applying a positive bias when the arc is detected.

Cathode poisoning can be prevented by using an rf (alternating current) power source or a pulsed dc power source, both providing the required alternating polarity of the cathode. Of the two systems, the pulsed dc source produces a much larger percentage of power to the actual sputtering process, yielding the higher sputtering rate. The pulse can be either unipolar, where the voltage is typically negative with a zero voltage-off time, or bipolar, where the voltage polarity alternates between negative and positive, or some combination of these two methods. Some possibilities are shown in Fig. 22.13 [Mattox 1998]. With the power supply operating in the range of 50 to 350 kHz, very rapid increases or decreases in the voltage are obtained. During the positive bias and/or off time, electrons from the plasma neutralize the charge buildup on the cathode, and the energetic ion bombardment can then take place during the negative part of the cycle, resulting in efficient sputtering.

A determination was made of the threshold energy of sputtering a number of conductive materials by light ion gases in the prethreshold energy region (from 10 to 500 eV) [Suvorov 2002]. The beryllium sputtering yields at room temperature as a function of energy of light ion

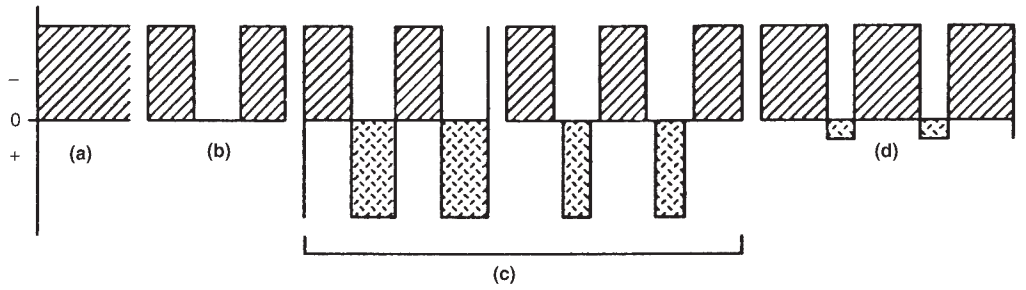

Fig. 22.13 Examples of typical pulsed direct current waveforms: (a) continuous, (b) unipolar, (c) bipolar, and (d) asymmetric bipolar. Source: Mattox 1998

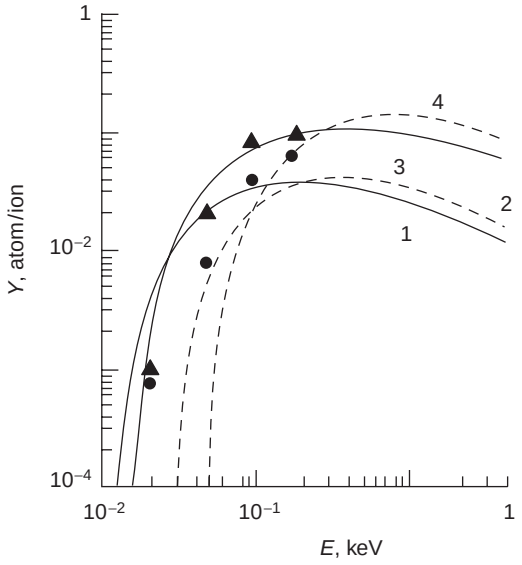

Fig. 22.14 Ion energy dependence of beryllium sputtering yields by D^+ and He^+ ions at room temperature: Be-D^+ data, ● and 2; Be-He^+ data, ▲ and 4. Theoretical calculations: Be-D^+, 1; Be-He^+, 3. Source: Bohdansky and Roth 1984

gases are shown in Fig. 22.14. Beryllium (99.4% purity) targets were irradiated with light ions (D^+ and He^+). Sputtering yields were independent of target temperature up to 700 °C (1290 °F) for ion energies above 1000 eV. At 760 °C (1400 °F), thermal evaporation became dominant. In the threshold region, at energies below 1000 eV, sputtering yield data at room temperature were influenced by an oxide layer. Above 300 °C (570 °F), beryllium diffuses sufficiently rapidly through the layer, and the sputtering yield becomes independent of temperature. The threshold energy is modified, resulting in an increase in the sputtering yield [Bohdansky and Roth 1984].

Ideally, the sputtering process ejects each surface atomic layer in sequence. The composition and degree of homogeneity of the deposit would mirror that of the target material. By contrast, the compositional distribution of a deposit formed by a thermal evaporation process will depend on the relative vapor pressure of the constituent elements, and for impure materials and especially alloys, it may vary significantly from the target. Characteristics of a film may be affected by too high a gas pressure, whereby gas-phase collisions take place, scattering particles and raising their temperature and energy, resulting in their bombarding and incorporating into the film.

The temperature of the substrate, as well as the gas pressure, that moderates the energy arriving at the substrate affects both the sticking coefficient (ratio of atoms adhering/atoms striking) and the film structure. Argon may become entrapped in the film. Generally, argon entrapment decreases with increase of temperature since the sticking coefficient is reduced. A positive bias on the substrate has the effect of attracting more electrons, heating the substrate, and, in turn, reducing the sticking coefficient for contaminating gases.

A number of studies have examined the sputtering operating parameters in producing superconductive amorphous beryllium films. Introduction of oxygen (up to 1 at.% added to argon) increased the thermal stability of the film by suppressing the growth of any crystallites (hexagonal close-packed structure) present [Takei et al. 1990]. The oxygen increased the resistivity of the film. The superconducting critical temperature (T_c) was found to vary between 1 and 7 K (−272 and −266 °C, or −458 and −447 °F), depending on the ejection angle from the target. In the study, a series of substrates were attached along a spherical arc within a holder so that the incident flux from the target was always normal to the substrate surface, as shown in Fig. 22.15.

The effect of the ejection angle between target and normal to the substrate was evaluated over a range of angles from 20 to 100°. The ion flux impinged the target at a fixed angle of 60° from the normal to the target (Fig. 22.15). A maximum T_c was obtained at an ejection angle of 30°; the lowest T_c was obtained at and near 90°. Crystallites formed at 30° were considerably smaller than those formed at 90°. Oxygen also increased T_c, depending on the ejection angle, with no effect of oxygen seen at 90°. The increase in T_c was attributed to the low-angle ejections (e.g., at 30°) from the target of high-energy-target (Be) atoms, which result from ions impacting the target at an off-normal angle. Film thicknesses ranged from 40 to 70 nm, depending on orientation, with the substrates at a temperature of 295 K (22 °C, or 71 °F). The pressure during deposition was 2×10^{-2} Pa (10^{-5} torr) [Takei et al. 1990].

The thermal stability of an ion-beam-sputtered beryllium film structure was illustrated by maintaining a 20 nm thick film at room temperature in a dry air atmosphere for one year [Maeda et al. 1987]. The superconducting critical temperature remained high (6 to 7 K, or −267 to −266 °C, or −449 to −447 °F). Transmission electron microscopy revealed a homogeneous, amorphous microstructure with some hcp crystallites. In the same study, it was observed that the critical temperature increased with increasing film thickness, reaching a maximum T_c of approximately 7 K (−266 °C, or −447 °F) at a thickness of approximately 20 nm. The subsequent decrease in T_c was attributed to a corresponding increase in the number of beryllium crystallites with increasing film thickness. A 30° incident angle to the beryllium target was used. Oxidized silicon wafers served as substrates. Argon ions were accelerated to an energy level of 5 keV with an ion beam current of approximately 0.2 mA. The argon pressure was maintained at 3×10^{-2} Pa (2×10^{-4} torr). The substrate temperature was kept at 295 K (22 °C, or 70 °F). The deposition rate was in the range of 0.2 to 0.5 nm/min, with the target-to-substrate distance at 3.5 cm (1.4 in.).

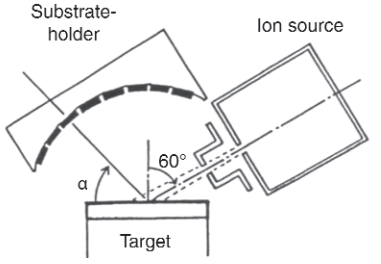

Fig. 22.15 Apparatus geometry for ion beam sputter deposition. Note that impingement (incident) angle is always normal to the substrate, independent of α. Source: Takei et al. 1990

The optimum angle of incidence on a target for maximum yield depends on ion mass, charge, and energy as well as other factors, such as target mass and crystallographic orientation. A calculation based on theoretical considerations gives a maximum sputter yield for beryllium at an incident-ion-bombardment target angle of 18° for ion energies of the order of 1000 eV [Sharp 1986]. A target design that would produce acute angles was evaluated. By generating an axial projection of an ion beam into a negatively biased cylinder (hollow cathode sputtering target), acute radial angles of impingement could be obtained, as illustrated in Fig. 22.16. The target used consisted of a pressed-and-sintered beryllium cylinder, using argon as the ion source. A negative potential of approximately 450 V was applied to the cylinder to establish the plasma. Typical grain sizes of 30 and 100 nm were obtained at ion-bombardment fluxes of 0.30 and 0.76 mA/cm^2, respectively. The substrate could be placed within the cylinder either at the opposite end of the incoming beam or at the center of the cylinder, with ion beams from two sources, one at each end, entering the off-cylinder axis, as illustrated in Fig. 22.17 [Sharp 1986].

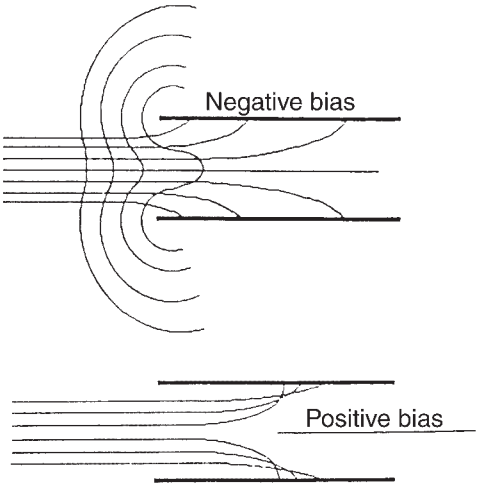

Fig. 22.16 Illustration of an ion beam entering a negatively biased cylinder and diverging as it passes through electrostatic fields emanating from the cylinder end (top). The addition of a positive field near the opposite end of the cylinder would enhance the effect. The combination of a negative cylinder bias and a positive substrate bias permits control of the cylinder area to be bombarded by the ion beams (bottom). Source: Sharp 1986

In contrast to the maximum yield at a low angle of incidence of 18° referred to previously, a maximum yield was reported for an incident beam angle of 75° where a range of angles from 0 to 85° were evaluated, with the yield falling off steeply from 75 to 85° [Guseva et al. 1997]. A Be^+ ion source of BeO together with beryllium targets heated to approximately 400 °C (750 °F) were used. The Be^+ ions were at an energy level of 1 keV. Both polished and unpolished targets were evaluated and showed little difference (approximately 10%) in yield. The sputtering of beryllium by the 1 keV Be^+ ions caused the carbon concentration to decrease and the oxygen concentration to increase in the subsurface layer. The effect of incident angle on yield is shown in Fig. 22.18 [Guseva et al. 1997]. The difference between a portion of the calculated and experimental curves was attributed to the topographical changes observed to have occurred during sputtering in the range of 60 to 80°. These changes effectively changed the incident angles to lower values, causing a reduction in the sputtering yields below the predicted values.

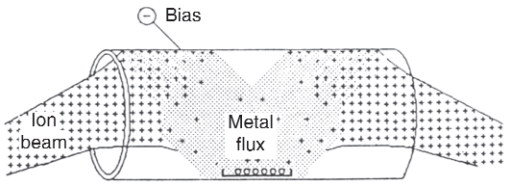

Fig. 22.17 Schematic illustration of the use of two guns symmetrically mounted such that the ion beams enter the cylinder off-axis. This reduces the direct bombardment of the substrate by the ion beam and permits the sputtered-metal flux to be partially directed downward onto a flat surface. Source: Sharp 1986

In a study on the effect of both roughness and angle of incidence on sputtering yield, the yield continuously increased with incidence angle from 0 to 85° (maximum reported) [Bohdansky and Roth 1984]. Ion energies of 0.3 and 3.0 keV were used. Some fraction of the atoms that were sputtered from the target were redeposited on the target surface. This was due to interference by the sides of surface depressions on being sputtered from low spots on the surface. This interference is illustrated in Fig. 22.19. Thus, the redeposition rate was lowest for the polished surface, especially at the lower incidence angles. In addition to surface conditions, processing methods, which may result in different crystallographic textures of the target, can affect yield and spatial distribution of the sputtered particles.

As with most metals, PVD-deposited beryllium tends to form a pronounced columnar grain structure, with the columns normal to the surface and often with a preferential crystallographic

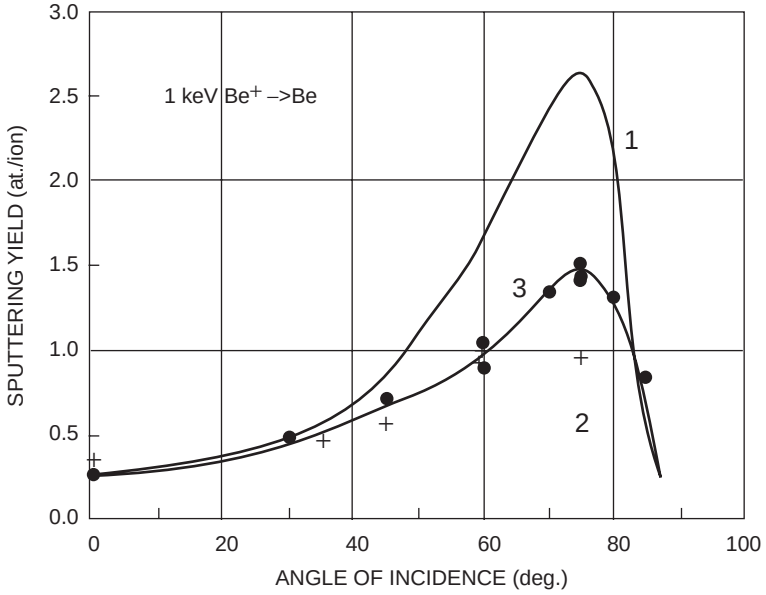

Fig. 22.18 Self-sputtering yield of beryllium as a function of the incident angle of 1 keV Be^+ ions. Curve 1 is calculated; curve 2 (+ + +) is from Hechtl et al. [1995]; curve 3 (•••) is experimental from TShP-type beryllium. Source: Guseva et al. 1997

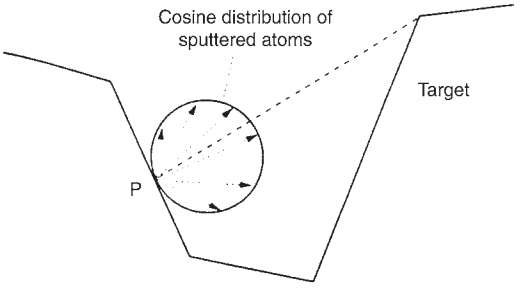

Fig. 22.19 Schematic illustration of target atoms being sputtered off by an incident ion at point "P" and leaving the surface with a cosine distribution. The region below the line from "P" to the edge cuts off the corresponding segment of this distribution such that some atoms are redeposited on the surface of the target. Source: Kustner et al. 1998

orientation. On planar surfaces, the grains tend to become larger with increasing film thickness, with a corresponding increase in surface roughness [McEachern 2001]. Short nitrogen bursts, with pressures up to 0.95 MPa (7100 torr) during sputtering of beryllium with argon, were found to reduce the grain size and suppress the preferential texture. The columnar growth was still present; however, it appeared to be limited in thicknesses to the intervals of successive nitrogen pulses. These effects were attributed to the formation of a nitride layer. In addition, the nitrogen pulsing increased the intrinsic compressive component in the film stress and shifted the compressive-to-tensile transition to higher sputtering pressures, as shown in Fig. 22.20(c) [Mutikainen 1992]. (Refer to inset in view (a) for symbol identification.) The stress-free transition occurred at 0.57 Pa (4×10^{-3} torr) using a 300 W magnetron power. An increase in pulse frequency shifted the crossover to still higher gas pressures. The figure also shows the effect of pressure on film growth rate and resistivity for different operating conditions, as well as the effect of dc magnetron power on film growth and resistivity. With dc magnetron sputtering, the sputtering power had only a minor effect on stress, and the preferred orientation was not affected by either sputtering pressure or power. By contrast, with rf diode sputtering at 250 W, which gave a sputtering self-bias voltage at the target that varied between 1.7 and 1.8 kV, the crystalline orientation normal to the surface was strongly affected, especially by the argon pressure.

Introducing metallic elements that are insoluble in beryllium, such as iron, copper, and nickel, as well as metallic-glass formers, such as boron, into the sputtering flux has been shown to reduce the deposited grain size of high-purity beryllium from micrometer to nanometer sizes. Transmission electron microscopy evaluation of the latter films showed no discernable grain structure. Extremely smooth films (1 nm rms roughness) were obtained with films of only several micrometers thickness. With increasing thickness, however, stresses were developed that caused buckling and delamination [McEachern 2001]. Impurity (carbon, nitrogen, and/or oxygen) gas doping during rf sputtering of high-purity beryllium results in smoother surfaces, finer stabilized structures, and random crystallinity. In the absence of these added impurities, large-grained, rough-surface (1060 nm deep defects) films were obtained on substrates at temperatures above 200 °C (390 °F). Impurity doping, low substrate temperatures, and low sputtering pressures (<1 Pa, or $<7 \times 10^{-3}$ torr) favor forming dense, smooth beryllium films [Burt et al. 1980].

Using a magnetron with three sputtering guns and three targets (two of beryllium and one of Be-6at.%Cu) with a bias voltage, films with thicknesses of 7 to 120 μm were deposited on polymer substrates [McEachern et al. 1997]. Except for a modest decrease in grain size, the microstructure changes little with thicknesses above approximately 7 to 14 μm. The roughness decreased somewhat with thickness/time (an rms of 140 nm for 26 μm thickness to 73 nm for 80 μm thickness). Increasing the bias voltage to within the range of 60 to 80 V and implanting argon resulted in a decrease in grain size (from 1 to 2 μm to 0.2 to 0.3 μm); in addition, the columnar structure becomes more oriented normal to the surface. Using magnetron sputtering of beryllium, both lower substrate temperatures and thicker deposits resulted in larger columnar structures; substrate temperatures were up to 150 °C (300 °F) [Egert and Allred 1990]. Some BeO may be required to prevent grain growth. Excessive BeO when concentrated in the grain boundaries can seriously impede polishing due to the difference in hardness between the oxide and the metal. The sputtering action results in an extremely fine distribution of the oxide throughout the matrix [Murray et al. 1991].

A microstructural model, shown in Fig. 22.21, was developed illustrating the combined effect of argon pressure and substrate temperatures on the different structures that are obtained by sputtering [Thornton 1977, Hill 1986]. The model that was presented originally was developed from evaluations made on deposits of titanium,

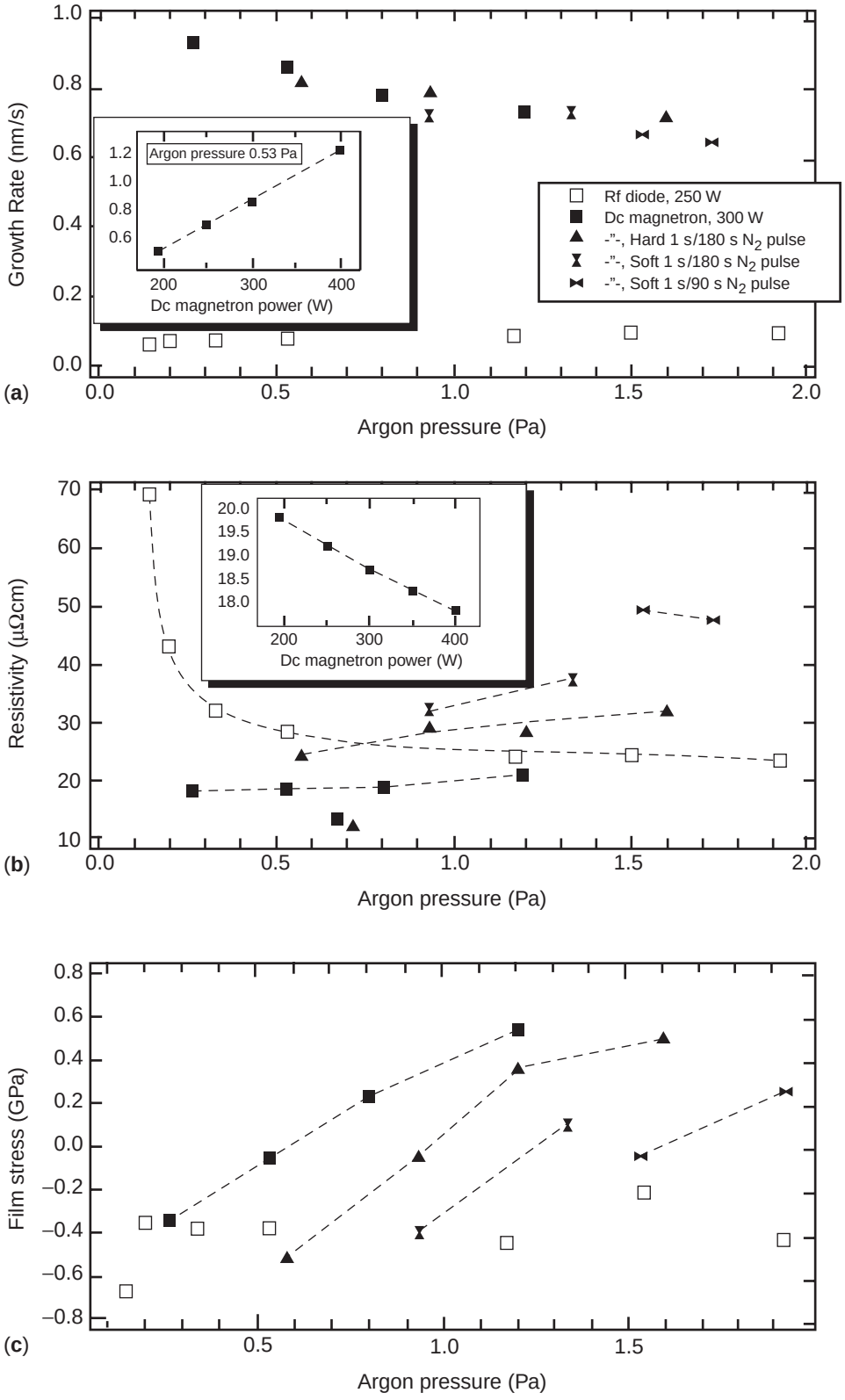

Fig. 22.20 Dependence of (a) growth rate, (b) resistivity, and (c) stress on the argon pressure for radio-frequency (rf) diode and direct current (dc) magnetron deposits. The insets show the dependencies on the magnetron sputtering power at 0.53 MPa (4000 torr). "Soft" refers to control of gas flow with a downstream leak valve, "hard" with a downstream shut-off valve. Source: Mutikainen 1992

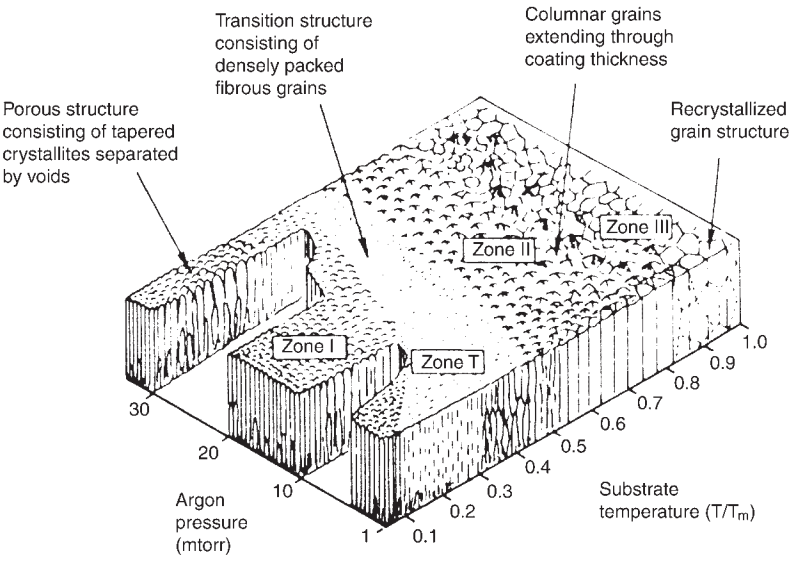

Fig. 22.21 Artistic presentation of a model illustrating the combined influence of substrate temperature and argon pressure on the microstructure of sputtered coatings. Source: Thornton 1977, Hill 1986

nickel, tungsten, iron, ZrO_2, and Al_2O_3 and was subsequently modified for sputtered metal coatings [Thornton 1977]. In the model, zone I consists of tapered columnar crystallites with domed tops separated by voided boundaries. Diffusion rates are very low; the grains have a high dislocation density, producing a high hardness with no ductility. The grain size increases with increasing substrate temperature. This structure is favored by substrate roughness, high argon pressure, and oblique deposition angles. A transition zone (T) between zones I and II consists of a dense array of poorly defined fibrous grains without voided boundaries. It has the internal structure of zone I crystallites. The hardness is still high, significantly above that of an annealed bulk material. The dislocation density and hardness decrease rapidly with increasing T/T_m (temperatures in degrees Kelvin; T_m refers to melting temperature) until zone II structure develops. Zone II consists of columnar-shaped crystallites/grains, which are separated by dense intercrystalline boundaries that extend through the coating thickness. The crystallites tend to have highly faceted surfaces. At high substrate temperatures, the surfaces are smooth with grooved grain boundaries. The columnar grains increase in width and may approach a near-equiaxed shape with an increase of temperature. Zone III, which refers to the highest substrate temperature range and where bulk diffusion has a dominant influence, consists of recrystallized grains. The grains may be equiaxed or columnar, depending on structure and stress distribution formed during deposition. As the columnar and equiaxed grain sizes increase with increasing temperatures in zones II and III, respectively, the hardness and strength decrease and ductility increases. Deposits in the high T/T_m region of zone III have mechanical properties similar to those of fully annealed bulk materials.

The voided (open) boundaries are attributed to shadowing, especially prominent when a significant oblique component is present. Shadowing occurs because of high points from surface irregularities or roughness and/or from preferential nucleation sites due to substrate inhomogeneities [Thornton 1977]. The voided boundaries present in zone I tend to disappear in the transition zone. The increase in diffusion rate due to the increase in temperature overcomes the effect of surface roughness and inhomogeneities of the substrate. An increase in surface roughness results in shifting the zone I boundary to higher temperatures. Since oblique deposition angles and surface irregularities favor the formation of zone I structures, it is difficult to achieve uniform dense microstructures in coatings deposited over complex-shaped substrates by vacuum deposition at moderate values of T/T_m.

Intense ion bombardment of the substrate was shown to suppress the development of the open zone I structure. Instead, structures that are similar to that of zone II were developed. This was

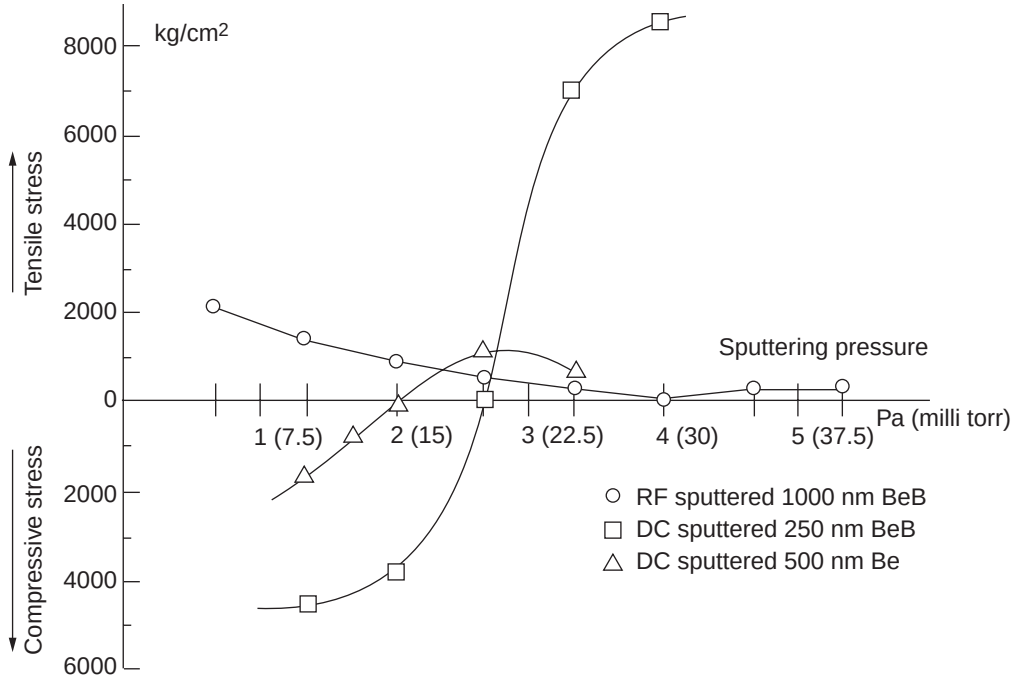

Fig. 22.22 Effect of sputtering pressure on residual stresses in beryllium and beryllium boride (BeB) sputter-deposited films. RF, radio frequency; DC, direct current. Source: Hseieh 1988

attributed to some back sputtering and redeposition of the coating, thus redistributing material into the voids [Thornton 1977]. Elevated gas pressures at low T/T_m cause grain boundaries to become more open and thus require increased substrate temperatures to obtain satisfactory structures. The influence of the inert gas disappears at the higher temperatures, which is attributed to a decrease in adsorption of the gas [Thornton 1977]. The transition of zone I to zone II occurs at $T/T_m \approx 0.3$. Recrystallized equiaxed zone III structures require temperatures of $T/T_m > 0.5$. If zone I-type structures persist to high T/T_m, the recrystallization will be limited to within the deposited grains because of the relatively open boundaries. Periodic doping with nitrogen combined with bias sputtering breaks up columnar growth and increases the tensile strength of the deposit [Hseieh 1988]. In sputtering deposition, bias sputtering can be used (by placing either an rf or dc voltage onto the substrate) to increase the ion bombardment on the substrate, to control the growth morphology, and to break up the columnar growth.

At the substrate, the deposition process is controlled primarily by surface diffusion, which depends on temperature. At sufficiently low substrate temperatures, where the atomic mobility is negligible, atoms come to rest at or near their point of impingement. An amorphous structure, or even a high-temperature phase or one similar to it, may be quenched in. With increasing substrate temperature, the tendency toward phase equilibrium and homgenization as well as annealing processes such as stress relaxation, recovery, grain growth, and/or recrystallization may occur. At the higher temperatures, these processes are controlled mainly by bulk and grain-boundary diffusion. A low-temperature deposit followed by a high-temperature anneal may be more effective in obtaining a particular particle/grain size and a desired distribution [Thornton 1977].

As pointed out earlier, either tensile or compressive stresses can be obtained by varying the sputtering gas pressure. An example of the dependence of stress on gas pressure is shown for beryllium and BeB films in Fig. 22.22 [Hseieh 1988]. Laser interferometry can be used to measure fringes on a film, from which one can calculate the stresses [Hseieh 1988]. Sputter deposition can produce films with the required internal stresses and surface smoothness at the same time. In studying the effect of residual stress of aluminum on beryllium, it was observed that the deposits with compressive stresses had the least

damage and greatest hardness. Thermally induced tensile stresses can arise on cooling from the deposition temperature due to mismatch between the deposit and the substrate. Thermal stresses can approach to near the tensile strength of the bulk beryllium [Hseieh 1988].

Failures of beryllium films were observed to be mainly by crazing (the formation of a network of fine cracks similar in appearance to those frequently seen on the glazed surface of pottery), as a result of thermal stresses caused by difference in the thermal expansion between the film and glass substrate [Hseieh et al. 1990]. The beryllium films were deposited by dc magnetron sputtering in 1.5 Pa (12 mtorr) of argon at a deposition rate of 1μm/h using an rf bias of 30 W. Columnar structure of the beryllium films deposited under normal conditions is inherently detrimental to the tensile strength of the films and may be responsible for failures when films are subjected to tensile stresses in service. Columnar growth was suppressed by incorporating nitrogen pulses of 100 ms duration at 2.5 to 10 min intervals. The interruption of columnar growth was attributed to the formation of a compound with the reactive gas. Ion bombardment tended to modify the preferential columnar growth by resputtering the deposited atoms and introducing new nucleation sites for new grain growth. The nitrogen pulsing was found to be more effective than the substrate-bias approach in modifying the grain structure. The nitrogen pulsing introduced contaminants of up to over 2% (mainly nitrogen and oxygen) at the greater pulse intervals. The pulse duration should be just long enough to supply sufficient reactive gas to form a compound layer in the growing film but not too long to introduce excessive contaminants in the resultant film. Thus, the minimum pulse frequency (largest interval) and pulse duration that provides sufficient grain refinement should be used [Hseieh et al. 1990, Price and Norberg 1989].

Attempts to sputter beryllium on large samples have been unsuccessful due to the continual appearance of porosity on successive polishing [Roybal et al. 1997]. This was believed to be inherent in films deposited on large samples, and, in the case of mirrors, it could result in excessive scattering of light. By first depositing a thin layer of electroless nickel onto the mirror, a smoother beryllium surface with less scattering could be obtained. To minimize any distortion that could occur by the mismatch in the coefficient of thermal expansion (CTE) between nickel and beryllium, both sides of the mirror should be plated with nickel of equal thickness. The nickel plating must be as thin as possible and symmetrical about the neutral mechanical axis. Addition of phosphorus, which reduces the CTE mismatch, can help to lessen the problem. Contaminants in the plating bath must be avoided, and, if improperly prepared, the nickel may peel off from the mirror. The largest precision optical component manufactured from beryllium (reported in 1997) is the 1.1 m Very Large Telescope secondary mirror. It is a nickel-plated mirror made from hot isostatic pressed I-220 Be. It had a surface roughness of λ/30 rms. The authors presented an overview on the status of beryllium as a substrate material for the manufacture of precision-reflective optical components with low-scattering optical surfaces [Roybal et al. 1997]. Various methods for measuring surface roughness and the resulting optical properties were described.

22.4 Ion Plating

Ion plating uses concurrent or periodic energetic bombardment of the depositing film by atom-sized energetic particles to modify and control the composition and properties of the depositing film [Mattox 1998]. The source of the material to be deposited can be evaporation, sputtering, arc erosion, laser ablation, or other evaporation sources. The energetic particles used for bombardment are usually ions of an inert or reactive gas. For every atom in a vapor cloud, there is a finite probability that it will ionize [Hill 1986]. The magnitude of this probability is a function of the ionization potential and temperature. In a dilute vapor phase, it is possible to deviate substantially from thermal and electronic equilibrium because the atoms are so far apart. This is usually the prevailing condition between source and substrate during physical vapor deposition. If ions are formed in this region, they have an excellent chance of reaching the substrate as ions. If the substrate is electrically biased, these ionized atoms are accelerated to the substrate, with improvements in properties of the deposits.

The most common form of ion plating is a plasma-based process where the substrate and/or its fixture is an electrode (cathode) used to generate a dc or rf plasma in contact with the surface being coated [Mattox 1998]. The plasma can be formed by ionization of an inert gas

when an elemental or alloy material is being deposited. Using argon, the energy of the bombarding ions should be greater than 50 eV and less than 300 eV to effectively modify the film properties. For lower ion energies, momentum transfer is insufficient to displace the film atoms. For higher ion energies, the bombarding species will be incorporated into the film unless the substrate temperature is high. In reactive ion plating, the plasma provides ions of reactive species, such as nitrogen, oxygen, or carbon, that are accelerated to the surface to form the desired compounds (nitrides, oxides, carbides, etc.).

A suitable vacuum system that had been proposed (1986) for high-pressure, nonmolecular flow in coatings and ion plating operations is schematically depicted in Fig. 22.23. It consists of a 50 kW, 10 kV, 270° magnetically deflected electron beam source evaporating from a 50 mm diameter rod-fed crucible [Hill 1986]. The vacuum system is separated into two volumes by a diaphragm, so that all pumping is in the lower chamber. This allows maintaining the pressure adjacent to the source at 2 orders of magnitude lower than in the coating chamber and permits deposition under pressures as high as 60 mtorr. Samples are loaded into the coating zone through a lock load and are mounted on a water-cooled shaft that can be operated at any voltage up to 5 kV negative. This negative-biased voltage could be maintained by a series-regulated, high-voltage supply that can deliver up to 1.4 A at any potential from 0 to 5000 V with 2% regulation. The temperature of the deposit during coating would be a balance between ion, radiant, and latent heat-energy input and radiant losses.

Concurrent or periodic particle bombardment during film growth modifies the film properties by affecting the nucleation of the depositing atoms, densifying the film by compaction or atomic peening, by introducing significant thermal energy directly into the substrate-surface region, and by sputtering and redeposition of the film material. Concurrent bombardment during film growth beneficially affects film properties, such as the film-substrate adhesion, density, surface cleanliness, porosity, surface coverage, residual film stress, index of refraction, and electrical resistivity.

The energetic particles can also come from the depositing source material, such as in plasma spraying or sputtering, by placing a negative bias on the substrate, thereby accelerating the positive metallic ions. In a vacuum (evaporation) environment, ions for bombardment are formed in a separate ion gun. Ion sources from plasma-based and vacuum-based systems are shown schematically in Fig. 22.24.

In plasma-based ion plating, the purpose is to produce a good-quality interface between deposit and substrate by the intermixing of the two

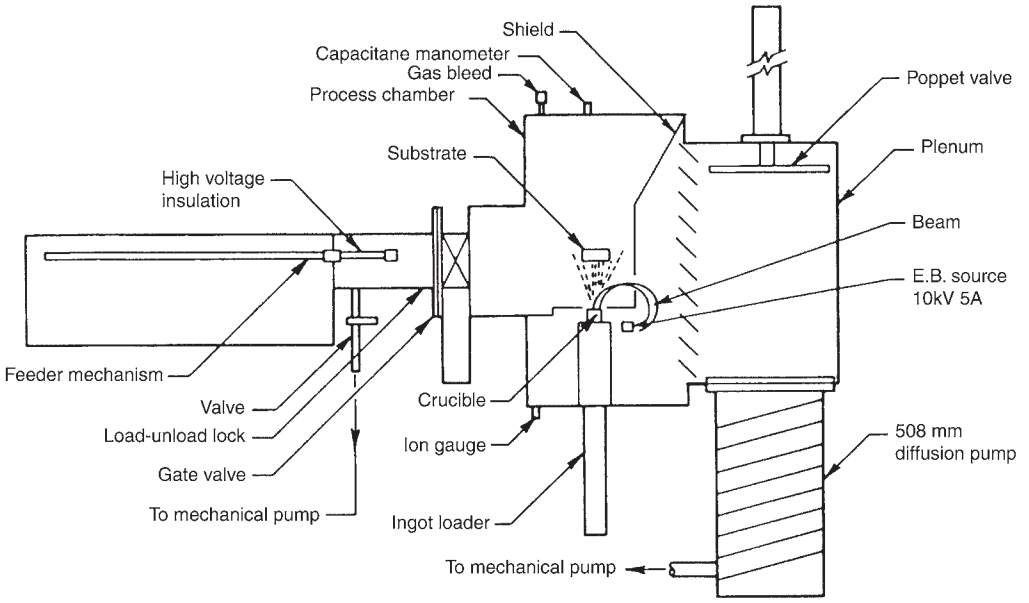

Fig. 22.23 Schematic of a rod-fed ion-plating system. EB, electron beam. Source: Hill 1986

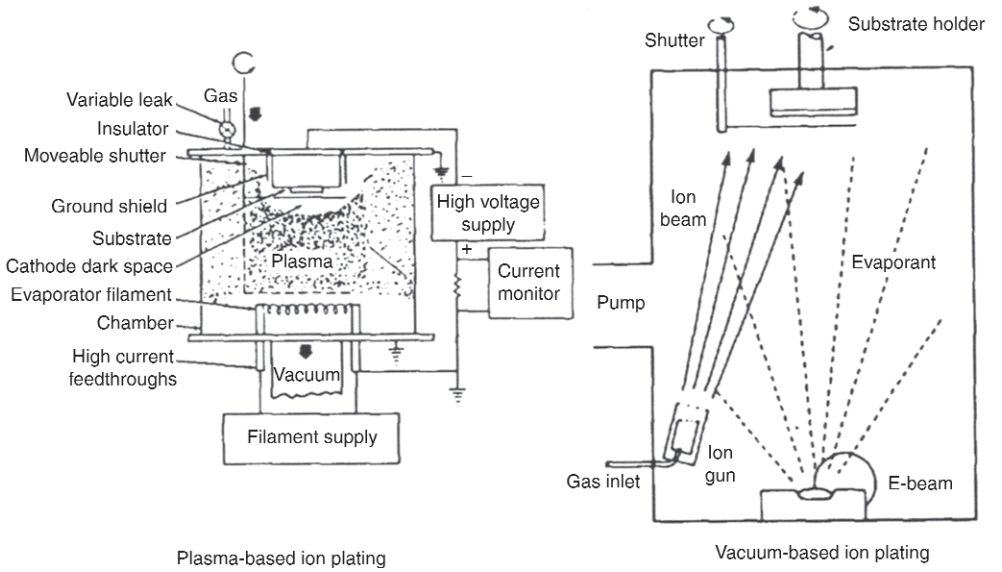

Fig. 22.24 Schematic illustrations of plasma-based ion plating, where the substrate fixture is the cathode of the direct current circuit, and vacuum-based ion plating using ion-beam-assisted deposition, frequently referred to as IBAD. Source: Mattox 1998

materials. The bias is frequently removed when a reliable interface is formed. If the bias is kept on continuously during deposition, the deposit may become porous due to micromelts occurring at the surface as a result of the excess energy transferred from the bombarding ions [Beat 2005]. In vacuum-based ion plating, the purpose of the ion bombardment is to continually massage the surface coating, resulting in enhanced surface mobility (diffusion) and reduction of stress. Considerable lower energies are introduced in vacuum-based ion plating than in plasma-based ion plating (current densities of approximately 0.01 W/cm^2 compared to 0.25 W/cm^2) [Beat 2005].

When resistance heating is used for vapor generation, relatively few ions are generated. By contrast, when using an electron beam as the heating source, deviation from the equilibrium population of ions can be achieved by the creation of ion-electron pairs resulting from the collision between the vapor atoms and the high-energy electrons of the primary beam. An additional, more powerful source of ions is from the collision of the atoms with the secondary electrons that are generated when the primary electrons strike the target. Depending on the operational parameters and on the magnetic field configuration, a high population of ions can be generated in the vapor cloud. If the substrate is biased, an electric field is developed between source and substrate that can further augment the production of ions. When these ions are accelerated by the substrate, their high-energy impact contributes substantially to the deposit adhesion. If either an inert or reactive gas is introduced and the voltage gradient is adequate, a plasma will be generated. This can substantially augment the population of ions, including both evaporant ions and ions of the introduced gas [Hill 1986]. One of the most important advantages of ion plating is its ability to produce adherent coatings. Using an elevated bias power at startup will generate an initial interface mixing of deposit and substrate materials and lead to improved substrate adherence.

Advantages of ion plating are:

- Significant energy is introduced into the surface of the depositing film by the energetic particle bombardment. The high-energy impact can contribute significantly to the adhesion of the deposit.
- Surface coverage can be improved over vacuum evaporation and sputter deposition due to gas scattering and sputtering/redeposition effects.
- Controlled bombardment can be used to modify film properties such as adhesion, film density, residual film stress, optical properties, and so on.
- Film properties are less dependent on the angle of incidence of the flux of depositing material than with the sputter deposition and

vacuum evaporation, due to gas scattering and sputtering/redeposition and atomic peening. (Peening refers to bombarding or impacting a surface with atoms, hard particles, laser beam, and so on, a surface in order to improve/impart certain properties to the surface.)

- Reactive ion plating can use the plasma to activate reactive species and create new chemical species that are more readily adsorbed, to aid in the reactive deposition process.
- For reactive-ion plating, bombardment can be used to improve the chemical composition of the film material by bombardment-enhanced chemical reactions (increased reaction probability) and the sputtering of unreacted species from the growing surface.
- The high-energy ionized atoms can also clean the surface of the substrate of any foreign atoms that may otherwise inhibit adhesion.

Disadvantages of ion plating are:

- It is often difficult to obtain uniform ion bombardment over the substrate surface, leading to film-property variations over the surface.
- Substrate heating can be excessive.
- Under some conditions, the bombarding gas may be incorporated into the growing film.
- Under some conditions, excessive residual compressive film stress can be generated by the bombardment.
- For plasma-based ion plating, the system pumping speed is limited, which can result in an increase in the film contamination problem.

22.5 Plasma Arc Spraying

A plasma is a hot ionized gas. Plasma (arc) spraying is a process in which the source powder is injected into a plasma jet stream that is produced by a low-voltage, high-current electrical discharge. The plasma stream heats the powder to near or above its melting temperature and accelerates it toward the substrate (workpiece) along a line of site from the plasma torch. A schematic diagram showing the essential elements of the process is illustrated in Fig. 22.25 [Tucker 1982]. As a gas is introduced between the cathode (usually tungsten) and anode (usually copper) electrodes, an arc is generated between the two electrodes to produce a plasma. The arc, which is initiated with a high-frequency discharge, is formed by a direct current and is continuously maintained. The power used varies from approximately 5 to 80 kW, depending on system design, type of torch, and operating parameters. The hot plasma consists of free electrons, ionized atoms, and some neutral atoms as well as undissociated diatomic molecules if nitrogen or hydrogen is used. The presence of undissociated diatomic molecules increases the enthalpy of the plasma, which will increase the heat transfer from the plasma to the powder. The gas injected into the torch to be ionized is usually argon or nitrogen or a mixture of these with hydrogen or helium [Tucker 1982].

Because of its toxicity, beryllium spraying needs to be conducted in a glove-box system, working in an argon atmosphere to minimize oxidation. For example, with a source powder containing 0.9 wt% BeO, spraying unprotected in air gave 1.5 to 2.5 wt% BeO compared to 1.2 to 2.0 wt% BeO obtained using an argon cover.

The electric power of the arc device varies widely, depending on the point of power injection. Downstream injection, external to the torch, makes for simple design and operation but inefficient heating. Deposition efficiency (deposit mass/sprayed mass) rarely exceeds 50% and is dependent on process parameters and the as-sprayed porosity required. There is no limit to the thickness of the sprayed part. The process is most cost-effective for thin parts where significant amounts of machining would otherwise be required. A constant or variable profile thickness with uniform texture can be built up on a substrate using a computerized program. Depending on the substrate material,

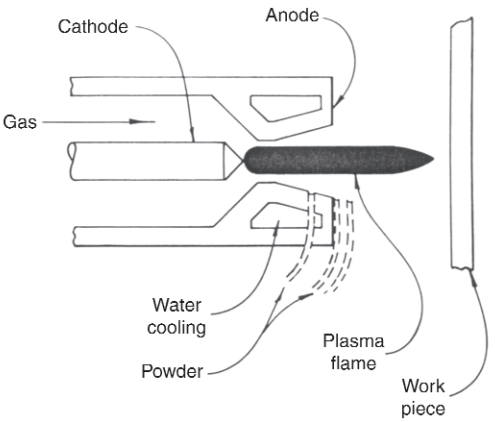

Fig. 22.25 Schematic illustration of a plasma-coating torch showing alternative powder-inlet positions. Source: Tucker, 1982

the deposit can then be removed by either machining, peeling, or chemical dissolution of the substrate.

In a study to develop a system for plasma-spray fabrication of thin-walled, free-standing structures, an acceptable beryllium powder size range was found to be −270 to +400 mesh (53 to 36 μm). Using argon for both the arc and powder-carrying gas systems, deposition efficiencies of approximately 50% were consistently obtained with an arc current of 30 V, an arc-gas flow rate of 1 standard m^3/h, and a stand-off distance of 10 cm (4 in.) between plasma gun and substrate [Northecutt and Hovis 1988].

Powders that are too small, less than approximately 10 μm, may cause blockage and subsequent buildup of crust in the torch nozzle and may be ejected and incorporated in the deposit. The upper particle size is limited by the ability of the system to transfer sufficient heat to the powder. Conduction is more likely to predominate if the powder is injected into the vicinity of the arc, which also increases the efficiency of the system. Generally, the further upstream the injection is, the more efficient is the heating. To maintain a smooth operation, however, more care is needed in the design of the system [Dunmur 1979]. Powder must be kept dry; moisture can be eliminated by incorporating a heater with the powder dispenser. Reduced pressures can substantially increase the as-deposited densities. At pressures less than 53 kPa (400 torr), as-deposited densities greater than 98% of theoretical density can be obtained. High particle velocities are attainable, which result in better impacting and splatting, especially of the liquid particles. (Splatting refers to the lateral spreading of the molten or near-molten material on impacting the substrate, the degree depending on the impact force.)

Plasma spraying offers a number of advantages. Large, thin-walled bodies requiring a minimum of machining can be made. The process provides the ability to introduce variations in wall thickness for stiffening or to reduce weight in less-stressed regions. The process eliminates the need for heavy tooling and gastight encapsulating, as required for isopressing. Plasma-sprayed structures may be readily repaired by plasma spraying. High deposition rates, of approximately 6 mm/h (0.2 in./min), can be achieved.

The many processing variables that can influence the properties and quality of the plasma-sprayed deposit are listed in Fig. 22.26 [Castro et al. 1995]. A set of operating parameters used for plasma-spraying studies of beryllium at the Los Alamos National Laboratory (LANL) is shown in Table 22.4. The LANL system uses a commercial SG-100 Plasmadyne torch mounted inside a vacuum chamber and located over a

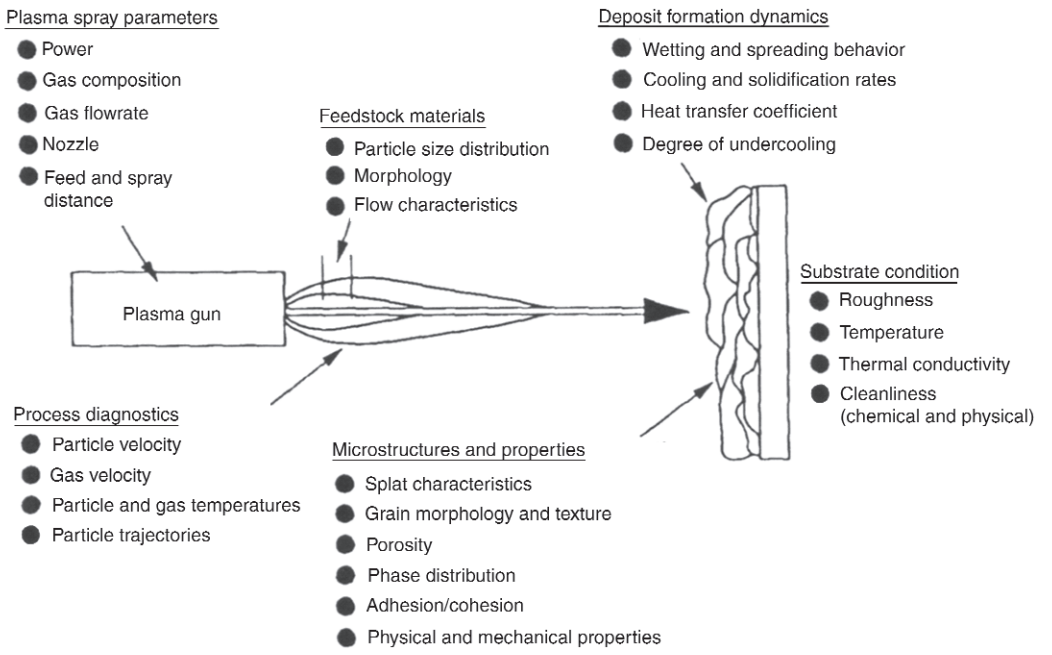

Fig. 22.26 Processing variables that can influence the quality of plasma-sprayed coatings. Source: Castro et al. 1995

Table 22.4 Operating parameters for plasma spraying of beryllium

Parameters	Settings
Current, A	800
Voltage, V	36
Primary gas (Ar), l/m	40
Secondary gas (He), l/m	10
Powder carrier (Ar), L/m	2.5
Chamber pressure, Pa	450
Powder feed rate, g/min	3.78
Spray distance, mm	7.6
Substrate translation, in./min	39
Anode/cathode	730/129
Gas injector	112

Source: Castro et al. 1995

translating copper-cooled substrate. An MKS 147 multigas flow controller served to regulate the processing gases used for spraying beryllium powders. The powder feed rate was controlled by a Masstron 200 unit. The powder was dispensed into the plasma torch using the Plasmadyne 1000 A powder feeder integrated with a weight scale.

Plasma spraying involves the successive buildup of deposited layers of hot and/or molten particles, which deform on impact with a substrate. The degree of deformation depends on temperature and velocity of the particles. The particles deform preferentially in directions normal to the impact direction, which is frequently referred to as splatting. There appears to be little or no metallurgical bonding. Particles are largely held in place by mechanical keying [Dunmur et al. 1977]. Some of the particles may have solidified prior to impact. If their temperature falls below 1250 °C, the body-centered cubic to hexagonal close-packed transformation point, the deformation on splatting will occur by basal slip, with the slip plane rotating toward the surface plane of the deposit, thus developing a preferred orientation. A columnar structure is frequently obtained. The apparent continuity of orientation between splatted particles is due to epitaxial seeding of the arriving molten particle impinging on the solidified particle. (Epitaxial seeding refers to a crystalline orientation of the crystalline material, or substrate, to nucleate, or seed, and grow into the crystalline material being deposited on it, such that substrate and deposit have the same crystalline orientation relative to a given axis and plane.) The degree of texturing may be affected by the standoff distance, since larger distances increase the chance of solidification prior to impact. More forceful impacts (higher plasma-jet velocities) will result in increased texturing. Dwell time in the

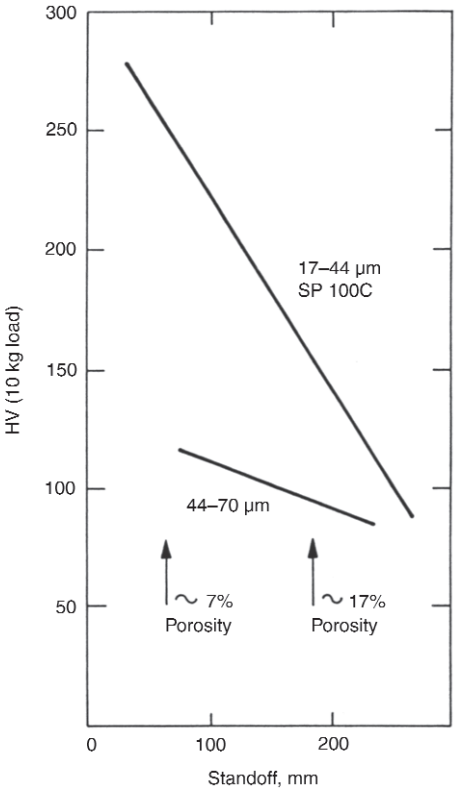

Fig. 22.27 Effect of torch standoff distance for a Metco torch on the microhardness of as-plasma-sprayed beryllium powder. Note that the porosity is lower at the smaller standoff distance. Source: Dunmur 1979

plasma (or flame in flame spraying), the electric arc power, and the chemical composition will also affect the microstructure [Dunmur 1979]. (Flame spraying is a spraying process in which fine powder is carried in a gas stream and is passed through an intense combustion flame, where it becomes molten. The gas stream, on expanding rapidly from the heating, sprays the molten powder onto the substrate.) The effects of standoff distance on hardness and tensile strength for a Brush Beryllium SP100C plasma-sprayed powder are shown in Fig. 22.27 and 22.28, respectively. The relatively high hardness of approximately 250 HV that is obtained at the smallest standoff distance (compared to approximately 180 HV for a fully dense beryllium) is attributed to the extensive deformation introduced by the corresponding severe splattering. The steep rise in tensile strength (ultimate tensile strength) is also attributed to the severe splattering [Dunmur 1979]. Note that the strength parallel to the spray (single value) is approximately one-fifth of that perpendicular to the spray.

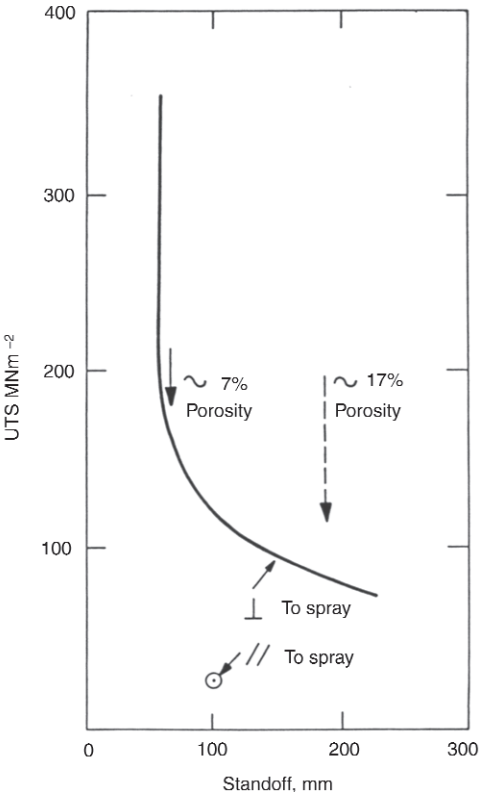

Fig. 22.28 Effect of torch standoff distance for a Metco torch on the ultimate tensile strength (UTS) of as-plasma-sprayed (17 to 44 μm) SP100C beryllium powder

The as-sprayed structure is inherently porous, with the porosity being largely interconnected. The quenched particles are held in place by conforming to the preexisting surface. Typical porosities of the order of 10 to 20% are obtained with relatively poor as-deposited mechanical properties, especially in the thickness direction of the deposit. Another illustration of the influence of the splatted structure is that the thermal conductivity of the as-sprayed beryllium can be approximately $^{1}/_{10}$ of that of the dense beryllium [Dunmur et al. 1977]. The nature of the layered, splattered structure and the cohesion between layers of sprayed beryllium deposits were shown to contribute to differences in the CTE, thermal diffusivity, flexture strength, and fracture toughness of different deposits. Differences in properties were also obtained between directions parallel and normal to the spray direction [Castro et al. 1998]. The CTEs of the deposits were found to be similar to those of S65B beryllium from room temperature to approximately 400 °C (750 °F). Above 400 °C (750 °F), the CTE of the deposit normal to the spray direction continuously decreased, while it still increased for the solid beryllium and the deposit parallel to the spray direction, although the latter increased at a slower rate (Fig. 22.29) [Castro et al. 1998]. This was attributed to the interaction between contiguous splat layers. At the elevated

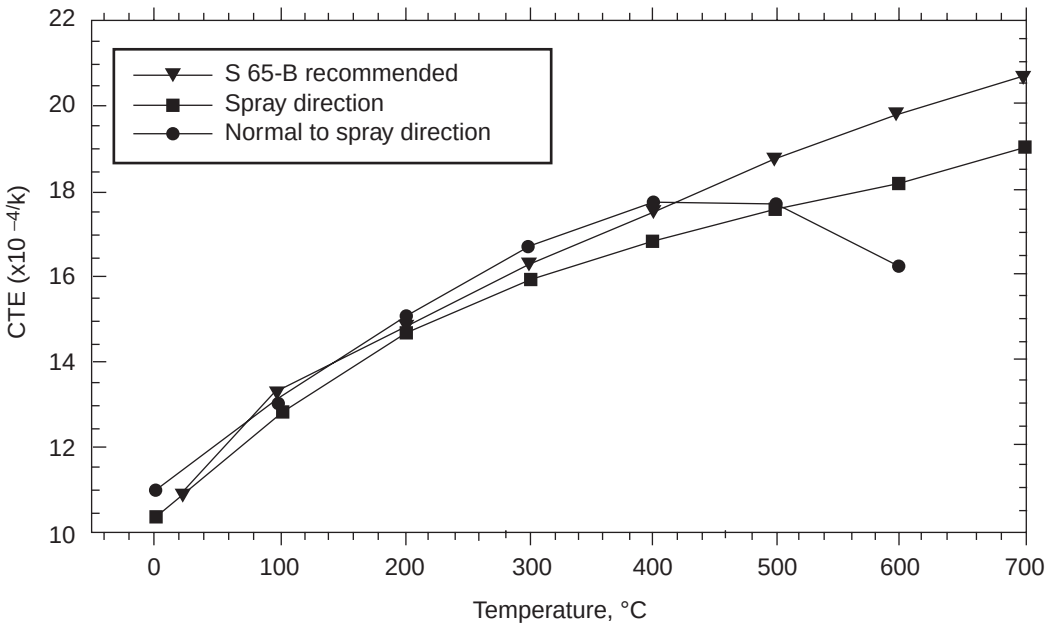

Fig. 22.29 Coefficient of thermal expansion (CTE) of plasma-sprayed beryllium deposited parallel and normal to the spray direction. Source: Castro et al. 1998

Table 22.5 Properties of plasma-sprayed-and-sintered beryllium compared to isostatically pressed beryllium

	*E**(b)		Yield strength, 0.2%		Ultimate tensile strength		Elongation, %	
Material(a)	GPa	ksi	MPa	ksi	MPa	ksi	Uniaxial	Biaxial
PSS P10	200	29,000	325	47	450	65	5.0	3.0
HIP-50 (HT)	205	29,700	340	49	500	73	4.5	2.1
CIP-HIP P1	100	14,500	270	39	440	64	. . .	. . .

(a) PSS, plasma sprayed and sintered; HIP, hot isostatic pressed; HT, heat treated; CIP, cold isostatic pressed. (b) *E**, tangent modulus. Source: Dunmur et al. 1977

temperature, some densification occurred. For many purposes, the as-sprayed beryllium is too weak, lacks ductility, and must be sintered. (Sintering refers to the heating of a material to a high temperature, sometimes under pressure, to decrease or eliminate porosity and increase density. Generally, the melting points of low-melting constituents at the grain boundaries are exceeded and the corresponding melting contributes to the elimination of pores and to the bonding between contiguous grains.) Dimensional changes due to sintering shrinkage must be taken into account, and internal or external forms may have to be used to control the final shape.

The as-sprayed deposit may subsequently be sintered at an elevated temperature, thereby approaching close to theoretical density with greatly improved mechanical properties. After sintering, the strength, tangent modulus, and ductility are comparable with the best hot isostatically pressed beryllium. Table 22.5 compares the mechanical properties of a plasma-sprayed-and-sintered deposit from a medium-purity beryllium powder with those of a cold and hot isostatically pressed (CIP-HIP) high-purity beryllium and a HIP product produced from an experimental powder (HIP-50) [Dunmur et al. 1977]. Another source reported achieving a yield strength of 410 MPa (59 ksi), an ultimate strength of 460 MPa (67 ksi), and an elongation of 2.3% for a sintered, plasma-sprayed deposit having a density of 99% [Dunmur et al. 1977].

The relative increase in density as a function of sintering temperature for different starting densities of several types of beryllium is shown in Fig. 22.30 [Dunmur 1979]. The time at temperature and the heating rate were not given. The densification has been normalized in terms of the relative decrease in porosity, namely, as $(P_{AS} - P_{HT})/P_{AS}$, where P_{AS} and P_{HT} refer to as-sprayed and as-heat-treated porosities, respectively. As can be seen, an increase in porosity requires an increase in sintering temperature. The powder composition will also affect the sintering requirements. The compositions of the

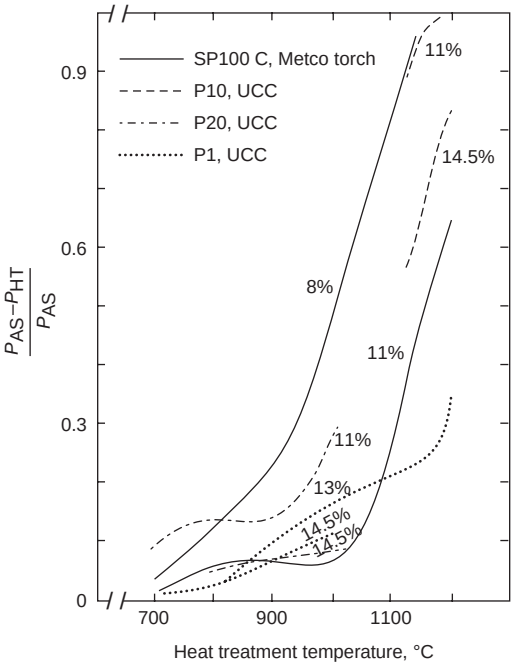

Fig. 22.30 Densification curves for various berylliums having different as-sprayed porosities. As-sprayed porosities are indicated. Source: Dunmur 1979

powders used for Fig. 22.30 are listed in Table 22.6. Referring to Fig. 22.30 and Table 22.6, it can be seen that the high-purity beryllium (dotted curve, P1) is difficult to densify at 1200 °C (2190 °F) and even at 1250 °C (2280 °F).

The achievement of nearly full density is assisted by having a high quenched-in lattice-strain energy, caused by heavy splattering, and by the presence of impurities such as silicon, which is believed to create a defect structure in the BeO surface coating, thereby enhancing the diffusion of beryllium. With evidence of silicon enhancing the sintering process, silicon additions varying between 0.1 and 0.5 wt% and in the size range of 4 to 30 μm were blended with beryllium powder particles in the size range of 36 to 53 μm. This resulted in having silicon in the form of small, discrete particles uniformly

Table 22.6 Beryllium analyses

Element(a)	P1(b)	P10(b)	P20(b)	SP100C(c)
Be	99.0	98.5	98.0	98.5
BeO	0.8	1.0	2.0	1.3
Al	100	800	1500	600–1000
C	300	1000	1500	120
Cr	25	. . .	. . .	80
Co	5	. . .	. . .	. . .
Cu	300	. . .	. . .	150
Fe	300	1500	1800	1300
Pb	5	. . .	. . .	. . .
Mg	60	800	800	40–100
Mo	30	. . .	. . .	60
Mn	10	. . .	. . .	10
Ni	200	. . .	. . .	300
Si	100	800	800	300
Others	. . .	400	400	. . .

(a) Be and BeO are in weight percent. (b) P1, P10, and P20 were produced by Berylco. (c) SP100C was produced by Brush Wellman. Source: Dunmur 1979

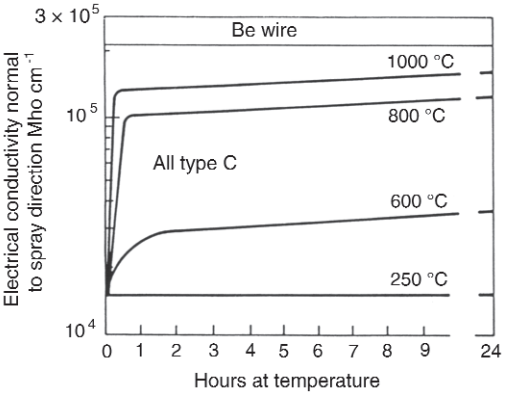

Fig. 22.31 Effect of sintering temperature on electrical conductivity of plasma-sprayed beryllium. Source: Dunmur 1979

dispersed within the sprayed structure. A negligible change in composition occurred. At least 0.3% Si was required to obtain consistently high-density parts after sintering. The sprayed material varied between 15 and 25 vol% porosity [Northcutt and Hovis 1988]. The as-sprayed porosities of four samples and those after sintering for 1 h at 1200 °C (2190 °F) were 14.05 and 0.33%, 15.87 and 0.07%, 19.44 and 1.24%, and 21.27 and 1.82%, respectively. As-sprayed porosities above approximately 20% resulted in poor sintered densities. In order to remove any volatiles from the as-sprayed condition, the samples were vacuum outgassed by heating up to 700 °C (1290 °F). To minimize loss of beryllium, argon was introduced to raise the pressure to approximately 17 kPa (125 torr) as the temperature continued to rise to 1200 °C (2190 °F).

The more heavily splattered deposits with impurities densify at lower temperatures. High-purity (low-silicon) beryllium deposits are difficult to bring to full density below the melting point. High sintering temperatures result in grain growth, nonuniform shrinkage, and significant evaporation of beryllium. A compromise between high-purity powder and less pure commercial-grade powder yields a sintered product with properties superior to those obtained from either powder. It is best to spray to the highest density (lowest porosity) and to optimize the purity content so as to minimize the sintering temperature.

The temperature at which densification started depends strongly on the as-sprayed density; for example, densification started at 650 °C (1200 °F) for 12% porosity and at 1000 °C (1830 °F) for 20% porosity. Because of the steepness of the densification curves (Fig. 22.30), very uniform heating of large bodies is required to prevent buckling by uneven shrinkage. In general, strengthening starts at a sintering temperature of approximately 800 °C (1970 °F) with an elongation of approximately 0.05%, and useful properties are achieved only on heating above 1000 °C (1830 °F) [Dunmur 1979].

Figure 22.31 shows the conductivity as a function of time at temperature [Dunmur 1979]. Two stages can be seen at the higher temperatures: a rapid initial rise followed by a slow, further increase with time. The rapid increase in conductivity is attributed to the growth of contact areas; the subsequent slow increase is attributed to pore reduction.

The use of laser processing to consolidate porous, thermal-sprayed beryllium deposits is a feasible option for in situ repairs [O'Dell et al. 1998]. Focused, localized melting of a damaged area permits consolidation with minimal shrinkage. Through local melting and quenching, a fine, recrystallized microstructure without voids was obtained, resulting in greatly enhanced physical, mechanical, and conductivity properties. Densities of over 99% were obtained. The penetration depth increased with the beam-energy density (energy/spot size) per pulse and with increased laser power. Shrinkage during solidification and cooling of the laser-treated material may cause it to pull away from the surrounding material and develop cracks normal to the surface [O'Dell et al. 1998]. The power and energy densities ranged from 49 to 614 W/mm^2 and 1 to 26 J/mm^2, respectively, using CO_2 and neodymium: yttrium-aluminum-garnet lasers. Maximum penetrations obtained were 1.2 and 1.6 mm, respectively, for the two lasers. The pulse rates were 10 to 200 Hz, and the spot sizes were 0.586 to 1.533 mm^2.

Studies are currently being conducted on developing methods to increase the density of plasma-sprayed deposits [Beat 2005]. The relatively high deposition rates and coverage of large surfaces compared to that obtained with other deposition methods are the main advantages in the use of plasma spraying. Of the physical vapor deposition methods, probably thermal evaporation comes closest to plasma spraying. Disadvantages of plasma spraying (PS) compared to thermal (vacuum) evaporation (TE) are given as [Anisimov et al. 1997]:

- The moderate rate of growth by atomic layers in the TE method allows for a more qualitatively dense and highly conductive coating compared to the PS droplet-spray method.
- Sticking efficiency of deposited material for TE is almost 100% compared to 50 to 80% for PS.
- The source beryllium can be much cheaper for TE than for PS. (Plasma spraying requires the use of spherical powders, whereas TE can use beryllium scrap, with appropriate composition.)
- Plasma spraying, which requires an electrical arc, cannot be used in a strong magnetic field.
- Dense, porosity-free PS deposits require further high-temperature heat treatment.

22.6 Chemical Vapor Deposition

Chemical vapor deposition (CVD) is a process where a volatile material (the precursor) is transported in the vapor phase, through a vacuum or by a carrier gas, to a heated surface (substrate) in the reactor chamber. Here, the precursor vapor decomposes or is reduced, the reaction leading to the deposition of a solid film. The volatile byproducts from the reaction and the excess carrier gas are exhausted from the chamber. The deposition species are atoms or molecules or a combination of these. Depending on the material to be deposited, various species are available as the gaseous precursor: fluorides, chlorides, bromides, iodides, hydrides, organometallics, hydrocarbons, phosphorus trifluoride complexes, and ammonia complexes [Blocher 1982a]. A few deposition reactions occur at substrate temperatures below 200 °C (390 °F). Most reactions, however, require temperatures above 800 °C (1470 °F). A schematic diagram of a typical CVD system is shown in Fig. 22.32. There are many variations of the apparatus, depending on the type of reactor and the application [Pierson 1999, ASM 2002].

Plasma-assisted chemical vapor deposition (PACVD) may be used where properties of the substrate and compatibility between deposit and substrate may be adversely affected by high temperatures. With PACVD, an electrical discharge is maintained in the gas phase adjacent to the substrate. Activated and ionic components in the discharge initiate the necessary chemical reactions in the gas, and deposition occurs at lower temperatures than would otherwise be required. Deposits at low substrate temperatures, typically below 300 °C (570 °F), are achieved. The PACVD method, which has a low deposition rate measured in angstroms per minute, is limited to thin films (<1 μm thick). The deposition rate in conventional CVD, which uses the heated target to initiate the reaction, is measured in micrometers per minute [Blocher 1982b].

Depending on the plating parameters, columnar grains with preferred crystallographic orientations relative to the substrate surface, similar to their occurrence in deposits formed by thermal evaporation and sputtering, are obtained in many materials. Decreasing substrate temperature or increasing supersaturation of the precursor (gas phase containing the depositing material) will influence the structure of the deposit according to the following sequence:

Epitaxial growth → platelets → whiskers → dendrites → coarse polycrystals → fine polycrystals → amorphous deposits [Blocher 1982a]

Refinement of the microstructure can be obtained by working the surface during deposition. This was first demonstrated by continuously rubbing the surface while depositing a

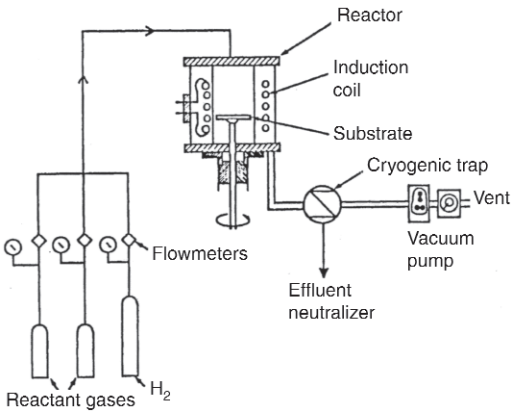

Fig. 22.32 Schematic illustration of a typical chemical vapor deposition system. Source: Pierson 1999

tungsten-rhenium alloy on the substrate [Holman and Huegel 1967].

The advantages of CVD are [Pierson 1999]:

- Deposition of refractory materials at temperatures far below their melting points or sintering temperatures
- Near-theoretical or controlled density of deposit
- Preferred grain/crystallographic orientation possible
- Controlled grain size of deposit
- Epitaxial grain growth possible
- Deposition is quite uniform, making CVD the best method for depositing in holes and recessed areas and other difficult three-dimensional configurations.
- Processing at atmospheric pressure possible
- With its high deposition rates, thick coatings (centimeters thick) are readily attainable.
- Changes in composition during deposition and the co-deposition of elements or compounds are readily attainable.
- Generally good adhesion

Limitations of CVD are [Pierson 1999]:

- High costs of some reactants
- Most reactants, as well as by-products, are corrosive, toxic, and/or moisture sensitive, necessitating a closed system.
- Scarcity of reactions available for low-temperature processing (<300 °C, or 570 °F)

Recent information on the use of CVD for beryllium is scarce. In an early review (1955) of numerous attempts at CVD of beryllium, it was concluded that "beryllium cannot be vapor deposited rapidly or efficiently by any known method" [Powell et al. 1955]. The main problems at that time appeared to be the very high temperatures (up to 1200 °C, or 2190 °F) required to efficiently decompose potential beryllium compounds and to eliminate any contamination of the deposit, especially by oxygen and/or carbon. In 1967, CVD of beryllium was attempted using the organometallic compound di-tert-butylberyllium as the precursor vapor [Wood and Frey 1967]. The study was sponsored by Lawrence Livermore National Laboratory. Decomposition of the vapor occurred at relatively low substrate temperatures. The best results were obtained at temperatures in the range of 280 to 305 °C (535 to 580 °F) at pressures of 133 Pa (1 torr) or less and using hydrogen as the carrier gas. Although the coatings were adherent, they were contaminated, primarily with carbon and hydrogen (97% Be). The coatings were described as "tiny scattered nodules, superficially smooth to the naked eye." The nodules became easily visible with thicknesses over 2.5 μm. A number of organometallic compounds and gas carriers were evaluated in this study.

The high (thermodynamic) affinity of beryllium for oxygen indicates the difficulty of avoiding oxygen contamination. By using organometallic compounds, it should be possible to eliminate oxygen contamination; however, carbon contamination due to the possible co-deposition of carbon with beryllium is still likely to occur. It appears that none of the elements in either group 1A or 2A (including beryllium) of the periodic table have been successfully deposited (uncontaminated) by CVD. A handbook (1999) on CVD devotes a chapter to elements that have been deposited by CVD "either on a production basis or experimentally," and beryllium is the only element of these two groups that is discussed [Pierson 1999]. In a more recent publication (2001), 80 elements were indicated on the periodic table that have been deposited by CVD, either as elements or in compounds. Some of these elements (including beryllium) are in groups 1A and 2A; no reference was made, however, that any of these elements were deposited in elemental form [ASM 2002]. (Elements in groups 1A and 2A listed as having been deposited using CVD are hydrogen, lithium, beryllium, magnesium, calcium, strontium, and barium.)

A recent attempt (2000) was made to coat beryllium on spherical capsules using CVD. Since this provides a non-line-of-site deposition, it should lead to the required uniform deposit on a spherical surface [Salazar 2005]. The precursor was $(C_5H_5)_2Be$, with argon gas as the carrier. The precursor reservoir was held at 35 °C (95 °F). A silicon substrate, heated to 150 °C (300 °F), was used. Although a continuous beryllium film was obtained, its macrostructure, microstructure, and impurities were unacceptable. The research was terminated. Problems were attributed to the extreme air sensitivity of beryllium, and the authors suggested that under a reducing atmosphere, $(C_5H_5)_2Be$ could still be a viable precursor candidate. A successful aluminum coating had been produced using $H_3Al:N(CH_3)_3$ as the precursor. The similarity of aluminum and beryllium in many of their chemical and electrochemical properties strongly suggested to the authors that using the analogous

$H_2Be:[N(CH_3)_3]_2$ complex as the precursor should produce "a very pure" beryllium coating. An attempt to verify this supposition was not made [Salazar 2005].

Good beryllium deposits were obtained by the following reaction for the pyrolysis of alkyls [Pierson 1999]:

$$(C_4H_9)_2Be \rightarrow Be + H_2 + 2C_4H_8 \qquad \text{(Eq 22.2)}$$

The deposition occurred within a temperature range of 280 to 305 °C (535 to 580 °F) under a pressure of less than 133 Pa (1 torr). This reaction, however, had a tendency to incorporate carbon in the deposit.

22.7 Electroplating (Electrodeposition)

The process of electroplating consists of transporting positively charged particles through an electrolyte bath from the source material to the object being plated. The electroplating system consists of four main components:

- Cathode, the negative electrode, which is the object that is to be plated. It is where positive ions are discharged and combine with electrons (plated).
- Anode, the positive electrode, where negative ions and electrons are discharged and positive ions (material to be plated) are created.
- Electrolyte, the conducting medium, where the current flow of positive ions is from anode to cathode. It usually consists of an aqueous solution such as an acid, base, or salt.
- Current source, a dc source that provides the external (negative) flow of electrons from anode to cathode and the (positive) current flow of ions in the bath from anode to cathode

In an early review (1963) on electroplating, when referring to the metals in group 2A, the authors stated that "it is doubtful that any of these strongly electronegative metals have been electrodeposited from aqueous solutions; however, they apparently have been deposited from nonaqueous baths" [Lowenheim 1963]. Deposits of beryllium from liquid ammonia and from organic compounds were reported; however, the presence of impurities made the deposits questionable. Questionable results on electrodeposits from beryllium salts in actimide and the unsuccessful attempts made with a series of anhydrous beryllium salts dissolved in alkylpyridinium or liquid ammonia were reported [Wood and Brenner 1957]. The claim for first electrodepositing beryllium from an organic solution was made in 1957 for a beryllium deposit of 95% purity [Wood and Brenner 1957]. More recent attempts at electroplating beryllium are described as follows.

Stating that it is impossible to electrodeposit beryllium from aqueous solutions, the electrodeposition from organic solutions was evaluated [Takei 1979]. A synthesized compound, $Be(CF_3COO)_2$, was used as the source for electrodeposition of beryllium onto a copper cathode plate, using platinum as the anode. Two different series of plating baths were investigated. One series consisted of $Be(CF_3COO)_2$ saturated in methyl hydroxide, with each bath containing a different additive, as given in Tables 22.7 and 22.8. The platings were performed at room temperature. The second series of baths consisted of $Be(CF_3COO)_2$ saturated in CF_3COOH-CH_3CN, using different current densities and/or bath temperatures. A constant amount of anhydrous Na_2SO_4 was added to all baths. The plating details are given in Tables 22.7 and 22.8.

The author concludes that a thin and uniform layer of beryllium can be "rather easily" electrodeposited with both types of baths. Thick layers were difficult to form. Smooth layers consisted of minute and irregular black or grayish-black particles. Uneven surfaces contained black blocks.

Numerous beneficial effects may be produced by the use of additives in electroplating solutions. The additives can be organic or metallic, ionic or nonionic. They are adsorbed on the plated surface and are usually incorporated in the deposit. The additives can be classified into four major categories: (1) grain refiners, (2) dendrite and roughness inhibitors, (3) wetting agents (surfactants), and (4) leveling agents. Surfactants

Table 22.7 Electrodeposition of beryllium in a MeOH bath with $Be(CF_3COO)_2$

Bath additive	Additive, mL/L	Current density, A/dm	Total electricity(a), C	Deposit color
...	...	0.38	120	Black
...	...	0.45	150	Black
...	...	0.68	200	Dark green
...	...	0.75	250	Green-black
CF_3COOH	0.6	0.68	250	Black
CF_3COOH	0.6	0.88	300	Black-brown
CF_3COOH	1.5	1.30	330	None
$NaClO_4$	0.3(b)	1.00	300	None
$(CF_3CO)_2O$	1.5	2.00	500	Gray

(a) C (coulomb) = 2.7772×10^{-4} amp hours. (b) Given in grams per liter. Source: Takei 1979

Table 22.8 Electrodeposition of beryllium in a CF_3COOH-CH_3CN bath saturated with $Be(CF_3COO)_2$

Bath additive	Additive amount, g/L	Current density, A/dm^2	Total electricity(a), C	Bath temperature,°C	Deposit color
Na_2SO_4	0.2	0.75	11	20	Black-gray
Na_2SO_4	0.2	0.50	100	25	Black
Na_2SO_4	0.2	0.75	17	25	Black
Na_2SO_4	0.2	0.50	18	30	Black
Na_2SO_4	0.2	0.50	17	40	Blue-black
Na_2SO_4	0.2	0.75	26	40	Dark gray
Na_2SO_4	0.2	1.00	30	40	Black
Na_2SO_4	0.2	0.50	50	40	Black
$(CF_3CO)_2O$	0.2(b)	...	...	...	Gray

(a) C (coulomb) = 2.7772×10^{-4} amp hours. (b) Given in grams per liter. Source: Takei 1979

are used primarily to prevent pits or pores by decreasing the surface tension of the surface deposit. Leveling agents are adsorbed preferentially on the peaks of a surface, inhibiting deposition. Otherwise, the peaks and valleys become more accentuated, because the current density is highest at the peaks since the electric fields are greatest in these areas. Potential benefits of additives include:

- Increase in surface brightness of the deposit
- Decrease in grain size
- Reduced tendency to treeing (formation of dendritic structure)
- Increased current density range
- Control of chemical and/or physical properties
- Promote surface uniformity (leveling)
- Reduce residual stresses
- Reduce pitting

An example procedure for preparing beryllium for plating was described by Nargi [1992]:

1. Soak clean
2. Cathodic clean
3. Cold water rinse
4. Desmut in nitric acid
5. Cold water rinse
6. Zincate (dilute type)
7. Cold water rinse
8. Plate

A cleaning and plating cycle recommended for beryllium was given as follows:

1. Clean
2. Anodic pickle in solution containing 10% by volume of phosphoric acid and 2% by volume of (38%) hydrochloric acid at 21 to 27 °C for 2 min
3. Do not rinse
4. Chemical pickle in concentrated nitric acid (70%) at 21 to 27 °C for 2 min and rinse

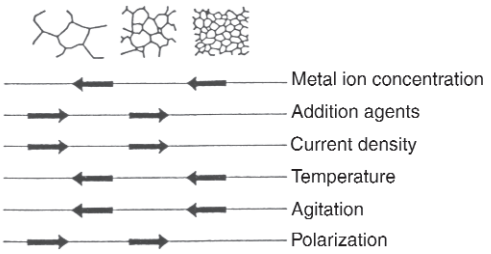

Fig. 22.33 Relationship of the microstructure of electrodeposits to the operating conditions of plating solutions. Source: Dini 1992

5. Plate in bath suitable for electrodeposition on active metals
6. Rinse and dry
7. Outgas if subsequent nickel plating will be done to avoid blistering when the plated metal is to be heated. Heating in an inert gas atmosphere for about 1 h at 500 °C is sufficient.

Electrodeposited material does not grow uniformly; rather, it becomes faceted, developing dendrites and other surface discontinuities. It can vary from relatively defect-free crystals to highly columnar and faceted structures. Organic additives may be added to modify the nucleating process and eliminate undesirable growth modes [Bunshah 1982]. The effect of operating conditions on the plating solutions is shown in Fig. 22.33.

REFERENCES

Adams, R.O., and Hurd, J.T., 1969. The Properties of Beryllium Surfaces and Films, A Review, *Less Common Met.*, Vol 18, p 399–409

Anisimov, A., Frolov, V., Komarov, V., Mazul, I., Moszherin, S., Pepekin, G., and Pirogov, A., 1997. Beryllium Armour Produced by

Evaporation-Condensation Technique, *Fusion Eng. Des.*, Vol 37, p 253–259

ASM, 2002. *Chemical Vapor Deposition*, Vol 2, *Surface Engineering Series*, J.H. Park and T.S. Sudarshan, Ed., ASM International

Beat, T.G., 2005. Lawrence Livermore National Laboratory, Livermore, CA, private communication

Blocher, J.M., Jr., 1982a. Chemical Vapor Deposition, *An Overview in Deposition Technologies for Films and Coatings, Developments and Applications*, Noyes Publications, Park Ridge, NJ, p 335–364

Blocher, J.M., Jr., 1982b. Chemical Vapor Deposition, *Surface Cleaning, Finishing, and Coating*, Vol 5, *Metals Handbook*, 9th ed., American Society for Metals, p 381–386

Bohdansky, J., and Roth, J., 1984. Light Ion Sputtering of Low Z Materials in the Temperature Range 20–1100 °C, *J. Nucl. Mater.*, Vol 122–123 (No. 1–3), p 1417–1424

Bunshah, R.F., 1982. Deposition Technologies, *An Overview in Deposition Technologies for Films and Coatings, Developments and Applications*, Noyes Publications, Park Ridge, NJ, p 1–18

Bunshah R.F., and Juntz, R.S., 1967. "The Purification of Beryllium by Vacuum Melting Followed by Distillation and Simultaneous Deposition to Sheet in an Electron-Beam Furnace," Preprint UCRL-14945, Lawrence Livermore National Laboratory, Livermore, CA

Burt, R.J., Meyer, S.F., and Hsieh, E.J., 1980. Radio Frequency Magnetron Sputtering of Thick Film Amorphous Beryllium, *J. Vac. Sci. Technol.*, Vol 17 (No. 1), p 407–410

Castro, R.G., Stanek, P.W., Elliot, K.E., Cotton, J.D., and Watson, R.D., 1995. Optimizing the Thermal Conductivity of Vacuum Plasma-Sprayed Beryllium for Fusion Applications, *J. Nucl. Mater.*, Vol 226, p 170–177

Castro, R.G., Vaidya, R.G., and Hollis, K.J., 1998. Characterization of Plasma Sprayed Beryllium ITER First Wall Mockups, *Proceedings of the Third IEA International Workshop on Beryllium Technology for Fusion* (Mito, Japan), 1997, p 137–145

Dini, J.W., 1992. "An Electroplater's View of PVD Processing," Preprint UCRL-JC-109419, Lawrence Livermore National Laboratory, Livermore, CA

Dua, A.K., Agarwala, R.P., and Desai, P.B., 1985. Preparation and Characterization of Beryllium Coatings, *J. Vac. Sci. Technol. A*, Vol 3 (No. 6), p 2612–2617

Dunmur, I.W., 1979. Plasma-Sprayed Beryllium, *Beryllium Science and Technology*, Vol 2, Plenum Press, NY, p 135–175

Dunmur, I.W., Davey, N., and Moules, T.R., 1977. The Nature of Plasma Sprayed Beryllium and the Effect of Heat Treatment, *Fourth International Conference on Beryllium, Met. Soc.* (London, England), The Royal Society, London, p 35/1–35/14

Egert, C.M., and Allred, D.D., 1990. Diffuse Absorbing Beryllium Coatings Produced by Magnetron Sputtering, *Proceedings of SPIE, Stray Radiation in Optical Systems*, Vol 1331, R.P. Breault, Ed., p 170–174

Guseva, M.I., Korshunov, S.N., Gureev, V.M., Martinenko, Y.V., Neumoin, V.E., and Stoljarova, V.G., 1997. Investigation of Beryllium Self-Sputtering, *J. Nucl. Mater.*, Vol 241–243, p 1117–1121

Hechtl, E., Roth, J., Eckstein, W., and Wu, C.H., 1995. Experimental Investigation of the Angular Dependence of Be Self-Sputtering, *J. Nucl. Mater.*, Vol 220–222, p 883

Hill, R.J., 1986. *Physical Vapor Deposition*, 2nd ed., Temescal, Berkeley, CA

Holman, W.R., and Huegel, F.J., 1967. "CVD Tungsten and Tungsten-Rhenium Alloys for Structural Applications," UCRL Preprints 70340, Parts I and II, Lawrence Livermore National Laboratory, Livermore, CA

Hsieh, E., 1988. Film Deposition and Status, UCID 21384, *Survivability of Coatings Program Review*, J.A. Rathkopf, Ed., Lawrence Livermore National Laboratory, Livermore, CA, p 53–71

Hsieh, E.J., Price, C.W., Pierce, E.L., and Wirtenson, R.G., 1990. Effects of Nitrogen Pulsing on Sputter-Deposited Beryllium Films, *J. Vac. Sci. Technol.*, Vol 8 (No. 3), p 2165–2168

Kustner, M., Eckstein, W., Hechtl, E., and Roth, J., 1998. Angular Dependence of the Sputtering Yield of Rough Beryllium Surfaces, *J. Nucl. Mater.*, Vol 265 (No. 1–2), p 22–27

Lowenheim, F.A., 1963. *Modern Electroplating*, The Electrochemical Society, Inc., John Wiley & Sons, Inc., NY

Maeda, Y., Takei, K., Okamoto, M., Nakamura, K., and Igarashi, M., 1987. Superconducting Beryllium Films Deposited by Ion-Beam Sputtering, *IEEE Trans. Magn.*, Vol 23 (No. 2), p 1022–1025

Mattox, D.M., 1998. *Handbook of Physical Vapor Deposition (PVD) Processing*, Noyes Publications, Park Ridge, NJ

McEachern, R.L., 2001. "Beryllium Materials for National Ignition Facility Targets LDRD Final Report," Final report UCRL-ID-142818, Lawrence Livermore National Laboratory, Livermore, CA

McEachern, R.L., Alford, C., Cook, R., Makowiecki, E., and Wallance, R., 1997. Sputter-Deposited Be Ablators for NIF Target Capsules, *Fusion Technol.*, Vol 31 (No. 4), p 435–441

Murray, B.W., Ulph, E., Sr., and Richard, P.N., 1991. Thick Fine-Grained Beryllium Optical Coatings, *Proceedings SPIE, Reflective and Refractive Optical Coatings for Earth and Space Applications*, Vol 1485, p 106–115

Mutikainen, R.H., 1992. Stress and Microstructure in RF-Diode and DC-Magnetron Sputtered Beryllium Thin Films, *Materials Research Society Symposium Proceedings, Thin Films: Stresses and Mechanical Properties III* (Boston, MA), p 45–50

Nargi, C.P., 1992. Preparing Metals for Plating, *Prod. Finish.*, Vol 57 (No. 1-A), p 106–108

Nieh, T.G., Karlak, R.F., and Vidoz, A.E., 1982. The Effect of the Atomic Incident Angle upon the Microstructure of Thick Deposits Produced by Physical Vapor Deposition, *J. Vac. Sci. Technol.*, Vol 21 (No. 4), p 980–985

Nieh, T.G., and Wadsworth, J., 1998. Improved Microyield Strength in Beryllium Produced by Vapor Deposition, *Scr. Mater.*, Vol 38 (No. 6), p 863–868

Northcutt, W.G., Jr., and Hovis, V.M., Jr., 1988. Thin Beryllium Structures by Powder Metallurgy, *Mod. Develop. Powder Metall.*, Vol 19, p 753–767

O'Dell, J.S., McKechnie, T.N., and Hanafee, J.E., 1998. Laser Processing of Thermal Sprayed Beryllium, *Mater. Manuf. Process.*, Vol 13 (No. 2), p 213–227

Pierson, H.O., 1999. *Handbook of Chemical Vapor Deposition: Principles, Technology and Applications*, 2nd ed., Noyes Publications, Park Ridge, NJ, p 150–151

Powell, C.F., Campbell, I.E., and Gopnser, B.W., 1955. *Vapor-Plating*, John Wiley & Sons, NY

Price, C.W., and Norberg, J.C., 1989. Analysis of Nitrogen-Pulsed Sputtered Beryllium, *Proceedings of the Seventh International Conference on Secondary Ion Mass Spectroscopy (SIMS 7)* (Chichester, U.K.), Wiley, p 727–730

Roybal, E.A., McIntosh, M.B., and Hull, H.K., 1997. Current Status of Optical Grade Sputtered, Bare Beryllium, and Nickel-Plated Beryllium, *Critical Reviews of Optical Science and Technology, Advanced Materials for Optics and Precision Structures*, CR67, p 206–235

Salazar, K.V., 2005. Los Alamos National Laboratory, Los Alamos, NM, private communication

Sharp, D.J., 1986. Confined Ion Beam Cylinder Sputtering: A New Approach, *J. Vac. Sci. Technol. A*, Vol 4 (No. 6), p 3165–3168

Suvorov, A.L., 2002. Precise Atomic Scale Studies of Material Sputtering by Light-Ion Gases in the Pre-Threshold Energy Region, *Phys. At. Nuclei*, Vol 65 (No. 11), p 2021–2028

Takei, T., 1979. Studies on the Electro-Deposition from Organic Solutions of Metals That are Difficult to Deposit from Aqueous Solutions, *Surf. Technol.*, Vol 9, p 285–302

Takei, K., Maeda, Y., Wbeag, Y.W., and Shimizu, R., 1990. The Effect of Ejection Angle in Ion-Beam Sputter Deposition of Superconducting Amorphous Beryllium Film, *Jpn. J. Appl. Phys.*, Vol 29 (No. 3), p 500–506

Thornton, G.A., 1977. High Rate Thick Film Growth, *Ann. Rev. Mater. Sci.*, Vol 7, p 239–260

Thornton, J.A., 1982a. Coating Deposition by Sputtering, *Deposition Technologies for Films and Coatings, Developments, and Applications*, R.F. Bunshah, Ed., Noyes Publications, Park Ridge, NJ, p 171–243

Thornton, J.A., 1982b. Sputtering, *Surface Cleaning, Finishing, and Coating*, Vol 5, *Metals Handbook*, 9th ed., American Society for Metals, p 412–416

Tucker, R.C., Jr., 1982. Plasma and Detonation Gun Deposition Techniques, *An Overview in Deposition Technologies for Films and Coatings, Developments and Applications*, R.F. Bunshah, Ed., Noyes Publications, Park Ridge, NJ, p 454–489

Wheeler, W., Karlak, R.F., Nieh, T.G., and Vidoz, A.E., 1982. Beryllium Optical Mirrors by Vapor Deposition, *Contemporary Methods of Optical Fabrication, Proceedings SPIE*, Vol 306, The International Society for Optical Engineering, p 71–78

Wood, G.B., and Brenner, A., 1957. Electrodeposition of Metals from Organic Solutions, Part IV: Electrodeposition of Beryllium and Beryllium Alloys, *J. Electrochem. Soc.*, Vol 104 (No. 1), p 29–35

Wood, J.M., and Frey, F.W., 1967. Chemical Vapor Deposition of Beryllium Metal, *Proceedings of the Conference on Chemical*

Vapor Deposition of Refractory Metals, Alloys and Compounds (Gatlinburg, TN), A.C. Schaffhauser, Ed., p 205–216

SELECTED REFERENCES

- O'Donnell, P.M., 1967. Beryllium Fluoride Coating as a Corrosion Retardant for Beryllium, *J. Corros. Sci.*, Vol 7, p 717–718
- Palatnik, L.S., and Fedorenko, A.I., 1964. Investigation of Condensed Beryllium Thin Films, *Fiz. Met. Metalloved.*, Vol 18, p 69–72
- Porembka, S.W., and Hanes, H.D., 1965. "Surface Damage in Machined Beryllium," Defense Materials Information Center, DMIC Memo 198, Batelle Memorial Institute, Columbus, OH
- Salazar, K.V., Pattilo, S.G., and Trkula, M., 2000. Progress Update on CVD Beryllium, *Fusion Technol.*, Vol 38 (No. 1), p 69–73
- Ward, W.V., Jacobson, M.I., and Matthews, C.O., 1961. Effect of Surface Finish on Properties of Beryllium Sheet, *Trans. ASM*, Vol 54 p 84–95

Beryllium Chemistry and Processing, p 401-439
By Kenneth A. Walsh
Edited by Edgar E. Vidal, Alfred Goldberg,
Edward N.C. Dalder, David L. Olson, and Brajendra Mishra

CHAPTER 23

Welding and Joining of Beryllium and Beryllium Alloys

Richard A. Patterson, Los Alamos National Laboratory
David L. Olson, Colorado School of Mines
Alfred Goldberg and Edward N.C. Dalder, Lawrence Livermore National Laboratory

BERYLLIUM has been successfully joined by fusion welding, brazing, solid-state bonding (diffusion bonding and deformation bonding), and soldering. These different processes are described, and the advantages, disadvantages, limitations, and precautions associated with each of these processes are discussed. Joining with mechanical fasteners is discussed in Chapter 24, "Adhesive Bonding and Mechanical Fasteners," in this book. Since beryllium has a high affinity for oxygen and nitrogen and readily forms oxides and nitrides, considerable care must be taken on heating the metal to protect it from the ambient atmosphere. Both the strongly adherent oxide film and the nitrided surface inhibit wetting, flow, and coalescence during welding or brazing. In addition, beryllium cannot be fusion welded by any process that uses fluxes or where heated metal is exposed to the atmosphere. Mating surfaces must be cleaned, and joints must be designed to minimize residual stresses and potential locations for stress concentration (notch effects).

In joining any two metals, the danger exists of having galvanic corrosion if the part is subjected to moisture or to any type of corroding environment. This becomes a problem if the less noble (anodic) metal has a significantly smaller area than the more noble (cathodic) metal, since the ions (positive charges) from the anodic (corroding) metal must correspond to the number of electrons (negative charges) involved at the cathode. Beryllium is anodic to almost all metals [CRC 2000–2001]; thus, when joined to other metals and exposed to an even mildly galvanic environment, it may be susceptible to corrosion. In designing a beryllium-metal joint, it is important to consider the environment to which the assembled component will be exposed in service.

Four joining methods are examined: fusion welding, brazing, solid-state bonding, and soldering.

23.1 Fusion Welding

23.1.1 Introduction

Beryllium has been successfully welded by several processes, including gas tungsten arc and electron beam welding. The welding operations should be designed to minimize heat input, thermal stresses, grain growth, and concentration of weld defects. Two principal concerns associated with the fusion welding of beryllium are the control of weld metal grain size and size of the heat-affected zone HAZ. Because of the inherent low ductility of beryllium, the cast metal is susceptible to cracking [Passmore 1964, Sanderson and Nightingale 1990]. Both the strength and ductility of weldments are influenced by the grain sizes of the weld metals and the HAZs. An average grain size of less than 30 μm is desirable. Welded joints with fine-grained structures exhibit better room-temperature properties than joints with coarse-grained structures. However, coarse-grained

materials have better mechanical properties at higher temperatures.

The most common problems associated with fusion welding beryllium are the susceptibility to cracking and control of grain size in the weld metal and in the HAZ. Three types of cracking commonly occur: hot cracking, cracking originating at defects, and cracking due to thermally induced stresses. Hot cracking is primarily due to a low-melting-point, aluminum-rich, grain-boundary film, which results from the rejection of aluminum during solidification [Passmore 1964, Fraikor et al. 1968, Hauser and Monroe 1968, ASM 1983].

23.1.2 Cracking

Solidification during welding occurs primarily by epitaxial growth, resulting in relatively large, highly oriented, columnar grains in the fusion zone and, to some degree, in the HAZ. A low effective heat input will minimize the grain size as well as provide a narrow HAZ (heat input (joules/meter) = [(current × voltage)/(welding speed)]; current × voltage is in joules/second, and speed is in meters/second). High travel speeds are to be avoided, because the elongation of the weld pool increases with an increase in travel speed. Elongated weld pools tend to cause grain growth to stop abruptly at the centerline of the weld with little change in grain orientation, producing a boundary-like structure, as illustrated in Fig. 23.1 [Devletian and Wood 1983]. Such welds have been found to have the poorest resistance to cracking and may be especially prone to hot cracking [Heiple 1972]. Thus, moderate travel speeds, designed to provide an optimal compromise between heat input and microstructure, may be best [Vaccarri 1991].

The high thermal conductivity of beryllium, which results in a low thermal gradient, increases the difficulty of maintaining a narrow HAZ. With the eutectic liquid being essentially aluminum (Fig. 23.2) and the final liquid to solidify, a high concentration of aluminum may

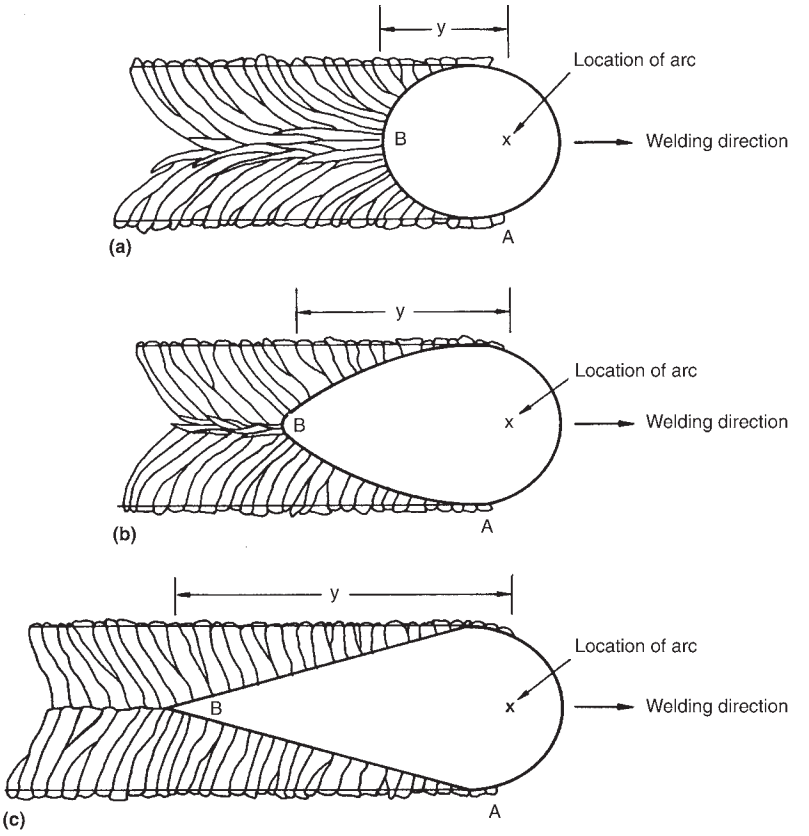

Fig. 23.1 Comparison of weld pool shapes. Travel speeds: (a) slow, (b) intermediate, and (c) fast. Source: Devletian and Wood 1983

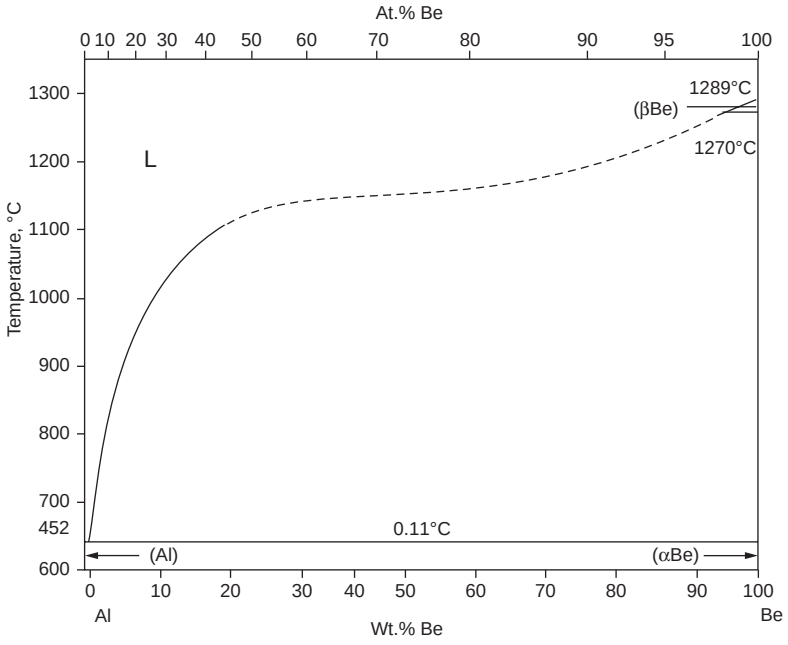

Fig. 23.2 Aluminum-beryllium phase diagram. Source: Massalski et al. 1990

form along the grain boundaries. The combination of coarse cast grains with aluminum-rich grain boundaries accentuates the hot cracking problem. The partitioning coefficient, *k*, of aluminum in beryllium is quite high, and the melting point of aluminum (660 °C, or 1220 °F) is much lower than that of beryllium (1289 °C, or 2355 °F). The problem is accentuated at the weld centerline due to the increased concentration of aluminum, grain-boundary orientation, and high tensile stresses perpendicular to the weld. Precipitates at the grain boundaries cause intergranular microcracking in welds. These precipitates are binary or ternary compounds associated with impurities in the beryllium. These impurities include aluminum, iron, and silicon.

The adverse effect of aluminum on beryllium welding can be reduced if the aluminum is present as the ordered compound $AlFeBe_4$. By weight, at least twice as much iron as aluminum must be in the starting material if the proper $AlFeBe_4$ stoichiometry is to be achieved. Insufficient aluminum will form the ternary compound while allowing the iron to remain in solution or to precipitate out as $FeBe_{11}$. The optimum ductility occurs at an iron/aluminum ratio of 2.4 [Hauser and Monroe 1968]. Also, high concentrations of $AlFeBe_4$ or iron in solid solution can result in increased cracking susceptibility [Heiple and Dixon 1979]. Therefore, the total amount of iron and aluminum should be limited. Figure 23.3 shows the range of iron and aluminum contents that have been shown to produce good welds [Heiple and Dixon 1979, Hill et al. 1990]. Figure 23.4 contains a bar graph showing the effect of impurity content of a number of impurities on the susceptibility to weld cracking in beryllium [Vaccarri 1991].

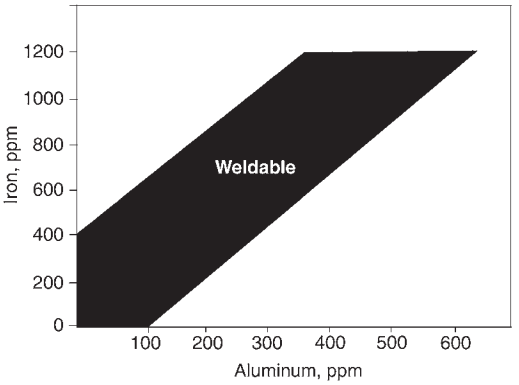

Fig. 23.3 Range of iron and aluminum contents in beryllium to produce good welds. Source: Heiple and Dixon 1979, Hill et al. 1990

As seen in Fig. 23.1, the grain macrostructure is influenced by the travel speed. Although

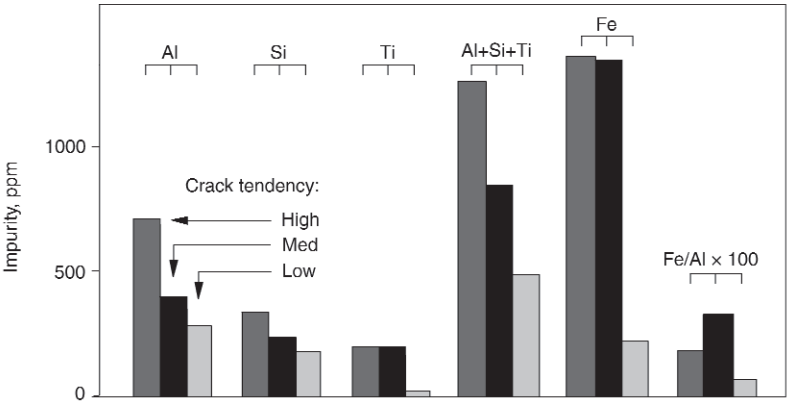

Fig. 23.4 Crack tendency of beryllium relative to its impurity content. Source: Vaccarri 1991

increasing the speed decreases the heat input, the resulting elongated weld pool caused the solidification and growth of the grains to advance more in a direction normal to the weld centerline. Thus, the grain growth from either side of the centerline stops abruptly at the centerline, producing a boundary-like structure. Such welds have been found to be the least resistant to cracking.

Cracking can originate at defects such as oxide particles, inclusions, voids, and surface markings. Machining defects, including deformation-induced twins may also act as crack nucleation sites. (Due to the small number of primary slip systems, beryllium is prone to twinning during machining.) Thus, it is best to remove a 0.10 mm (0.004 in.) layer of the machined surface before welding, and this is usually done by etching [Vaccarri 1991]. An increase in oxide content in the base metal was found to increase the occurrence of both undercutting and porosity. These defects are the result of the formation of an oxide film on the surface of the weld pool [Hauser et al. 1967]. This film, which has the appearance of a flux on the molten metal surface, interferes with the welding process by increasing the turbulence in the weld pool, which, in turn, mixes the oxide into the solidifying weld. The turbulence also causes an increase in weld-surface roughness over that achievable with lower oxide material [Hill et al. 1990] Furthermore, the increase in the oxide content increases the propensity to cracking.

The anisotropy of beryllium makes grain size a concern when welding. The grain size of powder-sheet beryllium is fine (20 μm), so the main limitations to its weldability are the iron/aluminum ratio and BeO content. However, the grain sizes of ingot material are typically large (50 to 100 μm), but the BeO content is quite low. This situation suggests that the ductility and weldability of the ingot sheet may be improved by a reduction in grain size. There are two methods that can be used to reduce the grain size: redundant working and roll bonding. Redundant working typically involves iterations of compression alternating in the principal three Cartesian orientations (90° directions) of the part [Heiple and Dixon 1979]. Grain sizes as fine as 2.3 μm have been reported in high-purity beryllium using redundant working. By diffusion bonding ten layers of 0.64 mm (0.025 in.) thick ingot-sheet beryllium, a grain size of 16 μm in a 6.4 mm (0.25 in.) thick sheet was achieved [Heiple 1972].

The low inherent ductility of beryllium perpendicular to the c-direction in the close-packed hexagonal unit cell, combined with the texture present in most product forms, results in very low base metal ductility. During welding, large, oriented grains are formed in the heat-affected and fusion zones. As a result, beryllium weldments may be subject to subsolidus cracking when thermal stresses created during welding exceed the material fracture strength in a direction associated with low ductility. This type of cracking could be at grain boundaries, where the long slip paths result in large dislocation pileups, stress concentrations, and microvoid nucleation. Beryllium is also prone to mechanical twinning during machining because of the small number of primary slip systems.

Cracking can also result from the inherently brittle beryllium not being able to accommo-

date the thermally induced stresses. High tensile stresses can be generated perpendicular to the weld along the weld centerline, where the microstructure is most susceptible to cracking. Thermally induced stresses are related to the high cooling rates and temperature gradients developed during welding. Weld cooling rates must be adjusted to avoid cracking whenever grain sizes above 10 μm are deemed unacceptable. Both types of stresses can be reduced by preheating (heating up a part to a predetermined uniform temperature prior to welding) the parts at some intermediate temperature for a period of time to allow transfer of heat throughout the parts prior to being joined. Preheating also increases the ductility, so that the thermally induced stresses are relieved by plastic flow rather than by cracking. Crack-free, full-penetration welds have been achieved in ingot-sheet beryllium up to 1.52 mm (0.06 in.) thick using a preheat of 400 °C (750 °F) [Heiple and Dixon 1979]. Beryllium made from low-oxide powder (0.5% BeO) has been successfully welded in thicknesses up to 2.5 mm (0.1 in.) with preheats of 340 °C (645 °F). In general, preheats should be used for autogenous welding (a fusion weld made without the addition of a filler metal) of beryllium in sections thicker than approximately 0.2 mm (0.008 in.) [Campbell et al. 1978].

A 2.54 mm (0.1 in.) thick product, made from powder having an oxide content of 0.5%, was successfully welded following a preheat at 340 °C (645 °F) [Vaccarri 1991]. If weld cracking cannot be avoided with autogenous welding, adding an Al-12Si filler alloy may help by creating an aluminum-rich, low-melting-temperature fusion zone, with the liquid being available to backfill cracks. Enrichment with aluminum, however, reduces the weld strength and lowers the service temperature of the beryllium.

Porosity, weld undercutting, and related cracking can be reduced by decreasing the oxide content of the base metal. The maximum permissible BeO content for single-pass, full-penetration welds in beryllium decreases with increasing thickness of the base metal. This is due to the increase in weld pool agitation and the more severe stress gradients associated with the increased heat inputs required with thicker materials. Successful single-pass, electron beam welds have been made with 1.6 and 3.2 mm (0.06 and 0.12 in.) thick beryllium parts containing 1.7 to 1.84 wt% BeO [Vaccarri 1991, Hill et al. 1990].

An investigation evaluated the source of centerline cracking in autogenous beryllium weldments [Cotton and Field 1997]. Centerline fusion-zone cracks were generated in rolled ingot-grade beryllium plates measuring 6.35 mm thick by 75 mm by 25 mm (0.25 by 3 by 1 in.). The fusion zone was formed by electron beam welding along the center of the plate, which was unrestrained. Optical, transmission electron, and scanning electron microscopy were performed on transverse and in-plane sections of the plate across and along the cracked weld. In addition, chemical analysis was performed. Typical of autogenous beryllium weldments, long, columnar grains formed, having nucleated epitaxially on partially melted base metal grains. (Epitaxial growth occurs when the crystallographic orientation of a deposited crystalline material follows the crystallographic orientation of the base material on which it nucleates.) The growth followed the direction of heat flow in the weld pool and was oriented nearly parallel to the welding direction along the centerline. The weld travel speed was between 2.5 and 4.2 mm/s (0.1 and 0.2 in./s), with 100% penetration of the plate. The directional growth and the crack that had formed at the intersection of the two growth fronts along the centerline can be seen in Fig. 23.5.

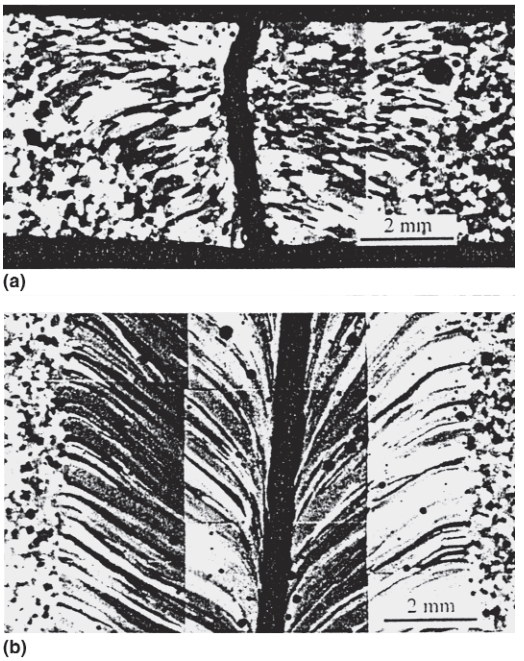

Fig. 23.5 Light optical photographs of typical weld sections, as imaged by polarized light. (a) Transverse cross section. (b) In-plane cross section. Source: Cotton and Field 1997

During solidification, impurities, following the direction of heat flow, are pushed toward the centerline and ultimately to the boundaries of the impinging dendrites and the associated columnar grains. (The word *dendrite* is derived from the Greek word meaning "of a tree." The treelike structure develops as solidification occurs by spikes or branches growing crystallographically into the liquid. The liquid in between the branches continually becomes enriched in those constituents that lower its melting temperature. The compositional gradients that develop as the liquid solidifies allow the dendritic structure to be revealed by etching.) Cracking was attributed to the formation along the columnar grain boundaries of a film of MBe_{12} (M refers to the metallic impurities in beryllium) along with low-melting-point, three-phase particles consisting of elemental silicon, elemental aluminum, and $AlFeBe_4$ formed along the columnar grain boundaries. Fracture characterization of the weld was obtained by extending an existing weld crack through the remaining intact (unaffected) metal and comparing it with the weld crack surface. Whereas the unaffected metal showed the characteristics of a typical brittle fracture, for example, cleavage facets, these characteristics were absent in the weld fractures. The latter exhibited a taffylike flow with width dimensions corresponding to those of the columnar grains, suggesting that the fracture is caused by the grain-boundary, low-melting phases and thus is due to hot shortness. (Hot shortness refers to the inability of a material to be worked or deformed at an elevated temperature as a result of disintegrating or fracturing due to the presence of a low-melting, grain-boundary film.) The gross difference between the two fractures can be seen in Fig. 23.6; the unaffected-metal fracture is seen in the lower left region of view (a). The taffylike feature is shown in view (b).

The selection of the welding process and process parameters has a significant effect on the weld composition and structure and on the thermal stresses developed. Thus, cracking susceptibility of beryllium can be overcome with careful control of welding process variables.

Thermal stresses result from temperature gradients induced during welding. Preheating can reduce these stresses. The preheat also increases the ductility so that the stresses are relieved by plastic flow rather than by cracking. A preheat of 400 °C (750 °F) allowed crack-free, full-penetration welds to be made in ingot sheet up to 1.52 mm (0.06 in.) thick. A 2.54 mm (0.1 in.) thick product, made from powder having an oxide content of 0.5 wt%, was successfully welded following a preheat at 340 °C (645 °F) [Vaccarri 1991]. In general, sections thicker than approximately 2 mm (0.08 in.) that are to be welded autogenously should be preheated. If weld cracking cannot be avoided with autogenous welding, adding an Al-12%Si filler alloy may help by creating an aluminum-rich, low-melting-point fusion zone, with the liquid backfilling the cracks. Enrichment with aluminum, however, reduces the weld strength as well as lowers the service temperature of the beryllium.

Decreasing the oxide content of the base metal can reduce porosity, weld undercutting, and related cracking. The maximum permissible BeO content for single-pass, full-penetration welds in beryllium decreases with increasing thickness of the base metal. This is due to the increase in weld pool agitation and the more severe stress gradients associated with the increased heat inputs required with thicker materials.

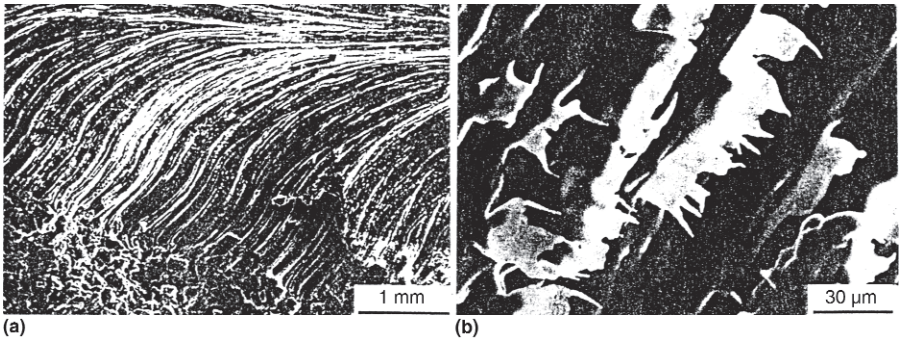

Fig. 23.6 SEM micrographs of the weld fracture surface. (a) Low magnification showing overall structure. (b) High magnification showing taffylike features of centerline weld crack. Source: Cotton and Field 1997

23.1.3 Selection of Welding Process

Various grades of beryllium are made with different powder sources, consolidation methods, and processing steps to produce the parts to be welded. These different parts will have correspondingly different chemical analysis, microstructures, degrees of anisotropy, and mechanical properties. Because of the relatively low tensile ductility (1 to 6%) of essentially all of these parts, small changes in properties will affect the weldability of the beryllium. Furthermore, improper surface preparation and/or contamination during the welding process may also adversely affect the weldability.

Fusion welding is limited to methods where either a vacuum or complete shielding from the ambient atmosphere is used. Welding operations should be designed to minimize heat input, thermal stresses, grain growth, and the concentration of weld defects. The process that produces the smallest weld zone usually provides the best results. The two most common methods used for fusion welding of beryllium are electron beam (EB) and gas tungsten arc (GTA), also known as tungsten inert gas (TIG), welding [Hill et al. 1990, Merlini and Bush 1978, Gilliland and Slaughter 1963, White et al. 1962]. (The electron beam welding process is a high-density fusion process that is accomplished by bombarding the joint to be welded with an intense, strongly focused beam of electrons. The instantaneous conversion of the kinetic energy of these electrons into thermal energy as they impact and penetrate into the workpiece causes the weld-seam interface surfaces to melt, producing the desired weld-joint coalescence. The gas tungsten arc welding process uses heat produced by an arc generated between a nonconsumable electrode, such as tungsten or tungsten alloy, and the workpiece. The electrode and weld region are shielded from the ambient atmosphere by a shielding gas that is supplied through the torch.) Beryllium can also be welded by gas metal arc welding (GMAW), also known as metal inert gas (MIG), and by pressurized gas metal arc welding (PGMA). (Gas metal arc welding is an arc-welding process in which the heat for welding is generated by an arc between the workpiece and a consumable electrode that is shielded by an externally supplied protective gas. The electrode is a bare solid wire, which serves as the filler metal, or metal added to the weld pool, that is continuously fed to the weld area. Pressurized gas metal arc welding is an adaptation of the GMAW process using pressurized gas.) Of these two, PGMA is preferred; however, both methods produce higher heat inputs than those obtained by GTA or EB. The benefits of pressure used with PGMA are the reduction of porosity and arc-column diameter [Hill et al. 1990] The GMAW process requires an aluminum-silicon filler wire and demands careful cleaning as well as good chemical homogeneity of the beryllium. Resistance spot welding is a process in which surfaces are joined in overlapping spots by the heat generated by resistance to the flow of electric current through workpieces.

Electron beam welding (EBW) appears to be the best fusion-welding process for joining beryllium. The EBW process produces welds with a high depth-to-width ratio (10:1 to 30:1) and a narrow HAZ. The sides of the weld are almost parallel. The narrow fusion zone and the relatively low heat input obtained by EBW lead to a reduction of thermal stress and distortion, thus reducing the tendency to crack. Also, it permits the welding of parts that already have been machined without the need for any further size adjustment. In addition, the high depth-to-width ratio often allows for single-pass welding, which results in a further reduction of the size of the HAZ. Because of the vacuum environment, the need for shielding of the molten metal from the ambient atmosphere is not needed. Because of the relatively high vapor pressure (3 Pa, or 25 μm Hg) at the melting point of beryllium, both heat input and vacuum should be limited, the latter to approximately a pressure of 13 mPa (10^{-4} torr). The EBW of beryllium is usually done at pressures between 0.1 and 130 mPa (10^{-6} and 10^{-3} torr), although the process can be adapted for pressures to as high as 13 Pa (10^{-1} torr). The higher-vacuum environments, however, are more effective at containing the toxic beryllium fumes and preventing oxidation. The penetration and the depth-to-width ratio are both reduced as the pressure is increased. For most materials, foil-to-plate thicknesses are weldable in one pass. The EBW process allows for high welding speeds (125 to 200 mm/s) on sheet material and requires no filler metal, flux, or shielding gas.

With EBW, a sharp focus must generally be used to minimize the size of the fusion zone. For the deeper welds, the weldability can be improved by a preheat treatment. The weldability is affected by weld metal contamination, where beryllium oxide is usually the major contaminant, primarily from powder-source material.

Lowering oxide content will improve weld ductility, so the beryllium oxide content is often required to be below 1.5 wt%. Aluminum content can also influence the weldability and susceptibility to hot cracking. To reduce cracking in autogenous welds, attention must be paid to appropriate fixturing, joint design, fit-up, and section thickness.

In the EBW process, an aluminum shim is placed between the two beryllium parts to be joined, the aluminum typically being high-purity1100 sheet. The aluminum shim must be in good contact with one of the parts, which can be problematic with large assemblies. An alternative method is to deposit the aluminum on the mating surface (or edge) using physical vapor deposition [Juntz 1986]. Surfaces that are not to be plated are carefully masked.

Single-pass EBWs have been made successfully in 1.6 and 3.2 mm (0.063 and 0.125 in.) thick beryllium containing 1.7 to 1.84 wt% BeO [Hauser and Monroe 1968, Hauser et al. 1967]. Commercially available grades now have oxide contents as low as 0.5 wt% BeO (0–50) (Brush Wellman designation for low-BeO grade of beryllium), and the BeO content of ingot and electrolytic beryllium are much lower still. However, the maximum permissible BeO content for single-pass, full-penetration welds in beryllium decreases with increasing thickness of the material due to the increased weld pool agitation and more severe stress gradients associated with the higher heat inputs. Therefore, BeO content must be kept as low as possible when welding thick sections.

In an early EBW investigation, it was observed that in order to obtain a satisfactory joint using a shim, it was necessary to melt the beryllium on both sides of the shim [Hicken and Sample 1967]. By focusing along the center of the joint, a fusion zone with nearly parallel sides was obtained. Focusing off the weld centerline resulted in poor wetting of the aluminum to the beryllium on one side of the weld and cracking in the beryllium on the other side. Throughout the fusion zone, the structure consisted of primary beryllium dendrites in an aluminum-beryllium eutectic matrix. (The term *eutectic* refers to a microstructure that forms due to the solidification of a liquid phase into two or more solid phases. The solid phases precipitate out of the liquid sequentially, continuously repeating the sequence until all the liquid has solidified, resulting in an intimate mixture of the solid phases.) The authors observed that the top of the joint consisted of a columnar structure, whereas at the bottom (root) of the joint the structure tended to be equiaxed as well as being finer than the structure at the top. (The term *equiaxed* refers to the grains of a microstructure having no morphological orientation; i.e., all axes drawn from the surface of any given grain through its center are essentially equal. Grain sizes would vary.) This was attributed to a decrease in the width of the fusion zone in going from top to bottom, resulting in a corresponding increase in the solidification rate. In addition, the beryllium content and hence the melting point were higher at the top of the joint than at the bottom of the joint. They noted that to produce a sound, crack-free, high-strength weld, the fusion zone had to contain over 30 wt% Al. Aluminum alloys 1100, 2024, 5052, 5083, 6061, and 718 were evaluated for use as shims. All except 2024 produced joint strengths equal to or greater than the strength of the beryllium. Alloy 718 showed the best fluidity.

Gas Tungsten Arc Welding and Gas Metal Arc Welding. Beryllium can be welded with limited success with GTA welding [Passmore 1964, Sanderson and Nightingale 1990]. The GTA welding process can be used for continuous welds, intermittent welds, and spot welds. It can be done manually or automatically. With GTA welding, the joint is produced by heating the abutting parts with an arc formed between a nonconsumable tungsten electrode and one of the parts. One or more electrodes may be used simultaneously. Protective inert gas shielding is required. Filler metal, if needed, can be used. The base metal thickness and joint design determine whether filler metal should be added to the joint. The parts being welded must be firmly secured relative to each other. Additional fixturing may be necessary when fit-up is marginal, parts are thin, shapes are complex, filler metal is not used, or when automatic or machine welding is used. The filler metal as well as the mating and adjacent surfaces must be clean. A typical weld line for the GTA (TIG) process is depicted in Fig. 23.7.

Welding with alternating current and argon shielding is recommended for manual welding. With automatic welding, direct current may be used. A low effective heat input and a high cooling rate are desirable. These conditions help to minimize the grain size in the weld metal and HAZ. When welding manually, the filler rod is added into the pool of molten metal ahead of the arc. Improper electrode and rod angles may de-

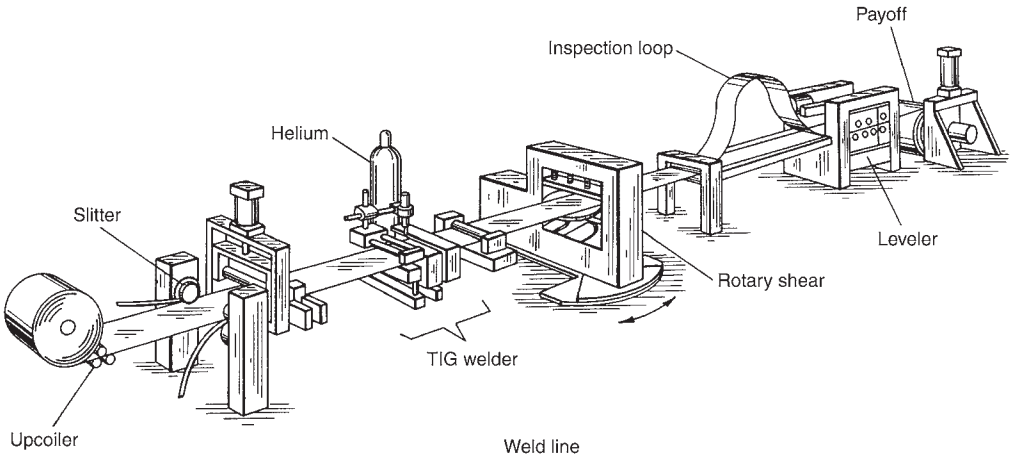

Fig. 23.7 Typical weld line for the gas tungsten arc (tungsten inert gas, or TIG) process

grade the weld. The recommended angles are 15° backward and 75° forward from the vertical to the work surface, in the travel direction, for the electrode and filler rod, respectively. All standard joints can be welded by this method. Generally, edges need not be beveled for thicknesses of 3.2 mm (0.1 in.) or less. Thicker base parts are usually beveled, and the aluminum filler metal is always added.

Because of the excellent control of heat input, the GTA process is good for joining thin parts. Another attractive feature is that the heat source and addition of filler can be controlled separately. Some disadvantages or limitations do exist. The process is slower than a consumable electrode process. Some transfer of tungsten from the electrode to the weld metal can occur, resulting in brittle tungsten inclusions. Costs are generally higher than those costs obtained for other welding processes.

In the gas metal arc (GMA) welding process, heat is generated by an arc developed between an electrode and the weld pool. The electrode is a bare solid wire that is continuously fed to the weld area, thus becoming the filler metal as it is consumed. An inert cover gas is fed through the welding gun and provides protective shielding from the ambient atmosphere. The arc must be protected against air drafts that could disperse the shielding gas. The process may be operated in a semiautomatic or automatic mode. Because of the continuous feed of filler metal, long welds can be made without interruptions. The process enables the attainment of relatively high deposition rates and welding speeds.

To further minimize cracking, the feasibility of welding beryllium by pulsed gas tungsten arc braze-spot welding with preplaced aluminum shims was evaluated [Banaim et al. 1988]. (Term created for an experimental process. The pulsed arc was obtained using the GTA welding process. The inclusion of *braze* is related to the use of a shim insert similar to its use in a brazing process.) The concept, based on thermodynamic calculations that a liquid miscibility gap exists in the liquid + solid region in the aluminum-beryllium system at high beryllium concentrations, was to induce rapid solidification that would result in a continuous and intimately mixed region of beryllium and aluminum. (A liquid miscibility gap refers to the region on the phase diagram where, over a temperature range, the liquid has separated into two liquids of different compositions in equilibrium with each other.) Welding experiments were performed on 2 mm thick, 20 mm diameter rings, machined out of beryllium rods. A schematic diagram of the joint design is shown in Fig. 23.8. The shims consisted of 0.3 mm thick 1100 aluminum strips. Both the aluminum and beryllium were cleaned by acid etching prior to welding. Welds were evaluated by radiographic inspection and optical and scanning electron microscopy of transverse sectioned samples.

Banaim et al. [1988] observed that the microstructure had a morphology that was typical of a pure eutectic, that is, a very fine dispersion of beryllium (primary phase) in continuous aluminum (secondary phase). The beryllium nucleated and formed dendrites, while the aluminum

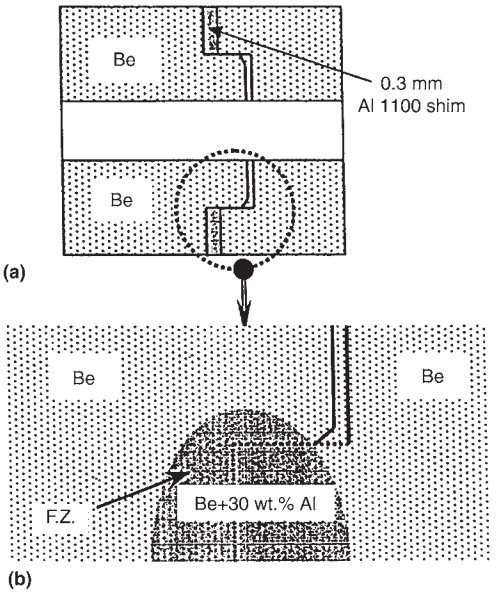

Fig. 23.8 Schematic sketch of joint design. (a) Before welding. (b) Enlargement of fusion zone (FZ) following welding. Source: Banaim et al. 1998

backfilled along the interdendritic zones. The aluminum from the fusion zone (FZ) extended along grain boundaries into the base metal HAZ, forming aluminum stringers. These stringers absorbed the thermal strain, thus inhibiting crack branching and crack propagation in the FZ. The surface of the FZ, however, was found to be sensitive to hot cracking.

Beryllium can be braze welded using either a gas-shielded electric arc or an electron beam as the heat source [Keil et al. 1960, ASM 1993]. Welds can be made with less than 30 wt% Al content, which requires proper melting of the beryllium edge. The best results are obtained using Al-12Si filler metal, which is typically added in the form of wire or preplaced shim stock.

Joint strengths equal to that of the base metal are achievable. However, the filler metal must fill the joint completely. The face of the weld and the root surface must blend smoothly with the base metal because of the notch sensitivity of beryllium. Discontinuities at the interfaces and excessive restraint can cause the beryllium to crack at those locations.

Hydrogen porosity will be a major problem if the heated filler metal is not kept under the shielding gas or if gas shielding coverage is inadequate. Maintaining proper voltage will help reduce the porosity; 23 V for cast/ingot stock or 21 V for powder-based stock have been cited as optimum values.

To reduce porosity, pressurized GMA braze welding is an option that should be considered. By welding in a chamber, which has been pressurized to 207 Pa, porosity is effectively eliminated. Additional beneficial effects are a more constricted arc column and increased current density, which combine to allow for a narrow weld groove that minimizes the level of impurities in the weld. To minimize distortion, a preheat of greater that 100 °C (212 °F) must be used. For multiple-pass welds, the aluminum oxide powder produced must be removed from the weld groove prior to subsequent passes.

Resistance spot welding can be used only for low-strength applications. At higher strengths, cracking will likely occur around fine-grained weld nuggets. When the weld heat input is adjusted to avoid cracking, a coarse-grained dendritic nugget of low strength is produced. Contact resistance is more critical for beryllium than for most engineering materials. Force must be controlled to provide a uniform and consistent contact resistance. Satisfactory results have been achieved with a contact resistance value of $3.6 \times 10^{-4}\ \Omega$.

23.1.4 Porosity in Welds

When welding the closure of beryllium pressure vessels, Dow Chemical Company reported having porosity in the MIG welds. Of special concern were those voids of macroscopic size, that is, discernable with the unaided eye. The porosity was attributed to the hydrogen dissolved in the molten aluminum filler metal. The drop in solubility on solidification and on cooling of the solid results in the formation of pores as the excess hydrogen is expelled from solution. The solubility of hydrogen in aluminum as a function of temperature is shown in Fig. 23.9. The hydrogen can originate from a number of sources: filler metal, moisture on the filler wire, beryllium, shielding gases, and greases and lubricants used in the manufacture of the wire or parts to be welded [Barker]. Calculations show that 10 ppm by weight of hydrogen will produce a volume of 1% porosity during solidification. An evaluation of the porosity of Al-12Si wires revealed 6 and 13 ppm of hydrogen for Alcoa and Allstate wire, respectively. Other gases were also present; of these, approximately 80% was hydrogen, and 20% was a mixture of methane and other gases. Cleaning the wire will reduce

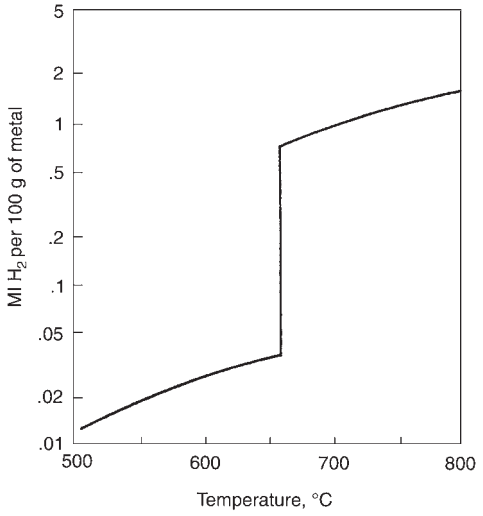

Fig. 23.9 Solubility of hydrogen in aluminum at atmospheric pressure. Source: Barker

the amount of porosity. However, if the cleaning agents are not completely removed, the porosity may increase. Trichloroethylene was suggested as a degreasing agent.

The most satisfactory welding process to minimize the effects of weld porosity is PGMA. It is suggested that the pressure increase tends to keep the dissolved gases in solution while the melt partially solidifies. The smaller gas bubbles that form are unable to readily migrate through the discontinuous melt and coalesce into larger bubbles, creating large voids. Significant reduction in macroporosity was realized by PGMA welding when the chamber pressure was raised to between 69 and 103 kPa (gage pressure) [Barker].

23.1.5 Surface Preparation

Surfaces must be carefully cleaned prior to welding. Contaminants can be removed by degreasing using a combination of acetone and alcohol wipes. Adherent refractory oxide films that can rapidly form on beryllium will inhibit wetting, flow, and fusion during welding and brazing. If the surfaces appear heavily oxidized or not properly degreased, they should be chemically etched with a 5% solution of hydrofluoric acid and deionized water. A slight tendency for pitting may occur. An alternative cleaning solution that has a lesser tendency for pitting is a solution of 70% phosphoric acid, 25% sulfuric acid, and 25% nitric acid. Care must be taken that the filler wire is not contaminated with lubricant.

The joining process and procedures must maintain contaminant-free joining surfaces and prevent oxidation during the operation by appropriate shielding media and techniques. Inert gas or vacuum is appropriate. This shielding is also a key in excluding hydrogen, which is the principal cause of porosity in beryllium weldments. The residual oxide content can also cause porosity and excessive crater development in the weld.

Cleaning, as reported in an early investigation evaluating EBW of beryllium using preplaced shims of various aluminum alloys, consisted of etching the beryllium with a hydrofluoric acid-malonic acid solution. The aluminum shims were treated with Tucker's etch. The aluminum alloys were etched until approximately 12 μm of material per side was removed.

Surface damage due to heavy tool forces in machining can provide nucleation sites for cracking during welding. Each of the final three cuts should be less than 76 μm (0.003 in.) deep.

23.1.6 Filler Metals and Feed Rates

Aluminum alloy filler wires have been used successfully for avoiding weld cracks in beryllium. The most successful of these is alloy 718 containing 12% Si, which, being close to the eutectic composition, results in a relatively high-fluidity, low-melting-point, aluminum-rich fusion joint. The melting point is sufficiently low to promote liquid formation and backfilling of cracks. The drawbacks of adding an aluminum alloy filler include a reduction of service temperature and a lowering of the tensile strength of the weld [Hill et al. 1990]. It is recommended that the filler wires contain at least 30 wt% (approximately 10 at.%) Al to suppress cracking at room temperature. A fusion zone content of 30 wt% Al is recommended to avoid microcracking [Hicken and Sample 1967].

Wire feed rate ranges from approximately 190 to 380 mm/s (7.5 to 15 in./s), depending on groove size [Weiss 1983]. The starting feed rate is approximately 25% of the continuous rate. The weld travel speed is on the order of 17 to 21 mm/s (0.7 to 0.8 in./s). Typical power settings are 30 to 32 V and 140 to 150 A direct current at the positive electrode. Welding machines with voltage characteristics of a medium slope perform somewhat better than one having a flat slope (constant potential). (Slope refers to the voltage-versus-amperage curve. It is a characteristic of the power supply. A flat slope refers to an essentially constant voltage supply attainable

with a power supply having a relatively low resistance. Power supplies are available to provide a range of slopes such that the amperage can be controlled with voltage changes. Different welding processes perform best at different slopes.) The former machines, having a slightly smaller arc length, avoid producing an arc blast at the start [Weiss 1983].

Satisfactory welds are made in two passes with the GMAW process using Alcoa 718 filler wire of 0.762 mm (0.03 in.) diameter, fed at a rate of approximately 380 mm/s (15 in./s) with a travel feed of approximately 38 mm/s (1.5 in./s). Other parameters include a reverse-polarity arc voltage of 22 V, and gas flows of helium at 2.83 m^3/h and argon at 0.51 m^3/h. Different numbers of passes are made with appropriate parameter changes. The PGMA process is similar to the GMAW process except that it is performed in an inert gas chamber that is at a pressure above atmospheric. Except for a slightly higher voltage with the PGMA process, both use similar parameters [Jacobson 1986].

Welding parameter ranges reported by Dow Chemical Company used in the GMAW process for welding equatorial closures of beryllium pressure vessels and using aluminum alloy 718 filler metal (0.762 mm, or 0.03 in., diameter) were 250 to 380 mm/s (9 to 15 in./s) wire feed speed; 18 to 51 mm/s (0.7 to 2 in./s) travel speed; 135 to 200 A direct current reversed polarity (DCRP) weld current (in DCRP, the electrons flow from workpiece to electrode instead of from electrode to workpiece); 22 to 30 V arc voltage; 120 to 210% joint fill; 1.42 to 2.83 m^3/h of helium and 0.38 to 0.51 m^3/h of argon; 0 to 69 kPa (0.01 ksi) (gage) pressure; and 6.35 to 9.53 mm (0.25 to 0.38 in.) for contact tip-to-work distance. It is suggested that the filler metal be deposited directly into a "V-" or "U-"grooved joint [Barker].

Improved strength was obtained using a two-step process. This consisted of depositing a layer of alloy 718 onto the mating surfaces. The surfaces were then machined to form an aluminum alloy "V-"joint at the closure area when the components were assembled to be welded. Such a joint is referred as a buttered joint.

A series of high-speed motion pictures were used to evaluate the effect of wire feed speed on the weld characteristics. The travel speed was adjusted to produce a constant 150% joint fill. The tests were performed using MIG welding, with alloy 718 filler metal, and at an arc voltage of 28 V. The films revealed that at low speeds (167 to 250 mm/s, or 7 to 10 in./s), the arc was very long, the puddle possessed little fluidity, and the beryllium bonded poorly to the aluminum weld metal. Increasing the feed speed to between 300 and 420 mm/s (12 and 17 in./s) results in a considerable shortening of the arc length, and good bonding was obtained. On further increasing the feed speed to 460 mm/s (18 in./s), the arc becomes increasingly shorter, with bonding occurring only at the root of the weld. Signs of arc instability appeared with rough surfaces of the weld deposits. At 22 V, the optimum feed speed was 340 mm/s (13 in./s).

Electron beam welds made without a filler metal usually tend to crack. Without a filler metal, the process is limited to sheet material approximately 0.58 to 0.76 mm (0.02 to 0.03 in.) thick. Typical welding parameters for a beam focused 6.35 mm above the joint, using an aluminum alloy filler, and requiring 2.54 mm (0.1 in.) penetration are 70 kV, 7.5 mA, and a travel speed of 6 mm/s (0.2 in./s) [Jacobson 1986]. To avoid any movement of the filler metal shim, the shim can be spot welded to the workpiece. Alternatively, the filler metal can be vapor deposited onto the part.

23.1.7 Shielding

Helium and argon gases are used to shield the molten and solidifying weld metal from the atmosphere. Weld metal porosity is lower with helium than it is with argon. However, some argon is required to obtain a smooth bead contour. In small amounts, the argon does not degrade the quality of the weld; thus, both gases are used together [Barker]. A combination of five parts helium to one part argon by volume is recommended as a gas shield. Typical flow rates are 1.4 to 2.8 m^3/h of helium and 0.28 to 0.57 m^3/h of argon, the rate depending mainly on the type of weld chamber. The higher flow rates should lead to contaminant-free welds.

23.1.8 Joint Design

The thermal stresses developed during welding are also affected by the design of the weld joint and fixturing. Whenever possible, joint designs should be selected to minimize the restraint of the part. Various joint designs have been used for 3.125 mm (0.125 in.) thick beryllium sheet including lap joints, tee joints, corner lap joints, corner butt joints, and butt joints between sheets of unequal thickness [Hauser and Monroe 1968,

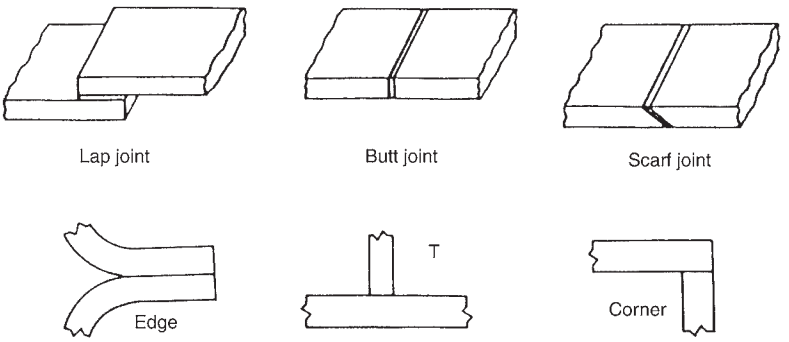

Fig. 23.10 Schematic examples of some common joints. Source: Heiple and Dixon 1979

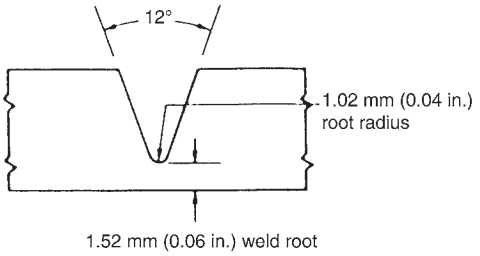

Fig. 23.11 Double-U-groove joint commonly used in gas metal arc welding of beryllium plate and tube. Source: Weiss 1983

Hill et al. 1990]. However, in lap, corner lap, and tee welds, a sharp notch is present at the interface that will limit the use of these structures to applications with low service stresses. Crack-free, full-penetration butt welds have also been made in ingot-sheet beryllium up to 3.8 mm (0.15 in.) thick [Heiple and Dixon 1979]. Some examples of joints are shown in Fig. 23.10. Additional illustrations of joints are presented in section 23.3, "Solid-State Bonding," in this chapter.

Joint designs and fixturing should be selected to minimize the restraint of the part. An example of a commonly used weld-joint design for plate and tube, based on butt joints prepared with a narrow "J" or "U" or with a narrow "V" with a root radius, is shown in Fig. 23.11. Each groove follows the shape of the welding arc to minimize thermal shock to the base metal. The weld root depth should not be less than 1.52 mm (0.06 in.). Weld penetrations of up to 6.35 mm (0.25 in.) may be obtained without preheat; for larger penetrations, preheating is necessary [Weiss 1983].

23.1.9 Weld Repair

Defects, such as porosity, can be repaired by machining out the defect, preheating to 100 °C (212 °F), and rewelding. If the pass is stopped, as may occur in a multiple-pass weld, then the part should be reheated before arc restart to reduce the possibility of cracking [Weiss 1983].

23.2 Brazing

23.2.1 Introduction

Brazing is an economically attractive process for producing high-strength metallurgical bonds while retaining the desirable properties of the base metal. Brazing of beryllium has been used in fabrication of complex, high-performance spacecraft structures and in instrument payloads [Keil et al. 1960, Maloof and Cohen 1964, Grant 1979, American Welding Society 1998]. In brazing, a joint is obtained by heating the parts to be joined and the filler metal to a suitable temperature that will not melt the workpiece and will avoid or limit the introduction of any undesirable microstructures. It is considered to be an economical process that produces a high-strength bond while preserving the base metal properties. A filler metal is used that has a liquidus above 450 °C (840 °F) and a melting point below the solidus of the parts to be joined. (The liquidus is the boundary between the liquid region and liquid-plus-solid region on a phase diagram; i.e., the material is completely molten above the liquidus temperature. The liquidus temperature varies with composition. The solidus is the boundary between the solid region and liquid-plus-solid region on a phase diagram; i.e, the material is completely solid below the solidus temperature. On heating, melting is initiated on reaching this temperature. The solidus temperature varies with composition.) The faying surfaces are first coated with a flux

that melts while the parts are being heated. The flux dissolves any metal oxides present as well as prevents new oxidation. Next, the filler is added at some point on the surface of the joint and then drawn into it. For this to occur, the filler metal must wet the base metal surfaces and be drawn into and held in the joint by capillary attraction, which is due to having an appropriate surface tension difference between base metal and filler. Thus, good wettability and fluidity are important characteristics of the filler. The filler metal must have a surface tension and density such that it displaces the flux, and, after cooling, the joint will be filled with solid filler metal, while the solid flux will be found at the joint periphery.

Capillary flow is the dominant brazing mechanism, provided that both faying surfaces are wetted by the molten filler metal. Furthermore, the joint must be properly spaced to enable the capillary action to be efficient. Metallurgical reactions between the base metal and the filler metal could change the flow characteristics.

Advantages of brazing over fusion welding include:

- Lower heating temperatures
- Minimization or elimination of warping
- Increased joining speed
- Higher production rates when simultaneously brazing several parts
- Reduction of the effects of expansion, contraction, and distortion
- Reduction of residual stresses
- More cost-effective

Brazing processes are generally designated according to the heating sources. Of industrial importance are furnace, induction, torch, resistance, dip, diffusion, and infrared brazing. (Furnace brazing is performed using a heated furnace. Induction brazing uses the heat from the resistance of the workpieces subjected to a voltage induced through one or more coils. Torch brazing is a brazing process that uses heat from a fuel-gas flame. Resistance brazing is a brazing process that uses heat from the resistance of the workpieces to current flow in an electrical circuit. Dip brazing is a brazing process that uses heat from a molten chemical or metal bath. The molten chemical bath may also serve as the flux, while the molten metal bath may serve as the filler metal. Diffusion brazing is a brazing process that forms liquid braze metal by diffusion between dissimilar base metals or between base metal and filler metal preplaced at the faying surfaces. The process is used with the application of pressure. Infrared brazing is a brazing process that uses heat radiated from an infrared source.) Other methods include blanket brazing and exothermic brazing. All these methods use a filler metal that has a melting point above 450 °C 840 °F) but below that of the base metal. The liquid filler metal spreads through the joint by capillary action. A brazing method that does not depend on capillary action is referred to as braze welding. Here, the filler metal is deposited directly to where it will be used. The distinction between brazing and soldering is based on the melting temperature of the filler. Solder filler metals melt below 450 °C.

23.2.2 Selection of Brazing Process

Selection of a proper brazing technique and filler metal depends on the service temperature, joint geometry, and required joint strength. Beryllium reacts rapidly with oxygen to form very stable oxides. It has a high solubility for oxygen, nitrogen, and hydrogen at elevated temperatures. Small amounts of any of these elements will result in an increase in hardness, notch sensitivity, and embrittlement. In addition, the oxidized and nitrided surfaces will impair the wettability and flowability of the brazing filler metals. A brazing filler metal that has a low melting temperature is recommended. To avoid these problems when brazing beryllium, surfaces of the parts to be brazed must be prevented from air exposure during heating. Therefore, beryllium must be brazed in vacuum (1.3 Pa, or 10^{-2} torr, or better) or in a high-purity inert gas. Induction and furnace brazing in inert gas or vacuum can be used successfully. Torch brazing should generally not be used for beryllium. It is difficult to control and requires special precautions and techniques. Induction brazing is favored for small, symmetrical parts because its speed minimizes reaction between filler metal and base metal. Furnace brazing is favored for large parts since the uniformity in temperature required throughout the heating and cooling cycle can be readily controlled [Schwartz 1983]. In general, a vacuum environment is preferred. To minimize the formation of intermetallics between beryllium and braze constituents, short heating, holding, and cooling times are recommended. This will also minimize the problem of alloying and penetration of grain-boundary constituents into the beryllium.

Furnace brazing is especially applicable to high production rates. Here, the filler metal must be preplaced at or near the joint. The filler metal can be in one of many forms: wire, foil, tape, paste, slugs, powder, or filings. Fluxes are used to protect the parts and brazing filler metal, except where an atmosphere of reducing or inert gases is used for the same function. A mixture of either stannous chloride or 60 wt% lithium fluoride and 40 wt% lithium chloride is a suitable flux for furnace or induction brazing. Beryllium and beryllium compounds residing in flux residues are toxic. Vacuum furnace brazing, by preventing oxidation, eliminates the need for a flux. This method is widely used when reactive metals are joined or when entrapped fluxes cannot be tolerated. Filler metals that contain constituents with high vapor pressures should not be used for brazing in vacuum. Only approved installations should be considered for brazing beryllium, regardless of the methods used.

During induction brazing, the filler metal is generally preplaced at the joint. To assure that all the faying surfaces reach the brazing temperature at the same time, the joint and coil setups must be carefully designed. Special attention must be given to the coil design for parts having widely varying thicknesses. Sheet thickness normally does not exceed 3 mm (0.1 in.), while bar thickness can be as high as 25 mm (1 in.). Brazing temperatures are reached in less than 10 s, allowing for high production speeds.

23.2.3 Surface Preparation

Beryllium surfaces must be thoroughly cleaned before brazing. Components should be degreased, pickled in an aqueous solution of hydrofluoric and nitric acid, rinsed in deionized water, and dried [American Welding Society 1991]. Because the presence of an oxidized or nitrided surface impairs the wetting and flow properties of brazing filler metals, high-temperature brazing should be done in a protective atmosphere, such as in argon, helium, or vacuum. Titanium hydride (TiH) flux is a very effective flux, especially for silver-containing braze alloys [Jacobson 1986]. The TiH can be painted onto the beryllium surface. (Additional references to fluxes are discussed in section 23.4, “Soldering,” in this chapter.)

Precoating the joint faying surfaces with silver, titanium, copper, aluminum, or American Welding Society (AWS) BAlSi-4 filler metal by either vacuum metallizing or electroplating prior to brazing is effective for improving wettability. For example, a vacuum-deposited titanium coating can be very effective in promoting wetting on beryllium. This coating drastically changes the surface of the beryllium and promotes extensive spreading and wetting when pure aluminum filler metal is used. Reoxidation of the precleaned surface can be prevented by applying a thin film of amyl acetate, which readily burns off at brazing temperatures [American Welding Society 1991]. Painting of titanium hydride may be used instead of vapor depositing. The hydride is mixed with commercial brazing cement (polyethyl methacrylate and 1,1,1-trichloroethane). The cement decomposes during brazing in vacuum at approximately 540 °C (1005 °F). The hydride decomposes at 660 °C (1220 °F), leaving a layer of titanium on the surface [American Welding Society 1991].

23.2.4 Filler Metals

Beryllium reacts with the constituents of most filler metals used for brazing, which may result in the formation of undesirable intermetallic compounds. Grain-boundary penetration into the beryllium may also be a problem. Brazing should be done under conditions that minimize the formation of intermetallic compounds: rapid heating and cooling cycles, low brazing temperatures, minimum time at brazing temperatures, and minimum amounts of filler metal. Beryllium reacts with oxygen and atmospheric nitrogen at conventional brazing temperatures. Oxidized or nitrided surfaces will impair the wettability and flowability of filler metals. Beryllium assemblies braze best in argon or helium gas. The choice of a specific filler metal or the need for a specific design can limit the choice of the optimum brazing procedures. Beryllium can be wetted directly by aluminum brazing alloys. Many of the filler metals, however, do not wet or flow well on beryllium. As a result, the filler metal must frequently be preplaced between the joint members in amounts sufficient to produce the brazed joint. Longer brazing times than desired may be required to ensure proper wetting and flow of the filler metal, which may adversely affect the joint properties. Surfaces may be plated with silver to improve wettability and flowability of the filler metals. In general, preplacement of the filler metal is recommended. Even so, outside corners and edges of the joint may show a lack of adequate filler metal flow, simulating a notch. Because of the severe notch sensitivity of beryllium, such

defects may have to be machined to a smooth surface after brazing.

Filler metals with narrow melting ranges or eutectic compositions, which behave similar to a pure metal during melting, are best for applications having small joint clearances (25 to 80 μm). With filler metals having a wide melting range, separation of solid and liquid phases may occur when using too slow a heating rate during brazing [American Welding Society 1991]. The compositions of the solid and liquid continually change as the temperature rises, because the liquation (initiation of melting) temperature of the unmelted (solid) portion rises, while the liquation temperature of the corresponding liquid portion decreases. Under these conditions (approaching equilibrium), there is sufficient time for some of the lower-melting liquid portion to escape, leaving behind an unmelted "skull" of the higher-melting solid, since its liquation temperature may be at the brazing temperature. This behavior is more likely to occur with a preplacement filler.

Metallurgical compatibility between the filler metal and beryllium as well as with any mating materials is mandatory. The likelihood of forming brittle intermetallic compounds, for example, beryllides, must be avoided. Only four metals do not form stable beryllides below 760 °C (1400 °F): aluminum, silicon, silver, and germanium [Grant 1979]. Intergranular penetration into hot pressed beryllium block was found not to be harmful. A two-phase structure formed consisting of primary beryllium grains surrounded by a silver matrix. Very limited mutual solubility, especially of beryllium in silver, exists between the two elements. This microstructure is reported as exhibiting outstanding strength and toughness properties [Grant 1979]. The penetration of silver into beryllium as a function of time above 760 °C (1400 °F) is shown in Fig. 23.12.

Filler metals used for brazing beryllium include silver, silver-base alloys, aluminum, and aluminum-silicon alloys. Silver and silver-base filler metals, such as BAg-18 (Ag-30wt%Cu-10wt%Sn), BAg-19 (Ag-7wt%Cu-0.2wt%Li), and BAg-8a (Ag-28wt%Cu-0.2–0.5wt%Li), are used for high-temperature applications. Lithium is added to the filler metal to improve wettability. It has been suggested that silver alloyed with less than 8 wt% Cu exhibits an improvement in wettability over that of unalloyed silver [Jacobson 1986]. The aluminum-silicon filler metals, such as BAlSi-2 (7% Si) and BAlSi-4 (12% Si), can provide high-strength brazed joints for service at temperatures up to 150 °C (300 °F). These are suitable for high-strength wrought beryllium because the brazing temperatures are below the recrystallization temperature of beryllium. However, these fillers exhibit poor flow behavior in capillary joints and must be preplaced in the joint. Another filler metal suitable for beryllium is 64Ag-34Cu-2Ti [American Welding Society 1991]. Silver-copper fillers that melt at relatively low temperatures may exhibit less grain-boundary penetration, although both elements can form brittle intermetallics at temperatures below the melting point of these fillers. These intermetallics cause low joint strengths.

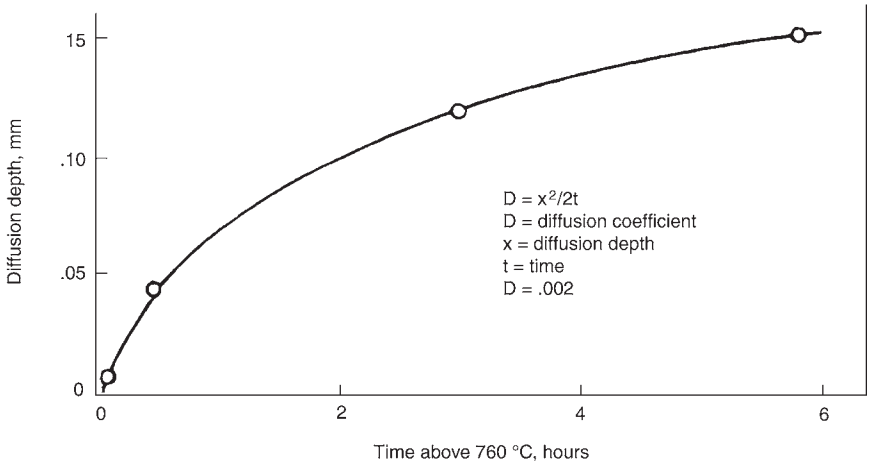

Fig. 23.12 Diffusion depth of silver from BAg-18 into beryllium as a function of brazing time just above 760 °C. Source: Grant 1979

Normally, at Lawrence Livermore National Laboratory (LLNL), silver and silver-base filler metals are used for high-temperature application; Ag-7Cu-0.2Li is an example. Small amounts of lithium may be added to pure silver to improve its wettability. Metallurgical problems related to excessive alloying, grain-boundary penetration, and intermetallics can be avoided or minimized by using copper-silver fillers that have small amounts of additives of either tin or lithium [American Welding Society 1991]. Silver brazing has many advantages over aluminum brazing. Many of the original beryllium brazing studies were done with silver [Grant 1979]. Silver brazing provides the ability to join beryllium to stainless steels and other alloys. Its major disadvantage is to cause a degradation of wrought beryllium sheet products by recrystallization when the brazing temperature exceeds 730 °C (1345 °F). Two filler metals currently being used at LLNL for vacuum brazing are Cusil (72wt%Ag-28wt%Cu eutectic) and Incusil-ABA (59.0wt%Ag-27.25wt%Cu-12.5wt% In-1.25wt%Ti); the "ABA" stands for active braze alloy. Cusil and Incusil are used to braze beryllium mainly to Monel; Cusil is also used for brazing to stainless steel. Additional braze compositions that have been used to vacuum braze beryllium joints are Ag-5wt%Pb, Ag-15wt%Pb-20wt%Cu, Cu-18wt%Pb, and Ti-6wt%Be.

Brazing-temperature ranges for several brazing-alloy compositions are given in the American Welding Society's handbook [American Welding Society 1991]:

- Zinc: 427 to 454 °C (800 to 850 °F)
- Aluminum-silicon: 566 to 677 °C (1050 to 1250 °F)
- Silver-copper: 649 to 904 °C (1200 to 1650 °F)
- Silver: 882 to 954 °C (1620 to 1750 °F)

Fluxes are essential in producing brazed joints when not using an inert atmosphere or vacuum. An important function is to dissolve and remove oxides present or formed during brazing. The flux must, however, be readily displaceable by the molten filler metal, and thus, it must have a sufficiently low viscosity. A flux consisting of 60wt%LiF-40wt%LiCl and one consisting of a tin chloride compound have produced good results when used for furnace or induction brazing [American Welding Society 1991]. However, these two fluxes should not be used when brazing in vacuum. Fluxes may also be used to prevent oxidation or eliminate oxides during low-temperature brazing in air.

Following brazing, the joint must be cleaned to remove any flux residue and any oxide scales that may have formed. Removal of flux residue is especially important, since many fluxes are chemically corrosive. Residual flux is removed with a hot water wash. If necessary, a wire brush may also be used.

23.2.5 Joint Design

Joint design, filler metal selection, and choice of brazing cycle are complicated due to the low ductility of beryllium as well as its reactivity with many of the filler metals used for brazing. The low ductility of beryllium is aggravated by the presence of structural discontinuities such as surface scratches, notches, and asymmetrical stress patterns produced by single-lapped joints. Joint configurations such as butt, scarf, step, and double-lap joints should be considered when designing beryllium joints [American Welding Society 1991]. Preferably, joints that contain no notches should be used to achieve maximum reliability [Schwartz 1983]. Asymmetrical stress patterns, such as those produced by single-lap joints, should be avoided.

The joint should be designed for proper stress distribution as well as accessibility for capillary flow of the filler metal when the parts are aligned for brazing. The design should provide for loads to be accommodated mainly by shear stresses across the deposited filler metal. The spacing between the mating surfaces must be sufficiently small to allow the filler metal to cover the entire surface by capillary action. A minimum amount of filler metal should be used, since a thin film of filler metal also provides for triaxiality strengthening. (Triaxiality results from the constraints imposed on the thin filler metal interlayer by the mating surfaces. Transverse stresses are imposed on the layer and keep it from contracting, which must occur in order for the layer to deform, or elongate, in the tensile direction. Thus, the tensile deformation of the layer follows along with the elastic tensile deformation of the beryllium mating parts.) Sufficient clearance, however, must be available to allow the escape of molten flux and gases during heating. Differences in the coefficient of expansion of the components must be taken into account.

Some examples of joints are shown in Fig. 23.10, 23.13, and 23.14. Additional illustrations

of joints are presented in section 23.3, "Solid-State Bonding," in this chapter.

23.2.6 Test Results of Brazed Joints

Screening tests of lap-shear specimens were performed to evaluate the potential use of four brazing alloys with beryllium for use at temperatures up to 650 °C (1200 °F) [Marschall 1990]. Information on the alloys is listed in Table 23.1. The shear strength results are shown in Fig. 23.15. Cusil ABA performed poorly, even at room temperature, due to poor wettability during brazing. Furthermore, many of the specimens brazed with this alloy frequently separated during final machining. Two of the alloys, BAg-18 and BAg-19, were further tested in compression panels. The results are shown in Fig. 23.16. BAg-18 was chosen over Palcusil-15 because its braze temperature had a much less degrading effect on the beryllium-base metal.

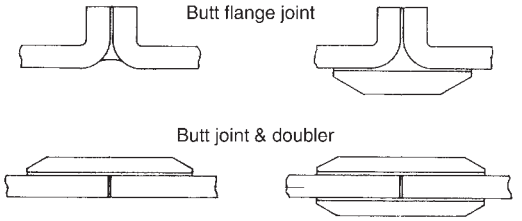

Fig. 23.13 Butt-joint designs for sheet metal brazements. Source: American Welding Society 1991

The mode of failure of the compression panels ranged from catastrophic brittle failure at lower temperatures to buckling at the higher temperatures. The shear strength as a function of temperature and braze thickness for a zinc-brazed beryllium is shown in Fig. 23.17 and 23.18, respectively.

An evaluation of silver brazing was performed by braze cladding a 50 μm thick foil of BAg-19 brazing alloy wrapped around a standard tensile bar, as depicted in Fig. 23.19. Only minor differences were seen in the tensile properties between the as-received (hot pressed) condition, following a brazing cycle only, and following the same brazing cycle that produced a brazed cladding. Results are given in Table 23.2 [Grant 1979]. In an attempt to avoid recrystallization by lowering the brazing temperature, a series of brazed beryllium specimens were made using a BAg-18 braze foil. Brazing was accomplished under a pressure of 1 to 3 kPa over a range of temperatures from 590 to 760 °C (1095 to 1400 °F), with times ranging from 2 to 45 min. Specimens were tested in single-lap shear. Optimum shear strengths ranging from 213 to 320 MPa were achieved at a brazing temperature of approximately 650 °C (1200 °F). Metallographic evaluation of a parallel study with BAg-18 braze alloy showed that higher strength values and lesser times led to minimum intermetallic formation; however, higher temperatures led to the formation of voids

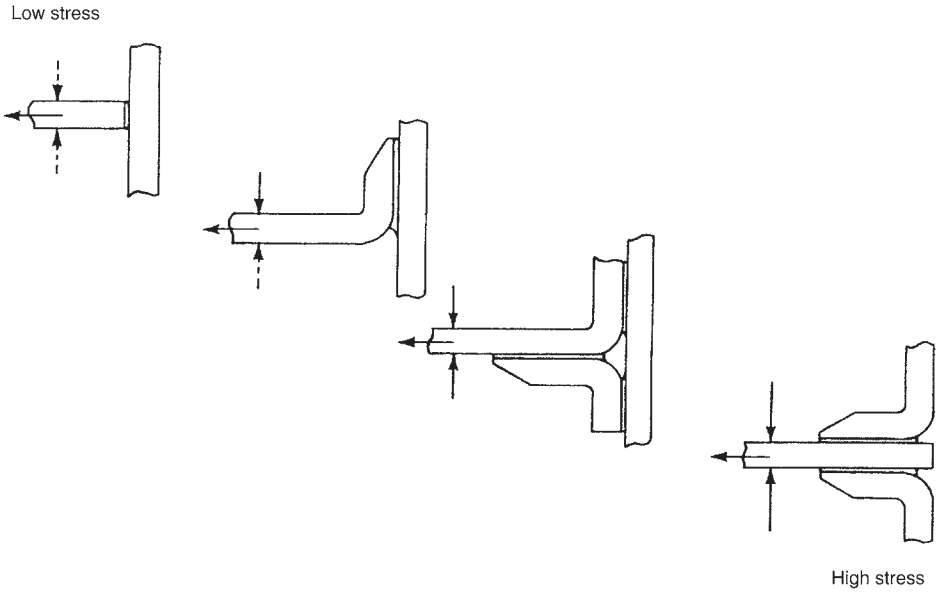

Fig. 23.14 Tee-joint designs for sheet metal brazements. Source: American Welding Society 1991

Table 23.1 Beryllium braze alloy compositions

American Welding Society class	Indicated element (nominal), wt%						Rationale for selection
	Ag	Sn	Li	P	Pd	Ti	
BAg-18	60	10	...	0.025	...	...	Extensive prior use
BAg-19	92.5	...	0.3	...	...	...	Higher silver contents expected to promote high-temperature strength
Palcusil 15	65	...	...	...	15	...	Palladium addition expected to increase strength and allow filling of large gaps and spanning of large braze interfaces
Cusil	63	...	...	...	...	1.5	Titanium addition expected to gather oxygen from surfaces and produce higher-strength joints

Source: Marschall 1990

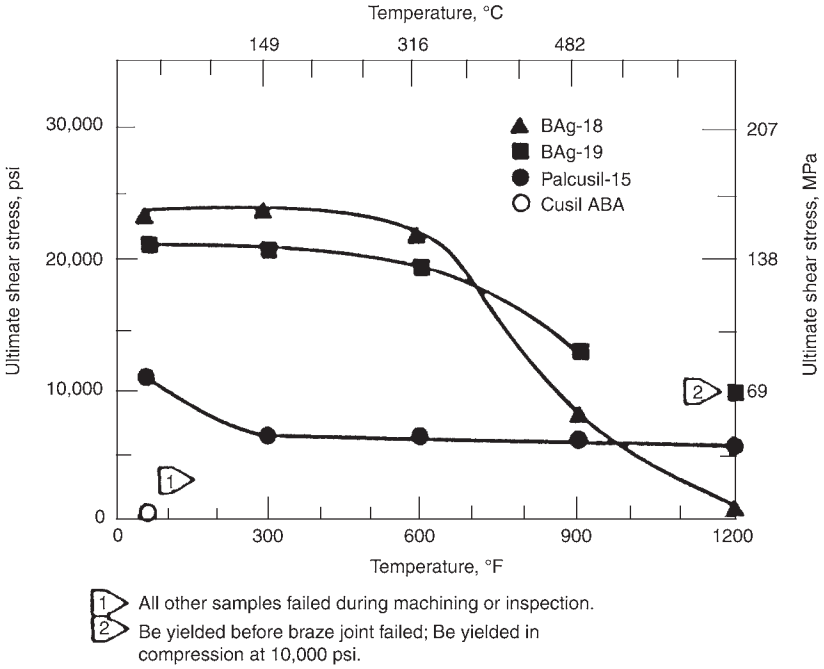

Fig. 23.15 Ultimate shear stress versus test temperature for lap-shear specimens of beryllium brazed to beryllium. Source: Marschall 1990

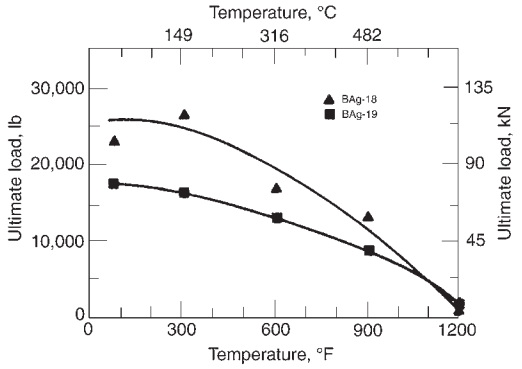

Fig. 23.16 Results of compression panel tests for two brazing alloys used with beryllium. Source: Marschall 1990

(Kirkendall voids) and more intermetallics due to the presence of the copper in the braze alloy [Grant 1979]. (The Kirkendall effect originally described the movement of an interface between two different bonded materials due to the unequal rate of diffusion of atoms from each material across the interface. Thus, one material had a net gain of atoms, while the other material lost atoms (mass). Similarly, the net microscopic movement of atoms locally can result in voids.) This effect can be seen from Fig. 23.20. A number of beryllium pin-and-base shear specimens (Fig. 23.21) with BAg-19 brazing alloy were brazed at 900 °C (1650 °F) for 10 min, followed by either 0.5 or 3 h at 760 °C (1400 °F). Brazed joints were made of several combinations of

three different grades of beryllium using BAg-19 brazing alloy. The brazed joints showed considerable scatter, with no consistent trends. The shear values ranged between a low of 171 MPa to a high of 301 MPa, with an average of 243 MPa [Grant 1979].

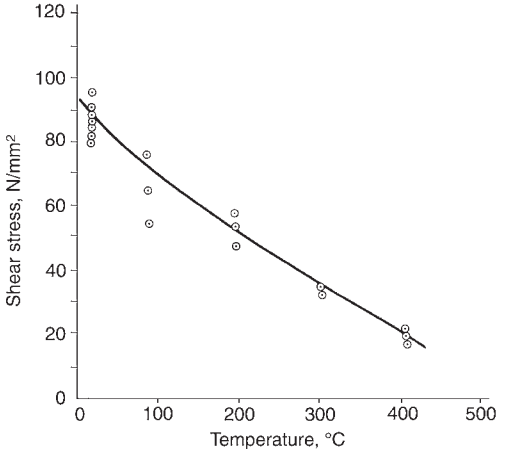

Fig. 23.17 Shear strength versus temperature for a zinc-brazed beryllium joint. Source: Marschall 1990

Aluminum-base brazing alloys are widely used fillers for brazing beryllium. Because of the lower brazing temperature that is used with these brazing alloys, the likelihood of recrystallization in beryllium, which occurs when brazing with silver-base alloys, is not a problem when brazing with aluminum-base alloys. The effect of brazing temperature, time, and joint gap on shear strength of brazed beryllium specimens using an aluminum-silicon eutectic alloy (Al-12wt%Si) is shown in Fig. 23.22, to 23.24, respectively. Figure 23.25 compares the shear strength of aluminum-brazed beryllium (EFC) with type 1100–0 aluminum as a function of temperature. Cylinder/ring push specimens, as illustrated in Fig. 23.26, were used [Grant 1979]. This design was adopted because it eliminated the tendency of the beryllium (due to its high modulus) to introduce a bending moment in conventional lap-shear specimens, which would distort pure shear values. The drop in shear strength with increasing temperature from approximately 20 to 200 °C (70 to 390 °F) parallels the drop in tensile strength in annealed pure aluminum.

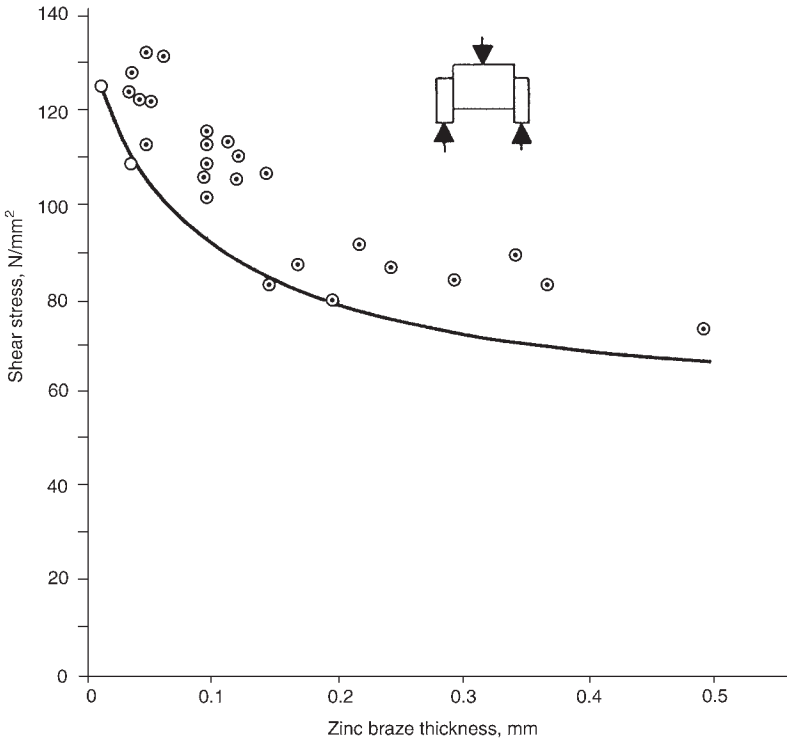

Fig. 23.18 Shear stress as a function of braze thickness for a zinc-brazed beryllium joint showing the specimen load configuration. Source: Marschall 1990

23.3 Solid-State Bonding

23.3.1 Introduction

Solid-state bonding is a generic term that encompasses a number of closely related processes that are dependent on diffusion, pressure, and/or deformation to different degrees and that do not involve melting. At one extreme, in deformation bonding, the transport of material takes place by mechanical means and may not involve diffusion. Significant deformations are required to break up oxide films, and sufficient pressures are required to cause fresh metal surfaces to come into contact and adhere between the fragmented oxides. Transfer of material across the interface between the two mating parts does not take place (this transfer of material depends on deformation temperature), and the interface is usually clearly identifiable. At the other extreme, in diffusion bonding, bonding takes place by interdiffusion across the mating surfaces, possibly with grain growth across the boundary obscuring the original interface. The process is enhanced by some deformation, which occurs due to the applied pressure, because it aids in achieving contact between the two surfaces. Surfaces must be carefully prepared to assure maximum contact between mating surfaces and to minimize interference with the diffusion process. For example, deformation bonding can be insensitive to a rough surface, whereas diffusion bonding requires a clean, flat, microscopically smooth surface. Beryllium, being very reactive in ambient atmospheres, forming oxides and nitrides, should be joined under vacuum when possible.

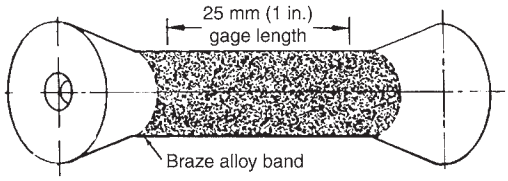

Fig. 23.19 Standard round tensile bar for evaluating BAg-19 brazing alloy foil that was braze-clad onto hot pressed block beryllium. Source: Grant 1979

The absence of a liquid phase and the lower process temperatures (relative to fusion processes) lead to several advantages for solid-state processes, especially those that do not involve any significant amount of deformation, including:

- Mechanical properties approaching base metal properties
- Reduced joining temperatures
- Minimum (or no) grain growth, depending on temperature
- Absence of cast microstructures
- Limited distortion
- Numerous welds can be made simultaneously.
- Bonding ability is largely independent of part thickness.
- Reduced weight relative to weldments obtained when using fillers
- Better heat transfer relative to that obtained when using fillers
- Joining and heat treating can occur simultaneously.
- More flexibility in joint design
- Less fixturing relative to that required in fusion processes

Some disadvantages may exist for processes in which the bonding relies mainly on diffusion:

- Long process times may be required.
- Increasing process temperature to reduce process time may cause excessive creep.
- Increasing process temperature to reduce time may induce undesirable microstructural changes.
- Increased heat and pressure requirements may increase costs.

Numerous solid-state bonding processes are available; some are referred to by different

Table 23.2 Surface-braze test results for BAg-19 brazing alloy (50 μm thick foil) braze-clad on hot pressed block (HPB) beryllium

Condition(a)	Yield strength, MPa	Tensile strength, MPa	Elongation, 25.4 mm gage, %
As-received HPB (hot pressed Be)	254	308	1.2
As-received HPB	267	347	2.7
Braze cycle only	242	351	2.8
Braze cycle only	239	320	1.7
Brazed with 6 mm band of BAg-19 foil	244	337	2.0
Brazed with 6 mm band of BAg-19 foil	240	311	6
Brazed with total band of BAg-19 foil	245	333	7
Brazed with total band of BAg-19 foil	222	373	8

(a) Braze cycle: 10 min at 900 °C (1650 °F) plus 3 h above 760 °C (1400 °F) in purified argon. Source: Grant 1979

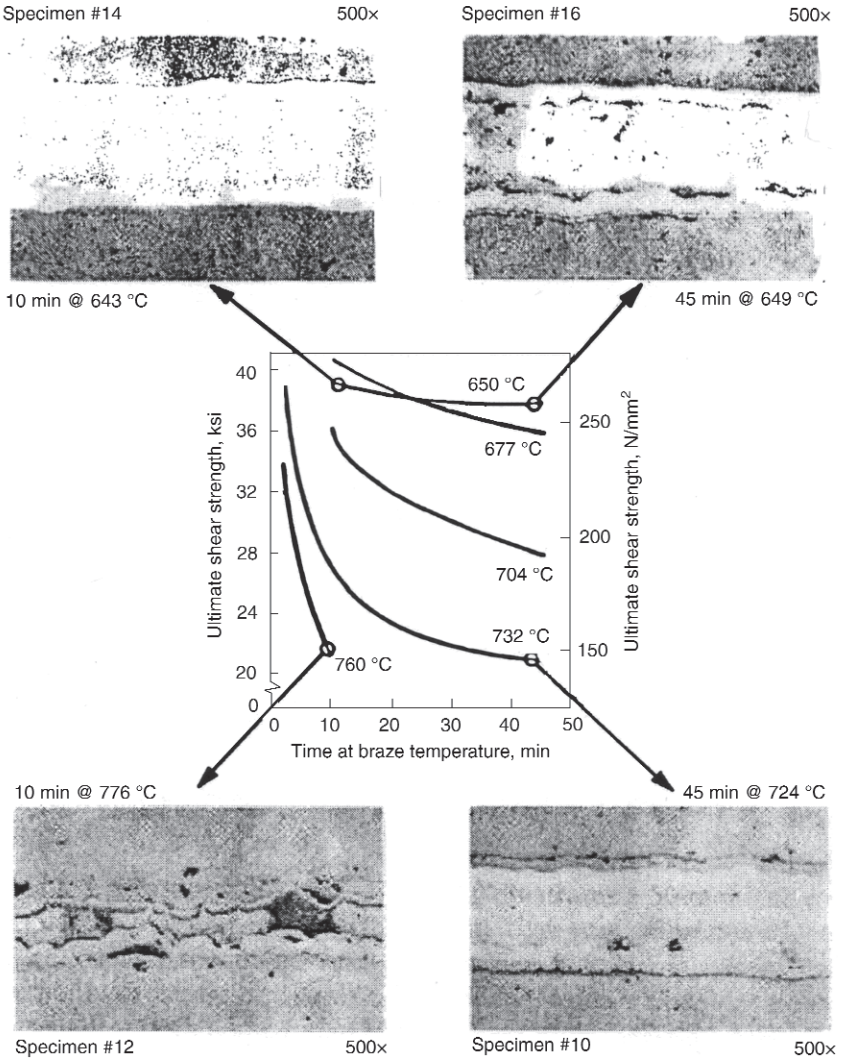

Fig. 23.20 Effect of brazing temperature and time on strength and braze joint microstructure of beryllium sheet brazed with BAg-18 alloy. (Microstructures reproduced at approximately 50 wt%). Source: Grant 1979

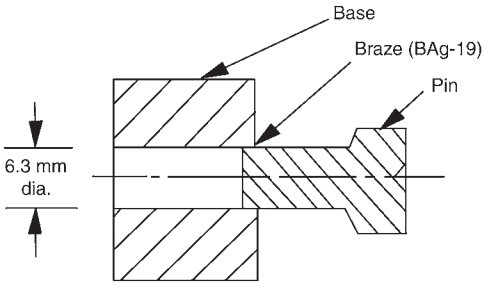

Fig. 23.21 Base-and-pin shear specimen used for testing BAg-19 brazing alloy. Source: Grant 1979

names, and the terms *welding* and *bonding* have been used interchangeably. Some examples are:

- Gas-pressure bonding—a diffusion process using pressurized gas
- Press bonding—joining pressure applied by a press
- Pressure bonding—any method that uses pressure to complete the bonding process
- Vacuum bonding—joining performed in a vacuum
- Forge welding—application of heat and pressure using a forging press

- Roll bonding—deformation bonding by rolling
- Explosive bonding—deformation bonding induced by shock waves
- Cold welding—pressure used to initiate the bond
- Differential thermal expansion (DTE) bonding—pressure induced by DTE of materials, either between mating parts or parts and fixture

23.3.2 Bonding Mechanisms

Diffusion bonding can be achieved either by having the workpieces in direct contact with each other or by having a very thin intermediate metal layer between the workpieces. In both cases, at times referred to as direct diffusion bonding and indirect diffusion bonding, respectively, the joint is heated to an elevated temperature and placed under pressure. Heating cycle times for processes can run from 4 to 5 h, with at least ½ h at the maximum temperature. Temperatures typically range from 815 to nearly 1100 °C (1495 to 2010 °F), with bonding pressures from approximately 35 to 70 MPa. Applied loads are usually considerably greater for the indirect process as compared to those used in the direct process. In both cases, mating surfaces must be clean and flat. A flatness of better than a half wavelength of light (0.3 μm interference) is generally recommended, especially for the direct diffusion process. Surface perturbations or lack of flatness can result in uneven

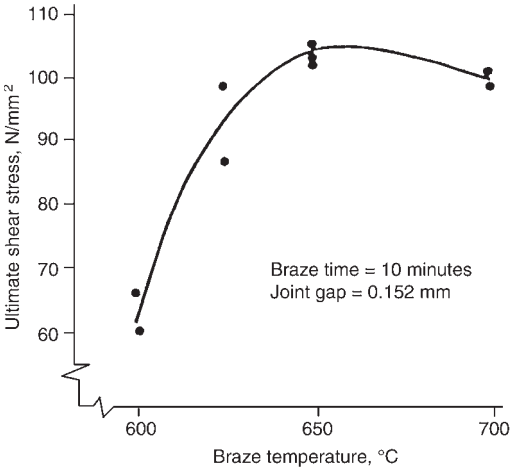

Fig. 23.22 Shear strength versus brazing temperature for aluminum-brazed beryllium. Source: Grant 1979

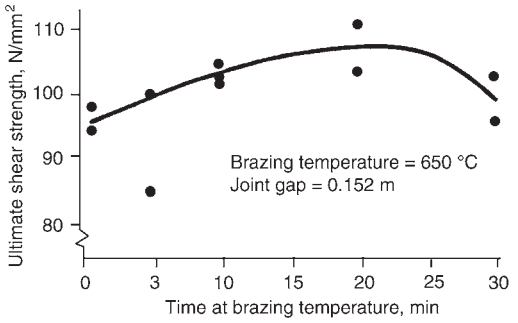

Fig. 23.23 Shear strength as a function of time at brazing temperature for aluminum-brazed material. Source: Grant 1979

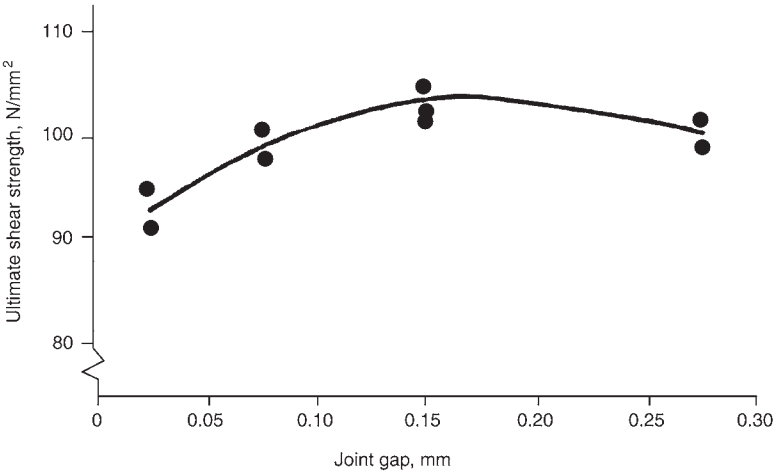

Fig. 23.24 Shear strength as a function of joint gap for aluminum-brazed beryllium. Source: Grant 1979

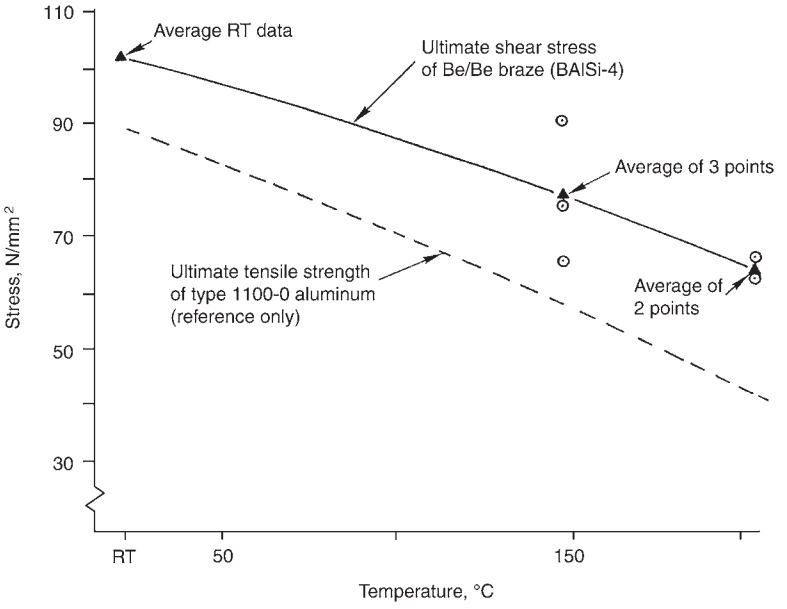

Fig. 23.25 Shear strength as a function of temperature for aluminum-brazed beryllium (EFC) . Source: Grant 1979

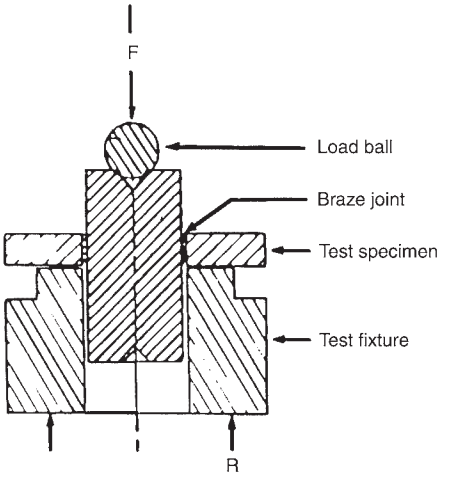

Fig. 23.26 Schematic illustration of cylinder/ring push specimen and test fixture for shear testing of brazed joints. Source: Grant 1979

bonding due to nonuniform pressures along the interfaces at the bonding temperature. An intermediate soft metal layer assures cleanliness as well as reduces problems due to surface asperities. The intermediate layer can also improve joint strength.

In addition to cleanliness, the oxide film normally present on beryllium must first be removed or penetrated before interdiffusion can take place between the metals in contact. Oxides can be removed, to a large degree, by abrasion or etching. The shearing deformation that occurs on the application of pressure during the solid-state diffusion process aids in furthering the breakup of the oxide films. It has been demonstrated that there is an optimum microscopic roughness for the most effective oxide breakdown. Furthermore, surfaces bonded at an angle to the load produced stronger bonds than those bonded normal to the load, especially for small deformations [Olson and Liby 1979]. In heating up the workpieces, care is taken that the elastic limit is not exceeded. Typically, only a light load is initially applied, which may be monitored (and even reduced) during heating; the required bonding load is then applied on reaching the bonding temperature.

Several mechanisms have been proposed for the bonding process [Olson and Liby 1979]. In one proposal, the stress resulting from the pileup of dislocations at the metal-oxide interfaces that are favorably oriented for plastic flow causes cracking of the oxide film and exposes the bare metal. When cracking and breakup of the oxide occurs on both sides of the interface and forms gaps where both bare metals are in contact, plastic flow occurs across these gaps, providing intimate contact for diffusion. In another proposal, it is suggested that the bonding

process occurs by void formation followed by void shrinkage, which is illustrated in Fig. 23.27. Initially, the applied pressure produces interface regions of intimate contact and irregularly shaped voids. The drive for minimization of surface free energy results in the voids tending toward a spherical shape through bulk and surface diffusion. With time, these voids will shrink and disappear. Generally, the greater the roughness of the surfaces, the longer the time required for the bonding process.

It was suggested that direct diffusion bonding requires temperatures of the order of 1120 °C (2050 °F) and applied stresses of approximately 10 kPa [Jacobson 1986]. Olson and Liby [1979] stated, however, that clean beryllium surfaces may be bonded together at temperatures as low as 700 °C (1290 °F), provided that the bonding time and pressure are sufficient. Lap joints in beryllium sheet and plate can be diffusion welded at 760 °C (1400 °F) or above with a minimum applied pressure of 10.3 MPa. A minimum deformation, ranging from 5% for 1.6 mm (0.06 in.) thick sheet to 15% for a 6.4 mm (0.3 in.) thick plate, is required to obtain a strong weld. The welding conditions and joint strengths appear to be related to the purity of the metal and the cooling rate from the bonding temperature. Cracking, excessive grain growth, and other problems associated with fusion welding are avoided with diffusion bonding.

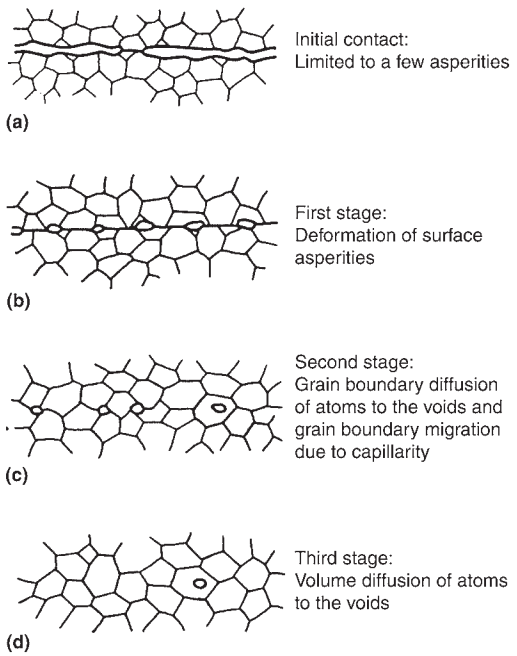

Fig. 23.27 Schematic of proposed stages of solid-state bonding. Source: Olson and Liby 1979

Bonds made at temperatures above 1000 °C (1830 °F) may suffer a loss of properties due to excessive grain growth. Furthermore, a high BeO content may interfere with the bonding process, and other impurities may influence bonding through precipitation reactions. Since diffusion rates increase exponentially with temperature, bonding times could be correspondingly reduced with increasing temperatures. If an intermediate metal is used between the beryllium parts, the maximum temperature would be limited by the possibility of forming undesirable intermetallics or a low-temperature liquid phase; for example, the silver-beryllium and aluminum-beryllium phase diagrams exhibit eutectic liquid at 881 and 645 °C (1615 and 1190 °F), respectively.

Results obtained by a number of investigators on direct diffusion bonding of beryllium are summarized in Table 23.3 [Olson and Liby 1979]; in their paper, Olson and Liby reviewed the results obtained by several of these investigators. Three studies reviewed in the Olson and Liby paper illustrate important aspects of solid-state bonding of beryllium.

Bonding of hot pressed and extruded QMV-grade beryllium with surfaces that were metallographically polished (some surfaces were only finish ground on 180-grit paper) was studied by Passmore [Olson and Liby 1979]. High-strength bonds were obtained with the polished specimens even though very little plastic deformation or disruption of the original surfaces was observed on the fractured surfaces. Maximum strengths were obtained by bonding in the range of 900 to 1000 °C (1650 to 1830 °F). The lower bond strengths were attributed to the lower diffusion rates and the higher material yield strengths at the lower bonding temperatures and to recrystallization at the higher bonding temperatures.

Parent metal strengths following solid-state bonding were obtained by Hodge et al. [Olson and Liby 1979]. The bonding was accomplished by sealing the assembled components in an evacuated expandable container that was placed into a high-pressure autoclave. The container was then subjected to isostatic pressure using an inert gas. Optimum bonding was obtained at 850 °C (1560 °F) for 4 h. Tests were formed at temperatures of 843 to 954 °C (1550 to 1750 °F) for 2 to 4 h. Prior blasting of the surfaces with chilled iron grit enhanced the bonding. The localized deformation introduced by the blasting

Table 23.3 Direct diffusion bonding of beryllium

		Bonding conditions									
		Temperature		Pressure				Maximum strength			
Investigators	Material	°C	°F	MPa	ksi	Time, h	Atmosphere	MPa	ksi	Comments	References(a)
Martin	Be	900–1200	1650–2190	Contact		2.5	Vacuum	193	28	Found transinterfacial grain growth	3
Atkins	Be	200–800	390–1470	Above yield		. . .	Argon	. . .		Determined temperature deformation curve for bonding beryllium	3
Monroe	Be	850	1560	20.7	3.0	. . .	. . .	275	40	Butt-welded rods	3
D'Annessa	Be	885	1625	13.8	2.0	0.25	Vacuum	. . .		. . .	5
Batzer and Bunshah	Be with 2% BeO	200–400	390–750	27.6–103	4.0–15	1	Vacuum	51	7.4	Ion bombardment surface cleaning	6
Hodge et al.	Be	843–954	1549–1749	69	10	2–4	Air	251	36	Surface treatment only	7
Bosworth	SR-200D PR-200D	730–790	1345–1455	10.4	1.5	3–6	Vacuum	379 Shear	55	Studied role of microalloying elements	15, 16
Hauser et al.	Be + 1–1.7% BeO	750–850	1380–1560	7–100	1.0–14.5	1–12	Vacuum	427	62	. . .	17
Albom	Be	800–1500	1470–2730	. . .		1	Vacuum	. . .		100% joint efficiencies have been achieved in butt joints.	1
Passmore	QMV hot pressed Be	800–1150	1470–2100	Above yield		1	Vacuum	275	40	Specimens were loaded by thermal expansion.	4
Passmore	QMV extruded Be	800–1150	1470–2100	Above yield		1	Vacuum	414	60	Difference between molybdenum clamps and beryllium	. . .

(a) Refers to references listed in Olson and Liby [1979]. Source: Olson and Liby 1979

promoted recrystallization at and grain growth across the interface [Hodge et al. 1966].

Solid-state bonding studies were performed on beryllium sheet containing 0.97 and 1.70 wt% BeO [Hauser et al. 1965]. Surface preparation was limited to chemical etching. Bond strengths exceeding 90% of the base metal properties at room temperature were obtained for the low-oxide material by bonding in the temperature range of 760 to 780 °C (1400 to 1435 °F) for 3 h under a pressure of 10.3 MPa. Such results were not achieved with the high-oxide material. In joining sheet material, the bond strength is influenced by the sheet thicknesses and their impurity content, especially BeO.

23.3.3 Intermediate Layers (Indirect Bonding)

An intermediate metal layer may be used to provide a clean mating surface as well as to reduce the effects of surface asperities. Nickel, gold, and silver are the main metals that are used for such purposes. Copper and copper alloy foils have also been used successfully. The intermediate layer may either be deposited on the beryllium mating surfaces or placed between the two surfaces. Silver-coated beryllium bonds usually produce excellent joints, with the failure most often occurring along the silver-silver interface. Silver, which does not form a very stable oxide, can be deposited on the beryllium by either electroplating or vacuum evaporation (deposition). Electron beam evaporation or magnetron sputtering evaporation are the two techniques most commonly used. Hot hollow cathode sputtering evaporation, which had previously been widely used in large-scale production, is less common now. With the latter technique, relatively thick deposits were formed, which were subsequently reduced to the desired thickness by machining. Machining stresses may be eliminated by annealing prior to bonding. Beryllium tensile specimens that were bonded together using electrodeposited silver have achieved strengths as high as 441MPa, with fracture occurring in the beryllium rather than in the joint [Olson and Liby 1979].

When a thin, separate layer is bonded to the beryllium and uniaxially loaded normal to the plane of the bond, the layer behaves mechanically similar to the beryllium in the elastic range of the beryllium. Because of the triaxial stress state developed in the thin layer, the layer is prevented by the beryllium from contracting (deforming) in the direction normal to the loading axis, even though the layer material may have a lower yield strength than the beryllium. Subsequent relaxation, which is due to the loss of stress triaxiality as beryllium yields, limits the joint strength, and fracture may occur in the layer. The same restraints may develop with a deposited layer.

The thinner the layer, the greater and more effective are the restraints. Table 23.4 lists the results of a number of investigations that experimented with bonding beryllium using intermediate layers [Olson and Liby 1979]. In their paper, the authors reviewed the results obtained by several of these investigations. Some of the details are presented in the following discussion.

Silver as an intermediate layer for solid-state bonding at relatively low temperatures was first demonstrated by Knowles and Hazlett [1970]. They bonded S-200C beryllium plated with a 12.7 μm thick layer of silver at 107 °C (225 °F) under a bonding pressure of 207 MPa (30 ksi) and obtained a bond strength of 120 MPa (17 ksi). They noted that over the bonding temperature range of 107 to 138 °C (225 to 280 °F), the bond strengths were insensitive to the environment, whether in vacuum (0.1 mPa, or 10^{-6} torr), helium, air, or oxygen. They also noted that the bond strength increased linearly with the plated-silver thickness with thicknesses, ranging from 14.7 to 76 μm. (The relationship also held for samples bonded at 204 °C, or 399 °F.) This increase is contrary to the effect normally observed, namely, that the triaxiality increases, and thus also the strength, with decreasing thickness of the interlayer. They attributed this contradiction to the increase in contact area obtained with increasing interlayer thickness [Knowles and Hazlett 1970]. The start of a rapid increase in bond strength with increasing bonding stress that occurred after plastic strain initiation was observed. This increase in bond strength was attributed to a corresponding increase in bond area with an increase in plastic strain. The plastic strain of the sample was measured adjacent to the bond. Higher bond strengths were obtained by maintaining the bonding stress while cooling to room temperature. It should be pointed out that the aforementioned results refer to relatively low-temperature bonding. The authors conclude that the bonding at these low temperatures occurred largely by cohesion (atomic bonding forces between surfaces in contact) rather than by diffusion. The limited role of diffusion was supported by the independence of

Table 23.4 Diffusion bonding of beryllium with intermediate layer

Investigators	Material	Bonding conditions: Temperature °C	Temperature °F	Pressure MPa	Pressure ksi	Time, h	Atmosphere	Intermediate layer	Maximum strength MPa	Maximum strength ksi	Comments	Reference(a)
Hauser, Howden, and Monroe	Be with 1–2% BeO	800	1470	17–32	2.5–8.6	4–6	Vacuum	Al, Al-Si	207	30	Aluminum intermediate foils did not assist bonding.	17
Hauser, Howden, and Monroe	Be with 1–2% BeO	. . .		. . .		. . .	Vacuum	Ni, Ni-Cu	Brittle		Nickel and copper-nickel foils resulted in brittle joints.	17
Knowles and Hazlett	S-200C	107–199	225–390	29	4.2	0.008–4	Vacuum, helium, and oxygen	Ag	275	40	Strength not a strong function of environment	8
O'Brien, Rice, and Olson	S-200E	200	390	138	20	0.167	Air	Ag	434	63	Both electroplated and vapor-deposited silver were used.	22
Naimon, Vigil, Villegas, and Williams	S-200E	200	390	138	20	0.167	Air	Ag	324	47	Study made of ion bombardment cleaning prior to coating	24

(a) Refers to references listed in Olson and Liby [1979]. Source: Olson and Liby 1979

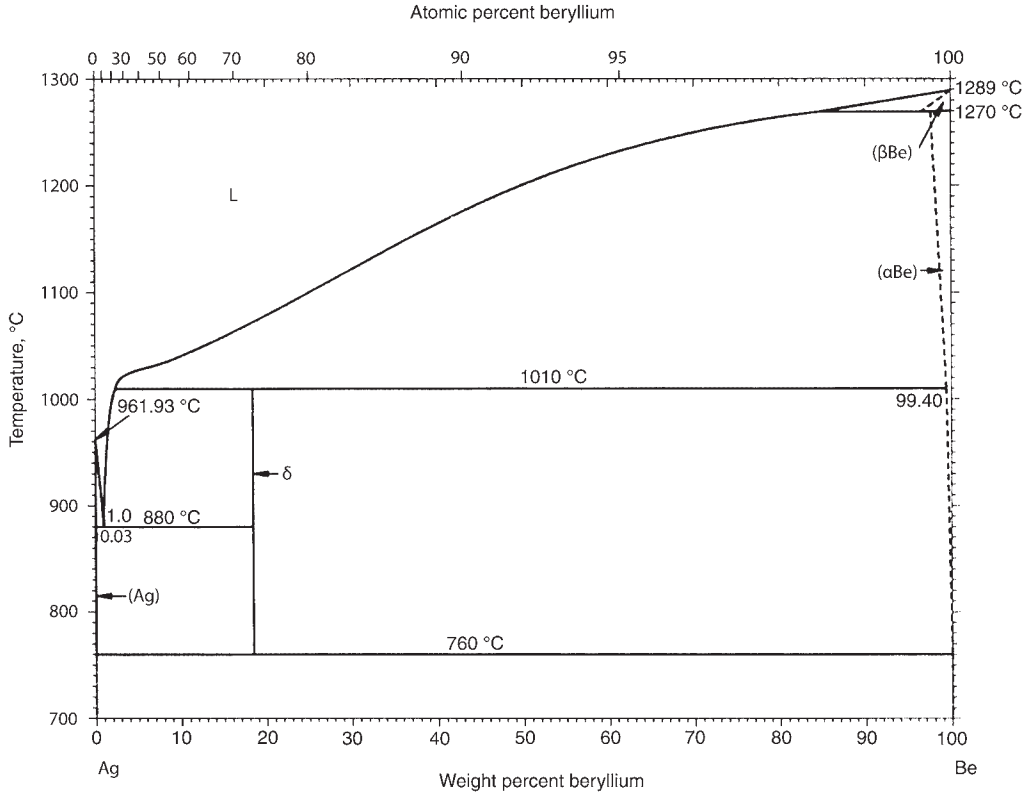

Fig. 23.28 Silver-beryllium phase diagram. Source: Massalski et al. 1990

bond strength on the time at the bonding temperature; the cohesion concept was supported by a linear relationship between bond strength and bonding pressure [Knowles and Hazlett 1970].

The silver-silver bond strength can be as high as 690 MPa, or approximately double the strength of beryllium [O'Brien et al. in Olson and Liby 1979]. This result was obtained by tensile testing silver-coated, solid-state-bonded, high-strength maraging steel in a manner ensuring that failure would occur at the silver interface. They also noted that the strength of the joint increased with decreasing joint thickness due to the increased restraint. With extremely thin layers, however, the strength can be reduced because of surface roughness, and lack of cleanliness reduces the effective contact area. In contrast to the successful bonding obtained at 107 °C (225 °F) reported by Knowles and Hazlett, O'Brien et al. found that the strength of silver bonds was drastically reduced for bonding temperatures below 150 °C (300 °F). At a bonding temperature of 400 °C (750 °F), similar bond strengths were obtained for both 1 and 10 min periods, suggesting that the bonding kinetics are extremely fast at this temperature. They also reported that a threshold bonding pressure was required to obtain an acceptable bond, and there was no bond strength improvement above this pressure (e.g., 69 MPa, or 10 ksi, at 200 °C, or 390 °F). Bonding pressures that are too high can reduce the bond strength due to edge deformation, which results in a reduction of contact area. As can be seen from the silver-beryllium phase diagram in Fig. 23.28 [Massalski et al. 1990], bonding temperatures should be kept below 760 °C (1400 °F) to avoid introducing the intermetallic delta (δ) phase, $AgBe_2$.

23.3.4 Surface Preparation

Adhesion of the silver coating to the beryllium substrate is essential for achieving reliable bonding. In studies using a hollow cathode source, the adhesion of the silver coating was found to be a function of the substrate current and bias. Lower currents and voltage levels may result in weaker adhesion of the silver to the beryllium. The importance of surface cleanliness prior to

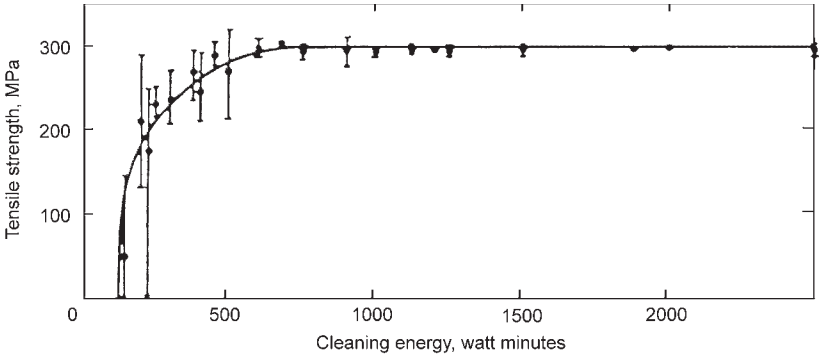

Fig. 23.29 Silver solid-state bond strength as a function of total energy used for cleaning by ion bombardment prior to silver deposition. Source: Olson and Liby 1979

coating is illustrated in Fig. 23.29, which shows the effect of cleaning energy used on bond strength during the ion bombardment cleaning stage when using the hot hollow cathode sputtering evaporation process [Olson and Liby 1979].

The application of a thin film of mercury over silver-coated beryllium was found to provide reliable, reproducible bond strengths. The mercury does not increase the maximum strength; rather, it reduces the scatter in bond strengths otherwise caused by contamination and roughness. A thin layer of mercury (e.g., 0.5 μm thick) is deposited using a cyanide electroplating solution. The mercury then rapidly migrates into the silver, forming a two-phase structure. The silver is thus strengthened by solid-solution hardening and by precipitation hardening of the silver-rich mercury precipitates. The mercury-activated silver allows reliable, reproducible, high-strength joints to be made between silver-coated parts that have been in long-time storage [Olson and Liby 1979].

A summary of various surface preparations for bonding beryllium reported by a number of investigators is given in Table 23.5 [Olson and Liby 1979]. In all cases, the first step is to obtain a flat surface. Both solvents and detergents have been used. Detergent cleaning of beryllium surfaces was shown to cause less contamination than solvent-cleaned surfaces. Corrosion pits can form if the beryllium is galvanically coupled to a more noble material, such as stainless steel, especially if chlorine ions are present in the cleaning solution. Tap water can also be a source of pitting. Corrosion pits have been identified as initiation sites of bond failures. As noted in the table, a 10% H_2SO_4 solution proved to be most effective at removing heavy oxide layers. Chemical etching that resulted in a matte surface was not conducive to achieving satisfactory bonds. Cleaning by ion sputtering facilitated direct beryllium bonding at temperatures as low as 200 °C (390 °F). Not listed in the table is the cleaning procedure used by Jacobson [1986] with a solution of 5%HF-45%HNO_3 in water. Grit blasting with chilled cast iron grit, followed by cleaning with dilute nitric acid to remove embedded grit, was found to be superior to other methods when used prior to forming joints by gas-pressure bonding. Smooth, mechanically prepared surfaces were found to recrystallize near 700 °C (1290 °F) prior to reaching the required bonding temperature and pressure. Numerous asperations were formed by grit blasting, resulting in additional deformation and causing additional recrystallization following the initial recrystallization. The two recrystallizations were accompanied by grain growth across 20 to 50% of the interface [Hauser et al. 1965]. This cleaning procedure would not be applicable when bonding under low pressures where surfaces must be flat.

23.3.5 Joint Design

The basic joints for diffusion bonding are butt and lap joints. Illustrations of various lap joints are shown in Fig. 23.30. An important consideration in designing a joint of dissimilar metals is the difference in their coefficients of thermal expansion (CTE). For example, a bar having a higher CTE than the plate to which it will be bonded should preferably be joined using an insert lap joint instead of a conventional tee joint (Fig. 23.31). Several examples of tee joints are shown in Fig. 23.32. Bond strengths can be increased by reinforcements, as illustrated in Fig. 23.30 and 23.32, or by increasing the interface area, as shown in Fig. 23.33. Joining of light

Table 23.5 Surface preparations studied for diffusion bonding of beryllium

Investigator	Grinding	Polishing	Cleaning	Etching	Inspection	Comments	Reference(a)
Passmore	Wet SiC paper	Cloth laps with levigated alumina in dilute oxalic acid	Volatile solvents	. . .	. . .	. . .	4
Hodge et al.	Both machined and abraded surfaces	. . .	. . .	Dilute H_2SO_4, dilute HNO_3-HF, or H_3PO_4-CO_3	. . .	10% H_2SO_4 appeared to be the best	7
Hodge et al.	Grit blasting	. . .	. . .	Dilute HNO_3	. . .	Promising	7
Bosworth	Machined and ground	. . .	Etch followed by hot water rinse	40% HNO_3 + 5% HF at room temperature	. . .	Etch to remove 20–25 μm from surfaces. Cleaned specimen remained exposed to shop atmosphere for 45 min before insertion into vacuum chamber.	15, 16
Albom	Wet SiC paper	Levigated Al in dilute oxalic acid	. . .	. . .	. . .	Chemical etch gave matte surface, which was not conducive to satisfactory bonding.	1
Albom	No. 1 gut emery paper	. . .	Acetone, at times followed with ether	. . .	. . .		
Hauser et al.	600-grit paper	. . .	Rinse in tap water plus acetone	40HNO_3-2HF-58H_2O, wt%	. . .	1 h between cleaning and bonding	17
Knowles and Hazlett	Ground flat	Hand polish with alumina and lap on thick to 0.5 μm abrasive or bonding surface	Cotton swab with acetone, followed by low- power ultrasonic cleaning in acetone for 0.157 h	. . .	Surface finish on bond surface of 2 rms	Procedure used for preparing specimens for silver-coating procedures	8
O'Brien et al.	Lapping machine with 3 μm alumina and light oil	. . .	Ultrasonic wash for 5 min in 3% Oakite NST aluminum-detergent-distilled H_2O solution, followed by 3–5 min ultrasonic cleaning in distilled H_2O	. . .	Flat to one light band after 20 min of lapping. Used Auger analysis to determine contamination level	Procedure for preparing surfaces for silver deposition procedures; also, surface is sputtered in vacuum system prior to silver coating.	22
Naimon et al.	On lapping machine with 3 μm alumina with a light oil vehicle	. . .	Detergent wash and alcohol rinse	. . .	Proved flat to one light band	Procedure for preparing surfaces for silver deposition procedures; also, surface is sputtered in vacuum system prior to silver coating.	23

(a) Refers to references listed in Olson and Liby [1979]. Source: Olson and Liby 1979

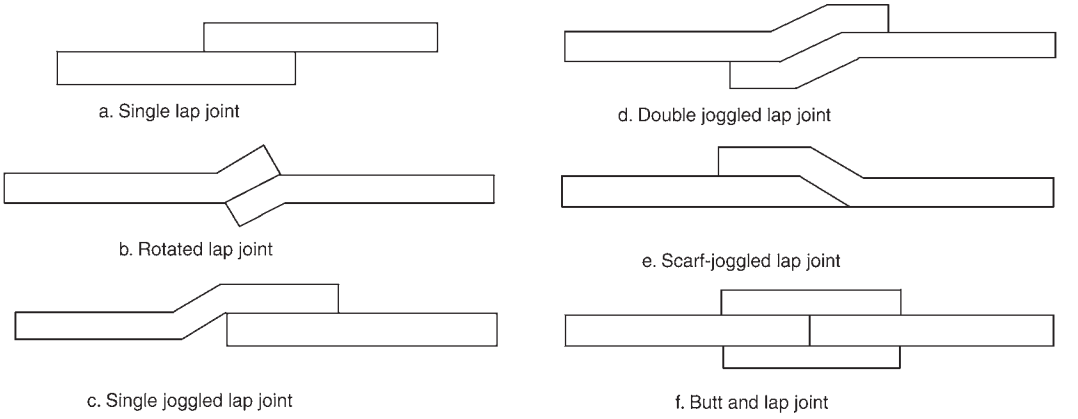

Fig. 23.30 Variations of lap joints for diffusion bonding. Source: Hauser et al. 1965

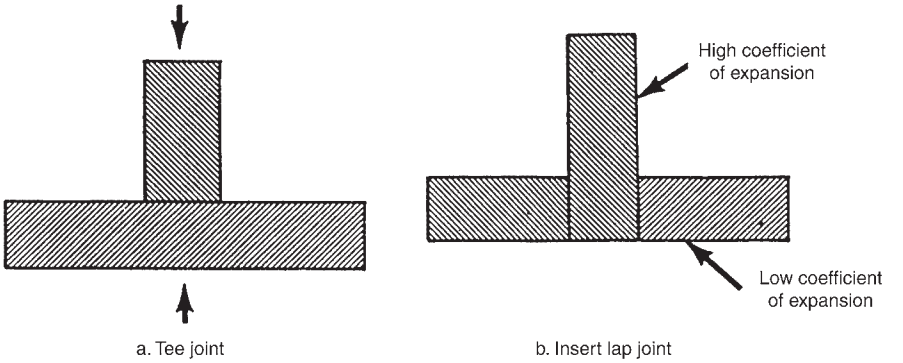

Fig. 23.31 Joint designs in diffusion bonding. (a) Conventional tee joint. (b) Insert lap joint to minimize residual stress due to differential coefficient of thermal expansion. Source: Hauser et al. 1965

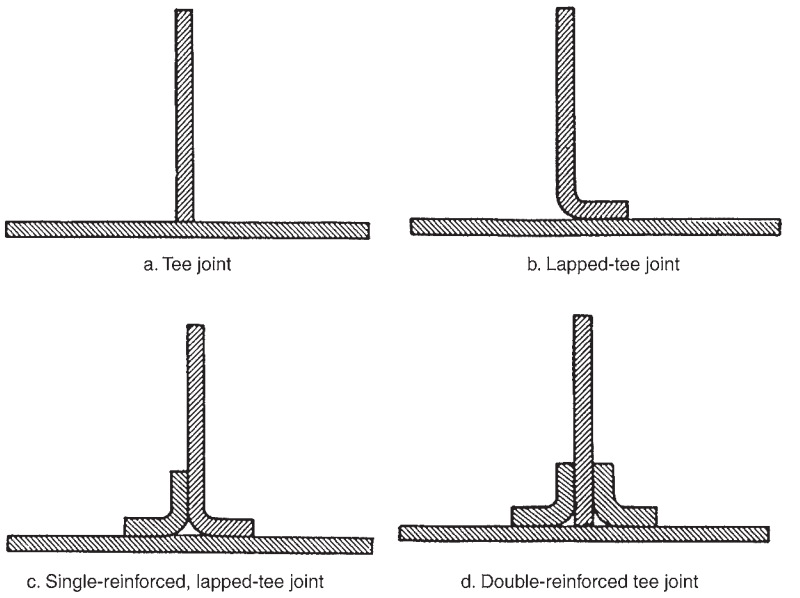

Fig. 23.32 Variations of tee joints for diffusion. Source: Hauser et al.1965

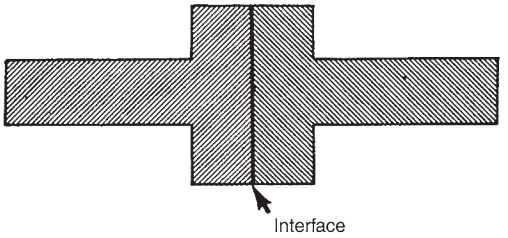

Fig. 23.33 Butt joint strengthened by increased joint area. Source: Hauser et al. 1965

and heavy sections should generally be designed with reinforcements.

23.3.6 Solid-State Bonding Equipment

Typical heating sources for solid-state bonding include radiation, induction, and self-resistance heating. Loads can be applied by hydraulic or mechanical means and by differential thermal expansion, usually with reference to a fixed jig. The disadvantage of loading by differential expansion is that control of the load is limited because the magnitude of the load is temperature dependent. Loads greater and more controllable than those obtained by thermal expansion may be required to optimize joint strength. The equipment used must protect the bonding surfaces from contamination from the ambient atmosphere. Solid-state bonding, however, has been achieved between silver surfaces at lower bonding temperatures without atmospheric protection. Deformation bonding of sheet may possibly be done by roll bonding. Although the bonding operation can readily be performed by adapting to existing facilities, such as a vacuum hot press, a mechanical testing system, or perhaps a modified furnace, for production purposes it is best to use equipment designed for a specific bonding operation.

Press welding, which consists of applying pressure to the parts placed between two platens or shaped dies held in a press, usually involves relatively simple procedures and equipment. The method is well suited for joining flat parts, parts having parallel opposite faces, sandwich composites, and butted rods or tubes. The latter two may have to be performed within a sleeve to prevent lateral deformation. An internal mandrel may also be used for the tube. The method offers the ability for good control and precise measurement of the loading.

Differential thermal expansion (DTE) bonding uses the stress developed due to the DTE between the joining pieces and the supporting fixture or between the pieces themselves. The equipment requirement is relatively inexpensive. Precise measurement and control of the bonding pressure is difficult.

Gas-Pressure Bonding Process. The joint components are fabricated or machined to final size and cleaned. The assembled components are then placed in a flexible, expendable container that is sealed or edge welded to produce a pressure-tight evacuated enclosure. Residual gases should be removed; otherwise, they may become entrapped in the weld interfaces and interfere with the bonding. The assembled components are then heated to the bonding temperature in an autoclave containing an inert gas under high pressure, which is transmitted uniformly to the components, forcing all the mating surfaces into intimate contact. Maximum allowable operating pressures are usually used to lower the temperature and/or time, to minimize grain growth and excessive diffusion. Because of the isostatic pressure, the process is especially suited for joining of brittle materials and decreases the risk of cracking.

Roll bonding, which does not depend on diffusion, requires some minimum amount of deformation, of the order of 40% or greater, depending on the material, surface preparation, rolling conditions, and temperature. Residual stresses, which develop when bonding materials having significant differences in the CTE, could be a limiting factor in using this process. Studies on roll bonding of aluminum showed that the shear strength of the aluminum-aluminum bond increased with increased deformation as well as by roughening (by wire brushing) and increased cleaning of the surfaces [Hauser et al.1965]. A threshold deformation of 40% at ambient temperature was reported to obtain a measurable strength for degreased and wire-brushed surfaces, compared to over 50% for an as-machined surface. Bonding was not obtained at 77% deformation for electropolished aluminum surfaces. The threshold value was reduced from 40 to 5% on increasing the temperature from ambient to 600 °C (1110 °F). By baking out, machining, and rolling in vacuum (within 5 s after rolling), the deformation threshold for aluminum at ambient temperature was reduced from 40 to 10%. As with aluminum, the high reactivity of beryllium with oxygen would require a limited exposure time of the surface between cleaning and rolling.

23.3.7 Evaluation of Bond Strengths

Defective diffusion bonds may be the result of:

- Total or partial lack of bonding at the interface
- Failure of intermediate layers to adhere to the beryllium
- Formation of brittle intermetallics at the interface
- Crack initiation (notch effect) at the edge of the bond interface due to deformation during bonding
- Crack initiation at etch pits formed during cleaning prior to bonding
- Lack of cleanliness, flatness, and/or smoothness of bonding surfaces

Because of the intimate contact of bonded surfaces, the integrity of a bond cannot readily be ascertained by conventional nondestructive evaluation methods, such as radiography or ultrasonics. High-sensitivity ultrasonic testing has shown potential under suitable conditions. Acoustic emission monitoring during proof testing also showed promise for assessing the integrity of bonds [Olson and Liby 1979].

23.3.8 Bonding of Beryllium with Dissimilar Metals

A number of investigations have been reported on bonding of beryllium with other metals. In many cases where intermediate layers were used, they consisted of materials other than silver.

Copper and Copper-Base Alloys. In one study, S-65C beryllium was bonded to dispersion-strengthened copper (DSCu) either directly or by using an interlayer insert of a 50 μm thick beryllium-copper (Cu-1.8%Be) foil [Makino and Iwadachi 1998]. The bonding was achieved by vacuum hot isostatic pressing at a pressure of 50 MPa (7 ksi). Bonding temperatures ranged from 600 to 850 °C (1110 to 1560 °F) for 1 h, except at 700 °C (1290 °F) where tests ranged from 1 to 6 h. Shear strength results as a function of bonding temperature are shown in Fig. 23.34. A slight drop in strength occurs with increasing bonding temperature. Consistent with this trend, an initial rise in strength followed by a drop was obtained with increased bonding time at 700 °C (1290 °F). Scanning electron and x-ray diffraction analyses of the joints revealed growth of diffusion layers with increasing temperature or time. Figure 23.35 shows the diffusion layer thickness as a function of temperature. Similar diffusion layer growth behavior was obtained with increasing time at 700 °C. In the absence of the insert, a Be_2Cu (δ) phase formed on the beryllium side, and a Cu + BeCu (γ) phase formed on the DSCu side. These same phases were obtained at the beryllium and DSCu sides when using the beryllium-copper foil. Makino and Iwadachi [1998] conclude that the shear strength is affected mainly by

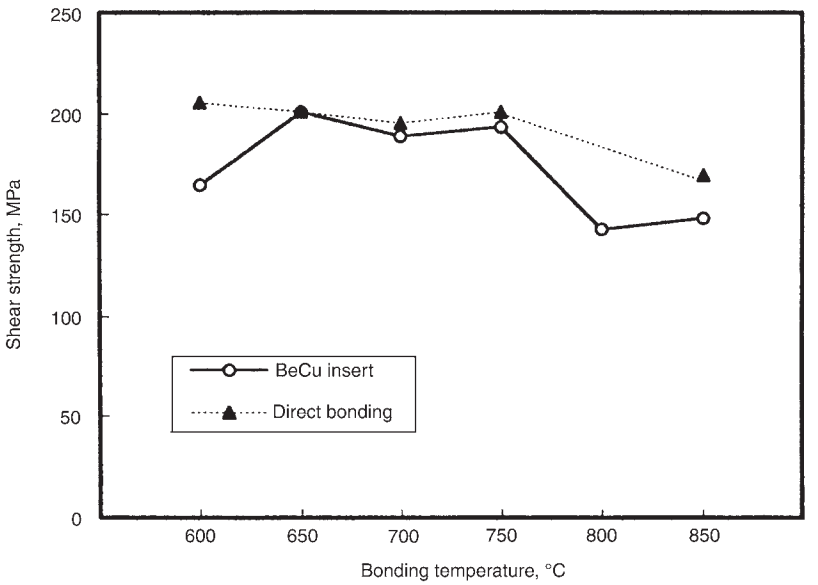

Fig. 23.34 Dependence of shear strength on bonding temperature for S-65C beryllium bonded to dispersion-strengthened copper. Source: Makino and Iwadachi 1998

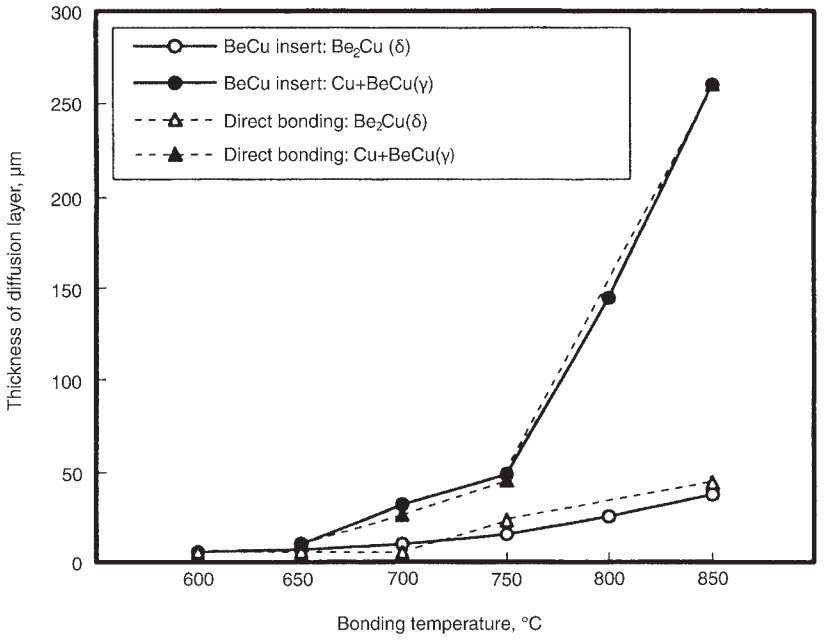

Fig. 23.35 Dependence of diffusion layer thickness on bonding temperature for S-65C beryllium bonded to dispersion-strengthened copper. Source: Makino and Iwadachi 1998

Table 23.6 Results of tensile testing beryllium-copper and Be-CuCrZr bonded samples

		Test temperature		Tensile strength			
Bonded materials	**Joining method**	**°C**	**°F**	**MPa**	**ksi**	**Failure zone**	**Comments**
Be-Cu	Brazing	20	70	81	12	Through brazing alloy	Brittle fracture
Be-Cu	Brazing	20	70	103	15	Through brazing alloy	Brittle fracture
Be-Cu	Brazing	350	660	125	18	Through brazing alloy	Mainly brittle
Be-Cu	Brazing	350	660	212	31	Through Cu	Ductile failure of Cu
Be-CuCrZr	Diffusion bonding	20	70	188	27	Through Be	Brittle fracture
Be-CuCrZr	Diffusion bonding	20	70	103	15	Through Be	Brittle fracture
Be-CuCrZr	Diffusion bonding	350	660	191	28	Through Be	Brittle fracture
Be-Cu	Diffusion bonding	20	70	...		...	Failed after machining
Be-Cu	Diffusion bonding	20	70	...		...	Failed after machining
Be-Cu	Diffusion bonding	20	70	21	3.0	Through Be-Cu bond line	Brittle fracture
Be-Cu	Roll bonding	20	70	53	7.7	Through Be-Cu bond line	Brittle fracture
Be-Cu	Roll bonding	20	70	70	10	Through Be-Cu bond line	Brittle fracture

Source: Gervash et al. 1996

the growth of the Be_2Cu phase at the beryllium interface and that the presence or absence of an insert is unimportant.

Preliminary results obtained to evaluate the usefulness of beryllium-copper and Be-CuCrZr bonds for beryllium-copper heat-sink structures are listed in Tables 23.6 and 23.7 for tensile and shear specimens, respectively [Gervash et al. 1996]. Brazing and roll-bonding results are included with the solid-state diffusion results. A silver-base brazing alloy was used for brazing, performed in vacuum at 760 °C (1400 °F). No intermediate layer was used for diffusion or roll bonding. The diffusion bonds were made in vacuum at 720 °C (1330 °F) under a pressure that corresponded to the initiation of plastic deformation of the copper.

It appears that direct bonding of beryllium to copper is not feasible, because of the formation of brittle beryllium-copper intermetallics. In addition, the high mismatch in the CTE results in corresponding high stresses. Interlayers should be used to both act as a diffusion barrier and to relieve these thermal residual stresses by plastic deformation.

Titanium. An evaluation was reported on the use of 50 μm thick titanium foil as an intermediate layer in diffusion bonding S-65C beryllium to Glidcop (99.5Cu-0.25Al, in wt%) [Saint-Antonin et al. 1998]. The copper and

Table 23.7 Results of shear testing beryllium-copper and Be-CuCrZr bonded samples

Bonded materials	Joining method	Test temperature °C	Test temperature °F	Shear strength MPa	Shear strength ksi	Failure zone	Comments
Be-Cu	Brazing	20	70	72	10.4	Through brazing alloy	Brittle fracture
Be-Cu	Brazing	20	70	123	17.8	Through brazing alloy	Brittle fracture
Be-Cu	Brazing	350	660	126	18.2	Through Cu	Ductile failure of Cu
Be-Cu	Brazing	350	660	213	31	Through Cu	Ductile failure of Cu
Be-CuCrZr	Diffusion bonding	20	70	43	6.2	Through Be	Crack in Be
Be-CuCrZr	Diffusion bonding	20	70	103	15	Through Be	Crack in Be
Be-CuCrZr	Diffusion bonding	350	660	107	16	Through Be-Cu bond line	Brittle fracture
Be-Cu	Diffusion bonding	20	70	82	12	Through Be-Cu bond line	Failed after machining
Be-Cu	Diffusion bonding	20	70	75	10.9	Through Be-Cu bond line	Failed after machining
Be-Cu	Diffusion bonding	20	70	152	22	Through Be-Cu bond line	Brittle fracture
Be-Cu	Roll bonding	20	70	123	17.8	Through intermetallic	Brittle fracture
Be-Cu	Roll bonding	20	70	141	20.4	Through Cu	Ductile failure of Cu

Source: Gervash et al. 1996

beryllium pieces each measured 10 by 10 by 5 mm (0.4 by 0.4 by 0.2 in.). Surfaces were chemically cleaned, and the bonding was performed by hot isostatic pressing. Two different bonding cycles were evaluated:

1. Heat to 850 °C (1560 °F) and 100 MPa (15 ksi) in 3 h, hold for 2 h, and cool to room temperature and 0.1 MPa (0.02 ksi) in 5 h
2. Heat to 850 °C (1560 °F) and 120 MPa (17 ksi) in 3 h, hold for 2 h, cool to 400 °C (750 °F) and 3 MPa (0.4 ksi) in 2 h, hold for 2 h

Ultimate shear strengths at room temperature were approximately 30 and 108 MPa (4 and 16 ksi) for bonds formed by procedures 1 and 2, respectively. Failure occurred at the interface between beryllium and the titanium-beryllium intermetallics ($TiBe_{12}$ and $TiBe_2$). Other phases that formed across the titanium foil were Ti_2Cu, TiCu, $Ti_2Cu_3 + Ti_3Cu_4$ (cracks were associated with these two latter phases), and $TiCu_4$.

Stainless Steel. The joining of hot pressed beryllium with type 316L stainless steel, both directly and with interlayers of copper and copper with nickel, was evaluated [Zhang et al. 2001]. The beryllium contained 6100 ppm BeO, 270 ppm Be_2C, and 800 ppm Fe. Bonding was achieved by hot isostatic pressing at 65 MPa (9 ksi) for 2 h at 930 °C (1705 °F) in argon. Evaluations of the joints were made using light microscopy, scanning Auger microscopy, nanoindenter hardness measurements, and tensile tests. Direct bonding led to the appearance of cracks due to the formation of brittle beryllium-iron intermetalllics; a tensile strength of less than 10 MPa (1.5 ksi) was achieved. Using a copper interlayer prevented the diffusion of iron into the beryllium. However, beryllium was able to diffuse through the copper into the stainless steel and led to cracking at the Cu-316L interface. No cracks formed at the Be-Cu-Ni-316L bond, which achieved a tensile strength of 50 MPa (7.2 ksi). The nickel layer impeded the diffusion of beryllium into the stainless steel, thus avoiding the formation of brittle beryllium-iron intermetallics. The diffusion widths ranged between 350 and 400 μm. Due to the intermetallics and solid-solution hardening, hardness values increased by as much as a factor of 4 across the diffusion regions relative to that of beryllium. Interlayer thicknesses were not given.

Iron, Nickel, Aluminum, Silver, and Vanadium. In forming a joint between beryllium and another metal, the difference in the CTE between the two metals can result in excessive residual stresses. To minimize this problem, iron or nickel interlayers (0.9 to 1.3 mm, or 0.04 to 0.05 in., thick) were used in solid-state bonding of beryllium to Cu-0.65Cr-0.1Zr (wt%) [Schneibel et al. 1997]. In addition, an interlayer of 130 μm thick silver foil was used as a reaction barrier to limit the formation of brittle beryllium intermetallics, since silver does not form any intermetallics below 760 °C (1400 °F). Bonding of beryllium to a V-5Cr-5Ti (wt%) alloy using silver as a reaction barrier was also evaluated. Instead of iron or nickel, an aluminum-beryllium interlayer (1.25 mm, or 0.05 in., thick) was used for the beryllium-copper bonding. The aluminum-beryllium layer was plasma sprayed onto the beryllium, attempting to obtain a gradation from 0 to 40 wt% Al. The CTEs as a function of temperature for these materials are shown in Fig. 23.36. The CTEs for both iron and nickel are close to that of beryllium over most of the temperature range, whereas the copper and beryllium curves are distinctly different from each other.

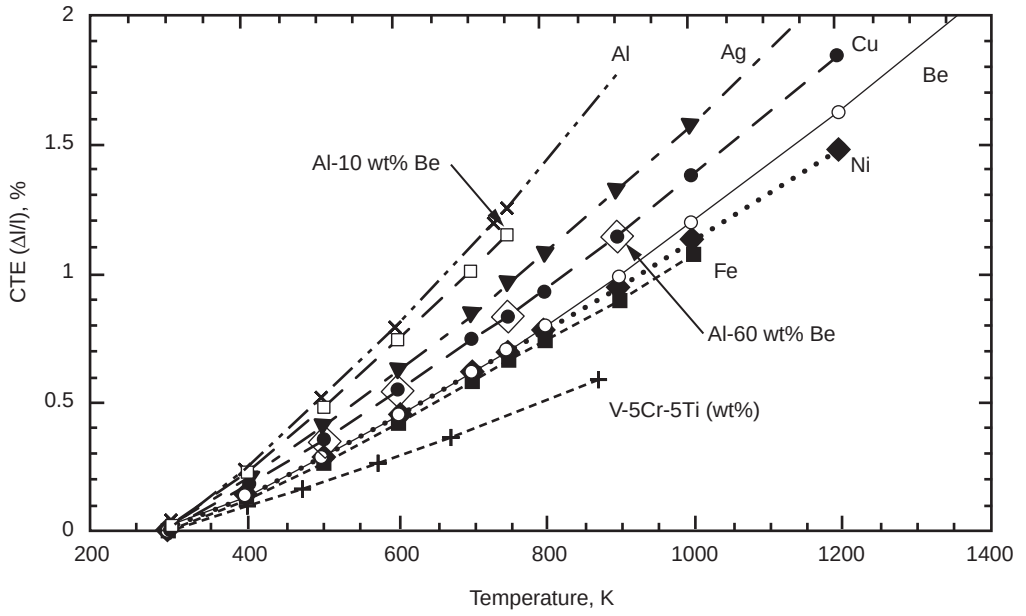

Fig. 23.36 Coefficients of thermal expansion (CTE) of beryllium compared to several possible inserts. Source: Schneibel et al. 1997

For evaluation, the different interlayer materials were cut into 25 mm discs, degreased, cleaned (including an initial 5 min etch in a $30HNO_3$-10HF-$60H_2O$ solution), stacked for bonding, and inserted into stainless steel cans that were then evacuated. The samples were then hot isostatically pressed for 0.5 h at 762 °C (1404 °F) at a pressure of 110 MPa (16 ksi). Some samples were sectioned for light microscopy and scanning electron microscopy; others were machined into compression-shear samples. The Cu-Ni-Ag-Be and Cu-Ag-AlBe-Be samples delaminated during machining, leaving only the Cu-Fe-Ag-Be and V-Ag-Be samples adequate for testing.

The load in the shear tests, following a small plastic strain (crosshead displacement of 10 to 20 μm), typically reached a maximum value followed by a sharp drop. In most cases, the load increased again during further deformation. A typical example is shown in Fig. 23.37. Reported shear strengths were 49 and 55 MPa (7 and 8 ksi) for the Cu-Fe-Ag-Be samples and 77 and 78 MPa (11.2 and 11.3 ksi) for the V-Ag-Be samples.

Interaction at the silver-beryllium interface in the Cu-Ni-Ag-Be and Cu-Fe-Ag-Be samples was not evident, even though the hot isostatic pressing temperature is very close to the temperature where $AgBe_2$ forms. The apparent lack of such interaction is consistent with the low

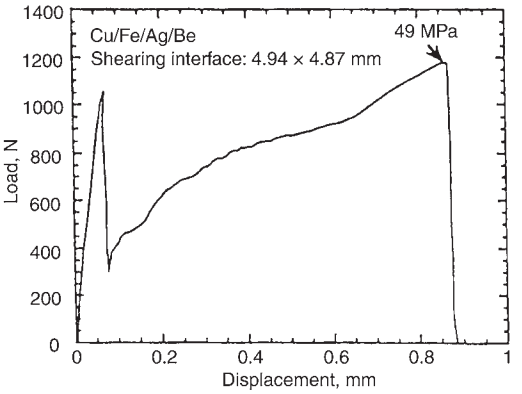

Fig. 23.37 Load displacement for a simple shear specimen of copper bonded to beryllium with interlayers of iron and silver as Cu-Fe-Ag-Be. Source: Schneibel et al. 1997

mutual solid solubility of silver and beryllium (Fig. 23.29). Failures usually occurred at the silver-beryllium interface. The authors conclude that achieving a minimum mismatch in the CTE will not necessarily lead to a maximum interfacial shear strength [Schneibel et al. 1997]. This observation was based on their results showing that the V-Ag-Be samples exhibited a higher shear stress than did the Cu-Fe-Ag-Be samples, although the CTE mismatch between the vanadium-base alloy and beryllium is much greater than it is between iron and beryllium.

23.3.9 Flash Welding

Flash welding is a resistance forge welding process in which the parts to be welded are securely clamped to electric current dies, heated by the current, and upset. It is a rapid, economical process that can produce a uniform, high-quality weld and is used primarily for production quantities. With beryllium (and other toxic metals), flash welding should only be used under stringent precautionary measures to prevent contamination of equipment, air, surroundings, and personnel by particles and dust.

23.4 Soldering

Soldering beryllium to beryllium and beryllium to copper has been successfully accomplished. Typical applications of soldering beryllium include those requiring high electrical conductivity with low stresses, applications requiring a mass spectrometer leaktight joint with low stresses, low-temperature applications where nonmetallic materials are not permissible, and high-voltage applications [Grant 1979]. Soldering of beryllium has been performed using indium-base solders, for example, 90%In-10%Ag. On the basis of strength, weldability, and flow, the use of high-zinc solders appears best for soldering beryllium. A reaction-type flux, which is suitable for aluminum, is recommended. The flux residue should be removed in a safe manner to avoid any health hazards [ASM 1993, American Welding Society 1998]. Minor defects or discontinuities in a brazed joint can be repaired by soldering. By first plating beryllium with copper and then nickel, beryllium surfaces can be joined to each other using silver solder [Jacobson 1986].

REFERENCES

American Welding Society, 1991. *Brazing Handbook,* 4th ed., American Welding Society, Miami, FL

American Welding Society, 1998. *Materials and Applications,* American Welding Society, Miami, FL

ASM, 1983. *Welding, Brazing, and Soldering,* Vol 6, *Metals Handbook,* 9th ed., American Society for Metals

ASM, 1993. *Welding, Brazing, and Soldering,* Vol 6, *ASM Handbook,* ASM International

Banaim, P., Zalkind, S., Eden, S., and Abramov, E., 1988. Joining of Beryllium by Braze Welding Technique: Preliminary Results, *Proc. of Third IEA International Workshop on Beryllium Technology for Fusion,* Japan Atomic Energy Research Institute Conference 98–01 (Milo City, Japan), p 93–101

Barker, R.B., "Beryllium Braze-Welding Porosity and Arc-Parameter Studies," RFP-287, Internal Document, Rocky Flats Division, Dow Chemical Company, Golden, CO

Campbell, R.P., Dixon, R.D., and Liby, A.L., 1978. "Electron Beam Fusion Welding of Beryllium," RFP-2621, Rockwell International, Rocky Flats Plant, Golden, CO

Cotton, J.D., and Field, R.D., 1997. Microstructural Features of Cracking in Autogenous Beryllium Weldments, *Metall. Mater. Trans. A,* Vol 28, p 673–680

CRC, 2000–2001, *Handbook of Chemistry and Physics,* D.D. Lide, Ed., The Chemical Rubber Company Press, New York, NY, p 8/21–8/31

Devletian, J.H., and Wood, W.E., 1983. Principles of Joining Metallurgy, *Welding, Brazing, and Soldering,* Vol 6, *Metals Handbook,* 9th ed., American Society for Metals, p 29

Fraikor, F.J., Hicken, G.K., and Grotsky, V.K., 1968. Precipitation in Electron Beam Welded Beryllium Sheet, *Weld. J. Res. Suppl.,* Vol 47, p 204s–211s

Gervash, A.A., Giniatouline, R.N., Mazul, I.V., Ganenko, A.A., Gitarskij, L.S., Sizenev, V.S., and Davydov, D.A., 1996. Metallographic Analysis and Strength Investigation of Different Be-Cu Joints in the Temperature Range RT–350 °C, *J. Nucl. Mater.,* Vol 233–237 (Pt 1), p 626–631

Gilliland, R.G., and Slaughter, G.M., 1963. Fusion Welding of End Caps in Beryllium Tubes, *Weld. J.,* Vol 42, p 29–36

Grant, L.A., 1979. Joining II: Brazing and Soldering, *Beryllium Science and Technology,* Vol 2, D.R. Floyd and J.N. Lowe, Ed., Plenum Publishing Corp., NY, p 249–273

Hauser, D., Kammer, P.A., and Martin, D.C., 1965. "Fundamentals of Solid State Welding and Their Application to Beryllium, Aluminum, and Stainless Steel," RSIC-437, Battelle Memorial Institute, Columbus, OH, July 15, 1965

Hauser, D., Mishler, H.W., Monroe, R.E., and Martin, D.C., 1967. Electron Beam Welding of Beryllium, Part 1, *Weld. J.,* Vol 46 (No. 12), p 525s–540s

Hauser, D., and Monroe, R.E., 1968. Electron Beam Welding of Beryllium, Part II, *Weld. J. Res. Suppl.,* Vol 47 (No. 11), p 497s–514s

Heiple, C.R., 1972. Mechanical Properties of Diffusion Bonded Beryllium Ingot Sheet, *Metall. Mater. Trans. B*, Vol 3 (No. 4), p 807–812

Heiple, C.R., and Dixon, R.D., 1979. Beryllium: Problems of Cracking and Environment, *Weld. Met. Fabr.*, Vol 47 (No. 5), p 309–316, 420

Hicken, G.K., and Sample, W.B., 1967. Joining Beryllium by an Electron Beam Braze Welding Technique, *Weld. J. Suppl.*, Vol 46 (No. 12), p 541s–550s

Hill, M.A., Damkroger, B.K., and Dixon, R.D., 1990. Beryllium Weldability, *Weldability of Materials*, R.A. Patterson and K.W. Manin, Ed., ASM International, p 331–339

Hodge, E.S., Gripshover, P.E., and Hanes, H.D., 1966. Properties of Gas-Pressure-Consolidated Beryllium Powder, *Beryllium Technology*, Vol 2, Gordon and Breach, p 703–728

Jacobson, L.A., 1986. "Joining Methods for Beryllium—A Survey," Report UCID-20750, Lawrence Livermore National Laboratory, Livermore, CA

Juntz, R., 1986. "PVD Aluminum on Beryllium," Lawrence Livermore National Laboratory, Livermore, CA, internal communication from J. West to R. Juntz

Keil, R.W., Hanks, G.S., and Taub, J.M., 1960. Brazing and Soldering of Beryllium, *Weld. J.*, Vol 39, p 406s–410s

Knowles, J.L., and Hazlett, T.H., 1970. High-Strength Low-Temperature Bonding of Beryllium and Other Metals, *Weld. J. Suppl.*, Vol 49 (No. 7), p 301s–310s

Makino, T., and Iwadachi, T., 1998. Interface Formation and Strength of Be/DSCu Diffusion Bonding, *J. Nucl. Mater.*, Vol 258–263, p 313–317

Maloof, S.R., and Cohen, J.B., 1964. Brazing of Beryllium for High Temperature Service, *Weld. J.*, Vol 43 (No. 3), p116s–125s

Marschall, C.W., 1990. "Testing of Beryllium Brazed Joints at Temperatures up to 1200 °F," Light Metals, Current Awareness Bulletin, Issue 201,Ceramic Information Center, p 1–3

Massalski, T.B., Okamoto, H., Subramanian, P.R., and Kacprzak, L., 1990. *Binary Alloy Phase Diagrams*, Vol 1, 2nd ed., ASM International, p 127

Merlini, R.J., and Bush, W.L., 1978. "Gas Metal Arc Braze Welding of Ingot Sheet Beryllium," RFP-1333, Rocky Flats Division, Dow Chemical Co., Golden, CO

Olson, D.L., and Liby, A.L., 1979. Joining III: Diffusion Bonding, *Beryllium Science and Technology*, Vol 2, D.R. Floyd and J.N. Lowe, Ed., Plenum Publishing Corp., p 275–296

Passmore, E.M., 1964. Fusion Welding of Beryllium, *Weld. J.*, Vol 43 (No. 3), p 116s–125s

Saint-Antonin, F., Barberi, D., Le Marois, G., and Laille, A., 1998. Development and Characterization of Be/Glidcop Joints Obtained by Hot Isostatic Pressing for High Temperature Working Conditions, *J. Nucl. Mater.*, Vol 258–263 (Pt 2), p 1973–1978

Sanderson, A., and Nightingale, K.R., 1990. High-Power EBW Equipment and Process Trends, *Weld. J.*, Vol 69 (No. 4), p 45–57

Schneibel, J.H., Haines, J.R., Snead, L.L., and Bloom, E.E., 1997. Solid State Bonding of Beryllium to Copper and Vanadium Using Transition Layers, *J. Nucl. Mater.*, Vol 250 (No. 2–3), p 216–222

Schwartz, M., 1983. Brazing of Reactive Metals and Refractory Metals, *Welding, Brazing, and Soldering*, Vol 6, *Metals Handbook*, 9th ed., American Society for Metals, p 1052

Vaccari, J., 1991. Welding Beryllium Takes Special Care, *Am. Mach.*, Vol 135 (No. 4), p 46–48

Weiss, H., 1983. Arc Welding of Beryllium, *Welding, Brazing, and Soldering*, Vol 6, *Metals Handbook*, 9th ed., American Society for Metals, p 461–462

White, S.S., Lander, H.J., Hess, W.T., and Bakish, R., 1962. A Study of Electron-Beam Welding, *Weld. J.*, Vol 41, p 279s–288s

Zhang, P., Bai, B., Shen, L., and Zhou, J., 2001. Distribution of the Composition and Micromechanical Properties of Be/316L Stainless Steel Following Diffusion Bonding, *Surf. Interface Anal.*, Vol 32, p 88–90

SELECTED REFERENCES

- Bosworth, T.J., 1972. Diffusion Welding of Beryllium, Part I: Basic Studies, *Weld. J. Res. Suppl.*, Vol 51 (No. 12), p 579s–590s
- Bosworth, T.J., 1973. Diffusion Welding of Beryllium, Part II, *Weld. J. Res. Suppl.*, Vol 52 (No. 1), p 38s–48s
- Passmore, E.M., 1963. A Solid State Welding of Beryllium, *Weld. J.*, Vol 42 (No. 4), p 186s–189s
- Ryczeck, L., and Parsonage, T., 2003. "Near Net Shape Technologies: AlBeMet NNSB and AlBeWeld," Technology Days in the Government

Beryllium Chemistry and Processing, p 441-457
By Kenneth A. Walsh
Edited by Edgar E. Vidal, Alfred Goldberg,
Edward N.C. Dalder, David L. Olson, and Brajendra Mishra

CHAPTER 24

Adhesive Bonding and Mechanical Fasteners

Alfred Goldberg, Lawrence Livermore National Laboratory

24.1 Introduction

Adhesive bonding of beryllium permits utilization of a combination of desirable physical and mechanical properties of beryllium while minimizing the inherent problems of high notch sensitivity (especially at fastener holes when using mechanical fasteners) and low ductility [Brush Wellman 2001, Norwood 1984]. Joining a thin section to a thick section enables the full strength of the thin section to be utilized, which is difficult to achieve with mechanical fasteners. In addition, adhesive joining produces a uniform load distribution over the bonded area, thus minimizing stress concentrations. The use of adhesives avoids distortions that would result with other joining methods and allows for the fabrication of complex shapes where other joining methods are not feasible. Adhesive bonding provides an assembly with lower weights than those obtained with mechanical fasteners. Properties of the adherents are not degraded. The adhesive reduces or prevents galvanic corrosion between dissimilar metals. Typically, adhesive bonding is used in applications where the structural strength requirements for shear are less than 35 MPa, temperatures are less than 235 °C (455 °F), outgassing requirements are not stringent, and lack of heat transfer across the joint is acceptable. Because adhesive bonds are not inherently strong, designs should provide for an adequate surface contact area. Also, designs should account for their susceptibility to failure by peeling. It is often difficult to apply adequate inspection to adhesive bonds.

When designing adhesive joints, the choice of adhesive and the potential for localized stress concentrations that could be produced in service must be considered. The four most important stresses that arise in adhesive bonds are illustrated in Fig. 24.1 [Pizzi and Mittal 2003]. These stresses are shear, tensile, peel, and cleavage.

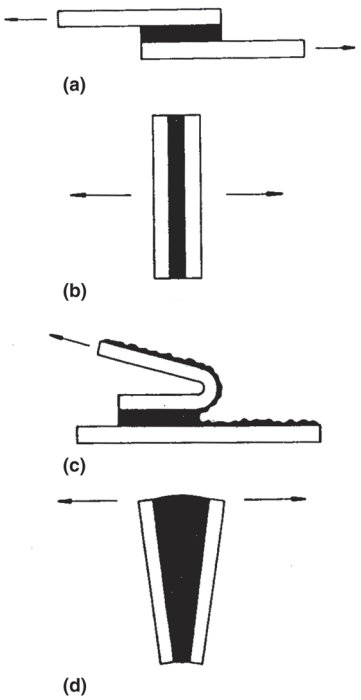

Fig. 24.1 Four important stresses to be considered in designing adhesive bonds: (a) shear, (b) tension, (c) peel, and (d) cleavage. Source: Pizzi and Mittal 2003

Most adhesive joints are lap joints in which a nonuniform stress pattern can be induced by a tensile load applied in shear, as illustrated in Fig. 24.2 [Sharpe 1990]. Examples of various lap joints are shown in Fig. 24.3 [Snogren 1970]. Some of the joints that are illustrated in this figure, such as the half-lap joint, ideally should result in a uniform stress pattern under tensile-shear loading. Several of these joints, however, would involve additional machining. An extensive discussion with corresponding illustrations of adhesive joints is presented in Pizzi and Mittal [2003]. (No attempt is made to educate the reader on the architecture, or molecular structures, of adhesives. Many handbooks are available on the subject, and several are referenced here.)

Differences in the temperature coefficient of thermal expansion (CTE) of the two metals being joined, the service temperature of the part, the cure temperature of the adhesive, and the transition temperature of the adhesive must be considered. For example, the CTE of aluminum and its alloys is almost double that of beryllium, while most steels have a value close to that of beryllium. (Values for the three materials will depend on their specific compositions and processing.) Thus, heating of an adhesive-bonded beryllium-aluminum structure may introduce a sufficiently high thermal stress to rupture the bond, whereas the beryllium-steel joint probably could have survived under the same conditions. Most adhesives are limited to an upper temperature of between 65 and 95 °C (150 and 200 °F) and some to temperatures up to 175 °C (345 °F). Several adhesives are available for limited use to 370 °C (700 °F) [Sharpe 1990]. Depending on the application of the bonded structure, specific adhesives covering a range of temperatures are available.

The strength of an adhesive bond depends on two elements: cohesion and adhesion. Cohesion is associated with the strength of the bonds between the various molecules of the adhesive layer. Adhesion refers to the strength of the bond between the adhesive and the substrates (adherents).

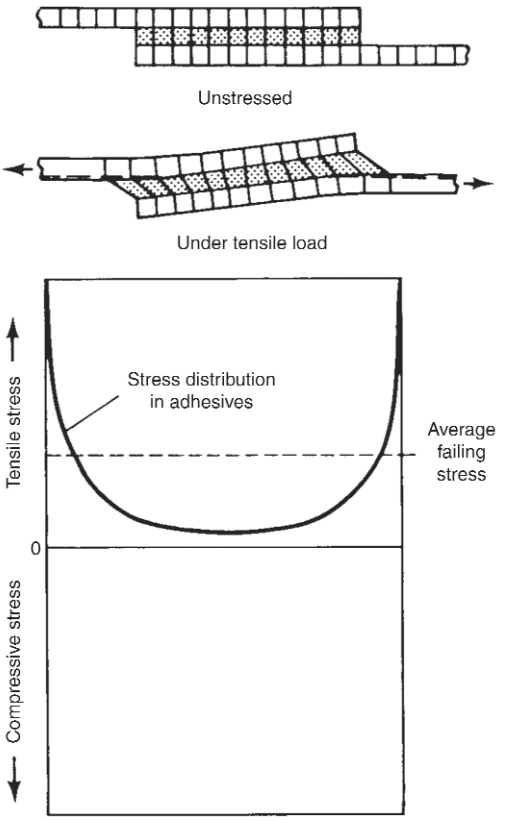

Fig. 24.2 Illustration of a nonuniform stress pattern introduced by a tensile load applied in shear to a plain lap joint. Source: Sharpe 1990

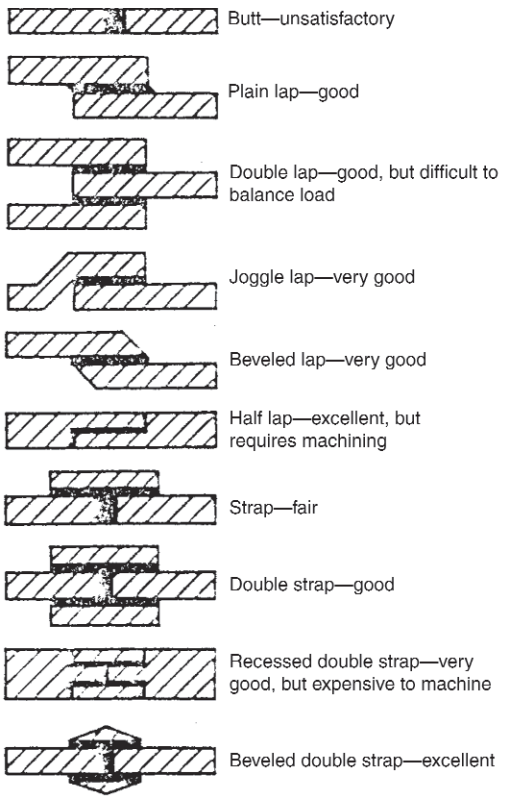

Fig. 24.3 Examples of possible shear-lap configurations. Source: Snogren 1970

As with metallic materials, the toughness or ductility of the adhesives can range between the extremes of being ductile to being brittle. Stress concentrations at voids can significantly reduce the strength of an adhesive bond, especially in a brittle adhesive, leading to premature, brittlelike failures. Although the damaging effect of stress concentration at flaws (such as a bubble) in a brittle material is obvious, there is some evidence that in some circumstances voids can toughen a ductile adhesive by involving larger volumes of the adhesive in plastic deformation during fracture. A study using a blowing agent to introduce voids into a polyethylene adhesive on copper showed that the voids resulted in a significant increase in peel strength. On the other hand, voids may also initiate crazing, which can grow and develop into cracks, leading to failure [Packham 1990].

Voids can readily form as a result of air entrapment during preparation of the adhesive as well as by failure to displace air from the substrate surface. The high viscosity of many adhesives in their liquid state makes the removal of air bubbles difficult, even when a vacuum is applied. Moisture, either in the adhesive or on the substrate surface, may also be a source for bubbles when the system is heated [Packham 1990]. Although there are several nondestructive techniques for detecting defects (ultrasonics, holography, thermal-wave imagining, and x-radiography), small voids with areas less than several square millimeters cannot readily be detected (if at all) by these techniques [Friedman 1989]. The nondestructive detection and characterization of defects is made especially difficult due to the thinness of the adhesive layer.

In some cases, a primer may be used, or the characteristic of the surface may be modified to improve the performance of the bond. A primer is usually a dilute solution of an adhesive in an organic solvent [Snogren 1970]. It is applied following surface preparation and dries to a film thickness that can range from approximately 1.5 to 50 μm (60 μin. to 0.002 in.). One purpose of the film is to protect the surface from the environment, extending the life between surface preparation and adhesive application by as much as six months, depending on the primer/adhesive system used. It is also used to increase the peel strength of structural adhesives. The primer can be dried at room temperature or force dried at 66 °C (150 °F); this provides a nontacky surface that can be protected from contamination and damage by either wrapping, sealing/bagging, or covering with a nontransferring adhesive-backed paper [Snogren 1970].

24.2 Classification of Adhesive Materials

There is a vast array of adhesive materials that are commercially available as well as extensive literature sources on this subject [Sharpe 1990, Packham 1990, Gauthier 1990, Acker 1990]. It was estimated that over 2500 different products were available [Snogren 1970]. The choice of adhesive is determined by the type of service stresses; joint design; environmental factors, such as temperature and humidity; potential exposure to other vapors or liquids; performance reliability; biological inertness; flammability; special requirements, such as electrical and thermal needs; and/or cost. In this book, reference to specific adhesives is usually made only with regard to the preparation, evaluation, and/or application of adhesives. Adhesives specific for beryllium joints, however, are presented.

Adhesives can be classified in a variety of ways. Benefits and limitations of various adhesive types are listed in Table 24.1 [Small and Courtney 2005]. A classification of structural adhesives based on chemical type, which also contains cure temperatures, service-temperature ranges, and strength values, is shown in Table 24.2 [Snogren 1970]. An additional classification system, which differs from Tables 24.1 and 24.2, is [Gauthier 1990]:

- Natural polymer base
- Synthetic base
- Thermoplastics
- Thermosets
- Physical forms (one or more multiple components, films, etc.)
- Functional types (structural, hot melt, pressure sensitive, water base, ultraviolet cured, electro beam cured, etc.)
- Chemical families (epoxy, silicone, phenolics, urethanes, polysulfides, etc.)

By the addition of certain additives and/or by a change in formulation, adhesives may serve other functions, such as electrical and/or thermal insulation, electrical and/or thermal conductors, electrochemical corrosion prevention at the joints between dissimilar metals, vibration damping, and smoothing of surfaces and contours (important for aerodynamic efficiency).

Table 24.1 Benefits and limitations of various adhesive types

Type	Anaerobics	Cyanoacrylates	Epoxies	Hot melts	Light cure	Silicones	Urethanes	Two-part acrylics(a)
Performance considerations								
Benefits	High strength	Excellent adhesion to most rubbers and plastics	Wide range of formulations	Fast, large-gap filling	Rapid cure and adhesion to plastic	Excellent temperature resistance	Excellent toughness and adhesion	Good impact resistance and ductility
Limitations	Metals only	Low solvent resistance	Mixing required	Low heat resistance	Light-cure system required	Low strength	Sensitive to moisture	Mixing required
Temperature resistance								
Typical temperature, °C (°F)	−54 to 149 (−65 to 300)	−54 to 88 (−65 to 190)	−54 to 82 (−65 to 180)	−54 to 121 (−65 to 250)	−54 to 149 (−65 to 300)	−54 to 204 (−65 to 399)	−54 to 121 (−65 to 250)	−54 to 121 (−65 to 250)
Highest-rated temperature, °C (°F)	450 (842)	121 (250)	204 (399)	165 (329)	177 (351)	316 (601)	165 (329)	204 (399)
Environmental resistance								
Polar solvents(b)	Very good	Poor(c)	Very good	Good	Good	Good	Good	Good
Nonpolar solvents(d)	. . .	Good	Excellent	Good	Very good	Poor to fair	Good	Very good
Adhesion to substrates								
Metals	Very good	Very good	Excellent	Good	Good	Good	Good	Excellent
Plastics(e)	Fair	Excellent	Fair	Very good	Excellent	Fair	Very good	Excellent
Glass	Excellent	Poor	Excellent	Good	Excellent	Very good	Good	Good
Rubber	Poor	Very good	Fair	Fair	Fair	Good	Good	Poor
Wood	Good	Good	Very good	Excellent	Poor	Fair	Fair	Good

(a) Two-step acrylic formulations are available for fast process speeds or high-temperature performance requirements. (b) Water, ethylene glycol, isopropyl alcohol, acetone. (c) Cyanoacrylates have very good moisture resistance on plastics. (d) Motor oil, toluene, gasoline, automatic transmission fluid. (e) Uncured liquid adhesives may cause stress cracking of certain thermoplastics, e.g., polycarbonate, acrylic, and polysulfon (special products and process techniques are available). Source: Small and Courtney 2005

Table 24.2 Classification of structural adhesives

Chemical types	Cure temperature, °C (°F)	Service temperature, °C (°F)	Lap-shear strength, MPa at °C (ksi at °F)	Peel strength at RT, g/mm
Epoxy formulated for room-temperature cure	16–32 (61–90)	−37 to 82 (−35 to 180)	17.2 at RT (2.49 at RT) 10.3 at 82 (1.49 at 180)	89.4
Epoxy formulated for elevated-temperature cure	93–177 (199–351)	−37 to 82 (−35 to 180)	17.2 at RT (2.49 at RT) 10.3 at 177 (1.49 at 351)	89.4
Epoxy-nylon	121–177 (250–351)	−253 to 82 (−423 to 180)	41.4 at RT (6.00 at RT) 13.8 at 82 (2.00 at 180)	1340
Epoxy-phenolic	121–177 (250–351)	−253 to 260 (−423 to 500)	17.2 at RT (2.49 at RT) 10.3 at 260 (1.49 at 500)	179
Butyral-phenolic	135–177 (275–351)	−37 to 82 (−35 to 180)	17.2 at RT (2.49 at RT) 6.9 at 82 (1.00 at 180)	179
Neoprene-phenolic	135–177 (275–351)	−37 to 82 (−35 to 180)	13.8 at RT (2.00 at RT) 6.9 at 82 (1.00 at 180)	268
Nitrile-phenolic	135–177 (275–351)	−37 to 121 (−35 to 250)	27.6 at RT (4.00 at RT) 13.8 at 121 (2.00 at 250)	1072
Urethane	24–121 (75–150)	−253 to 82 (−423 to 180)	17.2 at RT (2.49 at RT) 6.9 at 82 (1.00 at 180)	894
Polyimide	288–343 (550–649)	−253 to 538 (−423 to 1000)	17.2 at RT (2.49 at RT) 6.9 at 538 (1.00 at 1000)	53.6

RT, room temperature. Source: Snogren 1970

These functions would generally be unattainable using mechanical fasteners. Modifying the adhesive to obtain some of these objectives usually would also produce other changes in the properties of the joint, such as in mechanical properties and in peel resistance.

Although sealants are generally not discussed in this book, it should be pointed out that sealants

have many of the same characteristics as adhesives with respect to their molecular structures, storage limitations, surface preparations, curing, and so on. An exception is that an adhesive in a structural component would have a higher performance level than the corresponding sealant. Some adhesives serve equally well as sealants, especially where both bonding and sealing are required together.

24.3 Some Structural-Adhesive Types

In this section, only a very brief explanation/definition of some of the structural types of adhesives is presented [Messler 1993a]. A summary of the principal characteristics is listed in Table 24.3.

Epoxy adhesives are the reaction products of acetone and phenol. They are the most popular of all structural adhesives. Epoxies (epoxide adhesives) are thermosetting polymer resins that cure either by heating (in one-part systems) or by addition of a hardener or catalyst (in a two-part system) or by both with little or no need of pressure, becoming rigid through the formation of dense cross linking. The reaction is exothermic, and care must be taken to avoid overheating and causing voids. In addition to hardeners and catalysts, other additives may be used to modify the properties of the epoxy. The highest strengths (up to 77.2 MPa, or 11 ksi) are obtained with the heat-cured two-part epoxies. As a group, epoxies have low shrinkage, they tend to have low flexibility with poor impact strength, and they have low peel strength. Like most thermosetting polymers, they have good resistance to solvents.

The brittle behavior of the cured thermosetting polymer resins is overcome by incorporating various thermoplastics or elastomers that impart flexibility and toughness to the epoxy. The peel strength is also improved. These epoxies are known as modified epoxies; some examples are epoxy nylon, epoxy-polysulfide, epoxy-phenolic, and epoxy-nitrile (rubber).

Acrylic adhesives are based on acrylic monomers of ethyl acrylate, methyl acrylate, methacrylic acid, acrylic acid, acrylamide, and acrylonitrile. They are all two-part systems. They are not mixed for application; rather, the resin is applied to one adherent, and the accelerant applied to the other adherent. When mated, the bonding reaction occurs quickly (in minutes), even at room temperature. Pretreated parts can be stored separately for some time before bonding. Shear strengths can reach 28 MPa (4 ksi). Modified acrylics are adhesives in which the bonding

Table 24.3 Summary of principal characteristics of major structural adhesives

Adhesive	Type	Cure	Shear strength MPa	Shear strength ksi	Peel strength, N/m	Impact resistance	Solvent resistance	Moisture resistance	Substrates bonded
Epoxies	One(a) Two F&T(b)	Heat RT/heat H + P(c)	15.4	2.23	<525	Poor	Excellent	Excellent	Most
Polyurethanes	One One Two	Heat Moisture RT/heat	15.4	2.23	14,000	Excellent	Good	Fair	Most Smooth and nonporous
Modified acrylics	One	RT/heat	25.9	3.76	5250	Good	Good	Good	Most Smooth and nonporous
Cyanoacrylates	One	Moisture	18.9	2.74	<525	Poor	Good	Poor	Nonporous, metals, and plastics
Anaerobics	One	No oxygen	17.5	2.54	1750	Fair	Excellent	Good	Metals, glass, and thermosets
Silicones	One	Moisture	1.7–3.4	0.25–0.49	612	Good	Good	Excellent	Most
Phenolics	One Two F&P	Heat Heat H + P	N/A	N/A	N/A	Fair	Good	Good	Most
High-temperature	One F&P	Heat H + P	8–14	1.2–2.0	N/A	Fair	Fair	Poor	Thermoplastics and metals
Hot melts	One	Heat	4.3	0.62	N/A	Fair	Fair	Good	Thermoplastics and metals

RT, room temperature; N/A, not applicable (a) Numbers indicate number of components. (b) F&T, film and tape. (c) H + P, heat + pressure. Source: Messler 1993a

has been significantly enhanced by the addition of certain additives. They offer good peel, impact, and tensile-lap strengths over the temperature range of −110 to 120 °C (−165 to 250 °F). The modified acrylics, however, are quite flammable.

Examples of modified acrylics include acrylic-latex, acrylated silicones, acrylated urethanes, and acrylated silicone-urethanes. Silicone additions improve thermal stability, tensile strength, and resistance to solvents, abrasion, and ultraviolet light. Urethane additions increase toughness, thermal stability, and resistance to solvents, abrasion, and ultraviolet light.

Cyanoacrylates ("superglues") are composed of low-viscosity, liquid-acrylic monomers that polymerize easily in the presence of adsorbed water, especially if the adherent surface is slightly alkaline. Strong thermosetting bonds can be created with many materials with no added heat or catalyst, since most materials have adsorbed water present. Shear strengths up to 38.6 MPa (5 ksi) are attainable; peel strength and impact resistance are low, and moisture tolerance is poor. The principal advantage of cyanoacrylates is that they bond in seconds and will bond to almost any substrate. Methyl cyanoacrylate produces stronger and more impact-resistant joints than ethyl cyanoacrylate when bonding rigid materials. The latter, however, produces stronger and more durable joints than elastomeric, thermosetting, or thermoplastic polymer adhesives. The peel strength of cyanoacrylates is poor, they tend to be brittle, and they have limited temperature resistance.

Anaerobic adhesives and (more properly) sealants are single-component monomeric liquids that harden satisfactorily only in the absence of oxygen (air). They must be stored in the presence of oxygen. They have high fluidity, readily flow into small crevices, and cure with little or no shrinkage, providing thorough sealing. Addition of some urethane overcomes brittleness and improves peel and impact strengths.

Urethanes, or polyurethanes, are basically thermoplastic polymers that have the ability to develop cross links under certain conditions, thereby making them fairly rigid thermosetting adhesives. These polymers are available in one- and two-part systems, having inherently better flexibility and higher peel strengths than do the epoxies. They are generally applied to both adherents and are brought together when the proper tackiness is reached. Curing, which is usually done at room temperature, should be initiated immediately and may take hours or days. Heat can soften the adhesive if it becomes too dry before bonding.

Silicones are one- or two-component systems that cure to thermosetting solids. One-component systems cure at room temperature when exposed to atmospheric moisture. Two-component systems that cure by condensation polymerization are prone to polymerization reversion or decomposition. Silicones have good peel strength over the temperature range of −60 to 250 °C (−75 to 480 °F), and some survive limited exposure up to 370 °C (700 °F). Flexibility, impact resistance, and resistance to moisture, hot water, oxidation, and weathering are very good. Lap-shear strengths tend to be low. They are relatively expensive but are versatile and bondable to almost any material.

Phenolic or (more properly) phenolic-formaldehyde adhesives rely on penetration of the pore or cell structure (e.g., wood) of the adherent to develop bonding forces. They can be used as a primer on metals. They are frequently combined with other polymers to produce adhesives having one or more enhanced properties: higher bond strength, higher fatigue strength, higher service temperature, and better resistance to water, humidity, salt, and/or weather. For example, epoxy-phenolics offer excellent long-term service between 150 and 260 °C (300 and 500 °F) and down to −260 °C (−435 °F) if specially formulated.

Polyimides and the polybenzimidazoles are two specific high-temperature structural adhesives that are largely based on synthetic organics with open-ring structures that close on exposure to heat. Thus, instead of softening or decomposing, they become stronger on heating. These polymers are both expensive and difficult to handle in that they have long cure times and emit considerable volatiles. Polyimides offer superior long-term strength retention in air up to 260 °C (500 °F), while polybenzimidazoles are stable up to 288 °C (550 °F), but only for short times. Both are prone to degradation by moisture. This bonding scheme has been used in aerospace structures for metal-to-metal or metal-to-composite bonds.

Copolymers of polyethylene with polyvinyl, polyolefins, polyamides, polypropylene, nylon, polyester, and thermoplastic elastomers are used as hot-melt adhesives. These copolymers are 100% thermoplastic; that is, they will soften on heating and harden on cooling. These copolymers tend to soften at temperatures between approximately 80 and 100 °C (175 and 212 °F).

Some types will soften at temperatures of over approximately 100 °C (212 °F). They are applied in the molten state at temperatures mostly between approximately 150 and 400 °C (300 and 750 °F), depending on the adhesive. Most hot melts contain a diluent and/or filler. These hot-melt adhesives can be formulated to make either flexible or rigid bonds, and they will reach 80% of their bond strength in seconds after application. They can bond to either permeable or impermeable surfaces and are quite resistant to moisture. There are high-performance hot melts, such as polyamides and polyesters, that can produce bonds to withstand limited loads at elevated temperature without undergoing significant creep.

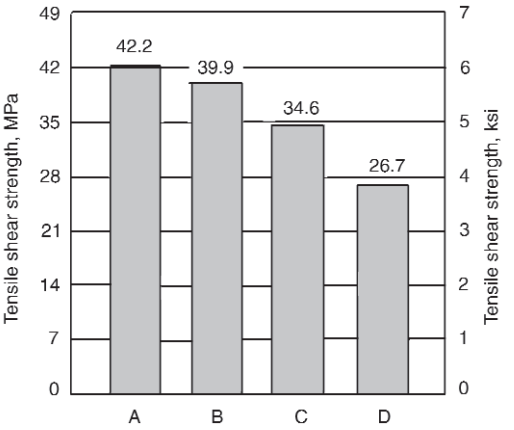

Fig. 24.4 Effect of aging conditions on an epoxy-film adhesive. A, fresh adhesive; B, cured after 90 days at 24 °C (75 °F); C, cured after 90 days at 32 °C (90 °F); D, cured after 1 h at 50 °C (122 °F) in a 95 to 100% humidity chamber. (Normal 120 °C, or 248 °F, cure cycle used after aging). Source: Acker 1990

24.4 Storage Life and Exposure of Adhesives

Adhesive and sealant materials have finite lives in storage. After being compounded, their useful lives are further limited. Shelf life can vary from a few days to approximately a year, depending on the components used in the mixture and the handling. Generally, the two-component products have much longer shelf lives than the one-component ones. Storage temperatures can be as low as −18 °C (−0.4 °F), which allows for storage of most materials for six months to a year [Acker 1990]. Premixed two-part systems, such as epoxy adhesives that contain a catalyst and resin, are stored at temperatures below −40 °C (−40 °F) until used. The premixing is done under vacuum to avoid moisture/air entrapment. Quick-setting epoxies should generally be avoided. Because of their limited pot life, bonding operations must be completed within an hour [Switz 1979].

Some materials cannot tolerate subzero temperatures; for example, freezing can damage the emulsions of aqueous solutions and dispersions. Because some of the components may react exothermically (heat evolution), it is important not to store them above their specified maximum storage temperature. After mixing, an exothermic reaction may provide sufficient heat for curing or even cause overaging. The stored materials may also be adversely affected by light and humidity. Some materials must be stored in the dark or in opaque containers [Messler 1993a]. Resins and curing agents for thermosetting adhesives should be stored apart to prevent accidental contamination if container breakage or leakage occurs. Exposure of a sealant in an uncovered container for just a day may result in the adsorption of excessive moisture. Unsealing a container too soon after removal from cold storage may cause excessive condensation. If the stored product deteriorates, the curing behavior, which depends on the characteristics of the product (e.g., a viscosity increase of liquid or paste, or lack of tack of films, etc.), is affected, resulting in a degraded adhesive bond. An example of a loss in strength due to aging of an epoxy-film adhesive is shown in Fig. 24.4 [Acker 1990]. The change in viscosity as a function of time for a paste adhesive is shown in Fig. 24.5. The increase in viscosity is initiated just before the expired shelf life [Acker 1990].

24.5 Surface Preparation

Adhesive-joint failure can be caused by a number of factors, such as poor design, improper adhesive selection for either one or both of the substrates, the operating environment (especially temperature), service overload or inadequate bond strength, and/or inadequate surface preparation [Small and Courtney 2005]. Surface preparation is claimed to be by far the most important factor in producing a good adhesive bond [Brush Wellman 2001, Switz 1979]. The main steps are degreasing, acid cleaning, neutralizing, drying, applying the adhesive, and subjecting the joint to the recommended heat and pressure. An appropriate fixture should be used

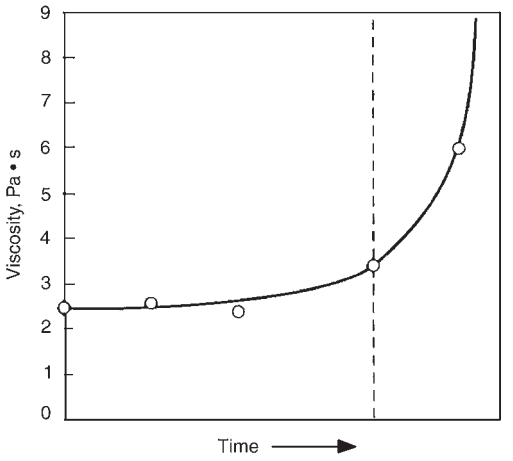

Fig. 24.5 Change in viscosity of a paste adhesive as a function of time at room temperature. Shelf life is indicated by the vertical dashed line. Source: Acker 1990

to restrain the joint during curing. If service temperatures are between –50 and 120 °C (−60 and 250 °F), it is best to select an adhesive curable at room temperature [Switz 1979]. Because of the great importance given to surface preparation, several examples of adherent (substrate) surface preparation are summarized. A handbook on adhesives lists a number of methods that have been investigated and are expected to be promising [Cagle 1973]. For all methods, adherents had first been vapor degreased:

- Method A (Method also suggested by Althouse 1976. Degreasing was done by wiping with trichloroethylene.):
  1. Immerse for 3 to 4 min in a solution of 20 wt% sodium hydroxide in distilled water maintained at 77 to 82 °C (170 to 180 °F).
  2. Rinse with cold water.
  3. Oven dry at 135 to 149 °C (275 to 300 °F) for approximately 15 min.
  4. Bond or prime as soon as possible.
- Method B:
  1. Immerse for 8 to 10 min in a solution of 283 g of Prebond 200 (American Cyanamid Company) to 3.8 L (1 gal) of water.
  2. Rinse thoroughly.
  3. Oven dry at 79 to 93 °C (175 to 200 °F) for 15 min.
- Method C:
  1. Immerse for 8 to 10 min in the same Prebond 200 solution used in method B.
  2. Rinse.
  3. Immerse for 10 min in a 20 vol% chromic acid solution maintained at 82 to 93 °C (180 to 200 °F).
  4. Water rinse at 54 to 60 °C (130 to 140 °F).
  5. Force dry at 82 to 93 °C (180 to 200 °F) for 30 min.
- Method D:
  1. Spray clean with liquid carrying Burr-al, 220 grit.
  2. Alkaline clean (using method B).
- Method E:
  1. Degrease with methyl ethyl ketone (MEK), followed with a vapor degrease.
  2. Etch for 30 s in a solution of (by weight) 45 parts nitric acid, 7 parts hydrofluoric acid, and 260 parts distilled water maintained at 21 to 27 °C (70 to 80 °F).
  3. Rinse thoroughly.
  4. Dry for 20 to 30 min at 71 to 82 °C (160 to 180 °F).
- Method F:
  1. Immerse for 3 min in a solution of (by weight) 420 parts hydrochloric acid, 44 parts phosphoric acid, and 32 parts hydrofluoric acid maintained at 21 to 27 °C (70 to 80 °F).
  2. Remove smut (if any) with MEK.
  3. Rinse thoroughly.
  4. Dry at 82 to 88 °C (180 to 190 °F).
- Method G:
  1. Apply the following paste to the faying surface for 3 min at room temperature: (by weight) 10 parts sulfuric acid, 1 part sodium dichromate, and 30 parts water. Add Cab-o-Sil (Cabot Corp.) to make a thixotropic paste, or it may be used as a hot solution maintained at 66 to 71 °C (150 to 160 °F).
  2. Rinse.
  3. Dry thoroughly.

The tensile-shear strengths of beryllium-beryllium bonds using various adhesives following the surface preparation of method G and tested at a series of temperatures are shown in Fig. 24.6. The tensile-shear strengths of the beryllium bonds using epoxy-phenolic and four different surface-preparation methods are shown in Fig. 24.7.

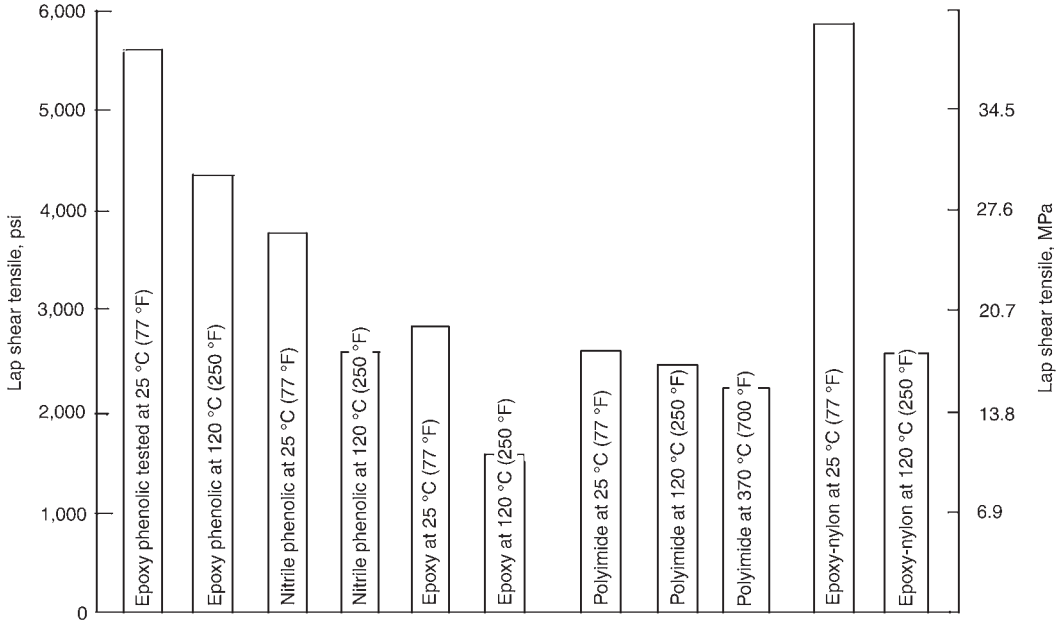

Fig. 24.6 Tensile-shear strengths obtained at a series of temperatures for beryllium-beryllium bonds using various adhesives and a sulfuric acid-sodium dichromate paste (method G). Test temperatures are shown. Source: Cagle 1973

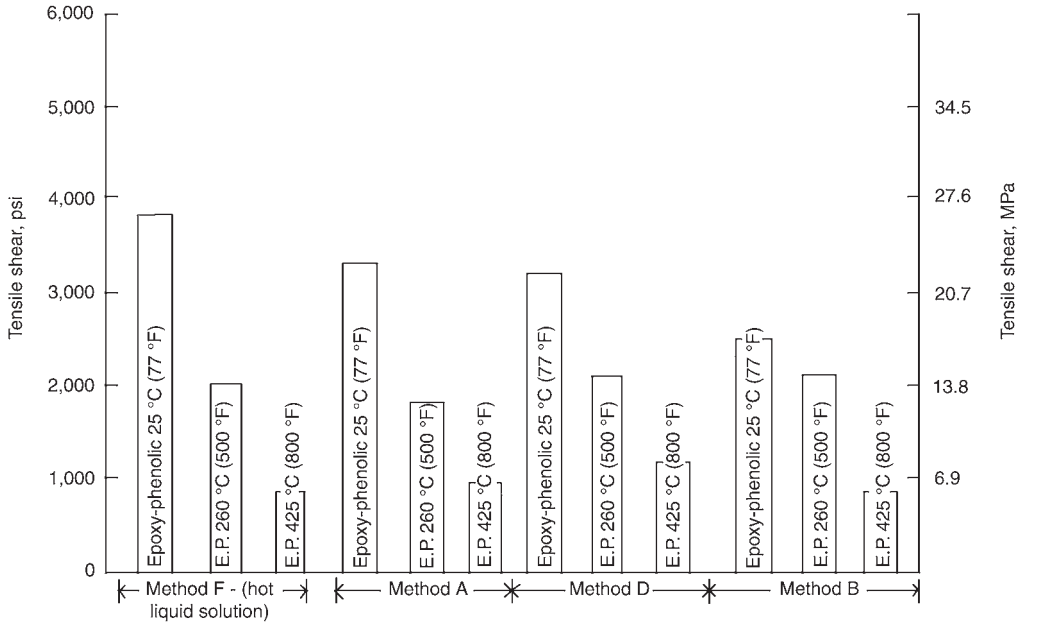

Fig. 24.7 Tensile-shear strengths obtained at a series of temperatures for beryllium-beryllium bonds using an epoxy-phenolic (E.P.) adhesive and four different surface-preparation methods (see text). Test temperatures are shown. Source: Cagle 1973

Cagle [1973] offers yet another set of surface preparation steps for beryllium:

1. Degrease with trichloroethylene.
2. Immerse for 5 to 10 min in a sodium hydroxide solution (one part NaOH to 6 to 8.5 parts distilled H_2O, by weight).
3. Wash in tap water.
4. Rinse in distilled water.
5. Oven dry for 10 min at 122 to 177 °C (250 to 350 °F).

Another method reported for surface preparation was to coat the beryllium surface with an epoxy-based paint primer within 8 h after etching [Switz 1979]. Etching was used to remove the machining-damaged surface. Priming provides protection from corrosion and significant storage time prior to bonding. The etch process provides a matte finish that results in good adhesion bonding. A strippable primer can also be used to protect the surface. All that will be required prior to bonding is a thorough wipe with either MEK or acetone. If a primer is not used, the surface should be thoroughly scrubbed with a cleansing powder free from halogens until a water-break-free surface is obtained. The part should then be etched to remove 3 to 5 μm of surface metal, rinsed, oven dried, and bonded within 2 h. Scrubbing and rinsing should be done with deionized water to avoid any corrosive attack. A slightly acidic water is suggested to avoid corrosion problems [Switz 1979]. Surface abrasion may add to the bond strength by facilitating mechanical interlocking. Surface abrasion would generally be limited to the use of relatively inactive materials such as stainless steel.

An evaluation of etchants used in a surface-preparation procedure for beryllium was reported using the following procedure [Fullerton-Batten 1977]: degrease in a proprietary solution of P3 VR580–4 (buffered alkaline solution) at 80 °C (175 °F) for 20 min, rinse in running water, etch, rinse in running water, final rinse in deionized water, dry in an oven at 70 °C (160 °F), apply primer, cure primer, and store in sealed polyethylene bags. Four different etchants were evaluated based on control of the etching reaction, having a water-break-free surface (no interference of flow of rinsing water), surface appearance, and the relative shear-strength values obtained with a single-lap bond test.

The etchant reactions and surface appearances obtained for the different etchants are:

1. Etching at room temperature for 2 to 3 min using dilute concentrations of potassium dichromate plus sulfuric acid (90 g $K_2Cr_2O_7$ + 200 mL H_2SO_4 + 3800 mL H_2O) gave an extremely vigorous reaction, rapidly removed metal, and developed rough surfaces. Use only with cooling or in large baths.
2. Etching 5 min at 90 °C (195 °F) with sodium hydroxide (20 wt%) gave a controllable reaction with minimal metal removal, developed an even matte surface, and formed a loose surface deposit that was easily removed on rinsing.
3. Etching 8 min at 90 °C (195 °F) with Prebond 700 gave a controllable reaction with minimal metal removal, developed a clean, even matte surface, and was the least problematic of the four treatments.
4. Nitric acid (28 wt%) + hydrofluoric acid (2 wt%) + H_2O (70 wt%) gave a somewhat vigorous exothermic reaction and developed an even matte surface, although rougher than with treatment 2 or 3 and less rough than with treatment 1.

Prior to etching, all parts (sheets) were degreased at 80 °C (175 °F) for 20 min using a proprietary buffered alkaline solution (P3 VR580–4), rinsed in running water, and then etched using the previously mentioned procedures. The parts were then rinsed again in running water, followed by a final rinse in deionized water, and oven dried at 70 °C (160 °F). The parts were then primed and stored in sealed polyethylene bags until bonded.

All four treatments exhibited good water-break-free surfaces. Procedures 2 and 3 produced the best shear-strength values of 35.5 and 36.7 MPa (5.1 and 5.3 ksi) (average of seven tests each), respectively. The adhesive system FM 1000/BR 1009–8 was used with curing in an autoclave. Values of 45.4 and 48.5 MPa (6.6 and 7.0 ksi) (average of seven tests each), respectively, were obtained using the adhesive system FM 123–5/BR 127. Additional tensile, sheer, and fatigue tests were performed, evaluating different adhesive systems and comparing adhesive bonding with riveting and with the combination of rivets and adhesives. Adhesive bonding proved to be best [Fullerton-Batten 1977].

24.6 Applying Adhesives

Adhesives may be applied either as a liquid, paste, film, or tape. The transportation industries are the largest users of adhesives, with the aerospace industry featuring the most critical applications [Acker 1990]. For structural components, the aerospace industry commonly uses a one-component, film-type adhesive, which is applied to chemically prepared substrates under environmentally controlled conditions. The resultant assembly is cured in a heated autoclave under controlled temperature and pressure conditions. The use of liquid or paste adhesives in the transportation industries is largely confined to secondary bonding, repair, or rework activities. The liquid must be able to wet the adherent and, in some cases, change its state or react with it. This situation is most obvious with organic adherents.

Various methods are described for applying liquid adhesives [Pizzi and Mittal 2003].

Brushing. Uneven films are likely. For selected areas or complicated shapes, use a stiff brush.

Flowing. Use for flat surfaces. Fast assembly is possible by using pressure-fed flow guns, which allows for better thickness control than with brushing.

Roll Coating. Use for wide sheet and film. The material is coated with adhesive as it passes between the transfer roller (for adhesive) and the pressure roller (controls adhesive thickness). It is the best method for speed and uniformity.

Knife Coating. An adjustable knife blade, rod, or bar controls both the adhesive flowing onto a moving sheet and the adhesive thickness.

Silk screening is useful for bonding selective areas or patterns.

Melting. Hot-melt-type adhesive is heated to a fluid state and dispensed by suitable nozzles onto the workpiece. It can be applied to knife-coating techniques.

Fluidity is one of the most important properties of an adhesive. Too little flow produces patchy, void-containing bonds with low-strength areas. Excess flow results in variable bond-line thickness and unreproducible strengths in metal-to-metal bond joints [Pizzi and Mittal 2003].

24.7 Curing Adhesives

Curing variables (temperature, time, mechanical restraint, and applied pressure) will depend primarily on the type of adhesive [Pizzi and Mittal 2003]. A number of heating methods can be used: ovens, hot presses (or platens), liquid baths such as silicone oil (with care to avoid contact with the bond), infrared radiation, metal or graphite conductor strips embedded in the adhesive, wrap-around heating tapes, heat from ultrasonic activation energy at the bond interfaces, and induction heating. The use of graphite conductor strips produces bond strengths comparable to strengths obtained by oven curing and offers a number of advantages, such as easy access of heat to localized regions, uniformly sized strips to avoid hot or cold spots, less distortion, rapid heating, close control of bond-line temperature, the complete assembly need not be heated, and reduced processing time [Pizzi and Mittal 2003]. A constant pressure should be sustained to allow for dimensional changes during curing, such as shrinkage. Some adhesives contain volatile components to improve their viscosity, and provisions should be made for their removal as well as for the possibility of by-products being formed during curing.

To avoid squeeze-out during clamping and curing, spacing beads (0.05 to 0.15 mm, or 0.002 to 0.006 in. diameter), which are usually made out of ceramic, can be used to keep the mating parts from touching. The beads, which should amount to only approximately 0.5 wt% of the adhesive weight, do not affect the bond strength [Switz 1979]. The wet adhesive can be spread with a comblike tool to assure a uniform thickness. To minimize runout after assembly, it is best to allow the adhesive to gel slightly before assembling the mating surfaces. When assembling the parts, sliding or swiping movements must be avoided to prevent introducing bubbles into the adhesive. For room-temperature curing systems, a 16 h period is the minimum time for keeping the parts in a restrained position before handling; maximum loads should not be applied for seven additional days, when full strength should be reached [Switz 1979]. Epoxies can frequently be cured by holding at 90 °C (195 °F) for 1 h, still following the 16 h restrained-position period. The times and temperatures should be verified for each adhesive system. If a bond is found to be defective and not repairable, the joint can be disassembled by heating the part to 350 °C (660 °F) for 1 h, which will crystallize most adhesives and facilitate separation of the mating surfaces. The beryllium should not be affected by the heating.

Surfaces must be properly prepared, as before, for rebonding [Switz 1979].

24.8 Mechanical Properties

The effect of operating temperature on the tensile strength of a beryllium joint bonded with a polyimide adhesive is shown in Fig. 24.8 [Snogren 1970]. Also, using the epoxy adhesive Dexter-Hysol EA9330 with the surface-preparation and epoxy-application procedures described by Salazar et al. [1999], butt-adhesive-bonded tensile samples had fracture strengths of 60.5 ± 3.4 MPa (8 ± 0.5 ksi) at room temperature, which increased to approximately 131 MPa (19 ksi) at −269 °C (−450 °F). Pressurized burst tests on adhesive-bonded beryllium hemispheres indicate burst strengths of approximately 24 and 172 MPa (4 and 25 ksi), without prior stress relief and following a stress-relief treatment, respectively. It was proposed that the thin oxide layer formed during the stress-relief treatment (in spite of the high vacuum) was better suited chemically for the adhesive bonding than was a metallic beryllium surface. The preparation of the epoxy adhesive is given as:

1. Mix small quantities of adhesive vigorously for five minutes using 33 parts B to 100 parts A (of Dexter-Hysol EA9330).
2. Degas in vacuum at 560 mm of mercury for five minutes.
3. Apply adhesive to the substrate as quickly as possible.
4. Cure samples under a pressure of approximately 97 kPa (applied by weight or spring) for 16 h at 23 °C followed by 2 h at 82 °C.

Adhesives applied to beryllium in the manufacture of the space shuttle orbiter navigation base are listed in Table 24.4 [Norwood 1984]. Bonding was performed on 36 detail parts in 6 different stages using 5 different adhesives. All the beryllium components were etched and primed with BR 127 primer. The effect of using different adhesive systems on the strength of beryllium joints can be seen in Table 24.5 [Brush Wellman 2001]. Two adhesives that have been successfully applied to beryllium in space-hardware applications are EA934 (Hysol Corporation) and Epon 825 (Shell Chemical). Two adhesive systems that were successfully used in an evaluation investigation on bonding beryllium are FM 1000, an unsupported polyamide epoxy film adhesive with a curing temperature of 175 °C (345 °F), and FM 123–5, a supported nitrile epoxy film adhesive with a curing temperature of 125 °C (255 °F). Both adhesives were used with compatible primer systems, FM 1000/BR 1009–8 and FM 123–5/BR 127, respectively [Fullerton-Batten 1977]. (Adhesives and primers

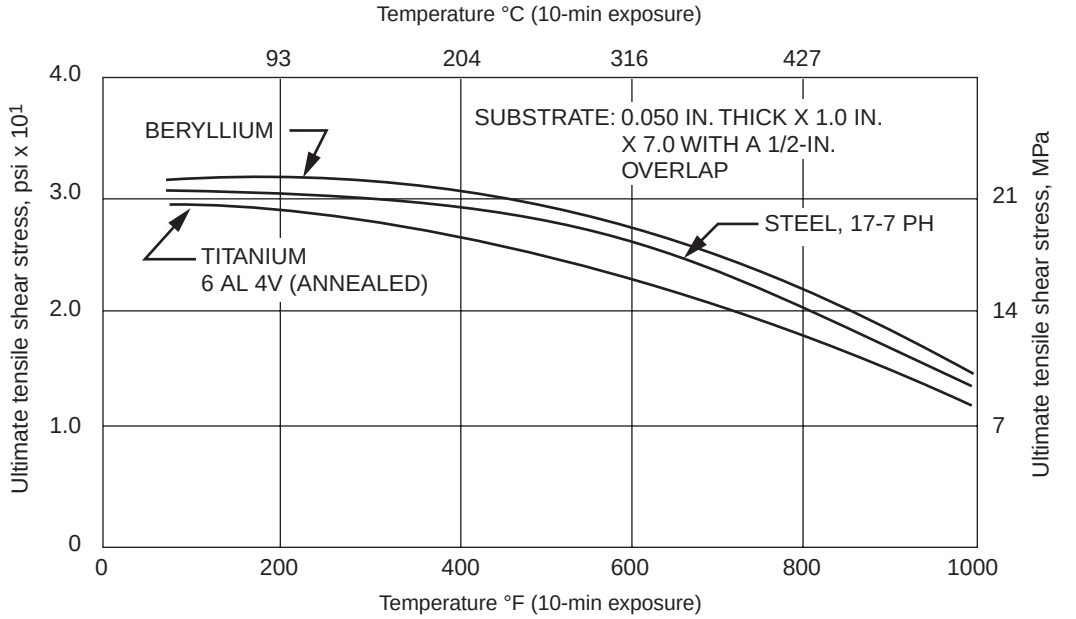

Fig. 24.8 Effect of operating temperature on the tensile strength of beryllium, steel, and titanium bonded with polyimide adhesives. Source: Snogren 1970

Table 24.4 Adhesives used in multistage bonding of the space shuttle orbiter

Adhesive	Type of joint	Cure temperature °C	Cure temperature °F	Cure time	Pressure kPa	Pressure psi
Epoxy-phenolic HT424	Be splices to Be fitting	171 ± 5.6	340 ± 10	60–90 min	69 (min)	10 (min)
Nitrile epoxy FM 123 and FM 37	Be honeycomb panel	121 ± 5.6	250±10	60–90 min	310	45
FM 123	Be splices to Be panel	88±5.6	190±10	6–7 h	69–103	10–15
Epoxy No. 206	Be splice to edge panel	Room temperature or		72 h	69–103	10–15
		82±5.6	180±10	1–2 h	69–103	10–15
EA934	Small tool holes and gaps	Room temperature or		24 h	Contact	
		46–82	115–180	6 h	Contact	
Epoxy No. 206	Titanium and Corrosion-resistant steel fittings to Be upper surface	Room temperature or 82 ± 5.6	180 ± 10	72 h 1–2 h	69–103 69–103	10–15 10–15

Source: Norwood 1984

Table 24.5 The influence of adhesive system on the strength of adhesive-bonded beryllium joints

Adhesive system	Average strength	Type of test
EA9309-BR 127 primer	32.4 MPa (4.70 ksi)	Lap shear
HT424-BR 127 primer	17.2 MPa (2.49 ksi)	Lap shear
FM 123-BR 127 primer	24.1 MPa (3.50 ksi)	Lap shear
FM 123-BR 127 primer	985 kg/m (662 16/ft)	Honeycomb peel
EA934-BR 127 primer	75 Shore D	Hardness
Epoxy No. 206-grade A	24.1 MPa (3.50 ksi)	Lap shear
BR 127 primer	716 kg/m (481 16/ft)	90° peel

Source: Brush Wellman 2001

were obtained from the Bloomingdale Division of American Cyanamid Company.)

In a study on the strength of beryllium/stainless steel adhesive bonds, various adhesives and several types of beryllium were evaluated [Cooper et al. 1977]. The stainless steel consisted of two threaded grips with flat faces, between which either a disk or square beryllium sample 2 to 3 mm (0.08 to 0.12 in.) thick was bonded to the steel. The samples, which were oversized to prevent edge effects, were grit blasted, degreased, and bonded within 24 h. The adhesives used were:

- Epoxide—Epikote 828, 100 parts by weight (pbw) resin, and Versamid 125, 100 pbw polyamide
- Polyimide—Keramid 500 (Rhone-Poulenc Paris)
- Urethane—CS 8097, two-part polyurethane, and Bostik Quickset
- Cyanoacrylate—IS 150 (thickened version) Loctite

A polyamide curing system was used for the epoxide to avoid the possible corrosive effect of amine hardeners on beryllium. The beryllium samples were:

- Fully dense cold isostatic pressed/hot isostatic pressed P-1-grade (electrolytically refined) beryllium
- 95% dense hot pressed P-10-grade (commercial purity) beryllium
- 90% dense, plasma-sprayed and sintered (PSS) P-10-grade beryllium

After storing 14 days at room temperature, they were tested in tension (1.27 mm/min, or 0.05 in./min) at crosshead speed. The urethane and epoxide adhesives were found to have marginally superior strengths, roughly of the order of 30 to 40 MPa (4 to 6 ksi), with the epoxide giving the most consistent higher strengths for all beryllium grades. Poor tensile results were obtained for the PSS P-10 beryllium when bonded with cyanoacrylate. This result was attributed to the high porosity of the PSS beryllium and the poor gap-filling properties of this class of adhesive. Preliminary aging studies with epoxide and urethane for up to six months at 60 °C (140 °F) indicated that significant strength increases are attainable by aging.

24.9 Mechanical Fasteners

Mechanical fasteners for beryllium generally fall into two categories, namely, bolts and rivets. In both categories, a hole must first be created in the metal. Producing holes that are free from cracks and delamination is considerably more difficult with beryllium than with other metals [Switz 1979]. A more complete list of mechanical fasteners and other mechanical fastening methods, many of which may not normally be applicable to beryllium, are described in considerable detail in the reference and include fasteners,

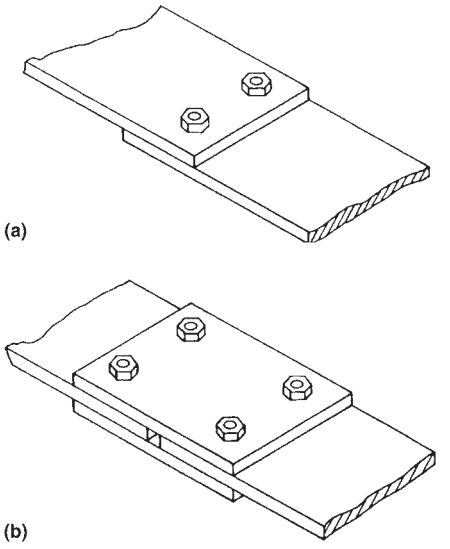

Fig. 24.9 Illustrations of two mechanical fastener, shear-loaded joints. (a) Lap joint. (b) Butt-type (or double-lap) joint. Source: Messler 1993b

such as bolts, screws, rivets, dowels, pins, nails, keys, retaining rings, eyelets and grommets, stapling, stitching, snap fits, and clips; and integral design features, such as flanges, interlocking members (tongue-and-groove, teeth, and tabs), roughened gripping surfaces, and deformed features (crimps, hems, punch marks, and stakes) [Messler 1993b].

In a mechanically fastened assembly, the load is transferred between components through the fasteners such that high stress concentrations are developed at the fasteners and surrounding metal. With poor designs, these high stresses can lead to premature failure. In addition, the stress concentrations can lead to distortion of the fastener hole and/or the fastener, especially in a component that exhibits viscoelastic behavior. Some of the loading may be carried by friction between the joined members. Simple examples of mechanical fastener joints are shown in Fig. 24.9 and 24.10, the latter figure illustrating some stress patterns. As in the case with adhesive joints, differences in the coefficient of thermal expansion between the beryllium and the

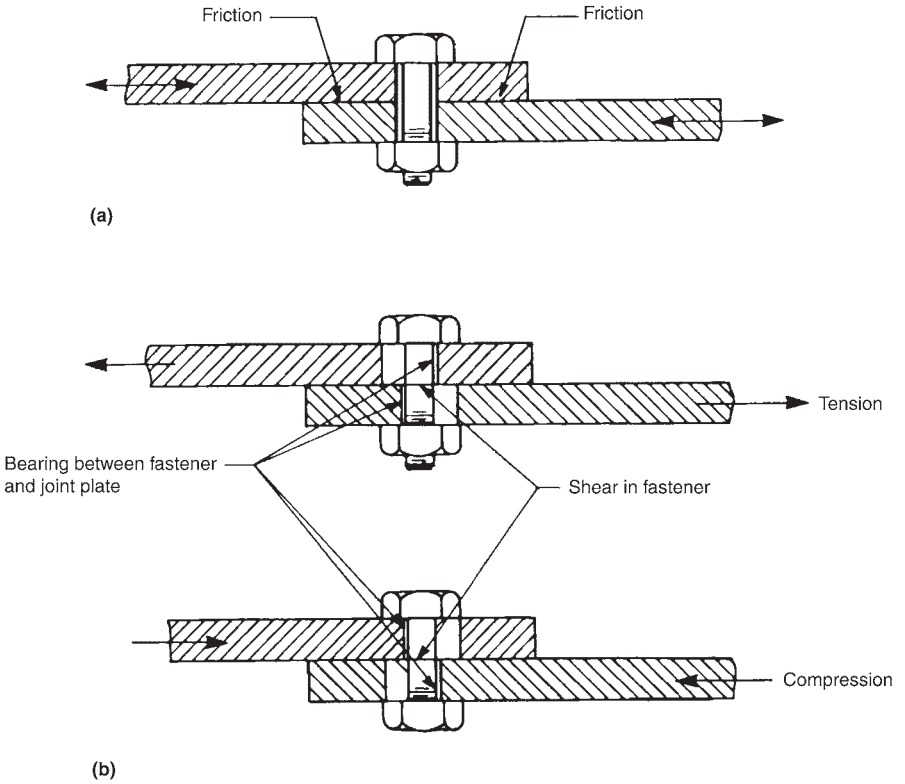

Fig. 24.10 Illustrating differences between (a) friction-type joints and (b) bearing-type joints. In the latter case, the load is transferred essentially through the fastener, thus introducing a shear stress across the fastener. Source: Messler 1993b

fastener as well as between the beryllium and the mating component should be considered with reference to the service-temperature range.

Some advantages of mechanical fasteners over adhesive bonding are [Messler 1993b]:

- Disassembly with little or no destruction of the component
- Relative motion is possible.
- No change in chemical composition or microstructure
- Dissimilar materials can be joined.
- Damage tolerant
- Does not require any special joint preparation
- Relatively low cost (unless large installation costs occur)
- Adaptable to automation

Some of the disadvantages of mechanical fasteners over adhesive bonding are [Messler 1993b]:

- Significant stress concentrations
- Fluid intrusion or leakage possible
- Potential entrapment of corrosive agent, accelerating corrosion
- May involve high labor-installation costs
- Joints can loosen in service under vibration, flexing, thermal cycling, and so on.
- Increased weight
- Utility limited with some materials
- Possible fastener pull-through or pull-out
- Vacuum system must be used to collect machining chips when drilling holes in beryllium components.

Holes in beryllium can be produced either by drilling or by electrical discharge machining (EDM). The advantages of EDM over drilling are that it offers the possibility of creating many holes simultaneously, and noncylindrical holes can be made. Minimum radial clearance for bolts and rivets is given as 0.025 mm (0.001 in.); the clearance must also allow for expansion of the rivet [Switz 1979]. If holes must be threaded, it is best to use a torque-controlled machine rather than hand threading. The drill tool must have a rounded-root configuration. It is suggested, when eliminating machining damage, that a stress-relief heat treatment is preferable to etching, because the etching may alter thread configuration. A recommended stress-relief schedule for a threaded hole is shown in Fig. 24.11 [Switz 1979].

Following a stress-relief treatment, the thread configuration, dimensions, and tolerances must conform to specifications (such as MIL-S-7742). Structural inserts can be used to prevent

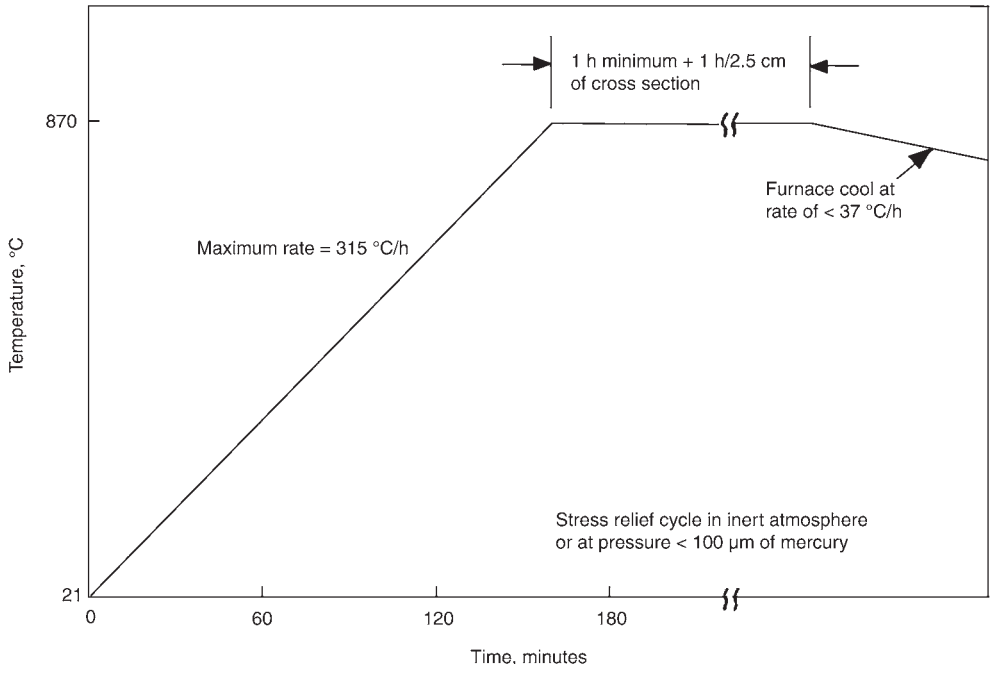

Fig. 24.11 Stress-relief cycle for removing machining damage of a threaded hole following cycle used for beryllium hot pressed block. Source: Switz 1979

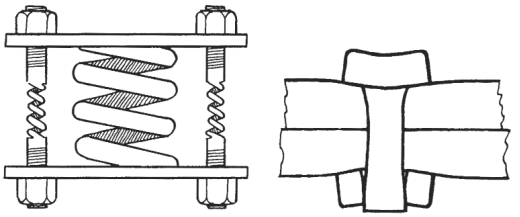

Fig. 24.12 Illustration of distortions developed by clamping. Components represented by heavy spring during bolting being compressed by a group of small springs (bolts). Distortion of the solid spring (components) is shown greatly exaggerated on the right. Source: Bickford 1990

wear and damage (galling, stripping, corrosion) of the beryllium threads. A helical-coil-type insert is suggested, because it does not require any staking into the part for retention and thus avoids any installation-impact forces on the beryllium [Switz 1979]. Where nut plates are used (instead of tapping into the beryllium), it is best to bond the plates to the beryllium rather than attach them with rivets. Using nut plates will usually require fewer drilled holes in the beryllium, because each nut could be loaded to higher stresses than would be accommodated in a threaded beryllium hole.

A bolt acts as a pin in preventing relative slipping between the joined components and as a heavy spring clamping the components together. It should be noted that the behavior and life of a mechanical joint would depend as much, if not more, on the correctness of the clamping force holding the components together as on any other design factor or environmental factor [Bickford 1990]. In general, the maximum clamp forces that the components can withstand should be used. In addition to the tensile stresses introduced by tightening of the nut, the frictional forces between nut and bolt threads introduce torsional forces, and bending stresses may develop due to any misalignment of the bolts and nuts with component surfaces. This behavior is shown in Fig. 24.12, where the interaction between components is represented by a heavy spring being compressed by a group of small springs (bolts) [Bickford 1990].

Rivets are the most commonly used unthreaded fasteners for structural joints. A rivet consists of a head and a smaller-diameter shank made from plastically deformable material (metal or thermoplastic). After inserting the rivet through the aligned holes of the components to be joined, the protruding portion of the shank is upset, creating a second head. The principle is illustrated

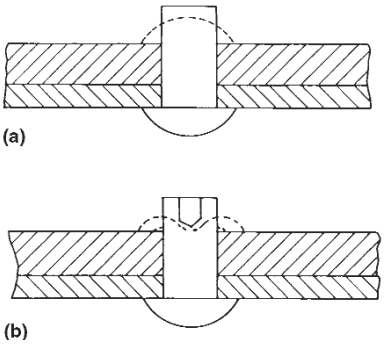

Fig. 24.13 (a) Solid and (b) tube rivets in a joint, before and after upsetting. Solid line, before upsetting; dashed line, after upsetting. Source: Messler 1993b

in Fig. 24.13 for solid and tubular rivets. There are many types of rivets with a variety of head shapes used for different applications [Messler 1993b]. The solid shape shown in the figure is the standard structural rivet and can be either hot or cold driven. The upsetting force depends on the material, size, and temperature of upsetting. The use of squeeze-type rivets is preferred for beryllium in contrast to those requiring an upset force [Messler 1993b].

Although extensive information is available in the literature on mechanical fasteners, very little was found that pertained to beryllium. This observation suggests that the use of adhesive is largely preferred over the use of mechanical fasteners for joining of beryllium. Probably, the largest use for beryllium has been in aerospace and transportation applications, and here, the weight factor is an important criterion in selecting the joining methods to be used.

REFERENCES

Acker, R.S.C., 1990. Manufacturing Use, *Adhesives and Sealants,* Vol 3, *Engineered Materials Handbook,* ASM International, p 681–725

Althouse, L.P., 1976. UCID 16997, Lawrence Livermore National Laboratory, Feb 2, 1976

Bickford, J.H., 1990. *An Introduction to the Design and Behavior of Bolted Joints,* Marcel Dekker, Inc., New York, NY

Brush Wellman, 2001. "Designing with Beryllium," Brochure 517, Cleveland, OH

Cagle, C.V., 1973. Surface Preparation for Bonding Beryllium and Other Adherents, *Handbook of Adhesive Bonding,* McGraw-Hill Book Company, NY, p 21/1–21/10

Cooper, R.E., Kerr, C., and Walker, P., 1977. Adhesive Bonding of Beryllium, *Proceedings of Beryllium, Fourth International Conference on Beryllium* (London, England), Oct 4–7, 1977, The Metals Society, London, England, p 39/1–39/6

Friedman, H., 1989. Photochemical Machining, *Machining*, Vol 16, *Metals Handbook*, 9th ed., ASM International, p 387–393

Fullerton-Batten, R.C., 1977. The Adhesive Bonding of Beryllium Structural Components, *Fourth International Conference on Beryllium* (London, England), Oct 4–7, 1977, The Metals Society, London, England, p 40/1–40/17

Gauthier, M.A., 1990. Adhesive Materials, *Adhesives and Sealants*, Vol 3, *Engineered Materials Handbook*, ASM International, p 73–93

Messler, R.W., Jr., 1993a. Adhesives and the Bonding Process, *Joining of Advanced Materials*, Butterworth-Heinemann, Boston, MA, p 143–180

Messler, R.W., Jr., 1993b. Mechanical Fastening, *Joining of Advanced Materials*, Butterworth-Heinemann, Boston, MA, p 23–61

Norwood, L.B., 1984. Application of Beryllium on the Space Shuttle Orbiter, *SAMPE J.*, Vol 20, p 7–15

Packham, D.E., 1990. Microstructural Analysis (of Adhesives), *Adhesives and Sealants*, Vol 3, *Engineered Materials Handbook*, ASM International, p 406–419

Pizzi, A., and Mittal, K.L., 2003. *Handbook of Adhesive Technology*, 2nd ed., revised and expanded, A. Pizzi, and K.L. Mittal, Ed., Marcel Dekker, Inc., NY

Salazar, M.A., Hermes, R., and Margevicius, R.W., 1999. Effects of Joining and Testing Parameters on the Adhesive Strength of Epoxy-Bonded Aluminum and Beryllium, *Fusion Technol.*, Vol 35 (No. 3), p 119–122

Sharpe, L.H., 1990. Overview: Adhesives Technology, *Adhesives and Sealants*, Vol 3, *Engineered Materials Handbook*, ASM International, p 33–38

Small, D.J., and Courtney, P.J., 2005. Fundamentals of Industrial Adhesives, *Adv. Mater. Process.*, Vol 163 (No. 5), p 44–47

Snogren, R.C., 1970. Space-Age Bonding Techniques—Part 2, Adhesive Bonding, *Mech. Eng.*, Vol 92 (No. 5), p 33–38

Switz, R.J., 1979. Joining I: Mechanical/Adhesive, *Beryllium Science and Technology*, Vol 2, D.R. Floyd and J.N. Lowe, Ed., Plenum Press, NY, p 231–247

Beryllium Chemistry and Processing, p 459-483
By Kenneth A. Walsh
Edited by Edgar E. Vidal, Alfred Goldberg,
Edward N.C. Dalder, David L. Olson, and Brajendra Mishra

CHAPTER 25

Aqueous Corrosion of Beryllium and Beryllium Alloys

Alfred Goldberg and Edward N.C. Dalder, Lawrence Livermore National Laboratory
Edgar E. Vidal, Brush Wellman, Inc.
Brajendra Mishra, Colorado School of Mines

25.1 Corrosion in Various Environments

Corrosion in beryllium is generally not a serious problem. Beryllium has a high affinity for oxygen, and in dry air, a protective, nonporous oxide (BeO) film forms. It reaches a limited thickness of approximately 100 Å, although thicknesses of approximately 30 Å are often quoted. The oxide occupies a volume 1.68 times that of the metal consumed in forming the oxide. Thus, being in compression, the oxide does not have any tendency to spall. The oxide film will decrease interdiffusion and chemical interaction rates between the metal and the environment.

Sanchez et al. [1999] consider three stages of corrosion of beryllium in the evolution of storage conditions. In the first stage, "dry" general corrosion and pitting corrosion may occur because of the existence of sufficient oxygen and aggressive anions such as Cl^-. In the second stage, starting immediately after being enclosed, either "dry" or aqueous general corrosion may occur depending on the humidity in the container, while pitting corrosion may continue until all the oxygen is consumed. In the third stage, general corrosion becomes dominant, and slow pitting corrosion is absent.

Beryllium is attacked by fluorine, HF, HCl, H_2SO_4, and HNO_3 at room temperature. Chloride and sulfate ions are the most critical contaminants in aqueous corrosion. Nitrate and chromate ions are comparatively innocuous unless present in amounts sufficient to substantially increase the conductivity of the water [Darwin and Buddery 1960b]. Cupric and ferric ions can exert a strongly corrosive effect. The normally passive beryllium oxide film is soluble in concentrated acids, fuming bases, and some chlorine-containing solvents. Beryllium chlorides are very soluble in water as well as in ethyl alcohol, ethyl ether, chloroform, and carbon disulfide [Birkbeck et al. 1999]. In the presence of chloride ions, beryllium is susceptible to pitting, occurring at localized sites in a sporadic and random manner. Because most of the surface remains passive, it can occur unnoticed and lead to catastrophic failure. In humid environments, however, beryllium in the presence of chlorides is especially susceptible to pitting attack. Severe stress amplification can occur at these pits [Vaidya et al. 1999]. Cold concentrated HNO_3 passivates beryllium, whereas the dilute acid will attack the metal. Cold dilute (1 *M*) H_2SO_4 attacks beryllium slowly, with the evolution of hydrogen. The more concentrated acid (e.g., 5 *M*) can react violently. If hot, the concentrated acid, in reacting with beryllium, forms SO_2, sulfur, and/or H_2S.

The free energies of reaction of beryllium with the halogens are strongly negative and therefore

are correspondingly favorable to reaction. The basic reactions are:

$$\mathrm{Be} + 2HX \rightarrow \mathrm{Be}X_2 + \mathrm{H}_2$$
$$2\mathrm{Be} + 4HX \rightarrow \mathrm{Be}_2X_4 + 2\mathrm{H}_2$$

at above and below its boiling point, respectively; X is the halogen. Beryllium is attacked by all the halide acids in all concentrations.

Beryllium is attacked by alcohol and ketone, as indicated in the following examples [Miller and Boyd 1967]:

Environment	Chemical reaction
Methyl alcohol and distilled water	Immediate
Methyl alcohol and Freon (E.I. du Pont de Nemours and Co.)	Strong
Methyl alcohol and perchloroethylene	Chemical reaction
Methyl ethyl ketone and Freon	In 3 min
Methyl ethyl ketone and distilled water	Starts immediately

The pH-potential range over how beryllium behaves in water at 25 °C is illustrated in Fig. 25.1 [Pourbaix 1966]. Potential-versus-pH diagrams of this type are known as Pourbaix diagrams. The significance of potential (electromotive force) as related to corrosion is discussed later in the chapter, but as used here refers to the electrode potential. The diagram represents the theoretical conditions of corrosion, immunity, and passivation of beryllium in the presence of solutions free from complexing substances and insoluble salts. The diagram assumes the same dissolved concentrations of each of the components. The boundaries will be displaced slightly with a change in the concentrations. The region between the dashed lines "a" and "b" is the domain of thermodynamic stability of water under a pressure of 1 atm. The two lines represent, respectively, the equilibrium conditions for the reduction of water (hydrogen ions) to gaseous hydrogen and the oxidation of water to gaseous oxygen:

$$2\mathrm{H}^+ + 2e^- = \mathrm{H}_2$$
$$2\mathrm{H}_2\mathrm{O} = \mathrm{O}_2 + 4\mathrm{H}^+ + 4e^-$$

The chemical and electrochemical equilibrium of the beryllium-water system is described using the Pourbaix (E versus pH) diagram. This diagram is useful in the extractive and corrosion fields to predict the dominant compound in a beryllium-water system. The only difference between the diagram used by the corrosion engineer and the extractive metallurgist is the location of the dominance line between one dissolved species and one solid species. The extractive metallurgist uses 10^{-3} mol/L to describe the ionic content for dominance to define this line, where the corrosion engineer uses 10^{-6} mol/L. Figure 25.1 is given for the corrosion engineer.

Because the whole of its domain of stability lies well below that of water (Fig. 25.1, line "a"), beryllium is theoretically a very base metal. It is a strong reducing agent and very unstable in the presence of water and aqueous solutions. In the presence of acid solutions, it vigorously decomposes water, with the evolution of hydrogen, dissolving as beryllium ions Be^{2+}; in the presence of strongly alkaline solutions, it dissolves once again, with the evolution of hydrogen, and gives rise to diberyllate ions $Be_2O_3^{2-}$ and beryllate ions BeO_2^{2-}. Figure 25.1 shows stability lines (9′,6, and 10′) plotted for ionic concentrations of 1 (10^0), 10^{-2}, 10^{-4}, and 10^{-6} g/L.

In the presence of water or noncomplexing solutions whose pH is approximately 4 to 6, beryllium can become covered with a layer of oxide or hydroxide. Figure 25.2, which is deduced from Fig. 25.1, represents the theoretical conditions of corrosion, immunity, and passivation of beryllium in the presence of solutions free from complexing substances and insoluble salts.

The corrosion resistance of beryllium is determined by the behavior of the layer of oxide (or hydroxide) with which it is almost invariably covered. Water has no action, even when the red-hot metal is treated with boiling water or steam, which must be due to the protective action of a layer of oxide (or hydroxide), because a freshly filed piece of metal maintained for a few hours in boiling water becomes covered with bubbles of gas and tarnishes with increase of weight [Pascal 1958].

Dilute and concentrated solutions of hydrochloric acid and dilute solutions of sulfuric acid attack beryllium, with the evolution of hydrogen; weak organic acids, such as acetic, citric, and tartaric acids, attack beryllium initially, with the evolution of hydrogen, until a protective layer of $Be(OH)_2$ is formed [Pascal 1958]. Beryllium is a very powerful reducing agent, reducing warm concentrated sulfuric acid to SO_2 or even to sulfur or H_2S; with nitric acid, it gives NO and NH_3.

Figures 25.1 and 25.2 show that beryllium is fairly resistant to slightly alkaline solutions of pH below approximately 11, but it does not generally resist the action of very alkaline solutions. A 50% solution of potassium hydroxide (approximately $10^{1.15}$ M) reacts in the cold, but

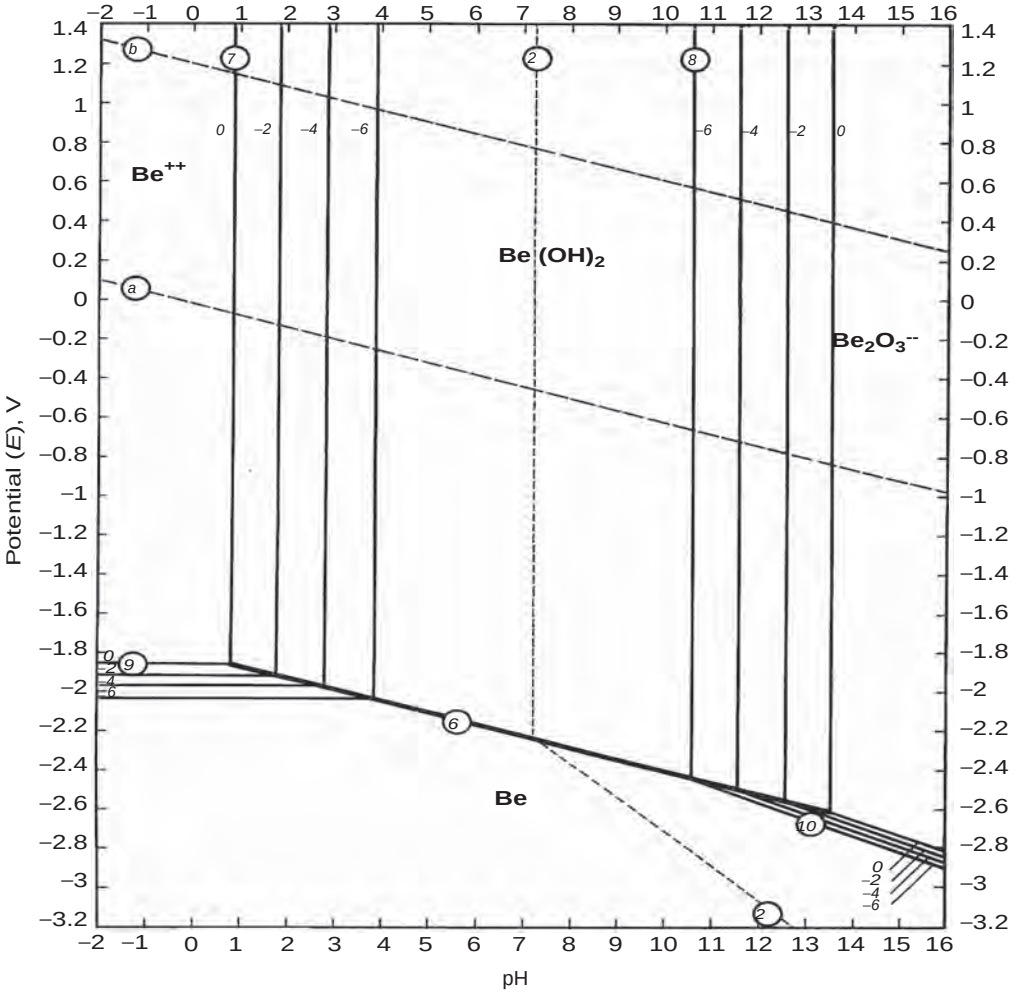

Fig. 25.1 Theoretical conditions of corrosion, immunity, and passivation of beryllium for the Be-H_2O system at 25 °C. Passivation is obtained by the β-form of $Be(OH)_2$. Source: Pourbaix 1966

heating is necessary for evolution of hydrogen to be noticed with a 10% solution (approximately $10^{0.18}$ *M*). Beryllium is clearly more resistant to alkalis than aluminum. It follows from Fig. 25.1 that, as is the case with all very base metals, direct determination of the equilibrium potential of the reaction $Be = Be^{2+} + 2e^-$ using an isolated beryllium electrode dipping into an aqueous solution of its salts is not possible, because the metal corrodes with the evolution of hydrogen.

The cathodic protection of beryllium is difficult, because of the very low protection potential (approximately −2 V). It has been known that pitting of passivable metals due to chlorides may sometimes be avoided by a cathodic treatment, bringing the metal into a state of perfect passivation. For the same reason of low protection potential, its electrolytic deposition cannot be brought about in aqueous solutions.

25.1.1 Stability of the Oxide and Hydroxide of Beryllium

Beryllium oxide, or glucine (BeO), is a substance whose chemical properties depend on the temperature reached during its preparation. As a general rule, it becomes less reactive the longer it is calcined and the higher the temperature. If it is heated to a high temperature, glucine becomes practically insoluble in acids and bases (in the same way as alumina and magnesia). If an alkali is added to an acid solution of a beryllium salt, a precipitate of gelatinous hydroxide

is obtained, which, after thorough drying, is shown to be amorphous.

The $Be(OH)_2 \cdot nH_2O$ formula has been attributed to the hydroxide [Pascal 1958] for simplicity, although this formula does not correspond to its constitution, particularly when the precipitate is fresh. On the other hand, $Be_2O_3H_2$ or $Be_2O(OH)_2$ represents freshly precipitated beryllium hydroxide [Latimer 1952].

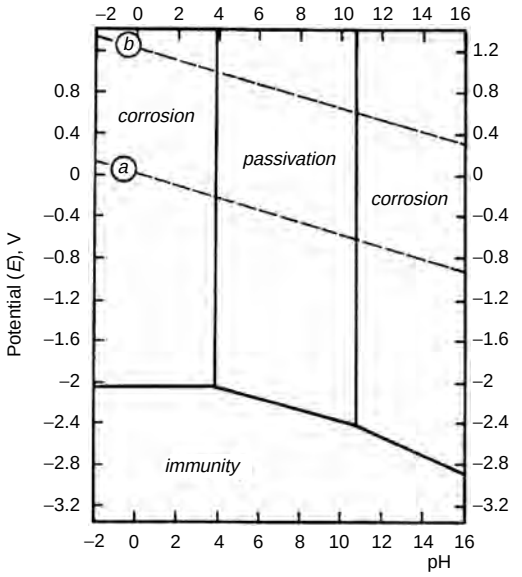

Fig. 25.2 Theoretical conditions of corrosion, immunity, and passivation of beryllium at 25 °C (passivation by the hydroxide β-$Be(OH)_2$)

The gelatinous (amorphous) hydroxide can be dissolved very easily in the common acids, even when they are dilute. Its dissolution in caustic alkalis is more difficult to bring about and depends on the alkali concentration; moreover, the solubility measurements are not reproducible, because the medium favors the conversion of the amorphous hydroxide into various crystalline varieties, whose solubilities are very much lower than the solubility of the amorphous compound.

The amorphous hydroxide is not a stable product as it slowly crystallizes in air or cold water. Two crystalline varieties of the chemical species $Be(OH)_2$ exist; the α-variety is metastable, and the β-variety is stable. The conversion of amorphous hydroxide into crystalline α-hydroxide can be speeded up by boiling an aqueous suspension of amorphous hydroxide; if it is kept in the presence of a concentrated solution of NaOH and KOH for a sufficiently long time, the α-variety changes completely into the β-variety.

The successive crystalline varieties of beryllium hydroxide formed during this "aging" are characterized by an increasing stability, with an accompanying variation in all their properties, notably their solubility in acids, bases, and pure water. In Fig. 25.3, a series of curves have been drawn showing the influence of pH on the solubility of the oxide and the three hydroxides of beryllium in the four dissolved forms: Be^{2+}, Be_2O^{2+}, $Be_2O_3^{2-}$, and BeO_2^{2-}.

According to Fig. 25.3, the most stable form of the hydroxide should be the amorphous one,

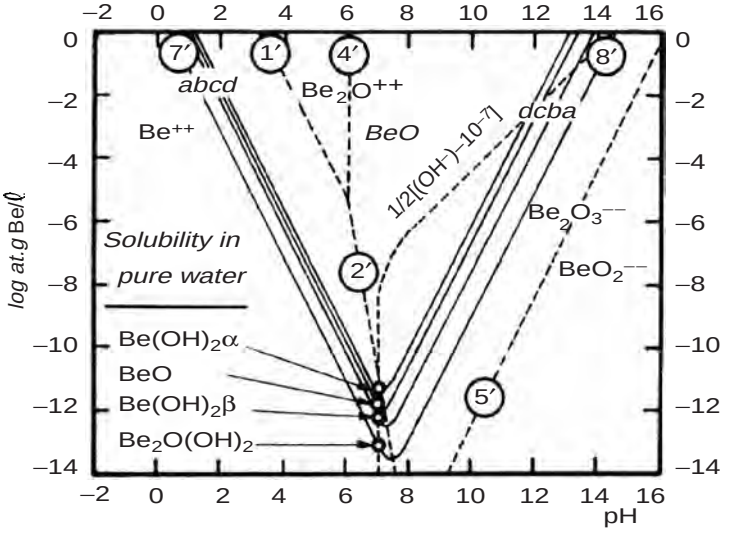

Fig. 25.3 Influence of pH on the solubility of BeO and its hydrates at 25 °C. Source: Latimer 1952

but this form is unacceptable in view of its experimentally established instability. The disagreement probably arises from an inaccuracy in the value of the free enthalpy of formation for the amorphous hydroxide [Latimer 1952]. Experimental data relating to the minimum solubility of the oxide and hydroxides of beryllium are practically nonexistent. The literature gives only a few values for the solubility of the amorphous hydroxide in pure water that lie between $10^{-6.85}$ and $10^{-4.10}$ mol/L and are therefore very noticeably greater than those given by Fig. 25.3 ($10^{-13.6}$ to $10^{-11.4}$).

The portion of Fig. 25.3 included between lines "7′" and "8′"] corresponds to unstable solutions supersaturated with $Be(OH)_2$, and the lines "1′" and "4′" drawn in this figure correspond to nonequilibrium states. At the equilibrium, no domain of predominance of the ion Be_2O^{2+} exists.

25.2 Corrosion of Beryllium in Rainwater and Seawater

The benign nature of pure water vapor, when the beryllium surface is uncontaminated and free of exposed beryllium carbide particles, was demonstrated by exposing beryllium coupons to an atmosphere of 95% relative humidity at 38 °C for 30 days. No evidence of corrosion was detected either microscopically or by weight measurements. The corrosive attack in good-quality water for beryllium that is clean and free of surface impurities and contaminants is typically less than 25 μm per year. By contrast, rainwater, which may contain pollution products, can cause premature corrosion if transported into an otherwise protected environment. Table 25.1 shows corrosive agents commonly found in rainwater [Mueller and Adolphson 1979]. Corrosion results of beryllium in NaCl solutions and in seawater from two different investigations are listed in Tables 25.2 and 25.3, respectively [Miller and Boyd 1967]. Table 25.2 refers to intermittent immersion tests of cross-rolled, surface-ground, flash-pickled ($HF\text{-}HNO_3$) sheet of commercial purity. For continuous immersion, the average corrosion rate decreased with time, as seen from Table 25.3. Figure 25.4 shows corrosion as a function of time of pickled beryllium sheet in synthetic seawater [Miller and Boyd 1967]. One can see the decrease in corrosion rate with time, typical of that for a passive film. Corrosion data in 5% salt spray at 38 °C of forged beryllium are shown in Table 25.4.

Because of its high electropositivity relative to most metals, it would be expected that beryllium would corrode in contact with most metallic materials. Not much information of such

Table 25.1 Corrosive agents in rainwater

Agent, source	Location	Concentration, mg/L
Chloride (Cl^-) ions; major source is sea spray	Over seas or near coastlines	Average: 2 to 20; with extreme winds, may increase up to 100
	500 miles or more inland	Average: 0.1 to 0.2 but at times higher than 1.0
Sulfate (SO_4^{2-}) ions; major sources in industrial areas	Large cities, industrial areas	Average: 10 to 50; higher under extreme conditions such as smog
	Other areas	1 to 5
Nitrate (NO_3^-) ions	Over land	0.5 to 5
Hydrogen (H^+) ions	Over land	Average: approximately 5; may decrease to 3 near industrial centers

Source: Mueller and Adolphson 1979

Table 25.2 Corrosion of beryllium in salt solutions at approximately 16 °C

Environment	Overall corrosion rate(a), μm/year	Maximum pit depth, μm
Distilled water	20.3	20.3(b)
Synthetic water	348	103(a)
Natural seawater	467	103(a)
3 wt% NaCl solution	546	. . .
3.5 wt% NaCl solution	848	173(c)

(a) 30 days. (b) 18 days. (c) 8 days.

Source: Miller and Boyd 1967

Table 25.3 Corrosion in natural seawater at approximately 16 °C

Time, days: with continuous total immersion	Corrosion rate, μm/year	Maximum pit Depth, μm	Percent of surface pitted
2	. . .	38	Negligible
5	. . .	41	1
20	330	76	5
30	267	76	12
40	229	64	15
60	165	76	20

Source: Miller and Boyd 1967

behavior has been found. Accelerated corrosion of beryllium coupled to aluminum and its alloys and to type 347 stainless steel has been reported. It was concluded that, in general, the corrosion rate of beryllium increases by approximately five times by coupling it with aluminum or stainless steel [Miller and Boyd 1967].

Atmospheric corrosion is usually more severe than aqueous corrosion. In atmospheric corrosion, a very thin electrolyte consisting of salts from the environment is deposited and becomes concentrated on the surface. Oxygen can readily diffuse through the electrolyte to the surface and contribute to the cathodic reaction, thus accelerating the corrosion that may be induced by these salts, for example, chloride salts. The term *atmospheric* is used generically; for example, it would also apply to storage tanks. Since corrosion would probably be less severe in an aqueous solution than in the atmospheric case, both containing the same salts, it is important to perform evaluation tests under conditions simulating the latter state. Several different tests, such as the Atmospheric Corrosion Rate Monitor, have been designed for such evaluations [Hill et al. 1996].

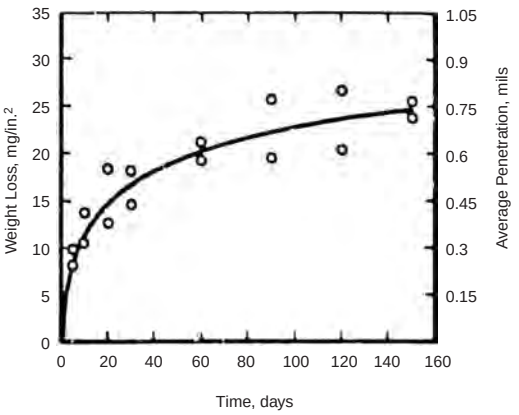

Fig. 25.4 Corrosion of unstressed pickled beryllium sheet exposed to synthetic seawater at 25 °C. Source: Miller and Boyd 1967

25.3 Observations Related to Carbides and Other Inclusions

Beryllium, which typically contains approximately 0.1 to 0.2 wt% of carbon, combines with carbon to form Be_2C particles. Such carbide particles, if exposed on the surface of a beryllium part following a machining operation, can slowly react with moisture in the air, forming hydrocarbons. The most common product is methane, formed according to the following reactions:

$$Be_2C + 2H_2O \rightarrow 2BeO + CH_4\,(gas)$$
$$Be_2C + 4H_2O \rightarrow 2Be(OH)_2 + CH_4\,(gas)$$

The second reaction has been suggested as an intermediate reaction to the first reaction that results in a flowery-white buildup of BeO [Mueller and Adolphson 1979]. The authors present a number of examples of this phenomenon:

- White corrosion products and blisters formed on the surface of extruded beryllium that had been exposed to humid air for approximately six months. The corrosion products were identified as being caused by carbide inclusions that lay parallel to the extrusion axis.
- A corrosion attack leading to similar products was observed on a finished precision-machined component during shelf storage. This occurred at disruptions of the finished unetched surfaces.
- An instrument-grade beryllium material corroded in service in a controlled gas environment containing a fixed value of relative humidity. A spotty white buildup and disruption of the surface occurred at carbide sites.
- Beryllium, which developed flowery corrosion spots during extended storage, yielded a similar pattern of corrosion within hours of immersion in an aqueous bath.
- The degree of corrosion and damage depends on the size and distribution of the carbides. A component may have a dual distribution of both fine and coarse carbides. For

Table 25.4 Weight loss of coupons (25 × 51 mm) from forged beryllium exposed to 5 wt% salt fog spray at 38 °C

	Weight loss, mg, at indicated exposure time, days							
Specimen	1	2	4	7	14	21	30	30, removed scale(a)
3-4	0.33	0.50	0.90	1.6	3.8	5.6	7.3	23.1
5-4	0.42	0.7	0.89	1.2	2.3	2.7	3.1	27.2
5-5	0.40	0.7	0.90	1.2	2.0	2.4	2.9	17.6
1-1	. . .	0.5	0.71	0.9	1.9	2.6	3.3	22.5

(a) Weight loss of corrosion products stripped from coupons following 30 days. Source: Miller and Boyd 1967

example, a large carbide inclusion, approximately 13 mm in diameter, had been exposed to the atmosphere at the machined surface of a 76 mm diameter component. The volume expansion at the large particle, resulting from the reaction with moisture in the air, caused a sizable piece of beryllium to break off from the component. The same reaction with the smaller particles caused surface disruptions only, such as blistering.

Free carbon inclusions would probably set up carbon-beryllium couples in which the surrounding beryllium would be anodically dissolved. Hydrolysis of chlorine or chloride impurities can cause swelling and rupture of beryllium. Aluminum and silicon inclusions are hydrolyzed at 20 °C. Purity variations in standard beryllium products generally have little effect on corrosion compared to variations in the environment. However, with high impurity contents, substantial variation effects may be obtained, especially at elevated temperatures.

25.4 Polarization Studies

The electrical potential difference developed between different sites within a metal and its environment, or between two metals and their environment, is the driving force for corrosion to occur. A conductive path must exist between the metal sites or the metals for current to flow in order to sustain the corrosion (dissolution of metal). The potential (electromotive force) relative to some standard potential is different for every metal. When two dissimilar metals are placed in a conductive solution in contact or electrically connected, this potential difference will result in a flow of electrons from the less noble to the more noble metal. The less noble metal (anode) will corrode (dissolve) more rapidly and the more noble metal (cathode) less rapidly than the rate at which either one alone would corrode in the same solution. Because of heterogeneities inherent in a metal and which can range over macroscopic to microscopic in size, differential potentials can develop within the metal itself, with some sites becoming anodic and other sites becoming cathodic. At the anodic sites, a metal, such as beryllium, will dissolve according to:

$$Be \rightarrow Be^{2+} + 2e^{-}$$

with a corresponding evolution of hydrogen at the cathodic sites as follows:

$$2H + e^{-} \rightarrow H_2$$

Each reaction is referred to as a half-cell reaction. The standard potential for a half-cell is given with reference to a standard hydrogen electrode (H_2/H^+) taken as zero potential. The standard conditions are a one molar (1 *M*) aqueous solution of both the metal and the hydrogen ions at 25 °C. A list of standard half-cell potentials of the different metals relative to hydrogen (hydrogen electrode) as zero is referred to as the standard electromotive force (emf) series. Table 25.5 contains the standard emf series covering a number of metals.

The cell potential of any metal or alloy will depend on the type, concentration, and temperature of a solution in which the measurements are made. This gives rise to a number of potential (galvanic) series, for example, "Galvanic Series" for seawater. The metals (and alloys) are listed in order of their tendency to dissolve (corrode) in seawater, such that the top of the list is the most noble and the bottom the most active of the metals. The greater the separation on the list between any two metals in contact, the greater the tendency for the lower-listed metal to corrode (becomes anodic). The measured potential values are not listed, because the results

Table 25.5 Standard electromotive force series—electrode potential (V) versus hydrogen potential in aqueous solution at 25 °C and 1 atm

Metal-ion equilibrium	Electrode potential, V
$Au–Au^{+}$	1.692
$Au–Au^{3+}$	1.498
$Pt–Pt^{2+}$	1.20
$Pd–Pd^{2+}$	0.987
$Ag–Ag^{+}$	0.799
$2Hg–Hg_2^{2+}$	0.788
$Cu–Cu^{2+}$	0.337
$H_2–2H^{+}$	0.000
$Fe–Fe^{3+}$	−0.037
$Pb–Pb^{2+}$	−0.126
$Sn–Sn^{2+}$	−0.136
$Ni–Ni^{2+}$	−0.250
$Co–Co^{2+}$	−0.227
$Cd–Cd^{2+}$	−0.403
$Fe–Fe^{2+}$	−0.447
$Cr–Cr^{3+}$	−0.744
$Zn–Zn^{2+}$	−0.763
$Al–Al^{3+}$	−1.662
$Be–Be^{2+}$	−1.847
$Mg–Mg^{2+}$	−2.363
$2Be–Be_2O_3$(a)	−2.63
$Na–Na^{+}$	−2.714
$K–K^{+}$	−2.925
Li–Li	−3.045

(a) $2Be + 6OH^{-} = Be_2O_3^{2-} + 3H_2O + 4e^{-}$. Source: CRC 2000–2001

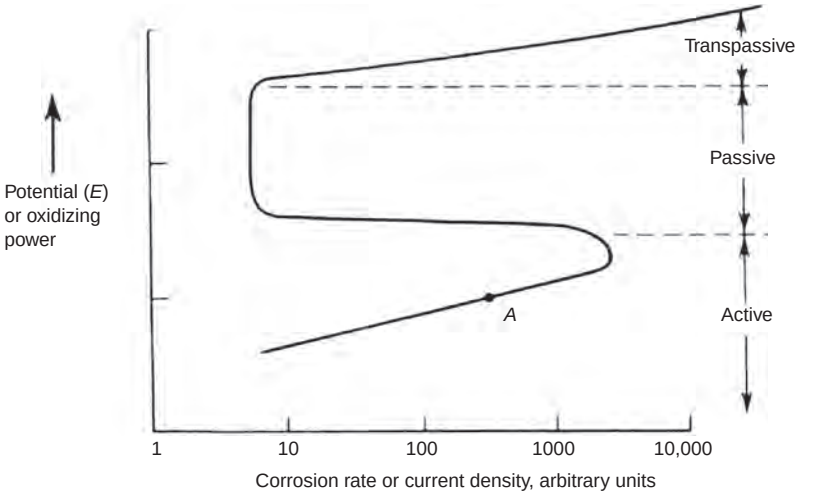

Fig. 25.5 Corrosion characteristics of an active-passive metal as a function of solution oxidizing power (electrode potential). Source: Fontana 1986

obtained by different investigators are not performed under any standardized conditions.

Under equilibrium conditions, the total number of electrons produced (metal dissolution) must be equal to the number removed (hydrogen formed). A departure from equilibrium is referred to as polarization and is manifested in a shift in the potential from the equilibrium potential; the amount of shift is known as the overvoltage. The overvoltage can be caused by a number of factors. For example, if the cathodic area is considerably smaller than the anodic area, then a relatively higher concentration of cations (ions consuming electrons at the cathode) must diffuse to the cathode area, since the current (flow of electrons) in the cathode and anode must be equal. Polarization at the cathode can occur if the diffusion rate is too slow to maintain the required concentration of cations at the cathode. The result is to slow down the corrosion rate at the anode. The reverse difference in relative size between anode and cathode will accelerate the corrosion. If the electrochemical reaction involves several steps and is controlled by a slow step, for example, adsorption on the cathode surface, this will cause polarization. Addition of an external negative voltage will also result in polarization providing cathodic protection.

In acid solutions, hydrogen ions are reduced at the cathode (or cathodic areas) and form hydrogen atoms, which plate out on the surface, polarizing the cathode and decreasing the potential between the cathode and anode. Subsequent formation of molecular hydrogen (H_2) then depolarizes the surface. In neutral or alkaline solutions, where the cathodic reaction is:

$$O_2 + 2H_2O + 4e^- \rightarrow 4OH^-$$

exhaustion of oxygen or an excess of hydroxyl ions may cause polarization. Oxygen can be removed from the solution by deaeration, by various inhibitors, or by scavenger additions, for example:

$$2Na_2SO_3 + O_2 \rightarrow 2Na_2SO_4$$

Excessive removal of oxygen, however, may interfere with the passivation action of a protective oxide film.

Passivity occurs when the rate of metal dissolution decreases upon increasing the potential to more positive values relative to the corrosion potential (open-circuit potential). Thus, low corrosion rates can be obtained at potentials above the open-circuit potential. This corrosion rate is illustrated in the polarization curve in Fig. 25.5 for an active-passive metal. The corrosion rate increases as the potential is increased to the point where an oxide-stable film begins to form, creating a passive region having a relatively very low corrosion rate. The films are usually extremely thin; for example, they are of the order of 20 Å thick when formed in aqueous chloride solutions [Hill et al. 1998]. The oxide film is resistant to cracking or spalling because it is in compression due to an increase in volume by 68% on forming. Most films are either

oxides or hydrated oxides, for example, BeO and $BeO \cdot (H_2O)_x$. At a neutral pH, the protective layer is $Be(OH)_2$.

At some polarizing potential, a breakdown in passivity occurs, and the protective film starts to break down. Numerous theories have been proposed attempting to explain this breakdown. Pitting is initiated at the breakdown potential, becoming more severe with further increase of potential. The potential at the conversion from the passive to transpassive region is referred to as the pitting potential. The point "A" on the curve represents the corrosion potential, where the anodic and cathodic current rates are equal. This representation is schematically illustrated in Fig. 25.6, where the two main components are represented by hydrogen and zinc. A similar behavior will be observed for beryllium. The corresponding half-cells are shown with the reduction and reverse oxidation reactions intersecting at its equilibrium current rate, in each case at their respective half-cell potentials, E (H_2/H^+ and Zn/Zn^{2+}). The intersection point at which the reduction of hydrogen and the oxidation of the metal produce the same current density corresponds to the corrosion current and corrosion potential. It should be pointed out that for a given environment, there is no relationship between the corrosion potential and the current density (corrosion rate). Thus, of two metals, the one with the more negative potential (more anodic) could have a lower rate of corrosion, contrary to what may be expected.

Polarization curves for S-200F beryllium in deaerated salt solutions ranging in concentration from 10^{-4} to $10^{-1}M$ NaCl are shown in Fig. 25.7 [Hill et al. 1996]. Beryllium is passive in these solutions until reaching the pitting potential (breakdown potential). This potential is seen to become more negative (more anodic) with increasing chloride concentration. The pitting results, which are plotted in Fig. 25.8, show a logarithmic relationship between pitting potential and chloride concentration. There does not appear to be any trend between the passivation-current density and the concentration. The extent of passivation and the corrosion potentials will differ in different environments. The polarization curves of S-200F beryllium in nonchloride aqueous solutions over a range of pH are shown in Fig. 25.9. Extensive ranges in passivity with low dissolution (anodic current) rates may be seen. The relationship obtained between the passive current density and pH is plotted in Fig. 25.10.

25.5 Pitting Corrosion

Pitting corrosion seen in beryllium components has been attributed to attack in areas that

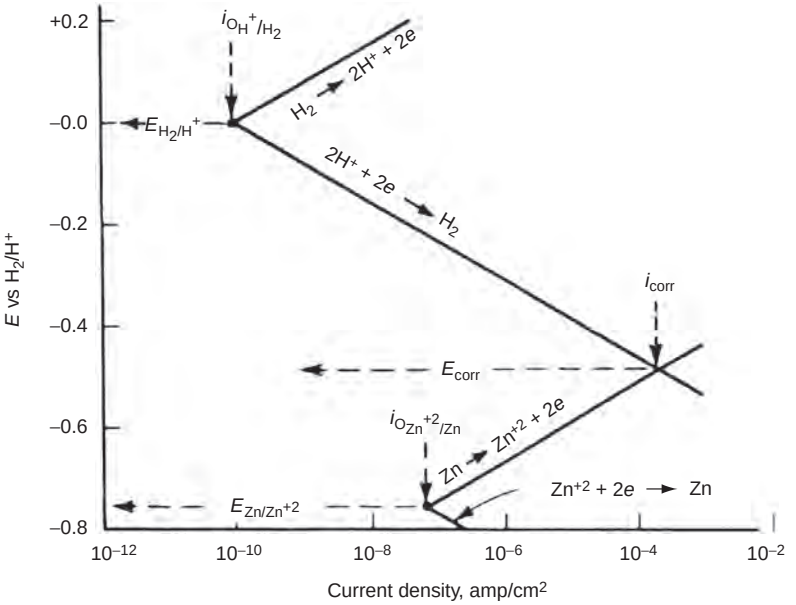

Fig. 25.6 Illustration showing the corrosion potential and corrosion current at the intersection of the anodic and cathodic reactions as represented schematically by zinc in acid solution. Source: Fontana 1986

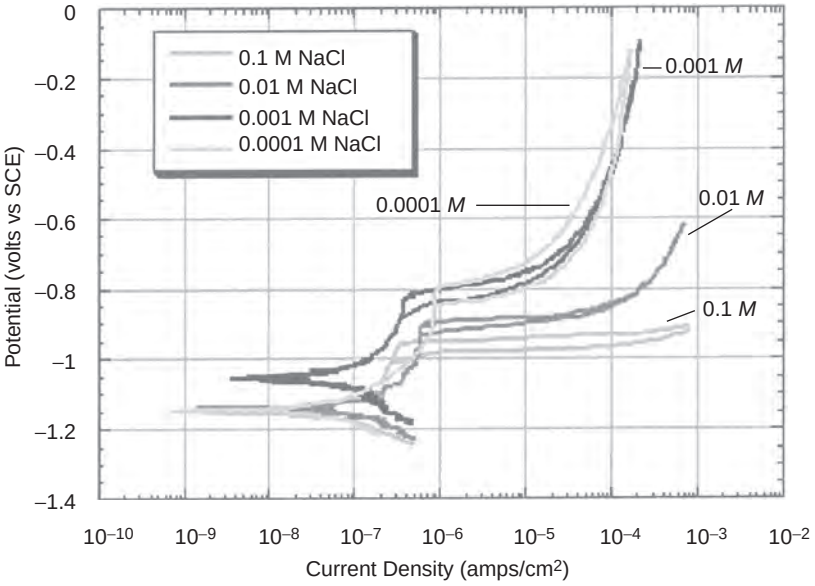

Fig. 25.7 Beryllium polarization curves for S-200F beryllium as a function of NaCl concentration, showing an increase in pitting potential with an increase in NaCl concentration. SCE, saturated calomel electrode. Source: Hill et al. 1996

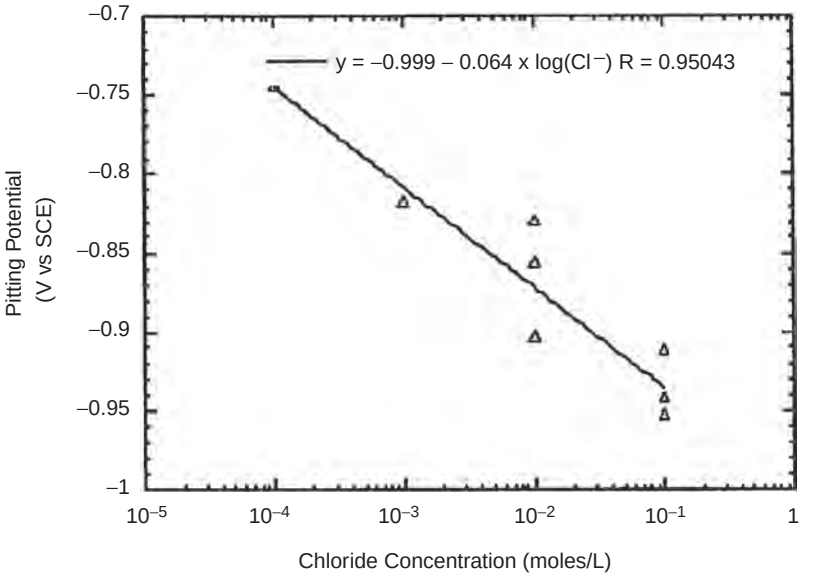

Fig. 25.8 Pitting potential of S-200F beryllium as a function of chloride concentration, displaying a logarithmic relationship. SCE, saturated calomel electrode. Source: Hill et al. 1996

were anodic to the bulk of the metal. Addressing this conclusion, studies were performed in aqueous solutions containing 200 ppm chloride ion, 400 ppm sulfate ion, and 50 ppm carbonate ion to produce an accelerated pitting attack of beryllium. Microprobe analysis showed that the localized pitting occurred at sites rich in either aluminum or silicon. Based on this analysis, the following conclusions were made [Mueller and Adolphson 1979]:

- Pitting corrosion is determined by the distribution of alloy impurities.
- Sites that have a high concentration of iron, aluminum, or silicon (probably in solid solution) tend to form corrosion pits.

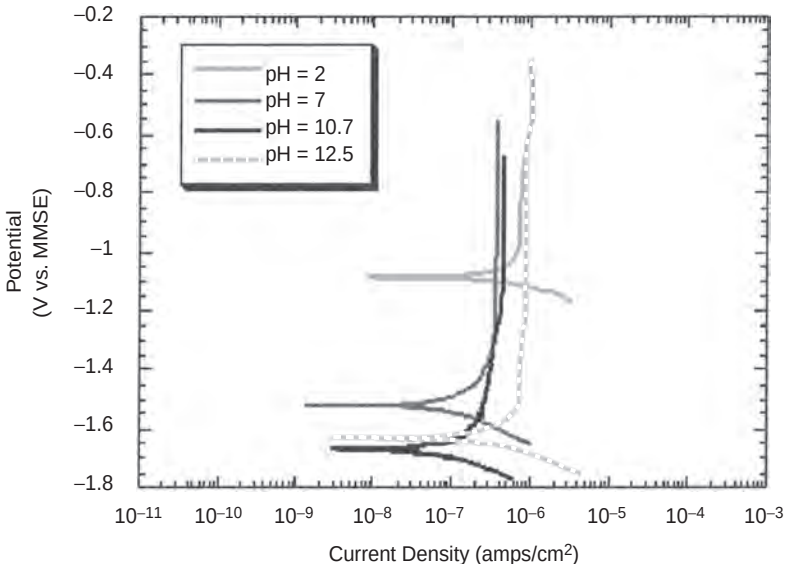

Fig. 25.9 Beryllium polarization curves as a function of pH, showing that the metal is passive over an extensive potential range in the absence of an aggressive species such as the Cl^- ion. MMSE, mercury/mercurous sulfate electrode. Source: Hill et al. 1996

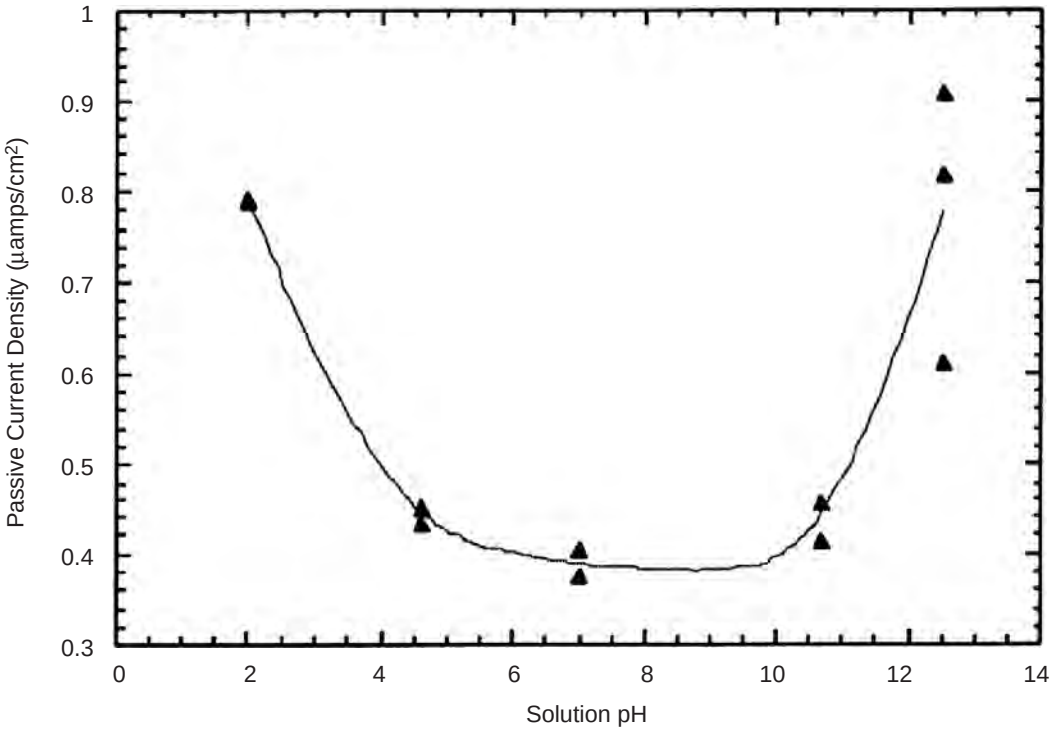

Fig. 25.10 Passive current density as a function of pH for S-200F beryllium, exhibiting a minimum in the pH range between a pH of 7 and 9. Source: Hill et al. 1996

- The corrosion sites are often characterized by the presence of alloy-rich particles, which are probably beryllides; however, the particles themselves did not appear to be corrosion active.
- Pitting density is believed to be related to the number of segregated regions in the matrix containing concentrations of either iron, aluminum, or silicon higher than concentrations present in the surrounding areas.

Segregated impurities such as carbide particles, intermetallic compounds, or alloy-rich zones can lead to localized attack when present in an exposed surface. With increased purity and improved technology of controlling segregation, the problem of localized corrosion and pitting at segregated particles and inclusions has been correspondingly decreased.

Using polarization curves, Hill et al. [1998] studied the effect of pH (1 to 12.5), chloride concentration, and chloride combined with pH (0.1 *M* HCl, pH = 1; 1 to 10^{-4} *M* NaCl, pH = 7; and NaOH/0.1 *M* NaCl, pH = 12.5) on the passivity of polycrystalline S-200D beryllium (98.0 wt% Be). A minimum in the current density as a function of pH at both the corrosion potential and the passive region was obtained, as shown in Fig. 25.11. The pitting potentials as functions of pH and chloride concentration are shown in Fig. 25.12 and 25.13, where the chloride solutions were deaerated. Note that linear and logarithmic relationships are obtained for the pitting potential as a function of pH and chloride concentration, respectively.

In buffer solutions, the beryllium was found to be spontaneously passive over a wide range of pH values from 2 to 13, with passive current densities of the order of 0.5×10^{-6} to 0.9×10^{-6} A/cm^2 [Hill et al. 1998]. The open-circuit corrosion current densities were of the order of 0.3×10^{-7} to 3.0×10^{-7} A/cm^2. Below a pH of 2, active corrosion of beryllium was obtained at the open-circuit potential. The difference between the minimum and maximum corrosion-pitting potential at any chloride concentration was of the order of 0.05 to 0.07 V. The corrosion pits, rather than being hemispherical, were usually morphologically similar to the size and shape of the grains. Scanning electron microcopy evaluations revealed a structure of parallel plates of unattacked metal separated by trenches, suggesting the presence of a preferred attack of certain crystallographic planes.

The pitting that was observed following exposure of beryllium in water at 85 °C for 12 months was attributed to the lack of metal purity. In a different study, on the basis of the examination of pitted surfaces by microprobe analysis, the following conclusions were made [Mueller and Adolphson 1979]:

- Pitting corrosion is determined by the distribution of alloy impurities.

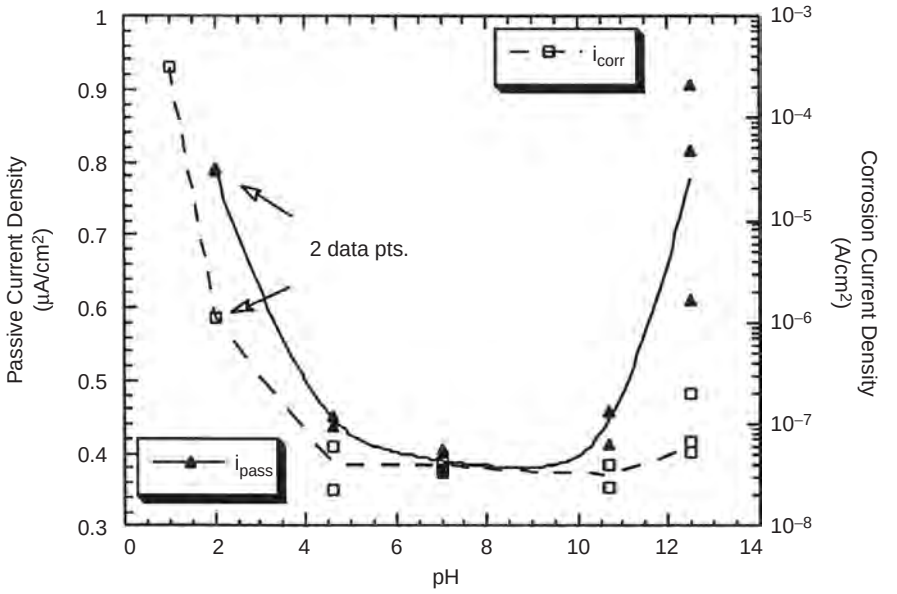

Fig. 25.11 Passive current density, i_{pass}, and corrosion current density, i_{corr}, as a function of solution pH for S-200D beryllium. A minimum in i_{pass} and i_{corr} exists between a pH of 4.5 and 10.7. Source: Hill et al. 1998

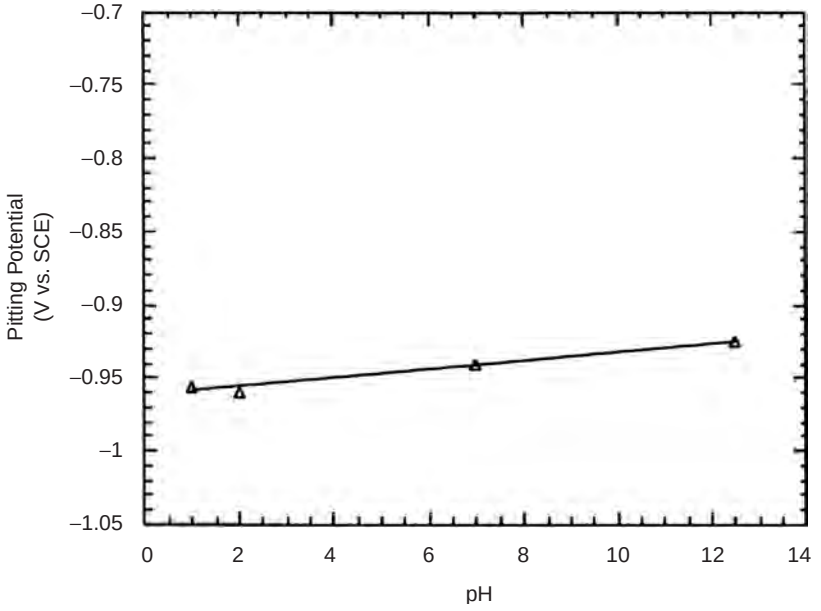

Fig. 25.12 Pitting potential as a function of solution pH in 0.1 *M* NaCl for S-200D beryllium, showing a small linear increase in E_{pit} with increasing solution pH. SCE, saturated calomel electrode. Source: Hill et al. 1998

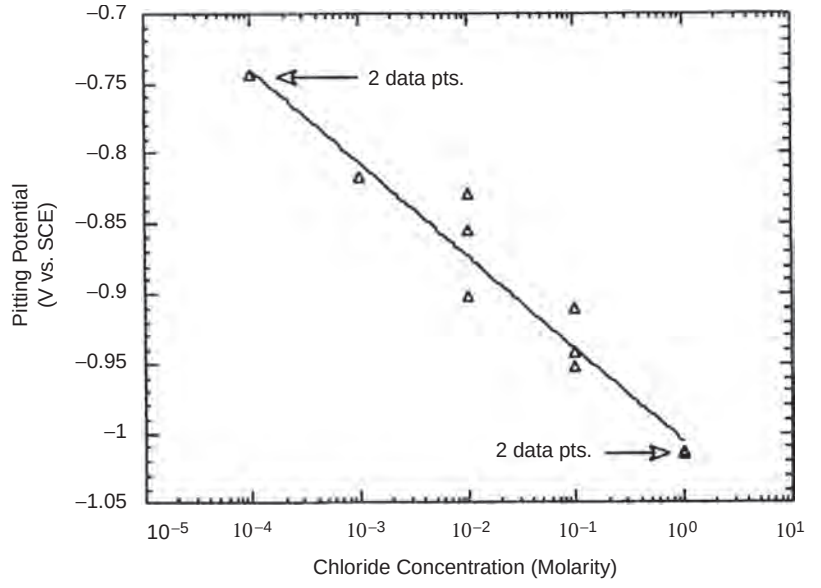

Fig. 25.13 Pitting potential as a function of chloride concentration, displaying a logarithmic relationship between E_{pit} and $[Cl^-]$. SCE, saturated calomel electrode. Source: Hill et al. 1998

- Sites that have a high concentration of iron, aluminum, and silicon (probably in solid solution) tend to be where corrosion pits preferentially form.
- The corrosion sites are often characterized by the presence of alloy-rich particles, which are probably beryllides; however, these particles do not appear to be corrosion active.
- The pitting density seems to be related to the number of segregated regions in the matrix containing iron, aluminum, or silicon higher than concentrations in the surrounding areas.

It should be pointed out that many of the observations and conclusions on corrosion and pitting of beryllium are based on studies made over a number of years. During this time, the control of impurities and uniformity of beryllium products has continually improved, such that with currently made products, the problem related to impurities and nonuniformity should have also diminished over this time period.

Figure 25.14 shows the typical pits produced in S-200 beryllium after being polarized in chloride-containing solutions [Hill et al. 1996].

25.6 Crystallographic-Orientation Effect on Corrosion

In many metallic systems, the degree and nature of pitting corrosion has been shown to be related to the crystallographic plane in the single crystal and to the crystallographic orientation of the surface grains in the polycrystalline material. Thus, a component that has a preferred crystallographic orientation, such as that obtained by rolling, may exhibit different pitting behavior on differently oriented surfaces. Several studies on such crystallographic effects on corrosion have been reported. Lillard [2002], doing potentiodynamic polarization studies using S-200F beryllium electrodes with a near-neutral, deaerated 0.01 *M* solution of NaCl, reported that compared to other crystallographic planes, the basal plane (closest-packed plane) exhibited the highest pitting potential. The author noted, however, that, in beryllium, the samples with the highest pitting potential showed the greatest amount of damage (charge passed) below the pitting potential (onset of stable pitting).

Friedman and Hanafee [2000], in performing potentiodynamic polarization studies, evaluated the corrosion characteristics of high-purity polycrystalline beryllium at 25 °C. The authors also studied a high-purity single crystal alloyed with 0.3 at.%Cu, from which several crystals with different orientations were extracted. These were the basal $(000\bar{1})$, type-1 prism $\{10\bar{1}0\}$, and type-2 prism $\{11\bar{2}0\}$ planes. The two prism planes intersect at 30°, both being parallel to the *c*-axis of the hexagonal crystal with the $\{10\bar{1}0\}$ planes, forming the three-dimensional hexagonal shape. The corrosion of the polycrystalline material was evaluated as a function of pH and NaCl concentration, whereas the single crystals were only evaluated in a 0.01 *M* NaCl solution at

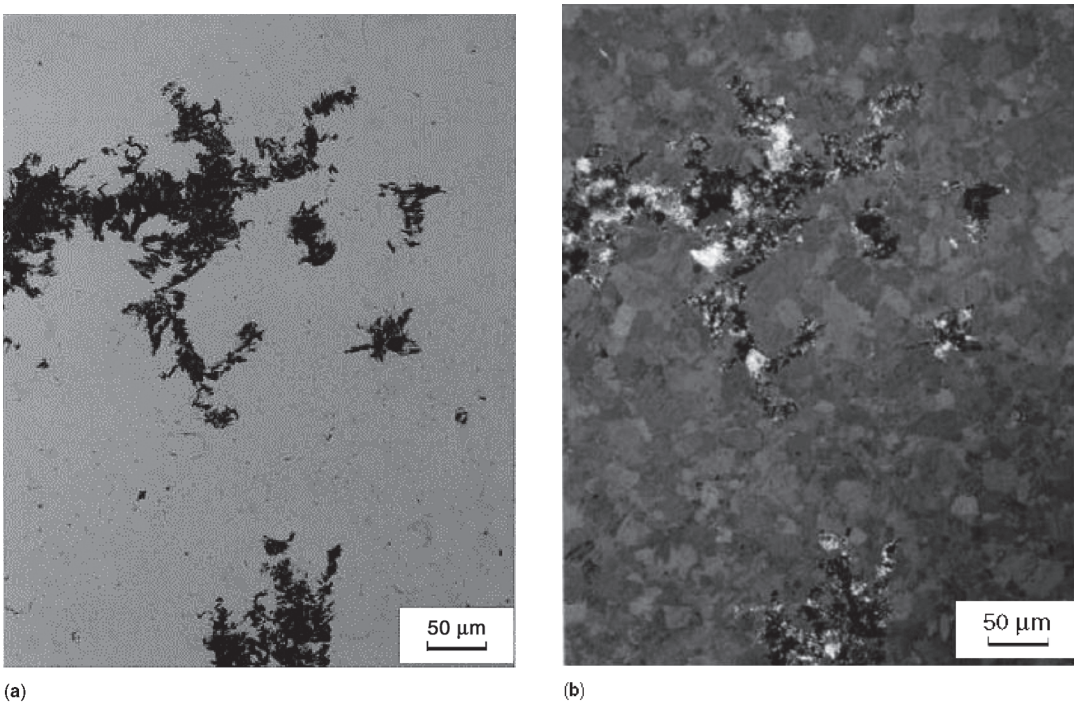

(a) (b)

Fig. 25.14 Micrographs (unpolarized and polarized light) of S-200 beryllium after being pitted in chloride solutions. Source: Hill et al. 1996

a nominal pH of 7. For the polycrystalline material, the corrosion potential was inversely proportional to the pH (range of pH 3 to 9), while the pitting potential and the passive range were directly proportional to the pH.

The magnitude of the passive range is a measure of the resistance to the breakdown of the oxide film as the potential is increased, while the pitting potential is the point at which the film is penetrated, as manifested by a large increase in the corrosion current. The effect of pH on the corrosion behavior was found to be much greater than the effect of chloride concentration (0.001 to 0.1 *M* NaCl). The corrosion and pitting potentials decreased while the passive range increased with an increase in chloride concentration. The single-crystal results showed that the passive range for the basal plane was considerably less than that obtained for the two types of prism planes, which differed much less between them. The differences were attributed to the relative atomic densities of the planes, the basal plane having the greatest atomic density of the three planes. The authors claim that the observations made on the morphology of the corrosion pits of both polycrystalline and single-crystal samples indicated that the corrosion in beryllium is strongly dependent on crystallographic orientations.

Lillard [2001] examined the role of the crystallographic orientation of the metal surface on the transition from metastable to stable pitting in single crystals of beryllium. Polarization tests in near-neutral 0.01 *M* NaCl solution showed that the pitting potential decreased (more negative) in the order (0001), (10$\bar{1}$0), and (11$\bar{2}$0). Pit geometries were different between the first and latter two crystallographic planes. In the numerous tests run, metastable pitting in the passive region was always observed for the first two planes and only once for the (11$\bar{2}$0) plane. For the latter plane, stable pitting was always preceded by a single damage event that did not passivate; instead, it transitioned directly to a stable propagating pit. The metastable behaviors were analyzed by running potentiostatic (current versus time at constant voltage) tests at voltages between the open-circuit potential and the pitting potential. The test was terminated shortly following repassivation in order to examine the pit formed by the metastable event. The frequency and magnitude of the damage in the pitting events increased with increasing applied potential for any given orientation. The accumulated damage was greatest for the (0001) plane. This was to be expected because it was the orientation having the highest (least negative) pitting potential.

Lillard [2001] reported some results of the potentiodynamic polarization studies, which are shown in Fig. 25.15. A scanning electron

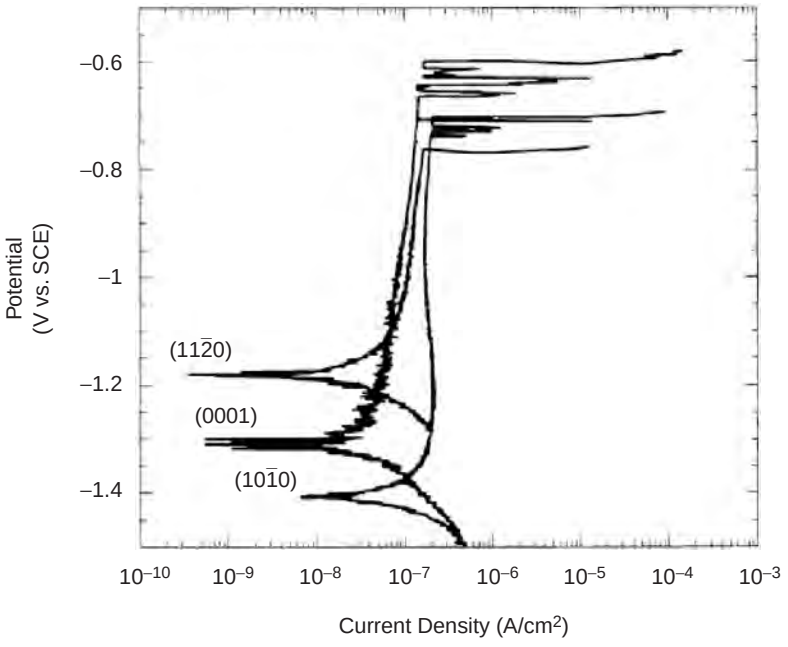

Fig. 25.15 Potentiodynamic polarization curves of single-crystal beryllium with different crystallographic orientations in deaerated 0.01 *M* NaCl solution. SCE, saturated calomel electrode. Source: Lillard 2001

micrograph of S-200 hot pressed beryllium powder after being pitted is shown in Fig. 25.16. It is evident that there is preferred attack in the material, depending on the crystallographic orientation.

25.7 Contamination Sources and Corrosion Prevention

Contaminants, which are frequently in the form of chlorides or sulfates, are common sources of corrosion. The use of tapwater or a chloride- or sulfate-contaminated water bath, without adequate cascade rinsing in deionized water prior to drying, can result in corrosion during subsequent processing or storage. Therefore, where tapwater is used, final rinses must be made in deionized water. Residual contaminants become concentrated during drying, and subsequent condensation of any moisture may provide active sites for corrosion. Residual dye penetrants from a nondestructive test can, on subsequently seeping out of crevices, lead to localized corrosion. Hand contact with semifinished and finished components should be avoided, because fingerprints can be a source of contamination, leading to etching and corrosion. Salt in a fingerprint may severely etch a beryllium surface. The etching may also interfere with the application of any subsequent passivation coatings, in that the continuity of the coating may be disrupted and thereby decrease its effectiveness. An alkaline detergent-type bath, such as Oakite NST, with a superimposed ultrasonic treatment can be used to remove all types of normal soils, with the exception of silicone greases. In the latter case, a solvent for silicone grease must be used prior to the alkaline treatment [Mueller and Adolphson 1979].

Other sources of chlorine ions, in addition to tapwater, can be chlorinated solvents used to remove oils and greases. Plastic piping in the cleaning system is also found to lead to chloride contamination. Contact with various plastic objects, such as polystyrene (Styrofoam, Dow Chemical Company), plastic folders, plastic routing sheets, and so on, can result in localized etching and possibly subsequent corrosion. The use of a polyethylene bag provides an effective

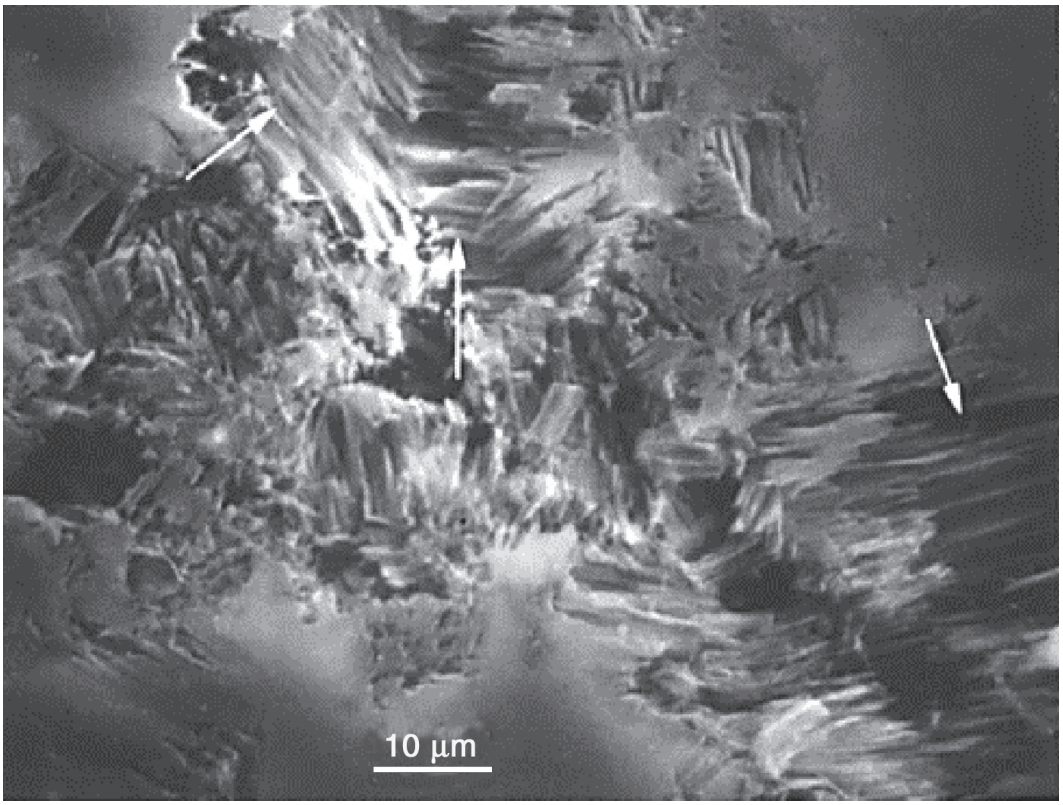

Fig. 25.16 Scanning electron micrograph of corrosion pits in S-200D-grade beryllium. Source: Lillard 2001

barrier between a beryllium part and these chloride-containing materials. In general, contact with materials of nonproven compatibility should be avoided. Storage should be in a moderately dry and noncondensing environment free of corrosion-causing contaminants. In moist environments, local corrosion can occur at inclusions of beryllium carbides.

The following recommendations for storage are given [Mueller and Adolphson 1987]:

- Ensure that the component entering storage is free of corrosion-causing contaminants.
- Maintain a moderately dry and noncondensing environmental atmosphere.
- Ensure against contact with materials of nonproven compatibility.

Heating a storage cabinet with a light bulb, raising the temperature to approximately 50 °C, was found to be effective for long-time (dry) storage. Humidity-controlled storage rooms have also been effectively used to prevent corrosion for several years of storage. For both shipping and storage, a desiccant can be used with the beryllium in a compatible container.

In a study, the effect of surface treatment on corrosion of machined beryllium immersed in demineralized water at 85 °C was evaluated [Mueller and Adolphson 1987]. Three surfaces were examined: 1) as-machined, 2) pickled in chromic-phosphoric acid (H_2CrO_4-H_3PO_4) after machining, and 3) machined and reannealed in vacuum for 1 h at 825 °C. The results showed the pickled samples corroded at the highest rate during the first 60 h of exposure, while the as-machined surface exhibited the slowest rate. With extended corrosion times, however, the magnitude of attack for all surfaces was similar, reaching within a range of 0.0025 to 0.005 mm/year.

Inadvertent galvanic coupling would result in corrosion. An example is given for such localized corrosion of a beryllium part. The problem was traced to a cutoff operation in which the beryllium was in contact with the steel blade under a coolant. Contact with an apparently dry material (e.g., placement on a mat or mesh to protect the surface) has also been found to be the source of corrosion or undesirable etching [Mueller and Adolphson 1987].

A comparison of results obtained between cleaning with alkaline and nonalkaline (including chlorinated solvents) detergents showed that, of the two types, the former produced the cleaner surface. The conclusion was based on scanning electron microscopy observations and on surface outgassing (e.g., of water vapor held by the surface contaminants) measurements.

Normally, machined surfaces are acid etched to remove machining-induced microcracks. Precision components that cannot be acid etched, however, are lapped to final size, which can result in residual microcracks, thus being susceptible to corrosion due to subsequent penetration of surface contaminants. In addition, any residual contaminants could be smeared over by the surrounding material during lapping. To overcome this problem, a free-cutting diamond paste has been recommended as the lapping agent.

Lillard et al. [1997] showed that beryllium in contact with polyisocyanurate (Celotex) and moisture may undergo pitting corrosion. This was based on the pitting potential of beryllium obtained from potentiodynamic polarization studies using a solution of ground Celotex soaked in deionized water for three weeks. Sanchez et al. [1999] suggested that the chloride ions causing corrosion come from three sources that contain the ion:

- From the beryllium metal itself
- From the packaging material, such as Celotex
- From chlorinated solvents used in cleaning the components

The chlorinated solvents are 1,1,1-trichloroethylene (TCA) and 1,1,2-trichloroethane (TCE). Using the property diagrams of BeO in TCA, TCE, and carbon tetrachloride, the authors predicted the corrosion of beryllium by the chloride ion in these environments. The property diagrams are developed using the Thermo-Calc Code [Sanchez et al. 1999], which is based on thermodynamic properties and phase diagrams. The results predicted that $BeCl_2$ formed by exposing BeO to TCE but not when exposed to TCA. This formation suggested that the H/Cl ratio in the solvents may play an important role in forming the $BeCl_2$ corrosion product. The authors then developed property diagrams for 20 chlorinated solvents with H/Cl ratios from zero to five. The solvents were of the form $C_xCl_yH_z$. The results, which are shown in Table 25.6, suggest that carbon is essential in order to form $BeCl_2$ from BeO and that the H/Cl ratio must be less than 1. With a ratio ≥ 1, no $BeCl_2$ is formed, suggesting that HCl is the more stable and preferred product. A series of curves show the relationship between the amount of $BeCl_2$ formed and the solvent concentration in H_2O for several different H/Cl ratios. Based on their results, the authors suggest that the solvents used in the

Table 25.6 Prediction of the formation of $BeCl_2$ in different solvents

Solvent	Formula	$BeCl_2$ predicted	H/Cl in solvent	C in solvent
Carbon tetrachloride	CCl_4	Yes	0/4	1
Chloroform	CCl_3H	Yes	1/3	1
Dichloromethane	CCl_2H_2	No	2/2	1
Methyl chloride	$CClH_3$	No	3/1	1
Tetrachloroethylene	C_2Cl_4	Yes	0/4	2
Trichloroethylene	C_2Cl_3H	Yes	1/3	2
Dichloroethylene	$C_2Cl_2H_2$	No	2/2	2
Vinyl chloride	C_2ClH_3	No	3/1	2
Hexachloroethane	C_2Cl_6	Yes	0/6	2
Pentachloroethane	C_2Cl_5H	Yes	1/5	2
Tetrachloroethane	$C_2Cl_4H_2$	Yes	2/4	2
Trichloroethane	$C_2Cl_3H_3$	No	3/3	2
Ethylene dichloride	$C_2Cl_2H_4$	No	4/2	2
Ethylene chloride	C_2ClH_5	No	5/1	2
Hexachlorobenzene	C_6Cl_6	Yes	0/6	6
Pentachlorobenzene	$C_6Cl_5H_1$	Yes	1/5	6
Tetrachlorobenzene	$C_6Cl_4H_2$	Yes	2/4	6
Trichlorobenzene	$C_6Cl_3H_3$	No	3/3	6
Diachlorobenzene	$C_6Cl_2H_4$	No	4/2	6
Monochlorobenznene	C_6ClH_5	No	5/1	6

Source: Sanchez et al. 1999

cleaning process should have low carbon and a high H/Cl ratio.

Corrosion may result from contamination during handling, transportation, and storage, for example, on exposure to rainwater or high humidity in an industrial area or near seawater. Corrosion protection during handling, transportation, and storage of beryllium may be provided by surface treatments and by surface coatings. As applied to essentially any metal, the following are the main considerations in selecting the proper corrosion-resistant coating: environmental resistance, surface preparation, substrate to be coated, design life, cost, safety, consequences of coating failure, available equipment, available skill, accessibility to future repairs, and appearance.

Chromate-type coatings provide reasonable protection for beryllium during handling and storage and against attack by salt-containing environments for moderately long time periods. A chromate passivation treatment involves a simple dip procedure, for example, a 30 min dip in a solution of 25% H_3PO_4, 25% saturated solution of KCr_2O_3, and 50% H_2O [Mueller and Adolphson 1979, Morana 1967]. Exposure to 100% relative humidity at 70 °C increased specimen life that had a chromate coating from 1 day to between 10 and 14 days. Coatings can be extremely thin, being virtually immeasurable by conventional techniques. A patented chromate coating of less than 0.01 μm resulted in a reduction in corrosion rate by a factor of 50 when tested in distilled water at 95 °C for 30 days [Hill et al. 1996].

Fluoride coatings, which are produced by treating beryllium in fluorine above 520 °C, were shown to be very effective in resisting corrosion in chloride-containing water and in distilled water. A glass-appearing water-insoluble coating is formed. A coating thickness of 0.2 μm was found to provide effective protection in water containing 150 ppm of chloride ion.

Anodized coatings can improve resistance to corrosion in normally corrosive aqueous solutions and to air oxidation at elevated temperatures. Ingredients common to the numerous anodizing baths that have been used are HNO_3, H_2CrO_4, $Na_2Cr_2O_7$, and NaOH. The anodizing parameters and components used depend on the desired protection required for one or more specific environments. The anodized film thickness can range from approximately 2.5 to 50 μm. Examples of formulations that produce a uniform, adherent coating are the following: 50 wt% HNO_3 solution with a current density of 2.15×10^{-6} A/mm^{-2} (0.20 A/ft^{-2}) for 5 min, and 7.5 wt% NaOH solution with a current density of 1.08×10^{-4} A/mm^{-2} (10 A/ft^{-2}) for 20 min. Anodized coatings were found to effectively protect beryllium from corrosion in the following environments: 100 days in a humidity cabinet, three months at 40 °C in tapwater, and 2000 h in ASTM International substitute sea water. With a 5 μm coating produced in H_2CrO_4, corrosion was undetected after exposure to 5% salt fog spray at 40 °C for 30 days. In a different study, an anodized coating showed favorable performance in 5% salt spray tests at room temperature; however, poor performance was indicated at 50 °C. In synthetic seawater, unprotected beryllium corroded at a rate 21 times that of the anodized samples. An important application of anodizing is for beryllium mirrors. In addition to its resistance to corrosion, the anodized film has a high thermal emissivity and absorptivity. The lapping compound, in moving to the rim of a mirror, has a tendency to cause corrosion. The anodizing prevents this from occurring [Mueller and Adolphson 1987].

Organic coatings are used to provide electrical insulation between beryllium and another metal component. The coating also prevents any galvanic action in the event of condensation or water entering between the two metals [Mueller and Adolphson 1979]. Epoxy primers have been successfully used as coatings for year-duration storage of fabricated structures. Surfaces are flash etched and immediately coated with the primer, then baked to effect its cure. All ex-

posed surfaces are coated, and then the individual components are joined by adhesive bonding or mechanical fasteners [Mueller and Adolphson 1987].

Plated coatings are used for specific applications, such as for electrical contacts, improved wear resistance, and improved polishing results, but rarely alone for corrosion protection. The coatings can be applied by electrolysis or by electrolytic plating. Numerous metals, including copper, tin, silver, chromium, aluminum, iron, nickel, and zinc, have been successfully electroplated onto beryllium. Care must be taken, however, in the use of beryllium at elevated temperatures when coated with some of these metals. Extended exposure at elevated temperatures may allow sufficient diffusion to occur, resulting in the formation of undesirable intermetallics. Other plating/coating methods that could be used are hot dip coating, thermal spraying, chemical vapor deposition, physical vapor deposition, vacuum sputtering, vacuum ion implantation, plasma spraying, and ceramic coating. Plasma spraying is discussed in Chapter 22, "Beryllium Coating Processes," in this book.

Studies on exposing chlorinated vapor (TCA, TCE) and liquid (CCl_4) degreasing solvents to polished-and-cleaned surfaces of S-200D beryllium were performed at the Pantex Plant in Amarillo, Texas [Birkbeck et al. 1999]. These three solvents, which react with beryllium, have been used during cleaning processing and possibly machining of beryllium prior to use in the nuclear industry. The solvents are listed in Table 25.7. Cleaned beryllium coupons were air dried for 4 h to form a native oxide and then exposed to the vapor solvents. The polishing and rinsing used distilled/deionized (DD) water. Cleaned coupons were also either scraped, machined, or further polished under liquid TCA or CCl_4, simulating processing, to assess whether the metal was attacked. Following exposure, the coupons were then analyzed using x-ray photoelectron spectroscopy.

Low-resolution spectroscopy showed the following approximate (semiquantitative) chlorine content, in atomic percent, following exposure of the cleaned coupons: polished in DD water, less than 0.03%; TCA vapor, 0.5%; TCE vapor, 4.8%; and scraped in TCA liquid and rinsed in DD water, 0.2%. In scraping or polishing the metal under the chlorinated liquid, the oxide is physically removed, exposing fresh metal to the chloride environment. In vapor degreasing, the oxide is dissolved, with a similar exposure of fresh metal. In both cases, the result is to form chlorinated surfaces consisting of a combination of organic and inorganic chloride compounds. The latter is susceptible to attack by water and can lead to corrosion. Table 25.8 is a summary of the chlorine content for the organic and inorganic compounds based on the high-resolution spectroscopic scans. Doublet peaks due to spin-orbit splitting are obtained for both types of compounds. The mechanism of forming the two types of chlorides involves partial dissolution of the protective oxide film, with the beryllium bonds then reacting with the carbon-chlorine bonds of the solvent, forming chlorides that become incorporated into the passivated layer. The following (bond) reaction is proposed [Birkbeck et al. 1999]:

$$\text{Be-Be} + \text{C-Cl} \rightarrow \text{Be-C} + \text{Be-Cl}$$

An alternative reaction with a passivated (beryllium-oxygen bonds) surface could be:

$$\text{C-Cl} + \text{Be-O} \rightarrow \text{Be-Cl} + \text{C-O}$$

Calculated bond energies show that, of the two reactions, the first reaction is thermodynamically

Table 25.7 Chlorinated solvents used for S-200D study

Solvent	Supplier	Grade	Impurities
1,1,1-trichloroethane (TCA)	American Chemical Enterprises, Inc.	Technical in accordance with Federal Specification O-T-620 Issue C	≥90% TCA by volume ≥2% all other halogens by volume Inhibitors(a) 100 ppm H_2O max
1,1,2 trichloroethylene (TCE)	Burdick & Jackson Labratories, Inc.	Reagent grade	0.006% K-F H_2O 0.28 ppm residual Inhibitors(b)
Carbon tetrachloride (CCl_4)	Matheson, Coleman, & Bell	Spectroquality grade	+99 mol% CCl_4 0.03% H_2O max

(a) Inhibitor package added that performs the following functions: absorbs ultraviolet light, scavenges acid, and prevents solvent from reacting with bare metal. (b) Only trace amounts of these inhibitors. Note: Other proprietary inhibitors (stabilizers) may also be present, e.g., nitromethane, which prevents breakdown of the solvent; 1,3-dioxolane, which promotes formation of a protective oxide on a reactive metal; and butylene oxide, which reacts with acid to form an alcohol that protects the metal against acid attack. Source: Birkbeck et al. 1999

considerably the more favorable one. When placed in a humid environment following exposure to the solvents, the corrosion of the beryllium accelerates; that is, the oxidation rate increases. As revealed by spectroscopy, the chlorides could be minimized by final rinsing with copious amounts of DD water, followed by a light wipe with a Kimwipe (Kimberly-Clark) saturated with DD water [Birkbeck et al. 1999].

Table 25.8 Summary of high-resolution scans of Cl 2p (electron state) of beryllium coupons.

Following water polishing, coupons were vapor degreased in or scraped under TCA or TCE.

Electron/ spin state	Chemical state	Sample treatment(a)	Cl intensity, at.%
Cl $2p_{3/2}$	Organic (C-Cl bond)	As water polished	<0.02
		TCA vapor degreased	0.25
		TCE vapor degreased	2.40
		TCA scraped	<0.02
		TCA scraped, water rinse	0.05
Cl $2p_{1/2}$	Organic (C-Cl bond)	As water polished	<0.01
		TCA vapor degreased	0.12
		TCE vapor degreased	1.20
		TCA scraped	. . .
		TCA scraped, water rinse	0.02
Cl $2p_{3/2}$	Inorganic chloride	As water polished	<0.02
		TCA vapor degreased	0.08
		TCE vapor degreased	0.74
		TCA scraped	1.60
		TCA scraped, water rinse	0.08
Cl $2p_{1/2}$	Inorganic chloride	As water polished	<0.01
		TCA vapor degreased	0.04
		TCE vapor degreased	0.37
		TCA scraped	0.80
		TCA scraped, water rinse	0.04

(a) All water refers to distilled/deionized water. TCA, trichloroethylene; TCE, trichloroethane. Source: Birbeck et al. 1999

25.8 Effect on Mechanical Properties

The effect of corrosion on mechanical properties of hot pressed S-200F beryllium has been reported [Vaidya et al. 1998]. Tests were performed according to ASTM standard C-203-05 using four-point-bend samples [ASTM C203-05]. The samples (2.5 by 5 by 25 mm) were electrodischarged-machined and 400-grit finish polished. Prior to testing, they were exposed 168 h to either 0.01, 0.1, or 1 *M* NaCl-aerated solutions. Typical results are shown in Fig. 25.17, which showed that corrosion can result in a significant loss of ductility and fracture strength. The yield strength and strain-hardening rate were essentially unaffected. Much scatter was obtained. Scatter in the results of the exposed samples was greatest for the 0.01 *M* solution, which exhibited the most degradation, and smallest for the 1 *M* solution, which exhibited the least degradation in the mechanical properties.

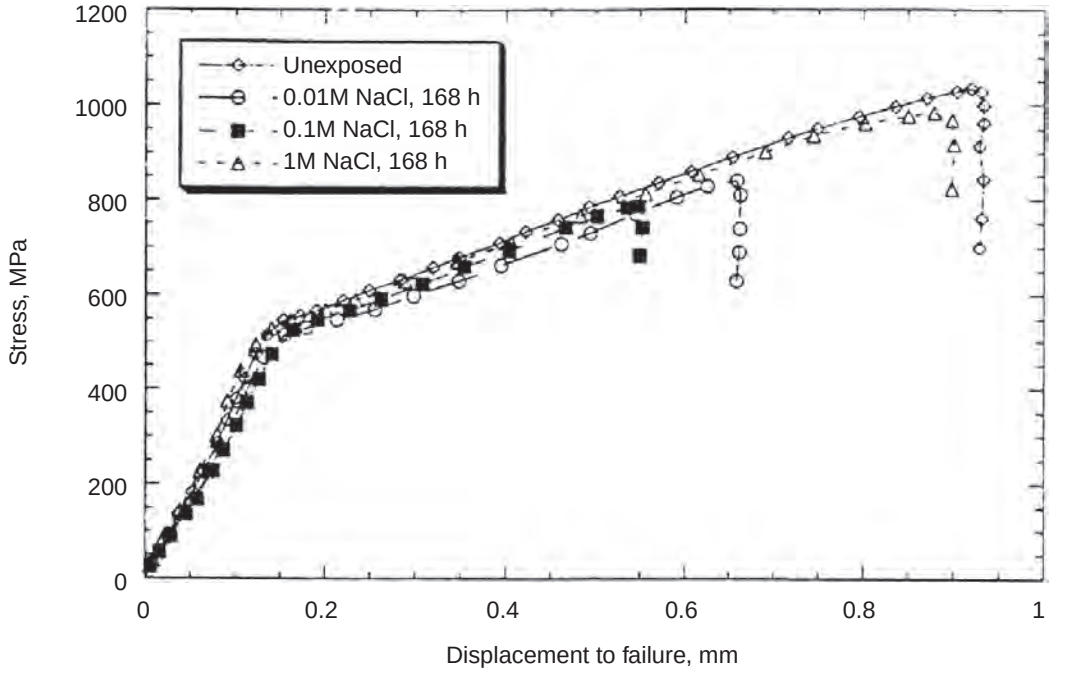

Fig. 25.17 Representative stress-displacement plots for as-received and corroded S-200F beryllium four-point-bend beryllium samples. Source: Vaidya et al. 1998

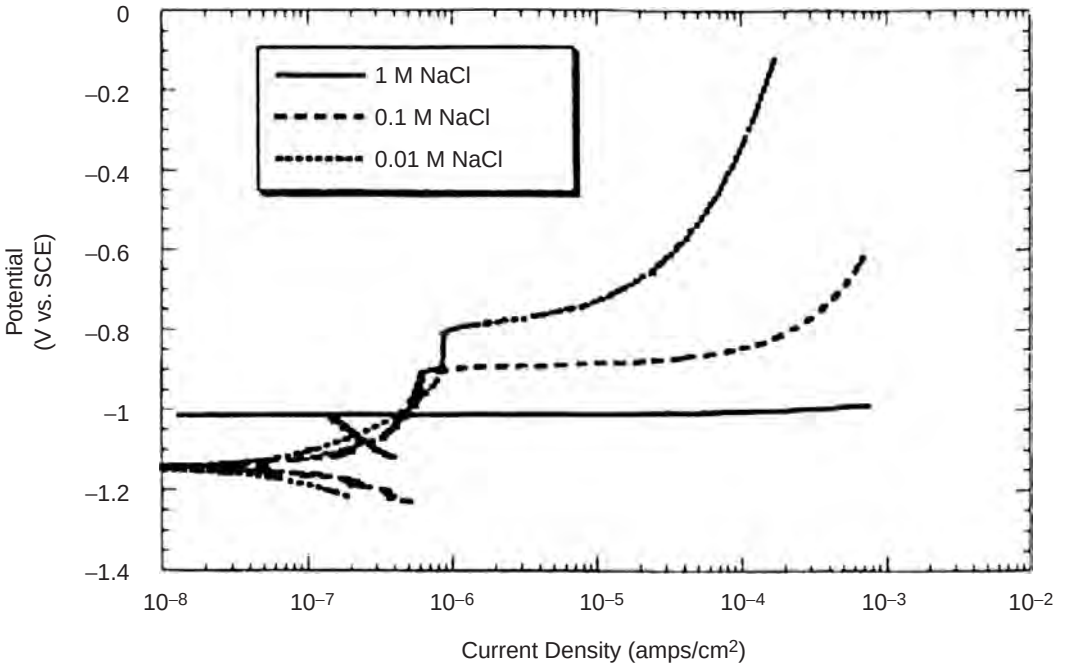

Fig. 25.18 Polarization curves for S-200F beryllium in NaCl solutions. SCE, saturated calomel electrode. Source: Vaidya et al. 1998

Polarization curves of the beryllium in the three NaCl solutions are shown in Fig. 25.18. Whereas the 0.01 and 0.1 *M* solutions showed a passivation regime prior to pitting, pitting of the 1 *M* solution continued at essentially the open-circuit potential without showing any indication of passivation. The increase in the negative potential at which pitting is initiated or where it is indicative by the high current density are consistent with an increase in the chloride concentration. As can be seen from the failure results in Fig. 25.18, this trend, however, is inconsistent with the mechanical property results.

Surface evaluation, using scanning electron microscopy, revealed that differences in pitting morphology could explain these results. Exposure in the 1 and 0.01 *M* solutions resulted in shallow pits approximately 1 to 3 and 5 to 20 μm deep and approximately 15 and 250 μm apart, respectively. Exposure to the 0.1 *M* solution gave intermediate pit measurements. Profilometry measurements showed that the minimum and maximum surface roughnesses were obtained for the 1 *M* solution and the 0.01 *M* solution samples, respectively. Furthermore, the former sample showed a uniformly roughened surface, whereas the latter sample showed significant variations in roughness along the profilometer profile. Thus, the beryllium exhibited a propensity for increased uniform surface dissolution and decreased localized pitting with an increase in NaCl concentration. Considering the pits as flaws and thereby sources of stress concentration, the deepest pits would result in the highest stress concentrations and thus yield the greatest degradation in the mechanical properties, as was obtained. Therefore, it is not only the amount of pitting but also, and more significantly, the morphology of the pits that is important in determining the life of a loaded structure exposed to a corrosive environment.

A study reported on determining whether there was any microbiologically induced corrosion in beryllium, as has been observed for many other metals [Vaidya et al. 1999]. Such corrosion negatively affected the mechanical properties of these metals. The study was performed on hot pressed S-200F beryllium using four-point-bend samples, as described previously. An aerobic bacterial strain, *Pseudomonas* species NCMB 2021, was selected for the bacterial source because of its abundance in nature and its propensity to enhance corrosion in a number of alloys and composites. The bacteria were grown from this source in 1 *M* NaCl solution containing 1.5 g yeast extract and 1 g dextrose per liter of solution (for inoculation). Tests were performed on as-polished samples, following exposure for 168 h

in 1 *M* NaCl solution and following exposure for 168 h in the bacteria-containing solution; both solutions were at 22 °C.

Relative to the results obtained for the as-machined samples, only slightly lower values in the crosshead displacement (3%) and in fracture stress (4%) were obtained for the samples that had been exposed to the NaCl solution. By contrast, the samples exposed to the bacteria exhibited a 30% drop in displacement (ductility) and a drop of 23% in the fracture strength relative to the values obtained for the as-machined samples. The strain-hardening rates (stress against displacement slope) were virtually identical for the three groups of samples. The samples exposed to the NaCl solution showed a high concentration of closely spaced, small, shallow pits, which the authors consider as equivalent to the removal of a uniform surface layer. Exposure to the bacteria resulted in the formation of tubercles that led to heavy localized pitting and the subsequent degradation in mechanical properties. By applying a monolayer coating of silane to the samples, estimated at 26 Å thick, prior to immersion in the bacteria-containing solution, the tubercles did not form, and the degradation in properties did not occur.

The results of numerous stress-corrosion tests in seawater, saltwater, and in many other more corrosive environments, with sustained stress levels of 80 to 90% of the yield stress, have been reported [Miller and Boyd 1967]. Although a loss of ductility and a decrease in failure stress are obtained due to prior corrosion/pitting, beryllium does not appear to be susceptible to stress-corrosion cracking in environments in which most metals exhibit this behavior. In general, failure is attributed to an increase in stress concentration at pits and/or to a decrease in cross-sectional area. Although an applied stress accelerates the corrosion, this stress does not increase the pit density relative to that seen in unloaded specimens; rather, just one or a few pits became more active and penetrates the metal more rapidly than the rest of the pits [Miller and Boyd 1967].

The effect of sustained constant loads on time to failure is shown in Fig. 25.19 for commercial-

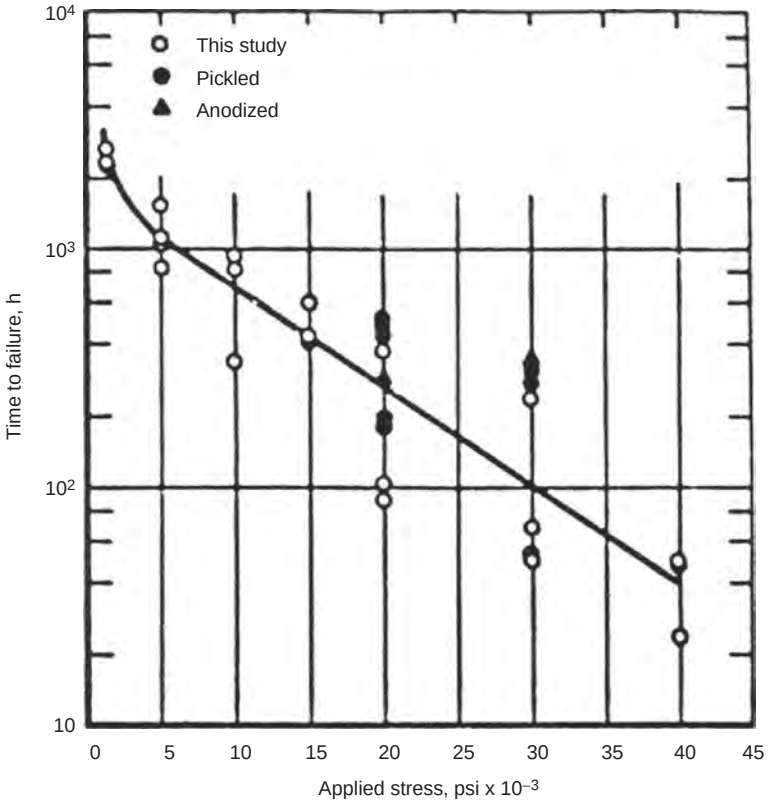

Fig. 25.19 Effect of applied stress on the time to failure for pickled beryllium sheet immersed in synthetic seawater at 25 °C. Source: "This study," Miller et al. 1967; Pickled and anodized data, Prochko et al. 1966

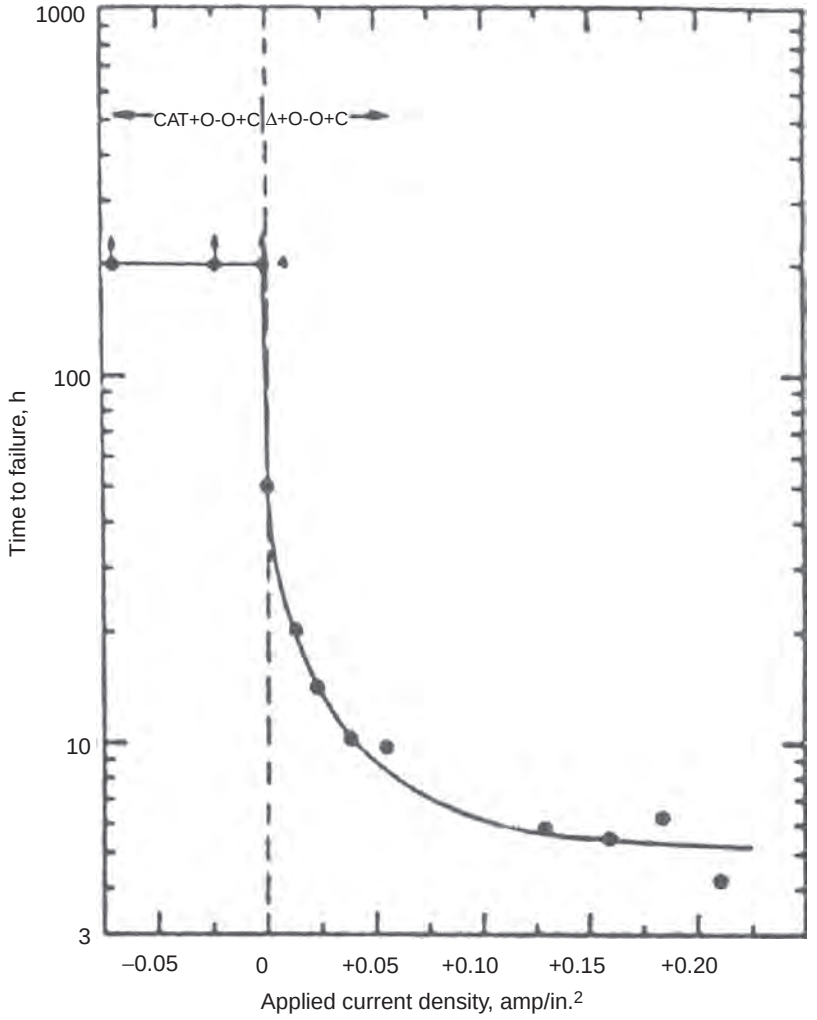

Fig. 25.20 Effect of impressed currents on failure time of beryllium in aerated synthetic seawater under a constant stress of 207 MPa. Source: Miller and Boyd 1967

purity beryllium (98.3 wt% Be containing 1.63 wt% BeO). Specimens, which were obtained from cross-rolled, 1.52 mm thick sheet, were surface ground and flash pickled prior to total immersion testing in synthetic seawater. The material had a yield strength of approximately 440 MPa, with applied stresses ranging from approximately 9 to 276 MPa. Failure was always transgranular and normal to the applied stress. The failures were attributed to stress-accelerated corrosion and associated with pitting. The effect of applied anodic currents, which increase the corrosion rate, on the time to failure of beryllium is illustrated in Fig. 25.20. The failure time for beryllium under a constant stress at 207 MPa decreases with an increase in the anodic current. By contrast, on applying a cathodic current, which protects against corrosion, the failure time remains invariant with current.

REFERENCES

ASTM C203-05. "Standard Test Methods for Breaking Load and Flexural Properties of Block-Type Thermal Insulation," *Annual Book of ASTM Standards*, Vol 4.06, ASTM International

Birkbeck, J.C., Kuehler, N.L., Williams, D.L., and Moddeman, W.E., 1999. X-Ray Photoelectron Spectroscopic Examinations of Beryllium Metal Surfaces Exposed to Chlorinated Solvents, *Surf. Interface Anal.*, Vol 27 (No. 4) p 273–282

CRC, 2000–2001. *Handbook of Chemistry and Physics*, D.D. Lide, Ed., The Chemical Rubber Company Press, New York, NY, p 8/21–8/31

Darwin, G.E., and Buddery, J.H., 1960b. Beryllium, *Metallurgy of the Rarer Metals*, Butterworths Scientific Publications, London, U.K., p 11–99

Fontana, M.G., 1986. *Corrosion Engineering*, 2nd ed., McGraw-Hill, NY

Friedman, J., and Hanafee, J.E., 2000. "Corrosion/Electrochemistry of Monocrystalline and Polycrystalline Beryllium in Aqueous Chloride Environment," Report UCRL-ID-137482, Lawrence Livermore National Lab

Hill, M.A., Butt, B.P., and Lillard, R.S., 1996. "The Corrosion/Electrochemistry of Beryllium and Beryllium Weldments in Aqueous Chloride Environments," LAUR-96-3669, Los Alamos National Laboratory, Los Alamos, NM

Hill, M.A., Butt, D.P., and Lillard, R.S., 1998. The Passivity and Breakdown of Beryllium in Aqueous Solutions, *Electrochem. Soc.*, Vol 145 (No. 8), p 2799–2806

Latimer, W.M., 1952. *Oxidation Potentials*, Prentice-Hall, NY

Lillard, R.S., 2001. Factors Influencing the Transition from Metastable to Stable Pitting in Single-Crystal Beryllium, *J. Electrochem. Soc*., Vol 148 (No. 1), p B1–B11

Lillard, R.S., 2002. "Relationships Between Pitting Corrosion and Crystallographic Orientation, An Historical Perspective," 201st Electrochemical Society Meeting

Lillard, R.S., Hill, M.A., and Butt, P.B., 1997. "Preliminary Investigation into the Corrosion of Beryllium Exposed to Celotex and Water," LAUR-97-0854, Los Alamos National Laboratory, Los Alamos, NM

Miller, P.D., and Boyd, W.K., 1967. "Corrosion of Beryllium," DMIC Report 242, Defense Metals Information Center, Battelle Memorial Institute, Columbus, OH

Miller, R.A., Meyers, J.R., and Saxer, R.K., 1967. Stress Corrosion of Beryllium in Synthetic Sea Water, *Corrosion*, Vol 23, p 11–14

Morana, S.J., 1967. "Surface Passivation Coating for Beryllium Metal," AFML-TR-67-329, Proc. 15th AFML Technical Conference on Corrosion of Military and Aerospace Equipment

Mueller, J.J., and Adolphson, D.R., 1979. Corrosion, *Beryllium Science and Technology*, Vol 2, D.R. Floyd and J.N. Lowe, Ed., Plenum Press, NY, p 417–433

Mueller, J.J., and Adolphson, D.R., 1987. Corrosion of Beryllium, *Corrosion*, Vol 13, *Metals Handbook*, 9th ed., ASM International, p 808–812

Pascal, P., 1958. *Nouveau Traite de Chimie Minerale, Glucinium*, Vol 4, Masson and Cie, Paris

Pourbaix, M., 1966. *Atlas of Electrochemical Equilibria in Aqueous Solutions*, Pergammon Press, NY, p 135

Prochko, R.J., Myers, J.R., and Saxer, R.K., 1966. Corrosion of Beryllium by Salt Water, *Mater. Prot.*, Vol 5, p 39–42

Sanchez, J., Landsberger, S., and Zhao, L., 1999. "Modeling of Beryllium Corrosion," ANRCP-1999-30, Amarillo National Resource Center for Plutonium, Texas Tech. University

Vaidya, R.U., Deshpande, A., Hersman, L., Brozik, S.M., and Butt, D.P., 1999. Protection of Beryllium Metal Against Microbial Influenced Corrosion Using Silane Self-Assembled Monolayers, *Metall. Mater. Trans. A*, Vol 30 (No. 8), p 2129–2134

Vaidya, R.U., Hill, M.A., Hawley, M., and Butt, D.P., 1998. Effect of Pitting Corrosion in NaCl Solutions on the Statistics of Fracture of Beryllium, *Metall. Mater. Trans. A*, Vol 29, p 2753–2760

SELECTED REFERENCES

- Billone, M.C., Dalle Donne, M., and Macaulay-Newcombe, R.G., 1995. Status of Beryllium development for Fusion Applications, *Fusion Eng. Des.*, Vol 27, p 179–190
- Booker, J., Paine, R.M., and Stonehouse, A.J., 1964. Studies on the Vapor Pressure and Oxidation of Certain Beryllides, *Symposium on Compounds of Interest in Nuclear Reactor Technology* (University of Colorado), sponsored by The Metallurgical Society of AIME, p 477–493
- Burnham, J.B., and Bartz, M.H., 1953. "Corrosion of Aluminum and Beryllium in MTR Channel Water," Report AECD-3923, U.S. Atomic Energy Commission
- Demant, J.T., Wiggins, R.E., and Gibson, P., 1963. "The Corrosion of Beryllium and Some Beryllium Alloys by High-Temperature Steam," Report AERE-R-4422, U.K. Atomic Authority
- English, J.L., 1949. "Interim Report on the Corrosion of Beryllium in Simulated Cooling Water for the Proposed Development

Reactor," ORNL-298, Oak Ridge National Laboratory
- English, J.L., 1950. "Corrosion of Beryllium in Simulated Cooling Water for the Materials Test Reactor," Report ORNL-772, U.S. Atomic Energy Commission
- Gilpin, C.B., and Mackay, T.L., 1967. "Corrosion Research Studies on Forged Beryllium," Report AFML-TR-66-294, Air Force Materials Laboratory, Wright-Patterson AFB, OH, p 27–54
- Griess, J.C., Saveage, H.C., English, J.L., Neumann, P.D., Fairchild, L.L., Rainwater, J.G., Hess, D.N., Rice, L., Mauney, T.H., and Winesetter, J.F., 1962. "Corrosion Behavior of QMV Beryllium in Heavy Water at Elevated Temperatures," Report ORNL-3262, U.S. Atomic Energy Commission, p 91
- Gulbransen, E.A., and Johansen, A.M.J., 1994. A Study of the Passive Behavior of Beryllium in Aqueous Solution, *Corros. Sci.*, Vol 36, p 1523
- Hays, W.J., 2005. Corrosion of Beryllium and Aluminum-Beryllium Composites, *Corrosion: Materials*, Vol 13B, *ASM Handbook*, ASM International, p 363
- Hill, M.A., Butt, D.P., and Lillard, R.S., 1997. "The Passivity and Breakdown of Beryllium in Aqueous Solutions," LAUR-97-5007, Los Alamos National Laboratory, Los Alamos, NM
- Hill, M.A., Hanrahan, R.J., Haertling, C.L., Schulze, R.K. and Lillard, R.S., 2003. Influence of Beryllides on the Corrosion of Commercial Grade Beryllium, *Corrosion*, Vol 59 (No. 5), p 424–435
- Levy, D.J., 1961. "The Electrolytic Polarization of Beryllium," LMSC-6-90-61-75, Lockheed Missiles and Space Division, Sunnyvale, CA
- Logan, H.L., and Hessing, H., 1955. "Summarizing Report on Stress-Corrosion of Beryllium," NBS-6, National Bureau of Standards, Washington, D.C., p 12
- Olsen, A.R., 1952. "The Effect of Metallurgical Variables on the Corrosion of Extruded Beryllium," ORNL-1146, Oak Ridge National Lab
- Phennah, P.J., Davies, M.W., and Woodfine, B.C., 1963. The Oxidation of Beryllium in Carbon Dioxide, *The Metallurgy of Beryllium*, Institute of Metals Monograph 28, Chapman and Hall Ltd., London, p 294–313
- Reed, J., 1953. "The Corrosion of Hot-Pressed, Extruded, and Vacuum Cast Beryllium in Simulated Cooling Water for the Materials Testing Reactor," Report ORNL-942, Oak Ridge National Lab
- Sheth, K.G., Johnson, J.W., and James, W.J., 1969. The Anodic Dissolution of Polycrystalline Beryllium, *Corros. Sci.*, Vol 9 (No. 3), p 135–144
- Smith, R., Stuart, W.I., Van Peer, V.J., and Price, G., 1963. The Inhibition of a Breakaway Oxidation of Beryllium in Carbon Dioxide, *The Metallurgy of Beryllium*, Institute of Metals Monograph 28, Chapman and Hall Ltd., London, p 325–334
- Stonehouse, A.J., and Beaver, W.W., 1965. Beryllium Corrosion and How to Prevent It, *Mater. Prot.*, Vol 4 (No. 1), p 24–28
- Stonehouse, A.J., and Beaver, W.W., 1965. Surface Treatments and Coatings, *Beryllium: Its Metallurgy and Properties*, H.H. Hausner, Ed., University of California Press, Berkeley, CA, p 155–177
- Straumanis, M.E., and Mathis, D.L., 1962. The Dissolution Reaction and Attack of Beryllium by HF, HCl, and H2SO4, *J. Electrochem. Soc.*, Vol 109 (No. 5), p 434–436
- Venugopal, A., Macdonald, D.D., and Varma, R., 2000. Electrochemistry and Corrosion of Beryllium in Buffered and Unbuffered Chloride Solutions, *J. Electrochem. Soc.*, Vol 147 (No. 10), p 3673–3679

Beryllium Chemistry and Processing, p 485-492
By Kenneth A. Walsh
Edited by Edgar E. Vidal, Alfred Goldberg,
Edward N.C. Dalder, David L. Olson, and Brajendra Mishra

CHAPTER 26

High-Temperature Corrosion of Beryllium and Beryllium Alloys

Kenneth A. Walsh, Brush Wellman Inc., Retired
David L. Olson, Colorado School of Mines
Alfred Goldberg, Lawrence Livermore National Laboratory
Warren Haws, Brush Wellman, Inc.

THE MOST COMPREHENSIVE reviews on the corrosion of beryllium were written by English [1955], Darwin and Buddery [1960a,b], Jepson et al. [1963a,b, 1965], Mueller and Adolphson [1979, 1987], and Haws [2005]. Special articles specifically on gas corrosion [Mrowec and Werber 1978] and stress corrosion [Logan 1966] are also available in the literature. A general summary of all beryllium corrosion investigations is that the oxidative behavior is influenced by impurities in the beryllium and the fabrication history. The reported corrosion results for beryllium often do not appear to be consistent or reproducible. This inconsistency is most likely due to the wide range of different grades of beryllium being investigated. The impurities in normal commercial grades of beryllium vary from 1 to 4.5 wt% and include oxygen, carbon, iron, chromium, nickel, silicon, aluminum, and copper. These impurities can exist in solid solution, as separate phases, or as particulates [Bunshah 1965]. For corrosion testing of beryllium, it is especially important to report the material source, content, and fabrication history [Jepson et al. 1963a,b, 1965].

26.1 Beryllium in Gaseous Atmospheres

26.1.1 Oxygen

Typically, the kinetics of oxidation of beryllium in pure oxygen has two identifiable regimes when weight gain is plotted against elapsed time at temperature. The first regime is linear, followed by an accelerating rate. The oxidation rate and time at temperature to reach the change in the time dependence is influenced by inherent variables of the beryllium, especially the impurity content and microstructure [Ervin and MacKay 1964a,b]. The source of the beryllium itself plays a role in its oxidation rate, as shown in Fig. 26.1.

It has been reported by Gulbransen and Andrew [1950a,b] that the initial period of oxidation has a parabolic time dependence for weight gain, W, for the temperature range of 500 to 750 °C, which is expressed as:

$$W^2 = k_p t + c \qquad \text{(Eq 26.1)}$$

where k_p is the parabolic rate coefficient, t is the time at temperature, and c is a constant.

The oxidation behavior, being very sensitive to impurity levels and fabrication practice, can exhibit a broad range of behaviors. After performing tests for up to 5000 h in flowing oxygen (containing less than 12 ppm water) at 1 atm and at temperatures between 600 and 1000 °C (1110 and 1830 °F), Higgins and Antill [1962] reported that some batches reached the breakaway time for an accelerated rate during the 5000 h at temperatures as low as 700 °C (1290 °F). Other batches were more resistant to oxidation and did not break away, even at temperatures as high as

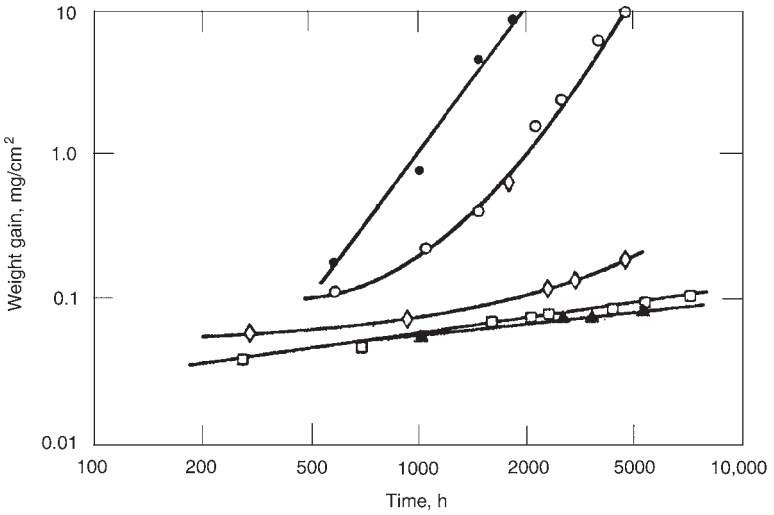

Fig. 26.1 Oxidation of beryllium at 700 °C (1290 °F) in a pure oxygen atmosphere with less than 12 ppm water. □, beryllium powders fabricated by Brush Wellman; ▲, ○, and ●, Pechiney beryllium from different fabrication methods; ◊, vacuum-distilled beryllium. Source: Higgins and Antill 1962

850 °C (1560 °F). However, other investigators [Aylmore et al. 1960, Draycott et al. 1961] observed breakaway at 750 and 800 °C (1380 and 1470 °F). Ervin and MacKay [1964a,b] showed that the length of period of satisfactory protective film barrier is dependent on oxidation temperature, microstructure (e.g., grain size), and the impurity level of the beryllium. The weight gain expression for lower temperatures between 300 and 500 °C (570 and 930 °F) will quickly establish a logarithmic relationship:

$$W = A \ln [1 + Bt] \qquad \text{(Eq 26.2)}$$

where A and B are constants.

The parabolic rate coefficient, k_p, has been further analyzed and found to follow the Wagner rate law for oxidation. Gulbransen and Andrew [1950a,b] reported the heat and entropy of activation for the assumed Be^{2+} ion diffusion through the oxide film. Ervin and MacKay [1964a,b] have shown the parabolic rate coefficient, k_p, to be a function of oxygen pressure to the $^1/_{4.6}$ power, which supports the model that the rate-controlling step is the diffusion of Be^{2+} vacancies throughout the oxide film. The coefficient k_p is also assumed to have an Arrhenius temperature dependence, allowing for the determination of the activation energy (heat) for this diffusion rate-controlling step. The initial phase of oxidation for the higher temperature range, above 500 °C (930 °F), appears to fit well with established analytical mechanistic interpretation.

According to Wagner's oxidation model, the charged defects migrate across the oxide layer under a gradient of chemical potential. This behavior can occur only if the defect concentrations are sufficiently large for the space-charged regions to be fully developed at each interface in the oxide. It is not clear that this condition has been met during beryllium oxidation. It is likely that impure ions influenced the defect concentration.

When oxidation reaches the transition from the parabolic to the accelerated rate, the beryllium disintegrates into a powdery mass of beryllium oxide and unattached metal [Ervin and MacKay 1964a,b, 1965].

26.1.2 Nitrogen

Gulbransen and Andrew [1950a,b] measured the weight gain of beryllium exposed to pure nitrogen (with less than 100 ppm oxygen) at various temperatures for 2 h at 0.1 atm and reported a weight gain of 3 μg/cm^2 at 650 °C (1200 °F) and 112 μg/cm^3 at 925 °C (1700 °F). Up to 900 °C (1650 °F), the reaction rate exhibited parabolic time dependence. For a given temperature, the nitridation rate was less than the rate of oxidation with pure oxygen. When Gulbransen and Andrew [1950a,b] exposed beryllium to lower pressures (2×10^{-4} atm) at 850 °C (1560 °F), the beryllium specimen lost weight with time. This behavior was related to competing rates; the loss due to metal sublimation exceeded the gain in weight due to nitride formation.

Bradshaw and Wright [1963] reported on beryllium nitridation between 980 and 1070 °C (1795 and 1960 °F) in pure nitrogen at 0.8 atm. The highest rate at 1 mg/cm^2 was reported after 4 h tests at 1070 °C (1960 °F).

26.1.3 Air

English [1955] described the surface appearance of beryllium after heating in air for 1 h at temperatures from 600 to 1000 °C (1110 to 1830 °F). The time to produce a noticeable surface tarnish was reported. Sinelnikov et al. [1963] reported that at temperatures above 600 °C (1110 °F), the water content of the air influences the inception of intergranular attack. In general, beryllium has been reported to have acceptable resistance to atmospheric corrosion at ambient temperatures. There have been occasional observations of localized corrosion on compounds after storage for a long period of time [Beaver and Stonehouse 1963, Stonehouse and Beaver 1965]. The use of anodized coatings on parts to be stored has been suggested as a solution [O'Boyle 1961, Steele 1962].

High-temperature oxidation of beryllium in air up to the melting temperature (1283 °C, or 2340 °F) was investigated by Bradshaw and Wright [1963]. Figure 26.2 shows their results in air at 1 atm. After an initial low rate of oxidation, a threshold occurs, followed by a much higher linear rate. The threshold time for the linear rate reduces with increasing temperature. This induction period indicates the progressive breakdown of a protective oxide film. An Arrhenius plot of the linear rate over the temperature range of 930 to 1295 °C (1705 to 2365 °F) results in two regions of different activated processes. An activation energy of 114 kcal/mol for temperatures between 930 and 1295 °C and 13 kcal/mol above 1050 to 1295 °C (1920 to 2365 °F) was determined. Below 1050 °C (1920 °F), the specimens were partially oxidized with intergranular corrosion. Above 1050 °C (1920 °F), the metal surface was totally oxidized. The corrosion product was primarily beryllium oxide with a few percent of beryllium nitride. Anodizing the beryllium in chromic acid before high-temperature oxidation lengthened the induction period.

The structure and orientation of beryllium oxide film formed on beryllium during high-temperature oxidation in air has been characterized [Kerr and Wilman 1956, Scott 1959]. Oxide film growth on both oriented polycrystalline surfaces and on a single-crystal surface has been investigated. The oxidation of beryllium [001] cleaved surface in air at different temperatures was characterized. Epitaxial growth was achieved between 300 and 400 °C (570 and 750 °F). The proportion of randomly oriented beryllium oxide increased with increasing temperature up to 600 °C (1110 °F). Between 600 and 800 °C (1110 and 1470 °F), only random growth was observed in the upper regions of the layer. Above 800 °C (1470 °F), a pronounced [001] habit of the randomly oriented beryllium

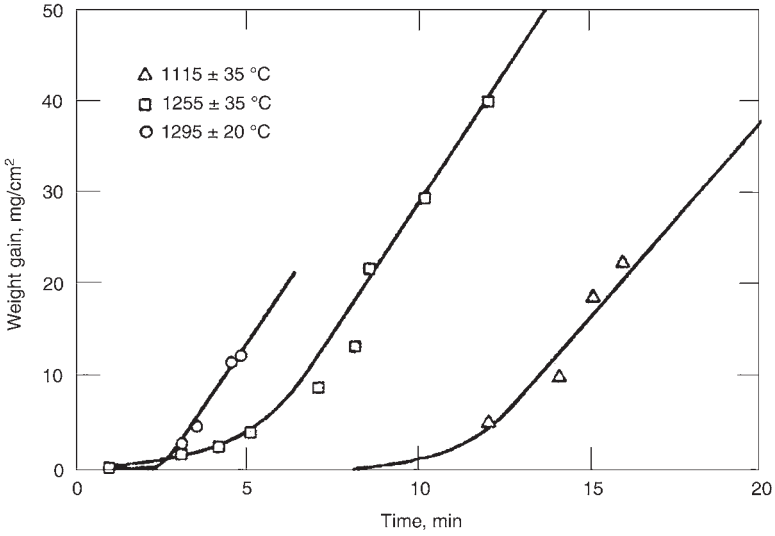

Fig. 26.2 Effect of temperature on the beryllium oxidation rate in air at 1 atm. Source: Bradshaw and Wright 1963

oxide crystals occurs. Grain growth of the oxide crystals associated with the product film also occurs. Below 300 °C (570 °F), the oxide crystals are several thousandths of angstroms. Above 600 °C (1110 °F), prospecting needles and flashes grew out from the substrate.

26.1.4 Carbon Dioxide

Gregg et al. [1960, 1961a,b] described the oxidation of beryllium in carbon dioxide and beryllium oxide film growth, which was accompanied by carbon deposition. The reactions involved are:

$$Be + CO_2 = BeO + CO$$
$$2Be + CO_2 = 2BeO + C$$

Over the temperature range of 500 to 750 °C (930 to 1380 °F), the reaction of carbon production was found to predominate; the ratio of carbon pickup to weight gain was approximately 1 to 10. Forty percent of the carbon becomes beryllium carbide [Gregg et al. 1960, Scott 1960]. Gregg et al. [1961a,b] suggested that this beryllium carbide is formed by the reaction:

$$2Be + C = Be_2C$$

rather than directly by:

$$4Be + CO_2 = 2BeO + Be_2C$$

McCoy [1963] reported that the deposited carbon becomes part of the reaction product and does not transport into the beryllium substrate.

With the presence of water, the carbon dioxide reactions already discussed must also involve the reaction:

$$Be + H_2O = BeO + H_2$$

Gregg et al. [1961a,b] estimated that, on average, twenty molecules of water reacted for every seven molecules of carbon dioxide. Of the seven molecules of carbon dioxide, six molecules reacted according to the CO_2 reaction, which produced CO, and one molecule of CO_2 reacted according to the CO_2 reaction, which produced carbon.

Gregg et al. [1961a,b] demonstrated that Be_2C reacts with water to transfer carbon back to the gas phase. This reaction is given by:

$$Be_2C + 2H_2O = 2BeO + CH_4$$

This reaction is slow but has been proposed to explain the blistering and intergranular attack observed after oxidation of beryllium in a carbon dioxide-water mixture at elevated pressure.

Draycott et al. [1961] have reported an unidentified phase in the corrosion product formed during carbon dioxide-water mixture exposure to beryllium. Inclusions of beryllium carbides present in the as-received beryllium also react with water vapor to form oxide products [Gregg et al. 1961a,b]. Raine and Robinson [1962] suggested that these may be suboxides of beryllium.

The high-temperature corrosion of beryllium in carbon dioxide depends on its fabrication history. The weight gain for beryllium corrosion in carbon dioxide also exhibits the initial low rate period prior to a breakaway to much higher rates. The time elapse before breakaway increases with decreasing concentration of water. The rate of oxidation after breakaway increases with increasing water concentration in carbon dioxide [Phennah et al. 1963], as shown in Fig. 26.3. Beryllium exposed to carbon dioxide containing a fixed concentration of water vapor exhibits a time to breakaway that decreases with increasing temperature of oxidation (Fig. 26.4). The deleterious effect of the water depends on its partial pressures, not the concentration in the carbon dioxide. It has also been reported that the addition of carbon monoxide to the carbon dioxide-water mixture delays the onset of breakaway corrosion under some conditions of exposure [Phennah et al. 1963].

Smith [1961] reported that breakaway corrosion occurred after a shorter time with etched surfaces than with machined surfaces. Tyzack et al. [1963] recommended specific surface treatment to retard breakaway corrosion. Vachon [1962] reported that anodizing resulted in less weight gain for the same length of testing time at 700 °C (1290 °F).

Van Peer [1961] characterized the surface of beryllium after oxidation for increasing time at 700 °C (1290 °F) in wet carbon dioxide. The beryllium oxide grew in mean preferred [001] orientation. As the oxidation progressed, needles and flakes of oxide grew outward from the substrate. The oxide needles are similar in appearance to those reported for beryllium after oxidation in air.

Breakaway corrosion is associated with small, circular eruptions on the beryllium surface. Underneath, such blisters have undergone intergranular attack. After the breakaway corrosion, there is deep penetration of oxide into the beryl-

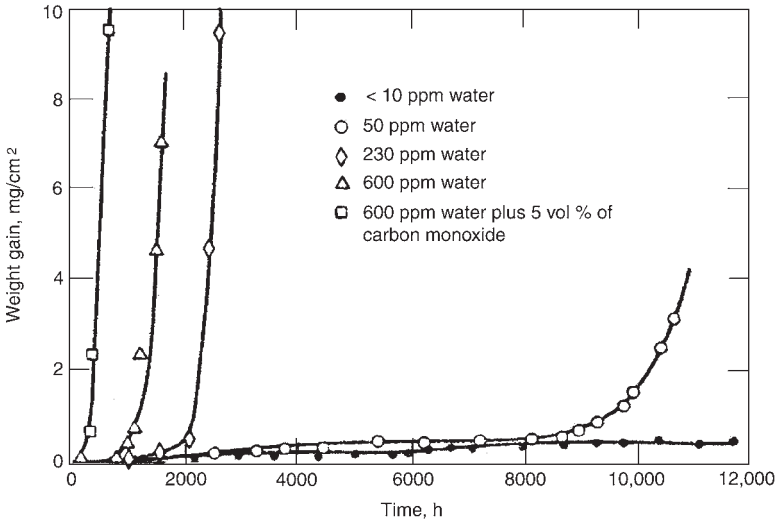

Fig. 26.3 Effect of water concentration in a carbon dioxide-water mixture on the oxidation of beryllium at 650 °C (1200 °F). The total pressure of the tests was kept at 11.2 atm. Source: Phennah et al. 1963

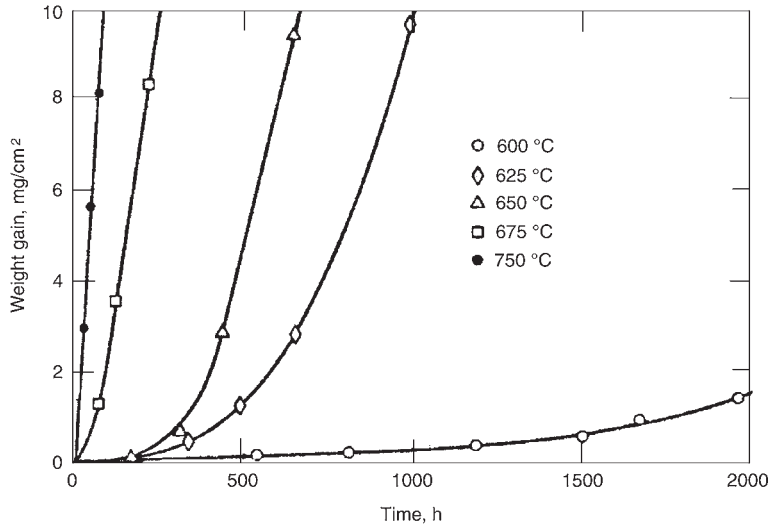

Fig. 26.4 Effect of temperature in a carbon dioxide-water mixture containing 600 ppm water on the oxidation of beryllium. The total pressure of the tests was kept at 11.2 atm. Source: Phennah et al. 1963

lium, and the blisters increase in size and height. Swelling accompanies the intergranular corrosion, resulting in porosity. As the intergranular attack proceeds, the beryllium distorts and eventually disintegrates into a powdery mass [Tyzack et al. 1963].

The mechanistic interpretations for these observations of breakaway and intergranular attack have been classified into two categories. In one category, the cause has been related to the chemical attack on the beryllium carbide inclusions [Higgins and Antill 1962]. Werner and Inouye [1963] reported that decarburization is directly associated with the breakaway behavior. Raine and Robinson [1962] suggested that the oxide blisters are associated with the aforementioned reaction between beryllium carbide and water vapor.

The second category of explanations relates the breakaway corrosion behavior to cracking of

the protective film. Cracking has been related to hydrogen effects [Aylmore et al. 1961, Phennah et al. 1963]. Recrystallization of the worked layers of the beryllium has been suggested by Menzies [1963] to cause the cracking. Cracking has been reported at 700 °C (1290 °F) in carbon dioxide by Gregg et al. [1961a,b], but cracking did not occur at 650 °C (1200 °F) [Scott and Ranzetta 1963]. Beryllium exhibits an oxide-to-metal volume ratio that is greater than 1. This volume ratio likely contributes to the mechanical weakness between adjacent grains, leading to the intergranular attack [Moore and Summerling 1962].

With the proper set of environmental conditions of temperature, water content, and a total pressure, beryllium oxidized in carbon dioxide can achieve a protective film that remains passive in excess of 10,000 h. This behavior has been related to the nature of the growth of the oxide layer. When the growth rate of a continuous oxide layer on the beryllium in carbon dioxide is similar to the growth rate in oxygen [Aylmore et al. 1960, Gregg et al. 1961a,b], acceptable protective film is produced. The difference that occurs in the ability to form a protective film is caused by the pressure dependence of the oxidation rate coefficient, since, in carbon dioxide, there is no apparent pressure dependence as is seen for the oxidation rate in oxygen [Werner 1960].

26.1.5 Carbon Monoxide

Pechiney beryllium was not able to maintain a protective film above 550 °C (1020 °F) [Gregg et al. 1961a,b]. The oxidation reaction produced a mixture of beryllium oxide, beryllium carbide, and elementary carbon [Scott 1960]. The primary reaction is given by:

$$Be + CO = BeO + C$$

In carbon dioxide with a 7.5 vol% carbon monoxide mixture, beryllium at elevated temperature (700 °C, or 1290 °F) will follow the same reaction as if it was in pure carbon dioxide. It appears that the carbon monoxide content of approximately 90% must be exceeded before the aforementioned reaction occurs. In low pressure, for example, in a carbon monoxide-water (5.3×10^4 ppm water) mixture at a total pressure of 0.13 atm, beryllium is oxidized by the following reaction:

$$Be + H_2O = BeO + H_2$$

with the beryllium-carbon monoxide contributing less than 10% of the weight gain. For these beryllium samples, intergranular attack occurred above 650 °C (1200 °F).

26.2 High-Temperature Corrosion-Resistant Alloys

Two types of special beryllium alloys have been investigated to increase the corrosion resistance of beryllium in high-temperature carbon dioxide containing traces of water. This effort studied beryllium with beryllium oxide at its grain boundaries and beryllium-calcium alloys. The beryllium with high oxide content showed some evidence of a significant improvement in the time to breakaway corrosion when compared to similar tests on beryllium with low oxide content. These preliminary results indicated a mechanism to inhibit intergranular attack [Higgins and Antill 1962]. Further work showed that corrosion resistance requires the beryllium oxide to be present as an almost continuous grain-boundary network in the fabricated material [Tyzack et al. 1963].

Tyzack et al. [1963] reported that a semicontinuous network is not retained in beryllium fabricated by hot pressing and extrusion. The oxide inclusion network can be destroyed by annealing the beryllium at 1200 °C (2190 °F), resulting in a loss in the corrosion resistance [Higgins and Antill 1962]. It has also been reported that attempts to make corrosion-resistant beryllium material by consolidating a mixture of beryllium and beryllia powders were not successful [Smith et al. 1963].

Beryllium-calcium alloys have been investigated for their corrosion resistance in high-temperature carbon dioxide environments, for example, as improved canning materials in carbon-dioxide-cooled nuclear reactors [Raine and Robinson 1962]. Calcium has a very low solid solubility (0.07 wt% at 650 °C, or 1200 °F) in beryllium, and excess calcium forms the intermetallic compound $CaBe_{13}$. The angular intermetallic particles are uniformly distributed intragranularly throughout the beryllium. No segregation of $CaBe_{13}$ to the grain boundaries has been observed [Scott and Ranzetta 1963]. Beryllium alloys containing 0.5 and 0.72 wt% Ca exhibited a corrosion resistance superior to base beryllium material when oxidized under the same conditions of carbon dioxide, water content, temperature, and pressure [Raine and

Robinson 1962]. A calcium-rich layer in the surface of the beryllium-calcium alloy has been reported [Scott and Ranzetta 1963]. This calcium-rich sublayer is thought to improve the adhesion between the protective oxide film and beryllium by allowing the oxide film to deform.

REFERENCES

Aylmore, D.W., Gregg, S.J., and Jepson, W.B., 1960. The High Temperature Oxidation of Beryllium, Part I: In Dry Oxygen, *J. Nucl. Mater.*, Vol 2, p 169–175

Aylmore, D.W., Gregg, S.J., and Jepson, W.B., 1961. The High Temperature Oxidation of Beryllium, Part IV: In Water Vapor and in Moist Oxygen, *J. Nucl. Mater.*, Vol 3, p 190–200

Beaver, W.W., and Stonehouse, A.J., 1963. "Beryllium: Surface Treatment and Coatings," Report NP-14783, Brush Beryllium Co.

Bradshaw, W., and Wright, E.S., 1963. Kinetic Reactions of High Temperature Corrosion of Beryllium in Air, *The Metallurgy of Beryllium, Institute of Metals Monograph 28*, Chapman and Hall Ltd., London, p 314–324

Bunshah, R.F., 1965. Future Trends in Beryllium Metallurgy Research, *Beryllium—Its Metallurgy and Properties*, H. Hausner, Ed., University of California Press, Berkeley, CA, p 279

Darwin, G.E. and Buddery, J.H., 1960a. *Beryllium*, Academic Press Inc., New York, NY

Darwin, G.E., and Buddery, J.H., 1960b. Beryllium, *Metallurgy of the Rarer Metals*, Butterworths Scientific Publications, London, U.K., p 11–99

Draycott, A., Nicholson, F.D., Price, G.H., and Stuart, W.I., 1961. "Study of the Variables Affecting the Corrosion of Beryllium in Carbon Dioxide," Report AAEC/E-83, Australian Atomic Energy Commission, p 34

English, J.L., 1955. Chap. IX, *The Metal Beryllium*, D.W. White, Jr. and J.E. Burke, Ed., American Society for Metals, p 530

Ervin, G., Jr., and MacKay, T.L., 1964a. "Beryllium Oxidation Research Relative to the SNAP-8 Reactor," Report NAA-SR-9672, U.S. Atomic Energy Commission

Ervin, G., Jr., and MacKay, T.L., 1964b. Catastrophic Oxidation of Beryllium Metal, *J. Nucl. Mater.*, Vol 12, p 30–39

Ervin, G., Jr., and MacKay, T.L., 1965. The Influence of Dislocations on the Oxidation of Beryllium Metal, *Fifth Int. Symposium on Reaction of Solids*, Elsevier, New York, p 290–302

Gregg, S.J., Hussey, R.J., and Jepson, W.B., 1960. The High Temperature Oxidation of Beryllium, Part II: In Reaction with Carbon Dioxide and Carbon Monoxide, *J. Nucl. Mater.*, Vol 2, p 225–233

Gregg, S.J., Hussey, R.J., and Jepson, W.B., 1961a. The High Temperature Oxidation of Beryllium, Part III: In Carbon Dioxide, Carbon Monoxide, and Mixtures Thereof, *J. Nucl. Mater.*, Vol 3, p 175–189

Gregg, S.J., Hussey, R.J., and Jepson, W.B., 1961b. The High Temperature Oxidation of Beryllium, Part V: In Moist Carbon Dioxide and Moist Carbon Monoxide, *J. Nucl. Mater.*, Vol 4, p 46–58

Gulbransen, E.A., and Andrew, K.F., 1950a. The Kinetics of the Reaction of Beryllium with Oxygen and Nitrogen and the Effect of Oxide and Nitride Films on its Vapor Pressure, *J. Electrochem. Soc.*, Vol 97, p 383–395

Gulbransen, E.A., and Andrew, K.F., 1950b. The Kinetics of the Reactions of Vanadium with Oxygen and Nitrogen, *J. Electrochem. Soc.*, Vol 97, p 396–404

Haws, W.J., 2005. Corrosion of Beryllium and Aluminum-Beryllium Composites, *Corrosion: Materials*, Vol 13B, *ASM Handbook*, ASM International, p 360–369

Higgins, J.K., and Antill, J.E., 1962. Oxidation of Beryllium in Carbon Dioxide and Oxygen, *J. Nucl. Mater.*, Vol 5 (No. 1), p 67–80

Jepson, W.B., 1965. The Corrosion Behavior of Beryllium, *Beryllium*, Atomic Energy Research Establishment, Harwell, England, p 221–256

Jepson, W.B., Myatt, B.L., Warburton, J.B., and Antill, J.E., 1963a. Some Topographical Observations on the Oxidation of Beryllium, *J. Nucl. Mater.*, Vol 10, p 224–232

Jepson, W.B., Warburton, J.B., and Myatt, B.L., 1963b. High Temperature Oxidation of Beryllium and the Fate of Beryllium Carbide Inclusions, *J. Nucl. Mater.*, Vol 10, p 127–133

Kerr, I.S., and Wilman, H., 1956. The Structure and Growth of Oxide Layers Formed on Beryllium, *J. Inst. Met.*, Vol 84, p 379–385

Logan, H.L., 1966. The Stress Corrosion of Metals, *Corrosion Monograph Series*, John Wiley and Sons, Inc., NY, p 259–263

McCoy, H.E., Jr., 1963. "Observations on the Oxidation of Beryllium CO_2 by Use of C_2 and Autoradiographic Techniques," Report ORNL-TM-622, U.S. Atomic Energy Commission

Menzies, I.A., 1963. Observations on the Oxidation of Beryllium in Carbon Dioxide at 600–700 Degrees, *Corros. Sci.*, Vol 3, p 35–49

Moore, D., and Summerling, R., 1962, unpublished work reported by Jepson, W.B., Warburton, J.B., and Myatt, B.L., 1963. The High Temperature Oxidation of Beryllium and the Fate of Beryllium Carbide Inclusions, *J. Nucl. Mater.*, Vol 10, p 127

Mrowec, S., and Werber, T., 1978. "Gas Corrosion of Metals," Report TT 76–54038, National Bureau of Standards, Washington, D.C., p 438–443 (translated from Polish in 1975)

Mueller, J.J., and Adolphson, D.R., 1979. Corrosion, *Beryllium Science and Technology*, Vol 2, D.R. Floyd and J.N. Lowe, Ed., Plenum Press, NY, p 417–433

Mueller, J.J., and Adolphson, D.R., 1987. Corrosion of Beryllium, *Corrosion*, Vol 13, *Metals Handbook*, 9th ed., ASM International, p 808–812

O'Boyle, D., 1961. Surface Coatings for Beryllium Parts, *Mach. Des.*, Vol 33, p 147–150

Phennah, P.J., Davies, M.W., and Woodfine, B.C., 1963. The Oxidation of Beryllium in Carbon Dioxide, *The Metallurgy of Beryllium, Institute of Metals Monograph 28*, Chapman and Hall Ltd., London, p 294–313

Raine, T., and Robinson, J.A., 1962. The Corrosion of Beryllium and Alloys of Beryllium with Calcium in Carbon Dioxide, *J. Nucl. Mater.*, Vol 5 (No. 3), p 341–343

Scott, V.D., 1959. Structure and Growth of Beryllium Oxide on Single Crystal of Beryllium, *Acta Cryst.*, Vol 12 (No. 2), p 136–142

Scott, V.D., 1960. Formation of Beryllium Carbide during the Corrosion of Beryllium in Carbon Monoxide and in Carbon Dioxide Gas, *Nature*, Vol 186, p 466–467

Scott, V.D., and Ranzetta, G.V.T., 1963. Electron Metallography of the Corrosion of Beryllium and Beryllium Calcium Alloys, *J. Nucl. Mater.*, Vol 9 (No. 3), p 277–289

Sinelnikov, K.D., Ivanov, V.E., and Vasyutinsky, B.M., 1963. The Oxidation of Be in Air at 500 °C, *The Metallurgy of Beryllium, Institute of Metals Monograph 28*, Chapman and Hall Ltd., London, p 355–361

Smith, R., 1961. *Fuel Element Fabrication*, Vol 2, Academic Press, London, U.K., p 147

Smith, R., Stuart, W.I., Van Peer, V.J., and Price, G., 1963. The Metallurgy of Beryllium, *The Metallurgy of Beryllium, Institute of Metals Monograph 28*, Chapman and Hall Ltd., London, p 325–334

Steele, J.R., 1962. Beryllium Corrosion, *Mater. Prot.*, Vol 1 (No. 7), p 59–62

Stonehouse, A.J., and Beaver, W.W., 1965. Beryllium Corrosion and How to Prevent It, *Mater. Prot.*, Vol 4 (No. 1), p 24–28

Tyzack, C., Campbell, C.S., and Trowse, F.W., 1963. *J. Br. Nucl. Energy Soc.*, Vol 2, p 95

Vachon, L.J., 1962. Protection of Beryllium Metal by Anodic Films, *J. Nucl. Mater.*, Vol 6 (No. 1), p 139–141

Van Peer, W.J., 1961. The Oxidation of Polycrystalline Beryllium in Carbon Dioxide, *Aust. J. Phys.*, Vol 14 (No. 1), p 191–192

Werner, W.J., 1960. "Beryllium Oxidation Studies," Report ORNL-2988, U.S. Atomic Energy Commission, p 424–425

Werner, W.J., and Inouye, H., 1963. Reactions of Beryllium with Wet Carbon Dioxide, *The Metallurgy of Beryllium, Institute of Metals Monograph 28*, Chapman and Hall Ltd., London, p 283–293

SELECTED REFERENCES

- Kneppel, D.S., 1957. "Corrosion of Beryllium in 600 °F Water," Report NMI-1190, U.S. Atomic Energy Commission
- Peoples, R.S., and Bulkowski, H., 1949. "Corrosion of Beryllium in 525 °F and 600 °F Distilled Water," Report BMI-HAP-101, Battelle Memorial Institute

Beryllium Chemistry and Processing, p 493-498
By Kenneth A. Walsh
Edited by Edgar E. Vidal, Alfred Goldberg,
Edward N.C. Dalder, David L. Olson, and Brajendra Mishra

CHAPTER 27

Beryllium Waste Recycling

Mark N. Emly and Edgar E. Vidal, Brush Wellman, Inc.

27.1 Introduction

Salient beryllium statistics are based mostly on the beryllium content of beryllium-copper alloys and beryllium metal (Table 27.1). In 2000, approximately 130 metric tons of beryllium contained in postconsumer old scrap was generated; approximately 5 metric tons of beryllium was recycled or reused (1 metric ton = 1000 kg = 1.102 short tons). The old scrap recycling efficiency was calculated to be approximately 7%, and the recycling rate approximately 10%. Beryllium contained in new scrap consumed was about 30 metric tons. Although little beryllium-bearing old scrap is recycled for its beryllium content, new scrap materials, such as beryllium alloys and beryllium metal, reclaimed at manufacturing plants that produce beryllium-related components are an important source of beryllium supply [Cunningham 2004].

A beryllium recycling efficiency of approximately 7% was estimated to have been reached in 2000. The recycling efficiency would have been higher if not for the lack of a concerted program to reuse beryllium from its major end use, beryllium-related electrical and electronic components manufactured from beryllium-copper alloys (containing approximately 2% beryllium).

Beryllium-containing by-products and wastes are generated in the manufacture of beryllium metal, beryllium oxide ceramics, and beryllium alloys. As a whole, these materials contain significant amounts of beryllium and copper. The recovery of these metal values is desirable both economically and environmentally. Significant work has been done at Brush Wellman, Inc. to recycle both copper and beryllium from their waste streams. This chapter is a compilation of work performed by Emly at Brush Wellman, Inc. [Emly 1994].

Table 27.1 Salient statistics for U.S. beryllium scrap in 2000

Old scrap	
Generated(a), t (b)	130
Consumed(c), t	5
Consumption value(d)	$1,800, 000
Recycling efficiency(e)	7%
Supply(f), t	140
Unrecovered(g), t	130
New scrap consumed(h), t	30
New-to-old-scrap ratio(i)	86:14
Recycling rate(j)	10%
U.S. net exports of scrap(k), t	5
Value of U.S. net exports of scrap(l)	$700, 000

(a) Beryllium content of products theoretically becoming obsolete in the United States in 2000; this excludes dissipative uses. (b) t, metric ton (1000 kg). (c) Beryllium content of products that were recycled in 2000. (d) Value of beryllium in materials used in calculating total value of contained metal in scrap. (e) (Old scrap consumed plus old scrap exported) divided by (old scrap-generated plus old scrap imported). (f) Old scrap generated plus old scrap imported. (g) Old scrap generated plus old scrap imported minus old scrap consumed minus old scrap exported. (h) Including prompt industrial scrap but excluding home scrap. (i) Ratio of quantities consumed, in percent. (j) Fraction of beryllium-apparent supply that is scrap on an annual basis. (k) Trade in scrap is assumed to be principally in old scrap. (l) Value of U.S. net imports of scrap is the value of beryllium scrap imports minus value of exports as reported by the U.S. Census Bureau. Source: Cunningham 2004

27.2 Resource Recovery and Process Facility

In the 1980s, Brush Wellman built a facility dedicated to the recovery of copper and beryllium from internal and customer-generated beryllium-containing wastes. For the initial recovery efforts, by-products generated during

beryllium-copper production were treated. These by-products constitute the largest volume of recoverable material, which include spent caustic and acid pickling solutions, furnace drosses, mill scale, alloy melting skulls, and collector dusts.

Copper was recovered via electrowinning technology and beryllium via solvent (liquid-liquid) extraction technology. To start, copper and beryllium are dissolved from the by-product materials, followed by copper electrowinning and/or electrorefining. The soluble beryllium is then extracted from the copper-depleted solution and reinserted into the main beryllium production stream. A seven-cell copper-electrowinning system, four electrorefining cells, and a six-stage beryllium solvent extraction circuit provide a capacity of 907 metric tons (2 million lb) of copper and 23 metric tons (50,000 lb) of beryllium per year. The process flowsheet for this facility is shown in Fig. 27.1.

Various beryllium-copper by-product feeds composition are shown in Table 27.2. The copper oxide and hydroxide represent the largest single feed, followed by the furnace dross, mill scale, and melting skull streams. During processing of wrought beryllium-copper alloys, parts are chemically milled (pickled) to improve surface finish. At Brush Wellman, most of the

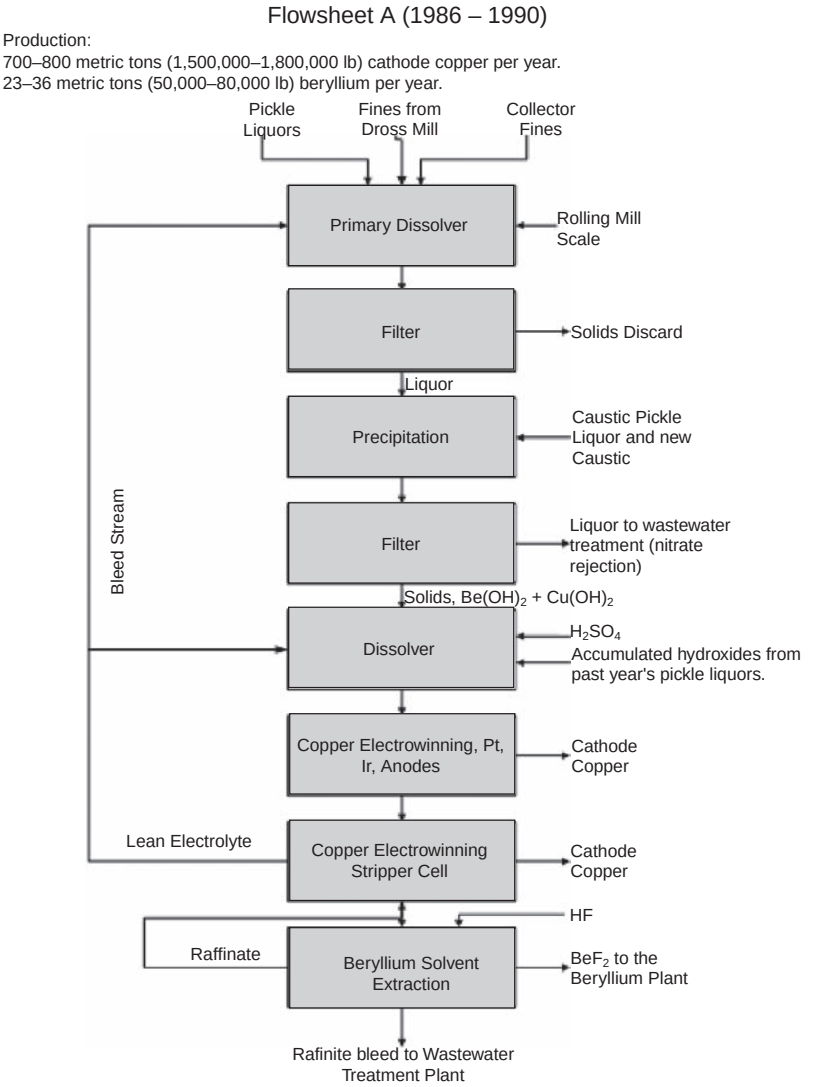

Fig. 27.1 Resource recovery flow sheet for copper and beryllium. Source: Emly 1994

pickling is done in a nitric acid or sulfuric acid-peroxide bath. The spent acid liquor is neutralized with a caustic solution to precipitate the copper oxide and copper hydroxide.

Dusts collected from ventilation equipment are recycled during master alloy production operations, with the exception of small quantities that are periodically removed to control the buildup of impurities.

Prior to casting, oxide inclusions are removed from molten beryllium-copper alloys by skimming the melt (furnace dross). Melting skulls from ladles and mill scale after mechanical milling have very similar compositions to the furnace dross. These materials are treated separately with fresh or spent nitric pickle liquors to yield a solution of beryllium and copper.

Chips, saw cuttings, and grinding and polishing residuals are liberated during the manufacturing process of beryllium and beryllium oxide ceramics. When plausible, these by-products are collected without additional contamination and recycled directly back into the manufacturing process. When these by-products are contaminated with other metals and organic fluids, they cannot be recycled directly. Dissolution and recovery of beryllium must be performed through the resource recovery facility described previously. If the beryllium oxide ceramic is metallized (molybdenum, manganese, nickel, and copper), the metals must be chemically milled before recycling. The beryllium oxide is then crushed and recycled to the arc furnace.

A dross processing operation separates true dross components from entrapped metallics in alloy furnace dross. The liberated metallics (>20 mesh) are recycled back to beryllium-copper alloy operations, while the dross and undersized metallics (<20 mesh) are dissolved in acid. Customer scrap that does not meet specifications in terms of impurities is melted and cast as anodes for electrorefining.

Table 27.2 Analysis of typical by-product feeds

Compound or element	Composition, wt%
$CuO/Cu(OH)_2$	
Cu	51.2
Be	0.78
O	16.0
Na	1.10
Si	0.36
Mg	0.13
Nitrate	2.57
Chloride	0.10
Other	<0.10
Moisture (loss on drying)	23.9
Furnace dross, mill scale, and melt skulls	
Cu	80–88
Be	3–4
O	6–12
Other	<1.0
Collector dusts	
Cu	30–35
Be	10–12
O	22–35
C	3–4
Other	<2

Source: Emly 1994

27.2.1 Copper Recovery

Caustic solutions are used for treating scrap dissolver solutions and spent nitric acid pickle liquors to precipitate impure copper oxide/hydroxide. Precipitation and wash are necessary to reject nitrates that interfere with the electrowinning step. The precipitates contain roughly 1 wt% Be. The washed precipitate is dissolved in sulfuric acid to form a copper-sulfate-base electrolyte. After electrolysis, lean electrolyte solutions typically have a composition as given in Table 27.3. Rich electrolyte is similar except for higher concentrations of copper and lower concentrations of acid. The copper electrolyte is polish filtered before electrowinning.

Copper is deposited for seven days before harvesting. The 70 to 100 kg (150 to 220 lb) copper plates are stripped from the stainless steel cathode sheets, weighed, and inventoried for use in beryllium-copper production.

Indium-coated titanium anodes have been used in the electrowinning circuit. The relatively high concentration of nitrates present in the electrolytes (5 to 6 g/L) prevents the use of standard lead-base anodes. Stainless steel cathodes were

Table 27. 3 Typical composition of electrolytes in flowsheet A (Fig. 27.1) process

Element or compound	Lean electrolyte, g/L	Rich electrolyte, g/L
Cu(a)	23–25	27–30
Be	5	5
Na	3	3
Mg	1	1
Fe	1.2	1.2
Ca	0.7	0.7
Co	0.5	0.5
Al	0.3	0.3
H_2SO_4(a)	75–80	70–75
Si	0.3	0.3
Ni	0.6	0.6
Nitrates	5–6	5–6
Chlorine	0.13	0.13
Fluorine	0.07	0.07

(a) After electrolysis, rich electrolyte solutions typically were similar to the lean electrolyte except for higher concentrations of copper and lower concentrations of acid.

used in place of copper starter sheets. Solids postprecipitated in the electrolysis cells and adhered to the cathodes.

The standard practice within the copper industry is to use solvent extraction with electrowinning to achieve a high-quality copper cathode. Research at Brush Wellman using LIX (Cognis Corp.) reagents demonstrated the feasibility of adopting this technology. Using LIX 84 substantially improves the quality of copper electrolyte by rejecting most impurities, including nitrates. By elimination of nitrates, it is possible to use lead-base anodes at a considerable cost-savings compared to the iridium-base titanium anodes.

Figure 27.2 shows the process flow diagram considering the use of solvent extraction. The purity of copper electrolyte has been significantly improved by the use of LIX 84 solvent extraction. A typical lean and rich electrolyte

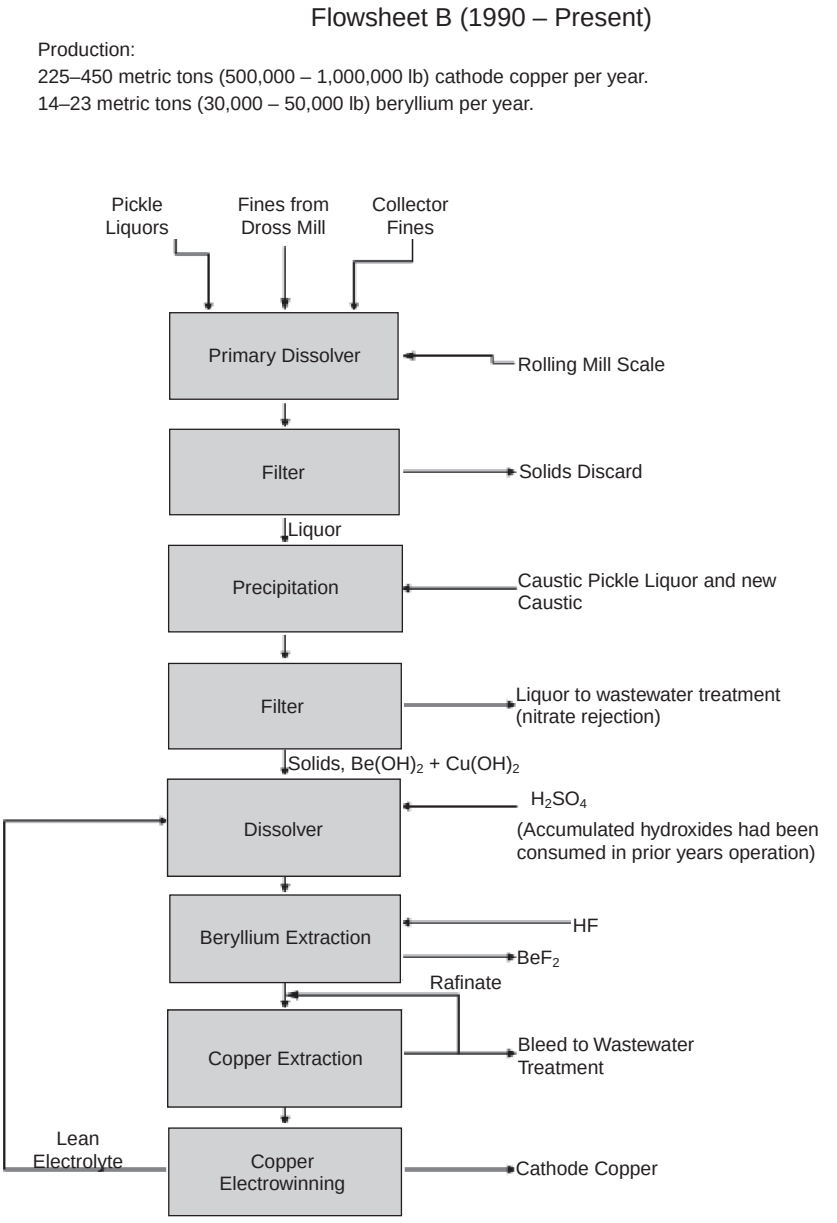

Fig. 27.2 Modified resource recovery for copper and beryllium. Source: Emly 1994

composition is shown in Table 27.4. The differences observed are in Copper content and sulfuric acid concentration. A McCabe-Thiele diagram for the copper-LIX1 84 system is shown in Fig. 27.3. By diluting the copper feedstream to 1 g Cu/L, three stages of solvent extraction were necessary to recover 97 wt% of the copper.

27.2.2 Beryllium Recovery

The copper-depleted solution is mixed with additional scrap beryllium solutions and diluted to 1 g Be/L with either fresh water or recycled raffinate. Caustic is added to adjust the pH of the solution to 1.0 ± 0.1. Beryllium is extracted into a kerosene solution of diethylhexylphosphoric acid and back-extracted or stripped into an aqueous HF solution. Figure 27.2 shows the schematic of the six-stage beryllium solvent extraction circuit. Loading occurs in three stages; stripping occurs in two stages. The stripped organic must be water washed in the sixth stage to prevent HF carryover into the loading stage.

Table 27.4 Typical composition of the electrolytes used after solvent extraction

Element or compound	Lean electrolyte, g/L	Rich electrolyte, g/L
Cu	25–30	35–40
Fe	0.5	0.5
Co	0.1	0.1
Other metallics	0.02	0.02
H_2SO_4	125–135	110–120
Nitrates, chlorides, and fluorides	0.01–0.03	0.02

Source: Emly 1994

The beryllium-loading circuit base on a McCabe-Thiele diagram is shown in Fig. 27.4. A pH of 1 is necessary to avoid the co-extraction of aluminum, nickel, copper, cobalt, and other impurities. When recycling a fraction of the raffinate, approximately 98 wt% of the beryllium values can be recovered. The final raffinate is neutralized with lime and sent to final water treatment prior to discharge.

A typical hydrofluoric acid strip liquor contains 40 to 60 g Be/L, 10 to 15 g Fe/L, 80 to 100 g HF/L, 1 g Al/L, $<$ 0.01 g Cu/L, and minor traces of other impurities. This liquor is processed along with the normal feedstreams used in the extraction of beryllium metal. The excess hydrofluoric acid is recycled in the downstream extraction and does not incur additional cost. It is estimated that the cost of recovering the beryllium from the acid strip liquor is roughly half of that by normal extraction techniques from the ore.

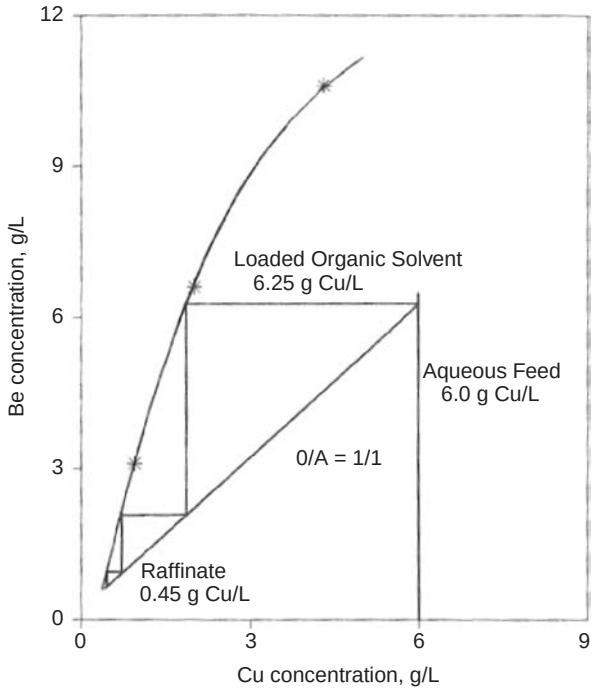

Fig. 27.3 McCabe-Thiele diagram for the copper-LIXI 84 system Concentration in organic solution for Be, concentration in aqueous solution for Cu. Source: Emly 1994

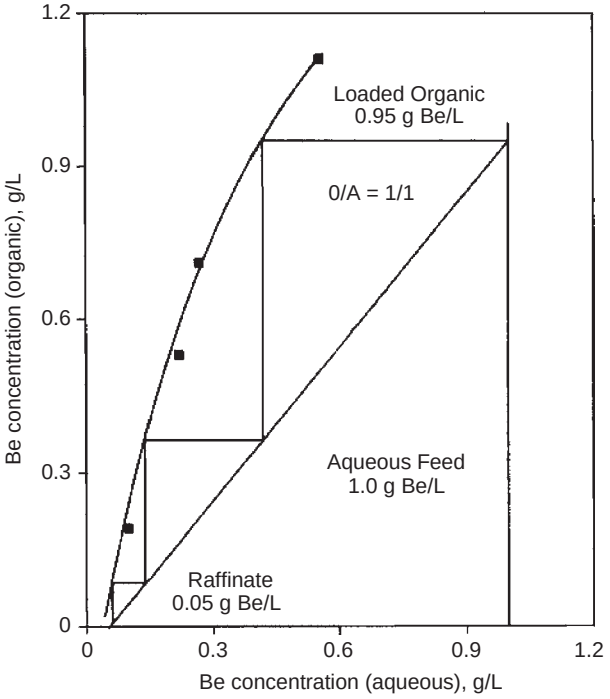

Fig. 27.4 McCabe-Thiele diagram for diethyl hexyl phosphoric acid and 1 g/L of beryllium at pH 1.0. Concentration of Be is in aqueous solution on *x*-axis and in organic solution on *y*-axis. Source: Emly 1994

27.3 Summary

Nearly 1364 metric tons (3,000,000 1b) of copper and 22.7 metric tons (50,000 1b) of beryllium can be recycled annually at the Brush Wellman facilities. Alternate disposal options for beryllium-containing wastes are expensive and pose a significant long-term environmental liability. Only the ventilation collector dusts remain in inventory, awaiting a process option.

REFERENCES

Cunningham, L.D., 2004. "Flow Studies for Recycling Metal Commodities in the United States," Beryllium Recycling in the United States in 2000, U.S. Geological Survey Circular 1196—P, U.S. Department of the Interior, U.S. Geological Survey

Emly, M.N., 1994. Recycle of Beryllium-Containing Waste, *Miner. Process. Extr. Metall. Rev*., Vol 13, p 165–176

Beryllium Chemistry and Processing, p 499-512
By Kenneth A. Walsh
Edited by Edgar E. Vidal, Alfred Goldberg,
Edward N.C. Dalder, David L. Olson, and Brajendra Mishra

CHAPTER 28

Medical Aspects of the Toxicity of Beryllium and Beryllium Alloys

George Fulton and Alfred Goldberg
Lawrence Livermore National Laboratory

28.1 Introduction

European researchers first reported beryllium-related lung diseases in the 1930s, several years after the emergence of beryllium in manufactured products. The first American reports came out in 1943, referring to a "rapidly appearing chemical pneumonia" that became known as acute beryllium disease (ABD) [Fields 2001]. It has been estimated that in the 1970s, 30,000 workers had been exposed to beryllium in the United States, while more recent (2003) estimates of exposure to beryllium by workers in the United States are between 200,000 and 800,000 [Infante and Newman 2004]. The exposure to beryllium can lead to the more-common chronic beryllium disease (CBD) and/or to beryllium sensitization. (Sensitization is not a disease; it is a reaction similar to a chronic allergy in which white blood cells in the blood or lungs react to the beryllium. It results in a heightened immune response to beryllium on subsequent exposures. It may be at least partly genetic. It has no symptoms. On inhalation of beryllium, the reaction of the white blood cells to the beryllium may lead to CBD.) The sensitization and CBD are immune-system responses to a foreign substance. Chronic beryllium disease was first described in 1946 with reference to fluorescent-lamp workers exposed to insoluble beryllium compounds used in fluorescent lamps, the disease then being named delayed chemical pneumonitis [Sawyer et al. 2002, World Health Organization 1990, Herr 1997]. The use of beryllium in the production of fluorescent lamps was discontinued in 1949 [World Health Organization 1990]; however, some of these lamps may still exist and remain in use.

In 1971, the Occupational Safety and Health Administration (OSHA) adopted a worker-protection permissible-exposure limit (also referred to as occupational-exposure limit) for beryllium of 2 $\mu g/m^3$ measured as a time-weighted average (TWA) [U.S. Department of Energy 1999]. TWA is obtained by measuring the concentration, c, during a given length of time, *t*, at various intervals during a work period, w, such that TWA = $[\Sigma(c \times t)]/w$.) This limit was established in 1949 by the then Atomic Energy Commission (AEC), and it was still in effect (1999) by the Department of Energy (DOE) [U.S. Department of Energy 1999]. In 1949, the AEC also set an ambient-air standard of 0.01 $\mu g/m^3$, which was adopted by the Environmental Protection Agency (EPA) in 1973. In 1979, the National Institute for Occupational Safety and Health recommended to OSHA an exposure limit of 0.5 $\mu g/m^3$ and classified beryllium as a carcinogen [U.S. Department of Energy 1999]. In December 1998, the American Conference of Government Industrial Hygienists proposed an 8 h TWA limit of 0.2 $\mu g/m^3$. The timing of this proposed limit change was preceded by the DOE Notice of Proposed Rulemaking, which instead contained the then-accepted 2 $\mu g/m^3$ limit. A maximum exposure limit of 5 $\mu g/m^3$ over a 30 min period and a 25 $\mu g/m^3$ peak limit at any time had also been established [Infante and Newman 2004].

In reviewing the technical information available up to that time, the DOE concluded that it was difficult to determine the exposure level necessary to eliminate the risk of contracting CBD. In 1996, the DOE initiated a number of surveys involving beryllium usage, the type and number of beryllium tasks, the estimated number of workers exposed during each task, and the estimated exposure levels associated with each task. The results of these surveys are detailed in the DOE December 1999 Rules Report on the CBD Prevention Program (CBDPP) [U.S. Department of Energy 1999]. While waiting for the OSHA proposal addressing this question, the DOE was establishing a 0.2 $\mu g/m^3$ limit that would trigger certain workplace precautions and control measures. The DOE also required its contractors and any covered DOE employers to establish in their CBDPP the exposure reduction and minimization measures designed to reduce potential levels to below the action level. In a recent Lawrence Livermore National Laboratory (LLNL) document (December 2004 Revision) [LLNL 2004], which was recommended for approval by the Environmental, Safety, and Health Working Group, it was also proposed that the action level be at 0.2 $\mu g/m^3$, and that all places should be maintained below this level. In a publication (partial reference given as Yoshida et al. 1997) by authors from Japan's Fujita Health University School of Medicine, it was concluded that if exposure was kept below 0.01 $\mu g/mm^3$, workers would not become sensitized to beryllium [Fields 2001]. A concentration limit of beryllium in the atmosphere in the vicinity of beryllium plants in the United States had also been set at 0.01 $\mu g/mm^3$ [Sawyer et al. 2002]. At LLNL, for an 8 h TWA, the permissible-exposure limit is 2 $\mu g/m^3$, and the permissible-action level limit is 0.2 $\mu g/m^3$.

The Brush Wellman Material Safety Data Sheet, No. M10, revised on January 1, 2002, indicated an 8 h TWA permissible-exposure limit of 2 $\mu g/m^3$. (Brush Wellman, Inc. is the sole current producer of beryllium in the United States.) In their Safety Facts Sheet (SF9/0997), they state: "Beryllium-containing materials, in solid form and as-finished parts, present no particular health hazard." They further state: "Breathing very fine particles may cause a serious lung condition in a small percentage of individuals." They also indicate that to be hazardous, the airborne particles must be less than approximately 10 μm in diameter, a size that cannot be seen with the unaided eye. (It is suggested that particles greater than 10 μm are too large to penetrate far into the lungs and so pose little health risk.) Brush Wellman suggests that instead of particle weight, the criteria for exposure limit could better be based on size and number of particles. A significant relationship was reported as existing between deposits in the alveolar region in the lung of particles less than 10 μm (as well as less than 5 μm) and the prevalence of CBD and sensitization. This study suggested that the concentration of particle sizes less than 10 μm may be more relevant than the total mass concentration of the airborne beryllium [Kent et al. 2001]. Another study suggested that inhalation of particle sizes of less than 1 μm in diameter causes the greatest risk for developing CBD [U.S. Department of Energy 2002]. This greater risk may be that, for the same mass, the finer the particle size, the larger would be the area coated for immune-cell attack. The most current (2004) CBDPP presented by LLNL to the DOE stipulated using a 0.2 $\mu g/m^3$ TWA limit.

28.2 Beryllium Diseases

Chronic beryllium disease is usually a slowly developing disease that gradually worsens with time. By contrast, ABD develops following a relatively short exposure to a high concentration of beryllium (dust). (The acute reaction immediately following inhalation of soluble-beryllium compounds is also known as acute pulmonary disease or acute chemical pneumonitis. It is a fulminating inflammatory reaction of the entire respiratory tract, and in the severest cases it can develop into acute fulminating pneumonitis; the severity is dose related [Goyer and Clarkson 2001].) Acute beryllium disease has many of the same symptoms as seen in CBD; however, the symptoms appear much more rapidly with ABD than with CBD. By not having further contact with the beryllium dust, recovery from ABD is possible within weeks or a few months, although symptoms could persist and possibly lead to CBD [Sawyer et al. 2002]. Approximately 30% of ABD sufferers eventually developed CBD [Fields 2001], and approximately half of these died of CBD. Many who died had been exposed to airborne-beryllium concentrations of 1000 $\mu g/m^3$ [Fields 2001]. No ABD cases were reported for beryllium exposures of less than 100 $\mu g/m^3$, and the last case in the United States was reported in 1967 [Fields 2001,

Newman et al. 1996]. Because of current engineering practices and controls, it is very unlikely (although still possible) to have beryllium exposures high enough to cause ABD. While ABD can be reversed, there is no cure for CBD, since it is not reversible. A comprehensive history of beryllium sensitization and CBD, the symptoms developed, and the diagnostics used covering the period from the 1940s to the mid-1990s were presented at a conference on beryllium-related diseases [Newman et al. 1996]. Only a very small percentage (2 to 5%) of people will become sensitized after a low-level exposure, although this would be increased to a higher percentage (10 to 12%) with higher levels of exposure (e.g., for machinists). There is no known exposure level that is safe for everyone [U.S. Department of Energy 2002].

Chronic beryllium disease is primarily a granulomatous lung disease caused by the inhalation of dust, mist, or fumes containing beryllium (as metallic, oxide, salt, etc.). (A granulomatous disease is a disease in which a tumorlike granulation or scarring is developed as a reaction to chronic inflammation from a foreign body. This can also develop in an open wound that is exposed to beryllium.) The disease is mostly caused by the relatively insoluble forms of beryllium-containing materials. The disease results when beryllium particles are inhaled and come into contact with lymphocytes (a cell class that produces antibodies to attack infected or cancerous cells and is responsible for rejecting foreign bodies) in the lungs, thus triggering the cells to become sensitized and then proliferate. (The proliferation of the cells is initiated by the normal response of the immune system in its effort to get rid of foreign matter. Cells in the lung will attempt to eliminate or destroy the beryllium particles in the air sacs. If unsuccessful, more cells will be activated, and cell clusters will form and grow around the particles. The resulting scarring or formation of granulomas on adjacent lung tissue decreases the lung's elasticity for expanding and contraction necessary for the exchange of oxygen and carbon dioxide between air sacs and blood vessels [U.S. Department of Energy 2002].) It is suggested that beryllium binds to a cell protein or peptide (a chemical compound containing amino acids), making the cell appear foreign, which then initiates a hypersensitivity reaction [Fields 2001]. According to Brush Wellman, the inhaled particles must be small enough to reach the air sacs deep in the lungs, and the person must be sensitive or allergic to beryllium. The lung tissues become inflamed. The inflammation may cause scarring that can restrict the exchange of oxygen between the lungs and bloodstream. The development of scarring and/or granulomas can best be detected by a biopsy, although the granulomas can sometimes be seen in a chest x-ray [U.S. Department of Energy 2002].

It is difficult to predict the progression of CBD. The clinical course of CBD is highly variable; it can cause either a rapid deterioration or, more commonly, a long, slow-growing illness of a person. Chronic beryllium disease can cause one or more of many symptoms and/or diagnostic evidences that are typical of other illnesses. For example, evidence of granulomas in lung tissue that could be attributed to CBD tissue may also be attributed to other lung diseases. The disease can also be present without symptoms. The most common symptoms are shortness of breath with physical exertion, and persistent coughing. Additional symptoms can be fatigue, chest and joint pain, blood in sputum, rapid heart rate, loss of appetite, fever, and night sweats [U.S. Department of Energy 2002, Trichopoulos 2005, LLNL 2002]. Some of these symptoms, especially shortness of breath, coughing, and chest pain, also occur with ABD. The symptoms for ABD may occur within three days after a massive short-term exposure or within weeks following a prolonged exposure to relatively lower beryllium concentrations. The symptoms have often suggested the presence of other diseases, such as bronchiolitis, pneumonitis, and dermatosis [World Health Organization 1990]. Both ABD and CBD have only been seen in individuals who have been exposed to beryllium particles, dust, or fumes [U.S. Department of Energy 2002].

Generally, inhalation exposure results in long-term storage of appreciable amounts of beryllium in lung tissue, particularly in pulmonary lymph nodes. The more soluble compounds are also translocated to the liver, abdominal lymph nodes, spleen, heart muscle, kidney, and skin. Persons with impaired pulmonary function, airway diseases, or conditions such as asthma, emphysema, chronic bronchitis, and so on may incur further impairment if beryllium particulates are inhaled. Other existing diseases (nervous, blood, kidney, etc.) may also be adversely affected from exposure to beryllium [U.S. Department of Energy 1999]. The biological half-life of beryllium in humans was calculated to be 180, 120, 270, 540, and 450 days in the total

body, kidneys, liver, spleen, and bone, respectively [World Health Organization 1990]. Beryllium may also impair some vascular endothelial (layers of cells lining the blood vessels) functions and alter the interaction between platelet and endothelial mediators (the transfer medium between the blood platelets and the endothelia) [LLNL 2002].

Controversy has existed as to whether CBD can be induced only by inhalation or whether exposure through other pathways (dermal or oral) are possible [Deubner et al. 2001]. Most of the literature on the subject indicates that ingestion and dermal uptake are unimportant routes of exposure. However, with beryllium contamination of the hands and work clothes, it is suggested that hand-to-face activity may contribute to the total inhalation of beryllium.

Following oral ingestion of beryllium, less than 1% of the dose is generally absorbed into the blood and finally stored in the skeleton, with small amounts also found in the gastrointestinal tract and liver. A considerable amount of the absorbed beryllium is rapidly eliminated, mainly in the urine and, to a small extent, in the feces. Most of the orally ingested beryllium passes through the gastrointestinal tract unabsorbed and is eliminated in the feces [World Health Organization 1990]. Part of the inhaled beryllium is also eliminated in the feces. The skeleton and lungs have a long beryllium storage period, with the half-life for the skeleton calculated (as stated previously) as 450 days [World Health Organization 1990].

Swallowing of beryllium has not been reported to cause effects in humans, because very little beryllium can move from the stomach and intestines into the bloodstream. Furthermore, from a toxicological viewpoint, the ingestion of beryllium is thought to be of minor importance [World Health Organization 1990]. Also, ingested beryllium is not believed to cause either sensitization or CBD [Sawyer et al. 2002].

Absorption of beryllium by the gastrointestinal tract is assumed to be less than 1%. Animal research indicated that systemic beryllium toxicity is limited. Oral ingestion of beryllium sulfate in rats over two years showed no effects on their cardiovascular system, lungs, eyes, skin, liver, or gastrointestinal tract [Deubner et al. 2001].

Contact dermatitis is the most common beryllium-related toxic effect. Exposure to soluble beryllium compounds may result in inflammation and papulovesicular lesions on the skin, which is a delayed type of a hypersensitivity reaction that is cell-mediated. If contact is made with an insoluble beryllium compound, an achronic granulomatous lesion develops, which may be necrotizing or ulcerative. If an insoluble beryllium-containing material becomes embedded under the skin, and not removed, the lesion will not heal and may progress in severity [Goyer and Clarkson 2001]. Absorption of beryllium into the blood through the skin is negligible, because beryllium will be bound by epidermal (the outermost layer of the skin) constituents [World Health Organization 1990]. A very small number of CBD cases have resulted from skin implantation [LLNL 2004].

A beryllium-induced lymphocyte proliferation blood test (BeLPT), which is highly specific for beryllium sensitivity, has a high predictive value for beryllium disease. (Lung T-cell lymphocytes, which are taken from a peripheral lung venous-blood sample or lung lavage cells, are cultured in a medium containing the DNA precursor, thymidine, which has been labeled with tritium, the radioactive isotope of hydrogen. The cell uptake of the radioactivated thymidine reflects the degree of immune-response-driven proliferation of T-cells when stimulated by exposure to three different concentrations of a beryllium-salt solution [Stange et al. 2004, Frome et al. 2003]. An increase in the rate of cell division and proliferation with increased beryllium concentrations is indicative of beryllium sensitization. The results are indicated by the ratio of beta counts of the stimulated cells divided by the counts of the unstimulated cells for the same degree, or period, of culture. In the absence of sensitization, the rate of division and proliferation is not affected by the salt solution. The test would be repeated to confirm the results [U.S. Department of Energy 1999, 2002]. BeLPT has been described as an in-vitro measure of beryllium antigen-specific, cell-mediated immune response [Stange et al. 2004]. An antigen is a substance, usually a protein, that stimulates the production of an antibody.) In severe cases, the affected person may be permanently disabled, and it could lead to their death. By contrast, people who are only sensitized to beryllium are asymptomatic, and, although not physically impaired, they could be more susceptible to CBD on subsequent exposures to beryllium [U.S. Department of Energy 1999]. Both false-positive and false-negative test results can occur. If the first test is positive, a second test is performed. If the second test is negative, a third test may be offered. If the first test is negative, subsequent yearly tests are

offered as part of routine monitoring [U.S. Department of Energy 2002]. With two confirmed BeLPTs, follow-up pulmonary tests are performed at LLNL to determine the possibility of having CBD [Trichopoulos 2005]. Evidence of any lung damage should also be determined. Although the BeLPT may be positive, there is a latent period that can vary between several weeks and as many as 20 [World Health Organization 1990] or even 40 years [Herr 1997] before manifestation of the disease.

The BeLPT was first used in the 1980s as a clinical diagnostic tool and subsequently further developed in the late 1980s as currently used. It is the best diagnostic tool for examining large populations. Studies have been performed involving extensive statistical evaluations of the test [Stange et al. 2004, Frome et al. 2003].

Although beryllium was shown to produce cancerous tumors in some animals and some indications of a slight increased chance in humans, there is some controversy as to whether it should be considered as a carcinogen relative to humans [Fields 2001, Sawyer et al. 2002, Herr 1997, Goyer and Clarkson 2001, Trichopoulos 2005, Sanderson et al. 2001]. A significant problem in the analyses is isolating the contributions of other potential sources of cancer, such as smoking, alcohol, and so on. Unlike CBD, which can surface in some cases just months after exposure, lung cancer rarely developed earlier than twelve years after exposure to beryllium, and often took longer [Fields 2001]. The International Agency for Research on Cancer, which lists beryllium as a known human carcinogen, noted that the work environment of workers involved in the refining, producing, and machining of beryllium metal was associated with an increased risk of cancer [Brush Wellman 2002]. Persons identified as having ABD were statistically more likely to develop lung cancer [World Health Organization 1990].

In an attempt to determine the association of lung cancer with CBD, a study was initiated in 1992 for 3569 male employees who worked at a beryllium processing facility located in Reading, PA, from January 1, 1940, to December 31, 1969, with disease and work history follow-up status through December 31, 1992 [Sanderson et al. 2001]. Eliminating confounding of smoking was addressed, but information on only 10% of the workers was available. The study found that individuals who had developed lung cancer had experienced higher cumulative, average, and maximum exposures at 10 and 20 years before death than had controls of the same age. Lagged-data analyses showed significant positive-exposure response trends, while unlagged analyses did not. This result assumes having a latency period (10 or 20 years) before detecting the cancer (as found with other occupational lung cancers), discounting exposures during these periods. Because tenure tended to be relatively short for workers in the early 1940s, the study primarily addressed short-term, relatively high beryllium exposures. To reduce confounding by smoking, the study was mostly limited to the nonprofessionals, since they had much higher beryllium exposures than did the professionals. Although they smoked more than the professionals smoked, the association between lung cancer and beryllium exposure remained the same for both groups.

There is no known treatment for curing beryllium disease, although the symptoms of the disease can be reduced by treatments such as medications to suppress the inflammatory and immune response to beryllium. Corticosteroids, such as prednisone, are the most commonly used medications for this purpose. Side effects occur that include the susceptibility to infections and their slower healing, fluid and salt retention, an increase in blood cholesterol, and loss of bone density [U.S. Department of Energy 2002]. Individuals with insufficient levels of oxygen in their blood as a result of CBD may also need supplemental oxygen to prevent damage to their organs due to lack of oxygen [U.S. Department of Energy 2002]. Generally, persons who are sensitized to beryllium or who have CBD should terminate any possible contact with beryllium [Brush Wellman 2002]. It should be noted that some individuals diagnosed with CBD may never become sick enough to require treatment [U.S. Department of Energy 2002, LLNL 2002].

28.3 Some Statistical Observations

To evaluate the beryllium-exposure risk, tens of thousands of air samples have been taken at LLNL since 1960. The concentrations were typically well below the action level of 0.2 $\mu g/m^3$. In the 1960s and 1970s, occasional samples were above this level. From the time that medical monitoring of beryllium workers was initiated at LLNL in 1967, sensitization was identified in three individuals, one of whom was diagnosed with CBD. In addition, one LLNL retiree was

diagnosed with CBD [LLNL 2002]. With the much-improved engineering controls and practices currently employed, it is now unlikely that anyone working in beryllium operations at LLNL would be exposed to concentrations sufficiently high enough in beryllium to cause CBD [LLNL 2002].

In a 2002 DOE document, an estimate was given that 20,000 individuals may have been exposed to beryllium in DOE facilities. Of the 15,327 workers and former workers who had been screened by April 2001, 483 had tested positive. Of these workers, 156 were diagnosed either definitely with CBD or showed symptoms of CBD [U.S. Department of Energy 2002].

Studies have shown that inhalation of even small amounts of particles small enough to have been breathed deeply into the lungs has triggered an allergy-like sensitivity in 2 to 5% of individuals so exposed, and 2% of all exposed to beryllium develop CBD. Furthermore, working in occupations such as beryllium machining, where exposure to airborne beryllium was historically greatest, between 8 and 16% of those exposed were diagnosed with CBD [U.S. Department of Energy 2002].

Although CBD is most prevalent for occupations having the greatest exposure to beryllium, the disease does not occur in everyone with high exposure. Furthermore, the disease can develop for some with almost no detectable level of beryllium exposure. There does not appear to be a simple direct dose-response relationship. No correlation has been found between the intensity of exposure and the severity of the disease. This paradox has often been attributed to a genetic predisposition, whereby this allergy-like immune reaction occurs only in a very small portion of the population. This reaction could explain the observation that even under severe exposure conditions, only a few percent of exposed workers were affected [Petzow et al. 2002b]. A study (with a limited number of subjects) indicated that exposure and genetics were at least additive in predicting disease progression [Sawyer et al. 2002]. The relationship and the strength of the relationship between sensitization and CBD are not completely understood. There are unresolved issues regarding defining beryllium sensitization and CBD. It is generally thought, however, that before CBD can develop as a full-blown, symptomatic disease, a person must become sensitized (or develop an allergic reaction) to beryllium. It was suggested that 10% of any newly sensitized group will develop CBD within a year, 10% of the remaining group within the following year, and continuing at the same rate with each subsequent year [Fields 2001]. Chronic beryllium disease has a latent period from several weeks up to more than 20 years; it is of long duration and is progressive in severity [World Health Organization 1990].

The U.S. EPA has estimated the daily beryllium intake from background environmental exposure to be 420 ng for the general population. The EPA also estimated, based on their toxic-chemical-release inventory, that 22,144 kg of beryllium and beryllium compounds were released to the environment in 1996 from nine facilities involved with the production, processing, and use of beryllium and beryllium-containing materials. Of this amount, 97.4% was released to the land, approximately 0.07% to water, and nearly 2.6% to air [U.S. Department of Health and Human Services 2002]. Atmospheric-beryllium concentrations at rural sites in the United States ranged from 0.03 to 0.06 ng of beryllium/mm^3 (1990), with the principal sources being from the combustion of fossil fuels [World Health Organization 1990]. Another source reported that the atmospheric concentration of beryllium in the urban areas of the eastern United States measured 0.3 to 3.0 ng of beryllium/mm^3, with the concentrations in the rural regions measuring one-twelfth of these values [U.S. Department of Health and Human Services 2002]. The average air concentration of beryllium at the LLNL Livermore site is 0.012×10^{-1} ng/m^3. (This value and the following value are inconsistent with the aforementioned values.) At LLNL site 300, it is 0.015×10^{-1} ng/m^3.

Beryllium occurs naturally in rocks and minerals, with concentrations ranging between 0.038 and 11.4 mg/kg. The range of beryllium found in the soil in the Livermore Valley is reported as 0.33 to 1.2 μg/g [LLNL 2001]. An average of 0.6 μg/g was reported for 847 samples of agricultural soil collected throughout the United States to a depth of 20 cm, with samples ranging from less than 1 to 7 μg/g. The U.S. EPA geochemical surveys indicated an average of approximately 6 μg/g. Significantly higher levels of beryllium were found in soils overlying beryllium-containing rocks, for example, up to 300 μg/g at Lost River Valley, AK. Beryllium contents in plants were reported as being generally less than 1 μg/g dry weight [World Health Organization 1990].

The U.S. EPA calculated a total daily consumption of 423 ng of beryllium, coming mostly

Table 28.1 Hypothetical calculated results of workday-beryllium doses: Ingestion versus inhalation

	Ingestion, μg/workday					
	Hand-to-mouth	Tracheobronchial-mucociliary-aided ingestion	Head airways ingestion	Total dose via ingestion	Alternative ingestion scenario(a)	Inhalation, μg/workday
Lower limit	0.0330	0.0003	0.0032	0.0365	10	0.116
Maximum value	4.02	0.0041	0.0865	4.11	20	1.63

(a) The alternative ingestion values were calculated using the following inputs: 10 mg dust transferred from hand to mouth per event; beryllium constitutes 10% of workplace dust (professional judgment); two events per day (professional judgment); 0.5 to 1% gastrointestinal absorption per day (Agency for Toxic Substances and Disease Registry). Source: Deubner et al. 2001

from food (120 ng/d) and water (300 ng/d), with negligible amounts from air and dust [World Health Organization 1990]. Tobacco smoking, with a reported concentration of beryllium in the smoke of up to 0.074 μg/cigarette, was suggested as a probable major source of beryllium intake in the general population [World Health Organization 1990]. The mean urinary level of beryllium in the general population was reported as 0.26 μg/L [LLNL 2001], and levels of up to 2 μg/g were reported for smokers [World Health Organization 1990]. OSHA reported that approximately 25,000 U.S. workers have been exposed to beryllium (cited in Hazardous Substance Data Bank) [U.S. Department of Health and Human Services 2002].

Chronic beryllium disease has been identified in workers whose average exposure levels were between 0.02 and 0.10 $\mu g/m^3$, levels that are 20 to 100 times lower than the permissible level [Infante and Newman 2004]. These exposure levels are still below the proposed new allowable levels of 0.2 μg/g. In modern plants complying with the 2 μg permissible-exposure limit, prevalence of CBD ranged from 2 to 15%, depending on the job being surveyed. Based on the 2% number, it was estimated that between 4,000 and 16,000 undiagnosed cases of CBD existed in the United States. Also, between 46 and 100% of surveillance-identified workers with an abnormal BeLPT result already may have had CBD at the time of the initial assessment [Infante and Newman 2004].

An evaluation was made as to whether the total exposure to beryllium was important in developing CBD [Deubner et al. 2001]. Although specific data on beryllium loading to the skin and work clothes and by ingestion are unavailable, calculations based on reasonable assumptions suggested significant exposure could occur through pathways other than by inhalation. Furthermore, the authors conclude that their calculations suggest that exposure from alternative pathways may contribute to beryllium exposures that are as much as 2 orders of magnitude higher than exposure from direct inhalation of workplace air. For example, the absorption of beryllium into systemic circulation that may occur from dermal exposure through a large area of damaged skin could be significant compared to inhalation exposure. It is suggested, however, that more important than its contribution to the total dose is the immunological sensitization reaction that could be induced by the dermal exposure, because this sensitization may cause an inflammatory response to even minute levels of beryllium deposited in the lungs. The question arises as to whether there is a dermal threshold exposure for beryllium sensitization and the relative effect of contamination by insoluble versus soluble forms of beryllium. Also, a question that needs to be addressed is the relative importance of the total area contaminated versus the concentration (μg/area). Studies on other metals showed that diseases from these other metals can be induced through both oral and dermal contamination [Deubner et al. 2001].

Table 28.2 Hypothetical calculated results of workday-beryllium doses: Dermal versus inhalation

	Dermal, μg/workday		Inhalation, μg/workday
	Undamaged skin	Damaged skin	
Lower limit	0.0036	0.0318	0.116
Maximum value	1.68	5.36	1.63

Source: Deubner et al. 2001

The results of hypothetical calculations of the intake of beryllium over a workday for ingestion versus inhalation and dermal versus inhalation are reproduced as Tables 28.1 and 28.2, respectively. The inhalation levels correspond to those measured at Brush Wellman (Elmore, OH). Detailed assumptions incorporated into the calculations are presented in the publication by Deubner et al. [2001]. Inhalation following resuspension of beryllium-containing particulates from contaminated surfaces would contribute to the total inhalation exposures to beryllium in the workplace. Lapel gross samplers were shown to produce consistently higher estimates than those

obtained by 1-day TWA air samples. Resuspension of dust from clothing was believed to be the main cause for the discrepancy. Some findings showed that the highest air concentration of beryllium was obtained in the changing and laundry areas [Deubner et al. 2001]. The resuspension from clothing may also result in exposure to others who otherwise have negligible exposure (meeting room, lunchroom, offsite, etc.). Hypothetical calculated results comparing estimated doses from resuspension and inhalation are shown in Table 28.3. The values given suggest that resuspension can contribute a nontrivial amount of the total exposure, and, in fact, in certain circumstances it may contribute a major portion of the exposure [Deubner et al. 2001].

28.4 Contamination Sources

Exposure to beryllium can occur by inhalation, ingestion, and skin contact. Activities that may lead to beryllium exposure in working with beryllium include melting, casting, dross handling, pickling, chemical treatment, heat treating, abrasive cutting, welding, grinding, sanding, polishing, milling, crushing, and, in general, any type of activity that may generate particulates/powders. Exposure can also occur when repairing or maintaining beryllium-contaminated equipment, during housekeeping of work areas, and in the decontamination and decommissioning of beryllium facilities. Persons have been exposed to beryllium, often unknowingly, in the recycling of scrap from electronics, computers, and certain beryllium-containing alloys.

Beryllium contamination can occur from operations involving materials ranging from very high (approximately 95 to 100 wt% Be) to quite low beryllium contents. (Small quantities of beryllium may be added to copper, aluminum, nickel, zinc, and zirconium for various purposes. The most widely used of these materials are the copper-base Berylco alloys, which contain between 0.4 and 2.0 wt% Be and are used for numerous applications [U.S. Department of Energy 2002].) These materials include metals, ceramics, glasses, and soluble salts. Some soluble beryllium salts that are used in nuclear reactors, in glass manufacturing, and as catalysts for certain chemical reactions are sulfates, chlorides, and fluorides. Occupational exposure to beryllium occurs in nuclear-related activities; in aerospace, automotive, electronics, ceramic, and telecommunication industries; in the manufacturing of some sporting equipment (e.g., golf and bicycles); in the medical and dental fields; in machine-shop operations; and in the production of beryllium and beryllium-containing alloys and the manufacturing of their products [Infante and Newman 2004].

Table 28.3 Hypothetical calculated results of workday-beryllium doses: Resuspension from clothing versus inhalation

	Resuspension from clothing, μg/workday	Inhalation, μg/workday
Lower limit	0.0926	0.116
Maximum value	0.461	1.63

Source: Deubner et al. 2001

Generally, beryllium and beryllium-containing products are harmless if not damaged (e.g., scratched, scored, sawed, crushed) so as to produce airborne beryllium-containing particles or fumes. Contact with water-soluble beryllium salts, however, may cause an inflammatory reaction of the skin. A comprehensive experimental study on the hazards and precautions taken associated with fabricating (machining, welding, and brazing) of beryllium-copper alloys was reported by Senn [1977].

Particulates deposited on hands, gloves, and clothing can be transferred to the breathing zone by normal hand-to-face motions and by coughing and sneezing, and then inhaled. Ingestion of beryllium from contaminated hands and clothes can similarly be affected during eating, drinking, smoking, nail biting, and so on. Eyes can be affected by contact with contaminated hands as well as by airborne particulates, leading to irritation or damage of the eyes [Brush Wellman 2002].

The diagnosis of CBD in an employee at the North Las Vegas facility was attributed to beryllium contamination inadvertently introduced from an outside source. The employee was not a beryllium worker, and there was no reason to believe that he had otherwise been exposed to beryllium. There were other similar cases at that facility of workers being diagnosed with beryllium sensitization. The beryllium may have been introduced by contaminated vehicles, documents, personal items, and/or clothing coming from sites having had beryllium exposure [U.S. Department of Energy 2003]. A study on inadvertent beryllium contamination by workers showed that many workers leaving beryllium sites had beryllium particles on their hands, and of these workers, the machine-shop operators had the largest amount [U.S. Department of Energy 2002].

The concentration of airborne beryllium particulates should be monitored in the person's breathing zone and workplace (environment). If airborne-particulate concentrations exceed accepted limits, approved and fitted respirators must be used. Sampling surfaces by swiping should also be done. Gloves should be used when handling materials having sharp edges, rough surfaces, and/or surfaces covered with particulates, preferably gloves that are resistant to being pierced and cut. Eye shielding (safety glasses, face shield, welder's helmet) that is appropriate for the job should be used. Protective overgarments or work clothes should be worn if there is any danger of clothing being contaminated by particulates, and such clothes should be managed to prevent them from contaminating other clothes or persons.

Possible sources of exposure to beryllium and beryllium oxide (BeO) are listed in Tables 28.4 and 28.5, respectively [Brush Wellman 2005a,b]. (BeO (solid) is used as a ceramic for a number of

Table 28.4 Possible beryllium-exposure sources when working with beryllium metal products

Low inhalation-concern operations(a)	Likely inhalation-hazard operations(b)		
Anodizing	Atomizing	Dross handling	Powder handling
Assembly	Abrasive blasting	Electrical discharge	Pressing
Handling	Abrasive processing	machining (EDM)	Rolling
Hand solvent cleaning	Attritioning	Electrochemical	Sanding
Inspection	Bonding	machining (ECM)	Sawing
Painting	Brazing	Extruding	Sintering
Plating	Brushing	Filing	Sizing
	Buffing	Grinding	Slitting
	Casting	Heat treating	Sputtering
	Chemical etching	High-speed machining	Tapping
	Cold isostatic pressing	Honing	Turning
	Coolant management	Hot isostatic pressing	Vapor deposition
	Crushing	Lapping	Welding
	Cutting	Laser cuting	Ventilation maintenance
	Destructive test	Melting	
	Drawing	Mixing	
	Drilling	Polishing	

(a) Operations in this category represent operations that typically release nonrespirable (>10 μm) particles, are not expected to generate significant ultraline particulate, and/or are not expected to result in exposures in excess of the Occupational Safety and Health Administration (OSHA) permissible-exposure limit (PEL). (b) Operations in this category represent those operations that may release respirable (<10 μm) particles, may generate ultraline particulate, may generate beryllium oxide, and/or may result in exposures in excess of the OSHA PEL. Note: This list is not all-inclusive, and variation can exist within specific processes. Determine, then verify, the adequacy of engineering and work practice controls by conducting an exposure characterization of all beryllium processing operations. Effective ventilation, work practices, and personal protective equipment use can control a likely inhalation hazard. When evaluating operations, consideration must be given to potential exposures from activities in support of these operations, such as setup, preparation, cleanup, and maintenance. Source: Brush Wellman 2005a

Table 28.5 Possible beryllium-oxide-exposure sources when working with beryllium oxide products

Low inhalation-concern operations(a)	Likely inhalation-hazard operations(b)		
Assembly	Abrasive blasting	Extruding	Sanding
Handling	Abrasive processing	Firing	Sand blasting
Inspection	Brazing	Grinding	Sawing
Metallizing	Breaking	Honing	Sectioning
Painting	Brushing	Lapping	Sintering
Plating	Buffing	Laser cutting	Sizing
Soldering	Coolant management	Laser machining	Slitting
Ultrasonic cleaning	Chemical etching	Laser scribing	Spray drying
Unfired tape	Crushing	Machining	Tumbling
	Cutting	Milling	Turning
	Deburring (grinding)	Mixing	Ventilation maintenance
	Destructive festing	Polishing	
	Dicing	Powder handling	
	Drilling	Pressing	

(a) Operations in this category represent operations that typically release nonresplrable (>10 μm) particles, are not expected to generate significant ultraline particulate, and/or are not expected to result in exposures in excess of the Occupational Safety and Health Administration (OSHA) Permissible-exposure limit (PEL). (b) Operations in this category represent those operations that may release respirable (<10 μm) particles, may generate ultraline particulate, may generate beryllium oxide, and/or may result in exposures in excess of the OSHA PEL. Note: This list is not all-inclusive, and variation can exist within specific processes. Determine, then verify, the adequacy of engineering and work practice controls by conducting an exposure characterization of all beryllium processing operations. Effective ventilation, work practices, and personal protective equipment use can control a likely inhalation hazard. When evaluating operations, consideration must be given to potential exposures from activities in support of these operations, such as setup, preparation, cleanup, and maintenance. Source: Brush Wellman 2005b

applications, including electrical and electronics. It is present as a dispersion in metallic beryllium. The oxides originate from the surface oxidation of the powders that are used in the production of the metal billets.) Although finished products of both the beryllium metal and its oxide in their solid forms are claimed to not present any special health risks, they do present a health risk if improperly handled. The BeO powder as dispersed in a properly handled solid-beryllium-finished product also does not present any health risk. In all the operations listed in the tables, proper precautions must be taken to minimize the danger of the person being contaminated. The degree of the hazard will depend on the form of the beryllium and how it is processed and handled. Proper (approved) ventilation and exhaust systems [Brush Wellman 2005c], protective clothing and respirators (if necessary) and means for their decontamination, proper handling and cleaning of work tools, and proper housekeeping of equipment and associated support systems to prevent excessive buildup of beryllium-containing materials must be available. High-vacuum, with a high-efficiency particulate air vacuum cleaner, and wet-cleaning methods should be used for removal of particulates from surfaces. (The air filter should be capable of trapping and retaining at least 99.97 wt% of dispersed particles of 0.03 μm diameter [Sanderson et al. 2001].) Approved methods of handling the hazardous waste and recyclable material (scrap, chips, powder) must be used. Work practices and control measures for particle-producing operations involving beryllium-containing materials are detailed by Brush Wellman [Brush Wellman 2005a,b].

Some beryllium-monitored data obtained at LLNL for an 8 h TWA are [LLNL 2001]:

- Machining beryllium metal: <0.0083 to 0.23 $\mu g/m^3$
- Milling high-fired BeO: <0.08 to <0.1 $\mu g/m^3$
- BeO parts cleaning: <0.05 $\mu g/m^3$
- Laser welding beryllium metal: <0.035 $\mu g/m^3$

In 1987, the EPA reported that the release of beryllium to the environment largely results from coal combustion. The combustion of oil and especially coal contributes approximately five times the amount of beryllium pollution caused by industrial production. The major industrial processes that release beryllium into the environment are beryllium extraction plants, ceramic plants, and manufacturers of beryllium and its alloys. Tobacco smoking is suggested as also being a likely important source for beryllium exposure. Copper-base alloys containing up to 4 wt% Be are used for a wide range of industrial applications. Aluminum and nickel-base alloys containing beryllium have also been developed. The Ni-Cr-Be alloys, as alternatives to the more expensive prosthetic gold alloys, are used as crowns and bridges. The beryllium improves castability of the alloys and their adhesion to the dental porcelain. Beryllium has also been found in the cements used to fix dental crowns and bridges [World Health Organization 1990]. After testing samples ($1\ cm^2 \times 0.1$ cm thick) of these alloys in 5 mL of human saliva for 120 days at 37 °C, the concentration of beryllium was between 0.3 and 3.48 μg/mL of saliva at pH 6 and between 12.4 and 43 μg/mL at pH 2, depending on the alloy composition. The normal pH of human saliva is between 5.8 and 7.1 [World Health Organization 1990].

Work-exposure standards recommended for approval by the Environmental, Safety, and Health Working Group and applicable to LLNL are shown in Table 28.6 (December 2004) [LLNL 2004]. The concentration limit of 0.002 $\mu g/cm^2$ referred to in footnote "d" in the table also applies to the decontamination of equipment prior to its release for use in a beryllium-free area. This limit also applies to the surface contamination limit where the equipment was located. In addition, the maximum permissible beryllium concentration in air was established by the EPA (for the general public) as 0.01 $\mu g/m^3$ averaged over a 30 day period, and the maximum beryllium level in drinking water was to be 4 μg/L.

28.5 First-Aid Procedures and Precautions

The entry routes for the beryllium-containing materials are through breathing, skin contact, skin wounds, mucous membranes, and swallowing. First-aid procedures/precautions for specific contaminated regions are [Brush Wellman 2002]:

- Inhalation of particulates that results in breathing difficulty requires immediate removal to fresh air. If breathing has stopped, artificial respiration should be performed, and emergency medical help must be obtained.
- Ingestion of beryllium-containing material must be immediately addressed by induced

Table 28.6 Occupational exposure, housekeeping, and release standards

Standard	Limit	Source
Personnel-exposure		
Action level (8 h, time-weighted average concentration)	0.2 μg Be/m^3(a)	10 CFR 850.23
Permissible-exposure limit (PEL) (8 h, time-weighted average concentration)	2 μg Be/m^3(a)	10 CFR 850.22, 29 CFR 1910.1000
PEL (acceptable ceiling concentration)	5 μg Be/m^3(b)	29 CFR 1910.1000
PEL (peak above acceptable ceiling)	25 μg Be/m^3, for no more than 30 min(b)	29 CFR 1910.1000
Surface contamination		
Housekeeping		
Maximum removable surface contamination for beryllium work areas	3 μg Be/100 cm^2(c,d)	10 CFR 850.30
Release criteria		
Maximum removable surface contamination for release to nonberyllium work area	0.2 μg Be/100 cm^2(d,e)	10 CFR 850.31

(a) Measured without regard to the use of respiratory protection. (b) For soluble compounds not subject to 10 CFR 850. (c) At the end of operational periods. (d) These are the units prescribed in 10 CFR 850; when expressed in the units typically used in analytical laboratory reports, these values are 0.03 μg Be/cm^2 and 0.002 μg Be/cm^2, respectively. (e) When there are visible accumulations of dust on accessible surfaces (for example, if a piece of equipment has been stored outdoors for an extended period of time), the release criteria are based on a bulk sample of the dust, and the applicable standard is the concentration of beryllium in the soil at the point of release (i.e., micrograms of beryllium per gram of soil, or μg Be/g). Source: LLNL 2004, Code of Federal Regulations

vomiting, as directed by medical personnel. Note that an unconscious person should never be given anything by mouth.

- Skin cuts or wounds must be thoroughly washed as soon as possible to remove all beryllium-containing material. After cleaning, the affected areas must be disinfected and covered. If cuts/wounds cannot be thoroughly cleaned or if irritation persists, medical help must be obtained. Any material implanted or lodged under the skin must be removed.
- Eyes must be immediately flushed with plenty of water for at least 15 min, lifting both lower and upper eyelids occasionally. Medical attention must be obtained immediately.
- Spills of beryllium powder should be taken care of as follows: Evacuate and isolate the area. Move upwind. Wear a respirator equipped with a high-efficiency dust filter. If practical, wet down the spill and cover with sand, a tarpaulin, or some other suitable material. Contact the hazardous materials response team.

28.6 Protective and Preventive Actions

A program exists at LLNL to ensure employee safety and minimize (control) beryllium exposure to all employees, consistent with federal agencies' requirements [LLNL 2004]. There are three main focuses: engineering controls, administrative controls, and personal protective equipment. There is also a CBD prevention program. The engineering controls program is designed to physically prevent any beryllium particles from entering the atmosphere. Some preventive examples are:

- Enclose all beryllium work
- Employ exhaust hoods and high-efficiency particulate air (HEPA) filters
- Capture beryllium dust at the machine-tool interface
- Employ wet-machining techniques and sticky coolants
- Perform wet grinding in a ventilated negative-pressure enclosure
- Prevent allowing beryllium particles that can be airborne, and were left from drying liquids, to remain on surfaces

The administrative controls program is concerned with minimizing exposure. Some control examples are:

- Post signs where beryllium is used
- Place warning labels on containers of beryllium and beryllium compounds and on items (clothing, papers, scrap, waste, miscellaneous debris, etc.) contaminated with beryllium
- Clean active beryllium areas every 24 h using wet wipes, wet floor mops, and vacuums with HEPA filters
- Treat beryllium clean-up material as contaminated hazardous waste
- Train workers

The personal protective equipment program is aimed at protecting an individual from the harmful effects of beryllium. Protective clothing

and equipment are required where airborne levels of beryllium are at or above the level where preventive action must be taken or where surface contamination is at or above 3 μg/100 cm^2. All protective clothing and equipment should be clean, available each day, and put on before beginning work. Protective items must be properly fitted, otherwise they may not provide adequate protection. Disposable clothing and equipment must be disposed of as hazardous waste. Some equipment examples are:

- Respirators
- Gloves
- Laboratory coats
- Safety glasses
- Hardhats and other headgear
- Safety shoes, shoe covers, or booties
- Hearing protectors
- Coveralls or laboratory coats

Respiratory protection must be used in unknown work-area exposures that have a potential for airborne exposure. The protection must be maintained until an appropriate evaluation of the condition is performed. Table 28.7 lists the type of respirator required for different exposures [LLNL 2004].

The DOE mandates that all DOE and DOE-contractor sites with beryllium activities institute a CBDPP that is consistent with the beryllium rule 10 Code of Federal Regulations (CFR) 850. The LLNL maintains a website for CBDPP, which contains current information on the following:

- Facts about beryllium
- Beryllium controls employed at LLNL
- A beryllium occupation exposure survey
- Frequently asked questions
- Other useful websites

The objective of 10 CFR 850 is to strengthen the program protecting workers from beryllium hazards at DOE sites. The requirements imposed by the CFR include:

- Limit access to beryllium locations and operations
- Prevent beryllium release and capture particles before they can be inhaled
- Conduct medical surveillance of exposed and potentially exposed workers
- Monitor the effectiveness of the new programs in preventing CBD

The various practices, procedures, preventions, and/or facilities at LLNL pertaining to protective clothing, hygiene, exposure monitoring, housekeeping, waste disposal, and criteria for release of equipment are summarized in the LLNL chronic beryllium disease prevention program document [Fulton 2005]. References to the regulations in the CFR for each of these activities, as well as of other pertinent agencies, are cited in that document.

Numerous methods were reported for analyzing beryllium concentrations in air samples and in biological samples; an extensive list of applications for beryllium as a metal, in alloys, and as an oxide is also presented [World Health Organization 1990].

Actions for reducing the risk of developing CBD are documented by the Beryllium Health Risk Communication Task Force (U.S. Department of Energy 2002). Some of these actions that can be done on the job to reduce the risk are:

- Read/consult the material safety data sheets on beryllium
- Wear the protective equipment required for the work area and operation
- Follow safe work practices
- Follow established work procedure
- Follow the site's procedure for disposing of beryllium-containing materials, scraps, dust, and other wastes according to DOE, EPA, and state requirements
- In maintenance, clean every item before removing it from a beryllium work area
- Be aware of exposure-monitoring results for the work area
- Inform the site medical department if any signs of CBD develop

Table 28.7 Required respiratory protection

Exposure(a)	Required respirator
<0.2 μg Be/m^3	None
<2.0 μg Be/m^3 (<10 × AL)	Half-mask, negative-pressure respirator with P100 filter
<10 μg Be/m^3 (<50 × AL)	Full-face, negative-pressure respirator with P100 filter or half-mask PAPR(b) with P100 filter
<20 μg Be/m^3 (<100 × AL)	Full-face PAPR with P100 filter
<200 μg Be/m^3 (<1000 × AL)	Supplied-air, full-face respirator operated in pressure-demand mode
>200 μg Be/m^3, unknown concentration, or firefighting	Full-face self-contained breathing apparatus in positive-pressure mode

(a) "Exposure" means measured exposure or potential for exposure at the indicated level. AL, action level. The level of air borne concentration of beryllium established persuant to 10 CFR 850.23 that, if met or exceeded, requires the implementation of worker-protection provisions specified in that code. (b) Powered, air-purifying respirator. Source: LLNL 2004

- Get regular medical examinations
- Be aware of the right to a safe work area
- Follow established personal hygiene practices
- Wash hands thoroughly after working with beryllium and before bringing them near to or touching the face
- In showering, wash the whole body thoroughly to prevent taking beryllium particles outside of the work area
- Do not bring any contaminated clothing near the face
- Remove protective clothing and equipment before entering clean areas or leaving the facility
- Do not wear jewelry while working with beryllium. Beryllium particles entrapped in the jewelry could be carried home
- Do not eat, drink, smoke, or apply any cosmetics in work areas

Medical monitoring and surveillance at a DOE facility must include the following:

- Keep an updated roster of workers at risk for CBD
- Collect work histories and medical histories
- Provide each worker examined with test results, an explanation of the findings, and a medical opinion on the need for more testing
- Analyze medical, job, and exposure data to identify other workers at risk for CBD
- Test for beryllium sensitization using the BeLPT
- If two positive BeLPT results are obtained, seek further evaluation tests and monitor for early detection of CBD

28.7 Acronyms

ATSOR	Agency for Toxic Substance and Disease Registry (Atlanta)
ABD	Acute beryllium disease
ACGIH	American Conference of Government Industrial Hygienists
AEC	Atomic Energy Commission
BeLPT	Beryllium-induced lymphocyte proliferation blood test
CBD	Chronic beryllium disease
CBDPP	Chronic beryllium disease prevention program
CFR	Code of Federal Regulations
DHHS	U.S. Department of Health and Human Services
DOE	U.S. Department of Energy
EPA	U.S. Environmental Protection Agency
EHC	Environmental Health Criteria
ES&H	Environmental, Safety, & Health (Working Group)
HEPA	High-efficiency particulate air filter
IARC	International Agency for Research on Cancer
LLNL	Lawrence Livermore National Laboratory
NIOSH	National Institute for Occupational Safety and Health
NNSA	National Nuclear Security Administration
NOPR	Notice of proposed rule making
OEL	Occupational-exposure limit
OSHA	Occupational Safety and Health Administration
PEL	Permissible-exposure limit (for worker protection)
TWA	Time-weighted average

REFERENCES

Brush Wellman, 2002. "Material Safety Data Sheet No. M10," Cleveland, OH

Brush Wellman, 2005a. "Safety Practices for Working with Beryllium Products," Brush Wellman Safety Facts, SF201-Version 1.2, Brush Wellman, OH; http://www.brushwellman.com/EHS/Safety%20Facts/SF201.pdf

Brush Wellman, 2005b. "Safety Practices for Working with Beryllium Oxide Products," Brush Wellman Safety Facts, SF301-Version 1.2, Brush Wellman, OH; http://www.brushwellman.com/EHS/Safety%20Facts/SF301.pdf

Brush Wellman, 2005c. "Ventilation of Operations Generating Beryllium Particulate," Brush Wellman Safety Facts, SF9-Version 1.1, Brush Wellman, OH

Code of Federal Regulations. http://www.gpoaccess.gov/CFR/index.html

Deubner, D.C., Lowney, Y.W., Paustenbach, D.J., and Warmerdam, J., 2001. Contribution of Incidental Exposure Pathways to Total Beryllium Exposures, *Appl. Occup. Environ. Hyg.*, Vol 16 (No. 5), p 568–578

Fields, S., 2001. Toxic Beryllium: New Solutions for a Chronic Problem, *Environ. Health Perspect.*, Vol 109 (No. 2), p A74–A79

Frome, E.L., Newman, L.S., Cragle, D.L., Colyer, S.P., and Wambach, P.F., 2003. Identification of an Abnormal Beryllium Lymphocyte Proliferation Test, *Toxicol.*, Vol 183, p 39–56

Fulton, G.P., 2005. "LLNL Chronic Beryllium Disease Prevention Program (CBDPP) Implementation of 10 CFR 850," UCRL-AR-144636-Rev-2, Lawrence Livermore National Laboratory, Livermore, CA

Goyer, R.A., and Clarkson, T.W., 2001. Toxic Effects of Metals, Chap. 23, *Casarett and Doull's Toxicology—The Basic Science of Poison*, C.D. Klaassen, Ed., McGraw-Hill, New York, NY

Herr, M., 1997. "Defense Program's Beryllium Good Practice Guide," UCRL-ID-127871, Lawrence Livermore National Laboratory, Livermore, CA

Infante, F., and Newman, L.S., 2004. Beryllium Exposure and Chronic Beryllium Disease, *The Lancet*, Vol 363 (No. 9407), p 415–416

Kent, M.S., Robins, T.G., and Madl, A.K., 2001. Is Total Mass or Mass of Alveolar-Deposited Airborne Particles of Beryllium a Better Predictor of the Prevalence of Disease? A Preliminary Study of a Beryllium Processing Facility, *Appl. Occup. Environ. Hyg.*, Vol 16 (No. 5) p 539–558

LLNL, 2001. "Beryllium Worker Training," UCRL-MA-144469-HS 4256, Lawrence Livermore National Laboratory, Livermore, CA

LLNL, 2002. "Beryllium Awareness: Beryllium at LLNL," Lawrence Livermore National Laboratory, Livermore, CA; https://www-training.llnl.gov/training/hc/HS4258/index.html

LLNL, 2004. Implementation of the Chronic Beryllium Disease Prevention Program Requirements, UCRL-MA-133867, Revision 4, *ES&H Manual*, Vol II, Part 14: Chemical, Lawrence Livermore National Laboratory, Livermore, CA

Newman, L.S., Lloyd, J., and Daniloff, E., 1996. The Natural History of Beryllium Sensitization and Chronic Beryllium Disease, *Environ. Health Perspect. Suppl.*, Vol 104 (Supplement 5), p 937–943

Petzow, G., Aldinger, F., Jonsson, S., and Preuss, O., 2002b. Toxicology and Occupational Health, *Ullmann's Encyclopedia of Industrial Chemistry*, 6th ed., Wiley-VCH Verlag Chemie, Weinheim, Germany

Sanderson, W.T., Ward, E.M., Steenland, K., and Peterson, M.R., 2001. Lung Cancer Case—Control Study of Beryllium Workers, *Am. J. Ind. Med.*, Vol 39 (No. 2), p 133–144

Sawyer, R.T., Maier, L.A., Kittle, L.A., and Newman, L.S., 2002. Chronic Beryllium Disease: A Model Interaction Between Innate and Acquired Immunity, *Int. Immunopharm.*, Vol 2 (2–3), p 249–261

Senn, T.J., 1977. "Evaluation of the Hazard Associated with Fabricating Beryllium-Copper Alloys," UCRL-52258, Lawrence Livermore National Laboratory, Livermore, CA

Stange, A.W., Furman, J.F., and Hilmas, D.E., 2004. The Beryllium Lymphocyte Proliferation Test: Relevant Issues in Beryllium Health Surveillance, *Am. J. Ind. Med.*, Vol 46 (No. 5), p 453–462

Trichopoulos, D., 2005. "On the Alleged Human Carcinogenicity of Beryllium," Brush Wellman Safety Facts, SF002-Version 1.2, Brush Wellman, April

U.S. Department of Energy, 1999. "Chronic Beryllium Disease Prevention Program; Final Rule," Federal Register, 10 CFR 850, 64, No. 235, Occupational Health and Safety Association, p 68854–68914

U.S. Department of Energy, 2002. "Communicating Health Risks: Working Safely with Beryllium," Training Reference for Beryllium Workers and Managers/Supervisors, Facilitator Manual, Prepared by the Health Risk Communication Task Force

U.S. Department of Energy, 2003. "Investigation of Beryllium Exposure Cases Discovered at the North Las Vegas Facility of the National Nuclear Security Administration"

U.S. Department of Health and Human Services, 2002. "Carcinogens," 10th Report on Carcinogens

World Health Organization, 1990. "Beryllium Environmental Health Criteria 106 (EHC 106)," International Program on Chemical Safety

Yoshida, T., et al., 1997. *Ind. Health*, July1997

SELECTED REFERENCES

- IARC, 1994. Beryllium, Cadmium, Mercury and Exposures in the Glass Manufacturing Industry, *IARC Monographs on the Evaluation of Carcinogenic Risks to Humans*, Vol 58, International Agency for Research on Cancer, Lyon, France, p 444
- McInerney, J.R., 2003. "Beryllium Health Surveillance," Rocky Flats Environmental Technology Site, Golden, CO
- Meyer, K.C., 1994. Occupational and Environmental Lung Disease: Beryllium and Lung Disease, *Chest*, Vol 106, Sept 1994, p 942–945
- Rossman, M.D., Preuss, O.P., and Powers, M.B., 1991. *Beryllium: Medical and Environmental Aspects*, Williams and Wilkins, Baltimore, MD

Beryllium Chemistry and Processing, p 513-521
By Kenneth A. Walsh
Edited by Edgar E. Vidal, Alfred Goldberg,
Edward N.C. Dalder, David L. Olson, and Brajendra Mishra

CHAPTER 29

Hygienic Practices for Handling Beryllium and Its Components

George Fulton and Alfred Goldberg, Lawrence Livermore National Laboratory
Frank Gibbs and Curtis Salmon, Colorado School of Mines

29.1 Introduction

The use of beryllium is associated with potential health problems in workers exposed to beryllium dust. Operations that produce beryllium particulates, such as machining, grinding, or facility decommissioning, when not managed properly, have been linked to both acute and chronic lung diseases. Proper management of the beryllium hazard includes measures to eliminate exposure through inhalation, ingestion, or puncture. These measures are similar to engineered and administrative controls established for other particulate hazards, such as asbestos or ionizing radiation, and include steps such as ventilation, containment, personnel protective equipment, and personnel practices such as elimination of food and tobacco products from work areas.

29.1.1 Regulatory Requirements

The regulatory requirement for management of the beryllium hazard was initially defined by the Atomic Energy Commission in 1949 and set at a permissible exposure limit (PEL) of 2.0 $\mu g/m^3$ for an 8 h time-weighted average (TWA). The Occupational Safety and Health Administration (OSHA) subsequently adopted this standard in 1971 with the passage of the Occupational Safety and Health Act [Pohanish and Greene 1996]. The American Conference of Governmental Industrial Hygienists recommends a threshold limit value set at 2.0 $\mu g/m^3$ per 8 h TWA, and the National Institute for Occupational Safety and Health recommends a PEL of 0.5 $\mu g/m^3$ per 8 h TWA. A recognized best practice to conservatively control worker exposure is to establish an "action" level at 10% of the PEL (0.2 $\mu g/m^3$); that is, work controls are evaluated when personnel or area sampling exceed 10% of the PEL. In this way, steps can be taken to improve work controls before exposure limits exceed regulatory values.

In 2001, the Department of Energy (DOE) implemented the new Chronic Beryllium Disease Prevention Program (CBDPP) by way of the Code of Federal Regulations 10 CFR Part 850. The Final Rule can be obtained from the DOE website currently listed as http://www.hss.energy.gov/healthsafety/wshp/be/. The CBDPP defines a structured program to integrate worker medical testing, training, engineering controls, and handling practices, with the goal of elimination of worker exposure.

29.2 Implementation of Handling Practices

A useful tool in the implementation of integrated beryllium-handling requirements is a work form, an example of which is given in Fig 29.1. Similar formats are used in the management of radiological particulates, and it provides a mechanism to document the type of work performed,

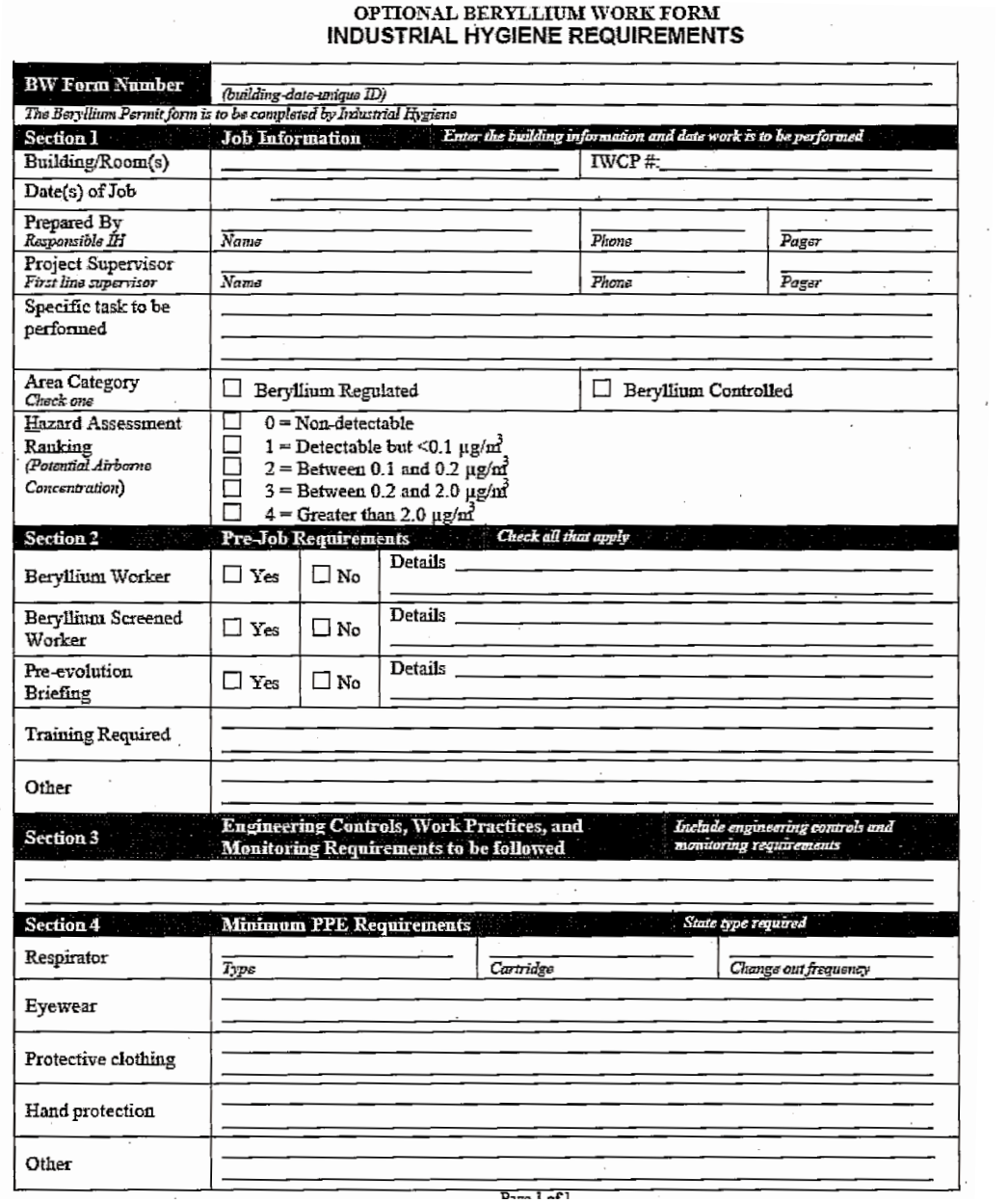

OPTIONAL BERYLLIUM WORK FORM
INDUSTRIAL HYGIENE REQUIREMENTS

BW Form Number	*(building-date-unique ID)*		
The Beryllium Permit form is to be completed by Industrial Hygiene			
Section 1	**Job Information**	*Enter the building information and date work is to be performed*	
Building/Room(s)		IWCP #:	
Date(s) of Job			
Prepared By *Responsible IH*	*Name*	*Phone*	*Pager*
Project Supervisor *First line supervisor*	*Name*	*Phone*	*Pager*
Specific task to be performed			
Area Category *Check one*	☐ Beryllium Regulated	☐ Beryllium Controlled	
Hazard Assessment Ranking *(Potential Airborne Concentration)*	☐ 0 = Non-detectable ☐ 1 = Detectable but <0.1 µg/m³ ☐ 2 = Between 0.1 and 0.2 µg/m³ ☐ 3 = Between 0.2 and 2.0 µg/m³ ☐ 4 = Greater than 2.0 µg/m³		
Section 2	**Pre-Job Requirements**	*Check all that apply*	
Beryllium Worker	☐ Yes ☐ No	Details	
Beryllium Screened Worker	☐ Yes ☐ No	Details	
Pre-evolution Briefing	☐ Yes ☐ No	Details	
Training Required			
Other			
Section 3	**Engineering Controls, Work Practices, and Monitoring Requirements to be followed**	*Include engineering controls and monitoring requirements*	
Section 4	**Minimum PPE Requirements**		*State type required*
Respirator	*Type*	*Cartridge*	*Change out frequency*
Eyewear			
Protective clothing			
Hand protection			
Other			

Page 1 of 1

Fig. 29.1 Industrial hygiene beryllium work form

work environment, training, medical testing, and a permanent record, as required in the regulations.

Similar to radiological protection practices, beryllium areas are defined at various levels based on the potential for exposure to personnel. The level of hazard control and personnel protective equipment is defined accordingly. Table 29.1 provides definitions of each area, the corresponding potential for exposure, and typical hazard controls. Prior to conducting work in any of these areas, workers are required to undergo a medical evaluation, including the beryllium lymphocyte proliferation test. Personnel showing no sensitivity to beryllium and who have undergone training, referred to as beryllium-screened workers, may be allowed access to beryllium areas in the course of their job. Personnel conducting hands-on work, referred to as

Table 29.1 Signage for areas of potential exposure to beryllium dust and typical hazard controls

Classification	Criteria	Example posting	Work controls
Beryllium-regulated area	Airborne or the potential for airborne beryllium contamination at or above 0.2 μg/m^3 as an 8 h time-weighted average (TWA)		Work control procedure including hazard analysis and controls. Respiratory protection and personnel protective equipment (PPE) Personal air monitor Worker entry log
Beryllium-controlled area	Surface contamination at or above 0.2 μg/100 cm^2 and/or reasonably expected to have airborne greater than or equal to 0.1 μg/m^3 but less than 0.2 μg/m^3 in an 8 h TWA	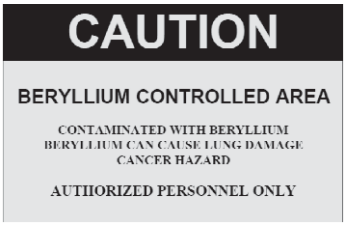	Work control procedure including hazard analysis and controls. Respiratory protection and PPE may be required if airborne potential is greater than 0.1 μg/m^3. Worker entry log
Potential beryllium-contaminated equipment and/or systems	No external Be contamination measured	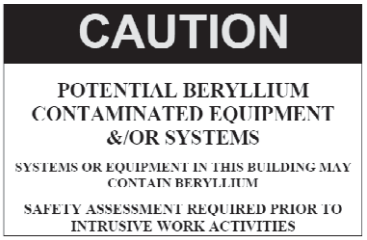	Activity dependent

beryllium workers, undergo additional training to ensure proper work practices that will protect them from exposure.

29.2.1 Hazard Analysis

Work with beryllium requires a detailed hazard analysis beginning with characterization of the hazard, including both surface and air sampling. A common method for surface samples is using paper smears similar to that used in radiological areas. This method is productive in decommissioning activities where both beryllium and radiological data can be collected and analyzed from the same smear samples. Random and biased surface sampling is conducted by taking 100 cm^2 smears (nominally), and beryllium analysis is commonly performed using inductively coupled plasma/atomic emission spectroscopy (ICP/AES). Air sampling is conducted using personal sampling pumps, with filter cassettes placed on the worker's lapel. The filters are analyzed for beryllium using ICP/AES. Figure 29.2 shows a technician conducting a smear sample on a recently used respirator to verify that it is free of beryllium prior to release. Also shown on the table is a color-coded map indicating routine sampling results, for review by beryllium workers prior to conducting work. The analytical analysis program is very important to a robust beryllium program requiring rapid sample result turnaround (~24 h) to maintain an up-to-date understanding of the hazard, provide personnel sampling data to workers, and to quickly identify and characterize the extent of potential upset conditions.

Industrial hygienists typically take a conservative approach when characterizing the beryllium hazard and defining hazard controls. In grinding or decommissioning activities, surface contamination is assumed to become completely airborne when initially defining protective equipment or engineering controls. For example, surface samples shown to be at levels of 5 μg/100 cm^2 will be assumed to produce 5 μg/m^3, and the area would be defined as a beryllium-regulated area. Application of engineered controls, such as the use of fixatives, allows for less conservative assumptions.

Fig. 29.2 Technician taking a smear sample for beryllium analysis from a recently used respirator. Also shown is a characterization survey map of the facility, listing results from routine surveys.

29.2.2 Hazard Controls

Hazard controls are best implemented through detailed procedures, with engineered controls preferentially applied over administrative controls or personnel protective equipment (PPE), which are normally considered a last line of defense. A key engineering control is the use of ventilation, including laboratory hoods, glove boxes, or point-source ventilation. In decommissioning applications, such as application of paints, foams, and fixatives, using some of the technologies developed for asbestos remediation has been shown to be very effective. Contamination control and cleanup are effectively accomplished with wet methods and the use of high-efficiency particulate air filter vacuums.

Personnel protective equipment is an important part of worker protection. In laboratory hood and protective atmosphere box applications, workers' hands must be protected to prevent puncture and exposure through injection. For operations outside fixed containment, PPE typically includes plastic coveralls, rubber booties, full-face respiratory protection (29 CFR 1910.134), and two pairs of protective gloves. Personnel lapel samplers and air pumps are set to monitor worker breathing space in the vicinity but outside of respiratory protection. Separate clothing change areas, laundry facilities, and eating areas are required and monitored routinely.

29.3 Applications

29.3.1 Dismantlement of Process Piping

Effective implementation of beryllium hygiene practices is best illustrated in decommissioning activities, because this type of work poses significant challenges in protecting workers. Figure 29.3 illustrates the use of point-source ventilation and wet methods to drill into beryllium-containing process piping. The PPE includes impervious coveralls sealed at the openings, full-face respiratory protection, and work gloves worn over the top of latex gloves. Figure 29.4 shows a mock-up demonstration of the use of

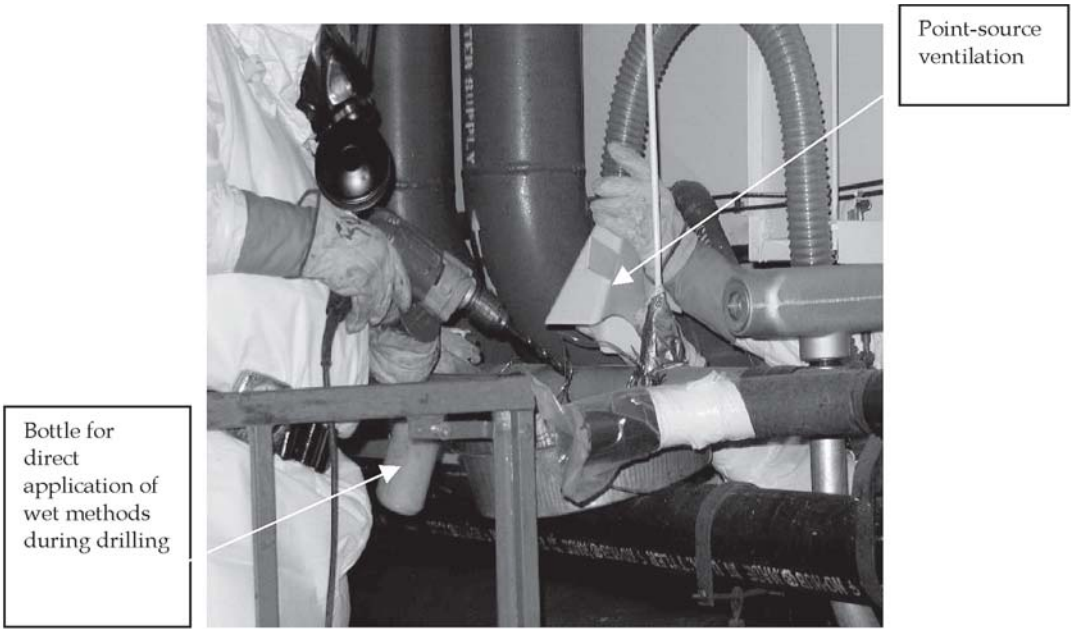

Fig. 29.3 Illustration of the use of wet methods and point-source ventilation to drill into beryllium-containing process piping

foam to contain beryllium contamination prior to cutting. Foam is introduced through a small hole until the pipe is filled in the area to be cut. The foam serves to "fix" the contamination and contain it during the cutting process. When combined with wet methods and the proper use of PPE, this set of controls effectively protects workers.

29.3.2 Decommissioning

Liberal application of fixatives has been demonstrated to contain beryllium contamination during demolition. The fixative shown in Fig. 29.5(a) (colored light green to improve inspection) is used to contain contamination. Fixative was also applied to equipment that has been wrapped in preparation for waste disposal. Figure 29.5(b) illustrates the use of a fixative (colored orange) during facility demolition. Traditionally, contamination is mechanically removed using scabbling and grinding equipment prior to demolition. Aggressive use of fixatives removes workers from the source of the hazard and allows for the use of heavy equipment to accomplish demolition. Air samples taken around this facility during demolition showed no airborne beryllium.

29.3.3 Waste Disposal

Waste handling and packaging poses risks similar to those seen in decommissioning. Extensive use of fixatives and wet methods are equally effective, but elimination of the need to size-reduce waste for the purpose of packaging completely eliminates the hazard. This approach was implemented successfully in the disposal of very large pieces of contaminated manufacturing equipment. Instead of size-reducing the equipment for disposal, a robust poly-urea-based coating was applied to serve as the "waste container" and to protect the equipment during transportation and ultimate disposal. Similar to the demolition example discussed previously, this removed workers from direct contact with the contamination, made the operations significantly safer, and reduced the time and cost for waste disposal. Figures 29.6(a) and (b) show a 100 ton press that was contaminated with uranium and beryllium. It has been coated and prepared for transportation to an appropriate repository. A key element in the success of this approach was in obtaining approval from the waste repository to receive a large, nonstandard waste package.

29.4 References of Regulations

The latest U.S. Code of Federal Regulations (CFR) for the Chronic Beryllium Disease Prevention Program (10 CFR 850) can be

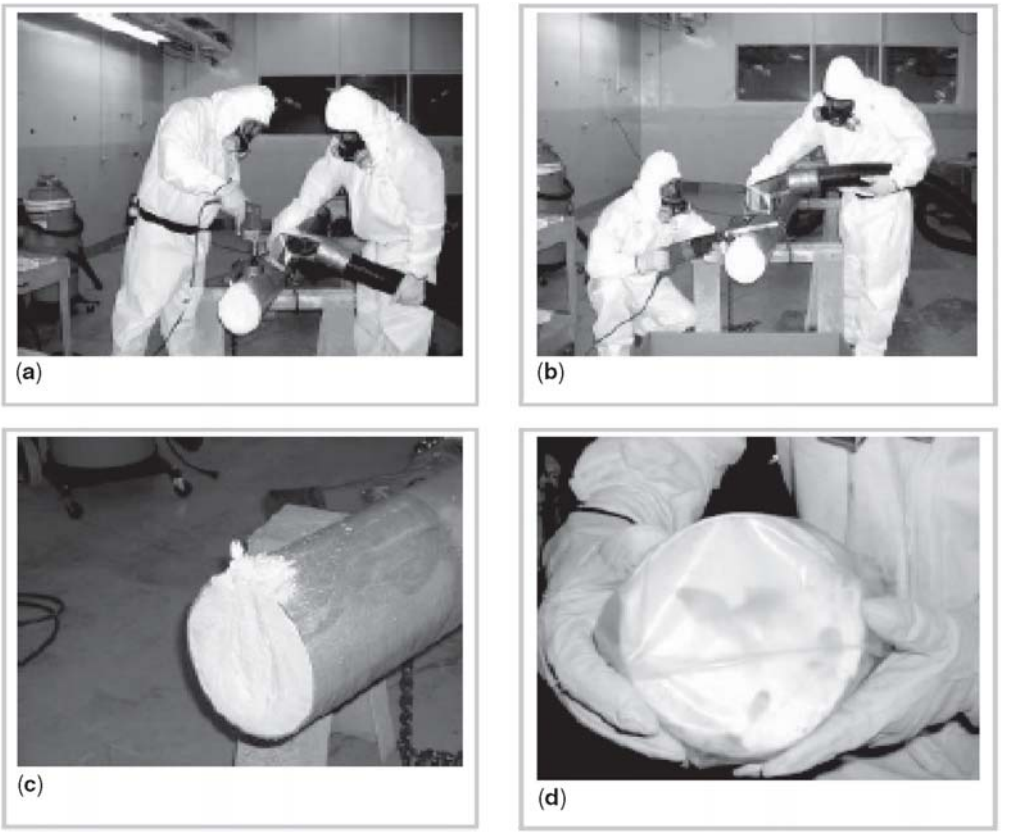

Fig. 29.4 Mock-up demonstration of the use of foam to contain beryllium contamination in process piping prior to cutting. (a) Drilling into duct. (b) Cutting duct after foaming process. (c) Cut end of duct after foaming. (d) Capping off duct

found at http://www.hss.energy.gov/healthsafety/wshp/be/.

All of the CFRs are collectively searchable and available at http://www.gpoaccess.gov/cfr/index.html.

The OSHA regulations (29 CFR) are available at the OSHA website, http://www.osha.gov/, under "Standards." Some of these regulations are:

- 29 CFR 1910, Subpart I, Personal Protective Equipment
- 29 CFR 1910 and 1926, Subpart Z, Toxic and Hazardous Substances
- 29 CFR 1910.141, Sanitation
- 29 CFR 1910.132, Personal Protective Equipment General Requirements
- 29 CFR 1910.134, Respiratory Protection
- 29 CFR 1910.1020, Access to Employee Exposure and Medical Records
- 29 CFR 1910.1200, Hazard Communication
- 29 CFR 1910.1450, Occupational Exposure to Hazardous Chemicals in Laboratories, the American Conference of Governmental Industrial Hygienists, Threshold Limit Values for Chemical Substances and Physical Agents in the Work Environment

REFERENCES

Pohanish, R.P., and Greene, S.A., 1996. *Hazardous Material Handbook,* Van Nostrand Reinhold, New York and London

SELECTED REFERENCES

- Brooks, R.O.R., 1958a. Beryllium Handling. Reducing the Health Risk, *Nucl. Power,* Vol 3, p 112–114
- Frey, C., 2004. "Workers at the Energy Department's Gaseous Diffusion Plants in Kentucky and Ohio Have Been Exposed to Beryllium," cfreyssi-group.net

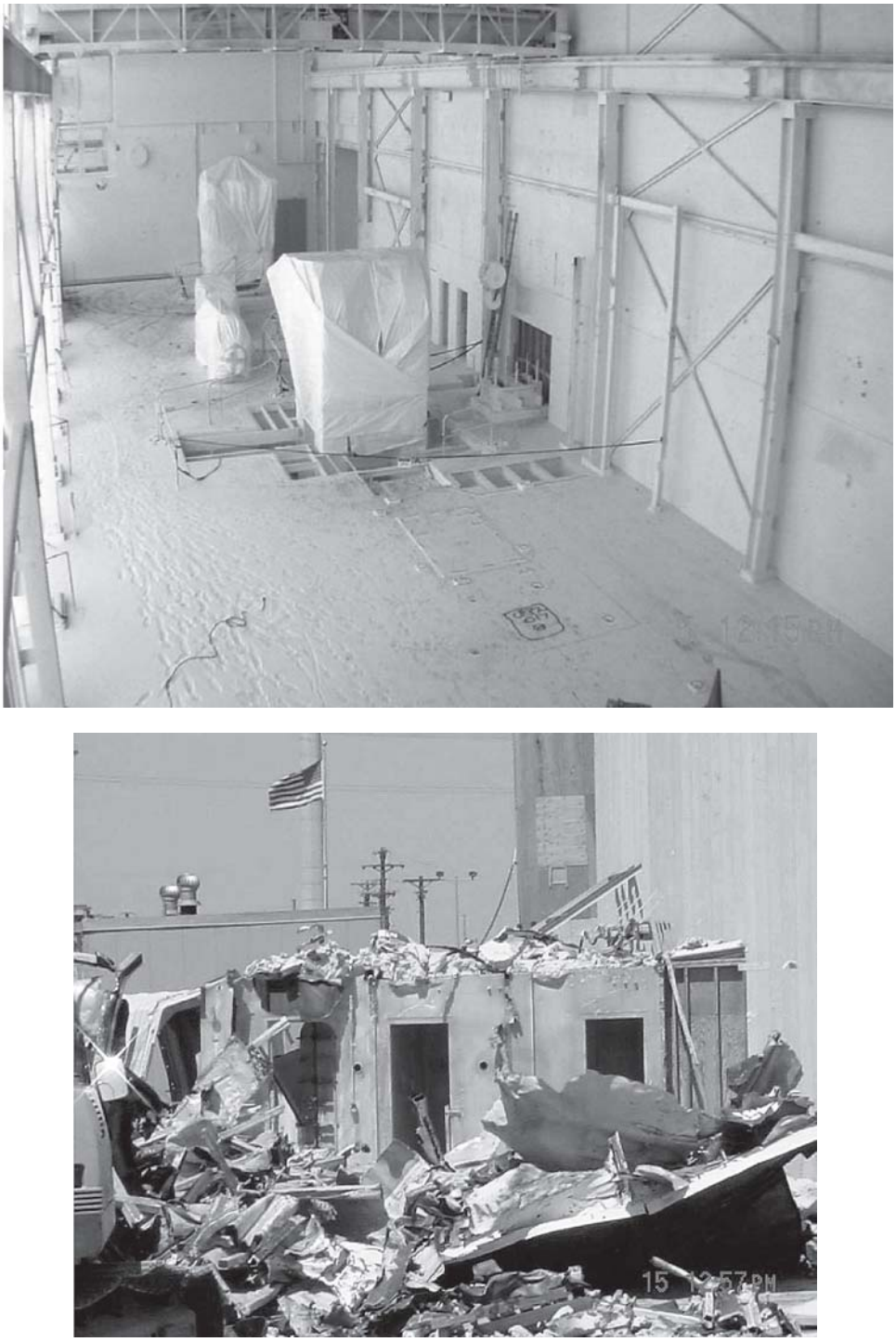

Fig. 29.5 (a) Application of fixatives (colored light green to improve inspection) to contain beryllium contamination is an effective method to control exposure to beryllium. (b) Control of beryllium contamination through the application of fixatives (colored bright yellow/orange) during facility demolition has been demonstrated to effectively contain beryllium and eliminate the need for higher-risk and labor-intensive manual decontamination.

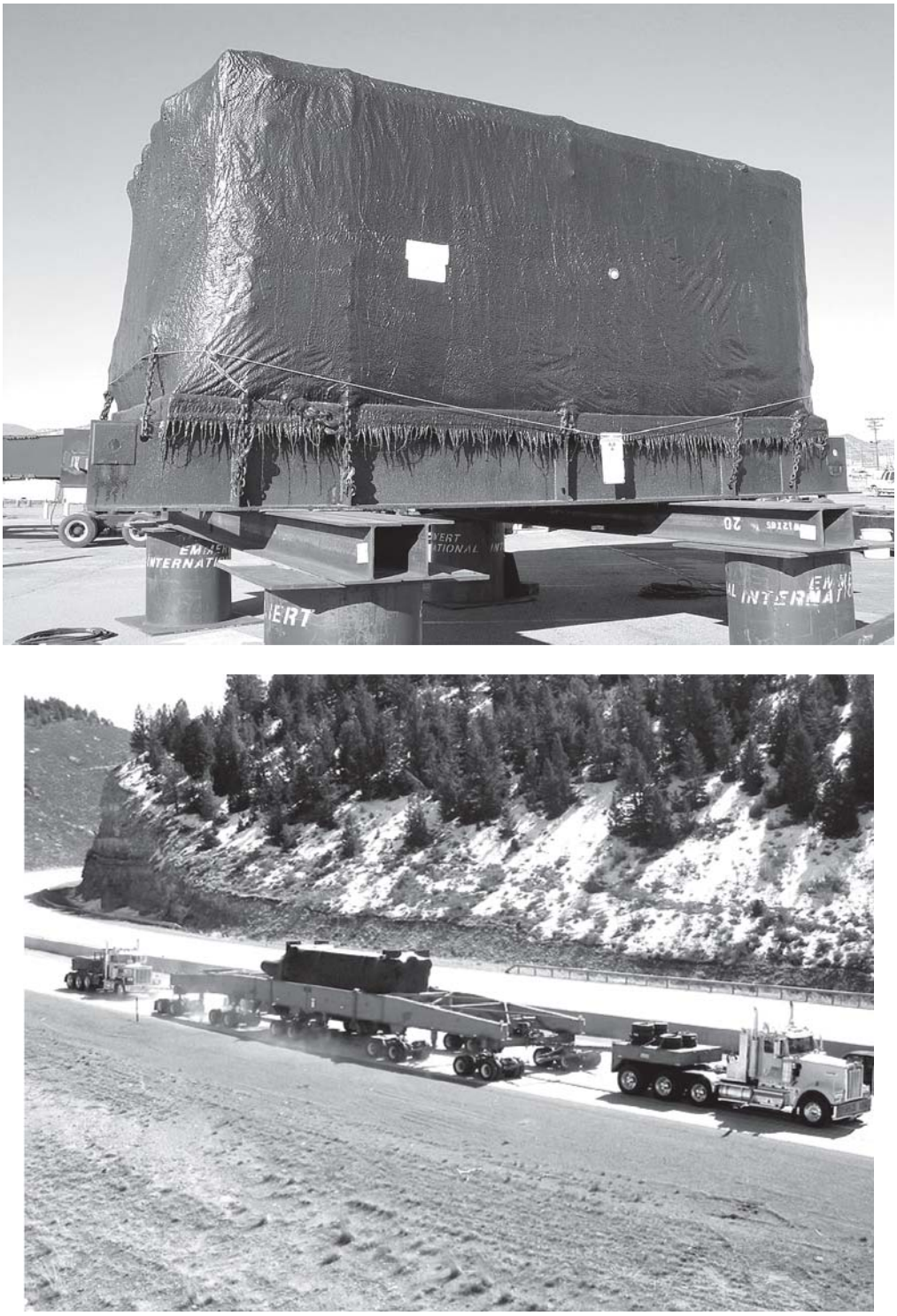

Fig. 29.6 (a) Large press contaminated with uranium and beryllium. It has been coated with a poly-urea-based coating and prepared for transport to a waste repository. (b) Large press, contaminated with uranium and beryllium and coated with a poly-urea-based coating, being transported to a waste repository

- IARC, 1994. Beryllium, Cadmium, Mercury and Exposures in the Glass Manufacturing Industry, *IARC Monographs on the Evaluation of Carcinogenic Risks to Humans,* Vol 58, International Agency for Research on Cancer, Lyon, France, p 444
- McInerney, J.R., 2003. "Beryllium Health Surveillance," Rocky Flats Environmental Technology Site, Golden, CO
- Narayan, R., and Ramamurthy, A., 1994. A Health and Safety Aspects of Beryllium Operations, *Miner. Process. Extr. Metall. Rev.,* Vol 14 (No. 1), p 301–318
- U.S. Department of Energy, 2003. "Investigation of Beryllium Exposure Cases Discovered at the North Las Vegas Facility of the National Nuclear Security Administration"
- U.S. Department of Labor, 1974a. "Access to Employee Exposure and Medical Records," 29 CFR 1910.1020, Federal Register 39:23502, Occupational Safety and Health Administration
- U.S. Department of Labor, 1974b. "Personal Protective Equipment General Requirements," 29 CFR 1910.132, Occupational Health and Safety Administration
- U.S. Department of Labor, 1974c. "Sanitation," CFR 1910.141, Federal Register 39: 23502–29, Occupational Health and Safety Administration
- U.S. Department of Labor, 1990. "Occupational Exposure to Hazardous Chemicals in Laboratories," 29 CFR 1910.1450, Occupational Safety and Health Administration
- U.S. Department of Labor, 1994. "Hazard Communication," 29 CFR 1910.1200, Federal Register 59:6126–6184, Occupational Health and Safety Association
- U.S. Department of Labor, 2003. "Standard on Personal Protective Equipment (PPE) for General Industry," 29 CFR Part 1910, Subpart I, Federal Register 68:14262–14263, Occupational Safety and Health Administration
- U.S. Department of Labor, 2004a. "Threshold Limit Values for Chemical Substances and Physical Agents," 29 CFR 1910.1450, American Conference of Governmental Industrial Hygienists, Cincinnati, OH
- U.S. Department of Labor, 2004b. United States Department of Labor, Occupational Safety and Health Administration, available from http://www.osha.gov/ (Accessed April 22, 2004)

Index

A

acrylic adhesives, 445–446
acute beryllium disease (ABD), 499, 500–501
adhesive bonding
  applying, 451
  benefits/limitations, 444(T)
  classification of, 443–445(T)
  curing, 451–452
  exposure of, 447, 448(F)
  introduction, 441–443(F)
  lap joints, 442(F)
  mechanical properties, 452–453(F,T)
  storage life, 447, 448(F)
  structural adhesive types, 445–447(T)
  surface preparation, 447–451(F)
    etchants, 450
    methyl ethyl ketone (MEK), 448
adhesive types, structural
  acrylic adhesives, 445–446
  anaerobic adhesives, 446
  characteristics of, 445(T)
  copolymers of polyethylene, 446–447
  cyanoacrylates (superglues), 446
  epoxy adhesives, 445
  phenolic (phenolicformaldehyde) adhesives, 446
  polybenzimidazoles, 446
  polyimides, 446
  polyurethanes, 446
  silicones, 446
  urethanes, 446
Agency for Toxic Substance and Disease Registry (ATSOR), 511
alloying of beryllium
  alloys, 163–164
  aluminum-beryllium production, 165, 167–170(F,T), 171(T)
  beryllium-aluminum alloys, 164–165(F), 166(F)
  beryllium-antimony alloys, 170–171
  beryllium-copper alloys, 171–173(F)
  beryllium-iron alloys, 173–174
  beryllium-titanium composites, 174–176(F,T)
  composites, 163–164
  introduction, 163
  Lockalloy, 164, 165, 167(F)
  transition metals, 173
aluminum-beryllium production, 165, 167–170(F,T), 171(T)
American Conference of Government Industrial Hygienists (ACGIH), 511
American Welding Society (AWS), 415
amorphous alloys
  applications, 148(F)
  early work on, 145–147(F,T)
  introduction, 145
  recent efforts, 147–148
anaerobic adhesives, 446
analytical chemistry (beryllium)
  beryllium analysis, radiometric methods for, 111–112
  beryllium determination
    colormetric methods, 108–110
    fluorometric methods, 108–110
    gravimetric methods, 107–108
    volumetric methods, 108
  beryllium separation, 110
  emission spectrometry, 112(T)
  introduction, 107
  polarographic methods, 113
  radiochemical separation procedures, 110–111
  sample preparation, 107
  spectrometric methods, 112(T)
aqueous corrosion
  atmospheric corrosion, 464
  carbide inclusions, 464–465
  contamination sources, 474–478(T)
  corrosion prevention, 474–478(T)
  crystallographic-orientation effect, 472–474(F)
  environments (in various), 459–461(F), 462(F)
  free carbon inclusions, 465
  hydroxide of beryllium, stability of, 461–463(F)
  mechanical properties, effect on, 478–481(F)
  metallic materials, 463–464
  oxide of beryllium, stability of, 461–463(F)
  pitting corrosion, 467–472(F)
  polarization studies, 465–467(F,T), 468(F), 469(F)
  rainwater, 463(T)
  saturated calomel electrode (SCE), 468(F), 471(F), 473(F), 479(F)

aqueous corrosion (continued)
seawater, 463(T), 464(F,T)
trichloroethane (TCE), 475, 477(T), 478(T)
trichloroethylene (TCA), 475, 478(T)
Argentina
beryl, sources of, 21, 23
production, history of, 12, 15, 17
atmospheric, use of term, 464
atmospheric corrosion, 464
Atomic Energy Commission (AEC), 499
atomic number, 1, 2(F)
atomic peening, 385, 387
atomic weight, 1, 2(F)
atomization
gas, 269–270
high-pressure gas atomizer (HPGA), 270
introduction, 269
attrition or attritioned, 269

B

ball milling, 246, 269, 270, 296
ball-milled powder, 216(F), 269, 329
bare rolling, 304, 305(T)
barns, 43–44, 47
bend
ductility, 283, 299
four-point bend, 219, 368, 478, 479
notched, 228, 229(F), 230(F)
roll, 308–310(F)
single-edge-notched, 220
test data, 228, 241(F)
bend-plane splitting, 154, 156(F)
bertrandite, 21
bertrandite flotation, 65–66
beryl
Brazil, 23
China, 24–25
introduction, 20–21
Russia, 25
variation in the chemical composition, 24(T)
beryllia ceramics, 1, 123(T)
beryllium, introduction
alloys, numbers limited by, 4
application of, 1, 3–4(T)
atomic number, 1
atomic weight, 1
beryllia ceramic ware, 1
chemical properties, 4–5
nuclear properties, 1
periodic table, 1, 2(F)
physical properties, 4
physico-chemical properties, 5(T)
radioisotopes of, 3(T)
symbol (Be), 1
beryllium, wrought, 347–348
Beryllium Alloy committee, 17
beryllium borides, 117
beryllium carbide, 117–118
beryllium carbonates, 118
beryllium carboxylates, 118
beryllium chloride, electrolysis of, 102–103
beryllium chloride-beryllium fluoride fused salt electrolysis process, 3
beryllium compounds
beryllium borides, 117
beryllium carbide, 117–118
beryllium carbonates, 118
beryllium carboxylates, 118
beryllium halides
beryllium bromide, 118
beryllium chloride, 118–119
beryllium fluoride, 119
beryllium iodide, 118
introduction, 118
polymorphism in, 120–121(F,T)
preparation of, 119–120
beryllium hydride, 121(F)
beryllium hydroxide, 121
beryllium nitrate, 121–122
beryllium nitride, 122
beryllium oxalate, 125(F)
beryllium oxide, 122–123(T)
beryllium oxide carboxylates
introduction, 123–124(T)
normal beryllium carboxylates, 124–125
beryllium perchlorate, 126
beryllium phosphates, 125–126
beryllium sulfate, 126–127
beryllium sulfide, 127
Beryllium Corporation, 8, 9
beryllium fluoride
glass, 99–101(F)
introduction, 99
metal production from, 101–102
preparation of, 99
beryllium fluoride-lithium fluoride fused salt electrolysis, 3
beryllium halides
beryllium bromide, 118
beryllium chloride, 118–119
beryllium fluoride, 119
beryllium iodide, 118
introduction, 118
polymorphism in, 120–121(F,T)
preparation of, 119–120
beryllium hydride, 121(F)
beryllium hydroxide, 121
beryllium hydroxide precipitates, 95
beryllium industry, current status, 17–18
beryllium ingot-sheet process, 260
beryllium intermetallic compounds
background/historical information, 131–132(T)
beryllides, fabrication of, 142
beryllides, structures of, 133(T)
$M2Be_{17}$, 132
MBe, 133
MBe_{12}, 132
MBe_{13}, 132
MBe_{2}, 133
MBe_{22}, 132

MBe_3, 132–133
MBe_5, 132
beryllium intermetallics, other, 133–134(F)
coefficients of thermal expansion (CTE), 139(T)
conclusions, 142
diffusion, 140–141
electrical properties, 140(F)
future work, 142
hydrogen storage, 141–142
mechanical properties, 134–138(F,T)
oxidation behavior, 138–139
sputter deposition, 140
thermal properties, 139–140(T)
beryllium minerals, 19(T)
beryllium nitrate, 121–122
beryllium nitride, 122
beryllium oxalate, 125(F)
beryllium oxide, 122–123(T)
beryllium oxide carboxylates
introduction, 123–124(T)
normal beryllium carboxylates, 124–125
beryllium pebbles, 295–296
beryllium perchlorate, 126
beryllium phosphates, 125–126
beryllium radio chemistry, 111
beryllium sulfate, 126–127
beryllium sulfide, 127
beryllium-aluminum alloys, 164–165(F), 166(F)
beryllium-antimony alloys, 170–171
beryllium-copper alloys, 171–173(F)
beryllium-induced lymphocyte proliferation blood test (BeLPT), 502–503, 505
beryllium-iron alloys, 173–174
beryllium-titanium composites, 174–176(F,T)
beta phase, 146, 151, 181, 182, 186
beveling (chamfering), 350
billets, 286(T), 295, 303, 305, 328
binary phase diagrams
beryllium-aluminum (Al-Be), 180(F)
beryllium-barium (Ba-Be), 181, 183(F)
beryllium-boron (B-Be), 180–181, 182(F)
beryllium-calcium (Be-Ca), 181, 184(F)
beryllium-cobalt (Be-Co), 181–182, 184(F)
beryllium-copper (Be-Cu), 182, 185(F)
beryllium-gallium (Be-Ga), 183, 186(F)
beryllium-germanium (Be-Ge), 183, 187(F)
beryllium-gold (Au-Be), 180–181(F)
beryllium-iron (Be-Fe), 182, 185(F)
beryllium-lithium (Be-Li), 183, 188(F)
beryllium-magnesium (Be-Mg), 183, 189(F)
beryllium-molybdenum (Be-Mo), 183, 185, 190(F)
beryllium-nickel (Be-Ni), 186, 191(F)
beryllium-niobium (Be-Nb), 186–187, 192(F)
beryllium-plutonium (Be-Pu), 187, 192(F)
beryllium-silicon (Be-Si), 187, 193(F)
beryllium-silver (Ag-Be), 179–180(F)
beryllium-sodium (Be-Na), 186, 191(F)
beryllium-tin (Be-Sn), 187, 193(F)
beryllium-titanium (Be-Ti), 187–188, 194(F)
beryllium-tungsten (Be-W), 188–189, 195(F)
beryllium-uranium (Be-U), 188, 194(F)
beryllium-yttrium (Be-Y), 189, 195(F)
beryllium-zinc (Be-Zn), 189, 196(F)
beryllium-zirconium (Be-Zr), 189–190, 196(F)
blistering, 277, 396, 465, 488
blisters, 464, 488–489
block (in contrast to billet), 295
body-centered cubic, (bcc), 5(T)
boiling point, 5(T), 33(T), 56(T), 85(T)
bonding
explosive bonding, 423 (*see also* solid-state bonding; welding)
gas pressure bonding, 422, 430, 433
press bonding, 422
pressure bonding, 422
brass
cathode, 354
electrode, 354, 355
fixtures, 339, 340, 348
mill products, 9
structure, 186
braze welding, 409–410. *See also* brazing
Brazil, 12, 17, 20, 21, 23
brazing
brazed joints, test results of, 418–420, 421(F,T), 422(F), 423(F), 424(F)
filler metals, 415–417(F)
fluxes, 417
furnace, 414–415
induction, 414, 415
introduction, 413–414
joint design, 417–418
process, selection of, 414–415
surface preparation, 415
temperature ranges, 417
torch, 414
Brush Beryllium Company, 8, 9–10
Brush Wellman, Inc., 11, 493–498(F,T)
buffing, 507(T)
butt welds, 325, 413

C

cancerous tumors, 503
carbide inclusions, 464–465
cast billets, 318
casting (beryllium)
beryllium, solidification of, 253–255(F)
cast structure, 255
centrifugal casting, 262
chill zone, 253, 254(F), 255
equiaxed zone, 255
grain refinement, 255–257(f)
melting techniques
centrifugal casting, 262
electron beam melting (EBM), 261–262(T)
introduction, 257
static casting, 257–258
vacuum arc melting (VAM), 260–261
vacuum induction melting (VIM), 258–260(F)

casting (beryllium) (continued)
metal purification, 262–263(T)
solid-liquid (S/L) interface, 253, 254, 255
static casting, 257–258
vacuum arc melting (VAM), 257
vacuum induction melting (VIM), 257, 259, 261, 262–263
cathode poisoning, 376
cathodes, 15, 62, 85, 495–496
CBD Prevention Program (CBDPP), 500
centrifugal casting, 262
chemical machining, 355–357(F)
chemical vapor deposition (CVD), 393–395(F)
chemistry of beryllium
beryllium chloride, electrolysis of, 102–103
beryllium fluoride
glass, 99–101(F)
introduction, 99
metal production from, 101–102
preparation of, 99
chemical behavior of, 103–104
chemical character
basic carbonate, 95
beryllium basic carbonate, decomposition of, 96–97
beryllium basic carbonate preparation, 96
beryllium hydroxide, 95
beryllium hydroxide precipitates, 95
beryllium hydroxide, thermal decomposition of, 95–96
hydrolytic complexes in aqueous beryllium solutions, 95(F)
introduction, 93–94(T)
metallic beryllium, reactions of, 94
hydrated Be^{2} ions, solution chemistry of, 97–99(F)
chill zone, 253, 254(F), 255
China
beryl, source of, 20, 21
beryl in, 24–25(T)
Kjellgren-Sawyer sulfate extraction, 73
production, history of, 12–13
variation in chemical composition of beryl, 24(T)
chronic beryllium disease (CBD), 499, 500–503
Clifton Products Incorporated, 8, 9, 10–11
coating processes (beryllium)
chemical vapor deposition (CVD), 393–395(F)
coatings
adhesion, 362–363
chemical vapor deposition (CVD), 362
electroplating, 362, 363(T)
introduction, 361
physical vapor deposition (PVD), 361–362
plasma spraying (PS), 362–363
thickness, 362–363
electron beam melting (EBM), 363–364
electroplating (electrodeposition), 395–396(F,T)
introduction, 361
ion plating, 384–387(F)
laser processing, 392
physical vapor deposition (PVD)
introduction, 363, 364(F)
thermal (vacuum) evaporation, 363–370(F,T)
plasma arc spraying, 387–393(F,T)
plasma-assisted chemical vapor deposition (PACVD), 393
sputtering, 371–384(F,T)
advantages, 374(T)
cathode poisoning, prevention, 376
disadvantages, 374–375(T)
introduction, 370–371
magnetron, 372–374(F,T)
microstructure, 379–383(F)
optimum angle of incidence, 378–379(F)
oxygen, effect of, 376
planar diode, 371(F)
pulse, 371–372(F)
radio-frequency (rf), 371–372(F)
superconductive amorphous beryllium films, production of, 377–378(F)
threshold energy of, 376–377(F)
triode, 371–372(F)
yield, 375–376(F)
Code of Federal Regulations (CFR), 510
coefficients of thermal expansion (CTE), 139, 384, 430
cold isostatic pressing (CIP), 269, 272–273(T), 274(F), 275(T)
cold welding, 423
compressibility, 28(T), 32, 33(F)
compressive strength, 123(T), 136
compressive yield strength, 176, 213, 287–288, 316
computer-aided design (CAD), 333
computer-aided drafting, 357
contact dermatitis, 502
Copaux-Kawecki Fluoride Extraction, 74–78
copolymers of polyethylene, 446–447
copper
beryllium-copper (Be-Cu), 182, 185(F)
beryllium-copper alloys, 171–173(F)
copper/copper-base alloys, 434–435(F,T), 436(T)
dispersion-strengthened copper (DSCu), 434–435
recovery, 495–497(F,T)
corrosion
aqueous corrosion, 459–484(F,T)
atmospheric, 464
high-temperature, 485–492(F)
pitting, 467–472(F)
prevention, 474–478(T)
stress-corrosion tests, 480
cost savings, 330, 331(T)
countercurrent decantation (CCD) process, 80(F)
creep
forming, 310–311(F)
strength, 231–233, 237(F), 238(F), 239(F), 240(F)
critical resolved shear stress (CRSS), 153, 154(F), 157(F), 158(F)
cross rolling, 280, 283, 298(F), 300, 304
crystallographic-orientation effect, 472–474(F)
cupping, 305
cupric-ferric, 107–459
curling, 303–304
cylindrical billets, 324

D

deep drawing, 305–308(F)
Degussa extraction of beryllium, 73–74, 75(F)
Degussa process, 15
delta phase, 182
dendrite, 395, 406
density, 1, 2(T)
Department of Energy (DOE), 499
Deutsche Gold und Silver Scheideanstalt (DEGUSSA), 14, 15–16
di-(2-ethylhexyl) phosphoric acid (HDEHP), 80, 81(F), 82, 83
die threading, 325
dies, 311, 317(F), 325, 438
differential thermal expansion (DTE) bonding, 433
diffusion, 40–41, 140–141
direct current reversed polarity (DCRP), 412
diseases
  acute beryllium disease (ABD), 499, 500–501
  acute pulmonary disease or acute chemical pneumonitis, 500
  beryllium-induced lymphocyte proliferation blood test (BeLPT), 502–503
  cancerous tumors, 503
  chronic beryllium disease (CBD), 499, 500–503
  contact dermatitis, 502
  lung cancer, 503
  treatment, 503
dislocation pileups, 156(F), 404
dispersion-strengthened copper (DSCu), 434–435
distilled beryllium, 13
domestic industry, origin of
  Beryllium Corporation, 8, 9
  Brush Beryllium Company, 8, 9–10
  Brush Wellman, Inc., 11
  Clifton Products Incorporated, 8, 9, 10–11
  introduction, 8–9
  Kawecki Berylco Industries (KBI), 11
  Kawecki Berylco Industries (NGK Metals), 11
dose-response relationship, 504
double-cantilever beam (DCB), 220, 221(F), 223(F)
draw ring, 307
drawability, 325, 326
drilling, 352–353
ductile-to-brittle transition temperature (DBTT), 134(T)
ductility
  adhesives, 443, 444(T)
  anisotropy, 297
  as-sprayed beryllium, 391
  bend, 283, 299
  beryllides, 134
  beryllium-titanium composites, 174
  biaxial, 290, 314
  contaminants, effect on, 333
  corrosion, 480
  directional, 290
  foils, 301
  grain size, 209, 235–236, 246(F)
  heat treatment, 326
  hot pressed block and sheet, 159(F), 160(F)
  HP21, 214, 217(F)
  improving, 154, 155, 163
  irradiated beryllium, 44
  Lockalloy, 165
  loss of, 44, 243, 246(F)
  oxide, 207, 298
  polycrystalline beryllium, 153
  powder production, 268
  powder sheet, 300
  preheating, 405, 406
  purity, 325
  rolling, 300, 301, 305
  S grades, 212, 213
  S-200E, 212(F), 213(F)
  S-65B, 212(F), 213(F)
  strain rate, 299
  structural castings, 206
  temperature, influence on, 218(F), 280, 283, 367
  twinning, 154, 341
  uniaxial, 298, 314
  vacuum hot pressing, 298
  vacuum induction melting (VIM), 258
  welding, 401, 403, 404, 407, 408
Dulong-Petit rule, 7

E

elastic modulus
  aerospace industry, 315
  aluminum-beryllium alloy, 164, 165, 168(T)
  copper-beryllium alloys, 171
  elastic properties, 152(T)
  optical components, 332
  physico-chemical properties, 5(T)
electric current dies, 438
electrical conductivity, 3(T), 5(T), 48(T), 85, 136(T), 326, 392(F)
electrical discharge machining (EDM), 354–355
electrical resistivity, 43(F), 48(F,T), 49(F,T), 50(T), 123(T), 160(F)
electrochemical, exposure sources, 507(T)
electrochemical grinding, 355
electrochemical machining (ECM), 355, 356(F)
electrodes
  brass, 354
  casting (beryllium), 261
  electrical discharge machining (EDM), 354
  electrochemical machining (ECM), 355
  mercury/mercurous sulfate, 469(F)
  saturated calomel electrode (SCE), 468(F), 471(F), 473, 479(F)
  sawing (cutting), 354
  standard emf series, 465(T)
  triode sputtering, 371–372(F)
  welding, 407, 408–409, 412
electroforming, 333
electroless plating, 363(T)
electrolysis, 270
  beryllium chloride, 102–103
  halides, 62
  solid cathode electrolysis cell, 86(F)
  soluble anode, 76

electrolytic
  extraction, 85–86(T)
  polishing, 202
  reduction, 62
electrolytic extraction, 85–86(T)
electromotive force (emf), 465
electron beam gun, 364
electron beam melting (EBM), 261–262(T), 363–364
electron beam welding (EBW), 407–408
electron microscopy, 206–207
electroplating (electrodeposition), 362, 363(T), 395–396(F,T), 427
electrorefining, 76–77, 90–91, 494, 495
elongation
  as-machined, annealed, and etched grade S-200E, 345(T)
  as-machined S-200E beryllium, 211(T)
  BAg-19 brazing alloy, 421(T)
  beralcast alloys, 171(T)
  beryllium cross-rolled sheet, 301(T)
  beryllium wire, 327(T)
  beryllium-antimony alloys, 171
  consolidated beryllium powders, 329(F)
  copper additions, 173
  effect of grain size on the temperature dependency, 244(F)
  extruded beryllium, 320(T)
  forged beryllium powder parts, 288(F)
  grain size, room-temperature tensile yield strength, fracture strength minus yield strength, comparisons between, 242(F)
  hot isostatic pressing (HIP), 328(T)
  hot-pressed block, grade S-200F, 209(F)
  of hot-pressed blocks, 215
  hot-pressed HY beryllium, 223(F)
  HP21 beryllium, 217(F)
  isopressed and sintered beryllium compacts, 289(T)
  longitudinal and transverse elongations, comparison of, 323(F)
  longitudinal tensile elongation, variations in, 245(T)
  plasma-sprayed-and-sintered beryllium, 391(T)
  S-200F consolidated by near-net shape processes, 330(T)
  S-200F vacuum hot-pressed beryllium, 214(T)
  smooth bar specimens, 213(F)
  tensile, 159(T)
  transverse tensile elongation at 556 °C (1033 °F), 246(F)
  vacuum hot pressed beryllium powders, 285(T), 286(T)
  vacuum hot pressing (VHP), 328(T)
  vacuum hot-pressed grade S-65B beryllium, 211(T)
  vacuum hot-pressed (VHP) beryllium, 223(F)
  vacuum-sintered beryllium slip castings, 290(T)
  warm-rolled beryllium sheet and plate, 301(T)
embrittlement, 138, 163, 222, 304, 414
emission spectrometry, 112(T)
emissivity, 363, 476
end milling, 350–351
Environmental, Safety, & Health (Working Group) (ES&H), 511
Environmental Health Criteria (EHC), 511
Environmental Protection Agency (EPA), 499
epitaxial, 366
epoxy adhesives, 445
equiaxed, definition of, 408
equiaxed zone, 255
Eriochrome Cyanine R, 109–110
etchants, 344, 355, 357, 450
ethylenediamine tetraacetic acid (EDTA), 107–108
eutectic, 205(T), 408
exit-edge milling, 350
explosive bonding, 423
extraction, thermodynamics of
  BeI_2, thermal decomposition of, 62(T)
  BeO, reduction of, 59–61
  beryllium halides, reduction of, 61(T)
  distillation, refining of beryllium by, 63(T)
  electrolytic reduction, 62
  hydrogen reduction, 61–62(T)
  introduction, 55
  thermodynamic data, 55, 56(T), 57(F)
  thermodynamic data, sources of
    Be_2SiO_4, 58
    Be_3N_2, 58
    $BeBr_2$, 58–59
    $BeCl_2$, 58–59
    BeCl(g), 59
    BeF_2, 58
    BeI_2, 58–59
    BeO, 58
    beryllium, 56, 58
    BeS, 58
    Br_2, 58
    Cl_2, 58
    F_2, 58
    I_2, 58
    N_2, 58
    O_2, 55–56
    S_2, 58
extractive metallurgy
  bertrandite, extraction from, 78, 80(F), 81(F)
  beryl, extraction from, 71
  cell configuration, 86(F)
  Copaux-Kawecki Fluoride Extraction, 74–78
  Degussa Extraction of Beryllium, 73–74, 75(F)
  electrolytic extraction, 85–86(T)
  electrorefining, 90–91
  Kjellgren-Sawyer sulfate extraction, 71–73
  leaching, 78–79, 80(F), 81(F)
  settling, 78–79
  solvent extraction, 78
  sulfate solutions, solvent extraction from, 79–85
  theoretical rate expression, 86–90(F)
extrusion
  canning, 317–319(F)
  conditions, 321–322
  conical-approach extrusion die, 317(F), 318
  cutoff block, 317
  dies, 317(F)
  extruded beryllium, mechanical properties of, 319–321(F,T), 322(F), 323(F)
  input billets, 316–317
  introduction, 316–319(F), 320(F)
  limitations, 322

reduction ratios, 319
temperatures, 319, 320(F)
warm extrusions, 317–318

F

fabrication, 142
face milling, 350
face-centered cubic, (fcc), 5(T)
filler metals
brazing, 415–417(F)
fusion welding, 411–412
film
anodized, 104, 476
epitaxial, 374
epoxy film adhesives, 47(F)
oxide, 4, 279, 404, 424, 466, 487
superconductive amorphous beryllium films, 377–378(F)
finished products, 508
flame spraying, 142, 389
flash
etched, 476
pickled, 463, 464(F), 481
removing, 325
flash welding, 438
fluorescent-tube industry, 10
fluxes, 417
foreign beryllium production (history of)
Argentina, 12
Brazil, 12
China, 12–13
former Soviet Union (FSU), 13–14
France, 12
French Morocco, 12
Germany, 14–16
India, 17
introduction, 12
Italy, 16–17
Japan, 17
Madagascar, 12
forge welding, 422. *See also* flash welding
forging
anisotropy, 315–316(F)
forgeability tests, 315
introduction, 311–314(F)
powder forging, 314
triaxial (redundant) forging, 313–314
unclad forging, 314–315
formability
composition, 298
deformation characteristics, 299
equipment, 299
fabrication history, 298
grain size, 297
introduction, 297
lubrication, 299–300
oil canning (or excessive warpage), 300
preheat treatment, 298
strain rate, 299
stress relieving, 300
temperature, 298–299
texture, 297–298(F)
tooling, 299
triaxial (redundant) forging, 298
former Soviet Union (FSU), 13–14
production, history of, 13–14
forming
creep forming, 310–311(F)
deep drawing, 305–308(F)
draw ring, 307
introduction, 305
roll bending (three-roll forming), 308–310(F)
stretch forming, 310–311(F)
fracture toughness, 219–228(F,T)
France, 7, 12
free cutting, 339, 475
French Morocco, 12
fritting, 80, 107
furnace brazing, 414, 415
furnace dross, 494, 495
furnaces
batch rotary fusion furnace, 75(F)
casting, 15
chlorinating furnace, 75(F)
conveyor furnace, 16
electric arc furnace, 60, 171, 495
electrolytic furnace, 75(F)
gas-fired rotary furnace, 74
graphite-lined, 102
Heroult type, 72
high-vacuum furnace, 345
induction furnace, 102
inert-atmosphere annealing furnace, 304
in-line furnace, 304
muffle furnace, 73
refractory linings of, 72
sublimation furnace, 75(F)
tilt-pour induction furnace, 258
vacuum induction furnace, 258, 262
fusion welding
cracking, 402–406(F)
feed rates, 411–412
filler metals, 411–412
introduction, 401–402
joint design, 412–413(F)
porosity (in welds), 410–411(F)
shielding, 412
surface preparation, 411
weld repair, 413
welding process, selection of, 407–410(F)
fusion zone, (FZ), 410

G

gamma background radiation, 111
gamma prime, 181, 186
gamma rays, 46, 47(T)
gamma source, 111, 112
gamma-alumina powder, 201
garimperos (illegal or freelance miners), 23
gas metal arc welding (GMAW), 407, 409, 412
gas pressure bonding, 422, 430, 433

gas tungsten arc (GTA) welding, 165, 407, 408–409(F)
geological outcroppings, 22–23
Germany
  Degussa extraction of beryllium from beryl, 73–74, 103
  Deutsche Beryllium GmbH (DEBEGE), 15
  Deutsche Gold und Silver Scheideanstalt (DEGUSSA), 14, 15–16
  production, history of, 8, 12, 14–16, 17
glucinium or glucinum (Gl), 1, 7
glykys, 7
gold
  beryllium-gold (Au-Be), 180–181(F)
  gold-plated mirrors, 333
  intermediate layers (indirect bonding), 427
  microconstituent, 205(T)
grinding, 353
Guinier-Preston zones, 180

H

half-cell reaction, 465
Hall-Patch (H-P) equation, 233
Hall-Patch (H-P) relationship, 227–228(F), 233–234, 240(F), 241(F,T), 242(F), 331(F)
hardness, 3(T), 4, 134, 135(T), 146(T), 453(T)
hazard analysis, 515, 516(F)
hazard controls, 516
heat affected zone (HAZ), 401–402
heat treatment, 156–157, 160(F), 163, 209, 298, 327(T)
heavy fermion, 132
hexagonal close-packed (hcp), 5(T)
high-density stringers, 254
high-efficiency particulate air filter (HEPA), 509
high-pressure gas atomizer (HPGA), 270
high-temperature corrosion
  beryllium in gaseous atmospheres
    air, 487–488(F)
    carbon dioxide, 488–490(F)
    carbon monoxide, 490
    nitrogen, 486–487
    oxygen, 485–486(F)
  high-temperature corrosion-resistant alloys, 490–491
  introduction, 485
high-temperature corrosion-resistant alloys, 490–491
history
  domestic industry, origin of, 8–11
  early, 7–8
  foreign beryllium production, 12–17
  industry, current status, 17–18
holes
  producing, 453, 455
  threading, 349(F), 354, 455(F)
hot isostatic pressing (HIP), 33
hot pressed block, 347
hydrofluoric acid activation, 66, 68(F)
hydrogen
  reduction, 61–62(T)
  storage, 141–142
hygienic handling practices
  applications
    decommissioning, 517, 519(F)
    process piping, dismantlement of, 516–517(F), 518(F)
    waste disposal, 517, 520(F)
  implementation of
    hazard analysis, 515, 516(F)
    hazard controls, 516
    introduction, 513–515(F,T)
  industrial hygiene beryllium work form, 514(F)
  introduction, 513
  personnel protective equipment (PPE), 515(T), 516–517(F)
  regulations, references of
    Code of Federal Regulations (CFR), 517–518
    OSHA, 518
  regulatory requirements
    American Conference of Governmental Industrial Hygienists, 513
    Chronic Beryllium Disease Prevention Program (CBDPP), 513
    Department of Energy (DOE), 513
    Occupational Safety and Health Administration (OSHA), 513
    permissible-exposure limit (PEL), 513
    time-weighted average (TWA), 513

I

impact resistance
  beryllium, 316
  cyanoacrylates (superglues), 446
  silicones, 446
impurities, control/effect of, 243–246, 247(F), 248(F)
inclusions
  carbide, 464–465
  free carbon, 465
  oxide, 202, 210, 495
India
  international beryllium sources, 21
  production, history of, 12, 17
  variation in chemical composition of beryl, 24(T)
ingot sheet, 300
ingots, 253
ingot-source rolling, 302
input billets, 316–317
interdendritic zones, 410
International Agency for Research on Cancer (IARC), 511
International Union of Pure and Applied Chemistry, 7
ion-beam assisted deposition (IBAD), 364, 364(T), 386, 386(F)
isotopes, 42, 47(T), 151
Italy
  production, history of, 12, 16–17
  SAPPI, 16–17

J

Japan
  Japanese Engineering Standard (JES), 17
  Nippon Gaishi Kaisha (NGK), 17
  production, history of, 12, 17
  Santoku, 17
  Yokozawa Chemicals, 17

Japanese Engineering Standard (JES), 17
joining. *See* welding
joint design, 409, 410(F)

K

Kawecki Berylco Industries (KBI), 11
Kawecki Berylco Industries (NGK Metals), 11
kinetics
  bonding mechanisms, 429
  evaporation, 366
  oxidation, 485
Kirkendall effect, 419
Kirkendall voids, 418–419
Kjellgren-Sawyer sulfate extraction, 71–73, 79, 84

L

lap joints, 442(F)
laser processing, 392
Lawrence Livermore National Laboratory (LLNL), 417, 500
leaching, 78–79, 80(F), 81(F)
lead, 202–203(T)
lead screw tappers, 358
  lead-based anodes, 495–496
lead-tin alloys, 255, 256(F)
liquid phase sintering, 276, 279, 280
liquidus, 413
Lockalloy, 164, 165, 167(F)
Los Alamos National Laboratory (LANL), 270, 388–389(T)
lubricants
  conventional, 300, 305
  drawing, 325
  glass, 328
  solid film, 317–318
  tapping, 358
lubrication
  can rolling, 304
  deep drawing, 305, 306(F), 308
  forging, 313
  kerosene, 199, 200–201
  metalworking, 299–300
  spinning, 328
lung cancer, 503

M

machinability, 339
machining. *See also* metal removal
  guidelines, general, 341–342, 343(F)
  machining-surface damage, 342–347(F,T)
    hot pressed block, 347
    wrought beryllium, 347–348
  operations
    beveling (chamfering), 350
    chemical machining, 355–357(F)
    cutting speeds, 354
    drilling, 352–353
    electrical discharge machining (EDM), 354–355
    electrochemical grinding, 355
    electrochemical machining (ECM), 355, 356(F)
    feed rates, 354
    grinding, 353
    introduction, 348
    milling, 350–352(F)
    photochemical machining (PCM), 357(F)
    sawing (cutting), 353–354
    tapping, 358
    thread cutting, 354
    trepanning, 357–358(F)
    turning, 348–350(F)
macroexamination, 206
Madagascar, 12
magnetic susceptibility, 48(T), 171
mast-mounted sight structure (MMSS), 330–331
McCabe-Thiele diagram, 497(F), 498(F)
mechanical fasteners
  advantages, 455
  bolts, 456
  clamping force, 456(F)
  disadvantages, 455
  electrical discharge machining (EDM), 455
  holes, producing, 453, 455
  holes, threading, 455(F)
  introduction, 441
  joints, 454–455(F)
  rivets, 456(F)
  structural inserts, 456
mechanical properties (beryllium)
  creep strength, 231–233, 237(F), 238(F), 239(F), 240(F)
  double-cantilever beam (DCB), 220, 221(F), 223(F)
  ductile-to-brittle transition temperature (DBTT), 222
  fatigue properties, 229–231(T), 232(F,T), 233(F), 234(F), 235(F), 236(F)
  fracture toughness, 219–228(F,T)
  grain growth, 233, 242
  grain size effects, 233–243(F,T), 244(F), 245(F)
  Hall-Patch (H-P) equation, 233
  hot isostatic pressing (HIPing) temperature, 213
  hot-isostatic-pressed properties, 213–214, 216(F,T), 217(F)
  hydrostatic tests, 246–247, 248(F), 249(F)
  impurities, control/effect of, 243–246, 247(F), 248(F)
  introduction, 209
  microyield properties, 217–219, 220(T)
  notched-bend properties, 228, 229(F), 230(F)
  notched-tensile properties, 228, 229(F), 230(F,T)
  notch-free strength ratio (NSR), 228, 230(T)
  Portevin-Le Chatelier (PLC), 214, 216, 219(F,T)
  recrystallization, 233, 234, 239–240, 242, 243(F)
  tapered double-cantilever beam (TDCB), 220, 221(F), 223(F)
  vacuum hot-pressed block properties, 209–213(F,T), 214(T), 215(F)
  yield-points, 214–216, 218(F), 219(F,T)
mechanical twinning, 344, 404
melting point (MP), 36(F), 37(F), 44(F), 45(F)
melting techniques
  centrifugal casting, 262
  electron beam melting (EBM), 261–262(T)

melting techniques (continued)
introduction, 257
static casting, 257–258
vacuum arc melting (VAM), 260–261
vacuum induction melting (VIM), 258–260(F)
metal inert gas (MIG) welding, 407, 410, 412
metal removal
etchants, 344, 355, 357, 450
machining guidelines, general, 341–342, 343(F)
machining operations
beveling (chamfering), 350
chemical machining, 355–357(F)
cutting speeds, 354
drilling, 352–353
electrical discharge machining (EDM), 354–355
electrochemical grinding, 355
electrochemical machining (ECM), 355, 356(F)
feed rates, 354
grinding, 353
introduction, 348
milling, 350–352(F)
photochemical machining (PCM), 357(F)
sawing (cutting), 353–354
tapping, 358
thread cutting, 354
trepanning, 357–358(F)
turning, 348–350(F)
machining-surface damage, 342–347(F,T)
hot pressed block, 347
wrought beryllium, 347–348
overview, 339–341
polytetrafluoroethylene (PTFE), pure form of Teflon, 340
wet cutting, 340, 348
metallography, beryllium/alloys
beryllium, microstructures of, 207
constituents, identification of
microconstituents, 205(T)
minor constituents, 206
principle constituents, 205–206
electron microscopy, 206–207
etching procedures, 202, 204–205(T)
grinding procedures, 199–200, 201(T)
introduction, 199
optical microscopy
macroexamination, 206
microexamination, 206
polishing procedures
electrolytic polishing, 202
electropolishing, 202, 204(T)
mechanical polishing, 200–202
specimen extraction, 199
toxicity issues, 207
metalworking
beryllium pebbles, 295–296
computer-aided design (CAD), 333
cross rolling, 298(F)
extrusion
canning, 317–319(F)
conditions, 321–322
conical-approach extrusion die, 317(F), 318
cutoff block, 317
dies, 317(F)
extruded beryllium, mechanical properties of, 319–321(F,T), 322(F), 323(F)
input billets, 316–317
introduction, 316–319(F), 320(F)
limitations, 322
reduction ratios, 319
temperatures, 319, 320(F)
warm extrusions, 317–318
forging
anisotropy, 315–316(F)
forgeability tests, 315
introduction, 311–314(F)
powder forging, 314
triaxial (redundant) forging, 313–314
unclad forging, 314–315
formability
composition, 298
deformation characteristics, 299
equipment, 299
fabrication history, 298
grain size, 297
introduction, 297
lubrication, 299–300
oil canning (or excessive warpage), 300
preheat treatment, 298
strain rate, 299
stress relieving, 300
temperature, 298–299
texture, 297–298(F)
tooling, 299
triaxial (redundant) forging, 298
forming
creep forming, 310–311(F)
deep drawing, 305–308(F)
draw ring, 307
introduction, 305
roll bending (three-roll forming), 308–310(F)
stretch forming, 310–311(F)
ingot sheet, 300
introduction, 295
mast-mounted sight structure (MMSS), 330–331
near-net shaping, 328–333(F,T)
powder consolidation, 295–297(F,T)
powder sheet, 300
rapid net-shape forming, 333
rolling
bare rolling, 304, 305(T)
can rolling, 302–304(F)
foil, 301, 302(T), 304–305
ingot-source rolling, 302
introduction, 300
powder-source materials, 300
sheet and plate, 300–301(T)
spinning, 327–328(F)
wire drawing
introduction, 322
materials, 325–326
mechanical properties, 326(F)
microstructure, 326–327(T)
technology, 323–325(F)

Metglas, 145–146(T)
methyl ethyl ketone (MEK), 290, 448
microexamination, 206
microhardness, 369(F), 389(F)
microyield strength, 217, 218, 219, 220(T)
milling, 350–352(F)
  basic milling operations, 351(F)
  beveling (chamfering), 350
  cutters, 351(F)
  end milling, 350–351
  exit-edge milling, 350
  face milling, 350
  metal removal, 350–352(F)
  roller/slab milling, 350–351
mineral processing
  bertrandite, tall oil fatty acid flotation of, 69(F)
  bertrandite flotation, 65–66
  beryllium ores, 66–68(F)
  hydrofluoric acid activation, 66, 68(F)
  introduction, 65
  low-grade deposits, 66(F)
  pegmatitic gangues, 66(F)
  phenacite, tall oil fatty acid flotation of, 69(F)
  phenacite flotation, 65–66
minerals of beryllium, 23(T)
miscibility gap
  metastable, 180(F), 183(F), 188, 194(F)
  subliquidus, 168, 183(F), 187, 192(F), 193(F), 409

N

National Institute for Occupational Safety and Health (NIOSH), 499
National Nuclear Security Administration (NNSA), 511
near-net shape (NNS), 328
near-net shaping, 328–333(F,T)
necking, 326
Nippon Gaishi Kaisha (NGK), 17
nondestructive
  analysis, 111–112
  detection/characterization of defects, 443
  evaluation methods, 434, 443
  test, 474
notch tensile strength, 230(T)
notch-free strength ratio (NSR), 228, 230(T)
notice of proposed rule making (NOPR), 511
nuclear properties, 1, 42–46, 47(T), 48(F)
nuclear-grade powder (NP), 269

O

Occupational Safety and Health Administration (OSHA), 499, 505, 507(T), 513, 518
occupational-exposure limit (OEL), 511
off-axis tensile strength, 174, 176(F)
oil canning (or excessive warpage), 300
order-disorder transition, 124
organometallics, 393–394
overaging, 447
oxidation behavior, 138–139
oxidation reaction, 467, 490
oxide inclusions, 202, 210, 495

P

peening, 387
pegmatites, 20, 22, 23, 24(T), 25
periodic table, 1, 2(F)
peritectic reactions, 179(F), 182(F), 185(F), 186(F), 187(F), 188(F), 189(F)
permissible-exposure limit (PEL), 499, 507(T), 509(T), 513
personnel protective equipment (PPE), 515(T), 516–517(F)
phase transformations, 151
phenolic (phenolicformaldehyde) adhesives, 446
photochemical machining (PCM), 357(F)
physical metallurgy (beryllium)
  alloying, 157–160
  beryllium phases, 151
  beryllium physical properties, 151–153(F,T)
  beryllium transformations, 151
  heat treatment, 156–157, 160(F)
  mechanical properties
    deformation mechanisms, 153–154(F), 155(F), 156(F), 157(F), 158(F)
    hexagonal crystal structure, 153(T)
    polycrystalline beryllium, 154–156, 159(F,T), 160(F)
physical properties
  atomic/crystal structure, 27(T), 28(F)
  elastic, 27–32(F,T)
  introduction, 27
  miscellaneous, 46–49(F,T), 50(T), 51(F), 52(F,T), 53(F)
  nuclear, 42–46, 47(T), 48(F)
  precision elastic limit (PEL), 29
  thermal, 32–42(F,T), 43(F), 44(F), 45(F,T), 46(F)
physical vapor deposition (PVD)
  introduction, 361, 363, 364(F)
  ion plating, 362
  sputter deposition, 362
  thermal (vacuum) evaporation, 361–362, 363–370(F,T)
pickling, 284, 312, 318, 324, 325, 495
pitting corrosion, 467–472(F)
plasma sprayed and sintered (PSS), 391
plasma spraying (PS), 284–285, 362–363, 388(F), 389(T), 393
plasma-assisted chemical vapor deposition (PACVD), 393–395(F)
plate, 300–301(T)
polishing
  electrolytic polishing, 202
  electropolishing, 202, 204(T)
  mechanical polishing, 200–202
  rough, 200
polybenzimidazoles, 446
polyimides, 446
polytetrafluoroethylene (PTFE), pure form of Teflon, 340
polyurethanes, 446
porosity
  argon, 412
  gas, 258
  helium, 412
  hydrogen, 410

porosity (continued)
repairing, 413d
in welds, 410–411(F)
Portevin-Le Chatelier (PLC), 214, 216, 219(F,T)
powder billets, 319
powder consolidation
cold compaction, 271
cold isostatic pressing (CIP), 272–273(T), 274(F), 275(T)
die pressing, 271–272(F)
explosive compaction, 276–277
slip casting, 275–276
vibration packing, 273–275(F), 276(F)
powder metallurgy
elevated-temperature consolidation
extrusion, 284
forging, 284
hot isostatic pressing (HIP), 283–284
introduction, 280
plasma spraying (PS), 284–285
vacuum hot pressing, 280–282(F,T)
introduction, 267–268
powder consolidation
cold compaction, 271
cold isostatic pressing (CIP), 272–273(T), 274(F), 275(T)
die pressing, 271–272(F)
explosive compaction, 276–277
slip casting, 275–276
vibration packing, 273–275(F), 276(F)
powder production
ablation method, 270–271
atomization, 269–270
ball milling, 270
electrolysis, 270
grades, 269
impact grinding, traditional, 268–269(T)
splat cooling, 271
standard commercial structural beryllium powder, 271(T)
vapor, 270
properties of
forged powder, 288(F)
hot isostatic pressing (HIP), 286–288(T)
introduction, 285
plasma-sprayed powder, 288–289(T)
sintered powder, 289–291(F,T)
vacuum hot-pressed (VHP), 285–286(T)
sintering
conventional, 277–278(F,T)
introduction, 277
pressureless, 278–280(F,T)
wrought forms, 290–291(T)
powder production
ablation method, 270–271
atomization, 269–270
ball milling, 270
electrolysis, 270
grades, 269
impact grinding, traditional, 268–269(T)
splat cooling, 271
standard commercial structural beryllium powder, 271(T)
vapor, 270
powder sheet, 300
precipitates, 95, 204(T), 403, 495
precipitation hardening, 244, 245, 246, 430
precision elastic limit (PEL), 29
preheat treatment, 298
press bonding, 422
pressure bonding, 422
pressurized gas metal arc welding (PGMA), 407, 411, 412
pulsed gas tungsten arc braze-spot welding, 409

R

radio-frequency (rf), 371–372(F)
radioisotopes, 1, 3(T)
rainwater, 463(T), 476
Raoult's law, 60, 367
rapid net-shape forming, 333
rapid solidification technique, 164, 168, 259, 409
recovery. *See* waste recycling
recrystallization, 233, 234, 239–240, 242, 243(F)
recycling. *See* waste recycling
reserves, world, 19, 20(T)
resistance butt welding, 325, 426(T)
resistance spot welding, 410
rod
cathode, 90
extruded, 241(T), 320(T)
filler, 408–409
history, 50(T)
rod-fed ion-plating system, 385(F)
roll bending (three-roll forming), 308–310(F), 404, 423, 433, 435(T), 436(T)
roller/slab milling, 350–351
rolling
bare rolling, 304, 305(T)
can rolling, 302–304(F)
foil, 301, 302(T), 304–305
ingot-source rolling, 302
introduction, 300
powder-source materials, 300
sheet and plate, 300–301(T)
rough machining, 348
rough polishing, 200
Russia, 14, 20(T), 24(T), 25

S

salt bath, 90
Santoku, 17
SAPPI, 16–17
saturated calomel electrode (SCE), 468(F), 471(F), 473(F), 479(F)
sawing (cutting), 353–354
scrap. *See also* metal removal; waste recycling
beryllium ingot-sheet process, 260
contamination source, as a, 507–508
conversion of, 90
near-net shaping, 328
reclaiming, 10

seawater, 463(T), 464(F,T), 476, 480(F)
segregation
  in alloys, 4
  aluminum, 212
  cooling rate, effect of, 253, 254(F)
  impurity, 262
  removing, 261, 262
  titanium, 259
  V-segregation, 254
self-diffusion, 40–41
sensitization, 499
shapes
  casting, 262
  circular, 327
  complex, 275, 276, 277, 284, 318, 451
  curved, 354
  cylindrical, 308
  deep drawing, 299, 307
  direct pressing of, 280
  fabrication, 142
  head, 456
  hollow, 267, 275, 283, 313, 314
  intricate, 354
  irregular, 272, 309
  powder metallurgy, 267
  simple, 276, 319, 327
  slip casting, 275
  special, 312
  structural, 316
  triaxial forging, 315
  tubular, 279
  U-shapes, 319
  weld pool shapes, 402(F)
shear strength
  aluminum-aluminum bond, 433
  bonding, 434–435(F), 436(F)
  brazed joints, 418, 419(T), 420(F), 423(F), 424(F)
  cyanoacrylates (superglues), 446
  lap-shear, 444(T), 446
  structural adhesives, 445(T)
  tensile strength, relationship of, 300, 448–449(F)
  ultimate, 436
shear stress
  braze thickness, as a function of, 420(F)
  in fasteners, 454(F)
  vs. shear strain, 248(F), 249(F)
  tensile, 452(F)
  ultimate, 419(F)
sheet and strip, 300
silicones, 446
single-edge-notch (SEN), 224–225(F), 227(F)
sintering
  conventional, 277–278(F,T)
  introduction, 277
  liquid phase, 276, 279, 280
  plasma arc spraying, 391–392(F)
  powder, 289(T)
  pressureless, 278–280(F,T), 289–290(F)
slabs, 301
slip planes, 153, 297
slip systems, 153, 154(F), 172, 299, 404
slope, definition of, 411–412
smelting, 60, 61
soldering, 438, 507
solid solutions, 60, 138, 163
solidification (beryllium), 253–255(F)
solid-liquid (S/L) interface, 253, 254, 255
solid-state bonding
  bond strengths, evaluation of, 434
  bonding mechanisms, 423–425(F), 426(T)
  dissimilar metals, bonding with
    aluminum, 436–437(F)
    copper/copper-base alloys, 434–435(F,T), 436(T)
    iron, 436–437(F)
    nickel, 436–437(F)
    silver, 436–437(F)
    stainless steel, 436
    titanium, 435–436
    vanadium, 436–437(F)
  equipment
    differential thermal expansion (DTE) bonding, 433
    gas-pressure bonding process, 433
    introduction, 433
    press welding, 433
    roll bonding, 433
  flash welding, 438
  intermediate layers (indirect bonding)
    introduction, 427, 428(T)
    silver, 427, 429
    silver-silver bond strength, 429(F)
  introduction, 421–423
  joint design, 430, 432–433(F)
  parent metal strengths, 425, 427
  QMV-grade beryllium, bonding of extruded, 425
  QMV-grade beryllium, bonding of hot pressed, 425
  surface preparation, 429–430, 431(T)
solidus, 413
solvent
  adhesives, 444(T)
  beryllium radio chemistry, 111
  chlorinated, 475–476(T), 477(T)
  copper industry, 496–497(F,T)
  direct beryllium extraction, 110
  extraction, 78, 79–85, 496(F)
  hand solvent cleaning, 507(T)
  methyl ethyl ketone (MEK), 348
  organic, 118, 123, 124, 443, 497
  resistance, 445(T), 446
  volatile, 431(T)
sources
  bertrandite, 21
  beryl, 20–21
  beryllium minerals, 19(T)
  Brazil, 23
  China, 24–25
  geological outcroppings, 22–23, 24(T)
  international, 21–22(F,T)
  introduction, 19–20(T)
  mineralogy, 20
  minerals of beryllium, 23(T)
  quaternary composition map of the Be-Al-M-Si-O system, 22(F)

sources (continued)
Russia, 25
summary statement, 25
variation in the chemical composition of beryl, 24(T)
world mine production, reserve and reserve base, 20(T)
space age, role in, 14
specific heat
application of beryllium/alloys, 3(T)
beryllides, 140(T)
covering a wide temperature range, 41(F)
as a function of temperature, 39(F), 40(F), 152(F)
physical properties of AlBEMet 140 and 162, 168(F)
physico-chemical properties, 5(T)
properties of high-purity beryllium oxide, 123(F)
room temperature thermal properties, 33(F)
thermal properties, 152(T)
spectral reflectance, 48, 52(F,T)
spectral transmittance, 49, 53(F)
spinning, 327–328(F)
splat cooling, 271
spoolers, automatic, 325
springback, 304, 311
springs, 3(T), 4, 10, 456(F)
Sputnik, 3
sputtering, 371–384(F,T)
advantages, 374(T)
cathode poisoning, prevention, 376
disadvantages, 374–375(T)
introduction, 370–371
magnetron, 372–374(F,T)
microstructure, 379–383(F)
optimum angle of incidence, 378–379(F)
oxygen, effect of, 376
planar diode, 371(F)
pulse, 371–372(F)
radio-frequency (rf), 371–372(F)
superconductive amorphous beryllium films, production of, 377–378(F)
threshold energy of, 376–377(F)
triode, 371–372(F)
yield, 375–376(F)
stacking faults, 363
standards, work exposure, 508, 509(T), 518
static casting, 257–258
stress-corrosion tests, 480
stress-strain curves, 210(F), 211–212, 213(F)
strip and sheet, 300
superconducting, 377, 378
surface tension, 296, 396, 414
swaging, 311–312
symbol (Be), 1
synthetic seawater, 476, 481(F)

T

tapered double-cantilever beam (TDCB), 220, 221(F), 223(F)
tapping, 358
tarnish, 4, 94, 460, 487
Teflon, polytetrafluoroethylene (PTFE), 340
tensile strength, 123(T), 167(T), 175(T), 287(T), 290(T), 421(T), 435(T), 452(F)
tensile yield strength, 155, 211(F), 214(F), 233, 242(T), 247(F), 248(F), 286(T), 305(T)
thenoyltrifluoro-acetone (TTA), 111
thermal (vacuum) evaporation (TE), 393
thermal conductivity
AlBEMet 140 and 162, 168(T)
application of beryllium and its alloys, 3(T)
beralcast alloys, 171(T)
beryllides, 140(T)
as a function of temperature, 42(F), 43(F)
high-purity beryllium oxide, 123(T)
normal-purity beryllium block and sheet as a function of temperature, 42(F)
physico-chemical properties, 5(T)
room temperature thermal properties, 33(T)
well-annealed high-purity beryllium, 44(F)
thread cutting, 354
three-roll forming machines
pinch-type, 308, 309(F)
pyramid-roll-type, 308–309(F)
three-roll forming (roll bending), 308–310(F)
time-weighted average (TWA), 499
toxicity, medical aspects of (beryllium /beryllium alloys)
acronyms, 511
Atomic Energy Commission (AEC), 499
beryllium diseases
acute beryllium disease (ABD), 499, 500–501
acute pulmonary disease or acute chemical pneumonitis, 500
chronic beryllium disease (CBD), 499, 500–503
treatment, 503
beryllium-induced lymphocyte proliferation blood test (BeLPT), 502–503
cancerous tumors, 503
CBD Prevention Program (CBDPP), 500
contact dermatitis, 502
contamination sources, 506–508(T), 509(T)
Department of Energy (DOE), 499
Environmental Protection Agency (EPA), 499
first aid procedures/precautions, 508–509
inhalation exposure, 501–502
introduction, 499–500
Lawrence Livermore National Laboratory (LLNL), 500
lung cancer, 503
Occupational Safety and Health Administration (OSHA), 499
oral ingestion, 502
permissible-exposure limit (PEL), 499, 507(T), 509(T)
protective/preventive actions, 509–511(T)
sensitization, 499
statistical observations, 503–506(T)
time-weighted average (TWA), 499
transgranular cleavage, 222
transgranular failure, 481
trepanning, 357–358(F)
triaxial (redundant) forging, 291, 298, 313–314, 315, 316(F)
trichloroethane (TCE), 475, 477(T), 478(T)
trichloroethylene (TCA), 475, 477(T), 478(T)

tubular
  blanks, 278
  extrusion, 318, 319
  rivets, 456
  shapes, 279
tungsten inert gas (TIG) welding, 407, 408(F)
turning, 348–350(F)
twinning, 153–154(F), 156(F), 200, 341, 343(F), 347, 348(F)
twinning, mechanical, 344, 404

U

ultimate shear strength, 436
ultimate tensile strength (UTS), 159
unclad forging, 314–315
urethanes, 446
U.S. Department of Health and Human Services (DHHS), 511
U.S. Strategic and Critical Materials Stock Piling Act of 1946, 19

V

vacuum arc melting (VAM), 257, 260–261
vacuum furnace brazing, 415
vacuum hot-pressed (VHP), 29
vacuum induction melting (VIM), 258–260, 261, 262–263
valency, 7–8, 117
vapor degreasing, 477
viscosity
  adhesives, 443, 446
  change as a function of time, 447, 448(F)
  high melt, 1
  molten fluoride, 100
voids, 259, 410, 411, 425, 443, 445
V-segregation, 254

W

waste recycling
  beryllium recovery, 497–498(F)
  copper recovery, 495–497(F,T)
  introduction, 493(T)
  McCabe-Thiele diagram, 497(F), 498(F)
  summary, 498
wedge-opening load (WOL), 225(F)
welding
  braze welding, 409–410 (*see also* brazing)
  brazing (*see* brazing)
  butt welds, 325, 413
  electron beam welding (EBW), 407–408
  fusion welding
    cracking, 402–406(F)
    feed rates, 411–412
    filler metals, 411–412
    introduction, 401–402
    joint design, 412–413(F)
    porosity (in welds), 410–411(F)
    shielding, 412
    surface preparation, 411
    weld repair, 413
    welding process, selection of, 407–410(F)
  gas metal arc welding (GMAW), 407, 409, 412
  gas tungsten arc (GTA) welding, 408
  introduction, 401
  joint design, 409, 410(F)
  metal inert gas (MIG) welding, 407, 410, 412
  pressurized gas metal arc welding (PGMA), 407, 411, 412
  pulsed gas tungsten arc braze-spot welding, 409
  resistance butt welding, 325, 426(T)
  resistance spot welding, 410
  soldering, 438
  solid-state bonding (*see* solid-state bonding)
  tungsten inert gas (TIG) welding, 407, 408(F)
wet blasting, 298
wet cutting, 340, 348
wire
  annealed, 327
  applications, 291
  beryllium, 175, 327
  filler, 407, 410, 411–412
  fine, 174, 327
  hot, 62
  wire-drawing process, 327(T)
wire drawing
  introduction, 322
  materials, 325–326
  mechanical properties, 326(F)
  microstructure, 326–327(T)
  technology, 323–325(F)
wire-drawing process, 327(T)
work hardening, 272(F), 311, 339, 342
world mine production, reserve and reserve base, 20(T)
wrought
  alloys, 171, 494
  beryllium, 347–348
  forms, 290–291(T)
  high purity wrought ingot, 241(T)
  hot pressed beryllium ingot, 290–291(T)
  unclad forging, 314
wrought beryllium, 347–348

Y

yield strength
  compressive, 176, 213, 287–288, 316
  microyield, 217, 218, 219, 220(T)
  tensile, 155, 211(F), 214(F), 233, 242(T), 247(F), 248(F), 286(T), 305(T)
yield-points, 214–216, 218(F), 219(F,T)
Yokozawa Chemicals, 17

Z

zones, 180, 255, 382, 404, 410, 470

ASM International is the society for materials engineers and scientists, a worldwide network dedicated to advancing industry, technology, and applications of metals and materials.

ASM International, Materials Park, Ohio, USA
www.asminternational.org

Publication title	Product code
Beryllium Chemistry and Processing	05223G

To order products from ASM International:

Online Visit www.asminternational.org/bookstore

Telephone 1-800-336-5152 (US) or 1-440-338-5151 (Outside US)

Fax 1-440-338-4634

Mail Customer Service, ASM International
9639 Kinsman Rd, Materials Park, Ohio 44073, USA

Email Cust-Srv@asminternational.org

In Europe American Technical Publishers Ltd.
27-29 Knowl Piece, Wilbury Way, Hitchin Hertfordshire SG4 0SX, United Kingdom
Telephone: 01462 437933 (account holders), 01462 431525 (credit card)
www.ameritech.co.uk

In Japan Neutrino Inc.
Takahashi Bldg., 44-3 Fuda 1-chome, Chofu-Shi, Tokyo 182 Japan
Telephone: 81 (0) 424 84 5550